DEEP FOUNDATIONS INSTITUTE

44th ANNUAL CONFERENCE

CHICAGO

Future Forward

Hilton Chicago | Illinois | October 15-18, 2019



2019 PROCEEDINGS

PREFACE

On behalf of Deep Foundations Institute (DFI) and the 2019 Annual Conference Organizing Committee, we would like to extend our thanks and appreciation to all attendees, exhibitors, underwriters, invited speakers, presenters and session moderators who helped make the 44th Annual Conference on Deep Foundations a success. This year's conference was held October 15-18, 2019, in Chicago, Illinois. Chicago has a rich history of contributions to geotechnical practice and foundation engineering and construction; and was a fitting location to look ahead to the future.

When the Organizing Committee was working to develop the central theme of the 44th Annual Conference, we explored the potential significance of the conference's number. Through numerology, or the study of the relationship between numbers and coinciding events, we discovered that the number 44 relates to business, and especially business which builds something that benefits many generations. The number 44 represents building for both the present and the future: it seeks for rewards for present work and a large positive effect on the future. Considering the conjunction of the legacy of Chicago in global foundation practice and the "meaning" of the conference identifier, we settled on a theme of ***>Future >Forward***. The intention of the conference was to promote the development of forward-thinking plans in deep foundation practice and related areas through technical presentations and panel discussions.

We believe we succeeded.

Our conference began with The Chicago Legacy which included a local celebrity, Geoffrey Baer who presented his impressions of the history, culture and people that have shaped the Chicago River corridor. We then followed with a panel of geotechnical experts who gave insight and offered predictions into the future of the geotechnical work which is integral to the magnificent high-rise structures of the Chicago skyline. Our spirited panel included Rich Finno, P.E., Ph.D., D.GE, Tony Kiefer, P.E., Steve Scherer, Bob Schock, Bill Walton, P.E., S.E., and Mike Wysockey, Ph.D., P.E.

>Future >Forward is also about the next generation of engineers and contractors and we were grateful to have former professor and current contractor, Rick Deschamps, Ph.D., P.E., present on the intricacies of the Mentor/Mentee relationship. Our final first-day plenary session theme was DFI and Technology which included presentations by the leaders of the DFI Project Information Management Systems (PIMS) committee which was formed in response to the industry trend towards digitalization of data, the increased use of data management and geospatial tools. The innovative panel, moderated by Gianfranco DiCicco, included Massimo Mucci, Vanessa Bateman, P.G., P.E., Mark Petersen, P.E., G.E., and Jamey Rosen, P.Geo.

The conference also hosted the Manufacturer Supplier and Service Provider (MSSP) Trade Expo Sessions in the Exhibit Hall and showcased presentations by DFI corporate members on services and products. The conference closed with our theme of ***>Future >Forward*** in mind with plenary sessions on Safety in Geo-Construction and The Digital Future. The conference welcomed undergraduate and graduate students throughout the Midwest with a formal program, including a networking session with participating industry professionals.

This publication contains peer-reviewed technical papers in the session areas selected by the Conference Organizing Committee: Crawl, Walk, Run - Improving Future Practice, Deep Foundations, The Digital Future, Developments in Safe Geo-Construction, Pile Foundations, Complex Excavations, Alternative Foundations, Earth Support, Underpinning and Soil Nailing, Ground Improvement, Drilled Shafts and Exploration and Testing.

As with past conferences, this event could not have been a success without the significant contributions and dedication of all stakeholders. We are grateful to the DFI Staff, Conference Organizing Committee, Session Chairs and Moderators, authors, reviewers, underwriters, exhibitors and volunteers. Finally, the

Chicago Organizing Committee is grateful for the opportunity to contribute to the success of the 44th Annual Conference on Deep Foundations.

Conference Chair: Dhooli Raj, P.E., Collins Engineers, Inc.

Program Co-Chairs: Ray Franz, P.E., D.GE, Hayward Baker Inc.
Cassandra Rutherford, Ph.D., P.E., Iowa State University

Session Moderators: Joel Dellaria, S.E., P.E., Hayward Baker Inc.
Darren Diehm, P.E., GEI Consultants, Inc.
Fei Han, Ph.D., P.E., Purdue University
Bernie Hertlein, FACI, M. ASCE, GEI Consultants, Inc.
Brandon Hughes, S.E., P.E., Thatcher Foundations, Inc.
Hannah Iezzoni, P.E., GeoStructures, Inc.
Sara Knight, P.E., Strata Earth Services, LLC
Robert Kruger, P.E., McDermott
Justin Lewis, P.E., Hayward Baker Inc.
Patrick Lydon, P.E., Bencor Global, Inc.
Todd Schraeder, BSCE, Hardman Construction, Inc.
Mark Stephani, P.E., WSP-USA, Inc.
Dan Woeste, P.E., Geosyntec

Student Activities: May El Khattab, P.E., Arup
Fawad Niazi, Ph.D., P.E., Purdue University Northwest

DFI - Finding Common Ground®

Mission Statement

To bring together multidisciplined individuals and organizations to find common ground and create a shared vision and a consensus voice for continual advancement in the deep foundations industry.

CASE STUDY: STABILITY ANALYSIS FOR AN EXISTING BRIDGE EXPERIENCING RIVERBANK EROSION

William Bohlen, P.E., BGE, Inc., Houston, TX; (281) 558-8700; wbohlen@bgeinc.com
Brandon Smith, P.E., BGE, Inc., Houston, TX; (281) 558-8700; bsmith@bgeinc.com

Abstract

Riverbank erosion along the Brazos River has modified the structural support conditions for an existing bridge structure in Southeast Texas. The 8-span, 1,200-foot long bridge was completed in 1992 along Highway 99, a key corridor for the Houston area. Foundation support conditions have been altered due to natural, ongoing river morphology for three bents on the affected riverbank. Recent events include three storms within a three-year period that each exceeded the 500-year return probability. This resulted in accelerated erosion along the northern riverbank. Over forty vertical feet of soil has been removed in some locations. Drilled shaft foundations are now functioning as columns. This review considers the behavior of columns and deep foundation elements due to the modified support conditions. The review ultimately presents a rational methodology for the review of the present and anticipated future bridge configuration with respect to current strength, service, and extreme event limits, with corresponding safety factors for the design.

Keywords: Drilled shafts, bridge columns, scour evaluation, bridge asset management, reliability based design

Introduction and Background

The Fort Bend Grand Parkway Toll Road Authority (Owner) oversees the State Highway 99 Judge Jodie Stavinoha Bridge over the Brazos River. The 8-span, 1,200-foot long bridge was originally designed with four southern approach spans of 115 feet; a three-span continuous river crossing with span lengths of 195 feet-235 feet-195 feet; and a single northern approach span of 115 feet. Figure 1 provides an overview of the northern portion of the bridge. Table 1 provides a summary of the original bridge substructure configuration. When the bridge was completed, the centerline of the Brazos River was located at midpsan of the main span and the northern high bank was originally located at Bent 7. Erosion process has forced the northern high bank to Abutment 9 (also called Bent 9), and the river centerline during normal flow conditions is located south of Bent 8. The overall estimated river excursion at present day is approximately 270 feet to the north from its original location. An erosion wall that was installed in 2017 limits further erosion of the north river bank within the 300-foot width of the roadway corridor right-of-way. This study was developed to better understand the existing conditions, and to forecast the need, nature, and criteria for potential future improvements.

The Brazos River is in a meandering alluvial river plain that naturally migrates over time. The processes of bank erosion and meander migration were ongoing before the bridge was constructed and will continue in the future. While some movement was always anticipated, recurring major flood events rapidly increased the rate of erosion in just a few years, as shown in Figure 1. Table 2 summarizes the impact of the riverbank erosion for Bents 6, 7, 8 and 9. The natural flowline of the Brazos River at the bridge is approximately Elevation +3.0. As the river shifts to the north, portions of the existing structure that were previously below ground are now above ground. Not only does this change the bridge support boundary conditions, but the exposed structures will be subjected to additional lateral loads due to wind and waterflow. Although the river seems calm with low current velocities most of the time, the currents were estimated at upwards of 12 knots during the flood events.

© 2019 Deep Foundations Institute

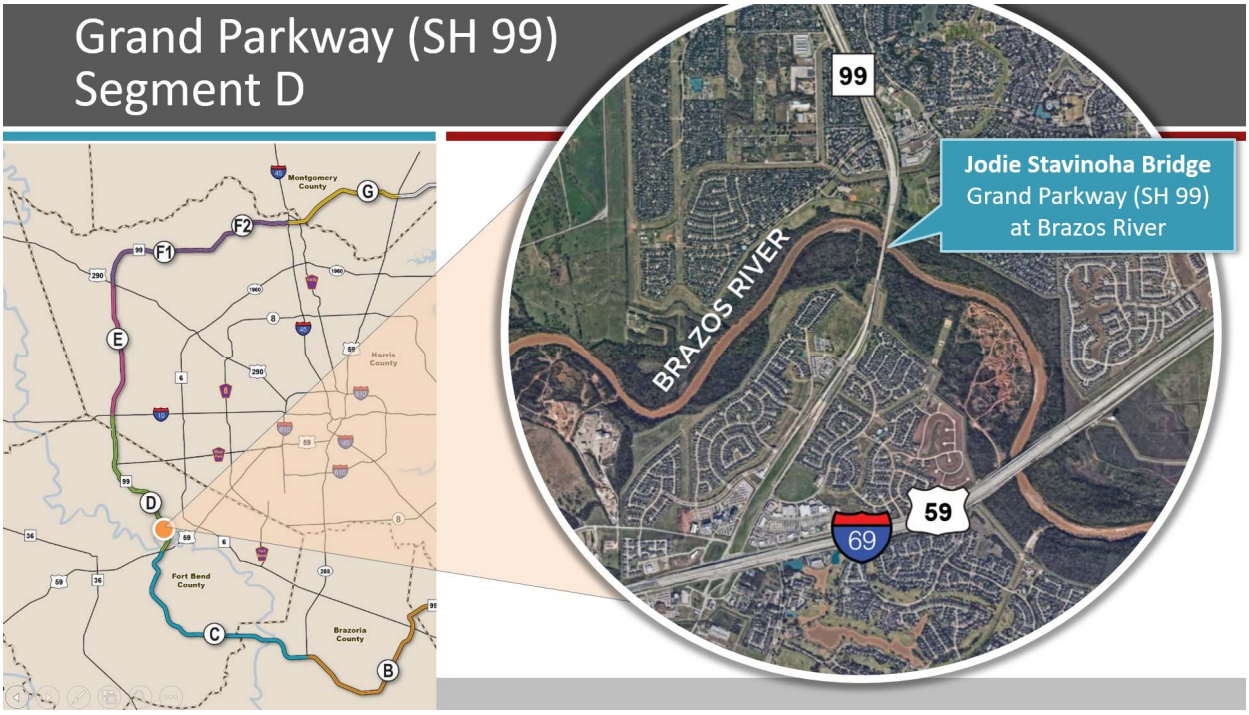


Figure 1. Vicinity Map and Location Map

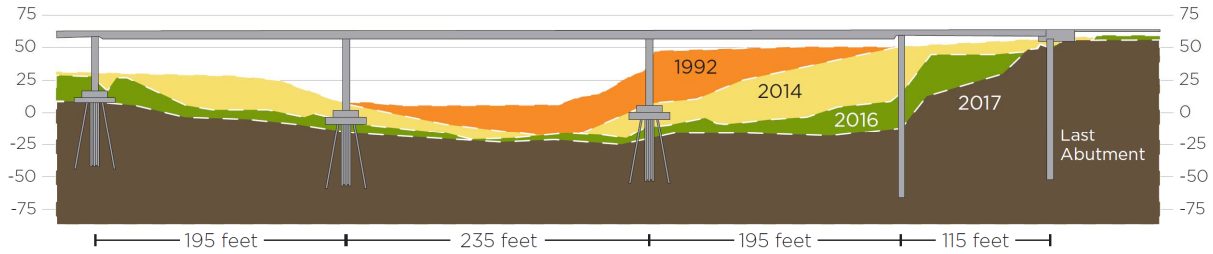


Figure 2. Bridge Profile Showing Scour Progression from 1992 to 2017 (Bents 5, 6, 7, 8, and 9)

Note that the elevations shown in Figure 2 require a vertical datum shift of approximately 15 feet to correspond to the elevations provided in the report, and the north bank is located on the right side.

Table 1. Original Bridge Substructure Configuration

Bent	Bridge Station	Column Description	Foundation Description	Foundation Tip Elevation
1	732+50	Abutment Backwall	5 Pairs of Battered 16” Concrete Piles	EL +33
2	733+65	3 EA @ 3’-0” Diam.	3 EA w/ 6 Battered PC Concrete Piles	EL +0
3	734+80	3 EA @ 3’-0” Diam.	3 EA w/ 6 battered PC Concrete piles	EL -27
4	735+95	3 EA @ 3’-0” Diam.	3 EA w/ 6 battered PC Concrete piles	EL -14
5	737+10	2 EA @ 5’x8’ Oval	2 EA w/ 14 battered PC Concrete piles	EL -31
6	739+05	2 EA @ 5’x8’ Oval	2 EA w/ 18 battered PC Concrete piles	EL -31
7	741+40	2 EA @ 5’x8’ Oval	2 EA w/ 18 battered PC Concrete piles	EL -31
8	743+35	Column Bent Cap	4 EA @ 5’-0” Diam x 121-ft long Shaft	EL -45
9	744+50	Abutment Backwall	4 EA @ 5’-0” Diam x 110-ft long Shaft	EL -35

Table 2. Ground Elevation Changes at Bents 7, 8, and 9.

Bent	Original Ground Elevation	Lowest Measured Ground Elevation	Calculated Scour Depth	Original Column Height	Present Effective Column Height	Original Foundation Length	Present Effective Foundation Length	Foundation Tip Elevation
6/7	72.50	+10	62.5 ft	n/a	n/a	55’ piles	45’ piles	EL -31
8	72.50	+20	52.5 ft	4.5 ft	56.5 ft	117.5 ft	65.0 ft	EL -45
9	72.50	+40	32.5 ft	3.5 ft	35.5 ft	107.5ft	75.0 ft	EL -35



Figure 3. Flooded Jobsite on August 30, 2017 (Hurricane Harvey)



Figure 4. Judge Jodie Stavinoha Bridge During Normal Flow Conditions, Showing Bent 8 in the Foreground and Bents 7, 6, and 5 Beyond

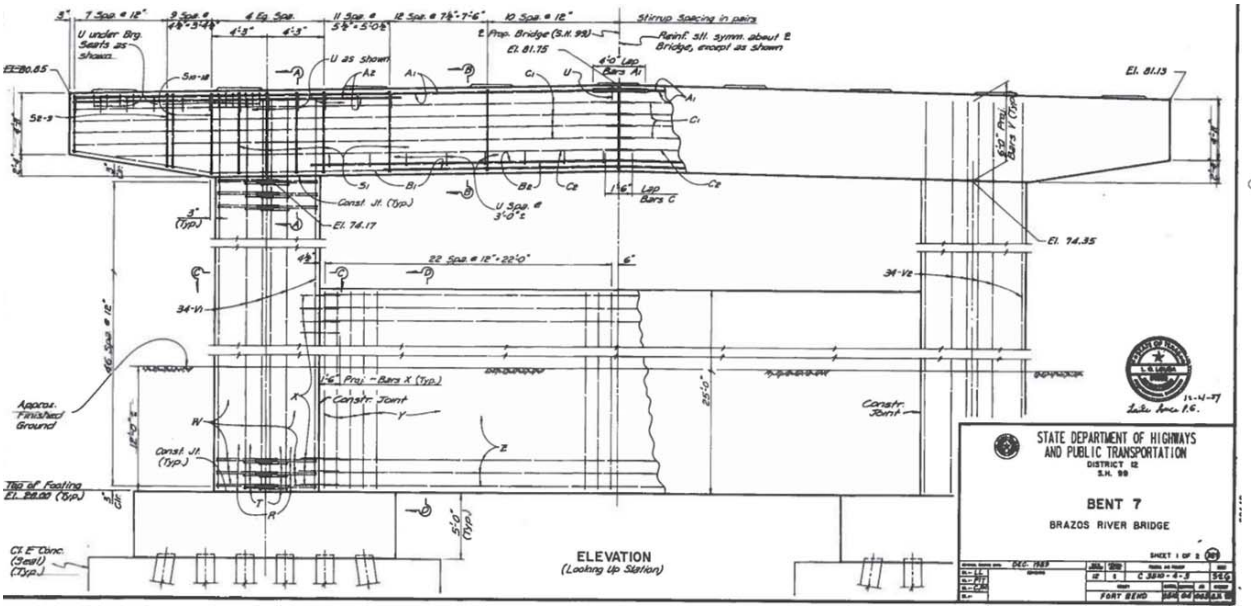


Figure 5. Typical Section at Bents 7

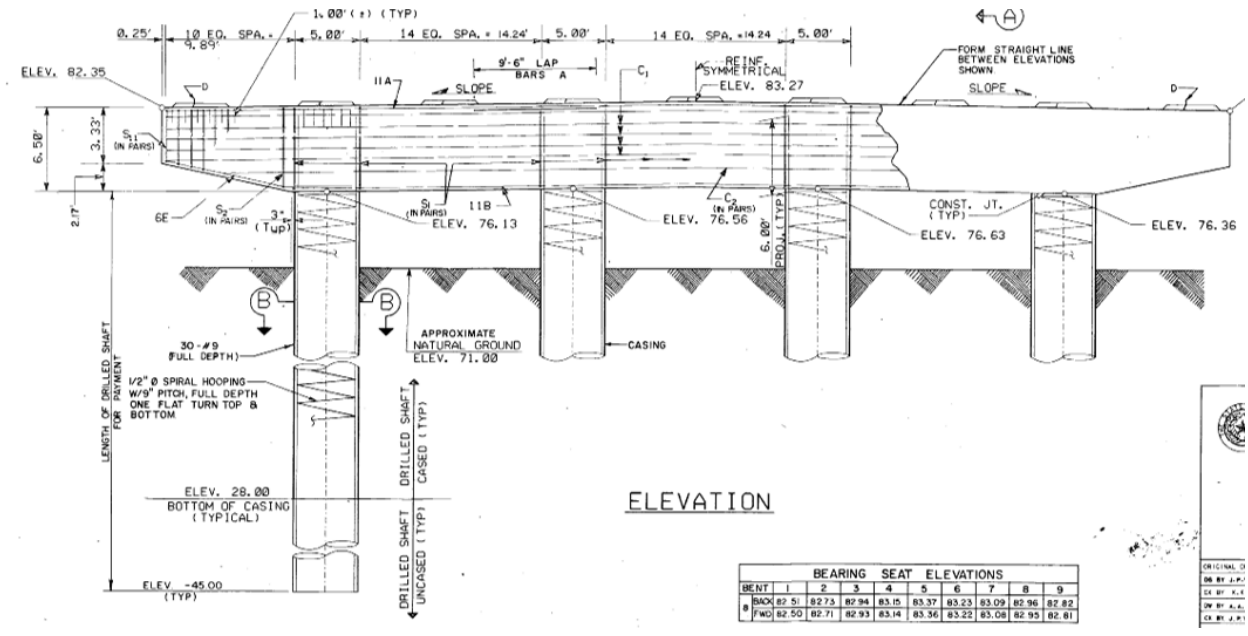


Figure 6. Typical Section at Bents 8 and 9

During previous studies at Bents 6 and 7, a scour hole was present. The upper portions of the precast piles were exposed. As the river continued northwards, the scour holes at Bents 6 and 7 were naturally filled, the piles were no longer exposed, and the river flowline has continued towards Bent 8. The potential for further erosion at Bent 8 and 9 is anticipated, although the extent is not fully understood at this time due to the overall impact of the new riverbank erosion wall. For the sake of this review, it is considered that the flowline may travel all the way to the bottom of the riverbank erosion wall located directly north of Bent 9. Under this advancement scenario, scour may cause ground elevations to be approximately +3.0.

Methodology for the Stability Analysis

The original bridge was designed using the Texas Department of Transportation (TxDOT) Bridge Design Manual, as well as the AASHTO Guide Specifications for Highway Bridges (AASHTO). The intent of the prior codes provided the design and details necessary to ensure structural integrity for reasonably conceived design loads. Typical calculation methodology revolved around providing foundation design using allowable stress design procedures, with structural calculations developed using either service load design method for allowable stress design or strength design method using load factor design procedures. Starting in the mid 1990's and continuing into the 2000's, bridge design methodology focused more on an overall reliability-based design approach, considering specified limit states in which force effects caused by factored loads are not permitted to exceed the factored resistance of the components.

Thus, the modern adaptation of the bridge design standards includes a combination of service limit states, strength limit states, and extreme event limit states. Service limit states are taken as restrictions on stress, deformation, and crack width under regular service conditions. Strength limit states are considered to ensure local and global strength are provided for statistically significant load combinations anticipated during the service life of the structure. Extreme event limit states are taken to ensure the survivability of a structure during a major event, in this case for a bridge during a flood under scour conditions.

An important factor that typically needs to be considered is the operational importance of the bridge. The Stavinoha Bridge is a vital thoroughfare for the region. However, this factor is mainly significant for seismic studies, which are not critical for this bridge due to its location on the gulf coast plains of Texas.

The applied loads for the bridge evaluation are the bridge permanent loads, superimposed dead loads, vehicular live loads, wind loads, water current loads and potential additional loads due to debris build-up during a high-water event, earth pressure loads, and the potential for force effects due to superimposed deformations.

The anticipated load effects are analyzed on the present and proposed future structural configurations using the following computer programs: VBENT, STAAD.Pro V8i, LPILE+, and SP Column. Additional calculations are developed using MathCAD and Microsoft Excel. A systematic approach is used to determine the relevant performance for the present conditions, and for future scour conditions where the reliability analysis for service, strength, or survivability no longer meets the desired objective.

Desktop Review of Existing Geotechnical Data

The study for the Stavinoha Bridge was conducted using existing geotechnical data from the original construction plans as well as additional data collected for the Owner in 2017. The site was typically characterized by approximately fifty feet of soft silt and sand (EL +75 to +25); underlain by twenty-five feet of medium to dense sand, with characteristics of cemented sand (Elevation +25 to +0); and a relatively deep layer of medium to stiff clay (Elevation +0.0 to -50.0 and below).

Axial capacities were determined for the drilled shafts at Bents 8 and 9 using the Texas Cone Penetrometer (TCP) blow count values from the boring logs and guidelines set forth in the TxDOT Geotechnical Manual. Additional vertical capacity estimates for varying ground elevation were performed to determine critical scour elevations for service, strength, and extreme event limit states.

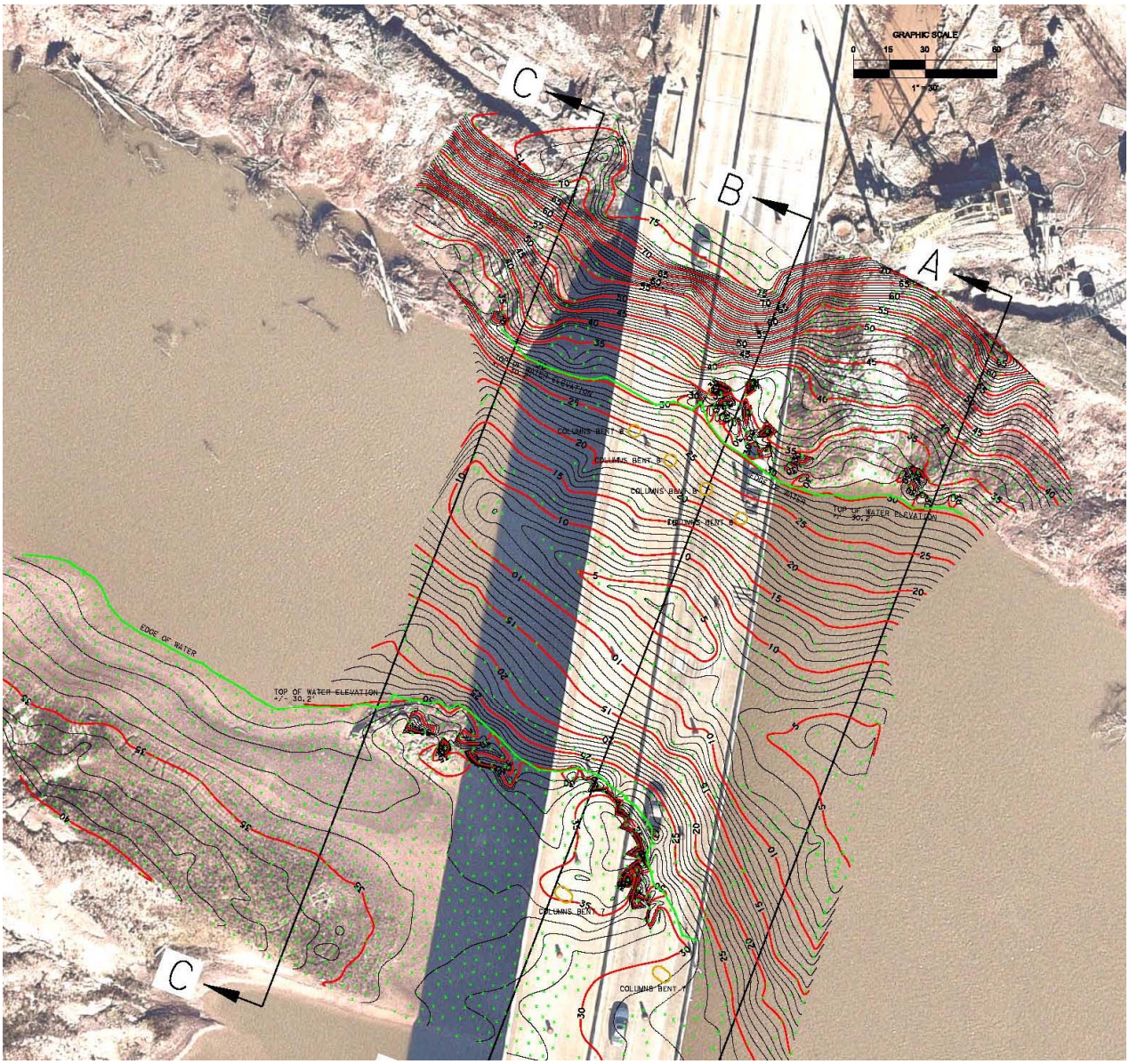


Figure 7. Post Hurricane-Harvey Riverbed Survey

Additional lateral pile behavior analyses were performed for the critical scour elevations to evaluate the relative ability of the remaining soils to resist lateral displacements and rotations at the base. Lateral soil spring values are developed for each soil strata and input into LPILE plus for the lateral stability analysis. The LPILE analyses are important to verify the unbraced length coefficients used in the structural evaluation of the columns, as well as to predict lateral displacements from the support locations up to the top of the superstructure.

Bent 7 required some additional consideration as the structure has experienced scour and subsequent in-fill. It remains unknown exactly what the nature of the new soil deposits are around the upper portions of the piles. However, the most conservative analysis will be to consider that the newly deposited material does not contribute to the support of the structure in any way. However since the bent is founded on two 18-pile groups of 16-inch square precast prestressed concrete piles, the primary concern appears to be the structural integrity of individual piles. Ultimately, the same principals apply for the piles at Bent 7 as for the drilled

shafts at Bent 8. Boring log data for the various soil layers was calibrated. Various methods are useful in determining load distributions in pile groups. The initial studies for Bent 7 have focused on the effective slenderness ratios at which the 16-inch piles begin to experience capacity reductions, in accordance with design procedures available in the Precast-Prestressed Concrete Institute (PCI) Design Manual.

Computer Analysis Methods

Due to the continued migration of the river channel to the north, erosion around Bent 7 appears to have halted while significant erosion has exposed drilled shafts at Bent 8. As the river channel moves north, Abutment 9 is also expected to experience scour around its drilled shafts. A bridge engineering design software (VBENT) was used to model Bent 8 and Abutment 9 to determine vertical downward loads as well as lateral loads on the structure. Following AASHTO LRFD Bridge Design Specifications, multiple load combinations were calculated considering the cases of various loads and positioning of live loads on the structure.

The bridge structure was analyzed at Bent 8 and Abutment 9 considering current ground elevations due to scour. Additional analyses were performed to determine the critical scour elevation that results in an ultimate vertical foundation capacity factor of safety (FS) of 1.0 utilizing both skin friction and end bearing on the drilled shafts. Using this approach, the maximum vertical loads on the drilled shafts were calculated as shown in Table 3.

The VBENT model was also used to calculate the structural capacity of the bent cap and columns of each substructure. Included in the models were: the complete geometry of each substructure, material properties for concrete and reinforcing steel, and the application of all permanent and transient load combinations. Over the life span of the bridge, no additional dead loads have been added, and no modifications to the bridge have resulted in an increased live load to the bents. By inspection, the bent caps would still be structurally adequate. Analysis results from VBENT have confirmed this assumption.

Table 3: Vertical Foundation Loading of Bent 8 and Abutment 9

Structure	Dead Load (Tons)	Dead + Live Load (Tons)	Dead + Live + Water + Wind Load (Tons)
Bent 8 Current Geometry (Scour Elev=+20.0)	451	626	660
Bent 8 Critical Geometry (Scour Elev=+10.0)	466	640	674
Abutment 9 Critical Geometry (Scour Elev = -1.0)	317	436	445

Analyzing the extreme event load scenario (Dead + Live + Wind + Water), the existing geometry of Bent 8 and Abutment 9 was evaluated to determine the structural capacity of the columns based on the current erosion conditions and the critical scour depth for the drilled shaft vertical capacity. Structural demands on the columns were checked for governing conditions resulting in combined axial loads and moments in both the transverse and longitudinal directions. SP Column was used to check the structural capacity of the columns for combined interaction of axial loads and moments. The calculated interaction diagram from SP

Column and loads from the analysis in VBENT are presented in Figure XX below. The results indicate the structural capacity of the columns is acceptable for current conditions (Points 1 and 2) and the critical scour depth (Points 3 through 6).

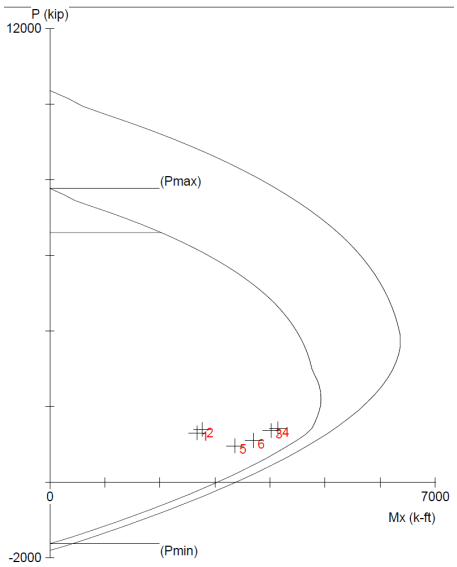


Figure 8. Column Interaction Diagram with Maximum Loads

Lateral stiffness for Bent 8 and Abutment 9 will be affected by the removal of soil around the foundations due to scour. The structural analysis evaluated the structural capacity of the foundations to take vertical and lateral loads based on current conditions and critical scour. As the Brazos River continues to erode the soil around Bent 8 and Abutment 9, the height of the substructure columns increases and the loads that are applied to the drilled shafts are increased as well. As a result, lateral deflections increase at the top of the drilled shafts, and potential displacement or rotation may result at the bottom of the shafts.

A lateral load foundation analysis program, LPILE, was used to analyze the lateral deflection of the foundations for both substructures. The program computes deflection, shear, bending moment, and soil response with respect to depth using a model with nonlinear soils for a single drilled shaft. The model in LPILE included the entire length of the drilled shaft up to the bottom of the cap. Individual loads were applied to the drilled shafts in LPILE both at the top of shaft and along the exposed length to represent the lateral loads due to wind and water from the analysis performed in VBENT.

Bent 8 was also modeled as a two-dimensional frame in STAAD to include the entire substructure, consisting of all 4 drilled shafts and the cap. Loads were applied based on the analysis performed in VBENT. Results were compared to the analysis performed in LPILE, and the drilled shaft support conditions were adjusted in STAAD to achieve similar results.

The analyses performed in LPILE and STAAD were used to determine approximate lateral deflections in both the longitudinal and transverse directions of the bridge. As expected, lateral deflections were found to increase as scour continues down to the critical scour elevation. The bottom of the drilled shafts did not show displacement or rotation for the conditions analyzed in LPILE, which indicates the tip of the shafts is

fixed. Presented in Table 3 are results for lateral deflections in the transverse and longitudinal directions for Bent 8.

Table 3: Bent 8 Computed Deflections

Scour Elevation	Lateral Load Direction	Top of Shaft Deflection (in)
+20	Longitudinal	2.0
+20	Transverse	0.6
+10	Longitudinal	3.1
+10	Transverse	0.8

Lateral deflections at Abutment 9 can be calculated using the same approach as Bent 8 considering vertical and lateral loads. However, additional lateral loading should be considered at the abutment due to the adjacent erosion mitigation retaining wall that was installed in 2017-18 to mitigate additional erosion under the northern embankment approach. The erosion wall is a tangent pile wall consisting of 10-foot diameter drilled shafts with 24-inch augered cast-in-place grout piles to act as the seal shafts. The gap between existing Abutment 9 and the erosion wall was specified based on the combined displacements of the wall structure towards the river, and Abutment 9 towards the shore, with an assumed multiplier of 1.50.

Given the close proximity of the cantilever wall to the abutment, effects from load transfer and soil response between and around the two structures will be challenging to calculate and is not part of this study. A detailed 3D soil structure interaction analysis using software such as Plaxis3D or FLAC would likely be required to determine the behavior of the structures subjected to river scour.

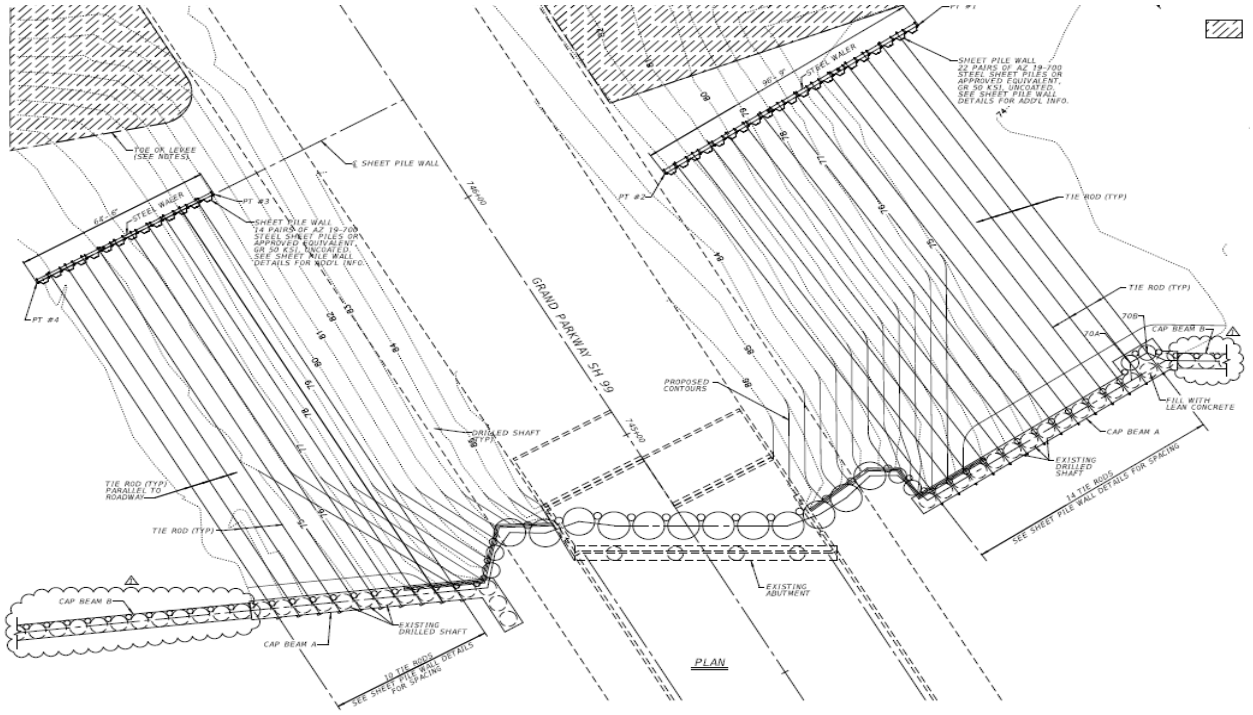


Figure 9. Modified Site Arrangement -Showing Abutment 9 and the Erosion Wall Installed post-Hurricane Harvey

Summary and Conclusions

Many bridges experience the effects of erosion and scour over the course of the design life. The original design calculations are not always available for review, or the erosion is beyond what may have been reasonably anticipated at the time of design. For these situations, it is important to follow a rational methodology to determine and assess the impacts of erosion on the bridge structure. This approach typically considers a global overview of the effects of the scour, but requires an individualized study program for a bridge based on the specific details that were included in the original bridge design

Current bridge code philosophy considers service limits, strength limits, and extreme limit event scenarios. It is important to assess the relative contributions of the component loads (dead, live, wind, water, etc.) that participate for each limit state.

The structural configuration likely changes due to erosion. Portions of the structure that were originally buried foundation elements may function as free-standing columns. Relative support locations will change, design loads will typically increase, corresponding internal design forces will increase, and structural deformations will increase.

Fundamental structural behavior may be altered due to the changes in overall supporting conditions for a structure effected by erosion. For example, deep foundation elements may lose fifty percent or more of their available embedment into the ground. As a result, a structure that previously achieved effective fixity against lateral movement and rotation may now experience lateral movement and rotation at the base. A careful review of the geotechnical support conditions, as well as the buckling behavior of columns and shafts, must be considered.

The functionality of the bridge appurtenances, such as the bearings, expansion joints, and utility connections, should be verified based on the anticipated bridge movements.

CONCRETE FILLED STEEL TUBES FOR DEEP FOUNDATIONS OF TRANSPORTATION STRUCTURES

Dawn E. Lehman, Professor, Civil & Environmental Engineering, University of Washington, delehman@uw.edu
Charles Roeder, Professor Emeritus, Civil & Environmental Engineering, University of Washington, croeder@uw.edu
Amy Leland, Foundations Specialist, Washington Department of Transportation, lelanda@wsdot.wa.gov

Keywords: Concrete Filled Tubes, Shear Strength, Connections, Seismic Design

ABSTRACT

Concrete filled steel tubes (CFSTs) are composite members that are commonly used in many countries today. CFST components are used in the United States, but they are more common in Asia, in part because the connections used in Asia are quite labor intensive and there are not standard connections in the U.S. In addition, US design specifications are prepared by separate groups for structural steel and reinforced concrete structures and so composite systems that use CFST components are not overseen by a single group and as such there are several, conflicting design standards. In the US, steel tubes used for CFST are more slender (i.e., the diameter-to-thickness, D/t, ratio is larger) than some other countries, and labor practices (structural steel labor is different than reinforcing steel labor) also cause potential conflicts in construction. As a result, CFST has had some use in tall building construction in the US, but very limited use in bridge construction. A research program at the University of Washington has been in progress to address many of these issues with an eye towards universal design expressions, simpler, standardized connections and promotion of accelerated bridge construction (ABC). The research has resulted in recent changes to the American Association of State Highway Officials (AASHTO) bridge design specification as well as state departments of transportation (DOTs), which supports the increased use of CFST in bridge pile and drilled-shaft foundations. An experimental research study which investigate the flexural strength, shear strength and connections was conducted. These connections provide good performance under both seismic and gravity loads and address the concerns of US construction. These connections, their design rules and requirements, and their impact on composite behavior and system performance are discussed. These results permit rapid and economical construction of CFST bridge piers, piles and drilled shaft foundations. They encourage the use of more slender and economical tubes, while achieving the benefits of composite construction.

INTRODUCTION

Concrete filled steel tubes (CFSTs) are widely used for bridge and building construction in Asia, but the use of CFST in bridge construction is limited in the US. The historical use of structural steel and reinforced concrete in US bridge construction have resulted in more developed design expression for those construction methods, which has limited the use of CFST. Bridge construction in the US is inherently different than in Asia because of differences in codes, labor costs and construction practices. As a consequence, design and construction practices that are economical and practical in other countries may not be practical for US bridge construction.

CFSTs offers many potential advantages for US bridge construction, because of its high strength, stiffness and ductility. Further, accelerated bridge construction (ABC) is very important in US bridge construction, and CFST can facilitate ABC, because it significantly shortens field construction time, reduces materials and labor requirements. The steel tube is prefabricated and delivered to the job site as a finished component. In comparison to precast columns, the steel tube is light and can be placed without requiring large cranes. CFST avoids the requirements of tying and placing slender rebar

© 2019 Deep Foundations Institute

cages, and building temporary formwork and shoring. The concrete fill can be placed quickly without vibration if self-consolidating concrete is used, because there is no interfering reinforcement inside the tube. Finally, CFST can provide lighter more economical structures, because less material is required to achieve the same strength and stiffness developed in a reinforced concrete (RC) component. This paper provides a brief review of the current use of CFST in US bridge construction, recent research into the use of CFST in bridges and a discussion of potential future use of these composite members.

USE OF CONCRETE FILLED TUBES IN US BRIDGES

Bridge design in the US employs a range of structural foundations. Spread footings are considered the most economical alternative, and they are used whenever possible. However, bridges designed for seismic loadings and/or in weak soil often require deep foundations. Seismic design induces large lateral loads on the bridge and its foundation. US bridges are designed to an expected seismic hazard with a recurrence interval of approximately 1000 years, which is much larger than the seismic design hazards (often a 100-year recurrence interval) considered 15 to 20 years ago. The combination of the large seismic forces and relatively weak and flexible soils found in sedimentary deposits increasingly require deep pile or drilled shaft foundations.

Pile foundations may use precast concrete piles, steel H-piles, or steel tube piles; typically, simple embedded shear connections are used to provide force transfer. Although these connections may develop moment resistance, the flexural resistance of the connection is often neglected in design.

Steel tube piles can be vibrated or driven, cleaned of soil for a portion of their depth, and then filled with concrete, and they are commonly used today. The concrete may increase the end bearing capacity and stiffness the pile, but bridge design engineers currently do not consider the composite stiffness and resistance of the pile. Instead a reinforcing cage may be inserted into the pile to provide a calculable flexural RC resistance, and the reinforcing cage may extend into the pile cap to provide limited moment transfer at the connection.

Bridges are often constructed on deep, soft soil, and large deep drilled shaft foundations are also increasingly used. Today, drilled shaft foundations may be 2m or 3m in diameter and more than 80m to 90m in depth for seismic design. A steel tube is inserted to hold back any loose soil and facilitate construction (see Fig. 1a). A steel reinforcing cage is then inserted into the tube and the tube is filled with concrete. The resistance of the shaft is often evaluated as a RC member with no consideration of the composite action or the strength and stiffness provided by the steel tube.

a)  b) 

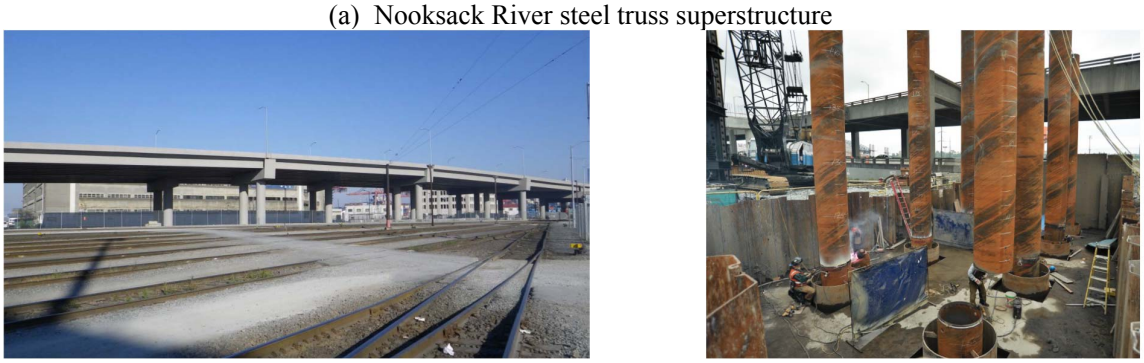
Figure 1. Deep drilled shaft foundations: a) Inserting the steel tube, b) Inserting the reinforcing cage.

In bridges, CFSTs can be used in the superstructure or foundation. In foundations, CFSTs piles or shafts are most common. Use of CFSTs as foundation elements allows for smaller diameter components than their cast-in-place or precast counterparts because of their superior flexural strength and stiffness, as demonstrated in Stephens et al. 2016. In cases of significant lateral spreading or

liquefaction, piles are subjected to significant lateral loading, resulting in large shear demands, which can dictate the shaft diameter. Use of CFSTs is the right solution in those cases because of the large shear strength. The Washington State Department of Transportation (WDOT) has utilized CFSTs to overcome design challenges resulting from significant lateral forces. Some examples of the WSDOT projects with CFSTs include the following.



(a) Nooksack River steel truss superstructure



(b) Alaskan Way Viaduct precast concrete superstructure



c) Ebey Slough steel plate girder superstructure

Figure 2. Examples of WSDOT Projects with CFSTs

- The Nooksack River bridge. The superstructure was a steel truss (Figure 2a). The use of CFST piles allowed overcoming the design challenges of supporting the vertical and lateral seismic loads on liquefiable soils conditions. The CFST pile group was composed of telescoping piles. Reinforcing bars were used in the upper portion of CFST for seismic resistant connection capable of developing plastic hinges. The CFST was both an economical and accelerated construction solution to this project.
- The Alaskan Way Viaduct has a precast concrete superstructure (Figure 2b). The CFST piles was the unique solution to overcome design challenges of bridge deep foundation subjected to liquefiable soils conditions along with lateral spread. Permanent casing was required for caving soil and CFST was the preferred solution providing permanent casing and increased strength.

- Ebey Slough has a steel plate-girder superstructure (Figure 2c). CFST piles were the only solution to support bridge vertical and lateral loads on challenging soil conditions with deep liquefaction and lateral spreading. Conventional concrete piles or shafts could not be used due to excessive self-weight. The use of CFST allowed to accelerate bridge construction and was a practical design solution to this project.

REASEARCH ON CFT CONNECTIONS

Standard connections of other structural elements have limited the use of CFST in bridge construction. Significant research has been performed on CFST connections with primary funding provided by the California Department of Transportation. Three CFST column-to-foundation or pile cap connection, illustrated in Fig. 3, have been evaluated (Stephens et al. 2014). In all, twenty-seven large-scale CFST connections were tested (Lehman and Roeder 2012, and Stephens et al. 2014 and 2015) and extensive nonlinear analyses were performed (Moon et al. 2012 and 2013).

Three types of connections were studied. All three use a corrugated metal pipe to form a recess in the cap beam. The first is the embedded ring (ER) connection, where the tube is embedded into the recess. The second uses headed reinforcing bars as the load transfer mechanism; the bars are welded to the inside of the tube and debonded to permit large drift capacity without strength degradation (WD connection for welded dowel). The last connection utilizes a reinforcing cage within the steel tube; again the RC gage is grouted into the recess (RC connection).

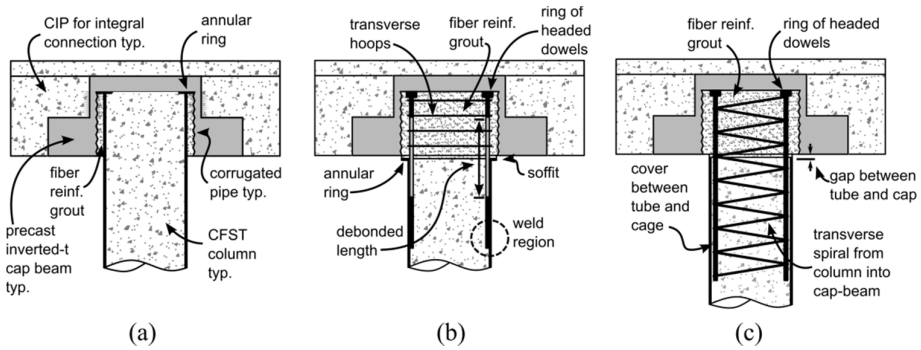


Figure 3. CFST connections; a) ER connection, b) WD connection, c) RC connection.

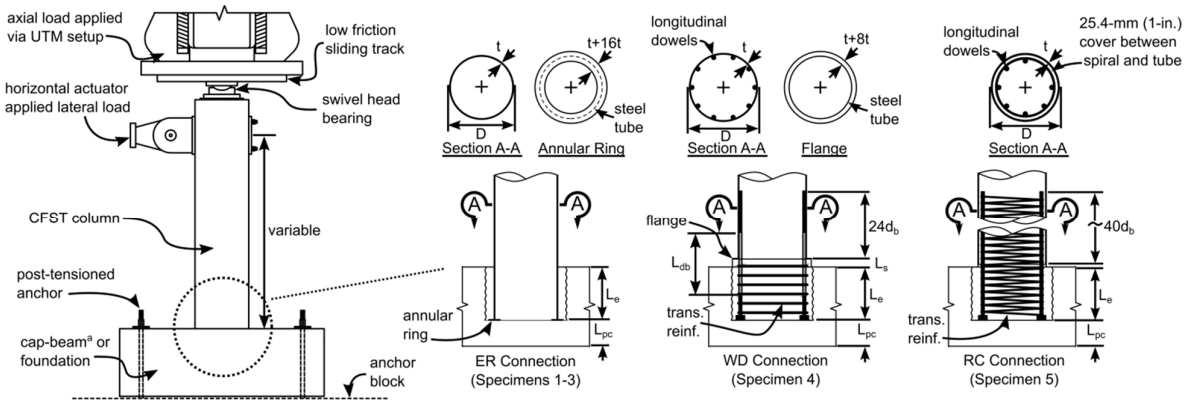
Eighteen large-scale ER foundation connection specimens were tested to evaluate the performance of the connection under reversed cyclic lateral and constant axial load. All specimens were approximately half-scale bridge columns to the point of inflection of the column, and were tested using a self-reacting test frame with a horizontal actuator to apply lateral load and a 2.4 million pound capacity Baldwin Universal Testing Machine to apply a constant axial load, as shown in Fig. 4. The specimens had typical reinforcing details for foundations, with an emphasis on reinforcing details used in high seismic regions. Due to the many tests in the research program, only specific foundation tests which directly impact key design expressions and recommendations for the ER foundation connection are highlighted here (Specimens 1 and 2 in Fig. 4 and Table 1). Significant instrumentation was used to monitor global response, local strains and deformation as described in detail elsewhere (Stephens et al. 2015). Various parameters were evaluated, including D/t, the embedment depth (L_e), and the axial load ratio P/P_o.

The performance of the ER connection is strongly influenced by embedment depth and the depth below the ring, since these quantities (in addition to the concrete strength and reinforcement) determine the punching shear capacity and cone pullout of the tube in flexure, and these issues were a focus of the research. Specimens with shallow embedment depths resulted in lower capacity, as shown in the normalized moment-story drift plot of Fig. 5a, and significant damage (the moments were normalized to the theoretical plastic capacity of the CFST). Specimens with adequate

embedment depth sustained virtually no damage to the footing, and large inelastic deformations with no deterioration in resistance as shown in Fig. 5b. The concrete inside the tube is very well confined, and damage to the concrete fill only occurred after severe local buckling of the tube. This is because the compressive concrete is less well confined in the buckled region, and crushing of the concrete in this local area occurs with increased inelastic deformation. Severe local buckling occurs only after relatively large inelastic deformation, because the steel tube must have sufficiently tensile yield elongation for the buckled shape to form. After multiple large deformation cycles, the concrete fill in the local area of local buckling of the tube is large pulverized and pours out of the tear as damage to the tube occurs. The required embedment depth and footing thickness required for punching shear were established from this research and are described in detail in reference material (Lehman and Roeder 2012; Stephens et al. 2015). A minimum cap width of two times the outside diameter of the CFST is currently recommended.

Table 1. Summary of Selected Experimental Specimens and Key Experimental Results

Specimen Summary									Experimental Results	
Spec.	**Connection Type**	**D mm**	**t mm**	**D/t**	**L_e mm**	**Long. dowels**	**Trans. Reinf.**	**(P/P_o)**	**$M_{max}/M_{P,PSDM}$**	**Failure Mode**
1	ER Foundation	2032	6.35	80	305	-	-	0.1	0.88	Cone Pullout
2	ER Foundation	2032	6.35	80	457	-	-	0.1	1.13	Ductile Tearing
3	ER Pier Cap	610	6.35	96	508	-	-	0.1	1.19	Ductile Tearing
4	WD Pier Cap	654	6.35	103	508	10 No. 11	No. 5 at 127-mm	0.05	1.1	No Failure Through 12% Drift
5	RC Pier Cap	2032	6.35	80	356	Eight No. 9	No. 3 at 63.5-mm	0.1	0.92	Fracture of Longitudinal Dowels



(a) test setup (b) specimen connecton details

Figure 4. Test Setup (Testing in Inverted Configuration to Facilitate Load Application)

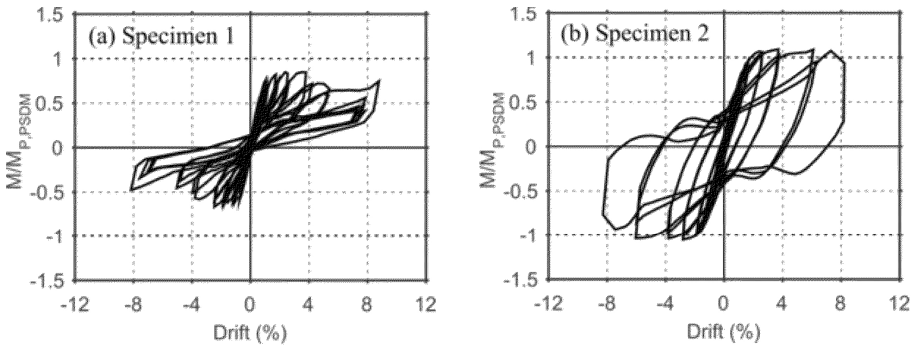


Figure 5. Typical response: a) Shallow, inadequate embedment, b) Adequate embedment

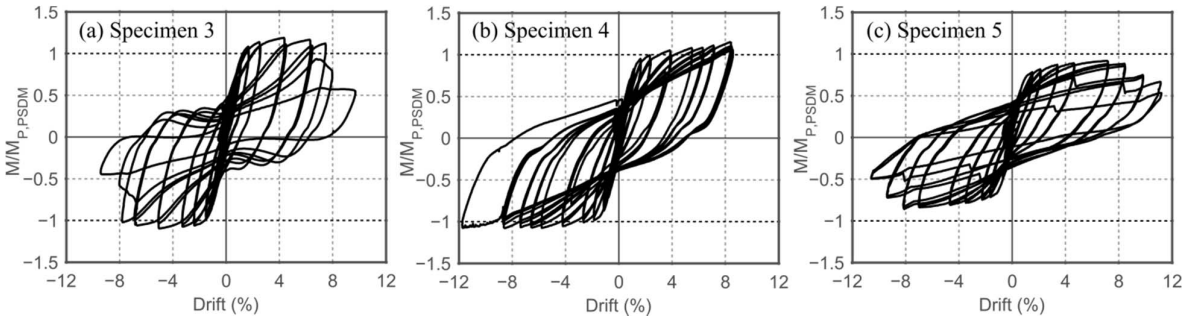


Figure 6. Force-deflection behavior of precast pier cap connections; a) Embedded connection, b) Welded dowel connection, and c) RC connection.

A total of four specimens were tested to evaluate the performance of the alternate connections with in RC cage. The WD connection shown in Fig. 4 was developed because a weaker connection to limit the demand to the adjacent components. Its strength depends upon the size and spacing of the rebar, and these parameters are limited by available space on the insider perimeter of the tube. The WD connection will normally be significantly stronger than a RC connection, because the diameter of the reinforcing bars is optimized and concrete cover is not required. The steel tube does not penetrate into the pier cap of the WD connection. Figure 6b, shows a WD connection with unbonded longitudinal dowels to increase the deformation capacity of the connection and reduce damage to the pier cap. However, WD connections with bonded bars were tested and significant damage to the pier cap; debonding the longitudinal dowels provided better inelastic performance with limited damage to the pier cap as illustrated in the moment-drift plot in Fig. 6b for Specimen 4, which utilized 10 No. 11 bars debonded in the connection region. The resistance of the WD connection in Fig. 6b is fairly close to that of ER connection, because the internal reinforcement had 87% of steel area of the tube and the specified yield stress of the rebar was 45% larger than that of the tube.

The placement and design of the weld was a critical issue for this connection. The recommended weld is a flare bevel weld designed to develop the tensile strength and inelastic deformation capacity of the rebar. An experimental study of this weld was completed prior to testing of the full connection to assure that the performance goals were achieved. Design and placement of the weld was completed in accordance with American Welding Society (AWS) Bridge Welding Code (AASHTO/AWS 2010). A total of 16 No. 7, 4 No. 9, and 4 No. 11 dowels were welded to inside of four 508-mm diameter steel tubes with 6.35-mm wall thickness, and the tubes were filled with self-consolidating low shrinkage concrete. The primary test parameters included weld strength, bonding or debonding the dowels from the concrete, and the embedment depth of the bar into the steel tube. Weld strengths ranging from 80% to 120% of the dowels strength and embedment depths of $16d_b$ and $24d_b$ were evaluated. The bars were pulled to failure using a hydraulic ram placed into a self-reacting system. The failure mode in all tests was characterized by dowel yielding followed by strain hardening and fracture. Debonding the reinforcing bars maximizes the deformability, and minimizes damage (Stephens et al. 2016).

SHEAR TESTING PROGRAM

The experimental study undertaken at the University of Washington was developed to (1) test large-scale specimens, (2) understand the relative contribution of the concrete fill and the steel tube, and (3) determine the impact of salient design parameters on the CFT capacity. Twenty-two specimens were built and tested (Table 2). The test specimens focused on construction issues (e.g., mud or grease on the interface to investigate bond transfer), configurations (e.g., D/t ratio and internal reinforcement), material properties, tube type and the impact of the length past the maximum moment to restrain slip.

Twenty of the test specimens were straight seam tubes made of steel conforming to API 5L X42 and ASTM A53B standards. Two specimens were spirally welded from ASTM A1011 HSLAS Gr 70 C1/C2 coil steel using a double submerged arc weld. Specimens 6 and 22 were tested using the higher strength steel tube. The steel tube for Specimen 22 was galvanized and filled with a high-strength, self-consolidating, low-shrinkage concrete mix with a 28-day design strength of 10,000 psi. It was previously fabricated for use in an earlier research program (Roeder et al. 2009) and was used as an initial test to validate the testing apparatus and procedure. Specimen 6 used the same steel tube and was filled with concrete as part of the current testing program. The reinforcing bar used in the four RCFSTs conformed to either ASTM A615 Gr 60 or ASTM A706 Gr 60. Three concrete design mixes with normal weight aggregate were used in the testing program.

The test specimens exhibited one of four failure modes: flexure, shear, bond or flexure-shear where the last category was the most difficult to determine. Specimens failing in shear are the focus of this paper were specimens failing in flexure are used as comparison and to determine shear failure. Table 2 presents primary results for all of the test specimens including: (1) primary study parameter, (2) a/D, (3) failure mode, (4) measured maximum moment and shear (M_{exp}, V_{exp}), (5) normalized strengths, and (6) slip. In addition, the table indicates whether or not shear deformations were visible and if the failure tear was inclined; these two observed response parameters indicate shear failure. The results are presented for example specimens that demonstrate shear failure modes.

Table 2 Test Matrix on Shear Testing

Specimen	a/D	a		t		D/t	F_{ydm}		f_{cm}'		P/P_0	L_T	ρ_{int}	Interface
		in.	mm	in.	mm		ksi	MPa	ksi	MPa				
10	0.375	7.5	190.5	0.25	6.35	80	42	289.6	6.0	41.4	0%	2D	0%	Clean
1	1.0	20	508.0	0.25	6.35	80	42	289.6	6.0	41.4	0%	2D	0%	Clean
2	0.5	10	254.0	0.25	6.35	80	42	289.6	6.0	41.4	0%	2D	0%	Clean
3		10	254.0	0.25	6.35	80	42	289.6	6.0	41.4	0%	D/2	0%	Clean
4		10	254.0	0.25	6.35	80	42	289.6	6.0	41.4	0%	D	0%	Clean
5		10	254.0	0.25	6.35	80	42	289.6	6.0	41.4	0%	2D	0%	Muddy
6		10	254.0	0.25	6.35	80	70	482.6	6.0	41.4	0%	2D	0%	Spiral
9		10	254.0	0.25	6.35	80	42	289.6	6.0	41.4	0%	2D	0%	Greased
12		10	254.0	0.25	6.35	80	42	289.6	6.0	41.4	0%	2D	1.13%	Clean
17		10	254.0	0.25	6.35	80	42	289.6	12.0	82.7	0%	2D	0%	Clean
18		10	254.0	0.375	9.53	53.3	42	289.6	12.0	82.7	0%	2D	0%	Clean
19		10	254.0	0.375	9.53	53.3	42	289.6	12.0	82.7	0%	2D	1.07%	Clean
7	0.375	7.5	190.5	0.25	6.35	80	42	289.6	6.0	41.4	0%	2D	1.04%	Clean
8		7.5	190.5	0.25	6.35	80	42	289.6	6.0	41.4	0%	2D	2.01%	Clean
11		7.5	190.5	0.25	6.35	80	42	289.6	6.0	41.4	0%	D/2	0%	Clean
13		7.5	190.5	0.25	6.35	80	42	289.6	6.0	41.4	8.5%	D/2	0%	Clean
16		7.5	190.5	0.25	6.35	80	42	289.6	12.0	82.7	0%	2D	0%	Clean
21		7.5	190.5	0.25	6.35	80	42	289.6	0.0	0.0	0%	2D	0%	Clean
14	0.25	5	127.0	0.25	6.35	80	42	289.6	12.0	82.7	0%	2D	0%	Clean
15		5	127.0	0.25	6.35	80	42	289.6	12.0	82.7	0%	5/8D	0%	Clean
20		5	127.0	0.25	6.35	80	42	289.6	2.5	17.2	0%	2D	0%	Clean

A good representative specimen of the shear failure mode is Specimen 8, the internally reinforced specimen for a/D = 0.375. Specimen 8 reached a moment and shear force magnitude of $1.02M_{PSDM}$ and $1.6*2V_s$, respectively (Figure 7). The complete moment and shear vs. displacement relationships

are shown in Figures 7c and 7d. Visible shear yielding was observed in the tube and dense diagonal cracking in the concrete of the north shear span. There was also a notable amount of diagonal cracking of the concrete in the south shear span, with limited flexural cracking in the midspan region.

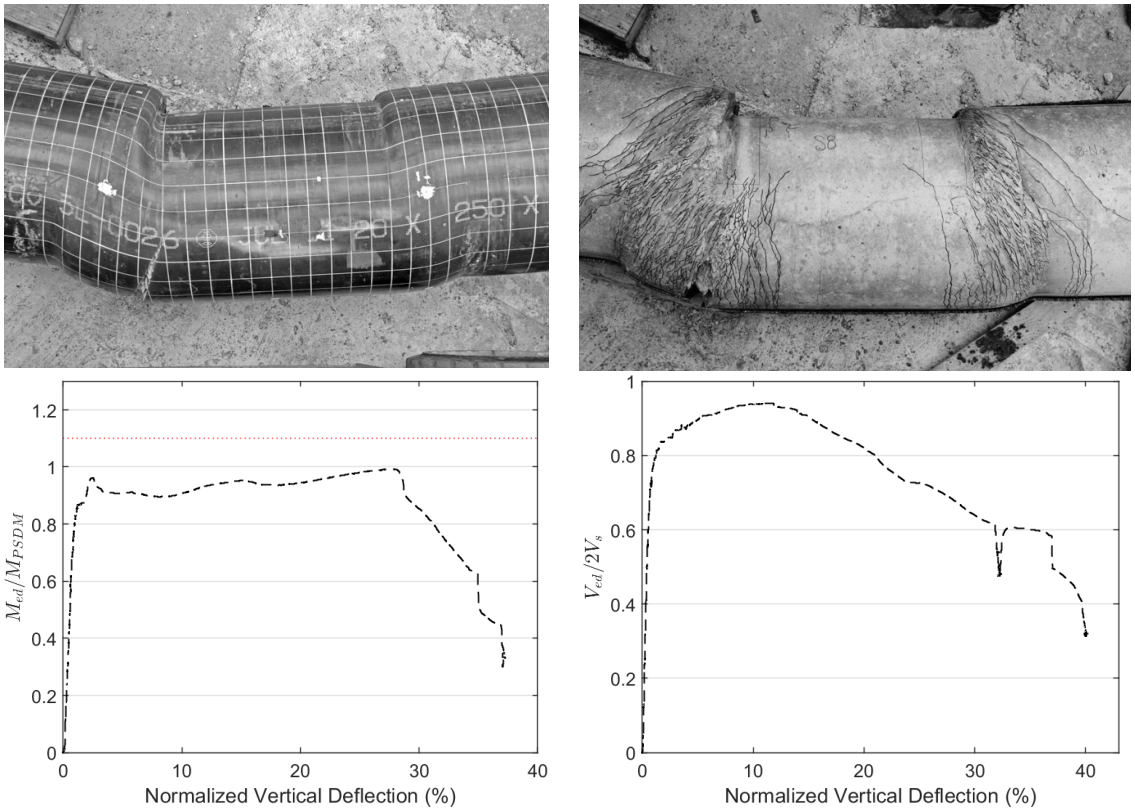


Figure 7. Shear Response (Specimen 8): (a) Damage to Tube, (b) Damage to Concrete (emphasis on shear region, (d) Moment-Drift Response and (e) Shear Force-Drift Response

The results indicate that specimens exhibiting a shear failure had diminished moment capacities, less than $1.1M_{PSDM}$. The majority of the specimens failing in shear had an a/D ratio of 0.25. Specimen 8 was the only specimen to fail in shear with a/D = 0.375; this specimen had internal reinforcement. In some cases, the specimens initially exhibited flexural response but the end failure mode was mixed in that the tear in the tube was inclined but buckling of the tube was also present. These mix-mode, flexure-shear specimens are not included in either the flexural or shear set.

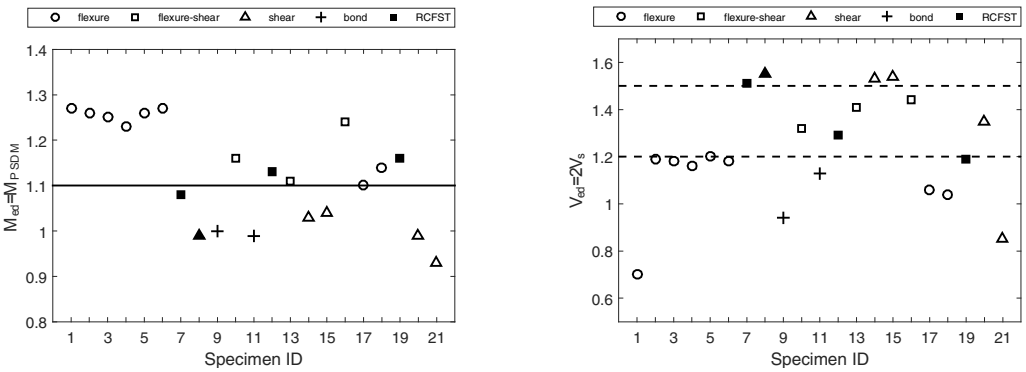


Figure 8. Normalized Maximum Moment and Shear Forces of All Specimens

Finally, three specimens are exceptions. Specimen 21 was filled with gravel in the shear spans; this specimen relied solely on the steel to sustain the shear and had a shear capacity of approximately

$1.7V_s$ where V_s is the shear strength of the steel computed as $(0.6F_{yt})*(0.5A_{st})$ where F_{yt} is the yield strength of the steel and A_{st} is the cross-sectional area of the steel tube. This represents the lowest-bound to the shear strength of a CFST (Table 2).

Two specimens exhibited a bond failure as a result of inadequate development length beyond the maximum moment (Specimen 11 had a tail length of D/2 and a/D = 0.375) or a frictionless interface (the interface between the steel tube and concrete fill was greased for Specimen 9). These two specimens failed to reach the expected moment capacity. However, this is not a shear failure mode and these specimens were not included in the development of the shear strength expression.

For the specimens failing in shear, the shear demand exceeds $2V_s$ where $V_s = 0.6F_{yt}(0.5A_{st})$, as given in Eq. 4a. This result indicates that: (1) the specimens failing in shear sustain a larger shear demand than the specimens failing in flexure, as expected, (2) using V_s greatly underestimates the shear capacity of CFST and RCFTs and (3) the concrete contributes to the shear strength, and this contribution may be approximated as $V_c = V_{ed} - V_{st} + V_{sr}$.

To develop the shear expression, the following form of the equation was used:

Proposed Shear Expression

$$V_{n\,(Proposed)} = V_c + V_{st} + V_{sr} \quad (3)$$

where

$$V_{st} = 0.6F_{yt}A_{st} \quad (4a)$$

$$V_{sr} = 0.6F_{yr}0.4A_{sr} \quad (4b)$$

$$V_c = 4\sqrt{f_c'}A_c \quad (4c)$$

SUMMARY AND CONCLUSIONS

This has been a brief overview of the use of CFST in US bridge construction. It is clear that the use of CFST in bridge construction is less advanced in the US than in many other countries. Nevertheless, significant advances have been made in recent years, and it is expected that the use of CFST in US bridge construction will increase significantly in the future. The primary usage of CFST has been and will likely continue to be for piles, drilled shafts and bridge pier columns. CFST have larger flexural strengths since the steel tube is at the optimal location; the plastic stress distribution method is recommended for calculation of the flexural capacity. The proposed connections are practical and economical, they facilitate accelerated bridge construction and can sustain the full strength of the CFST. Comparison of the cap beam experiments clearly demonstrates the different behaviors of the proposed connections as well as the influence of varying parameters on each connection type. The ER cap beam connections exhibited larger stiffness and strength than the WD and RC connections. Further, the ER connection has many advantages in terms of facilitating ABC. Finally shear testing of CFST and RCFST indicate that the shear strength is primarily dependent on the tube, with contributions from the concrete fill and internal reinforcement (if present). The new shear expression provides an accurate shear strength which is at least twice the shear strength of existing equations.

REFERENCES

American Association of State Highway and Transportation Officials (AASHTO) (2012) AASHTO LRFD Bridge Design Specifications, Washington, D.C.

American Association of State Highway and Transportation Officials (AASHTO) (2014) AASHTO LRFD Bridge Construction Specifications, 3rd Edition with 2010 through 2014 Interims, Washington, D.C.

American Concrete Institute (ACI) (2011) Building Code Requirements for Structural Concrete (ACI 318-11), Farmington Hills, MI

American Institute of Steel Construction (AISC) (2010). Specification for Structural Steel Buildings, AISC, Chicago, Illinois.

American Welding Society (AWS) (2010) "Bridge Welding Code," *AASHTO/AWS D1.5:2010 Standard*, Miama, FL.

Bishop, E. (2009) Evaluation of the Flexural Resistance and Stiffness Models for Circular Concrete-Filled Steel Tube Members Subjected to Combined Axial-Flexural Loading, a thesis submitted in partial fulfillment of the Master of Science in Civil Engineering Degree, University of Washington, Seattle, December 2009.

Lehman, D.E. and Roeder, C.W. (2012) "Foundation Connection for Circular Concrete Filled Tubes," *Journal of Constructional Steel Research*, Vol. 78, November 2012, pgs. 212-25, Elsevier.

Lehman, D.E., Kuder, K., Gunnarsson, A.K., Roeder, C.W., and Berman, J.W. (2013) "Circular Concrete Filled Tubes for Improved Sustainability and Seismically Resilience", *Journal of Structural Engineering*, ASCE, Reston, VA, ISSN 0733-9445/B4014008(12).

Moon, J., Lehman, D.E., Roeder, C.W., and Lee, H-E (2013) "Evaluation of Embedded Concrete Filled Tube (CFT) Column-to-Foundation Connections," *Engineering Structures*, Vol. 56, pgs 22-35, Elsevier.

Moon, J., Lehman, D.E., and Roeder, C.W. (2012) "Strength of Circular Concrete Filled Tubes (CFT) with and without Internal Reinforcement Under Combined Loading," *Journal of Structural Engineering*, ASCE, Reston, VA, DOI:10.1061(ASCE)ST1943-541X.000078.

Moon, J., Roeder, C.W., Lehman, D.E., and Lee, H-E (2012) "Analytical Modeling of Bending of Circular Concrete-Filled Tubes," submitted for publication review, Engineering Structures, Elsevier.

Priestley, M.J., Seible, F., and Xiao, Y. (1994) "Steel jacket retrofitting of RC bridge columns for enhanced shear strength; test results and comparison with theory," *ACI Structural Journal*, Vol 91, pp 537-551.

Roeder, C.W., and Lehman, D.E. (2012) "Initial Investigation of RC Filled Tubes for use in Bridge Foundations," Washington State Dept. of Transportation Report WA-RD 776.1, Olympia, WA.

Roeder, C.W., Lehman, D.E., Stephens, M. (2014) "Concrete Filled Steel Tubes for Accelerated Bridge Construction," *Transportation Research Record No. 2406, Vol. 1*, Washington, DC, pgs 49-58.

Roeder, C.W., Lehman, D.E., and Bishop, E. (2010) "Strength and Stiffness of Circular Concrete Filled Tubes," ASCE, Journal of Structural Engineering, Vol 136, No. 12, pgs 1545-53, Reston, VA.

Stephens, M. T., Berg, L. M, Lehman, D.E. and Roeder, C.W. (2014) "Circular concrete filled tube bridge pier connections for accelerated bridge construction," *Proceedings: 2014 National Accelerated Bridge Construction Conference*, Miami, FL, pgs 354-363.

Stephens, M.T., Lehman, D.E, and Roeder, C.W. (2015). Concrete-Filled Tube Bridge Pier Connections for Accelerated Bridge Construction. Report for the California Department of Transportation. Report Number CA15-2417.

Stephens, M., Berg, L., Lehman, D., and Roeder, C. (2016). "Seismic CFST Column-to-Precast Cap Beam Connections for Accelerated Bridge Construction." *J. Struct. Eng.* , 10.1061/(ASCE)ST.1943-541X.0001505 , 04016049.

DUCTILE IRON PILE FOUNDATION SOLUTION FOR INTERIOR RETROFIT PROJECTS

Gregg Piazza, PE, GeoStructures, Inc., Purcellville, VA 20132, 540-751-5023,
gpiazza@geostructures.com
Keithe J. Merl, PE, GeoStructures, Inc., Purcellville, VA 20132, 862-754-0438,
kmerl@geostructures.com
Brendan FitzPatrick, PE, DuroTerra, Braintree, MA 02184, 781-817-6053,
bfitzpatrick@duroterra.com

ABSTRACT

Urban and industrial construction projects commonly involve interior work within buildings, warehouses and manufacturing facilities. Renovations of these existing structures must address both structural and geotechnical engineering challenges while also balancing the practicality of implementing solutions within site constraints including limited site access, overhead clearance restrictions, vibration tolerances and uninterrupted facility operations. This paper highlights two projects for an international shipping company where mezzanine level additions within active shipping facilities required construction of new foundations. Construction requirements included low vibration levels, as well as rapid and clean installation to limit impacts on the active shipping operations. The selected system also needed to adjust to both variable ground conditions and differing overhead clearances. This paper describes the installation, design and performance of Ductile Iron Piles used to meet the project challenges. The low vibration, driven pile system offered the ability to work within restricted overhead environments while successfully delivering working compression capacities ranging from 45 to 75 tons (41 to 68 tonnes) as well as lateral and tension resistance. The paper also presents the results of site-specific load testing (and pile capacity) for various termination criteria.

Keywords: Ductile Iron Pile, interior, overhead clearance,

INTRODUCTION

Urban and industrial construction projects commonly involve interior work within buildings, warehouses and manufacturing facilities. Renovations of these existing structures must address both structural and geotechnical engineering challenges associated with the new construction. Foundation solutions must also balance the need to achieve design requirements with the practicality to be installed within the particular site constraints including limited site access, overhead clearance restrictions, vibration tolerances and uninterrupted facility operations.

A staple in European construction for over 30 years, Ductile Iron Piles (DIP) are often used on projects to meet the many design and construction challenges, while providing the benefit of cost and time savings compared with other piling systems. The low vibration, driven pile system offers the ability to work within restricted overhead environments while delivering moderate to high capacities. The system was recently used on four separate projects across the Northeast U.S. for an international shipping company where mezzanine level additions were planned within active shipping distribution facilities. The projects involved support for new column foundations subjected to compression, tension and lateral demands. In addition to the technical design requirements, of particular importance to the owner, was the deployment of a foundation system that involved low vibration, rapid construction and clean installation to limit impacts on the active shipping operations. The selected system was also required to adjust to both variable ground conditions as well as differing overhead clearances within the structures. Details of installation, design and testing at two of the facilities are described herein.

© 2019 Deep Foundations Institute

DUCTILE IRON PILES

Ductile Iron Piles are a low vibration, driven pile system pictured in Figure 1. The modular, small-diameter piles have been manufactured by Austrian-based Tiroler Rohre GmbH for over three decades and used extensively throughout Europe. With diameters ranging from 3.8 in (98 mm) up to 6.7 in (170 mm) and wall thicknesses of 0.24 in (6 mm) to 0.51 in (13 mm), working structural capacities range from 25 tons (23 tonnes) to more than 100 tons (91 tonnes). Piles are manufactured using a centrifugal-casting process to transform the lamellar graphite cast iron into spheroidal graphite or ductile cast iron to improve strength and impact resistance for durability during driving. The piling material exhibits a design yield stress of 46 ksi (320 MPa) and modulus of elasticity of 24,600 ksi (170,000 MPa) (TRM 2014). Each pile is cast with a bell and spigot to form a Plug-and-Drive connection mechanism. The connection develops strength through a combination of the tapered compression fit as well as a friction (cold) weld that occurs during the high-frequency driving process, thereby eliminating the need for field splicing. The connection also exhibits full moment capacity of the nominal pile section based on the results of bending tests confirming the stiffer load-deflection response of both the bell-spigot and coupler drive connections compared with the nominal straight-line pipe section (DuroTerra 2018). The piling comes in standard 16.4 ft (5 meter) lengths and delivered in compact bundles containing between 8 and 18 pile sections depending on pile diameters. The bundles can be easily transported to congested urban or interior sites and offloaded into limited laydown areas to allow ease of installation on constrained sites.

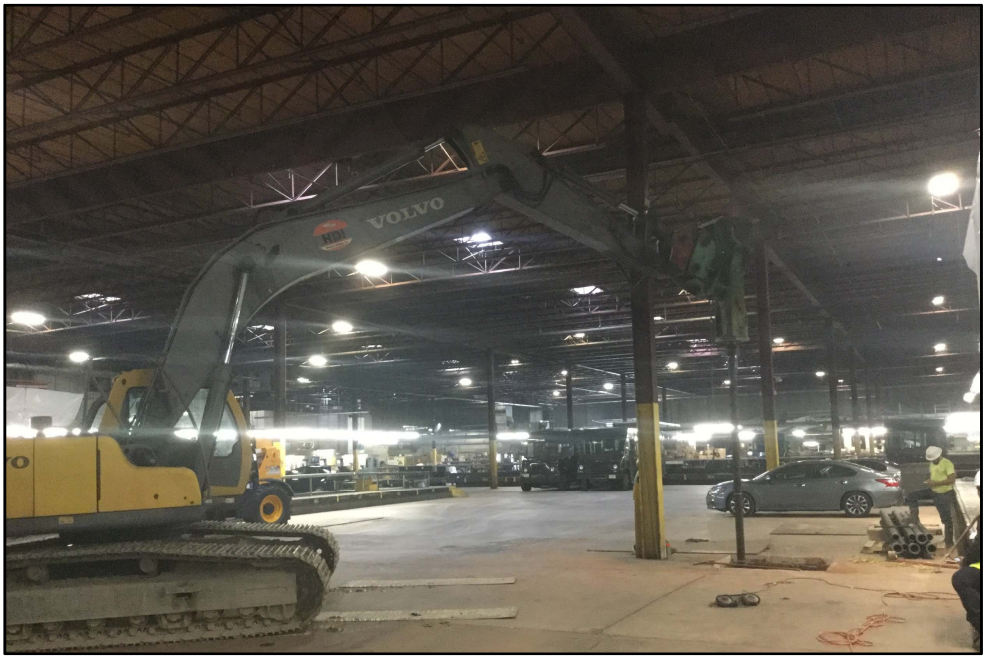


Fig. 1. Ductile Iron Pile Installation at Shipping Facility

Installation

The system is installed using an excavator-mounted, hydraulic breaker hammer. The hydraulic hammer uses a modified drive shank that seats into the pile bell. Using the hammer's percussion energy, the closed-ended pile segment is driven into the ground while monitoring rates of advancement. Using the same excavator, a second pile section is swung into place and inserted into the Plug and Drive (bell and spigot) connection and then driven. This process is repeated until the design length or pile termination ("set") criteria is reached, where the set is a maximum rate of advancement (i.e. 1 inch or less in 50 seconds). The hammer size (energy) is matched with the size of the Ductile Iron Pile and the driving conditions to develop

the most efficient installation while not overstressing the pile material. Hammer sizes typically range from 3,000 ft-lb to 7,000 ft-lb class hammers for typical range of pile sizes.

Vibration measurements of the high frequency driving energy recorded on various project sites with multiple pile diameters, all at distances of less than 5 feet (1.5 m) from installation, are shown in Figure 2. Results of the monitoring illustrate that the majority of vibrations are in the high frequency spectrum and exhibit peak particle velocities less than 1 inch/second (25 mm/s). Monitoring also shows high frequency vibrations rapidly decrease with distance from the pile location.

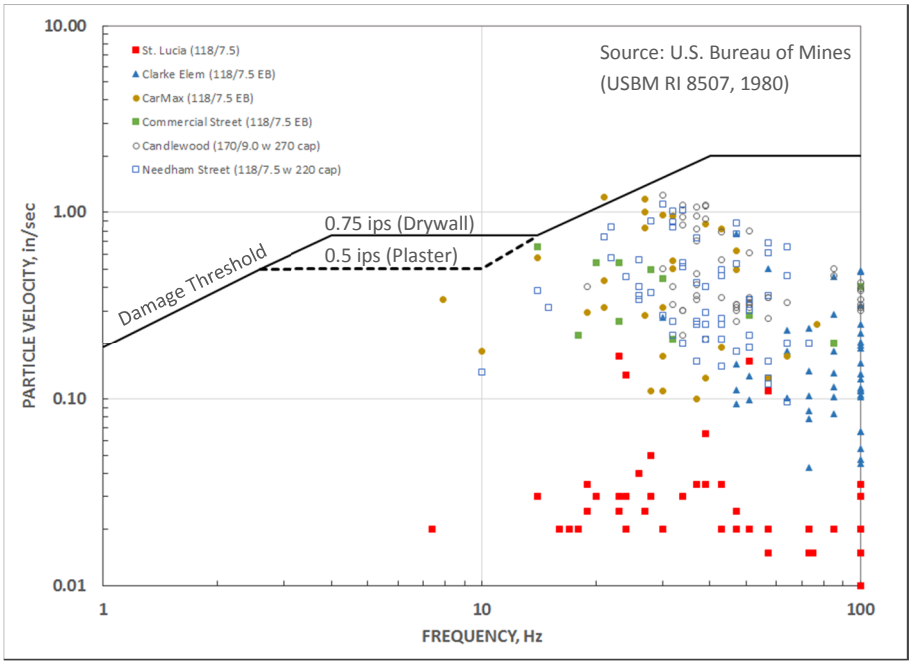


Fig. 2. Vibrations Measurements near Ductile Iron Pile installation

Geotechnical Application

Ductile Iron Piles can develop geotechnical capacity in either end-bearing or in friction depending on the installation technique. End-bearing piles are outfitted with a flat or pointed drive shoe and are driven through problem soils to terminate by achieving set in very dense soil or rock. A common recommended set criterion for end-bearing piles is less than 1 inch of movement in 50 seconds. Soil conditions exhibiting SPT N-values on the order of 50 blows per inch [50 bpi] are often required to achieve typical set thresholds. After achieving set, the remaining pile is cut to elevation and the completed pile is filled with neat cement grout. A center reinforcing bar may be placed into the wet grout, if required by the design. The remaining cut section including the bell is used as a starter pile section to minimize waste.

Friction Ductile Iron Piles are used to generate compression or tension resistance by bonding between the soil and cement grout interface. At the start of driving, an oversized conical grout shoe is placed over the end of the hollow pile. The grout caps are 5.9 in (150 mm) up to 14.6 in (370 mm) in diameter and create an annular space around the pile during driving. The pile is driven into the ground while continuously pumping cement grout through the hollow pile. The grout exits through the grout ports in the conical cap, immediately filling the annular space around the pile exterior during driving. The pile shaft becomes encapsulated in grout, developing a grout-to-ground bond zone. Additional pile sections are driven until the pile extends to the design length within the bond zone. Monitoring of drive rates provides useful

information to determine when the pile encounters the design bond zone. After completion of driving, a center reinforcing bar is inserted into the wet grout if required for compression or tension capacity.

SHIPPING FACILITY, HARTFORD, CT

Renovations at an existing shipping facility in Hartford, Connecticut included construction of a new 25,000 sq. ft. (2,323 sq. meter), steel-framed mezzanine level within the existing high-bay warehouse. The existing building was constructed in the 1970s and supported on driven piles (either timber or steel based on original design documents). Typical overhead clearances were on the order of 30 feet (9.1 m), although limited areas were between 20 and 25 feet (6.1 to 7.2 m). Loading conditions at the new column footings were up to 400 kips (181 tonnes) in compression. Footings were also subjected to tension loads of up to 120 kips (54 tonnes) based on pile design requirements. To construct new mezzanine foundations, the existing concrete floor slab would be saw-cut to accommodate the new pile foundations. Following pile installation, new pile caps would be formed and poured. Management of the facility required operations to be moved in and out daily and work zones to be covered overnight. In addition, temporary shutdowns were required in the morning to allow for the daily departure of trucks. These aspects presented substantial logistical challenges to be addressed by the selected foundation system.

Geotechnical Conditions & Recommendations

Subsurface soil conditions described in the Geotechnical Engineering Report prepared by GZA GeoEnvironmental, Inc., (2017) consisted of medium dense to dense granular fill to depths of 3 to 9 feet (0.9 to 2.7 m) followed by very soft to stiff clay, silt and organic silt extending to depths of 16 to 27 feet (4.9 to 8.2 m) below grade. The cohesive layer was underlain by loose sand and silty sand followed by a 2 to 6 foot (0.6 to 1.8 m) thick layer of dense glacial till. Rock depths encountered during explorations ranged from about 26 feet (7.9 m) up to 40 feet (12.2 m) below grade. Groundwater was measured at 4 to 9 feet (1.2 to 2.7 m) below grade.

Project plans and specifications were prepared based on 7-inch (177 mm) diameter drilled micropiles installed through the fill, clay and organic soils and terminating by bonding in glacial till / rock to develop a capacity of 50 tons (45 tonnes) in compression. Alternative foundation options presented by the Geotechnical Engineer also included Ductile Iron Piles and helical piles.

Pile Selection and Design

Selection of the pile type by the project team was based on factors including anticipated pile performance, vibration limitations, duration, cost, cleanliness and field support requirements. As noted in the geotechnical report, helical piles would require a reduction in the working capacity and therefore increase both pile quantities and pile cap sizes and impact the zone of renovation. While drilled micropiles would develop the working capacities, the rate of installation would slow the project schedule and grouting operations would create undesirable spoils management requirements within the existing facility. The project team selected Ductile Iron Piles as a more-rapid and cost-effective alternative to 50 ton (45 tonnes) micropiles. Prior project experience in similar conditions was used as a baseline to confirm acceptable vibration levels and the cleanliness of the operation.

Ductile Iron Piles were designed to terminate on glacial till or rock to resist compression loading in end-bearing. As described in LeDo et al (2016), the structural design is based on a composite strength approach that is similar to micropiles with the pile material ($P_{ironpipe}$), interior grout (P_{grout}) and high-strength center bar (P_{bar})(if used) contributing to the ultimate capacity as described in Equation 1,

$$P_{dip} = u_{dip} F_{y-dip} A_{dip-final} + f'_{c-all} A_{grout} + u_{bar} F_{y-bar} A_{bar} \quad [1]$$

where u_{dip} and u_{bar} are the corresponding allowable stress factors for the pipe and bar, respectively, which range from 0.4 to 0.5 depending on load testing, $F_{y\text{-}dip}$ and $F_{y\text{-}bar}$ are the corresponding material yield strengths, $f'_{c\text{-}all}$ is the allowable grout compressive strength and $A_{dip\text{-}final}$, A_{grout} and A_{bar} are the respective areas of the pipe, interior grout and center bar (if used). As illustrated in Figure 3, a Series 118/7.5 Ductile Iron Pile section (4.65 inches or 118 mm outer diameter with 0.30 inches or 7.5 mm wall thickness) was used along with 4,000 psi (28 MPa) cement grout to achieve a working capacity of 50 tons (45 tonnes). To provide 15 tons (14 tonnes) of allowable tension resistance, all piles were installed with an over-sized grouting shoe to create an annular space around the pile that was filled with cement grout by continuously pumping through the pile and out the grouting shoe during installation. Piles were driven to achieve a rate of set of 1-inch (25 mm) or less in 50 seconds on glacial till or rock but developed an exterior grouted zone within the annular space created while driving the oversized shoe. This grouted zone provided grout-to-ground bonding to achieve sufficient geotechnical capacity for tension resistance. A full-length #8 Williams Grade 75 ksi (525 MPa) center bar was installed in the wet grout to meet the structural tension requirements.

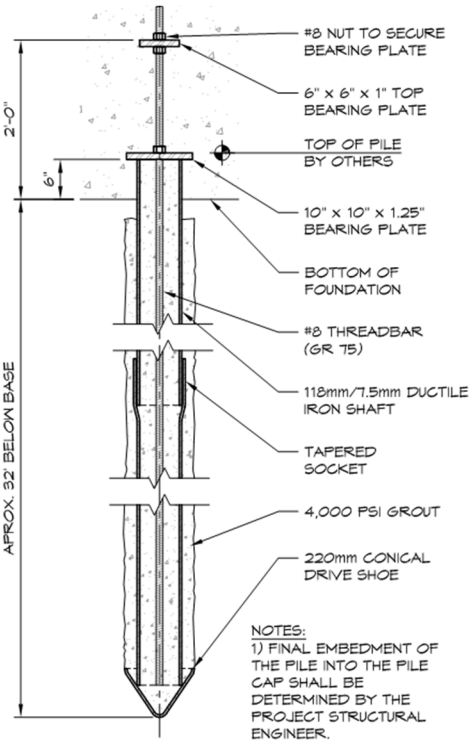


Fig. 3. Ductile Iron Pile Detail

Load Testing and Construction

Pre-production load testing was performed at the start of construction by design/build pile contractor Helical Drilling, Inc. One compression test pile and four tension reaction piles were all installed in a similar manner as the production piles. Piles extended 37 feet (11.3 m) below grade before achieving set. The test was performed in accordance with ASTM D-1143. In addition to monitoring the compression response of the test pile, reaction piles were also monitored to verify the tension load-deflection response. Figure 4 shows the results of the load testing which confirmed the design capacities with less than 0.2 inches (5 mm) of deflection at 100 tons (91 tonnes) in compression and less than 0.25 inches (6 mm) of deflection at 25 tons (23 tonnes) in tension. Following the completion of the test program, installation of the 73 production piles was performed in only 8 working days. Pile lengths averaged 29 feet (8.8 m) due to the variable rock depth. Select locations with limited overhead clearance of 20 feet (6.1 m) required the cutting of piles and use of drive-on couplers similar to the bell-spigot configuration to complete the installation.

AIR HUB SHIPPING FACILITY, PHILADELPHIA, PA

Facility upgrades consisted of doubling the size of an existing mezzanine inside a 1,000,000 square foot (92,903 sq. meter) international shipping logistics warehouse adjacent to the Philadelphia International Airport. Originally constructed in the late 1980's, the 500,000 square foot (46,451 sq. meter) mezzanine expansion was in response to the recent, unprecedented growth in eCommerce.

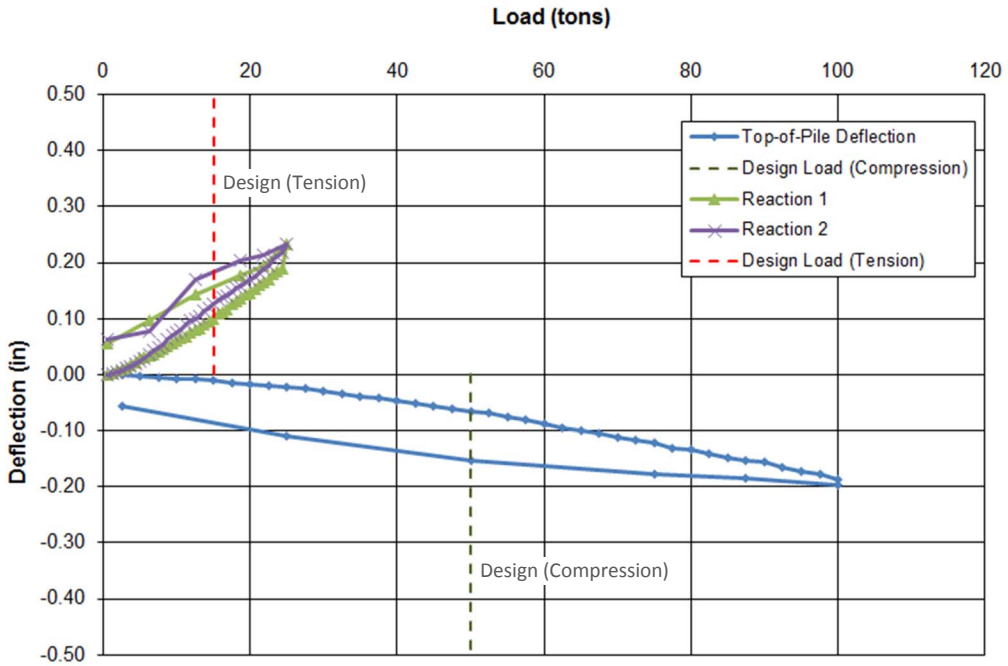


Fig. 4. Results of Compression and Tension Load Testing in Hartford, CT Facility

The existing building, consisting of pre-engineered steel and tilt-up precast concrete wall construction on grade beams, is supported on 60 ton (54 tonne) capacity step tapered piles driven about 75 ft. (23 m) into dense, lower alluvial deposits. The slab is conventional ground-supported construction. The project design team was headed by CVM. New pile-supported column footings were designed to support up to 258 tons (234 tonnes) in compression and lateral loads up to 18 tons (16 tonnes). The new mezzanine columns were located inline and between the existing column supports, which also encompassed the conveyor processing and truck loading platforms. In all, 74 new pile caps supported by a total of 288 piles were designed to support the new mezzanine.

Overhead clearances varied to a maximum of 35 feet (11 m) with areas adjacent to the existing mezzanine limited to 20 feet (6 m). Horizontal clearances were as low as 18 inches (0.5 m). The new mezzanine foundations were earthen formed by precise slab and platform removal with temporary infill prior to pile installation to maintain minimal to no downtime at the facility. Second and third shifts are the primary working hours, therefore construction commenced during modified daytime hours and did not allow for the impact of more than the areas that could be constructed during that shift. This included any sort of piping, hoses, wires, or cables extending outside of the work zone. These tight working constraints and minimal impact requirements on active operations presented construction challenges that the selected piling system needed to be compatible with while achieving the design working load capacity.

Geotechnical Conditions

USDA maps the underlying site soils within the proposed mezzanine retrofit area as made land, gravelly materials and Tidal Marsh deposits, common along the tidally influenced sections of the Delaware River. The Geotechnical Engineering Report prepared by Dynamic Earth, LLC, (2018) describes the history of site development and subsurface conditions.

Three borings were performed which generally encountered fill up to a depth of 10 feet (3 meters) below the warehouse slab. Below the fill, stratified natural alluvial deposits consisting of sand, silt and clay extend up to a depth of about 65 ft (20 m) with N-values averaging 7 blows/foot (bpf). Below these “upper” alluvial

deposits were medium dense to very dense “lower” alluvial deposits consisting of sand, gravel and varying amount of silt with N-values from 18 to 79 bpf, averaging 38 bpf. Beneath the alluvial deposits are natural residual soils extending to boring termination depths of 85 to 90 ft (26 to 27 m) with N-values ranging from 13 to 51 bpf, averaging 32 bpf.

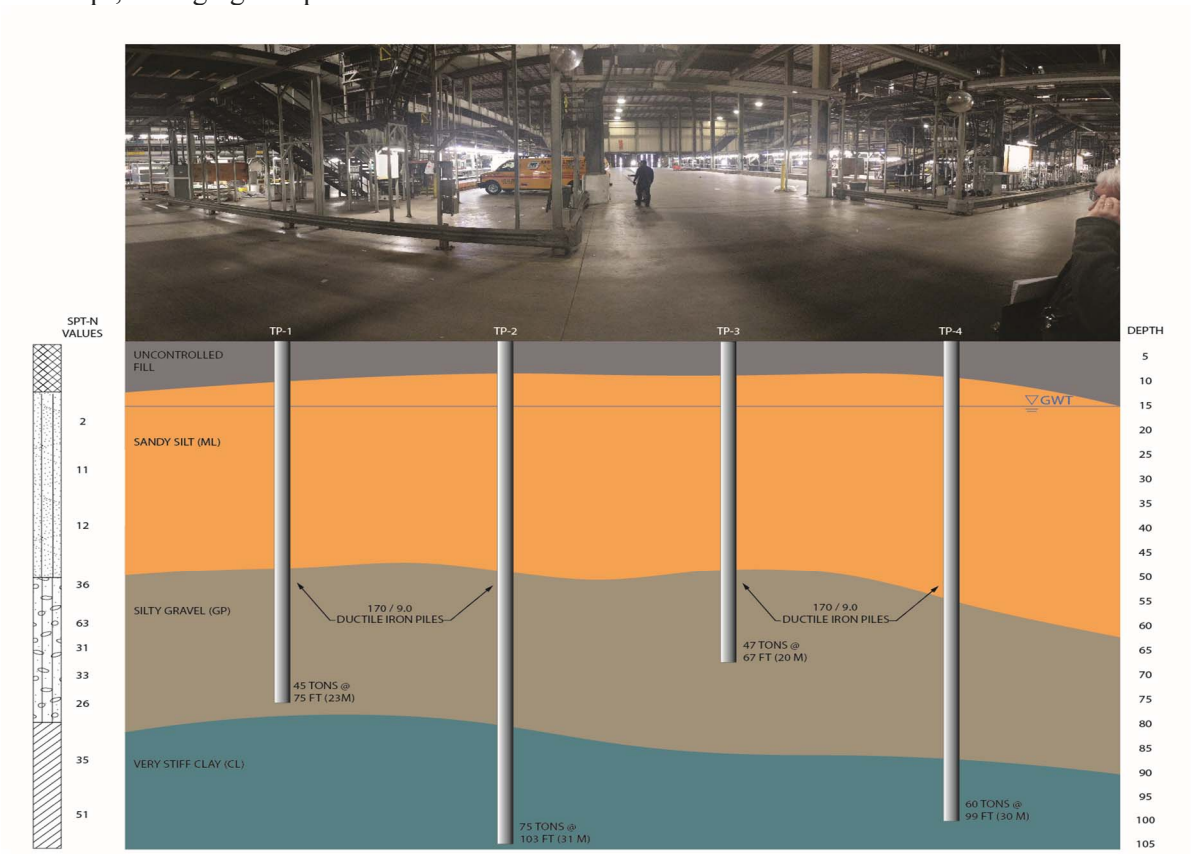


Fig. 5. Test Pile Tip Elevation and Confirmed Allowable Capacity (F.S. =2)

Pile Selection and Design

Based on site logistics, constraints, headroom, spatial limitations, active facility operations, and soil conditions, the project design team selected Series 170/9.0 (6.9 inch or 170 mm OD with 0.35 inch or 9 mm wall thickness) Ductile Iron Piles installed to develop capacity in end-bearing for new column support. End bearing DIPs, which do not require pressure grouting the exterior of the pile, were considered advantageous over grouted friction DIPs, based on site constraints, concerns over grout management within the active facility and on account of previous success driving end bearing DIPs inside the Hartford, CT facility.

Typically installed where rock is within reachable depths to maximize pile structural capacity, little data exists utilizing small-diameter, end-bearing DIPs in looser soils where traditional set rates are not achieved. During the project’s Design Development phase, geotechnical design using the Nordlund Method (FHWA 1996) estimated end bearing DIP ultimate capacity of 110 tons (100 tonnes) for 75 ft (23 m) long piles terminating in the lower Alluvial stratum. The design estimated approximately 75% capacity in end bearing and the remaining 25% of capacity in side friction between the pile casing and soil. Post contract award column load modifications required up to 120 tons (109 tonnes) ultimate capacity per pile based on the structural engineers pile lay-out, which consisted of 2-pile to 5-pile caps. It was, therefore, decided to perform a pile load test to 120 tons (109 tonnes) to confirm a 60 ton (54 tonnes) allowable capacity with a factor of safety of 2.0 for a 75 ft. (23 m) long DIP.

The 6.7 inch (170 mm) diameter Series 170/9.0 DIP was filled with 2,000 psi (13.8 MPa) grout giving it a maximum ultimate structural capacity of 166 tons (150 tonnes), meaning the estimated geotechnical capacity would govern the performance since the piles were to bear in soil rather than on rock. A flat end plate was installed at the tip of each pile and cap plate on the top of each pile.

Load Testing and Construction

Design-build contractor, GeoConstructors, Inc., performed test and production pile installation and performed pile load testing. Pile load testing occurred on non-production piles installed outside the southwest entrance to the facility. In all, four load tests were performed on variable length piles, illustrated in Figure 5.

Initially, one static axial load test was performed in accordance with ASTM D1143 to confirm 120 ton (109 tonne) ultimate capacity. The initial test pile (TP-1) was driven 75 feet (23 m) into the lower Alluvial deposits (silty gravel), to a set of 1.9 seconds per inch (0.75 seconds/cm). The target ultimate capacity of 120 tons (109 tonnes) was not achieved and a lesser ultimate capacity of 90 tons (82 tonnes) was confirmed. With the looser conditions and high advancement rate (set) at 75 feet (23 m), the project design team directed the DIP installer to install a second test pile (TP-2) deeper into the very stiff Residual (clay) stratum in an attempt to successfully confirm the 120 ton (109 tonne) ultimate capacity. The second test pile was driven 103 feet (31 m) to a set of 50 seconds per inch (20 seconds/cm). TP-2 was successfully tested to 150 ton (136 tonne) ultimate capacity. While TP-1 results confirmed the ultimate capacity was 25% lower than the target ultimate capacity, TP-2 results were 25% higher.

Not wanting to re-design many of the pile caps that were already being prepped for production work, the project design team decided to have two additional piles installed and tested. TP-3 was driven 67 feet (20 m) into the lower Alluvial deposits to a set of 3.2 seconds per inch (1.3 seconds/cm), and TP-4 was driven 99 feet (30 m) into the very stiff Residual stratum to a set of 7.6 seconds per inch (3 seconds/cm). TP-3 was tested to 94 ton (85 tonne) ultimate capacity, mirroring TP-1 which was also bearing in the lower Alluvial stratum. TP-4, bearing in the Residual stratum similar to TP-2, was tested to 120 ton (109 tonne) ultimate capacity. Figure 6 plots the results of the load tests for each of the test piles. A graph of DIP allowable capacity (incorporating a factor of safety of 2.0) versus set time for these tests is shown in Figure 7.

The load test data was used to optimize pile caps with minimal changes in pile cap size and orientation. Many of the 5-pile caps were reduced to 4-pile caps and 4-pile caps reduced to 3-pile caps by utilizing piles bearing collectively per cap in either the lower Alluvial or the Residual strata to meet the required load demand.

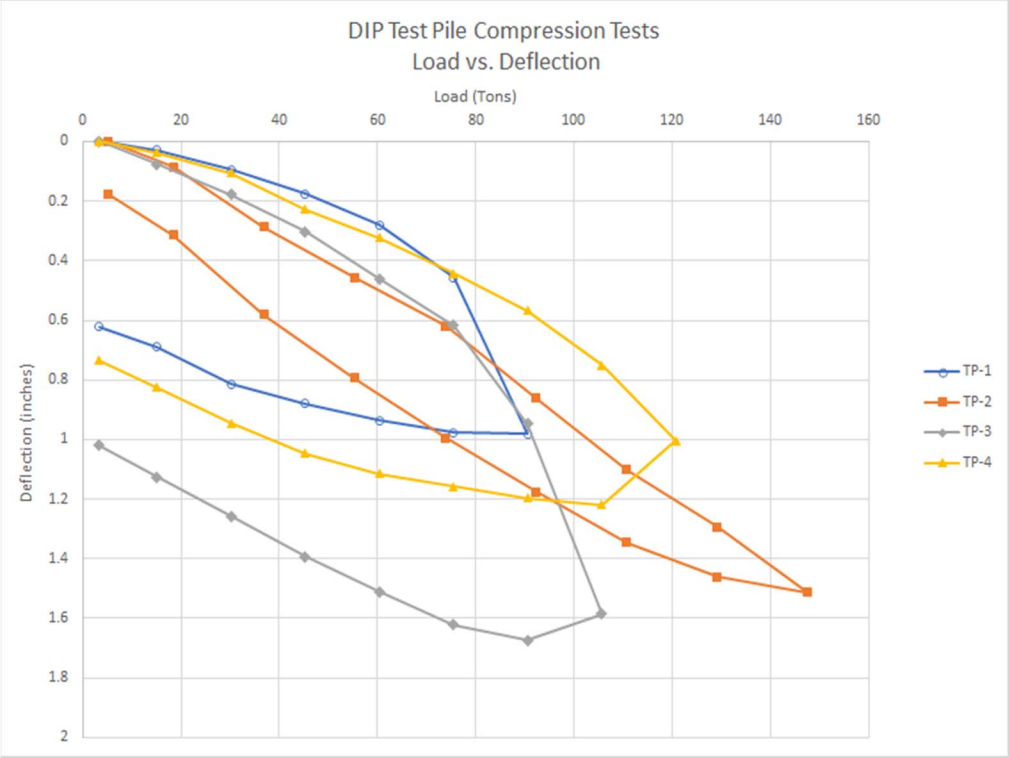


Fig. 6. Results of Compression Load Testing in Philadelphia, PA Facility

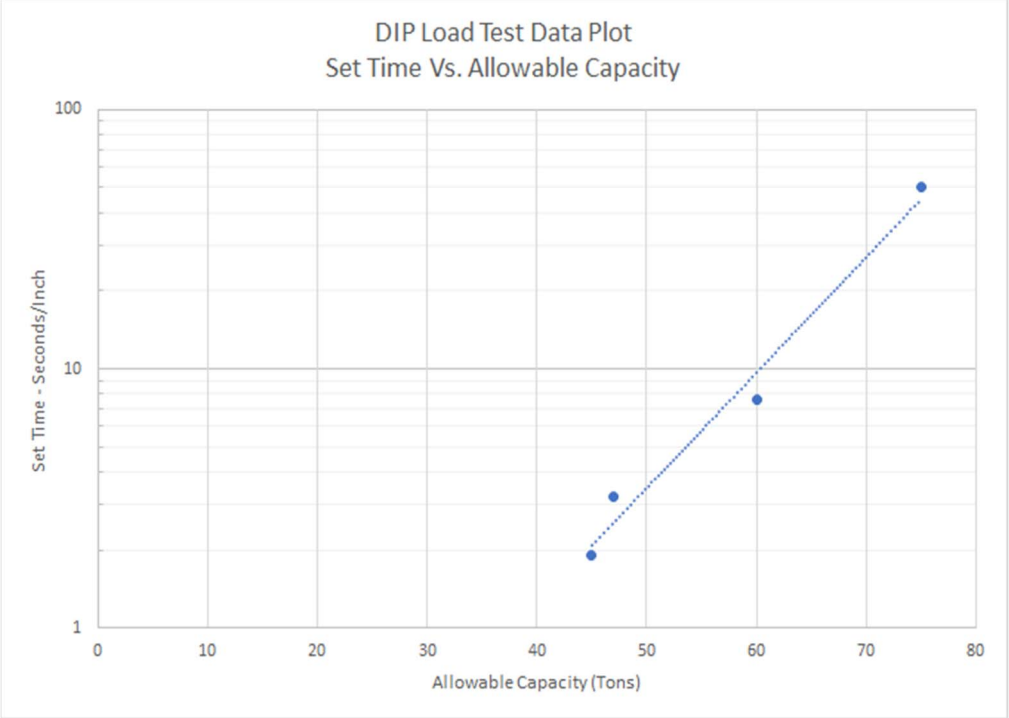


Fig. 7. Test Pile Allowable Capacity vs. Set Time

SUMMARY AND CONCLUSIONS

Ductile Iron Piles are a proven pile solution to support moderate to high loads. Installed with a high frequency hammer mounted on an excavator, they are particularly effective on constrained sites, in areas with low vertical and horizontal clearance and where vibrations are a concern. DIPs can be driven with a closed end plate to develop their capacity in end bearing, typically where rock is reachable to maximize pile structural capacity. They can also be installed by grouting through a conical grouting cap to create a column of grout on the pile exterior and develop load capacity in friction via the grout-soil interface.

Two interior retrofit projects, consisting of mezzanine expansions in shipping facilities in Hartford, CT and Philadelphia, PA, utilized end-bearing DIPs to support new construction in low headroom warehouses. The DIPs were selected over equivalent capacity micropiles based on cost and production and over helical piles by providing greater capacities at reduced cost. In Hartford, CT, DIPs were driven 26 to 40 feet (8 to 12 meters) to rock to develop allowable capacities of 50 tons (45 tonnes) compression, 15 tons (14 tonnes) tension. In Philadelphia, PA, 45 to 75 ton (41 to 68 tonnes) allowable compression capacity DIPs were successfully set in soil, ranging in depths from 67 to 103 feet (20 to 31 meters), with the lower capacities bearing in shallower dense granular soils and the higher capacities in a deeper very stiff clay strata.

REFERENCES

DuroTerra, LLC. 2018. “Technical Brief: Bending Resistance of Ductile Iron Piles.” Dated January 18, 2018.

Dynamic Earth. “Report of Geotechnical Investigation, Proposed Mezzanine Expansion.” Dated May 7, 2018.

Federal Highway Administration. 1996. “NHI Course Nos. 13221/13222: Design and Construction of Driven Pile Foundations. Publication No. FHWA-HI-97-013. December 1996.

GeoStructures, Inc. 2015. “Ductile Iron Pile Load Test 1 and 2 Results”, dated August 16, 2018.

GeoStructures, Inc. 2015. “Ductile Iron Pile Load Test 3 and 4 Results”, dated August 16, 2018.

GZA GeoEnvironmental, Inc. 2017. “Geotechnical Engineering Report. New Mezzanine, 90 Locust Street, Hartford, Connecticut.” Dated February 13, 2017. Project No. 05.0045956.00.

International Code Council, Inc. (ICC). 2015. International Building Code 2015. Country Club Hills, IL.

LeDo, D., Billups, T., Carchedi, D. and FitzPatrick, B. 2016. Innovative Deep Foundation Support Using Ductile Iron Piles. Proceedings of the DFI International Conference on Deep Foundations, Seepage Control and Remediation. New York, NY. October 12 - 15, 2016.

Siskind, D.E., Stagg, M.S., Kopp, J.W. and Dowding, C.H. (1980). “Report of Investigators 8507: Structural response and damage produced by ground vibration from surface mine blasting.” United States Department of Interior - Bureau of Mines. P.73. 1980.

Tiroler Rohre Gmbh (TRM). 2014. “Piling Systems for Deep Foundations.” October, 2014.

EMERGENCY JACKING TUNNEL IN COMPRESSIBLE SOIL

Michael McNicholas, P.E., Moretrench, Rockaway, New Jersey, USA, (973) 627-2100, mmcnicholas@moretrench.com
James C. McIntyre, Melcar Underground, Oxford, New Jersey, USA, 484-653-8259, james@melcar.biz
Tai Luu, P.E., Moretrench, Rockaway, New Jersey, USA, (973) 627-2100, tluu@moretrench.com

ABSTRACT

The Jersey City Municipal Utilities Authority (JCMUA), discovered that an existing sewer pipe had collapsed under the New Jersey Transit Conrail Railroad between Pine Street and Ash Street in Jersey City New Jersey. Immediate action was taken to abandon the pipe in place and install a new sanitary sewer. The borings showed 10-20 ft (3.04 m.- 6.09 m) of competent fill overlaying approximately 8 ft. (2.44 m.) of compressible peat and organics. Groundwater was at 8 ft (2.44 m) below ground level. The poor condition of the soils at subgrade could not withstand the extreme weight of the jacking machine or the thrust force required to push the casing from the launching pit to receiving pit. The support of excavation (SOE) would therefore not only need to retain the soil to allow the jacking equipment to reach subgrade at 14 ft (4.27m) below working grade, but also the back wall of the SOE would need to be sufficiently robust to function as the reaction block for jacking operations. The alignment and allowable tolerance for the jacked casing was minimal, therefore the performance of the SOE was extremely critical to the success of jacking operations. This paper will discuss in detail the design concepts that were developed and implemented by the team to overcome these obstacles.

Keywords: constructability, pipe soldier piles, micropiles, support of excavation, thrust block, deep foundations, load testing, jacked piles.

HISTORY

The discovery of a collapsed section of an existing sanitary sewer led the Jersey City Municipal Utilities Authority to act on an emergency contract. The project design team was tasked with developing an abandonment plan for the broken pipe and installation of the new pipe through challenging geology. The new 180 ft.(54.96 m) long, 54-in. (1.37 m) . diameter sewer pipe was designed to be contained within a 72-in. (1.83 m) protective steel casing. The installation of the new sewer pipe would require a detailed understanding of the geology. The geotechnical subcontractor assembled a subsurface investigation report on November 2nd, 2017. It was quickly realized that the only way to replace the pipe was with a jacked pipe system since the large grade change and the Conrail Right of Way created no other alternative. Delaying or closing the railway was absolutely not an option as that particular railway served as the main heavy-haul route to and from Jersey City. It became apparent that a major obstacle to pipe jacking was the challenging geology present across and beneath the proposed sanitary sewer. The following challenges faced the design team prior to the installation of the replacement pipe:

- Explore the subsurface soil and groundwater conditions within the proposed machine support area.
- Estimate the geotechnical engineering properties of the encountered subsurface materials
- Evaluate the support requirements for the jacking machine, considering the anticipated structural loads.
- Recommend an appropriate type of foundation for the support of the proposed machine and final sanitary sewer in place.
- Estimate the post construction performance of the foundation system.

© 2019 Deep Foundations Institute

The General Contractor was tasked with assembling the design and construction team. The scope of work would include the correct measures to install a jacked pipe under the existing Conrail line without disturbing anything in its path. The job scope was split between two specialty subcontractors, one to discuss and construct the SOE and foundation system, and the other tasked with installing and jacking of the proposed pipeline.

SUBSURFACE CONDITIONS

The subsurface program consisted of three soil borings, B1 through B-3, as shown in Figure 1. These borings extended to depths of 50-85 ft (15.24 – 25.91 m) from the existing ground surface and documented the change in soil strata and elevation of the water table. Each boring encountered 10-20 ft (3.04 - 6.09 m) of fill overlaying 5-10 ft (1.52 - 3.05 m.) of low blow count compressible peat above weight-of-hammer silts and clays. These are challenging materials, even for a basic support of excavation system. The immense weight of the tunnel boring machine also had to be taken into consideration. Vertical or horizontal bearing resistance against the geology present would be challenging, and additional measures would need to be considered while planning the remediation of the pipe. A cross-section through the three borings is shown in Figure 2. For clarity, the limits of the jacking pit have been shown in blue and the new pipe has been shown in yellow.

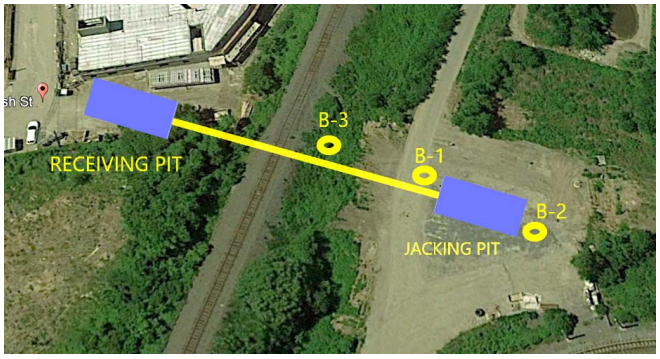


Fig. 1. Arial view of jacking pit and receiving pit

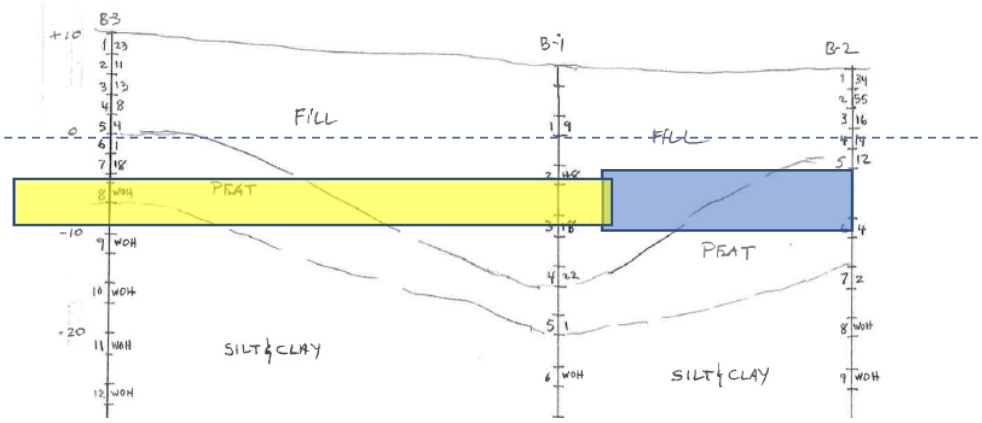


Fig. 2. Cross-section of geology

The high water table noted by the blue line extending across Figure 2 would have to be addressed by a series of dewatering wells installed around the perimeter of the proposed excavation pit. The soil would be analyzed to determine where the water would be pumped from to allow for the largest drop in water

levels. As the pumps pull water into the wells, they create a cone of depression. Installing wells around the perimeter of the pit allows for a uniform drop in the water table. The system would need to stay active until all the construction was complete and the hole was backfilled.



Fig. 3. Deep well system around jacking pit

PHASES OF EXCAVATION SUPPORT

In addition to the challenging geology, the pipe would have to cross under an existing train line operated by NJ Conrail system. This eliminated open trenching on either side of the pipe and guaranteed it would have to be a horizontal drilling method of construction. The new pipe would be installed by pilot-guided auger boring from an excavated jacking and receiving pit.

The design of the excavation system required evaluating different construction phases. Each phase had a critical issue to be resolved.

Phase 1. Excavation to Subgrade: Resisting the active pressure of a 14 ft (4.27 m) vertical cut in soft soil with and high-water table

P**hase 2. Jacking Phase:** Resisting a high jacking force to push the 72-in. (0.635 m) diameter casing through the virgin soils

Phase 3. Final Backfilled Conditions: Support the new pipe and sewer system and backfill on the structural slab

The goal was to create a highly efficient design that was cost effective and constructible. Each phase was evaluated individually but it became apparent that the entirety of the phased support needed to be taken into consideration.

The system could be supported by either a driven sheet pile or drilled-in system. The driven sheet system was eliminated due to vibration concerns based on the proximity of the railroad. Also, the difficulty of cutting through the sheet during jacking and the depth required to toe the sheets into a denser material made this option uneconomical. An additional drilled-in system approach that was evaluated was large diameter helical piles functioning as cantilevered soldier piles, with a wooden lagging system. This scenario was costly and would require specialty material to be ordered and shipped, resulting in a lead time outside of the project timeframe. Ultimately, a drilled-in pipe system with internal bracing was chosen for the jacking pit.

SUPPORT OF EXCAVATION CHALLENGES

During the conceptual phase of the design, the SOE system needed to overcome several challenges. The objectives for the design included: creating a large open hole to 14 ft (4.27 m) deep with minimal interferences to allow for equipment to be set in the hole, prevention of ground loss during lagging, provision of slab support, and a means to tie the system together in anticipation of the jacking force.

The pipe soldier piles were installed on varied spacing around the perimeter (Fig. 4). The soil in between the piles would be retained by the lagging.

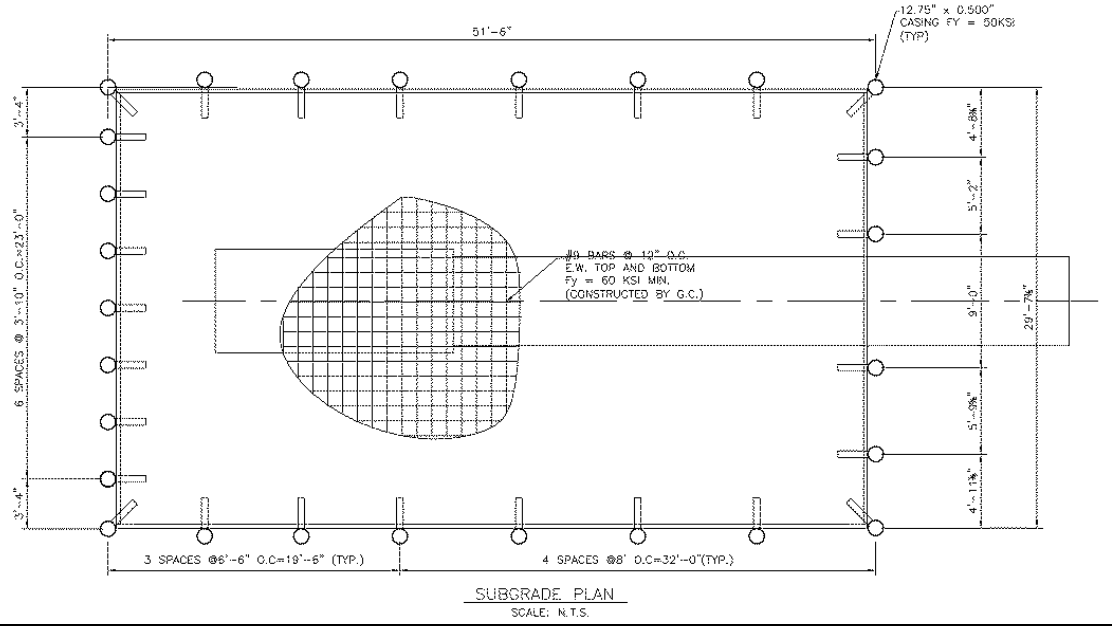


Fig. 4. Base Foundation System
1 ft = 0.305 m

Due to the soft peat layer, excavation of material and installation of lagging was accomplished at a slower rate than a typical installation. Any loss of material would jeopardize the integrity of the soil at grade. To reach subgrade, the excavation was designed to be supported by a structural beam wrapping around the perimeter of the excavation at two different elevations. A single support, referred to as a strut, was located in the middle of each tier of beams. The top support would be approximately 1 ft (0.304 m) from grade and the temporary second tier would be 8 ft (2.44 m) from grade. The second-tier strut was removed after the 18 in. (0.45 m) slab was poured at subgrade. There was added benefit to keeping the structural steel wrapping around the excavation as it provided additional rigidity to the SOE.

OVERCOMING FOUNDATION CHALLENGES

The soft peat layer was present both behind and beneath the support of excavation system. The peat would not be a suitable bearing material for the jacking equipment or the sub-base for the new sanitary system. Any settlement of the slab would directly result in a change in the alignment of the jacked pipe. An 18 in. (0.45 m) structural slab, supported on micropiles, would be able to carry the temporary structural load and the final load. The slab was intentionally poured tight to all four walls. Each soldier pile surrounding the excavation included a small w-section. The steel section would allow for the base of the SOE to aid in generating lateral resistance.

The new slab foundation had to support multiple phases of loading during construction, from temporary loading of the jacking equipment to the final backfilled phase with the 72-in. (0.635 m) pipe, cradle and box sewers and backfilled soil. In order to support such heavy loading requirements, rock-socketed micropiles were specified for the job. The micropiles were not only designed for the axial load required but also the lateral load imposed during the jacking of the 72-in. (0.635 m) pipe. Figure 5 shows the micropiles prior to the slab being poured.

Prior to production work, a sacrificial micropile was successfully tested to twice the intended design load to verify design assumptions. Strain gauges allowed for interpretation of the rock socket bond stress capacity.

The foundation was constructed to temporarily and permanently support its design objective.

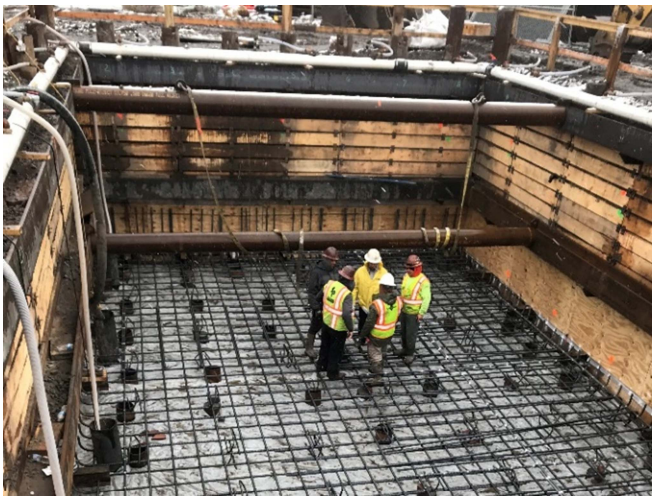


Fig. 5. Base foundation system

THRUST BLOCK DESIGN

Initial conversations between the jacked pipe specialty subcontractor and SOE contractor indicated that the reaction force needed to jack the 72-in. (0.635m.) pipe from the receiving pit was approximately 600 k (2668.9 kN). The geology at the application of force (approximately 12-ft (3.66 m) down is compressible, weak organic silt and clay material with a high propensity for movement. A series of options were discussed to remediate the soil behind the jacking force in order to increase the soil resistance behind the SOE during the jacking process. Options included mass soil mixing behind the SOE and tiebacks to counteract the force from the pilot guided auger or to tie the support of excavation and

foundation system together to create combined resistance. There were pros and cons for each approach; however connecting the SOE system and permanent foundation system together proved to be the most feasible and most economical solution.

With the SOE system and permanent system tied together, the thrust force needed to be absorbed into the back wall of the SOE. In order to absorb the jacking force into the system, a concrete block and beam was designed to spread the load to the soldier piles. The system was tied together with welded shear studs, collars and rebar. The internal forces, such as moment and shear of the jacking block and beam, were checked against the passive pressure of the soil behind the SOE. Essentially, the SOE system was designed to work as a large passive wall to dissipate the jacking forces into the surrounding soil. The thrust block is shown in below in Figure 6. The system was designed to have a considerable amount of robustness and conservatism build in to account for unforeseen variability such as additional jacking pressure needed to overcome obstructions.. The wet, heavy peat formations resulted in higher than normal thrust pressures. In addition, because of train traffic, the calculations had to account for the added axial load and pulsations caused when the heavy-haul cars were passing overhead.



Fig. 6. Thrust block and SOE system

SELECTION OF JACKING METHODOLOGY

The primary objective during jacking was to minimize the risks involved in the casing installation. Risks to be calculated included:

1. ***Unknown ground conditions:*** The closest boring was drilled +12 ft (3.66 m) ft to the north of the bore path at the base of the grade going up to the tracks. This boring could not be used as a valid source of information, only as a reference.

2. ***The high potential for underground obstructions***: The area had been raised previously. In the 1970s, the area which the entire project encompassed was used as a distribution area for a minimum of five rail lines. These rail lines have no record of being properly removed, and there are no records of what materials were used to geotechnically support these five lines or the existing raised heavy-haul rail line. Given this information–the knowns and the unknowns– it was highly probable obstructions would be encountered in the bore path.

   With such soft and wet ground, various drilling options needed to be weighed, as summarized in Figure 7 below.

Options for Technology	Pros	Cons
Microtunneling	1.Fast installation time 2.Equipment availability 3.Small jacking pit 4.One pass system 5.Guided via laser	1.Over budget 2.Head weight of 25,000lbs plus soils 3.Slurry to be disposed of 4.Limited face access for obstructions
Tunnel Boring Machine	1.Small jacking pit 2.Easy of excavation 3.Face access 4.Guided via laser 5.One pass system 6.Equipment availability	1.Head weight of 25,000lbs 2.Too close to budget
Horizontal Directional Drilling	1.Fast installation 2.Limited site preparation 3.Low head weight – drill rod would guide the tunnel upwards to hold grade. 4.Obstructions can be bored through	1.Unsupported bore below railway 2.No guarantee of line or grade accuracy
Auger Boring vs. Small Boring Unit	1.Meets budget 2.Single Pass system 3.Bore hole supported by steel casing	1.Operated from inside the tunnel 2.Head weight of 14,000 lbs. 3.Slow progression 4.Limited face access
Pilot Guided Auger Boring	1.Meets or is under budget 2.Bore hole continuously supported 3.Laser guided 4.Head is less than 1200 lbs plus soils 5.Speed of installation 6.Full face access plus maintained face support – ONLY after pilot tube installation	1.Equipment availability (to match timeline) – not on the market 2.Three pass system – adding 2 time the variables 3.Technical challenges facing Melcar during execution

Fig. 7. Drilling Technologies Evaluated

Pilot guided auger boring was chosen due to the ability of the technology to perform the needed operations with respectively no head weight. The weight was a critical factor due to the softness and unknowns that were to be encountered. The boring process consists of the drive element, either a pilot rod or casing, the guidance machine and the auger tracks. As the casing is advanced the guidance machine locks into the tracks and pushes against the thrust block at the back of the SOE. An operator rides on the guidance system as it progresses along the length. As each new piece or casing or rod is added. the soil that is augered out of the hole is cleaned and stockpiled. Figure 8 shows the jacked system in action.



Fig. 8. The jacked system in action

Once the methodology was determined, it was found that the necessary equipment and machinery was not available on the open U.S. market, and the lead time to have a unit manufactured was a three-month minimum. However, the pilot guidance machine was located and procured from Abu Dhabi, United Arab Emirates. A member of the jacking subcontractor's team flew to Abu Dhabi to inspect, purchase, and ship the equipment back to the United States.

The 60/72-1200 auger boring machine was brought in from Louisiana, while the cutting heads and knife reamers were produced and shipped from Ohio. Both the 30 in. (0.762 m) and 72-in. (1.83 m) casings were brought in from Missouri.

With the logistical hurdles overcome, the technical operations team focused on the engineering challenges. As mentioned in the risk assessment above, the unknown ground conditions coupled with the known softness and wetness to be encountered had to be evaluated extremely closely. The pitch angle for the pilot guidance tube had to be calculated to account for the weight-drop factor. Figure 9 shows the instrumentation used to measure the jacked piles alignment.



Fig. 9. Instrumentation (left) and pipe being pushed (right)

With soils that showed 4-10 blow counts per foot, the weight-drop factor of the pilot tube, the intermediate 30 in. (0.762 m) guidance pipe and the final calculations for the 72-in. (0.635m) casing pipe had to be compounded.

INSTALLATION

Following installation of the pilot tube jacking frame and ancillary equipment, the pilot tube was installed at a +3 degree angle, aligning it to reach the exit pit 7 in. (177 mm) above centerline. This would allow for the weight-drop factor of both of the following pipes. The pilot tube jacking equipment and tracks were disassembled and replaced with the 60/72-1200 auger boring machine, capable of a thrust force of 1,200 k (5337.87 kN). The capability of this machine was necessary to ensure that face pressure in a wet and heavy soil environment could be held at all times once the bore had surpassed the influence zone of the dewatering system. The maximum force that was calculated to be required was 535 k (2379.79 kN), not accounting for any obstructions. At the time of switching the pilot tube installation equipment with the auger boring machine, it was then known that there was a hard formation and obstruction at invert level where the slope to the tracks began, and another obstruction in the center of the railway tracks. It was estimated that a force of 750 k (3336.16 k.) would now be needed to overcome the restriction that the obstruction would put on the casing and jacking equipment. Careful pre-planning from all parties

allowed for the design of the thrust block, SOE, and back-wall support system able to withstand the entire capability of the 1200 k (5337.87 kN) machine.

The 30 in. (0.762 m). casing was installed to follow the same path as the pilot tube. At the same two aforementioned locations, the casing struck obstructions but the auger bore machine and head technology were able to work together to break through successfully. Upon entering the exit pit, the 30 in. (0.762 m) casing came in at 4 in. (101.6 mm) above centerline (Figure 10). A cribbing support system would ensure that further drop in the 30 in. (0.762 m) casing would not be possible.

Working against ever increasingly wet ground conditions due to large amounts of rainfall and seventeen inches of snowfall, the team began the preparation for the installation of the final 72-in. (1.83 m.) casing. All alignments were dually checked, equipment inspected, and calculations verified. The seventy-two-inch casing was installed following the 30 in. (0.762 m) casing and attached via a knife reamer – the same as the 30 in. (0.762 m) was to the pilot tubes. At the location of the first obstruction, the head excavated fragmented boulders, wood, and traces of metal along with other nonorganic debris. The machine and head were able to work through the obstruction at a slow but progressive rate.



Fig. 10. 30 in. (0.762 m) jacked casing

Once the obstruction was overcome, the bore was able to resume at the normal rate. The second obstruction site was reached during night operations at approximately three a.m. The crew spent two hours using the machine and head to attempt to work through the obstruction. After three hours without progression, an early morning meeting was called to address possible ways forward. It was quickly determined that face access was the best option. With the 30 in. (0.762 m) guidance pipe accessible from the receiving pit, face access was able to be gained to properly address the situation without going through the extensive operation of removing the tunnel internals including the augers and head assembly. The obstruction was confirmed to be a rock shelf that encompassed the entire top half of the 72-in. (1.83 m) casing. The bottom third of the head and casing pipe was under the water table since the effects of the dewatering system had to be minimized directly under the railway to prevent settling. The previous bores [pilot and 30 in. (762 mm)] had been able to go below the majority of the obstruction, only being slightly hindered.

The tunnel had to be gutted of the head assembly and augers to allow for a team to access the face and manually remove the rock obstruction. Once the team was at the face, they began to break the rock, discovering large amounts of steel and rebar along with wooden pylons. Obstructions of this nature would have crippled a bore being installed by another method. Within a total turn-around time of three hours, the tunnel had been gutted, obstruction removed, tunnel internals reinstalled and the steel casing thrusted forward once again. To advance the casing forward, the auger bore machine had to reach a thrust of 900 k

(4003.39 kN). Once the tunnel began to advance again, the pressures went back down to the 300 – 400 k (1334.47 – 1779.29 kN) range.

At break-through of the 72-in. (1.83 m)steel casing into the reception pit (Figure 10), the invert came in very slightly above target. Achieving such line and grade accuracy on a bore that presented so many challenges and technical milestones is a testament to the expertise of all involved.



Fig. 10. 72-in. (1.83 m) jacked casing entering receiving pit

SUMMARY

The key benchmarks that come from the success of the boring/thrusting scope of this project are:

1. Utilization of a pilot guided system to install 72-in. (1.83 m) x 1-in. (25.4 mm) wall casing.
2. Maintaining line and grade accuracy in soil that does not support the weight of the installed pipe.
3. Coordination between multiple contractors, engineers and the client over 8-9 months.
4. Thrusting pressures of 900 k. (4003.39 kN) with no movement or alteration in the thrust block or back wall with ground conditions of 4 blow counts per foot.

CONCLUSIONS

Overcoming the multiple design and installation challenges was a tremendous accomplishment for the entire project team. Individually, each design phase showed the professionalism and skill of the project team; however when combined it showcased the creativity and brilliance of specialty construction. Implementing a cost-effective and safe design resulted in an expedited remediation of the problem. Key to the smooth running of the entire operation was the experience of the foundation and jacking teams, and the continuous inter-cooperation from the planning stages through execution of the work that ensured that any issues that arose were able to be immediately addressed and resolved.

RECENT DEVELOPMENTS IN WIND TURBINE FOUNDATION DESIGN: POST TENSIONED SINGLE PIER

Mohamed Alrowaimi, Ph.D., NV5, 201 S Bumby Ave, Orlando, Florida, USA, mohamed.alrowaimi@nv5.com
Amr Sallam, Ph.D., P.E., NV5, 201 S Bumby Ave, Orlando, Florida, USA, amr.sallam@nv5.com
Xuebing Zheng, P.E., NV5, 201 S Bumby Ave, Orlando, FL 32803, USA, xuebing.zheng@nv5.com
Ahmad Mohamed, Ph.D., NV5, 201 S Bumby Ave, Orlando, Florida, USA, ahamad.mohamed@nv5.com
Mohsen Elsayed, P.E., NV5, 201 S Bumby Ave, Orlando, Florida, USA, mohsen.elsayad@nv5.com

ABSTRACT

The foundation is an essential component of the wind turbine that ensures continued operation under stable and safe conditions. Both shallow and deep foundations are utilized to support wind turbines including gravity spread foundation, anchor foundation, pier or drilled shaft foundation and pile and pile cap foundations. Conventional methods were typically utilized to design the wind turbine foundations. With the advances in numerical modeling in the geotechnical field, foundation designers may utilize numerical analysis to design wind turbine foundations. Geotechnical numerical packages allow modeling structural components and soil-structure interaction that is usually neglected in conventional methods. Furthermore, the subsoil conditions, geometries, stress-strain behavior, boundary conditions and load staging can be modeled, minimizing the assumptions and generalization. This results in better understanding of the stress strain behavior of the foundation leading to optimized foundation designs. This paper includes a brief review of current foundations used to support wind turbines with an emphasis on post tensioned single pier foundations. The current conventional foundation design methodologies and state-of-the-art foundation design utilizing numerical modeling of the single pier foundation will be discussed. Two case histories where the single pier foundation, designed using numerical modeling, were utilized to support the wind turbines will be presented.

Key words: wind turbine foundations, Post Tensioned Single Pier foundation design, numerical modeling

INTRODUCTION

The foundation is an essential component of every wind turbine that ensures continued operation under stable and safe conditions. Turbine manufacturers provides load specifications for designers to be utilized for wind turbine foundations design. Loads include bending moments, torsional moments, lateral forces and vertical forces in both operational and extreme wind conditions. Essential specifications under seismic conditions might also be provided in seismic prone areas. Turbine manufacturers also include foundation design criteria including minimum rotational stiffness, minimum horizontal stiffness, maximum allowed inclination and maximum allowed lateral movement under both operational and extreme loads.
Geotechnical explorations and evaluations are typically performed at early stages of the wind development projects. The field explorations usually include Standard Penetration Test (SPT) borings, Cone Penetration Test (CPT) Soundings, geophysical surveys, and laboratory tests to define soils stratification system and soil strength and compressibility characteristics. The most critical soil parameters for turbine foundation design are shear strength parameters (cohesion and friction), shear modulus, Poisson's ratio, and unit weight. The depth to the groundwater table is also a crucial parameter in design. Advanced field explorations techniques such as Dilatometer Tests and Pressuremeter Tests may also be utilized. Laboratory tests for foundation design typically include index parameters, consolidation and triaxial tests.

© 2019 Deep Foundations Institute

Both shallow and deep foundations are utilized to support wind turbines, including Gravity Spread Foundation (GSF), anchor foundation, pier or drilled shaft foundation, and piles. For GSF, vertical loads and overturning moments are resisted by the weight of the foundation, the soil ballast and bearing capacity of the foundation soil. Horizontal loads are resisted by friction between the foundation base and the supporting soil. For soil/rock anchor or pile cap foundations, axial loads and overturning moment are resisted soil/rock anchors or piles. The foundation soil under the cap provides additional bearing resistance increasing the overturning safety factor. Lateral loads are resisted by the friction under the concrete cap and shearing resistance of the anchors/piles. Post tensioning the soil/rock anchor guarantees that the foundation will withstand extreme wind load. For post tensioned single pier foundation, horizontal loads and overturning moment are resisted by the passive earth pressure and friction of the soil surrounding the foundation and by bearing on the foundation base. The single pier foundation may be considered as a natural extension of the turbine tower similar to direct embedded poles. Post tensioning the tower/pier anchor guarantees the pier structural concrete will not have any tension stresses under operational wind loads. It is effectively a tensionless pier, which substantially increase the fatigue lifetime of the foundation. Figure. 1 shows different examples of wind turbine foundation types.

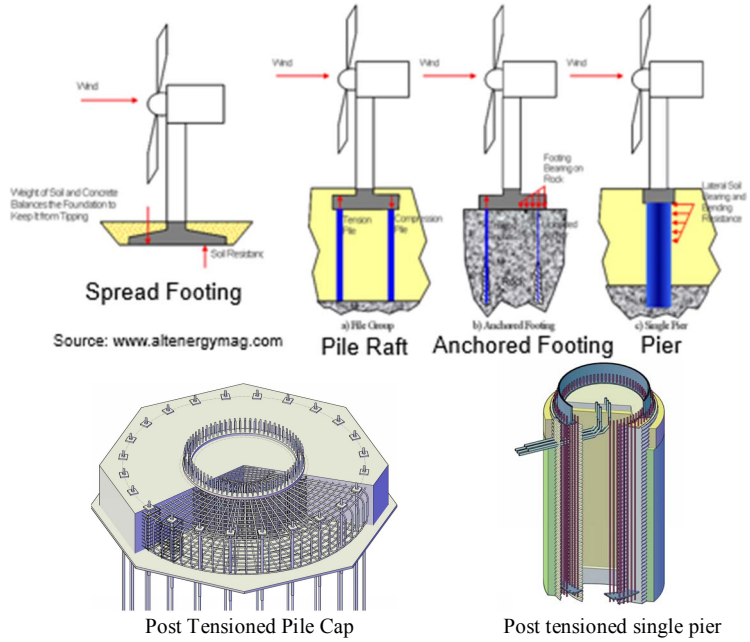


Fig. 1. Examples of wind turbine foundation types

With the current high demand of renewable energy, wind turbine generators are getting larger each year to ensure the economic viability of wind projects. Wind turbine generators larger than 3 Megawatts (MW) have started to penetrate the market and proved to be a more economical option than smaller turbines that were more common during the last decade. The foundation cost is an integral part of the overall wind turbine projects cost. For smaller turbines, the difference in cost between traditional shallow spread foundations and other foundation options is small. However, for larger foundations with substantially higher bending moments and lateral forces, the size of the GSF becomes substantial and the amount of required concrete and steel becomes a challenge for suppliers. The construction time also increases substantially. The single pier foundation provides not only an economical advantage over the GSF but also a durable foundation, which if constructed and maintained properly, could have a very long design life and potential for re-use (re-powering). This paper presents an in-depth explanation of the post tensioned single pier foundations' geotechnical design, optimization, stress strain behavior using finite element analysis, and provides two case histories, which are representative to the presented design methodologies and approach.

POST TENSIONED SINGLE PIER MECHANISM AND CONSTRUCTION

The post tensioned single pier is an innovative foundation to support wind turbines supported on monopole towers. The single pier foundation may be considered as a natural extension of the tower. The foundation consists of a large diameter, cast-in-place post-tensioned concrete annular pier.

The single pier consists of two Corrugated Metal Pipes (CMPs) to provide a stay-in-place form for the concrete annular pier. The hollow interior of the single pier foundation is backfilled with the un-compacted natural soils resulting from the foundation excavation eliminating the need for overhaul excavated soils. A concrete plug is poured at the bottom of the foundation and an 18-inch thick structural slab across the top of the annular space provides the top of the pier. The embedded depth of the single pier foundation varies depending on Wind Turbine Generator (WTG) size, turbine loads and subsoil conditions at the site. The tower bolts are extended for the full length of the pier, which are used to apply the required post-tensioned to ensure that the annular pier remains in compression under the extreme wind loading. Figure 2 shows different components of the post tensioned single pier foundation.

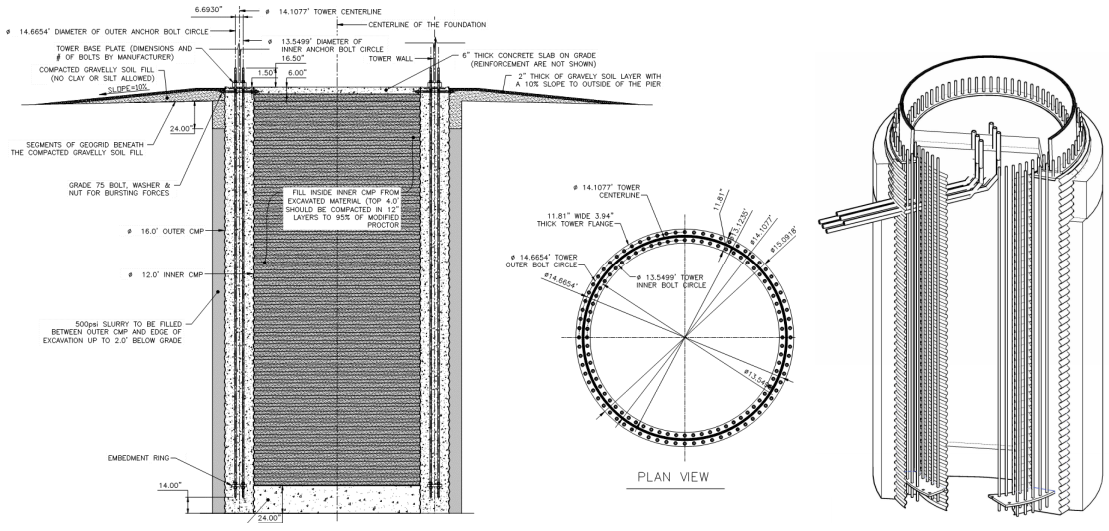


Fig. 2. Post tensioned single pier foundation components and construction pictures

Construction of the pier begins by excavating a hole slightly bigger than the outer diameter of the pier with an excavator or a drill. A crane is used to set the two CMPs concentrically within the hole. Sand-cement slurry is placed in the space between the outer CMP and the excavation sides. A 3-foot (0.9-meter) concrete plug is poured inside the inner CMP then the excavated spoils are placed within the central casing, thus reducing the volume of left-over spoils. Threaded steel bolts, encased in PVC sleeves, are arranged with a template that matches the base flange of the tower. The bolts are set vertically in the annular space between the two CMPs. Structural concrete is then placed between the two CMPs. The tower is bolted to the threaded rods above the concrete. After structural concrete set, the rods are post-tensioned to the design lock-off load to keep the concrete in compression during loading to ensure no tension stresses in the pier, which substantially increase the fatigue life time of the foundation.

DESIGN OF THE POST TENSIONED SINGLE PIER FOUNDATION

The design of post tensioned single pier includes two main components; geotechnical stability/stiffness and internal structural analysis of the pier. The single pier foundation needs to ensure adequate stability against extreme wind load with a sufficient safety factor. The foundation also needs to satisfy the serviceability requirements including lateral movement, rotational stiffness and horizontal stiffness specified by the turbine manufacture.

The design methodology of the single pier foundations utilizes a combination of national and international codes and standards. The stability of the single pier foundation is based on the principles of engineering statics, limit equilibrium at the fully plastic state and the principles of soil and rock mechanics. The geotechnical analysis is based on design manuals, text books and peer reviewed technical journal articles. The "Guidelines for Design of Wind Turbines" published by DNV and RisØ National Laboratory in Denmark also provides general design guidance (DNV and RisØ 2002). The moment capacity is the sum of the ultimate passive soil or rock reaction above and below a point of rotation. This point of rotation occurs when the sum of lateral forces is at equilibrium, usually determined by iteration (Davidson 1982). Figure three presents the applied forces and applied moments compared to the resisting lateral earth pressure, side and base friction on short rigid piers.

For granular materials, a modified method introduced by Broms (1964) may be used. The original Broms' method assumes that at the ultimate limit state, the pier rotates near the base and develops 3 times the Rankine passive pressure because of soil arching effects (Broms 1964). Hansbo (1995) calculates the ultimate lateral passive pressure of sand. The 3-D wedge effect and soil/pier friction is also considered. Broms originally developed the undrained lateral load analysis for cohesive soils for small diameter piles, but it may be implemented with modification to large piers. However, Broms simplified assumption to neglect the upper 1.5 times the diameters of the upper clay becomes extremely conservative for large diameter piers (Broms 1964). For the post tensioned single pier foundation, the modification proposed by Randolph and Houlsby (1984) should be considered for a fully rough face.

The vertical side shear provides additional moment capacity. A loss of contact opposite to loading is assumed. The lack of development of the ultimate lateral resistance near the point of rotation is considered. Additionally, there is a base resistance that is developed by shear and bearing.

The design of the tower considers the equivalent damage fatigue load based on a time spectral analysis of varying wind velocities. Foundation stiffness is evaluated to avoid resonance and excessive vibrations leading to premature fatigue of the tower. There are several analytical tools to evaluate dynamic stiffness including: Classical elastic half space (EHS) theory (DNV and RisØ 2002), finite difference methods based on the Beam of Elastic Foundation (BEF) method (Hetenyi 1946), and Finite Element Models (FEM).

The dynamic soil properties are derived for estimated average values of the soil or rock profile over the depth of the foundation. The maximum (low-strain) shear modulus (G_o) is the most relevant property for dynamic analyses. The maximum shear modulus is usually estimated from the shear wave velocity (V_s) or from soil empirical correlation with basic soil indices and field penetration resistance. The dynamic shear modulus is dependent on the cyclic shear strain amplitude. The reduction in the dynamic shear modulus comes from published empirical relationships of G/G_o versus shear strain (Ishibashi and Zhang 1993). The shear modulus will not be affected by fatigue if the amplitudes remain in the low shear strain range.

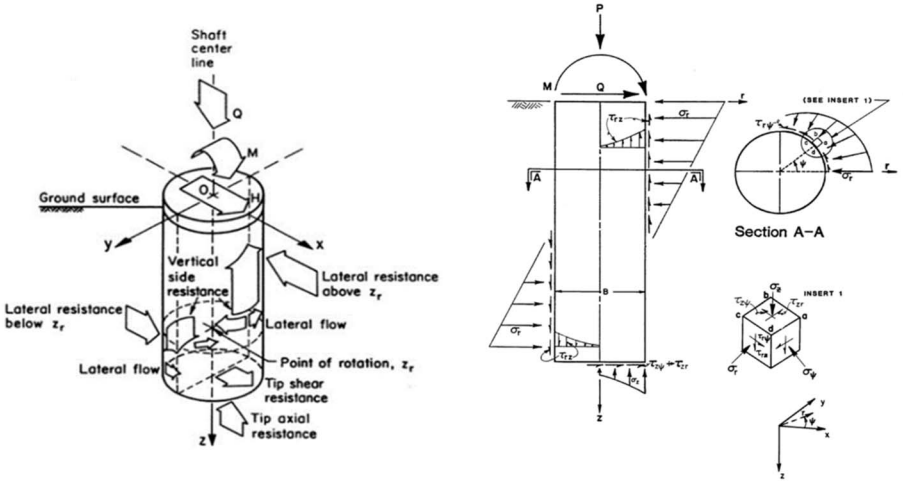


Fig. 3. Applied and resisting forces and moments on short rigid piers (adopted from Kulhawy and Chen 1995 and Davidson 1982)

Dynamic spring stiffness may be derived from the classical, closed form equations for an embedded rigid block within an elastic half space (EHS) theory. This method is used commonly for design of machine foundations and spread footings for wind turbines. The EHS method is generally applicable for footings that have a depth to width ratio of less than one. Embedment factors assume perfectly rigid foundations and are limited generally to an embedded length/diameter (L/D) ratio of 1. Despite this limitation, EHS method may be extended to the geometry of a single pier with some modifications since the embedment greatly increases the stiffness of the foundation. The dynamic spring stiffness values may be derived using published equations found in the Guidelines for Wind Turbines (DNV and RisØ 2002).
In the typical design, we follow: Serviceability Limit State (SLS) design which is based on normal wind loading events, Ultimate Limit State (ULS) design which is based on extreme wind loading events or seismic loads, whichever governs, and Fatigue Limit State (FLS) or Damage Equivalent Load (DEL).
Based upon the ACI 318, IEC 61400-1, and ASCE 7-10, three load cases are required to be considered in the design of the post tensioned single pier foundation: 1) Foundation Stability: overturning and bearing strength for the foundation under un-factored extreme wind loads, 2) Foundation Strength: strength of the foundation under factored extreme wind loads, and 3) Subgrade Strength: overturning and bearing strength for the foundation under un-factored operating wind loads. Details of design, analysis, results of the post tensioned single pier foundation are presented under the Case Histories section.

CASE HISTORIES

In this section, two case histories for post tensioned single pier wind turbine foundation designed using conventional geotechnical calculations and numerical modeling are presented. The first case is located in area with shallow rocks, while the second case is located area with rock deeper than the foundation base depth.

CASE 1

The wind turbine farm is located at Sweetwater, Texas. It consists of one hundred (100) wind turbine generators which were built in 2001 utilizing the post tensioned single pier with foundation depths of 18, 19, and 20 ft (5.5, 5.8, and 6.1 m) and excavation diameter ranged from 19 to 30 ft (5.8 to 9.1 m). Blasting was used to facilitate the foundation excavation. The thickness of overburden soil on top of the competent limestone ranged from 1 ft (0.3 m) to 4 ft (1.2 m). The hollow piers were constructed with 14 ft (4.3 m) outside diameter and 10 feet inside diameters. The typical design life of the wind turbine generators and their foundations are twenty years.
In 2017, it was decided to repower the whole site to extend the design life to another 20 years by replacing the existing turbines with more efficient turbines. In addition to repowering the existing foundation, it was also decided to construct seventeen (17) new turbines at the project site. A post tensioned single pier foundation 28 feet (8.5 m) deep and 16 ft (4.9 m) outside diameter and 12 ft (3.6 m) inside diameters was designed for the new turbines.
The selected pier foundation for this case history was analyzed for the applied loads provided by the turbine manufacturer. The selected turbine was the GE 1.7MW w/103m Rotor on a 79.7 meter Hub Height Tower. The provided wind loads are summarized in Table 1.

Table 1. GE 1.7MW wind turbine load.

GE 1.7MW Wind Turbine Load	Extreme Load Case	Operational Load case
Load Factor	1.1	1.0
Horizontal Load (F_{xy}), kip (kN)	149 (664)	74 (329)
Vertical Load (F_z), kip (kN)	517 (2298)	532 (2367)
Torsion Moment (M_z), kip-ft (kN-m)	-1320 (-1790)	-39 (-53)
Overturning Moment (M_{xy}), kip-ft (kN-m)	37117 (50324)	18144 (24600)

The serviceability criteria for this wind turbine generator was 36.9 x 10^6 kip-ft/rad (50 GN-m/rad) for the rotational (dynamic rocking) stiffness, 68.5 x 10^3 kip/ft (1 GN/m) horizontal (translation) stiffness, and 0.036 in/ft (3 mm/m, 0.17°) uneven settlement, which varies based on the turbine size and loads.
The typical subsoil layers, measured properties, and estimated properties for the selected location for the 28-feet-deep foundation is summarized in Table 2.

Table 2. Summary of the soil layers and properties

Material Description	Depth ft (m)	Unit Weight pcf (kN/m^3)	Cohesion psf (kN/m^2)	Friction Angle (deg)	Poisson's Ratio	Maximum shear modulus ksf (kN/m^2)
Top soil*	0 to 2 (0 to 0.6)	125 (19.6)	0	34	0.35	7500 (35.9 x 10^4)
Limestone	2 to 15 (0.6 to 4.6)	130 (20.4)	2000 (95.8)	38	0.3	27000 (12.9 x 10^5)
Limestone	15 (4.6) to BTD**	130 (20.4)	1000 (47.9)	40	0.25	30000 (14.4 x 10^6)
* Top soil consists of Silty Clayey, Sand Silty, Gravel with Sand, Clayey Sand, or Silty Sand ** BTD: Boring termination depth Groundwater was not encountered.						

As stated above in the design section, the foundation design includes foundation stability, foundation strength, and subgrade strength in which the geotechnical calculations, structural calculation, fatigue analysis, and finite element analysis are considered. In this case history, the emphasize will be on the finite element analysis and results.
The design team performed 3D Numerical Modeling utilizing Finite Element Analysis (FEA) for the geotechnical calculations of the post tensioned single pier foundation for this project. The 3D FEA code "midas GTS NX" by midaSoft was utilized in the analysis and evaluation for this single pier foundation. The purpose of the FEA of the geotechnical aspects of the single pier foundation is to i) Estimate the rotational (rocking) stiffness of the pier foundation, ii) Estimate the total, vertical, and horizontal movements; iii) Estimate the lateral spring stiffness (translation stiffness), and iv) Estimate the stresses and strains in the pier and foundation soils and ensure there is no tension in the pier shaft.
The post tensioned single pier was modeled as 3D solid elastic structural element, while soil and rock were modeled as 3D solid using the elastic perfectly plastic Mohr Coulomb model. Five inputs are used to define the Mohr Coulomb model. Modulus of elasticity and Poisson's ratio for elasticity and stiffness. Cohesion and angle of friction for plasticity and dilatancy angle for dilatancy. It is a first-order approximation model with a constant average stiffness.

Drained condition was selected for the soil models to represent the long term behavior of the foundation. In addition, the groundwater table was below the foundation base. The modeling was accomplished in three stages which are self-weight stage, structural installation and post tension stage, and loading stage. In the self-weight stage, all soil layers were defined and activated as soils with self-weight and boundary conditions to represent field conditions prior to the excavation. Displacements are cleared at the end of this stage. The structural installation and post tension stage includes activating the foundation component to its corresponding materials (concrete and steel) and the application of the post tension forces. This stage represents the period prior to the full operation of the wind turbine. The final stage includes applying operational wind loads and calculating the corresponding stresses, strains and displacements. Since the movement of the foundation is very small, no large displacement, separation or gaping is expected. Therefore, adding interface elements to simulate the soil-structure interaction is not crucial and should not affect the accuracy of the model.

In general, the post tensioning was taken into considerations by applying two equal and opposite vertical pressures on the top and bottom of the pier, respectively as shown in Fig. 4. Given the thickness of the pier (24 in, 610 mm) and the tower flange (about 12 in or 300 mm), and assuming the stress distribution in the pier follows a 1:1 slope, the post tension stress should be uniform across the pier thickness in about 8 inches into the pier. Figure 4 demonstrates the 3-D mesh sets for the single pier foundation and soil layers.

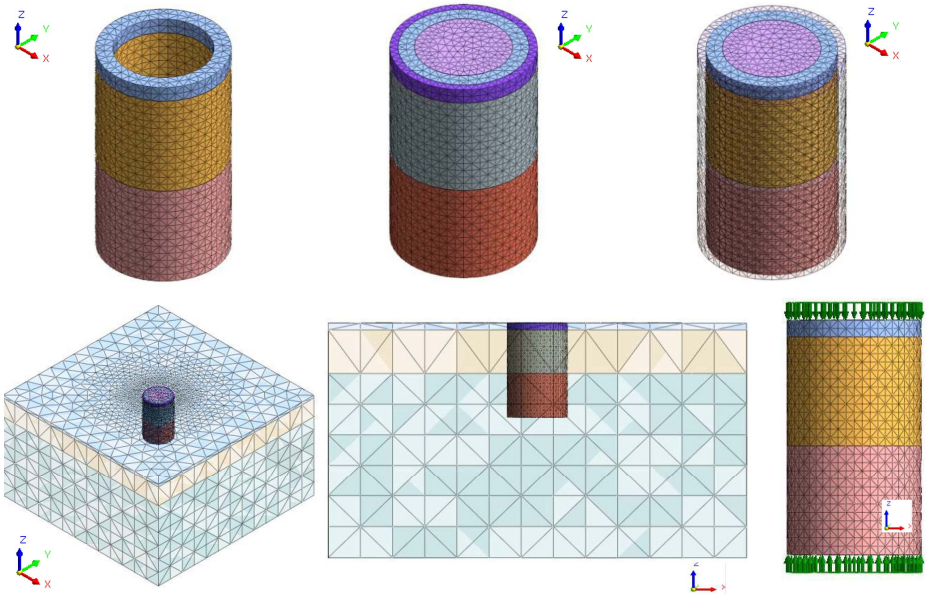


Fig. 4. 3-D mesh sets for post tensioned single pier foundation, soil layers, and post-tension applied pressure

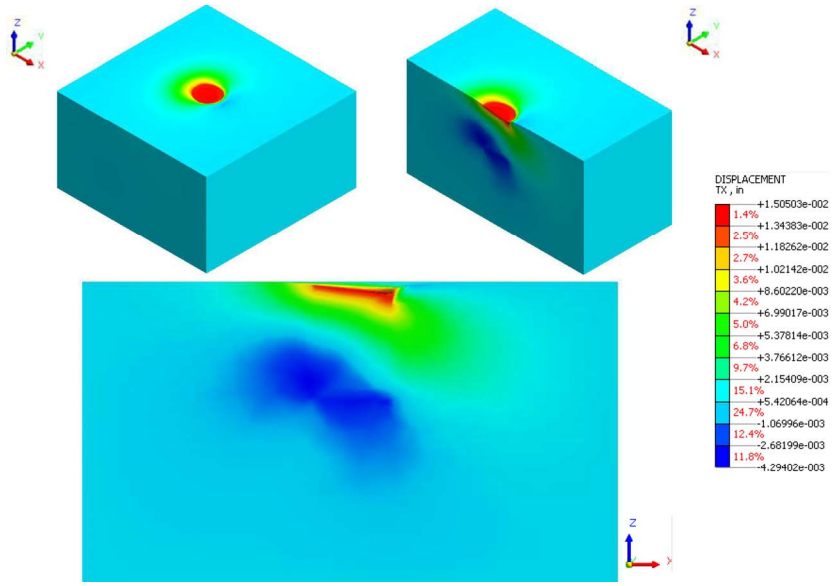
The post tensioning pressures were applied after the self-weight of the model was applied. Settlements resulted from the post tensioning were eliminated before applying the load cases. Per the construction plan and specification, if 10% of the anchor blots have relaxed more than 10%, then all bolts shall be re-tensioned back to 100%. This post-tension maintenance of the anchor shall be performed annually. In order to consider the potential 10% post-tension loss in the anchor bolts, the FEM was only modeled with 90% of the post-tension force. Table 3 summarizes the results of the 28 ft (8.5 m) single pier foundation design calculations using both the conventional geotechnical method and the finite element analysis.

Table 3. Results of the FE model and the conventional geotechnical calculations.

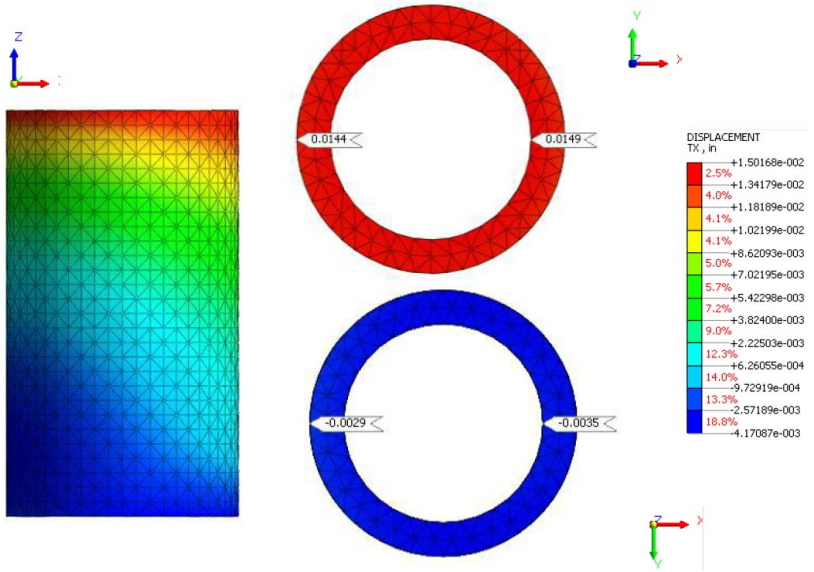
Analysis Method	Loading	Rotational Stiffness ft-kip/rad (GN-m/rad) at Pier Top	Maximum Lateral Movement in (mm) at Pier Top	Unenven Settlement (deg)	Translation Stiffness kip/ft (GN/m) at Pier Top	Overturning Safety Factor *	Axial Safety Factor*
3D Finite Element Analysis	Operation Load	11.6×10^7 (158)	0.02 (0.4)	0.0002	74×10^4 (10.8)	Not required	Not required
	Extreme Load	11.1×10^7 (151)	0.03 (0.8)	0.0003	80.9×10^4 (11.8)	-	-
Conventional Geotechnical Calculations	Operation Load	18.1×10^7 (246)	0.02 (0.6)	0.006	12.3×10^5 (18)	Not required	Not required
	Extreme Load	Not required	0.05 (1.3)	0.01	Not required	4.0	7.7
* FEM was not utilized to evaluate the ultimate geotechnical capacity, instead the conventional geotechnical was used.							

The results show that the FE model better represent the behavior of the single pier foundation. It should be noted that the conventional geotechnical calculations of the rotational and translation stiffness derived from the classical, closed form equations for an embedded rigid block within an elastic half space (EHS) theory with some modifications to be applicable to the pier geometry.

Figure. 5 (a and b) shows the horizontal displacement in the model and the pier in the direction of the highest moment (M_{xy}) and highest horizontal (shear) force (F_{xy}) under the operational load case (serviceability case). All of the displacement values were within tolerable limits.



(a) Horizontal displacement in the whole model and cross-section of the model



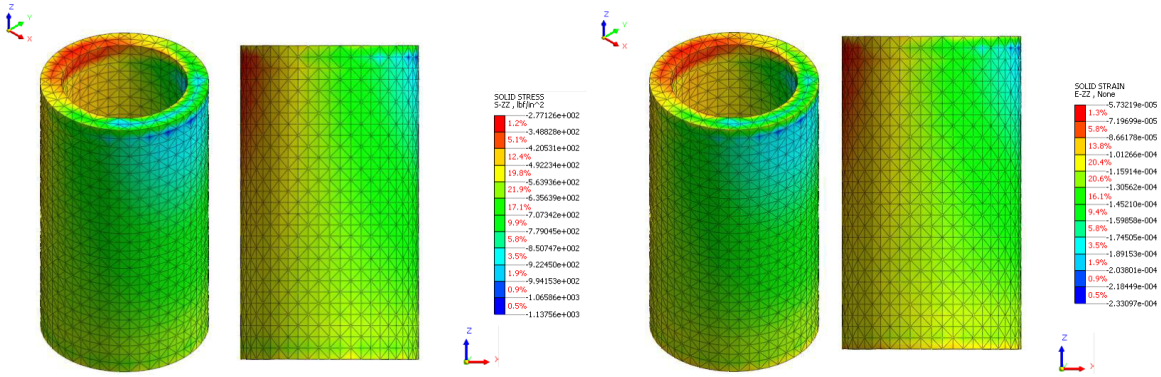
(b) Horizontal displacement (Top and Bottom) of the pier

Fig. 5. The horizontal displacement in the model

Vertical stresses and vertical strains, as shown in Fig. 6, were within the required design criteria. In addition, no tensile stresses were captured in the model which confirmed post tension was enough to maintain a tensionless pier.

The geotechnical design calculations and FEA demonstrated that the post tensioned single pier foundation has an adequate overturning stability against extreme load with factor of safety in excess of 2 and a rotational stiffness greater than the turbine manufacture specified requirement of 36.9 x 10^6 kip-ft/rad (50 GN-m/rad).

The structural design analysis for the reinforced concrete pier and the anchor bolts are performed using spreadsheets that utilize traditional design methods of the American Concrete Institute (ACI). Also, the fatigue analysis was performed using Eurocode 3 to check the steel bolts and using CEB-FIB Model Codes 2010 to check the concrete and grout in the single pier structure for the design life time of 20 years. The results of the cumulative damage index were ranging from 0 to 0.021 for the steel bolts, concrete, and grout compared to the critical cumulative damage index of 1. The structural calculations showed that the accomplished foundation design in 2017 has adequate strength to withstand design loads and meets serviceability requirements.



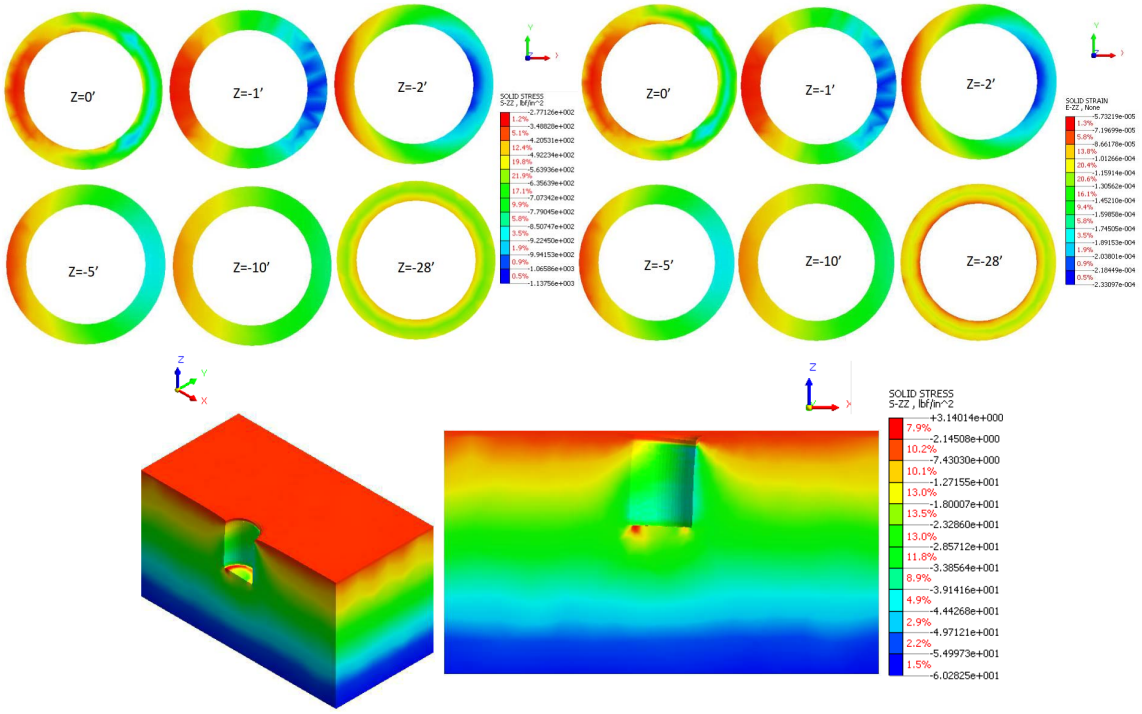


Fig. 6. The vertical stress and vertical strain of the post tensioned single pier

CASE 2

This second case for a wind farm located at Cochran County, Texas. It consists of sixty-seven (67) wind turbine generators. It was constructed in the last quarter of 2018. The selected foundation was the post tensioned single pier with foundation lengths of 30 and 32 ft (9.1 and 9.8 m) and excavation diameter of 18 ft (5.5 m). Similar to the first case history, the hollow piers were constructed with 16 ft (4.9 m) outside diameter and 12 ft (3.7 m) inside diameters. The typical design life of the wind turbine generators and their foundations are twenty years.

The selected pier foundation for the case history (32- foot (9.8 m) deep foundation) is analyzed for the applied loads of a GE 2.3 MW W/ 116M Rotor, 90 meter Hub Height Tower. These loads are higher than Case 1. The wind loads are summarized in Table 4.

Table 4. GE 2.3MW wind turbine load

GE 2.3 MW Wind Turbine Load	Extreme Load Case	Operational Load case
Load Factor	1.1	1.0
Horizontal Load (F_{xy}), kip (kN)	152 (676)	92 (411)
Vertical Load (F_z), kip (kN)	598 (2660)	609 (2709)
Torsion Moment (M_z), kip-ft (kN-m)	-1771 (-2401)	-673 (912)
Overturning Moment (M_{xy}), kip-ft (kN-m)	41614 (56422)	26167 (35478)

Also, the serviceability criteria for this GE 2.3 MW is 36.9 x 10^6 kip-ft/rad (50 GN-m/rad) for the rotational stiffness, 68.5 x 10^3 kip/ft (1 GN/m) horizontal stiffness, and 0.036 in/ft (3 mm/m, 0.17°) uneven settlement. The established subsoil conditions based on the geotechnical investigation report for 32- foot (9.8 m) deep foundation is summarized in Table 5.

Table 5. Summary of the soil layers and properties

Material Description	Depth ft (m)	Unit Weight pcf (kN/m^3)	Cohesion psf (kN/m^2)	Friction Angle (deg)	Poisson's Ratio	Maximum shear modulus ksf (kN/m^2)
Clayey sand	0 to 12 (0 to 3.7)	110 (17.3)	240 (11.5)	29	0.35	705 (33.8×10^3)
Silty sand	12 to 24 (3.7 to 7.3)	110 (17.3)	240 (11.5)	29	0.35	3,134 (15×10^4)
Clayey sand	24 to 32 (7.3 to 9.8)	120 (18.9)	180 (8.6)	31	0.35	4,407 (21.1×10^4)
Groundwater was not encountered.						

Similar to case 1, the case 2 analysis was established and the results are summarized in Table 6. All of the results were within the allowed design criteria

Table 6. Results of the FE model and the conventional geotechnical calculations.

Analysis Method	Loading	Rotational Stiffness kip-ft/rad (GN-m/rad) at Pier Top	Maximum Lateral Movement in (mm) at Pier Top	Unenven Settlement (degree)	Translation Stiffness kip/ft (GN/m) at Pier Top	Overturning Safety Factor*	Axial Safety Factor*
3D Finite Element Analysis	Operation Load	42,778,605 (58)	0.13 (3.3)	0.036	11×10^4 (1.6)	Not required	Not required
	Extreme Load	Not required	0.28 (7.0)	0.072	Not required	-	-
Conventional Geotechnical Calculations	Operation Load	39,828,356 (54)	0.2 (5.1)	0.039	27.4×10^4 (4)	Not required	Not required
	Extreme Load	Not required	0.32 (8.1)	0.061	Not required	1.9	5.3
* FEM was not utilized to evaluate the ultimate geotechnical capacity, instead the conventional geotechnical was used.							

CONCLUSION

Due to the high demand for renewable energy, wind turbine generators are getting larger year after year to ensure the economic viability of wind projects. This demand leads to the design of more economical and durable structures to withstand the massive loads imposed by large WTGs. Geotechnically, deep foundations such as the post tensioned single pier or any pile cap system provide better overall stability for higher lateral and moments when compared to shallow Gravity Spread Foundation (GSF). Structurally, the increase in reinforcement is substantial in a spread foundation when compared to post tensioned single pier or to the pile cap foundation for larger turbines.

The fatigue resistance is also a distinct advantage of post tensioned single pier foundation when compared to GSF, which allows repowering of existing foundations to extend power generation for double the design life.

Numerical analysis is utilized to optimize the design of the post tensioned single pier wind turbine foundations. Different boundary conditions, various load staging, and scenarios with adding the effect of the soil-structure interaction is modeled. The numerical modelling provided an optimized foundation and better evaluation of the stress-strain behavior of the foundation component. Based on overall design of the post tensioned single pier and the case histories, the results show that the finite element model was able to capture the behavior of the foundation. The tensionless pier is not covered in literature and is a unique innovative wind turbine foundation.

REFERENCES

American Concrete Institute, 2014. Building Code Requirements for Structural Concrete (ACI 318-14): Commentary on Building Code Requirements for Structural Concrete (ACI 318R-14): an ACI Report. American Concrete Institute. ACI.

American Society of Civil Engineers, 2013. Minimum Design Loads for Buildings and Other Structures, Standard ASCE/SEI 7-10.

Broms, B. B., 1964a. Lateral Resistance of Piles in Cohesionless Soils. Journal of the Soils Mechanics and Foundation Division, ASCE, Vol. 90, No. (SM2).

Broms, B. B., 1964b. Lateral Resistance of Piles in Cohesionless Soils. Journal of the Soils Mechanics and Foundation Division, ASCE, Vol. 90, No. (SM3).

Davidson, H. L, 1982. Laterally loaded drilled pier research, Vol 1: Design methodology, Vol. 2: Research documentation. Final Report by GAI Consultants Inc., to Electric Power Research Institute (EPRI).

Det Norske Veritas (DNV) and RisØ National Laboratory, 2002. Guidelines for Design of Wind Turbines. 2nd Edition, Copenhagen, Denmark.

Hansbo, S., 1995. Ultimate Resistance of Laterally Loaded Piles. Proceedings: Bengt Broms Symposium in Geotechnical Engineering, Singapore, 165-170.

Hetenyi, M., 1946. Beams on Elastic Foundations. The University of Michigan press, Ann Arbor.

IEC 61400-1 (International Electrotechnical Commission, International Standard,). (2005) Wind Turbine Generator Systems, Part 1: Safety Requirements. Third Edition, Geneva 20, Switzerland.

Ishibashi, I. and Zhang, X., 1993. Unified dynamic shear moduli and damping ratios of sand and clay. Soils and foundations, 33(1), 182-191.

Kulhawy F. and Chen, Y, 1995. A Thirty Year Perspective of Broms. Lateral Loading Models, as Applied to Drilled Shafts, Proceedings Bengt Broms Symposium in Geotechnical Engineering, Singapore, 225-240.

Randolph, M.F. and Houlsby, G.T., 1984. The limiting pressure on a circular pile loaded laterally in cohesive soil. Geotechnique 34 (4), 613–623.

SUSTAINABILITY ASSESSMENT OF DEEP FOUNDATIONS: CASE STUDY

Girish Kumar[1], Jyoti K. Chetri[2], and Krishna R. Reddy[3*]

[1]Graduate Research Assistant, University of Illinois at Chicago, Department of Civil and Materials Engineering, 842 West Taylor Street, Chicago, IL 60607; e-mail: gkumar6@uic.edu
[2]Graduate Research Assistant, University of Illinois at Chicago, Department of Civil and Materials Engineering, 842 West Taylor Street, Chicago, IL 60607; e-mail: jkc4@uic.edu
[3]Professor, University of Illinois at Chicago, Department of Civil and Materials Engineering, 842 West Taylor Street, Chicago, IL 60607; e-mail: kreddy@uic.edu (*corresponding and presenting author)

ABSTRACT

Geotechnical engineering encompasses a major portion of the civil and infrastructure projects. The large amounts of energy and resources typically used in these projects leads to undesirable emissions and wastes which contribute substantially towards global environmental impacts (e.g., global climate change). This could further include secondary economic and societal issues which are often unaccounted in traditional engineering design of the geotechnical projects. In order to address this issue, it is imperative to integrate the broader environmental, economic and social implications into decisions of a geotechnical project. Recent years have seen a major impetus on life cycle assessment to evaluate the environmental sustainability of the geotechnical designs. However, there are no tools that can quantify the life cycle triple bottom line sustainability of potential design alternatives in a project with holistic considerations towards broader economic (indirect costs and benefits) and social impacts (stakeholder preferences, socio-environmental and socio-economic impacts). This study presents a new framework for quantitative assessment of life-cycle sustainability (QUALICS) for alternative designs in engineering projects. The framework integrates two multi-criteria decision analysis methods namely, the Integrated Value Model for Sustainable Assessment (MIVES) and Analytic Hierarchy Process (AHP), to support decision making on the potential design alternatives. In this study, a brief overview of the framework is presented. A case study demonstrating the use of QUALICS framework is discussed with its application to the sustainability assessment of two deep foundation systems, caissons and piles, over their design life. The technical designs of both systems are developed based on bearing capacity, both primary and secondary settlements, and structural integrity. The results from the sustainability assessment of the two deep foundation systems are discussed, and the most sustainable option based on different stakeholder preferences and site-specific conditions are identified.

Keywords: caissons, carbon footprint, life cycle assessment, multi-criteria decision analysis, pile foundations, sustainability, triple bottom line

© 2019 Deep Foundations Institute

INTRODUCTION

Geotechnical engineering involves projects that make extensive use of the earth and its resources. In the light of ever-growing global population and rapid urbanization, there has been a significant growth in the need for construction of high-rise buildings. In this regard, the design and construction of deep foundations has become inevitable due to poor subsoil conditions and the large loads that needs to be supported from the super structure. In the current practice, the pile foundations and drilled shafts (also referred as caissons) are the two most common alternatives for deep foundation systems. However, the choice of either of the systems is solely based on the preference, construction cost, ease of design and implementation, and construction time with no regard to broader environmental, economic and social impacts across the design life of the deep foundation system installed. The different stages involved in the design and implementation of the deep foundations involve several activities that have substantial impacts on the environment (e.g., greenhouse gas emissions and waste water), economics (e.g., costs from materials, labor, and equipment), and the society (e.g., quality of life of residents) which are often unaccounted.

In recent years, there is a major impetus on taking conscious decisions and incorporating sustainable designs at the project scale to contribute towards global sustainable development. Several studies in the literature have used qualitative and quantitative tools to assess the environmental sustainability of design alternatives in different geotechnical engineering projects to recommend the option that is technically sound and yet environmentally friendly for construction (Reddy et al. 2018; Reddy et al. 2019). However, a sustainable design must ensure environmental care, economic feasibility, and societal well-being across the entire design life of the system. Moreover, the sustainability of the design alternatives must be quantifiable for a rational and appropriate decision on the choice of the design alternative that can be implemented in a project.

In this study, a new quantitative tool/framework named quantitative assessment of life cycle sustainability (QUALICS) developed by Trentin et al. (2019) was used for sustainability assessment of pile foundations and drilled shafts for a deep foundation construction project and provide decision support on the choice of the most sustainable deep foundation system for the specific site conditions assessed. The framework integrates two multi-criteria decision analysis methods namely, the Integrated Value Model for Sustainable Assessment (MIVES) and Analytic Hierarchy Process (AHP) to support decision making on the design alternatives in a project. A brief overview of the QUALICS framework is presented. Finally, a case study involving the application of QUALICS to a deep foundation construction project is discussed to demonstrate the applicability of the framework to geotechnical engineering projects.

METHODOLOGY

Project site description

The project site is located in the city of Chicago in Illinois, USA. The generalized subsurface soil profile at the site is shown in Fig. 1. The functional unit for the sustainability assessment of the two deep foundation systems was assumed to be five columns with each column carrying a load

of 4448 kN (~1000 kips). Thus, the assessment compared the design and construction of five pile groups (i.e., 5×14=70 steel piles) and five caissons to support the five columns. The depth of both foundation systems required was 16.8 m (~55 ft.), which is the depth at which the base of the foundation was sufficiently within the hard clay. Further, the settlement limit was established at 0.0254 m (1 in.).

The geotechnical engineering properties of soil layers including the shear strength (angle of internal friction (ϕ) for sands, and undrained shear strength (c) of clays), and the unit weight of the soil layers (γ) required for the technical design of the pile groups and caissons were determined based on the available site boring logs and laboratory/field testing (see Fig. 1). Using these properties and the principles for design of pile foundations and caissons, the pile group and caisson designs were finalized. A detailed description of the technical design is provided in the following section.

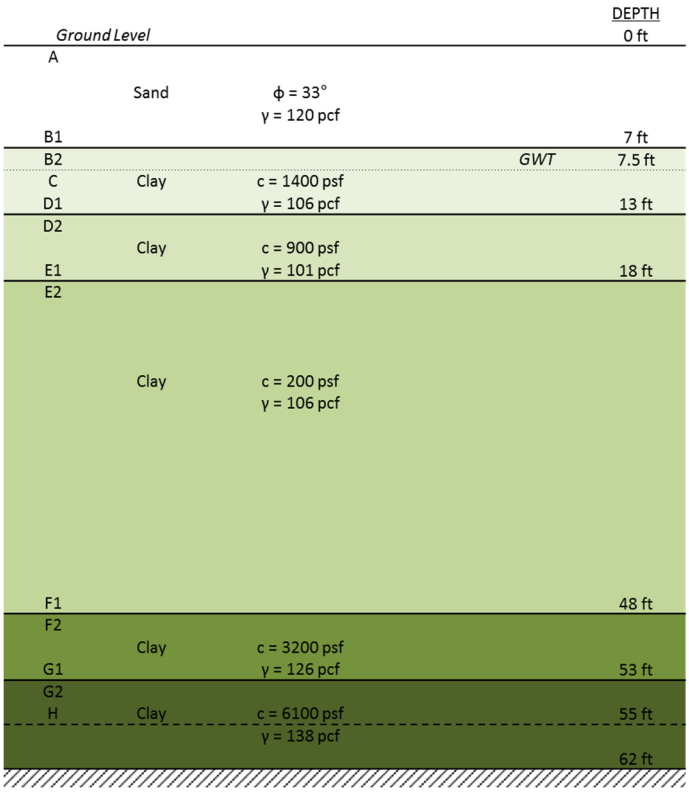


Fig.1 Subsurface soil profile considered for the technical design

Technical design

Technical design of the pile foundations and caissons were carried out based on load transfer mechanism by evaluating side frictional resistance and end bearing capacity. Suitable assumptions were made in order to normalize the comparison between the two foundation systems. The factor of safety for both structures was given a value of three. A dead load of 600 kips and a live load of 400 kips were assumed on each column for both the alternatives. Further, it was assumed that the loading is purely concentric (zero eccentricity) meaning that there will be no moment induced by the load on the column.

The total capacity of piles and the caisson was as a result of skin friction and the toe bearing resistance. Since both foundations are considered to be the same depth, the size was a key factor for the resistance. A detailed step by step procedure of the calculation of the foundation skin friction and toe bearing resistance for both alternatives was used based on Coduto (2001). The final design of each pile foundation was a group of fourteen pipe piles with an outside diameter of 0.51 m (20 in.) and a wall thickness of 0.009525 m (0.375 in.). The caisson's final design was a 1 m (3 ft.) diameter shaft with a 1.22 m (4 ft.) high bell with an 8 ft. diameter at the bottom (i.e., at 55 ft. depth). Both the pile group and the caisson had a length of 16.76 m (55 ft.). A total capacity of 4626 kN (1040 kips) and 4537 kN (1020 kips), respectively, was obtained for pile groups and the caisson systems designed. In addition, both foundation alternatives resulted in settlements below one inch and were therefore considered satisfactory. A pile cap made of reinforced concrete with nominal reinforcement was provided for the pile groups.

Once the technical design proved to be satisfactory, calculations to determine the amount of materials required for construction of five pile groups and five caissons were performed (see Table 1). The equipment needed for the construction of the foundations and their fuel consumption rates are provided in Table 2. The data presented in Table 2 is obtained based on the common industry practice.

Table 1: Material quantities required for construction of five pile groups and five caissons as per the design

	Five pipe pile groups			**Five caissons**	
Materials	Steel	Concrete	Rebar	Concrete	Rebar
Quantity	280,995 lbs.	4,500 ft^3	18,000 lbs.	2,430 ft^3	5,000 lbs.

Note: Pipe pile weight/foot length = 78.6 lbs/ft.

Table 2: Equipment needed and their fuel consumption rates

Piles			**Caisson**		
Equipment	**Fuel (Diesel) consumption rate (gal/hr)**	**Total operation duration (hrs)**	**Equipment**	**Fuel (Diesel) Consumption (gal/hr)**	**Total operation duration (hrs)**
100T Crawler Crane	34	40	Drill Rig (150,000)	20	10
400-600 CFM Air Compressor	17	40			
924 Loader with Forks	8.5	40	Crawler Crane (100T)	17	10
Air Hammer	NA	40			
Welders	1.25	80	Track Loader	8.5	10
Box Leads	NA	40			

Sustainability assessment framework

The sustainability assessment of the two alternative deep foundation systems involved the quantitative assessment of environmental, economic and social sustainability using the QUALICS framework. The QUALICS framework entails evaluating the environmental sustainability by performing life cycle assessment (LCA) using the standard procedure established by International Organization for Standardization (ISO 14040; ISO 14044). The life

cycle inventory analysis was performed using SimaPro v8.5 developed by PRé Consultants. The US life cycle inventory (LCI) database available in SimaPro v8.5 was used for the materials used in the construction. The Tool for the Reduction and Assessment of Chemical and other environmental Impacts (TRACI), a midpoint life cycle impact assessment (LCIA) method developed by USEPA was used for the environmental impact analysis and to evaluate the environmental sustainability.

The economic sustainability was assessed by evaluating the direct costs (e.g. cost of materials, equipment and machinery, labor and fuel) and indirect costs (e.g. social cost of carbon) associated with the design and implementation of the foundation system. The indirect costs were essentially based on an estimate of the monetized damages caused by an incremental increase in the carbon dioxide (CO_2) emissions in a given year (Raymond et al. 2017; USEPA, 2017).

Social sustainability is a subjective field which makes it difficult to quantify the social impacts of any activity. However, a few semi-quantitative approaches such as Social Sustainability Evaluation Matrix (SSEM) have been developed to quantify the social impacts of an activity in a project (Reddy et al. 2014). In this study, based on adaptation of SSEM approach the functional and social impacts of each deep foundation system were assessed by conducting an online survey among professionals and academicians familiar with the two foundation systems. Questions for the survey were structured to evaluate the social impact of each of the deep foundation alternative on aspects at the functional, individual, community, economic and environmental category. Each category consisted of project specific indicators which serve as the metrics to evaluate the social impacts under that category level. The survey results were analyzed and scores ranging from 1 – 4 (1 representing the best, preferred, or most positive impact case and 4 representing the worst, least preferred, or least positive impact case) were assigned to each indicator under each category. The survey was performed using a Google survey with the indicators as shown in Table 3.

Table 3: List of indicators used to assess social sustainability

Category	Indicator description
Functional Indicators	Relative level of advancement in design methodology
	Relative ease of design (e.g. specialty designs)
	Relative ease of construction (e.g. equipment, skilled field labor, no. of skilled field personnel, specialty construction technique)
	Relative duration of construction
	Relative ease of performance testing (e.g. load testing)
	Relative flexibility to change design during construction for changed site conditions
Socio-Individual (workers, residents)	Relative level of noise during construction
	Relative level of vibrations during construction
	Relative exposure to dust (if applicable)
	Relative risk of accidents (safety during construction)
	Relative opportunities for skill development
Socio-Community	Relative traffic congestion during construction
	Relative involvement of community or community organizations in the project
Socio-Economical	Relative use of local materials (e.g. available within approximately 30 mile radius)
	Relative impact on the local economy (e.g. employment opportunities, material supply/manufacturing)
	Relative impact on project cost
	Relative potential for reuse/recycle of the foundation system/materials at the end of project

	life cycle
Socio-Environmental	Relative impact on surrounding local water resources (e.g. groundwater, surface water)
	Relative air emissions (air pollutants, GHG) during construction
	Relative use of renewable/alternative resources (e.g. energy, materials)

Finally, the sustainability index was calculated for each design alternative following the Spanish Integrated Value Model for Sustainability Assessment (MIVES) methodology as explained in Reddy and Kumar (2019) and Trentin et al. (2019). The MIVES methodology assists with normalizing the scores obtained from the environmental, economic and social impact analysis in the range of 0 to 1 making the comparison between the indicators with different metrics possible. In this methodology, the overall sustainability of a design alternative is a function of the weightages assigned to each of the indicators, the criteria under which the indicators categorize into, and the three pillars of sustainability. The overall sustainability of a design alternative can then be assessed by evaluating the sustainability index on a scale of 0 to 1. The sustainability index is evaluated by performing the value function analysis. This method involves establishing representative value functions which convert all the quantitative and qualitative variables (environmental, economic or social indicators/metrics) into a set of variables with same units. Each indicator is assigned a weightage (in terms of percentage) depending upon the preference of the stakeholder.

The AHP process is employed into the QUALICS framework to determine weights for each indicator/criterion/requirement (Saaty, 2008). However, in this study, the weightage was distributed equally among different indicators. The value function obtained for each indicator (e.g., greenhouse gas emissions, NO_x, SO_x) ($V_{indicator}$) is multiplied by the respective weightage ($W_{indicator}$) assigned to the indicator. Each of the indicator can be grouped into a criterion (e.g., air pollution, water pollution, land contamination). The sum of the products of the $V_{indicator}$ and $W_{indicator}$ of the indicators given under a criterion becomes the value of the criterion ($V_{criterion}$). Further, the sum of the product of value obtained for criterion and their corresponding weightages ($W_{criterion}$) gives the value for each sustainability requirement level (e.g., environmental, economic and social) ($V_{requirement}$). The final value (V_{final}) for each sustainability pillar is obtained by the product of $V_{requirement}$ and its corresponding weightage ($W_{requirement}$) assigned to each of the requirement. The sum of the V_{final} values of the environmental, economic and social pillars give the final sustainability index for a design alternative. The same procedure can be followed for each design alternative to arrive at their respective sustainability indices. The most sustainable option among the different design alternatives can be assessed by comparing the individual sustainability indices obtained for each design alternative.

RESULTS AND DISCUSSION

Environmental sustainability

Fig. 2 shows the relative environmental impacts associated with the construction of five pile groups and five caissons for the same load carrying capacity. The environmental impacts are evaluated across the different life cycle stages of the foundation construction including the raw material acquisition, manufacturing of the materials, transportation till the end of construction. The use and end-of-life phases were not considered in the environmental impact assessment performed in LCA. The environmental impacts across the various impact categories of the

TRACI LCIA in Fig. 2 shows that the pile foundations have far more negative environmental impacts than the caissons. For the purpose of comparison, the carbon footprint is also assessed using a well-known carbon footprint calculator for deep foundation techniques and projects, the EFFC-DFI Carbon Calculator Tool v2.3 (2014), which showed nearly 300 tons and 38 tons of CO_2 eq. emissions for pile foundation and caissons, respectively. These values were found to be reasonably close to the CO_2 eq. emissions estimated from TRACI LCIA which was nearly 321 tons and 33 tons of CO_2 eq. for pile foundations and caissons, respectively. The high CO_2 emissions for piles primarily stems from the extensive use of steel in the pile foundations which involved fourteen steel pipe piles in each pile group resulting in significant carbon footprint associated with pile foundation design.

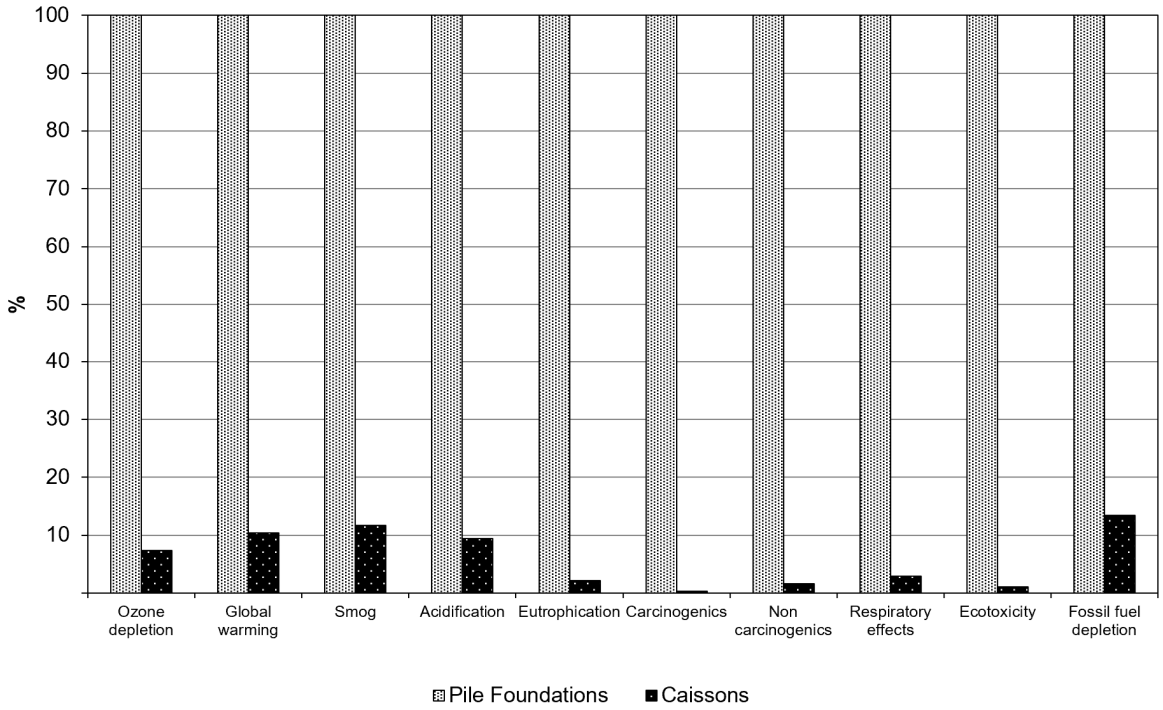


Fig. 2: Relative environmental impact of piles and caissons from the LCA

Further, steel making is a highly energy and resource intensive process along with generation of significant amounts of emissions. Although, caissons involve the use of concrete and cement, which are as well derived from energy intensive processes, the amount of material needed for constructing five caissons was significantly less, thus reducing its net negative environmental impacts when compared to pile foundations. Most of the negative environmental impacts were due to the steel in the case of pile foundations and cement in the case of caissons. In addition, the diesel used in operating the machinery and equipment during the construction also contributed substantially to the environmental impacts of both pile foundations and caissons.

Economic sustainability

The economic sustainability assessment comprised of evaluating the direct costs (due to materials, labor, equipment and fuel and lube) and the indirect costs associated to the damage caused by the broader environmental impacts (e.g. social cost of CO_2 emissions from production

of steel, cement and concrete). The materials and equipment transportation/mobilization was included in the materials and equipment costs, respectively. Fig. 3 shows the direct costs, under each category, and the social cost of carbon for both the pile foundations and caissons. The cost of construction of five pile foundations in each category and consequently the total cost was invariably higher than the cost of construction of five caissons. The material costs dictated the total cost of construction which was mainly driven by the high amount of steel used in pile foundations. Consequently, the amount of greenhouse gas emissions was also significantly higher for the pile foundations when compared to caissons and thereby the indirect costs. The social cost of carbon was considered as the indirect cost in terms of dollars per metric tons of CO_2 emission as per USEPA (2017). In all the categories of costs (direct and indirect), pile foundation was found to have higher negative economic impact.

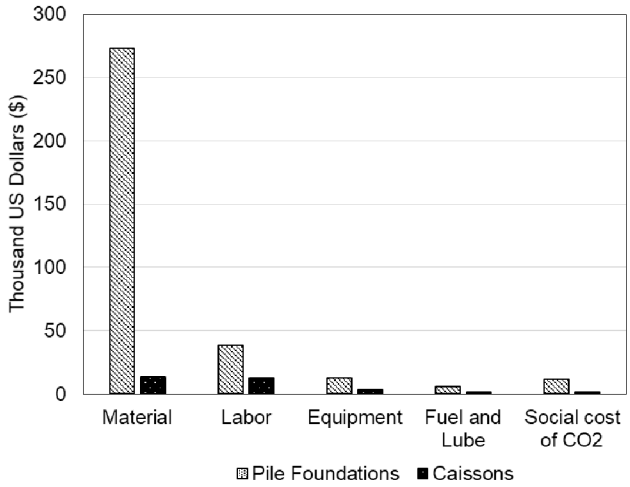


Fig. 3: Direct costs and indirect costs comparison associated with the two foundation systems

Social sustainability

Social sustainability of the two foundation systems was assessed based on the scores obtained from the Google survey. A total of seven responses were received for the survey which was largely from contractors/designers with more than 10 years of experience. Each indicator was scored in a range of 1 to 4 (1 being the best and 4 being the worst) by the respondents. The scores received by each foundation system under each indicator category was summed to arrive at a total score which quantifies the social sustainability of each foundation system as shown in Fig. 4. The caisson system received lower score which means it is more sustainable socially in comparison to the pile foundation system. Since the scores obtained by the foundation systems is dependent on the opinions and choice of the stakeholders or experts, the final outcome may vary with the increase in the number of the diverse respondents.

Overall sustainability

The overall sustainability assessment comprised of integration of environmental, economic and social sustainability by implementing QUALICS framework. The sustainability index value indicates the overall sustainability of the foundation system. Fig. 5 shows the sustainability index obtained by each foundation system when equal weightage was given to environmental,

economic and social aspects. Sustainability index of caisson is 0.83 and pile is 0.15, which means caisson is 5.5 times more sustainable than the piles system. Similarly, caisson received highest sustainability index under each category: environmental, economic and social (Fig. 5). It clearly shows that the caisson is more sustainable than the piles system.

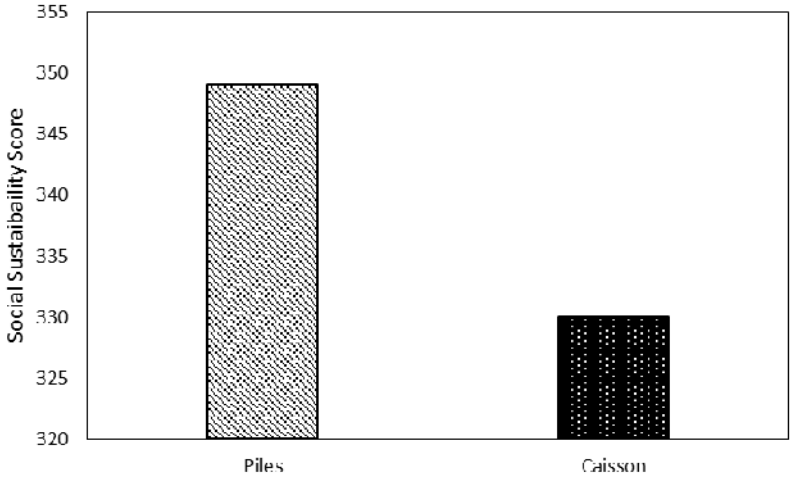


Fig. 4: Scores obtained by foundation systems in social sustainability assessment survey
Note: Lower score = more sustainable

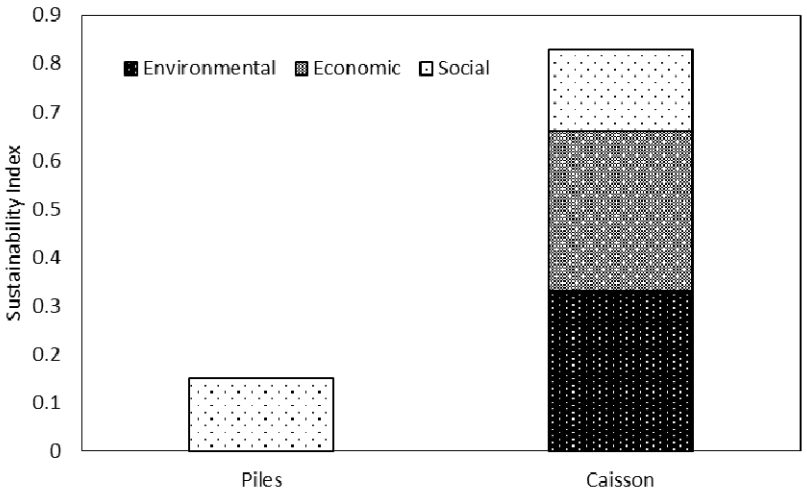


Fig. 5: Overall sustainability assessment of the foundation systems

FINAL REMARKS

The sustainability assessment performed in this study was limited in size and scope and the conclusions are relevant only in the context of the inherent biases for the case study project. The outcome may be different in different cases such as the drilled shaft appeared to be more sustainable system in the current case and geologic conditions examined in this study; however, in a scenario where the loads are lighter and the soils are of a poorer quality, drilling may be prohibitive and it is very possible a different outcome could be realized. Nevertheless, the

methodology could be applied to any project or site to evaluate sustainability of the proposed foundation systems as well as facilitate the decision making process. The triple bottom line sustainability assessment takes into account the environmental and social impacts apart from economic impacts which are otherwise not considered in the design and construction industry in general.

Overall sustainability assessment is dependent on the weightages assigned to the criteria at each level of assessment such as requirement level, criterion level and indicator level. An extensive analysis with experts and stakeholders involved is of utmost importance to arrive at more realistic weightages. In this study, equal weightages were assigned to each indicator for simplicity. The environmental assessment covered broader impact categories addressing the impacts on air, water and energy use. The economic assessment covered direct costs and indirect cost from CO_2 emissions. The indirect costs of other emissions such as SO_x, NO_x etc. can also be included in the assessment to reflect the climatic impacts of the various construction activities on the economy. The social impacts assessment covered the broader impacts of the activity on various aspects of the society. The indicators can be varied based on their relevance to the project. Overall, the triple bottom line sustainability assessment using QUALICS framework makes the decision-making process more rational and transparent.

ACKNOWLEDGEMENT

The authors are greatly thankful to Mr. Partrik Lydon for his assistance during this study.

REFERENCES

Coduto, D. P. 2001. Foundation Design Principles and Practices 2nd Ed., Prentice-Hall, New Jersey

EFFC-DFI Carbon Calculator Tool v2.3. 2014. European Federation of Foundation Contractors, UK, and Deep Foundations Institute, Hawthorne, NJ, USA.

Raymond, A. J., Pinkse, M. A., Kendall, A., and Dejong, J. T. 2017. Life-cycle assessment of ground improvement alternatives for the Treasure Island, California, redevelopment. Geotechnical Special Publication, (GSP 276), 345-354.

Reddy, K. R., Cameselle, C., and Adams, J. A. 2019. Sustainable Engineering: Drivers, Metrics, Tools, and Applications. Wiley, Hoboken, New Jersey.

Reddy, K. R., and Kumar, G. 2019. Application of triple bottom line sustainability framework to select remediation method at industrial contaminated site. Proceedings of Eighth International Conference on Case Histories in Geotechnical Engineering, GeoCongress-2019, Geotechnical Special Publication, (GSP 312), 241-251.

Reddy, K. R., and Kumar, G. 2018. Addressing sustainable technologies in geotechnical and geoenvironmental engineering. In Geotechnics for Natural and Engineered Sustainable Technologies (pp. 1-26). Springer, Singapore.

Reddy, K. R., Sadasivam, B. Y., and Adams, J. A. 2014. Social sustainability evaluation matrix (SSEM) to quantify social aspects of sustainable remediation. Proceedings of ICSI2014, ASCE, Reston, Virginia, 831-841.

Saaty, T. L. 2008. Decision making with the analytic hierarchy process. International journal of services sciences, 1(1), 83-98.

Trentin A.D.S., Reddy, K.R., Kumar, G., Chetri, J.K., and Thomé, A. 2019. Quantitative assessment of life cycle sustainability (QUALICS): framework and its application to assess electrokinetic remediation. Chemosphere, 230, 92-106.

United States Environmental Protection Agency (USEPA). 2017. The social cost of carbon: estimating the benefits of reducing greenhouse gas emissions. Available at: https://19january2017snapshot.epa.gov/climatechange/social-cost-carbon_.html (accessed on April 5, 2019)

THE FINAL PIECE OF THE PUZZLE: RE-DESIGN OF GROUTED CLOSURES FOR A DAM CUTOFF WALL

James C. Myers P.E., Moretrench, Rockaway, New Jersey, USA, (973) 627-2100, jmyers@moretrench.com
Lucian P. Spiteri P.E., Moretrench, Rockaway, New Jersey, USA, (973) 627-2100, lspiteri@moretrench.com
Daniel P. Stare P.E., Gannett Fleming, Harrisburg, PA, USA, (717) 763 - 7212, dstare@gfnet.com
Christopher M. Hallahan P.E., Gannett Fleming, Harrisburg, PA USA, (717) 763 - 7212, challahan@gfnet.com

Keywords: jet grouting, seepage control, permeation grouting, dam

ABSTRACT

Buckeye Lake Dam was substantially remediated between 2015 and 2018 as a result of unacceptable dam safety performance. A permanent seepage cutoff, consisting primarily of a soil mixed cutoff wall (SMCW) with occasional sections of steel sheet piling, was constructed along the dam alignment. Closures were required at the terminus of the soil mix elements with existing structures or coffer cells, and at locations where new sheet piling was constructed parallel to the new soil mixed cutoff wall, creating a short circuit seepage path. The original proposed design to construct these closures included permeation grouting methods with chemical grouts. However, a combination of multiple chemical grout types, multiple grout pipes, and an extensive post-grouting verification program was required to ensure the design intent was achieved. After award of the project, the specialty grouting contractor elected to evaluate jet grouting as an alternative closure construction method. The advantages of the jet grouting option offered potential schedule and cost savings to the project as well as a superior product for seepage reduction, given the mixed soil conditions at the site. This paper presents an examination of the site conditions and project goals for the construction of the proposed closure elements for the rehabilitation of Buckeye Lake Dam. Descriptions of the original and alternative treatment methods are provided, with expected performance results. A description of the relative strengths and deficiencies of each method, as well as the feasibility and constructability of each method is provided. The implementation of the jet grouting program is presented, including a discussion of the design elements, quality control test methods, movement monitoring, and verification test methods. This paper also examines the risks associated with jet grouting and how those risks were mitigated during the grouting operations.

HISTORY

Buckeye Lake is situated approximately 28 miles east of Columbus, Ohio and is managed and operated by the Ohio Department of Natural Resources (ODNR) as part of the Ohio State Parks system. The lake is impounded by natural features that exist along the south and east banks of the reservoir, and by the embankment structure constructed along the north and west banks of the reservoir (see Fig. 1). The reservoir site was originally a natural swamp and the original purpose of the constructed dam and reservoir was to provide water to the Ohio and Erie Canal System. Several dam alignments and configurations were constructed during its early history; however, the original embankment is comprised of homogeneous earthen fill. The embankment is 15 ft (4.6 m) high and extends 4.1 miles (6.6 km) from the North Shore abutment along the east, continuing to the abutment at Lieb's Island to the West. Several spillway and outlet structures exist along the embankment alignment. Most noteworthy are Seller's

© 2019 Deep Foundations Institute

Spillway and Amil Spillway. Fig. 2 is a Plan View of the embankment alignment and appurtenant structures at Buckeye Lake.



Fig. 1. Aerial photograph of Buckeye Lake, pre-construction



Fig. 2. Plan view of Buckeye Lake Dam

Prior to recent rehabilitation efforts, the original embankment consisted of fine-grained soils obtained from local excavations. The original embankment also had a steep (near-vertical) masonry wall constructed along the upstream slope. Later, various sections of the embankment had sheet piling extensions added upstream of the embankment, with tendons connected to dead-man anchors set along the masonry wall. These extensions were then backfilled with poorly compacted silty sand (bank run) material (Rizzo 1997).

SITE GEOLOGY

The foundation soils at the Buckeye Lake Dam site are generally composed of various interbedded layers of alluvial, lacustrine and glacial till deposits. Therefore, the foundation soils are highly variable and include intermixed zones of both permeable and relatively impermeable coarse and fine-grained strata (ODNR 2017) Bedrock (not encountered during the project) is reported to consist of shale, limestone and sandstone was reported around one hundred ft (30 m) below existing grade. The general stratigraphic profile of the native materials at the site consist of the following layers as shown on Fig. 3:

- Surficial Lake Bed Sediments (Brown) – Recent lake sediments of up to several ft (1 m) in thickness. Sediments generally consist of fine-grained soils, silts, and clays and include moderate organic content.
- Lacustrine Soils (Green) – Fine-grained soils deposited by glacial lakes, typically 10 to 30 ft (3 to 9 m) in thickness and having frequent sandy stringers.
- Fluvial/Alluvial Soils (Red) – Coarse-grained soils deposited by higher energy glacial action, with various fine-grained stringers, typically 10 to 30 ft (3 to 9 m) thickness.
- Glacial Till (Yellow) – Predominately fine-grained soils with some zones of coarse-grained materials. Stiff silts and clays with gravel extending to bedrock.
- Bedrock (Not shown)– Sedimentary rock approximately 100 feet (30 m) or more below ground surface. Bedrock not encountered during rehabilitation work.

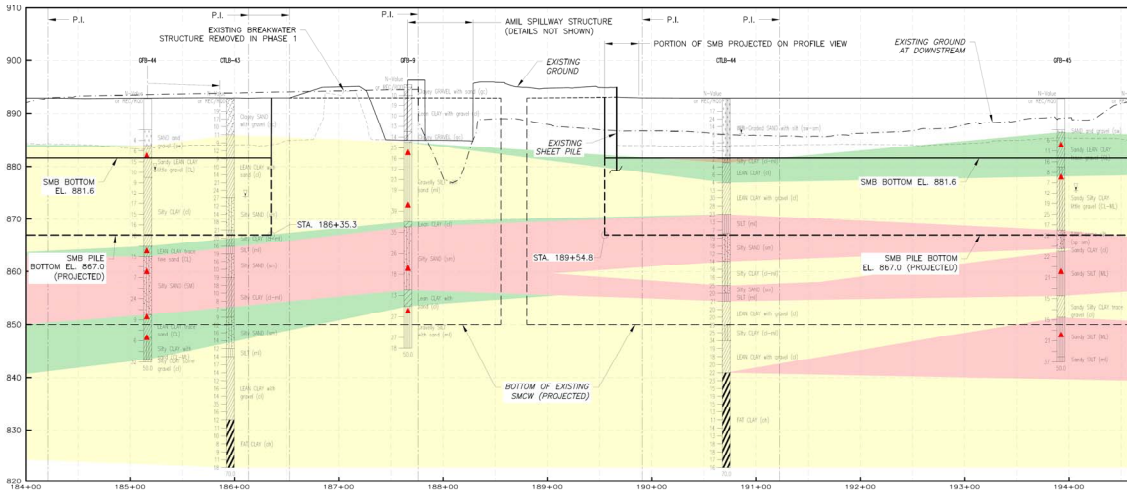


Fig 3. Example of Interbedded Soils at Amil Spillway

The different soil strata also varied in fines content along the embankment alignment. Table 1 summarizes the range and average fines content observed in the soils tested during the most recent subsurface exploration program (ODNR 2016).

Table 1: Summary of Foundation Soils at Buckeye Lake Dam

Stratum	Range of Fines Content (Passing the #200 Sieve)	Average Fines Content (Passing the #200 Sieve)
Lake Bed Sediments	11.6% - 99.6%	74.9%
Lacustrine Soils	51.6% - 99.9%	88.5%
Fluvial/Alluvial Soils	0.4% - 98.0%	33.3%
Glacial Till	3.7% - 72.3%	50.3%

EMBANKMENT DEFICIENCIES

Review and analyses of the existing conditions of the original dam and subsequent additions were provided through Gannett Fleming (USACE 2015). The analyses determined that principal failure modes for Buckeye Lake Dam included unacceptable seepage through the embankment, internal instability of the embankment and structures, and overtopping. In order to address these deficiencies rapidly while allowing the reservoir to remain in service, ODNR decided to implement a Construction Manager At Risk (CMAR) design and phased construction approach.

PHASE I CONSTRUCTION

Phase I construction of the Buckeye Lake Dam Improvements Project included Interim Risk Reduction Measures and site preparation work for Phase II. These included temporary lowering of the operating pool elevation from EL 891.5 ft (271.7 m) to EL 880.0 ft (268.2 m), construction of an embankment stability berm (ESB) upstream of the dam, lining of the ESB slope with rip-rap, and construction of a soil mix cutoff wall (SMCW) extending into underlying foundation soils to a depth of 43 ft (13 m). An illustration of the Phase I construction cross-section is provided in Fig. 4.



Fig. 4. Typical Phase I construction cross-section

PHASE II CONSTRUCTION

Phase II construction included installation of a soil mix buttress (SMB), coffer cells at various existing structures and terminus of the SMB, a final cap of the new composite embankment structure, final grading, and landscaping of the completed embankment. A typical cross-section of the Phase II construction (included with previously constructed Phase I elements) is provided as Fig. 5.

Due to the constraints of the soil mixing equipment and the presence of existing structures, such as spillway walls and existing sheet pile cutoffs, a contiguous seepage cutoff could not be created across the dam and appurtenant structures. Therefore, additional coffer cells were constructed at select structures These were constructed as open cut mass concrete cells that extended to the same depth as the constructed soil mix buttress and connected to the adjoining spillway abutment walls.

Several locations remained where the combined structures did not provide a contiguous seepage cutoff. These paths had the potential to short-circuit the newly constructed embankment and create unmitigated seepage and instability which need to be addressed.



Fig.5. Typical Phase II construction cross-section

CLOSURES - SEEPAGE CUTOFF PROBLEM

In order to cut off the remaining seepage paths along the newly constructed embankment, various discrete closure elements needed to be designed. A total of eight locations were identified for closure at Sellers Spillway, Amil Spillway and the North Shore Abutment. Few options existed that could provide adequate cutoff in confined areas at very critical structure locations and at depths up to 45 ft (13.7 m) below the crest of the ESB and in a cost-effective manner given the soil conditions and logistics of accessing the treatment areas. Given the challenges presented by the existing structures and site soils coupled with the always present concern for dam safety, a conservative solution was proposed by Gannett Fleming, the Engineer representing ODNR. After the successful bidder had been awarded the general contract, which included the closures, the grouting specialty geotechnical contractor proposed a modification to the scheme which considered jet grouting as an alternate.

INITIAL SOLUTION - CHEMICAL GROUTING

Chemical grouting/permeation grouting is a technique that refers to the process of injecting a fluid into the pore space of the target soils and replacing the air or water in that volume with the grout binder, without disrupting the soil matrix. This results in an improved soil zone with increased strength and cohesion as well as reduced permeability. This grouting method favors having a clean, sandy target soil through which the grout can be readily injected. Permeation grouting can be performed utilizing relatively low pressures and injection rates, therefore limiting potential negative effects created by fluid pressure within an earthen embankment dam This was critical in the method selection.

Acrylate grouts were selected as the best possible permeation grout type for treating the mix of foundation soils illustrated in Table 1. The fines content of the target soil is ultimately the determining factor as to which type or types of chemical grout are viable for permeation grouting. Based on the potentially high fines content that these soils could have, the lowest viscosity grout available (acrylate) was selected. One disadvantage of using acrylates is that they do not perform well over long periods of time if subjected to wet-dry cycles. This presented a problem for treatment of the embankment stability berm that would be subjected to seasonal fluctuations in pool elevation. Therefore, an alternative grout type would need to be used to treat the ESB zone. The gradation of the ESB material indicated that it was potentially groutable with polyurethane grouts. Although polyurethane grouts are a higher-viscosity chemical grout compared to acrylates, they are not susceptible to degradation from wet-dry cycles.

Both chemical grouts could be injected into the soils at the closure locations through a line of multiple sleeve port pipes (MPSP). The use of MPSP would also permit re-grouting of a zone without additional drilling. Multiple injection holes along the closure alignment would help to address variability of the soils and provide confinement of the grouting effort.

The chemical grout solution was a conservative, low pressure, low risk (in terms of dam safety) concept. However, the concept was also likely very tedious, cumbersome, and expensive, resulting from the injection of two chemical grouts within the same MPSP, particularly due to the use of polyurethane which expands when contacted with water. This would require supplemental measures and substantial care to prevent the MPSP's from fouling during injection.

A robust verification program was required to determine the results of the chemical grout injection. The program was clear that testing would be performed to measure the change in permeability rather than specify problematic and inappropriate verification methods such as coring or a target unconfined compressive strength.

The chemical grouting program would require an iterative process of grouting, testing to determine the change in permeability, and additional grouting. The iterative process of the specified program introduced additional layers of complexity and time in order to grout several relatively small treatment zones, especially if additional holes were needed to meet permeability targets. The combination of these issues would likely contribute to a costly grouting program. But most importantly, the biggest drawback to the chemical grout solution was that the results of the grouting program were unlikely to produce a decreased uniform permeability due to marginally groutable soil with higher fines content. Site soils with lower fines content would likely be interbedded in nature, making them more difficult to fully treat, and could have permeabilities of up to 20 gpd/ft^2 ($1x10^{-3}$ cm/sec) which would compromise the cutoff.

Despite the potential drawbacks, the chemical grout solution was included in the Phase II work package. However, the matter of implementation of the final solution was left to the specialty grouting contractor's expertise to propose a viable alternative in terms of performance, cost and overall risk to the structure.

PROPOSED ALTERNATIVE - JET GROUTING

Jet grouting refers to the process of utilizing a high energy fluid jet to break up and erode the target soil while mixing and replacing it with a grout binder, typically cement. This high energy ground improvement technique is applicable across a wider range of soil types ranging from gravelly soils through soft clays. Fig. 6 below shows gradation sizes that various grouting techniques and materials are effective in, including jet grouting and permeation grouting with synthetic solutions (i.e. acrylate), sodium silicates and cementitious mixes.

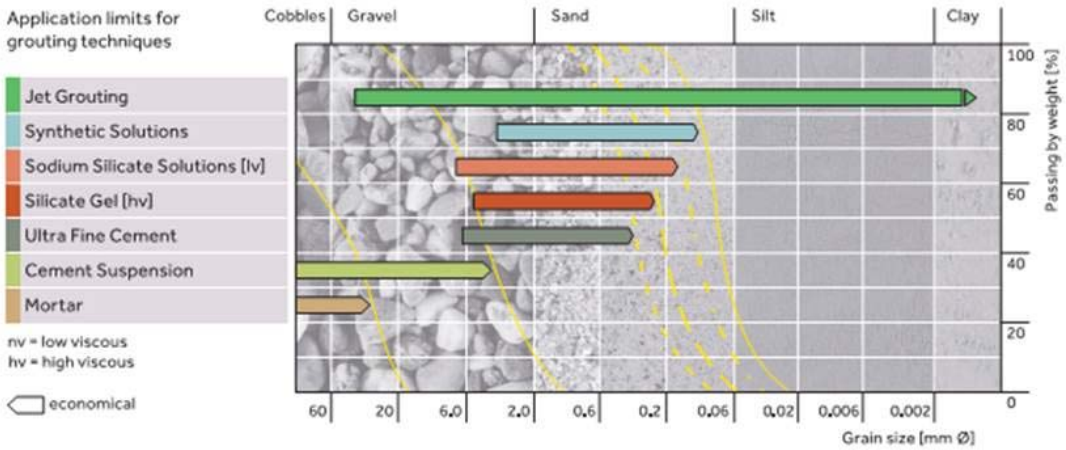


Fig. 6. Application limits for various grouting techniques (Courtesy of Hayward Baker Inc.).

The jet grouting option presented several advantages over the permeation grouting option, including effectiveness over a much wider range of soils, the production of a higher strength mass of improved ground, and a more uniform treated mass with lower permeability. While strength was not a requirement, the increased strength of the treated mass provided greater assurance of treatment and long-term durability. The higher strength and higher degree of improvement also allowed for additional means of quality control such as verification coring to be included in the program.

The site soils included various interbedded layers of sands, sandy lean clays, and silty sands. According to the specialty grouting contractor's review of the project, when considering the effectiveness of chemical grouting with acrylates and polyurethanes, an assumption was made that the Engineer had considered that some of these soils were treatable (sands), some were marginally treatable (silty sands), and some were not treatable (lean clays). It was the specialty grouting contractor's assumption that this situation was acceptable, since the goal of the grouting program was to treat/improve the higher permeability soils and increase cohesion to facilitate closure.

It was recognized that some of the soils on site may not be practically treatable using jet grouting methods. As such, some untreated zones of clay may remain in the target area. However, these zones were already naturally low permeability and cohesive. The specialty grouting contractor therefore anticipated that if these soils remained untreated, the final product would still be acceptable to the engineer given favorable permeability testing results across the target zone. An additional advantage to a jet grouting program included time and schedule savings since the jet grouting program proposed was essentially a one-pass treatment of each closure element, unlike the iterative chemical grouting process.

Although there were several advantages for a jet grout solution, there were a few risks with the jet grouting operations that needed to be addressed and mitigated, especially for work on or near a dam embankment. Unlike permeation grouting's lower pressure/energy approach, jet grouting uses very high energy that would need to be carefully monitored and controlled. Space and access considerations were also a concern for delivery and staging of materials and equipment, work zones had to be integrated into the difficult to access site (Fig. 7). Key risks associated with jet grouting operations on dam structures are discussed below.



Fig.7. Jet grout equipment setup with a bulk cement delivery in process.

REDUCTION AND MITIGATION OF RISKS WITH JET GROUTING

Although the jet grouting solution offered a potential superior final product, there were still several risks that needed to be addressed prior to approval by the owner and engineer. Development of a jet grouting specification and the submittal process addressed means to mitigate most of the risks. Several of the key concerns are discussed below.

Hydraulic Fracture/Break-out: The potential for hydraulic fracture or damaging of the dam embankment material was considered very low. Most of the closure elements were confined upstream by steel sheet pile cutoff elements and downstream by the Soil Mix Cutoff Wall or by reinforced concrete walls of the spillway structures. These structures provided bulkheads that limited the travel and damped the erosive effects of the jet grouting operations.

Movement: In order to provide assurances that excessive movement did not occur at critical structures adjacent to the jet grout elements, a movement monitoring program was provided by the general contractor at the request of the engineer. The general contractor provided real-time monitoring of survey points located at critical structures and survey points with before and after measurements at SMCW and SMB locations adjacent to jet grout elements. Upon any signs of movement (measured or visual) of adjacent structures, all jet grouting operations would cease, and notification of project personnel would take place, including the owner, engineer, and construction manager.

Contamination – Spoils Handling: Contamination of the site and Buckeye Lake by jet grout spoils was controlled with a plan using the conventional method of trenches and shallow collection pits to work with the relatively high water table. Once spoils reached a collection pit, they would be allowed to set up overnight and then excavated and removed for offsite disposal.

The concerns of the various stakeholders were addressed by the specialty grouting contractor by the work plan process and by a pre-construction meeting with all relevant stakeholders. Methods of installation, expectations of the specialty grouting contractor, program goals, review of acceptance criteria and verification procedures were all addressed, and a consensus was reached to allow the program to move forward.

FINAL JET GROUT DESIGN

The first step of the design process was to review the geometry of the various closure locations to select optimal jet grout column sizes. Review of geometry at the closure locations yielded results that a 4-ft (1.2 m) diameter column was a very practical size and could be used for all the locations. To ensure closure, multiple adjacent columns were placed in a linear arrangement as shown in Fig. 8. This pattern mimicked the original arrangement of the permeation grout pipe locations in plan and depth.

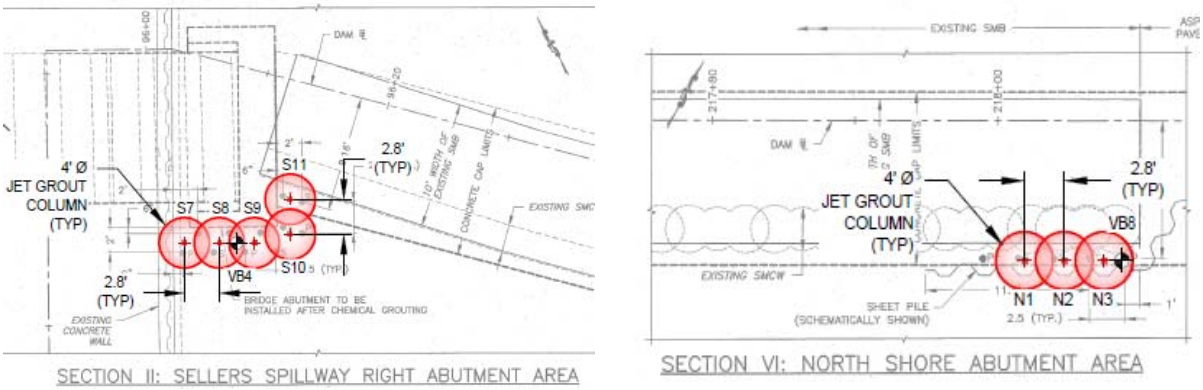


Fig. 8. Sample of jet grout column configurations.

As discussed above, the jet grout design assumed that full treatment of the clayey soils was not required. Therefore, the jet grout element design was initiated using soil parameters for a very low plasticity clay. Using these soil parameters to develop the energy required to erode, mix and replace the target soils allowed the program to be more cost effective because the higher energy required for full treatment of the clay was not necessary. Once the depth, arrangement, location and preferred diameter of the columns was established the process moved on to energy requirements for the preferred diameter. The resulting jet grout parameters developed for the site were as follows:

Nozzle Size =	0.16 in (4.0 mm)	Withdrawal rate =	16 in/min (40 cm/min)
Grout pressure =	5800 psi (400 bar)	Rotation speed =	12-15 rpm
Air pressure =	72-87 psi (5-6 bar)	Grout flow rate =	86 gpm (325 l/m)

PROGRAM EXECUTION

Mobilization and setup of equipment at Buckeye Lake began on May 14, 2018 and production jet grouting operations began on May 31. The final jet grout elements were completed at the North Shore abutment on June 14. Verification coring operations began on June 11 and were completed on June 20, with falling head testing completed on June 21. A total of 26 jet grout elements were installed ranging in depths between 15 ft (4.6 m) and 45 ft (13.7 m). Jet grouting operations were able to be performed while various other construction operations were ongoing at the Amil Spillway and without adversely affecting the adjacent work.

Test Program

Prior to installing production jet grout columns, a test program was completed to verify the selected jet grout parameters, prove out the monitoring program and ensure the spoils handling methodology was sufficient for the site constraints. The test program consisted of installing three columns of the planned 4-ft (1.2 m) diameter at the Amil Spillway location. The three columns were installed in a linear

arrangement with 1.2 ft (0.37 m) of overlap to mimic the production geometry. After approximately two weeks of curing, the two overlap locations were cored using a P sized triple tube barrel. Retrieved core samples as well as wet grab samples from the installation were tested for unconfined compressive strength (UCS) to verify that the strength criteria had been met. To test for permeability of the jet grouted soil, a piezometer was constructed within the borehole created during the verification coring process. Each piezometer was constructed with 2-in. (5 cm) diameter PVC screen and riser pipe, filter sand extending approximately two ft (0.6 m) above the top of screen, and a bentonite seal above the filter sand.

All information gathered during the installation of the test columns, the verification coring, and from the laboratory USC testing indicated that the test columns achieved the desired geometry and exceeded the minimum strength requirement of 100 psi (0.7 MPa). Falling head testing completed in the piezometers did yield results exceeding the specified requirement of 0.2 gpd/ft^2 (1x10^{-5} cm/sec). The permeability results were a function of the piezometer construction, namely the interface between the filter sand and the bentonite seal ended up being located extremely close to the top of the jet grout columns and possibly above them. This configuration created unrepresentative results of the jet grouted soil because the untreated soil above the jet grout zone was subjected to the permeability testing. During the production verification coring program, the piezometer screen length was shortened to ensure a proper bentonite seal would be constructed within the soilcrete borehole.

Observations During Jet Grouting Operations

Effects of jet grouting were confined at most locations as described above; however, surface connections were observed during grouting operations at two locations. The first grout connection occurred while installing element A5 at the Amil Left Forebay location. The surface connection was due to the intersection of a portion of removed sheet pile cutoff wall that crossed the path of the newly installed Forebay sheet pile adjacent to the jet grouting elements. The connection was likely caused by a defect in the foundation soils left by the removal of the former sheet pile sections. When the connection was observed by the specialty grouting contractor, the grouting pressures were immediately reduced, the borehole reamed, and the surface connection was monitored while the jet grout element was completed. The connection was significantly decreased once the jet grout monitor was lifted above the bottom of the Forebay sheet pile which blocked the connection.

The second connection occurred during the grouting of Seller's Right Abutment element. Minor connections to the upstream slope of the ESB below the pool elevation were observed as bubbles and turbulent water. Once connections were observed, the specialty grouting contractor reduced grout and air pressures and continuously reamed the borehole in an effort to reduce the strength of the connections to the upstream slope. The connections were believed to be a release of compressed air only and due to the granular nature of the ESB material. The ESB at the Seller's Right Abutment was also unconfined upstream of the jet grout elements due to the absence of a sheet pile wall, as was the case at the other closure locations. Although there were connections to the upstream slope of the ESB material, the berm material was not a critical member of the seepage cutoff system at the dam and therefore was not considered a dam safety concern. Visual inspections of the abutment during jet grouting operations confirmed there were no break-outs or connections downstream of the SMB at the Seller's Right Spillway Abutment closure location.

During installation of jet grout element S5 at the Seller's left abutment and coffer cell, slight movement was observed by the real-time measurements of survey pins set at the right abutment and outlet structure vault. Grouting operations were immediately suspended, and the owner and engineer were notified. A survey of the movement monitoring pins installed at the right abutment and outlet vault was performed. Results of the survey indicated there was approximately 0.25 in. (6.35 mm) of heave that occurred only at the corner of the abutment (closest point to the jet grouting). Although the measured heave was below the

allowable threshold levels determined for the grouting operations, additional inspection of the vaults and testing of the gates were initiated by the engineer in coordination with the CM and ODNR as an additional measure. No disruption was found, and work was allowed to proceed.

Observation of the verification cores showed continuous, generally uniform closure elements from top to bottom of each element cored. Permeability testing was conducted in piezometers installed in each of the verification core holes. Permeability was measured by falling head permeability tests and applying the appropriate equation from Hvorslev (1951). Results of the permeability testing for all of the closure locations were less than 0.2 gpd/ft^2 (1x10^{-5} cm/sec) and met acceptance criteria. Results of unconfined compressive strengths indicated that all samples were well over 100 psi (0.7 MPa) and also met specified acceptance criteria. Table 2 provides a summary of the results of the verification core drilling and testing.

Table 2: Summary of Verification Hole Drilling and Testing Results

Verification Hole	Depth of Verification Hole (ft), (m)	Core Recovery (%)	Falling Head Test Permeability (gpd/ft^2), (cm/sec)	Unconfined Compressive Strength 28-Day (psi), (MPa)
VB1	28.8, 8.8	99.2%	0.06, 2.7x10^{-6}	570, 3.9
VB2	29.1, 8.9	100%	0.10, 4.6 x10^{-6}	1040, 7.2
VB3	31.5, 9.6	98.9%	0.07, 3.4 x10^{-6}	535, 3.7
VB4	29.0, 8.8	98.9%	0.18, 8.5 x10^{-6}	1220, 8.4
VB5	15.0, 4.6	99.1%	0.07, 3.3 x10^{-6}	865, 6.0
VB6	26.4, 8.0	78.0%	0.13, 5.9 x10^{-6}	660, 4.6
VB7	35.7, 10.9	100%	0.02, 9.8 x10^{-7}	655, 4.5
VB8	43.7, 13.3	99.8%	0.11, 5.3 x10^{-6}	290, 2.0
VB9	13.5, 4.1	95.4%	0.11, 5.3 x10^{-6}	445, 3.1

LESSONS LEARNED

During the execution of jet grouting and verification testing programs, several lessons were learned. The first was that real-time movement monitoring is critical for evaluating performance of jet grouting elements adjacent to critical structures, especially for dam embankments. Passive surveys (i.e. before and after grouting operations) are not enough to assess the effects of the jet grouting operations. By the time information is collected and reported, the movements have already occurred and cannot be addressed immediately to prevent additional or excessive movements. In addition, real-time monitoring should also be automated. While the real-time measurements collected during jet grouting at Buckeye Lake were performed manually by a technician in a continuous manner, the process was still subject to potential human error. Automation of this process with the use of laser levels, automated instruments, robotic total station, or similar equipment eliminate the human error and increase the level of accuracy and expedite reaction times.

Always be mindful of the potential effects of jet grouting on known or suspected defects in the surrounding soil such as those caused by the removal of sheet piles or other demolished structures. Also, be mindful of low confining stress in soils caused by presence of vertical elements or rock features. These low confining stress zones are susceptible to the erosive energy of jet grouting pressures. Be mindful of the potential for weak, soft, or unsupported soils that are also susceptible to jet grouting pressures.
Expect the unexpected and be ready to act quickly. Always be ready to halt jet grouting operations immediately for any reason. Have a plan developed ahead of grouting operations to address potential issues. Have a contact list of all critical personnel created and distributed to all site personnel. Contact critical personnel if any surface connections, break-out, or movement is observed. Review procedures and adjust grouting methods as needed to achieve project goals while avoiding adverse effects.

Collaboration between the owner, engineer, and specialty grouting contractor at all phases of work (from submittal to execution to verification) is key to successfully achieving project goals and design intent while maintaining the principles of dam safety. Communication between all stakeholders of the project (owner, engineer, construction manager, specialty grouting contractor) during grouting operations is necessary for clear understanding of the work being performed as well as maintaining dam safety.

CONCLUSION

Jet grouting works can be performed safely in and around existing dam structures if the risks are understood and mitigated properly by trained, experienced personnel and robust monitoring. Design personnel should choose the situation and locations for jet grouting at a dam site carefully and all risks should be adequately understood and address prior to implementation. Experience is critical. Don't hesitate to reach out to design professionals or specialty geotechnical contractors that have extensive experience with jet grouting to help with assessment of its capabilities.

REFERENCES

Hvorslev, M. J. (1951). "Time lag and soil permeability in ground-water observations". Technical bulletin No. 36, Us Army Corps of Engineers Waterways Experiment Station, Vicksburg, VA

Paul C. Rizzo Associates (May 1997), *Buckeye Lake Dam Stability Study, Buckeye Lake State Park, Fairfield, Licking and Perry Counties, Ohio*, DNR 736 730-96-034, Project No. 95-1590.

U.S. Army Corps of Engineers (USACE) (March 2015), *Review of Past Reports and Existing Conditions and Recommendations for Interim Risk Reduction Measures, Operation and Maintenance*, Huntington District, Great Lakes and Ohio River Division.

Ohio Department of Natural Resources (ODNR) (June 2016), *Geotechnical Data Report, Buckeye Lake Dam Improvements*, Gannett Fleming Engineers and Architects, P.C.

Ohio Department of Natural Resources (ODNR) (2017):

– February 2017. *Phase II – Package A – 100% Design Report*, *Buckeye Lake Dam, Ohio*, Project No. DNR-150080.

– August 2017. *Buckeye Lake Dam Improvements: Package B – Subsurface Treatments*, *Buckeye Lake State Park*, Project No. DNR-150080, Division of Engineering

– September 2017. *Phase II Basis of Design Report*, *Buckeye Lake Dam, Ohio*, Project No. DNR-150080.

THE USE OF RIGID INCLUSIONS TO SUPPORT LARGE SPANS

By Sonia Sorabella Swift, Nina Carney, David Tarasovic, and Michael Shedlosky

ABSTRACT

Rigid inclusions were used to support roadway fills and mechanically stabilized earth (MSE) walls for the South Capitol Street Corridor project. The first phase of this two-phase, nearly $1 billion project will include the replacement of the Frederick Douglass Memorial Bridge, including two approach ovals east and west of the Anacostia River, the replacement of the I-295/Suitland Parkway Interchange, and the construction of several traffic ramps. The bridge itself carries over 70,000 drivers daily and is expected to open in 2021.

Ground improvement is required over a portion of the project footprint. Within the ground improvement area, the construction includes MSE walls up to 35 feet high and embankment fills up to 28 feet for which CMC rigid inclusions (RIs) were used to mitigate settlement and stability. The proposed construction runs over multiple old, in-service utilities that the project requirements indicate could not tolerate any stress or settlement due to the construction. As such, solutions that spanned the utilities were required.

A concrete slab of varying thickness was used to span a fragile 108-inch-diameter sewer pipeline and 48-inch-square-precast-concrete box beams were used to span twin utilities that were buried just a few feet below current working grades on site. Unreinforced RIs were used to support these structures. The center to center spacing of the RIs perpendicular to the pipe run was 26.5 ft for the concrete slab and 62 feet for the precast--concrete box beams. The axial forces on the RIs were up to 267 kips. The RIs were not structurally connected to the slab or box beams. A single-element load test was performed to confirm the load-carrying capacity of the RIs. This paper will focus on the utility protection slab over the twin utilities and provide an overview of the design of the structural and geotechnical solutions and will present the results of the load test performed.

KEYWORDS: rigid inclusions, settlement, Frederic Douglass Memorial Bridge

INTRODUCTION

The new Frederick Douglass Memorial Bridge (FDM Bridge) and reconstruction of the Suitland Parkway/ I-295 interchange (South Capitol Project) is a part of the Anacostia Waterfront Initiative (AWI) Program, whose goal is to transform the shores of the Anacostia River. The existing FDM Bridge is approximately 70-years old and has been classified as "functionally obsolete". The completed South Capitol Project will improve the multi-modal transportation options, increase pedestrian and vehicular safety and provide additional green space. The proposed FDM Bridge, a rendering of which is shown in Fig. 1, is designed to become a landmark bridge in the Washington, D.C. area.

The ideas behind this project are not novel ones as congested urban areas seek ways to streamline travel, shorten commutes, and increase tourist appeal. However, when making such drastic changes in cites with aging infrastructure, the projects increase in complexity and cost. Building a new landmark bridge doesn't just involve a bridge design but rather the design for the roadways leading up to the bridge, the bridge abutment, the on and off-ramps, and, sometimes the most complex aspects of the project are the interactions between all of these items. For this project, Menard worked as a Subcontractor to South Capitol Bridgebuilders (SCB), a joint venture between Archer Western Construction LLC (Walsh Group) and Granite Construction Company**.** Menard's scope of work was limited to providing ground improvement in two areas on the project – the East Oval and Retaining Walls 6&7. The soil conditions and proposed

© 2019 Deep Foundations Institute

structures in each of these areas varied significantly; however, rigid inclusions (RIs) were used throughout the ground improvement zone.



Fig. 1 Rendering of Proposed FDM Bridge taken from the National Capital Planning Commission Concept Review Submittal dated March 2, 2018

Rigid inclusions are small-diameter concrete columns that are installed through soft or variable soils to reduce settlement and increase bearing capacity. Menard's patented variation of a rigid inclusion is the Controlled Modulus Column (CMC), which is a 12.5-, 15.6-, or 17.75-inch diameter fully-grouted column installed with a displacement auger. CMCs are typically unreinforced, though structural steel can be added, as necessary to resist compressive, tensile, or flexural forces. As ground improvement elements, CMCs are not generally connected to the structure they are supporting unless it is required to resist the applied forces (in the case of an uplift element). Throughout the remainder of this paper, we will refer to the CMC ground improvement elements more generally as RIs.

This paper focuses on the ground improvement installed in the East Oval and, more specifically, the RIs that were used to support the structural protection system that spans the twin utilities. The twin utilities are two separate concrete structures, one of which is reinforced and one of which is unreinforced, supported by timber piles. This section of utilities was constructed as early as 1905 for the transport of sewage. The utilities run along the entire length of the East Oval and beyond, yet approximately 170 feet of the twin utilities run directly beneath the proposed East Oval fill. Because the utilities are old, fragile structures, the owner of the utilities, District of Columbia Sewer and Water Authority (DC Water), posed stringent requirements on the allowable stresses applied to the twin utilities during construction. As such, SCB worked with Menard, ECS Mid-Atlantic LLC, the geotechnical engineer of record on the project, engineers from AECOM, the bridge designer, and structural engineers from SAI Consulting Engineers, Inc (SAI) to design a structural protection system to span the utilities. The structural protection system required elements to span approximately 62 feet – the width of the twin utilities, including the space between the

two (46 feet) and the RIs had to maintain an 8-foot clearance from the edge of the timber piles supporting the twin utilities. The change in grade due to construction was approximately 14 feet, which resulted in an applied load of approximately 2,000 psf. With such a high uniform sustained load applied and a large unsupported length, a traditional reinforced concrete slab would not suffice, leading the team to more complex solutions.

STRUCTURAL DESIGN CHALLENGES

Since this was a design/build project several parties were involved with the development of the approach roadway and final grade elevations used to determine the design heights. Coordination with all team members, both construction and design, was crucial to the advancement of the support system design. Together, the team evaluated several different support options which involved reinforced concrete deck slab supported by either steel girders or spread pre-stressed box beams and adjacent pre-stressed concrete box beams with no reinforced concrete deck slab. All options would span the twin utilities and rest on a reinforced concrete grade beam supported by RIs. The use of geofoam and/or lightweight fill to reduce the applied load was also evaluated but found not to be cost effective. Ultimately, the adjacent pre-stressed concrete box beam structure running perpendicular to the twin-utilities was selected.

Twin Utility Design:

An early design option for the twin utilities was to use pre-stressed concrete T-beams, similar to what is found in parking garages. This was removed from consideration based on structural adequacy after a depth of 10' of fill including live load surcharge was proposed. Based on the fill height needing support and the span length required to span the twin utilities, a more robust load carrying system was required.

As a team, we discussed and reviewed several superstructure options:

Option 1: Rolled Steel Girders (W40 x 397) spaced at 6'-6" with a 7-1/2" concrete deck slab. We selected the beam spacing based on a preliminary spacing of the RIs needed to support the load applied by the fill.

Option 2: Spread Prestressed Box Beams (48" x 48") spaced at 6'-6" with a 7-1/2" concrete deck slab. We selected the beam spacing based on a preliminary spacing of the RIs needed to support the load applied by the fill. .

Option 3: Adjacent Prestressed Box Beams (48" x 48") with no concrete deck slab.

SCB performed a cost evaluation and selected to move forward with Option 3, the Adjacent Prestressed Box Beams.

To support the superstructure, we designed a continuous grade beam supported by RIs equally spaced along the length of the grade beam. Initially, we intended to place an RI beneath every concrete box beam (spaced 4'-0" on center) in the system, but to avoid pile group effects and limit the loads applied to the RIs, their spacing was limited to 4'-6"; thus requiring a more refined grade beam design model due to the misalignment of the beam centerline of bearing to the center of the RIs. While alignment would have caused compression in the grade beam with a direct transfer of load to the RI below, misalignment causes force distribution within the grade beam to transfer the beam reactions to the RIs. Moment and shear was induced in the grade beam and accounted for by strength design for loads extracted from a refined STAAD analysis. The refined analysis more accurately modeled the designed condition to limit the required grade beam thickness and reinforcing.

The resulting utility-slab-support-solution resembled a traditional displacement pile supported embankment solution. However, since the majority of project site was supported with displacement RIs, (>2000 RIs), we explored the use of RIs to avoid mobilizing additional equipment to the site.. Initially, we discussed designing the RIs as piles and connecting the RIs and the superstructure together. However, as design progressed, we realized that by keeping the two elements separate allowed for more economical and simpler designs of both the RIs and the superstructure.

By eliminating a positive connection between the RIs and the grade beam, we were able to transfer only axial load to the RIs while limiting the lateral load and moment transferred to the RIs. Consequently, the cost of the RIs was reduced - both because of the time and material savings in keeping the grade beam and RIs as separate elements. Thermal movement of the superstructure was not considered because we expect it to be nominal based on the 10 feet of fill (4'-0" minimum fill height) above the superstructure. We controlled lateral movement from the earth surcharge to the structure by doweling the superstructure to the grade beam, ensuring the position of the grade beam over the RIs. To avoid transfer of any vertical load to the existing utility, we placed a void beneath the superstructure and set it to the depth of the grade beam (2'-0").

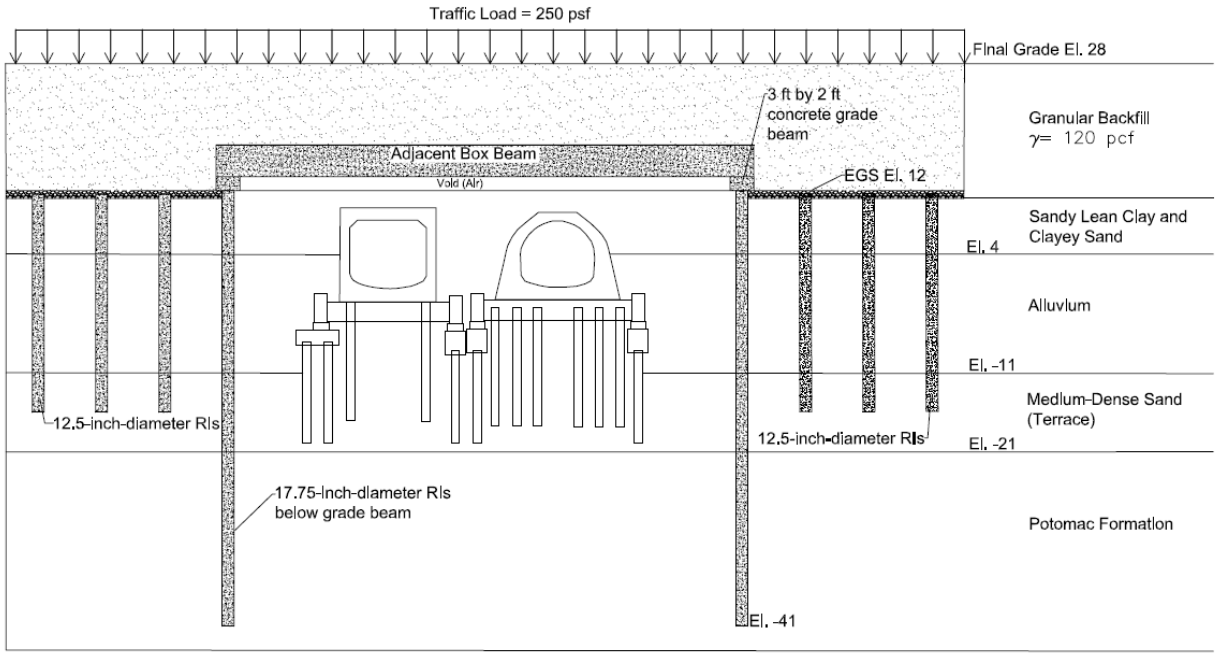


Fig. 2 Preliminary design concept for twin utility structural support system

GEOTECHNICAL DESIGN OF THE RIGID INCLUSIONS

As the structural design was being prepared, we were simultaneously designing the RIs that would support the structural protection system. SAI provided Menard with the maximum reactions for the RIs based on the structural design of the grade beam and Menard performed the design of the RIs and estimated the settlement associated with the proposed construction. Because of the large span for the structural system, the design of the RIs was controlled not by settlement, but by the structural and geotechnical capacity of the RIs. The RI design was further impacted by the need to minimize differential settlement between the soil directly above the twin utilities and the soil (embankment) adjacent to twin utilities. The project specifications for the long-term settlement of the twin utilities is 1 inch; however, the long-term settlement

of the surrounding roadway and embankments was 2 inches. Therefore, we designed the rigid inclusions surrounding the twin utility structure to gradually transition from 2 inches of long-term settlement to 1 inch of long-term settlement.

To evaluate the interaction between the area adjacent to and directly above the structural protection system, we built a 3-dimensional (3D) finite element model of the system in Plaxis. The model included the structural protection system including both the box beam structure and the concrete grade beams. Both the box beams and concrete grade beams were modeled as rectangular concrete structures. We did not explicitly model the reinforcement or exact shape of the concrete box beams, but we did reduce their unit weight to account for the fact that they are mostly hollow. We modeled the surrounding embankment and the RIs adjacent to the structural protection system and modified the spacing of the RIs moving outward from the centerline of the utility to minimize differential settlement at the ground surface. See Figs. 3 and 4 for the soil profile and RI layout modeled in our 3D Plaxis model.

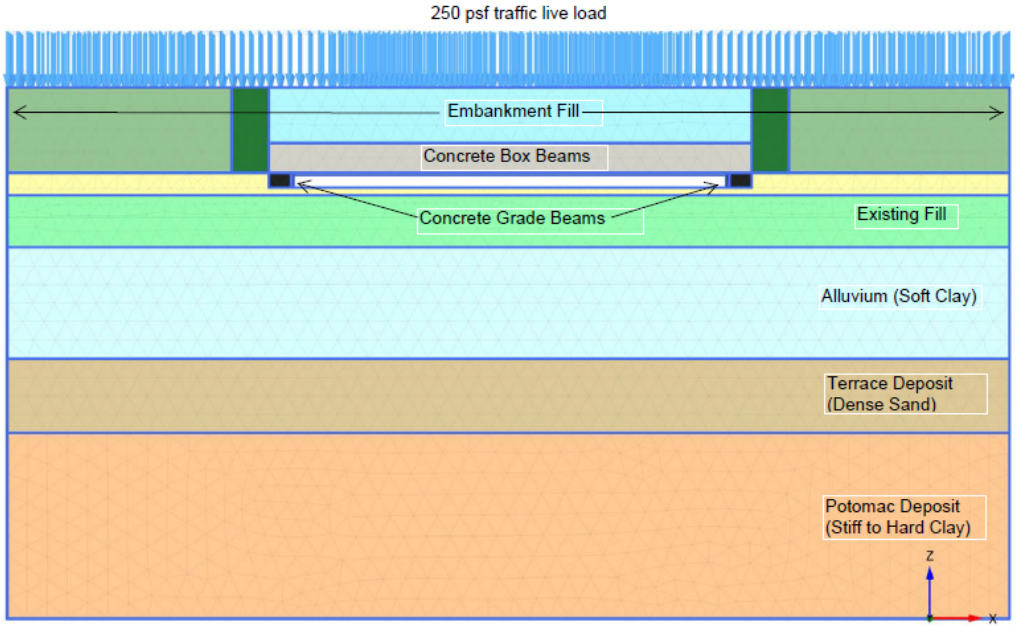


Fig. 3 Soil profile modeled in 3D Plaxis

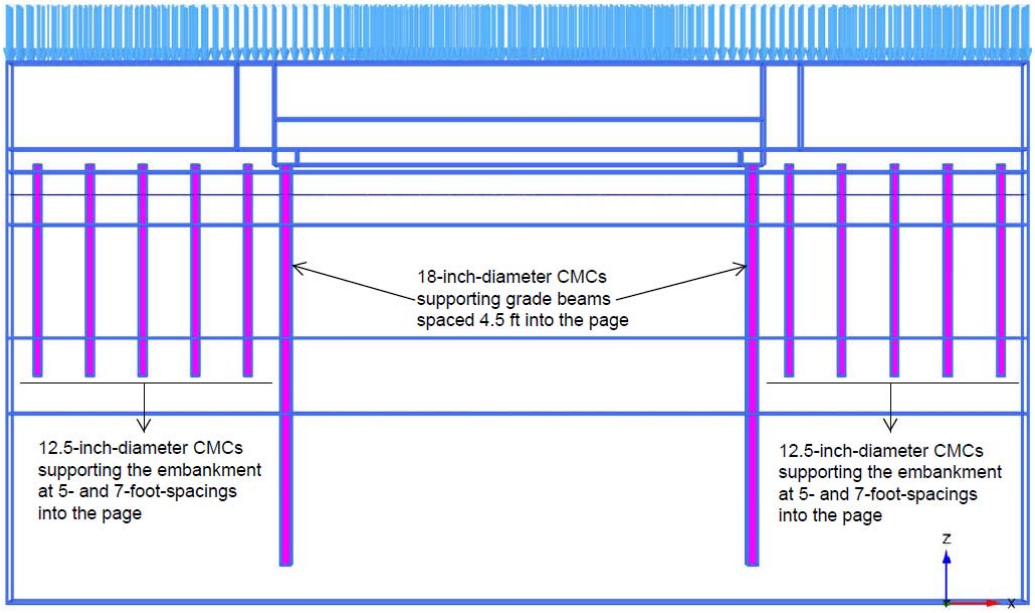


Fig. 4 RIs modeled in 3D Plaxis

Our model represents one row of RIs running perpendicular to the twin utilities. The 18-inch-diameter RIs supporting the grade beams are spaced 4.5 feet on center (this spacing is along the length of the grade beam, parallel to the twin utilities). The RIs directly adjacent to the box beam structure are spaced at 5 feet on center and then the spacing transitions to 7 feet. This gradual transition in RI spacings minimizes the differential settlement at the ground surface.

To reduce model complexity, we did not model the actual twin utility structures. The addition of horizontal tunnels into the 3D model would have likely increased model run-time and decrease the likelihood of model convergence. However, the presence of the twin utility structures in the model does not significantly increase the amount of information we have about how the structures will perform, if our main concerns are settlements and stress changes. Instead, we reported the settlements and stress changes at the top and bottom elevations of the utilities.

Figure 5 shows the resulting settlements estimated by the 3D Plaxis model. The post-construction settlement ranges from 0.15 inch to 0.8 inch across the 135-foot-width of the model. The differential between the center of the utility and the edge of the model, which represents the conditions about 35 feet away from the edge of the utility protection system is approximately 0.65 inch. The project criteria required that the post-construction settlement was 1.0 inch or less.

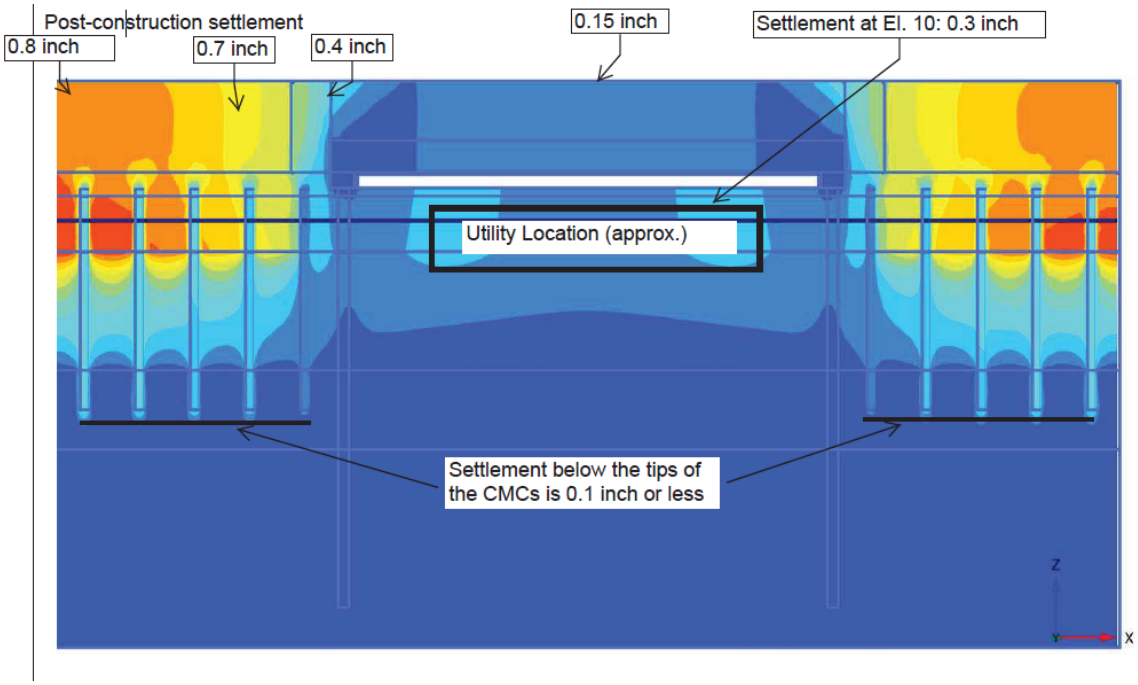


Fig. 5 Estimated post-construction settlement in 3D Plaxis

We also obtained the RI forces from the 3D model, shown in Figure 6 and compared them to the structural reactions provided by SAI. The maximum applied service load for an 18-inch-diameter RI was 290 kips, which is a larger load than we typically design the RIs to support. Generally, we design 18-inch-diameter RIs for loads ranging from approximately 160 kips to 220 kips (or less). We performed hand calculations of the geotechnical capacity of the RI assuming that the RI had the same embedment length in the soils that resulted in acceptable settlements in the 3D Plaxis models. Those hand calculations resulted in a factor of safety on geotechnical capacity just over 1.0. After considering the types of soils at the site, we proceeded with our design as suggested by the 3Dmodel but indicated that we would rely on the results of an instrumented load test at the location of the twin utilities to estimate the final length of the installed rigid inclusions. If the results of the load showed more movement than allowed by the design, we would have increased the length of the RIs for production. We instrumented our test CMC with strain gauges along its length, and more heavily within the deeper soil strata, so that, if required, we could use the frictional resistance of the soil obtained during the load test to estimate the required length of the RI.

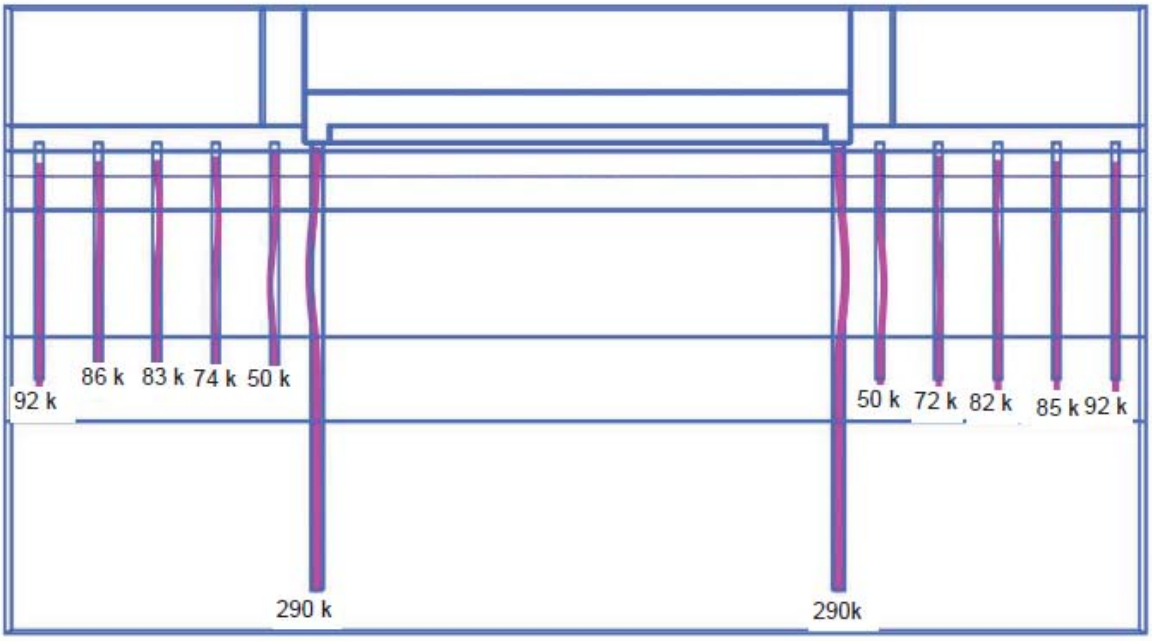


Fig. 6 Axial load in RIs based on the 3D Plaxis model

STRUCTURAL DESIGN OF THE RIGID INCLUSIONS

Rigid inclusions are generally made of unreinforced grout, though they can be reinforced with a single center bar or a center bar and a cage depending on loading or construction considerations. Rigid inclusions are also generally separated by the structure they are supporting by a load transfer platform, which can range from 6 inches thick to 3 or more feet thick. The load transfer platform is generally a dense-graded aggregate that is placed and compacted in an engineering manner. The purpose of the LTP, which was used throughout this project in area with RI support, is to distribute the loads from the point of application to the RIs without causing stress concentrations or the need for a pile cap.

Based on the allowable stresses given in IBC for unreinforced concrete elements, we have the required structural capacity from the grout alone, if we increased the grout strength beyond the 3,000 psi mix we typically use. However, the owner of the utilities expressed concerns about having unreinforced elements and requested that we provide some reinforcement within the top portion of the RIs. The design team agreed to provide a 35-foot-long No. 10 steel reinforcing bar in each RI supporting the grade beam. This reinforcement provides additional capacity, both for the long-term and it provides the RIs with additional ductility to minimize damage during construction activities after the CMCs are installed. A total of 77 RIs supported the twin utility support slab, 37 on the west side and 40 on the east side.

As discussed previously, we decided to leave the RIs and the grade beam as separate elements without a structural connection between the two. However, to minimize settlement, we eliminated the load transfer platform and decided that the grade beam could be placed directly on top of the RIs. As discussed previously, the grade beam was designed structurally to resist the point loads from the RIs and span between them, as appropriate.

LOAD TEST

We performed a static load test on a single 18-inch-diameter non-production RI in the vicinity of the twin utilities.

The soil profile encountered during installation of the test column was consistent with nearby borings. We installed the test column to a total length of 58 ft. Based on the installation log, soft soils were encountered until a depth of 31 feet. Based on our review of the RI installation log and the nearby borings, we estimate the profile contained the following soils:

- 5 feet of medium-dense to dense sand, known as the Granular Terrace Deposit,
- 13 feet of a silt/clay mixture known as the Cohesive Terrace Deposit, and
- 8 feet of embedment in a stiff clay, known as the Potomac Deposit.

We performed the test according to ASTM D-1143 and followed the procedure for the Quick Test. We installed strain gauges at six distinct elevations within the column to record the load at each depth during the loading increments. The strain gauges were located in the locations listed below to allow us to back-calculate the frictional resistance of each soil layer, if necessary to adjust the column length for production.

- Three feet from the top of the test column
- Near the top and bottom of the Granular Terrace Deposit
- Within the Cohesive Terrace Deposit
- At the top of the Potomac Deposit and
- Three feet from bottom of the test element.

The design load for the test element, as discussed before was 290 kips and our test load is equal to 150% of the design load (435 kips). During the test, we applied a maximum load of 580 kips, at which the test was terminated due to safety concerns. At this load, which is equal to 200% of the design load, the top of the RI deflected about 0.36 inch. The deflection at the design load and the test load, 150% of the design load, was approximately 0.15 and 0.2 inch, respectively. The deflection was less than the deflection observed in our model for a RI with a design load of 290 kips. Our models predicted 0.5 inches of post-construction settlement at the 290 kip design load. See Fig 7 and 8 for the load deflection test and the strain gauge graph.

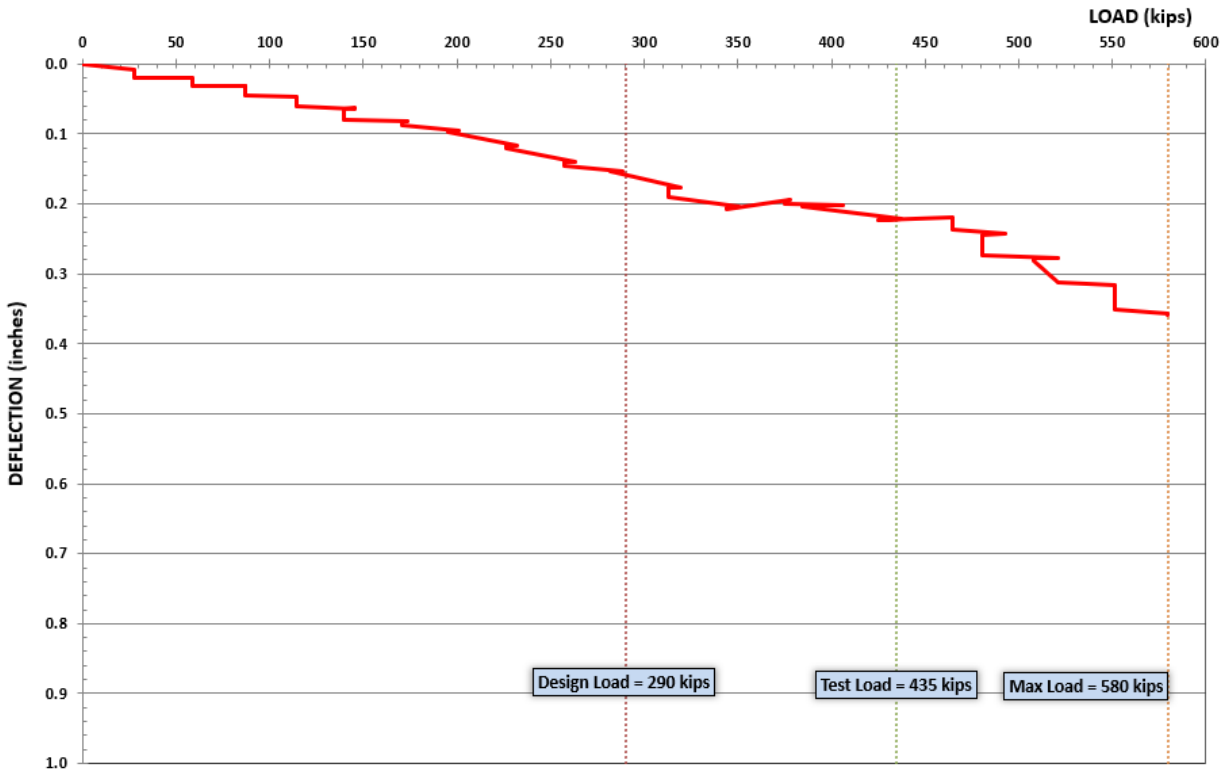


Fig. 7 Load-Deflection plot from single-element load test

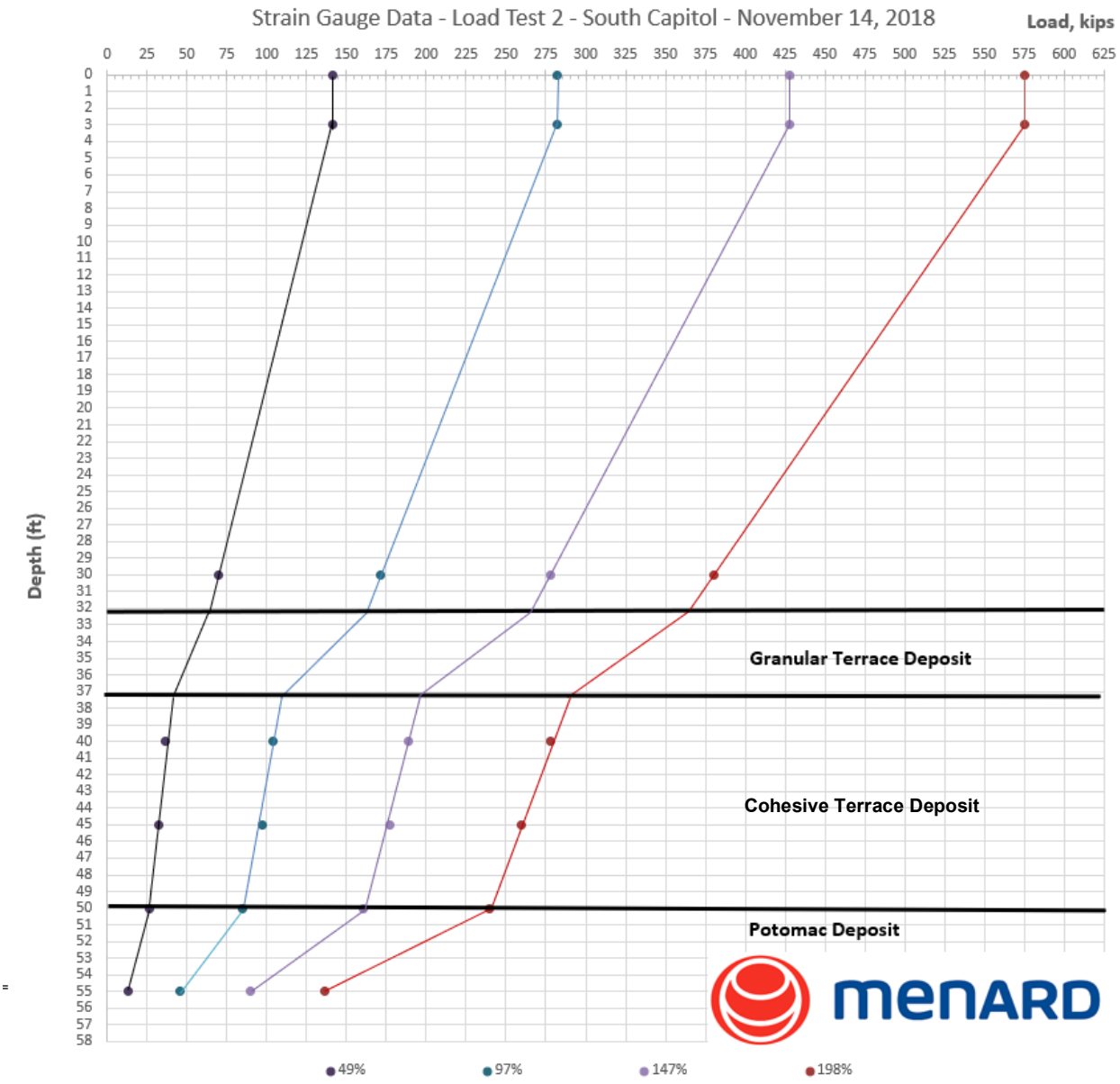


Fig. 8 Strain gauge data from single-element load test

Based on the strain gauges, we calculated the frictional resistance of the granular terrace deposit and the Potomac deposit and compared them to hand calculations. The frictional resistance of those layers was higher than anticipated based on our hand calculations. However, the frictional resistance of the Cohesive Terrace Deposit was similar to what we estimated in hand calculations. As such, we could not reduce the total column length significantly because the test results showed that the production columns needed to tip into the Potomac layer to have adequate capacity.

Since the load test showed a minimum factor of safety of 2 on the design load with movements smaller than estimated in our models, we set the termination criteria for the production RIs to be the same as they were for the test.

CONCLUSION

We approached a complex problem with an open mind and considered many different alternatives to achieve a technically sound, buildable, and cost-effective solution, both structurally and geotechnically. While piles with traditional reinforcement and a positive connection between the piles and the grade beams or pile caps could have been used, the use of RIs allowed for cost and schedule savings and met the same settlement criteria as a pile-supported system. The key to the success of this design was combining the complex structural and geotechnical calculations and evaluating the interaction between the different components to confirm that the result would meet the long-term settlement criteria. For this design, we used the models to provide us with confidence that our design was valid but the load test results confirmed our modeling and provided additional assurance to the project team about the long-term performance of the system.

CHALLENGES AND LESSONS LEARNED FROM SHORING DESIGN OF 2ND/BROADWAY METRO STATION

Pirooz Barar, PB&A Inc., San Rafael, CA, USA, (415) 259-0191, pbarar@pbandainc.com
Babak Mamaqani, PB&A Inc., San Rafael, CA, USA, (415) 259-0191, babak.mamaqani@pbandainc.com

ABSTRACT:

Regional Connector Transit Corridor (RCC) is part of the Los Angeles metro expansion project under construction which adds three new stations into the system. PB&A was responsible for the design of the support of excavation (SOE) systems for two stations, 2nd/Broadway and 2nd/Hope, in RCC. In this paper, challenges and lesson learned from SOE design of 2nd/Broadway station with a main focus on underpinning design are discussed. 2nd/Broadway station required to cut and cover excavation of 500 ft long by almost 100 ft deep, underneath 2nd Street. SOE systems consisting of drilled soldier beams with tiebacks and/or struts. The main challenge in 2nd/Broadway station was to underpin the LA Times building which was partially protruded into the station. A chellenging underpinning system consisted of concrete panels and ground anchors was designed to support the building surcharge and prevent settlement. The underpinning system was designed based on METRO design criteria and the deflection was evaluated by Finite Element Analysis (FEA) program, PLAXIS 2D. A maximum deflection of 0.4 inches was calculated to occur at the top of the underpinning system. Data from settlement and tilt sensors showed minimal movements which aligned with PLAXIS outputs.

Keyword: support of excavation, retaining wall, underpinning, tieback, soldier pile

PROJECT DESCRIPTION

The Regional Connector Transit Corridor (RCC) is Los Angeles Metro's ambitious Light Rail Project. It runs under the City's main thoroughfares, Flower and 2nd Streets, and when complete will alleviate traffic and parking congestion in downtown Los Angeles. The Regional Connector will connect thousands of residents living in the bedroom communities of the Inland Empire and Long Beach to their jobs Downtown. The rail line will serve 1.9 miles, using the $1.756 Billion budget to construct the underground rail line, including 3 new stations, at 2nd & Hope Street, 2nd & Broadway, and 1st St. & Central Ave (Fig. 1).

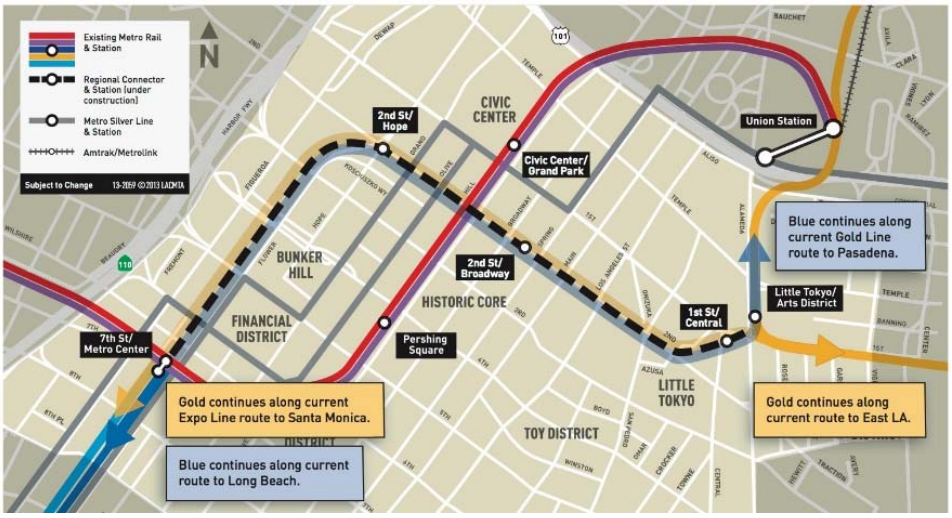


Fig. 1. Regional Connector Transit Corridor (RCC)

© 2019 Deep Foundations Institute

The 2nd/Broadway station is 500 ft long which required almost 100 ft of excavation underneath 2nd Street. The shoring systems were comprised of drilled soldier beams with internal bracings (i.e., struts and wale) and tiebacks. The typical drilled hole diameter was 36 inches to accommodate the installation of W24 structural steel sections as soldier beams. The shoring system design was made challenging by the depth of excavation and the need to keep 2nd street operational during the excavation, along with the proximity of buildings to the station, underground utilities, City of LA's tie back de-tensioning requirement and underpinning the Los Angeles Times Buildin. This paper mainly discusses underpinning design for the LA Time building. The plan view and an aerial photo of the station are shown in Fig. 2.

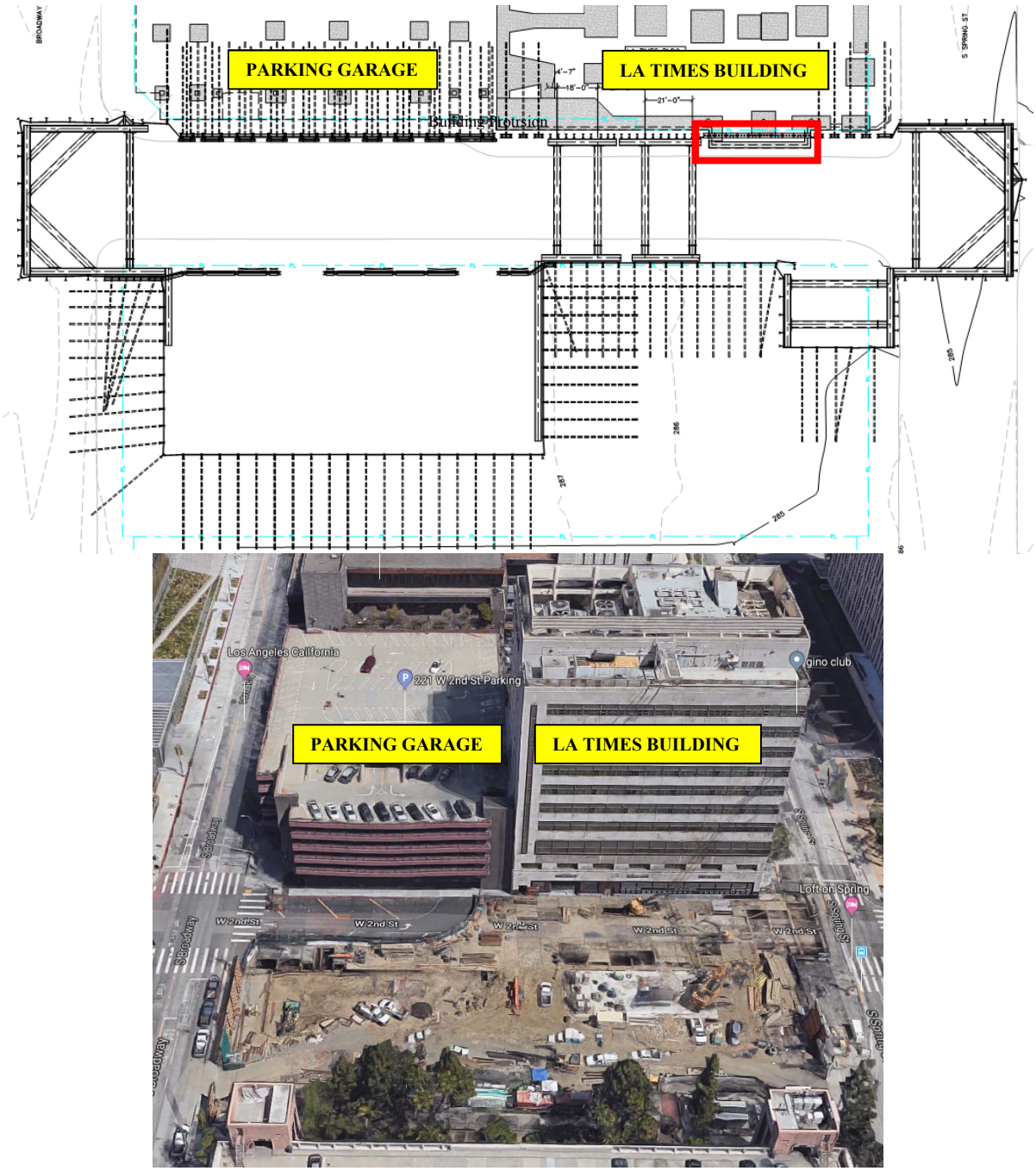


Fig. 2. 2nd/Broadway Station; Top) Plan View, Bottom) Aerial Photo

SITE STRATOGRAPHY

Site stratigraphy of the 2nd/Broadway station consisted of 15 ft of artificial fill and alluvium underlain by the Fernando Formation. The Fernando Formation is essentially the bedrock that consists of siltstone and claystone. Since the depth of excavation for the project was almost 100 ft, the majority of the excavation was within Fernando Formation as shown in Fig. 3.

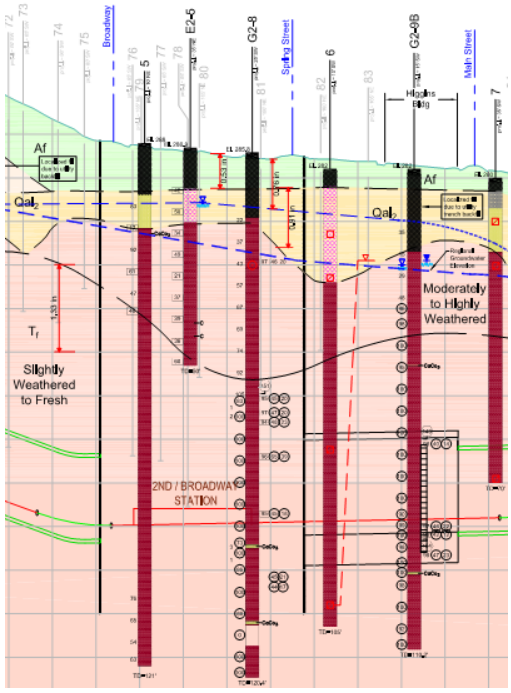


Fig. 3. Stratigraphy of 2nd/Broadway Station

Comprehensive geotechnical investigations were conducted and properties were recommended at each soil layer as shown in Table 1.

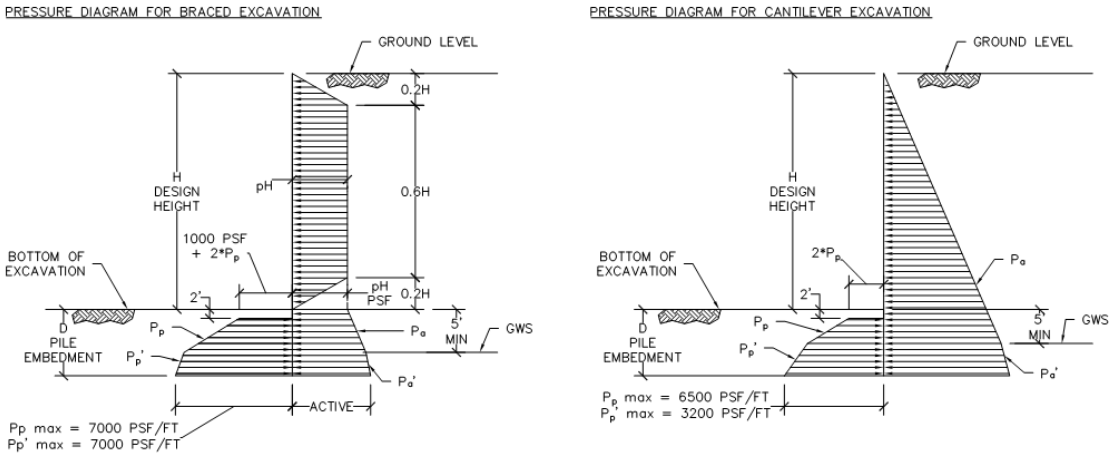
Table 1. Soil Properties

Soil Layer	Top Elev. (ft)	E_{50} (ksf)	E_{oed} (ksf)	E_{ur} (ksf)	m	OCR	F (deg.)	c (psf)	Ψ	K_o	γ (pcf)
Artificial Fill	0	750	750	2,250	0.75	NA	28	0	0-5	0.53	105
Alluvium	8	1,500	1,500	4,500		NA	32	150		0.47	118
Fernando mon / Moderately Weathered	15	1,700	1,700	5,100		5.0	19	2,300	7-15	0.67	120
Fernando mon / Slightly Weathered	50						27	3,620		0.55	120

SUPPORT OF EXCAVATION (SOE) DESIGN CRITERIA

Support of Excavation (SOE) needed to be designed based on design criteria developed by METRO (Los Angeles County Metropolitan Transportation Authority, 2010). One of the main criteria was active and passive pressures. As shown in Fig. 4, trapezoidal and triangular pressures were recommended to be used for braced (struts or tiebacks) and cantilever cases respectively. The active pressure width below the bottom

of the excavation was equal to the drill hole diameter while the passive pressure was allowed to be applied over two times of drilled hole diameter.



STATION NAME	CONDITION	P (PCF)	PA (PSF)	PA' (PSF)	PP (PSF)	PP' (PSF)
2ND/BROADWAY	Braced	24	30	15	300	300
	Cantilever	30				

Fig. 4. Active and Passive Pressure for SOE Design

METRO (Los Angeles County Metropolitan Transportation Authority, 2010) required additional lateral surcharge including traffic, seismic and building surcharges to be considered for SOE design. The seismic load was modeled as an equivalent rectangular surcharge of 6H applied over the height of the SOE. The passive pressure and yield strength of the soldier beam were allowed to increase by 33% under seismic event. The SOE system was needed to be checked for both static and seismic events and designed for the highest possible load.

Another considered surcharge in SOE design was traffic surcharge. The traffic surcharge consisted of 600 psf of vertical surcharge applied over 20 ft which was equivalent to 240 psf of the lateral surcharge at first 10 ft followed by 100 psf at second 10 ft.

Another considered lateral surcharge was the equivalent lateral surcharge (E_b) due to building contact pressure (q_f). E_b was calculated using following equations (Los Angeles County Metropolitan Transportation Authority, 2010):

$$E_b = 0.4 * n * (1-a/H1) \quad \text{for} \quad a/H1 \leq 1 \qquad [1]$$

$$E_b = 0 \quad \text{for} \quad a/H1 > 1 \qquad [2]$$

Where E_b = equivalent lateral surcharge (psf), n = building net contact pressure (psf), a = building distance from the face of the excavation (ft), H1 = depth from the bottom of the building to bottom of the SOE (ft).

The seismic force due to building was a rectangular load acting over Df on the SOE and was calculated as follows (Los Angeles County Metropolitan Transportation Authority, 2010):

$$P_e = 100 \text{ psf} \quad \text{for} \quad a \leq Df \qquad [3]$$

$$P_e = 50 \text{ psf} \quad \text{for} \quad Df < a \leq 2*Df \qquad [4]$$

$$P_e = 0 \text{ psf} \quad \text{for} \quad a > Df \qquad [5]$$

Where P_e = building equivalent seismic load (psf), Df = depth of the building foundation from ground level (ft) and a = building distance from the face of the excavation (ft).

The lateral surcharges and parameter definitions are shown in Fig. 5.

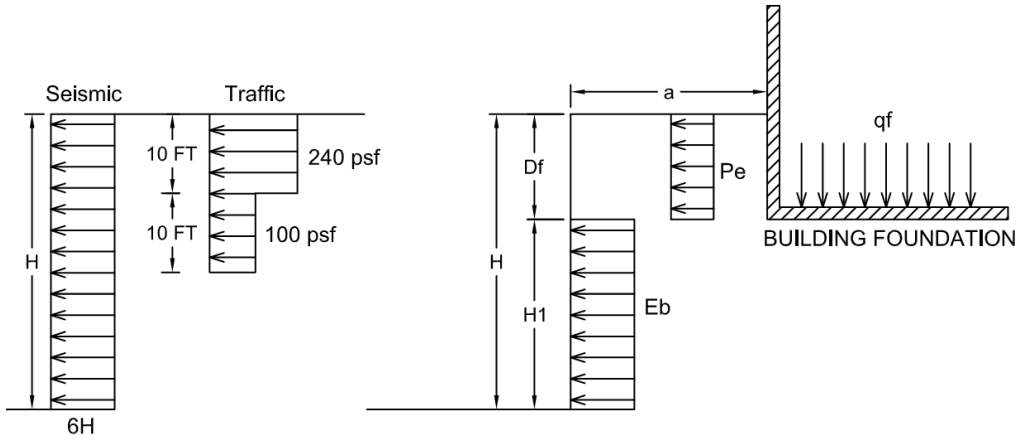


Fig. 5. Additional Lateral Surcharges for SOE Design

The soldier beams were required to be modeled as a simply supported beam between lateral supports (i.e., tieback or struts). This assumption ignores the presence of negative moment generated at the lateral support location which reduces positive moment occuring between lateral supports. To account for positive moment reduction due to negative moment at lateral support locations, the positive bending moment from the simply supported beam model was allowed to be reduced by 20% ($wL^2/10$ was used instead of $wL^2/8$ for moment calculation in simply supported beam where w is the lateral pressure and L is the distance between two lateral supports) at intermediate stages until excavation reaches the bottom of the final excavation.

When a structural slab is poured against the SOE system during station construction at backfill stages, it was allowed to reduce moment at simply support beam model by 33% ($wL^2/12$ instead of $wL^2/8$) to account for fixity provided by the structural slab.

The limit equilibrium method was adopted to design the SOE system. Since the SOE lateral bracings needed to be removed and/or de-tensioned during main station construction, all construction stages needed to be modeled to capture the highest possible load exerted to the SOE. DeepEX (Deep Excavation, 2019) software program was extensively used to model all construction stages and design the SOE system. Lateral bracing (i.e., strut and tieback) loads were extracted at each construction stage and used as benchmarks to make sure actual loads do not exceed calculated loads. This helped to verify the assumptions that were made during the design process of SOE in terms of lateral pressures being valid. Also, the results were used to develop contingency plans in case an excessive load is observed during construction.

Two of the construction stages, final excavation and roof level construction stages, with traffic and building surcharges are shown in Fig. 6 on which the demand moment and shear, as well as bracing loads, were calculated at each stage. As shown the second level bracing experiences 26% higher load (42.76 klf vs 33.78 klf) once the third level bracing is removed for roof level construction. This proves how important it is to model all intermediate construction stages to capture maximum possible load and design the SOE accordingly.

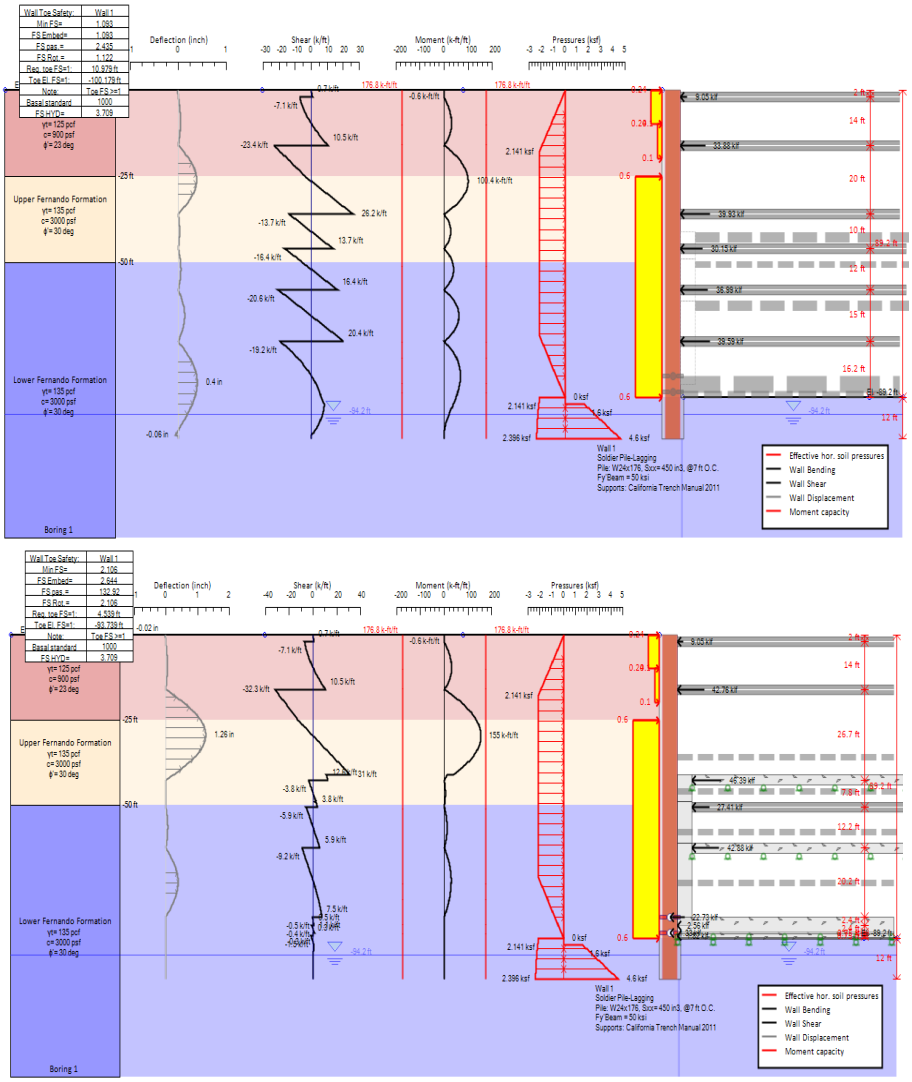


Fig. 6. DeepEX Model of SOE; Top) Final Excavation Stage, Bottom) Roof Level Stage

UNDERPINNING LA TIMES BUILDING

The LA Times building is a 10-story building that sits next to the station and part of the building at the basement protruded into the station. Therefore, an underpinning system was integrated into the SOE system to support the vertical load from the basement wall and prevent lateral movement and settlement due to surcharge from building foundations behind the underpinning system.

Geometry and Construction

A challenging underpinning system consisted of the ground anchors with precast concrete panels/diaphragms were designed to support the building vertical and lateral surcharges as shown in Fig. 7. The first two rows typically consist of 5 ft X 6 ft precast concrete panels to expedite the construction procedure. Since higher lateral surcharge from the LA Times building was expected based on the Boussinesq Equation, ground anchors were installed on every panel at first two rows. The excavation was conducted locally under the basement wall to install only one panel at a time to assure minimum settlement occurs during underpinning construction.

As shown, the first two rows were followed by hand-dug pit where reinforced concrete was constructed prior to excavation and then ground anchors were installed once the excavation reached almost 3 ft below each ground anchor elevation.

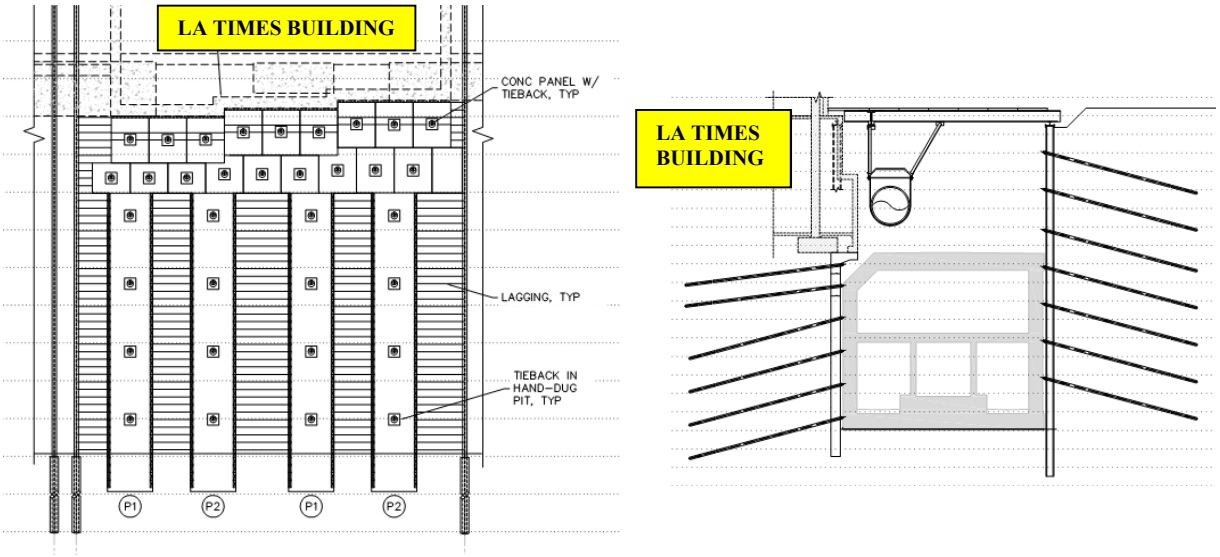


Fig. 7. Underpinning System for LA Times Building; Left) Elevation, Right) Cross Section

The first row of the panels was an inverted L shape to support the bottom of the basement wall footing and transfer the vertical load into the ground anchors as shown in Fig. 8. As shown, each concrete panel were connected to each other with a series of plates and bolts to make sure the loads from the LA Times Building were distributed evenly and the whole system works together as a single unit.

Spiles (breasting boards) were installed prior to excavation for concrete panels to prevent soil behind the wall footing from collapsing into the excavated area for concrete panels. Spiles are closely spaced steel bars that are mainly used in tunneling to provide temporary protective support for soil. Spiles for the underpinning system are shown in Fig. 8 at top of the first row right below the wall footing.



Fig. 8. LA Time Building Underpinning System

Limit Equilibrium Analysis

A DeepEX (Deep Excavation, 2019) model was generated for the underpinning system based on the METRO criteria discussed previously as shown in Fig. 9. The lateral surcharge from the building was calculated with Boussinesq Equation which showed maximum lateral surcharge of 4.8 ksf at 3 ft below the top of the underpinning. Although the lateral surcharge can dissipate rapidly by depth based on the Boussinesq Equation, the minimum lateral surcharge was limited to 1.9 ksf per METRO criteria for the building to achieve a conservative design.

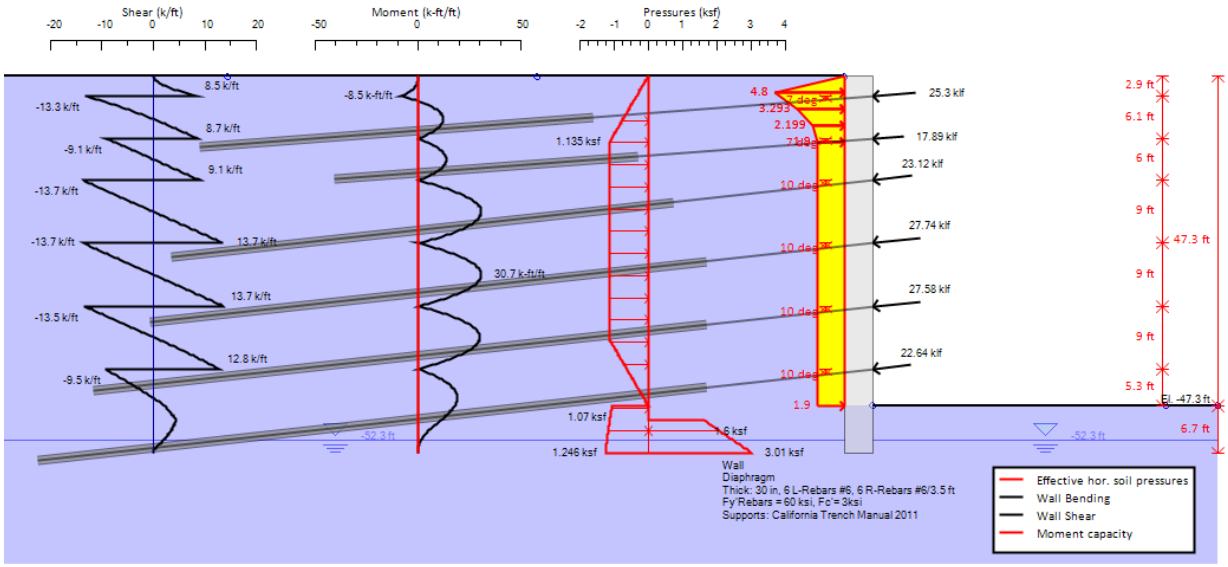


Fig. 9. DeepEX Model for Underpinning

Calculated loads from DeepEX model were then used to design concrete planks/diaphragms and to determine the number of strands required at each ground anchor elevation. Based on the METRO criteria, the anchors were tested for 2 times of design load and locked off at design load.

Finite Element Analysis (FEA)

Finite Element Analysis (FEA) with PLAXIS 2D (PLAXIS, 2019) was conducted to evaluate deflection of proposed underpinning system. All intermediate construction stages were modeled in order to calculate the cumulative deflection of the underpinning system. Based on geotechnical information, the top two rows were located within moderate to highly weathered Fernando Formation while the rest of the underpinning was within slightly weathered Fernando Formation. The un-bonded and bonded lengths of anchors were modeled with node-to-node anchor and embedded beam row elements. Hardening soil was used to model the soil behavior.

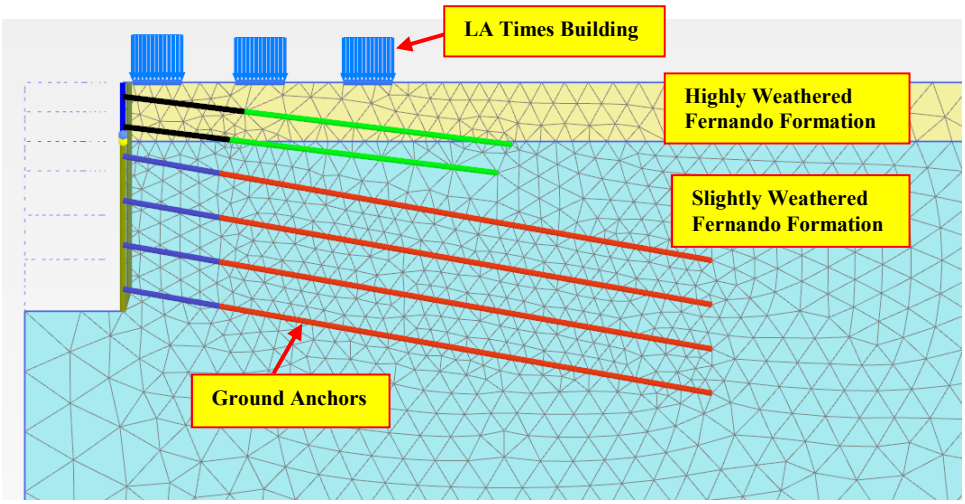


Fig. 10. PLAXIS Model for Underpinning

The soil deflection profile was extracted and saved at each stage of the construction as shown in Fig. 11. The soil shows positive deflection (i.e., backward) at the initial stages of and as excavation proceeds the deflection becomes negative (i.e., inward). This is because anchor design loads were based on maximum possible load during construction stages which in the underpinning system occurred at the final excavation stage. Therefore, anchor lock-off load is higher than the actual load at initial stages which theoretically pushes the wall back into the soil.

As shown, the maximum deflection of 0.41 inches (0.07% of the wall height) occurs at the final excavation stage which is less than METRO maximum allowable deflection of 1 inch (Los Angeles County Metropolitan Transportation Authority, 2010). The data from inclinometer and tilt sensors at top of the LA Times building showed minimal settlement which aligned with calculated deflection.

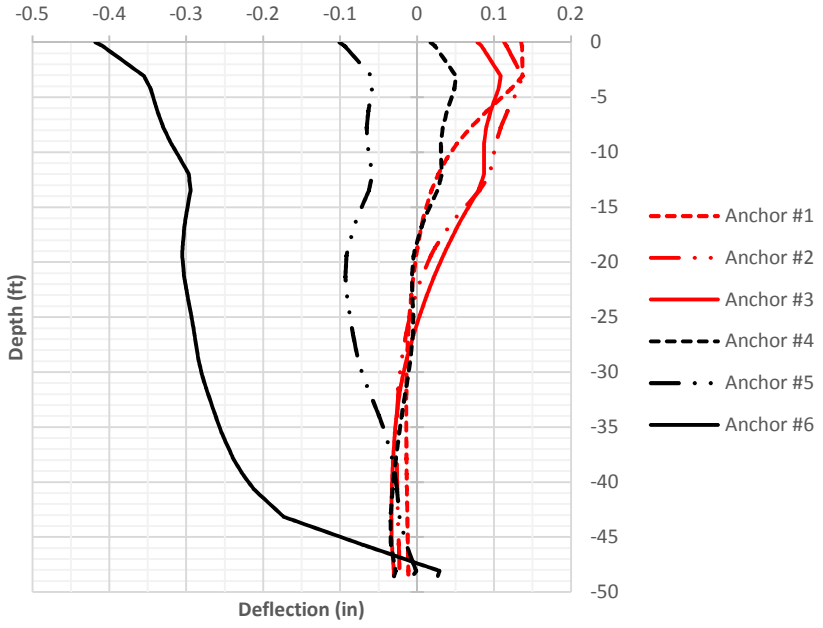


Fig. 11. Underpinning Deflection Profile

CONCLUSIONS

The support of excavation (SOE) system for the 2nd/Broadway station was designed based on METRO criteria using the limit equilibrium method. It was shown it is extremely important to model all construction stages to calculate maximum possible loads in the SOE system. Calculated lateral bracing loads at every construction stage were used as benchmarks to verify assumptions made during the design process. They also helped to develop contingency plans in case excessive loads were observed.

A challenging underpinning system consisted of ground anchors and concrete panels/diaphragms were designed and constructed to support part of the LA Times building that protruded into the station as well as building foundations that sit adjacent to the station. The underpinning elements were designed based on results from the limit equilibrium method and then the deflection was checked with finite element analysis (FEA). Data from settlement and tilt sensors showed minimal movement which was aligned with FEA model outputs.

REFERENCES

Deep Excavation, 2019, http://www.deepexcavation.com/en/deepxcav-2011

Los Angeles County Metropolitan Transportation Authority, 2010, Metro Rail Structural Standard Cut & Cover Underground Structures, Los Angeles, CA.

PLAXIS, 2019, https://www.plaxis.com/product/plaxis-2d/

DEEP FOUNDATIONS FOR TOP-DOWN CONSTRUCTION OF HIGH-RISE PROJECT

Kenneth S. Hudson, Wood Environment and Infrastructure Solutions, Inc., Los Angeles, California, USA, 323-208-2572, kenneth.hudson@woodplc.com
Martin B. Hudson, Ph.D. Wood Environment and Infrastructure Solutions, Inc., Los Angeles, California, USA, 310-497-5033, marty.hudson@woodplc.com
Gwendolyn Arreguin, Wood Environment and Infrastructure Solutions, Inc., Los Angeles, California, USA, 323-365-8473, gwendolyn.arreguin@woodplc.com

Keywords: High-rise, Osterberg load cells, drilled shafts, end-bearing, construction, Los Angeles

ABSTRACT

A twin high-rise project site in Century City posed several foundation engineering challenges for the design team. One portion of the twin high-rise project site was required to utilize top-down construction in order to allow a driveway to remain open during construction of the project's 40-foot deep excavation. The challenge was compounded by the need to utilize a mat foundation to support the high-rise construction and yet have temporary drilled shafts through the mat foundation area that would not create excessive differential settlement. This was accomplished by constructing a deck supported by eight drilled end-bearing drilled shafts with Osterberg load cells and five 7-foot-diameter end-bearing drilled shafts. The Osterberg load cells served to verify the capacity of each of the drilled shafts and preload the soils at the drilled shaft tips. The 7-foot-diameter shafts were constructed with bond breakers to prevent skin friction but instead mobilize end bearing (for settlement compatibility with the surrounding mat foundation). After the drilled shafts were placed, then top-down construction began beneath the driveway, leaving the driveway supported on the drilled shafts. Construction challenges included drilling of the shafts through previously abandoned tieback anchors from an adjacent parking structure basement, as well as cemented layers within the rock materials. The paper describes the use of the various analytical methods used to calculate capacities and check settlement compatibility, the construction and testing methods utilized, and the construction challenges encountered.

INTRODUCTION

Wood Environment and Infrastructure Solutions, Inc. (hereafter referred to as Wood) performed a geotechnical investigation for the New Century Plaza currently being constructed in the Century City District of Los Angeles, California. The New Century Plaza project consists of the construction of two new towers (designated as North and South Buildings) and the rehabilitation of the existing Hyatt Regency Century Plaza Hotel. The existing hotel tower is 15 stories in height above the existing grade and is underlain by four subterranean basement parking levels. The new North and South Buildings will stand approximately 46 stories in height above the existing grade to accommodate residential use. The new towers are planned west of the existing hotel. The site was previously occupied by the existing hotel subterranean parking structure and overlying podium structure, and a loading dock in the southwest portion of the site. The former western portion of the podium and subterranean parking structure west of the existing hotel building western edge were demolished to allow for new subterranean levels, a new podium structure, and the new towers. The lowest floor of the proposed subterranean level required excavation on the order of 35 to 80 feet.

The geologic materials at the site consist of fill soil underlain by Late to Middle Pleistocene-age alluvial fan deposits. The alluvial fan deposits are in-turn underlain by marine deposits identified as the San Pedro formation. The San Pedro formation consists of silty sand, sand, and clayey sand with layers of clay and silt and local gravel and cobbles deposited in a marine setting. The deposits are dense to very dense throughout the depth explored. Localized cobbles and highly cemented beds are present throughout the

© 2019 Deep Foundations Institute

alluvial fan and marine deposits. In the boring performed in close proximity to the subject area, the raw blow counts obtained in the very dense, poorly graded sand with a Standard Penetration Test sampler, near the planned shaft tip elevation, were 77 blows per 9 inch penetration (refusal) at a depth of 56 feet, and 98 blows per 9 inch penetration (refusal) at a depth of 66 feet in the boring.

Groundwater encountered is generally perched and semi-perched occurring as seepage in the permeable layers of the older alluvium and marine deposits. Little to no seepage was encountered in the fill zones. Groundwater was measured at approximately 69 feet below ground surface in the recent borings. Borings drilled at the site in 1962 indicated groundwater seepage encountered at depths ranging from 40 feet to 74 feet below the then-existing ground surface.

The existing hotel tower had been supported originally on spread footing foundations. For support of the new towers, Wood recommended a mat foundation be used. The structural design of the mat foundation was performed by Englekirk Structural Engineers. The mat is thickest under the core of each tower (13 feet thick), tapering to 3.5 feet thick near the perimeter of the new basement structure. Wood performed three-dimensional finite difference evaluation of the settlement characteristics at the site using FLAC3D and estimated that the settlement of the tower would be about 4 inches at the center of the towers, decreasing to about 2 inches at the edge of the mat.

TOP-DOWN SECTION

The western portion of the site contained a driveway to an adjacent building loading dock that needed to remain open during construction of the project. However, part of the new basement structure needed to be constructed under a portion of the driveway, and foundations for a portion of the new structure needed to be constructed beneath the driveway. Therefore, it was decided to use a top-down technique wherein a temporary deck could be constructed and left in service during construction of the project, while the new construction took place below the deck. Figure 1, Location Plan, shows the approximate area of the loading dock and temporary driveway.

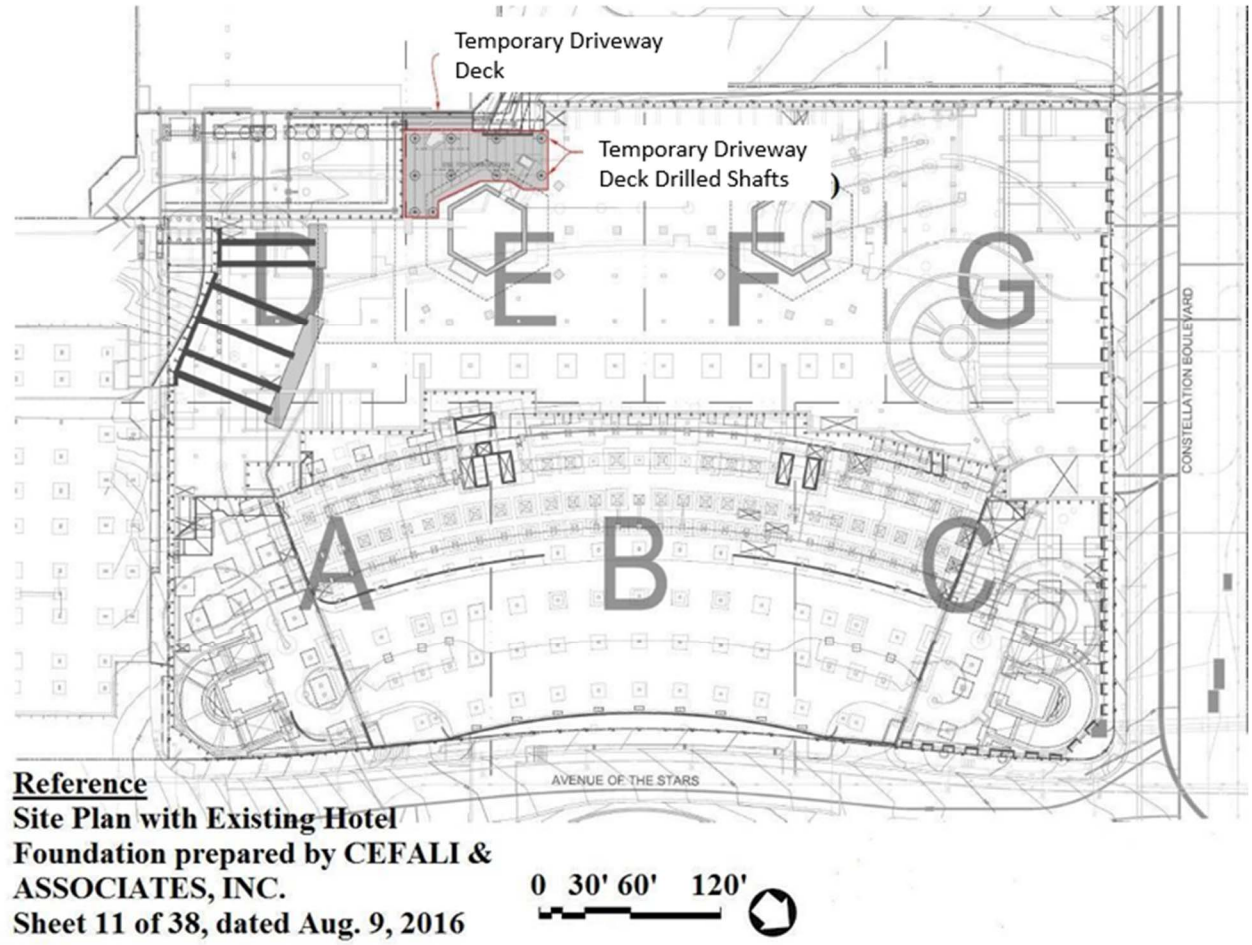


Fig. 1. Location plan showing loading dock deck and drilled shaft locations

In order to leave the driveway in place, a temporary deck was needed. Therefore, a separate foundation system had to be constructed for support of the temporary driveway deck and allow for the eventual construction of the underlying mat foundation when excavation of the basement was completed. The temporary deck foundation consisted of drilled shaft foundations, which allow for the top-down sequence. The upper portion of the drilled shaft foundations within the depth to become subterranean levels consisted of H-beams surrounded by sand-cement slurry. The sand-cement slurry allowed the H-beam to be exposed as excavation progressed under the temporary deck. The sequence of construction was as follows, and is illustrated on the following pages.

Step 1: drill shaft/subterranean column foundations, as illustrated in Figure 2.

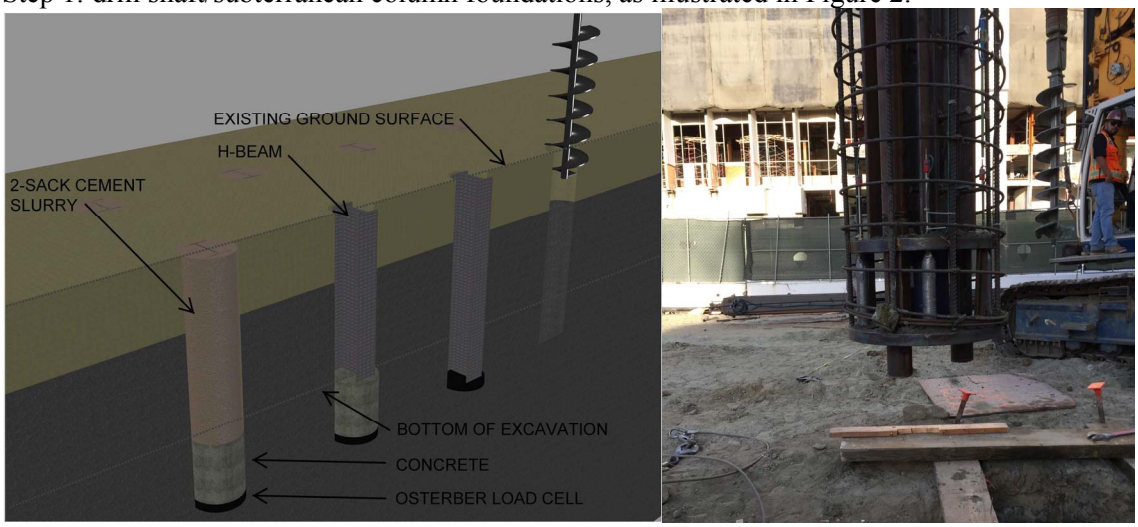


Fig. 2. Step 1 - construct drilled shaft/columns from ground surface

Step 2: construct temporary deck supported by drilled shaft foundations, as illustrated in Figure 3.

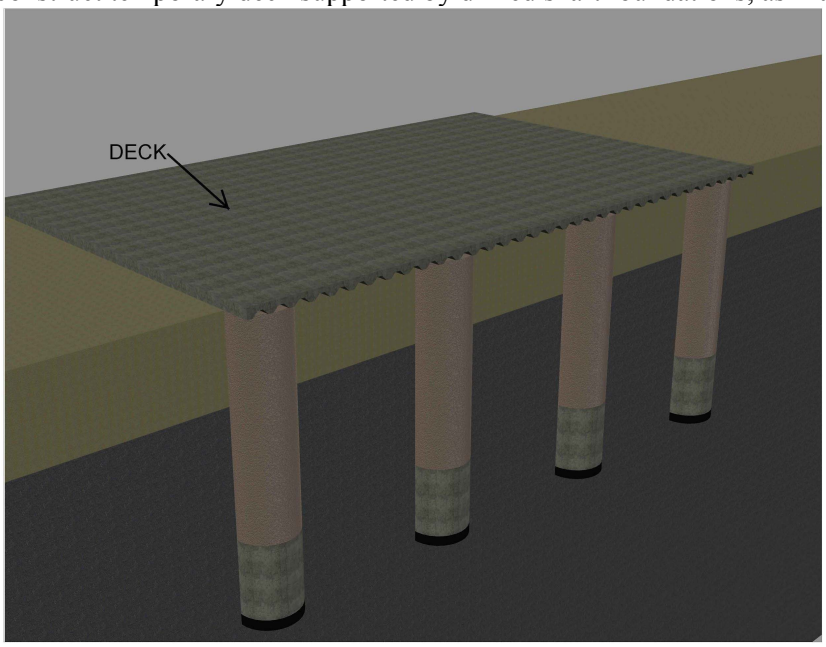


Fig. 3. Step 2 - temporary deck

Step 3: excavate first level below deck, as illustrated in Figure 4.

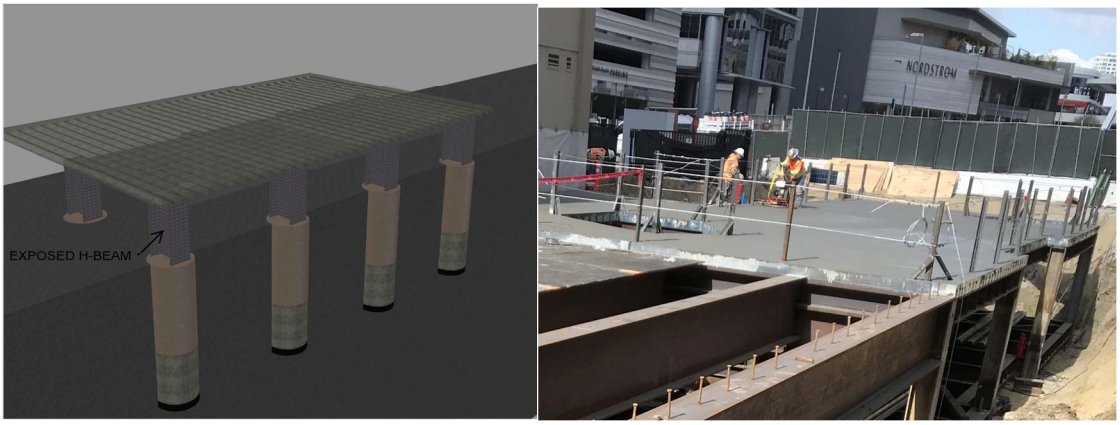


Fig. 4 - Step 3 - excavation below deck

Step 4: construct beams between columns at elevation of bottom of first subterranean level, as illustrated in Figure 5.

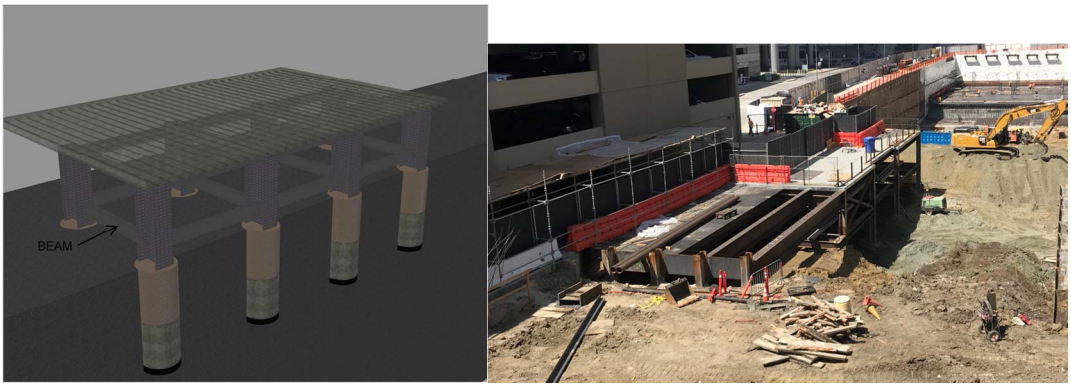


Fig. 5. Step 4 - construct beams between columns as excavation progresses

Step 5: excavate second level below deck, as illustrated in Figure 6.

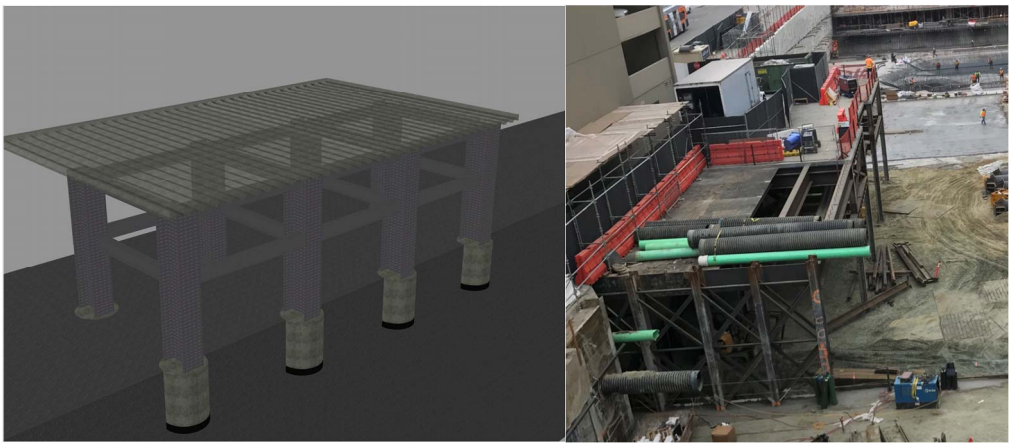


Fig. 6. Step 5 excavate second level

Step 6: construct mat foundation around columns, as illustrated in Figure 7.

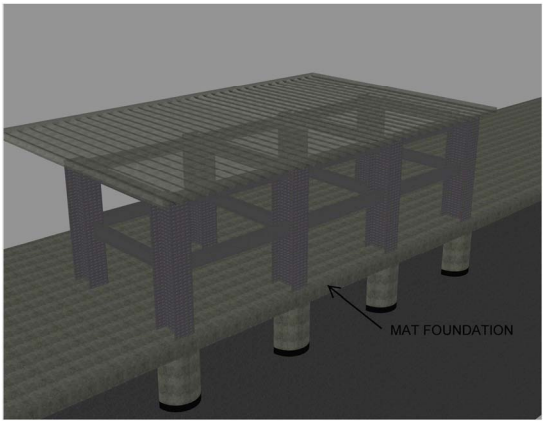


Fig. 7. Step 6 construct mat foundation

In this area, the top-down drilled shaft foundations needed to be designed with just sufficient capacity (i.e. no more than minimum Factor of Safety) to support the temporary deck and the intermediate structural elements during construction. However, after the eventual structural connection of those drilled shafts with the surrounding mat foundation, the drilled shafts would be required to eventually have settlement matching the settlement of the mat foundation at the location of the drilled shafts. Hence, the drilled shafts had to be designed in a manner that, after connection to the mat foundation, the shafts would plunge when the planned mat foundation is anticipated to settle due to the weight of the eventual high-rise superstructure. This criterion was necessary to prevent the temporary drilled shafts from becoming "hard spots" that could potentially result in too little settlement in those locations, potentially resulting in excessive differential settlement across that portion of the planned mat foundation. This set of constraints required that the capacity of each drilled shaft be evaluated and tested as precisely as possible, then design the drilled shaft length with no more than required to support the temporary loads until connected to the mat foundation. The decision was made to utilize Osterberg Load Cells for these purposes as described below.

DESIGN OF DRILLED SHAFTS

A design allowable bearing pressure of 43 kips per square foot was recommended for the drilled shafts at the top down section. This value was based on drilled shaft end bearing for shaft tip deflection equal to 10% of shaft diameter ($q_{b,10\%}$) using Lee and Salgado 1999, Salgado, 2006a, 2006b, and Salgado and Prezzi, 2006, and a Factor of Safety of 2.0. This computation was based on a relative density, D_R, of 92.5 (based on the corrected SPT blow counts indicating very dense sand), an assumption of $K_0 = 0.5$, and embedment of 5 feet (representing the condition after excavation for the basement and mat foundation), an effective friction angle of 43 degrees, and a unit weight of 120 pounds per cubic foot. Similarly, the total allowable skin friction was estimated using Navy Facilities Engineering Command, 2012, for 5 feet of embedment below the excavation bottom, to be between 2 and 3 kips (using a soil/shaft friction angle of 0.75*43 = 32 degrees, and $K_{HC} = 0.7$, and a Factor of Safety of 2.0). Elastic settlement of the drilled shafts was calculated to be in the order of 1 to 1½ inches under service loads of the deck alone. After connection of the drilled shafts to the mat foundation, and after loading of the mat foundation, the drilled shafts will cease to serve their original function, and the drilled shafts will settle along the mat, up to about 4 inches.

OSTERBERG TESTING OF DRILLED SHAFTS

First, three non-production test drilled shafts were installed with total depths of 70, 60 and 42 feet to test the capacity of drilled shafts of varying length, and to understand the variability of capacity with depth. The

load tests were performed using Osterberg down-hole hydraulic load cells (O-cell) placed at the bottom of the drilled shafts to measure the capacity of the drilled shafts, and to preload the base of excavation (end bearing) of the drilled shafts. In addition, the capacity confirmation and end bearing pre-loading of the production drilled shafts was performed using O-cells. The load cell testing was performed by LoadTest.

The test drilled shafts were instrumented with vibrating wire strain gages (Geokon 4911 "sister bars") attached to the to the longitudinal steel reinforcement to allow for monitoring of the axial strain at selected depths in the drilled shafts during the load tests. The tests were performed in accordance with ASTM D1143 (Procedure A: Quick Test (which has now been superseded by ASTM D8169)). As each cell was expanded, an equal load is applied to the movement of the jack plate and the bottom of the drilled shaft. Displacement versus upward drilled shaft friction and downward end bearing of each drilled shaft was recorded to determine the drilled shaft behavior. The displacement of the bottom and top plate of the O-cell was independently measured. The details of test drilled shafts as shown on Table 1.

Table 1. Test Drilled Shaft results

Test Drilled Shaft Designation	As-Built Elevation of Base of O-Cell	As-Built Drilled Shaft Diameter (in)	Elevation of Tip of Test Drilled Shaft (ft)	As Built Length of Test Drilled Shaft (ft)	O-Cell Maximum Load Applied (kips)	Calculated Ultimate End-Bearing Capacity (Kips)*
TP-1	200.0	32.0	197.6	70.0	1,017	780
TP-2	217.9	34.0	216.0	60.0	976	750
TP-3	225.5	28.5	223.2	42.7	296	560

*Capacities calculated for a 24-inch diameter drilled shaft and lengths 30, 61, 66 feet below current grade.

The ultimate bearing capacity of the test drilled shafts was taken as the load at which end displacement reached 10% of the diameter of the drilled shaft. Based on the test results, the 10%-diameter bearing capacities of TP-1, TP-2, and TP-3 were 500, 1017, and 85 kips, respectively. See an example of the load-deflection test results for one of the test drilled shafts, TS-1, as shown on Figure 8.

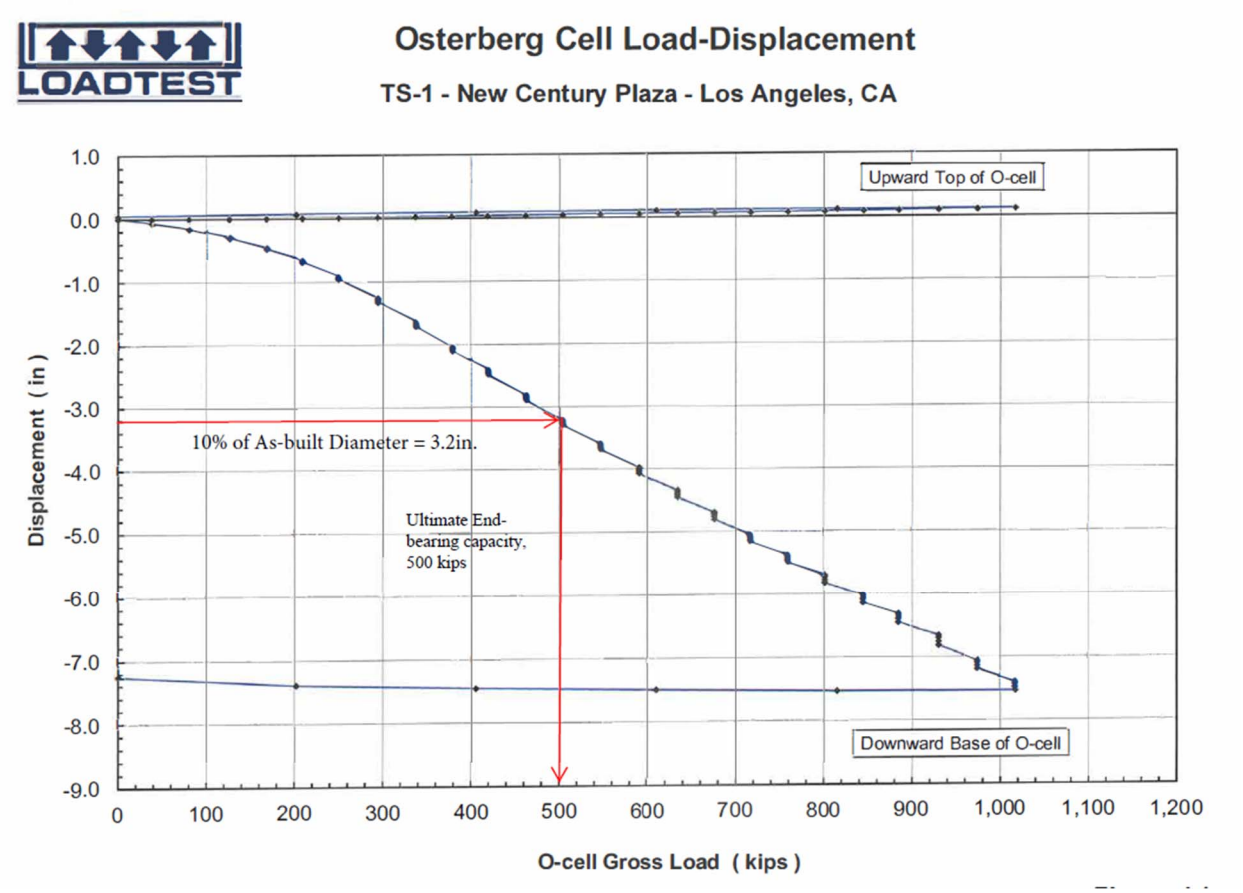


Fig. 8. O-Cell test load results for test drilled shaft TS-1

The ultimate skin friction capacity corresponding to the upward movement of the O-cell top plate was evaluated based on the Brinch-Hansen 90% criterion as described in FHWA-RD-99-170 and Dotson (2013). The Brinch-Hansen 90% Criterion defines the ultimate drilled shaft capacity as the load that is associated with twice the drilled shaft head deflection as obtained for 90% of the ultimate load. The Brinch-Hansen 90% Criterion allows for the interpretation of ultimate capacity from load tests which do not achieve failure (i.e. drilled shaft ultimate capacity), using a methodology based on an assumed stress-strain relationship for the soil near ultimate capacity.

An example plot of the upper plate of the load cell and strain gauges at different depths within the drilled shaft, used to interpret the ultimate skin friction capacity at varying depths in the drilled shaft, are presented on Figure 9 for TP-1.

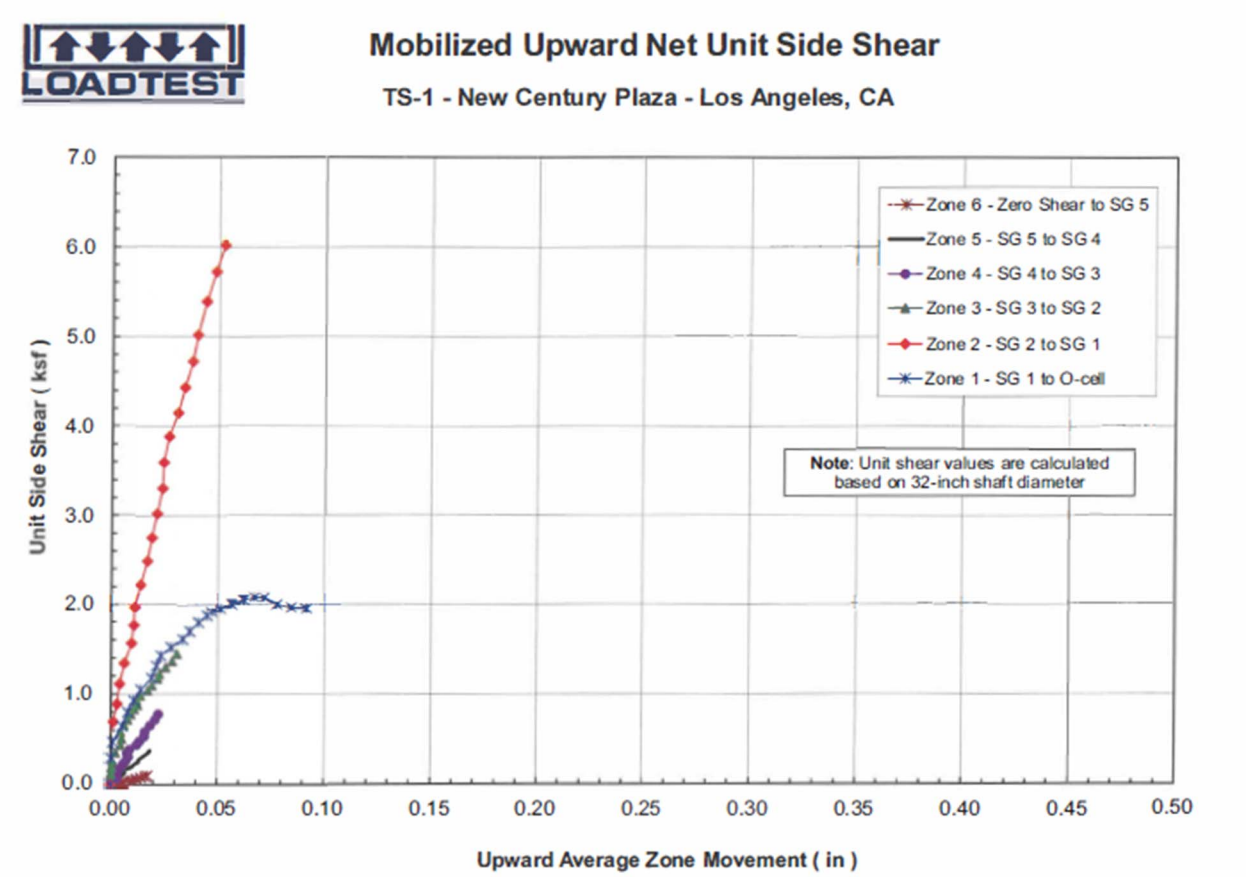


Fig. 9. Skin Friction test results using O-cell and strain gauges

The mobilized unit skin friction capacities for TP-1 through TP-3 within the zone of interest are shown in Table 2 and were calculated using the data obtained from the unit side shear graphs and transformed using the Brinch Hansen Transformation method.

Table 2. Skin friction capacity results

Test Drilled Shaft Designation	Side Friction Depth Interval of Interest (ft)	Mobilized Unit Skin Friction* (lb/ft^2)	Drilled Shaft Head Upward Deflection (in)
TP-1	60 to 70	246	0.09
TP-1	49 to 60	N/A	0.05
TP-1	38 to 49	7,169	0.03
TP-2	45 to 52	515	0.31
TP-2	39 to 45	4,305	0.27
TP-3	33.5 to 45	10,788	0.04

* Some values shown are estimated ultimate values using Brinch-Hansen 90% Criterion

Based on the interpretation of the drilled shaft load tests described above, Table 3 presents the recommended drilled shaft lengths for the eight production drilled shafts. These final recommended lengths represented higher end bearing capacities and skin friction than estimated using engineering and empirical methods computed before the testing. The recommended capacities were based on the average ultimate unit skin friction and average end bearing from the load testing, with a factor of safety for end bearing and skin friction of 2.0. Some of the drilled shafts were drilled to a slightly greater depth than originally intended, and thus the O-cell loads were increased to account for the skin friction that would develop (in addition to the end bearing) for the length of drilled shaft below the O-cell.

Table 3. Summary of Recommended Drilled Shaft Lengths and O-cell loads

Drilled Shaft Designation	P1	P2	P3	P4	P5	P6	P7	P8
Drilled Shaft Diameter (in)	48	42	36	30	33	33	30	30
Load Demand (kips)	595	361	255	129	152	105	149	91
Drilled Shaft Length Below Bottom of excavation	17.5	11.0	10.0	9.5	7.3	5.0	10.5	7.0
O-cell Loads (Kips)	566 628*	433 488*	318 365*	221	266	210	221	182
*O-cell jack load to account for skin friction for drilled shaft length below O-cell								

The eight drilled shafts were installed at the existing ground surface prior to excavation. After the drilled shafts were installed and tested in Step 1, the temporary loading dock was established at the existing ground surface (Step 2). In this manner the contractor was able to excavate beneath the loading dock and around the supporting drilled shafts – chipping out the sand-cement slurry surrounding the drilled shafts, leaving the steel columns to support the deck – until the excavation reached the planned mat foundation bottom for the permanent structure below the loading dock.

The use of O-cells at (or near) the base of the production drilled shafts also verified the end-bearing capacity of each of the production drilled shafts without the need of personnel to descend into the borehole to verify firm and cleared bottom.

7-FOOT-DIAMETER DRILLED SHAFTS

A portion of the podium structure at the west end of the project (south of the previously-described temporary O-cell loaded top-down drilled shafts) was designed to be supported on five 7-foot-diameter end bearing drilled shafts. These drilled shafts served both as permanent support of a portion of the structure, and a secondary purpose during construction as support for the temporary driveway. In this area, there was no need to excavate basement levels beneath the ground surface, and therefore top-down techniques were not required. The drilled shafts were designed to be fully end bearing to achieve reduced differential settlement between the drilled shaft-supported portion of the new development and the mat foundation-supported portion of the new development. In order for the drilled shaft to achieve settlement comparable to the mat

foundation, a bond-breaker was used along the shaft so that skin friction was not mobilized. The bond-breaker was achieved by installing a steel casing and coating the interior with bitumen. Cleaning and inspection of the bottom of the shafts was necessary to confirm a firm, clean surface was achieved. In order to safely allow personnel to clean and inspect the base of these large-diameter shafts, steel casing was used, with an air supply. The bond-breaker material was manually applied to the interior of the steel casing after placement of the casing in the excavation. The casing extended to the bottom of the shaft with a vertical separation of at least 3 inches between the bottom of the drilled shaft cap and the top of the casing to prevent engagement of the top of the casing by the drilled shaft cap. Furthermore, the vertical separation at the top of the drilled shaft had a sonotube used to prevent overpour of concrete over the casing, to avoid engaging the casing by the drilled shaft. See Figure 9 for photographs of the large-diameter drilled shafts.



Fig. 9. Large Diameter Drilled Shafts during construction - view looking down shaft, and view of top of shaft.

SUBSURFACE CHALLENGES

In addition to the challenges of the foundation design, there were challenges due to subsurface conditions at the locations at which the drilled shafts were installed. The drilled shafts were drilled close to the property line with pre-existing tie-back anchors that had been installed to temporarily support excavation during construction of the basement at the adjacent property. Therefore, during drilled shaft drilling, core barrels had to be used to grind through the grout and steel of the tie-backs. The shafts also had to be particularly straight - including being measured with a sonic caliper after completion - because of the tight fit of the O-cell; therefore, the grinding through tie-backs with the core barrel was a slow process so that the hole would not lose verticality.

Limited, relatively thin cemented layers within the San Pedro dense sand formation also presented similar difficulties for drilling as the tiebacks presented. There was one zone approximately 2 ft thick of highly cemented fossiliferous sandstone to conglomerate at approximately 50 ft below the ground surface. There were shells in the cemented zone up to 3 inches in diameter; the cementitious material in the sandstone was identified as calcite. Above and below the cemented layer was an uncemented, poorly graded sand. Amec Foster Wheeler's interpretation for the existence of the cemented zone is that the layer was deposited by a turbid current that brought the coarser sand, cobbles, and shells to the deep marine setting of the San Pedro formation. As it was buried, the shells leeched calcite into the pore space of the surrounding soil which cemented it into a very hard layer. This hard layer had to be cored-through using the core barrel similarly to the coring through tie back anchors.

CONCLUSIONS

The use of O-cells in temporary drilled shafts allowed for top-down construction to occur while also allowing settlement compatibility with the permanent mat foundation used for support of the structure. Testing and analysis was performed to reduce drilled shaft length to as short as possible, because in this case, excessively long temporary drilled shafts would potentially increase the differential settlement of the mat foundation. The use of large diameter end bearing shafts was successfully performed in order to provide compatible settlement between a portion of the structure and the mat foundation. The analytical techniques utilized to analyze the various foundation types were found to be successful in reasonable estimates of capacity of the top-down drilled shafts.

ACKNOWLEDGEMENTS

Thanks are given to Mr. Rick Arambulo and others at Next Century Partners, Englekirk Structural Engineers, Webcor Builders, Cefali & Associates Inc., Calex Engineering Co., and LoadTest for their skillful work and contribution to this project. In addition, thanks are given to Dr. Marshall Lew, Ms. Rosalind Munro, and Ms. Lan-Anh Tran of Wood for their involvement in the project prior to and during construction.

REFERENCES

Amec Foster Wheeler, 2015. "Report of Geotechnical Investigation, Proposed New Century Plaza, Avenue of the Stars, Century City, Los Angeles, California. Project No. 4953-14-1151."

Amec Foster Wheeler, 2016. "Supplemental Consultation - Drilled Shafts for Temporary Loading Dock Deck, Proposed New Century Plaza, Avenue of the Stars, Century City, Los Angeles, California. Project No. 4953-14-1151."

Amec Foster Wheeler, 2017. "Supplemental Geotechnical Consultation -Temporary Loading Dock, Pile Load Test Results and Recommended Pile Capacities, proposed New Century Plaza, Avenue of the Stars, Century City, Los Angeles, California. Project No. 4953-14-1151."

Amec Foster Wheeler, 2017. "Supplemental Geotechnical Consultation - Temporary Loading Dock, O-cell Test Loads, Proposed New Century Plaza, Avenue of the Stars, Century City, Los Angeles, California. Project No. 4953-14-1151."

Amec Foster Wheeler, 2017. "Supplemental Geotechnical Consultation - End Bearing Drilled Shafts, Proposed New Century Plaza, Avenue of the Stars, Century City, Los Angeles, California. Project No. 4953-14-1151."

ASTM International, 2007. Standard Test Methods for Deep Foundation Under Static Axial Tensile Load.

ASTM International, 2013. Standard Test Method for Deep Foundations Under Static Axial Compressive Load.

Dotson, Don W. 2013. "Direct Solution of the Brinch-Hansen 90% Pile Ultimate Failure Load." Deep Foundation Institute Vol. 7, No.1.

Federal Highway Administration, 1999. Extrapolation of Pile Capacity From Non-Failed Load Tests. FHWA-RD-99-170.

Lee, C. J., and R. Salgado, 1999. “Determination of Pile Base Resistance in Sands.” Journal of Geotechnical and Geoenvironmental Engineering, Vol. 125, No. 8, 673-683.

Navy Facilities Engineering Command, 2012, Navfac DM 7.02.

Salgado, R., 2006a, “The Role of Analysis in Pile Design,” in Modern Trends in Geomechanics, Wei Wu and H.-S. Yu (eds.), Spring Proc. Physics, Vol. 106, 521-540.

Salgado, R., 2006b, “Analysis of the Axial Response of Non-Displacement Piles in Sand,” Geomechanics II: Testing, Modeling and Simulation. Proc. 2nd Japan-U.S. Workshop, Geotechnical Special Publication, ASCE.

Salgado, R., and M. Prezzi, 2006, “Computation of Cavity Expansion Pressure and Cone Resistance in Sand,” International Journal of Geomechanics.

DESIGN AND CONSTRUCTION OF PERMANENT SHEET AND PIPE PILE BASEMENT WALLS WITH THE PRESS-IN PILING METHOD

Takefumi Takuma, Giken Ltd., Orlando, FL, 407-380-3232, ttakuma@gikenamerica.com
Tsunenobu Nozaki, Giken America Corp., New York, NY 916-340-5600, nozaki@giken.com
Masashi Nagano, Giken America Corp., New York, NY, 212-597-9331, nagano@giken.com

Keywords: press-in, permanent basement wall, sheet pile, pipe pile, low noise, low vibration

ABSTRACT

Using sheet piles and pipe piles for permanent earth retaining is one of the most economical methods for constructing basement walls since they can also work as temporary shoring during construction. A major mixed-use redevelopment project in the UK, encompassing two to three large city blocks, utilized both sheet and pipe pile walls for a two-level subterranean parking structure. The 290m (950ft) x 100m (330ft) basement's steel walls were designed to temporarily support excavation during construction and eventually to become a load carrying permanent structure in order to expedite the construction process and to achieve cost reduction. Two types of press-in piling machines, one for sheet piles and the other for pipe piles, were used for the job because of their abilities to press in sheet and pipe piles within tight tolerances for finished walls, for difficult installation conditions with very hard soil, and for its very low noise and practically zero-vibration operation; an essential factor for the job in close proximity to other businesses and residents.

BACKGROUND

Steel sheet pile and pipe piles have been used for many purposes including earth retaining. They are produced at steel mills and spirally welded at a fabrication yard to their corresponding specifications under strict quality control measures. Therefore, they can form highly reliable walls to its design capacity with proper installations. Their advantages as underground walls are:

- They can form a high level of water cut-off function with their interlocks sealed by welding or with hydrophilic materials. See Figure 1 for a few examples for a sheet pile application.
- They can carry vertical loading in addition to horizontal load and bending moment.
- They can be a self-standing and temporary/permanent wall with flexible design and construction processes; bottom-up, top-down or hybrid sequences can be chosen per the project's needs.
- They can form a thinner wall than other wall types, creating larger inner space. See Figure 2.



Figure 1 Typical Interlock Sealing Methods for Sheet Piles (Original Source: Nucor Skyline)

© 2019 Deep Foundations Institute

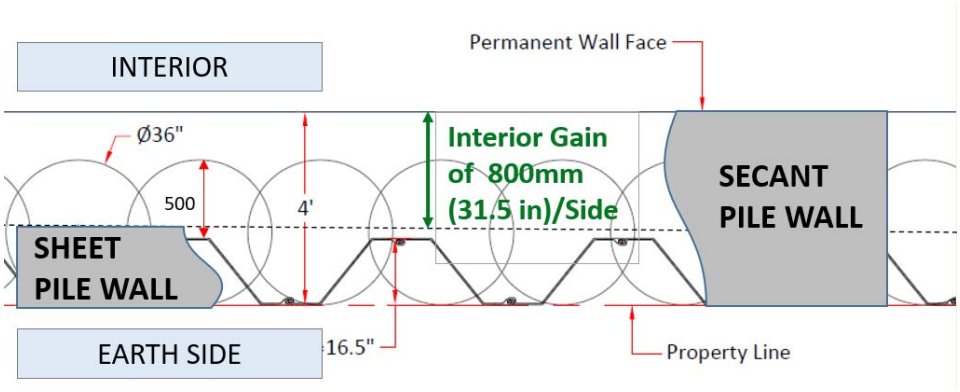


Figure 2 Comparison of Typical Sheet Pile and Secant Pile Wall Thickness
(Original Source: Nucor Skyline)

- They can be installed with low noise and practically no vibration if pressed in.

About 20 underground steel wall structures have been built in major U.S. cities.

Speaking of press-in piling, it utilizes a hydraulic force to push piles into the ground, thus practically eliminating the noise and vibration issue associated with typical pile driving. Conventional pile driving utilizes either percussive or vibratory pile driving methods, both of which generate high levels of noise and vibration, causing nuisance and potential damage to nearby structures. A commnly used press-in machine sits on top of already installed piles and is anchored with its own weight and additional counter weight when starting as shown in Figure 3. Once the first few piles are pressed in this way, the equipment grips on top of the already installed piles and moves forward on its own as the pile installation progresses without counter weights. This method does not use a vibratory or percussive force to install piles.

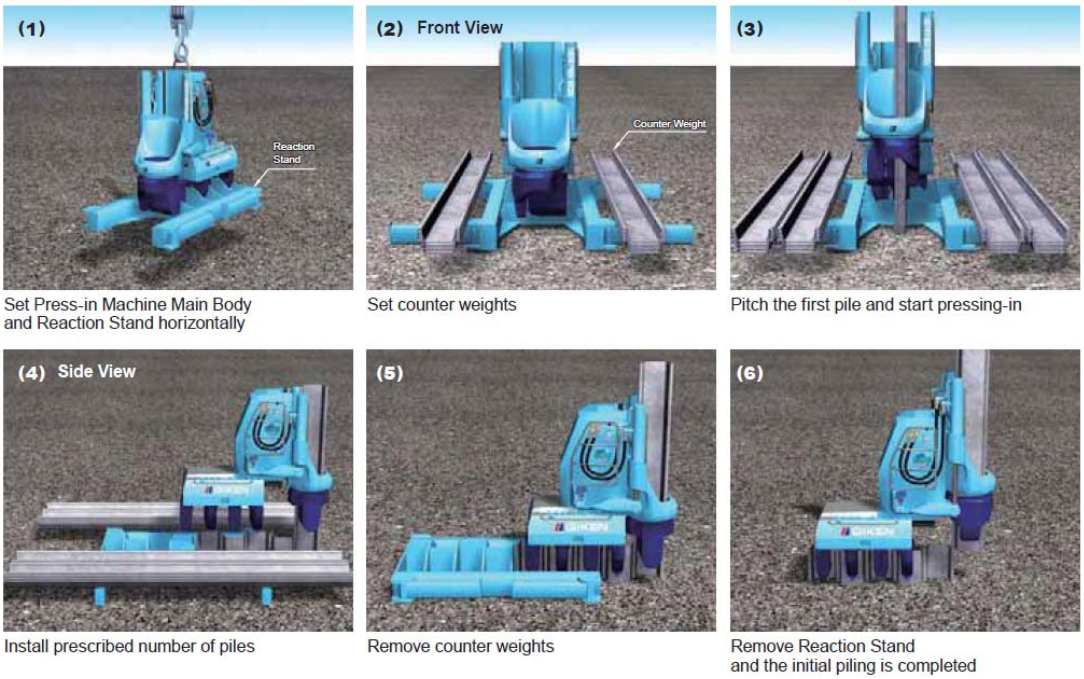


Figure 3 Starting of Press-in Piling

Main features of press-in piling are:

1. Low noise and practically vibration free (White et al., 2002). It enables piling projects close to

houses, schools, hospitals, and other sensitive structures as well as in the areas where sensitive fish and/or animals are around. This was one of the primary reasons that the piling method was adopted for the case study project to be discussed later in this paper.

2. The equipment size is relatively small while its clamping points are much lower than those of other pile driving methods. This feature enables the equipment to work in physically tight working conditions, both horizontally and vertically, such as an area under railway girders (Takuma et al., 2015) or right next to existing sensitive structures (Takuma et al., 2013).
3. With attachments, it can press in piles into hard soil effectively. A high pressure water jet or continuous flight auger attachement allows the piles to be installed simultaneously as the attachment loosens the hard soil without having to bring in a large predrilling machine. The latter attachment can work in dense sand, gravel, and cobbles with N-values much higher than 50 (Takuma et al., 2018). The case study project to be discussed used the auger attachment to facilitate its pile installation in siltstone with the SPT value close to 500.
4. It can achieve highly accurate pile installation due to a combination of the machine's ability to control the pile position/direction and lower clamping points.
5. Most of hot-rolled U- and Z-shaped sheet piles and pipe piles with its diameters ranging from 600mm (23.6 in) to 2,500mm (98.4 in) can be pressed in with the piling machines of this type in varying sizes and weight (https://www.giken.com/en/products/silent_piler/).

Case Study: Underground Parking Structure for St. David's 2 Mixed-use Redevelopment Project in Cardiff, the U.K.

Cardiff is the capital city of Wales, located in the southwestern part of Great Britain. Its St. David district once was an old-fashioned dense arcade shopping area. With recent redevelopment, the district has turned into one of the largest and most modern shopping centers in the country. St. David's 2, a part of this redevelopment project, built a four story building with 304 units of high-end apartments and 200+ retail spaces on top of two levels of an underground parking structure, completed in 2009. The design architect describes the project in the following manner, "Attracting more than one million visitors in its first week of trading, St. David's 2 is a major, retail-led, mixed-use city centre development in the heart of Cardiff" (https://www.chapmantaylor.com/projects/st.-davids-2). See Figure 4 for the plan view of the project site in relationship with the rest of the redevelopment and the surrounding environment, Figure 5 for the cross section of the structure, and Figure 6 for the plan view of the underground structure with the locations of the permanent sheet and pipe pile walls. Figure 7 shows the completed basement with the sheet pile wall.

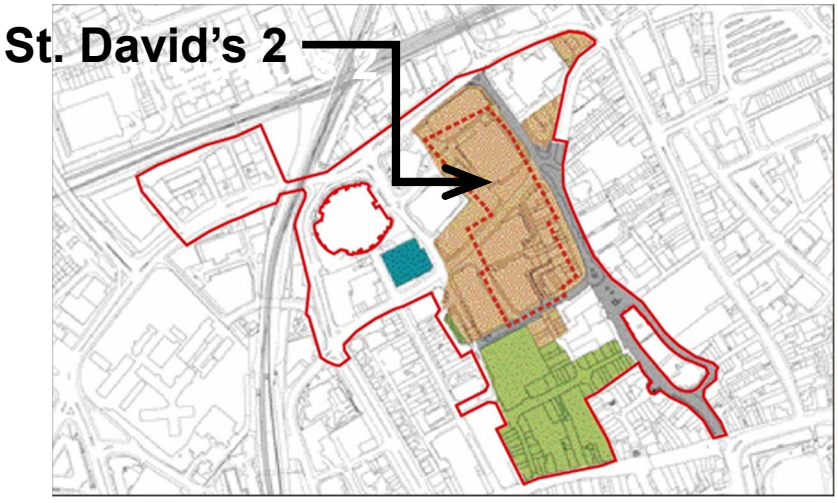


Figure 4 St. David's 2 Project Location (dotted red line) & Master Redevelopment Envelope

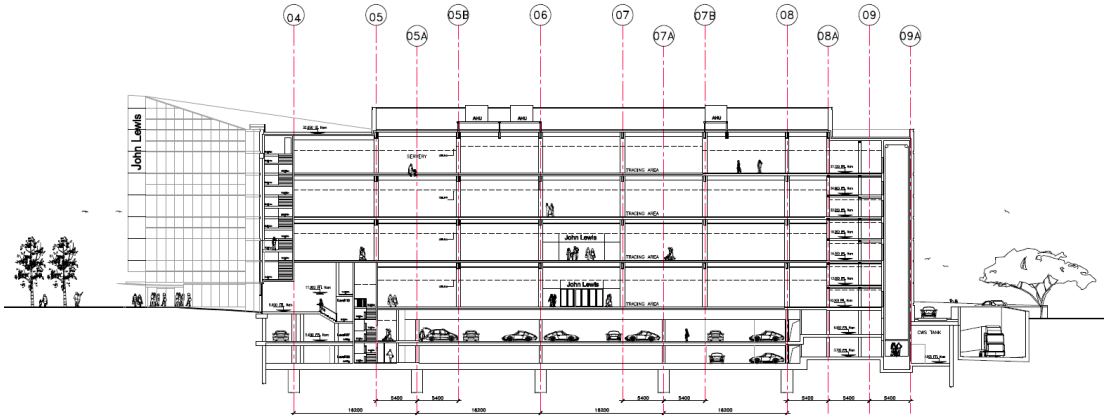


Figure 5 Cross Section of St. David's 2 Structure w/ 2 Levels of Basement

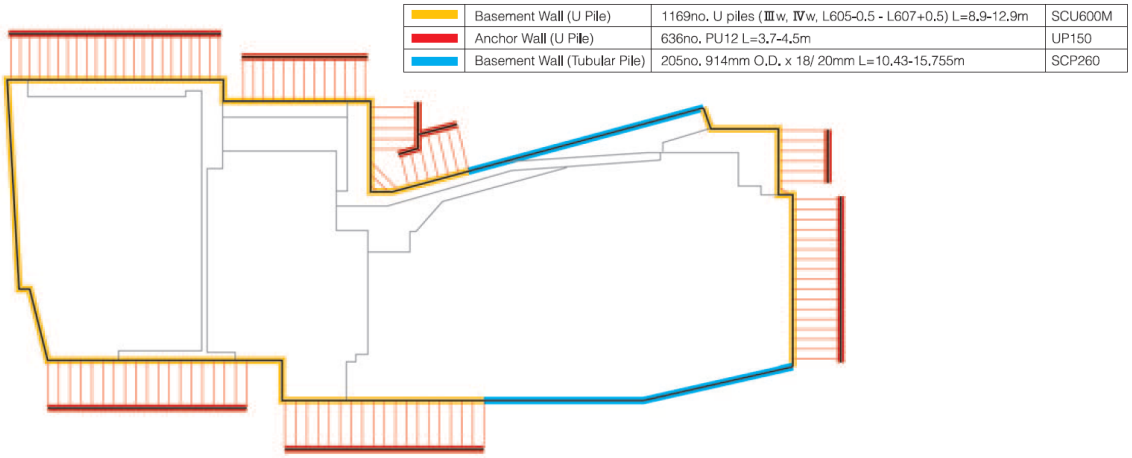


Figure 6 Plan View of Sheet and Pipe Pile Basemant Walls

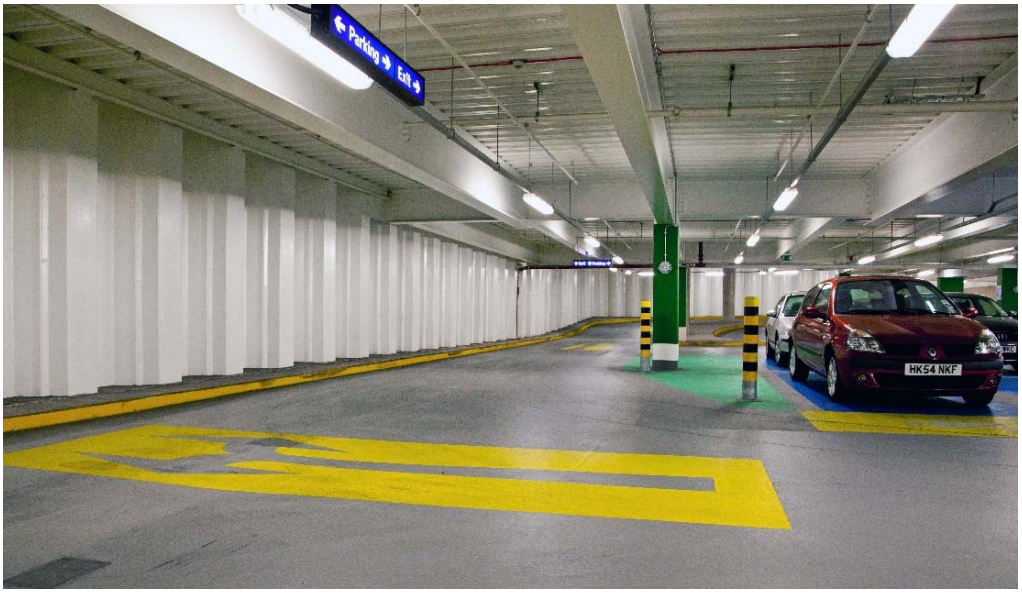


Figure 7 Completed Sheet Pile Wall Section of Basement Parking Space

Although secant pile walls had been first considered for the basement walls, steel pile walls were constructed for the following reasons.

- It was feared that many concrete mixer trucks for secant pile wall construction would generate extra traffic volume, noise, and dust in the highly congested project and surrounding areas.
- Steel pile walls would shorten the construction period with cost advantages over secant pile walls per the project team's comparison.
- The press-in piling method would be able to provide realtime monitoring of a pile's ultimate bearing capacity even in the project's complex and changing geological conditions.

Figure 8 shows the project's typical geological conditions with the sheet pile and pipe pile walls. Mudstone and underlying siltstone as bedrock, both of which are categorized as Marcia Mudstone Group at -8m (26 ft) and below, had the SPT values between 100 and 500; necessitating the use of an auger attachment for both sheet and pipe piles' press-in installation. The ground water table was at about -6m (20 ft) where the B2 level would be, requiring a high level of water cut-off measures to meet the specifications.

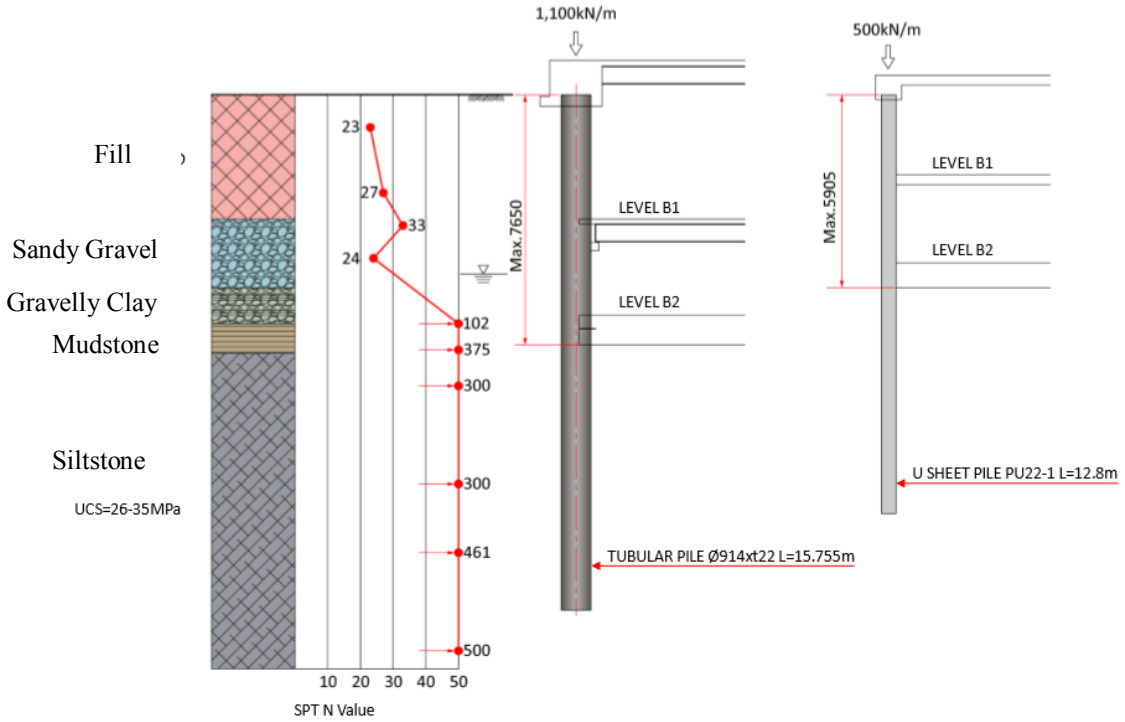


Figure 8 Typical Geological Conditions and Basement Wall Arrangement

The basement was designed based on the design criteria summarized in Table 1. Basement Grades as referred to on line 2 are corresponding to the intended use of the basement. Underground automobile parking structures are categorized as Grade 1 and commercial/residential areas are as Grade 3 per British Standard 8102:2009. Some seepage and dampness are tolerable in Grade 1 structures while they are not acceptable for Grade 3. Further, Line 3 shows vertical loading conditions that would be carried by the wall piles as permanent structures.

Table 1 Basement Design Criteria

Design Life of Retaining Wall	100 years
Basement Grade (BS 8102:2009)	Grade 1 (Car Park) and Grade 3 (Other area)
Working Load on Retaining Wall	500kN/m run (300kN/pile) on U sheet pile wall and 1,100kN/m run (1,075kN/pile) on tubular pile wall
Surcharge Loading behind Retaining Wall	10kN/m^2
Movement under Lateral Loads	Limit of vertical movement of wall elements; 25mm
	Limit of horizontal movement of wall elements; 20mm
	Limit of differential movement between adjacent columns and basement; 1 in 500
Piling Tolerances	Deviation in plan normal to the wall line at the top of the pile; ±25mm
	Deviation of verticality along line of piles; 1 in 100

The press-in force monitoring system, as part of the press-in piling machine, records the press-in and extraction force realtime. When a pile is pressed in, the measured press-in force is a combination of toe resistance and surface friction with surrounding soil. When extracted by counteracting the surface friction, the recorded force is equivalent to the friction plus the pile's weight. By comparing these two readings, one can calculate the amount of net toe resistance.

At the project, in order to determine the piles' bearing capacity and also to establish a quality assurance procedure for the production piles' capacity, test piling including a static load test was conducted on eight unconnected U-shaped sheet piles at different locations on the project site prior to construction. Two of them were installed to the depth of the planned excavation for the basement construction while six others were driven down to the design toe elevation, giving two sets of friction values; one for the depth of the excavation and the other for the entire penetration. A pile extraction test was done 7 days after installation so the surrounding soil would form an increased bond to the pile (time effect), yielding a higher friction value at the time of extraction. The counterweight used for static load testing was weighing 680kN (153 kips), which was based on twice (reflecting 2.0 of the factor of safety) the specified working load of 300kN (67 kips)/pile plus the 80kN (18 kips) friction contribution above the bottom of the excavation. See Figure 9 for the static load testing on site. Figure 10 shows one of the load v. dispalcement results with the maximum settlement of 5.58mm (0.22 in) and residual settlement of 4.21mm (0.17 in).



Figure 9 Static Load Testing on Sheet Pile

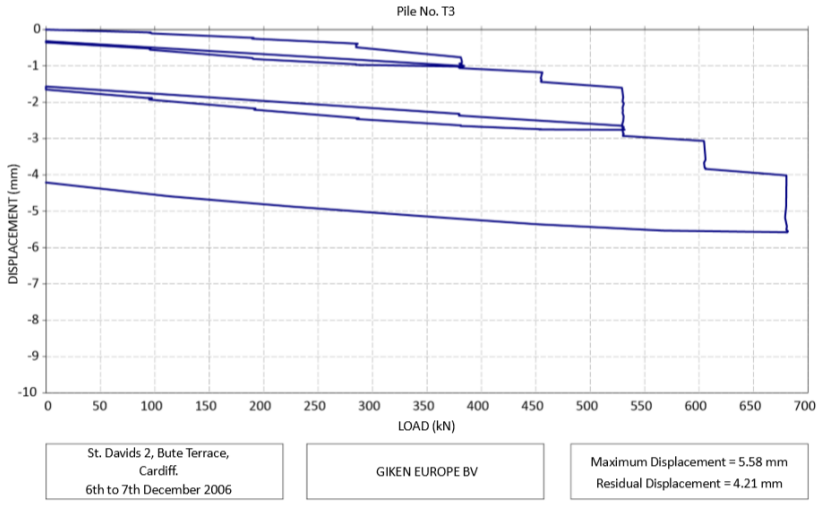


Figure 10 Load vs. Settlement Result by Static Load Test

The test piles' settlement was assessed with the Fleming's Method (1992), which was originally developed for bored piles. The test pile shaft and base diameters were adjusted to apply the method for this analysis for preparation of the ultimate loading capacities with static and dynamic friction. It was so concluded that a net toe resistance value of 230kN (52 kips) be required to satisfy the specified 300kN (67 kips) per pile loading capacity including skin friction. Similar testing and analysis were done on two pipe piles during the initial stage of pipe pile installation, resulting in the required net toe resistance value of 650kN (146 kips) per pile.

As mentioned earlier, an integraded auger attachment was utilized for facilitating pile installation into the siltstone bedrock. In order not to disturb the load bearing base, the auger's drilling operations was holted right at the pile's design toe level with the actual pile kept at a higher level. Then the auger was raised slightly while the pile was pressed down to the design toe level. Figure 11 shows this operation after the auger attachment was raised upon completion of drilling.

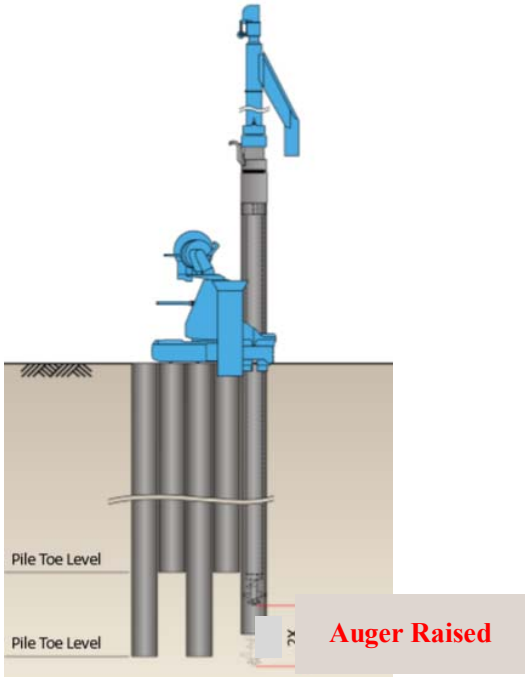


Figure 11 Pressing in Pipe Pile to Design Toe Level with Auger Attachment Raised

Since the press-in piling operation could monitor realtime press-in force all the way down to the pile's design toe elevation, the loading capacity of each and every pile was verified by comparing the aforementioned net toe resistance at ending against the required value of 230kN (52 kips) for sheet pile and 650kN (146 kips) for pipe pile. The average net toe resistance of production piles at refusal was 283kN (64 kips) for sheet piles and 1,041kN (234 kips) for pipe piles.

Speaking of seepage control, a combination of welded interlocks, water stop plates along with secure slab connections, and the application of hydrophilic materials were used. Figures 12 and 13 show the sheet pile wall's slab connection preparation while Figures 14 and 15 show that of the pipe pile wall.

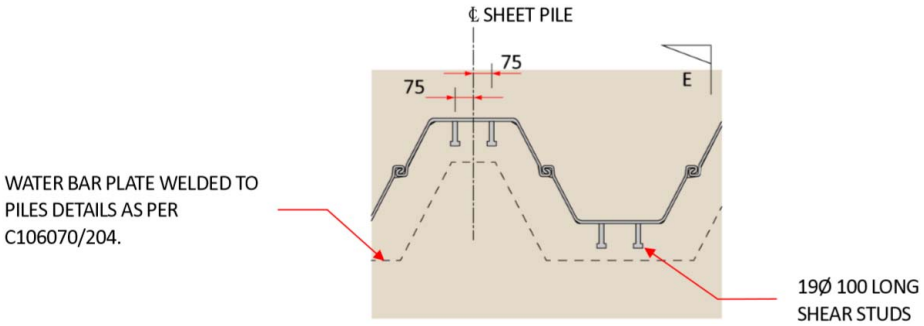


Figure 12 Plan View of Sheet Pile Wall's Slab Connection



Figure 13 Sheet Pile Wall's Slab Connection with Water Stop Plate and Hydrophilic Tape

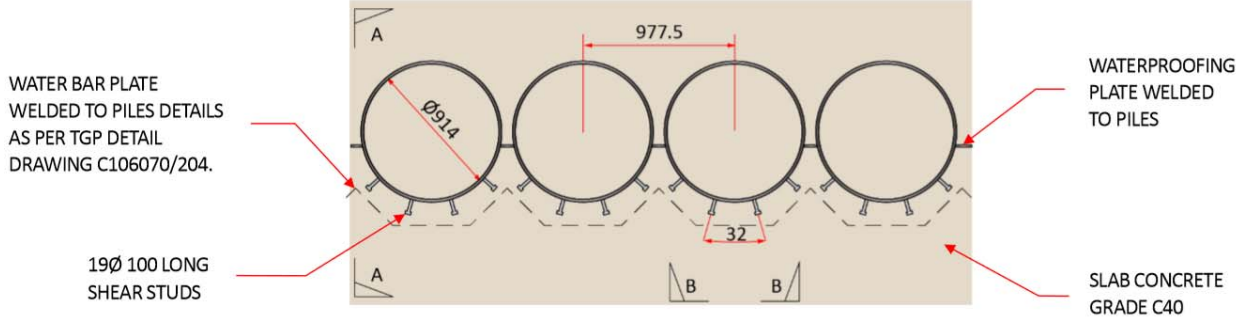


Figure 14 Plan View of Pipe Pile Wall's Slab Connection



Figure 15 Sheet Pile Wall's Slab Connection with Water Stop Plate and Shear Studs

The steel pile walls were used as temporary shoring during construction and later as permanent structural components, with interior surface finally painted white for an aesthetic purpose as shown in Figures 7 and 16.



Figure 16 Finished Pipe Pile Wall along the Ramp Way

CONCLUSIONS

Underground steel pile walls both as temporary shoring members and permanent structural components that carry vertical and horizontal loading can shorten a construction period with a resultant cost reduction as realized on the case study project. If coupled with press-in piling, each and every pile's bearing capacity can be verified at the time of their installation and drastically reduce noise/vibration/dust associated with other piling methods.

ACKNOWLEDGEMENT

The authors appreciate the support and assistance provided by the following individuals.

Denis Guimond, Nucor Skyline
Ian Vaz, Giken America Corp.

REFERENCES

Fayad, A., Takuma, T., and Kambe, S., (2015), Levee Repair and Upgrade by Dual Sheet Pile Walls and Accordion Sheet Pile Wall, Proceedings of Deep Foundations Institute 2015 Annual Conference

Fleming, W.G.K., A New Method for Single Pile Settlement Prediction and Analysis, (1992), Geotechnique, Vol. 42, Issue 3, pp. 411-425

Takuma, T., Nishimura, H., and Kambe, S. (2013), Low Noise and Low Vibration Tube Pile Installation by the Press-In Piling Method, Proceedings of Deep Foundations Institute 2013 Annual Conference

Takuma, T., Nishimura, H., and Kambe, S., (2015), Development of Very Low Head Room Sheet Piler Press in Driver, Proceedings of 2015 International Foundations Congress and Equipment Expo

Takuma, T., DellAringa, C., and Nagano, M., Retrofitting Drainage Systems with Pressed-In Sheet Piles in Very Hard Soil in Southern California, (2018), Proceedings of Deep Foundations Institute 2018 Annual Conference

White, D., Finlay, T., Bolton, M., and Bearss, G. (2002), Press-in piling: ground vibration and noise during piling installation, ASCE Special Publication 116.

HUDSON'S REVITALIZATION: THE USE OF ROBOTICS IN THE WORK PLACE

Dave P. DeClerck
Hardman Construction
Ludington, MI USA
(231) 845-1236
david@hardmanconstruction.com

ABSTRACT
Hardman Construction was faced with the challenge of completing a large earth retention project on a constricted downtown Detroit site, while maintaining a safe and productive worksite. To do so, new technologies using robotic equipment was instituted.

HISTORY
The historic J.L. Hudson Building (Hudson's) in Detroit, Michigan was the premier retailer in the city's downtown district from the 1890s through the 1960s. The massive flagship store sat at 1206 Woodward Avenue, one of the busiest streets in the Detroit area. Hudson's broke ground in 1891 and would go through twelve renovations and expansions. The last renovations took place in 1946, which gave the building the title of being the largest department store in the world at the time. It spanned an entire city block and boasted 2.2 million square feet of retail space. By the 1970s, Detroit was in an economic downturn. The Hudson's department store finally closed its doors in 1983. Besides a few working offices, the building sat vacant. The building was unique in that it had four levels underground, offices, mechanical areas, and equipment storage.

Following years of neglect, the Hudson's building was seized by the state and transferred into the hands of the city. The city had it demolished in 1998, (shown in Fig. 1) to construct a new, four-level underground parking garage as well as a potential future above-grade development (Sewlck, 2017). The building was imploded in one of the largest implosions of that time. The building rubble filled the underground rooms and helped to stabilize the exterior concrete walls and keep them from collapsing.



Fig. 1. Hudson's Building Pre-Demolition, 1988

© 2019 Deep Foundations Institute

The new underground parking structure utilized the existing 19th-century concrete walls as earth retention. The design consisted of excavating and unloading the soil around the site to reduce the lateral loading on the existing walls; then as the excavation/rubble cleanup was performed, three rows of permanent earth anchors were installed and locked off. The anchors were permanent, double corrosion protected, and consisted of 1-1/4" and 1-3/8" diameter grade 150 threaded bars. Numerous existing utilities around the site and a city mandate, required that a depth of 15' be reached before earth anchors could be installed. Once the bottom depth of 40' was reached, the parking structure was constructed. The lower three levels of parking deck were internally post tensioned, meaning no attachment nor loading were transferred to the existing concrete walls. The top deck was a poured-in-place, two-foot thick concrete slab, which was used to resist the lateral loading from the soil and to withstand the loading from the parking deck. The concrete walls varied in thickness from two to three foot thick. This work was completed from 1998 to 2001.

OPERATION OF THE SITE, AND FUTURE PLANS

The garage would remain operational until early 2017. It was plagued with operational issues during this period. The existing concrete walls continually wept water and caused flooding on the bottom floor. The weeping water helped speed the corrosion of the concrete walls and anchors. Some attempts were made to correct spalled concrete at localized locations, only to have the weeping water migrate to the next closest corroded concrete area. By 2017 the site needed major repairs. The property was purchased by the Bedrock Development Group in 2017. Bedrock had been planning for a new development in this location for years. Construction was slated to start on the new Hudson's building in December of 2017. Once completed, the 890' tall building will be the tallest building in Detroit and in the state of Michigan. It will pay homage to the prior building with multiple retail stores in the mixed-use development.

DESIGN AND CONSTRUCTION

The location of the development, along with city codes, required the developer to create numerous parking spaces. Initial design had the new structure sitting on the existing parking structure and existing caissons. Due to the state of the existing structure, as well as the unknown state of the caissons, it was determined that the best plan would be to demolish the existing parking structure and install new deep foundations for a below grade parking structure. The Urban environment and proximity to surrounding streets and buildings meant earth retention would need to be utilized. The existing foundation walls were a 240' x 430' rectangle. These existing walls would act as the current earth retention but needed some serious repair and revitalization. The plan was to make the repairs necessary to use the existing walls as permanent earth retention for the new structure, as well as install new deep foundations. (Figure 2 shows the footprint prior to mobilization)

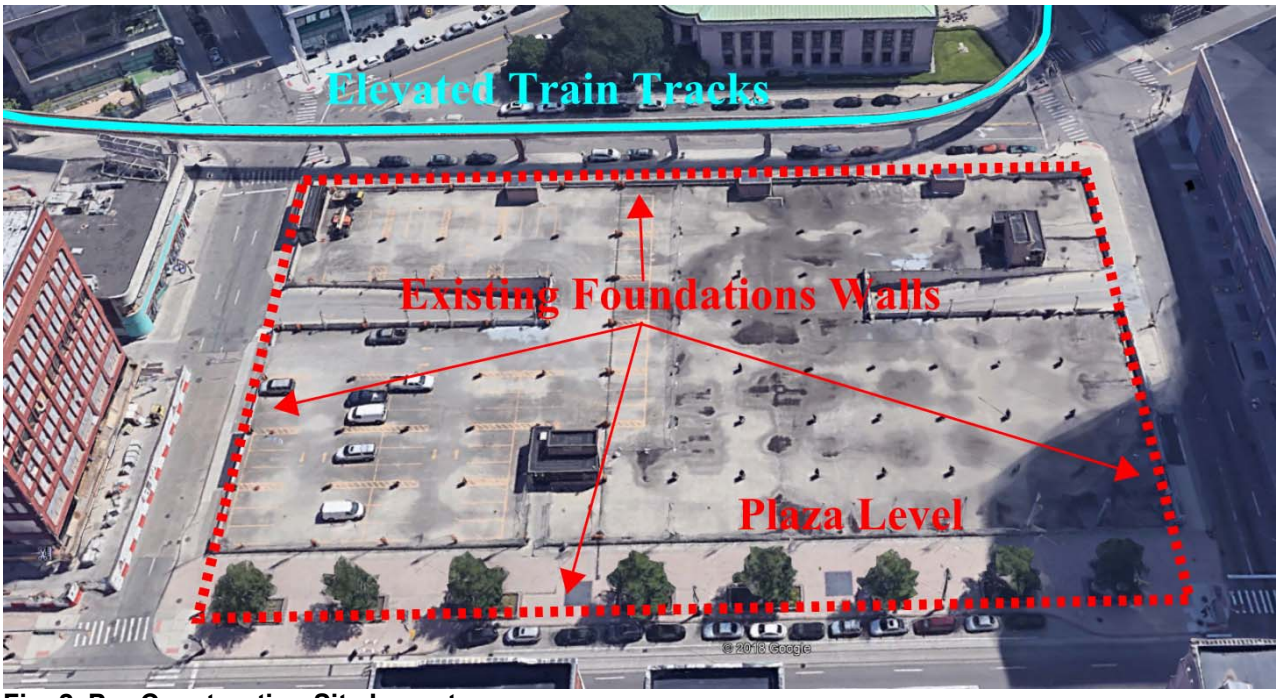


Fig. 2. Pre-Construction Site Layout

EARTH RETENTION PROCESS

There were major concerns about the condition and integrity of the anchors, as well as the original 19th century concrete walls. The walls had numerous spalled areas that exposed 19th century steel. These areas constantly wept water. Calcium deposits encased the ties, making it difficult to evaluate their integrity. The plan to make the 40' excavation safe was a four-step process. First, the perimeter walls would be stabilized to allow demolition to commence. Second, the four underground floors and top plaza level would be demolished. Third, existing anchors were to be inspected, tested, and in some cases repaired, depending on their condition. Fourth, all existing walls would be hydro-demoed, repaired, and the walls sprayed with shotcrete.

STABILIZATION OF THE EXISTING WALLS

The existing perimeter walls were 40' tall with five parking levels; ground floor, first through third, and the top level or what is called the Plaza Level. Stabilization would begin by pinning the existing walls at the top, near the Plaza Level. Pinning would need to take place prior to the Plaza Level being removed. The Plaza Level acted as a lid on a box; it was a cast-in-place concrete slab that not only supported vehicular traffic but also withstood the lateral loading from ground surface to the first earth anchor. If the top was removed prior to the stabilization of the existing walls, there would have been catastrophic failure. Stabilization of the perimeter walls consisted of a series of structural beam members being fastened to the existing walls. Pinning the walls created a hinge loading by transferring the loading from the top of the wall to below the first anchors. Beams were spaced at the typical 6 feet on center unless special loading criteria required the beam spacing to be reduced. Beams included W8x58, W10x49, and W12x45. (Figure 3 illustrates a detailed section of the structural beams)

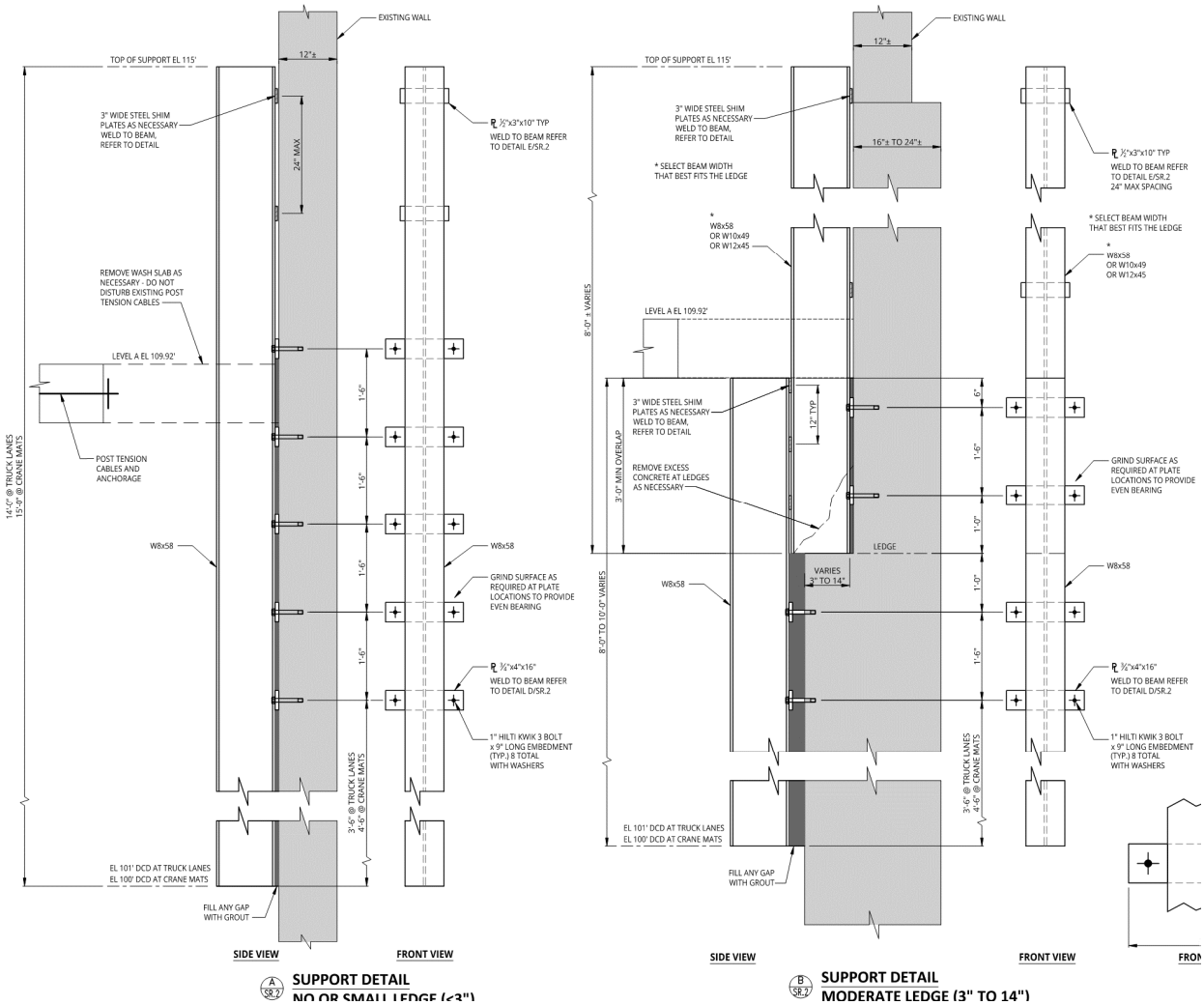


Fig. 3. Structural beam sections

Prior to mobilization, field discovery of wall integrity was completed. This allowed the construction team to create shop drawings for structural steel. All beams were fabricated prior to mobilization. Since the pinning and setting beams had to take place prior to demolition of any floors, approximately 240 structural beams up to 17' long were placed in a space with no more than eight feet of headroom at any level. This meant the Plaza Level and Level A needed to be saw cut to allow the beams to be lowered in from the top down. This created a unique challenge, as Level A was a post-tensioned deck. The post-tension strands ran through the area of the floor that needed to be saw cut to allow for the structural beam-installation. With safety as a main concern, Hardman Construction knew that if the wrong strands were cut, there was a potential for the Level A deck to collapse onto Level B. Engineering controls were put in place to ensure the Level A deck was safe from collapse prior to coring holes. Shore jacks were placed between Level A and Level B. Jacks were placed on 10-foot centers across the entire span. Once Level A was supported, cutting and coring began. The Plaza Level got 2' diameter holes, and Level A had a 2.5'-wide strip cut out along the perimeter. This allowed the beams some wiggle room. With the post tension strands cut on Level A deck, it was now being supported by Level B deck. This limited the load-carrying capacity that could be put on Level A deck. General construction equipment, like Sky Traks, could no longer be used due to loading restrictions. Smaller equipment needed to be used to set the structural steel. The use of an electric Brokk 180, a medium range demolition robot with a grappler clamp was chosen. The beams were lowered in from the holes in the Plaza Level. The small, electric

Brokk sat on Level A and secured the beams to the wall while carpenters fastened them in place. The robotic Brokk was valuable for a couple of reasons. First, its light weight allowed compliance with the load restrictions, and second, it was electric. This meant there was no contention with poor air quality. Air quality was a major safety concern since all electricity was cut to the property. This meant the ventilation fans would be shut off as well, not allowing harmful gases created by combustion engines to be removed from the work space. The Brokk's job was to clamp onto the Structural beams as they were lowered into position by the equipment from above. Once the Brokk had ahold of the beam, the rigging would be removed from above. The Brokk's arm had full range of motion, similar to a human arm. This allowed carpenters to maneuver the large beams into place with finesse. Once in the desired location, beams were fastened to the existing wall using 1"x12" anchor bolts. Carpenters fastened beams to the existing wall from Level A deck. The carpenters were tied off for fall protection due to the 2.5'-wide open strip along the perimeter of Level A deck. A horizonal lifeline capable of supporting two people was anchored to the existing columns inside the structure, roughly 10' behind the working area. A no-access zone was established 10 feet from the work area, for anyone who was not tied off. Once the beams were anchored in place, grouting began. The void area between the beams and existing uneven walls would be grouted. Beams were required to maintain intimate contact with the existing concrete walls. Non-shrink 4,000 PSI grout was used to fill the voids between the beams and the concrete.

EXISTING ANCHORS

Part of the wall stabilization process included checking the integrity of the existing anchors. Most of the 494 anchors were visually distressed. (Figure 4 shows the condition of the anchors) Calcium scale, caps, and grease needed to be removed. The integrity of the anchor would then be examined by the geotechnical engineer. Each anchor was then assigned one of four treatment methods.



Fig.4. Typical anchor head prior to cleaning and inspection

ANCHOR TREATMENT METHODS

Method A meant the anchor was in good condition and would remain tensioned. The steel on the anchor head was prepped for a shotcrete coating, prepping which entailed cleaning the anchor head to bare metal. This was accomplished by a variety of methods, from sand blasting, to grinding, to needle cleaning. Anchors had to meet a type SSPC-SP-3 surface. An epoxy coating was then painted on the heads to prevent rusting prior to shotcrete application. A steel box was placed over the anchor after shotcrete was applied and remained on the anchors to allow future access if there was ever an issue with the wall or anchors.

Method B meant the anchor head was inspected and deemed insufficient to hold the load. These anchors were then de-tensioned. Anchor head components were removed and replaced with new components. The anchors were re-tensioned, and the surfaces prepped for shotcrete. Steel boxes were placed over these anchors as well.

Anchors deemed by the engineer as no longer needed were designated as Method C. These anchors were abandoned in place. Anchors would remain tensioned, and the surface prepped for a shotcrete coating. Shotcrete was applied over the anchor heads.

Method D anchors were those that stood in the way of the future building and were no longer needed to support the existing loads. All Method D anchors were located at the very bottom of the excavation. These anchor heads were de-tensioned and completely removed from the wall, and trumpets were sprayed with shotcrete.

Method B anchors required the anchor to be de-tensioned. If an anchor was de-tensioned, no other anchor could be de-tensioned within twenty feet in any direction; up, down, or laterally until the prior anchor was re-tensioned. This made sequencing work and production difficult because there was uncertainty about which anchors needed to be de-tensioned until they were inspected. If an anchor needed to be de-tensioned, the crew needed to relocate all work materials to a new location. Tiebacks checkered the walls of the parking structure. Locations and bar sizes varied with no rhyme or reason. The anchors were epoxy DSI bar that ranged from 1”-1-3/8”. The bar also ranged between grade 75 and grade 150 steel. Most of the tieback restoration was tackled prior to demolition of the floors. Refurbishing the ties from the existing parking levels allowed for efficiency and safety. Unfortunately, not all ties could be accessed during the pre-demo stage. Roughly twenty percent of the ties were cast into the existing decks or in areas that were not accessible prior to demolition. The final anchors needed to be revitalized after the demolition took place. Demo of the floors allowed access to the final ties but also removed the working platform. The final anchors would need to be finished using ~~from~~ manlifts. This dramatically reduced production.

LOAD TESTING ANCHORS

All anchor~~s~~ heads determined by the geotechnical engineer to be not structurally sound, needed to be de-tensioned. New components, trumpets, plates, and heads would then be installed. The anchors would then be re-tensioned. By putting them through a performance test with cyclical loading, holding 133 percent of design load for a minimum of 10 minutes, or one hour if the anchor creeped more than 4 hundredths of an inch in the first 10 minutes. Fortunately, all the anchors that were tested passed.

ROBOTIC HYDRODEMOLITION

Hydro-demolition was the next step in the process. The existing concrete was deteriorated and spalled. This deteriorated concrete was removed prior to the application of shotcrete. Hardman’s scope was to hydro-demo 48,400 square feet, approximately 1.5” deep or as deep as the deteriorated concrete was found. The hydro-demo took place on seventy-five percent of the existing walls from top to bottom. Due to safety and access concerns, a robot was used for all hydro-demolition work. The hydro jet was capable of twenty thousand PSI and cutting concrete up to four foot thick. The goal was to remove the deteriorated and spalled concrete, not to blow through the wall with twenty thousand PSI. Multiple hydro-demo test runs were done to try to implement a standard and acceptable PSI range. (shown in Fig.5) Due to the differing nature of the concrete, it was difficult to achieve an exact PSI. The most acceptable PSI found, ranged from six to nine thousand PSI, two feet off the wall.

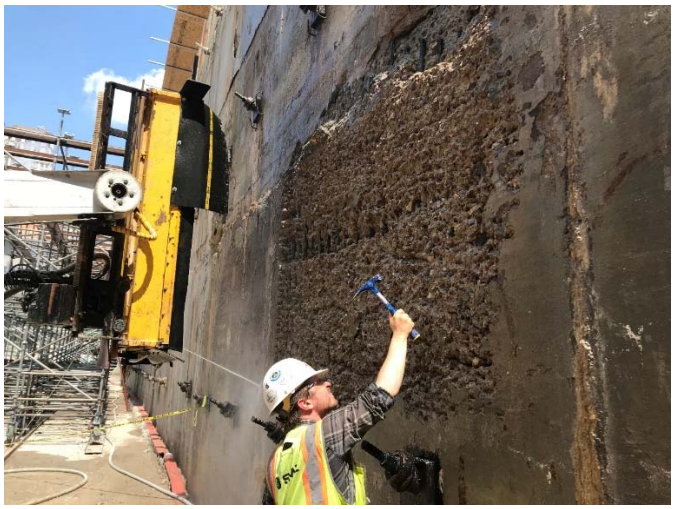


Fig. 5. Robotic hydro demolition. Testing the PSI Levels prior to production

In one pass the robot removed an area thirty-five feet long by three and a half feet tall. The hydro-demo was performed at the lowest level first and then progressed to higher levels. The robot could reach a vertical height of 22'. The project required hydro demolition up to 40' from the base mat. The demolition above 22' would require the use of an engineered scaffolding platform that would support the robot for the final 18'. The engineered platform was a rolling, scaffolding system, capable of supporting the robot at 22' above grade with the arm fully extended vertically, while in operation at twenty thousand PSI. The scaffold was ten-foot-wide by seventy feet long and weighed almost 30,000 pounds. The scaffold was designed to move with the hydro-demo robot on it. To move the scaffold, equipment was placed on both sides of the scaffold. One piece of equipment was rigged to pull the scaffold and the other piece was rigged to push it. The scaffold was positioned six feet away from the wall for optimal robotic placement. Once in position, the scaffold jacks were lowered and secured. With the robot on the platform, demo of the upper walls could be completed. Demolition of the upper walls took place within five feet of public pedestrian traffic. Flying debris was a major safety concern and an overhang protection shield was designed to defend the public from the flying debris. Hydro-demolition of the concrete wall generated roughly sixty gallons per minute. The resulting water from the demolition had to be collected in the bottom of the hole, pumped up to grade, treated, tested, and discharged into the city sewer. The water collected in low areas at the bottom of the work area, where it was pumped to a 21,000-gallon frac tanker. The tanker was a three-tiered system that allowed the solids to drop out. At the end of the frac tank, there was an osmosis water filter that lowered the pH levels. The last step of this process was to hold the treated water, in separate tanks, for final testing and then discharge into the City sewer system. The discharged water had to meet requirements of the Great Lakes Water Authority and the City of Detroit.

MESH & SHOTCRETE

The last step was to shotcrete the area that was just cleaned of spalled concrete. The steel mesh consisted of 6X6 D7.5xD7.5 wire mesh and hung on #4 steel dowels with a standard hook. The dowels were imbedded a minimum of twelve inches and were epoxied in place. Steel mesh was hung approximately three inches off the hydro-demoed concrete face and was tied to every dowel. Dowels were four feet on center. Crews had to install all dowels and hang all the mesh using man baskets. Shotcrete was sprayed four and a half inches thick, or three inches plus the one and a half inches that was removed from the hydro-demolition. To get the shotcrete finish as close to the four and a half inches as possible, steel wire was run vertically at four foot on centers. The steel wire acted as a guide for the nozzle man and finishers. This wire was critical for the finishers. With the

wire system, waste was dramatically reduced, and the finish was within a half inch tolerance. At the post bid, there was some concern about shotcrete over runs. Since shotcrete was a unit price number, the owner wanted to make sure we had a good way to measure the exact volume installed on the wall. Since the walls were rough after the hydro-demolition, ~~we~~ it was decided to use a three-dimensional laser scanning system, that had the ability to scan the walls before and after the shotcrete was applied. The scanning system measured millions of data points on the wall after hydro-demolition and prior to applying shotcrete. The difference in the distances at each point determined the volume of shotcrete on the walls. This was a great piece of technology that helped the contractor, as well as the owner to be able to accurately determine final quantities.

Hardman decided to use a wet mix that consisted of 750 pounds of cement, 1,900 pounds of sand, 800 pounds of stone, 100 pounds of fly ash, and 326 pounds of water. The mix was very temperamental and had to meet tight tolerances for slump. The mix needed to be held at a 1.5 – 2-inch slump for good pumpability, application, and finishing. It was determined that running four-yard loads was the most economical. If running larger loads, the shotcrete would dry up prior to getting the mix off the Redi-Mix truck. This would plug up pumping operations and shut the crew down for hours. The four-yard loads would need to be completely pumped out within forty minutes of reaching the pump. The workability of the four-yard loads was approximately one hour from batch time. Redi-Mix trucks would need to be scheduled to arrive just as the previous truck was finishing. If the shotcrete sat idle in the lines for more than ten to fifteen minutes, the shotcrete would set. Coordination of the trucks was key to the success of the shotcrete operation. On average, crew would shoot twenty-four to thirty-two yards a day. Shotcrete had to be pumped from the road as access to the bottom of the hole was not available. Steel pipes were bolted to the walls and run across the bottom of the excavation. The steel pipe was connected to a 2.5" rubber hose that was run up the side of the Sky Trak boom and ultimately into a man basket where two nozzleman would apply the shotcrete to the walls. Steel tubes could be added or taken away based on the distances needed to pump. The furthest run was around 600 feet of pumping. The crew for shotcrete consisted of ten people. One pump man at the top of the excavation, two nozzleman, six finishers, and one more person on the ground directing traffic. The decision to use a wet mix over a dry mix was strictly economical. Even though there's difficulties and struggles with the wet mix. It was substantially cheaper than a dry mix. (Figures 5 and 6 illustrate the above)



Fig. 5. Crews Meshing prior to shotcrete around the structural beams

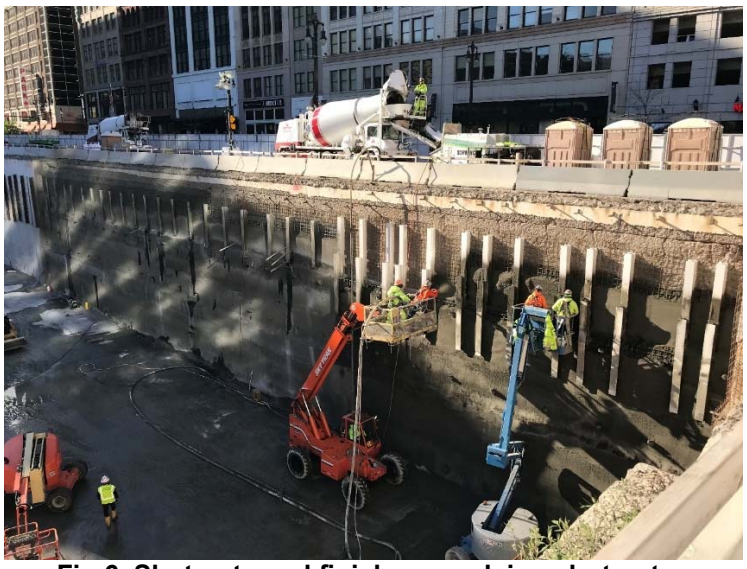


Fig.6. Shotcrete and finishers applying shotcrete

CONCLUSION

The four-step process of Structural Steel Installation, Repairing Anchors, Demolition, Hydro-Demo and Shotcrete was fraught with challenges, but the construction team was able to employ new technologies to help overcome these difficulties. The implementations of this new technology on the Hudson's site will allow for better preparation for all involved in future work with similar projects. Full excavation and stabilization of the work area was completed in October of 2018. The site is currently receiving drilled shafts for foundations.

As the Hudson Building was a testament to greatness and technology in its time, the use of new technology to revitalize this new building shows how far the construction industry has come. The new building will again be a significant and iconic symbol for Downtown Detroit.

REFERENCES

Sewlck, P., 2017. The past, present, and future of the Hudson's site. http://detroit.curbed.com. Accessed 4-1-19.

TOP-DOWN METHODS UTILIZING SECANT WALLS AT 110 N. CARPENTER: DESIGN AND CONSTRUCTION

David R. Sutfin, PE, SE, Michels Corporation, Kent, Washington, United States, 253-220-8004, dsutfin@michels.us
Joseph Lodde, Michels Corporation, New Berlin, Wisconsin, United States, 262-938-6060, jlodde@michels.us

ABSTRACT

110 N. Carpenter is new commercial building located in the West Loop neighborhood of Chicago, Illinois. The new home to the McDonalds Corporation work headquarters, accelerated project delivery methods were essential to meet the scheduling demands for this project along with other projects slated to start in the region. As such top-down construction methods were utilized to allow for above and below grade construction to proceed in parallel in lieu of more conventional bottom-up construction methods, thus compressing the project schedule. To achieve this plan, perimeter secant pile walls were constructed in conjunction with interior columns/drilled shafts and a shear wall core constructed from inside a temporary cofferdam. The use of secant pile walls allowed for efficient accommodation of a variety of loading conditions including: exterior curtain walls loads, perimeter column loads, tower crane foundation loads, and in-plane shear loads. Furthermore, this system allowed for efficient and fluid operation of equipment on site in order to accommodate the 90-day window allotted for initial foundation construction.

Keywords: secant, top-down construction

INTRODUCTION

110 N. Carpenter is a recently-constructed 9-story commercial building located on the old Harpo Studios property in the West Loop neighborhood of Chicago, IL. The construction of this 55,750m^2 (600,000 ft^2) structure is significant to the continued commercial development of Chicago as nearly 46,450m^2 (500,000 ft^2) of the building houses the new world headquarters for the McDonald's Corporation, which had moved from Chicago to the suburb of Oak Brook in 1971. McDonald's recommitment to this urban environment is not only a reinvention of the long-established fast food giant but the anchor for a broader redevelopment of the West Loop neighborhood. Since the opening of this building was seen by the developer, the City of Chicago and others as a key to future local projects, innovative solutions were required to showcase forward-thinking design as well as expedite the construction process.

The final result of the design/planning process is a structure consisting of nine levels of above-grade commercial space and two levels of below-grade parking, providing approximately 300 parking spaces. The above-grade structure consists of a reinforced concrete flat plate system, including two-way slabs, columns, and two core/shear wall systems for lateral support. With an average depth of 7m (23ft), the below-grade structure consists of interior components similar to the above-grade structure (structural slabs, columns, shear walls) but includes a perimeter secant pile wall that was designed to support lateral earth pressures; vertical forces from the exterior curtain walls, perimeter columns, and the construction tower cranes; and in-plane lateral forces to reduce the demand on and quantity of interior shear walls. The use of a secant pile wall is a key component to the project because it accommodated the use of top-down construction methods to accelerate the construction schedule.

TOP-DOWN CONSTRUCTION AND FOUNDATION SELECTION

From early on in the design/planning process, it was understood that schedule was going to be a primary driver for the project, leading to the push for use of top-down construction methods to expedite construction.

© 2019 Deep Foundations Institute

Using more conventional bottom-up methods of construction the project schedule is very linear, requiring excavation, foundation construction and above-grade construction to occur in series in order to complete the overall scope of the project. When top-down construction methods are utilized only the most critical substructure components are constructed from grade, thus allowing for construction of the above-grade structure to begin. From this point above-grade construction and the remaining substructure components are completed in parallel, thus reducing the overall project schedule. Below outlines a generalized sequence of operations for the top-down methods used for this project:

1. Construct the primary shear wall core within a temporary cofferdam utilizing conventional bottom-up construction methods. This phase often starts first as the core structure must be constructed to grade prior to beginning above-grade construction.
2. Construct perimeter foundations walls along with interior shafts and associated lower level columns from existing grade. For this project the lower level columns were essentially extensions of the drill shafts (circular reinforced concrete).
3. After completion of steps 1 and 2, construct the main level structural slab located at existing grade, including a perimeter cap beam to marry the foundation walls, interior columns, and shear wall core into a single structure.
4. Begin above-grade and remaining below-grade construction as parallel operations. Above-grade construction is performed in a similar manner to conventional construction methods. The remaining below-grade construction (excavation, lower level slab construction, infill walls) is performed using a mining-type excavation process where openings are left in the main floor structural slab, known as "glory holes," to allow for removal of site material followed by slab construction.

While the use a top-down construction was decided early in the planning process, the type of foundation wall to be utilized was not agreed to until just prior to beginning the permitting process. Original design discussions focused on the use of slurry walls as the means of foundation wall construction. Given the large footprint of the site, approximately 76m x 100m (250ft x 330ft), it was believed that slurry wall methods, which utilize wider panels in lieu of individual secant shafts, would yield the most efficient production rates in order to meet scheduling restraints. However based on internal design and production reviews, it was Michels' opinion that a secant wall system would be able to yield similar production rates to slurry wall construction but at a lower overall cost. There were a couple key factors that led to this conclusion and eventually to its selection as the system of choice for the final structure.

The first factor was related to the equipment utilized and logistics of working on site. Since the perimeter walls and the interior shafts/columns needed to be constructed simultaneously, utilizing slurry walls meant that two completely different equipment spreads were required to complete these tasks, with slurry wall construction in particular requiring a large footprint of the site to work efficiently. Utilizing a secant pile wall system allowed for the use of the same equipment to be utilized for both operations. This operation created a more fluid site condition in order to keep equipment working, particularly if any unforeseen conditions would arise.

The second factor involved the design efficiencies a secant wall provided for the loading requirements associated with the project. To address out-of-plane lateral load demands, the secant pile lengths could be optimized to where the unreinforced primary shaft length was minimized and the longer reinforced secondary shafts would be the means of stabilizing the toe of the wall, in a similar manner to a soldier pile wall. To address vertical demands the reinforced secondary shafts would vary in length depending on loads it was required to support, whether it be more typical curtain wall loads or more significant column or tower crane loads. This ability to fine tune the extent of excavation and material replacement required when

compared to the larger panels associated with slurry wall construction yielded significant savings. Refer to Figure 1, which summaries the final secant wall geometry selected for the project based on the efficiencies described above.

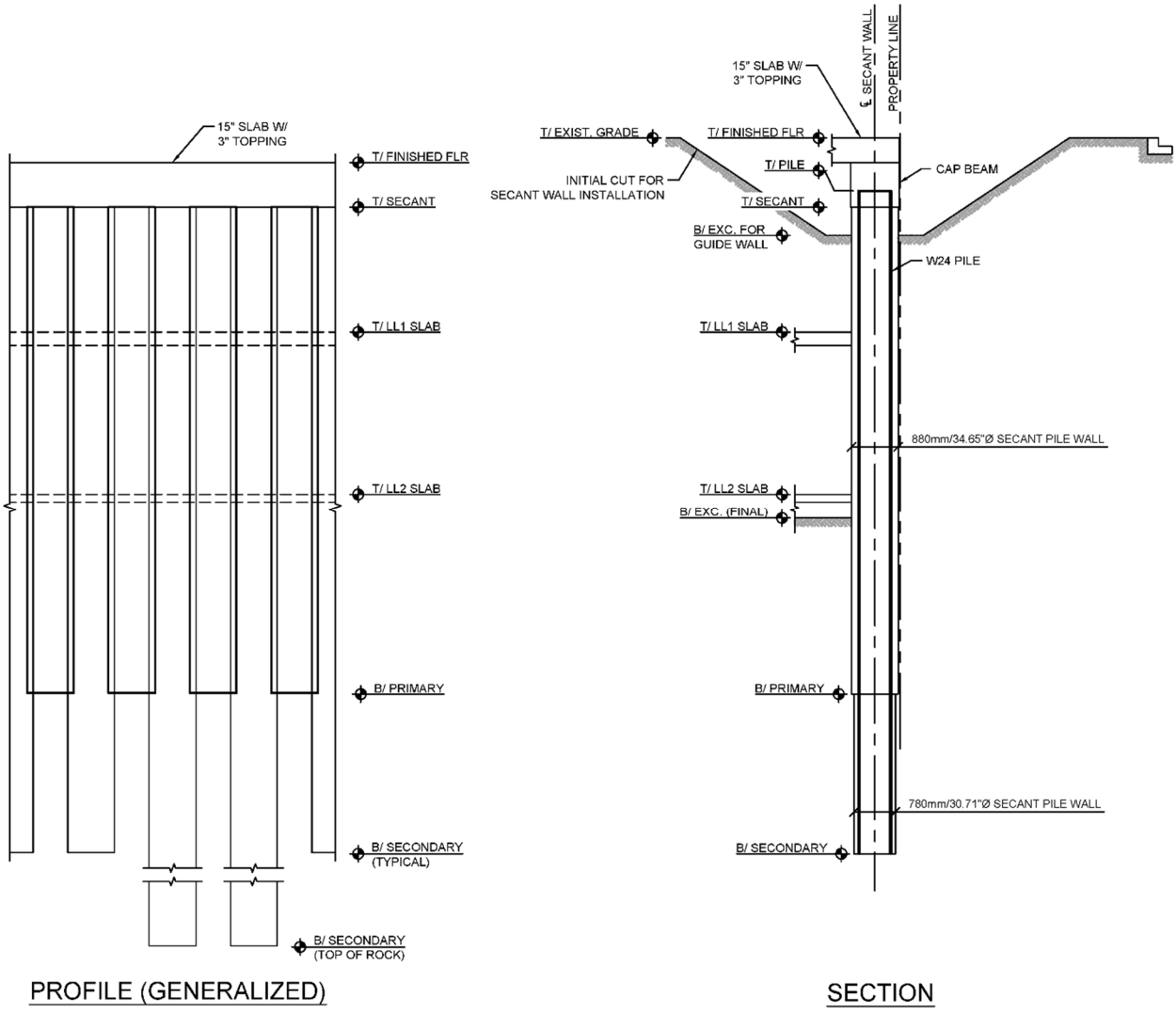


Fig. 1. Typical secant wall geometry

PERMITTING AND DESIGN SCOPE CHALLENGES

As was noted previously, the final decision to utilize secant pile walls as the foundation wall system was determined late in the design process and right before foundation permitting was to begin with the City of Chicago. Since the secant wall system was contractually established as a design/build portion of the project, it required significant and rapid coordination between the structural engineer of record for the building (Magnusson Klemencic Associates, MKA), the civil engineer of record for utility/infrastructure coordination (Terra) and the design/build foundation team (Collins Engineers, Inc./Michels) to ensure all parties understood critical aspects of the foundation system and how it would be married to the other aspects of the structure that were already under development.

To further complicate the project design methods, the building was being constructed using three separate permits in order for construction to begin prior to completion of design. The foundation permit would be

issued first so that the appropriate substructure work could commence. This was followed by permits for two tower cranes, designed by the general contractor, McHugh Construction Company, which were to be founded on the newly constructed secant pile wall and interior columns/drilled shafts thus allowing the tower crane structure to cantilever into the public right-of-way. This foundation scheme was chosen in order to avoid installing additional foundation elements outside of the property line, which would necessitate further approvals and create delays to the project schedule. The final permit issued addressed the construction of the building superstructure and civil improvements to occur in the public right-of-way.

The overlapping of construction schedules with design phases that were still in flux meant that the foundation system had to be able to facilitate a variety of design scenarios that could occur while attempting to minimize the use of conservative design assumptions to keep project costs down. While the superstructure loading was fairly well established during the design process for the substructure elements, there were tie-in substructure elements to be located in the public right-of way that could not be finalized until after issuance of the foundation construction permit. These elements included exhaust vaults to properly ventilate the below-grade parking, an electrical utility vault, and various utility tie-ins to the building. Each of these elements required significant penetrations through the secant wall system, thus requiring the wall design to be able to accommodate all potential configuration options. With schedule driving the project decisions, the option(s) that would be chosen was predicated solely on achieving the necessary approvals in the least amount of time.

GEOLOGY / SITE CONDITIONS

The geology that was sampled and tested on the project site is comparable to a majority of sites in or nearby the downtown region of Chicago, consisting of urban fill underlain by native silty clay (CL/ML) soils of varying strengths, the primary of which is typically classified as very soft to medium consistency based on standard testing methods, including SPT and pocket penetrometer tests. This soil strata is often referred to as *Chicago Blue Clay* and can create issues for the design of temporary or permanent earth retention systems as any excavation typically 6m (20ft) deep or greater can develop heave/base stability issues. This potential for a deep-seeded failure can generate significant lateral pressures on a proposed retention system and makes the selection of design soil parameters that more critical to provide an efficient, yet appropriately robust system. It is because of these needs that more refined methods of testing are typically implemented in Chicago in order to achieve efficient designs. While there are a variety of laboratory and in-situ methods that can be utilized, the use of in-situ vane shear testing has historically been the test method used to evaluate and define the soil parameters in this strata of cohesive soil.

At depths of approximately 15m (50 ft) below grade the soil transitions into significantly stiffer silty clays that can be more accurately characterized by standard SPT and pocket penetrometer testing. These stiff to very stiff clays are then followed by dense silt/clay “hardpan” layer at approximately 23m (75 ft) below grade and finally limestone rock at approximately 31m (103ft) below grade. The long-term ground water table was observed approximately 2.1m (7ft) below grade.

Figure 2 provides a generalized profile of the soils sampled on site, including total stress and effective stress properties that were used for design.

As this project site encompassed an entire city block, typical urban construction issues such as working directly adjacent to existing building structures did not dictate design requirements such as increased local surcharges or deflection/settlement restrictions. However there were a significant number of underground utilities in close proximity to or in conflict with the proposed project, be it the primary structure or planned civil improvements. Given that the success of this project rode on its ability to navigate its expedited schedule, coordination with the local agencies to identify and address the concerns of all parties was paramount to the project’s success. Refer to Figure 3 for an overall view of the project site.

Depth	Soils		Total Stress Properties		Effective Stress Properties	
			ϕ	c	ϕ'	c'
m (ft)	Description	Classification	degrees	kPa (psf)	degrees	kPa (psf)
0.0m to 1.8m (0ft to 6ft)	Urban Fill	-	30	0.0 (0)	30	0.0 (0)
1.8m to 3.4m (6ft to 11ft)	Stiff Clay	CL/ML	0	95.8 (2000)	28	0.0 (0)
3.4m to 10.7m (11ft to 35ft)	Medium Silty Clay	CL/ML	0	28.7 (600)	28	0.0 (0)
10.7m to 12.2m (35ft to 40ft)	Medium Silty Clay	CL/ML	0	33.5 (700)	28	0.0 (0)
12.2m to 15.8m (40ft to 52ft)	Medium Silty Clay	CL/ML	0	43.1 (900)	28	0.0 (0)
15.8m to 23.2m (52ft to 76ft)	Stiff to Hard Silty Clay	CL/ML	0	95.8 (2000)	28	0.0 (0)
23.2m to 31.4m (76ft to 103ft)	Very Dense Sand/Silt/Clay	ML/CL or SM	40	0.0 (0)	40	0.0 (0)
Below 31.4m (103ft)	Limestone	-	8.62 MPa (180ksf) Bearing Capacity based on O-Cell Testing			

Fig. 2. Generalized Soil Profile

DESIGN PROCESS

After design soil parameters and externally-applied lateral and vertical loads were established by the structural engineer, finalizing sizing and details of the secant wall system could be completed. The final secant wall structure consists of 880mm unreinforced primary shafts with 880mm secondary shafts reinforced with W24 beams. The longer secondary shafts were open-hole drilled after reaching the bottom of the previously-constructed primary shafts, resulting in an effective shaft diameter of 780mm over said length. The primary shafts were only extended deep enough to control heaving effects of the weakest clay soils observed on site. The secondary shafts were either founded on the underlying stiff to very stiff clay if supporting typical curtain wall loads or on bedrock if supporting concentrated loads from the exterior columns or tower crane foundations. The secant pile wall was designed to be laterally supported at two locations. The first location was the first floor structural slab and cap beam that were tied into the secant pile prior to commencing with the mining operation. The second location was at the structural slab at Lower Level 1, which was constructed and doweled into the secant wall system during the first lift of the mining operation. Considerations had been made to design the Lower Level 2 slab as structural slab in order to provide a third point of lateral support for the secant wall but due to concerns of potential long-term volumetric changes of the underlying soft clays it was decided to make that lowest slab a floating slab-on-grade independent of the secant wall system.



Fig. 3. Overall site (green line indicates location of proposed secant wall construction)

Geotechnical analyses performed to design the secant walls were primarily based on limit equilibrium methods, considering each stage of excavation/construction and its influence on the overall requirements for design. On the retained side of the wall, multiple pressure profiles were considered including: active pressures (Rankine), apparent earth pressures (Terzaghi) and at-rest pressures. Rankine passive pressures were utilized on the toe of the wall. Use of these pressure profiles were based on the stage of construction being evaluated and the magnitude of movement the wall could accommodate in order to mobilize said pressures. As the soils on site are primarily cohesive in nature, both total stress pressures and effective stress pressures were considered, with the former being considered both during construction and in the final condition and the latter being considered solely in the final condition. The general stage-by-stage methods used for design are as follows:

- Stage I – Secant piles and First Floor structural slab installed, mining operations completed to accommodate Lower Level 1 structural slab construction (total stress condition).
- Stage II – First Floor and Lower Level 1 structural slabs installed, mining operations completed to accommodate installation of subbase, drainage system, and Lower Level 2 slab-on-grade (total stress condition).
- Stage III – Substructure after installation is complete (total stress condition and effective stress condition).

The use of limit equilibrium methods has historically provided reasonable and reliable results for the geology typically encountered in the region. However, given the high wall stiffness and relatively shallow excavation depth utilized for a system of this nature, basic models considering soil-structure interaction were developed. These models were used to confirm limit equilibrium methods did not result in grossly over-conservative or under-conservative designs. The results of the initial modeling did confirm that limit equilibrium methods provided acceptable results.

As part of the project additional steel sheet piling shoring was required to construct the building core along with various vaults and civil structures located in or near the public right of way. The shoring required for the core construction was 14.6m (48ft) wide by 23.8 (78ft) long by 9.8m (32ft) deep and consisted of 2 levels of internal steel bracing. The shoring required for the miscellaneous right-of-way construction accommodated excavations of varying depths up to 4.4m (14.5ft) deep. For these conditions either cantilever or one level of internal bracing were utilized, dependent on the required excavation depth and the ability to pre-cut areas in close proximity to the shoring. All steel sheet piling shoring was designed using similar methods to those previously outlined but were limited to total stress conditions and basic active/passive pressures due to the short-term nature of their use. Refer to Figure 4 for as-built details of the core cofferdam shoring system.

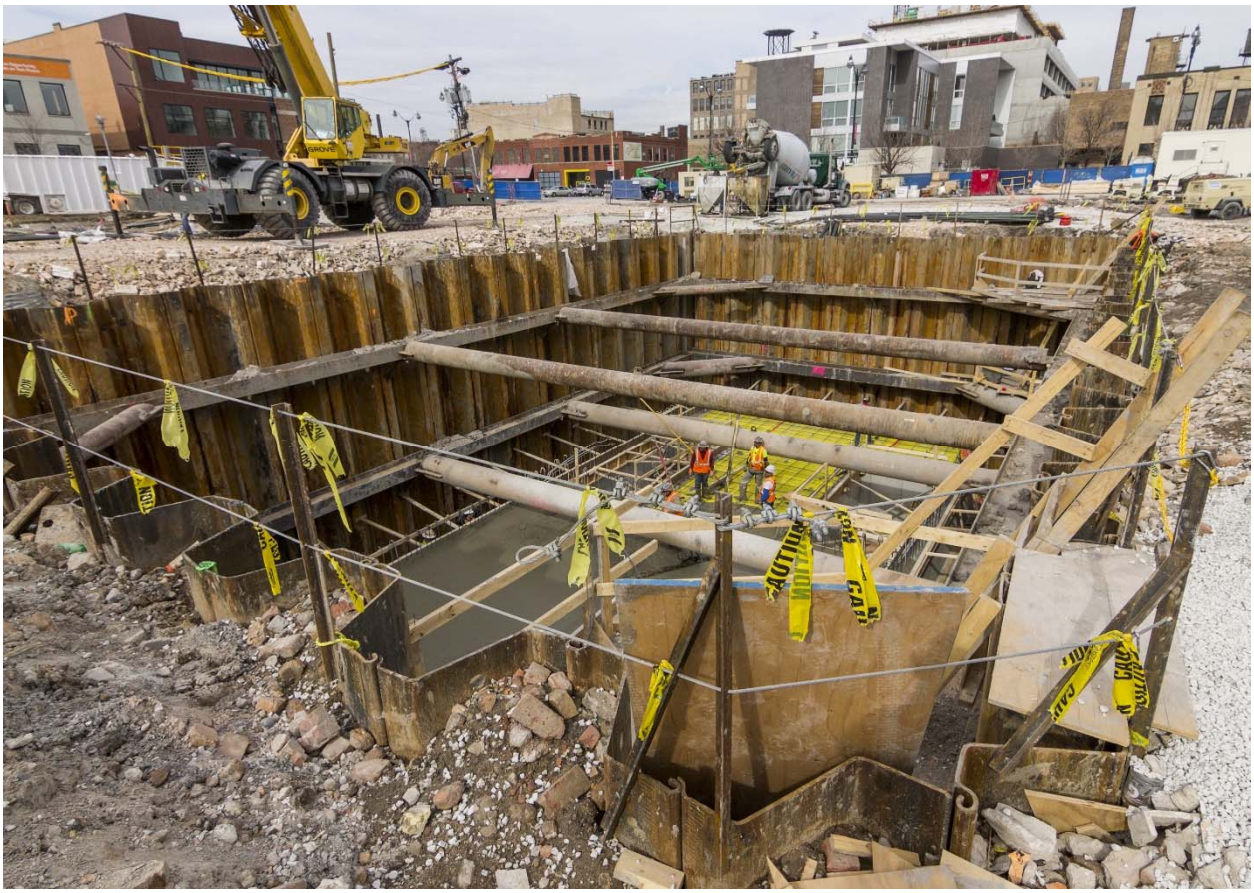


Fig. 4. Cofferdam for core construction

CONSTRUCTION

In November 2016 the foundation permit was issued by the City of Chicago and subgrade construction commenced. At this point in the project an upper bound on the superstructure loads applied to the substructure had been established but the final details for the tower crane had not yet been finalized. This lead to setting vertical loading limits in the region of the proposed tower crane based on the approved secant wall configuration. The tower crane designer was then required to finalize their work based on those established constraints. In the end the designer was able to work within the restraints of the secant wall design but modifications were required to nearby interior drilled shafts during the construction phase in order to safely support the tower crane demands.

Once on site the first tasks to perform after initial site preparations were completed included: excavate, form and pour the secant guide walls necessary to properly locate and construct the secant pile wall; construct and test an interior drilled shaft to confirm bearing capacity of rock; and install the sheet piling cofferdam needed to excavate and construct the building core. Despite having a relatively large site for an urban project, these initial tasks were located on a much smaller portion of the site and each task necessitated different pieces of equipment. Due to this congestion, careful coordination was required to ensure all tasks were completed efficiently and safely.

After these initial tasks had been completed, secant wall construction, interior drilled shaft construction, and the building core excavation/construction were all performed in parallel. To avoid project delays, these three tasks needed to be completed at the same time in order to proceed with the next task, construction of the structural slab located at grade, which ties all of the mentioned substructure components together. To meet these project schedule demands, four drill digs were typically working simultaneously on site. This initial substructure construction, consisting of 100 drilled shafts, 458 secant piles, and 252wf of sheeting cofferdam with subsequent core construction was completed within 90 days as required by the project schedule.



Fig. 5. Photo of as-built secant walls and drilled shafts during mining operation

At this point in the project both above-grade and below-grade construction tasks were allowed to proceed. By the time the two levels of below grade construction were completed, five of the nine above-grade floors has been completed, thus compressing the project schedule by several months.

MONITORING

As part of the project's QAQC process, movements of the secant wall were monitored through the use of six inclinometers located around perimeter of the project. The monitors were used to validate design parameters and to ensure the system performed as intended. During the design process the maximum lateral deformations were estimated to be approximately 2.87cm (1.13in) based on semi-empirical methods developed by Clough. The observed deformations were significantly less, with a maximum lateral deformation of 1.27 cm (0.50in) and typical deformations often under 0.64cm (0.25in). It is the Author's opinion that this difference between the theoretical and observed movements can most likely be attributed to conservative inputs (base stability factor of safety, wall stiffness) used as part of the analysis performed based on Clough's method. A more rigorous analysis method that accounted for actual construction methods and soil-structure interaction would most likely have yielded estimates closer to the observed movements.

CONCLUSIONS

The selection and implementation of foundation systems in modern building construction can vary significantly depending on numerous variables including but not limited to: geology, site conditions/constraints, facility requirements, local history of construction, schedule, and cost. For the 110 N. Carpenter project, rapid project delivery was paramount to its success and the viability of numerous projects scheduled to follow in the region. Through the use of innovative design/build methods, efficient use of materials and site logistics, as well as significant collaboration between owners, tenants, designers, contractors, and local agencies, the goals of this project were successfully implemented; creating a marquee structure that will be used to help reinvent a fast-food giant as well as the urban area it resides in.

ACKNOWLEDGEMENTS

The authors would like to extend their sincere gratitude to all of the operation and support personnel at Michels Corporation for taking on this significant project and making it a team success as well as a cornerstone for future growth of the company within the foundation construction industry. We would also like to thank all of the project partners that were instrumental in the conception, design and execution of this project including: Sterling Bay, James McHugh Construction Company, Roy Strom Company, Gensler, Terra Engineering, Magnusson Klemencic Associates, ECS Midwest LLC, and Collins Engineers, Inc..

INNOVATIONS AND CHALLENGES DURING URBAN DEVELOPMENT – SHORING AND FOUNDATIONS OF CANADA'S TALLEST RESIDENTIAL BUILDING

Shawna Munn, P.Eng,
Isherwood Geostructural Engineers, Mississauga, Ontario, Canada; 905-820-3480;
Shawna@isherwood.to

Nadir Ansari, P.Eng, D.GE, M.ASCE
Isherwood Geostructural Engineers, Mississauga, Ontario, Canada; Nadir@isherwood.to;

Toben Jerry, Senior Vice President
GFL Infrastructure Group Inc., Vaughan, Ontario, Canada; Tjerry@gflenv.com;

ABSTRACT

With ever increasing demands on space in urban environments and smaller available footprints, buildings are being designed to increasing heights to meet the need. This case study discusses the increasing challenges in developing projects within urban environments with smaller available footprints and increasing building heights. The One, Canada's tallest residential building under construction will stand at 85 storeys and is located at one of the most prominent and built up intersections in Toronto, Yonge Street and Bloor Street. This led to many challenges in design and construction of the shoring and foundation work, including the required design capacity of the foundations for the supertall building and proximity of the large diameter drilled shafts to the excavation shoring wall. This case history describes the shoring design option evaluation, performance, and lessons learned to date throughout construction of the building foundations within a small congested site.

Keywords: large diameter drilled shafts, performance based design, monitoring, design, excavation shoring, support of excavation, SOE, foundations, frost

PROJECT OVERVIEW

The One, Canada's tallest residential building under construction by Mizrahi Developments, is a supertall building that will stand at 85 storeys and 306 m (1005 ft). The first 18 floors will be comprised of retail, restaurants, and hotel with luxury residential condominium units in the tower above. The project is located on the Southwest corner of Yonge Street and Bloor Street, one of the most prominent and built up intersections in Toronto. The L-shaped excavation measures 58 m by 47 m (190 ft to 154 ft) and ranges from 22 m to 28 m (72 ft to 92 ft) in depth with one internal corner projecting 11 m (36 ft) into the site.



Fig. 1. Site at Yonge and Bloor (L), and Supertall tower in the Toronto skyline looking South (R)

© 2019 Deep Foundations Institute

EXCAVATION SHORING DESIGN OPTIONS AND CONSTRAINTS

The SOE design was driven by a design build tendering process allowing for innovation and design alternatives. This required evaluation of several design options that had to consider the following constraints:

- No encroachment underneath neighbouring buildings to the South and West
- Existing deep basements limiting space for tieback anchorage on the East, and Southwest
- Existing utilities underneath Bloor Street and Yonge Street on the North and East
- Limited access around and under existing heritage building section to be retained in place
- Limited space for the shoring footprint on the South and Northwest due to proposed building footprint proximity to existing buildings, and on the East due to heritage building proximity to existing hydro duct
- Maximizing access for installation of structural caissons from subgrade elevation
- Refer to Figure 2 for layout of building foundations and constraints

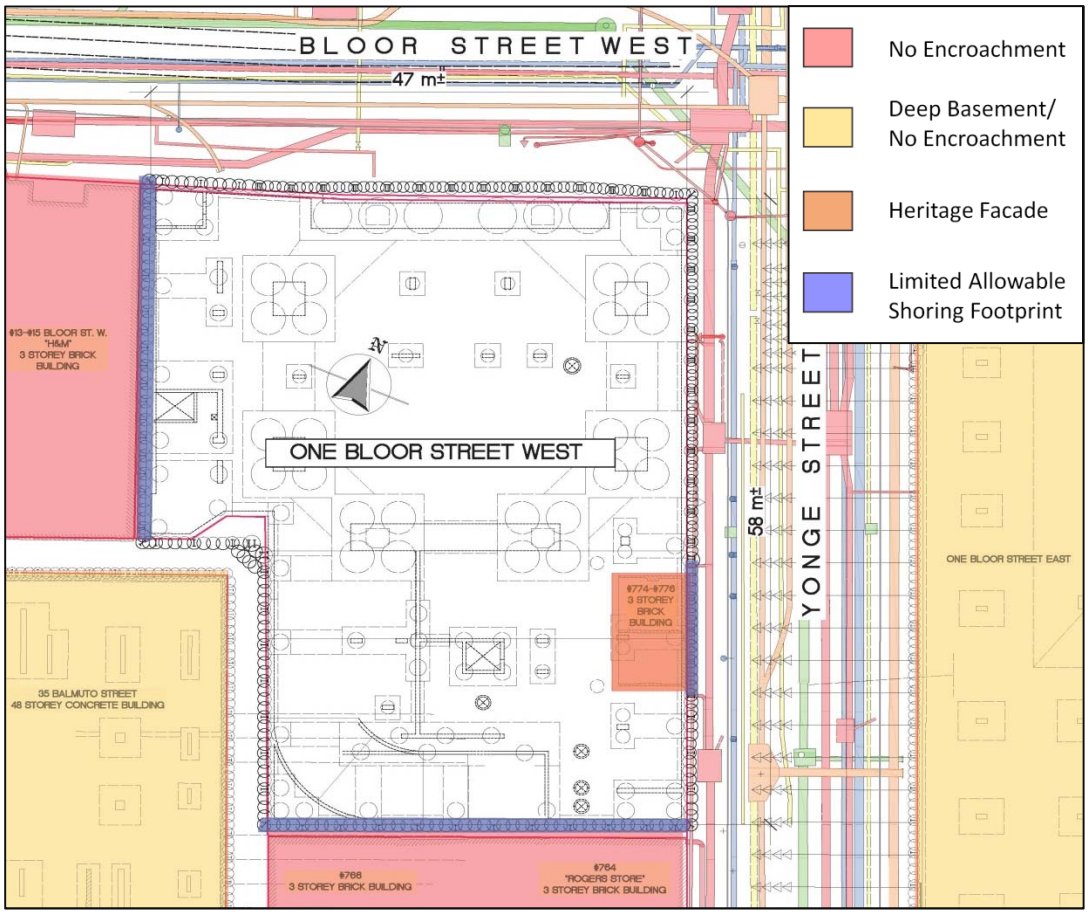


Fig. 2. One Bloor Street West Foundation Plan and Design Constraints

GEOLOGY

The site is generally underlain by shallow earth fill followed by glacial deposits down to the Georgian Bay shale at a depth of approximately 38 m (125 ft). From grade, the glacial deposits consist of stiff to hard varved silt and clay extending up to 15 m (50 ft) below grade (Queen's Park Clay), very dense to hard sand with some silt from 15 m to 38 m (Queen's Park Stratum), and hard layered clayey silt glacial till with gravel, cobbles, and boulders from 36 to 38 m (York Till) (Terraprobe 2016). The water table

was measured to be approximately 20 m below grade within the cohesionless sands and silts and mandated the use dewatering or impermeable shoring below the water table.

OPTION ANALYSIS

Temporary Cutoff Wall

The geotechnical conditions and spatial constraints limited effective dewatering and mandated installation of an interlocking secant pile wall sealed in rock all around the project site. Pile drill depths ranged from 40 m – 43 m below grade and were installed with three rotary drill rigs using segmental liners – two Bauer BG40's and one Bauer BG55.

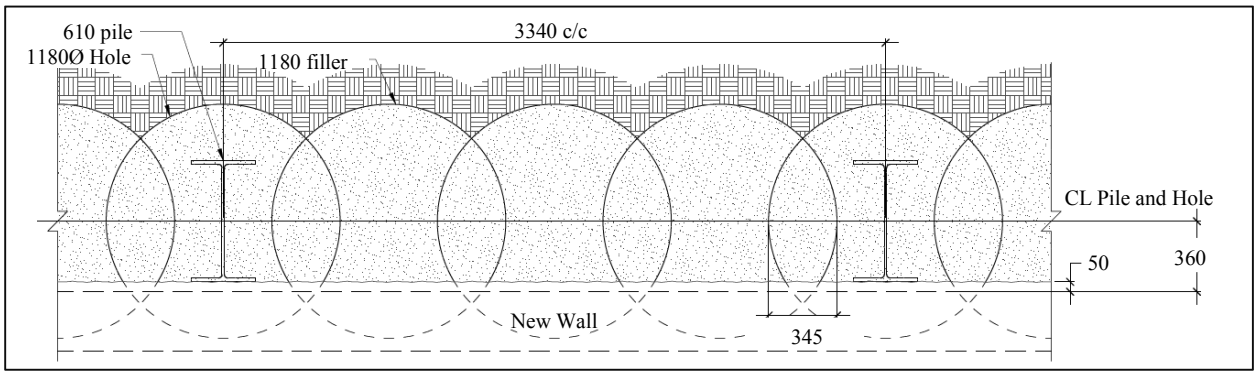


Fig. 3. Typical Secant Pile Wall Layout

Where space was limited between the proposed building and existing buildings on the West and South walls, the secant pile wall depth was limited to 580 mm (23") to allow for desired installation clearance to the adjacent building.

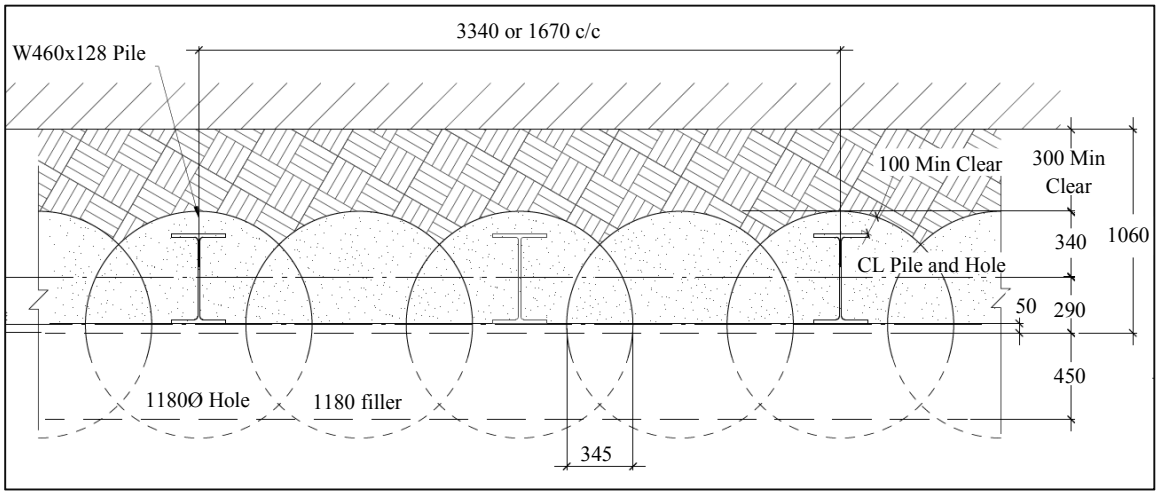


Fig. 4. Secant Pile Wall Adjacent to Existing Buildings on South and West Walls

Tied-back Shoring

Where geometry and encroachment agreements allowed, the preferred shoring bracing for design, installation, schedule, and performance reasons was tieback anchors. This design module was used adjacent to both Bloor and Yonge Streets. Anchor lengths were limited to maintain a minimum clearance of 1 m to adjacent structures. This option provided the most access within the site for both excavation and drilling of structural caissons at subgrade.

Internal Bracing

An internal bracing scheme was required where encroachment onto adjacent properties was not allowed or deep adjacent structures existed. A corner brace and cross site strut option with king piles was evaluated (Figure 5) but ultimately abandoned due to the excavation challenges and site access challenges it would impose for caisson installation at subgrade by effectively cutting the already small site into two smaller excavations.

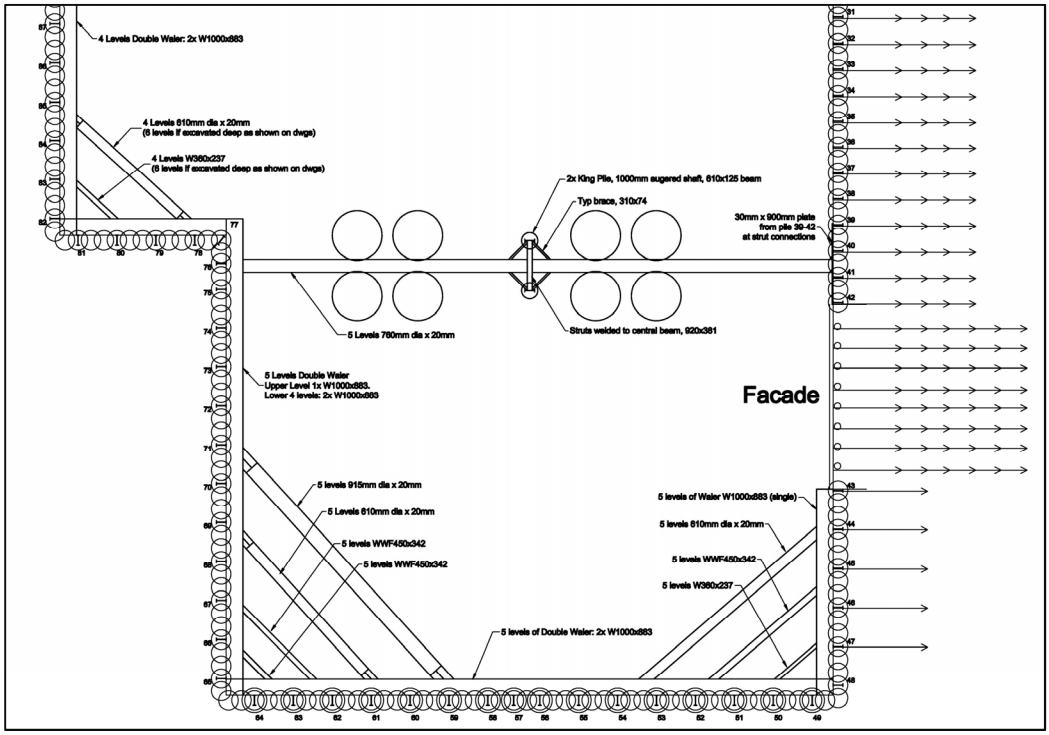


Fig. 5. Internal Bracing Scheme with Corner Bracing and Cross Site Strut/King Piles

Partial Hybrid Top Down

A hybrid top down approach was also evaluated for the West and South walls using a section of the permanent slabs as a deep beam to brace the shoring walls (Figure 6). Permanent slab width was limited to avoid conflict with larger diameter caisson locations and changes in the permanent structure geometry, for example the ramp location on South wall. This required the design of supplementary steel truss reinforcement to limit deflection and cracking of the permanent slabs in the temporary condition. Due to deflection compatibility, and therefore load sharing compatibility, the steel truss would have to be preloaded against the shoring wall prior to attachment to the concrete slab. The slab/truss would be braced back to the North and South shoring walls to limit deflection and transfer support load.

The slabs would also be used as construction staging areas due to limited space around the perimeter and no option of lane closure on either of the adjacent streets for the duration of the project. These slabs would be used for the excavator platform, material handling and loading, truck loading/unloading, concrete delivery, and concrete pump platform.

This option was ultimately passed over due to schedule pressure and constraints on excavation and the permanent structure design still being in-process at the time of design.

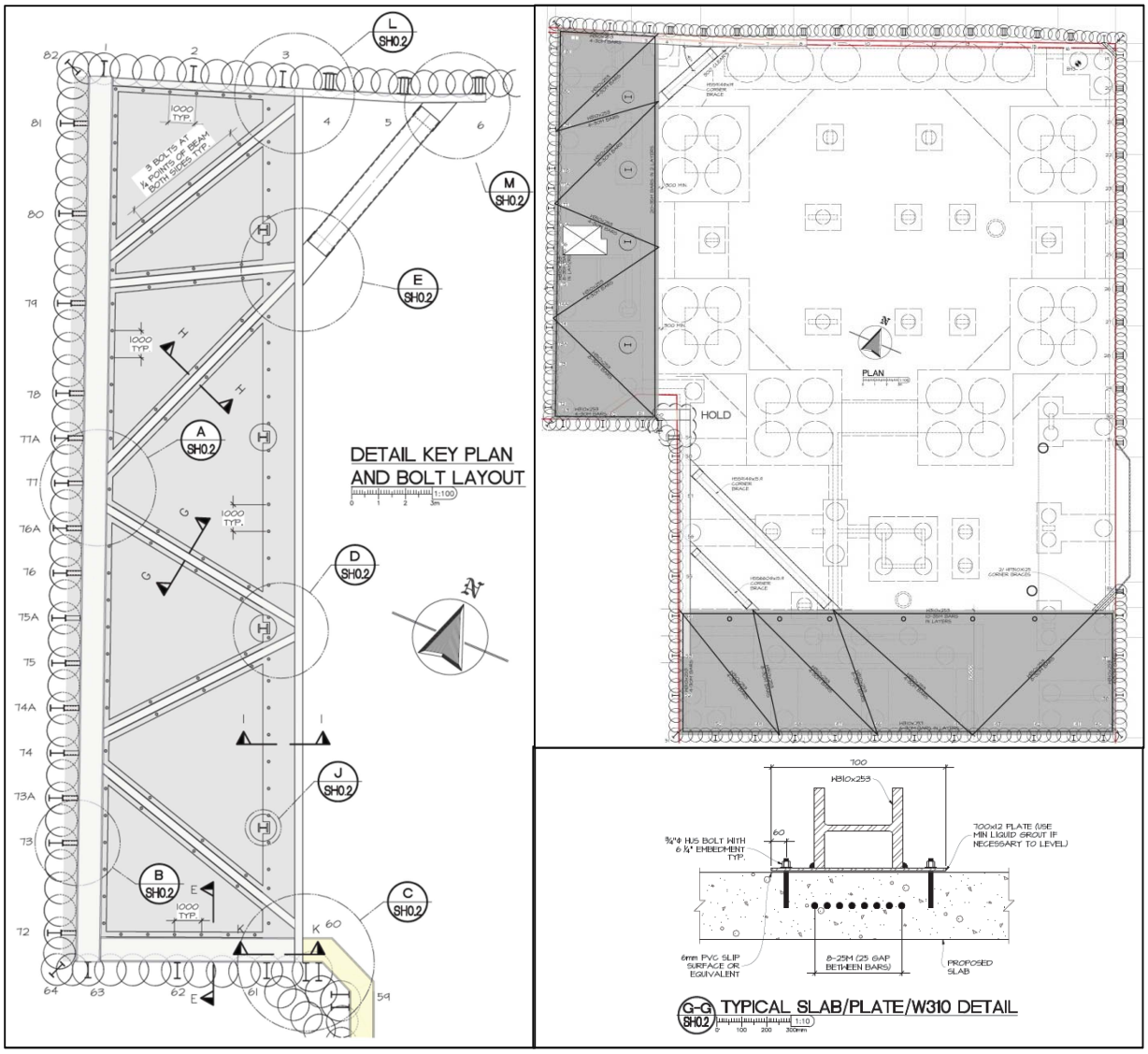


Fig. 6. Hybrid Top Down Scheme with Typical Example Details

The "Supercorner" and "Superpiles"

In order to facilitate an open excavation, removal of the cross site strut, and load transfer from the South slab bracing to the Northwest slab bracing, the concept of a "supercorner" with anchors through the public laneways was introduced. The supercorner has two double W760 (W30) piles in 1300 mm diameter drilled holes with six supplementary 1180 mm filler secants to transfer load from one section of the shoring to the other with limited deflection. Each superpile was designed with 13 anchors splayed from 15 to 45 degrees, each 1550 kN (348 kips) – the practical installation limit for a 12 strand anchor in a 150 mm (6 inch) post-grouted soil anchor and 115 mm (4.5 inch) rock anchor. The total horizontal anchorage force in each super pile is over 16,500 kN (3700 kips). Refer to Figure 7.

Shoring at Façade

A requirement for the development of the project at The One was to retain the building segment of the existing 774-776 Yonge Street building in place without relocation or dismantling and rebuilding. This did not leave sufficient space to the existing utilities, specifically an existing Toronto Hydro duct, along Yonge Street to install a secant pile wall from grade. Other options evaluated included an anchored

shotcrete wall, hybrid micropile shoring/anchor shotcrete wall (to achieve enough clearance with the anchors to existing utilities), and micropile shoring wall full depth with dewatering.

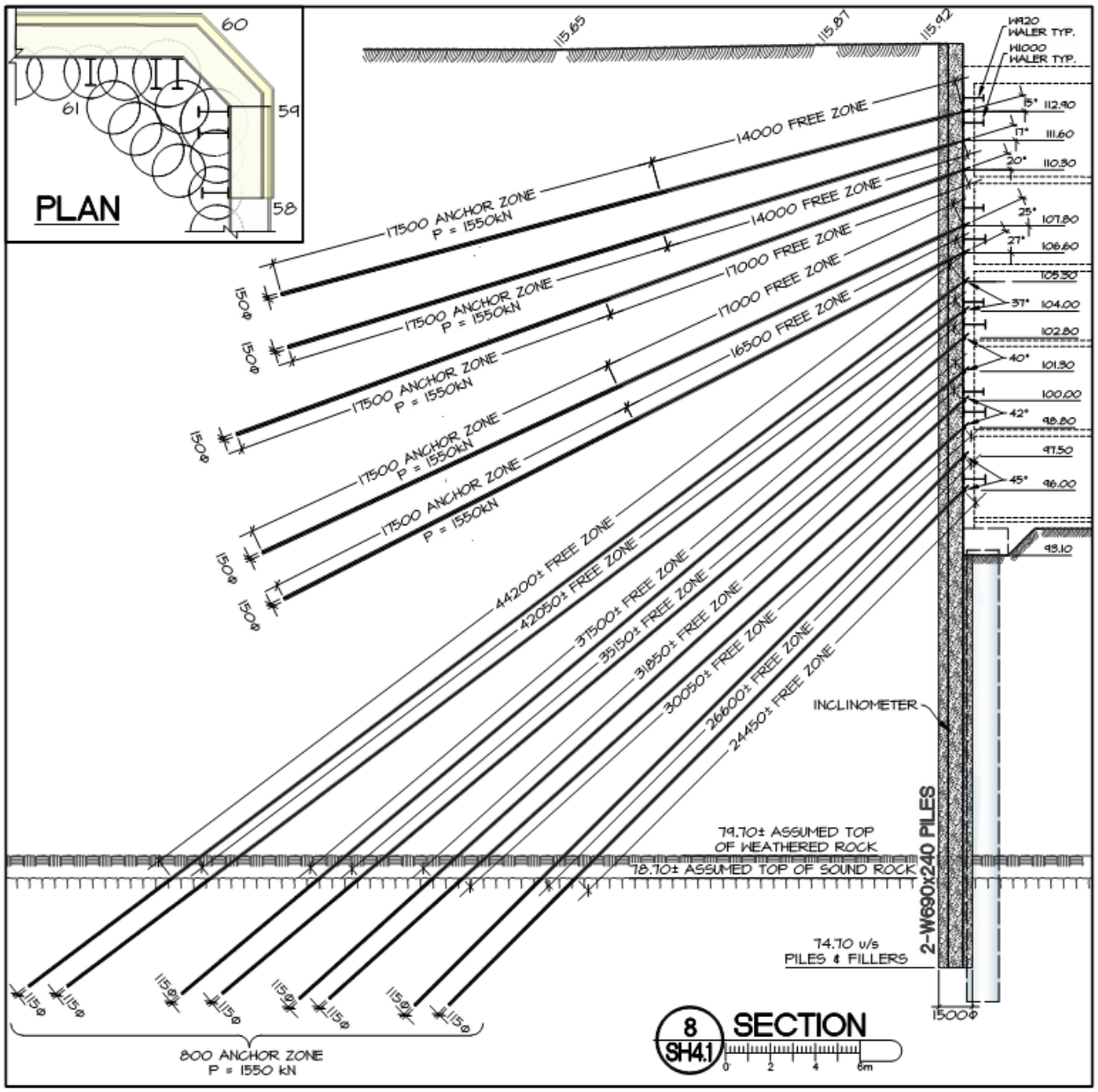


Fig. 7. "Supercorner" Layout and "Superpile" Section

Final Scheme

Ultimately encroachment negotiations were successful with the South neighbour allowing for tied-back shoring on the South wall and elimination of 11 anchors on one of the superpiles. On the Northwest side of the site, the super corner facilitated an internal bracing design with walers and corner braces from the West wall to the super corner and North wall. At the Heritage Building segment, anchored micropile-reinforced shotcrete shoring was used to an excavation depth of 20 m (65 ft) where a lower secant pile wall with anchors was installed to cutoff water for pile cap excavation. The final layout bracing layout is shown in Figure 8.

For construction staging, a temporary slab was constructed on the South wall to allow for construction access throughout the duration of the project. This temporary slab also provided bracing for the top of the piles on the South wall.



Fig. 8. Final Shoring Bracing Scheme – View looking South

LARGE DIAMETER DRILLED SHAFT FOUNDATIONS

The building foundation design consists of drilled shafts with up to a 6.5 m socket in rock. Due to the depth to rock, the decision was made to install the larger (>3 m/10ft) diameter caissons from a subgrade elevation near the base of final excavation. Overhead obstructions at the temporary slab, internal bracing, and heritage façade required the majority of the smaller diameter (<1.5 m) to be installed from grade using one BG40 (1.3 m dia. only) and one BG55 with segmental liner casing prior to excavation with the exception of the caissons located underneath the heritage building segment. The caissons located in the centre of the site were also installed from grade to advance the installation of the tower crane footing as it was planned to place the large equipment for subgrade caisson installation into the base of excavation. Table 1 provides a summary of the drilled shaft quantities and average drill depths.

Table 1 – Structural Foundation Summary

Drill Elevation	Diameter – mm (ft)	Average Drill Depth – m (ft)	Quantity
Grade (115 m ±)	1300 (4.25)	42.3 (138)	17
	1500 (5)	43.0 (141)	48
Subgrade (95 m ±)	1300 (4.25)	23.0 (82)	4
	3058 (10)	25.3 (83)	24
	3353 (11)	25.9 (85)	6

The large diameter caissons were installed from subgrade (-20 m/65 ft) using the APE 400 vibratory driver to drive casing to rock before drilling inside with a BG55 rotary drill. Due to low headroom underneath the heritage building and support structure, a modified low headroom BG24 rig was used to install both the lower secant pile wall and structural caissons (Figure 9).

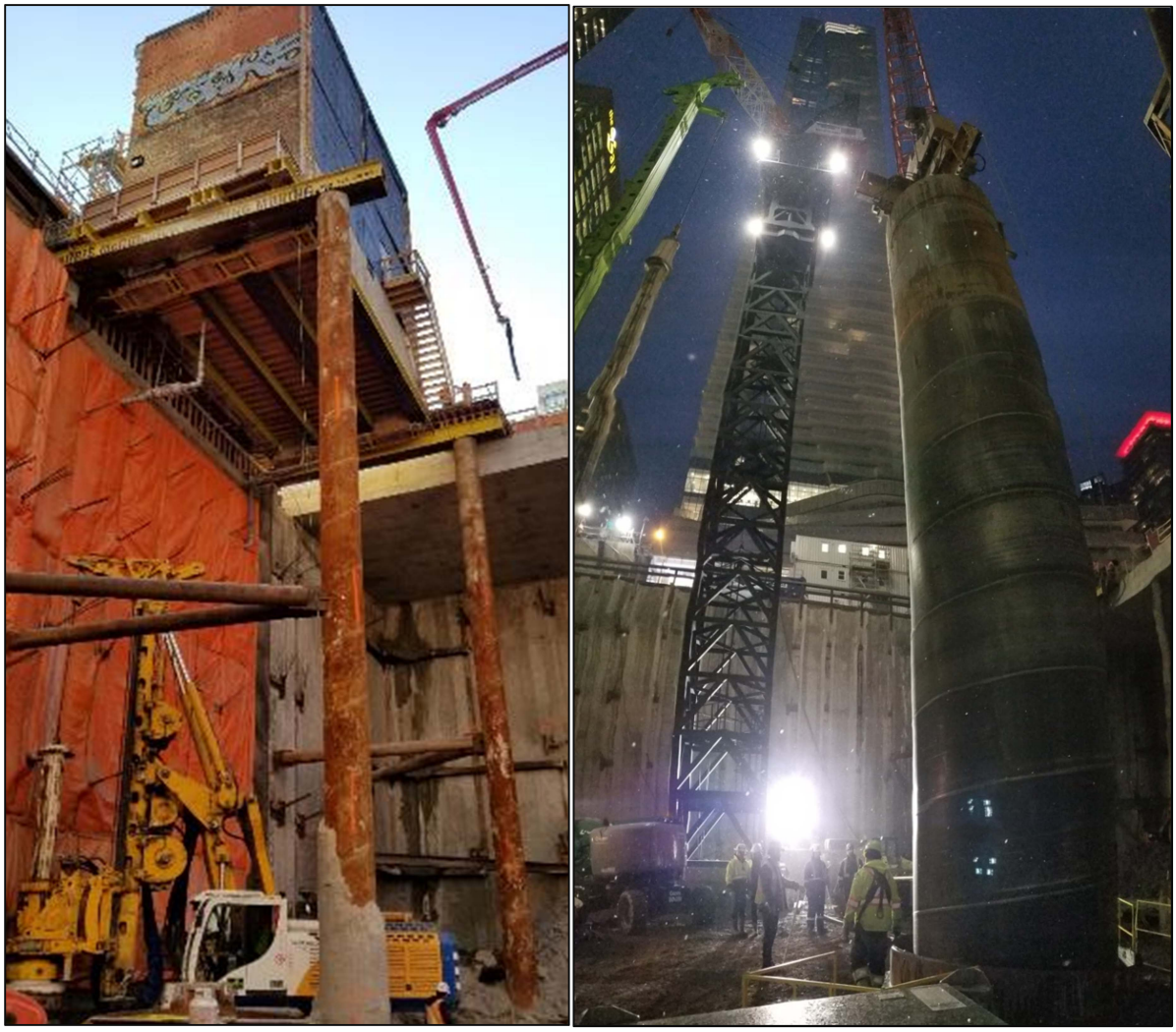


Fig. 9. Low Headroom BG24 under Façade (L); Driving 10' dia. liner at subgrade APE400 (R)

RISKS TO ADJACENT STRUCTURES

Using the vibratory driver installation method for the large diameter caissons involved a balance between efficient installation methodology and risks to adjacent structures including the active excavation shoring, heritage façade, and surrounding structures. The structural caissons adjacent to the shoring ranged in distance to the shoring walls from 6 m (20 ft) to 300 mm (1 ft), creating concern that installation could

cause disturbance within the sand layer and result in excessive shoring movement. At the heritage structure, structural caissons were located as close as 3 m from the supporting king piles. Of concern was vibration transmission through the king piles into the sensitive structure above. Finally, limiting vibration transmission through the shoring into adjacent structures to below City of Toronto mandated vibration limits (5mm/s) had to be managed.

MONITORING AND THE OBSERVATIONAL METHOD

Based on the known risks, a monitoring plan was developed to take advantage of the observational method to manage and converge on the areas of highest risk. Figure 10 outlines the excavation monitoring plan for the project including:

Inclinometer Monitoring: At 11 locations around the site to cover various design modules, and at locations adjacent to large diameter structural caissons
Shape Accel Array (SAA): At super corner location to provide real time inclinometer readings during tieback stressing, corner brace preloading, and excavation on the Northwest wall
Pile Survey Monitoring: Located at the top and mid-span of each pile to correlate inclinometer monitoring, and provide performance coverage between inclinometer locations
Slab Survey Monitoring: Along the edge of the South temporary slab support beams in lieu of pile targets due to site line challenges with reading pile targets below slab
Façade Survey Monitoring: To monitor façade structure movement during excavation
Precision Survey Building Monitoring: At adjacent buildings within the influence of excavation at the South and West
Real-time Vibration Monitoring (not shown): In adjacent buildings within the vibration influence and the heritage building

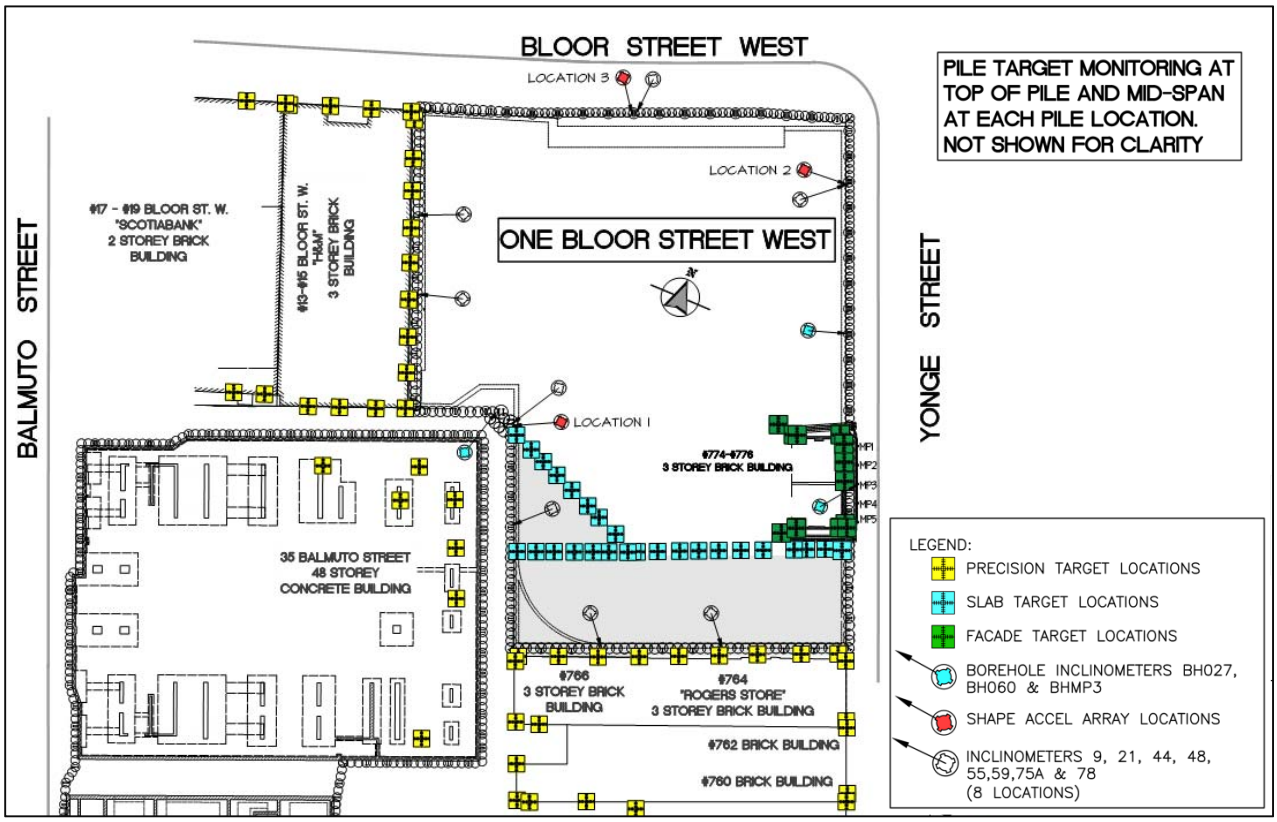


Fig.10. Monitoring Plan for One Bloor West

REAL-TIME RISK MANAGEMENT

In order to manage the risk from large diameter caisson installation, a sequence of installation was created to monitor shoring performance while converging on areas of the perceived largest risk (i.e. proximity to the shoring wall). This involved installing the first caisson at a test location to confirm installation methodology and impact to shoring at each new group of caissons as they were installed closer to the shoring wall i.e. at 6 m, followed by 2 m, and then 0.3 m. The SAA was relocated to each location using the tower crane to monitor real-time shoring performance at the test location and should unfavourable movement be observed, either methodology would be adjusted or additional bracing would be added to the remainder of the shoring wall prior to continuing caisson installation. Shoring performance remained within acceptable levels at each location and no additional bracing was required.

For installation adjacent to the heritage building, it was determined the calculated natural frequency of 10 – 15 Hz for façade support king piles was within the operating range of the APE 400 vibratory driver (6.7 – 23 Hz) (APE 2007). To control this risk, real-time vibration monitoring was installed on the king piles between the lateral brace elevation and base of excavation. For caisson installation adjacent to the king piles, vibration was closely monitored for amplification of readings at the king piles and overall vibration within the heritage façade.

FROST IMPACT ON SHORING

Frost forces behind and beneath exposed ground surfaces can be many times greater than the normal forces an excavation shoring system is designed to withstand. Frost, according to Environment Canada, can occur between November 1 and May 15 and has been known to heave entire buildings several inches. At local excavations, we have observed damaged lagging, cracked caisson walls, broken tieback connections (including projectiles), and monitoring results indicating pile movements greater than 40 mm (1½ inches) in one week and over 90 mm (3½ inches) total. This presents a safety concern, can cause site delays, require increased field presence and monitoring costs, and remedial actions. Our recommendation regarding frost movements is to protect shoring and soil faces from freezing between November 1 and March 31 by insulated blankets or tarps, heating tents, or sprayed on polyurethane foam. We know of no frost damage occurring on local sites where frost protection blankets (minimum R4 value) were deployed.

Prior to November 1 at The One, frost protection was installed on the micropile shoring wall only which showed little to no impact from frost throughout the winter. In our experience, frost traditionally develops from the top of the excavation downwards - a trend that was visible on the East wall of the project. However, the SOE system at The One posed an additional challenge for frost susceptibility: the “skinny” caissons walls on the Northwest and South walls. These 570 mm (22 ½” inch) walls were the first to show impact from frost and exhibited movement over the entire depth of the excavation. This difference in expected behavior of frost loading resulted in delay of problem identification and required remedial action to protect the integrity of the shoring. Insulated blankets and active heating were required on the Northwest and East walls, and the South wall was backfilled with a 7 m (23 ft) berm to the third tieback level to protect the anchors from yielding. The total additional movement due to frost ranged from 12 mm (1/2”) on the Northwest wall to 20 mm (3/4”) on the South wall. After active heating, frost induced movement was recovered on the North and East walls, and movement was recovered on the South wall after temperatures rose above 0°C. Frost movement had little to no impact on the North (i.e. South – facing) wall which receives the most sun exposure.

SHORING PERFORMANCE

Figures 11 – 14 below show overall SOE performance at the North wall, South wall, “Superpile”, and West wall. With the exception of frost induced movement, shoring performed within expectations and vibratory installation methods had minimal impact on overall shoring performance.

LESSONS LEARNED

Several lessons were learned throughout the excavation shoring of The One:

1. Inviting design build alternatives when tendering projects can lead to innovative solutions and have a tremendous advantage for constructability of projects;
2. Fast tracking of excavation shoring design in advance of final structural design barred incorporation of permanent structure into temporary shoring;
3. Vibratory installation methodology of large diameter structural caissons at subgrade had minimal impact on SOE performance in the stiff to hard silt/clay and dense to hard sand;
4. Thin caisson walls (<600 mm / 24 inch) have higher susceptibility to frost and can exhibit different behavior than thicker (800 mm/ 32 inch) secant pile walls; and
5. Lack of frost protection at shoring walls can cause overstressing of the excavation support bracing and require remedial action to protect the integrity of the excavation shoring system.

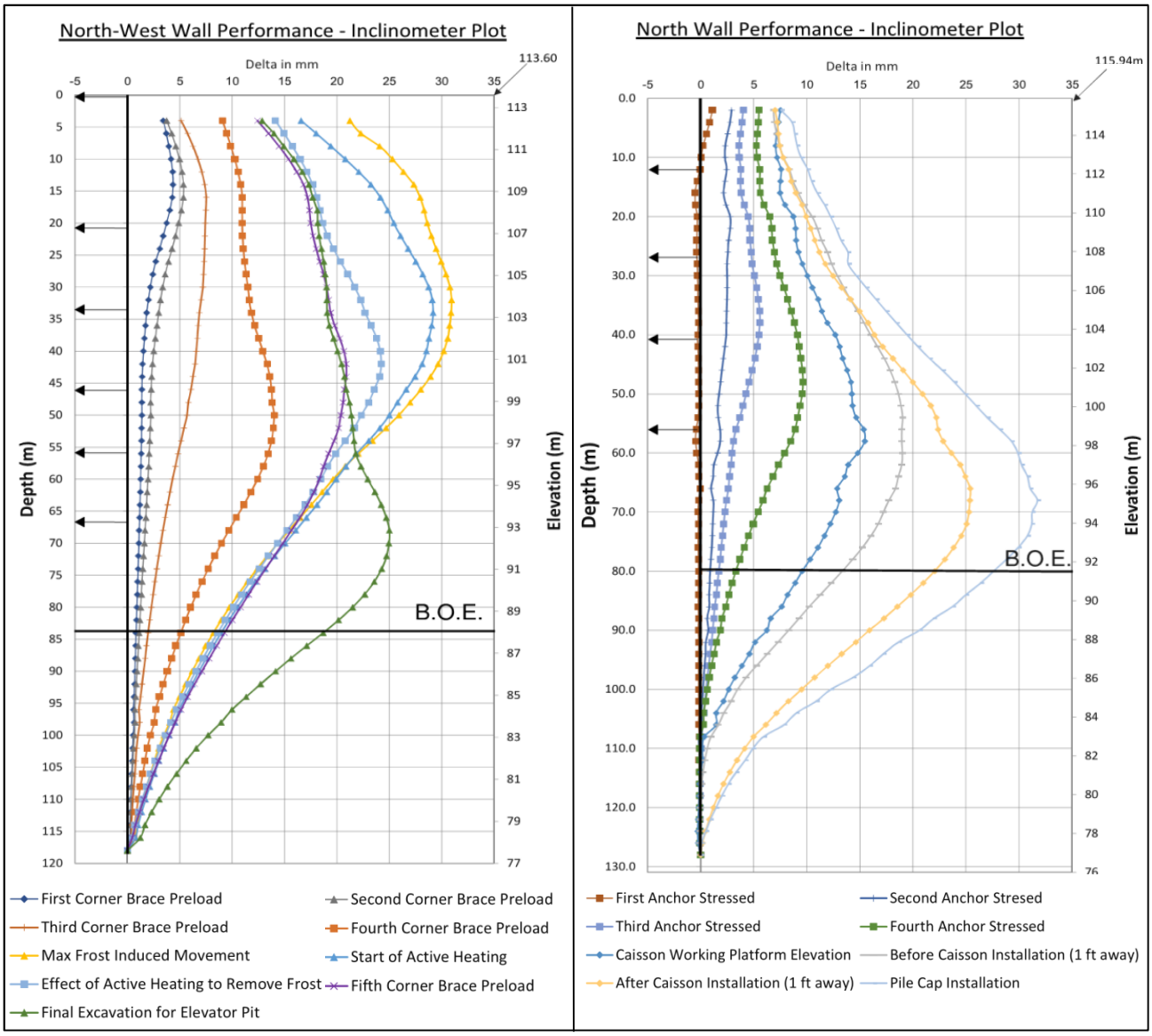


Fig. 14. Northwest Wall Performance (L), North Wall Performance (R)

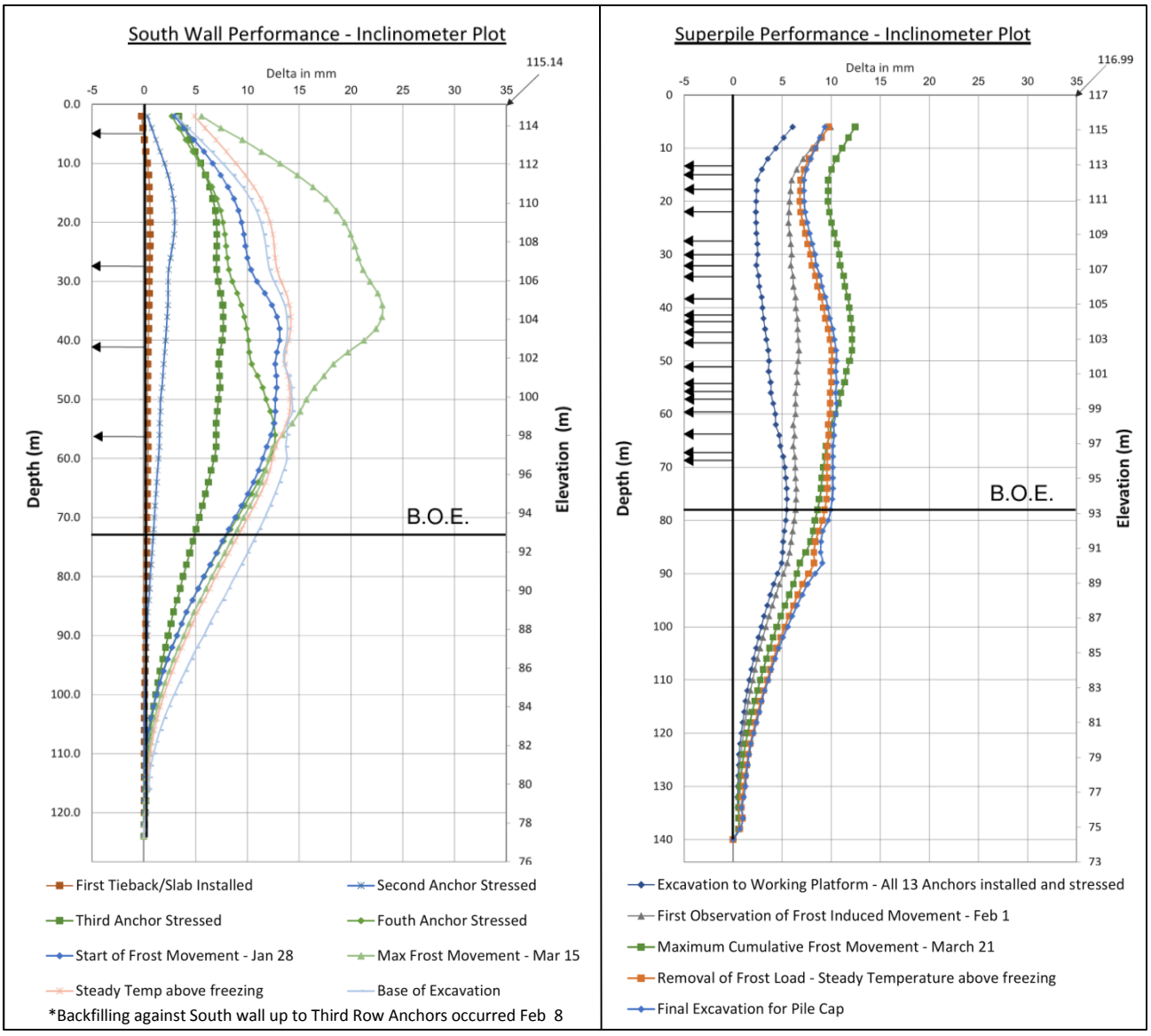


Fig. 15. South Wall Performance (L), Superpile Performance (R)

ACKNOWLEDGEMENTS

To Mizrahi and Clark Construction Management for undertaking Toronto's first supertall residence.

REFERENCES

1. Terraprobe, 2016. Detailed Geotechnical Investigation, The One, 1 Bloor Street West, Toronto, Ontario. 60 p.
2. APE, 2007. American Pile Driving Equipment Inc. Model 400 Vibratory Driver Extractor. http://www.americanpiledriving.com/manuals/APE/400_1050_11%2007_Spec.pdf. 2 p. Accessed 19.04.01.

EXCAVATION-INDUCED MOVEMENT OF ADJACENT FOUNDATIONS

Wystan Carswell, Haley & Aldrich, Inc., Boston, Massachusetts, +1 (617) 886-7357, wcarswell@haleyaldrich.com
Hugo Meggitt, Haley & Aldrich, Inc., Boston, Massachusetts, hmeggitt@haleyaldrich.com, +1 (617) 886-7474
Damian R. Siebert, Haley & Aldrich, Inc., Boston, Massachusetts, dsiebert@haleyaldrich.com +1 (617) 886-7399

ABSTRACT

Excavation-induced ground movements are a critical component in the design and construction of deep excavations in urban settings due to the potential adverse effects on adjacent structures and infrastructure. Ground movements are influenced by soil stratigraphy, soil properties, adjacent structures, and construction means and methods. The use of empirical relationships, computer models, and reliance on experience with similar excavations in similar soil conditions often provides a basis for predicting excavation-induced ground movements. In this paper, data from 21 deep excavations approximately 20 ft to 75 ft deep supported by concrete diaphragm "slurry" walls in the Greater Boston area are compared to published literature, considering how different foundation systems (e.g. shallow foundations, caissons, and piles) of abutting structures have been affected by adjacent excavations. The influence of construction method (conventional vs. top-down) on adjacent foundation movements indicate that top-down construction typically results in smaller foundation movements.

Keywords: Support of excavation, ground movement, settlement, piles, empirical correlation

INTRODUCTION

Estimation of ground movements due to excavation is a challenging endeavor, even with complex three-dimensional finite element modeling and high-order constitutive models that are increasingly available in modern engineering practice. Aside from the expense of the soil exploration and testing used to inform these higher-order models, the challenges of modeling past stress history, adjacent structures, and the groundwater conditions during excavation require not only large investments of time during design but also validation from past experience (to avoid a "garbage in, garbage out" paradigm). While site conditions such as soil stratigraphy, soil properties, groundwater conditions, and as-built conditions of adjacent structures can be obtained, measured, and estimated, the effects that means and methods of construction have on ground movements are difficult to quantify. During early phase design, assessments of predicted ground movement are unable to account for all aspects of project construction, nor is it cost-efficient to fully design an excavation while project parameters such as site size and excavation depth are under consideration by the design team. While construction is in progress, benchmarking support of excavation performance and associated ground movements in the context of successfully completed projects allows for a more nuanced view of system performance and provides the opportunity for more informed decision-making (if required) as construction proceeds. For these reasons, the use of empirical relationships and the collection of historical support of excavation performance holds high value for the practicing geotechnical engineer at all phases of the project.

Particularly for densely developed urban areas, the prediction of ground settlement is of high importance due to the potential impact on abutters and critical infrastructure during both the planning and construction stages of major excavation projects. Empirical correlation has often been used to inform the prediction of ground movements. This paper compiled data from 21 deep excavations approximately 20 ft to 75 ft

© 2019 Deep Foundations Institute

supported concrete diaphragm "slurry" walls using various construction methods (conventional construction, top-down construction) in various subsurface conditions (clays, organics, glacial soils, bedrock) in the Greater Boston area and compares the results to the seminal work by Clough and O'Rourke (1990). The effects of adjacent excavation on different foundation systems (e.g. shallow foundations, caissons, and piles) of abutting buildings is discussed.

SUBSURFACE CONDITIONS OF GREATER BOSTON

The subsurface conditions of Greater Boston typically consist of fill overlying organic deposits over marine deposits of sand, silt, or clay, with a layer of dense glacial soils followed by bedrock (e.g., Fig. 1). The depth to bedrock varies significantly across the city, from exposed outcrops in some areas (e.g., Roxbury) to over 200 ft deep (South Boston Seaport). Groundwater elevations vary but are typically on the order of 0 ft to 20 ft below ground surface. Depending on the depth of excavation and the soil conditions at the project site, excavation-induced ground movements may be governed by local movements (i.e., vertical soil movements due to the lateral movement of excavation support walls) or a combination of local and deep-seated, global movements (i.e., basal heave from soil unloading during mass excavation). Global movements are a more prevalent issue for large excavations in deep deposits of softer soil conditions; while no differentiation is made in this paper regarding the specific soil conditions of the project sites, it is worth noting the significant influence that global soil movements can play in excavation-induced ground movements.

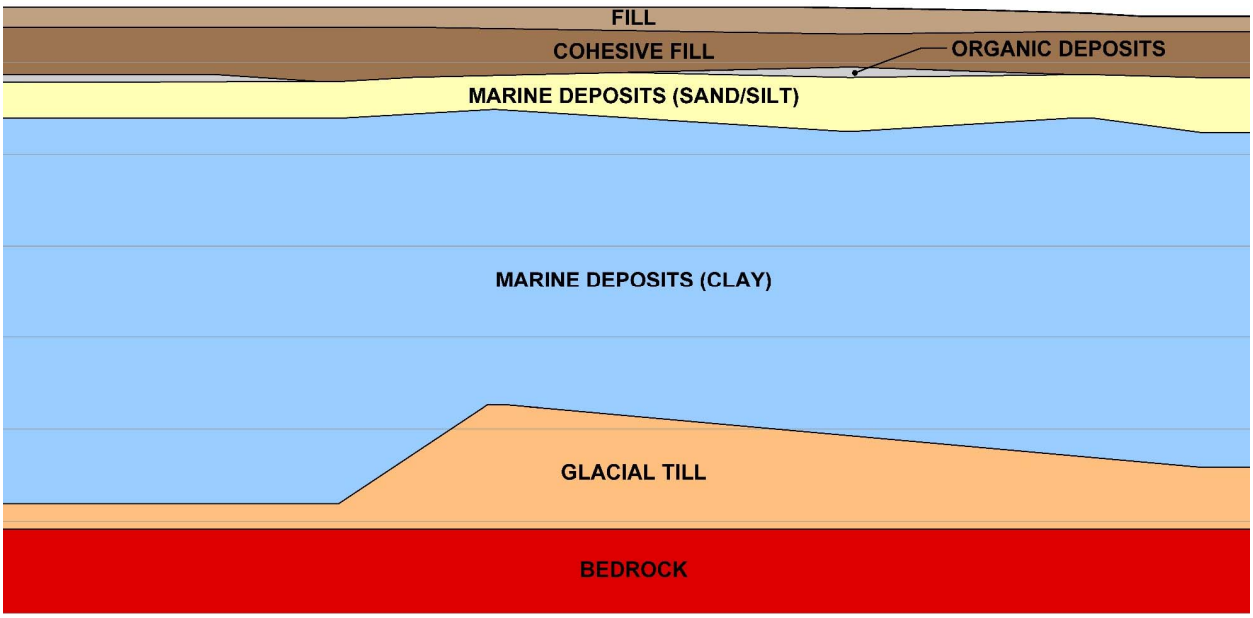


Fig. 1 Typical subsurface conditions for the greater Boston area

PROJECT DATABASE

The data presented in this paper was compiled from 21 projects located in the Greater Boston area (either Boston or Cambridge, Massachusetts), with excavations varying in depth from 20 ft to 75 ft below ground surface. The excavations were supported by concrete diaphragm "slurry" walls varying in thickness from 24-in. to 48-in. and internal bracing (pipe struts and external wales) and/or external bracing (tiebacks). Vertical movements from nearly 1000 survey points on 98 adjacent structures were recorded prior to and throughout mass excavation using survey points established on the structures.

Adjacent structures were supported on a variety of deep and shallow foundation types bearing in marine sand or clay, glacial till, or bedrock, discussed in more detail below. The approximate locations of the projects are shown in Fig. 2.

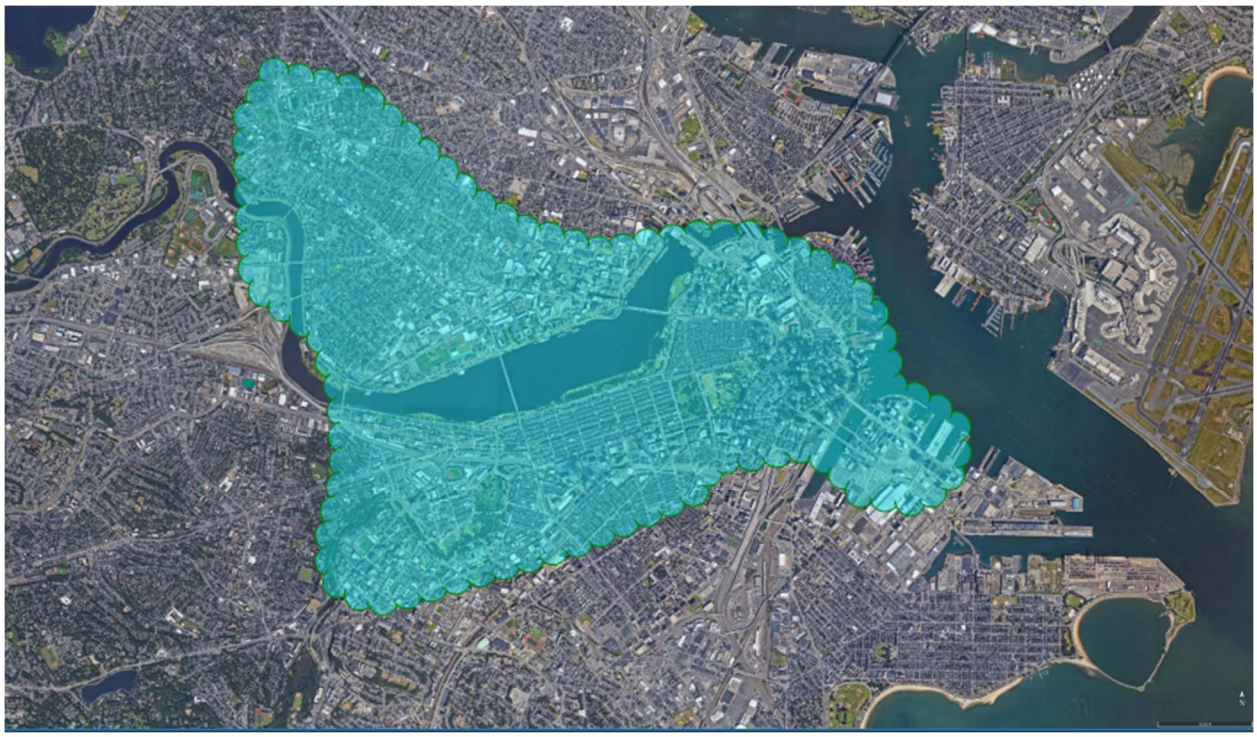


Fig. 2 Greater Boston support of excavation project database

CONSTRUCTION METHODS FOR CONCRETE DIAPHRAGM "SLURRY" WALLS

Reinforced concrete diaphragm "slurry" walls (slurry walls) are constructed in panels with the use of a clamshell excavator bucket. Excavation proceeds under a head of slurry (bentonite or polymer) which provides lateral stability of the panel side walls during excavation. Once excavation reaches the bottom of the panel, a reinforcement cage is lowered by crane into the panel excavation and concrete is placed via tremie tube from the bottom of the panel progressively toward ground surface while the slurry (displaced by concrete) is pumped from the top of the panel excavation. Once concrete has set in a "primary" panel, excavation can proceed for an adjacent "secondary" panel, until all panels have been excavated and concreted into a continuous wall. Mass excavation proceeds after the slurry wall has been completed using one of two construction methods which are referred to here as "conventional" and "top-down" excavation.

For conventional slurry wall construction (Fig. 3), mass excavation takes place after slurry wall construction is completed. Temporary internal or external bracing is constructed as mass excavation proceeds; once the bottom of excavation (B.O.E.) is reached, permanent structural features are constructed moving upwards towards ground surface. When floor slabs achieve design strength or other permanent bracing features are constructed to support the wall in the permanent condition, bracing is removed.

In top-down construction, permanent floor slabs are constructed with progressive excavation through "glory holes" left in the slabs (Fig. 3) and thus serve as both the temporary and permanent bracing for the foundation walls. Because excavation typically occurs in smaller increments – i.e., vertical between floor slabs is often less than the vertical distance between temporary bracing levels – and because diaphragm action from permanent floors slabs provide a significantly stiffer lateral bracing system than internal or

external bracing, top-down construction typically results in smaller excavation-induced movements of adjacent structures as compared to conventional slurry wall construction.

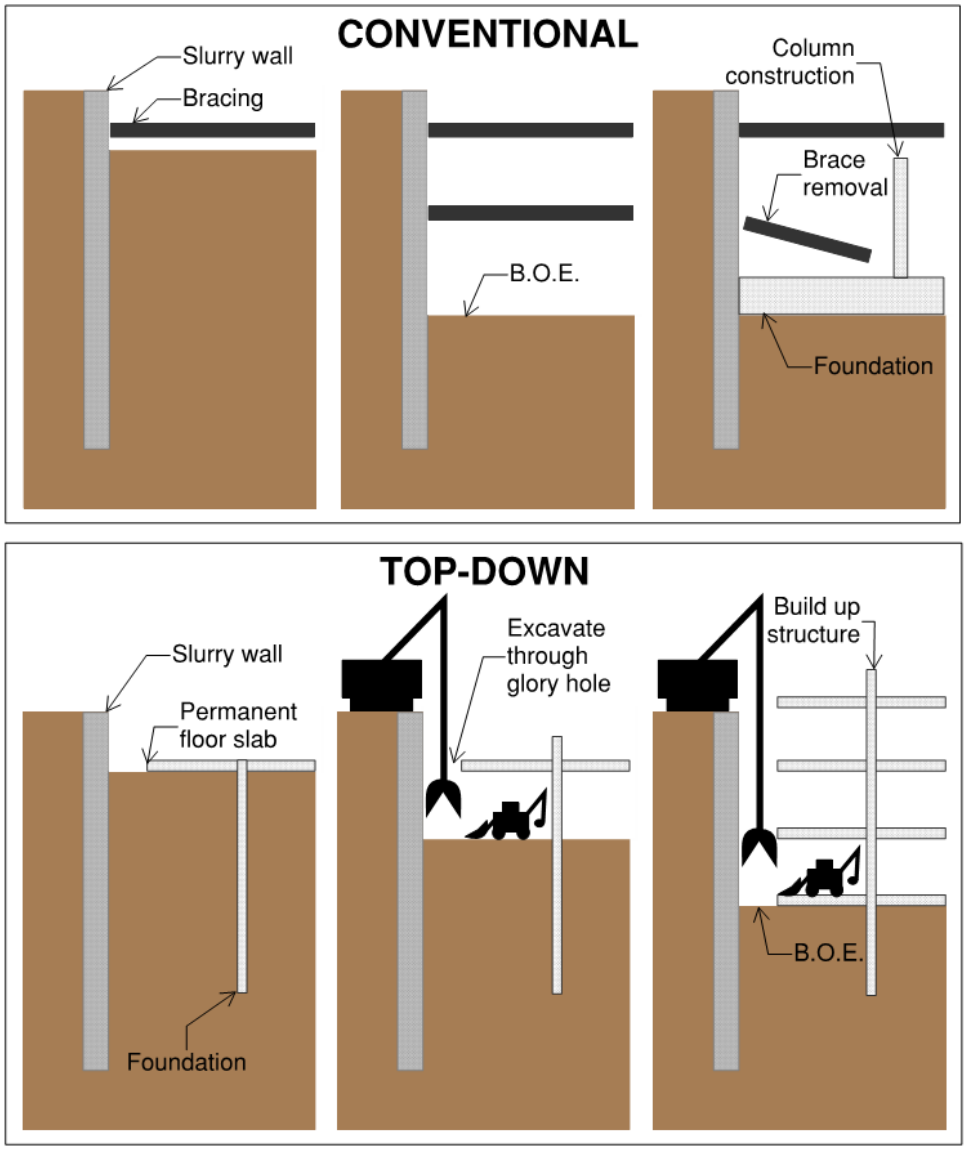


Fig. 3 Concrete diaphragm "slurry" wall construction methods

Of the 21 slurry wall-supported deep excavation projects considered, eighteen were constructed using conventional excavation methods and three used top-down construction methods.

ADJACENT STRUCTURES FOUNDATION TYPES

Excavation-induced movements of adjacent structures in this paper were subdivided by general foundation type: shallow foundations and deep foundations.

Shallow foundations include structures supported by spread footings and mat foundations. Bearing elevations for spread footings typically ranged from ground surface to 30-ft below ground surface (bgs). The bearing strata for the spread footings was typically marine clay, but also marine sand, fluvial soils, and

for one structure, fill. Spread footings include reinforced concrete and historic stepped granite blocks shallow foundations. Mat foundations supported typical structures and also underground transit tunnels (separated from typical structures) with bearing elevations typically between 20 ft and 40 ft bgs on marine clay, marine sand, glacial till, or bedrock.

Deep foundations for adjacent buildings included piles (timber, steel H-piles, and precast concrete), caissons, pressure injected footings (PIFs), slurry walls, and Load-Bearing Elements (LBEs).

- Timber piles bearing between 20 ft and 35 ft bgs founded in the marine clay strata.
- Steel H-Piles and precast, prestressed concrete (PPC) piles bear in either glacial deposits or bedrock and typically were below the bottom of adjacent slurry wall panels).
- Caissons included both straight shafts and belled caissons, bearing in the upper marine sand or clay stratum above the bottom of the excavations.
- The bearing elevation of PIFs was typically 20 ft to 50 ft bgs in marine sand and in all cases, above the bottom of excavation.
- Slurry walls and LBEs, founded in bedrock, were below the bottom of excavations.

EXCAVATION-INDUCED FOUNDATION MOVEMENTS

Foundation movements from excavations can be due to local effects (due to lateral excavation support wall movement) or a combination of local and global effects (lateral excavation support wall movement combined with basal heave due to mass excavation), depending on the soil conditions at the project site as well as the size (in plan area) and depth of the excavation. Global soil movements can significantly contribute to adjacent structure movements for large, deep excavations in areas with deep deposits of softer clay soils. Movements due to local effects are typically predicted during design, however movements due to global effects are often overlooked and difficult to capture and estimate.

Fig. 4 shows the vertical movement data (v) from survey points installed on structures with shallow foundations plotted against the distance of the survey point from the excavation (D), normalized by the maximum depth (or "height") of the excavation, H. Open markers indicate vertical movement data measured from projects excavated using conventional construction methods and solid markers indicate vertical movement data from projects excavated using top-down construction methods.

Clough and O'Rourke (1990) defined an approximate maximum boundary of vertical movements with a linear boundary from 0.3% v/H to $3D/H$ for stiff to very hard clays (indicated on Fig. 4). It should be noted that one of the projects considered by Clough and O'Rourke (1990) was an excavation near State Street in Boston, the data from which appears to largely inform the linear boundary selected for stiff to hard clays; when depicted relative to the greater Boston area excavation data, this linear boundary captures the majority (but not all) of the vertical movement data. The exceedance of this boundary for many of the excavations in Boston implies two factors:

1) Many excavations in the greater Boston area were in soils softer than excavations in stiff to very hard clay considered by Clough and O'Rourke (1990), and
2) The softer soils in greater Boston necessitate an examination of global soil movements due to excavation, which may significantly contribute to foundation movements within as much as five times the maximum depth of excavation ($5D/H$).

Consequently, a maximum boundary for excavations in greater Boston would be better captured by a linear boundary from 0.4% v/H to $5.5D/H$ (Fig. 4). Additionally, movements of shallow foundations from top-down construction methods are typically smaller relative to the range of movement data from conventional

excavation (less than 0.1% *v/H* typically, except for spread footings directly adjacent to the excavation, which are less than 0.17% *v/H*).

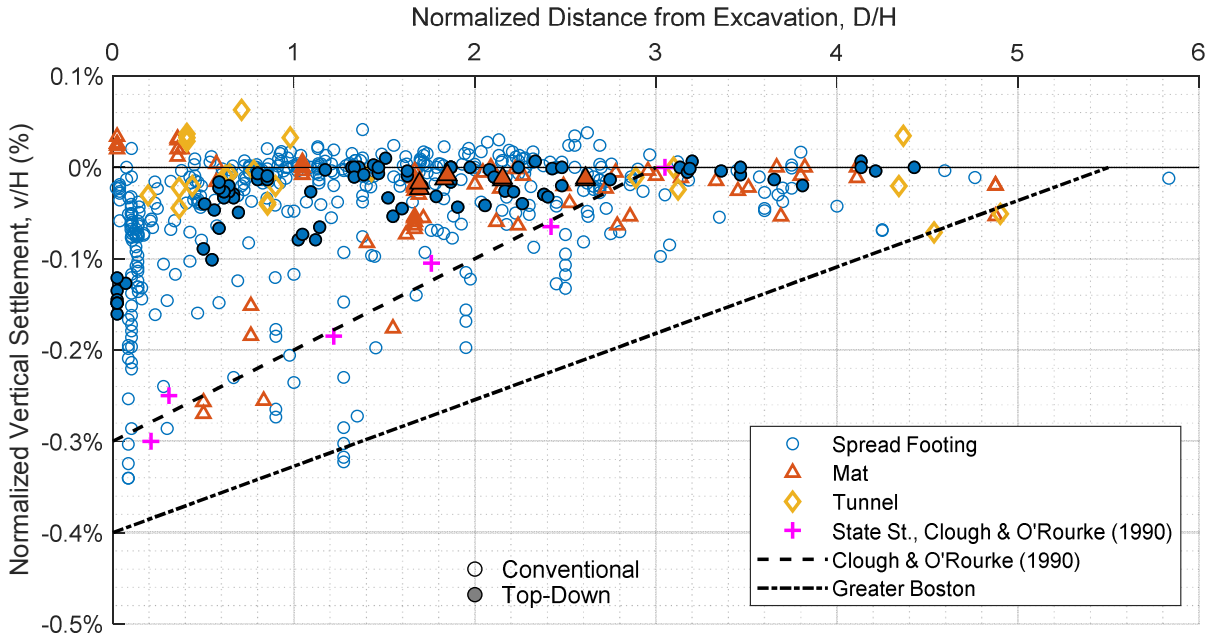


Fig. 4 Vertical movement of shallow foundations (*v*) vs. distance from excavation (*D*), normalized by depth of excavation (*H*).

Fig. 4 obfuscates the relative relationship between the bearing elevation of the shallow foundations and the bottom of excavation; intuitively, shallow foundations bearing at or near the bottom of excavation ought to move less than a shallow foundation that bears significantly higher than the bottom of excavation. Traditionally, geotechnical engineers have used empirical "zones of influence" to indicate the possible influence of an excavation on surrounding structures (or alternately, whether the bearing pressure from a shallow foundation may laterally surcharge an excavation support wall). These zones of influence are often taken to be diagonal lines in the range of 1 horizontal to 1 vertical (1Horiz:1Vert) to 2 horizontal to 1 vertical (2Horiz:1Vert). These zones of influence are shown on Fig. 5 at $D/dH = 1$ and $D/dH = 2$ (where *dH* is the difference in elevation from adjacent foundation bearing to bottom of excavation), and indicate that for the excavations in the greater Boston area, shallow foundations outside of these typical zones of influence may still be affected by nearby excavations.

It is interesting to note that the linear relationship visible in the data normalized by full excavation depth in Fig. 4 is, for the most part, lost when data is normalized by relative excavation depth (*dH*) as in Fig. 5. Instead, a maximum bound for vertical movements is better characterized by an envelope boundary from approximately 0.65% *v/dH* out to $2.5D/dH$ and then decreasing to 0 at $9D/dH$ (denoted as "Greater Boston Envelope" in Fig. 5).

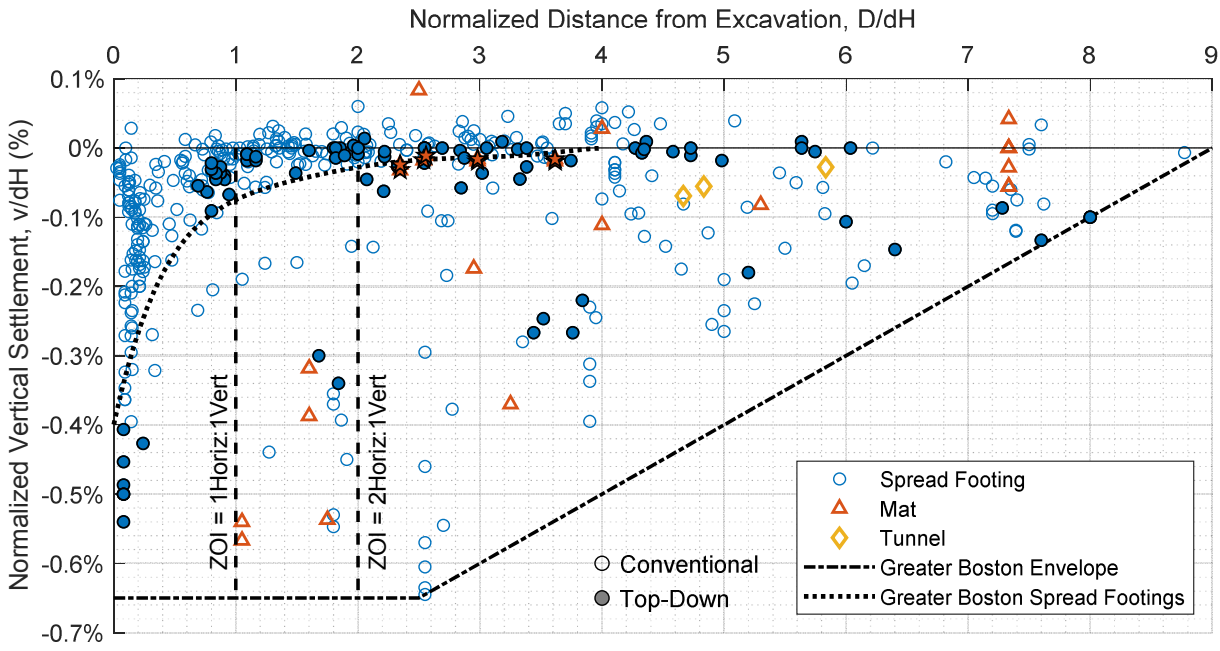


Fig. 5 Vertical shallow foundation movement (*v*) vs. distance from excavation (*D*), normalized by relative depth of excavation (*dH,* from foundation bearing elevation to bottom of excavation)

A large portion of the vertical movement data for spread footings appears to behave in an exponential manner, with maximum vertical movement at approximately 0.4% *v/dH* and a rapid decrease to negligible movement (< 0.01% of excavation depth) by approximately 4*D/dH* (noted with the dotted curve in Fig. 5, denoted as "Greater Boston Spread Footings"). This relationship may presumably capture excavation-induced movements from local behavior, while the outside scatter may indicate the effects of global soil movements, construction means and methods, or other unique project issues.

Clough and O'Rourke (1990) focused on soil movements adjacent to excavations rather than adjacent foundation movements; consequently, there was no differentiation in vertical movements based on foundation type and depth relative to the excavation. Fig. 6 illustrates the same maximum bound defined by Clough and O'Rourke (1990) from 0.3% *v/H* to 3*D/H* (as discussed in relation to the behavior of shallow foundations in Fig. 4) for vertical movement of adjacent structures supported by deep foundations. The Clough and O'Rourke (1990) boundary appears to capture the vertical movements of most of the deep foundation supported structures, with the exception of the structures supported by caissons.

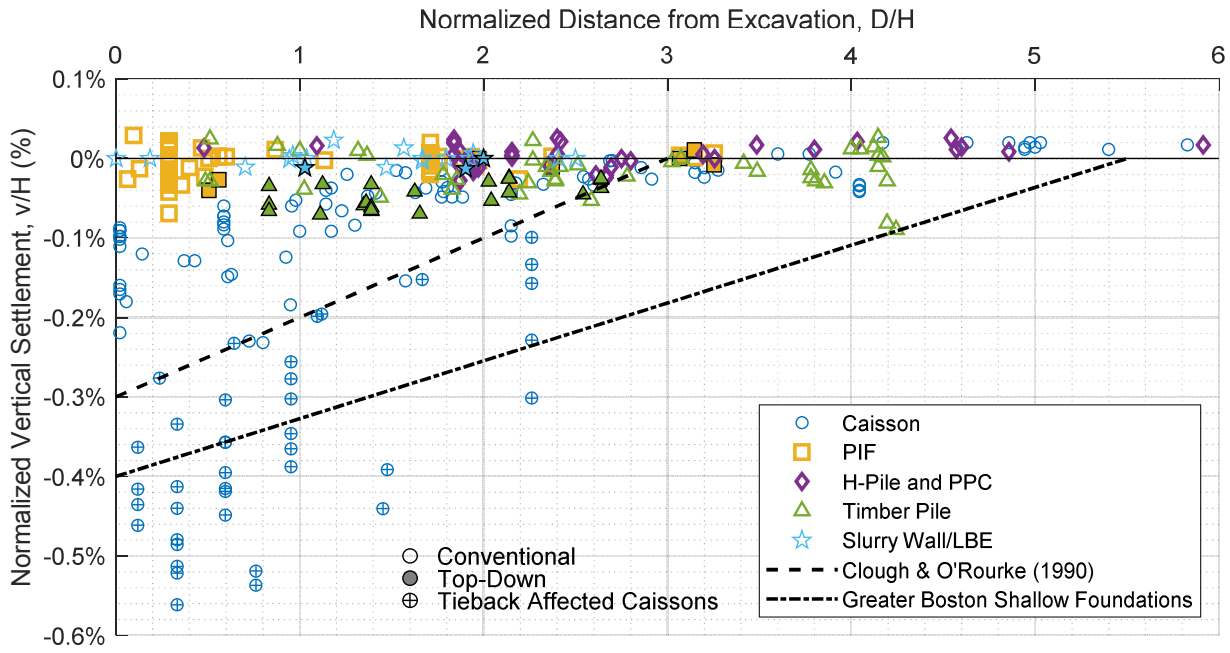


Fig. 6 Deep foundation movement (*v*) vs. distance from excavation (*D*), normalized by depth of excavation (*H*)

As mentioned previously in the descriptions of the foundation elements, all of the caissons assessed in this paper ended in marine sand or clay layers above the bottom of the excavation. The majority of the caisson data below the Clough and O'Rourke (1990) boundary were from a construction project where tiebacks were drilled (without internal flush) below the bottoms of the caissons and induced significant settlement independent of the effects from the adjacent excavation (these caissons are noted with a "+" symbol in Fig. 6).

Excavations adjacent to slurry wall and LBE-supported structures resulted in negligible movements (less than 0.02% of the excavation depth). This is unsurprising due to the fact that these deep foundation elements (for the projects considered here) were end-bearing in rock and are also significantly stiffer relative to the other deep foundation types. Similarly, structures supported by piling (PPC and H-Piles) down to glacial soils and rock below the bottom of excavation also showed negligible movement (±0.03% of excavation depth).

Construction method had less influence on the vertical movements for deep foundations than for shallow foundations, though no data was available for the movement of caissons from adjacent top-down excavations, which may have indicated a similar trend. The movements of timber piles adjacent to top-down and conventional excavations was approximately the same (in both cases, less than 0.1% *v/H*).

SUMMARY AND CONCLUSIONS

This paper collected excavation-induced vertical movement data of nearly 1000 survey points on 98 structures from 21 excavation projects in the Greater Boston area. Trends and discussion of movements considered general foundation system (shallow foundations and deep foundations) as well as further subdivision by specific foundation type (e.g. spread footings, mats, piles, etc.). The relationship between vertical movement, distance from excavation, and depth of excavation were compared to the observations made by Clough and O'Rourke (1990).

The conclusions of this paper are summarized as follows:

- In general, the majority of vertical movement data from Greater Boston excavations was captured by the maximum envelope of vertical movements identified by Clough and O'Rourke (1990) for stiff to very hard clays; however, because much of the data collected in this paper exceeded this envelope, revised bounds were proposed for use in the Greater Boston area.
- Many of the soils in the Greater Boston area are likely softer than the stiff to very hard clay soils examined by Clough and O'Rourke (1990); in line with previous observations, deep excavation in thicker softer soils are more susceptible to global movements (i.e., movements associated with basal heave) which would extend the zone of influence from an excavation further than typically accepted zones of influence (e.g., 1H:1V or 2H:1V).
- Excavations constructed using top-down methods typically resulted in smaller vertical movements for adjacent shallow foundations, but construction method had a less pronounced effect on the movement of adjacent deep foundations.
- Movements of deep foundations were well captured by the Clough and O'Rourke (1990) boundary for excavation-induced movements in stiff to very hard clays, with the exception of project data from caissons which experienced excess movement due to tieback installation beneath them.
- Negligible movement (less than 0.02% v/H) was observed for structures supported by piles (typically end bearing in stiff glacial layers), slurry walls, and LBEs (end bearing in rock).

REFERENCES

Clough, G.W. and O'Rourke, T.D., 1990. Construction Induced Movements of Insitu Walls. Proceedings of the ASCE Conference on Design and Performance of Earth Retaining Structures, Geotechnical Special Publication No. 25, New York, pp. 439-470.

HELICAL PILE-TO-PILE CAP CONNECTIONS SUBJECTED TO UPLIFT FORCES: IMPROVING FUTURE PRACTICE

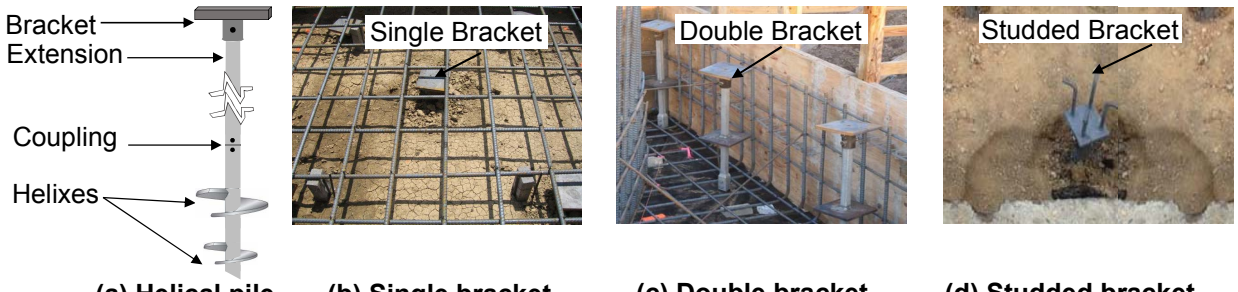
Sundar Chiluwal, The University of Toledo, OH, 567-970-1840, Sundar.Chiluwal@rockets.utoledo.edu
Serhan Guner, The University of Toledo, OH, USA, 419-530-8133, Serhan.Guner@utoledo.edu

Abstract. Although significant research has been conducted on helical piles, there is a lack of research and official design provisions on the helical pile-to-pile cap connections. These connections may govern the global response of pile cap systems—especially in tall and light structures where uplift forces dominate the response. To improve future industry practice, the objective of this study is to understand the influence of pile-to-pile cap connections on the global behavior of concrete pile caps and develop recommendations for their efficient design. For this purpose, 108 high-fidelity nonlinear finite element simulations are conducted to quantify the influences of bracket type, embedment depths, longitudinal reinforcement percentages, shear span-to-depth ratios, and loading conditions on the load, deformation, cracking, and failure behavior of concrete pile caps. The results indicate that the design configurations involving single bracket type may result in premature concrete cracking around the anchorage zones with a 25% reduction in the uplift load capacity. The investigations also confirm that high reinforcement percentages and low shear span-to-depth ratios result in higher load resistance in all bracket types, and that the load capacities of the double and studded bracket types are similar. For applications requiring the use of lower embedment depths, it is recommended that either double or studded bracket types be used. The research findings have applicability to both helical and micro piles given that both include similar connection types.

Keywords: Helical pile, helical pile-to-pile cap connections, single bracket type, double bracket type, studded bracket type, longitudinal reinforcement (ρ_x), embedment depth (h_e), shear span-to-depth (a/d) ratio

INTRODUCTION

Tall and light structures may experience significant uplift forces at their foundations due to large overturning moments from wind or other lateral loads. Helical piles (e.g., Fig. 1a) can provide a cost-effective, practical, and resilient solution for resisting significant uplift forces. In order to realize the full potential of helical piles, it is imperative that the helical pile-to-pile cap connections (see Figs. 1b, c and d for examples) are properly designed to resist the applied forces. However, there is a lack of research and associated knowledge on the influence of pile-to-pile cap connection detailing on the global response of pile caps.



(a) Helical pile **(b) Single bracket** **(c) Double bracket** **(d) Studded bracket**

Fig. 1. Helical pile-to-pile cap connections with different bracket types

The geotechnical literature primarily focuses on the axial load behaviour of isolated piles, and consistently demonstrates the suitability of helical piles for load cases including the tensile uplift loads (e.g., Elkasabgy and El Naggar 2013; Cerato and Victor 2009; Livneh and El Naggar 2008; El Naggar et al. 2007; Youssef

© 2019 Deep Foundations Institute

et al. 2006) and the compression loads (e.g., Elsherbiny and El Naggar 2013). The structural literature, on the other end, exclusively focuses on the behaviour of traditional pile caps supported by socketed piles, subjected to compression loads (e.g., Cao 2009; Suzuki and Otsuki 2002; Suzuki et al. 2000; Otsuki and Suzuki 1996; Adebar et al. 1990). There is a lack of understanding and official design guidelines for creating safe and efficient helical pile-to-pile cap connections. An experimental study conducted by Diab (2015) demonstrated that the connection behavior might govern the entire system response. In another study, Labuda et al. (2013) investigated the failure of an Olympic-size swimming pool supported by helical piles and found that the pool collapsed due to the connection failure under uplift water pressure. These examples highlight the importance of understanding and explicitly accounting for the connection response when designing foundation systems.

Objectives

In the theme of improving the future practice of helical pile connection design, the objective of this study is to understand the effectiveness of the commonly-used bracket types (e.g., Fig. 1) and predict their load, deformation, cracking, and failure behavior using state-of-the-art high-fidelity nonlinear analysis methods. For this purpose, 108 high-fidelity nonlinear finite element (NLFE) simulations are conducted to understand and quantify the influences of bracket type, embedment depths (h_e), longitudinal reinforcement percentages (ρ_x), shear span-to-depth (*a/d)* ratios, and the loading conditions (uplift and compression). A significant emphasis is placed on understanding the behavior of connections under *tensile uplift (i.e., pullout)* loads, as opposed to compression loads, and identifying undesirable failure modes and design configurations.

PILE CAP MODEL PARAMETERS

A foundation strip representative of commonly-used pile cap configurations (e.g., strip footings, grade beams, or a segment of pile caps) was designed, following the CRSI (2015) and Guner and Carriere (2016) recommendations. The strip is supported by two helical piles to create a one-way stress flow and better isolate the pile cap response (see Fig. 2). Helical piles are terminated with one of the three bracket types; namely, single bracket (see Fig. 2a), double bracket (see Fig. 2b), and studded bracket (see Fig. 2c). The square helical pile shaft supports the pile cap strip with dimensions of 2100 mm x 800 mm x 600 mm, where the compressive strength of the concrete is 20.7 MPa. The single bracket type has a Grade 50 plate with a size of 254 mm x 254 mm and 19-mm thick. The double and studded bracket types have plates with the same dimensions and properties to facilitate comparisons with the single bracket type. The studs are No.6 steel rebars of Grade 60. The pile cap strip supports the column load anchored by the bolts of Grade 105 steel, spaced 400 mm, with the length and the diameter of 460 mm and 38 mm, respectively.

Influencing parameters investigated include: three h_e for single bracket type [i.e., 460 mm (top), 300 mm (middle), 140 mm (bottom)]; one h_e for double bracket type [i.e., 460 mm (top)]; two h_e for studded bracket type [i.e., 300 mm (middle), 140 mm (bottom)]; three ρ_x for all bracket types [i.e., minimum 0.2% (5-#5 rebars) from ACI (2014), 0.4% (7-#6 rebars), and 0.8% (10-#7 rebars)]; and three *a/d* ratios for all bracket types [i.e., 1.68, 1.42, and 1.11] (see Fig. 2). When also considering two loading conditions, 108 pile cap design configurations were created [i.e., 3 x 3 x 2 x (3+2+1) = 108].

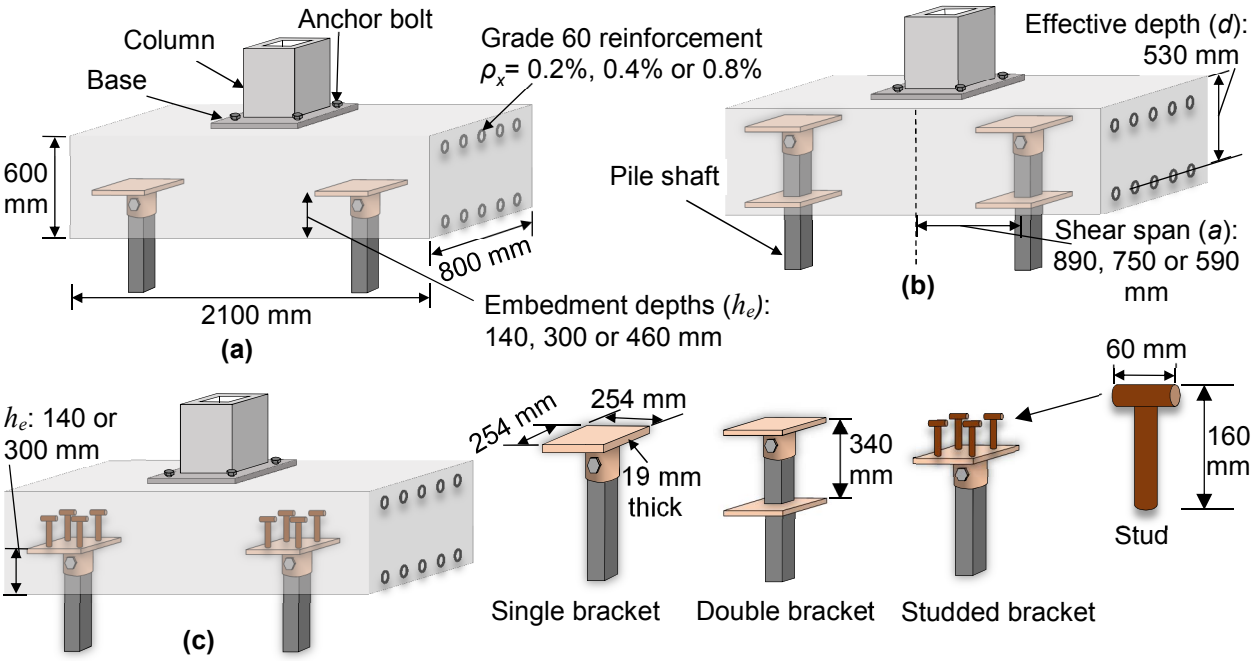


Fig. 2. Helical pile-to-pile cap connections for (a) single bracket type; (b) double bracket type; and (c) studded bracket type

NONLINEAR FINITE ELEMENT MODELING

A two-dimensional, continuum-type, plane-stress element is used for the finite element modeling through a computer program VecTor2 (VTAG 2019). The formulation is based on the Disturbed Stress Field Model (Vecchio 2000), which is an extension of the Modified Compression Field Theory (MCFT) (Vecchio and Collins 1986). The MCFT employs a smeared, rotating crack approach within a total-load, secant-stiffness solution algorithm and allows the consideration of the coupled flexure, axial, and shear effects.

One sample numerical model created is shown in Fig. 3a, where the concrete was modeled using a four-noded rectangular element with 8 degrees of freedom (see Fig. 3b), and the longitudinal reinforcement was modeled using a two-noded truss bar (see Fig. 3c) with 4 degrees of freedom.

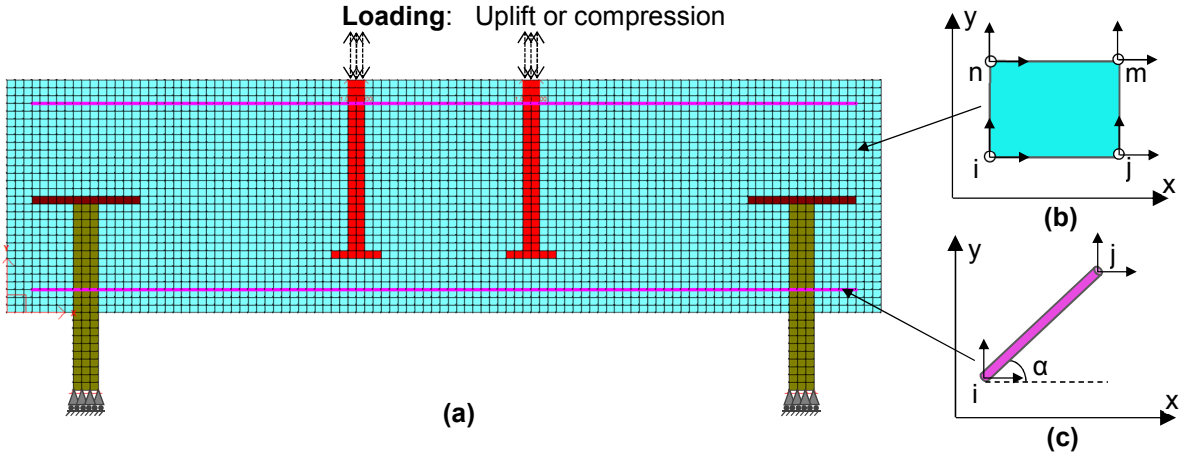


Fig. 3. (a) NLFE model developed in the study for the single bracket type; (b) Plane-stress rectangular element used; and (c) Truss bar element used

Tables 2 and 3 show the component properties in terms of their strengths and dimensions. VecTor2 incorporates several second-order material behaviors (Wong et al. 2013; Akkaya et al. 2019) as listed in Table 4, including the material responses shown in Figs. 4a and 4b as examples. A very fine mesh with a size of 20 mm x 20 mm was used where each helical pile was restrained with four hinges, to better isolate the pile cap response. A displacement-controlled analysis was employed, which is advantageous when simulating the post-peak response, ductility, crack patterns, and failure modes. A monotonic loading was applied uniformly with a displacement increment of 0.2. Sample models of double and studded bracket types are shown in Fig. 5.

Table 2. Continuum region properties

Region	Description	Color	f'_c (MPa)	f_y (MPa)	Thickness (mm)
1	Concrete		20.7	-	800
2	Helical Pile			552	44
3	Bracket Plate		-	345	260
5	Anchor Bolts		-	724	57

Table 3. Truss bar properties

Truss	Description	Color	f_y (MPa)	ρ_x
1	Longitudinal bars		414	0.2%, 0.4% or 0.8%

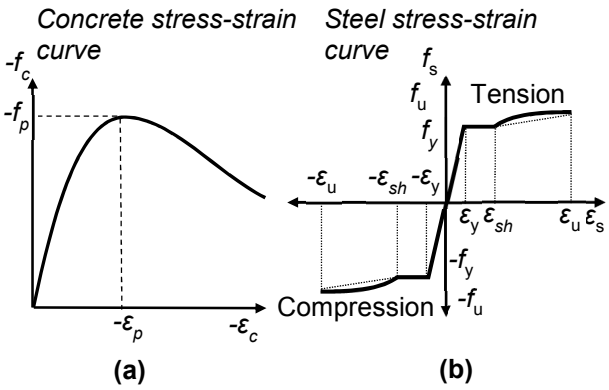


Fig. 4. Two of the material behaviors models used

Table 4. Concrete and reinforcement material models

Material Behaviour	Default Model	Material Behaviour	Default Model
Compressive Base Curve	Hognestad	Concrete Dilation	Variable-Isotropic
Compression Post-Peak	Modified Park-Kent	Cracking Criterion	Mohr-Coulomb (Stress)
Compression Softening	Vecchio 1992	Crack Width Check	Agg/5 Max crack width
Tension Stiffening	Modified Bentz 2003	Crack Slip	Walraven
Tension Softening	Linear	Hysteretic Response	Bauchinger Effect (Seckin)
Confined Strength	Kupler/Richart	Dowel Action	Tassios (Crack Slip)
Buckling	Akkaya et al. 2019		

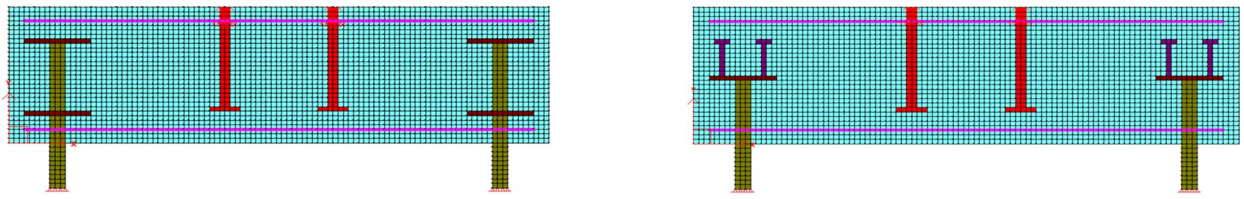


Fig. 5. Numerical models representing top h_e with a/d ratio of 1.68 (a) Double bracket type; and (b) Studded bracket type

UPLIFT BEHAVIOR

The overall uplift responses of all three bracket types are shown in Fig. 6. The maximum load capacities obtained are the same as all bracket types except the bottom h_e of the single bracket type, which provided a 15% less load capacity (see Fig. 6a) due to connection failures. A similar trend is observed for the failure displacements, with the bottom embedment depth sustaining failures under smaller deformation levels.

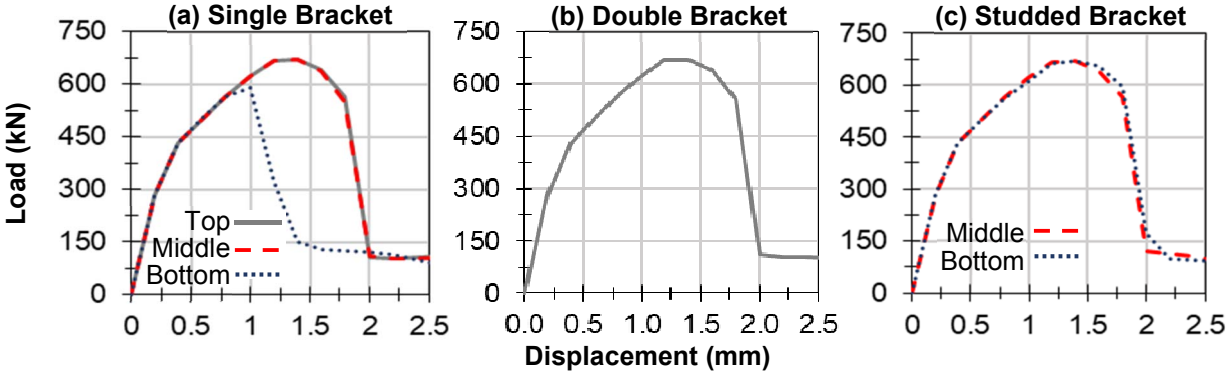


Fig. 6. Simulated responses for *a/d* ratio of 1.68 and ρ_x of 0.4% subjected to uplift

Figure 7 presents all 54 simulation results in terms of load capacities, h_e, a/d ratios, and ρ_x percentages subjected to uplift. The slopes of three blue lines (i.e., bottom h_e) in Fig. 7a are significantly lower than those of red (i.e., middle h_e) and gray lines (i.e., top h_e), which shows that the capacity increase is much smaller in bottom h_e when a/d ratio is reduced (i.e., pile cap is made deeper) or ρ_x percentage is increased as compared to other h_e. When the h_e is changed from bottom to middle, the capacity increases by an average of 32%. The further increase in h_e from middle to top does not affect the capacity, as shown by the overlapping of red and gray lines in Fig. 7a. The double bracket behaves similarly to the middle or top h_e of the single bracket, as their load capacities are similar (see Fig. 7b). For studded bracket type, the gray lines overlap the blue lines, which shows that the change in h_e does not influence the load capacity (Fig. 7c). Also, the capacity of the bottom or middle h_e for studded bracket type is found to be similar to those of the middle or top h_e of the single bracket type (compare Figs. 7a and 7c). If the bottom h_e must be used, the change of the bracket type from single to studded can improve the global capacity by an average of 29%.

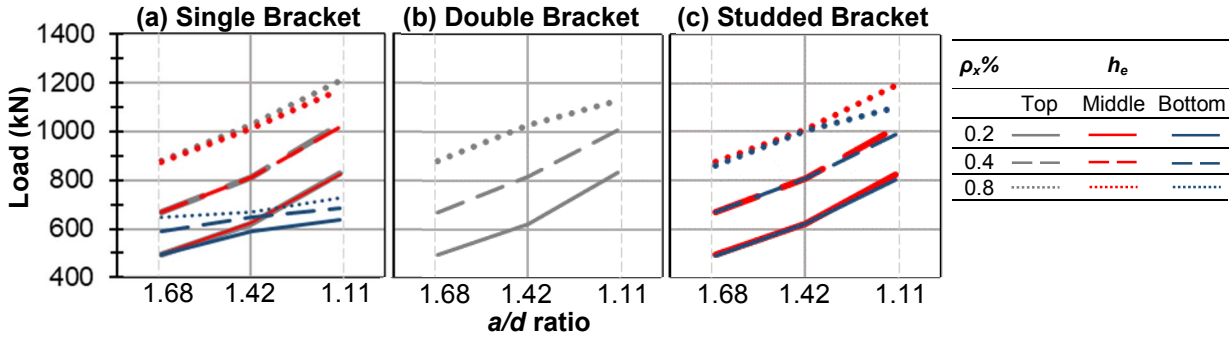


Fig. 7. Interaction among different parameters subjected to uplift.

The uplift capacity of all bracket types increases with higher ρ_x and lower a/d ratios (as shown by the increasing slopes in Fig. 7). For the single bracket type, the capacity increases by an average of 24% and 19% when the ρ_x is increased from 0.2% to 0.4% and 0.4% to 0.8%, respectively, and the capacity increases by an average of 17% and 19% when the a/d ratio is decreased from 1.68 to 1.42 and 1.42 to 1.11,

respectively. Other bracket types exhibit similar increase of capacity for h_e and a/d ratio change within a range of ±5%.

COMPRESSION BEHAVIOR

The overall compression responses of all three bracket types are shown in Fig. 8. The maximum load and deformation capacities obtained are the same as all bracket types.

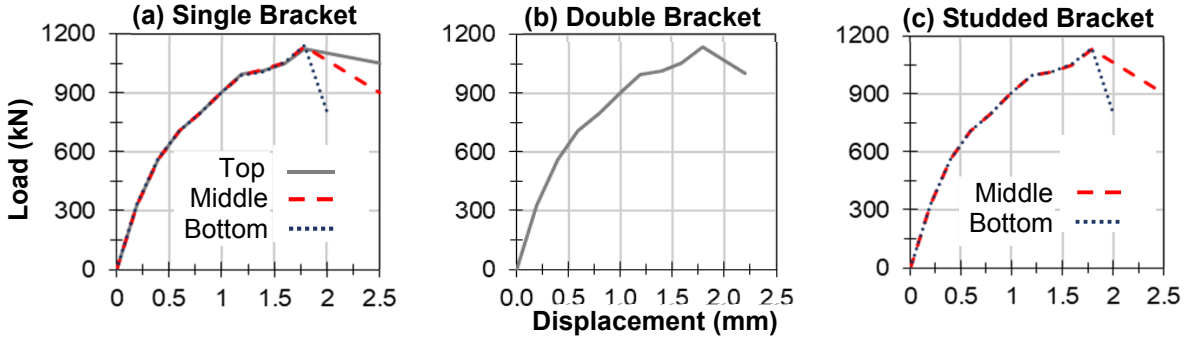


Fig. 8. Load-displacement responses for *a/d* ratio of 1.68 in ρ_x of 0.4% subjected to compression

Figure 9 presents all 54 simulation results in terms of load capacities, h_e, a/d ratios, and ρ_x percentages subjected to compression. The overlapping nature of lines with different colors demonstrates that the compressive load resistance is independent of the changes in h_e. This can be attributed to the absence of connection failures subjected to compression loading. The load capacity of all bracket types increases with the increase in ρ_x and decrease in a/d ratios. This increase is more pronounced for the lowest ρ_x, as apparent from the bilinear nature of the solid lines in Figs. 9a, 9b, and 9c. When the a/d ratio is changed from 1.42 to 1.11, the capacity increases for ρ_x of 0.2, 0.4, and 0.8 percentages are 43%, 29%, and 19%, respectively. For the single bracket type, the compressive capacity increases by an average of 24% when ρ_x is increased from 0.2% to 0.4%, or 0.4% to 0.8%, while the capacity increases by an average of 21% and 29% when the a/d is decreased from 1.68 to 1.42, and 1.42 to 1.11, respectively. The double and studded bracket types show similar increases in the load capacities within a range of ±5% for similar changes in h_e and a/d.

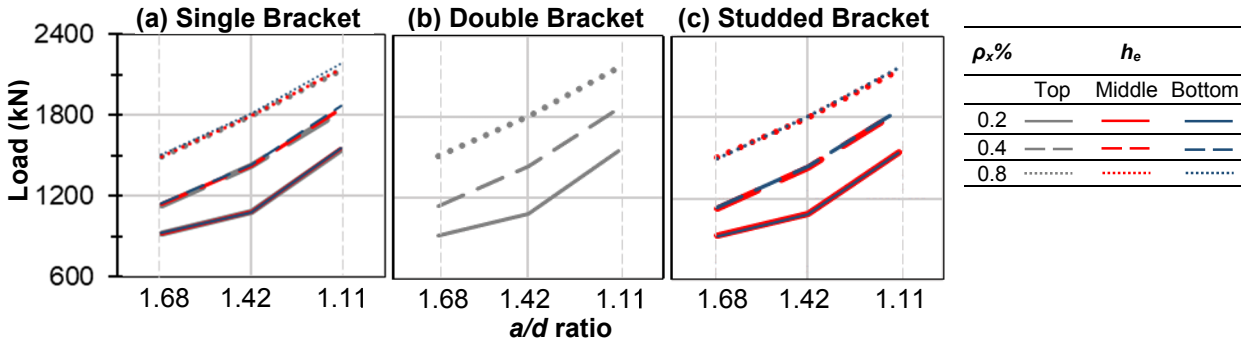


Fig. 9. Interaction among different parameters subjected to compression

DEFORMATION AND CRACK PATTERNS

Dominant concrete cracks are predicted around the connection zone for the bottom h_e of the single bracket type subjected to uplift loads (see Fig. 10a). Connection concrete cracks are concentrated over a small area and extended along the bottom longitudinal reinforcement. This type of failure is found to be the least preferable failure mode in this study because it results in a premature failure with no to very little redistribution of stresses. For the middle or top h_e, concrete cracking only along the top longitudinal

reinforcement are predicted (see Fig. 10b). This type of behavior provided better load redistribution and higher displacement ductility. Other parameters (i.e., ρ_x and *a/d* ratios) are found to not change the failure modes of the single bracket type. This confirms that h_e is the most influencing parameter for the single bracket type. For the double bracket type, the crack patterns are predicted to be the splitting of concrete along the top longitudinal reinforcement in most of the cases (see Fig. 10c). In the configuration involving higher ρ_x of 0.8% (see Fig. 10d), additional minor anchorage cracks are predicted, yet these cracks are found to not influence the global response of the pile caps in any significant way. For the studded bracket type, a similar cracking behavior is obtained (see Figs. 10e and 10f).

For all the bracket types subjected to compression loads, most of the failure modes involved splitting of the concrete along the bottom reinforcement (see Fig. 10g) where the cracks initiate from the tip of the anchor bolts and propagate to the helical pile anchorages. For the lowest *a/d* ratio of 1.1 with ρ_x of 0.4% or 0.8%, shear failures are predicted (see Fig. 10h). No signs of anchorage cracks are predicted in any of the brackets.

For all simulations, widespread concrete cracking is found to provide a more favorable global pile cap response than those from concentrated concrete cracking (e.g., Fig. 10a).

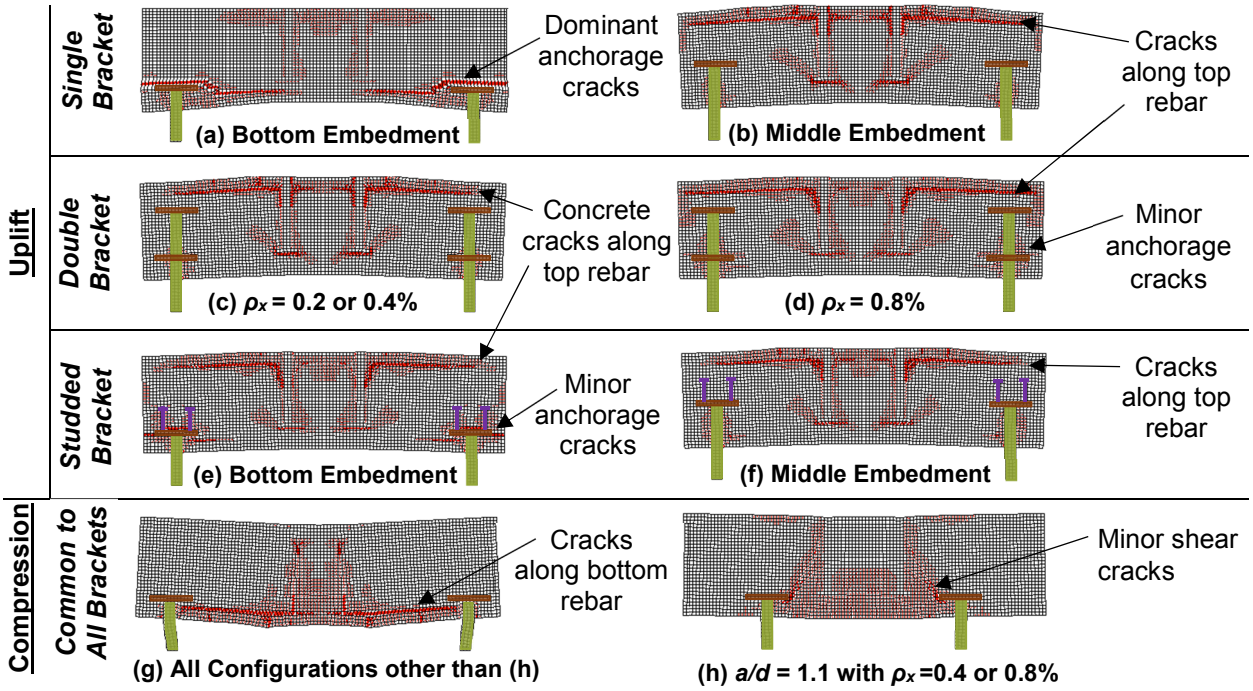


Fig. 10. Failure modes and crack patterns

SUMMARY AND CONCLUSIONS

This study performed 108 high-fidelity NLFE simulations to quantify the influences of key design parameters on the load, deformation, cracking, and failure response of concrete pile caps supported by helical piles. The analyses investigated: the influences of three bracket types (i.e., single, double, and studded); three embedment depths (h_e = 140, 300, and 460 mm); three longitudinal reinforcement percentages (ρ_x = 0.2, 0.4 and 0.8); and three shear span-to-depth ratios (*a/d* = 1.68, 1.42 and 1.11).

The results of the numerical investigations demonstrate that the helical pile-to-pile cap connections may govern the entire system capacity for the load conditions involving uplift forces. As such, it is recommended to perform an explicit check of the connection capacity in addition to the structural and geotechnical checks for the global pile cap and helical pile capacities. The findings of this study are also applicable to micro piles which incorporate similar connection details. Detailed conclusions and recommendations are provided below for uplift and compression load cases.

Uplift Behavior

- Connection (anchorage) failure is predicted only for the bottom h_e of single bracket type, which decrease the global tensile load resistance of the pile cap by an average of 25%. It is recommended that the bottom h_e should be avoided for the most efficient design when the single bracket type is used.
- The analysis indicates that h_e is the most influential parameter, which also dictates the effectiveness of ρ_x and *a/d* ratio on the uplift load resistance for the single bracket type.
- The uplift load capacity increases by an average of 29% when h_e is changed from bottom to middle for the single bracket type.
- The uplift load capacity remains similar when h_e is changed from middle to top for the single bracket type. Therefore, it is still recommended to use the middle h_e.
- The uplift load capacity increases by an average of 22% when ρ_x is increased from 0.2% to 0.4% or 0.4% to 0.8% for the single bracket type.
- The uplift load capacity increases by an average of 18% when the *a/d* ratio is decreased from 1.68 to 1.42 or from 1.42 to 1.11 for the single bracket type.
- The double bracket type has only one h_e, which provides satisfactory response with no anchorage failure. The load capacity increases similar to the single bracket type for ρ_x or *a/d* ratio changes.
- The studded bracket type has two h_e positions, and the change in h_e does not influence their capacities. Any one of these embedment depths could be used for efficient design. The load capacity increases similar to the single bracket type for ρ_x or *a/d* ratio changes.
- For the configurations involving bottom h_e, the change of bracket type from single to studded improves the pile cap capacity by 29%. Therefore, if the bottom h_e is required, the studded bracket type is recommended.
- To maximize the uplift load resistance, high ρ_x percentages and low *a/d* ratios should be used for all bracket types, along with the middle or top h_e for the single bracket type.
- Overall uplift behavior of double and studded bracket types is comparable to middle or top h_e of single bracket type, and the load capacity obtained for these brackets are similar within a range of ±5%.

Compression Behavior

- No anchorage failure is predicted for compression loads in any of the bracket types.
- The compressive load capacity increases by an average of 24% when ρ_x is increased from 0.2% to 0.4% or from 0.4% to 0.8% for the single bracket type.
- The compressive load capacity increases by an average of 25% when the *a/d* ratio is decreased from 1.68 to 1.42 or from 1.42 to 1.11 for the single bracket type.
- The double and studded bracket types exhibit load capacity increases similar to the single bracket type for similar changes in ρ_x or *a/d* ratios.
- To maximize the compressive load resistance, high ρ_x percentages and low *a/d* ratios is recommended, regardless of the h_e for all bracket types.

ACKNOWLEDGEMENT

The authors would like to thank Helical Piles and Tiebacks Committee of the Deep Foundation Institute (DFI) for providing funding for this study.

REFERENCES

ACI Committee 318, 2014. Building code requirements for structural concrete (ACI 318-14) and commentary (ACI 318R-14), American Concrete Institute, Farmington Hills, MI, USA, 524 p.

Adebar, P., Kuchma, D., and Collins, M.P., 1990. Strut-and-tie models for the design of pile caps: an experimental study. American Concrete Institute Structural Journal, 87(1): 81-92. Retrieved from https://trid.trb.org/view/307069 Accessed 23/03/2019.

Akkaya, Y., Guner, S., and Vecchio, F.J., 2019. A constitutive model for the inelastic buckling behavior of reinforcing bars. ACI Structural Journal, 116(3): 195-204. Retrieved from http://www.utoledo.edu/engineering/faculty/serhan-guner/docs/JP11_Akkaya_et_al_2019.pdf Accessed 23/03/2019.

Cao, J., 2009. The shear behaviour of the reinforced concrete four-pile caps. Ph.D. Thesis, School of Civil Engineering and the Environment, University of Southampton, Southampton, UK, 287 p. Retrieved from https://eprints.soton.ac.uk/73699/ Accessed 23/03/2019.

Cerato, A., and Victor, R., 2009. Effects of long-term dynamic loading and fluctuating water table on helical anchor performance for small wind tower foundations. Journal of Performance of Constructed Facilities, 23(4): 251-26. https://doi.org/10.1061/(ASCE)CF.1943-5509.0000013

CRSI., 2015. Design guide for pile caps (1st ed.). Concrete Reinforcing Steel Institute, Schaumburg, IL, 156 p. Retrieved from http://resources.crsi.org/resources/design-guide-for-pile-caps/ Accessed 23/03/2019.

Diab, M.A.M., 2015. Behavior of helical pile connectors for new foundations. Ph.D. Thesis, School of Civil and Environment Engineering, University of Western Ontario, London, Ontario, Canada, 638 p. Retrieved from https://ir.lib.uwo.ca/cgi/viewcontent.cgi?article=4736&context=etd Accessed 23/03/2019.

Elkasabgy, M., and El Naggar, M.H., 2013. Dynamic response of vertically loaded helical and driven steel piles. Canadian Geotechnical Journal, 50(5): 521–535. https://doi.org/10.1139/cgj-2011-0126

El Naggar, M.H., Youssef, M.A., and Ahmed, M., 2007. Monotonic and cyclic lateral behaviour of helical pile specialized connectors. Engineering Structures, 29(10): 2635–2640. https://doi.org/10.1016/j.engstruct.2007.01.018

Elsherbiny, Z.H., and El Naggar, M.H., 2013. Axial compressive capacity of helical piles from field tests and numerical study. Canadian Geotechnical Journal, 50(12): 1191–1203. https://doi.org/10.1139/cgj-2012-0487

Guner, S., and Carrière, J., 2016. Analysis and strengthening of caisson foundations for uplift loads. Canadian Journal of Civil Engineering, 43(5): 411–419. Retrieved from http://www.utoledo.edu/engineering/faculty/serhan-guner/docs Accessed 23/03/2019.

Labuda, T., Corley, G.W., and Murphy, M., 2013. Failure investigation of a helical anchor tie-down system supporting an olympic size swimming pool. Proceedings of the Seventh International Conference on Case Histories in Geotechnical Engineering, Chicago, April 29-May 4, Scholoars' Mine, Missouri University of Science and Technology. 7 p. Retrieved from http://scholarsmine.mst.edu/cgi/viewcontent.cgi?article=3223&context=icchge Accessed 23/03/2019.

Livneh, B., and El Naggar, M.H., 2008. Axial testing and numerical modeling of square shaft helical piles under compressive and tensile loading. Canadian Geotechnical Journal, 45(8): 1142-1155. https://doi.org/10.1139/T08-044

Otsuki, K., and Suzuki, K., 1996. Experimental study on bending ultimate strength of four-pile caps. Trans Jpn Concrete Inst, 482: 93-102. Retrieved from https://ci.nii.ac.jp/naid/110004303171 Accessed 23/03/2019.

Suzuki, K., Otsuki, K., and Tsubata, T., 2000. Influence of edge distance on failure mechanism of pile caps. Trans Jpn Concrete Inst, 22: 361-367. Retrieved from https://ci.nii.ac.jp/naid/10007467724/ Accessed 23/03/2019.

Suzuki, K., and Otsuki, K., 2002. Experimental study on corner shear failure of pile caps. Trans Jpn Concrete Inst, 23: 303-310. Retrieved from https://ci.nii.ac.jp/naid/10007251043/ Accessed 23/03/2019.

Vecchio, F.J., and Collins, M.P., 1986. The modified compression field theory for reinforced concrete elements subject to shear. ACI Journal, 83(2): 219–231. https://doi.org/10.14359/10416

Vecchio, F.J., 2000. Disturbed stress field model for reinforced concrete: formulation. Journal of Structural Engineering, 126(8): 1070–1077. https://doi.org/10.1061/(asce)0733-9445(2000)126:9(1070)

VTAG, 2019. VecTor2: Nonlinear finite element analysis software for reinforced concrete structures. VecTor Analysis Group (VTAG) Version 2.9 (Online), Retrieved from http://vectoranalysisgroup.com/ Accessed 23/03/2019.

Wong P.S., Vecchio F.J., and Trommels H., 2013. VecTor2 and formworks user's manual. Technical Report, Department of Civil Engineering, University of Toronto, ON, Canada, 347 p. Retrieved from http://www.vectoranalysisgroup.com/user_manuals/manual1.pdf Accessed 23/03/2019.

Youssef, M.A., El Naggar, M.H., and Ahmed, M., 2006. Monotonic and cyclic load behaviour of helical pile connectors in the vertical direction. Canadian Journal of Civil Engineering, 18(1996): 10–18. https://doi.org/10.1139/l05-074

MAKING FOUNDATION DESIGN COURSES MORE ENGAGING AND EFFECTIVE FOR STUDENTS

Evangelia Ieronymaki, Assistant Professor, Dept. Civil & Environmental Engineering, Manhattan College, Riverdale, NY, (+1)7188628145, ieronymaki@manhattan.edu

ABSTRACT

Civil engineering education relies on traditional methods of teaching, comprising mostly of deductive instruction by presenting the theory, followed by applications. This paper presents an alternative way for teaching foundation design to senior students, introducing a more inductive approach. The students are presented with a project/game adapted to a real-world problem at the beginning of the course. They are asked to identify the correct steps and methods throughout the lectures, for reaching an appropriate solution that they document and present at the end of the course. To make the project more enjoyable, the project has the format of a game where the students compete with each other on completing the task faster and more efficiently. The goal of this teaching approach is to enhance the ability of the students for problem solving and the engineering way of thinking, while playing a game. In the end, the students were requested to respond to a survey regarding the efficiency of this project/game on their learning. The results showed that students prefer more inductive methods for a design course, feeling that this project made them think more like engineers, while the 'game' twist of it made the whole course more fun.

Keywords: foundations, design course, education, inductive learning

INTRODUCTION

Most civil engineering courses are taught in 2019 the same way they used to be taught 40 years ago in the 80s. Classic methods are mostly deductive, where the instructor presents the theory first and then applications of that theory follow. Little or no attention is given initially to why the theory was developed or what are the problems it solves. The applications of the theory, and thus the purpose it serves, come only in the end and after methodologies have been presented, leading the students to show low interest in the material. As Albanese and Mitchell (1993) have reported, people are mostly motivated to learn things when they clearly see the need to know them. This explains the students' little motivation that, if any, comes mainly from the fact that the material may be useful either in other courses or in their future careers.

On the other hand, there are alternative inductive methods of teaching, where the role of the students is more active. A lot of researchers have highlighted the benefits of inductive methods in teaching engineering courses. Based on Prince and Fedler (2006), inductive methods include; a) inquiry-learning, b) discovery learning, c) problem and project-based learning (PBL), d) case-based teaching, and e) just-in-time learning. Inquiry-learning is maybe the most traditional method of inductive teaching/learning methods, where the instructor asks questions or poses problems and the students need to apply the theory they have learnt in order to find the solution (Bateman 1990; Prince 2004; Lee 2012). Similar to inquire-learning is the discovery learning, where students have to find the solution to a problem or answer to a question, while the instructor simply provides feedback to the students without guiding their efforts (Leonard 1988; Westbrook and Rogers 1994).

In the problem-based and project-based learning (PBL) method, the students are presented with a real-world open-ended problem and work in teams to develop a viable solution. The instructors do not provide guidance but have the role of facilitator (Dahlgren 2003; Weiss 2003; De Graaf and Kolmos 2003; Jensen, Helbo, Knudsen and Rokkjær 2003). In the case-based teaching, the students are presented with a case, real or hypothetical, and they are asked to find a solution or make a decision (Kardos and Smith 1979; Fitzgerald

 © 2019 Deep Foundations Institute

1995). Case-based teaching, frequently seen in courses offered by business schools, is similar to problem-based learning, however the problem/case presented here is more well-structured and with more details than the problem-based learning. Finally, a more modern method of teaching is the 'just-in-time teaching' (JITT) where the students are assigned with some questions to answer online before the class, the instructor reads through the answers and adjusts the lecture accordingly (just-in-time). This method can be combined with any other inductive method mentioned above (Maxim, Akingbehin and Modesitt 1999; Novak, Patterson, Gavrin and Christian 1999).

Many studies and brain researches have proven that the aforementioned inductive methods are more effective that the traditional deductive methods, by promoting student's intellectual development, critical thinking and problem solving, which are essential skills to scientists and engineers. However, if these methods are not implemented correctly or without the proper guidance from the instructor, they will not have the desired outcome for the students. Although, the inductive teaching methods can be more effective in helping the students understand the concepts and retain the information for longer, they don't guarantee that the students will be engaged throughout the length of the course.

Most of the above methods are applied to 'design' courses in engineering curricula. 'Foundations design' is a course that is offered usually in the senior year of civil engineering undergraduate studies. Most instructors teach this course by presenting first the different types of foundations, the design procedure and the construction method, followed by solving example problems to show the applications of these methods. Problem sets are often assigned at the end of each lecture so that students practice by applying the methods they learnt in class. Some instructors occasionally assign a term project, where the students are given a real or hypothetical case of a structure, along with all information they need (e.g. site characteristics, ground conditions, loading system etc.) in order to select the appropriate foundation system and design it.

This paper proposes an alternative 'design project' as a companion assignment in 'Foundations design' course for students that major in Civil Engineering. This assignment is a combination of a project-based learning method and a game with the following objectives; a) to help the future engineers become better problem-solvers, b) to improve their critical thinking, c) to foster team-working spirit and d) to keep them engaged and enthusiastic throughout the whole course.

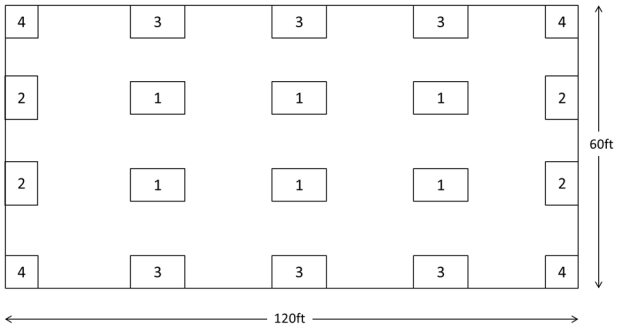
SUGGESTED EDUCATIONAL MODULE

The geotechnical design project is assigned to the students at the beginning of the course, during the first week of classes. It consists of a hypothetical case where the mayor of a big city in the United States requires the construction of a 3-story building for the new City Hall, that will include offices, conference rooms and exhibition spaces. A typical outlook and a simple plan view of the required building is provided (Figs. 1a and 1b). The students have to work in teams of 3 or 4 members, and act as the geotechnical engineering firm that will perform the design of the foundation system for the required structure. The design teams need to establish an efficient and constructible foundation system, following the strength and safety requirements for the anticipated loads and soil conditions.

To keep the students more engaged and entertained, the project is presented in the form of a game, where the goal of each team is to be the first one that will complete the project correctly. To do so, the students need to gather 'hints' for the design procedure by identifying the design steps from the lectures throughout the semester. In this example, the design procedure is divided in ten steps in total, and the students need to identify them in the correct order. For every correct step, the team gets 1 extra point in the total grade (maximum possible 10 points out of 100) and the first team that will complete all ten steps in the correct order, gets a bonus of additional 10 points (20 points in total). The competition among the students regarding which team will finish first, is also an effort to simulate the competition among the design firms in real life.



Fig. 1a. Indicative outlook of the building



1b. Plan view of the building to be designed

When the students identify a step, they have to verify it by asking the instructor who will provide them with the data to complete that design step. For example, the first design step is to gather information about the soil stratigraphy of the area where their structure is going to be built, and as a second step to request information about the soil properties. In this case, the instructor plays the role of the sub-contractor who performed the site investigation and provides the data (e.g. information from boreholes, Figs. 2 and 3). An example of a wrong design step would be to begin with deciding upon the type of the foundation, without prior information of the in-situ geological conditions. This would be considered as a wrong step and thus a missed extra point.

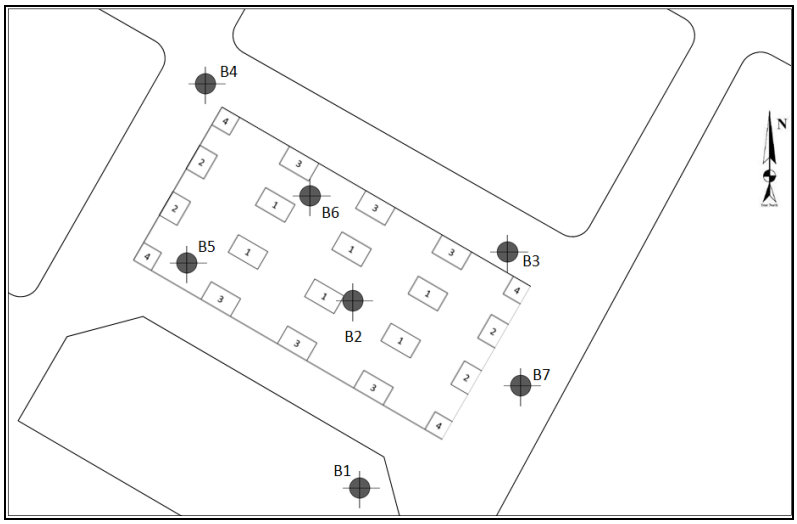


Fig. 2. Indicative plan view of the building showing location of the boreholes

It is up to the instructor to decide how to break down the design procedure (i.e. number of steps), how to incorporate this information in the lectures (e.g. one hint per lecture etc.) and select the appropriate reward system for the students (e.g. extra points). The lectures usually follow the classic curriculum of the 'Foundation Design' course that most schools offer, starting with site investigation, followed by performance requirements, shallow foundation, and finish with deep foundations. Given that the course is designed to basically follow the foundation design procedure, it is relatively easy for the students to guide themselves towards an adequate design, using information and the appropriate methods shown in the lectures. It has to be noted, that although it may be clear in some cases that piles are needed for given ground conditions, the students need to show why shallow footings would not be adequate.

Given that the completion of this project requires the knowledge from all lectures of the course, the students can work on it, either in stages throughout the semester, or as a whole in the end. However, it is suggested that the project is worked in stages so that students get continues feedback from the instructor and grow as

designers throughout the semester. Also, with the suggested reward system students have the incentive not only to follow the lectures closely in order to identify correctly the design steps, but also to work on it as fast as possible so that they are the first team to complete it and get the additional bonus points. Their motivation for learning the material increases as they get in the classroom already with the mentality to search for the desired information and therefore, the whole course (the set of lectures) becomes a pool of information, that the students use as a tool to solve their problem.

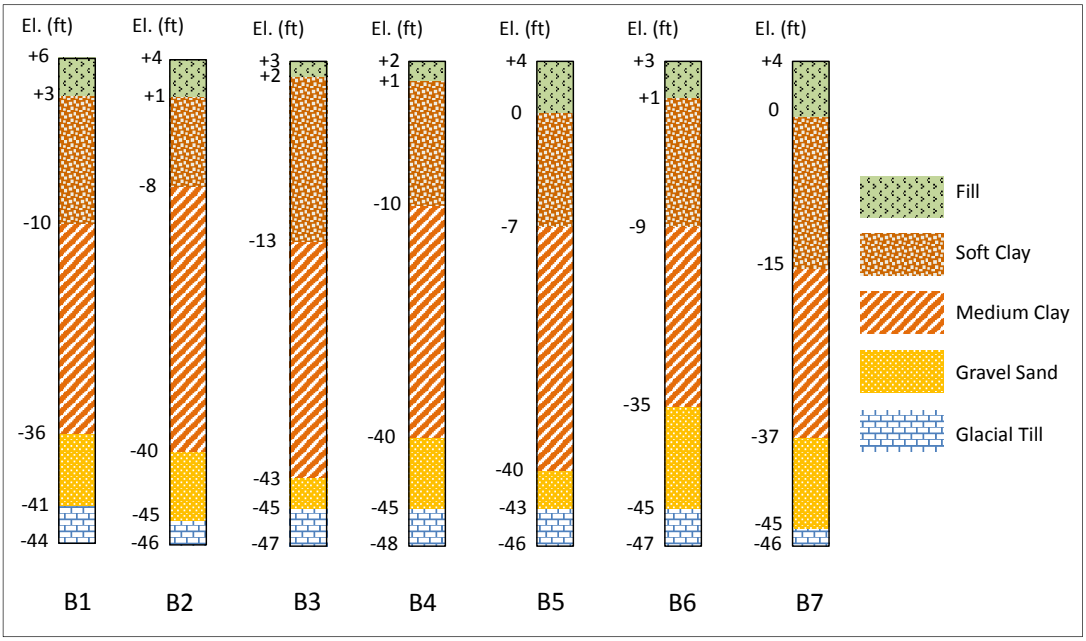


Fig. 3. Example of geological information from boreholes

Evaluation

Upon completion, each team has to submit a technical report, written in a professional manner, including all details about the ground conditions, the loading system on the structure, reasoning for choosing the selected foundation type, the design approach used, as well as the designs of the suggested foundations. The students are expected to divide the work among the team members, but each one of them is responsible for checking the work of the other members. They are also required to have a page at the beginning of their report with a table showing the different tasks, the name of the responsible student, as well as the names of the students who checked and approved them (e.g. Fig. 4).

	Performed by:	Checked by:	Checked by:
1. Site investigation	A.X.	B.Y.	C.Z.
2. Cross-sections with soil profiles	B.Y.	A.X.	C.Z.
3. Bearing capacity of footings	C.Z.	A.X.	B.Y.
Etc...			

Fig. 4. Example of reporting task allocation among team members

The students' work is evaluated based on; a) the logic and sequence of the design steps, b) the adequate foundation system selected, c) the appropriate methods used d) the correct designs presented and e) the professionality of the submitted report. If the students are unable to identify the correct sequence of the design steps, the instructor has to guide them, so that they can move to the next level performing

calculations, without getting extra points. Thus, the students still have the chance of getting 100 in their project, if they complete all parts of their report correctly.

STUDENT RESPONSES

To evaluate the effectiveness of the suggested educational approach on student learning and engagement, the students were asked to respond to a survey after the completion of the project. The project/game was assigned to two consecutive 'Foundation Design' courses (Fall 2017 and Fall 2018) and a total of 43 students participated, with a 25.5% being female and a 74.5% being male students. Demographic data regarding their race and whether they are first generation college-degree, have also been recorded, although they have not been associated individually with each question, at this stage. Figures 5 shows the race distribution of the participants.

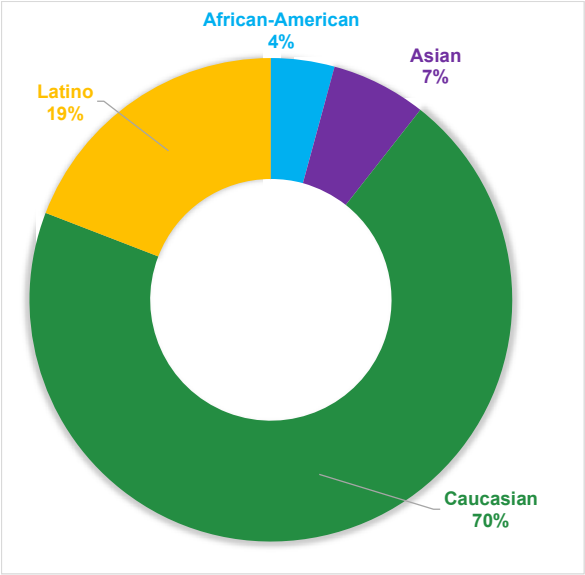


Fig. 5. Race distribution of participating students

The students were asked to respond to a set of six questions, using a system of five possible answers (strongly disagree, disagree, neutral, agree, strongly agree). The results are shown in Table 2. The first two questions aimed to evaluate the level of learning achieved using the specific assignment, based on the students' opinion. As it can be seen by the responses, the great majority of the students (~90% combined 'Agree' and 'Strongly Agree') believe that the suggested design project contributed to their learning, while a lower percentage (~55%) believe that the project was effective in helping them identify the important parts for foundation design.

The purpose of question 3 was to identify to what extend the project helps the students grow as engineers by improving their critical thinking and problem solving. The majority (70%) responded positively to this question, although when asked whether they prefer to be given the design steps instead of having to identify them through the lectures, 40% of the students agreed while another 40% was indifferent. A possible reason for this is that students are used to follow examples, guidelines, and procedures, but they are not used to self-driven assignments or open-ended questions. Therefore, not be given the steps to solve the project, may cause insecurity and anxiety, especially for the weak students. This is also confirmed by the response to whether they 'would prefer if projects in other courses were also self-driven', where only about 48% replied positively, with a 36% being indifferent, and a 16% being negative to this idea.

Finally, the students were asked to evaluate whether the game aspect of the project made it more entertaining for them. Although it would be expected that the students would strongly be in favor of the game, only 45% responded positively, with another 30% being neutral about it. Surprisingly, a significant 25% (combined 'Disagree' and 'Strongly Disagree') was against the 'game'. Based on the written comments of the students, this is attributed to the fact that the competitive aspect of the project (i.e. first team to find correctly all design steps and complete the project gets additional bonus points) exerted more stress on them than enjoyment.

Table 2. Student responses to the survey regarding

	Strongly Disagree	Disagree	Neutral	Agree	Strongly Agree
1. The design project contributed to my learning of designing foundation systems	2%	0%	9%	47%	42%
2. The project/game helped me identify the parts of the lectures that are most important for the foundation design	2%	9%	24%	49%	16%
3. The project/game helped me think like an engineer	2%	7%	21%	47%	23%
4. I would prefer if the design steps were given in the project	0%	20%	40%	26%	14%
5. I would prefer if other projects were self-driven too	0%	16%	36%	29%	19%
6. The 'game' aspect of the project made the assignment more fun	9%	16%	30%	23%	22%

At the end of the survey the students were asked to write what they liked most about the project and what they would suggest for improvement. The comments can be divided in three main categories, reflecting students' positive opinion about: a) teamwork, b) challenging and self-driven project and c) extra points. Table 3 shows some examples of the responses. Based on the written comments, it is evident that the project /game serves its purpose. Students found the project challenging and unique, that helped them think like engineers. They liked working in teams and the extra points gave them an additional motivation to follow the lectures meticulously and be precise on the design steps.

Table 3. Examples of student comments on what they liked about the suggested project – game

- "*The scavenger game helped me concentrate more in class.*"
- *"Extra-credit points motivated us to find all the steps. I liked the process of finding the steps."*
- *"It was nice to tie everything we've learnt together and design. The game itself was interesting and the fact we were getting extra points for it made it that much more engaging. I think the game is a great idea."*
- *"I liked that it was different and unique. We had to start from scratch with no steps, to think like engineers"*
- *"Multiple steps and you must figure it out like real life."*
- *"Creative thinking and working as a group was great!"*

On the negative aspects of the project, some students commented that the competitive feature was somehow stressful. The perception of the students on this feature depends on their personality, as some people find competition intriguing, while others feel nervous. Also, 'competition' is a feature that exists in the real world (e.g. bidding phase), maybe not in the same format (i.e. be the first team to complete the design), but incorporating it in the project, gives the students a first exposure to this condition. Another comment that

came along many times in the downsides of the suggested assignment, is some students face difficulties in distinguishing which part of the design procedure was considered as a 'step'. This is expected, as there is no clear definition of a 'design step' and it is up to the instructor to divide the design procedure into steps and determine the number of them. To bypass the frustration this may cause to the students, the instructor could give more constructive feedback when students request confirmation on their assumed steps (i.e. explain if they have suggested two steps as one etc.), and ask them to make a list with the steps they have identified correctly up to that point. Table 4 shows representatively the students' comments that reflect the aforementioned negative aspects of this project.

Table 4. Examples of student comments on what they liked less about the suggested project – game

- "*We were sometimes unsure how specific the steps or general should be."*
- *"The only thing I was a bit confused is about all the assumptions needed to be made in the project. I was not sure what things I could assume and which ones I couldn't.."*
- *"The scavenger hunt was unnecessary stress. It made us over think."*
- *"It was difficult to come up with the steps and it made our project become very time consuming."*

CONCLUSIONS

A new educational module is presented as an alternative method to teach foundation design to civil engineering college students. The suggested module consists of a hypothetical problem where the plan view of a structure is given, and the design of its foundation system is required. The project is given to the students at the beginning of the semester and comprises the core element of the course. The goal is to form teams and complete the project by gathering all required information presented in the lectures throughout the semester. To incorporate a fun aspect, the project is in the form of a game where the students compete with each other on completing it faster and more efficiently, having bonus points as a reward.

The objective of the suggested module is to help students take initiative in their learning, promote their critical thinking, enhance their problem-solving skills and build team spirit, while having fun by playing a game. The project was implemented in 2 Fall Semester 'Foundation Design' classes (a total of 43 students). Its effectiveness on students' learning was evaluated indirectly by students themselves through a survey. The results revealed that students appreciated the self-driven aspect of the project, feeling that this project made them think more like engineers while keeping them engaged throughout the semester. Although, the game side of the project was expected to be more entertaining and enjoyable for the students, quite a few found that to be rather stressful.

The presented module is a first attempt of the author to make 'Foundation Design' course more engaging and more effective for student learning. Despite the positive response from the student body, the sample is small to generalize the results of the survey. The next step would be to associate the demographics of the students with their responses in order to identify patterns in perception and learning styles among the different student groups.

REFERENCES

Albanese, M.A., and Mitchell S., 1993. Problem-Based Learning: A Review of Literature on its outcomes and Implementation Issues, Academic Medicine, 68, pp. 52–81

Bateman, W., 1990. Open to Question: The Art of Teaching and Learning by Inquiry, San Francisco, Jossey-Bass

Dahlgren, M., 2003. PBL through the looking glass: Comparing applications in computer engineering, psychology and physiotherapy. International journal of engineering education, 19(5), pp.672-681.

De Graaf, E. and Kolmos, A., 2003. Characteristics of problem-based learning. International Journal of Engineering Education, 19(5), pp.657-662.

Fitzgerald, N., 1995. Teaching with cases. ASEE Prism, 4(7), pp.16-20.

Jensen, L.P., Helbo, J., Knudsen, M. and Rokkjær, O., 2003. Project-organized problem-based learning in distance education. International Journal of Engineering Education, 19(5), pp.696-700.

Kardos, G. and Smith, C.O., 1979, March. On writing engineering cases. In Proceedings of ASEE National Conference on Engineering Case Studies, pp. 42-50.

Lee, V.S., 2012. What is inquiry□guided learning?. *New directions for teaching and learning*, *2012*(129), pp.5-14.

Leonard, W.H., 1989. An experimental test of an extended discretion laboratory approach for university general biology. Journal of Research in Science Teaching, 26(1), pp.79-91.

Maxim, B.R., Akingbehin, K. and Modesitt, K.L., 1999. Just-in-time learning in software engineering. Journal of Computers in Mathematics and Science Teaching, 18(3), pp.287-301.

Novak, G.M., Patterson, E.T., Gavrin, A.D. and Christian, W., 1999. Just in time teaching. Blending active Learning with Web Technology, Upper Saddle River, New Jersey: Prentice-Hall

Prince, M., 2004. Does active learning work? A review of the research. Journal of engineering education, 93(3), pp.223-231.

Prince, M.J. and Felder, R.M., 2006. Inductive teaching and learning methods: Definitions, comparisons, and research bases. Journal of engineering education, 95(2), pp.123-138.

Weiss, R.E., 2003. Designing problems to promote higher□order thinking. New directions for teaching and learning, 2003(95), pp.25-31.

Westbrook, S.L. and Rogers, L.N., 1994. Examining the development of scientific reasoning in ninth□grade physical science students. Journal of Research in Science Teaching, 31(1), pp.65-76.

SPECIALTY GEO-ENGINEERING IN A CAISSON TOWN

[1]Jeffrey R. Hill, P.E., Director, Hayward Baker, Inc. – Rail Services Division, 1530 South Second Street, St. Louis, Missouri, 847-343-2023, jrhill@haywardbaker.com
[2]Joel Dellaria, P.E., S.E. Senior Geo-Structural Engineer, Hayward Baker, Inc., 1350 West Lake Street, Roselle, Illinois, 630-339-4343, JBDellaria@HaywardBaker.com
[3]William H. Walton, PE,P.E., S.E., F.ASCE, D.GE, Senior Vice President, GEI Consultants, Inc., 400 Lakeview Parkway, Vernon Hills, Illinois, 847-226-7694, bwalton@geiconsultants.com

ABSTRACT

The City of Chicago has a world-renowned skyline and is known for its provocative architecture. The subsurface conditions in the city have allowed for construction of these significant structures. The skyline is supported on caissons as they are called in Chicago or drilled shafts in other locations. Despite the significant strides the industry has made in advancing the drilled shaft, the use of other specialty geotechnical construction techniques like micropiles has not been overlooked in Chicago and the surrounding areas. Micropiles have been utilized to underpin famous existing historic structures like Orchestra Hall any many others. Engineers have used 200 to 600 kip micropiles to underpin compromised, inadequate, or damaged caissons. The paper will discuss the use of drilled shafts, micropiles, and ground improvement over the last 30 years in Chicago using a curated collection of case histories. It will also examine advancing the industry beyond its current technical limitations using these techniques.

Keywords: Chicago, geo-engineering, caisson, deep foundations, micropiles

INTRODUCTION

20,000 years ago, glaciers from the Chicago region left behind sheets of glacial clay till underlain by dense, over consolidated glacial till below: limestone bedrock, found about 100 ft below street level. An unusual feature in this profile is the soft Chicago Blue Clay. Chicago has been called the birthplace of the Skyscraper and drilled shaft foundation, both of which came about in the 19th century. After the Great Fire of 1871, tall new structures were built rapidly and designing a successful foundation was trial and error. The first deep driven wood pile and caisson foundations bypassed the problem layer and found solid support on hardpan till or bedrock below (Schock and Risberg 2013).

Once the drilled shaft foundation became acceptable to the Chicago engineering and construction community, building heights and complexity grew dramatically. As the city grew, building foundations were being repurposed. There was also the need to underpin structures for additional loads and shallow foundations for adjacent construction. Hand-dug drilled shafts were an option for some of these restricted access and low headroom sites but a new technique, micropiles, would prove to be the future of retrofit and hard to construct foundations. Micropiles were introduced on a limited basis to the United States market in the 1970s and 80s. In the early 1990s, the Chicago market began to latch onto micropiles and their use has grown significantly as a solution to the most complex foundation problems a maturing skyline has to offer.

At about the same time, micropiles were starting to become a commercially viable deep foundation alternative to drilled shafts in difficult and challenging conditions. Micropiles have evolved as segment piling units adopting oil-field pipe meeting American Petroleum Institute high strength steel piping (e.g., API N80 or Grade 80 ksi steel) filled with tremie grout and often reinforced for tension using thread bar core steel. Micropiles are well suited for work in urban environments and can be drilled through grillage foundations and old footings that are common foundation elements for buildings constructed after the Great Chicago Fire without vibration or ground loss. This paper will walk through several case histories highlighting the evolution of micropile use in Chicago through four different phases. First phase: Fear and

© 2019 Deep Foundations Institute

Disbelief (prior to 1995) where micropile use was limited to small loads (less than 80 kips there was a Code limit of 40 tons and minimum steel pile diameters that were perceived threshold limit for pile design) and low-profile projects involving few clients and installers. The second phase: Education and Experimentation (1995 to 2002) saw the use of higher capacity micropiles expand to higher-profile projects and capacities grew to 220 kips, and awakened the Chicago construction industry to the potential of grouted steel pipe micropiles drilled into bedrock. The third phase: Acceptance and Increase (2003 to 2010) saw capacities rise to 400 kips and micropiles transitioned from an interesting value engineering idea to a plans and specification solution for many projects. Finally, we arrive in the current phase: Growth and Multi-Technique, where capacities continue to rise to 600 kips and higher. Furthermore, micropiles are now used in conjunction with other ground modification techniques to solve more deep foundation problems.

The authors have selected several sequential case histories highlighting each of these periods. The projects selected are not necessarily the largest sampling but rather ones that had in our opinion a profound influence on the local technology and engineering community.

NAVY PIER 1993 – 2018

Between 1914 and 1916, the Navy Pier was constructed as a pre-cast concrete deck structure supported on timber pile foundations driven into the stiff clay and hardpan beneath. It was renamed in 1927 to honor naval veterans of WWI. The pier extends 3,300 feet out from the Lake Michigan shoreline.

As the wood piles aged and deteriorated over time, foundation repair work was required. Renovations replaced the industrial strength timber decking with maintenance-free pre-cast reinforced concrete decking. This surface could not safely support the additional concentrated loads imposed by the large, heavy equipment typically required for the drilled shafts—the drilled shaft support (bell caissons on hardpan), a post 1920s historic deep foundation method of choice.

The use of rock-socketed shafts combined with excellent dolomitic limestone beneath the city allowed for the construction of the skyline. The shafts are often drilled through urban fill and at times debris from the Great Chicago Fire of 1871. Beneath the urban fill, foundation contractors and geotechnical engineers encountered a layer of native very soft Blue Clay that was not a suitable bearing stratum, as discovered during the 1890 (e.g., Auditorium Theater settled 17 inches). As time evolved, engineer constructed bells by hand at the base of shafts that rested on top of the competent glacial tills (hardpan) with more heavily loaded shafts extending through the hardpan and socketed into bedrock. Bedrock is generally about 100 to 140 feet below ground level.

When the Navy Pier Exposition Authority set about improving the amenities on the piers some 25 years ago, a decision was made to raise a two-level parking garage to six stories. This done by supplementing existing bell caissons with 200-kip drilled micropiles to bedrock with corbeled pile caps extending from the caisson caps and existing columns were required. Geotechnical contractor TCDI (predecessor to HBI) worked with general contractor Schal Bovis and structural engineer Rubinos & Mesia Engineers, Inc. to design and install six 50-kip capacity friction piles for the repurposing of the original Headhouse structure as the new home of the Chicago Children's Museum around 1993.

Micropiles were used in 1997 was to underpin the updated and renovated Shakespeare Theatre. Micropiling work in 2003 was the result of a garage floor collapse; a portion of the parking deck collapsed when overloaded by soil placed in preparation of a home and garden show. More recently, 400-kip micropiles were installed to support the new Giant Ferris wheel, as well as for ongoing construction of a new hotel. Today, the Navy Pier is one of the most visited tourist destinations in the Midwest.

Design loads on these piles have not been overly significant. However, the Navy Pier Hotel required a very interesting design for the micropiles, providing design capacity for both vertical and horizontal loads despite the micropiles extending some 20 feet through open water. Micropiles now support a parking garage, hotel, Ferris Wheel, and theatre. Without stable foundations for these structures, the Pier would be unrecognizable.



Fig. 1a. Navy Pier Parking Garage 1997.

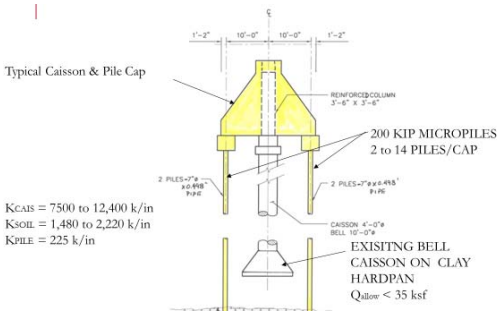


Fig. 1b. Navy Pier Parking Garage supplemental micropile support.



Fig. 1c. Installing micropiles from under garage floor beams.

ORCHESTRA HALL (SYMPHONY CENTER) 1995

In 1902, the property at the site of Leroy Payne's livery stable at 220 Michigan Avenue became available. After purchasing the lot, the building was started in May 1904 and opened a year later as the Orchestra

Symphony Center, designed by architect Daniel Burnham. Far too spacious for an orchestra, filling 4,000 seats twice weekly was a challenge and there were many scheduling conflicts with other ensembles. The hall has undergone numerous alterations to improve acoustical flaws of the original design. Designated a National Historic Landmark in April 1994, it has been listed on the National Register of Historic Places since 1978.

In June 1993, plans to renovate and expand Orchestra Hall were approved and the $110 million project resulting in Symphony Center began in 1995 and was completed in 1997 (Orchestra Hall at Symphony Center 2014). According to Walton (1996), the renovation included raising the existing building three stories to improve acoustical qualities of the Hall, renovating the Chapin and Gore building at Adams and Wabash, and constructing a new eight-story support building. Most of the work could only be performed during summer, and the only area available for the new foundations was in the 8-foot-wide alleys on each side of the building and in low overhead conditions.

According to Scherer et al. (1996), engineers used high-capacity micropiles as an alternative to hand-dug caissons. The challenge was the foundation system. The team consisted of Skidmore Owings and Merrill, Chicago; STS Consultants Ltd., Deerfield, Ill.; Turner Construction Co., Chicago; and The Concrete Doctor Inc., Lincolnshire, IL (Ill (TCDI now Hayward Baker Inc. [HBI]), and GEI Consultants as the micropile consultants.

Six new interior pile caps were required to support expanded balconies and acoustical walls with column loads ranging from 90 to 150 kips. Original contract documents required 30 kips service load capacity, 8-inch diameter, 3/8-inch thick, concrete-filled pipe piles to be installed using drilled-in-place procedures. Column loads for the new structure were as high as 720 kips. Foundation contractor TCDI/HBI (Hayward Baker) proposed an alternative: 210-kip (105 ton) capacity rock-socketed drilled steel micropiles consisting of 7-inch-diameter casing with 80 ksi grade steel, and hydraulically pushed micropiles consisting of 4-inch-diameter casing. This technique eliminated hand dug caissons, electrical or internal combustion driven pile or drilling equipment, ventilation provisions, and management of drill cuttings and fluids within a constrained basement.



Fig. 2a. New section of Orchestra Hall building under construction.



Fig. 2b. Completed Fascia perimeter frame and roof for Orchestra Hall in 1998.



Fig. 2c. Two load tests required.

SHEDD AQUARIUM 2003

Located on Lake Michigan, the aquarium contains 32,000 marine animals and was the largest indoor aquarium in the world with 5,000,000 gallons of water. In 1924, the Shedd Aquarium Society led by Chicago millionaire John G. Shedd asked the Chicago Park District for land at Roosevelt Road to build what would become the first permanent inland saltwater exhibit. The aquarium cost $3,000,000 to build and initially included 132 exhibit tanks (Bishop 1932). Completed in 1929, the first exhibits opened in 1930.

In 2003, TCDI/HBI installed micropiles for new foundation and excavation support. The first phase of restoration included renovating the existing Rotunda area exhibit and constructing two new exhibits—one of which would be located beneath the existing basement and connect with the other exhibits on the main floor via a below-grade corridor to an elevator lobby. Creation of the sub-basement level T-shaped corridor and elevator lobby required an excavation 20 feet deep, 120 feet long, and 27 feet wide. This required underpinning of portions of the existing building, provision support for the new foundations, and earth retention during excavation.

Typically, this type of low-headroom work would be accomplished by drilling and installing segmented soldier beams and lagging as earth retention and drilled or driven micropiles from within the newly-created space for the new foundation loads. HBI, in cooperation with general contractor Turner Construction Company, Ground Engineering Consultants, STS Consultants, Ltd., and Klein & Hoffman, proposed an innovative alternative that significantly reduced the schedule and cost and simplified the construction sequence. Support of the new foundation was achieved by installing hydraulically-pushed micropiles from the existing basement level using the existing floor slab as a reaction. HBI installed a soil-nailed earth retention system as excavation of the sub-basement progressed. This allowed other trades to continue working in the basement before beginning excavation.

The initial phase of the renovation program also included relocation of the existing loading dock entrance. HBI installed 24, 100-kip capacity end bearing drilled rock socket micropiles to a depth of 100 feet in bedrock to support the new entrance. Thirteen pushed micropiles were installed to provide additional support to the existing exterior grade beam at the new loading dock entrance.

Relocation of the loading dock entrance allowed construction of an access ramp to the sub-basement beneath the original entrance. Prior to excavation of the ramp, sixteen 50-kip design capacity pushed micropiles were installed to underpin the existing exterior grade beam. Pushed micropiles also provided support for the new corridor and elevator lobby. A reaction frame was set up and anchored to the existing concrete slab prior to installation. A total of sixty-one, 50-kip design capacity micropiles were hydraulically pushed in 3.5-foot segments to an ultimate load of 75 kips (1.5 times the design load) and to an approximate depth of 85 feet. Once the excavation was complete for the sub-basement, the piles were cut off to final elevation and tremie grouted.

While the micropile loading on this project did not move the allowable stresses in the micropiles forward, these were alternative uses of micropiles for underpinning and earth retention (laterally loaded). At this stage in the growth of micropiles in the City, this project strengthened the comfort levels of City Officials and engineering community. This was also another example of complex construction being completed on an expanding Chicago Landmark using the strength and limited space for the versatile use of the micropile.

An addition was later completed in the early 90s.



Fig. 3a. Micropiles used as soldier beams in limited access areas.



Fig. 3b. Completed renovation.

SOLDIER FIELD 2002

Plans for the stadium began in 1919 as a memorial to deceased American veterans. Soldier Field is multi-use stadium and an American football stadium and home field of the National Football League (NFL)'s Chicago Bears who moved there in 1971. From 1922 to 1928, the stadium was constructed by the South Park Commission (which later merged with other park commissions to become the Chicago Park District in 1934.) Soldier Field was built in three stages between 1922 and 1939 for $13 million. Though it opened in October 1924 as Municipal Grant Park Stadium, the name was changed to Soldier Field in November 1925 and wasn't completed until a third phase of construction concluded in 1939, giving it a capacity of nearly 75,000.

During the 1990s, the stadium's infrastructure was crumbling, its facilities outdated, and it was lacking club seating that generates substantial revenues for other NFL franchises. The old stadium sat on 10,000 timber piles driven through a landfill of Chicago Fire Debris and muck from 50 miles on Chicago Freight tunnel located 40 feet below the street. The timber pile fetched in very stiff clay and had an average depth of 62 feet. Supporting the new stadium built inside the colonnade of the original stadium required 2,200 vertical and battered H-piles driven 90 to 100 feet to hard hardpan or to top of bedrock, and more than 400 drilled micropiles drilled in-between the existing colonnade pile caps as driven pile were redistricted from being this close to the fragile colonnade. Seating tiers of precast-concrete risers span 40 feet to their structural steel supports. The rakers supported the upper grandstand cantilever 60 feet over the historic colonnades, one of the longest such cantilevers supporting crowds. The new stadium had a 13,000-ton structural steel frame (Burns and McLean 2004). While much of the new stadium was supported by the driven steel piles,

portions of the new stadium would be supported on vertical and battered micropiles to resist compression and base shear. The micropiles were installed immediately adjacent to the stone masonry columns to prevent damage to the columns that could occur if pile driving was executed nearby. The project team consisted of structural engineer Thornton Tomasetti, geotechnical engineer STS Consultants, general contractor Tuner/Barton Malow/Kenny (JV), geotechnical contractor HBI. Driven piles were installed by Thatcher Engineering.

The micropiles were installed to a design stress of 18 ksi in the grouted segmental API steel pipe and were the first 200-ton micropiles approved by the City of Chicago. This would be the first occurrence on a major high-profile project in which the Chicago Building Code limited 12 ksi in steel was adjusted upward, after an extensive pile load program. The micropiles were installed along the east and west colonnades after a significant pile test program verifying the design stress, which allowed for a grout filled 9-5/8-inch by 0.545-inch wall pipe for vertical and battered pile to be designed with a design load of 400 kips (200 tons). This allowed for the 18 ksi compressive steel stress and 400 kip to be the new standard of practice for high load capacity micropile work in Chicago.

The stadium's interior was mostly demolished and rebuilt as part of a major renovation project in 2002, which modernized the facility but lowered seating capacity and delisted it as a National Historic Landmark.



Fig. 4a. Soldier Field under construction.



Fig. 4b. Soldier Field on a summer day in 1954.



Fig. 4c. Production micropile installations.

1845 SOUTH MICHIGAN AVENUE 2003

In 2003, a new development was under construction on the South Side. The project consisted of a 19-story high-rise private residential condominium with five levels of parking and 14 levels of condominiums located above the parking levels. The original foundation design included rock socketed and steel cased caissons into sound dolomite. The contractor's value engineering option was to construct caissons under polymer slurry to top of rock designed for 100 ksf bearing. This was a first for the City of Chicago to design uncased drilled shaft to bear on top of bedrock.

The micropile installation were done here to repair a new drilled shaft that developed issues during construction. Micropiles were installed around the perimeter of a single drilled shaft that needed underpinning as it was determined the shaft was founded on boulders and not top of bedrock. The drilled shaft was shorter than other shafts on site. As a result of this change from rock socketed drilled shafts to a single shaft founded above top of rock, there were differences in the stiffness of the individual foundation units. The structural and geotechnical engineers determined micropiles should be installed around the perimeter of this single shaft to act as "settlement reduction load bearing elements". As such, they were not permitted by the Chicago Building Department and CDOT Office of Underground Coordination as deep foundations but were installed to provide supplemental stiff to the drilled shafts to match the adjacent shafts constructed directly on bedrocks. This may have marked the first time in the City that micropiles were installed as settlement reducers without a 48-hour pile load test.

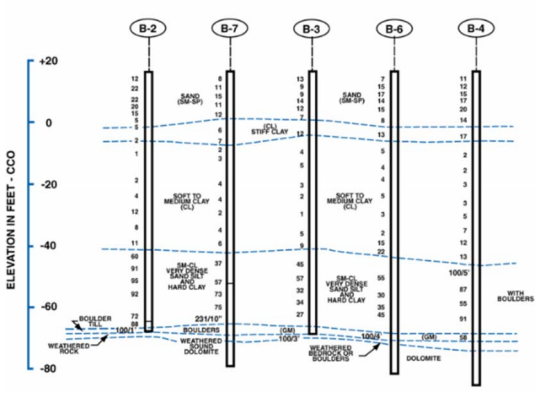


Fig. 5a. Drilling 6-inch augers with a Casagrande C8 drill rig.

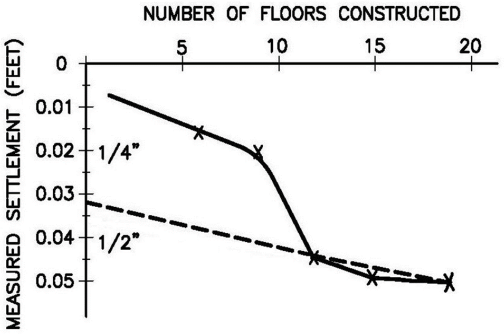


Fig. 5b. Average building settlement versus the number of floors built.

111 SOUTH WACKER DRIVE 2004

A 51-story concrete core and steel frame commercial office tower was recently constructed on the site of the former US Gypsum building in downtown Chicago, Illinois, USA. The structure foundation reused several caissons from the demolished US Gypsum building supplemented with new belled caissons bearing on silty clay hardpan. Extensive in-situ pressure meter testing was performed during the geotechnical investigation to determine allowable bearing capacity and better estimate building settlements. Problems during foundation construction along the south side of the building frame required remediation of two caissons. One caisson was supplemented with micropiles, while the second caisson was abandoned and replaced with a straight-shaft rock socketed caisson. To determine the effectiveness of the repairs, the building foundation settlements were monitored during construction.

The design geometry of Caisson D.5-5.9 consisted of a 7-foot-diameter shaft and an 18.5-foot diameter bell. The caisson flooded near the end of belling operations. Water inflow rates made the caisson bell sidewalls unstable, and the completed geometry was questionable.

Case Foundation Company attempted to form a grout plug in the bell under polymer slurry to reduce seepage. Two days later, at the request of STS, a larger diameter bell was constructed approximately 2.5 feet above the original bearing elevation. Only minor seepage was observed during re-belling.

STS performed a series of borings at varying distances from the caisson centerline which indicated the constructed grout pad was slightly undersized. In addition, the bearing soil in the region outside the grout pad had been disturbed by construction cleanout operations. Settlement predictions (both local and differential) based on PMT tests performed at, and below, the new bell exceeded the tolerance set by the structural engineer MKA.

To relieve a portion of the load, and thereby reduce settlement. STS designed 14 high capacity micropile “settlement reduces) which encircled the impacted caisson. The micropiles were designed as end bearing, rock socketed elements with full-length 9.625 inch diameter steel casing. Hayward Baker, Inc., a contractor locally experienced in high capacity applications, installed the micropiles at a 1H:1OV batter angle (see Figure 12). MKA re-designed the caisson cap to integrate the micropiles and the caisson shaft without altering the top-of-cap elevation. The total settlement of the micropile assisted caisson for the 11,800 kip design load was predicted to be less than 0.8 inch (2 cm).

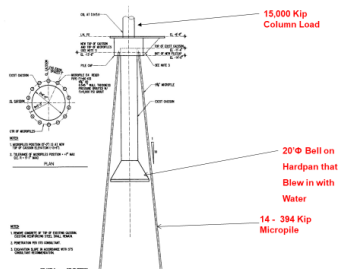


Fig. 6. Micropile support of hardpan caisson.

WRIGLEY FIELD 2013

Designed by architect Zachary Taylor Davis, construction of the 14,000 capacity ballpark began March 14, 1914 (Patt). The proposed length of the curved stand was to be 800 feet, breadth 100 feet, and height 56 feet. It was projected 160,000 bricks and 45,200 cubic feet of concrete, 1,900 cubic feet of hollow tile, and 1,700 yards of plastering were to be used for construction. By March 19, the workers erected steel and laid the brick for the right field bleacher stand. The foundations were complete shortly and by March 30, laying of the concrete slab for the grandstand seats was in progress. The laborers completed steel work by April 4 and were building the iconic brick wall for part of the outfield by April 9. By April 14, the concrete runways and seat slabs were finished and seats installed within six days (Kush).

The $250,000 ballpark opened April 23, 1914 as Weeghman Park for Charles Weeghman's Chicago Whales of the Federal League, which folded after the 1915 baseball season. The park is the home of the Chicago Cubs. Original dimensions at Weeghman Field were 310 feet (left), 440 feet (center), and 356 feet (right). It was the first ballpark to have permanent concession stands.

The structure needed a complete facelift to meet the revenue goals and fan comfort of a modern stadium. In order to, as well as meet modern building codes for strength and serviceability. To meet these modern day needs while keeping the historic and architectural aspects of the National Register of Historic Places Ballpark, creative underground foundation solutions would be needed to support gravity and wind loading for a "group assembly". Due to the historic designation and the fact that the park is landlocked in a busy urban neighborhood, any additional building square footage for amenities would either need to be above or below the existing stadium and fan areas. Earth retention was used to provide additional back of house storage areas and the Cubs locker room. Micropiles were used to reinforce existing foundations to allow additional loads from luxury boxes and wind loads. Drilled shafts were installed to increase the support new outfield bleachers. A secant pile wall was installed to allow for a deep basement for Cubs underground locker room and street grade front office needs and commercial sales. The tower and basement were constructed using top-down construction methods to speed construction.

Perhaps the cleverest design solution was to keep the single-story historic ground keeper house now has a deep basement for additional storage and the house sits atop the sheet pile wall. New players' storage rooms and future access from the ball field to the underground clubhouses were moved to the area just outside the walls in another below-grade storage area created by sheet piling. A tunnel was required to go beneath the concourse to allow the players free access to and from the clubhouse from the dugouts. This was accomplished with a cut and cover tunnel supported by jet grouting with micropiles acting as soldier piles with cross-lot bracing. A sophisticated real-time monitoring system was brought online prior to the foundation work beginning. This allowed for the project team to observe movement of the building without damaging the structure.

When the project team went to obtain Chicago Building Department and CDOT OUC approval for the micropiles, they would be the heaviest loaded micropiles completed to date at 550 kips. The higher design loads were needed to further economize the foundation package. More importantly, the micropiles were used to underpin existing foundations. Due to the congested site, there were locations where additional, lower-capacity micropiles simply could not be installed in the room allowed.

To make things more challenging, the baseball team would retain their normal season and post season schedules. Work had to be phased and planned to not interfere with the baseball schedule or with fans, meaning all work was done late fall through winter. The project was completed successfully over several off seasons in the middle of some of Chicago's harshest winters. The project team consisted of Pepper Construction, GEI Consultants, Thornton Tomasetti, Case Foundations, and HBI. GEO -Instruments was contracted to provide real time movement monitoring of the structure. This type of monitoring had been completed previously in the City, but this was perhaps the first time on such a fragile building that had to be ready and safe for one of America's favorite baseball teams.

The project improved the fan experience as well as the revenue for the Cubs. And as we all know; the Cubs were able to bring home a World Series victory in the new stadium in 2016



Fig. 7a. Wrigley Field expansion (aerial).



Fig. 7b. Column F; four 500 kip micropiles.



Fig. 7c. Wrigley Field expansion (close-up).

150 NORTH RIVERSIDE 2014

Architecture and structural design were done by Goettsch and MKA, respectfully. IT was built by Clark Construction as the 2018 ASCE Opal Award Winner. This high-rise building is 53 stories tall and sits on two acres on the west bank of the Chicago River. It holds 1.2 million square feet of leasable office space. Due to its unique superstructure design, the foundation encompasses approximately 25 percent of the lot. The building opened in 2017 and rises on a small base which slopes outward at an angle for the first eight stories and widens (Lully-Pop building). The designers chose a core-supported central concrete spine that holds the elevator and transfers the load of the upper floors down to the foundations (Chicago Architecture Center 2017).

In 2014, Clark Construction worked with Case Foundation and structural engineer MKA(MKA) for O'Donnell Financial Group to drill two lines of eight steel cased rock socketed caissons more than 110 feet below grade level and sink the shafts five (5) feet into Chicago's dolomite bedrock to provide a stable foundation on a very restricted footprint. The west side development is a podium structure that is restricted by the Amtrak and Metra ROW for foundation support location. In this area, there was no room for drilled shafts. Steel cased rock socketed micropiles were selected as an alternate here. The Grout filled 9.875 diameter by 0.625 inch wall outer pipe and 7.0 inch diameter by 0.5-inch wall inner pipe were installed by the team of Atkinson (a Division of Clark) and Thatcher Foundations. These micropiles would be the largest design loads permitted and then constructed in the city to date at 600 kips (Cassidy 2017). 81 floating barges were tied together to hold a 2,000-kip capacity ringer crane that lifted the giant steel trusses. The largest and longest hot-rolled steel beams ever used in the country allowed the building's width to splay out from 39 to 120 feet.

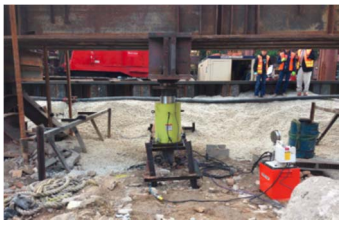


Fig. 8a. 1,200-kip load test.



Fig. 8b. Multiple casings (11.75, 9.875, and 7.0 API N80).

CONCLUSIONS

Micropiles in the City of Chicago do not carry the weight or notoriety of the traditional Chicago bell or rock socket caissons. However, over the last 25 years, micropiles and specialty geotechnical construction techniques have allowed structural and geotechnical engineers to support some of the most sophisticated projects in the world. These specialty techniques have allowed for repair of existing and new damaged foundations. The micropiles have allowed for new column loads to be placed in nearly impossible access confined work spaces. The specialty techniques have let Chicago's engineering and architecture community develop new methods to support one of the world's most iconic skyline. The authors hope as the micropile

transitions into its fourth phase, we will continue to see design loads pushed upward, design stresses evaluated more openly, and projects become more challenging. Using micropiles to supplement existing foundations for building reuse and redevelopment is a "green" idea that saves energy, time, and natural resources.

REFERENCES

150 North Riverside. 2017. Chicago Architecture Center. www.architecture.org/learn/resources/buildings-of-chicago/building/150-north-riverside/. Accessed 19-4-1.

Bishop, G.A. 1932. Chicago's marine wonder house The John G. Shedd Aquarium: where fishes of all sizes, shapes, and hues delight the visitor. Chicagology. https://chicagology.com/skyscrapers/skyscrapers025/. Accessed 19-4-1.

Burns, J. and McLean, D. July 2004. Field goals: Chicago's new Soldier Field tackles complex geometry and construction constraints in the NFL's fastest stadium construction. http://hirschfeld.wwafcosteel.com/sectors_structural_05_article.pdf. Accessed 19-4-1.

Cassidy, R. 2017. Nerves of steel: 150 North Riverside. Building Design + Construction. www.bdcnetwork.com/nerves-steel-150-north-riverside. Accessed 19-4-1.

Chicago Symphony Center. Trahan Architects. https://trahanarchitects.com/work/chicago-symphony-center/. Accessed 19-4-1.

Dellaria, J., Born, D. and Hill, J. 2018. Chicago's Navy Pier: moving into the future with micropile foundations. The International Association of Foundation Drilling, ADSC Foundation Drilling Magazine, pp 28-40. https://www.haywardbaker.com/uploads/news/ADSC-Foundation-Drilling-Chicago-Navy-Pier-Article.pdf. Accessed 19-4-1.

Kush, R.D. The building of Chicago's Wrigley Field. Society for American Baseball Research. http://research.sabr.org/journals/building-of-wrigley-field. Accessed 19-4-1.

Orchestra Hall at Symphony Center. 2014. Chicago: Rosenthal Archives of the Chicago Symphony Orchestra, pp 1-2. https://cso.org/globalassets/about/rosenthal-archives/pdfs/orchestra_hall_at_symphony_center.pdf. Accessed 19-4-1.

Patt, A. How much of Wrigley Field's original 1914 structure remains today? Medium. https://medium.com/the-wrigley-rapport/how-much-wrigley-fields-original-1914-structure-remains-today-af3a93b4e8cb. Accessed 19-4-1.

Scherer, S.D., Walton, W.H., and Johnson, R. 1996. Chicago's micropile debut. Civil Engineering ASCE, 66(8) 51-53. https://cedb.asce.org/CEDBsearch/record.jsp?dockey=0102387. Accessed 19-4-1.

Schock, R.E. and Risberg, E.J. 2013. 120 years of caisson foundations in Chicago, p. 6. International Conference on Case Histories in Geotechnical Engineering.

Soldier field renovation on tight schedule. Hammer & Steel. http://www.hammersteel.com/09-08-03-soldier-field-renovation-on-tight-schedule.html. Accessed 19-4-1.

Walton, W.H. and Scherer, S.D. 1996. Mini-pile foundations for Orchestra Hall renovation and expansion project. ASCE Newsletter – Illinois Section, 37(8) 1-2.

DEEP FOUNDATION ADVANCEMENTS IN FARGO

Matthew R. Glisson, PE, Braun Intertec Corporation, St. Louis, Missouri, USA, 314-569-9883, mglisson@braunintertec.com
Ezra Ballinger, PE, Braun Intertec Corporation, Fargo, North Dakota, USA, 701-492-5872, eballinger@braunintertec.com

ABSTRACT

Located in downtown Fargo, North Dakota, the Block 9 Redevelopment project site contains highly-compressible soils in the upper 100 feet with groundwater about 10 to 15 feet below the existing ground surface. The owner prohibited using driven piles to avoid disturbing neighbors of the project and historically, drilled shafts are used in Fargo as a reduced noise and vibration alternative to driven piles. However, developments over the last 20 to 30 years in drilling equipment, load testing and integrity testing resulted in the project team identifying augered cast-in-place piles as a suitable alternative for this project. To reduce the risks associated with using a relatively unproven foundation system in the area, the project team used the design-build delivery method for foundation design and construction. The team also specified compression load testing and higher-than-normal integrity testing. A successful bi-directional load test validated the design parameters for the augered cast-in-place pile while thermal integrity profiling gave the team confidence that these piles would perform similarly to the test pile.

Keywords: augered cast-in-place pile, bi-directional load test, thermal integrity profiling, urban redevelopment

PROJECT DESCRIPTION

The Block 9 Redevelopment project goal was to turn an existing, at-grade parking lot in downtown Fargo, North Dakota into a public outdoor plaza, a mixed-use building and a parking ramp. The project provides new offices, retail spaces, a hotel, a restaurant and private apartments. Situated in the southeast quadrant at the intersection of Broadway and 3rd Avenue North, the project site wraps around a bank building that was to remain. According to aerial photographs, the eastern portion of the site contained a public parking ramp that was constructed between 1952 and 1976, and subsequently demolished between 2009 and 2010. The western portion of the site had some combination of buildings and surface parking visible in aerial photographs taken between 1952 and 1979. Since 1984, aerial photographs show the western portion of the site being entirely surface parking.

The redevelopment included the construction of three structures: the Tower, the Podium and the Parking Ramp, as shown in Fig. 1. With plan dimensions of roughly 100 feet by 100 feet, the Tower has 1 level of below-grade parking and 19 above-grade levels rising to a height of about 230 feet above grade. The Tower contains eight levels of commercial office space, four levels of hotel, six levels of residences and a mechanical level. This configuration resulted in column service loads ranging between 435 and 2,685 kips. The Tower core area has a total service load of about 30,000 kips.

The Podium wraps around the west and south sides of the Tower, extending 50 feet out from the Tower on the west side and 80 feet to the south. With one level of below-grade parking, one level of retail, three levels of office space and the uppermost level being large-event space, the Podium has column service loads between about 435 kips and 700 kips.

The Parking Ramp is located to the east of the Tower and Podium, separated by a proposed alley. With eight levels of parking, the lowest level of the Parking Ramp is connected to the Tower and Podium by a tunnel. The Tower and Podium are also connected to the Parking Ramp by a skyway at the second level. Service loads for the Parking Ramp columns ranged from about 615 to 1,750 kips.

© 2019 Deep Foundations Institute

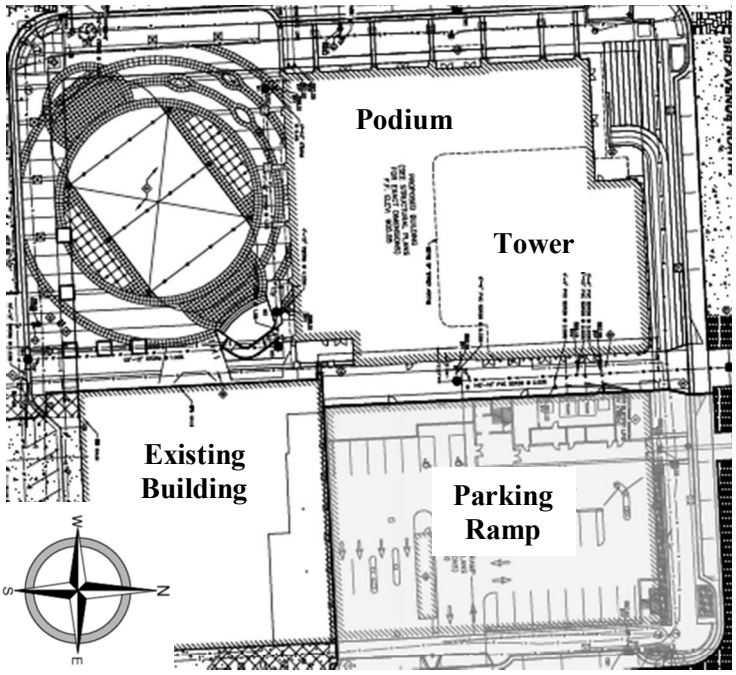


Fig. 1. Site layout

SUBSURFACE CONDITIONS

Fargo is in the Red River Valley region of eastern North Dakota and western Minnesota. The general soil profile of the Red River Valley consists of relatively weak, unconsolidated, glacial-lake deposits overlying glacial till. In the downtown Fargo area, most sites contain a layer of surficial fill. At the Block 9 site, the fill thickness was about 3 to 9 feet and it generally consisted of sand over clay with varying amounts of construction debris. The fill varied in strength with N-values ranging from 5 to 23.

Underlying the fill are the Glacial Lake Agassiz (GLA) deposits that extended to depths of about 100 feet below existing grade. The GLA deposits generally classify as fat clay with some silt layers also present. The N-values of the material generally fell between 2 and 5. Below the GLA deposits are glacial till soils classifying as lean clay with varying amounts of sand and gravel and having N-values generally between 47 and 81. Table 1 summarizes the results of laboratory testing performed on the retrieved samples.

Table 1. Laboratory Test Results

Material	Moisture Content, %	LL	PI	C_c	C_r	e_o	Po, ksf	Dry Unit Weight, pcf
Fill	14 - 37	---	---	---	---	---	---	77 - 109
GLA	28 - 79	54 - 113	32 - 87	0.87 - 1.27	0.041 - 0.059	1.36 - 1.90	2.48 - 3.10	55 - 109
Till	10 - 21	---	---	---	---	---	---	100 - 126

Table 2 summarizes the results of pressuremeter tests also performed as part of the Block 9 subsurface exploration program.

Table 2. Summary of Pressuremeter Test Results

Material	Yield Pressure, ksf	Limit Pressure, ksf	Modulus, ksf
GLA	7 - 13	12 - 15	81 - 121
Till	29 - 91	54 - 134	510 - 1,595

FOUNDATION SELECTION

Based on the loads and soil conditions, the project team determined that a deep foundation system was the best choice for supporting the Tower, Podium and Parking Ramp. The most common deep foundation system in Fargo is driven pile, usually steel H-pile or closed-end pipe piles sufficient to provide allowable resistances of 100 to 300 kips. The next most-common deep foundation systems in Fargo are drilled shafts followed by helical piles.

The Block 9 Redevelopment is part of a few projects the developer undertook in downtown Fargo, one of which is the Roberts Street Ramp. This project included static load testing on a helical pile bearing in the till. The test pile had a shaft diameter of 10-3/4 inches, a bottom helix with an 18-inch diameter and an upper helix with a diameter of 32 inches. The test pile was filled with concrete having a compressive strength of about 6 kips per square inch (ksi). This test did not include instrumentation along the shaft and was stopped at a maximum load of 787 kips with about 5 inches of measured movement at the pile top. For 1 inch of pile-top movement, the load-deflection curve indicated a resistance of about 415 kips. A plot of theoretical elastic deformation with the measured pile-top movement indicates that the pile deformation was elastic to about 0.75 inch at a load of about 340 kips. Beyond this load, the pile indicated increasingly plastic deformation. The permanent deflection of the pile top after unloading was about 1 inch.

The developer also performed a design-phase test pile program on driven pile specifically for the Block 9 project. The test program included high-strain dynamic testing of two closed-end pipe piles. One pile had an outside diameter of 12-3/4 inches and the other had an outside diameter of 16 inches. The testing program consisted of collecting dynamic test data during the initial drive and during a seven-day restrike. After the initial drive, the piles were filled with concrete such that the restrike tests were performed on piles with a greater impedance. High-strain dynamic testing experience in the Red River Valley has shown that testing concrete-filled pipe piles results in higher, estimated, ultimate resistances that more closely match values obtained from static load tests.

The 12 3/4-inch diameter pile was driven to a toe elevation of 774 feet, or about 25 feet into the glacial till. The contractor drove the 16-inch diameter pile to a toe elevation of 780 feet, which is about 19 feet into the till. Wave matching evaluations performed by others estimated the ultimate resistances of the 12 3/4- and 16-inch diameter piles to be about 928 and 1,096 kips, respectively.

Construction vibrations are a common concern with redevelopment projects in an urban setting. So, it is not uncommon for owners of redevelopment projects to require the use of relatively low-vibration foundation systems to be less disruptive to the project area and reduce the risk of claims from neighboring building owners and tenants.

In response to this potential risk, the driven pile test program included vibration monitoring at the perimeter of the site and near some of the adjacent buildings. Based on the results of the monitoring and discussions with owners and tenants of the adjacent buildings, the developer decided that driven pile foundations were not an option for the Block 9 project.

At this point in the project, the construction manager asked the authors' firm to perform a peer review of the geotechnical analyses and recommendations performed for the project so far. The request was due in part to the initial cost estimates for utilizing large-diameter helical pile or drilled shafts to support the

structures, which were the recommended options by the original geotechnical engineer for the project. As part of the peer review, we discussed the possibility of supporting the building on augered cast-in-place (ACIP) piles with the project team, as well as with some contractors. The project team was only aware of one other project that had used ACIP piles for foundation support in the Fargo area.

Based on preliminary discussions with ACIP pile contractors, this foundation system was more attractive from financial and schedule perspectives. Initial estimates for ACIP piles with diameters between 16 and 24 inches showed that ACIP piles could achieve an ultimate resistance of about 800 kips and an allowable resistance of about 400 kips, depending on the pile length in the till. These resistances were similar to the large-diameter helical pile tested on the developer's other project. The biggest drawback for ACIP piles was being an early-adopter of a relatively unproven foundation system to the area. To offset the resulting schedule and financial risks, the project team chose to utilize a design-build contracting approach for ACIP piles and to have quality control and assurance requirements that were higher than typical for ACIP projects in areas where this system is more commonly used.

HISTORICAL CHALLENGES FOR ACIP PILE IN FARGO

Early versions of ACIP piles were developed in the United States in the 1940s and formalized with Raymond Patterson's patent application in 1950 and award in 1956. A similar patent was awarded in Europe to Gaspar Coelius in 1960 (NeSmith, 2006). Despite being available for over 60 years and being commonly used in the surrounding regions of Minnesota and North Dakota, ACIP piles had not seen significant use in the Red River Valley. The Fargo Water Treatment Plant expansion project in 2015 is the only known project to use ACIP piles in the Fargo area. For this project, 18-inch-diameter piles were installed to a depth of about 100 feet below grade. ACIP piles were also installed during 2001 in the City of Grand Forks, North Dakota as part of a new gravity raw water intake pump station. The Grand Forks project utilized ACIP piles with a diameter of 24 inches installed to a depth of 121 feet before the upper 65 feet was excavated as part of the caisson installation (Kershaw et al., 2003).

There are two primary reasons that ACIP piles have not been widely used in the Red River Valley in general and particularly in Fargo. First are concerns that drill rigs will not be able to penetrate deep enough into the glacial till to obtain significant resistance. Second are concerns that the relatively weak, GLA soils will not allow construction of a continuous shaft. "Very soft soils" is the first unfavorable geotechnical condition listed for ACIP design in Geotechnical Engineering Circular No. 8: Design and Construction of Continuous Flight Auger Piles (Brown et al., 2007) published by the Federal Highway Administration.

Related to this second concern is the difficulty in performing non-destructive, integrity testing on ACIP piles that have lengths of at least 100 feet. Prior to about 2013, the widely-available techniques for integrity testing of ACIP piles included cross-hole sonic logging (CSL), gamma-gamma logging (GGL) and pulse echo or transient response. CSL and GGL both require the installation of access tubes to lower transmitters and receivers into the pile. These access tubes have diameters of about 2 inches. With the most common diameters for ACIP piles ranging from 16 to 30 inches and reinforcing cover requirements of 3 inches, there is not much space left for access tubes with ACIP piles that have a diameter of less than 30 inches. In addition, access tubes increase the difficulty of installing the reinforcing cage. Therefore, Brown et al. (2007) recommend CSL and GGL for ACIP piles with diameters of 30 inches or more. Single-tube testing is possible for both CSL and GGL. However, the effective diameter of testing around the access tube is roughly 2 to 4 inches. This could leave anywhere from 12 to 24 inches of the ACIP diameter being untested.

Low-strain integrity testing with pulse-echo or transient response methods are generally only capable of testing a length that is 30 times the pile diameter (Brown et al., 2007). This means that for the most-common diameters, this test method would only be able to evaluate the ACIP to a depth of 40 to 75 feet below the pile top. The authors have successfully tested ACIP piles with length-to-diameter ratios of 60, in relatively

homogeneous soils. While the GLA soils are relatively homogeneous, the difference in strength between the GLA soils and the till soils will likely result in a difference in the actual pile diameter between the two layers. This change in cross-sectional area would likely result in a reflection of the energy wave that might be too close to the toe for accurate determination of the piles' integrity. For cases where the pile toe is sufficiently deep into the till, the change in cross section might still result in a reflection that obscures the reflection from the pile toe.

The Grand Forks project did include pulse echo testing of the ACIP piles but only after the caisson excavation. So, the tested length of the piles was approximately 56 feet, which is just below a length-to-diameter ratio of 30 for a 2-foot-diameter ACIP pile (Kershaw et al., 2003).

ADVANCEMENTS IN ACIP PILE CONSTRUCTION AND QUALITY ASSURANCE

When first developed, ACIP pile rigs typically were able to generate a torque of about 15 kip-feet. By the 1970s, generated torque has increased to about 30 kip-feet. Today, crane-mounted systems typically range from about 15 to 90 kip-feet with a crowd pressure (downward force) of about 3 to 10 kips. Hydraulic rigs that used to be more common in Europe are now readily available in the United States. These rigs can develop a torque between 66 and 300 kip-feet. Perhaps more significant is the ability of the hydraulic rigs to generate crowd force of up to about 60 kips (Brown et al., 2007). These increases in torque and crowd pressure result in ACIP piles that can go deeper, have larger diameters and be constructed faster than was possible 30 to 40 years ago.

During the 1980s and into the early 1990s, ACIP piles saw a significant increase in use due to maturation of the design and construction techniques used. This was also the time when automatic monitoring equipment (AME) and the low-strain integrity testing methods were developed. These represented significant improvements to quality control and quality assurance. Although, not as much for projects in the Red River Valley due to the soil conditions.

AME utilizes computers and analog or digital sensors to measure auger tip depth, auger rotation rate, hydraulic pressure applied to the gearbox, grout volume and grout pressure. This allows both the contractor and third-party observer to have more accurate and detailed records of a pile's construction than is possible by relying on just the visual observations of a human. The rig operator can also see the data in real time, which allows alerts when certain variables are outside of the desired range, like grout volume.

As early as the 1980s, another method of integrity testing that would use the thermal characteristics of the concrete curing was identified. Initially developed for drilled shafts that might be subject to thermal cracking due to mass concrete effects, this approach resulted in the development of a thermal probe in the early 2000s that proved an effective alternate to CSL and GGL (Mullins et al., 2007). Subsequent developments in the late 2000s led to wires with thermal sensors at approximately 1-foot intervals that did not require access tubes, and thermal models that could interpret temperature measurements in elements that were not specifically mass concrete, like ACIP piles (Mullins, 2010; Piscsalko et al., 2011).

Dr. Jorj Osterberg performed the first bi-directional load test using what would later come to be known as an Osterberg cell, or simply an O-cell, in 1984. Receiving a patent in 1986 was just the start of this new approach to test deep foundations at loads previously beyond feasible reach (Hayes, 2012). The test method consists of placing a calibrated, hydraulic jack at the toe or at some point along the shaft of the pile, ideally where the estimated shaft resistance above the jack is equal to the shaft and toe resistance below the jack. This allows the system to use the test pile as the reaction system and effectively double the capacity of the jack. For example, a jack with a capacity of 400 kips can push the pile above the jack up with a force of 400 kips, while also pushing the pile below the jack down with a force of 400 kips. Summing the forces means that the gross total force on the pile is 800 kips.

Along with developments in bi-directional jacks since 1986 are improvements in vibrating wire strain gauges, linear-variable displacement transducers and computers that can automatically control load tests and record the data from the tests. These improvements in sensors and computers have decreased the costs of performing tests with sacrificial equipment and sensors, which has led to a more widespread use of them. Instrumentation that was once viewed as only practical for use on research-quality testing is now becoming viewed as the standard of care with load testing. This allows designers to utilize greater resistance with more reliability, thereby reducing the cost of deep foundations based on unit load/resistance.

CONTRACTOR SELECTION AND PRELIMINARY DESIGN

The final geotechnical evaluation report for the project provided recommendations for ACIP pile design and construction using a design-build approach with performance-based plans and specifications. The owner and project structural engineers perceived significant financial and schedule risk associated with the unproven nature of ACIP piles due to the limited number of ACIP projects in the region. The design-build approach allowed them to transfer some of this risk to the contractor. The final geotechnical report also provided initial estimates of ACIP pile lengths and resistances for common diameters ranging from 16 to 30 inches. These initial estimates were necessary for the structural engineer and general contractor to continue developing plans and cost estimates as the structural engineers would maintain engineering responsibility for pile caps.

The project documents required the ACIP pile contractor to use AME and to perform a static load test. The geotechnical engineer would provide and perform thermal integrity testing on one-third of the production piles, in addition to the test pile. Typical practice in the United States is to perform integrity testing on about 10 to 20 percent of the piles for an ACIP pile project (Brown et al., 2007). So, two to three times the normal amount of integrity testing was required for this project.

Once the design progressed far enough that foundation loads were relatively certain, the project team invited a pre-qualified group of contractors to submit proposals for the project. After submitting a cost proposal, each contractor was invited to an interview with the construction manager, the general contractor, the structural engineers and the geotechnical engineer. Although no formal, scoring system was used, each contractor was evaluated based on, in no particular order: safety, project understanding, schedule, proposed quality control program, proposed equipment, experience and cost.

The successful ACIP pile contractor then submitted a preliminary design for review by the project team. The design was based on a 20-inch diameter pile that would extend 4 feet into the underlying till and develop 400 kips of allowable resistance. The design used a safety factor of 2.0 against the geotechnical strength limit state meaning that the design would develop an ultimate resistance of 800 kips.

The preliminary design with 20-inch diameter piles resulted in a number of piles that were spaced less than three diameters apart, center-to-center in the Tower core. Once group effects were considered, a significant number of pile would need to be added to offset the reduced efficiency of the closely-spaced piles. The contractor re-evaluated their design and decided to decrease the ACIP diameter to 18 inches while increasing the length of pile in the till to 6 feet. These changes did not affect the allowable or ultimate resistance of the pile and resulted in only needing a few additional piles to offset reduced efficiency due to group effects.

ACIP PILE CONSTRUCTION AND TESTING

The ACIP pile contractor selected a crane-mounted drill system capable of applying more than 100 kip-feet of torque and up to 80 kips of crowd force. ACIP pile construction began with the installation of a sacrificial test pile. In accordance with their proposal and design submittal, the ACIP pile contractor performed a bi-

directional static load test in general accordance with ASTM International's Standard Test Methods for Deep Foundations Under Bi-Directional Static Axial Compressive Load (ASTM D8169-18). The test pile had a diameter of 18 inches and an overall length of 108.8 feet. The pile toe elevation was 792.7 feet, meaning that roughly 7 feet of the pile was embedded in the glacial till, based on the closest boring and observations during drilling. The bottom of the jack, which also corresponds to the break in the pile between upward and downward movement, was placed at an elevation of 801.5 feet. Instrumentation included in the test pile consisted of one strain gauge below the jack, three individual strain gauges at different elevations above the jack and telltales measuring movement of the jack top and of the jack bottom at an elevation of 797.2 feet. The four strain gauges were placed at the center of the shaft cross section. The ACIP pile contractor was unable to install the reinforcing cage all the way to the bottom, which resulted in the intended telltales for the toe not being at the bottom of the pile, the bottom of the jack assembly not being at the top of the till and the strain gauge below the assembly being approximately at the top of the till. Two automated digital survey levels and corresponding targets measured pile top movement.

The ACIP pile contractor performed the bi-directional static load test six days after installing the test pile. The maximum sustained load was 482 kips, with the net upward load being 457 kips of side shear resistance above the jack. The combined end bearing and side shear resistance below the jack was 482 kips. Table 3 summarizes the calculated unit side shear resistance above the jack along with the estimated unit shear for these layers from the geotechnical evaluation report and the ACIP pile contractor's preliminary designs.

Table 3. Summary of Unit Side Shear

	Unit Side Shear Resistance, ksf		
Elevation, feet	Geotechnical Evaluation	Contractor Design	Test Pile Result
901 – 876	0.15	0.80	0.6
876 – 848.5	0.40		0.7
848.5 – 821.5	0.70		0.6
821.5 – 801.5	0.96		2.4
801.5 – 792.7	3.78	4.28	---

The unit side shear resistance of the till below the jack is unknown as the strain gauge data became unreliable during the test. Similarly, the end bearing resistance is unknown because the telltale for the toe did not actually extend to the toe. In addition, the strain gauge below the jack had unusual results and the data was determined to be unreliable. Figures 2 and 3 show the bi-directional load-displacement and equivalent top load-displacement graphs from the test.

Based on the load test results, the net, ultimate resistance of the test pile was 939 kips. At an equivalent, top load of 400 kips, the pile top movement was less than 1/2 inch. As previously stated, the ACIP pile contractor's preliminary design required the pile to extend 6 feet into the till. The actual test pile embedment in the till was 7 feet. Even though the load test was not able to determine how much of the resistance below the jack was from side resistance and how much was from toe resistance, the total resistance below the jack was more than needed. Given the design, ultimate resistance of 800 kips and the available side resistance of 457 kips above the jack, only 343 kips of ultimate resistance was needed below the jack. Therefore, the ACIP pile contractor chose to reduce the design length of the production piles in the glacial till from 6 feet to 5 feet.

Thermal integrity wires were installed on 95 of 286 production piles installed for the Tower and 30 of the 84 production piles for the Parking Ramp. Of the 125 piles with thermal integrity wires, 10 piles had data for only a portion of the pile. These piles were accepted based on reviewing the automated and manual field logs compared with the log for the test pile and with other piles having thermal integrity data.

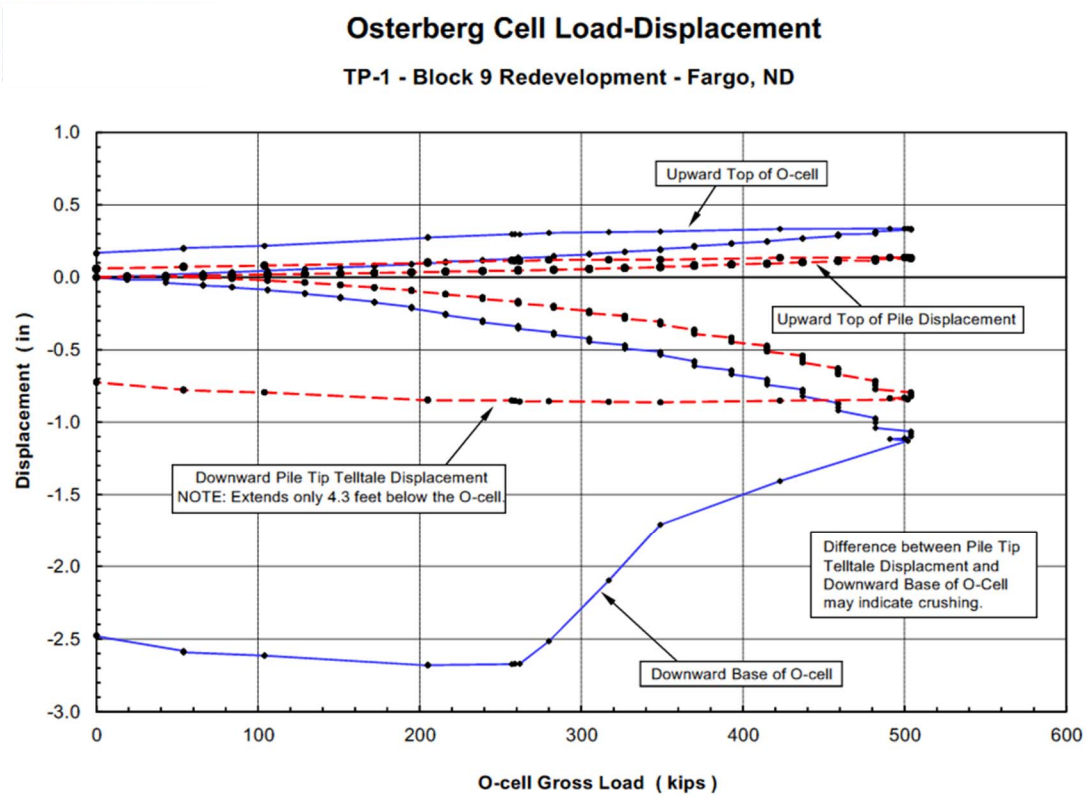


Fig. 2. Bi-directional load displacement graph

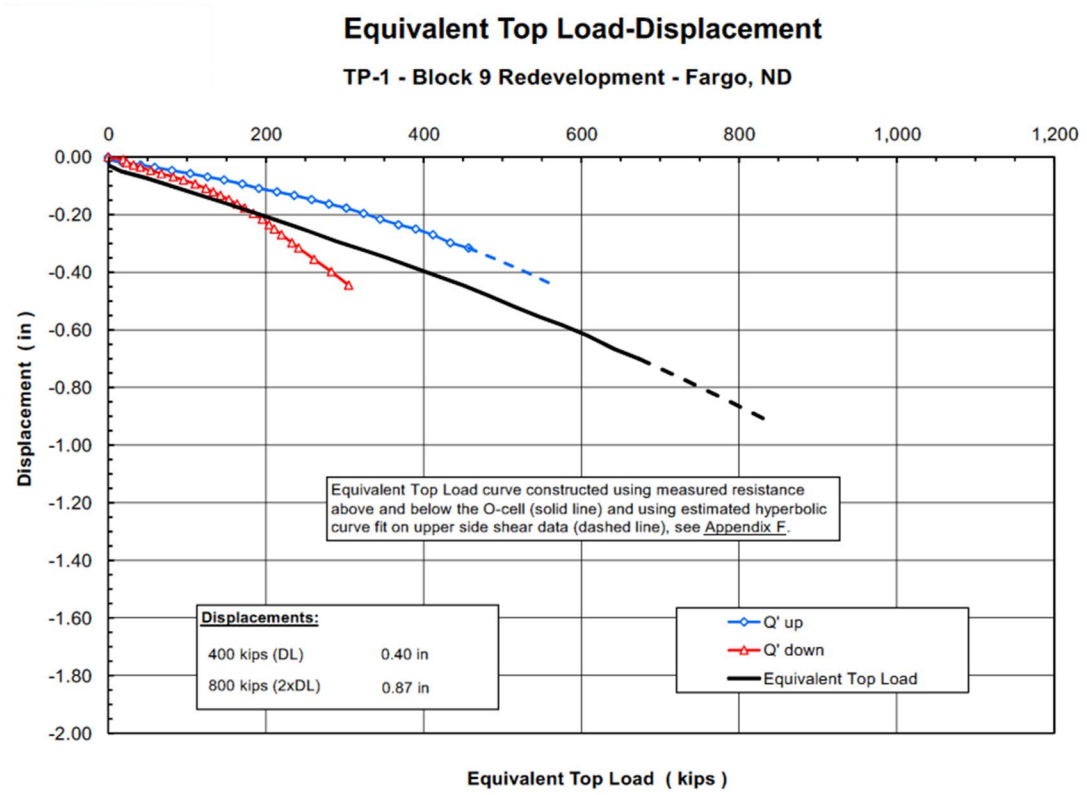


Fig. 3. Equivalent top load displacement graph

Thermal profiling of Piles 116 and 227 indicated potential anomalies consisting of diameters less than the design diameter for these piles. Figure 4 shows the temperature with depth profiles for Pile 116, with the potential anomaly, and Pile 115, which had a typical thermal profile.

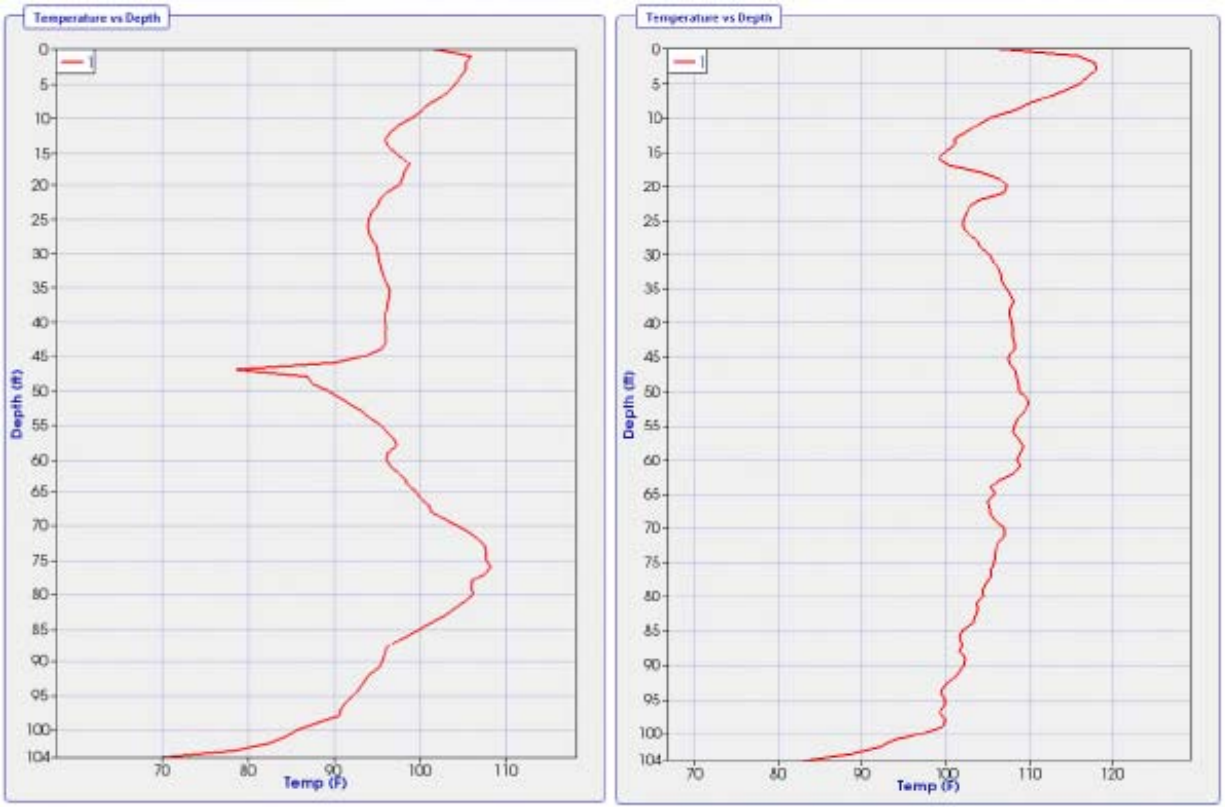


Fig. 4. Thermal integrity results for Pile 116 (left) and Pile 115 (right)

For Pile 116, the potential reduced-diameter was at a depth of about 47 feet below the top of the pile. Due to the potential anomaly being about 30 diameters below the pile top, the project team decided to perform pulse echo testing in an attempt to confirm the presence of an anomaly. Pulse-echo test results indicated a clear toe response at a depth of about 108 feet, as well as a decrease in impedance at a depth of about 50 feet below the pile top. Pulse-echo testing uses empirical correlations or known pile length to estimate the speed of a stress wave within the pile. For Pile 116, the installation records indicated the pile had a length of 108 feet. Knowing this length and the time from hammer impact to the toe response, the approximate wavespeed could be calculated. Due to the inherent inaccuracies of this method, it is generally assumed that length estimates with pulse-echo have an accuracy of about plus-or-minus 10 percent. Therefore, an impedance reduction at a depth of about 50 feet from pulse-echo testing and a reduced temperature around 47 feet from thermal profiling are at about the same depth. Based on these results, the ACIP pile contractor abandoned Pile 116 and installed an additional pile.

For Pile 227, thermal profiling indicated a zone of reduced temperature and possible anomaly between a depth of about 15 and 37 feet below the pile top. During grouting of this pile, the grout pump broke when the auger tip was at a depth of about 30 feet. There was a delay in grouting of about 1 hour. After a replacement grout pump was operational, the ACIP pile contractor redrilled to a depth of about 34 feet and resumed grouting and auger withdrawal. Ambient temperatures during construction of Pile 227 were between 30 and 40 degrees F, allowing significant heat loss for the grout that was in the hose lines and the portion of the auger that was above ground during the delay. The estimated grout volume subject to ambient

temperatures during the delay and the AME-indicated volume of grout placed between the depth of 15 and 37 feet were within 10 percent of each other. Therefore, the project team concluded that the zone of reduced temperature was the result of the delay in grouting and not a reduction in cross-sectional area of the pile or other anomaly and the pile was maintained as a production pile.

CONCLUSIONS

Twenty years ago, ACIP pile construction in the Red River Valley was seen as impractical and highly risky. Developments in drilling equipment, monitoring equipment, load testing, integrity evaluation and contracting methods have reached the point where ACIP piles are a viable, deep foundation system in this region. Driven pile may still be a less expensive option on projects. However, when construction vibrations are a concern, like they are with urban redevelopment, ACIP piles can be more attractive for cost and time than drilled shafts or large-diameter helical pile. The risk of using a relatively unknown foundation system can be offset by using the design-build contracting method, which allocates more risk to the contractor, who is likely better equipped to understand and control the risk. The risk can also be offset with increased integrity testing and by using instrumented load tests that allow the designer to understand where resistance is coming from. As a result of these advancements in contracting and technology, the Fargo area now has another option for deep foundation to use for development and/or redevelopment.

ACKNOWLEDGEMENTS

The authors appreciate the support and contributions of the project team working both on the project and with the development of this paper: Block 9, LLC; BC Contracting; Skidmore, Owings & Merrill, LLP; Collaborative Design Group, Inc.; McGough Construction; and Richard Goettle, Inc.

REFERENCES

Brown, D.A., Dapp, S.D., Thompson, W.R., and Lazarte, C.A., 2007. Geotechnical engineering circular no. 8 design and construction of continuous flight auger (cfa) piles. Federal Highway Administration, Washington, 228 p.

Hayes, J.A., 2012. The landmark osterberg cell test. Deep Foundations, November/December, pp. 45-49.

Kershaw, K.A., Fischer, G.R., Brand, J., Johnson, K.M., Yavarow, M.K., 2003. Augered cast-in-place pile installation grand forks north dakota. Proceedings of the 28th Annual Conference on Deep Foundations, Miami Beach, October 22-24, DFI, pp. 163-176.

Mullins, G., Johnson, K., Winters, D., 2007. Thermal integrity testing of drilled shafts. Florida Department of Transportation, Tallahassee, 214 p.

Mullins, G., 2010. Thermal integrity profiling of drilled shafts. DFI Journal, 4(2) 54-64.

NeSmith, W.M., 2006. A historical perspective on current cast-in-place piling practice. DFI's Augered Cast-In-Place Pile Committee Specialty Seminar: Augered Cast-In-Place Piles, Los Angeles, May 5, DFI, pp. 1-6.

Piscsalko, G., Cotton, D., 2011. Non-destructive testing methods for drilled shaft and acip piles. Proceedings of the 36th Annual Conference on Deep Foundations, Boston, October 18-21, DFI, pp. 525-532.

OVERCOMING CONSTRUCTABILITY CHALLENGES FOR DRILLED DISPLACEMENT PILE INSTALLATION IN DIFFICULT GEOLOGY

Yaser Taheri, P.E., Moretrench, Rockaway, New Jersey, USA, (973) 627-2100, ytaheri@moretrench.com
A. Rod Kern, Moretrench, Rockaway, New Jersey, USA, (973) 627-2100, rkern@moretrench.com
Michael A. McNicholas, P.E., Moretrench, Rockaway, New Jersey, USA, (973) 627-2100, mmcnicholas@moretrench.com

ABSTRACT

Deep foundations were required for construction of an 18,000 ft^2 (1,672 m^2) 4-story office building and an adjacent 23,750 ft^2 (2,206 m^2) 5-story parking garage in Queens, New York due to an existing uncontrolled fill layer ranging from 15-20 ft (4.6 - 6.1 m) in thickness beneath the building footprint. The geotechnical engineers for the project initially selected auger cast-in-place (ACIP) piles over driven piles to limit the impact of noise and vibrations on the surrounding neighborhood. Ultimately, drilled displacement piles (DDP) were installed since this method offered a more economical solution that would generate the required pile capacity with shorter drill depths and would also mitigate spoils volume. During installation of test piles by the geotechnical contractor retained for the foundation work, multiple unanticipated soil conditions were encountered that would adversely affect the constructability of the piles. The existing fill contained significantly more natural and manmade obstructions than expected and the underlying glacial soil became too dense to penetrate at shallower depths than anticipated. This paper discusses how these issues were overcome through pre-drilling and the use of detailed instrumented test pile data coupled with in-house engineering capability to proactively re-evaluate minimum pile lengths at any given location and keep the project on track.

Keywords: constructability, drilled displacement pile, augered cast in place piles, deep foundations, load testing, urban fill

INTRODUCTION

Geotechnical work in the New York City market presents soil conditions that can be highly variable and challenging due to the presence of uncontrolled urban fill placed over the native soils. Construction in this area can therefore pose many unforeseen challenges, even with detailed geotechnical analysis being performed at project sites. A case in point is a construction site in Queens, New York. The proposed site development consisted of construction of a 4-story office building with a footprint of 18,000 ft^2 (1672 m^2) and a stand-alone 5-level parking garage with a footprint of 23,750 ft^2 (2206 m^2), together with associated new pavements and utilities. The site is bordered by a mix of commercial buildings and residential properties on all sides.

Depth of the uncontrolled nature of the fill extended up to 20 ft (6.1 m) below street grade. Given the significant cost associated with removal and replacement, deep foundations were recommended to bypass the unsuitable soils and support the structures at depth where good bearing material existed.

GEOTECHNICAL CONDITIONS

According to the geotechnical report (Whitestone 2017), the existing geology indicated man-placed fill materials overlying marshland deposits consisting of organic soils. The organic soils are underlain by glacial deposits. Review of historic aerial photographs and maps indicate that the site formerly consisted of marshlands associated with the adjacent Mill Creek which flowed southwest and discharged into Flushing Bay. The original site elevation was raised approximately 15 to 20 ft (4.6 to 6.1 m) up to the

© 2019 Deep Foundations Institute

current elevation during the 1960s as part of an urban renewal program. The site was reported to be filled with miscellaneous construction debris, incinerator ash, cinders and scrap metal.

Eighteen borings were performed at the site by the project geotechnical engineer. The New York City Building Code defines seven classes of soil in correlation to the USCS soil classification system. All borings performed in the NYC area are classified according to the building code system and design considerations are based on these classifications accordingly. These borings indicated that soil of NYC Class 7 (existing fill materials) extended up to 15 to 20 ft (4.6 to 6.1 m) below ground surface. The existing fill consisted of silty sand with up to 50 percent debris. Beneath the fill, two of the borings encountered NYC Class 6 soil (organic deposits) extending 2 to 8 ft (0.6 to 2.4 m) below the fill material. The organic deposits were described as a fibrous peat with a soft/compressible consistency. NYC Class 2a, 3a and 3b soils (glacial deposits) were encountered underlying the fill or organics up to the maximum boring depth of 65 ft (19.8 m) below ground surface. The glacial deposits consisted of a mixture of sand, silt, clay and gravel that typically became denser with depth.

FOUNDATION RECOMMENDATIONS AND SELECTION

The initial geotechnical report (Whitestone 2016), available at the project budgetary stage, recommended driven closed-ended pipe piles installed to approximately 50 to 60 ft (15 to 18 m) below ground surface. It was noted that these driven piles would require predrilling through the existing fill layer to allow installation. The initial report also proposed auger cast-in-place (ACIP) piles as an alternate to driven piles, noting that they could be less expensive and would limit noise and vibrations.

Upon review of the project and initial geotechnical report, the eventual geotechnical contractor offered drilled displacement piles (DDPs) as another alternative. DDPs offered the same benefits as ACIP piles in that they would limit the noise and vibration concerns on the surrounding buildings and neighborhoods when compared to driven piles. In addition, the DDPs would present advantages over ACIP piles in that they would not be limited by the same concerns of bulging or necking and down drag in the soft organic layer. As a displacement rather than removal technique, DDPs would produce significantly less spoils, a major consideration on urban sites, and would allow for a higher pile capacity with a shorter pile length. Overall, installing DDPs would create a cleaner and therefore safer work environment and have less neighborhood impact..

Following additional soil sampling and analysis, the geotechnical engineer subsequently released an updated report (Whitestone 2017) that recommended the deep foundations to be either DDPs or closed-ended pipe piles. Ultimately, DDPs were selected.

DESIGN CONSIDERATIONS

The DDPs were designed in accordance with FHWA guidelines (FHWA GEC NO. 8) and the New York City Building Code (New York City Building Code 2014). The design of the building foundation called for the piles to be designed for three load components – axial compression, axial tension and lateral loading. Factored design compression loads ranged from 25 to 80 tons (22.6 to 72.6 tonnes), tension loads ranged from 15 to 50 tons (13.6 to 45.3 tonnes), and lateral loads ranged from 2 to 10 tons (1.8 to 9.1 tonnes). The geotechnical design for the axial compression and axial tension elements was based on the method described in FHWA GEC-8.

When accounting for the contribution from the side-shear resistance, the fill and organic layers are ignored in the design process so that the side-shear resistance and end bearing are assumed to come from the glacial soils. The axial compression and tension elements must also be designed for structural stability, accounting for the center bar reinforcement and grout in compression while the tension accounts

for only the reinforcement. Finally, the lateral load is designed for structural stability by checking combined stress and geotechnical support utilizing L Pile Software to determine lateral capacity based on p-y curves for soil strength and the bending stiffness of the pile, EI. The lateral load on the pile is designed assuming partial fixity of the pile head.

LOAD TESTING PROGRAM

The 2014 New York City Building Code has specific requirements for the quantity and types of load tests that are required. Given the combined footprints of the structures being between 30,000 ft^2 (2,788 m^2) and 50,000 ft^2 (4,645 $m^{2)}$, four different pile designs, and the moderately different subsurface conditions between the parking garage and office building locations, it was determined that three axial compression load tests would be appropriate for this project. Due to all of the lateral loads being greater than one ton (0.9 tonne), two lateral load tests were required for this project. Uplift load were designed with a factor of safety of three, satisfying the requirements of the building code. All load tests were performed using sacrificial test piles.

Axial Compression Load Tests

All three compression load tests were set up in the same manner. Each consisted of four reaction piles and one compression test pile. Two of the reaction piles would also be used as lateral load test piles. Figure 1 shows a typical compression test set-up. Compression tests were run following the ASTM D1143 – Quick Load Test Procedure. Each test pile was equipped with vibrating wire sister bar strain gauges attached to the center reinforcing bar as a means of monitoring load shedding during the load test. The strain gauge locations consisted of two gauges at the top, one or two gauges at the pile cutoff, one immediately above and below the top of the glacial soil, and one at the pile tip. See Fig. 2 below for typical test pile instrumentation details.



Fig, 1. Typical compression load test set-up

In addition to the strain gauges, the pile movements were monitored through dial gauges and piano wire on top of the pile while the load was monitored through a calibrated load cell between the jack and the reference beam. Upon completion of the quick load test procedure, the contractor opted to continue the

load tests, running a second cycle until pile failure was reached at each location. Taking each pile to failure provided the ultimate pile capacity. Using the ultimate pile capacity with a safety factor of two yielded the allowable pile capacity based on the load test results. Table 1 provides a summary of the axial compression load test results and how they relate to the design loads. It should be noted that the 60 ton test pile experienced significantly more deflection than the other two test piles. This is attributable to the 60 ton test pile experiencing a geotechnical failure while the other two piles experienced structural failures.

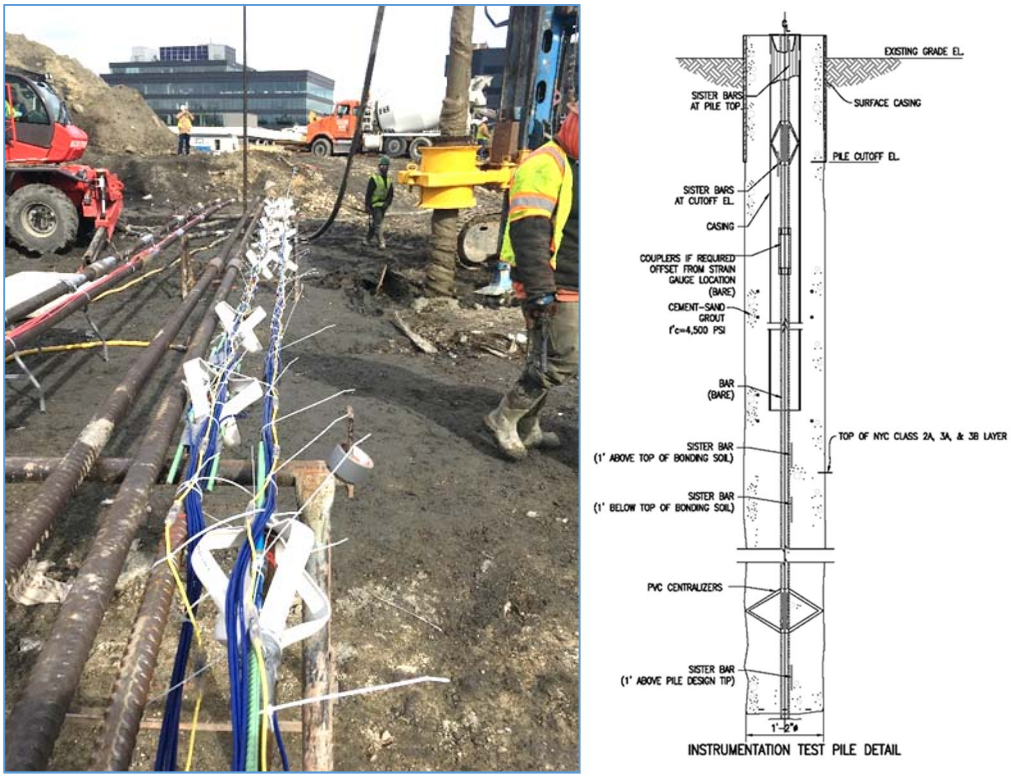


Fig. 2. Instrumented Bars (Left) and Instrumentation Test Pile Typical Detail (Right)

Table 1. Results and Analysis of Axial Compression Load Tests

Axial Compression Design Load (DL) (tons)	Site Location	Pile Length (ft)	Pile Test Load at 200% DL (tons)	Deflection at 200% DL (in)	Pile Test Load at Failure (% of DL)	Pile Test Load at Failure (tons)	Deflection at Failure (in)	Allowable Design Load (tons)	Additional Safety Factor Above Design
80	Parking Garage	25	160	0.231	370%	296	0.697	148	1.9
60	Office Building	32	120	0.411	430%	258	3.721	129	2.2
25	Office Building	35	50	0.070	740%	185	0.846	92.5	3.7

1 ton = 0.9 tonne
1 ft = 0.3 m

CONSTRUCTABILITY CHALLENGES

Two major constructability challenges were encountered at the beginning of the drilling process: excessive obstructions in the upper fill and impenetrable glacial soils at shallower depth than anticipated.

These two issues would have extremely detrimental effects to the start of this project and could have significantly impacted the schedule if they were not handled efficiently.

Drilling for installation of the first group of load test piles was at much slower rates than typical for DDPs and caused the starter drill bits to wear out. Replacement was required after the complete installation of one or two piles (Fig. 3). In addition, all five piles hit penetration refusal before their target tip elevation. Penetration refusal is commonly defined as a rate of auger penetration of less than 1 ft (300 mm) per minute of drilling. The four reaction piles were to be installed to El -25 ft (-7.6 m). The test pile was to be installed to El -15 ft (-4.5 m). The four reaction piles encountered refusal between approximately El -19 ft (-5.8 m) and El -22 ft (-6.7 m) while the reaction pile reached refusal at approximately El -13.5 (-4.1 m).



Fig. 3. Photo of New Starter Bits (Left) and Worn Out Starter Bit (Right)

Following completion of the parking garage test piles, the drilling operation was moved to the office building area and attempts were made to install another five piles. Obstructions were encountered at shallower depth at the second load test area. As a result, test piles were not able to be installed. The drill rig was then moved over to the next load test location. Similar ground conditions were also encountered there which resulted in no pile installation. The site work contractor dug a test pit to the depth where piles hit refusal and a layer of large boulders was encountered. Additional excavation at the parking garage test piles showed significant amounts of various obstructions including wood, boulders and miscellaneous steel (Fig. 4). It became obvious that continuing with the same installation system was not feasible and that solutions would have to be explored to keep the project on track.



Fig. 4. Various obstructions encountered

Overcoming Excessive Natural and Man-Made Obstructions in Uncontrolled Fill

Typically if obstructions are encountered within 10 ft (3 m) of the surface, they are dug out, and the hole backfilled. When an obstruction is encountered at a drill depth greater than 10 ft (3 m), the drill tool is extracted and the drill hole is grouted. If directed by the Engineer, the reinforcing steel is installed within the shortened pile that will now have less capacity. In these situations, a supplemental pile is required. Given the severe obstructions encountered during the test pile installation for this project, it was clear that an aggressive predrilling method had to be utilized prior to production DDP installation to overcome this.

The geotechnical contractor selected rotary-percussion duplex drilling method with internal air flush to overcome the obstructions (Fig. 5). With this method, the casing and drill rod are advanced simultaneously through the fill layer. The drill fluid and soil cuttings are returned to the surface through the annulus between the casing and drill rod. The inner drill rod is equipped with an air powered down-the-hole-hammer with an overburden bit, while the casing has continuous J-Teeth to facilitate drilling. The overburden bit cuts a slightly larger hole than the outer diameter of the casing, allowing it to advance down the hole uninterrupted. Any rough material that remains is cut through by the continuous carbide j-teeth on the casing. In this particular instance, a 1.75-in. (323 mm) outer diameter casing was selected since the overburden bit would cut an approximately 13-in. (330 mm) hole and would be drilled to a depth of approximately 20 ft (6.1 m) through the fill layer. This would break up and clear most of the obstructions, allowing the 14-in. (355-mm) displacement bit to pass through the fill and drill into the native soils.

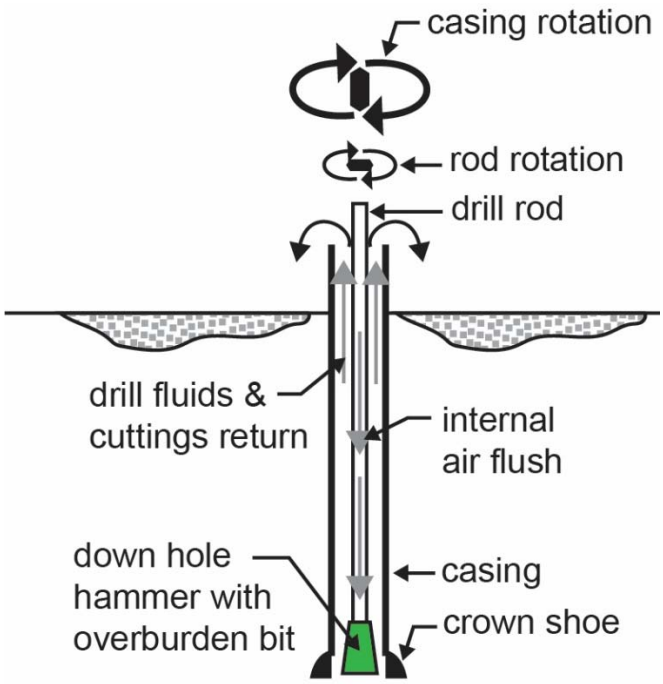


Fig. 5. Schematic of Rotary Percussive Duplex Drilling Method

It was determined based on the highly variable nature of the fill that all of the piles for the project would require predrilling. Once predrilling began with the rotary percussion drilling method none of the piles had to be relocated due to refusal in the existing fill. There was no clear way to determine which locations would encounter obstructions since piles drilled a few feet apart were observed to have significantly

different drilling conditions. It was also cost prohibitive and would negatively impact the schedule to attempt to drill the holes with the displacement auger and then only predrill the ones where obstructions were encountered. Once an obstruction was encountered, it would often immediately render the starter bit unusable, adding time to change the auger and cost to have it rebuilt. Taking a reactive approach would also impact the sequencing which if not properly maintained could add days on to the end of the project.

Having to employ this aggressive pre-drilling technique introduced a new set of issues since it compounded the already difficult sequencing scenario. The initial DDP set-up consisted of a drill rig and grout pump connected by 2-in. (50 mm) grout hose, with a concrete truck feeding the pump. The process also requires a rotating telehandler to set the reinforcing bar and casing. This pre-drilling method added another drill rig along with a large air compressor that would be connected by 2-in. (50 mm) air hose. Due to the close spacing of the piles in the caps, both of these operations would have to traverse the majority of the site each day. This required careful daily planning to ensure that materials were placed appropriately around the site and the predrilling operation would stay ahead of and out of the way of the DDP operation in order to keep the jobsite safe, avoid equipment damage, and keep production on schedule. Figure 6 shows a photo of the site with the entire pre-drilling and DDP operations under way.

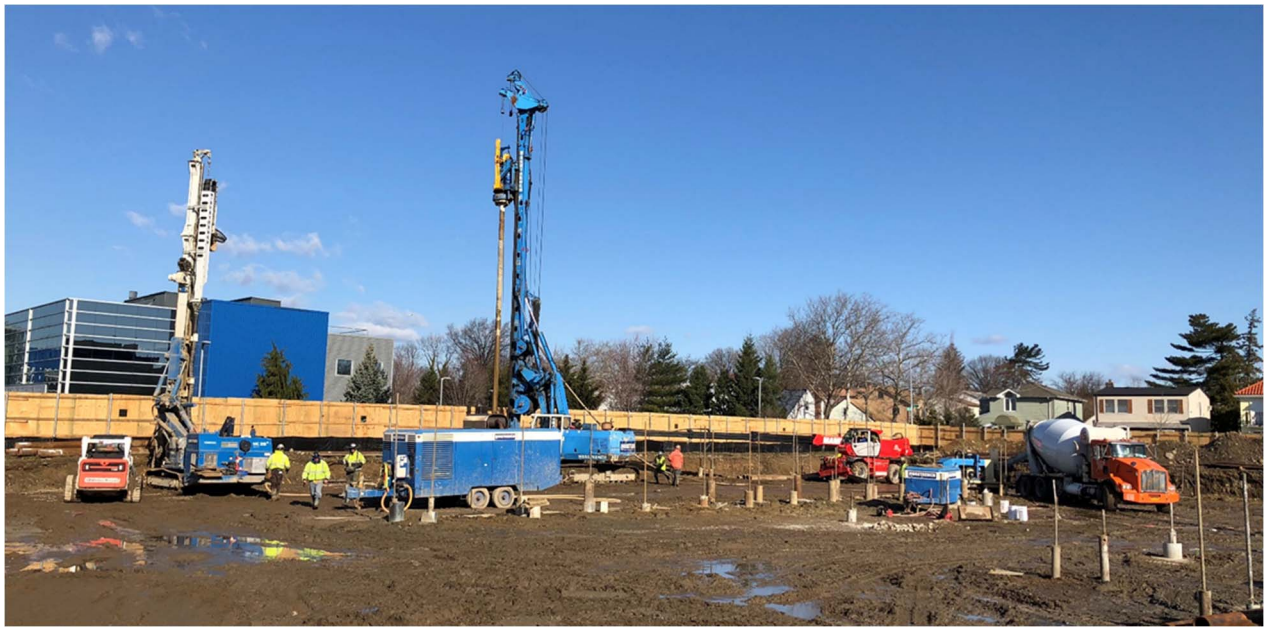
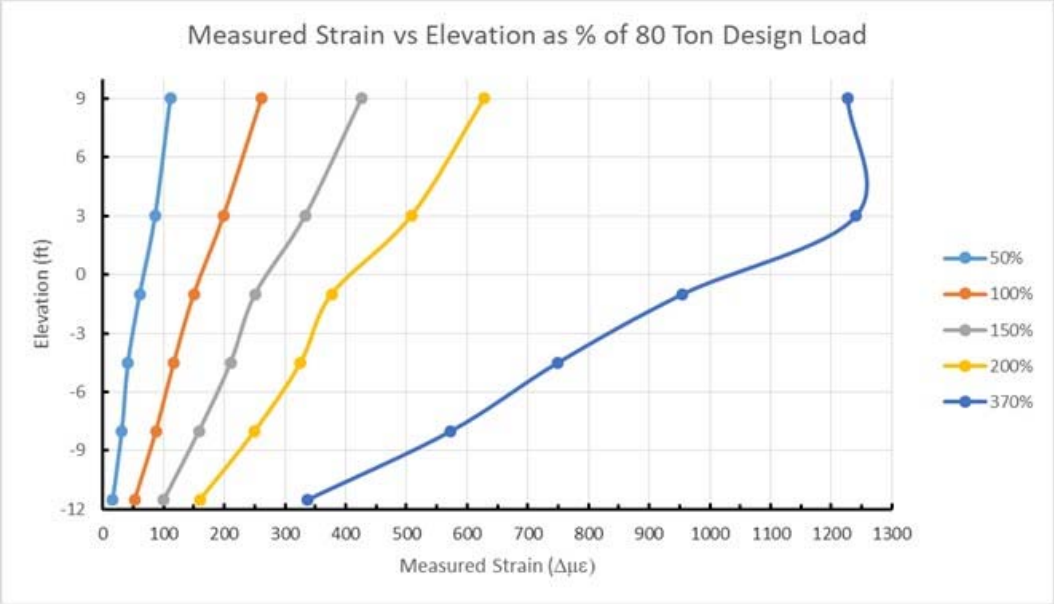


Fig. 6. After predrilling operation started, a once wide-open site became congested due to the multiple operations occurring and the closing in of space as piles are installed.

Overcoming Penetration Refusal Above Designed Tip Elevation

During the testing program phase, it was noted that six of the 15 piles installed for load testing purposes encountered penetration refusal at a higher elevation than anticipated based on the soil boring information. Once production piling in the parking garage started, it became a significant concern as nearly a third of the piles installed during the first week of production hit penetration refusal above their design tip elevation but below the fill layer. It was believed that this penetration refusal condition was a result of native denser glacial soils occurring at higher elevations than anticipated. To prevent any negative impact to the schedule and avoid adding cost by adding more piles, the geotechnical contractor's in-house engineering team expeditiously analyzed the results from the load tests to determine an acceptable solution.

Testing the piles to failure allowed an evaluation of the original calculated side-shear resistance and end bearing in comparison to the ultimate side-shear resistance and end bearing. The preliminary calculation where calibrated to conservatively reflect the ultimate side shear and end bearing values. The strain gauges data further assisted the engineering group to incrementally distinguish the load dissipation on a side-shear per foot basis in the glacial soil. The remaining load below the lowest strain gauge allowed for accurate interpretation of the ultimate end bearing. Fig. 7 shows the relationship of delta strain with depth observed from the strain gauges for one of the test piles. All three compression load test showed the same trends for the relationship between delta strain and depth. The 80 ton pile was chosen as a representative of all three tests.



1 ton = 0.9 tonne
1 ft = 0.3 m

Fig. 7. Relationship of delta strain vs depth for load on 80-ton (72.6-tonne) office building load test showing dissipation of load as pile depth increases.

The contractor's engineering group, together with the owner's engineer, arrived at a solution that piles could be considered acceptable above the design tip elevation. The guidelines set for the parking garage were that any pile reaching a minimum tip elevation of -8 ft (-2.4 m) would be deemed acceptable.

Encountering this issue in the production piles for the parking garage also encouraged a proactive approach to the office building piles. In the office building, it was determined that the 60-ton (54.4 tonne) piles would be acceptable at a minimum tip elevation of -10 ft (-3 m). The 25-ton (22.6 tonne) piles would be acceptable any time El-10 (-3 m) was reached or a minimum of 2 ft (0.6 m) embedment into the native glacial soils below the fill or organics was achieved, as determined based on the nearest boring.

The quick turnaround by the group regarding the solution allowed for the field team to determine if each pile would be acceptable as it was drilled. Due to the nature and timing of the solution, there was no down-time caused by this issue and the field team was able to keep the project moving on schedule.

SUMMARY AND RECOMMENDATIONS

Encountering NYC Class 7 fill is typical of nearly every project in the NYC area. Characterizing exactly what the fill contains across the entire site is impossible due to the extremely variable nature of this material and the relatively small amount of the surface area of a jobsite that is actually penetrated during a subsurface investigation (18 drill holes approximately 3 in. (76 mm) in diameter out of an over 40,000 ft^2 (93716 m^2) surface area).–The geotechnical report for this project indicated that there was miscellaneous debris and some locations where blows were greater than 50/6-in. or refusal was encountered. However this was the exception and is common with urban fill. Having experience working in similar subsurface conditions and a competent in-house design team allowed the geotechnical contractor to be proactive and find quick solutions to the constructability challenges that arose due to the unanticipated soil conditions.

It is the authors' considered opinion that it is always better to gain as much information as possible about the soil conditions on a specific site. The running of load tests to pile failure on piles that were thoroughly instrumented provided the tools and information necessary to redesign piles based on the observed subsurface conditions. Running a load test to failure to gain as much insight as possible is recommended even if not required. The geotechnical contractor's past experience in this market and with DDP technology allowed for a proactive response to the fill issues. It was determined that aggressive predrilling was the most feasible, cost-effective and schedule-minded option available. The operation was able to be mobilized to the site within days of encountering the issue and ultimately, the project was completed within a week of the anticipated schedule. This would not have been possible without cooperation and understanding between all parties involved.

REFERENCES

Brown, D. A., Dapp, S. D., Thompson, W. R. III., and Lazarte, C. A. (2007). "Geotechnical Engineering Circular No. 8: Design and Construction of Continuous Flight Auger (CFA) Piles." *Federal Highway Administration*

New York City Building Code. (2014) International Code Council

Whitestone Associates, Inc. (2016) "Report of Preliminary Geotechnical Investigation: Proposed Jetro/Restaurant Depot Corporate Headquarters."

Whitestone Associates, Inc. (2017) "Updated Report of Supplemental Geotechnical Investigation: Proposed Jetro/Restaurant Depot Corporate Headquarters."

URBAN HIGH CAPACITY DEEP FOUNDATION SOLUTIONS IN SITES WITH COMPLEX HISTORY AND GEOLOGY

Gisele R. Passalacqua, AECOM, New York, NY, USA, 1-212-377-8648, gisele.passalacqua@aecom.com
Joanna Smith, AECOM, New York, NY, USA, 1-212-377-8646, joanna.smith@aecom.com
Karen C. Armfield, AECOM, New York, NY, USA, 1-212-377-8652, karen.armfield@aecom.com

ABSTRACT

New York City is an urban environment with a history spanning over 200 years. The coastline of New York has changed over the years. In the East River, old bulkhead and remnant of relieving platforms together with variable bedrock elevations pose challenges in the design and construction of deep foundations. This paper presents a Case History of high capacity deep foundations along the Franklin D. Roosevelt (FDR) Drive on the Upper East Side in New York City. The project consists of a ramp that overpasses the FDR Drive allowing heavy trucks to access the Marine Transfer Station (MTS) facility built over the East River. Large diameter drilled shafts and mini-piles socketed to bedrock were designed and constructed. Remnant of old bulkhead was encountered at the site and a Ground Penetrating Radar (GPR) investigation was completed during the subsurface investigation phase of the design. This paper discusses details of the subsurface investigation program and design methodology of the high capacity drilled shafts and mini-piles. It also describes construction methods and results of Osterberg Load tests documenting the field values of skin friction through the rock socket. Other construction challenges include construction and drilling rock sockets for drilled shafts over sloping bedrock.

Keywords: deep foundation, drilled shafts, minipiles, design, construction, challenges, case history

1. INTRODUCTION

New York City is a renowned urban city that always calls for the most delicate, yet complex, and robust superstructures and most importantly substructure designs. The historic preservation of this large 200 years old city of 319 square miles is ever changing. Shorelines are often extended to accommodate new infrastructure and very often many miscellaneous structures are discovered below the ground surface. The East 91st Street Ramp was constructed to provide access to the East 91st Street Marine Transfer Station over FDR Drive and York Avenue. Another alternative ramp will be relocated to the South Bound (SD) of the FDR Drive at 92nd Street. A subsurface exploration program was completed in accordance with the New York City Department of Design and Construction (NYCDDC) general requirements, Section 4.5, to perform subsurface investigation along the FDR Drive in Manhattan, New York.

1.1 Subsurface Investigation

This section presents subsurface investigation program for the alternative ramp starting at 92nd Street. Subsurface investigations included eight (8) borings with Standard Penetration Test (SPT) sampling, one (1) rock core per boring, one (1) test pit, three (3) pavement cores and two (2) observation wells. The following laboratory tests were performed to evaluate soil and rock samples: three (3) grain size test per boring (ASTM D6913), one (1) Atterberg limit test (ASTM 4318), and one (1) rock core compressive strength test per boring (ASTM D7012). Borings B1 to B8 consisted of fill ranging from 4 to 33 feet below ground surface (BGS), followed by sand to a depth of 40 feet BGS. Silt and clay were encountered in borings B1 and B6, with an average thickness of 5 feet. Gravel was encountered within borings B2 and B3. Within boring B2, gravel was encountered from 12 to 20 feet BGS and in boring B3, gravel was encountered from 14.5 to 18.5 feet. Decomposed rock was encountered within borings B1 and B7. Within boring B1, decomposed rock was encountered from 20 to 25 feet BGS and in boring B7, decomposed rock was encountered from 35 to 40 feet BGS. Bedrock was encountered between 20 and 30 feet BGS.

© 2019 Deep Foundations Institute

Bedrock consists of mica schist and RQD range from 40% to 95%. See Figures 1 and 2 for the boring layout plan (BLP).

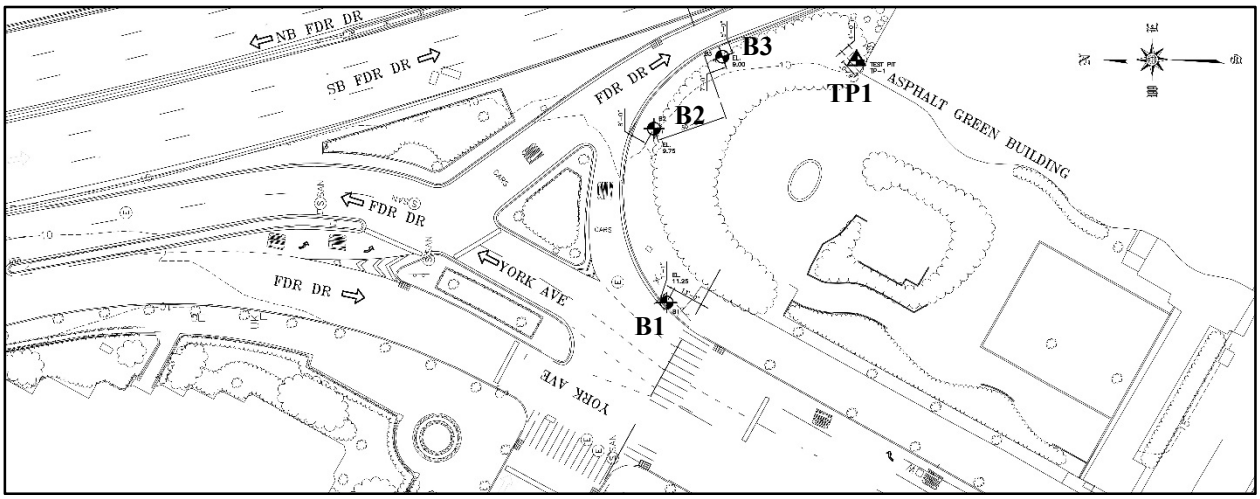


Figure 1. BLP of borings B1 to B3 and TP1 for the East 92nd Street ramp over FDR drive.

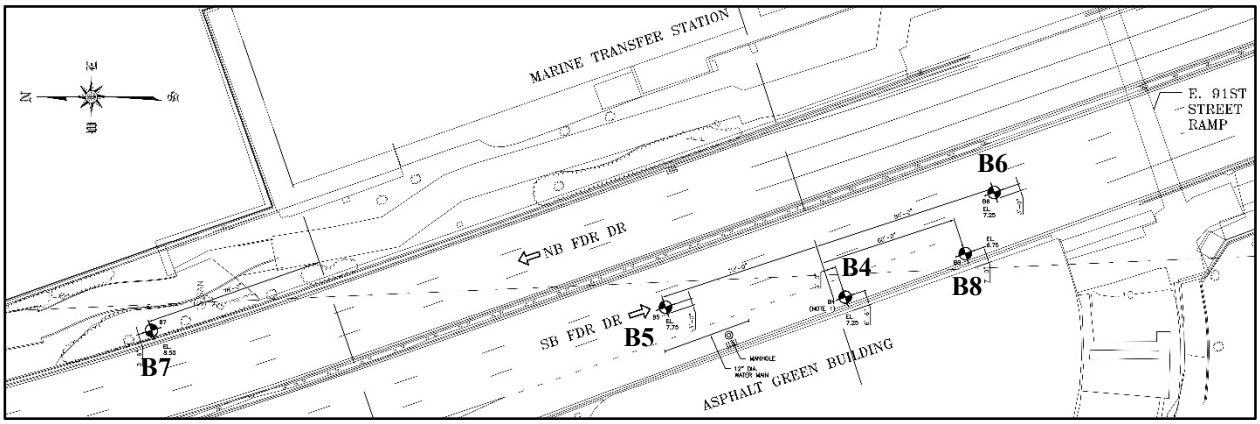


Figure 2. BLP of borings B4 to B8 for the East 92nd Street ramp over FDR drive.

During the subsurface investigation, an obstruction was encountered near boring B4 at the south bound of the FDR drive. Boring B4 had to be relocated. Further investigation was performed using Ground Penetrating Radar (GPR) technology which was able to detect possible utilities and a possible bulkhead. The bulkhead existence was then confirmed with a historical map showing its location. See the GPR survey layout plan in Figure 3 and the historical map showing the bulkhead in Figure 4.

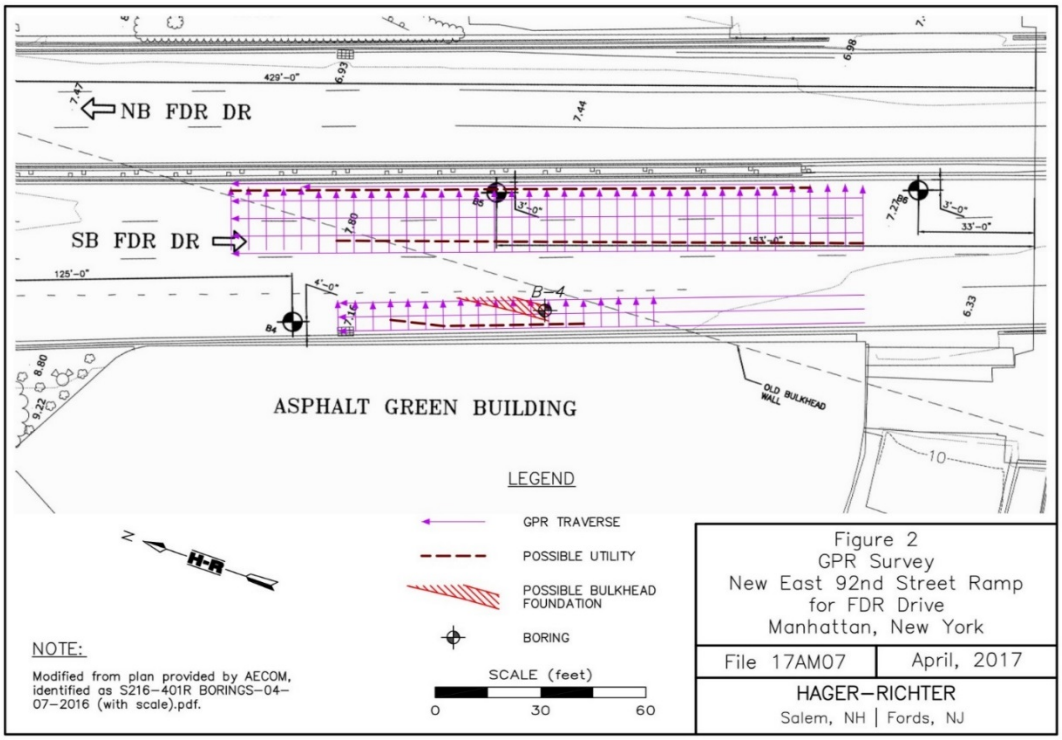


Figure 3. GPR survey layout plan for the East 92nd Street ramp over FDR drive, near B-4.

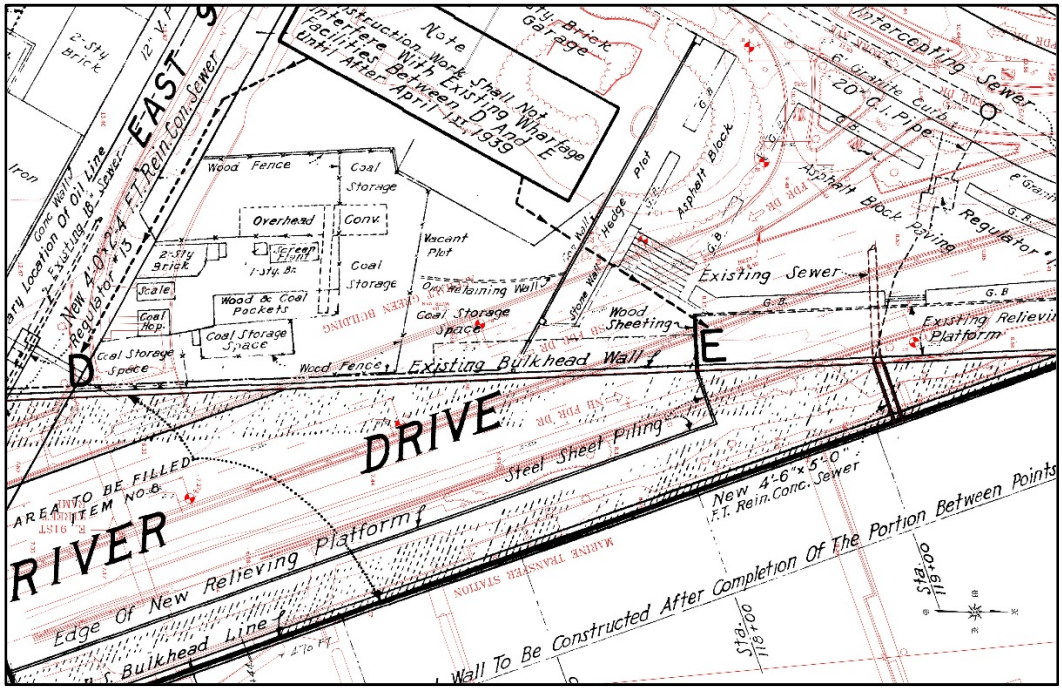


Figure 4. Historical map showing location of existing bulkhead wall near B-4.

The water table varies between 6 and 18 feet throughout the eight borings and two observation wells. The test pit was excavated to 12 feet BGS, approximately (4 x 8 x 12 feet). The water table was encountered approximately 12 feet BGS within the test pit. The soil encountered was fine-medium-coarse sand fill, with a trace of wood fragments and debris. The test pit was performed to investigate the foundation

condition of adjacent buildings. The test pit confirmed that foundation of adjacent buildings does not interferer with proposed foundation of the new ramp.

The general condition of the soil encountered was loose to medium dense silty soil. The fill layer was composed of mud, wood fragments, and debris. Borings B5, B6, B7, and B8 consisted of a loose layer of sand ranging from 4 to 24 feet BGS. A 5-foot layer of clay and silt was encountered 8 to 14.5 feet and 38.5 to 42.5 feet BGS. The rock was encountered between 20 and 42.5 feet BGS. A hydrocarbon odor was described within B5, B6 and B7. The groundwater table within borings B1 and B7 was 9 feet and 6 feet BGS, respectively. The top layer of pavement cores within B5, B6 and B8 consisted of 3 to 4 inches thick asphalt. The underlaid layer at B6 and B8 consisted of 18 inches thick concrete or rubble, while in B5 the asphalt was underlaid by 117 inches thick concrete.

2. FOUNDATION DESIGN

Drilled foundations such as minipiles and drilled shafts were both appropriate for this project. The presence of obstruction, man-made fill and close proximity to existing structures discredit driven piles as a suitable solution. The relatively shallow depth of rock required both drilled minipiles and drilled shafts to have rock socket. Drilled shafts have much higher resistance to lateral loads and bearing capacity in comparison to minipiles due to its larger size and lateral area. Foundations placed over water are subjected to higher lateral load and moments because of its unsupported length above the mudline. Therefore, drilled shafts were recommended for the foundation over water, and minipiles were used for the land portion of the ramp. For both drilled shafts and minipiles, permanent steel casing was placed until top of competent rock. This provides a stable drilling hole and prevents soils from collapsing into the drilled holes. In some cases, the casing length extended 1 foot into the bond zone (plunge length) to transfer the design load to the rock by the cased portion of the pile. Rock sockets were drilled utilizing a down-hole hammer until the required tip elevation was obtained. Vibration and noise monitoring were conducted during the foundation installation to measure the level of vibration and noise and ensure both meet contract requirements. The bedrock at the project site is the Manhattan schist and provides good bearing material for the foundation. For drilled shafts, both skin friction and end bearing of the rock socket were utilized to determine axial shaft capacity. For minipiles, only skin friction of the rock socket was utilized to determine axial capacity. An interesting aspect of the design is that the New York City Building Code recommends an allowable skin friction of 200 psi for rock. In the design, results of the field investigation and laboratory tests performed on the rock were utilized to determine rock design parameters. This includes the rock recovery ratio, rock quality designation ratio, and unconfined compressive strength. The results indicated that rock can be classified as Class 1.b according to New York City Building Code. Ultimate unit end bearing is 160 ksf as recommended. Considering a rock socket length of 10 feet and potential presence of weathered rock at the top 3 to 5 feet, an average ultimate skin friction of 28.8ksf (200psi) was assumed for the rock socket.

A different alternative to access the Marine Transfer Station was investigated. One option was accessing the MTS through 92nd Street. The proposed foundation for the 92nd Street ramp was located within the FDR median. Five (5) layout alternatives were initially studied for the 92nd Street ramp layout during the schematic design phase. For each layout alternative, two (2) different types of foundations were designed and evaluated: drilled shaft and minipiles. Large diameter shafts would limit potential contractors from bidding on work and would not be suitable for work within FDR drive enclosures. Generally, minipiles are preferred in urban areas where difficult access or limited headroom precludes the use of other deep foundations and where subsurface conditions (debris fill, cobbles, etc.) could hinder installation of driven piles or drilled shafts. Driven piles were not taken into consideration primarily due to the close proximity of a building near to the project area, where one (1) test pit was performed to investigate existing foundation of the building. Driven piles would create a potential for settlement, as a result of vibration during pile driving. The project is located in a premium residential area of New York City, the Upper East

Side, and the residents also played an integral role in minimizing noise and vibration during construction. Therefore, minipiles was the most practical foundation selected for the onshore aspect of this project. The final land design for the 92nd Street ramp included (see Figure 5):

- Five (5) foundation structures with a group of four (4) minipiles each
- Seven (7) foundation structures with a group of six (6) minipiles each
- Foundation structure including two (2) retaining walls and one (1) abutment, with a total of twenty-two (22) minipiles

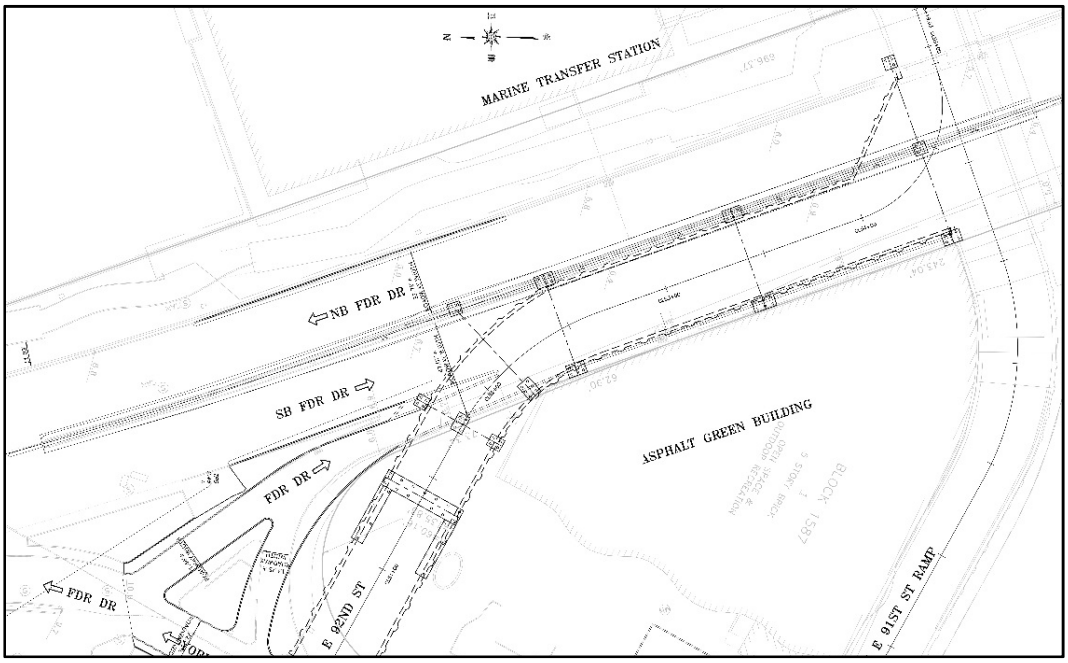


Figure 5. Foundation layout for the 92nd Street ramp.

3. INSTRUMENTATION AND LOAD TESTING

The overwater ramp foundation consisted of 36-inch diameter cased drilled shaft with a 30-inch diameter rock socket. In order to ascertain the load carrying ability of these foundation elements, a production shaft was fitted with an Osterberg Load Cell. This method of testing was chosen mainly due to the over water location which makes it difficult to perform a traditional load test. A test shaft (PT-6) was selected to be load tested (see Figure 6).

This nominal 30-inch diameter shaft was drilled to elevation -37.88 feet. Casing through the overburden soils consisted of a 36-inch diameter casing inserted with the use of a twister bar. The 10-foot rock socket was completed with a down-hole hammer. Airlifting was used to clean the hole upon drilling completion. Once approved, the rebar cage was inserted. A seating layer of concrete was pumped beneath the O-cell and the remainder of the concrete was delivered by pump through a 6-inch tremie pipe. Bedrock at the site was composed of mica gneiss bedrock and the rock socket was 10 feet into bedrock (tip el. -37.88ft MLW). The design intent was for the rock socket to carry the axial load. Therefore, the strain gauges were spaced within the socket at approximately 1.5 +/- foot intervals for use in the Osterberg Load Test analysis. The single 16-inch diameter O-cell test assembly was placed 0.96 feet above the base of the shaft and the general configuration can be viewed in the Figure 7 below.

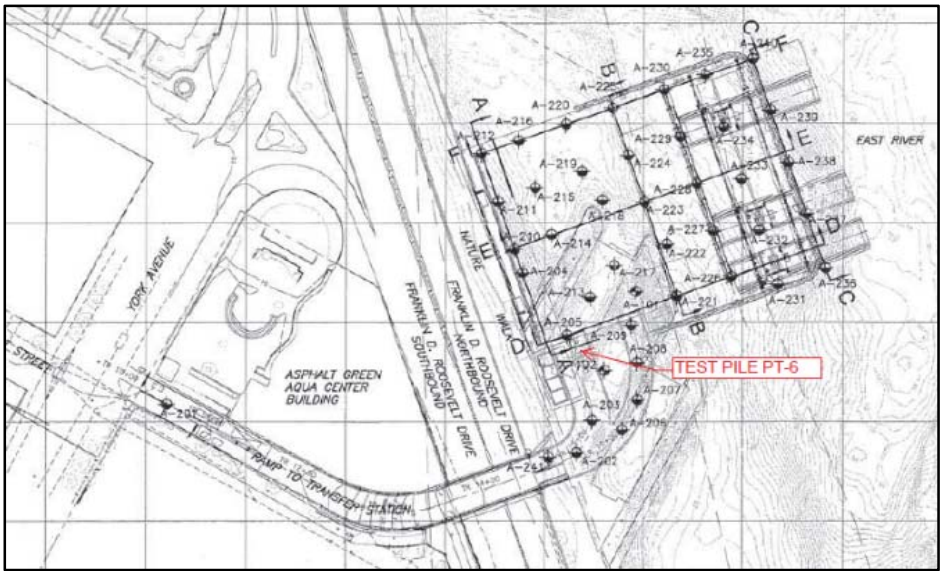


Figure 6. Location of test shaft PT-6.

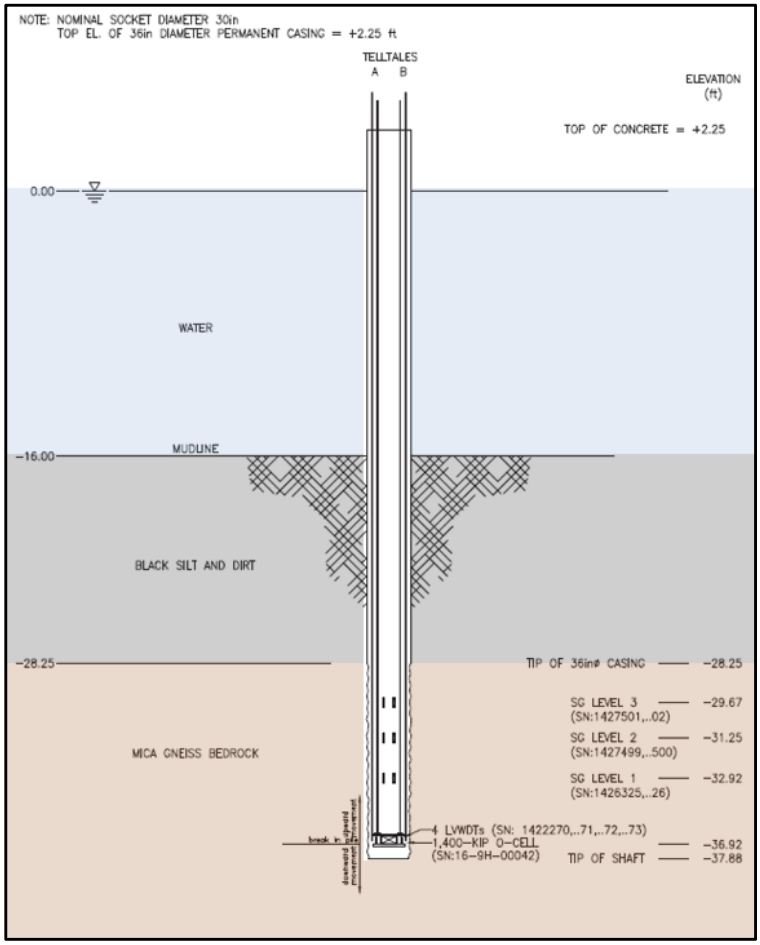


Figure 7. Schematic section of test shaft PT-6.

The instrumentation for the load test consisted of the following combination: three (2) levels of two (2) sister bar vibrating wire strain gages in the socket (Geokon Model 4911 Series) used to measure strain

along the socket; four (4) linear vibrating wire displacement transducers (LVWDT) positioned between the upper and lower load cell plates used to measure the expansion of the O-cell assembly; and paired ½" upper telltale casings to measure compression displacement. All instruments were assembled around the rebar cage. There was also a cable bundle, hydraulic hoses and a vent pipe for post-test grouting added to facilitate the testing. The pressure at each interval was measured using both a Bourdon pressure gage and a vibrating wire pressure transducer. The configuration of instruments can be viewed in Figure 8.

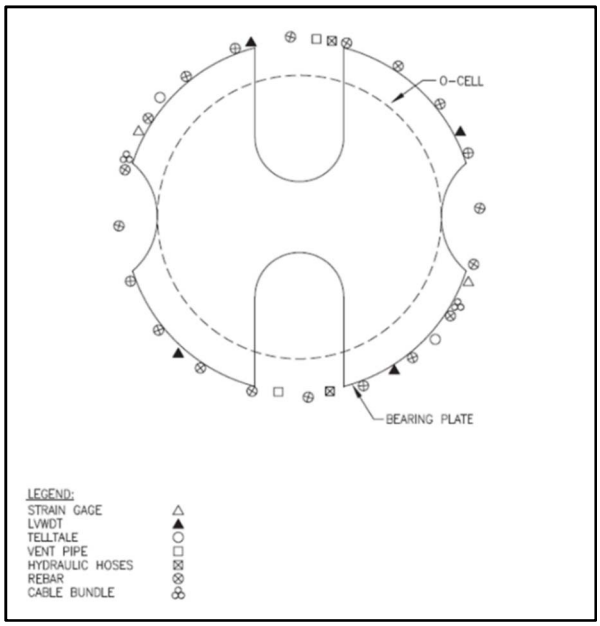


Figure 8. Instrumentation layout.

The test was performed on October 28, 2014 on test shaft PT-6. The maximum sustained bi-directional load applied to the shaft was 907 kips. The load increments were applied using the Quick Load Test Method for Individual Piles (ASTM D1143 Standard Test Method for Piles Under Static Axial Load). All instrumentation was attached to a data logger for compilation of the results. Each successive load increment was held constant for eight minutes by manually adjusting the O-cell pressure. Approximately one minute was used to move between increments. The data logger automatically recorded the instrument readings every 30 seconds, but herein only the 1, 2, 4 and 8-minute readings during each increment of maintained load are reported. At the maximum load, the displacements above and below the O-cell assembly was 0.093 inches and 0.127 inches, respectively.

One benefit of an O-cell test is the ability to independently test the end bearing and frictional resistance of the shaft. In this case, in evaluation of the upper side shear resistance, a maximum upward net load of 878 kips was applied which corresponds to the 0.093-inch displacement. The analysis determines the net unit side shear at each increment between strain gages. Please see Table 1 for average net unit side shear values. Figures 9 to 14 depict the Osterberg O-cell test results.

Table 1. Average Net Unit Side Shear Values.

Load Transfer Zone	Displacement[1]	Net Unit Side Shear[2]
Zero Shear to Strain Gage Level 3	↑ 0.08 in	0.9 ksf
Strain Gage Level 3 to Strain Gage Level 2	↑ 0.09 in	8.7 ksf
Strain Gage Level 2 to Strain Gage Level 1	↑ 0.09 in	14.7 ksf
Strain Gage Level 1 to O-cell	↑ 0.09 in	15.3 ksf

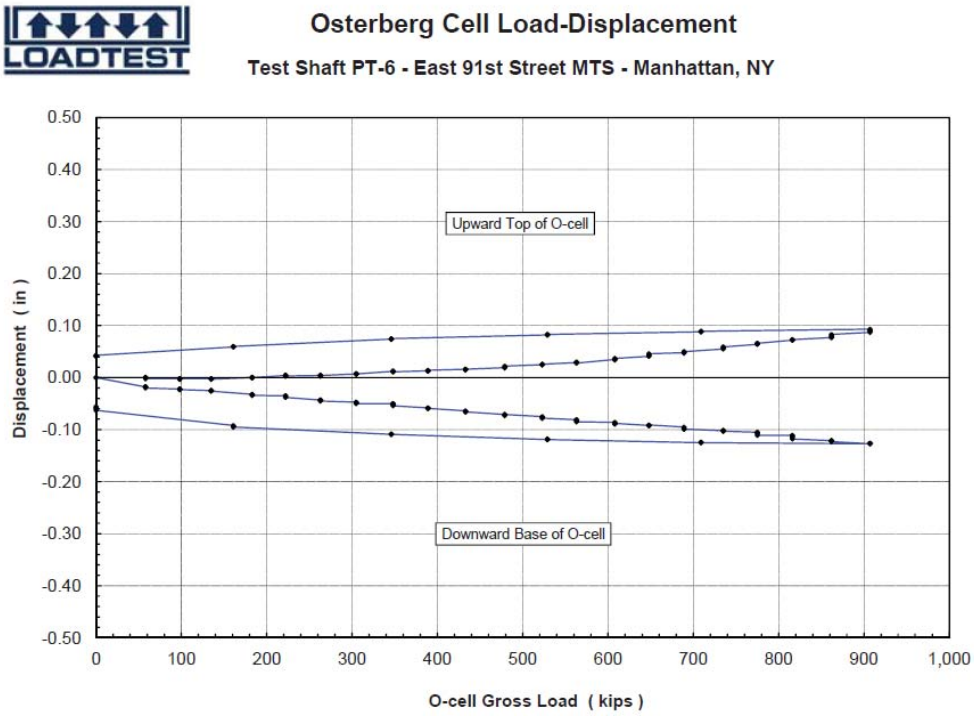


Figure 9. Osterberg Cell Load-Displacement Test Shaft PT-6.

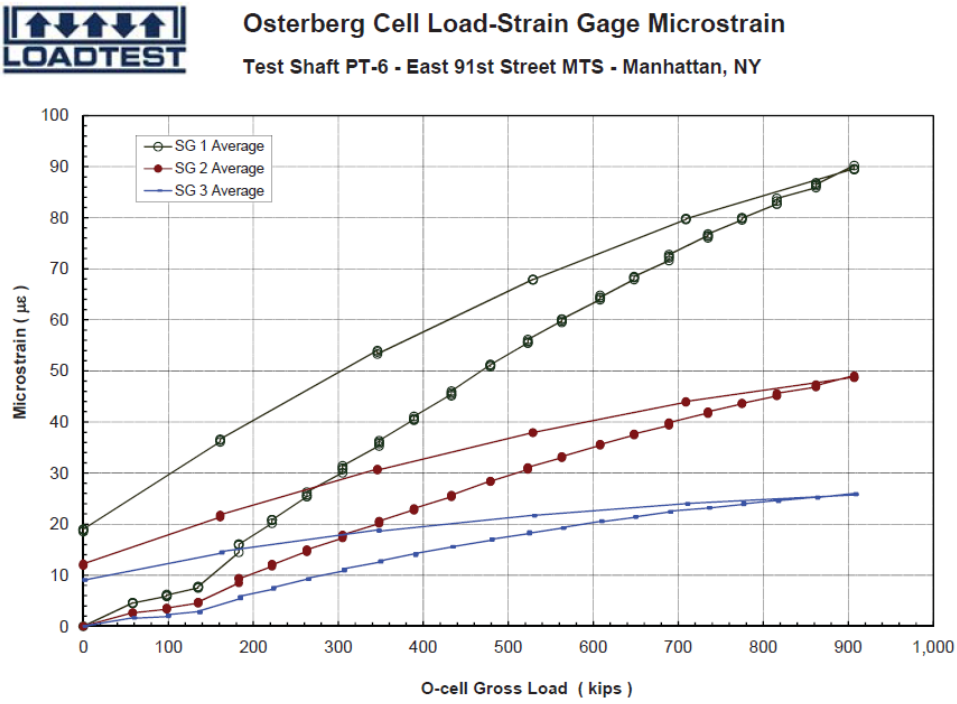


Figure 10. Osterberg Cell Load Strain Gage Microstrain Test Shaft PT-6.

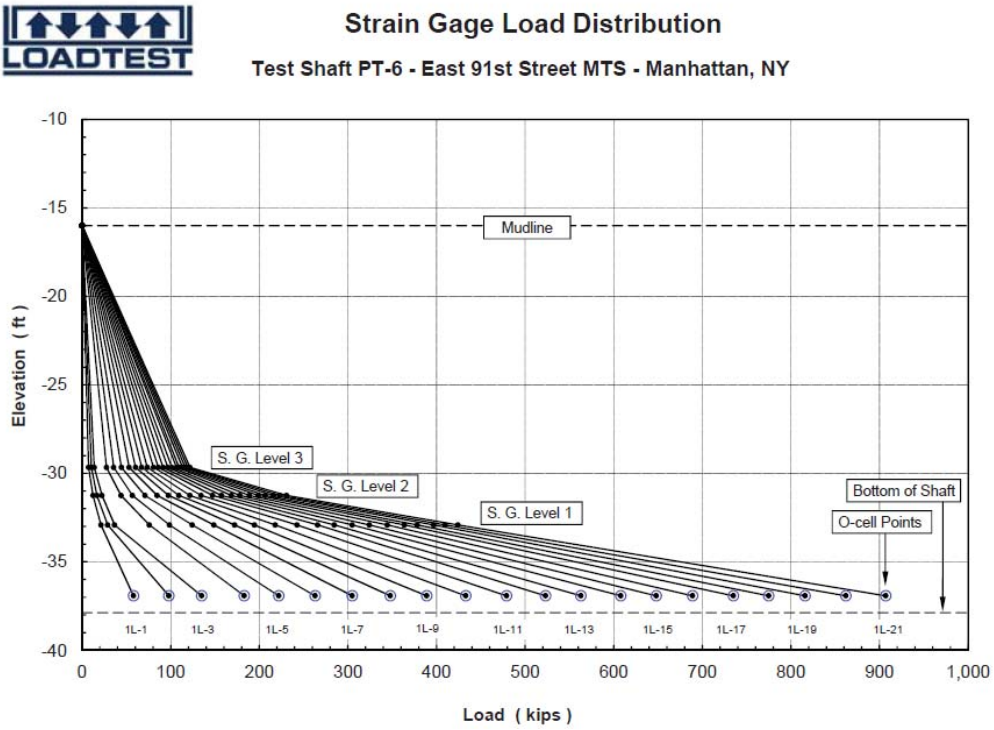


Figure 11. Strain Gage Load-Distribution Test Shaft PT-6.

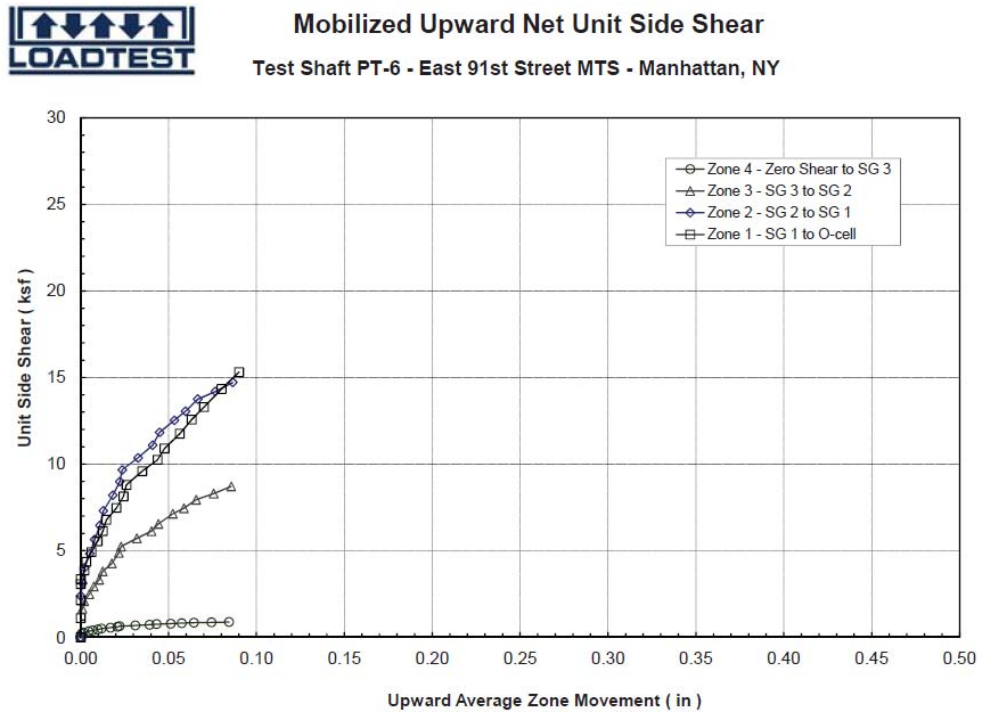


Figure 12. Mobilized Upward New Unit Side Shear Test Shaft PT-6.

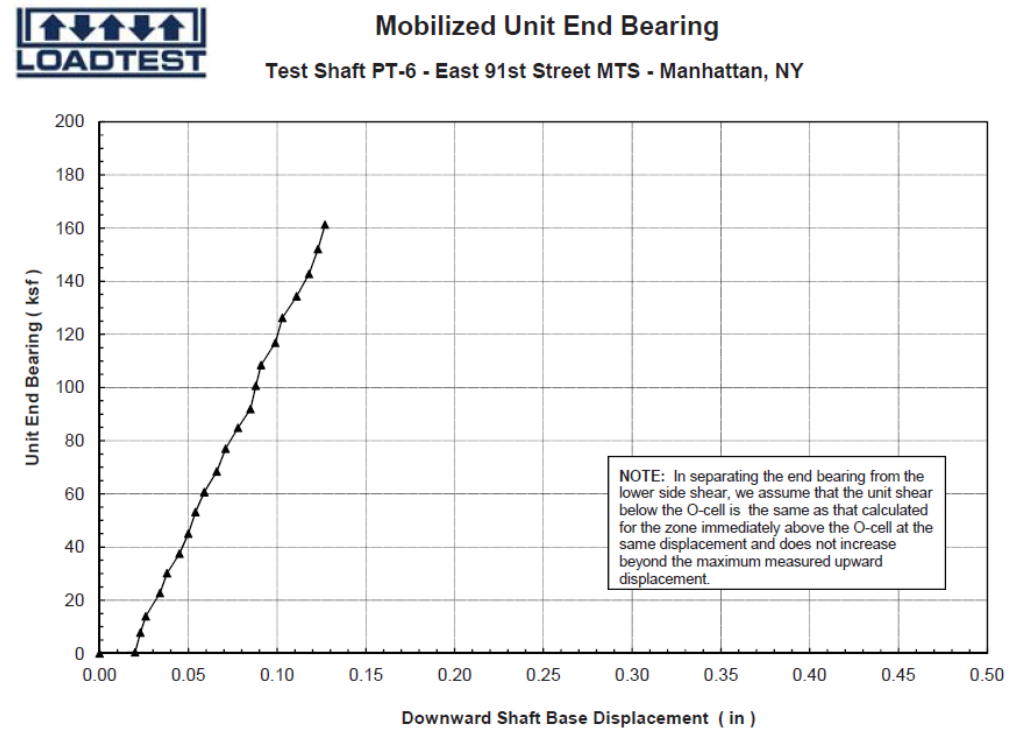


Figure 13. Mobilized Unit End Bearing Test Shaft PT-6.

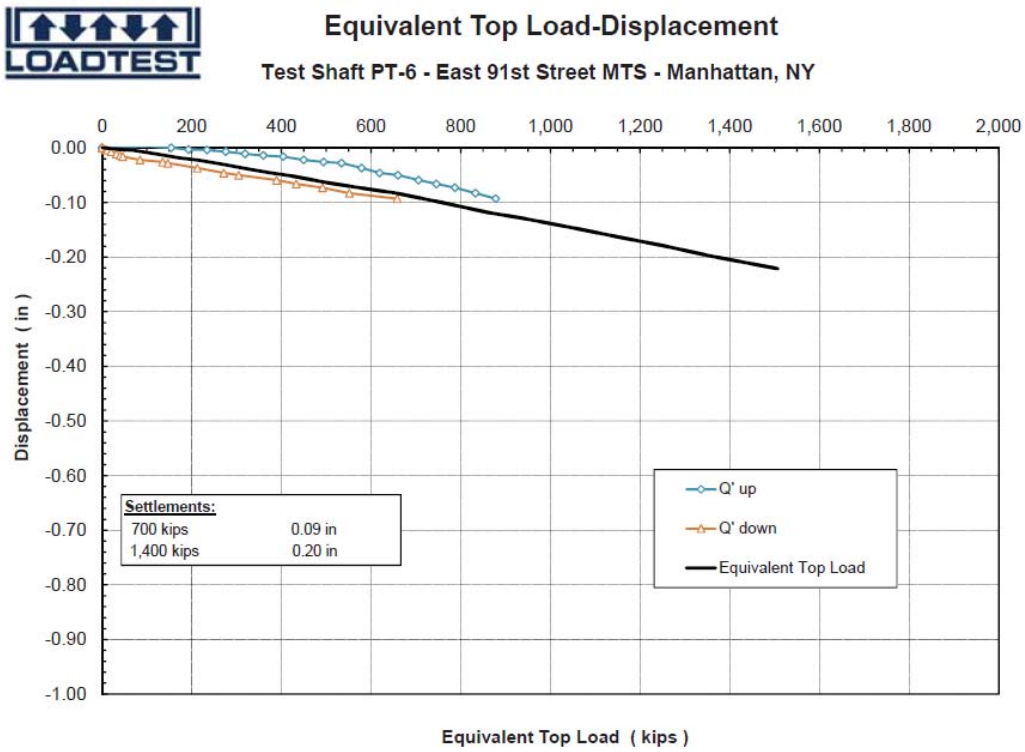


Figure 14. Equivalent Top Load-Displacement Test Shaft PT-6.

4. CONSTRUCTION CHALLENGES

One of the major construction challenges was the limited project site space which was surrounded by existing structures, and the dense traffic of the FDR. The over water location was also challenging upon performing traditional load tests. The subsurface investigation gave insight to the man-made reclaimed fill and buried debris which also helped to identify the remnant bulk heads. Obstructions are important to be identified early on the project in order to place the foundation at the appropriate location. Selection of adequate number of borings helped the Design Engineer better identify the changes in bedrock elevation especially by the water side. By doing so, the contractor was able to select the appropriate equipment to install the drilled shafts. Steel casing was equipped with carbide teeth that allow the casing to bite into rock and provided an adequate seal which will prevent surrounding soils from migrating inside the rock socket. The carbide teeth allowed the casing to be seated on the sloping rock encountered in the river.

5. SUMMARY AND CONCLUSION

Local knowledge of the site geology is an important factor for a successful foundation design. In this paper, understanding the history of water front structures in New York City and the constant changes of coast line enabled the engineers to come up with detailed subsurface investigation program. GPR was used to locate unknown and anticipated obstruction within the project site. Minipiles foundations are becoming more attractive foundation alternative. When socketed to rock, minipiles can carry very large axial loads. The use of the Osterberg load tests in lieu of standard load tests was appropriate for this project because of the limited space and access. The design and construction of the 91st Street ramp giving access to the Marine Transfer Station over the FDR drive and the design of the proposed 92nd Street alternative ramp were possible possible due to the collaboration of the designer and the contractor. The Osterberg tests were used to evaluate load displacement, end bearing, net unit size shear and strain. Vibration and noise monitoring program helped reducing the adverse impact of construction on the surrounding structures. Lessons learned on how to create solutions for Urban high Capacity Sites with complex history and geology can be applied anywhere in the world especially once done successfully in New York City.

Results of the Osterberg load test were comparable to values from the New York City Building Code (NYCBC). For instance, NYCBC recommends an allowable end bearing of 80 ksf of rock class 1.b (medium hard rock). Figure 13 shows a mobilized end bearing of 160 ksf corresponding to 0.13 inches of settlement. Considering that the shaft can undergo 0.5 inch settlement safely, it is clear that you can utilize an allowable end bearing of more than 80 ksf. As far as the skin friction in rock, Figure 12 shows unit side shear of 15 ksf corresponding to 0.1 inch vertical movement. Considering that full skin friction can be mobilized with movement of 0.3 inch to 0.5 inch, it can be concluded that full skin friction can achieve 25-30 ksf. Our design for drilled shafts and minipiles assumed ultimate end bearing of 160 ksf and ultimate unit skin friction of 28.8 ksf. Therefore, the Osterberg load tests confirmed the design assumption. Lastly, the NYCBC recommends an allowable unit skin friction of 28.8 ksf and if the load test continues with higher loads, NYCBC values can be achieved.

6. REFERENCES

1. History, New York Times, May 24, 2018

CONSULTANTS CAN BE SAFE, TOO – A COLLABORATIVE APPROACH

Michael J. Weaver, P.E., Haley & Aldrich, Inc., Boston, Massachusetts, USA, 617.886.7373, mweaver@haleyaldrich.com
Brian FitzPatrick, CHMM, Haley & Aldrich, Inc., Bedford, New Hampshire, USA, 781.685.2132, bfitzpatrick@haleyaldrich.com

ABSTRACT

Everyone has a role in site safety, even consultants. This paper presents a summary of how a geotechnical and environmental consulting firm, with field staff on construction and subsurface explorations sites, engaged their staff and leveraged relationships with contractors to assess the construction related risks to which its staff members are exposed. These findings were then integrated into their technical training materials for both new staff and those needing a refresher, so that safety is discussed at the same time as the technical work and not treated as a separate topic. The paper outlines the process of identifying and evaluating the construction related risks that staff members face and presents examples of how the consultant can engage contractors in the process. By doing this, knowledge can be shared and there is a better mutual understanding of the risks associated with common construction and exploration related field tasks. The work resulted in an increase in staff engagement in safety, a better understanding of the true risks that staff face in the field, better relationships with contractors, and lower safety metrics.

Keywords: safety, integrated, knowledge sharing

HISTORY

At Haley & Aldrich, Inc., we renewed our safety journey in May 2012. Like many others, we had concerns over injuries our staff experienced in the three previous years, and a potentially significant utility strike we experienced while excavating a trench. In 2009, 2010 and 2011 we experienced an increase in recordable injuries, including two significant injuries, which caused our Experience Modification Rate (EMR) (see note below), Total Recordable Incident Rate (TRIR), and Days Away-Restricted, and Transferred Rate (DART) to rise significantly. See Fig. 1 for details. This caused us to step back and review our approach to safety, and our "safety culture". The rise in reportable incidents and injuries also corresponded to the beginning of a growth period for the company.

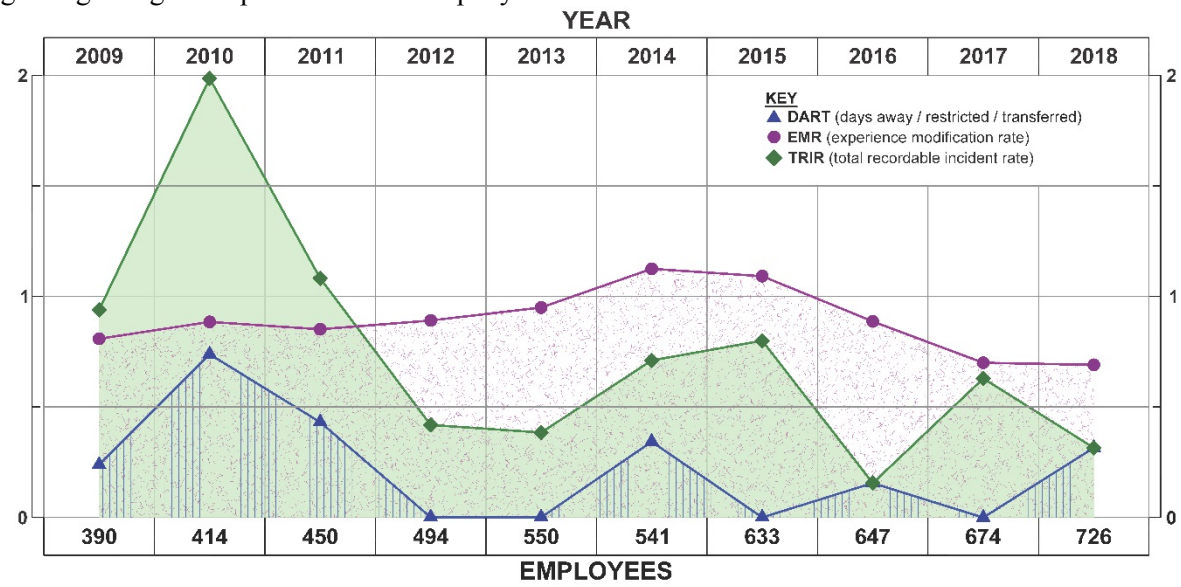


Fig. 1 Graph of Safety Statistics 2009 – 2018

© 2019 Deep Foundations Institute

Note: EMR is a 3-year lagging indicator calculated by Workers Compensation insurance, based upon claims, and consists of three years of data excluding the prior year (e.g. 2014 EMR is developed from injuries experienced in 2010, 2011, and 2012).

When we stepped back and critically reviewed our approach to safety, and our culture, we found flaws in policies and programs, and in our culture. We looked at why those flaws existed, and we found some interesting facts:

1. Our staff members were not "risk competent."
2. Separating safety from operations inhibits the adoption of safety as an important aspect of our culture: "Safety is the Safety person's job, not mine."
3. Our Health and Safety policies and programs were outdated compliance documents, written to impress our clients, but not to help guide those that do the dangerous work.

"Risk competence" is a phrase coined by our CEO. In early 2015, he wrote an internal document to the company entitled, "Safety in Everything We Do, Managing Risk in Our Business". In this document our CEO went on to write that the reality of our business is that there is risk in everything we do. We could either become risk averse and not perform work, or we could become risk competent and safely work in our industry. To be risk competent, we must be aware of and trained to recognize and mitigate the risks we face. We must continually educate our staff on the nature of the risks involved in our business.

At the same time, we revised our Health and Safety Policy to reflect the idea of risk competence. In doing so, we made a conscious effort to integrate safety as an important aspect of our work. Our current policy states:

> *Our goal is to protect our staff by improving the safety performance of every staff member, every project, and across our Company by:*
>
> - *improving our safety systems, tools, and training;*
> - *improving the ability of all staff to inherently recognize unsafe systems, processes, situations, and behaviors; and*
> - *empowering all staff to intervene to improve safety and our underlying systems, processes, and behaviors.*
>
> *We will know we have achieved success when our continually improved key performance indicators consistently outperform those of our industry, but more importantly, when each person returns home as healthy as when he or she came to work that morning.*

We knew that changing a policy statement alone would not address the changes that were necessary in our organization. We needed to take action that aligned with this shift in thought. This paper discusses the approach we took to engage our staff and our partners to collaboratively improve our policies, our programs, and our culture. The benefits of working collaboratively with staff and our partners is that we are able to understand the processes and risks associated with the work from multiple perspectives. In fact, we used the collaborative approach to initiate the culture change, while making program improvements. What better way to integrate safety into how we work—and empower staff to intervene and improve safety—than to give them ownership of the safety programs? We were able to address all three of the issues we identified above through this one collaborative approach.

LEVERAGING EXPERIENCE

As consultants, our role on construction sites and field exploration projects is primarily as inspectors, so we are not operating equipment or preforming work tasks. However, our staff are working in proximity to all types of construction and exploration equipment. The inspector's job is to observe the work being performed by others, and that sometimes means being within a meter and half of a micro-pile rig to observe cuttings, counting blows on a pile as it is being driven, or measuring the depth and sounding the bottom of a caisson or slurry wall panel (see Fig. 2). The consultant inspector is typically the only representative from their firm on-site. As such, they are in risky situations every day. The inspector's job requires them to be close to the work, but they are not in control of the operations going on around them. Also, they may not be familiar with the operation of equipment being used and the risks associated with it.



Fig. 2. Photograph of inspector near a pile driving rig.

As we set out to redefine our safety culture and programs, we decided to take a bottom-up rather than a top-down approach. Our company has been working in the built environment for more than 60 years and has some staff with more than 40 years of experience working on construction sites and around subsurface exploration rigs. In addition to our staff, we also have long standing relationships with many geotechnical specialty subcontractors and subsurface exploration contractors that have been in business for decades. What better way to learn than to engage these experienced staff and business partners and see what they do day in and day out to stay safe.

We started by identifying the most common field tasks that our inspectors were engaged in, such as observing pile driving, micro-pile installation, subsurface exploration drilling, slurry wall excavation, groundwater sampling, earthwork, etc. We engaged our experienced field inspectors (not the senior office staff who have been out of the field for 10+ years) to understand how they do their jobs, and what risks they are exposed to on a day-to-day basis and how they plan for them.

We conducted job hazard analyses (JHAs) with small groups of our experienced field staff. We got them talking with our safety staff, who facilitated and recorded the discussion. We heard plenty of "war stories" of near-misses and other incidents over the course of decades. Who knew that a wood pile, loosened by construction, acts like a missile when coming out of a slurry-filled trench! We also learned some of the tricks of the trade, like where to stand during pile driving to lessen the risk of things falling on them, or where not to stand near a micro-pile rig that is pressure grouting to avoid being injured or covered in grout when a hose breaks.

In addition to talking with our staff, we also engaged geotechnical contractors and subsurface exploration contractors to better understand how the work actually gets performed in the field and what those risks are. As an example, we worked with two test boring contractors to better understand the risks associated with drilling test borings. On one occasion, we sent some experienced field staff and safety staff to the drillers yard (See Fig. 3) and ran through a typical project from start to finish. We recorded the operations, including mobilizing the rig to the site, off-loading equipment, checking Dig Safe markings, setting up the rig, drilling, retrieving samples, and demobilizing the rig. Because this was not done during a production day of drilling, we were able to record the information and engage the driller and the driller's helper in conversations about their responsibilities at each stage of the operation. This allowed us to better understand the process from their perspective and to understand the risks they look for and try to mitigate.



Fig. 3. Photograph of consultant's inspector reviewing hazards associated with mobilization of a drill rig.

We learned that during certain operations (such as when the driller is booming up the rig or taking a standard penetration test [SPT]), they are very focused on the mechanics of the job and are not focused on where our inspector is or what they are doing. This type of feedback is invaluable for us as consultants, so we can coach our staff to better understand the mechanics of the operations and the inherent risks. We can identify times when our staff members need to position themselves farther from the operations, and when they need to have a heightened sense awareness of their surroundings. As a result of this working session with the driller, we were able to produce an internal drilling safety video that covered the various stages of the process and the risks associated with each stage.

To further leverage our staffs' experience, we improved our near-miss reporting program so staff can document safety observations in real-time. We now utilize a software program that allows staff to input near-miss reports on their phones or tablets while in the field. See Fig. 4 for a picture of the input system The near-miss reports are reviewed by our safety staff, and the results are summarized to look for trends that can be used in updating our safety policies and procedures. Significant near misses and incidents are reviewed by a team which includes the staff who entered them. The team performs an incident investigation and root-cause analysis shares the lessons-learned in our monthly company-wide mandatory safety meetings. We also share the information with contractors we work with. This can help them identify risks that they may have become immune to or complacent about as they are engaged in the day-to-day work on the site

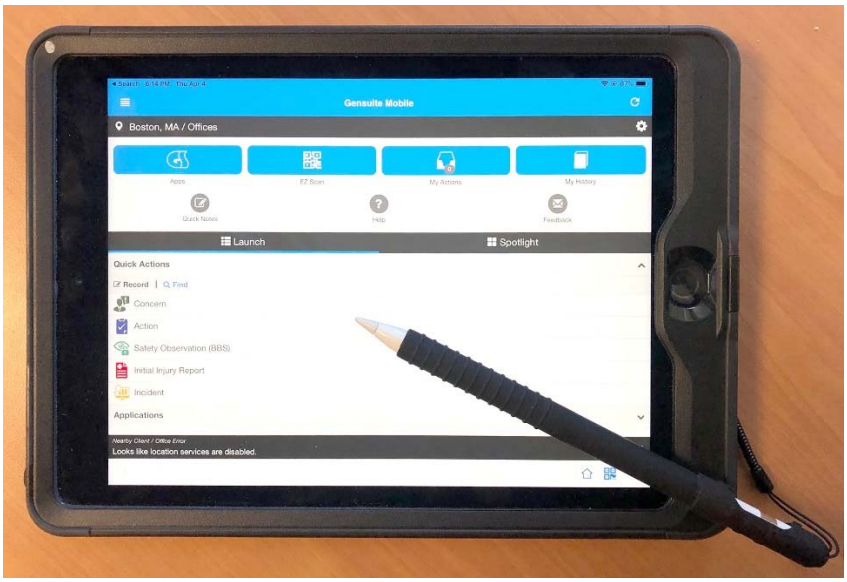


Fig. 4. Photograph of input for near-miss reporting on a tablet

INTEGRATED SAFETY

To avoid the idea that safety is just something that the safety person does, we integrated the safety feedback we got from our staff and our business partners directly into our technical how-to training. Prior to 2017, our firm had separate technical and safety operating procedures. The technical procedures were focused on the technical how-to of a task, such as what information to gather, what kinds of different piles there are, how to determine if a pile had achieved final driving resistance, or how to record a SPT on a boring log. We had separate safety policies that were compliance documents. This system was sufficient for a long time, as many of our field personnel had many years of experience with the tasks they were performing. However, as the company grew in size and geographic footprint, we encountered issues with this approach, as we found we were sending newer, less experienced staff into the field as inspectors. Many had a good grasp on the technical issues they were observing but were oblivious to the safety issues that surrounded them. *You don't know what you don't know*.

As a result, we looked for ways to better integrate safety into our training and technical operations to make it one conversation not two separate ones, and safety was neither separated nor subordinated to performance. We asked our staff if the current operating procedures (both technical and safety) were helpful. The feedback was that they were good references, but they lacked instructions on how to complete the tasks, pictures to illustrate what was being discussed, safety considerations, and tips and tricks of things to look for and be aware of. We again turned to our staff and said, "Instead of us telling you how to do your job why don't you tell us how it's done best." We formed committees for our most common field tasks comprised of approximately 4 to 8 people that included a mix of experienced field staff, health and safety personnel, and practitioners from across our offices and asked them to summarize information for each task (i.e. pile driving observation, micro-pile installation, or subsurface explorations) including:

- **What and why** – what is the process and why is what they are observing/doing important.
- **What is needed** – a checklist of supplies and personal PPE required to complete this task.
- **How** – how do they complete the tasks, what information do they need to record, what are the risks with performing the work/observing the work, and how do they mitigate those risks to complete it safely.
- **What it means and why is it important –** what do the results or observations mean, is the information they collected reasonable, and how will it be used by others.

Working with our learning and development staff, we developed a graphical template to summarize the information into two- to six-page "field guides." The field guides provide a summary of what our field inspectors are supposed to do on site, and what they are supposed to look for. The guides also have tips and tricks that our experienced staff have learned along the way, like how do you tell silt from clay in the field, and where is the best place to stand when observing pile installation. Safety considerations are woven directly into the step by step guidance so new inspectors can not only review what they need to do from a technical perspective, but are reminded of the specific safety concerns at each step. The safety information includes everything from the appropriate personal protective equipment (PPE) to don, to identifying potential hazards for each step, such as potential slips, trips, and falls, "struck by" hazards, and where to stand and not to stand while observing the work. If used on a computer, tablet, or phone, the documents also contain links to our full operating and health and safety procedures, including publications like the OSHA trenching guidelines. Once the committee compiled each guide, they were peer reviewed by 2-6 other subject matter experts in the company and finalized.

These guides are used as the outline for our training of new staff. Staff review the materials prior to going out in the field with more experienced staff for training. Training checklists generated from the guides are used when staff are trained so they cover all the safety and technical topics at the same time. In addition to the checklists, we also outline a few real-life scenarios that the trainer and trainee discuss, such as what happens if a cable breaks on the rig, or what to do if soil is pumping and weaving under compaction. The scenario portions of the training allow our staff to talk through issues that may arise, so they are prepared to deal with them or recognize the risks if they come up in the field.

The process of creating the field guides was a valuable knowledge-sharing event for our company. It also allowed us to collaborate across our offices to revise our "standard way" of doing things. Figures 5 and 6 show examples of sections from the field guides.

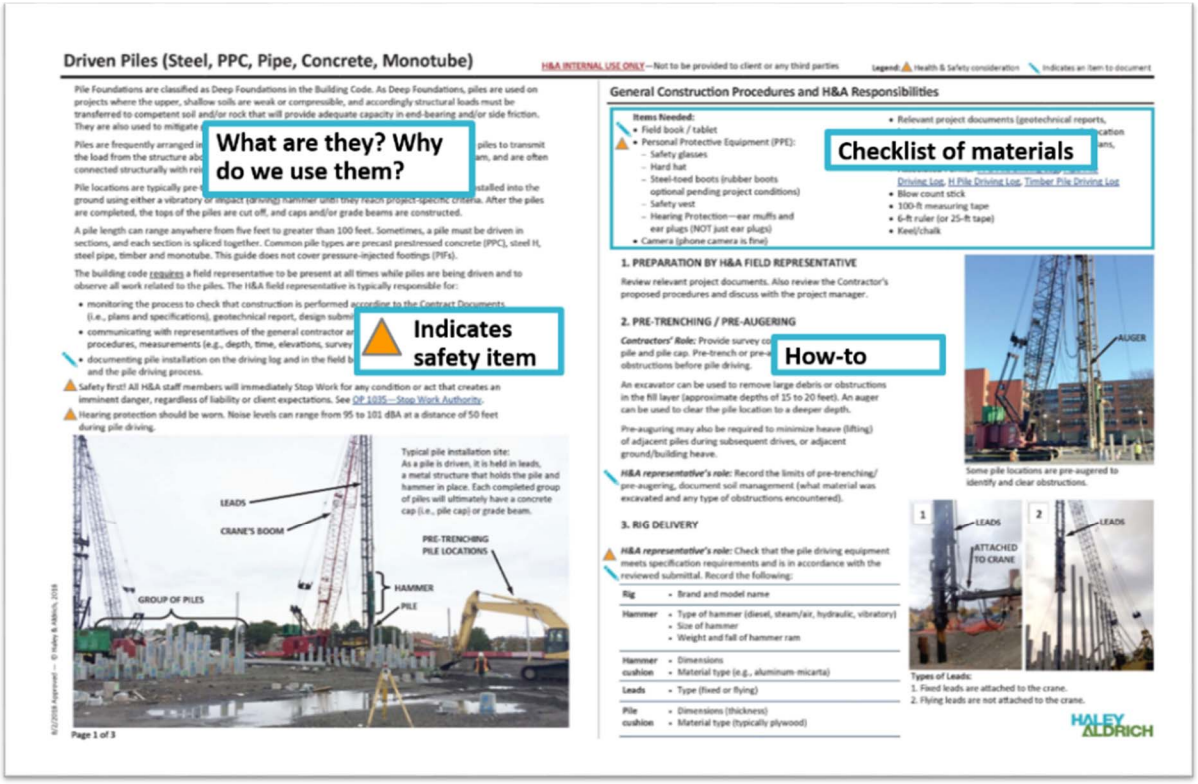


Fig. 5. Example of Field Guide

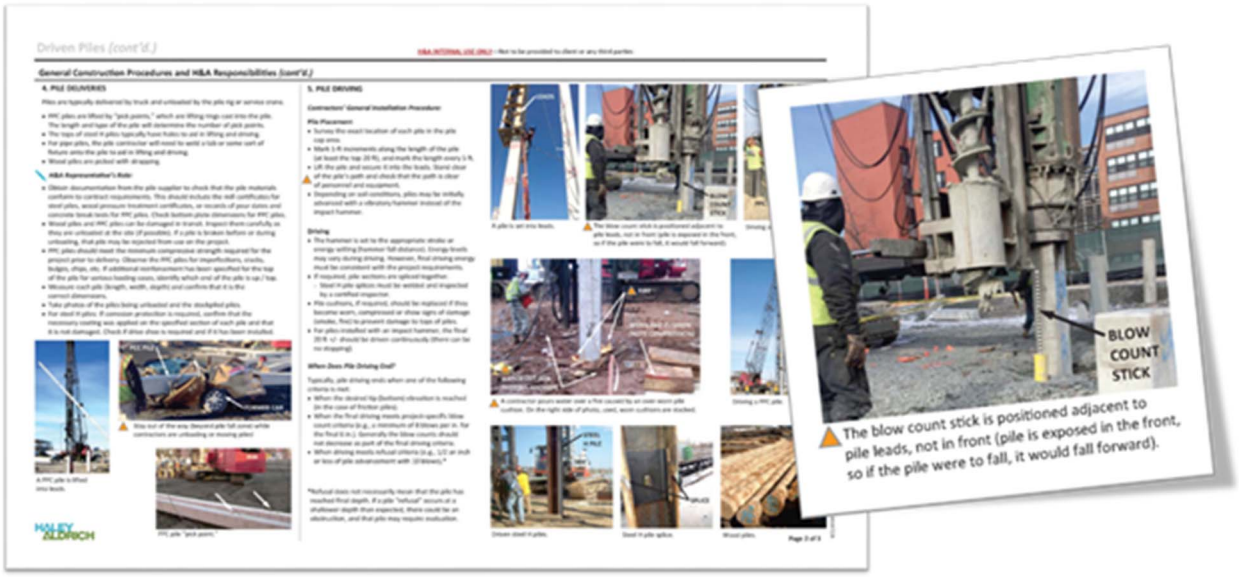


Fig. 6. Example of field guide and safety-specific information

In training our staff, we also looked to the contractors we work with for assistance. As an example, we had a group of 10 new staff that needed training on test boring drilling. We engaged one of the test boring contractors that we work with, and they provided a drill rig and a crew for the day (and even offered a site that they owned). Two of our most experienced geologists led the training along with the driller, the driller's helper, and a project manager from the drilling company. The basics of drilling were reviewed, including drilling safety for each step in the process. This collaboration on training was a huge success, in that our staff were able to learn on a non-production drill day and were able to hear firsthand experiences from our senior staff as well as the drillers. Our staff reported feeling much better prepared to observe drilling activities and to understand the risks associated with the work. They now understood the equipment better (See Fig. 7) after we focused part of the day on explaining the rig and tooling used as well as the hazards that exist, such as pressurized lines, rotating parts, and blind spots (i.e. where the driller can't see when operating the rig).



Fig. 7. Photograph of drill training

However, training and feedback cannot be a one-and-done event. We conduct periodic training for our field inspectors, focusing on engaging staff in safety discussions rather than only lecturing. As part of the training, we pair up senior staff with newer or less experienced staff and engage them to perform Job Hazard Analyses (JHA) on the common tasks they perform. We found this approach is beneficial as the younger staff get to learn from the more experienced staff, and the more experienced staff get to see a whole new perspective on the tasks they have been involved with for years. This type of reverse mentoring is beneficial for both parties, and it helps keep the safety discussion fresh and ongoing as staff learn and ask questions. The results of these periodic JHA assessments are used to check our field guides and Health and Safety policies to see if improvements and changes are needed as new construction technologies and processes are developed and implemented in the field.

BENEFITS

Through these efforts, we have seen many expected benefits unfold. By collaborating with our staff and the contractors we partner with, we have been able to effectively integrate safety into the everyday technical work we do, which has led to rapid improvement, shifting our safety culture from compliance focused to shared responsibility. This is evidenced by the 82 percent increase in near-miss reporting we have seen over the past year. This is also shown through our lower TRIR, EMR, and through the reduction in serious injuries and days away from work that we recorded in 2018 (see Fig. 1).

We have seen rapid improvement in all areas. Staff report feeling better equipped to handle the technical and safety challenges they face each day in the field. Training staff on how to be safe while performing technically competent work in the field has become more efficient. We have seen better communication between field staff, project managers, and safety staff because of the working relationships they have developed.

We have also experienced many unexpected benefits. Our staff are more empowered to say something when they see something and feel an ownership for safety. By involving the staff in the improvements, they see that they have control over their work and now own the safety that they helped develop. Our field staff report feeling they have a voice and are heard. By working collaboratively, the work itself has helped change the culture. We have also seen that there were gaps in how our office and safety staff planned work and how our field staff performed work. There are many safety benefits to exploring the gap in work-as-planned versus work-as-performed, and it is in these gaps where safety and technical issues exist. Lastly, by working collaboratively, relationships (both between staff and our partners) have been formed, and trust was gained, which promoted a greater exchange of ideas and concerns resulting in more productive conversations.

SUMMARY AND CONCLUSIONS

Our firm made measured improvements in our collective risk competence and safety culture by engaging staff in the process of identifying risks and mitigation measures, and by integrating safety into the everyday flow of technical work. By integrating technical and safety discussions into one conversation and documenting with the field guides, safety has become part of the everyday conversation among our staff. Junior staff report they feel more confident in the work they are being asked to observe/perform and more "risk competent." With the performers/observers of the field work engaged in assessing the field risks and identifying potential mitigation measures, they feel more invested in the subsequent policies and procedures that are put in place. They are more likely to adhere to them and to report issues. They are also more vocal when they see something wrong or see something that could be improved. This bottom-up approach to safety creates more buy-in from staff.

Also, by collaborating between consultants and contractors, two different viewpoints of the same work task can be reviewed together. Consultants and contractors already work very collaboratively (most of the time!) on technical client challenges. By using that same collaborative approach to identify and mitigate risks, there is a shared responsibility for safety among all the parties involved. Through collaboration, both parties risk-competence is increased, which benefits everyone!

Consultants can be safe too, but only if we stop making safety a separate discussion. We need to take the time to listen to and engage with our staff and collaborate with the contractors they work with each day.

ACKNOWLEDGMENTS

The authors would like to thank their colleagues at Haley & Aldrich for working day in and day out to improve our safety culture by finding ways to integrate a "safety in everything do" mentality into their daily work. We also want to acknowledge the assistance of our contractor partners New England Boring, Inc., Geologic-Earth Exploration, Inc., Hayward Baker Inc., and DGI-Menard, Inc., for their willingness to help us better understand safety.

DESIGN AND CONSTRUCTION OF MIXED GROUND WORKING PLATFORM FOR A CCR SURFACE IMPOUNDMENT

Daniel J. Woeste, P.E., Geosyntec Consultants, Chicago, Illinois, DWoeste@Geosyntec.com
William Tanner, P.E., Geosyntec Consultants, Kennesaw, Georgia, WTanner@Geosyntec.com
Juan M. Pestana, Sc.D., P.E., Geosyntec Consultants, Boston, Massachusetts, JPestana@Geosyntec.com
Paul J. Sabatini, Ph.D., P.E., D.GE, Geosyntec Consultants, Chicago, Illinois, PSabatini@Geosyntec.com
Jeremy M. Gasser, P.E., Geosyntec Consultants, Kennesaw, Georgia, JGasser@Geosyntec.com
Cuneyt Gokmen, P.E., Geosyntec Consultants, Kennesaw, Georgia, CGokmen@Geosyntec.com

ABSTRACT

An access pathway and working platform were designed and constructed for equipment access for a Deep Soil Mixing (DSM) pilot study over a coal combustion residual (CCR) surface impoundment (SI). The DSM pilot study was conducted to evaluate slurry mix designs and construction techniques for installing DSM columns up to 95 feet deep. Two-dimensional (2-D) limit equilibrium and 2-D finite element analyses were used to evaluate multiple failure mechanisms including: (i) bearing capacity, (ii) punching shear of mixed ground and underlying CCR, (iii) effect of fluidized DSM columns on working platform stability, and (iv) liquefaction. The analysis results were used to design ground improvement required to increase bearing capacity and stability of the CCR under the proposed equipment access route. A long-reach excavator was used to perform shallow bucket mixing and walk onto the CCR SI atop previously mixed cells following a minimum cure time and acceptance of quality control test results. Prior to mobilizing the DSM rig, a static load test was conducted to evaluate performance of the working platform. Both the access pathway and working platform demonstrated acceptable performance under the design loads during the DSM pilot study. This case study emphasizes the economic and safety benefits that can be realized by appropriately designing critical temporary work items such as access pathways and working platforms in difficult ground conditions.

Keywords: working platform, CCR, ground improvement, soil mixing, finite element

INTRODUCTION

A Deep Soil Mixing (DSM) pilot study was conducted at a coal combustion residual (CCR) surface impoundment (SI) to evaluate slurry mix designs and construction techniques for closure design of the SI (Site). Sluicing of CCR at the facility ceased and closure will be initiated based on requirements in the final United States Environmental Protection Agency (USEPA) Rule for Disposal of Coal Combustion Residuals from Electric Utilities, 40 CFR 257, effective October 19, 2015. The proposed closure approach involves constructing a DSM containment structure (DSM Wall) to separate the SI into two areas: (i) a closure by removal area; and (ii) a consolidate and cap-in-place area. The proposed DSM Wall would retain the CCR within the consolidated closure footprint and provide a barrier between the two areas of the SI. The predominant CCR in the SI where the pilot study was conducted were fly ash and bottom ash. CCR materials in surface impoundments are generally soft and saturated as a result of being sluiced into place and can present stability and safety challenges when performing earthwork activities.

The goals of the DSM pilot study were to: (i) assess potential slurry mix designs in-situ with respect to achieving target design strengths; and (ii) evaluate DSM construction techniques that could reach the design mixing depths, estimated to be up to 95 ft deep along the proposed DSM Wall alignment. To achieve these goals, DSM test columns were to be installed on the CCR delta approximately 500 ft from the nearest dike (Figure 1). This location was selected based on the following considerations: (i) proximity to the proposed DSM Wall alignment; (ii) subsurface conditions (e.g., thickness of CCR, presence of fly ash vs. bottom ash); and (iii) access and stability with nearness to the CCR delta/pond edge interface.

© 2019 Deep Foundations Institute

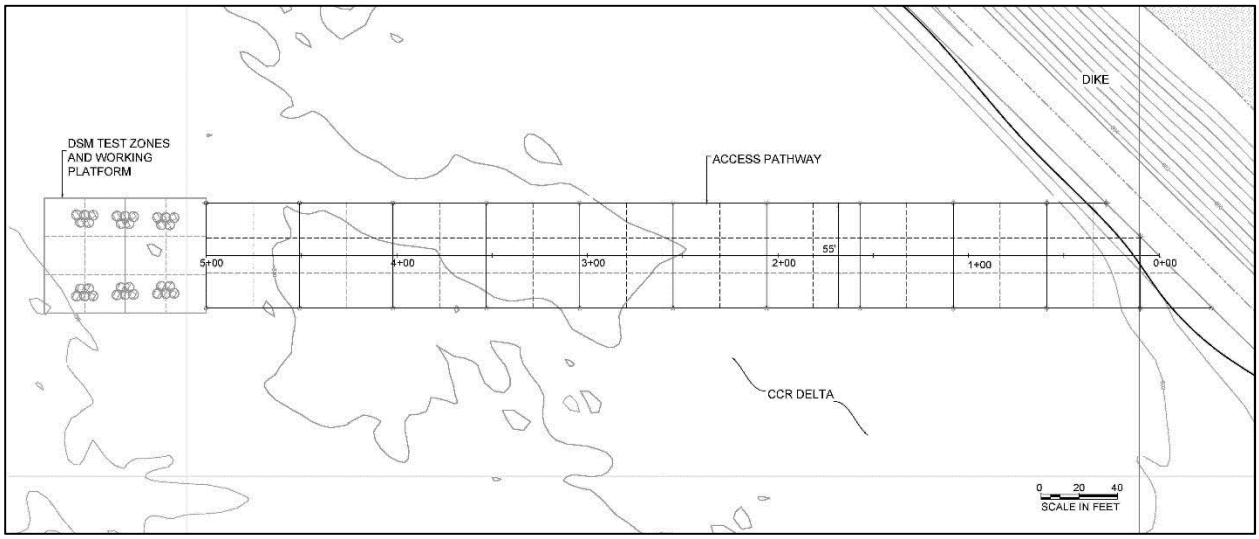


Fig. 1. Site Plan

The soft CCR deposits in the area of the proposed DSM pilot study required that an improved ground access pathway and working platform be constructed to allow the DSM rig and support equipment to reach the location of the pilot study. These temporary work items represented a significant portion of the project cost and risk. This paper focuses on the design and construction of the access pathway and working platform portion of the DSM pilot study.

SUBSURFACE CONDITIONS

The subsurface conditions at the Site were assessed from existing data including: boring logs, geologic maps, investigation reports, and a geotechnical field investigation and laboratory testing program previously conducted by Geosyntec to support closure design.

Four primary lithologic units are encountered at the Site including: (i) CCR; (ii) native soil (saprolitic soils and alluvial deposits); (iii) partially weathered rock (PWR); and (iv) metamorphic crystalline bedrock. The generalized subsurface stratigraphy in the area of the pilot study includes 70 to 80 ft of CCR underlain by more than 20 ft of native soil. Soil units below this depth were not considered as part of this study since the DSM test columns were designed to terminate in the native soil.

The depth to water on the CCR delta ranged from approximately 0 to 6 feet below ground surface and was primarily controlled by the SI pool level. Water levels in the CCR were verified prior to beginning work and monitored throughout construction.

DESIGN ANALYSES

A preliminary design for the access pathway and working platform was submitted by the subcontractor with their project bid. Following the contract award, Geosyntec finalized the design in collaboration with the subcontractor to ensure that analyses were consistent with the proposed construction methods and loading conditions. The subcontractor's preliminary design included 10 ft of mixed ground improvement overlain with a biaxial geogrid and covered with 1.5 ft of compacted aggregate. Two-dimensional (2-D) limit equilibrium and finite element analyses (FEA) were used to prepare the final design. The results of these analyses indicated that the mixed ground improvement thickness could be reduced from 10 ft to 5 ft,

resulting in significant schedule and cost savings. Analyses were performed for the following two construction loading conditions:

1. Excavator Loading: This condition occurred during mass mixing of CCR, prior to placement of the geogrid and the aggregate base with the excavator working from 4 ft x 1 ft x 24 ft hardwood timber mats. The total equipment weight of 70 kips was assumed to act over the track length and overall width (i.e., out-to-out track width), resulting in a ground pressure of 560 pounds per square foot (psf).

2. DSM Rig Loading: This condition occurred while trafficking the DSM rig on 4 ft x 1 ft x 24 ft hardwood timber mats over the completed access pathway and working platform. The total equipment weight of 290 kips was assumed to act over the track length and overall width (i.e., out-to-out track width), resulting in a ground pressure of 1,100 psf.

Limit equilibrium analyses

Two-dimensional (2-D) limit equilibrium analyses were conducted to evaluate potential failure mechanisms, including: (i) global stability, (ii) bearing capacity, and (iii) mixed ground shear and bearing strength. The analysis results indicated that the subcontractor's bid design of 10 ft of mixed ground could be reduced to 5 ft of mixed ground.

Global stability

Two-dimensional static global stability analyses were performed using Spencer's method (Spencer, 1973) as implemented in the computer program Slide 2018, version 8.016 (Rocscience, 2018). The analyses were performed assuming: (i) a groundwater level within the SI located 3 ft below ground surface; (ii) the beneficial effect of the geogrid is not modeled; (iii) full-depth tension cracks are present within the previously mixed CCR (to account for the effects of localized, potential overstress that could result from eccentric loadings from the equipment); and (iv) freshly mixed (i.e., fluidized) CCR has a unit weight of 100 pcf and zero shear strength (i.e., modelled as a fluid pressure). The optimized 5 ft of mass mixed CCR exceeded the target minimum factor of safety (FS) of 1.3. The results also indicated that the excavator would be required to maintain at least three feet of clearance between the edge of the tracks and the edge of mass mixing operations, and the DSM Rig was required to maintain at least five feet of clearance between the edge of the tracks and the edge of the access pathway.

Bearing capacity

Bearing capacity of the unmixed CCR material below the mass mixed CCR was analyzed for: (i) general shear; (ii) local shear; (iii) and punching shear failure. For these analyses, it was conservatively assumed that the water table was located at the ground surface and that equipment loads were transmitted directly to the bottom of the mass mixed CCR. The target minimum FS of 2.0 was met for all bearing capacity checks.

Shear and bearing strength

The required unconfined compressive strength (UCS) of the mass mixed CCR was calculated for the two loading conditions described above. Calculations were performed using the methodology for structural plain concrete (ACI, 2011) with adjustments for soil cement. Results of the mixed ground shear and bearing strength analyses are summarized in Table 1.

Table 1. Required compressive strength of mass mixed CCR

Loading Condition	Min. Req. UCS (psi).
Excavator	12
DSM Rig	28

Finite element analyses

PLAXIS 2D was used to evaluate global stability of the working platform and verify the limit equilibrium analysis results. Multiple load cases were considered, including the presence of a fluidized CCR column and eccentric loading during auger retraction. A simplified Mohr-Coulomb model was used for all materials. The model used 15-noded triangular elements which are useful in the analysis of failure mechanisms. The FS analyses in PLAXIS was used wherein the software performs a progressive reduction of material shear strength properties until failure is achieved. Failure is defined as a condition in which the numerical solution cannot converge. For these analyses, the ratio of peak strength to the strength that causes failure provides a FS that is comparable to those obtained through more conventional slope stability limit equilibrium analyses.

Figure 2 shows the contours for incremental shear strain and total deformation (blue contours indicate essentially no deformation) for the critical load case during auger retraction. The areas with large total deformation represent a soil-body that is unstable, and the contours of incremental shear strain provide a representation of the failure surface (i.e., concentration of shear strains) and can be equated to the critical failure surface from a limit equilibrium analysis. The analyses show a shallow rotational failure mechanism constrained by the location of the drill rig with a computed FS value of 2.80. The global stability failure mechanism and FS value matched closely with the corresponding limit equilibrium analysis.

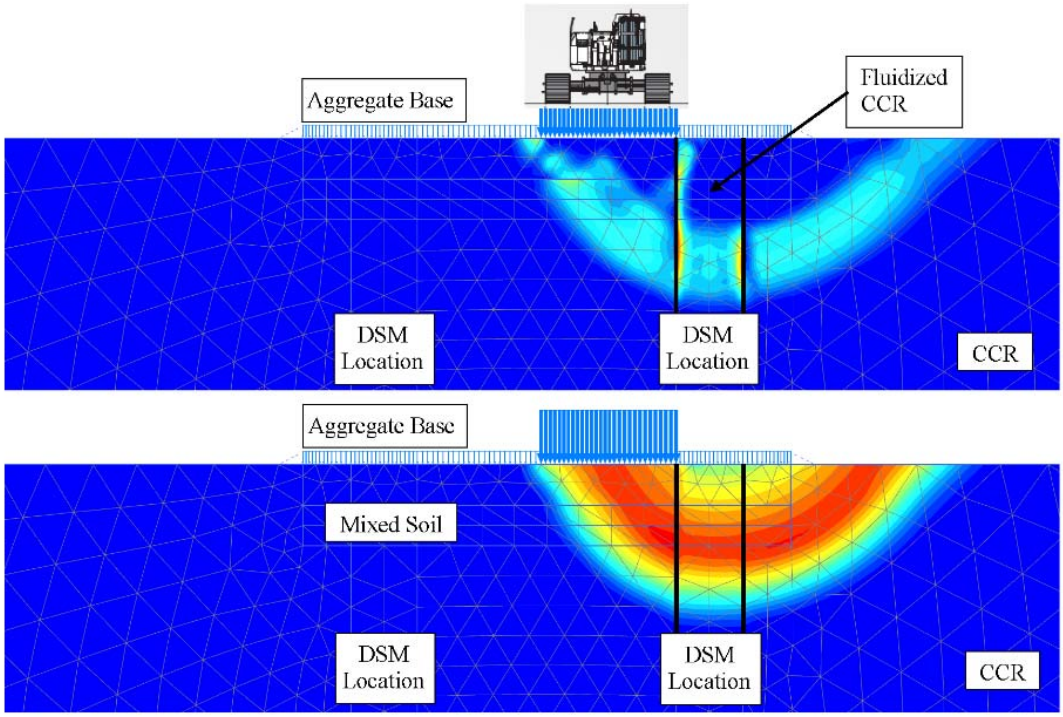


Fig. 2. FEA analysis results for DSM rig loading: Contours of incremental shear strains (top); Contours of total deformation (bottom)

ACCESS PATHWAY AND WORKING PLATFORM CONSTRUCTION

The access pathway and working platform were constructed with in-situ bucket mixing using a long-reach excavator to blend grout into the CCR. The construction sequence required that the long-reach excavator sit atop previously mixed cells as the work progressed onto the SI. Mixing was completed in a cellular manner based on a contractor-proposed primary and secondary cell configuration (Figure 3). This mixing sequence was selected to allow enough cure time between mixing cells and to help limit the amount of fluidized CCR adjacent to the equipment loads. During construction, however, the actual mixing sequence deviated to include mixing of adjacent cells based on variations in the production rate. This deviation was allowed since the material setup time was observed to be much faster than expected, thereby eliminating concerns about sloughing of adjacent cells.

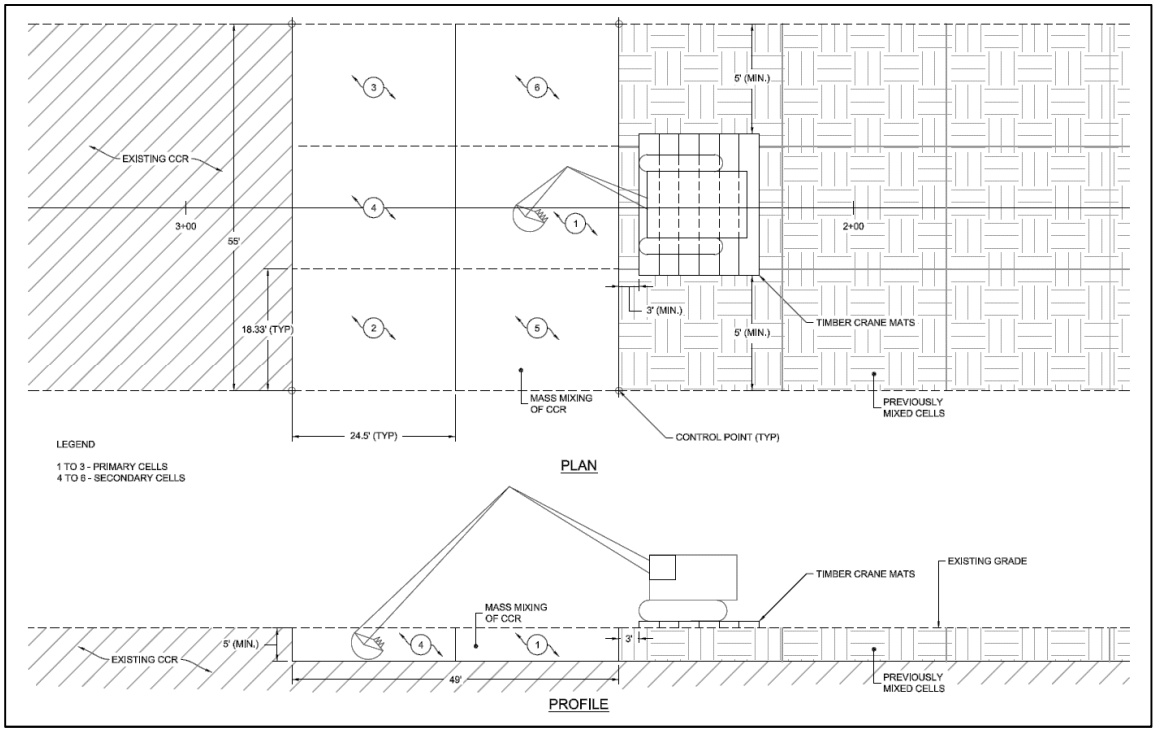


Fig. 3. Access pathway construction sequence

The water level within the CCR was verified in each cell prior to mixing by excavating a sump in the middle of the cell and observing if water was present. One to two feet of free water was observed at the bottom of cells beginning half way through access pathway construction, a condition that had been considered in the stability analyses. The grout water to cement ratio was lowered for the remaining cells to account for the extra free water.

The access pathway and working platform were instrumented with vertical and horizontal inclinometers, vibration monitoring units (VMU), and nested vibrating wire piezometers (VWP) to monitor performance of the mixed ground. Data were collected from the instruments with data loggers and sent to a remote server where the data was accessed and monitored real-time. The presence of excess pore pressures was of interest since liquefaction due to rapid loading and equipment vibrations has been documented for other saturated CCR sites. During DSM rig mobilization, settlement was measured to be less than 0.1 inches and rebounded almost immediately, a maximum peak particle velocity (PPV) of 0.12 inch per second (frequency of 6 Hz) was measured, and the maximum excess pore pressure was 30 psf (pore pressure ratio = $\Delta u/\sigma_v'$ of 0.03) and dissipated approximately 20 minutes after it reached peak value (Ahmadipur et al., 2019).

Observations during construction included the following:

- Lack of bulking: volumetric increase (i.e., swell) is usually observed during wet mixing ground improvement. However, essentially no bulking was observed at the Site and, in some cases, volumetric loss (i.e., shrinkage) was observed. This phenomenon is suspected to be associated with densification of the very low density CCR material during construction (i.e., surficial CCR material within approximately 5 ft of the ground surface appeared to be loosely deposited).
- Faster cure time: The grout-CCR mixture had sufficient strength after two to four hours allowing for construction of adjacent cells in the same day. For the Type III cement, moderate to significant force was required to scrape/key into adjacent cells with the excavator bucket.
- No observed signs of liquefaction: The CCR material experienced dynamic loading due to the excavator rocking onto track toes/heels during mixing and the excavator bucket being thrust into cured material. Moderate increases (i.e., "spikes") in pore pressure (i.e., 1 to 2 ft of head) were measured in the piezometers. Most excess pore pressures dissipated within minutes and no signs of liquefaction (e.g., CCR boils or pumping ground surface) were observed.

Mix Design

The grout mix design at the start of construction included 10 percent Type III Portland cement by dry weight of CCR with a one-to-one (1:1) water to cement ratio. Type III cement was selected with the goal of achieving high early strength to allow equipment to advance and maintain the project schedule. Because very high strengths were achieved using the Type III cement, a field study was conducted to evaluate whether Type I/II Portland cement could provide the requisite strengths and reduce project costs. The field study indicated that Type I/II Portland cement would meet the project objectives and the remaining portion of the access pathway and working platform were constructed with this type of cement. The water to cement ratio was adjusted a few times during construction based on observed groundwater and measured operations variables; values ranged from 1.25:1 to 0.8:1. Actual cement dosages per cell during production ranged from 10 to 25 percent.

Static Load Test

A static load test was conducted on the completed working platform prior to mobilizing the DSM rig. The load was applied by positioning two, 17,850-gallon (gal) frac tanks at the middle of the working platform and filling them with water in load steps. Each tank had a footprint of 8 ft wide by 19 ft long, corresponding to a ground pressure of 1,175 psf when full, approximately equal to the DSM rig average ground pressure.

The load test was monitored with vertical inclinometers, settlement profilers, and nested VWPs. Three settlement profilers were used: two extending in the longitudinal direction at the edge of the frac tanks and one extending through the centerline of the short axis of the frac tanks. The settlement profilers were horizontal ShapeArrays (SAAX) manufactured by Measureand, Inc. In addition, seven survey targets were installed on the upper rim of the frac tanks and read manually during each loading and unloading interval.

The load test was conducted in general accordance with ASTM D1143, Standard Test Method for Deep Foundations Under Static Axial Compressive Load, Procedure A. The frac tanks were filled in load steps corresponding to 1 ft of water fill depth. Each load step was held for approximately 30 to 60 minutes while instrumentation data was collected. The maximum test ground pressure was maintained for approximately two weeks while automated instrumentation readings were collected. The tanks were then emptied in five equal load steps.

The observed response of the working platform during the load test was generally consistent with the anticipated performance which indicated sufficient capacity to accommodate the DSM rig loading. Additional load test and instrumentation details and results are provided in Ahmadipur et al., (2019).

CONSTRUCTION QUALITY CONTROL AND QUALITY ASSURANCE

Geosyntec provided full-time construction quality assurance and health and safety oversight during the work. Our field activities included record keeping, material qualification, field evaluation and monitoring, and sample collection and testing. Construction progress was tracked via Geosyntec's internally developed construction information management (CIM) project website which allowed data to be efficiently and securely shared with the involved parties. The website was updated daily with items such as daily field reports, sampling summaries, field testing results, material quantities, and photos, all of which were accessible via an interactive webmap. The webmap included a color-coded display to visualize the work progress and access results. An example of the webmap is provided in Figure 4.



Fig. 4. Construction information management system webmap example

Wet grab samples were field tested for moisture content in general accordance with ASTM D4643 and cast into 3-in. by 6-in. cylinder molds. The day after collection, samples were tested in the field with a pocket penetrometer and a custom proving ring device. The proving ring device was capable of testing samples up to 64 pounds per square inch (psi) unconfined compressive strength (UCS) and provided an index of sample strength. These field tests were used to estimate the one-day UCS and to assess if equipment could advance onto the freshly cured cells. A minimum pocket penetrometer value of 2.0 tons per square foot (tsf) was established as the threshold prior to allowing equipment to advance. The pocket penetrometer and proving ring UCS test results on one-day samples are summarized in Figure 5. These data indicate that a pocket penetrometer reading of 4.5 tsf corresponds to a UCS value of at least 40 psi (resulting in a pocket penetrometer to UCS ratio of approximately 1.5). The standard deviation for these data is 7 psi (0.5 tsf) which indicates that the acceptance criteria of achieving a minimum pocket penetrometer reading of 2.0 tsf (for a 12 psi excavator loading design value) was appropriate.

Because samples were tested with less than 24 hours of cure time, cylinder molds were pre-cut and duct taped to facilitate removal of the samples with minimal disturbance. An example pre-cut cylinder mold with extruded sample and the proving ring device are shown in Figure 6. Samples that were not tested in the field were hand delivered to the construction quality control laboratory after at least three days of curing and a minimum pocket penetrometer reading of 4.0 tsf. Laboratory UCS testing was performed in general accordance with ASTM D2166 on selected samples after 3 to 28 days of curing; these UCS test results are summarized in Figure 7.

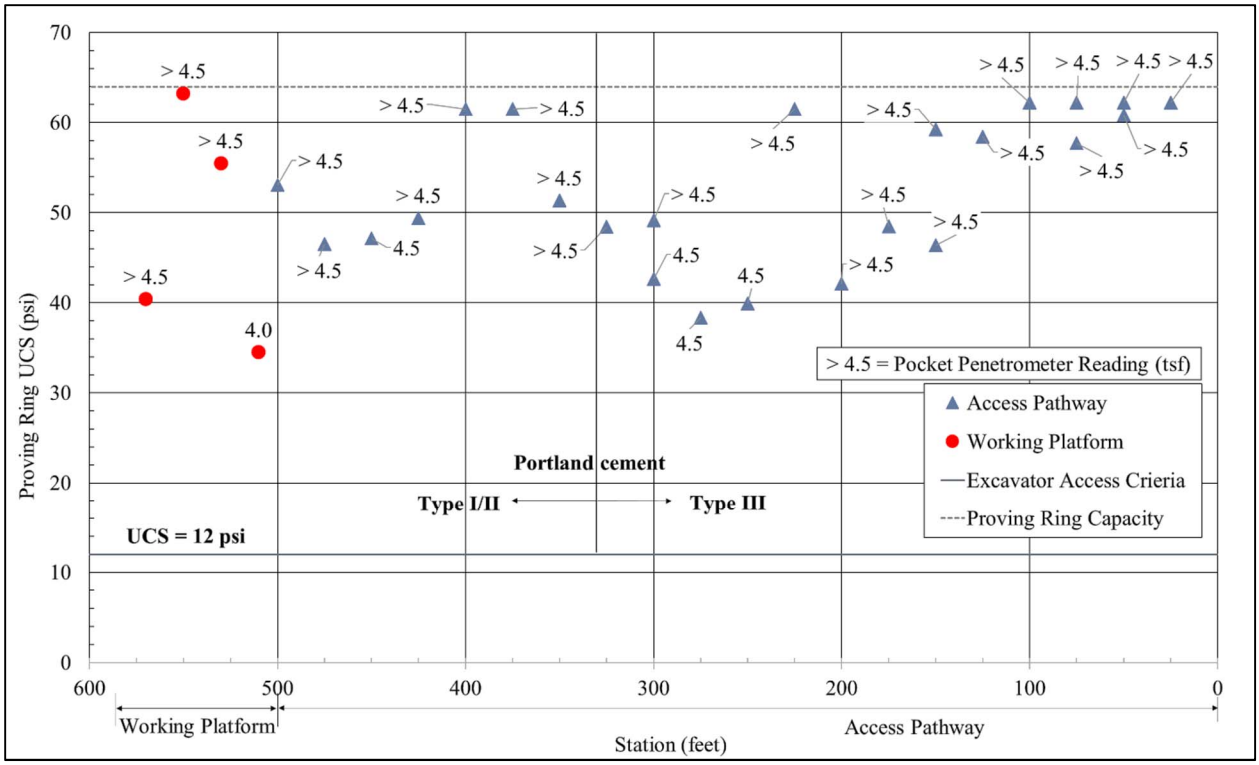


Fig. 5. Proving ring UCS test results with pocket penetrometer readings



(a) **(b)**

Fig. 6. (a) Wet grab pre-cut mold and extruded sample, (b) Sample testing in proving ring device

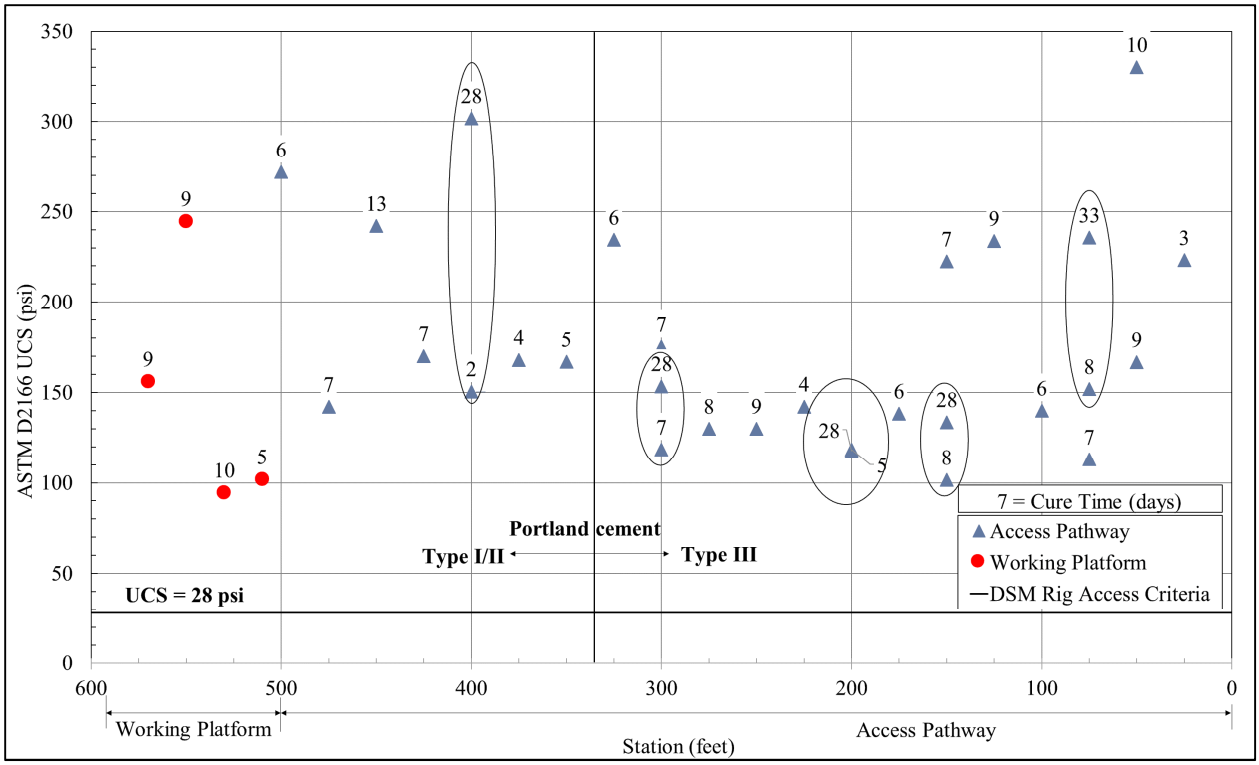


Fig. 7. Laboratory UCS test results with cure time

The data in Figure 7 indicates little correlation between cure time and UCS for the Type III cement. The circled data represent tests from the same suite of samples. These data generally suggest that approximately two-thirds of the strength gain is achieved within the first five to eight days of curing for Type III cement.

CONCLUSIONS

The following conclusions can be made based on this case history of access pathway and platform design, construction, and observations:

- The use of Type I/II and/or Type III cement with just one day of cure time was sufficient to develop a mass mixed CCR layer that could safely support construction equipment.
- Volumetric reduction (i.e., shrinkage) observed during in-situ mixing of the surficial CCR (upper 5-ft) is believed to be the result of the densification of very loosely deposited CCR material. Volumetric bulking/shrinkage behavior is expected to be a site-specific behavior, which may also vary with depth and location based on CCR SI operations.
- The pocket penetrometer test and a simple UCS device (e.g., proving ring) were effective in providing timely and appropriate information in the field for work product acceptance and to support critical construction decisions such as advancement of construction equipment onto the freshly cured cells.
- Pore pressure increases observed during construction were not sustained and dissipated quickly thereby indicating little potential for equipment and vibration induced liquefaction.

Significant concerns related to safely traversing across wet and saturated CCR materials required a comprehensive design, oversight, and instrumentation program. The specific destabilizing behavior of vibration-induced liquefaction of CCR materials was addressed through appropriate consideration of

equipment geometry and loading, drainage potential of CCR material, and pore pressure monitoring. This project demonstrates how an engineer-led design of critical temporary work elements, such as access roads and working platforms over difficult ground, can decrease project cost by reducing contractor risk and compressing the project schedule.

ACKNOWLEDGMENTS

The authors would like to thank their client for the opportunity to be involved with this project and their subcontractor, Geo-Solutions, Inc., for their contributions to the design and efforts throughout construction.

REFERENCES

ACI Committee 318. (1999). "Building code requirements for structural concrete: (ACI 318-99); and commentary (ACI 318R-99)". Farmington Hills, Michigan: American Concrete Institute.

Ahmadipur, A., Ebrahimi, A., Das, R., Tanner, W., Sabatini, P.J., Gasser, J.M., and Gokmen, C. (2019). "Performance Monitoring of Mixed Ground Working Platform for a CCR Surface Impoundment", Submitted to the 44th Deep Foundations Institute (DFI) Conference, Chicago, Illinois.

Rocscience (2018), "Slide® – 2-D Limit Equilibrium Slope Stability for Soil and Rock Slopes," User's Guide, Rocscience Software, Inc., Toronto, Ontario, Canada.

Spencer, E. (1973). "Thrust line criterion in embankment stability analysis." Geotechnique, 17:11-26.

EXCAVATION RISKS ADJACENT TO EXISTING STRUCTURES IN ILLINOIS AND URBAN ENVIRONMENTS - IDENTIFYING AND MANAGING TECHNICAL AND LEGAL ISSUES

Gregory R. Meeder, Partner, Holland & Knight LLP, Chicago, IL, 312-928-6022, gregory.meeder@hklaw.com

James P. Chivilo, Partner, Holland & Knight LLP, Chicago, IL, 312-715-5895, james.chivilo@hklaw.com

Scott J. DiFiore, P.E., Principal, Simpson Gumpertz & Heger Inc., Waltham, MA, 781-907-9320, sjdifiore@sgh.com

Matthew H. Johnson, P.E., Principal, Simpson Gumpertz & Heger Inc., Chicago, IL, 312-754-7500, mhjohnson@sgh.com

ABSTRACT

New construction in metropolitan areas has direct impacts on immediate neighbors and abutters. While noise and dust are generally nuisance concerns, demolition, vibrations, excavation, and dewatering can cause structural damage to adjacent structures. Different cities, states, or jurisdictions have different regulations that dictate requirements, roles, or responsibilities for varying parties during construction. The authors will introduce and discuss risks of new construction adjacent to existing structures, and the legal framework in Illinois which requires the owner of the new construction project to provide adequate protections for adjacent existing structures. The authors, who are engineers and attorneys, will discuss technical and legal concerns, and will highlight the importance of early and frequent communication among project participants to manage risks, despite whether or not any local regulations exist to drive the process.

Keywords: abutter, adjacent construction, excavation-induced movements, demolition, vibration, claims, regulations, ALEPA

RISKS IN ADJACENT CONSTRUCTION

New construction in metropolitan areas inherently involves some combination of noise, dust, ground-borne vibrations, earth excavation, and subgrade dewatering. These issues have potential to directly and adversely affect abutters and their property. Noise and dust can be nuisance concerns, while vibrations, excavation, and dewatering can result in damage to abutters' structures. Noise and dust are unlikely to lead to physical damage to abutters' property, and can be controlled with limited work hours and good housekeeping practices. Vibrations and excavations, however, if not well understood, planned for, and mitigated, can result in serious damage to abutters' structures. In turn, this damage introduces additional and often significant costs and schedule delays.

Vibrations can be caused by a wide range of construction activities including, but not limited to, blasting, excavation, demolition, driven shoring, and/or driven foundation elements. Vibrations can cause soils to densify or liquefy, and can damage archaic or fragile structures. Excavations can lead to a wide range of problems associated with abutters' property, particularly due to horizontal or vertical movement of the existing foundations. Movements can result from a support-of-excavation with insufficient strength and stiffness, dewatering that lowers the water table, and/or direct undermining of abutters' structures.

© 2019 Deep Foundations Institute

THE IMPORTANCE OF PLANNING AND COMMUNICATION

The success of a construction project adjacent to existing structures ("adjacent construction project") is based in proactive planning and communication. Leaving the responsibility to a single party leads to a reactive response to issues, impacts schedule, adds costs, and frequently results in claims.

Overall, the most prevalent risk for adjacent construction projects is lack of planning and communication between the project team members and the abutters. Methods and processes for mitigating the effects of adjacent construction projects are well established; lack of planning and lack of communication are typically the origin of problems.

A well-organized and proactive project addresses the potential effects of adjacent construction projects during the design phase. The owner/design team for the new construction can identify the potential impacts of vibration and/or excavations, and evaluate existing adjacent structures to understand the type of construction and potential response to the new construction work. Preconstruction evaluations are often part of this work to document the existing materials, structural systems, and conditions. This information can be shared with the abutters and the construction teams bidding the project.

While the construction team may ultimately be responsible for the means, methods, and sequences of construction, the owner/design team for the new construction needs to provide guidance at the bidding stage through either performance or prescriptive specifications. The geotechnical report for the project, which is typically issued prior to developing bid/construction documents, should address not only design recommendations but also construction considerations associated with vibration-inducing activities or support of excavation systems. The design team can then use the information to develop an instrumentation program, acceptable thresholds for vibration and movements (of existing structures, support-of-excavation system, and ground), acceptable thresholds for groundwater levels, limitations on construction means, methods and sequences, and a process for addressing construction-phase modifications when threshold values are reached. While the means, methods, and sequences of construction ultimately fall to the construction team, communication during the design phase will allow all parties to become educated on important issues, and appropriate limitations can be set forth in the project specifications to allow each party to perform its job better.

LOCAL REGULATIONS FOR ADJACENT CONSTRUCTION

Some cities, states, or jurisdictions have regulations that dictate requirements, roles, or responsibilities for varying parties during construction. However, not all have established or codified requirements for adjacent construction practice; the risks of damage to adjacent structures can be highest in in the absence of guidance. Regardless of local code requirements, it is incumbent upon the design and construction team to be knowledgeable about the adjacent construction, the risks that are introduced by the new construction, and the appropriate protections and monitoring of the adjacent structures.

EXCAVATION LAW AND LIABILITY ISSUES IN ILLINOIS

Introduction.

There is significant property damage risk associated with excavations under (1) the risk allocation clauses contained in procurement contracts for design professionals and contractors, (2) common negligence law, and (3) individual state statutes. For the purposes of the subsequent discussion, we define the following terms:

- Strict Liability. Strict liability is generally defined as one's liability that does not depend on an actual negligent act or an intent to harm. This is liability that is created as result of an act without

intent and whether caused negligently or by other means. For example, the party committing the act is liable for the mere commission of the action regardless of what the intent or mental state at the time of the occurrence.

- Negligence Liability. Negligence liability results when someone fails to act with the level of care that someone of ordinary prudence would have exercised under the same or similar circumstances. Negligent liability arises when there is a duty on one party's part to act with this level of care and a resulting failure to act resulting and causing damages to another party. Negligence liability is based upon actions which are not directly intentional.

- Statutory Claim. A statutory claim is a claim based upon a direct written state statute or law.

- Tort Claim or Tort Liability. A tort claim or tort liability is understood as a civil wrong (as opposed to criminal) which results in legal liability for the person who commits a negligent or intentional act resulting and causing damages to another party.

- Common Law. Common law is known as judge-made law or case law and is a body of law derived from legal decisions of courts or similar tribunals.

Excavations, which can impact abutters in dense metropolitan areas, carry design and construction obligations under the law and contract clauses. Different cities, states, or jurisdictions also manage property damage risk allocation differently for owners of new construction owners and abutters. It is, therefore, necessary to examine excavation risks under the law in the relevant jurisdiction before performing design and construction in dense metropolitan areas. The excavation risks for property damage to adjacent structures include, but are not limited to, the following general areas of significant risk:

- What is the new construction owner's procurement philosophy with respect to allocating risk for property damage caused by excavations (to whom is the risk assigned)?

- Has the new construction owner assigned the risk of protecting the adjacent structures to the design professional, the contractor, or no one?

- What are the contract or statutory deliverables required from design professionals and contractors with respect to the protection of abutters' property?

- What indemnifications have the design professional and/or contractor given to the new construction owner or third parties with respect to damage to abutters' structures?

- Is the new construction owner's, professional engineer's or contractor's self-insured retention under applicable insurance policies so large that it renders insurance coverage meaningless (i.e., the $10,000,000 self-insured retention)?

- Is a contractor generally aware that certain deliverables are required of a design professional in designing the project to protect abutters' property (has the contractor seen or asked for these deliverables)?

- What notice to abutters needs to be provided (and who has to give that notice) for new construction projects, so that the abutters can review the intended design or construction?

- What are the impacts to adjacent multi-unit condominium owners, where some of the owners are close to the new construction, and some are remote? Does liability extend to remote adjacent owners?

- Are both individual condominium owner's claims for property damages and the condominium association's claim for common element property damages recoverable?

- What common law negligence theories permit property damage recovery from designers or contractors for new construction projects?

- Does the state or local government unit have a statute or ordinance for risk allocation for new construction and property damage to abutters (i.e., is any property damage covered on a strict liability basis)?

- What sovereign immunity defenses and limitations do public owners of new construction projects possess in a given jurisdiction with respect to direct claims against public owners from abutters?

- Will sovereign immunity of public owners of new construction projects affect claims against design professionals and contractors?

- What defenses to liability for property damage to abutters' structures exist in both the public and private sectors for design professionals and contractors?

- How is a defect determined to be a design defect or a construction defect when multiple tiers of contractors and design consultants are involved in executing large metropolitan projects?

- How are delay claims by contractors impacted when property damage to an abutter's structure interrupts a construction schedule and project?

From the foregoing risk management issues, excavations in dense metropolitan areas carry significant legal and monetary risks. Different cities, states, or jurisdictions have different regulations, statutes, and procurement risk allocation programs which dictate the requirements, roles, and responsibilities of various design professionals and contractors both before and during construction. Given the nature of high-density construction and excavations in metropolitan areas, these risks also often play out in the context of high-profile and newsworthy events involving significant and important buildings.

Illinois deep excavation law – Adjacent Landowner Excavation Protection Act (ALEPA).

In 1957, Illinois joined a number of other states by enacting a state statute that provides that abutters to construction projects are legally and statutorily entitled to continuous lateral and subjacent support received from adjoining land. It is through this statute that contractors and design professionals become secondarily liable through procurement contracts and common law.

Under the Adjacent Landowner Excavation Protection Act (ALEPA), Chapter 765 of the Illinois Compiled Statutes (ILCS) Section 140, rights are conferred upon abutters to adjacent construction projects and duties are placed upon owners of excavation projects to make proper excavation for purposes of construction or improvements to property. In nearly all cases, new construction owners do their best in their contract procurement documents to pass this obligation to their contractors, subcontractors, architects, engineers, and other service providers. This usually includes standard contractual indemnification clauses that require the contractor and design professionals of the new construction to contractually defend and indemnify the owner of the new construction projects, which would include liability under ALEPA.

ALEPA notice provisions and requirements.

ALEPA requires new construction owners or possessors of land intending to excavate their property to give "due and reasonable notice in writing to the owner or owners of adjoining lands and of adjoining buildings

and other structures stating: (1) the depth to which the excavation is intended to be made and (2) when the excavation will begin." 765 ILCS 140/1(1).

Required time and duty for abutters to protect property under ALEPA.

If the excavation is of a depth greater than 8 ft below the established grade of the street (or, if there is no established grade, if it is below the surface of the abutters' land), and if it appears that the excavation is to be of a greater depth than the walls or foundations of any abutters' building or other structure and is to be so close as to endanger the abutters' building or structure, then abutter shall be allowed a reasonable time (not less than thirty days) to take measures to protect the abutters' land, building and structures from damage or to extend the foundations, and for that purpose the abutter must be given a license to enter onto the land on which the excavation is to be or is being made. 765 ILCS 140/1(1), (4).

The new construction owner of the excavated land, if provided a license by the abutter, shall protect the adjoining land and any building or other structure thereon, without cost to the abutter, by furnishing lateral and subjacent support" to the adjoining land and all buildings and structures thereon to protect them from damage by reason of the excavation, and the new construction owner shall be liable to the abutter for any damage to the land or to any buildings or other structures including liability to occupant and tenants. 765 ILCS 140/1 (2), (5), (6).

The language of this statute expands damages to more than just repairs to the adjoining land and structures, and also to business losses and economic related expenses of occupants and tenants which are usually excluded under common law.

This liability also extends to state and local governmental agencies. There is no case law that concludes that sovereign immunity (the rule of government immunity to legal action for liability) prevents the application of ALEPA to state and local government.

The City of Chicago excavation lateral support regulations which exceed ALEPA.

The City of Chicago (the City) has its own excavation regulations which may create additional liability. *Bockweg v. Konopiots*, 2013 IL App. (1st) 121112 is an action brought under Illinois Municipal Code and Chicago Municipal Code regarding excavation requirements. The Chicago excavation regulations contain additional requirements for notice, bracing and liability when compared to the state law of ALEPA. See Chicago Municipal Code §13-124-380 et seq.

The City regulations include requirements for thirty days advance notice of excavation to neighboring properties and the alderman, §13-124-390; bracing of neighboring structures within 5 ft of the excavation, §13-124-400; fencing in certain circumstances, §13-124-411; and insurance requirements, §13-124-420.

Unlike ALEPA, the City regulations allow declaration of liability upon contractors as well as new construction owners. As a result both owners and contractors can be declared to be jointly liable for "any damage, death, or injury caused by sagging, settling, cracking or collapsing of the public way or of the foundation or walls of a structure located within 5 ft of the excavation, due to absent or insufficient reinforcement or bracing or due to any other act or omission in the performance of such excavation." §13-124-410. This would include costs of salvage, relocation, temporary housing and costs incurred by the City.

Additionally, violators are subject to penalties including fines from $1,000-$10,000 for each offense not resulting in the injury or death of any person and misdemeanor criminal liability; and a fine of at least $10,000 for excavation resulting in the injury or death of any person, and license revocation. §13-124-440.

The Chicago regulations expressly exempt the City, but not its contractors, from the notice and insurance requirements under the City Municipal Code. §13-124-450.

The strict liability problem under ALEPA and the City's Municipal Code.

Generally, the doctrine for strict liability does not apply to construction activities in Illinois. Construction activities in most construction projects do not meet the definition of a "product" under Section 402A of the Restatement of Torts, and, therefore, such activities should not give rise to strict liability actions. Typically, legal texts such as the Restatement of Torts provide that strict liability is usually involved in litigation over the manufacture of "products." If a construction project is not considered a "product," one would presume that there cannot be strict liability which would result from construction activities.

Some might determine that this universally removes strict liability (or the risk of liability without negligent acts) from the construction context altogether. However, the obligations under ALEPA and City's ordinance are statutory obligations, which if breached, give rise to strict liability for new project owners based upon the language of these written laws.

The Illinois Appellate Court explored the history and intent of ALEPA in the case of *Proud v. W. S. Bills & Sons, Inc.*, 119 Ill. App. 2d. 33 (1970). Based upon a reading of the *Proud* case, it is possible to read ALEPA as a combination of a statutory claim and a tort claim. This means that statutory liability could arise based upon failure to meet the requirements of the written statute or tort liability could arise if a new project owner fails to meet the common law. The mere fact that a new construction owner unintentionally fails to meet the requirements of the written statute (ALEPA) would be construed as strict liability.

Therefore, the response from the affected abutters thus may be that there are indicators that ALEPA creates its own statutory right of action under strict liability. For example, ALEPA provides specific damages for injuries arising out of violations of its terms.

Remedies for abutters under ALEPA parallels common law relief but does not state that it authorizes a type of tort claim directly, and thus ALEPA can be construed to create strict liability. There is anecdotal support for this interpretation in that ALEPA claims are often asserted in lawsuits against violators with a combination with, and separate from, a tort claim. See for example the case of *Chicago Province of Society of Jesus v. Clark and Dickens*, LLC, 383 Ill. App. 3d 435 (1st Dist. 2008), in which claims are alleged including ALEPA, negligence, and Illinois Municipal Code and Chicago City Code violations regarding building collapse caused by neighboring excavation.

Commercial insurance products to cover third party and abutter liability risks.

The type of insurance and exclusions under insurance coverage are also important to review before engaging in an excavation project. A self-insured retention (SIR) is an amount that must be paid by the insured before the insurance policy will apply to a covered loss under a commercial general liability policy (which policies provide coverage for third party claims). An SIR is a form of coinsurance commonly used in the construction industry to offset premium costs, but creates a level of coinsurance on the part of the insured which the insured must pay, up to the SIR limit, before insurance takes effect under the policy. Contractors should be aware of these coinsurance limits because they can apply per claimant. In the case of a large SIR limit, combined with an event involving multiple parties, the SIR could eliminate insurance coverage and passing of risk to a contractor's or design professional's insurance company.

One should also review the scope and provisions of coverage under an insurance policy. Various endorsements to the policy which change the policy terms may eliminate coverage. For example, some insurers endorse liability policies to eliminate coverage for property damage caused by earth subsidence or movement. When a contractor is performing work that might be implicated, especially when performing

foundation work, it is particularly important to specify that coverage for earth subsidence and movement are included in the policy terms.

Attention should also be paid to Explosion, Collapse, or Underground coverage, which is usually modified by insurance carriers. Many carriers eliminate this coverage by endorsement to eliminate coverage for explosion, collapse, or underground risks (known as XCU risks). If those risks are implicated in a project, it is good practice to specify that the XCU endorsement eliminating coverage will not be allowed.

BEST PRACTICES

There is a spectrum of approaches to protecting abutters' structures and mitigating the potential for damage and delay. The project team for the new construction is in the best position to establish criteria and expectations for the work. Approaches can range from reactive to proactive; a proactive approach invariably sets better project expectations and provides enhanced awareness and protections for existing adjacent structures. The two extremes are presented in the table below.

Table 1 – Approaches to Mitigate Issues Associated with Adjacent Construction

Potential Action	Reactive Approach	Proactive Approach
Open Communication with Neighbors	No discussion of means and methods of the work, and potential impacts on neighboring structures.	Establish meetings prior to construction with neighbors to explain potential impacts on neighboring structures, and expectations to mitigate those impacts.
Knowledge of Construction of Adjacent Building	No research or investigation to understand conditions or potential risks.	Obtain information on superstructure and substructure through walkthroughs, construction drawings, test pits, or other methods.
Knowledge of Soil and Groundwater Conditions	No understanding or effort to obtain this information.	Obtain information through existing records or through subsurface explorations.
Documentation of Before and After Conditions	No site walkthroughs of neighboring structures.	Perform pre-construction condition assessments, with photos, to compare with conditions during- and post-construction.
Instrumentation to Monitor Performance of New Work and Adjacent Structures	No instrumentation program established to evaluate ground movement, structure movement, earth support system movement, groundwater levels, or vibration levels.	Develop an appropriate instrumentation and monitoring program to evaluate ground movement, structure movement, earth support system movement, groundwater levels, and/or vibration levels. Establish response levels for instrumentation data to provide early warning when adjustments in new construction might be necessary. Share data with abutters to encourage open communication.

The proactive approach results in educated and informed parties, including the project team for the new construction and the abutters. As a result, all parties are in a better position to understand and mitigate risks, identify problems, and collaborate to make corrections as the work proceeds. This collaborative and informed approach can effectively mitigate damage, associated costs and delays, and potential litigation.

CASE STUDY OF A PROACTIVE APPROACH

On an urban site where two buildings partially share the property line, a developer planned to demolish an old building and replace it with a new structure with a 25 ft deep basement/parking area. The existing, adjacent structure consists of load-bearing, mass-masonry walls supported by shallow footings. The basement for the new structure extended more than 15 ft below footings of the existing building, and in some locations the footings were right on the property line. Fig. 1 illustrates site conditions.



Fig. 1 – Building to be demolished on right, adjacent structure to the left.

Before construction, the developer understood the risks of the construction process, and actively engaged in discussions with the abutter about potential risks. The abutter's engineer reviewed the proposed demolition and excavation support plans and worked collaboratively with the developer and developer's engineer prior to and during construction. As a group, the team defined risks, developed expectations, and set requirements for the construction work to mitigate potential impacts from the adjacent work. Involvement of the abutter and the abutter's engineer positively affected the protection and monitoring of the adjacent structure, and included the following:

- Review of pre-construction condition surveys and supplemented the surveys with photo and video documentation.
- Periodic monitoring during demolition to assess if the work was being performed in accordance with the approved submittal.
- Performance of test pit excavations to confirm existing foundation assumptions and documented the soil and foundation conditions in the pits.
- Analysis of potential excavation-induced building movements, which led to modifications to the excavation support design (Fig. 2) and building movement monitoring during construction.



Fig. 2 – Proximity of excavation to existing adjacent structure.

- Identification of threshold and limiting movement values to minimize potential distress that may manifest on the adjacent structure.

- Review of survey data to evaluate building performance during the excavation work.

- Evaluation of post-construction photographs of the adjacent structure to identify changes from pre-construction conditions that could have been related to the construction activity.

This collaborative and proactive approach, while adding costs and time to the construction process, effectively identified concerns, set expectations, and allowed the construction to proceed without significant incidents. It is the uncollaborative and reactive approach that is far more likely to result in problems. Problems that develop during construction have the potential to substantially increase construction costs, introduce unexpected repair costs due to adjacent structure damage, and in turn cause costly construction delays and potentially litigation.

In situations where the abutter is not willing to engage with the team for the new construction, the owner, contractor, and design team should still be proactive in communicating to the owner the process and measures taken to protect against damage. Detailed planning and records are a strong hedge against future claims.

SUMMARY AND CONCLUSION

Construction professionals need to be aware of the risk associated with adjacent construction projects, particularly excavation projects, adjacent to existing structures. In Chicago, strict construction liability for owners, contractors and engineers exists based upon state statutory and local city ordinances and regulations. These risks are passed on by new construction owners to contractors and construction professionals through the procurement documents. Failure to be aware of state and local laws and taking proactive approaches can result in third-party damages, increases in project costs, and repairs that escalate construction costs and cause delays. In certain cases, project costs can further escalate from damage to abutters' property, as attorney's fees (especially under the Chicago Municipal Code) can also be awarded.

Best practices for a successful project include understanding and planning for the technical, legal, and insurance risks, engaging and educating abutters prior to and during construction, and monitoring construction to allow for appropriate course correction as issues arise.

NUMERICAL ANALYSIS IN ASSISTING CRANE PAD DESIGN AND UNDERGROUND UTILITIES EVALUATION

Yao Zhang, Ph.D., P.E., Terracon Consultants, Louisville, Kentucky, USA, (502)-365-9733, yao.zhang@terracon.com
Yazen Khasawneh, Ph.D., P.E., Terracon Consultants, Louisville, Kentucky, USA, Yazen.Khasawneh@terracon.com

ABSTRACT

Upgrading and maintenance programs were proposed at a power generating plant in Indiana. To perform construction activities associated with the proposed upgrading and maintenance, a LR11350 crawler crane with a dead load of 1,500 ton was required in the vicinity of existing plant structures. The contact pressure from the crane tracks for the heaviest lift, maximum reach and angle (worst loading condition) were estimated by the rigging engineer to be on the order of 84 psi. Several concerns were raised regarding the total and differential settlements while the crane is in operation and the induced stresses on existing underground utilities due to crane loads. Three-dimensional finite element simulations were conducted using hardening soil model for the subsurface soils and elastic model for the other structural elements (underground utilities and crane mats) to optimize the configuration of the proposed crane foundation. It was found 1-foot thick engineered steel mats underlain by a 1.5-foot thick crushed stone pad will provide enough support to the crane. It will also control the settlement to the allowable limit and maintain the stresses in the underground utilities within tolerance.

Keywords: Crane Pad, Underground Utilities, Finite Element Analysis, Local Buckling, Ovality

INTRODUCTION

A LR11350 heavy lift crawler crane was proposed as part of an upgrade program at an existing power plant in the state of Indiana. The proposed crane will be sitting on an open ground in the vicinity of existing plant facilities, with multiple underground utilities going beneath the proposed footprint of the new crane pad. The existing utilities are of diverse kinds, including sanitary sewer corrugated metal pipes, electrical conduits and variable steel water/oil drain pipes. The safety and functionality of these underground utilities are critical to maintain the proper operation of the power plant. Therefore, the design of the new crane pad foundation system is of essential to control the ground settlement and the imposed stresses to the existing utilities (Davie et al., 1998, Scott 2017).

To ensure all utility locations and depths are identified, the proposed footprint was thoroughly surveyed. Information in regard to each identified utility was provided by the owner. Subsurface explorations were conducted using geotechnical soil borings and soundings to evaluate the ground conditions and generate soil profiles. Numerical simulation and analysis utilizing finite element method were performed to design the crane pad foundation system and evaluate the responses of the utilities. This paper summarizes project information, geotechnical conditions and then focuses on the finite element analysis in assisting the design of crane pad and the utilities evaluation.

CRANE DESCRIPTION

The proposed crane to be erected is a LR11350 crane manufactured by Liebherr with a dead load of 1,500 tons, shown in Fig. 1. The contact pressure from the crane tracks for the heaviest lift, maximum reach, and angle (worst loading condition) was estimated to be 84 psi (12,096 psf). The general information of the

© 2019 Deep Foundations Institute

crane is listed in Table 1.

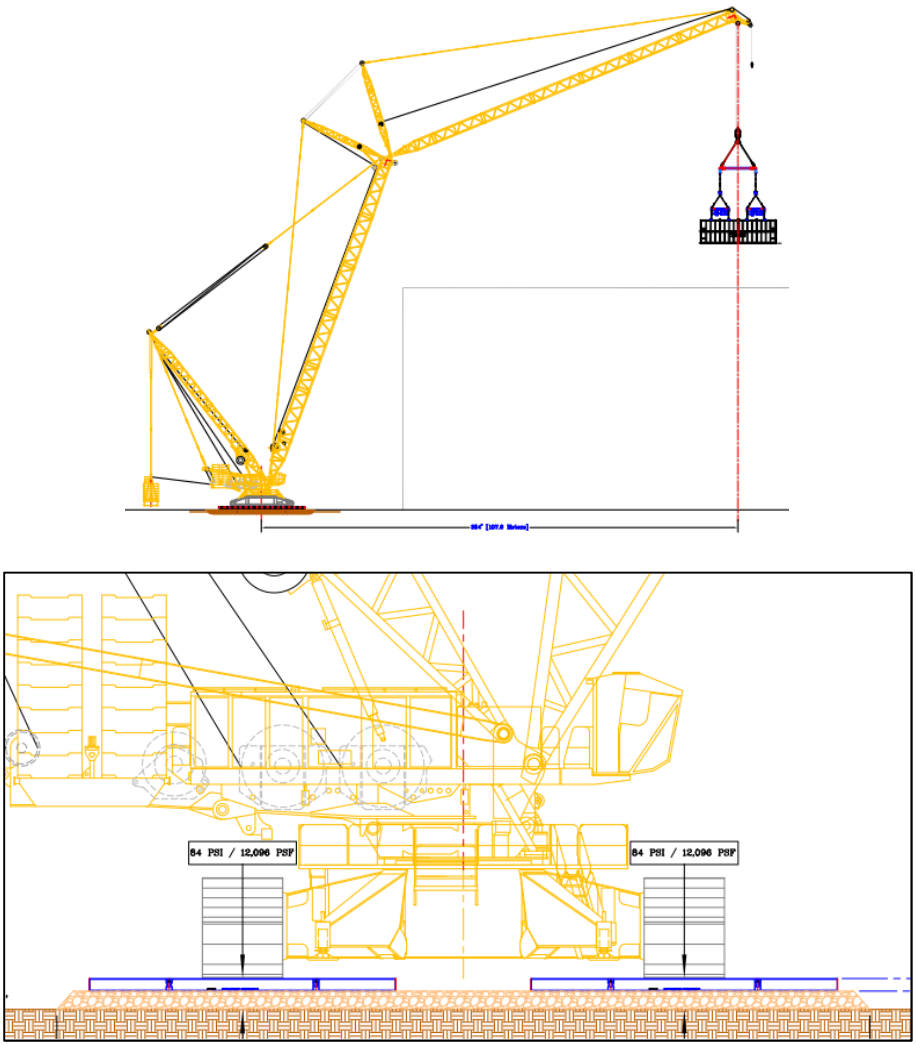


Fig. 1 LR11350 crane and foundation

Table 1. Maximum Contact Pressure and Track Dimensions

Crane	Max Contract Pressure (psi/psf)	Track length (ft)	Track Width (ft)
LTR11350	84 / 12,096	50	5.9

SUBSURFACE CONDITIONS

Three geotechnical soil borings with Standard Penetration Testing (SPT) were advanced to 100 feet below ground surface and four Automatic Dynamic Cone Penetration sounding (ADCP) were conducted to depths of 5 to 30 feet below ground surface at the site to explore subsurface soil conditions. In general, the test borings encountered approximately10 feet of existing fill, which was comprised of poorly graded sand trace gravel. Native soils underlying the fill generally consisted of poorly graded sand with gravel and silt. The water levels observed at the soil borings were at about 33.5 ft below ground surface. The soil profile is summarized in Table 2.

Table 2. Subsurface Soil Conditions

Layer No.	Soil Layer Bottom (ft)	Soil Description	Averaged SPT Blow Counts	Density
1	10	Fill – Poorly graded sand, trace gravel	15	Medium Dense
2	25	Poorly graded sand with silt and gravel (SP-SM)	35	Dense
3	33	Poorly graded sand with gravel (SP)	80	Very Dense
4	37	Poorly graded (SP)	3	Very Loose
5	70	Poorly graded sand with gravel (SP)	15	Loose

UNDERGROUND UTILITIES

The underground utilities on site vary on diameter, cross-sectional area, and material with depths ranging from approximately 2.5 feet to 8 feet below existing grade. A list of the utilities considered in the analysis are shown in Table 3. The locations of utilities with respect to the proposed crane pad can be found in Fig.2.

Table 3. Underground Utilities

Utility No.	Description	Depth (ft)	Diameter (in)	Wall Thickness (in)	Material
1	Sanitary Sewer	8	10	1.8	ARMCO
2	Seal Water	5.5	3	0.22	Steel
3	Fire Protection	4.5	12	0.28	Steel
4	Electrical	5	15	0.35	Steel
5	CDTS	7.5	6	0.312	Steel
6	Storm Drain	2.5	18	0.079	Corrugated Metal
7	Ignition Oil Drain	5	3	0.25	Steel
8	BRNR Deck Drain	4.5	6	0.28	Steel
9	Ash Handling Water Supply	4.5	10	0.32	Ductile Iron
10	CDTS	6	2	0.25	Steel
11	DR Drain	4.5	4	0.26	Ductile Iron
12	Sanitary Sewer	8	6	1.0	ARMCO
13	Pyrites Tank Overflow	4	14	0.36	Ductile Iron

NUMERICAL ANALYSIS

Soil-structure interaction nonlinear analyses were conducted to estimate the ground settlement and the induced stresses on the underground utilities due to the crane loading.

Method of Analysis

The analyses were carried out using the 3-dimentional commercial Finite Element (FE) software MIDAS GTX NX. The model included the proposed engineered crane mats, newly placed crushed stone pad-on-grade, ground soil profile, and existing underground utilities. The element selection for the various parts of the model is presented in Table 4. The finite element model is shown in Fig. 2.

Table 4: Elements Utilized in the Analyses

Item	Modeled Element
Engineered Steel Mats	2D Shell Element
Pad and Subgrade Soils	3D Solid Element
Underground Utilities	1D Embedded Beam Element

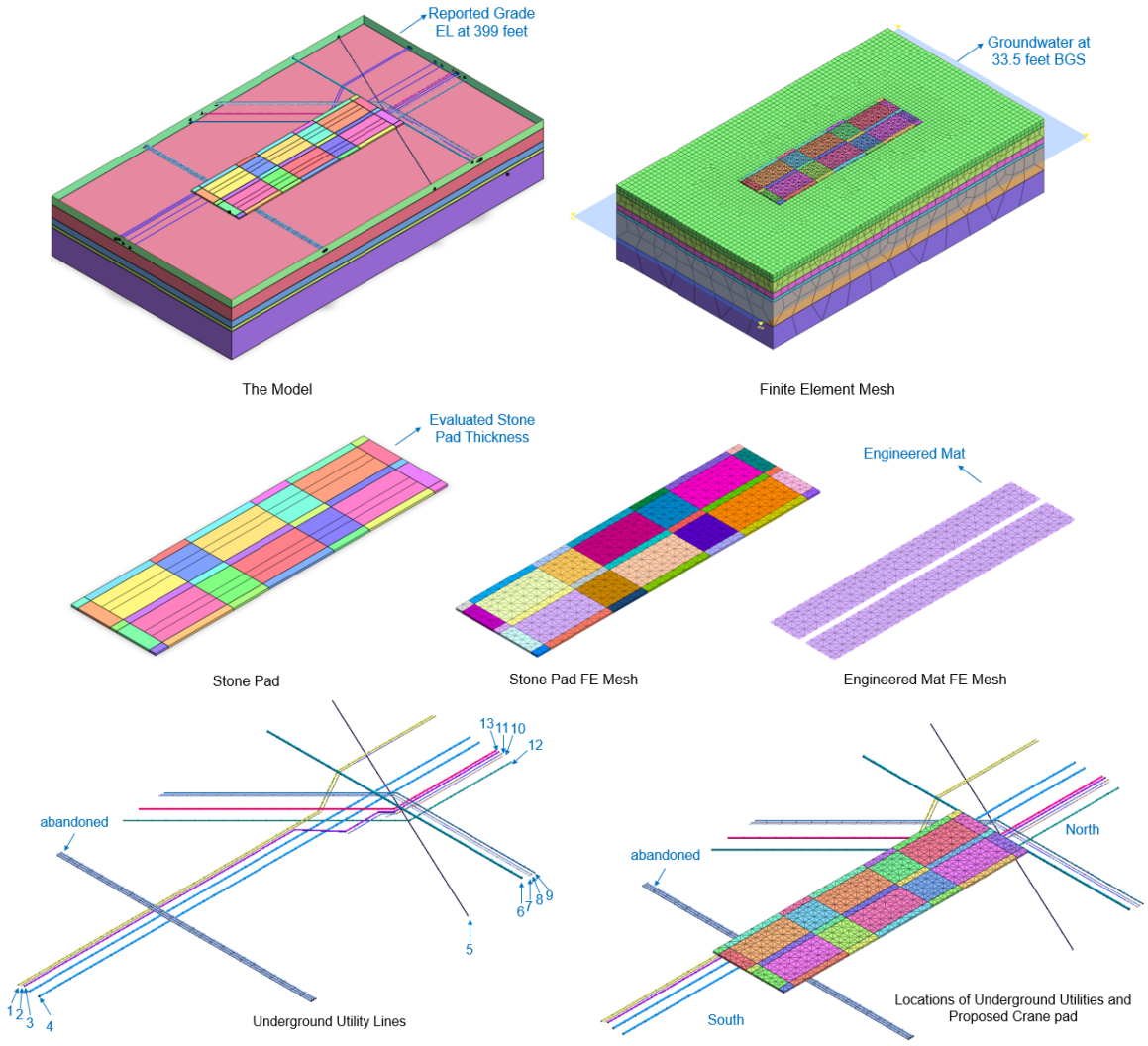


Fig. 2 Finite Element Model

Constitutive Models

The hardening soil constitutive model (Schanz et al., 1999) was used to model the behavior of the subgrade granular soils. The hardening soil model is a nonlinear elastic-plastic model with a hyperbolic stress-strain relation and associative flow rule. It requires three moduli values at a reference pressure to identify loading (E_{50}^{ref}), unloading/ reloading (E_{ur}^{ref}), and hydrostatic loading (E_{oed}^{ref}). The crushed stone pad was modeled as an elastic perfectly plastic material, which assumes a linear elastic relationship and obeys Mohr-Coulomb yield condition. The engineered crane mats and all underground utilities were modeled as isotropic elastic material.

Model Parameters

The hardening soil parameters were estimated based on empirical correlations using the subsurface exploration results (Khasawneh and Sabatini, 2017). The initial effective tangent modulus was calculated based on Kulhawy and Mayne (1990). The material parameters used in the analysis are shown in Table 5.

Table 5. Model Material Parameters

Subgrade Soils (Hardening Soil Model)										
Layer No.	Soil Layer Bottom (ft)	γ (pcf)	ϕ (°)	σ'v0 (psf)	κ	E_{50}' (psf)	E_{50}^{ref} (psf)	E_{ur}^{ref} (psf)	E_{oed}^{ref} (psf)	m
1	10	105	30	525	525	275625	1102500	3307500	1102500	1
2	25	110	36	1875	795	788765	834750	2504250	834750	0.5
3	33	110	40	3140	975	1251841	1023750	3071250	1023750	0.5
4	37	115	28	3716	435	607615	343340	1030025	343340	1
5	70	120	30	4772	525	830975	365685	1097060	365685	1

Crushed Stone Pad (Mohr Coulomb Model)				
Layer	γ (pcf)	E (psf)	ϕ (°)	c (psf)
Crushed Stone	140	1087470	45	0

ANALYSIS RESULTS

The finite element analyses were performed as a series of construction stages. These stages comprise:

- defining the geostatic stresses in the ground (considering ground water table at 33.5 feet bgs),
- installing all underground utilities,
- placing the crushed stone pad and installing the crane mats,
- applying the crane loads

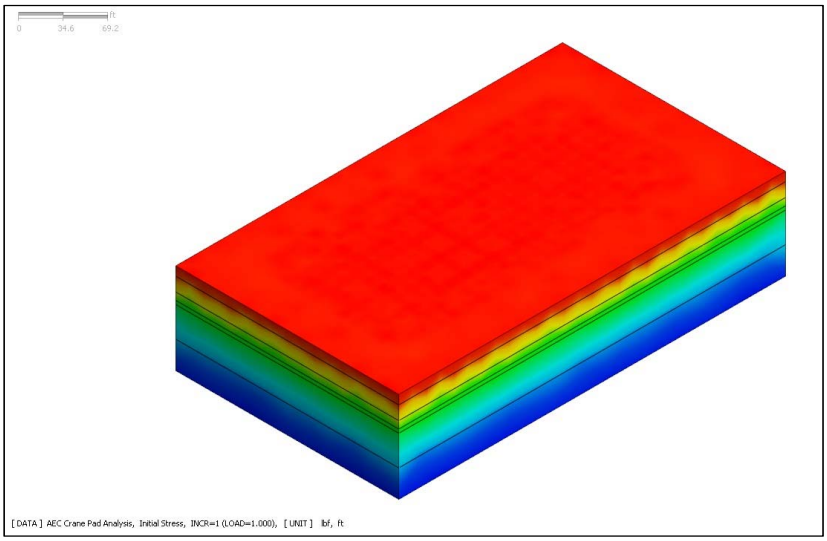
Ground Pressure and Settlement

Three loading cases were analyzed for the crane being seated on three different locations on the pad (North end, Center and South end). Cyclic loading was not considered as the crane moves very slow and is supposed to be sitting statically for operation. Based on the rigging engineer's instructions, the analyses were conducted for the worst-case scenario of 84 psi on both of the crane tracks (dead weight + maximum lift). Various foundation options were evaluated for the crane pad system to minimize the total and differential settlements and to control the ground pressure. The dimension of crane track, crane mat and stone pad used in the analysis are listed in Table 6. Options of 1-foot thick timber mat and 1-foot thick engineered steel mat with crushed stone layer were evaluated.

Table 6: Dimensions Used in the Analyses

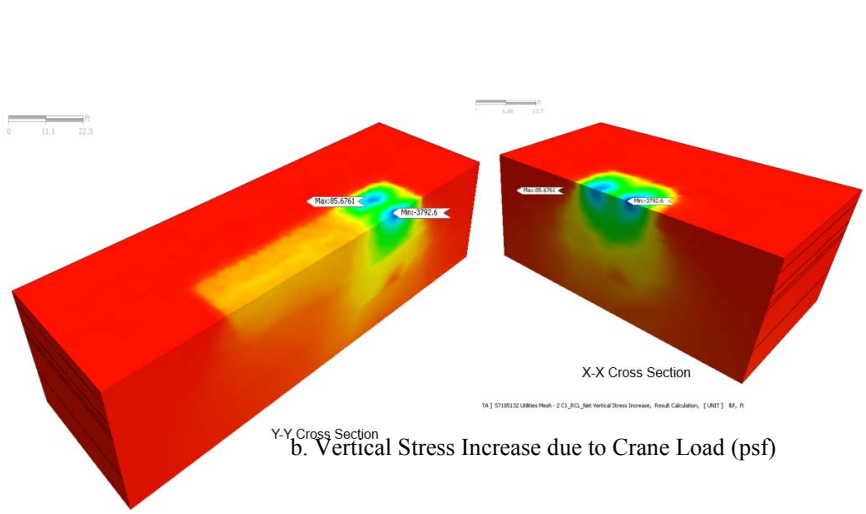
Item	Length (ft)	Width (ft)
Crane Track (X2)	50	5.9
Crane Mat (X2)	225	25
Stone pad	225	65

Based on the analysis, 1-foot in thickness timber mat would not reduce the imposed ground pressure to less than 4,000 psf as required for bearing capacity and the total settlement exceeds 2.0 inches. 1-foot thick engineered steel mat (I-beams) with 1.5-feet thick crushed stone pad was then evaluated and should provide sufficient thickness so that the total ground settlement is less than 2.0 inches. The induced maximum ground pressure from the crane lifts is approximately 3,500 psf. The analysis results for the crane being seated on the north end of the pad (worst case) are shown in Fig. 3.

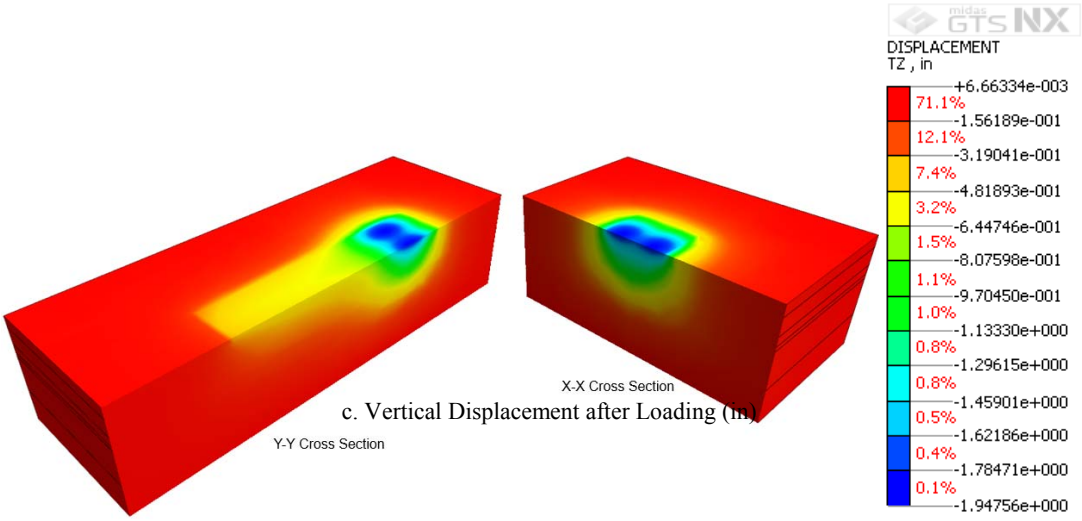


The % was to show the percentage of specific color out of all the colors.

a. Initial Vertical In-Situ Total Stress (psf)



b. Vertical Stress Increase due to Crane Load (psf)



c. Vertical Displacement after Loading (in)

Fig. 3 Finite Element Results

Responses of Underground Utilities

The analyses assumed that the underground utilities are in good condition with no leaks or severe defects.

Stresses and Deflections: The responses of the underground utilities under the crane load was obtained from the finite element analysis and the stress demands were evaluated to make sure they are within the capacity. Maximum stress and vertical deflection of the utilities induced by the increased ground pressure from crane load are shown in Fig. 4.

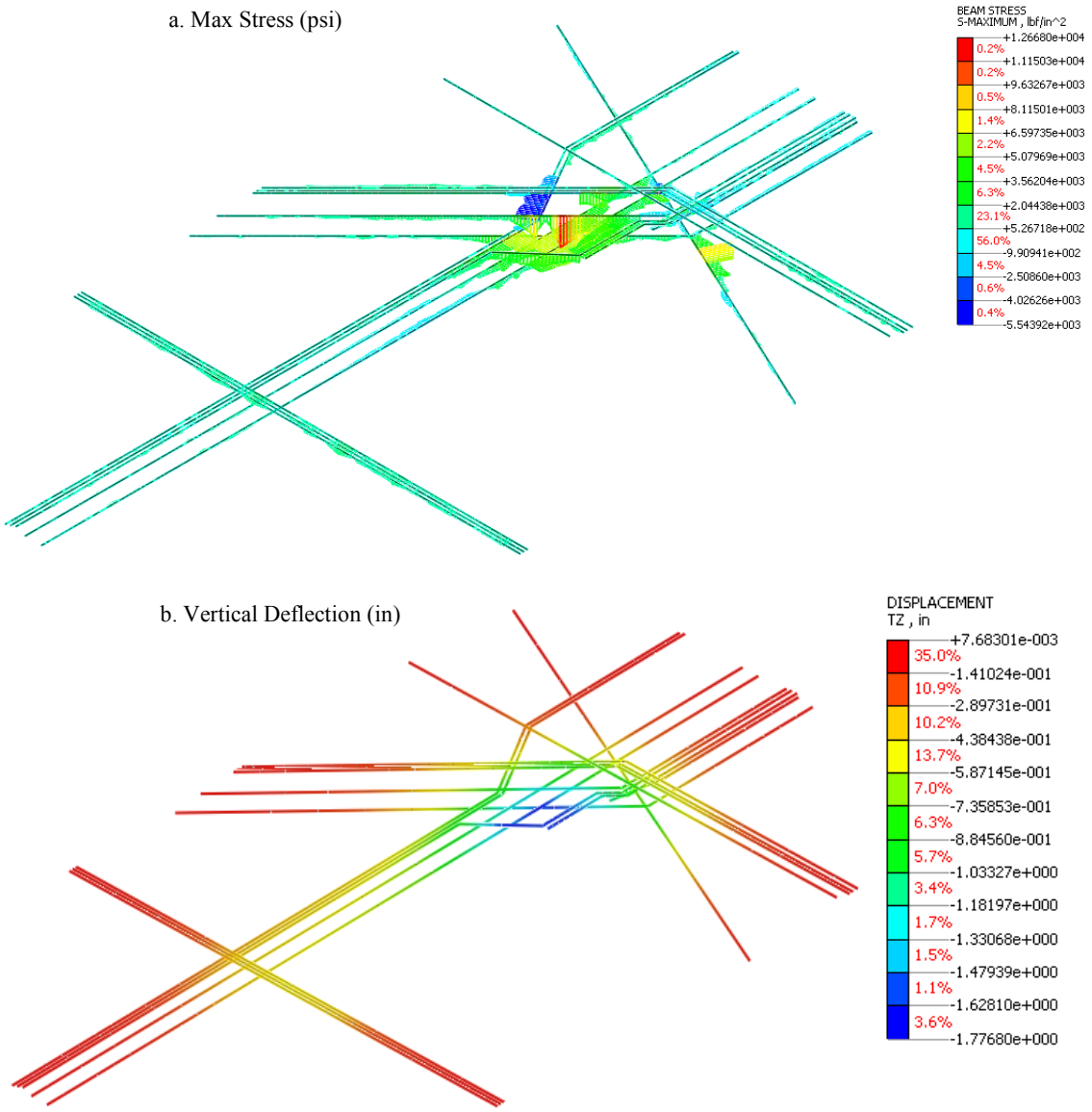


Fig. 4 Maximum Stress and Vertical Deflection in Utilities (FE Results)

The bending moment, shear forces, demand and deflection within each utility are summarized in Table 7.

Local Deformation and Buckling: Local deformation and buckling were analyzed based on the finite element results. For utility No.6 which was reported to be a corrugated metal pipe, the resistance to buckling

was evaluated based on *AASHTO LRFD Bridge Design Specifications, 2017, Section 12, Buried Structures and Tunnel Liners*. The critical buckling stress is calculated using the following equations.

$$IF\ S < \left(\frac{r}{k}\right)\sqrt{\frac{24E_m}{F_u}},\ \text{then}\ f_{cr} = F_u - \frac{\left(\frac{F_u kS}{r}\right)^2}{48E_m} \quad [1]$$

$$IF\ S > \left(\frac{r}{k}\right)\sqrt{\frac{24E_m}{F_u}},\ \text{then}\ f_{cr} = \frac{12E_m}{\left(\frac{F_u kS}{r}\right)^2} \quad [2]$$

where S is the diameter of pipe or span of plate structure (in); E_m is the modulus of elasticity of metal (ksi); F_u is the tensile strength of metal (ksi); f_{cr} is the critical buckling stress (ksi); r is the radius of gyration of corrugation (in); k is the soil stiffness factor taken as 0.22 as suggested in *AASHTO LRFD Bridge Design Specifications*, 2017.

The local ring buckling for all other utilities were evaluated based on the *AASHTO LRFD Bridget Design Specifications, published in 2017*. The local buckling critical pressure for each underground utility were calculated using equation 3.

$$\frac{1}{FS}\sqrt{32R_w B' E' \frac{(EI)_{eq}}{D^3}} \quad [3]$$

where *FS* is factor of safety, with the suggested value of 2.5 for C/D is equal or greater than 2 or 3.0 for C/D is less than 2. $R_w = 1 - 0.33(h_w / \mathrm{C})$, for $0 < h_w < C$ is water buoyancy factor; B' is empirical coefficient of elastic support (dimensionless). B' was given in *AWWA Manual 11*, *steel pipe – A Guide for Design and Installation* as in equation 4.

$$B' = \frac{1}{1 + 4e^{\left(-0.065\frac{C}{D}\right)}} \quad [4]$$

The local ring deformation, also known as ovality was evaluated using equation 5.

$$\frac{\Delta y}{D} = \frac{D_l KP}{\left(\frac{(EI)_{cq}}{R^5} + 0.061E'\right)} \quad [5]$$

where D is pipe outside diameter (in); Δy is vertical deflection of pipe (in); D_l is deflection lag factor (~1.0-1.5); K is bedding constant (~0.1); P is total pressure on pipe due to soil load P_v plus live load P_p

(psi); R is pipe radius (in); $(EI)_{cq}$ is equivalent pipe wall stiffness per inch of pipe length (in/lb.); E' is modulus of soil reaction (psi).

Table 7 below presents a summary of the result for each utility with combined stress demand from bending moment and shear force, estimated global and local deflections as well as factor of safety against local buckling.

Table 7. Model Material Parameters

Utility No.[a]	M (in*lb)	V_{max} (lb)	$\delta_{v,max}$ (in)	Demand [b] (psi)	Ring Deflection (%)	Buckling Critical Pressure (psi)	Buckling Pressure (psi)	Factor of Safety against Buckling
1	3700	180	0.9	30	0.17	59890	65	982
2	1700	50	1.25	4500	0.03	19735	145	136
3	87500	2600	2.05	4200	0.15	2510	450	5
4	250000	2500	2.0	8000	0.15	2450	450	5
5	16600	290	0.9	8300	0.06	10400	210	50
6	389000	6300	0.8	2800	0.02	50230	240	211
7	2300	70	1.0	5300	0.02	23130	125	185
8	25800	400	0.95	4500	0.08	7800	245	32
9	95000	1400	0.8	4200	0.13	4075	355	11
10	740	30	1.25	2200	0.01	52200	90	602
11	3100	140	2.0	3500	0.04	14110	175	81
12	517000	2800	1.90	8100	0.10	60890	70	925
13	557750	8240	1.7	12700	0.15	2795	430	6

a. See Fig.2 for Utility numbers and Table 3 for Utility information
b. Stress due to combined axial and bending moment

SUMMARY AND CONCULSIONS

A new heavy lift crawler crane was proposed in an existing power plant where a series of underground utilities of multiple kinds were presented. An appropriate crane pad foundation system was needed to support the proposed heavy crane as well as keep the underground utilities safe and functioning. This paper presents a method of utilizing finite element analysis in assisting making engineering decisions to evaluate the behavior of underground utilities under additional loading.

Depending on the complexity of the problem, three-dimensional finite element model is generally recommended as both global and local capacity of the utilities will need to be evaluated. One-dimensional beam element can typically be used to model small section utilities less than 3 feet in diameter, which is capable of providing all internal forces including axial forces, shear forces and bending moment from solving the boundary value problem to evaluate global capacity. Local buckling stress and ovality deformation of the utilities can be evaluated using AASHTO criteria referenced in this paper.

For this case history, finite element analyses were conducted to evaluate the ground settlements below crane pad and imposed stresses on existing underground utilities. Analysis results indicate that total and differential settlements of the crane pad system using 1-foot thick engineered steel mat and 1.5-feet thick crushed stone would meet the manufacture's requirement. The global and local responses of underground utilities were analyzed based on the finite element results. The resulted demand in all utilities were tolerable for worst case loading conditions. The calculations also showed that local ring deformation for all utilities were within tolerance and local buckling is less likely to occur.

REFERENCES

Antaki, G.A. and Hart, J.D., 2001. Guidelines of the Design of Buried Steel Pipe. Report of American Lifelines Alliance with FEMA and ASCE.

AASHTO LRFD Bridget Design Specifications, the Eighth Edition, 2017 (ISBN: 978-1-56051-654-5).

Davie, J.R., Bell, K.R., Fitzsimmons, M.B. and Haggerty D.A., 1998. Heavy Crane Foundations on Soft Clay. Proceedings of Fourth International Conference on Case Histories in Geotechnical Engineering 1998, St. Louis, Missouri, PP. 228-231.

Khasawneh, Y.A. and Sabatini, P.J., 2017. Evaluation of Crane Pad Performance on Partially Improved Ground Adjacent to a Seawall, Proceeding of DFI Annual Conference 2017, New Orleans, LA, PP. 256-265.

Kulhawy, F.H. and Mayne, P.W., 1990. Manual on Estimating Soil Properties for Foundation Design, EPRI EL-6800, Project 1493-6.

Schanz, T., Vermeer, P.A., and Bonnier, P.G. (1999). "The Hardening-Soil Model: Formulation and Verification." R.B.J. Brinkgreve, Beyond 2000 in Computational Geotechnics, Balkema, Rotterdam, pp. 281-290.

Scott, M.A., 2017. Soil Bearing Capacity for Crane Loads. Report to the U.S. Department of Energy Office of River Protection.

PERFORMANCE MONITORING OF MIXED GROUND WORKING PLATFORM FOR A CCR SURFACE IMPOUNDMENT

Amir Ahmadipur, Geosyntec Consultants, Houston, Texas, AAhmadipur@Geosyntec.com
Ali Ebrahimi, PhD., P.E., Geosyntec Consultants, Houston, Texas, AEbrahimi@Geosyntec.com
Roneet Das, Geosyntec Consultants, Houston, Texas, RDas@Geosyntec.com
William Tanner, P.E., Geosyntec Consultants, Atlanta, Georgia, WTanner@Geosyntec.com
Paul J. Sabatini, Ph.D., P.E., D.GE, Geosyntec Consultants, Chicago, Illinois, PSabatini@Geosyntec.com
Jeremy M. Gasser, P.E., Geosyntec Consultants, Kennesaw, Georgia, JGasser@Geosyntec.com
Cuneyt Gokmen, P.E., Geosyntec Consultants, Kennesaw, Georgia, CGokmen@Geosyntec.com

ABSTRACT

There are safety concerns related to operation of heavy equipment over coal combustion residual (CCR) impoundments during construction of the impoundment closure programs. As part of a pilot study prior to a full-scale closure construction, an access pathway and working platform were designed and constructed to facilitate equipment access for construction of deep soil mixing (DSM) zones on the ash delta of a CCR impoundment. The access pathway and working platform was constructed using shallow mass mixing with cement at the CCR surface to address safety concerns related to the geotechnical behavior of CCR. This paper describes the data from the instrumentation system which was implemented to monitor the geotechnical performance of the CCR during the pilot study. The instrumentation system included monitoring of the ground movement, vibration, and porewater pressure within the ash delta of the CCR impoundment during a pre-construction load testing, equipment mobilization over the access pathway, and DSM column installation over the working platform.

Keywords: performance monitoring, working platform, CCR impoundment, deep soil mixing

INTRODUCTION

A deep soil mixing (DSM) pilot study was conducted at a coal combustion residual (CCR) surface impoundment to evaluate mix designs and construction techniques for the regulatory closure. The DSM columns will create a wall which will separate and retain the CCR in a consolidated footprint separate from the closure by removal portion of the footprint and provide a barrier between the two areas of the surface impoundment. Historically, the surface impoundment received CCRs including fly ash, bottom ash, boiler slag, and gypsum, along with other byproducts produced from flue gas desulfurization (FGD). The predominant CCR in this impoundment were fly ash and bottom ash.

The primary goals of the DSM pilot study were to assess the mix design strengths and to evaluate DSM construction techniques that could reach the design mixing depths of up to 90 ft. The DSM test columns were installed on the CCR delta approximately 500 ft from the nearest impoundment dikes. Another objective of the pilot study was to develop, construct, and monitor an access pathway for safe passage and movement of construction equipment on the CCR delta.

The soft CCR deposits in the area of the proposed DSM pilot study required the design and construction of the access pathway and working platform to allow the DSM rig and support equipment to reach the DSM pilot study platform. The access pathway and DSM platform consisted of a 5-ft thick mass mixed stabilized CCR with minimum unconfined compressive strengths of 28 psi, overlain by a 1.5-ft-thick layer of coarse aggregate base. A layer of geogrid was installed between the coarse aggregate base and the mass mixed stabilized layer.

© 2019 Deep Foundations Institute

An instrumentation system was designed and implemented to monitor the geotechnical performance of the CCR during the DSM construction. The geotechnical instrumentation system included monitoring of the ground movement, vibration, and porewater pressure within the ash delta of the CCR impoundment during pre-construction load testing, equipment mobilization over the access pathway, and DSM column installation. The instrumentation system included a near real-time monitoring system to provide early alert notifications indicating unanticipated response.

SITE CONDITIONS

The subsurface stratigraphy at this site included, from top to bottom, up to 90-ft thick CCR layer, 20-ft thick alluvial deposits (native soil), partially weathered rock, and metamorphic crystalline bedrock.

The water level in the CCR delta was estimated for design based on a nearby monitoring well and the surface impoundment pool level, located approximately 1000 ft and 600 ft away from the work area, respectively. The depth to water level on the ash delta ranged from approximately 0 to 6 feet below ground surface and was primarily controlled by the surface impoundment pool level. The water level in the CCR was lowered to approximately 5 ft below the CCR surface at the working area prior to construction of the access pathway and was monitored throughout the construction and DSM pilot study.

SEQUENCE OF CONSTRUCTION

The access pathway and working platform were constructed with in-situ bucket mixing using a long-reach excavator to blend grout into the CCR. The construction sequence required that the long-reach excavator sit atop crane mats on previously mixed cells as the work progressed onto the ash delta. Mixing was completed in a cellular manner based on a proposed primary and secondary cell configuration.

After completion of the access pathway and working platform, a full-scale load test was conducted over the work platform using two tanks filled with water. The estimated equipment pressure from the DSM rig was approximately 1,000 psf. During a load test, the ground pressure of approximately 1,200 psf was applied by filling the tanks with water in 11 steps on a 21 ft by 8 ft contact area. Each load step was held for approximately 30 to 60 minutes while monitoring data was collected prior to consequent loading. The maximum load was maintained for approximately 2 weeks while automated instrumentation readings were collected. The tanks were then emptied in 5 load steps.

Following the completion of the first loading test (i.e., gradual step-wise test), a rapid load test was performed by filling the southern tank in one stage. The filling took approximately 48 hours.

The DSM rig was mobilized approximately 10 days after the completion of the working platform. The DSM rig was mobilized by placing 4 ft x 1 ft x 24 ft timber crane mats over the coarse aggregate base and gradually moving the rig from the perimeter dike toward the working platform with an approximate travel length of 500 ft. The DSM rig mobilization traversing the access pathway was completed in approximately 7 hours.

DSM column installation started 9 days after mobilization of the DSM rig on the working platform. Each DSM column was installed using two or three auger passes. Total of 6 DSM zones were constructed on the working platform. Zone 1 consisted of 3 DSM columns with a diameter of 8 ft and the other zones consisted of 5 DSM columns with a diameter of 5 ft. Different mix designs were used in the construction of each column.

GEOTECHNICAL INSTRUMENTATION SYSTEM

An instrumentation system was designed and installed along the access pathway and working platform to: (i) monitor the vertical and lateral deformation of CCR foundation along the access pathway to assess the capacity of CCR to carry the load from construction equipment during the DSM pilot study and construction activities; (ii) identify areas where unsafe conditions are developing (e.g., change in the rate of ground deformation, development of excess pore water pressure, or ground vibration); and (iii) provide real-time data when ground deformations or pore water pressures indicated unanticipated response or instability. The instrumentation system included monitoring of the ground movements, vibrations, and porewater pressures. Pore water pressures were monitored using grouted- vibrating wire (VW) piezometers. These piezometers were used to monitor the water level within the ash delta and subsequent increases in porewater pressure induced by construction equipment load or vibration. A total of 22 VW piezometers were installed at 6 nested locations. There were four nested piezometers under the access pathway, with each containing VW piezometers installed at 5 ft, 10 ft, and 20 ft below the mass mixed surface. The two nested piezometers within the working platform were installed at 5 ft, 10 ft, 20 ft, 30 ft, and 60 ft below the mass mixed surface. Figure 1 illustrates the location of each of these instruments and the location of DSM zones on the working platform.

Ground movements were measured using automated inclinometers and settlement profilers. Two settlement profilers (i.e., horizontal ShapeArrays) were installed along the access pathway and working platform centerline. The settlement profilers were installed at a 15-ft offset from the centerline of the access pathway in order to trace the two tracks of the DSM rig. Automated inclinometers (i.e., vertical ShapeArrays) were installed at two locations along the access pathway and three locations on the working platform.

Ground vibrations were measured to evaluate if construction equipment or operation of the DSM rig can cause vibrations and subsequently an unstable ground. Vibration monitoring units (VMUs) were installed at three location along the access pathway to monitor the ground vibration during the mobilization of the DSM rig to the working platform. Three VMUs were installed at the working platform to monitor the ground vibrations due to drilling and deep soil mixing.

Instrument data was recorded and monitored at various frequencies during the construction using Remote Monitoring Units (RMUs). Table 1 summarizes the frequency of data collection for various components of the instrumentation system using an automated data acquisition system.

Table 1. Frequency of data collection

Phase of Construction	Instrument	Data Collection Frequency
Load testing	Inclinometer	3 minutes
	Piezometer	
	Settlement Profilers	
DSM Rig Mobilization over Access Pathway	Inclinometer	30 seconds
	Piezometer	
	Settlement Profilers	
	Vibration Monitoring	Continuous (when peak particle velocity, PPV, exceeded 0.1 in/sec)
Installation of DSM Test zones	Inclinometer	3 minutes
	Piezometer	
	Settlement Profilers	30 minutes
	Vibration Monitoring	Continuous (when PPV exceeded 0.05 in/sec)

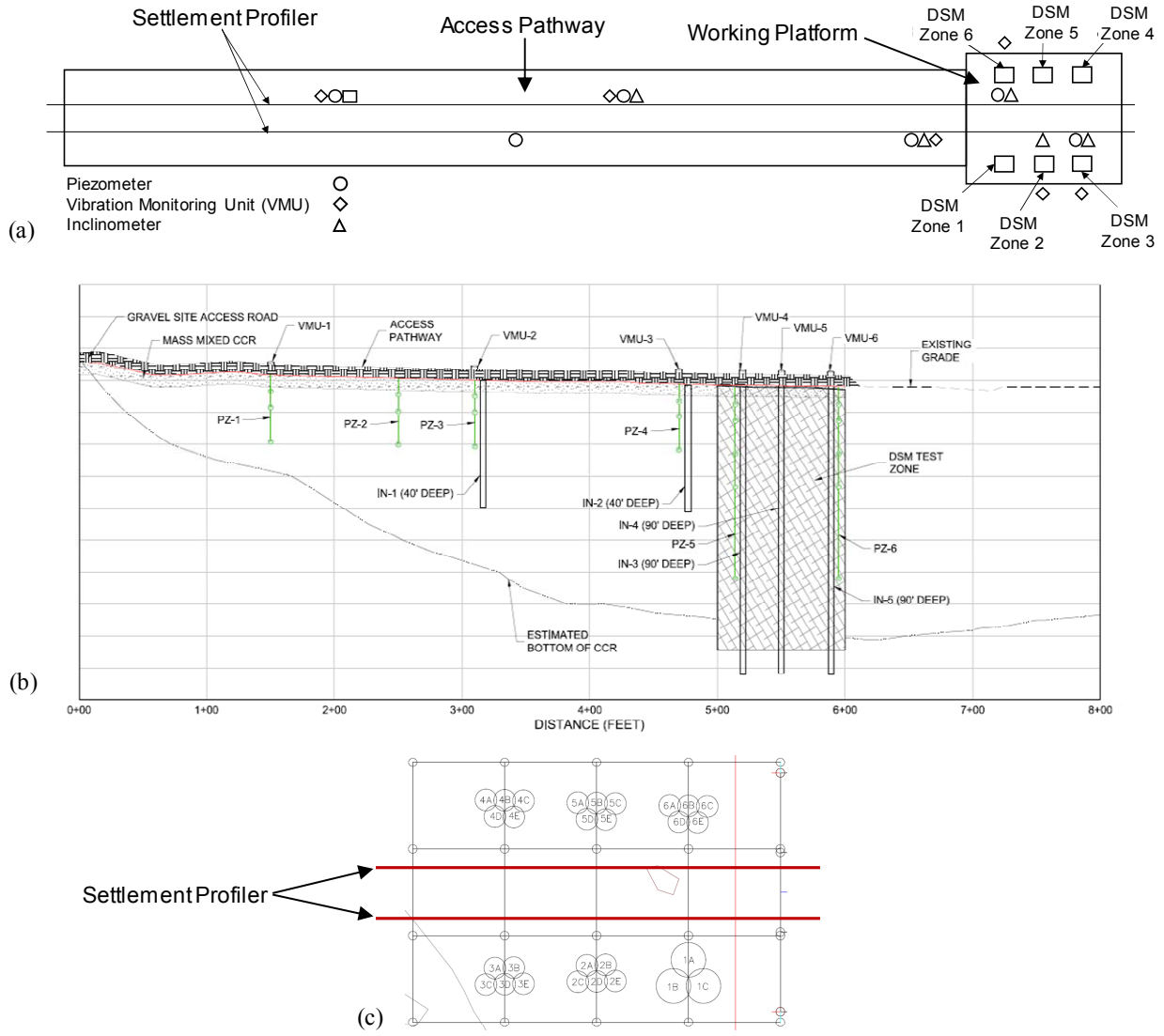


Fig. 1. (a) instrumentation plan view; (b) instrumentation profile, (c) DSM column locations

GEOTECHNICAL MONITORING RESULTS

Load testing

Figure 2 shows the development of pore water pressure and ground settlement during the load testing. In general, the maximum pore water pressure was measured at the end of load testing to be about 12 psf, equivalent to increased pore pressure ratio ($\Delta u/\Delta\sigma$) of 0.01. Δu is the developed excess pore water pressure due to total applied pressure of $\Delta\sigma$. The pore water ratio was due to the slow nature of the loading where most of the excess pore water pressure was dissipated after each loading step. The excess pore water pressure dissipation rate was in general quicker than the loading rate even at the rapid load test, resulting in approximately constant excess pore water pressure during loading. In Figure 2(b), the pore water pressure increase at day 10 when the load was constant, corresponds to the precipitation during the load test.

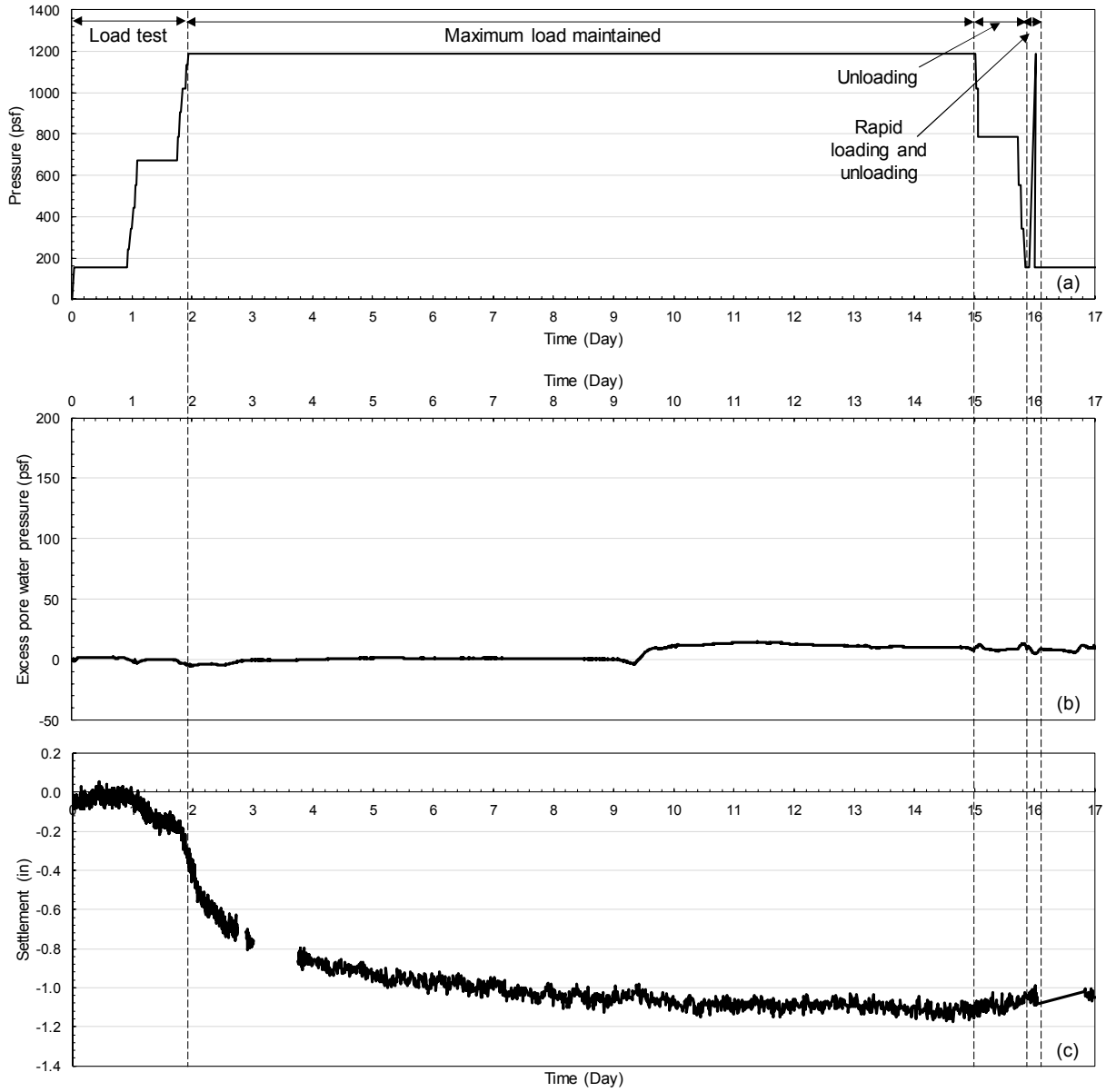


Fig. 2. (a) Load testing stages; (b) Pore water pressure variations during load test; (c) settlement at the middle of loading area during the load test

The settlement reached to approximately 0.2 inches at the completion of loading, however the settlement continued to 1.2 inches while the maximum load was maintained for 13 days. During unloading, approximately 0.05 inches of rebound was measured. During the rapid load test, settlement of less than 0.05 inches was observed, indicating over-consolidated CCR layers due to previous load test.

Figure 3 shows the settlement profile along the access pathway and working platform at the location of the load test. The measured maximum settlement of approximately 1.2 inches was directly under the load test with deformation reaching to 0.2 inches at about 40 ft from the center of the load test. The settlement measurement perpendicular to the working platform showed uniform deformation of 0.7 inches at the center of the load test.

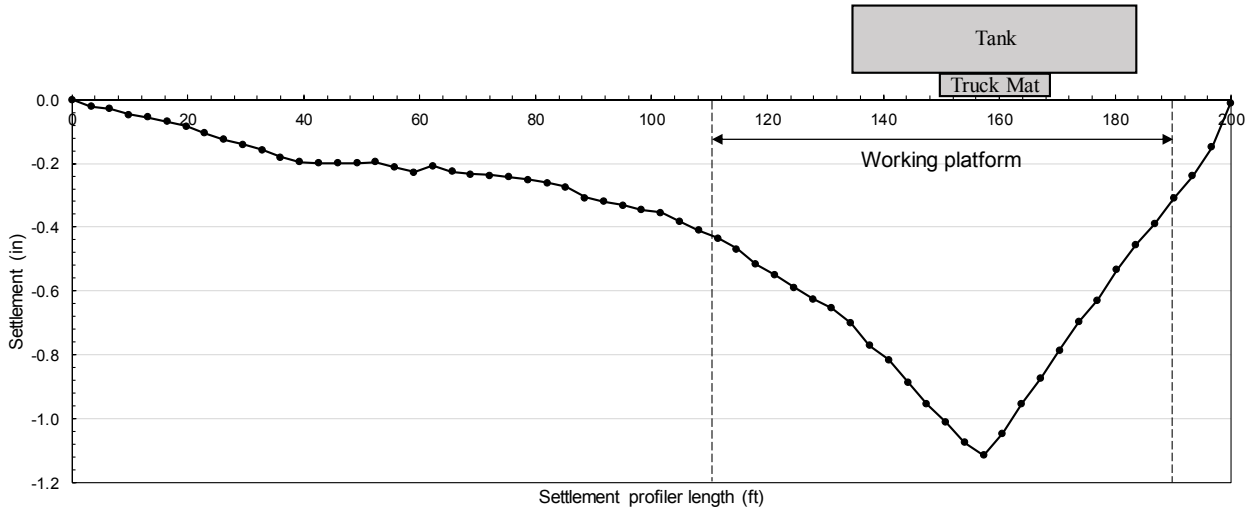


Fig. 3. Settlement profile along the access pathway and working platform

Construction equipment mobilization

The DSM rig was mobilized by placing timber crane mats over the coarse aggregate base and gradually traversing the DSM rig toward the working platform. Performance of the access pathway during DSM rig mobilization was monitored real time using the implemented instrumentation system.

Settlement was measured to be less than 0.1 inches during the DSM rig mobilization and rebounded immediately after the DSM rig traversed along the pathway, indicating elastic ground deformation. The measured excess pore water pressure induced by the DSM rig was about 30 psf ($\Delta u/\Delta\sigma$ of 0.03) from the VW piezometers at depths of 5 and 20 ft, and 50 psf $\Delta u/\Delta\sigma$ of 0.04) from the VW piezometer at a depth of 10 ft (Figure 4). The excess pore water pressure was dissipated approximately 20 minutes after it reached the peak value.

Lateral ground displacements were monitored at three locations using automated inclinometers. The rig was stopped at these locations for 10-15 minutes to allow for observation of lateral displacements. Lateral displacements of less than 0.05 inches were measured.

Three vibration monitoring units were installed along the access pathway to monitor the vibrations. The peak particle velocity (PPVs) and the frequencies were recorded when the PPV exceeded 0.1 inch per second. A maximum PPV of 0.12 inch per second corresponding to the frequency of 6 Hz was measured during DSM rig mobilization.

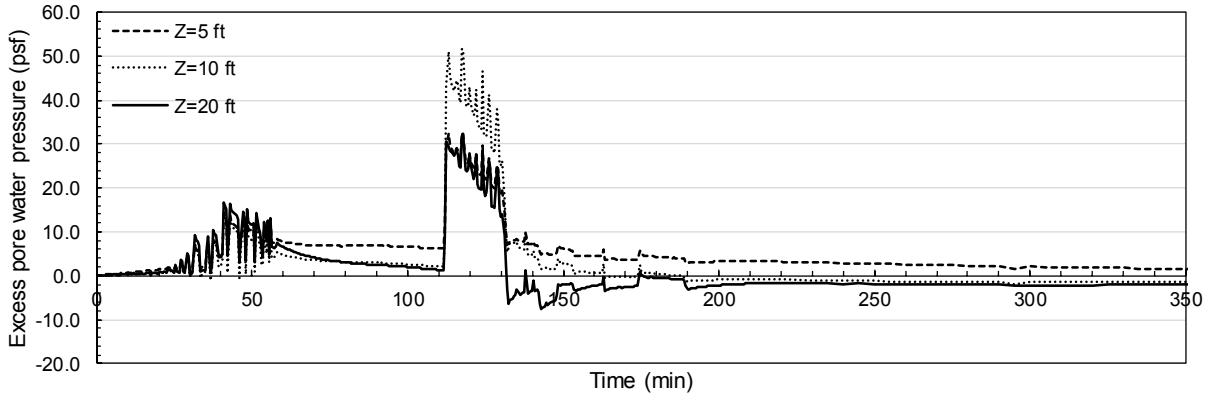


Fig. 4. Excess pore water pressure during DSM rig mobilization

DSM column installation

The locations of each DSM zone and the instruments installed on the working platform is illustrated in Figure 1. Figure 5 shows the development of excess pore water pressure in various depths during the construction of two DSM columns in Zone 3 (i.e., columns 3C and 3A). The distance between the edge of DSM columns and the piezometer borehole were about 5 ft and 10 ft, respectively. The pore water pressure increased during DSM auger penetration and reached the peak pressure when the auger reached the piezometer depths. Excess pore water pressure was then dissipated during the removal of the auger at the end of each pass. The maximum excess pore water generation occurs at the lowest piezometers at a depth of 60 ft which is consistent with the observation by Chen et al. (2013).

The change in excess pore water pressure in each pass is shown in Figure 5(c). The excess pore water pressure at depths of 20, 30, and 60 ft was measured to be about 15%, 16%, and 20% of the estimated effective vertical stress at that depth, respectively, where the pore water pressure spikes correspond to the end of the penetration stage. As presented in Figure 5, it takes approximately 10 hours for the excess pore water pressure to get fully dissipated.

Figure 6 shows maximum ground settlements after the construction of DSM columns at all six zones. A maximum settlement of approximately 2.4 inches was observed after DSM columns installation. This figure shows that the settlements are less than 0.05 inches before and after the completion of the DSM zones; however, deep soil mixing resulted in settlements of up to approximately 2.2 inches in the working platform. The construction of DSM columns at each zone, resulted in settlements ranging from 0.3 inch to 0.6 inch.

Figure 7 shows the lateral deformations perpendicular to the DSM zone due to the construction of Column 3C for various auger depths. The lateral deformations at various auger locations during the first drilling pass and the final lateral displacements after the third pass (i.e., completion of DSM) are depicted in this figure. Maximum lateral deformations occurred approximately at the mid length of the column. During the first pass, maximum deformations of 0.02, 0.05, 0.08, 0.13, and 0.22 inch occurred for the auger depths of 5 ft, 10 ft, 20 ft, 30 ft, 60 ft, and 90 ft, respectively. After the third pass was complete and the DSM column was constructed, a maximum lateral deformation of 0.5 inch was recorded at the depth of 37 ft below ground surface.

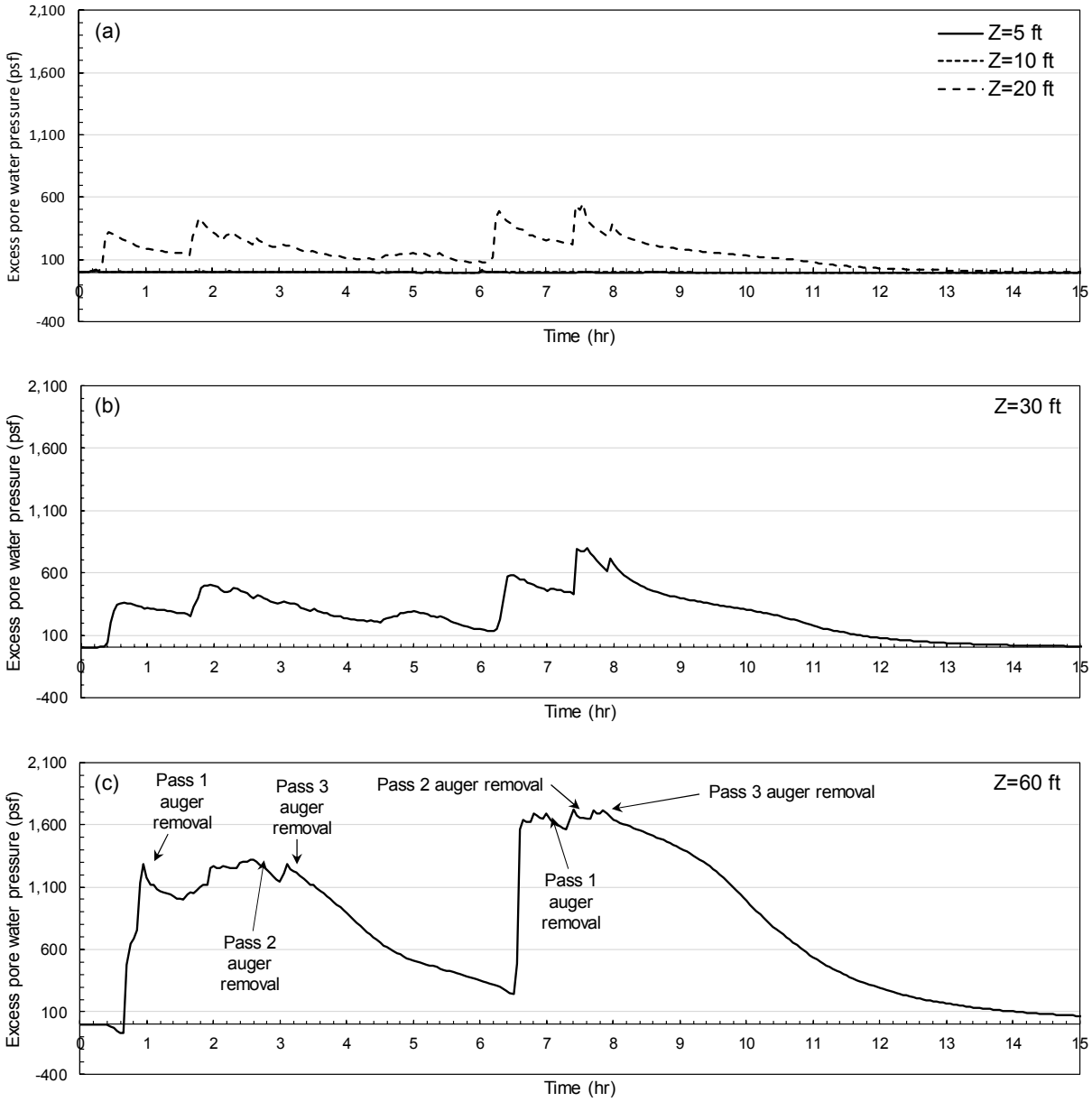


Fig. 5. Excess pore water pressure during construction of Columns 3C and 3A: (a) piezometer depths (Z) of 5 ft, 10 ft, 20 ft; (b) Z=30 ft; (c) Z=60 ft

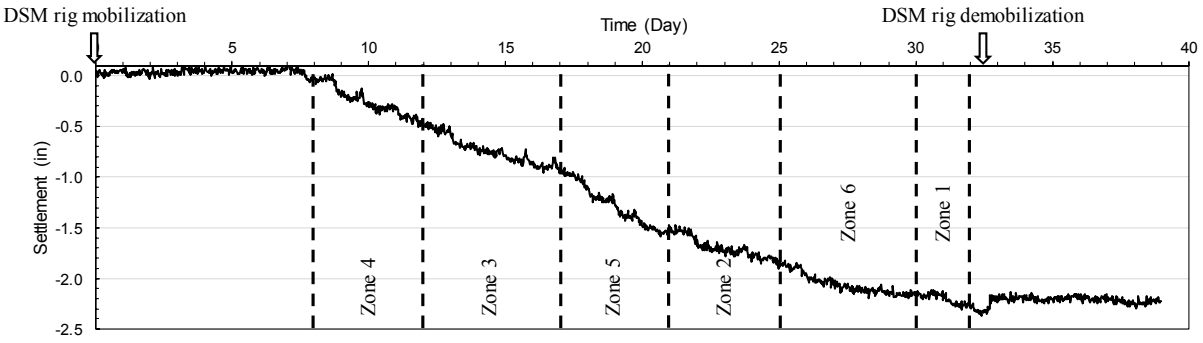


Fig. 6. Maximum ground settlements after the construction of DSM columns

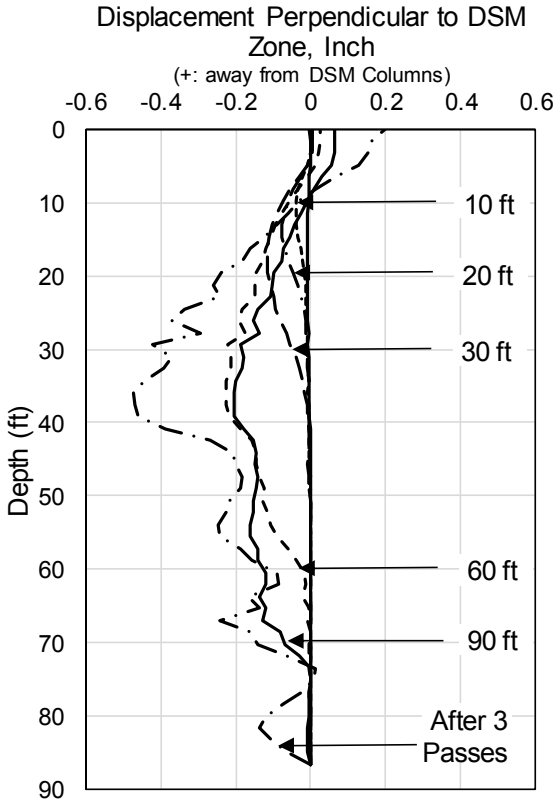


Fig. 7. Lateral deformations during construction Column 3C

Figure 8 shows the ground vibrations during the installation of Column 3E. The VMU was installed at about 10 ft from the edge of the DSM column. No PPV greater than 0.05 in/sec were recorded during the installation of the column since the VMU was installed at the ground surface; however, before and after deep soil mixing, PPVs as large as 0.52 in/sec and 0.28 in/sec were observed due to the DSM rig movements on the platform.

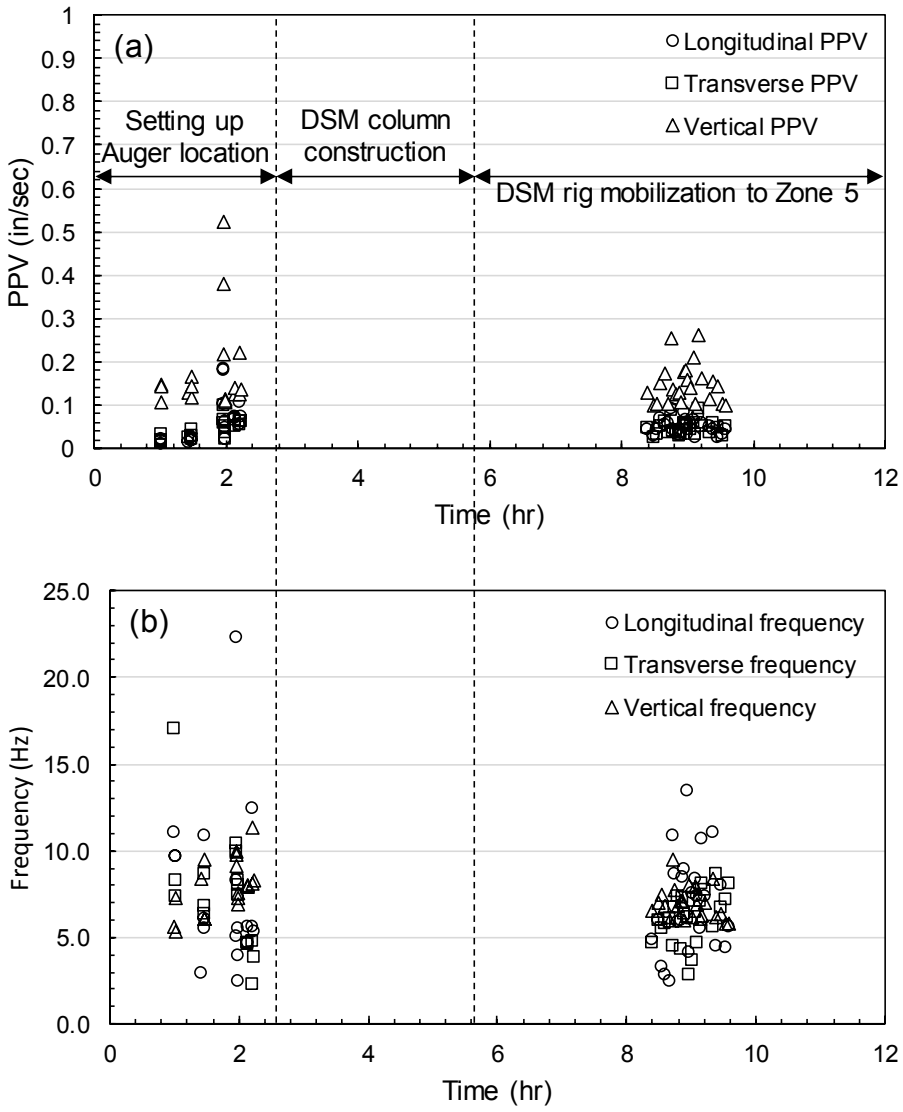


Fig. 8. Vibration measurements during construction of Column 3E

SUMMARY AND CONCLUSION

An instrumentation and monitoring system was implemented to assess the geotechnical performance of the working platform during the DSM pilot study. Pore water pressures, ground movements and vibrations were monitored to evaluate the safety of construction activities on a CCR impoundment. The following key conclusions and observations can be made from this study:

- Settlements less than 0.1 inches and excess pore water pressures of about 30 psf were observed during the mobilization of the construction equipment to the working platform. The excess pore water pressures were dissipated rapidly during the mobilization process.
- The load test was performed to assess the geotechnical performance of the working platform before the mobilization of the DSM rig and constructing the DSM columns. The results of load tests indicated up to 1.2 inches of settlement when 1.3 times equipment load is statically applied on the platform.

- Construction of DSM columns resulted in settlements of 2.4 inches and lateral deformations of 0.5 inches.
- Excess pore water pressure was generated due to the construction of the DSM columns. The excess pore water pressure was larger at higher depths (e.g., 550 psf, 800 psf, and 1,700 psf at 20 ft, 30 ft, and 60 ft below ground surface).
- No ground vibration was recorded during the construction of the DSM column as the VMU was installed at the surface. Borehole geophones will be useful for vibration monitoring at various depths during deep soil mixing.

ACKNOWLEDGMENTS

The authors would like to thank their client for the opportunity to be involved with this project and their subcontractor, Geo-Solutions, Inc., for their contributions to the design and efforts throughout construction.

REFERENCES

Chen, J. J., Zhang, L., Zhang, J. F., Zhu, Y. F., & Wang, J. H. (2012). Field tests, modification, and application of deep soil mixing method in soft clay. Journal of Geotechnical and Geoenvironmental Engineering, 139(1), 24-34.

Woeste, D., Tanner, W., Pestana, J., Sabatini, P., Gasser, J., Gokmen, C. (2019). Design and construction of mixed ground working platform for a CCR surface impoundment. Submitted to the 44th Deep Foundations Institute (DFI) Conference, Chicago, Illinois.

BI-DIRECTIONAL TESTING USING SUPER CELLS FOR THE JIAXING-SHAOXING RIVER CROSSING BRIDGE

Antonio Marinucci, PhD, MBA, PE, V2C Strategists, LLC, New York, N.Y., USA. +1 (347) 670.2006, amarinucci@v2cstrategists.com
Robin Mao, Ougan Group, Hangzhou, P.R. China, +86 571 28223950, robinyxmao@ougangroup.com
Diane Reid, RAND Engineering & Architecture, DPC, New York, N.Y., USA. +1 (646) 331.5213. drdianereid@gmail.com

ABSTRACT Super Cells are an innovative, open-shaped bi-directional static load testing device used to promote concrete flow during placement while utilizing greater cross-sectional area of the pile to achieve large applied axial loads at relatively low hydraulic pressures (≤ 250 bar). This paper describes the results of multi-level load testing performed on a sacrificial drilled shaft that was 3.8 m (12.7 ft) in diameter and 110.6 m (363 ft) in length for the Jiaxing-Shaoxing River Crossing Bridge that spans Hangzhou Bay in Shaoxing, China. The test shaft was instrumented with embedded strain gauges and telltale rods along with displacement transducers at the top of the pile to measure the load-induced displacements along the length of the shaft. Load testing was performed twice using a Super Cell placed near the tip of the shaft, prior and subsequent to tip post-grouting, and then again using a Super Cell placed higher in the shaft. The axial resistance for the tested conventional drilled shaft was more than 5 times greater than the estimated axial resistance. In addition, the axial resistance after tip post-grouting (347,100 kN (39,033 ton)) was about 5.3% greater than the ungrouted axial resistance (329,600 kN (37,050 ton)).

Keywords: drilled shaft, Super Cells, bi-directional static load testing, tip post-grouting

INTRODUCTION

During the past few decades, the magnitude of axial, lateral, and flexural loading has considerably increased due to updated design codes, larger superstructures, and the manner in which extreme event loading (e.g. seismic and scour) is incorporated into design. The diameter and depths to which bored piles or drilled shafts are constructed have increased considerably during the last three decades due to the advancements in equipment technology and capabilities. In addition, monoshaft foundations have become increasingly used, as one large drilled shaft is able to replace a group of smaller diameter piles connected by a cap. Correspondingly, adequate strata, for both side and end resistance, must be discovered/determined as well as achievable to be able to construct the required foundations to support the greater design demands.

As design demands have increased, the need to ensure integrity, quality, and performance of a constructed drilled shaft has become ever more crucial. Load tests are essential to validate design assumptions of side and end resistances, to assess the behavior and load transfer characteristics of the constructed drilled shafts, and to evaluate construction methods. Load tests utilizing a bi-directional static load testing (BDSLT) device can achieve considerably large applied axial loads and can be performed more economically, in less time, and in a much safer manner than conventional top-down static load testing methods.

In addition to the BDSLT device, other instrumentation (e.g., embedded strain gauges, load cells, telltale extensometers, fiber optic strain sensors, and digital survey levels) is utilized to measure the response due to the imposed loading to compute the end and side resistance of and load transfer distribution along the drilled shaft. Conventional top-down static load tests are sometimes unable to achieve or provide the axial loading needed to fully mobilize or geotechnically fail the drilled shaft. However, a bi-directional load test device can be designed to impart the required axial loading and its placement within the shaft chosen to either balance the axial capacity above and below the device's location or to evaluate the resistance within a specific region. Presently, there are various types of BDSLT devices, but a new load cell from China has addressed many concerns associated with using this type of test.

© 2019 Deep Foundations Institute

OVERVIEW OF SUPER CELLS

A Super Cell is a specially designed system that uses built-in hermetically sealed pressure cells, where the pressure is applied to the load cell through a flexible hose(s) from a hydraulic pump located external to the drilled shaft. The pressure in the load cell is measured by a pressure transducer and movements of the device and along the shaft are measured by displacement transducers connected to the load cell and at other locations along the length of the shaft by telltale rods embedded in the cast concrete. During testing, the internal movement of the hydraulic pressure cell results from the expansion of a stacked series of flexible circumferential flutes, which are compliant to non-uniaxial forces thereby reducing the risk of seizing of components as well as eliminating risk of damaged seals or leaking of O-ring seals.

There are three available types of devices: (1) donut shape, (2) multiple cell, and (3) solid cell. The donut-shaped device (Fig. 1a) is applicable for smaller diameter elements (≤ 1.2 m [4 ft]), while the multiple-cell device (Fig. 1b) is well suited for larger diameter shafts and consists of multiple units assembled to match the diameter of the drilled shaft and to provide the required axial loading. The solid cell is applicable and typically used to evaluate end bearing resistance (Fig. 1c), which will not be discussed further hereinafter. For the donut and multiple cell devices, which are embedded within a drilled shaft, concrete flow around and through a testing device is enhanced due to (1) cone-shaped flow guides, which facilitate concrete flow and reduce buildup of laitance below and above the cells and (2) the device being secured within and to the steel reinforcement cage without the use of bearing plates.



Fig 1. Three different types of Super Cell: (a) donut cell, (b) multiple cell, and (c) solid cell

The design configuration of these devices transfers the force of each cell directly to the shaft, effectively eliminating the need for large steel bearing plates. In addition, the design utilizes the entire cross-sectional area of the shaft, thereby enabling greater axial loads to be applied while using a lower hydraulic pressure of the fluid to activate the pressure cells. The pressure required to operate a pressure cell is only about 250 bar (3,625 psi), which can be considerably less than other devices.

Prior to affixing a device to the steel reinforcement cage, the inner conical space or annulus within a multiple or donut cell must be filled with concrete and let harden (Fig. 2). One side of the device is filled with concrete, rodded with vibration to ensure compaction of the concrete, and then left overnight to allow the concrete to harden or set, after which time the device can be flipped and the process repeated. Per the design of the assembly, the pressure cell is contained within an outer steel shell to protect the cell from damage during fabrication, lifting/placing, and installation; and to provide a surface to which other components can be welded so that the welding does not occur directly to the pressure cell.

The infill concrete placed within the annulus between the outer shell and the pressure cell is used to transfer the pressure/load effectively and efficiently from the cell to and together with the concrete comprising the drilled shaft to the surrounding soil/rock. After the concrete has cured, the device can then be incorporated into the steel reinforcement cage (Fig. 3). When installing a device into the cage, there is no direct welding to the pressure cell itself; welding is performed only to the brackets and metal cones supporting the pressure

cells, thereby eliminating excess heat and contamination problems. Once the minimum compressive strength of the concrete has been achieved, the bi-directional load testing can be performed. Since the BDSLT device and steel reinforcement were cast together, measurements from embedded instrumentation have shown that there is little-to-no relative movement between the device assembly (affixed to the steel reinforcement) and concrete. Current practice (where Super Cells have been used) has been to tighten the pitch of the spiral reinforcement to about 100 mm (4 inch) on either side of the BDSLT device for a distance of about 2 m (6.6 ft) to provide additional confinement and stiffness to the drilled shaft.



Fig 2. Concreting of inner conical space or annulus for (a) a multiple cell and (b) a donut cell

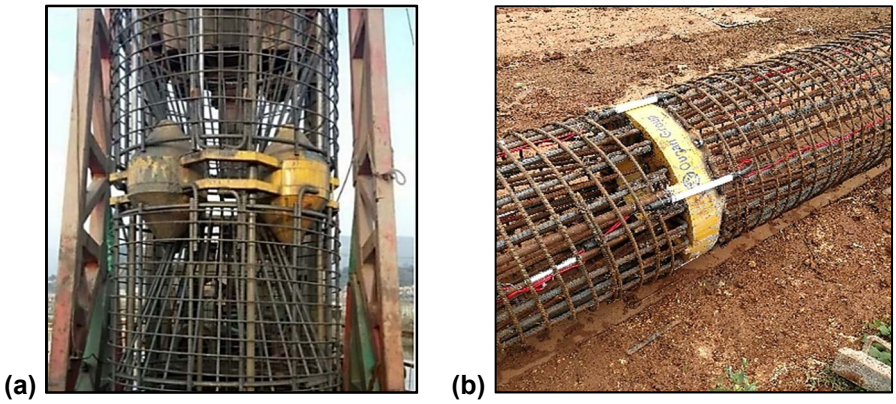


Fig 3. Attachment of (a) a multiple cell and (b) a donut cell to the steel reinforcement cage

PROJECT DESCRIPTION

The Jiaxing-Shaoxing Sea Bridge (Jiashao Bridge) is currently the world's longest and widest multi-pylon cable-stayed bridge in service. Due to considerable vehicle congestion on the nearby Hangzhou Bay Bridge, a new bridge was commissioned to alleviate the congestion and decrease drive times. It was reported that the drive time between Shaoxing and Shanghai, a distance of about 200 km (125 mi), could be reduced from about 3 hours to less than 2 hours. Construction of the bridge, which connects Jiaxing and Shaoxing, began in December 2008, was completed in February 2013, and was later opened to traffic in late July 2013. The Jiashao Bridge is about 10.14 km (6.3 mi) long, about 40.5 m (133 ft) wide, supported by six 227 m (745 ft) tall pylons, and can accommodate eight lanes of traffic (four in each direction).

SUBSURFACE CONDITIONS

For the portion of the project within the river, a site characterization program to define the subsurface conditions and establish engineering design properties was undertaken in two stages. In total, 27 boreholes were drilled with a total length of about 3,060 m (10,040 ft); numerous samples were collected: 57 rock samples, 595 undisturbed soil samples, 417 disturbed soil samples, and 6 water samples; 530 standard penetration tests and 99 conical dynamic penetration tests were performed; and wave velocity measurements within the boreholes were performed. As shown in Fig. 4, the generalized subsurface profile within the river beneath the bridge alignment is quite heterogeneous.

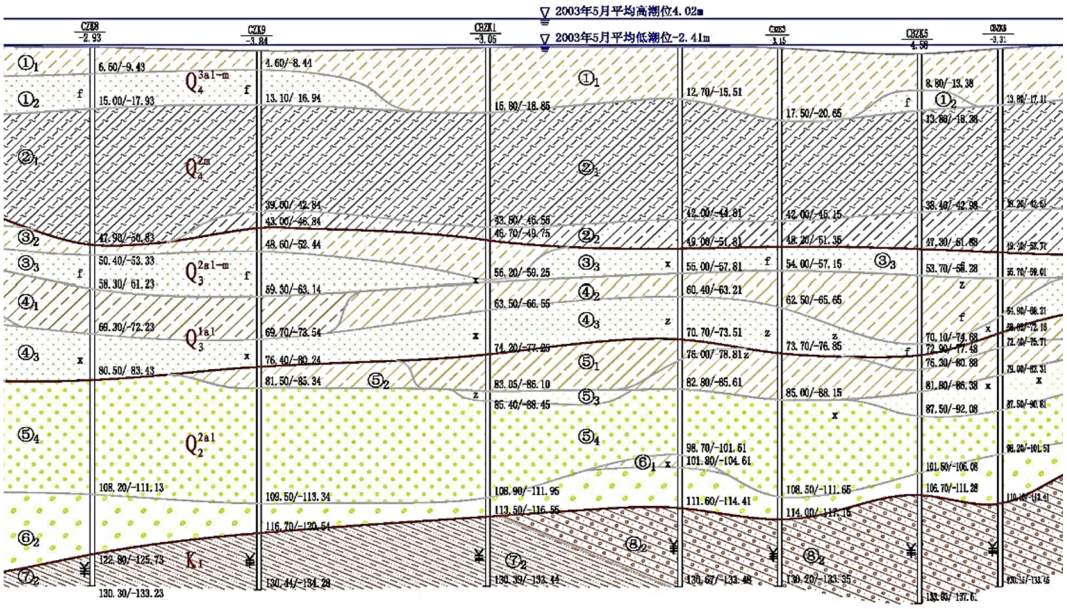


Figure 4. Generalized subsurface profile (excerpt)

Table 1. Subsurface profile and geotechnical resistance

Layer Desig.	Soil Layer Description	Bottom of Layer Elevation		Layer Thickness	
		(m)	(ft)	(m)	(ft)
---	Surface	+2.69	+8.83	0.0	0.0
①1	Sandy Loam	-8.31	-27.26	11.00	36.09
①2	Silty Sand	-17.31	-56.79	9.00	29.53
②1	Muddy Loam	-34.81	-114.21	17.50	57.41
②2	Loam w/ silty sand	-48.31	-158.50	13.50	44.29
③4	Loam	-56.71	-186.06	8.40	27.56
④3	Silty Sand	-60.91	-199.84	4.20	13.78
④3	Gravely Sand	-65.11	-213.61	4.20	13.78
④3	Silty sand	-68.51	-224.77	3.40	11.15
④3a	Loam	-70.31	-230.68	1.80	5.91
④3	Silty sand	-74.11	-243.14	3.80	12.47
⑤2	Loam	-75.31	-247.08	1.20	3.94
⑤3	Silty sand	-78.01	-255.94	2.70	8.86
⑤4	Round pebble	-83.11	-272.67	5.10	16.73
⑤4	Round pebble	-94.31	-309.42	11.20	36.75
⑥2	Pebble	-102.31	-335.66	8.00	26.25
⑦2	V. weathered sandstone	-104.11	-341.57	1.80	5.91
⑦3	Sl. weathered sandstone	-112.46	-368.96	8.35	27.39

The topography of the bed of Hangzhou Bay is relatively flat, with a water depth of about 5 to 10 m (16 to 33 ft). In general, the topography of the bridge site area is high on either side and low in the middle and can be divided into three main landforms: (1) alluvial plain area, (2) intertidal zone, and (3) underwater depression. As shown in Table 1, the profile was subdivided into 17 layers by the geotechnical engineer: a near surface layer of sandy loam and silty sand (Layers 1, 2, and 3), which is underlain by silty to gravelly sand (Layer 4), which is underlain by a layer of sandy loam to pebbles (Layers 5 and 6). The bottom of the pile is founded in a layer of highly to slightly weathered argillaceous sandstone (Layer 7). The upper and lower BDSLT devices were positioned or located in Layer 4 (silty sand and loam) and Layer 6 (pebbles), respectively. Based on the results of the site characterization and laboratory testing, the designers provided recommendations for the permissible axial compression resistance of a single 3.8 m (12.5 ft) diameter drilled shaft (Table 2).

Table 2 Estimate of permissible axial compression resistance of a single 3.8 m (12.5 ft) diameter drilled shaft

Bridge segment	Pile bottom elevation (m) [ft]	Effective Pile Length (m) [ft]	Name of Stratum at Pile Tip	Estimated capacity (kN) [ton]	Scour depth (m) [ft]
North approach Bridge	-76.3 [-250.3]	80.0 [263]	Fine sand	34,431 [3,870]	0
	-112.0 [-367.5]	82.8 [272]	Gravel	62,462 [7,021]	26.9 [88.2]
	-112.0 [-367.5]	81.7 [268]	Strongly weathered argillaceous sandstone	64,500 [7,250]	27.35 [89.4]
Main navigable orifice Bridge	-125.3 [-411.1]	84.8 [278]	Strongly weathered sandy conglomerate	76,675 [8,619]	37.7 [123.4]
	-125.3 [-411.1]	84.8 [278]		80,917 [9,095]	37.4 [122.5]
	-125.3 [-411.1]	84.8 [278]		77,415 [8,702]	35.9 [117.8]
	-122.3 [-401.2]	81.8 [268]		76,231 [8,569]	37.9 [124.4]
South approach bridge	-112.0 [-367.5]	84.8 [278]	Strongly weathered argillaceous sandstone	80,156 [9,010]	27.9 [91.5]
	-65.5 [-214.9]	70.0 [230]	Round gravel	39,699 [4,462]	0.0 [0]

TEST PILE DETAILS

The test pile (SZ1) and production piles were installed using the top-drive reverse circulation drilling method along with PHPA (partially hydrolyzed polyacrylamides) polymer slurry; where the drilling apparatus was mounted atop the permanent steel casing (Fig. 5a). The borehole was excavated using large diameter drilling buckets (Fig. 5b) and full-faced rotary cutters (Fig. 5c). A slurry plant system was used to prepare and recycle the drilling support fluid. Prior to the placement of the concrete, the hole was cleaned to ensure the thickness of the sediment at the bottom of the shaft was less than 100 mm (4 inch). Permanent steel casing was used for the upper portion of the shaft, where it extended about 2 m (6.6 ft) above the water surface to approximately Elev. +10 m (Elev. +32.8 ft). The tip of the 50 m (164 ft) long steel casing was located at about Elev. -40 m (Elev. -131 ft).

The two BDSLT devices were positioned (Fig. 6) to satisfy the following three criteria:

1. $R_{S,A} > R_{S,B}$ where $R_{S,A}$ = side resistance provided by uppermost section (Section A with length = L_a = 70.1 m [230 ft]) above the uppermost BDSLT device, and $R_{S,B}$ = side resistance provided by portion of shaft between the BDSLT cells (Section B with length = L_b = 28 m [91.8 ft])
2. $R_{S,B} + R_{S,C} > R_{S,A}$ where $R_{S,C}$ = sum of side and end resistance provided by lowermost section of the shaft below lower BDSLT device (Section C with length = L_c = 10.5 m [34.5 ft])
3. $R_{S,A} + R_{S,B} > R_{S,C}$.

The lower and upper multiple cells were positioned about 10.5 m (34.5 ft) and 38.5 m (126 ft), respectively, above the toe of the drilled shaft (Fig. 6) at El. -98.1 m (El. -321.8 ft) and El. -70.1 m (El. -230.0 ft). The configuration for the two levels of BDSLT devices included 6 individual unit cells connected together using

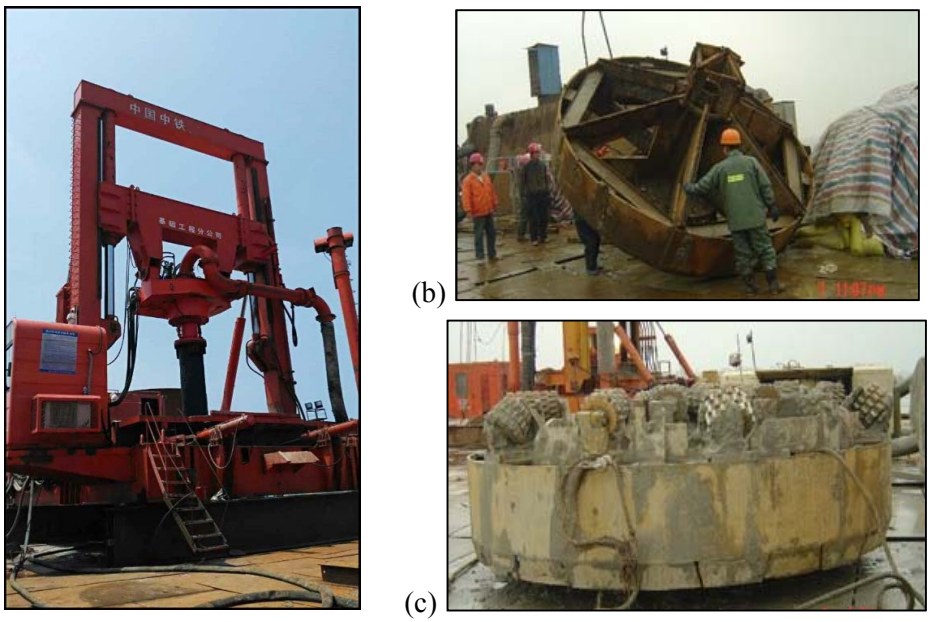


Fig. 5. Equipment and tooling used to install the test and production drilled shafts: (a) top-drive reverse circulation drilling system, (b) large diameter drilling bucket, and (c) large-diameter full-faced rotary cutter

integral brackets or struts welded to the cells for support within the reinforcement cage (similar to the arrangement shown in Fig. 1b). When fully fabricated, the outer diameter of each of the devices was about 3.6 m (11.8 ft).

The horn rebar (or funnel reinforcement) not only provides additional structural stiffness to the reinforcement cage and an additional means to distribute the applied axial loading, but also acts as a guide to ensure the tremie tube reaches the bottom of the borehole. On both sides of the BDSLT device, the horn rebar is welded to the cover plate (outer shell) of the Multiple Super Cell and the reinforcing cage or the tremie pipe hole (in the center of the array). The length of the horn rebar is typically twice as long as the annular width of the Multiple Super Cell assembly to ensure the angle between the device and the horn rebar is at least 60 degrees. In addition, the quantity of horn rebar used is usually greater than the quantity of the longitudinal steel reinforcement bars, which also ensures the spacing between each horn rebar is narrower than the outer diameter of the tremie pipe.

The concrete mix design conformed to grade C30, which comprised a mix ratio of 1:2:3 of cement-to-sand-to-gravel (by weight), in addition to water and admixtures (e.g., plasticizers and water reducers). The amount of steel reinforcement was increased (i.e., reduced spacing between the spiral reinforcement and use of the horn reinforcement) to stiffen the reinforcement cage, ensure structural integrity, and ensure proper load distribution to the drilled shaft from the applied axial loading. For the test shaft, strain gauges were installed at 15 elevations along the length of the shaft. At a given elevation, four strain gauges were installed for accuracy and redundancy. In addition, four displacement transducers were mounted to measure the movement of the top of the drilled shaft during the load testing. Crosshole sonic logging (CSL) was performed 14 days after placement of the concrete for the sacrificial test shaft was completed.

After the CSL testing was completed, the bi-directional static load testing program was initiated once the concrete had achieved its minimum unconfined compressive strength, as determined from compression testing of test cylinders. The planned sequence of activities was as follows:

1. Perform the bi-directional testing using the lower BDSLT device prior to performing post-grouting beneath the base of the shaft to determine the side and end resistance of lowermost section of the shaft

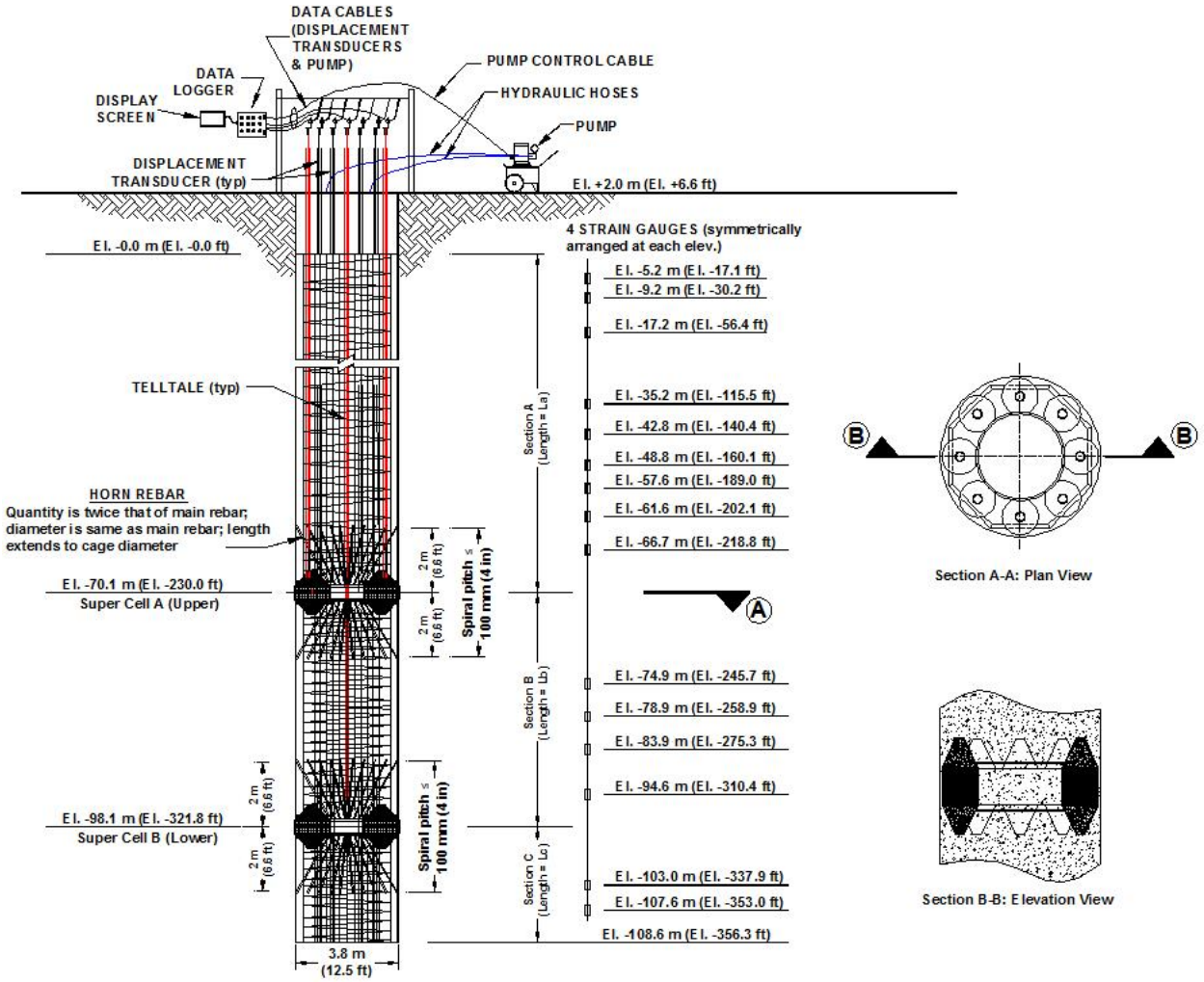


Fig. 6. Schematic of the sacrificial test pile and instrumentation including two levels of bi-directional load testing devices (not to scale; reinforcement not shown in Section B-B for clarity)

(Section C). The maximum expected applied axial test load was 70,000 kN (15,737 kip) and would be applied in 10 equal increments of 7,000 kN (1,574 kip). After completion of the testing, the pressure in the lower cell would be released.

2. Perform the post-grouting works beneath base of shaft.
3. Following a wait time of 20 days after the completion of the tip post-grouting, perform bi-directional testing again using the lower BDSLT device to determine the side and end resistance of lowermost section after post-grouting (Section C). The maximum expected applied axial test load was about 84,000 kN (18,884 kip) and would be applied in 12 equal increments of 7,000 kN (1,574 kip). After completion of the testing, the pressure in the lower cell would be released.
4. Following a wait time of 4 days after the completion of Part 3, perform the bi-directional testing using the upper device to determine the side resistance of the section of the shaft between the BDSLT devices (Section B). Up until a load of 65,000 kN (14,613 kip), the loading would be increased in increments of 6,500 kN (1,461 kip); thereafter, the load would be increased in increments of 3,250 kN (731 kip) until failure of Section B is achieved. Then, the pressure in the upper cell would be released.
5. Following Part 4, pressurize and maintain the pressure in lower device. Then, perform bi-directional testing using the upper device to determine the side resistance of the uppermost section of the shaft (Section A). Up until a load of 65,000 kN (14,613 kip), the loading would be increased in increments

of 6,500 kN (1,461 kip); thereafter, the load would be increased in increments of 3,250 kN (731 kip) until failure of Section A is achieved. The pressure in upper and lower cells would then be released.

TEST RESULTS

BDSLT using the Lower Cell Static load testing was performed prior to and after post-grouting beneath the base of the drilled shaft. The results of the BDSLT prior and subsequent to tip post-grouting are shown in Fig. 7. The response of the drilled shaft was slightly stiffer for the tip post-grouted condition than it was for the ungrouted condition. The end resistance was fully mobilized (i.e., achieved peak resistance) for both ungrouted and post-grouted conditions, as observed by the plunging response (i.e., continued displacement at constant applied load).

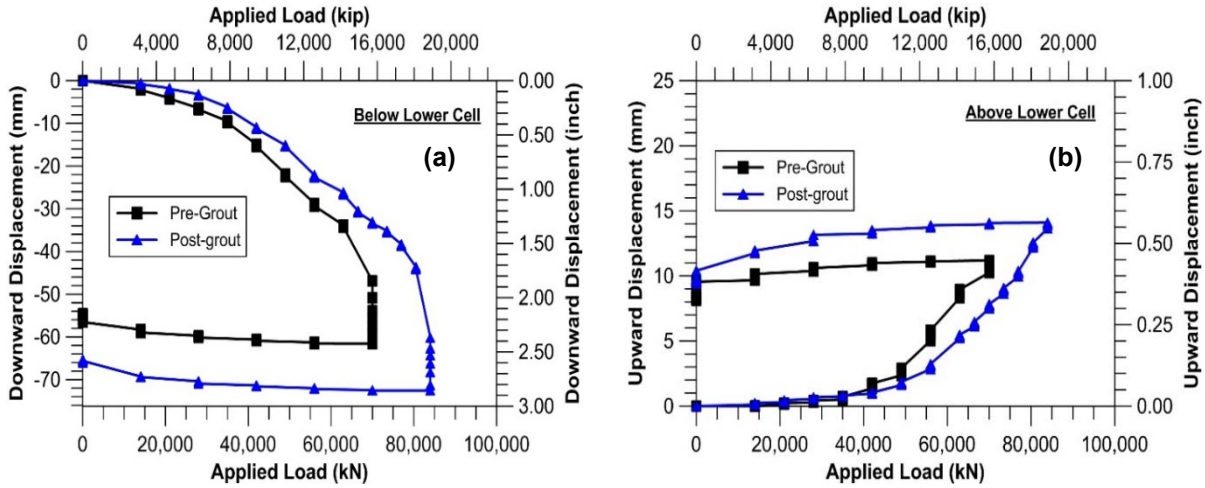


Fig. 7. Load-displacement results from the BDSLT using lower device (only) before and after tip post-grouting: (a) downward movement of lowermost portion of shaft (Section C), and (b) upward movement of shaft above device (Section B)

The maximum loads applied via the lower cell were 70,000 kN (15,737 kip) and 84,000 kN (18,884 kip) for the ungrouted and post-grouted conditions, respectively, which resulted in downward displacements of approximately 47 mm (1.8 in) and 60 mm (2.4 in). The upward movement above the lower cell and at the top of the shaft were 10.25 mm (0.40 in) and 6.7 mm (0.26 in) prior to the tip post-grouting and were 13.6 mm (0.54 in) and 8.6 mm (0.34 in) after the tip post-grouting, respectively. The ultimate axial resistance of the lowermost section of the test shaft prior to tip post-grouting ($Q_{u,C,bg}$) was determined to be approximately 189,850 kN (42,680 kip). After tip post-grouting, the ultimate axial resistance of the test shaft ($Q_{u,C,pg}$) was determined to be approximately 207,350 kN (46,648 kip), resulting in an increase in ultimate axial capacity of approximately 9.2% from the ungrouted condition.

The load transfer distributions from the BDSLT using the lower device (only) for the test drilled shaft prior to and after tip post-grouting are shown in Fig. 8. As expected, the majority of the resistance was developed in the pebble (Layers 5 and 6) and, especially, in the sandstone layers (Layer 7). Comparing the load transfer distribution for the same applied loading (i.e., 65,000 kN [14,613 kip]), the magnitude of computed load was less after than prior to tip post-grouting by an amount ranging from 0.5% to 13% for the strain gauges below Elev. -57.6 m (Elev. -189.0 ft), but there was an increase of about 64% and 16% in computed load at Elev. -42.8 m (Elev. -140.4 ft) and Elev. -48.8 m (Elev. -160.1 ft), respectively. One possible explanation of the decrease in load transfer could be the sequencing and repeated loading of the lower portion of the drilled shaft: load testing then tip post-grouting then load testing again. Nonetheless, as a result of the tip post-grouting, a much greater load could be applied by the Super Cell to the drilled shaft, which resulted in the mobilization of side resistance at higher elevations in the drilled shaft.

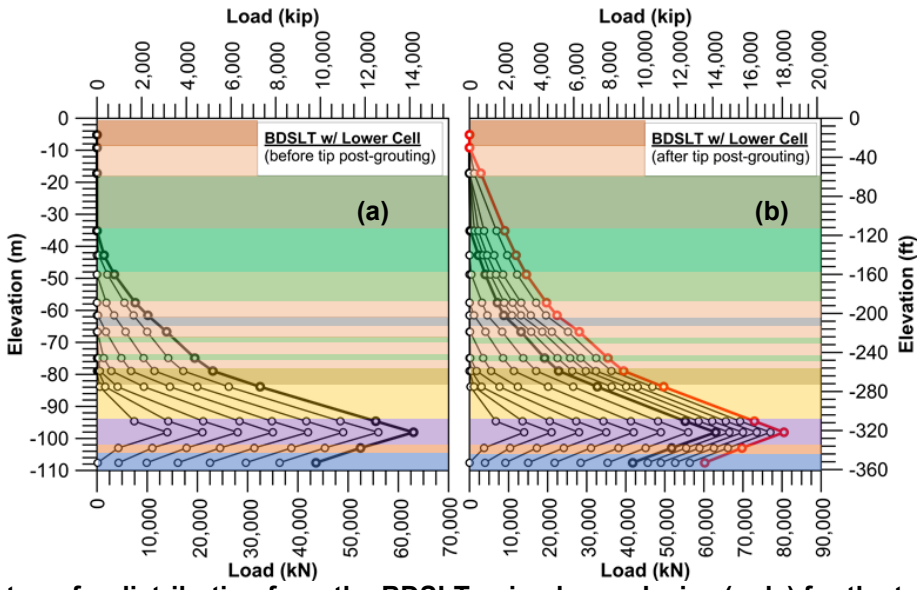


Fig. 8. Load transfer distribution from the BDSLT using lower device (only) for the test drilled shaft (a) prior to and (b) after tip post-grouting (layering corresponds to Table 1)

The t-z (unit side resistance) responses from the BDSLT using the lower device (only) for the test drilled shaft prior to and after tip post-grouting are shown in Fig. 9. Based on the computed t-z responses, it is apparent that the side resistance of only the lower portions of the shaft were fully mobilized during the testing. Prior to the tip post-grouting, the side resistance between strain gauge elevations Elev. -98.1 m and -103.0 m (Elev. –321.5 ft and -338.0 ft) and Elev. -103.0 m and -107.6 m (Elev. –338.0 ft and -353.0 ft) were fully mobilized, resulting in values of unit side resistance of about 182 kPa (3,800 ksf) and 163 kPa (3,400 ksf) and, respectively.

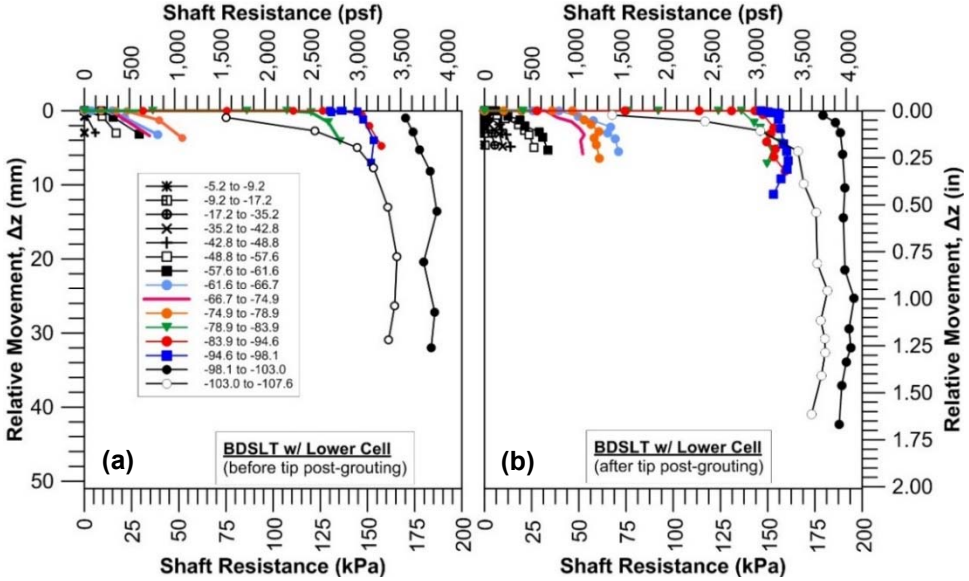


Fig. 9. t-z responses for the test drilled shaft (a) prior to and (b) after tip post-grouting

The BDSLT performed after the tip post-grouting indicated that not only was the side resistance fully mobilized below about Elev. -94.6 m (Elev. -310.4 ft), but also that increase in the side resistance below about Elev. -98.1 m (Elev. -321.5 ft) occurred and was likely due to the tip post-grouting (e.g., upward migration of grout and other general ground improvement below/around the lower portion of the drilled

shaft). The side resistance between strain gauge elevations Elev. -94.6 m and -98.1 m (Elev. -310.4 ft and -321.5 ft), Elev. -98.1 m and -103.0 m (Elev. –321.5 ft and -338.0 ft), and Elev. -103.0 m and -107.6 m (Elev. –338.0 ft and 353.0 ft) were fully mobilized, resulting in values of unit side resistance of about 153 kPa (3,200 ksf), 187 kPa (3,900 ksf), and 177 kPa (3,700 ksf), respectively.

BDSLT using Upper Cell With the pressure released in the lower cell, the portion of the drilled shaft between the two devices could be tested. The static load testing was performed after post-grouting beneath the base of the drilled shaft and after the testing using the lower cell. The results of the BDSLT following tip post-grouting and testing using the lower cell are shown in Fig. 10.

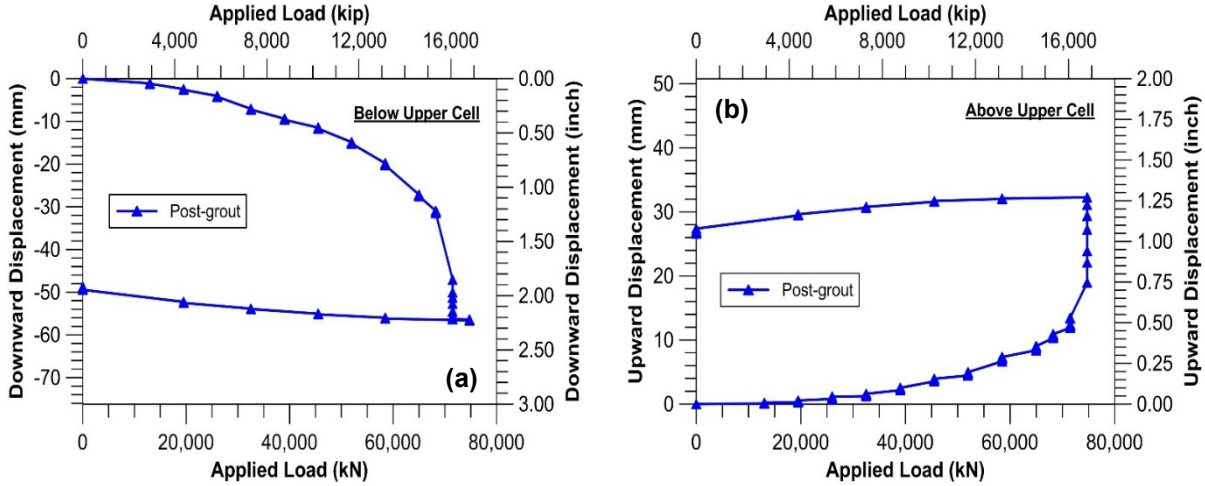


Fig. 10. Load-displacement results from the BDSLT using upper device (only) after post-grouting: (a) downward movement below device, and (b) upward movement above device

During the incremental loading, the drilled shaft behaved as anticipated based on the results from the loading with the lower cell. As the applied axial loading approached 65,000 kN (14,613 kip), the rate of induced both downward and upward displacement began to increase. In accordance with the governing specifications, the subsequent increment was reduced by 50%. At the applied load of 71,500 kN (16,074 kip), the downward displacement of the drilled shaft increased rapidly under the sustained loading. The side resistance below the upper cell was fully mobilized, as observed by this plunging response. The maximum load applied via the upper cell was 71,500 kN (16,074 kip), which resulted in a downward displacement of approximately 57 mm (2.2 in). The upward movement above the upper cell and at the top of the shaft were 19.0 mm (0.75 in) and 15.6 mm (0.61 in), respectively. From the results of the BDSLT, the ultimate axial resistance of the middle section of the test shaft ($Q_{u,B}$) was determined to be approximately 68,250 kN (15,343 kip).

For the last portion of the testing program, after the pressure in the upper cell was released and unloaded, the lower cell was again pressurized and the load maintained, which enabled the testing of the uppermost portion of the shaft by reacting against the lower sections (below the upper cell). At axial loads below 71,500 kN (16,074 kip), the drilled shaft behaved as anticipated. However, at an applied axial loading of about 74,750 kN (16,805 kip), the upward displacement of the uppermost section of the shaft increased suddenly and rapidly (by about 19 mm [0.75 in] from about 13 mm to 32 mm [0.51 to 1.25 in]). At this sustained load, the upward displacement would not stabilize, and the testing was terminated. As such, the ultimate axial resistance of the uppermost section of the test shaft ($Q_{u,A}$) was computed to be 71,500 kN (16,074 kip).

The load transfer distributions and t-z (unit side resistance) responses from the BDSLT using the upper device (only) for the test drilled shaft are shown in Figs. 11 and 12, respectively. The pebble layers (Layer

5-4) provided the greatest side resistance, about double the unit side resistance than the lower portion of silty sand (Layer 4). Based on the computed t-z responses and the plots shown on Fig. 12, it is apparent that the side resistance of the drilled shaft within Section B, between Elev. -70.1 m and -98.1 m (Elev. -230.0 ft and -321.8 ft), were fully mobilized during the testing using the upper cell only. As such, between strain gauge elevations Elev. -70.1 m and -74.9 m (Elev. –230.0 ft and -245.7 ft), Elev. -74.9 m and -78.9 m (Elev. –245.7 ft and -258.9 ft), Elev. -78.9 m and -83.9 m (Elev. –258.9 ft and -275.3 ft), and Elev. -83.9 m and -94.6 m (Elev. –275.3 ft and -310.4 ft), the values of side resistance were computed to be about 82 kPa (1,700 ksf), 105 kPa (2,200 ksf), 192 kPa (4,000 ksf), and 196 kPa (4,100 ksf), respectively.

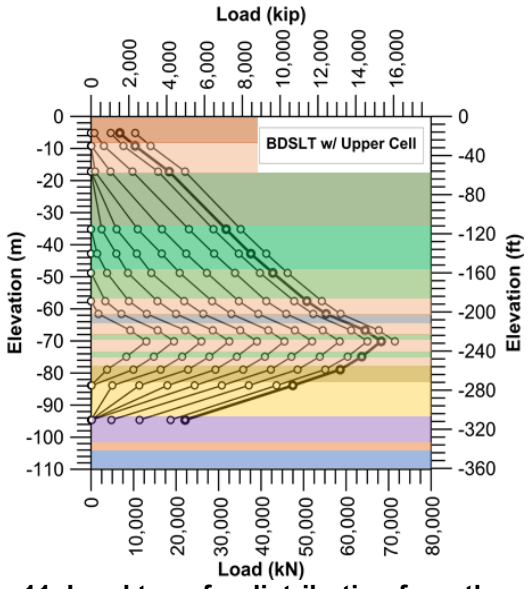


Fig. 11. Load transfer distribution from the BDSLT using upper device (only) for the test drilled shaft after tip post-grouting (layering corresponds to Table 1)

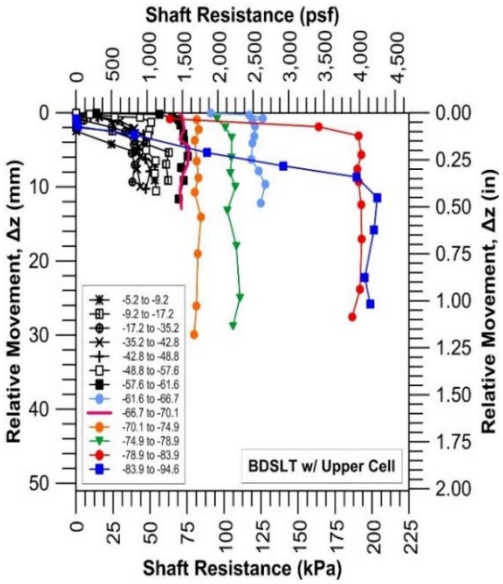


Fig. 12. t-z responses for the test drilled shaft after tip post-grouting (using loading from upper device)

CONCLUSION

The bi-directional static load testing of a 3.8 m (12.5 ft) diameter drilled shaft embedded to a depth of about 108.6 m (356.3 ft) into the Hangzhou Bay was successfully performed on a sacrificial pile. Two levels of super cell were used to confirm the assumptions used for the design of the drilled shafts for the Jiaxing-Shaoxing River Crossing Bridge. During each of the tests performed using the super cells, the side resistance of the different soil layers within the two lower portions of the drilled shaft (Sections B and C) as well as the end resistance was fully mobilized, as determined by the plunging behavior under sustained loading. The axial resistances in compression were computed to be about 329,600 kN (37,050 ton) and 347,100 kN (39,033 ton) for a conventional (ungrouted) and tip post-grouted drilled shaft, respectively. The computed axial resistance for the conventional (ungrouted) drilled shaft (329,600 kN [37,050 ton]) tipped in the weathered sandstone was considerably greater than the estimated axial resistance for the same layer (64,500 to 80,917 kN [7,250 to 9,095 ton]). In addition, the results of the testing indicated a slight increase of about 5.3% in total axial resistance of the drilled shaft due to the tip post-grouting, with an increase of about 9.2% in the lowermost portion of the shaft (Section C) alone.

BUILDING DRILLED SHAFTS TO BRIDGE THE MISSISSIPPI

Brian Koch, Michels Corporation, Brownsville, WI, USA 920- 539-7287, bkoch@michels.us

ABSTRACT

Michels installed 242 drilled shafts to support the piers for a new basket-handle, true-arch twin bridge across the Mississippi River from Moline, IL to Bettendorf, IA. The installation of the drilled shafts was completed with the simultaneous use of two Liebherr LB36 and one IMT 300 drill rigs. Utilizing barges, 233 drilled shafts were installed in the river. Michels crews also installed 7-ft to 10-ft permanent steel casing into the bedrock, and drilled to depths of 60 feet for each shaft. Despite working in strong currents, freezing temperatures and on rocking barges, Michels crews placed the shafts within 3 inches of plan position. Since the drilled shafts are the key piece in supporting the bridge structure, Michels provided cross-hole sonic logging to verify the integrity and strength of the concrete within the shafts and to add another level of quality control for the owner/customer. Extensive planning took place each day to ensure that tugboats, the linchpin of the project, were being efficiently utilized to shift the barges and materials daily. On any given day, Michels transported five concrete trucks by barge from shore to shaft sites to pour between 40 and 240 cubic yards of concrete. The Michels environmental team was diligent with preparing, discussing and implementing a water treatment plan that was accepted by all state and federal agencies and adhered to strict environmental regulations. Grain hopper barges were rented to control and treat the water that was used in the drilling operations. Another challenge crews ran into was the discovery of caverns when drilling into some parts of the bedrock. Michels worked with the engineer to develop a plan to construct the drilled shafts that encountered the caverns.

INTRODUCTION

Michels met the challenge of the Mighty Mississippi when called upon to install shafts for a new bridge carrying eight lanes of traffic over the river on Interstate-74 between Bettendorf, IA and Moline, IL. The new bridge will be an important link in the Quad Cities area, replacing a two-lane westbound bridge that opened in 1935 and the two-lane eastbound bridge that opened in 1960. Currently, the average daily traffic count on the bridges is about 75,000. By 2035, it is estimated to top 100,000.

The new bridge's visual highlight will be two 164-ft arches, but the foundation system is equally impressive. Michels scope of work was to install 242 7-ft to 10-ft outer diameter permanently cased drilled shafts to support the 28 piers that spanned the 3,370-ft section of the Mississippi River. The piers will support a basket-handle, true-arch twin bridge. The drilled shafts were installed with simultaneous use of four drill rigs, three working off marine barges. A load test was performed with an Osterburg Cell within a demonstration shaft to confirm the

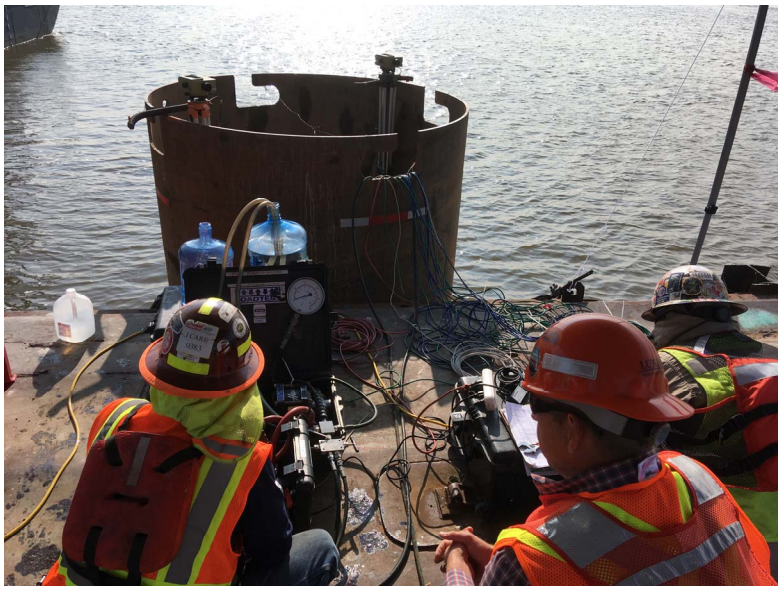


Fig. 1: A load test was performed with an Osterburg Cell to confirm constructed shafts met designed capabilities.

© 2019 Deep Foundations Institute

constructed shafts were meeting designed capacities. Prior to the load test, the design assumed a nominal bearing resistance of zero and a nominal side resistance of 2705 kips for Pier 10 - Eastbound, Pier 10 - Westbound, and Pier 11 - Eastbound. The load test concluded that a sustained upper side shear resistance of 2,515 kips was mobilized during the test. An end bearing resistance was estimated at 6,000 kips. Due to the information gained by performing a load test, 24 drilled shaft rock sockets were reduced by a cumulative length of 228'. By reducing the rock socket lengths, the schedule and cost of the project were also reduced.

Drilled shaft jobs are typically risky due to the unknowns of what lies below the ground surface. The risk on this project increased because the ground surface was below 10 to 25 ft of flowing Mississippi River water. This project's contract documents included better-than-average soil boring information; however, with more than 200 drilled shafts in the river, Michels was destined to uncover unknown features.

LOGISTICS

To be productive, each drilling barge island needed to be independent and self-sufficient since there were limited crew boats and it took approximately one hour for a round trip back to the dock. Additional planning went into stocking the supply trailers since the foreman couldn't walk over to their pickup truck and grab a screwdriver or pliers. Daily morning meetings with each barge foreman were held to plan the tugboats' movements for the day. There were limited hours each day for tugboats to push concrete trucks out to pour a shaft, push in excavated spoils, move drilling and crane barges to the next shaft location, and supply the barges with fuel, reinforcement cages, and permanent casing.



Fig. 2: Tugboats were used to bring concrete from shore to the drilled shafts. Scheduling of the tugboats was a critical component of the project.

WEATHER

The project schedule dictated that work to install the drilled shafts would run through the freezing winter and wet spring seasons. Michels Corporation reviewed historic river data prior to fabricating the permanent casing to allow for the river pool to fluctuate during the year. If the casing was too long, it would be inefficient to work around and would require cutting, which would take time; if it was too short, it would delay installation until the river levels receded. The summer season brought potential of thunderstorms and

lighting. Being isolated on a steel barge with a crane and drill rig sticking into the air increased the risk of lightning strikes. The winter season brought freezing temperatures and ice. Several weeks of production were lost due to the slough freezing over and losing the ability to reach the barges on the main river channel.

SCHEDULE

The baseline critical path method (CPM) schedule placed the demonstration shafts, Pier 12 Interior, Pier 12 Westbound, Pier 13 Interior, and Pier 13 Westbound drilled shafts on the critical path of the project. Critical path work is defined as durations that include less than five days of float on the schedule. The original duration of drilled shaft work on the project started Aug. 22, 2017 and finished Feb. 6, 2019. The actual duration of the drilled shaft work started on Aug. 21, 2017 and finished July 21, 2018.

SITE LOGISTICS

The Mississippi River is a unique jobsite. The jobsite had one personnel dock and one materials loading dock. Personnel were moved using closed cabin crew boats. Materials were loaded on barges and pushed out to location with tugboats. The tugboats were the linchpins of the project, and each day extensive planning took place to determine the schedule and hierarchy of the barge movements for the day. A dike/break wall was located approximately 1,050-ft from the Illinois dock. This dike/break wall was once used to separate the Moline pool from the main Mississippi River channel. The Moline pool was used to store logs being floated down the river to local mills. There was one main gap within the dike/break wall that all construction barge traffic utilized. The gap was several thousand feet upriver and added additional time to the transportation of concrete and materials. The existing bridge was west of the new construction. During periods of increased flow, two tugboats were utilized to transport barges to ensure the barge remained in control and spotted in the correct location for use.

EQUIPMENT

Two Liehberr LB36-410, one IMT 300 and one IMT 270 drill rig were utilized to complete the drilling on the project. Each drill rig had a support crane and multiple material barges assisting the drilling operation. The drill rigs excavated through overburden and then attacked the rock sockets with rock augers, core barrels and down-the-hole hammers (DHH) on Pier 12. The DHH were chosen to excavate limestone on Pier 12 due to the length of rock sockets and the critical path of the schedule that ran through Pier 12. In order to have the DHH run efficiently, seven 1170 CFM air compressors were used. Once the rock socket was opened to 96-in



Fig. 4: Michels built a casing kerf-cutting tool nicknamed "Kitchen Sink" to aid in the proper installation of casing.

with the DHH, conventional rock drilling tools were used to reach the planned 114-in outer diameters. Pier 12 and 13 were in the main river channel, and there was not any overburden material above the bedrock. This made it very difficult to place the casing in the correct location and seat it into the bedrock with the main channel river currents. A crude sketch turned into a casing kerf-cutting tool, which was nicknamed the "Kitchen Sink" by the crew members. This tool allowed for a kerf to be cut into the bedrock to allow the casing to be installed in the correct location, meeting the project specification location tolerances.

CHALLENGES

Michels Corporation's fundamental Core Value revolves around taking pride in a reputation for quality work performed safely and with care for the environment. Safety and environmental challenges were overcome on the project. With regard to safety, Michels crew members worked 39,000 man-hours on this job without an OSHA recordable incident. Daily safety discussions took place prior to the start of work each day. Once a week, a foundations-related safety topic was discussed with the group. Because falling into the Mississippi River was a concern of the crew members, a man-overboard drill was conducted and coordinated with local authorities. The response times were tracked and a Man Overboard Safety Plan was implemented. Fortunately, the plan did not need to be implemented during Michels' scope of work.

Environmental challenges were encountered and overcome throughout the duration of the project. The largest environmental challenge was containing, treating and disposing of drilling fluid. Michels utilized the river water as drilling fluid. However, during the rock socket drilling operation, the river water was mixed with the stone cuttings. These stone cuttings turned the water a cloudy white color and increased the turbidity and pH of the water. The Michels environmental team worked with the two local Department of Natural Resources agencies and within the EPA guidelines to generate a Water Treatment Plan. During the months with freezing temperatures, grain hopper barges were brought in to contain the drilling fluid prior to treatment and discharge. Prior to the arrival of the Michels drilled shaft operation, a team of divers relocated endangered clams.

WORK

The current northbound and southbound suspension bridges were constructed in 1935 and 1959, respectively. A visit by U.S. Transportation Secretary Ray LaHood in 2012 spurred the initial $34 million for engineering, design and land acquisition for the new I-74 Mississippi Bridge. The I-74 corridor project will be constructed for a cost of $1.3 billion. The design of the bridge called for 242 drilled shafts as the deep foundations that will support the 28 piers on the new bridge. Lunda Construction was the low bidder on the contract for $322,067,927.86, and Michels was chosen as the subcontractor to install the drilled shafts.



Fig. 3: A rebar cage is hoisted and set into an excavated drilled shaft from a barge in the river.

SHAFTS

The drilled shafts consisted of a steel outer permanent casing that was embedded into between 6-in and 2-feet of bedrock. The casing included carbide teeth that were welded to the bottom of the casing. These teeth cut through the bedrock while the casing was screwed in using the drill rig. Then the overburden soil was excavated inside the casing down to the top of bedrock. A rock socket was then excavated to a depth of 12 ft to 28 ft below top of bedrock. Once the rock socket was excavated, the bottom of shaft was cleaned, utilizing an airlift pipe or one-eye cleanout tool, to meet project specifications and approved by the onsite inspector. The steel reinforcement bar cage (rebar cage) was then hoisted and set into the excavated drilled shaft. Pier 12 and 13 drilled shaft rebar cages were designed as a double cage, which included an inner and outer cage. Next, a watertight concrete tremie pipe was assembled and inserted into the drilled shaft. The tremie pipe is a steel 10-in diameter pipe that allows the concrete to be placed at the bottom of the shaft without the concrete falling through the water column. A concrete pump truck was driven onto a barge and the barge was pushed into position by one of the tugboats. While the setting of the cage, tremie assembly and concrete pump truck priming was taking place, up to five concrete trucks were loaded onto a barge and were being pushed out to the drilled shaft that was being poured. By project specifications, the concrete trucks have a limited time to discharge their concrete into the drilled shafts, so the coordination of the previously mentioned steps was critical to the integrity of the drilled shaft. For Pier 12, the designed bearing was 4,789 tons, the nominal bearing resistance is 300 KSF, and the side resistance in 21 KSF for each drilled shaft. Cross Hole Sonic Logging (CSL) performed quality control testing of the drilled shaft. The integrity of the concrete was confirmed by the speed and strength of a signal passing through the concrete. Numerous false positives were encountered on the job using CSL testing. Concrete coring confirmed or denied the CSL results at a cost bore solely by Michels. Michels cored 53 shafts during the duration of the project. Of the 53 cored shafts, 12 shafts required remediation efforts, meaning CSL testing inaccurately detected a defect 77 percent of the time. The typical remediation efforts included coring additional holes to the defect zone, then pressure grouting the defect in accordance with an approved remediation plan. Several shafts were analyzed and accepted with 3-D tomography, a method that provides an enhanced evaluation of potential defects. Thermal integrity profiling, another drilled shaft quality control test, was proposed by Michels. However, the Iowa Department of Transportation denied the proposal.

COFFERDAMS

The top of the drilled shafts for Pier 12 and 13 were only several feet above the top of bedrock. Cofferdams were constructed from steel sheet pile and dewatered to allow access to the top of the drilled shafts. Rebar was placed and a concrete footing was then poured over the drilled shafts to create the footing for the basket handle sections of the bridge structure. The majority of the work on the cofferdams and footings took place during the winter months of 2017-18. The crews worked 24 hours a day to complete the schedule critical concrete footing pours.

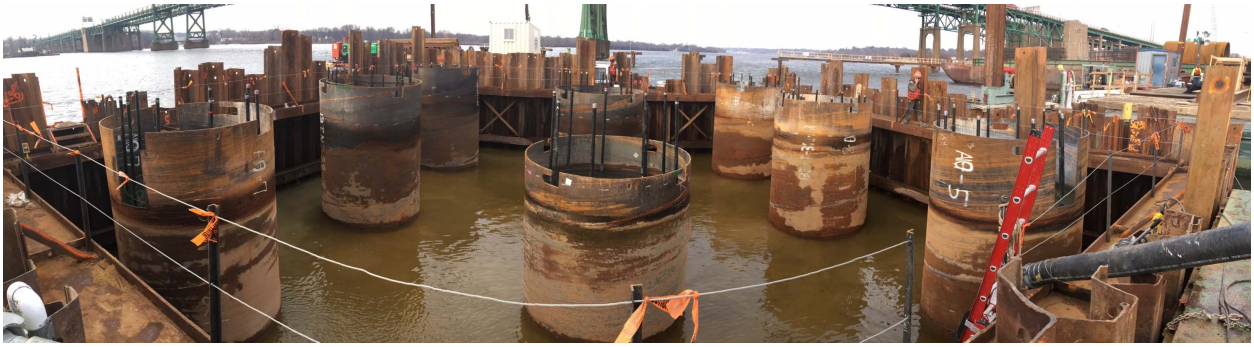


Fig. 5: Cofferdams were constructed from steel sheet pile and dewatered to allow access to the top of drilled shafts.

CONCLUSION

Michels successfully completed its portion of the contract six months ahead of Lunda Construction's schedule, setting Lunda up for future success. Teamwork was on display throughout the job from the pre-job planning to the daily coordination meetings. The crew took pride in their work and always took time to explain what Michels was doing on the river to curious local residents. At the end of the day, Michels was a critical part of building a bridge that will allow the traveling public to safely traverse the largest river in the United States, the Mississippi.

DRILLED SHAFT LOAD TESTING PROGRAM FOR DESIGN OF FOUNDATIONS FOR AN AUTOMATED PEOPLE MOVER

John C. Niedzielski, P.E., Gannett Fleming, Inc., Phoenix, Arizona, USA, 602-553-8817, jniedzielski@gfnet.com, Samer Rabab'ah, Ph.D., P.E, Civil Engineering Department, Hashemite University, Zarqa, Jordan, +962 (5) 390-3333, srababah@hu.edu.jo., Jason Valeria, P.E., Gannett Fleming, Inc., Jacksonville, Florida, USA, 904-988-9809, jvaleria@gfnet.com.

ABSTRACT

The PHX Sky Train is an automated people mover system located at Phoenix Sky Harbor International Airport. Phase II of the PHX Sky Train includes the design of over 150 drilled shafts for support of four guideway abutments, 75 guideway piers and three proposed stations. The soil conditions in this area generally consist of alluvial Sand, Gravel and Cobbles (locally known as SGC) deposited by the nearby Salt River. The foundation system will support relatively high axial loads, lateral loads and moments due to the height of the elevated guideway above the ground surface, where it needs to pass over roadways, parking lots, an existing terminal, and other buildings. Deep foundation design involves designing drilled shafts within the SGC deposits, some of which extend below the long-term groundwater table. Such extreme design loading conditions, together with difficult ground conditions at the site, result in several challenges for the design and construction of the deep foundation system for the project. This paper will present the results of a drilled shaft load test program implemented to provide site-specific measurement of the axial and lateral performance of the project drilled shafts. The load testing program consisted of a bi-directional load cell axial load test and a lateral load test performed on an instrumented test shaft 84 inches in diameter. The development and execution of the load test program and analysis of the test results are discussed. Comparisons were developed between predicted load capacities of drilled shafts using different design methodologies and the load capacity measured from the load tests. The load test results showed that underestimation of the capacity is evident using conventional methodologies. The load testing program was important for verifying the performance of the drilled shaft foundations on the project and was used to reduce the size of the drilled shafts.

Keywords: drilled shaft, load test

INTRODUCTION

The PHX Sky Train is a five-mile long automated people mover system situated at-grade and on an elevated guideway which connects terminals, parking facilities, a rental car center and the Valley Metro Light Rail system in Phoenix. The purpose of this automated train system is to provide a secondary transportation system within the airport to relieve roadway congestion, minimize wait times and travel times for passengers and provide climate-controlled waiting areas. Phase 1 opened to the public on April 8, 2013. Phase 1A opened on December 8, 2014.

Stage 2 of the project will extend west from the current Sky Train western terminus to connect Terminal 3, a future terminal, the proposed 24th Street Station and the Rental Car Center (RCC). The proposed elevated guideway will be cast-in-place concrete supported on precast pre-stressed concrete tub girders. The superstructure girders will be supported on piers, which will be founded on drilled shaft foundations.

The soil conditions in this area generally consist of alluvial Sand, Gravel and Cobbles (locally known as SGC) deposited by the nearby Salt River. Based on previous experience at PSHIA, shallow footings, mats, and drilled shafts were determined to be the best suited for the soil conditions encountered. Driven piles have not been used because of the anticipated difficulty in driving piles into dense soils that contain cobbles and boulders. The drilled shaft foundations supporting the piers will be either 72 inches, 84 inches or 96 inches

© 2019 Deep Foundations Institute

(6, 7, or 8 feet) in diameter. Piers will be supported on one pier column with one drilled shaft or two pier columns with two drilled shafts. There is a total of 75 piers supporting the elevated guideway, not including the 15 piers supporting the two proposed stations (24th Street Station and RCC Station) and one future station (West Terminal Station).

The foundation system will support relatively high axial loads, lateral loads and moments due to the height of the guideway above the ground surface, where it needs to pass over existing roadways, parking lots, an existing terminal, and other buildings. The potential presence of undocumented loose and compressible fill, potentially unstable excavation conditions in the granular SGC soil, and the presence of cobbles and boulders, which may be difficult to remove during excavation, are the primary considerations for foundation design. Most design techniques are based on test results in sands and clays and do not account for soil with cobbles and boulders. Allowable Stress Design was used for the design of this project.

SITE GEOLOGY AND GEOTECHNICAL INVESTIGATION

Phoenix is located within the Paradise Valley Basin in the Basin and Range physiographic province of Arizona. Alluvial fan deposits are predominant in this area, which result from sheet-flow erosion from the surrounding mountains and re-deposition in lowland areas. These alluvial materials have been deposited during the Holocene and Pleistocene periods in the arid climate of Southern Arizona, and as a result, are related to "flash-flood" events followed by drying and cementation. These conditions have produced a variable subsurface stratigraphy of generally coarse alluvium (sand, gravel, and cobbles) interbedded and overlain by finer-grained materials (clay, silt, and sand). Lateral and vertical variability of localized deposits of coarse gravel and cobbles typifies the high-energy alluvial depositional systems. Therefore, the materials described as predominantly coarse-grained soils (classified as SP, SW, GP, GW, GM, and GC) will also contain cobbles and boulders (Figure 1).

Gannett Fleming developed a subsurface investigation consisting of 116 borings for Stage 2 of the PHX Sky Train. Seventy-nine of these borings were performed for the elevated guideway. Most of the elevated guideway borings were extended to depths ranging from 80 feet to 100 feet below existing grades. Four borings were extended to 110-foot or 120-foot depths below grade. Nineteen borings were extended to depths of 130 feet to 135 feet below existing grades, and four borings were extended to depths of 140 feet to 146 feet below grade.

The rotosonic drilling method, which was used for this project, is a method of drilling by which a steel drill casing is vibrated while being pushed into the underlying formation. This method allows for the retrieval of continuous soil cores which are deposited into a plastic bag sleeve. The rotosonic boreholes were generally drilled using a 6-inch diameter inner barrel and an 8-inch diameter outer casing. At the bottom 10 to 30 feet of the borings, the inner barrel was changed to 4-inch diameter and the outer casing was 6-inch diameter. Prior to drilling, for safety reasons and in order to avoid possible conflicts with existing unmarked underground utilities, the first 10 feet of depth at the boring locations was excavated using air-knifing (potholing) methods.

In addition to the continuous core runs with the rotosonic drilling equipment, standard split-spoon samples (ASTM D 1586) were collected in some borings in general accordance with ASTM procedures. The split-spoon samples were typically only collected in the upper 15 feet of the subsurface in the alluvial soil deposits above the sand-gravel-cobble deposits (SGC).

Groundwater was encountered during drilling at depths ranging from 97 feet to 106 feet bgs (below ground surface). Within borings 90-feet deep or shallower, groundwater was not encountered either during drilling or immediately after drilling completion.



Fig. 1. Sand, gravel and cobbles (SGC) encountered during drilled shaft excavation.

DRILLED SHAFT LOAD TEST

As a means to demonstrate the installation plan and to provide site-specific measurement of axial performance for the as-built conditions, a load test shaft was designed and constructed in a non-production site area. Loading was by means of a bi-directional static load test utilizing AFT-Cell embedded hydraulic jacks performed by Applied Foundation Testing, Inc. on October 12, 2017. The test shaft was constructed with 87-inch O.D., 1-inch wall permanent casing, installed from grade to elevation 1099 feet, 4 feet below ground. Below the casing, the shaft was 84 inches nominal diameter and constructed to a tip elevation of 1041.5 feet. The top of shaft concrete was equal with the ground surface elevation of 1103 feet, resulting in an overall shaft length of 61.5 feet.

A single level of three bi-directional embedded hydraulic jacks was installed at elevation 1058 feet. Five levels of strain gages with four gages per level were also included within the shaft to measure load distribution. Four embedded Linearly Variable Differential Transformers (LVDTs) were also installed to obtain displacement data at the cell location. Figure 2 shows the elevation view of the instrumented test shaft. Figure 3 shows the AFT-Cell with top and bottom plates welded to the rebar cage along with the installed LVDTs and telltales.

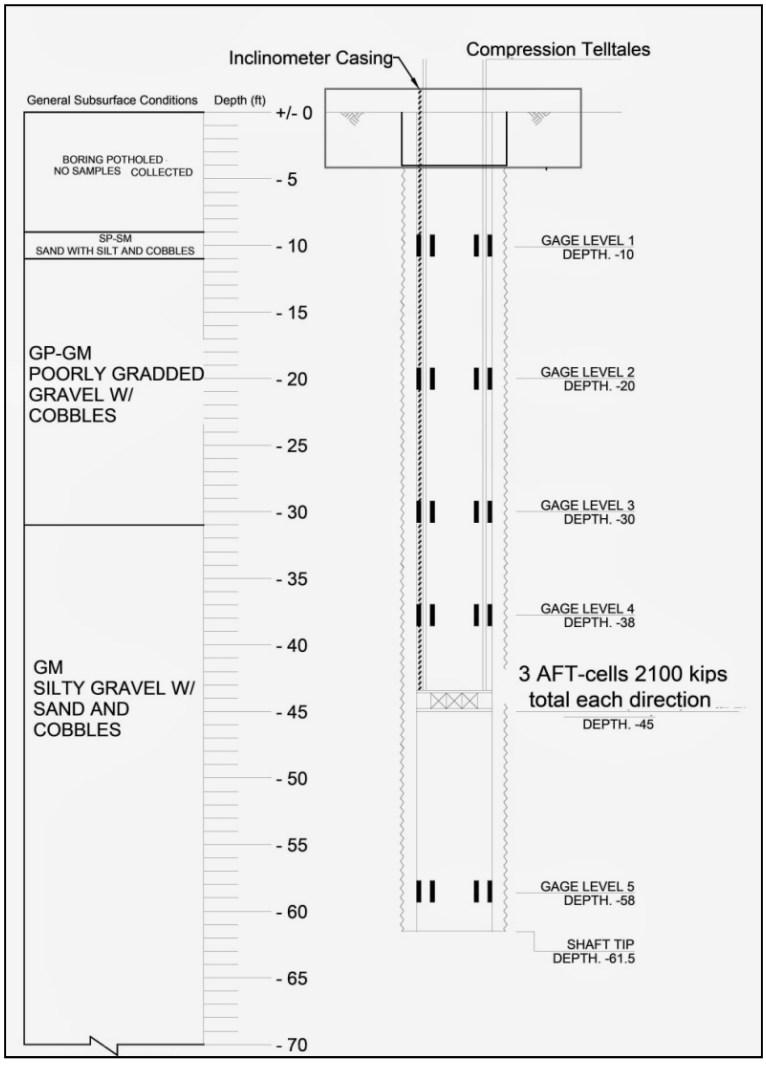


Fig. 2. Load test instrumentation (courtesy of AFT).



Fig. 3. ATF-Cells with top and bottom plates, telltales, and LVDTs.

The drilled shaft was constructed in the dry with the upper permanent casing provided as a means of supporting the upper sand layer and to prove attachment for the subsequent lateral test. Upon completing the excavation, the drilled shaft was subsequently checked for depth and inspected visually for verticality. Once the required depth was attained, the shaft bottom was cleaned using a standard clean-out bucket. Mechanical caliper testing was performed to determine the actual dimensions of the shaft excavation.

Shaft reinforcement consisted of a full-length rebar cage with 40-#11 Grade 60 vertical bars and #5 bar lateral ties with 12-inch center-to-center spacing. The single level embedded jacks, telltale and inclinometer casing, displacement sensors, and five levels of four sister bar strain gages were installed onto the rebar cage. A tremie pipe was installed in the center of the shaft following rebar cage placement with the tremie funnel facilitating its passage through the embedded jack assembly. Concrete was placed by the tremie method using a concrete pump truck, until sound concrete was observed at the top of the drilled shaft. The theoretical concrete volume calculated from the caliper data was 104.4 cubic yards, and the actual concrete volume placed was 110.5 cubic yards. Prior to axial and lateral load testing, integrity was evaluated on the test shaft using Crosshole Sonic Logging (CSL) and gamma-gamma density logging (GDL).

The test loading steps were performed in accordance with ASTM D1143 "Standard Test Methods for Deep Foundations Under Static Axial Compressive Load", Procedure A - Quick Test. Loads were applied in 30 increments until the maximum pressure of the loading system was reached. The maximum applied load was 4,050 kips, resulting in 0.012 inches of upward displacement and 0.078 inches of downward displacement. After accounting for the shaft weight above the AFT-Cell of 315 kips, the maximum applied bi-directional load applied during the test was 7,779 kips.

Figure 4 shows the load displacement curves obtained for the test shaft. Upward displacement above the load cell is shown as positive values on the y-axis and downward displacement below the load cell is shown as negative values.

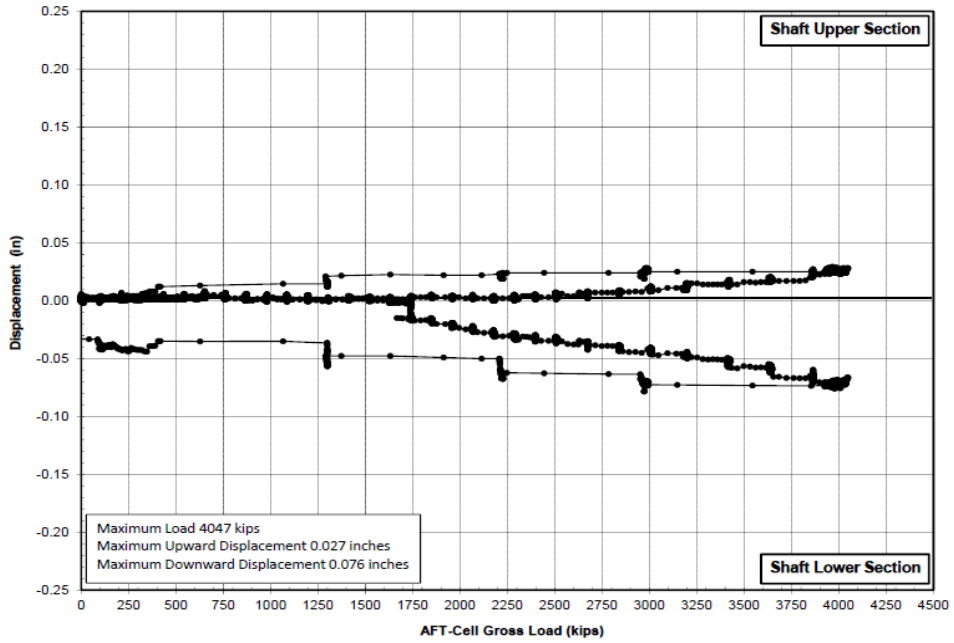


Fig. 4. Load-Displacement Curves (courtesy of AFT).

Unit side shear values obtained during the load test were calculated using strain gage data and are presented below in Table 1. The side shear increased with increasing depth from 0.84 kips per square foot (ksf) at approximately 15 feet bgs to 13.4 ksf at approximately 41.5 feet bgs. However, the unit shear values above

elevation 1065 feet were not mobilized during the load test, and these results were not used for drilled shaft design. The peak unit side shear resistances of 7.8 and 13.4 ksf compare with a previous load test performed for Stage 1 of the PHX Sky Train project where mobilized peak unit side shear resistances of 14.5 ksf and 17.9 ksf were achieved in SGC soils as described in Niedzielski et al., DFI Annual Conference Proceedings, 2010. Other recent unpublished load tests performed on SGC materials in Phoenix have shown mobilized peak unit side shear resistances in the 12 to 20 ksf range.

Table 1. Load Transfer Summary (Courtesy of AFT)

Elevation	Soil Type	Layer Displacement	Peak Unit Side Shear Resistance (ksf)	Calculated Side Shear Resistance using AASHTO*
1103' (TOS) to 1093'	Sand with Silt and Cobbles (SP-SM)	0.005	1.85**	0.81
1093'-1083'	Poorly Graded Gravel with Sand & Cobbles (GP-GM)	0.006	0.84**	1.98
1083'-1073'	Silty Gravel with Sand and Cobbles (GM)	0.009	1.62**	2.78
1073'-1065'	Silty Gravel with Sand and Cobbles (GM)	0.012	4.05**	3.27
1065'-1058'	Silty Gravel with Sand and Cobbles (GM)	0.018	13.4	3.53
Load Cell Level				
1058'-1043.5'	Silty Gravel with Sand and Cobbles (GM)	0.051	7.76	3.7
	End Bearing	0.030	31.2	

*AASHTO Standard Specifications for Highway Bridges, 2002
**Side shear resistance not mobilized

DESIGN FOR AXIAL CAPACITY IN COHESIONLESS SOIL

All methods for determining the axial capacity of drilled shafts are based upon the general equation:

$$Q_{ult} = Q_T + Q_S \quad [1]$$

Where, Q_{ult} is the ultimate axial load capacity of the shaft, Q_T is the ultimate tip resistance of the shaft, and Q_s is the ultimate side resistance of the shaft. Q_s is calculated by the following equation:

$$Q_s = f_s A_s \quad [2]$$

where f_s is the shaft resistance per unit area, and A_s is the surface area of the sides of the shaft in contact with the soil. This paper is focused on determining f_s for the SGC materials.

The unit side resistance for a given granular soil layer is given by Reese and O'Neill (1999) (Publication No. FHWA-IF-99) adopted by AASHTO (2002) as:

$$f_s = \beta\sigma'_z \leq 2 \text{ tsf (tons/ft.}^2\text{)} \quad [3]$$

Where β is given by the function $\beta = 1.5 - (0.245z)^{0.5}$; $0.25 \leq \beta \leq 1.20$, σ'_z is the vertical effective stress at the middle of a layer, and z is the depth to the middle of a layer in feet. In gravelly sand or gravel,

β is given by the function: $\beta = 2.0 - 0.15z^{0.75}$; $0.25 \leq \beta \leq 1.80$.

However, in gravelly sands or gravels, when $N_{60} > 50xB/1$ ft., Reese and O'Neill (1999) recommend treating the soil as a Cohesionless Intermediate Geomaterial (IGM) as follows.

$$f_s = k_o \sigma' \tan\phi \quad [4]$$

Where

$$k_{0i} = (1 - \sin\emptyset_i') \left[\frac{0.2 p_a N_{60}(\text{Layer i})}{\sigma_{vi}'}\right]^{\sin\emptyset_i'} \quad [5]$$

Comparisons between the measured axial capacity using the results from the load test and the β-method (FHWA 1999 and AASHTO 2002) for drilled shafts in cohesionless materials are shown in Figure 5.

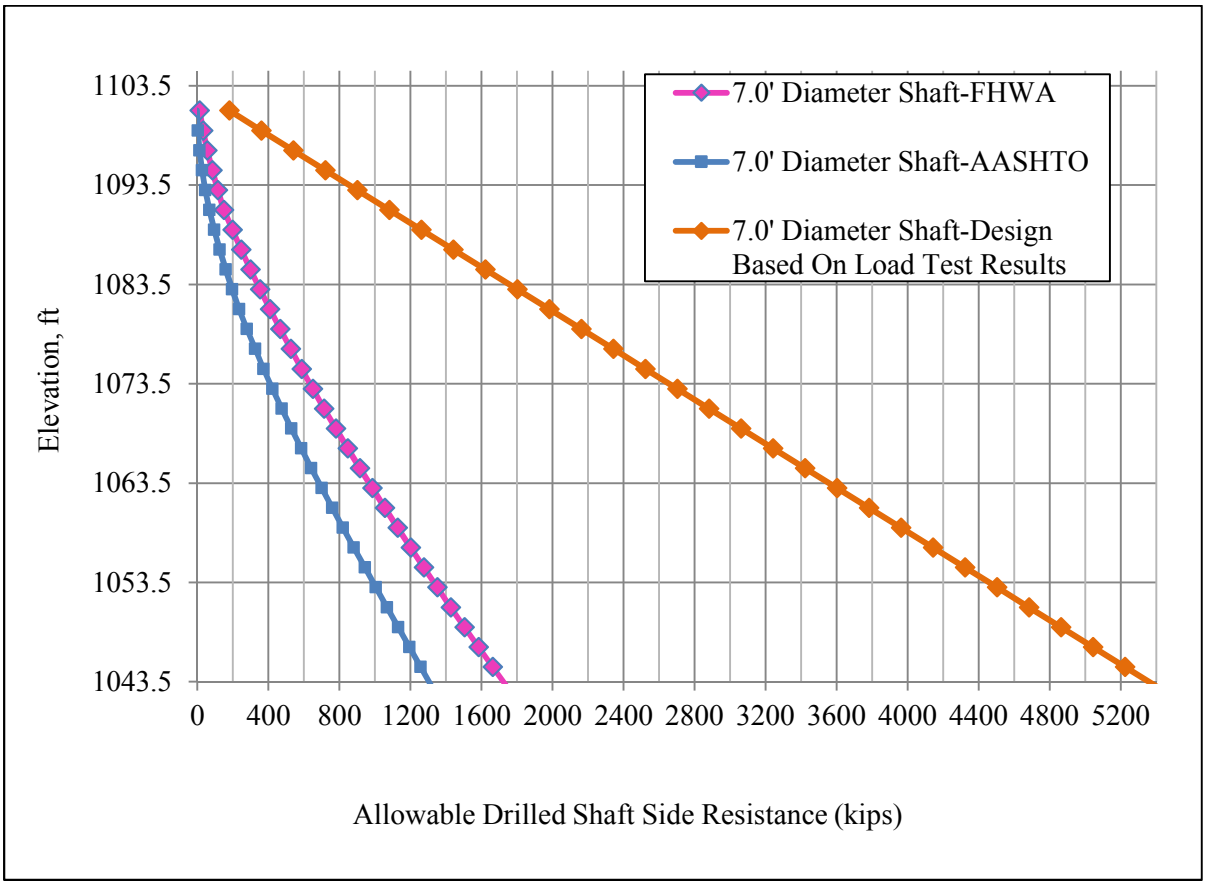


Fig. 5 Allowable drilled shaft side resistance using different prediction methods.

The Reese and O'Neill (1999) equation for cohesionless IGM resulted in a higher predicted side friction capacity compared to AASHTO but is much lower when compared to the side friction used for design. The design shaft side friction in Figure 5 was derived from the results of the axial load test. The load test report notes that the unit side friction values measured are not fully mobilized. This is evident in the very small amounts of movement measured by the instrumentation in the test shaft. As such, the values most representative of the ultimate unit side friction within the generally homogenous SGC deposit would be those experiencing the most movement, which would be captured by the instrumentation closest

to the load cell. The shaft segments directly above and below the load cell measured unit side friction values of 13.4 and 7.8 ksf, respectively. Considering these as the most representative estimates of the SGC unit side friction and understanding that even these values would likely be higher if allowed to fully mobilize, the design team selected a design unit side friction of 10.5 ksf.

LATERAL LOAD TESTING

Lateral load testing was performed in general accordance with ASTM D3966: "Standard Test Methods for Deep Foundations Under Lateral Load". The load test was performed on October 13, 2017. The test program included the installation of the test shaft, as described earlier, which underwent Bi-directional load testing followed by a lateral load test via jacking against a reaction shaft. The reaction shaft was 72-inches in diameter and 35 feet in length. Instrumentation for the lateral load test consisted of a calibrated hydraulic jack, five levels of strain gages, two LVDTs on an isolated reference beam to measure lateral displacement, and an inclinometer casing to facilitate deflected shape measurement. The strain gage pairs aligned along the lateral loading axis were monitored during the lateral load test to measure bending strains.



Fig. 6 Reinforcing cage with instrumentation.

The specified lateral test load for the shaft was 150 tons (300 kips). Loads were applied with a 300-kip hydraulic jack attached between the test shaft and reaction shaft with a clevis/pin connection, which allowed the drilled shafts to freely rotate during loading. During the load test, load increments of approximately 15 kips, at intervals of 8 to 10 minutes, were applied up to the test load of 300 kips. An additional load increment was then applied, reaching the maximum lateral test load of 338 kips. No additional load increments were able to be applied due to reaching the limits of the jacking equipment. The load was released in four decrements using 8-minute hold periods. The test shaft had a maximum lateral displacement of 0.036 inches as measured by the average of the two LVDTs attached to the reference beam at the rear face of the shaft.

The lateral loads imposed on the foundations controlled the design of the drilled shafts. The conventional

P-Y curves were used based on the API sand model that is internally generated using the soil parameter inputs in the LPILE 2015 (Ensoft, Inc.) computer program. The response of the drilled shafts to the horizontal and moment loading was analyzed using the LPILE program. The soil properties used for Stage 1 of this project were γ=135 pcf, ϕ=40°, and k=275 pci, where γ is the unit weight, ϕ is the friction angle, and k is a constant for the Young's modulus.



Fig. 7 Test shaft (background) and reaction shaft

Plots of lateral load versus deflection of the pile head are shown for both the lateral load test and an LPILE analysis in Figure 8. In the load test, the displacement measured at any given load was less than the displacement predicted using LPILE. The results show that LPILE overestimates the pile head deflection. Based on these results, the SGC soil showed higher lateral resistance than what is predicted by the LPILE software.

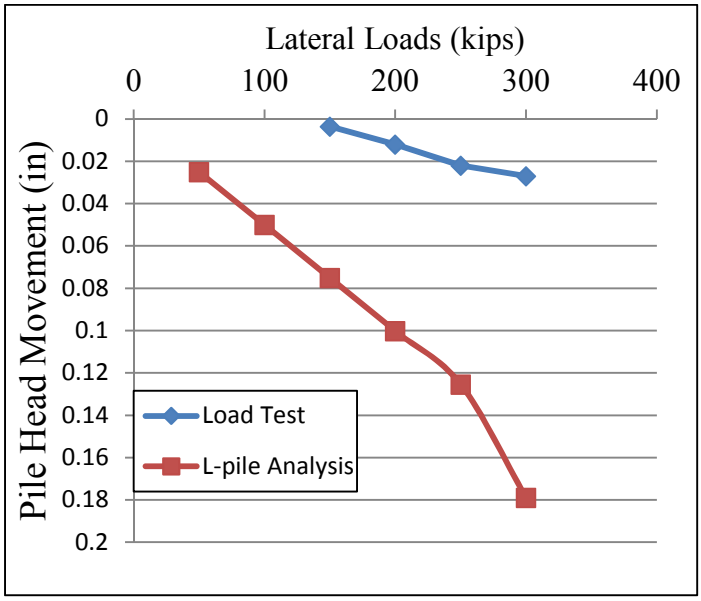


Fig. 8 Lateral load versus pile head displacement

The low lateral movement prevented the authors from being able to develop site-specific P-Y Curves. However, sensitivity analyses were performed to back-calculate the subgrade modulus k, based on load test results. Instead of k=275 pci that had been used for the Stage 1 design, the authors recommended a higher k value be used (k=500 pci) for the analysis and design of drilled shafts for Stage 2 of this project. This k value compares well with analyses of pressuremeter data collected during the pre-design phase of Stage 1.

The load test results indicated a much higher soil response, as shown in Figure 8, and therefore, much smaller shaft top deflection. Shaft lateral capacity design solely using conventional p-y curves would have resulted in much larger diameter and/or deeper shafts. Therefore, the use of the load test results for design produces substantial construction cost savings.

Costs associated with the load testing included the additional cost to construct the load test shaft and the reaction shaft and the cost of the vertical and lateral load tests. The total cost of the load tests was approximately $286,000. The cost savings to the project as a result of performing the vertical and lateral load tests is estimated to be approximately $3 million.

CONCLUSIONS

This paper presents a case history of a successful implementation of an in-situ load testing program to re-design conventionally designed drilled shaft foundations, which resulted in significant cost savings. In-situ testing provides a direct measure of performance using the actual construction means and methods planned for the project in the specific geologic formation in which the shafts will be founded. The overall reliability of the foundation is improved because of the site-specific verification of the design and construction methods. Measured side resistance of a drilled shaft from a load test was compared with various predictive equations currently employed for design purposes. The results demonstrate that the AASHTO design methods appear to be conservative for design of drilled shafts in SGC soils.

The use of the drilled shaft load test results was essential for axial and lateral capacity analyses; without the load test many of the drilled shafts would have needed to be extended deeper. Had this occurred, drilled shaft construction would have been more costly for the owner, and additional construction time and issues would have arisen for the contractor such as the potential for caving in drilled shaft excavations at greater depths, longer temporary casings and handling heavier reinforcing bar cages.

REFERENCES

AASHTO, 2002. Standard Specifications for Highway Bridges, 17th Edition, American Association of State Highway and Transportation Officials.

Applied Foundation Testing, 2017. Final Data Report of AFT-Cell Bi-Directional Load Testing, Phoenix Sky Harbor International Airport-Sky Train Stage 2.

Applied Foundation Testing, 2017. Final Data Report of Lateral Static Load Testing, Phoenix Sky Harbor International Airport-Sky Train Stage 2.

LPILE Plus 2015 for Windows, 2015, Ensoft, Inc., Austin, Texas.

Niedzielski et al., Foundation Design and Construction Challenges for the Phoenix Sky Train Project, Proceedings of the 35th Annual Conference on Deep Foundations, 2010, Hollywood, CA.

O'Neill, M. W., and Reese, L. C., 1999. Drilled Shafts: Construction Procedures and Design Methods, Federal Highway Administration Publication No. FHWA-IF-99-025.

INSTALLATION OF 10 FEET DIAMETER CIDHS IN SOFT CLAY USING ROTATOR/OSCILLATOR ON TRESTLE

Pirooz Barar, PB&A Inc., San Rafael, CA, USA, (415) 259-0191, pbarar@pbandainc.com
Babak Mamaqani, PB&A Inc., San Rafael, CA, USA, (415) 259-0191, babak.mamaqani@pbandainc.com

ABSTRACT:

The Moanalua trestle spanned over Moanalua Stream, Honolulu, HI and was designed to accommodate construction of five 10 feet diameter cast in drilled hole (CIDH) piers as a part of Honolulu Authority for Rapid Transportation (HART) project. Due to the proximity of piers to the existing bridge, the trestle was elevated 20 feet above grade. Stratigraphy of the site consisted of shallow depth of fill and 150 feet of loose to very loose recent alluvium (soft clay) underlain with stiff to hard old alluvium (stiff clay). CIDH casings were installed by a rotator or oscillator depending on the diameter of the piers. The challenge was to design the trestle, not only for heavy gravity loads, but also to resist significant lateral loads from rotator and oscillator with minimal deflection. Series of piles, called reaction piles, were integrated into the trestle at each CIDH pier location to provide adequate lateral support for the rotator/oscillator. Due to the lack of information regarding soil Young's modulus (E), a methodology was developed to calibrate and calculate E with two methods. Extensive analyses using LPILE and finite element analysis program, PLAXIS, were performed to model reaction piles and calculate lateral deflection.

Keyword: trestle, cast in drilled hole (CIDH), rotator, oscillator

PROJECT SPECIFICATIONS

The Honolulu Rail Transit includes 20-mile route and 21 stations to be built from East Kapolei to Ala Moana Center, with $1.55 billion construction budget. The project is divided into two phases as shown in Fig. 1: Phase 1 which connects East Kapolei to Aloha Stadium with expected operation in late 2020, and Phase 2 which connects Aloha Stadium to Ala Moana Center with expected operation in 2025.

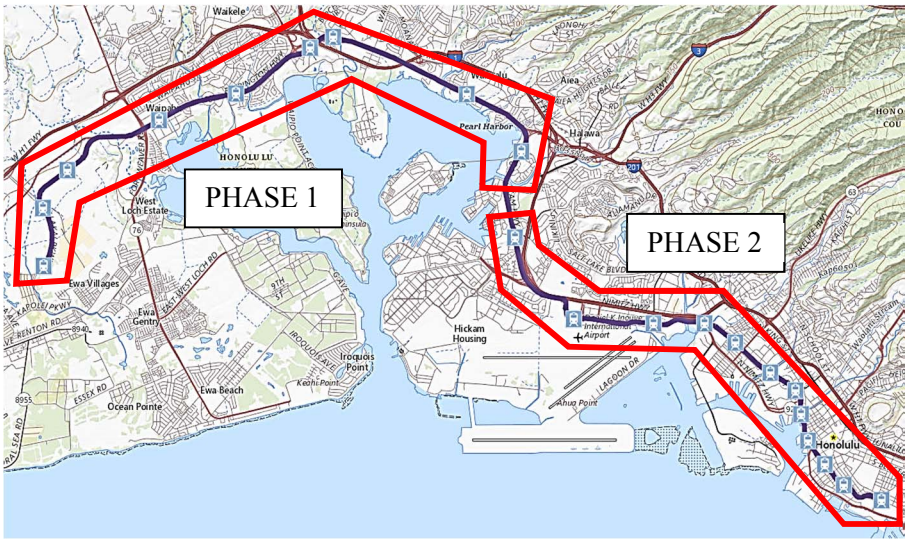


Fig. 1. The Honolulu Rail Transit Project, Honolulu, HI (HART, 2019)

© 2019 Deep Foundations Institute

Moanalua trestle was a temporary platform over Moanalua stream to construct five cast in drilled hole (CIDH) piers, namely piers 614 through 618, as a part of Phase 2 of Honolulu Authority for Rapid Transportation (HART) project. The diameter of piers typically was 10 feet with tip elevation at 250 feet below grade. Due to the proximity of piers to an existing bridge and required space for equipment, the trestle was elevated 20 feet above grade to clear conflicts. The location of the Moanalua trestle is shown in Fig. 2

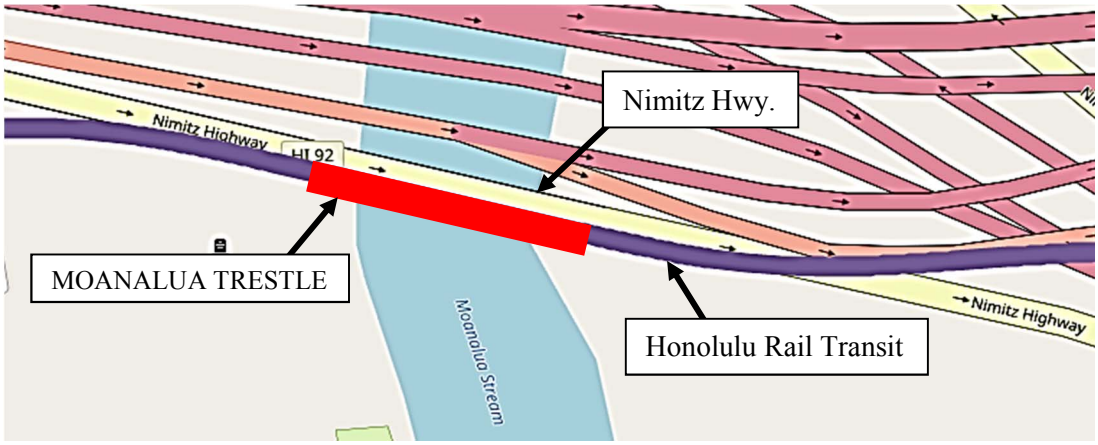


Fig. 2. Moanalua Trestle Location

SITE STRATIGRAPHY AND SOIL PROPERTIES

Per the geotechnical report, the stratigraphy of the job site consisted of shallow fill and almost 150 feet of loose to very loose recent alluvium (Ra) underlain with stiff to hard alluvium (Qa and Ql) as shown in Fig. 3.

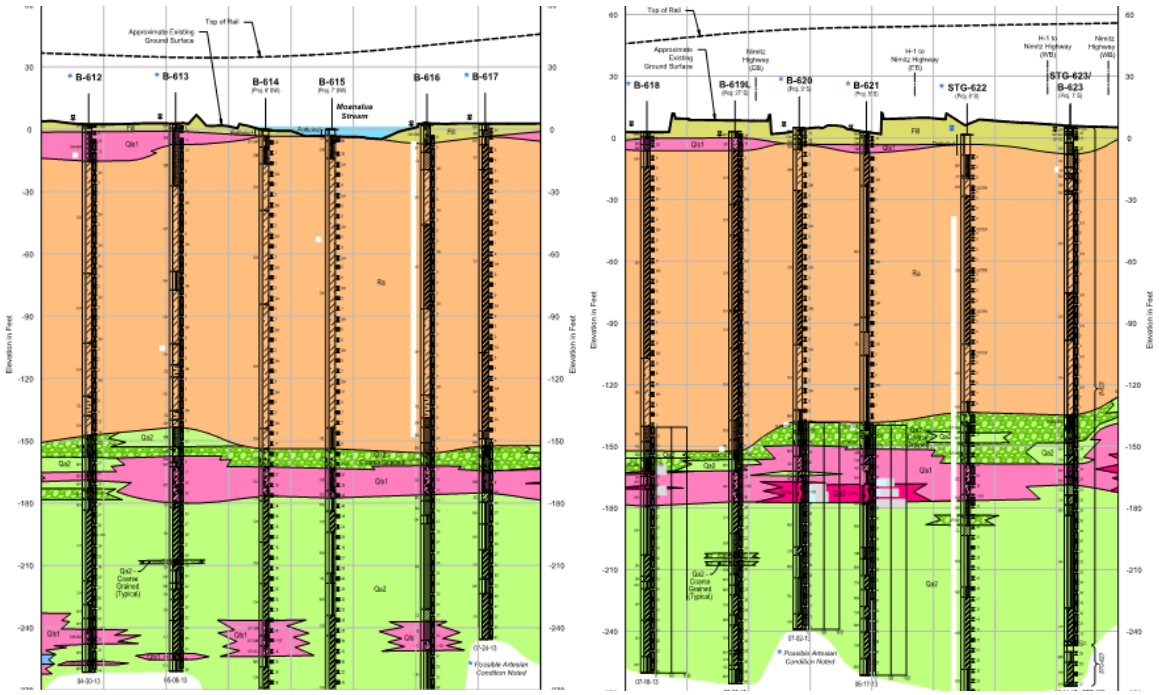


Fig. 3. Site Stratigraphy at Piers 614 Through 618

According to the standard penetration test (SPT) result, the N value for Ra layer is 0 and the hammer could penetrate the soil under its self-weight. Soil properties were developed to be used mainly for LPILE program as listed in Table 1. All the values in the geotechnical report were based on geotechnical investigations except soil Young's Modulus which was purely based empirical values in table C10.4.6.3-1 of AASHTO LRFD (2012).

Table 1. Soil Properties

Soil Type	Top Elevation (feet)	Soil Density γ (pcf)	Poisson Ratio ν	Young's Modulus E (ksi)	Friction Angle ϕ (degree)	Undrained Shear Strength S_u (psi)	Modulus of Subgrade Reaction k (pci)	Strain at 50% Max Stress ε_{50}
Fill	0	115	0.3	8.3	34	0	60	-
Ra	5	105	0.45	1.0	-	600	-	0.01
Qa2-CG	150.8	110	0.35	13.9	38	-	125	-
Qls1	160.3	110	0.25	6.9	32	-	30	-
Qa2	174.5	110	0.3	8.3	-	3,000	-	0.005

SPECIAL CONSTRUCTION EQUIPMENT

A BUMA rotator CR3000 was used to install CIDH casings for piers 614 through 617 using. The rotator uses clockwise or counterclockwise rotational force to drill and install casings through the soil. Per the manufacturer's specifications (BUMA, 2019), the rotator can exert up to 98,000 kip-feet of torque which translates into 260 kips of the lateral load if it is restrained at tongue end (point A) as shown in Fig. 4. The rotator can install up to 118.1 inch diameter casing and has the extraction capacity of up to 1180 kips.

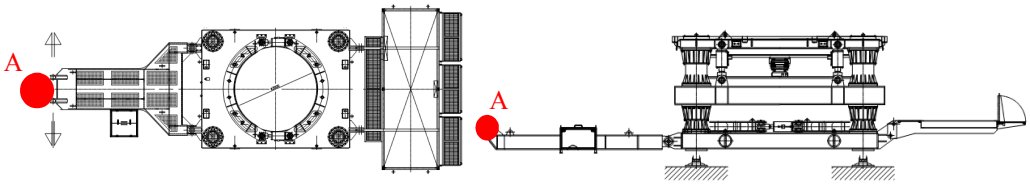


Fig. 4. Rotator BM-CR3000

CIDH casing for pier 618 was installed with a BUMA oscillator C3600. Unlike rotator, the equipment oscillates back and forth to install a casing. The oscillator has higher torque and extraction capacities compare to the rotator and can be used to install larger diameter casings. Per manufacturer's specification (BUMA, 2019), the oscillator can exert up to 14,000 kip-feet of torque which translates into 580 kips of the lateral load if it is restrained at tongue end as shown in Fig. 5. This equipment can install up to 141.7 inch diameter casing and has the extraction capacity of up to 28,000 kips. The self-weight of both rotator and oscillator is 195 kips. Per the manufacturer, rotator and oscillator displacement should be limited to maximum 2 inches to achieve optimum capacity and prevent any damages to the casing.

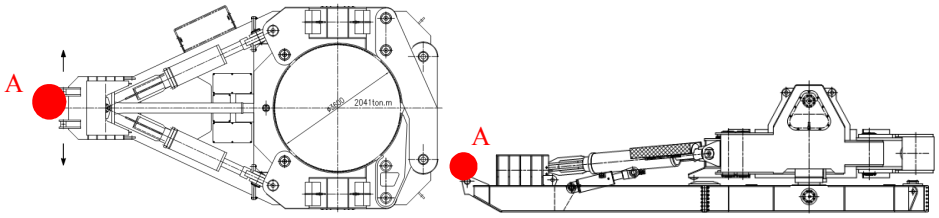


Fig. 5. Oscillator BM-C3600

TRESTLE GEOMETRY

Five and seven Pipe 42”X1” were initially assumed at rotator and oscillator reaction frames respectively to limit deflection to 2 inches as required by manufacturer’s specifications. These piles were connected by lateral bracings and cap beam to create a reaction frame at each pier location as shown in Fig 6.

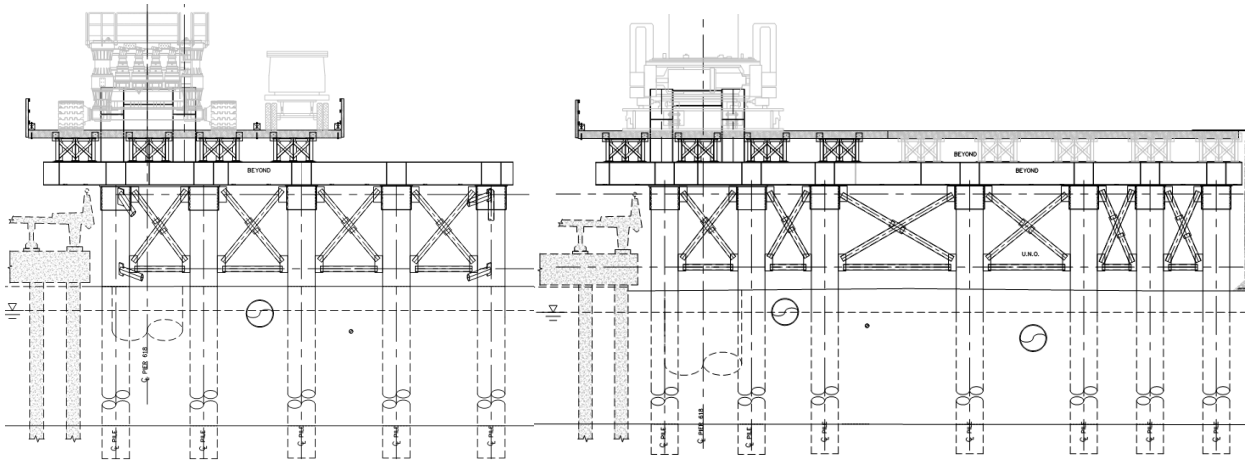


Fig. 6. Typical Reaction Frames; Left: Rotator Frame, Right: Oscillator Frame

LATERAL LOAD ANALYSIS

Trestle piles were divided into two main categories: 1) gravity piles which were mainly designed to resist and transfer gravity loads, and 2) reaction piles which were designed to resist lateral load exerted by rotator/oscillator with the minimal deflection on top of gravity loads. This section focuses on the design of reaction piles under lateral loads.

Due to the complexity and sensitivity nature of the project, finite element analysis (FEA) program, PLAXIS 2D, was selected to evaluate reaction pile deflection under the rotator/oscillator lateral load. Soil Young’s modulus (E) was needed to perform PLAXIS analysis. Therefore, Young’s Modulus in the geotechnical report needed to be verified since they were based on empirical values. A methodology was developed to calibrate and calculate accurate soil Young's Modulus.

Methodology

Recommended Young’s modulus in the geotechnical report was first calibrated using results obtained from LPILE and PLAXIS models with a single reaction pile. The calibrated Young’s modulus from this step is a constant value over the depth of the soil layer.

Second, Young’s modulus was calculated using the shear wave velocity value obtained from seismic CPT test in the geotechnical report. This resulted in variable Young’s modulus over the depth of the soil layer which was then idealized into three zones with constant E values to simplify the modeling procedure.

Finally, PLAXIS models were generated using both calibrated and calculated Young’s modulus and soil properties listed in Table 1 to investigate reaction frame deflection under lateral loads from rotator/oscillator. The adopted methodology in this paper is presented in Fig. 7.

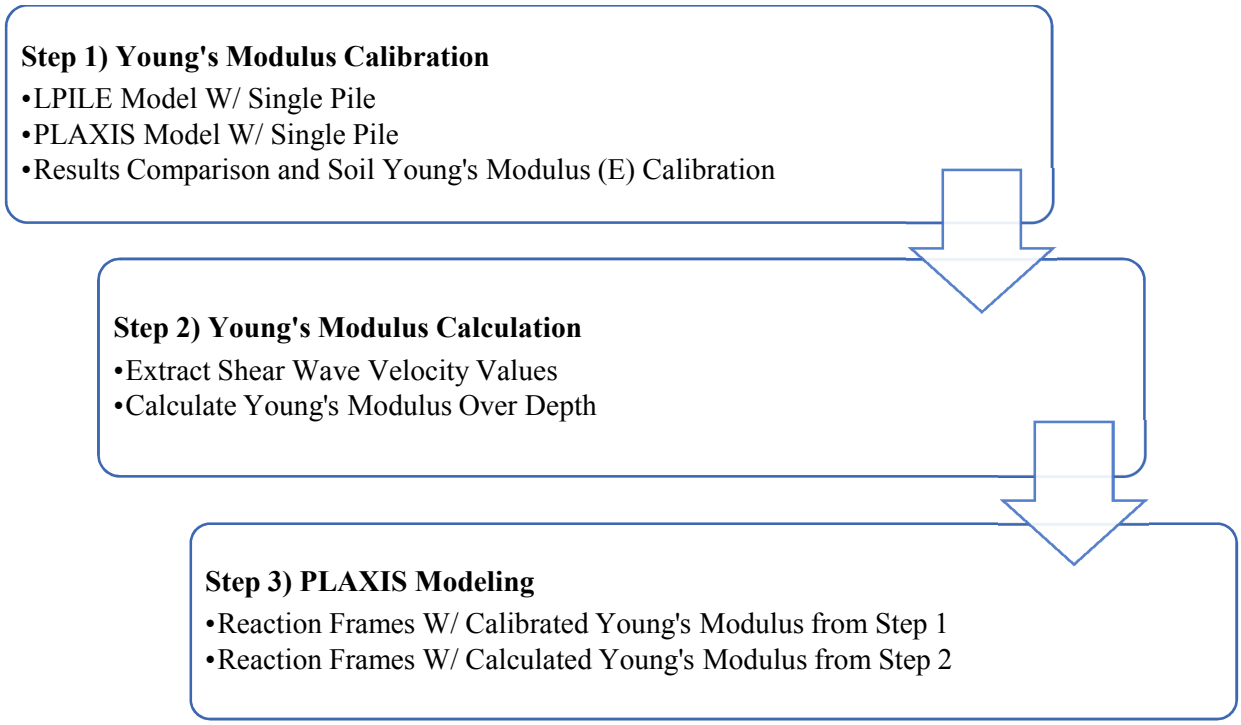


Fig. 7. Methodology to Evaluate Reaction Frame Deflection

Young's Modulus Calibration

LPILE is a powerful tool to investigate a single pile under lateral loads. One of the main advantages of LPILE over PLAXIS is that it can calculate pile deflection without input for soil Young's modulus. The program generates p-y curves over the depth of the pile which can be translated into soil Young' modulus. However, the program has two main limitations: 1) it can only model a single pile, and 2) it cannot accurately model pile head condition and multiple pile cross bracing frames.

Two identical models with a single pile were generated in LPILE and PLAXIS with properties listed in Table 1. Each model consisted of a single reaction pile with 52 kips of lateral load (260 kips for rotator/5 piles per reaction frame) applied at top of the pile. It was assumed that the pile head is fixed at the top, which means it is restrained against rotation but can freely move laterally. Only one pier was modeled since soil properties and stratigraphy were almost the same at all pier locations.

LPILE model results using soil properties listed in Table 1 showed that maximum deflection of 0.82 inches occurs at the pile head and then rapidly dissipates and reaches zero at almost 50 feet below the pile head within the top soil layer (Ra). This implied that Young's modulus of the top soil layer (Ra) only needed to be calibrated.

The identical PLAXIS model with recommended E value predicted 1.95 inches of deflection at pile head, which was significantly higher than the one calculated by LPILE as shown in Fig. 8. This meant that the recommended Young's modulus in the geotechnical report was significantly low considering other soil properties recommended in the geotechnical report. Therefore, the value for the Young' modulus (E) of the upper layer of soil (Ra) was increased gradually in an iterative process, and at each iteration, the results were compared to see whether the results of the PLAXIS and LPILE model would match. After several

iterations, a PLAXIS model with constant moduli value (E) of 4.9 ksi for the upper soil layer, Ra, yielded results that are aligned with the LPILE model as shown in Fig. 8.

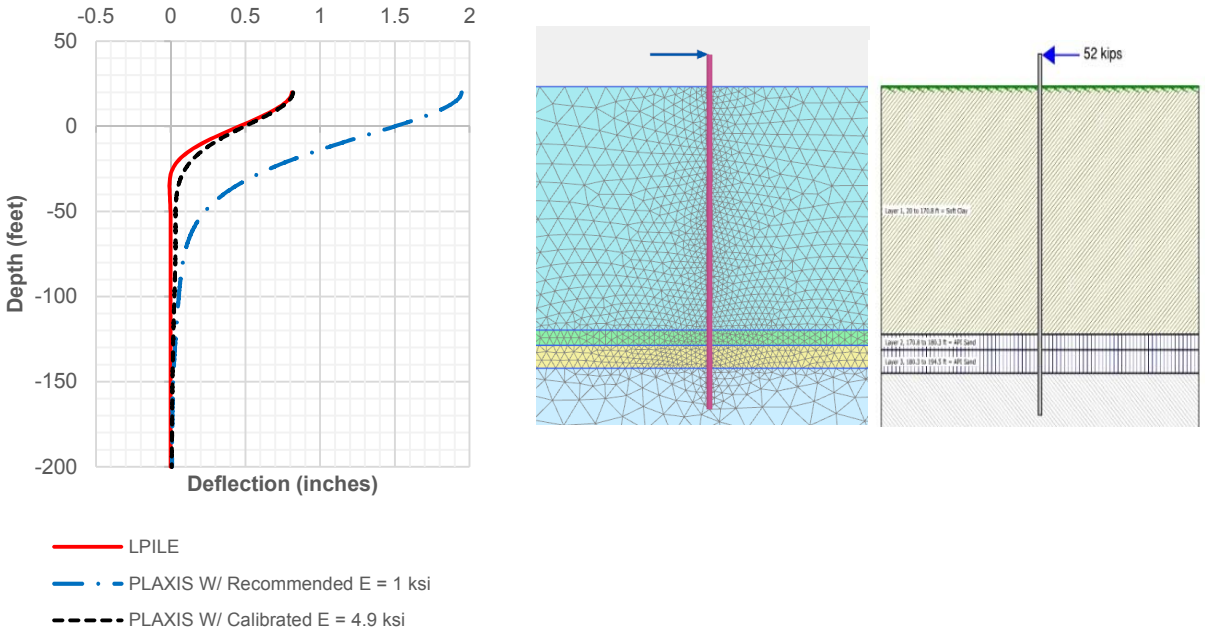


Fig. 8. Single Pile Models in LPILE (Right) and PLAXIS (Middle) with Results (Left)

Young's Modulus Calculation

Soil Young's modulus (E) can be caluacted using shear wave velocity results from seismic CPT tests. The first step was to calculate maximum shear modulus using the shear wave velocity as suggested by Kramer (1996) using the following equation.

$$G_{max} = \rho . V_s^2 \quad [1]$$

Where G_{max} is the maximum shear modulus, ρ is soil density and V_s is shear wave velocity.

Vucetic and Dobry (1991) suggested modulus reduction curves as shown in Fig. 9 for clay with OCR up to 15 that can be used to calculate soil shear modulus using G_{max}, cyclic shear strain, γ_c and plastic index (PI).

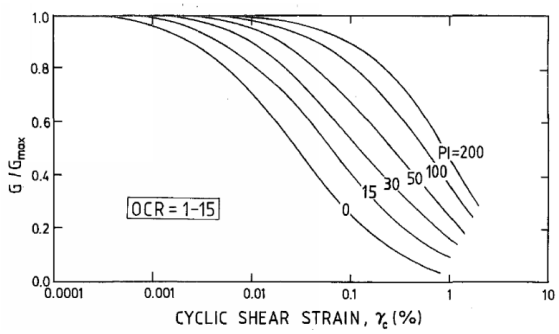


Fig. 9. Modulus Reduction Curves for Clay by Vucetic and Dobry (1991)

Shear strain ratio can be calculated as follow:

$$\varepsilon_{shear} = \frac{\Delta}{L} \quad [2]$$

Where ε_{shear} is the shear strain, Δ is pile deflection at grade, and L is the length of the pile.

The shear strain was calculated for three pile defelection values namely, 2 inch, 0.8 inch, 0.3 inch and corresponding G/G_{max} ratios were extracted from Fig. 9, using PI of 49 per geotechnical report for soil layer Ra as listed in Table 2. The LPILE model in the previous section showed that the pile deflection at grade is close to 0.3 inches (Case 3). Other cases were considered to investigate lower Young's modulus impact on determining reaction pile deflection.

Table 2. G/G_{max} Ratio

Case #	Pile Defelection Δ (inches)	Shear Strain ε_{shear} (%)	Shear Stress/Max. Shear Stress G/G_{max}
1	2	0.08	0.73
2	0.8	0.032	0.86
3	0.3	0.012	0.95

Then, the Young' modulus (E) can be calculated using the following the equation:

$$E = G * 2(1 + \vartheta) \quad [3]$$

Where E is Young's modulus, and ν is the soil Poisson's ratio.

Soil Young's modulus over depth of top soil layer (Ra) were calculated using shear wave velocity for each case as shown in Fig. 10.

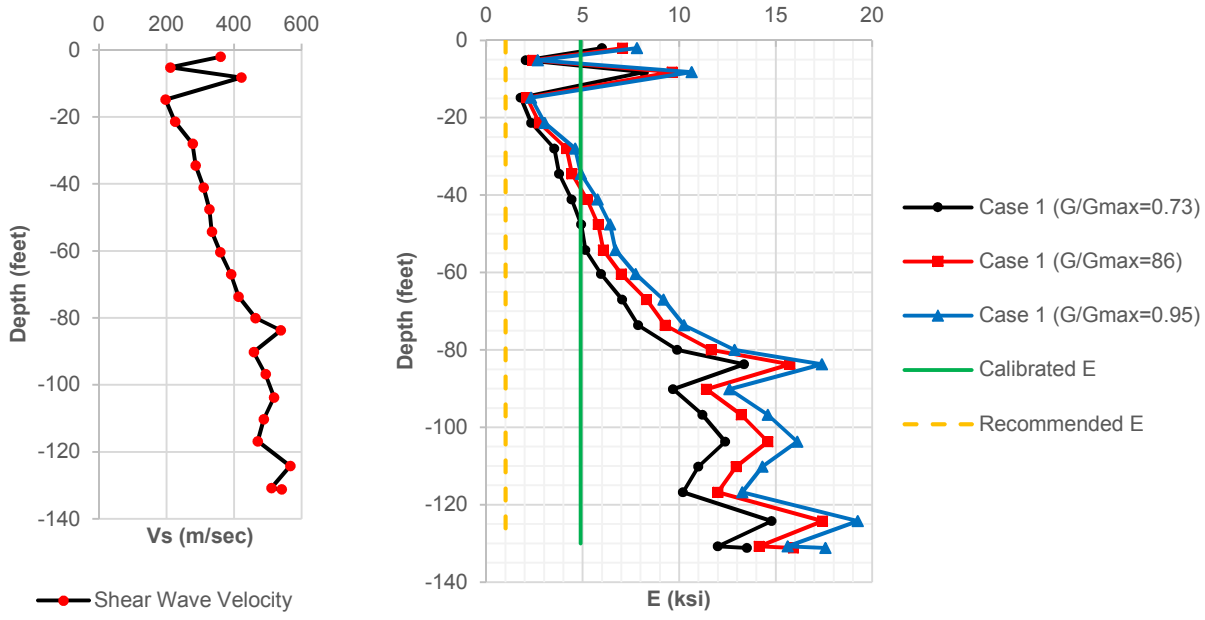


Fig. 10. Left) Shear Wave Velocity, Right) Calculated E value over Depth

Finally, Young's modulus over the depth was idealized into three zones with constant values to simplify the modeling process. Table 3 summarizes the calculated Young's modulus from this section, the calibrated Young's modulus from the previous section and recommended value in the geotechnical report per AASHTO LRFD (2012).

Table 3. Young's Modulus Values

Case #	Depth (feet)	Calculated E (ksi)	Calibrated E (ksi)	Recommended E (ksi)
1	0-20	2.1	4.9	1
	20-65	5.0		
	65-130	11.4		
2	0-20	2.4		
	20-65	5.9		
	65-130	13.5		
3	0-20	2.7		
	20-65	6.5		
	65-130	14.9		

PLAXIS Modeling

PLAXIS models for reaction frames under rotator and/or oscillator lateral loads were developed with calculated and calibrated Young's modulus (E) listed in Table 3 and soil properties listed in Table 1 as shown in Fig. 11. As shown, the piles are connected with a cap beam at pile head and lateral bracings were provided to distribute the lateral load among reaction piles equally and minimize lateral deflection.

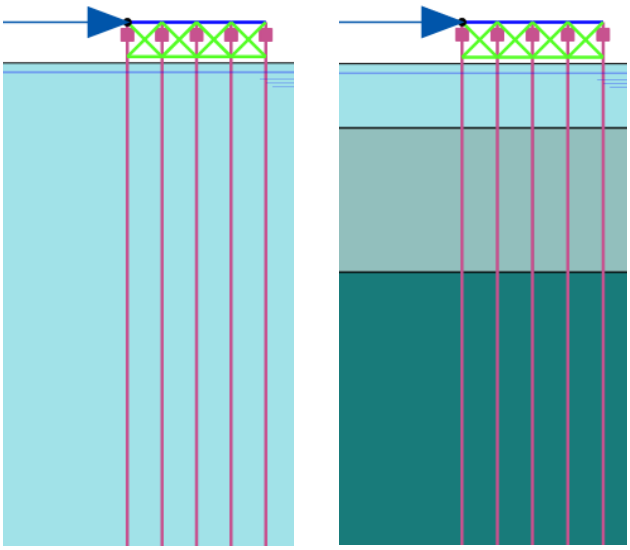


Fig. 11. PLAXIS Models for Reaction Frames: Left) Calibrated E, Right) Calculated E

As results show in Fig. 12, the deflection profiles with calculated and calibrated E values are consistent and they predict almost similar maximum pile deflection. Deflections in models with calculated Young's modulus dissipate faster than models with calibrated Young's modulus. This is because of higher Young's modulus over depth in the models with calculated Young's modulus. Also, results show that the deflection of the pile increases as G/G_{max} ratio decrease. This is because the lower G/G_{max} ratio corresponds with lower soil Young's modulus.

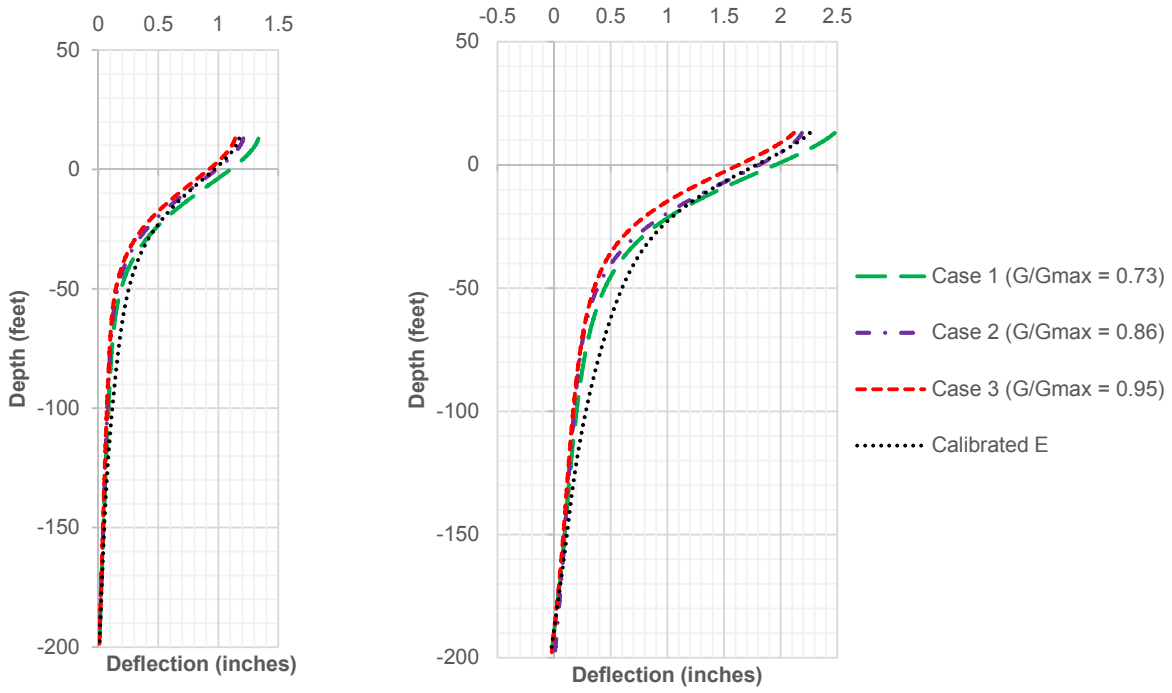


Fig. 12. Reaction Frame Defelection: Left) Rotator, Right) Oscillator

CONCLUSIONS

The calculations presented in this paper demonstrat that soil Young's modulus plays an important role in determining pile deflection under lateral load. Analyses proved that empirical values for soil Young's modulus in this project are significantly lower actual Young's modulus of the project and results in unrealistic pile deflection.

Results in this paper show that deflection of a pile under lateral load mainly occurs above grade and then dissipates rapidly over the pile depth into the soil. Calculations show that Young's modulus increases with depth and, therefore less deflection in the pile can be expected compared to a model with constant Young's modulus.

REFERENCES

AASHTO LRFD, 2012. Bridge Design Specifications, American Association of State Highway and Transportation Officials, Washington, DC

BUMA, 2019, BUMA Construction Equipment

HART, 2019, https://www.honolulutransit.org/

Kramer, S.L., 1996, Geotechnical Earthquake Engineering, Pearson Publishers

Vucetic, M., and Dobry, R., 1991, Effect of Soil Plasticity on Cyclic Response, ASCE Journal of Geotechnical Engineering, Vol 117 (1), DOI: https://doi.org/10.1061/(ASCE)0733-9410(1991)117:1(89)

FINITE ELEMENT AIDED DESIGN METHOD FOR FROZEN EARTH SHAFT SUPPORT

Joseph A. Sopko, Moretrench, A Hayward Baker Company, Rockway, NJ, USA, 973-627-2100 x 231, jasopko@moretrench.com

ABSTRACT

The first documented procedures for designing frozen earth structures are over 50 years old, implemented long before the introduction of the Finite Element Method (FEM). Since that time, the development of three-dimensional models has made the traditional and often over-conservative methods relatively obsolete. This paper discusses a new approach that is largely dependent on the analysis of internal stresses with the frozen structure and comparison to frozen soil laboratory tests. A specific design process is discussed related to initial field investigation, laboratory testing, structural and thermal analysis, and performance monitoring. The design results are compared to case histories in the field that verify the procedure.

Keywords: design, frozen, earth, structures, stresses

BACKGROUND

One of the first documented methods to designing frozen earth retaining structures was by Sangar (1968). Methodical refinements were published by (Harris 1995) and published by the International Symposium on Ground Freezing in 2002 (Andersland et al. 1991). The structural design or thickness of the frozen mass was based on the unconfined compressive strength of the frozen soils. Two simple equations for determining the thickness of a frozen shaft are shown in Fig. 1 and the first two equations below.

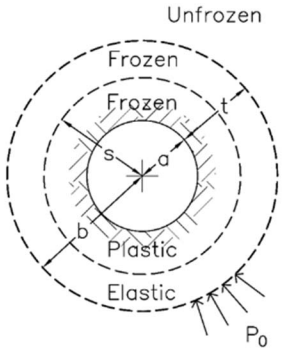


Fig. 1. Description of the variables used in the structural equations

$$t = a\left[0.29\left(\frac{P_0}{q}\right)+2.30\left(\frac{P_0}{q}\right)^2\right] \quad [1]$$

$$t = a\left[(0.29 + 1.42\sin\emptyset)\left(\frac{P_0}{q}\right) + (2.30 - 4.60\sin\emptyset)\left(\frac{P_0}{q}\right)^2\right] \quad [2]$$

Where $s = \sqrt{ab}$ and q is the unconfined compressive strength.

This method assumed the frozen earth structure was a thick-walled cylinder with shortcomings often leading to conservative results. Inconsistencies with this method (Sopko 1990) include the following. P_o is often the at-rest earth pressure and inconsistent with actual subsurface conditions; it does not account for

© 2019 Deep Foundations Institute

strain deformation of the frozen structure, pressure generated by the expansion of the soil during the freezing process, and the natural arching of the soils. Secondly, the structure is not a fully open cylinder, it is fixed at the bottom with a cantilevered effect as the soil or rock at the base absorbs some of the stress. Finally, the unconfined compressive strength does not represent the confined state of the frozen soil within the frozen mass.

Once the thickness of the frozen structure is determined, both methods describe a thermal analysis to determine the refrigeration pipe spacing, required freezing time, and associated refrigeration load. The methods for evaluating the thermal requirements are shown in Equations 3-7 and Fig. 2. The time required to have closure of the frozen wall is defined as t_1 while the additional time required to form the entire structure is defined as t_2. It is also necessary to evaluate the required refrigeration load (*Kw*) as shown in Equation 6.

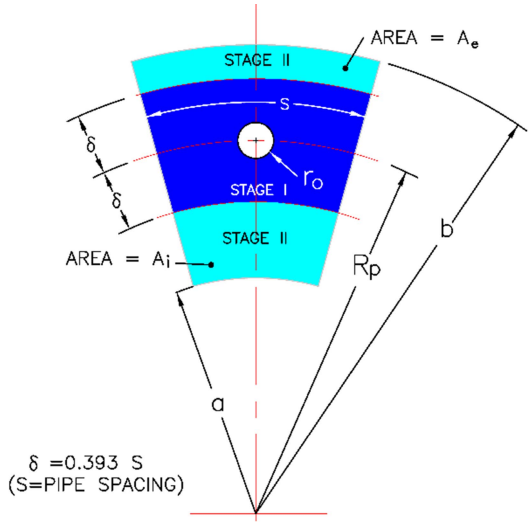


Fig. 2. Description of variables used in the thermal equations

$$t_I = \frac{R^2}{4K_1 v_s}\{(L_I)(2\ \ln\ R' - 1) + C_1 v_s\} \quad [3]$$

Where K_1 = frozen thermal conductivity of the soil, C_1 = frozen heat capacity of the soil, and v_s = degrees that the coolant temperature is below freezing.

$$L_I = (L + C_1 v_s + 3C_2 v_0) \quad [4]$$

Where L = latent heat of fusion and v_o = degrees that the initial ground temperature is above freezing and C_2 is the heat capacity of the unfrozen soil.

$$t = t_{IIe} = \frac{1}{2K_1 v_s}(L_{IIe})\left[b^2\ \ln\frac{b}{R_p+\delta} - \frac{b^2-(R_p+\delta)^2}{2}\right] + \frac{C_1}{2K_1}\left[\frac{b^2-(R_p+\delta)^2}{2}\right] \quad [5]$$

$$Kw = \frac{K_1 v_s}{6685}\frac{1}{\ln R^1}\ \text{kw per unit of pipe} \quad [6]$$

While these equations provide a somewhat reasonable estimate of the required time and heat load, inadequacies become apparent when applied to actual construction projects. Actual refrigeration pipe spacing after drilling is highly variable due to deviations. The equations are suited for a uniform spacing

around the shaft perimeter, are pure conduction, do not account for the convection associated with the circulation coolant flow, and use values for frozen and unfrozen thermal conductivity when the value is actually a function of temperature. The coolant temperature is typically warmer for the first week of freezing and then cools off. The equations only use one temperature. This method does not factor in groundwater velocity that can delay or even prevent the formation of a frozen earth wall.

With the advent of numerical methods (particularly the FEM), new methods have been developed and put into practice to perform the structural and thermal designs of frozen earth structures. The value of the numeric models, however, are highly dependent on the material properties used in the input files. These numeric methods have been used, modified, and verified with ground freezing projects since 1985. The standardization of these models in practice requires the standardization of evaluating the parameters which only through a standard practice of field investigation, laboratory testing, instrumentation, and field quality assurance.

FIELD INVESTIGATION

When ground freezing is specified as a method of temporary earth support or groundwater control in an underground project, frozen soil testing is typically included in the Geotechnical Baseline Report (GBR) or Geotechnical Data Report (GDR). In cases where these tests are excluded or ground freezing is selected after the contract documents are published, an additional sampling test and program must be implemented. The field investigation for a ground freezing project should include but not be limited to the following:

1. verification of strata type and elevations by conducting borings as close to the frozen structure as possible that may include standard penetration tests. Sonic drill however provides a clear definition of the strata is required without forgetting highly permeable strata are potential sources for lateral groundwater flow and clay strata are susceptible to time-dependent creep deformation during excavation. While the standard penetration test is good indicator of soil density, using correlations for other parameters can result in inaccurate values. The samples recovered in the sonic testing provide necessary quantity of soil needed for the laboratory testing to provide input parameters such as cohesion, friction angle and elastic modulus that are required for the structural analyses.
2. groundwater elevations should be measured through several tide cycles in the borings as monitoring wells or piezometers. Boring locations should be situated to measure any potential groundwater gradients across the site. Lateral groundwater flow can delay or even prevent the formation of the frozen earth wall. Borings completed with piezometers or monitoring wells across the site can be used to detect ground water gradient. A large gradient coupled with high permeability can result in excessive groundwater velocity;
3. verification of impermeable base stratum, key to vertical excavations. The frozen earth structure should extend into an impermeable rock or soil stratum deep enough to ensure hydraulic and basal bottom stability. In cases where such a stratum does not exist, it is possible to drill and install refrigeration pipes in the interior of the structure to form a frozen bottom plug;
4. collecting samples for compression testing;
5. an aquifer pumping test.

LABORATORY INVESTIGATION

It is highly important to obtain quality soil samples for testing. While it is possible to obtain quality relatively undisturbed cohesive samples, quality saturate sand samples are difficult to attain. In almost all cases, it is necessary to reconstitute the samples and correlate the SPT values with density using an accepted method. Quality sample preparations for testing are as important as the tests themselves. In addition to the density, water content and grain size distribution, two other key components will ensure the samples are fully saturated and frozen using a procedure that eliminates water and ice segregation. This can be

accomplished by exposing the base of the cylindrical sample and insulating the top and sides, forcing the freezing in one direction. Freezing from all sides could result in entrapped water and ice in the sample's center.

The laboratory tests conducted for the design phase include unfrozen triaxial testing and constant strain rate frozen soil compression testing. Typically consolidated, undrained, multi-stage (ASTM D4767-11) triaxial tests are conducted to evaluate the shear strength, friction angle, and elastic modulus of the unfrozen soil. These values are needed to evaluate the lateral earth pressure imposed on the frozen structure when the shaft is excavated. Constant strain rate unconfined compression tests (ASTM D7300-18) are conducted on the frozen soil, typically at -10°C and -15°C using a testing apparatus similar to those in Figs. 3a-b.

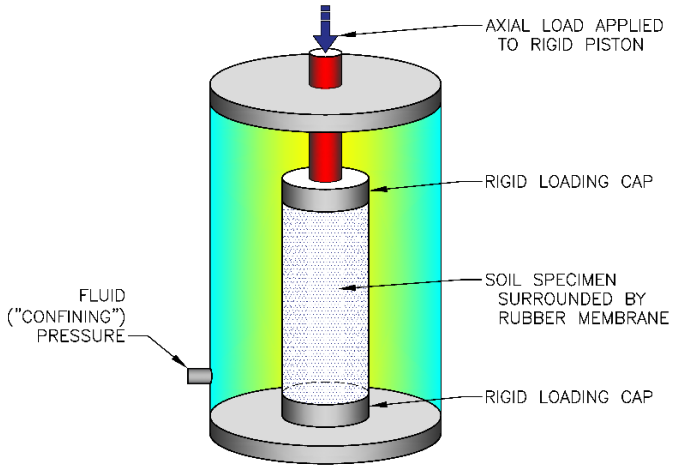


Fig. 3a. Triaxial Compression Cell



Fig. 3b. Compression test load frame in freezer

Testing strain rates can range from 1.0 to 0.1 percent strain per minute. The higher rate will yield a higher strength while the lower rate will yield a lower strength. Research indicates the strength and elastic modulus from this lower strain rate could replace the need for the constant stress creep tests. Results of the constant strain rate test provide an instantaneous or short-term strength and elastic modulus. Frozen soil exhibits time and temperature-dependent rheology; it is stronger at colder temperatures and strength decreases with time. The results of this are used to determine the stress levels in constant stress creep tests. Per ASTM

D5520, the recommended stress levels are 0.5, 0.3, 0.3, and 0.1 of the unconfined compressive strength determined by this test.

The constant stress (creep) frozen soil compression test (ASTM D5520-18) is used to evaluate the long-term compressive strength and elastic modulus of the frozen soil. The samples are typically tested as -10°C and -15°C. The results of the time versus strain values for each stress level is shown in Fig. 4.

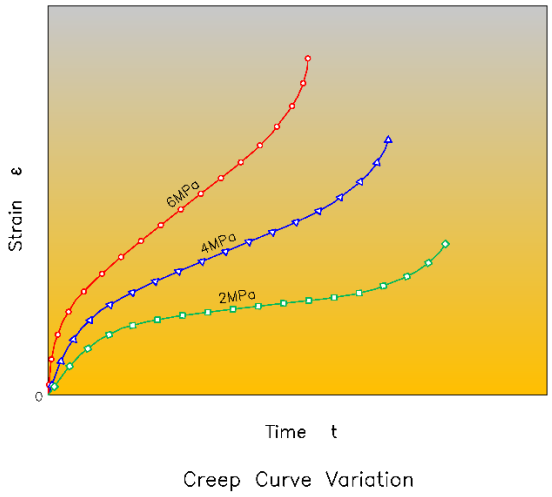


Fig. 4. Results of the constant stress creep tests

It is important the test is conducted long enough to fail the sample; 6 percent strain should be considered failure. It is not uncommon when the actual failure is not readily observed. The creep test data is used to determine the parameters A, B, and C as described by Klein (1981). These parameters cannot be computed unless the samples are run to failure or assumed 6 percent as failure. Once these parameters have been obtained, it is possible to evaluate the unconfined compressive strength (q_f) and elastic modulus E as functions of time as shown in Equations 7-8.

$$q_f(t) = \left(\frac{\epsilon_f}{A* t^C}\right)^{1/B} \quad [7]$$

$$E(t) = \left(\frac{\epsilon^{(1-B)}}{A* t^C}\right)^{1/B} \quad [8]$$

Where A, B, and C are creep parameters and ε_f is the strain at which the samples fail. Theoretically, the samples at all different stress levels should fail at the same strain. This does not typically occur in practice. This Becasue of this, the failure strains should be averages, or simply use 0.06 (whichever is lower).

FROST HEAVE AND THAW CONSOLIDATION

With more ground freezing projects conducted in urban areas, it is necessary to evaluate the effects of frost heave and thaw consolidation on structures, utilities, and roadways. There are no established and universally accepted laboratory procedures for determining these parameters. Frost heave is typically defined by the primary heave, which occurs instantly upon freezing when the pore water freezes and has a volumetric expansion of approximately 9 percent (note only the water expands 9 percent, not the entire soil mass), and secondary heave. Secondary heave occurs when ice lenses form in fine-grained, frost-susceptible soils. As the freezing front is formed, water migrates towards the front and freezes. Secondary heave is more common in natural, seasonal freezing when there are many freeze/thaw cycles.

The segregation potential test has been suggested as a method for evaluating frost effects on soils. The author has found it a complicated procedure and subject to laboratory mistakes. There is no ASTM standard for this test nor computer program available to use the results. A more positive approach is directly measuring the primary heave and settlement in a device like the one in Fig. 5. This device permits the application of a vertical load prior to freezing. Heave can then be measured followed by settlement upon thawing. Variations of this device are being developed that include a flexible member to permit variation of the later stress. Volumetric expansion and contraction can be determined and used in numerical analysis.

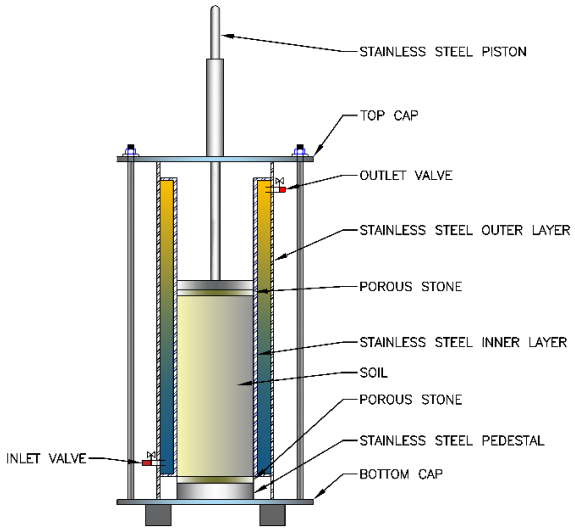


Fig. 5. Volumetric change cell

STRUCTURAL ANALYSIS

Numerical methods, particularly the FEM, permit evaluation of the frozen earth structure and compensate for disadvantages of the equations previously presented. An axis-symmetric model is the most straight forward approach to analyzing a frozen shaft as presented in Fig. 6. The internal stresses of the frozen earth wall section are presented in Fig. 7. The FEM requires an iterative process where different frozen wall thicknesses are evaluated. Fig. 7 shows the hoop stresses defined in Fig. 8.

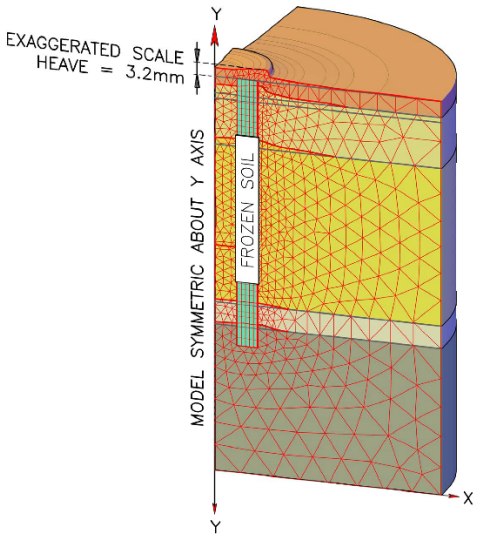


Fig. 6. Axisymmetric FEM model

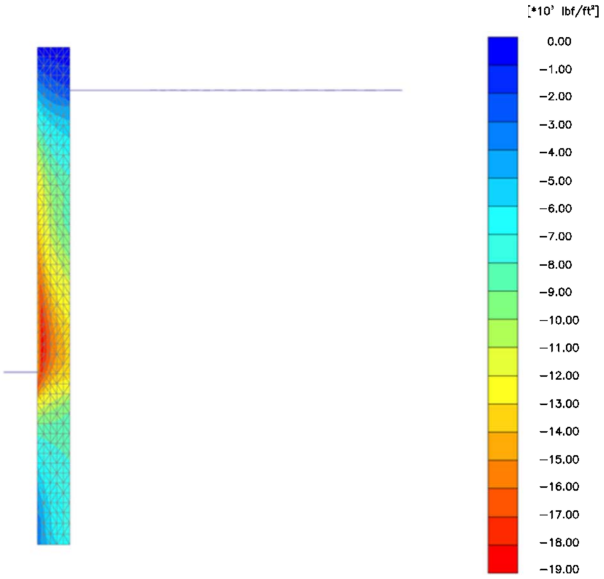


Fig. 7. Stresses within the frozen wall

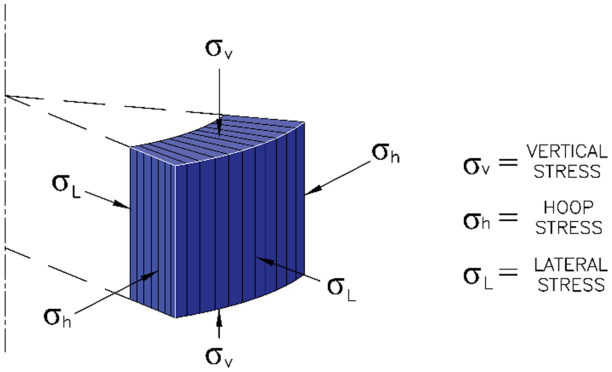


Fig. 8. Definition of Stresses

The hoop stresses are then compared to the long-term strength evaluated in Equation 7. This is a comparison to an unconfined strength when in fact the in-situ frozen soil is subject to lateral confining stresses displayed in Fig. 8. A new approach described by Sopko (2019) is to use this comparison as the factor of safety (F.S.):

$$F.S. = q_f(t)/\text{max hoop stress} \quad [9]$$

This approach is significantly different than the two traditional approaches. Those methods apply a factor of safety of 2.0 by dividing the unconfined compressive strength by two. This leads to additional conservatism, particularly when the inconsistencies are added to the design. The traditional approaches also consider only a thin-walled cylinder. In practice, it is not uncommon to line the frozen shaft sequentially as the excavation progresses. This method requires the use of staged construction approaches used in commercially available FEM programs.

THERMAL ANALYSIS

Once the thickness of the frozen mass is determined, it is necessary to provide a thermal analysis to determine the spacing of the refrigeration pipes, required time to freeze, and refrigeration capacity required to form the mass in a specified time frame. Figs. 9a-b illustrate a typical FEM mesh used on a recent shaft project. The refrigeration pipe coordinates were taken from a deviation survey completed after the drilling and installation of the pipes. The spacing is not equal, hence the need for the model. Results of the model present the temperature regime after approximately 30 days of freezing. A more specific evaluation of the time is presented in Fig. 10, where actual temperatures are calculated at a node located where the frozen zone extends to the required structural thickness. These figures also compare the modeled temperature to actual data from the project.

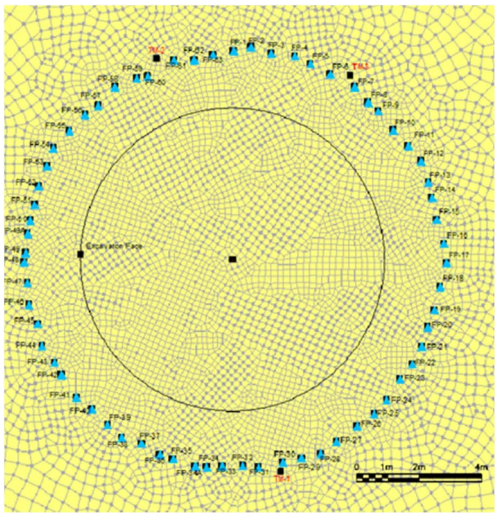


Fig. 9a. Thermal finite element mesh and computed temperature regime

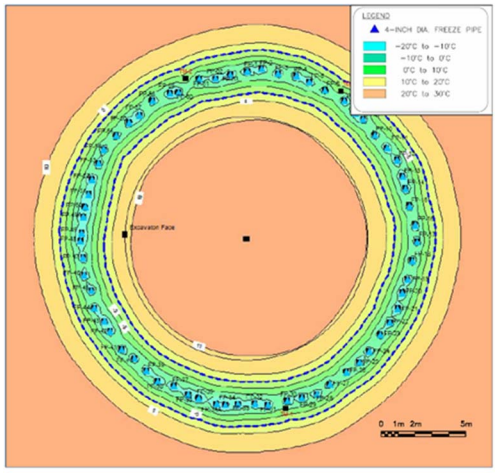


Fig. 9b. Thermal finite element mesh and computed temperature regime (2)

As previously mentioned, lateral groundwater flow introduces heat into the system and can delay or prevent the formation of the frozen wall. Certain FEM heat transfer programs permit the coupling of the thermal model with a groundwater flow program, permitting an evaluation of the heat introduced by the fluid. If the lateral groundwater flow exceeds 1 m/day, the frozen wall will not form using a single row of refrigeration

pipes. Fig. 10 illustrates the results of a heat transfer model coupled with groundwater flow. Fig. 11 shows temperature flow. These models provide evaluation of the heat extracted to be included in the design of the mechanical ground freezing system.

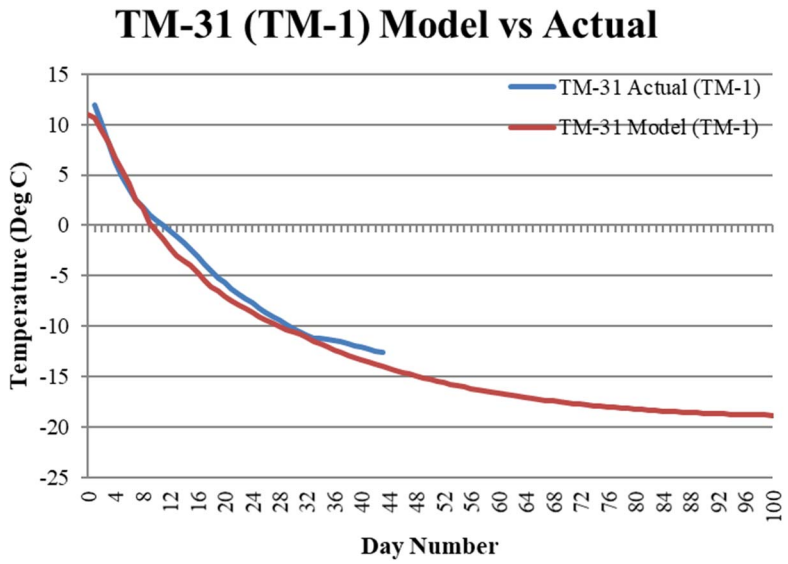


Fig. 10. Time vs temperature plot

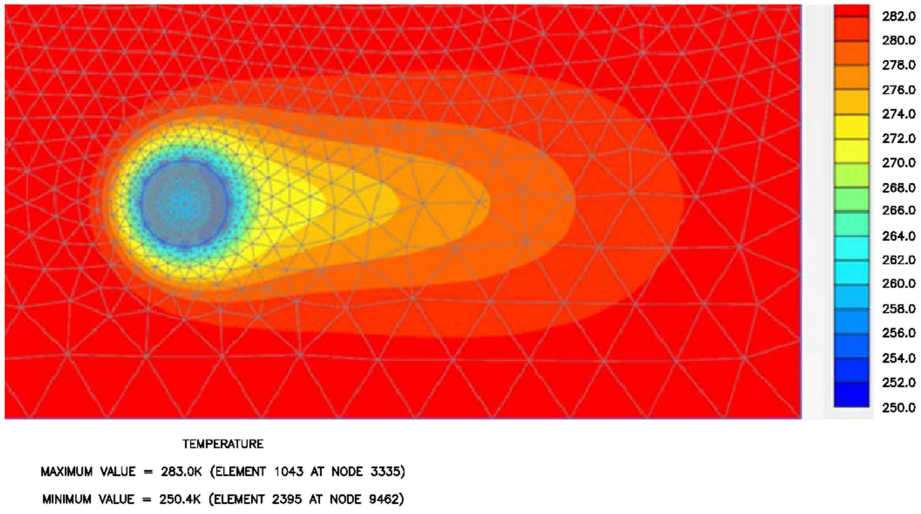


Fig. 11. Temperature plot

INSTRUMENTATION AND QUALITY ASSURANCE

A quality instrumentation system is required to ensure components of the design are implemented and correct. Ground freezing instrumentation systems should measure and record ground temperature and water level, coolant temperature, return temperature from each individual refrigeration pipe, flow rate, refrigeration plant data, and heave and settlement. The data must be evaluated as frequently as practical and compared to the behavior predicted in the analysis.

CONCUSIONS

The introduction of the finite element method for the structural and thermal design of frozen earth structures has shown advantages over the previously accept methods. It is now possible to model the actual frozen structure instead of free body diagrams that somewhat represent the in-situ geometry and stresses. These methods have been in practice for the last ten years by experienced ground freezing contractors and proven to be effective.

Additionally, given quality frozen soil laboratory tests, it is now possible to more reasonably evaluate the factor of safety. This paper presents a summary of the methods used and considers them a starting point for industry wide acceptance.

REFERENCES

Andersland. O.B., Berggren, A.L., Fish, A., Fremond, M., Gallavresi, F., Gonze, P., Harris, J., Jessberger, H.L., Jordon, P., Klein, J., Maishman, D., Ohrai, T., Rebhan, D., Ryokai, K., Sego, D.C., Shuster, J.A., Thimus, J.F., Changsheng, W., Williams, P., 1991. Frozen ground structures—basic principles of design. Proceedings of the Sixth International Symposium on Ground Freezing, Beijing, September 10-12.

American Society for Testing and Materials (ASTM), 2011. D4767, Standard test method for consolidated undrained triaxial compression test for cohesive soils.

American Society for Testing and Materials (ASTM), 2011. D-5520, Laboratory determination of creep properties of frozen soil samples at constant rate of strain.

American Society for Testing and Materials (ASTM), 2011. D-7300, Laboratory determination of strength properties of frozen soil samples by uniaxial compression.

Harris, J.S., 1995. Ground freezing in practice. Thomas Telford Services Ltd., London, pp. 74-74.

Klein, J., 1981. Dimensionierung von Eiswänden um Tiefkühlschächte, die unter Berücksichtigung der Zeit durch Sandformationen versenkt wurden. Juni, Gluckauf Forschungsh, pp. 42-43.

Sangar, J.S., 1968. Ground freezing in construction: pp. 139-141, Proceeding of the Soil Mechanics and Foundations Division. American Society of Civil Engineers.

Sopko, J.S., 2019. Factor of safety in ground freezing design. Proceedings of the World Tunnel Congress, Naples, May 3-9.

Sopko, J.S., 1990. New design method for frozen earth structures with reinforcement (Unpublished Ph.D. Thesis). Michigan State University, East Lansing, Michigan.

STRUCTURAL EVALUATION OF THERMAL INTEGRITY PROFILE RESULTS OF TRANSMISSION FOUNDATIONS

Travis Coleman, P.E., GRL Engineers, Inc, Lincolnwood, IL, (847) 213-0592, tcoleman@grlengineers.com

Ryan Weaver, P.E., Burns & McDonnell, Chesterfield, MO, (314) 682-1555, rjweaver@burnsmcd.com

ABSTRACT

The drilled shafts that support transmission lines and substations have been increasingly subject to testing to assess the integrity of placed concrete. Cross-hole Sonic Logging (CSL) has been used, but large diameter shafts with challenging site access are generally more favorable to Thermal Integrity Profiling (TIP) testing. TIP testing assesses the shafts based on measurements of the concrete temperature during curing. The TIP results provide assessment of integrity both within and outside the cage, along with information about the alignment of the cage and concrete cover. This data has allowed shafts with imperfect results to be subject to more detailed structural evaluations. However, it may not be well understood how to use this additional information by designers and engineers. The purpose of this paper is to present TIP results of transmission line foundations, both with and without issues with integrity, including cage shifting, minimal concrete cover, or soil inclusions. The intent is to provide general guidelines of the issues that merit additional investigation and those that should be recognized as inconsistencies inherent to underground construction.

KEYWORDS

Shaft Integrity, Thermal Integrity Profiling, TIP, Transmission Line Foundations

BACKGROUND

This paper is intended to discuss some of the drilled shaft evaluations made when TIP testing is performed. The authors of this paper were recently involved with a transmission line project that was designed and constructed for a Confidential Utility Client located in the Midwest United States. The project was delivered as an Engineering, Procurement, and Construction (EPC) contract with the electrical line construction company as the prime contractor. The contractor then subcontracted several parts of the work which included engineering for transmission line and foundation design, foundation construction, and third-party testing intended to evaluate the concrete homogeneity and integrity of the place concrete in the deep foundations. The testing method selected was Thermal Integrity Profiling Method B, which uses thermal sensors embedded in the concrete. The TIP testing was administered by Mr. Travis Coleman with GRL Engineers, Inc. Mr. Ryan Weaver with Burns & McDonnell served as the owner's engineer and technical consultant for the utility and was responsible for reviewing submitted TIP reports and providing recommendations to the utility on their acceptance, and if there were any issues that would warrant further discussion and analysis.

The utility specified a significant number of structures requiring TIP testing. The foundations tested were at all line deadend locations, any line angle structures that exceeded 3-degrees, and approximately 10% of the remaining structures, which were selected at regular intervals or at areas of interest (e.g. near waterways) along the transmission line route. In additional to the contractor's own administered quality control program, TIP testing was heavily relied upon to help ensure the foundation construction consistently utilized best practices, and provided the utility with information that the foundations were installed with as-expected concrete homogeneity, met specified concrete cover requirements, etc. The transmission line consisted entirely of steel monopole structures, and the nominal sizes of the drilled pier foundations varied from 5.5-ft in diameter and 15-ft in embedded depth up to 13.5-ft in diameter and 59-ft in embedded depth.

© 2019 Deep Foundations Institute

DESIGN OF TRANMISSION LINE REINFORCED CONCRETE DRILLED PIER FOUNDATIONS

Design of these types of foundations involve both the analysis of the pier-soil interaction and then the structural reinforcement design of the concrete section. The piers are considered as "beams" and are typically subject to high bending moments applied at the top of the pier. Pier to soil interaction generally doesn't rely on end bearing, but rather on lateral resistance of the soil which can be modeled using non-linear springs. The springs represent the ultimate soil passive pressure but can also include vertical side shear and base shear. Satisfactory lateral design of a drilled pier foundation requires that the ultimate capacity of the foundation must exceed the maximum expected applied loads and that the groundline deflection and rotation for design loads must remain within serviceable limits.

Typical design programs used are EPRI's Foundation Analysis and Design (FAD) Tools, which is an industry-specific program that is administered by DiGioia Gray & Associates, and LPILE by Ensoft, Inc., which is also a special-purpose program used for analyzing a single pile (or drilled shafts) under lateral loading using nonlinear lateral load-transfer (*p-y*) curves. Other internal design tools may be used as well, especially for reinforcement design, but these two programs are the most widely used in the Electric Power Transmission and Distribution industry. It should be noted that neither of these programs or ACI-based spreadsheet calculations account for situations where cage shift has occurred during construction.

TIP TESTING

TIP testing is based on the measurement of temperature as the concrete cures following placement. Determining the shaft's temperature to volume relationship allows for modeling of the effective radius of the shaft, including any bulges or reductions due to inclusions or reduced quality concrete. Additionally, diametrically opposite locations provide information on the alignment of the cage relative to the excavation and the concrete cover. The Thermal Wires® are tied along the full reinforcing cage length, and are equally spaced with a frequency of one wire per foot of diameter, with a temperature node every one foot of embedded wire length. Shortly after shaft placement, the Thermal Wires are attached to data logger boxes, and the temperature at every node is recorded every fifteen minutes. This allows for review of the shaft concrete temperature shortly after placement, increasing up to a peak shaft temperature, and then decreasing as the heat continues to dissipate into the soil. Analysis generally occurs at or slightly before the shaft reaches its peak temperature. The analysis is performed based on a relationship between the average temperature measurements and the placed concrete volume. Additional corrections must be made for the top and bottom roll-off, the zones where additional heat is dispersed longitudinally to the air and soil at the base of the shaft. These corrections are performed based on concrete, soil, and air temperatures at the time of analysis and the time for the concrete to reach peak temperature. Following these corrections, the results are presented as effective shaft radius, shown versus depth. The purpose of the term "effective" is to express that TIP results do not delineate between soil inclusions and reduced quality concrete.

PROJECT PROTOCOLS

For the shafts on this project, the typical shaft report submittal included the following items:

- Inspection field reports, which provided the as-drilled shaft dimensions, location of any temporary or permanent casings installed, depth at which the water table was encountered, depth to any rock layers that may have been encountered, use of water of drilling slurry used to maintain head pressure on the excavated hole, time and duration of both hole drilling and concrete placement, concrete strength and slump field testing data, specific locations of the TIP wires, and other items of interest from the construction of the shaft foundation.
- The TIP report with comments and recommendations provided by the TIP engineer.
- A cover letter by the design engineer indicating they had reviewed the report and also providing an opinion on any variations from the specified dimensions and placement requirements, any issues

apparent as noted either from the TIP report or the field reports, and then most often their acceptance of the installed foundation.

The owner's engineer reviewed the complete submittal. When all items appeared to be in agreement, a brief summary indicating findings and recommendation of acceptance of the shaft would be submitted to the utility. When variations were apparent, those issues would be noted along with an opinion regarding their acceptance, along with recommendations for further investigation or analysis.

A couple of items to additionally note that were unique to the construction of the foundations for this transmission line project: As part of stabilizing the upper strata of soil around the excavation, which then also assisted the foundation contractor in setting the full-length anchor bolts (which were used as the longitudinal reinforcement for the drilled pier shaft), a permanent corrugated metal pipe (CMP) casing was initially installed prior to drilling activities. This casing would then be grouted in to help fill any voids around it which then enabled appropriate soil-pier interaction to be applied in the upper layer(s) of the foundation. The use of the grouted-in CMP could influence the reported curing temperature of the pier in the upper portion of the shaft as many times the grout could still be curing when the remainder of the pier was being constructed.

REPRESENTATIVE PROJECT TIP RESULTS

Shaft 1

Figures 1 and 2 show a typical TIP result for a shaft without significant issues. The average radius is greater than the nominal radius over the full shaft length, with a bulge apparent in the upper portion of the shaft near the ground surface. This is typical, with oversized casings often used near the ground surface along with repeated passing of the drilling equipment during excavation. A close review of the upper 2 ft would indicate that one wire has an anomalous effective radius which is less than the cage radius 1 foot below the shaft top. The upper roll-off correction is applied to the average shaft temperature. Thus, any slight elevation changes in the first embedded node, which are circled in the temperature vs. depth figure, are exaggerated within the changes in boundary condition occurring in the shaft reveal. This limitation of the TIP results should be noted, along with a recommend to visually inspect the shaft top.

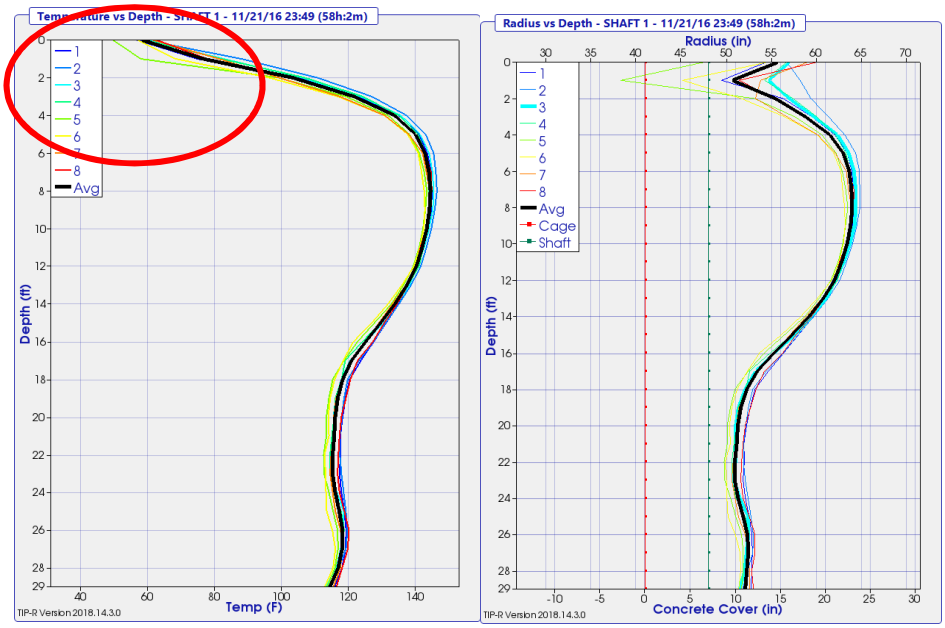


Fig. 1 and 2 – Shaft 1 Temperature and Effective Radius versus Depth

Owner's Engineer Comments: For this installation, it was apparent that the installed dimensions of the foundation were larger than the design dimensions. No further discussion was warranted for this foundation.

Shaft 2

To contrast, Figures 3 and 4 show the TIP results for Shaft 2, a shaft with clear indications of issues. Even without performing TIP analysis, an issue with the shaft is evident based on the temperature vs. depth results. A roll-off should be evident in the lower 7 ft to 9 ft of the shaft as seen at the shaft top and as projected at the shaft bottom with the dashed red line. Instead, a linear decrease in temperature is evident over the lower half of the shaft length. The average radius indicates an effective radius equal to the nominal radius at 24 ft, and less than the reinforcing cage from 28 ft to the bottom of the shaft.

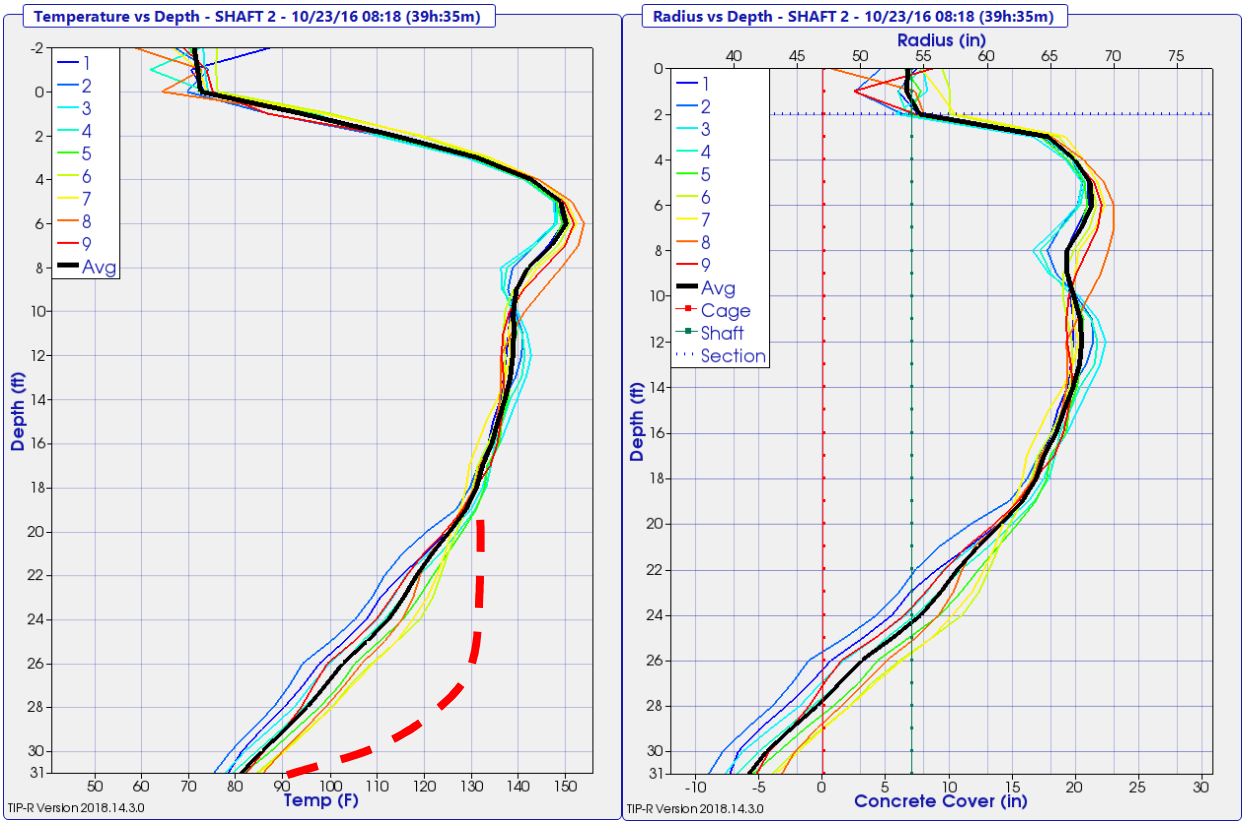


Fig. 3 and 4 – Shaft 2 Temperature and Effective Radius versus Depth

An important means of checking the data is to plot the theoretical versus placed concrete volumes, which are presented in Figure 5. While the placed concrete volume is greater than the theoretical volume in the lower portion of the shaft, the placed and theoretical volumes converge in the upper portion of the shaft. Whether the upper portion is permanently or temporarily cased, the placed volume should be at least equal to the nominal volume, as shown with the dashed line, and generally should be greater. The value of this plot is limited by the accuracy of the concrete depth measurements that can be taken in the field, but as a general rule any convergence of the theoretical and placed concrete volumes merits a closer review.

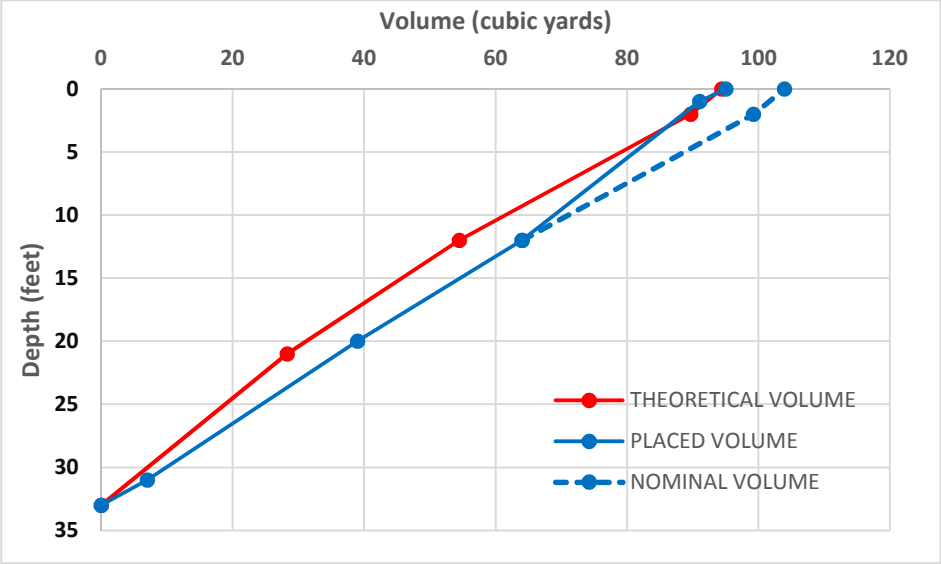


Figure 5 – Shaft 2 Theoretical Versus Placed Concrete Volume

A core was advanced outside of the bolt ring for this shaft. The core indicates concrete with sand lenses were encountered beginning at 25 ft below the shaft top. The final approximately 7 ft of the core are shown in Figure 6 below, with low concrete breaks, sand seams, and unrecoverable sections.



Figure 6 - Shaft 2 Core Results

Owner's Engineer Comments: Based on the TIP analysis and the follow-up rock coring, the design engineer further reviewed the foundation design based on revising the pier depth to be the estimated depth at where the concrete contamination became apparent, while also allowing for the larger as-constructed diameter to be included. A 9 ft diameter X 26 ft length pier design was evaluated where the initial design was for 8.5 ft diameter X 31 ft length. It was found that the revised design presented did not appear to meet the serviceability requirements (i.e. displacements), and applied loads were greater than design capacity. Ultimately the shaft was abandoned and re-drilled.

Shaft 3

Shaft 3 is an example of a shaft that required rigorous evaluation. The TIP results are shown in Figures 7 and 8. There are a number of issues to be addressed, which are noted on Figure 8 below:

1. A shift in the cage relative to the excavation. Between 27 ft and 32 ft the effective radius relative to the cage radius transitions from 16 in to 1 in in the vicinity of Wire 9. The opposite wire, Wire 3, transitions from 4 in to 13 in.
2. An area of reduced cover along one quadrant, with Wires 8 and 9 having an effective radius equal to the cage radius. These two issues indicate an eccentricity in the upper and lower portions of the excavation, as opposed to bending or sweeping in the cage, such that the lower portion of the cage is very close to face of the excavation on one side.
3. A localized reduction near the bottom of the excavation. The reduction indicates that in the vicinity of Wires 5, 6, 7, and 8 the shaft has an effective radius less than the cage radius over the lower 2 ft.

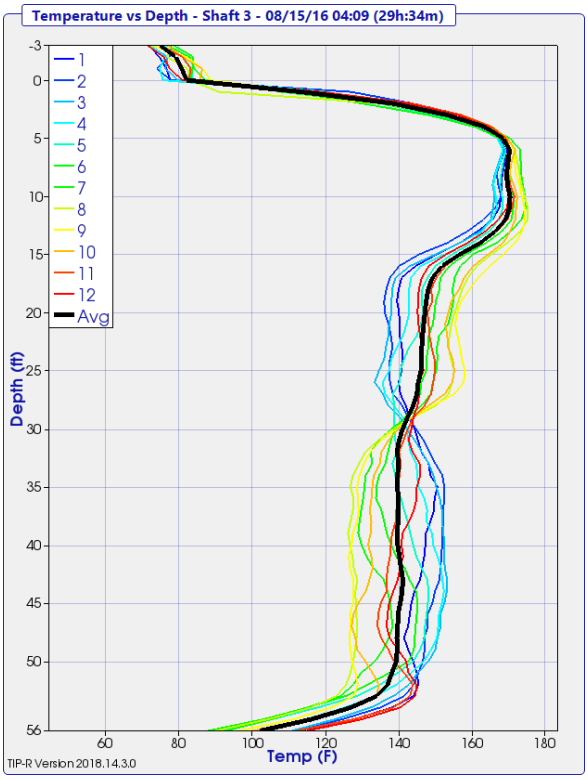


Fig. 7 – Shaft 3 Temperature versus Depth

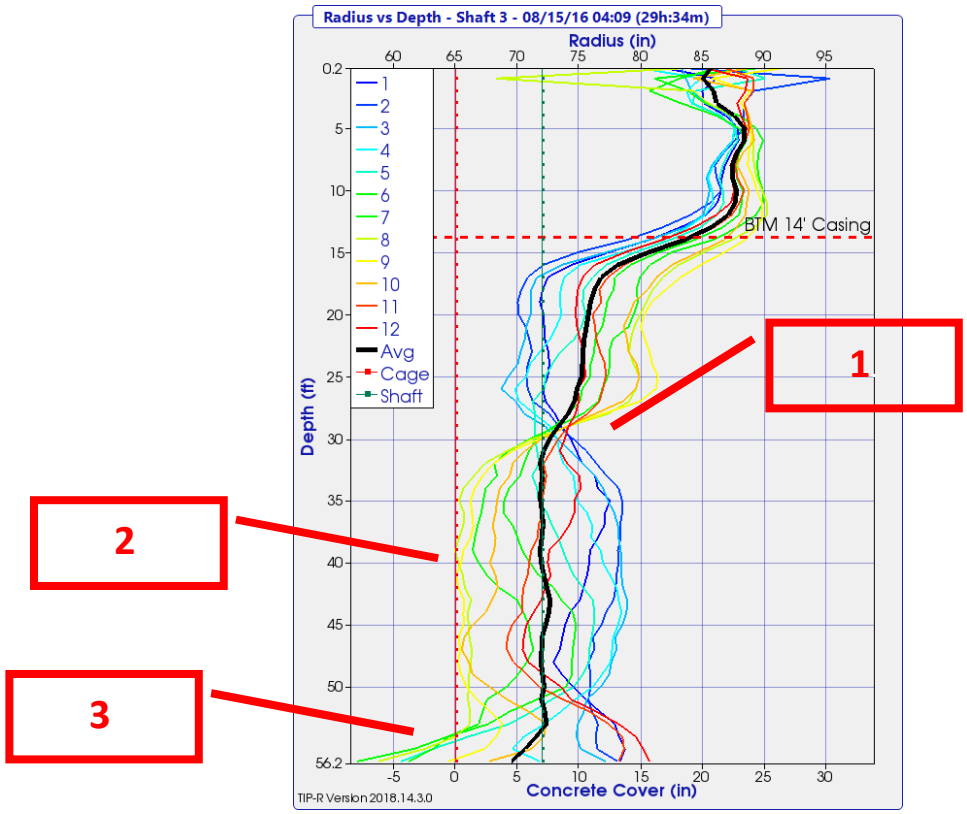


Figure 8 – Shaft 3 Effective Radius versus Depth

Owner's Engineer's Initial Comments: This was a significantly large shaft, with nominal design dimensions of 11.5-ft diameter X 56-ft length. The structure that is supported by the shaft is a deadend structure that is intended to support terminal line loads (i.e. line loading from only one side). This structure was located outside of the utility substation and thus would also typically handle large differential tension loading, with the line side being high tension and the substation side being low tension. Individual cross sections of the shaft at key locations were requested for further evaluation When evaluating the placement of the TIP wires, it was found that this area of insufficient cover happened to be on the compression side of the pier. See Figure 9 for the direction of the higher tension line load relative to the pier cross section at a depth of 36 ft.

There were considerable discussions on how to evaluate the pier and how the pier could be mitigated. An additional foundation analysis was performed, which also accounted for the oversizing of the upper section and as-tested higher concrete strength. Though the affected southeast/east section of the pier below a depth of 32 ft was expected to be in compression and not likely subject to tension-side loading in the pier, the highest range of expected shear was from 30 ft to 50 ft depth, with maximum shear at approximately 41 ft depth. The design engineer evaluated the shear requirements based on unreinforced concrete. The issue of shear rupture, where a significant section of the pier would be subject to high levels of shear without sufficient reinforcement across the entire pier section, could result in an abrupt and catastrophic failure of the foundation.

One item of mitigation was applied – the full -tension side of the line, going to the south-southeast, had its design tension load reduced by 6.7% (approximately 1,000-lbs per subphase, or 9,000-lbs total for all phase wires attached at the design line loading condition. Line clearances were checked for the line section impacted and no significant issues were identified.

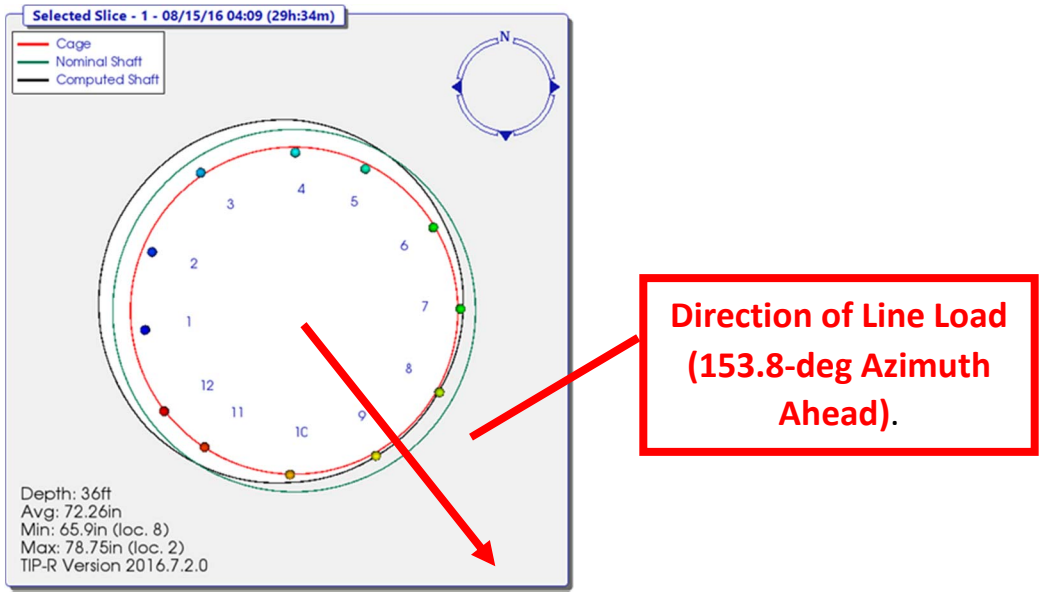


Figure 9 – Cross-Section of Shaft 1 at 36-ft Depth

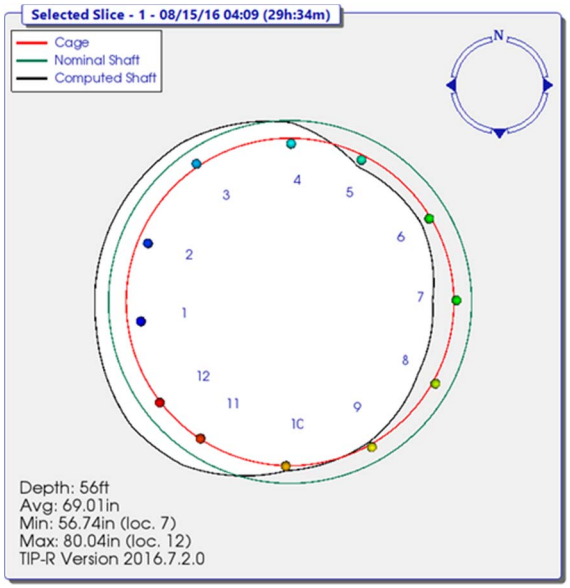


Figure 10 – Cross-Section of Shaft 1 at 56-ft Depth (Bottom of Pier)

Additional Testing Comments: This shaft was the first shaft analyzed for the project. As the project progressed, it was understood that a corrugated metal pipe (CMP) casing was permanently grouted into place, which normally took place the day before the shaft was placed. This heat contribution was initially attributed to the concrete placed for the shaft, thus incorrectly allocating placed concrete volume within the CMP cased section. Upon review a revised analysis was performed, with a correction in the boundary conditions accounting for the heat contribution from the grout, shown in Figure 11. The effective radius results were decreased near the shaft top, which allowed for an increase in effective shaft radius in the lower portion of the shaft. The portion of the shaft initially shown with zero cover had approximately two inches of cover. There was some slight improvement to the localized reduction at the bottom of the shaft, but the issue still remained.

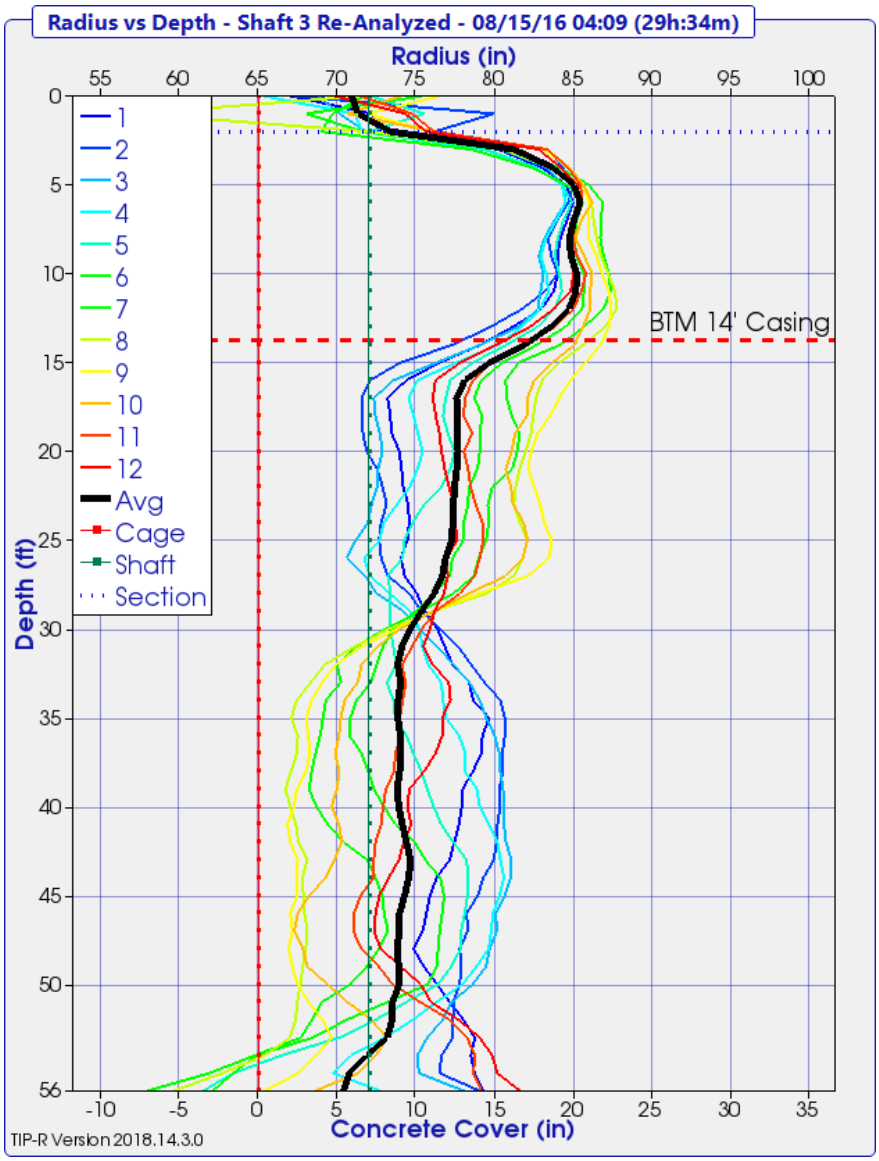


Fig. 11– Shaft 3 Revised Effective Radius versus Depth

Owner's Engineer's Follow-Up Comments:

With the re-evaluated and improved TIP analysis, it was determined that though concrete cover still did not meet the specified and ACI-318 requirements, there was expected to be sufficient cover to effectively encase the outer reinforcement and concerns about abrupt shear failure were abated. Though there was still an apparent inclusion in the bottom of the installed pier, by reducing the higher tension line loads as described previously the effective reduced embedment for the as-installed pier was then found to be acceptable. The re-evaluated pier was then found to have a sufficient factor of safety in terms of lateral capacity versus applied load and also met the specified serviceability requirements. As one final conditional check, the foundation contractor was to have the pier top regularly monitored for any unexpected displacement issues that may indicate insufficient pier performance during the contract warranty period.

SUMMARY

TIP testing is a valuable means of assessing the integrity of drilled foundations, and provides information that was previously unavailable by commonly used testing methods, particularly on the reinforcing cage alignment and concrete cover. The results indicate that even a shaft deemed "perfect" by other testing methods have some variations in effective radius, cover, alignment. A thorough understanding of the results can allow for detailed evaluation when the results are imperfect.

Though there were challenges in a few of the installations of the foundations for the subject project, by utilizing detailed field inspection reports and with the extensive use of TIP testing, the owner achieved a high degree of confidence in the foundation contractor's work plan and installations. Using tools like TIP advances the overall confidence of these types of installations and can only help the contractor's demonstration of their construction methods when employed properly.

ANCHORED DOUBLE-TIER RETAINING WALLS ON SLOPING EMBANKMENT

Chu E. Ho, Arup, New York, USA, Tel: 1-917-4388029, Email: chu.ho@arup.com
Paul Napoli, Arup, New York, USA, Tel: 1-212-8963269, Email: paul.napoli@arup.com

ABSTRACT

A new waterfront park was developed on Long Island in close proximity to the East River and Newtown Creek. The existing ground consisted of fill over soft organic clay, medium dense silty sand, glacial till and schist bedrock. The ground was initially raised to preload the underlying soft soils to stabilize the ground in preparation for site development. The ground was subsequently cut down to temporary grades for installation of foundation piles for the overlook structures and construction of reinforced concrete cantilever retaining walls forming pathways located adjacent to the water bodies. The retaining walls were located in two rows at different elevations along the sides of a steep embankment. Where the pathways converge, some of the walls were too close to each other, and were redesigned as a combined U-wall with a common base slab. The individual retaining walls were designed for adequate bearing, sliding and overturning resistance. Ground anchors were installed to enhance global stability of the retaining walls. This paper presents the design considerations for the retaining walls for various loading conditions, and evaluation of the trial and proof tests for the anchors.

Keywords: waterfront, cantilever retaining wall, global stability, ground anchor, trial test, proof test

INTRODUCTION

The New York City Master Plan included the transformation of an approximately 30-acre parcel of land in Long Island City, Queens, New York from a former manufacturing zone into a residential, commercial and recreational zone for middle-income community. The site was located at Hunters Point South along the eastern shoreline of the East River and Newtown Creek (Figure 1). The development included low to high-rise residential buildings, a public school, and retail structures. Open spaces were provided along the East River and Newtown Creek waterfronts in the form of a continuous park providing for recreational and community-related activities. Waterfront structures included small park buildings, walkways and viewing platforms. The shoreline was surrounded by revetments as part of the flood mitigation strategy. The project involved extensive site re-grading and several retaining walls were constructed. The earthwork volume amounted to approximately 47,000 cubic yard of imported fill and 93,000 cubic yard of cut. The exposed height of the retaining walls ranged from 3 to 15 feet. This paper focuses on the design and construction of the retaining walls for the project.

EXISTING SITE CONDITION

The project site was located on reclaimed land (Figure 2). The existing fill comprised of all sorts of dumped materials, including building demolition rubble, rip-rap and boulders. The fill had been placed during the last two centuries to expand the shoreline for industrial development. Based on available historical information, extensive reclamation took place between 1855 and 1898. After 1951, changes to the shoreline took place along the East River, including the removal of reclaimed land along the northern portion of the project site to allow for docking facilities. By 1977, these facilities had been removed and backfilled to form the current shoreline configuration. The current project was implemented in two phases, with Phase 1 construction completed in 2013. The existing plot of land in Phase 2 was used as a parking lot with stockpiles of fill mixed with construction demolition rubble of varying heights across the site. The existing ground surface elevation varied significantly up to approximately 25 feet. The stockpiles were removed and the site was re-graded to design elevations during the project.

© 2019 Deep Foundations Institute



Fig. 1. Hunters Point South site development

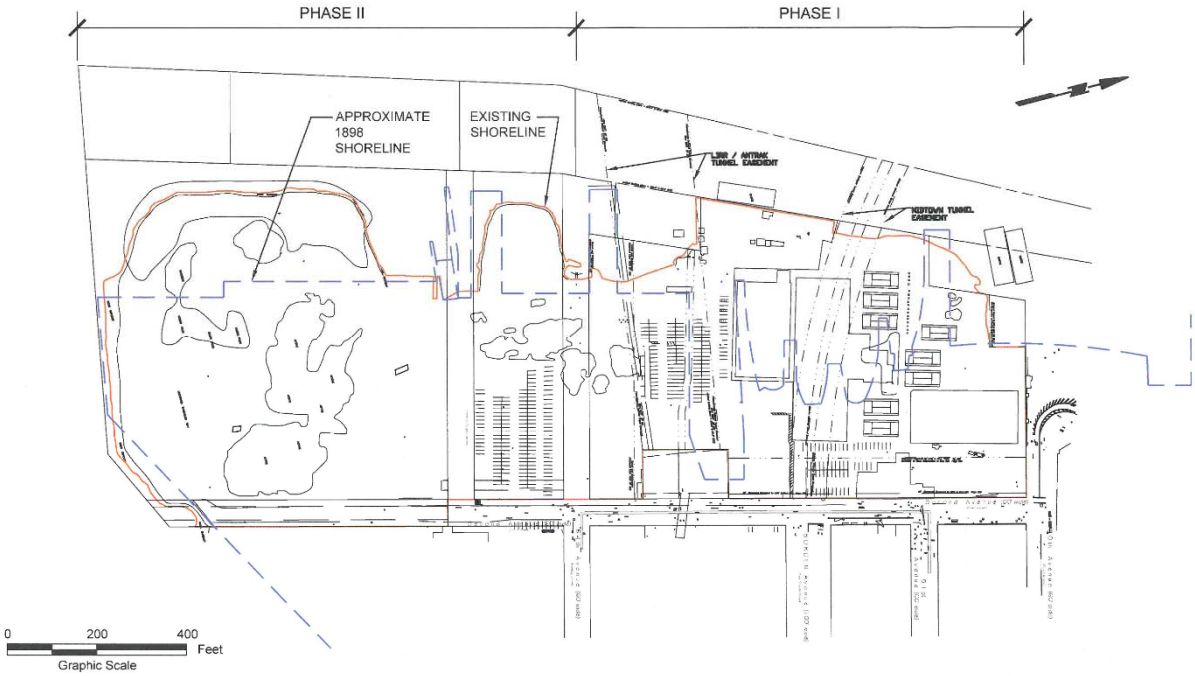


Fig. 2. Historic shoreline at Hunters Point South

Figure 3 shows the typical subsurface geologic profile based on historical and supplementary geotechnical investigations. The existing subsurface consisted of miscellaneous fill overlying soft organic clay, medium dense silty/clayey sand, glacial till, decomposed rock and schist bedrock. The elevation of groundwater table observed from monitoring wells ranged from EL+2.5 to -2.6ft, with an average elevation of EL+0ft. The groundwater regime was influenced by tidal action. Historical records indicated tidal fluctuation in the East River could be as high as EL+8ft. Based on FEMA Flood Insurance Charts, the 500-year flood event

is EL+12ft. The regional hydrogeology played an important role in the evaluation of groundwater levels for design. Reference was made to past records of observation well readings published by the United States Geological Society (USGS, 1999) to inform the drainage conditions over the various periods of site reclamation and redevelopment. The project site was classified as Seismic Site Class E based on the New York City Building Code (NYCBC, 2014) with a design peak ground acceleration (PGA) of 0.17g corresponding to a Maximum Considered Earthquake (MCE) with a 2% probability of exceedance in 50 years (or a return period of 2475 years). Table 1 summarizes the geotechnical parameters evaluated for the geologic materials identified.

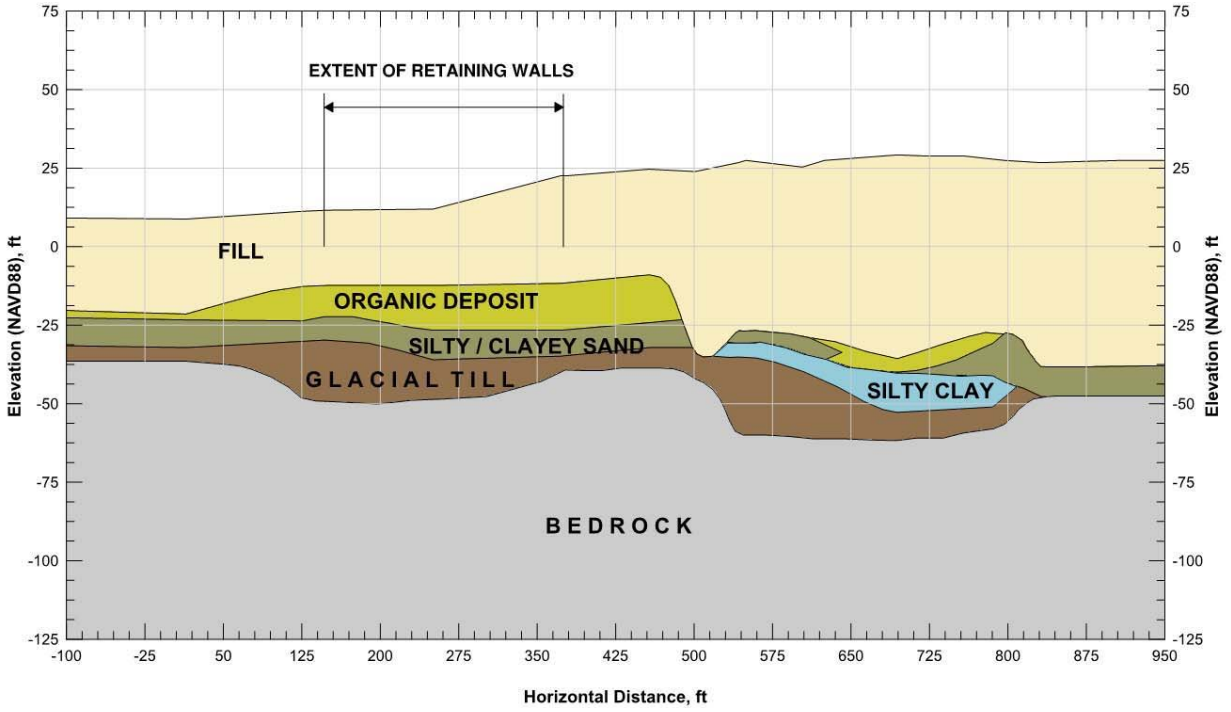


Fig. 3. Typical subsurface geologic profile

RETAINING WALL DESIGN

The greatest design challenge on the project was the retaining walls at the Major Overlook Structure and South Cove. The landscape architectural design called for a complicated series of retaining walls carrying huge concrete panels on a steep embankment facing the waterfront (Figure 4). Two rows of cantilever retaining walls were designed to run along the side slopes in a two-tier stepped fashion to provide earth retention for a pedestrian pathway from street level to the shoreline below. Due to the unique landscaping design, the pathway narrowed towards the lower elevations, resulting in the retaining walls being located very close to each other. Where the upper and lower tier wall structures clashed, some walls were combined as a U-section by linking them together with a common base slab (Figure 5). The retaining wall heights were up to 22 feet from the top of the base slabs. The retaining walls were excavated from the existing earth embankment and backfilled using compacted free draining granular soils to 90% of the maximum Proctor dry density. The compacted backfill was provided behind each retaining wall within the active soil wedge defined by a line sloping at 1H to 2V from the heel of the shear key. Subsoil drains were placed immediately behind the retaining walls to ensure no water pressure would build up behind it. All retaining wall foundation slabs were embedded a minimum 4 feet below final grade for frost protection.

Table 1. Geotechnical parameters of soil and rock units

Stratum	Thickness	SPT N_{60} (average)	Unit weight	Friction angle	Cohesion	Undrained shear strength
	ft	blows/ft	pcf	degree	psf	psf
Fill	14 to 65	0 to refusal[a] (24)	110	34 (above EL+0 ft) 30 (below EL+0 ft)	0	-
Organic Clays and Silts	2.5 to 22	0 to 24 (6)	106	-	-	700
Silty or Clayey Sands	4 to 25	2 to 55 (23)	120	31	0	-
Silty Clays	4 to 25	3 to 61 (19)	120	-	-	800
Glacial Till	3 to 51	16 to refusal[a] (55)	130	35	0	-
Decomposed Rock	4 to 7	40 to refusal[a] (refusal[a])	130	38	0	-
Bedrock	-	-	171	-	-	(UCS[b] 9 ksi)

Notes:
a. SPT blow count > 50 blows/6ins; b. Uniaxial compressive strength of rock

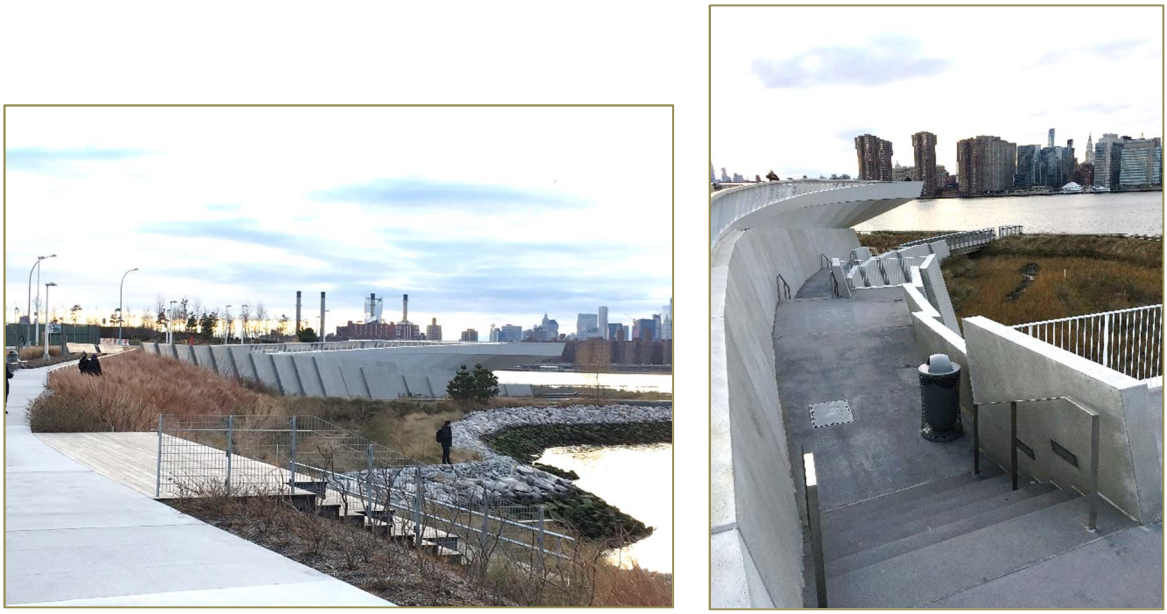
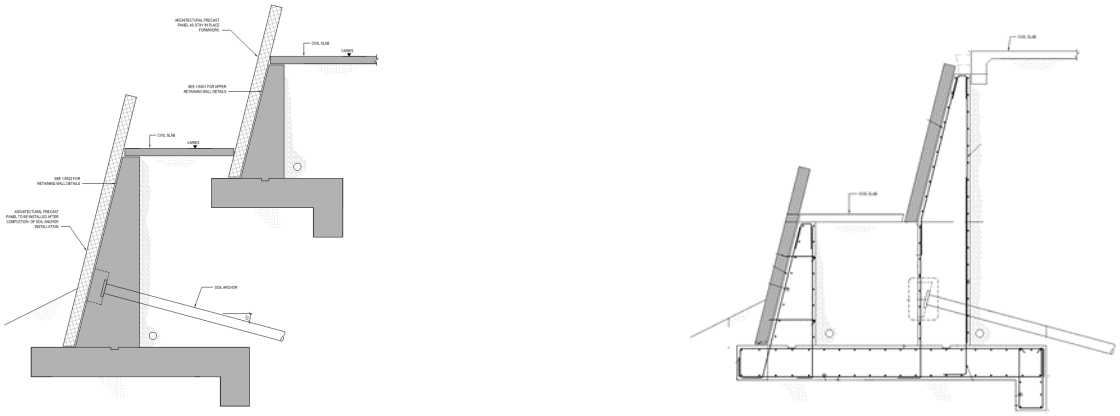


Fig. 4. Double-tiered retaining walls

Local Stability

Individual retaining walls were designed for lateral active earth pressures based on Rankine's earth pressure theory under permanent static dead and live loads. A friction angle, $\phi = 34$ degrees and bulk unit weight, $\gamma = 120$ pcf was assumed for the retained compacted backfill material. A factor of safety of 1.5 was required against sliding failure beneath the retaining wall base. A factor of safety of 2.0 was required for overturning

failure about the toe, with the resultant load acting within the middle third of the wall base. The allowable bearing capacity of the foundation soils ranged between 725 to 4500 psf depending on the width and height of wall sections, and the amount of preloading achieved at the location of the retaining walls. Nominal groundwater was assumed to be 10 feet on the retained side and zero at the base of the wall. Sliding failure mode governed the design for majority of the retaining walls and shear keys up to 4 feet deep were introduced to improve lateral resistance. Additionally, the lateral and overturning stability of the retaining walls under seismic earth loading were evaluated based on Mononobe-Okabe analyses (Mononobe and Matsuo, 1929; Okabe, 1926) assuming a seismic lateral earth pressure of 11 psf/ft applied as an inverted triangular distribution. A minimum factor of safety of 1.1 was achieved in all seismic cases.



(a) Double tier section **(b) U-section**

Fig. 5. Typical cross-section for double-tier and U-section retaining walls

Global Stability

Global stability checks were carried out to evaluate the conditions of the combined effect of the double tier walls and U-sections facing the water body at South Cove. Analysis was carried out using SLOPE/W based on Morgenstern-Price limit equilibrium method for circular failure surfaces (Morgenstern and Price, 1965). The base case loading condition assumed phreatic groundwater surface in the retained fill corresponding to the USGS historical water level contours and average water level in the South Cove at EL+4ft. Initial analyses assuming no ground anchors suggested the factor of safety was marginally less than 1.5 for the imposed dead and live loads, and was considered inadequate for permanent structures in accordance with New York City Building Code. Ground anchors were subsequently introduced to meet the stability requirements (Figure 6). The retaining walls were also checked for several other scenarios including rapid drawdown after potential heavy rainfall and storm surges due to its close proximity to the shoreline. The most critical case (factor of safety of 1.3) was determined for rapid drawdown for a 500-year flood elevation at EL+12ft (NAVD88) within the retained ground and EL +0ft (NAVD88) in the South Cove. Additionally, pseudo-static seismic stability analyses were also performed to verify that a minimum factor of safety of 1.1 was achievable for a lateral earth pressure coefficient, $K_h = 0.085$ (half of MCE PGA).

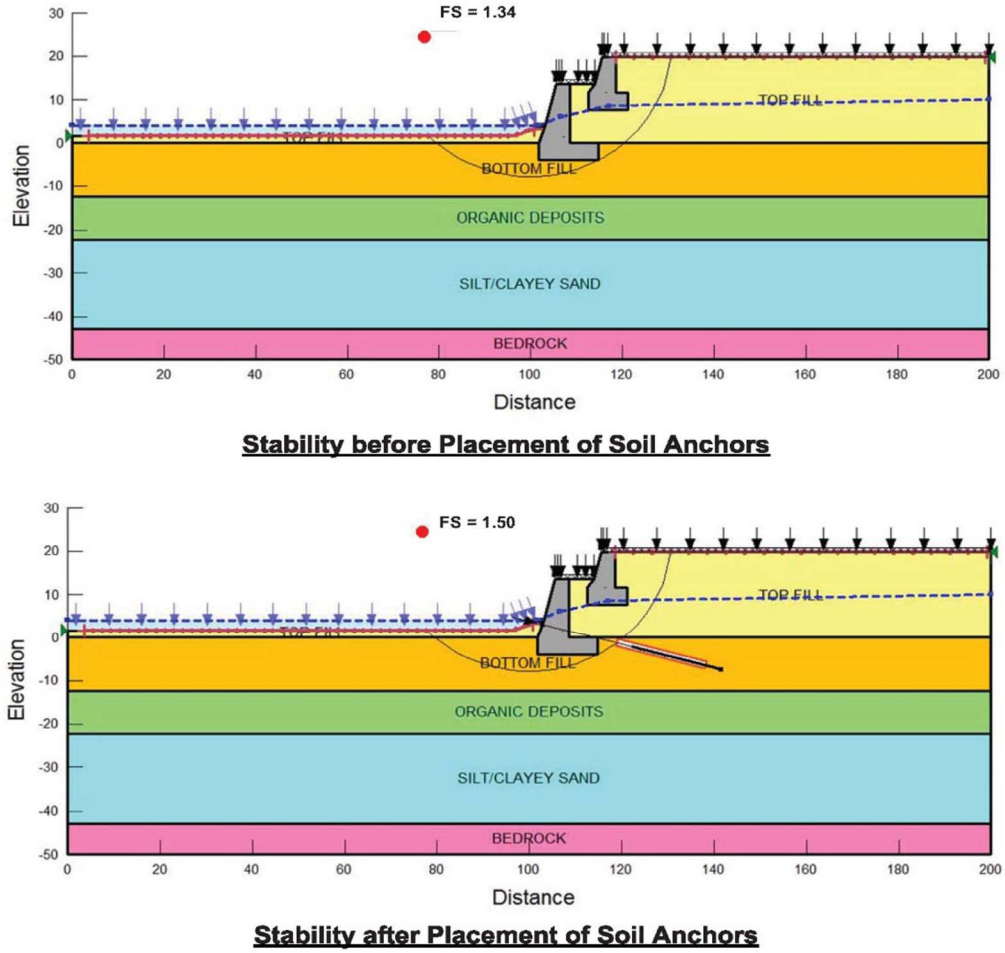


Fig. 6 Typical global stability analysis using SLOPE/W

GROUND ANCHOR DESIGN

Figure 7 shows the typical configuration and layout of ground anchors at the retaining walls. The anchors were inclined at 15 degrees from the horizontal. Twenty two ground anchors with a working load of 16 kips were originally designed to improve the stability of the retaining walls. Each anchor was reinforced with a single 40ft long No.11 Dywidag continuously threaded steel rod (yield strength Fy = 80 ksi) with nominal diameter of 1.375 inches (cross-sectional area of 1.56 square inches). The upper sections of the anchors were installed with a 9ft long permanent steel casing with 7.625 inch outer diameter (Fy = 80 ksi). The original anchor design specified a minimum 8 inches diameter borehole with 20 feet free length and 20 feet bond length, assuming an ultimate grout-soil bond strength of 750 psf within the fill material and a factor of safety of 2.0. The bond length was subsequently increased by the contractor to 25 feet for the final design of the production anchors. Grouting was carried out using neat cement with 5000psi unconfined compressive strength. The bond length was encased in an epoxy grouted corrugated PVC pipe for double corrosion protection. The top of the anchors were secured by a single 14 x 14 inches square steel plate with lock nut. At each anchor location, a 10 inches diameter PVC pipe (Schedule 40) was cast into the retaining wall stem for drilling access.

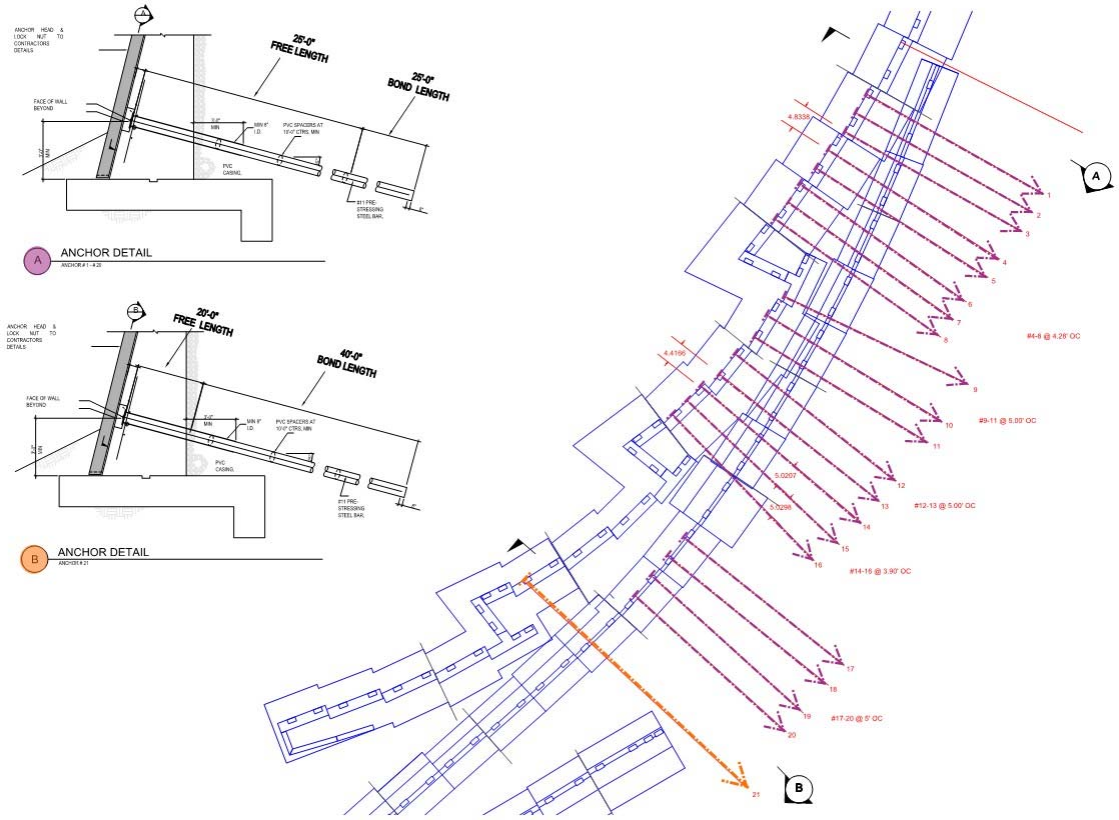


Fig. 7. Configuration and layout of soil anchors

The position of anchors were carefully chosen to avoid drilling through the base slab of the retaining wall behind it. Drilling was carried out from the front wall at double tier walls. For these walls, the anchors have to be drilled within the gap between the heel of the lower tier wall and the toe of the upper tier wall. A minimum gap of 2 feet was allowed in the design between the elevations of the upper and lower tier wall slabs to achieve this. For U-section retaining walls, anchors had to be installed from the back wall to avoid drilling through the base slab when drilling from the front. All anchors were aligned perpendicularly to the wall face as far as possible in plan and typically spaced horizontally at 3.9 to 5 feet on centers to ensure a minimum distance of 5 feet was maintained between anchors at the bond zone. This was to minimize interaction between the anchor bond zones, including due consideration for installation deviation of the anchors. At the lower wall elevations near the Major Overlook structure, the last two anchors had to be redesigned due to field constraints and were replaced by a single anchor (SA-21) carrying twice the original design load (32 kips). SA-21 was installed from the front wall in this case, with a free length of 20 feet and bond length of 40 feet. The borehole size and configuration of the central steel rod and permanent steel casing remained unchanged, except for the introduction of a coupler for extension of the steel rod.

GROUND ANCHOR PERFORMANCE

Preliminary Trial

The project specifications called for a sacrificial trial anchor to be installed prior to commencement of the production anchors to confirm the ultimate grout-soil bond strength that could be achieved on the site. An initial trial anchor (TP-1) was therefore installed approximately 5 feet away from the first anchor SA-01.

Prior to the scheduled trial test, the contractor elected to place a tensile load on the installed sacrificial anchor as a preliminary check of its performance. However, while applying the load the upper anchor segment decoupled and pulled out, rendering it impossible to reapply load to the trial anchor. Meanwhile, the contractor had progressed with installation of the initial five anchors (SA-01 to SA-05) at their own risk.

Due to the failure of TP-1, some uncertainty was cast over the installation methodology for the installed production anchors. The contractor opted to carry out the alternate trial testing on SA-01 instead of installing another sacrificial anchor. Prior to the trial test, the contractor decided to conduct an informal quick pull test on SA-01 to three times the design load (48 kips) in an attempt to verify the anchor capacity. Loads were applied incrementally in steps of 25% of design load without cycling and without extended hold times. The residual displacement upon unloading to zero load was not measured. The quick pull test confirmed that the intended test load of 48 kips could be resisted at a displacement less than 0.6ins, giving confidence that the installed production anchors were likely to be satisfactory.

A full scale trial was subsequently carried out on SA-01 after a waiting period of two weeks to three times the design load per the original project specifications (Figure 8). An alignment load of 2 kips was initially applied. Five load cycles were conducted in incremental steps up to 1.2 times design load (Point A) to check for elastic behavior at anchor working condition. The load for each cycle was reduced to 4 kips each time. The applied load was subsequently monotonically increased in six steps to the full test load (Point C) to confirm the design grout-soil bond resistance. Elongation for each load step was observed for 10 minutes hold periods. The trial indicated that the anchor successfully sustained the loads up to maximum test load. The elongation at 1.2 times design load (19.2 kips) was 0.89 inches and at three times design load (48 kips) was 2.0 inches. There were some issues with elongation measurements during unloading (Point D to D') therefore it was difficult to interpret the final condition of anchor behavior.

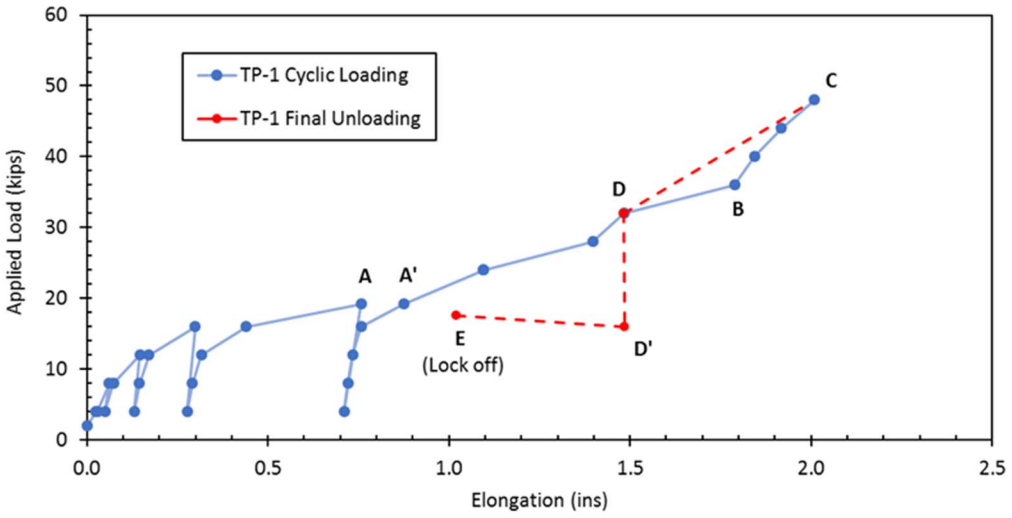


Fig. 8. Trial test on Anchor SA-01

Figure 9 shows the separation of the elastic and plastic deformation components of the measured anchor elongations based on FHWA procedure. In the analysis, it was assumed that the rebound elastic deformations for loads beyond Point A will follow the same slope as that for point A. It can be seen that the elastic deformations were small and plastic deformation dominated the anchor behavior. The elastic deformations were less than the 80% of the calculated elastic elongation based on extension of the design

anchor free length alone (20 feet) with allowance for the jack length (1.5 feet). This implies that either the anchor free length was not adequately de-bonded or frictional resistance have developed within the free lengths due to bending of the anchor tendon or misalignment of the test equipment set up. The small elastic component of the anchor deformation was indicative of the rigidity of the anchor body in relation to the soil stiffness (note that the upper section of the anchor was installed with a permanent steel casing 9 feet long). On this basis, the elastic performance of the anchor was considered not unreasonable.

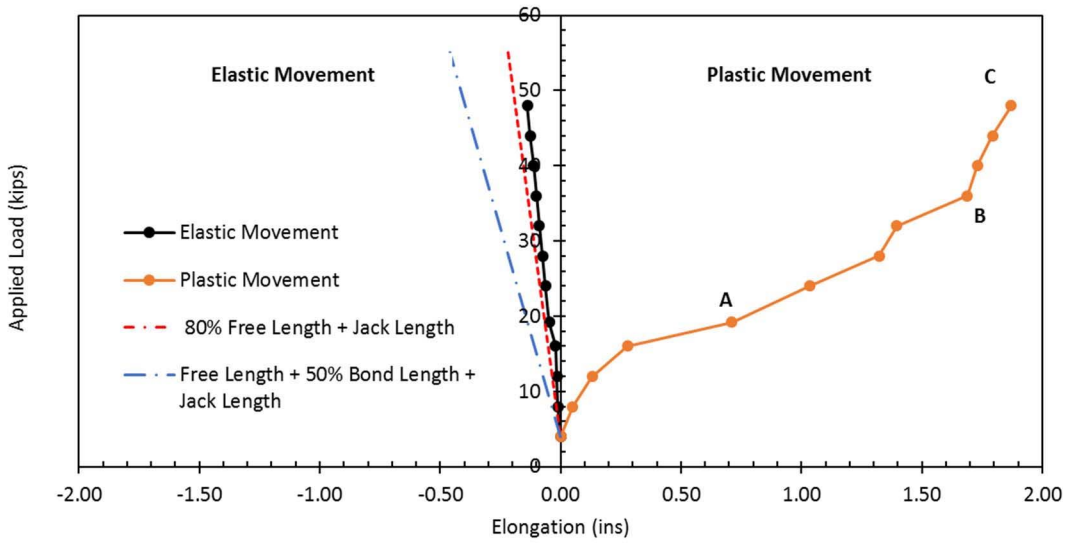


Fig. 9. Elastic and plastic elongation for trial test on Anchor SA-01

Because of the contrasting rigidity of the anchor body in relation to the soil stiffness in this case, an alternate method of investigating anchor behavior was adopted using the inverse hyperbolic plot commonly used for evaluation of piled foundations (Chin, 1976). Figure 10 shows the inverse load-elongation relationship for the trial results. As can be seen, anchor behavior can be separated into three types using this alternate plot. The initial straight line with an approximately constant slope (up to point A') suggests that the early mobilization of the interface shear resistance along the anchor body followed an approximately hyperbolic function. This was consistent with typical shearing behavior in soils. Beyond this point the plot flattens out to an approximately horizontal line (A' to B), implying elastic deformation likely dominated during this loading period. It was possible that this elastic behavior resulted from additional extension of the tendon at constant load due to slippage taking place at the grout-soil interface within the design free anchor zone. The decreasing slopes of the plot beyond point B indicates a subsequent stiffening effect as the anchor is loaded to the maximum test load (point C). This stiffening behavior may be attributed to the engagement of the anchor bond length as the extension of the anchor free length becomes increasingly developed. Assuming the bond zone is fully engaged at the maximum test load of 48 kips, the estimated ultimate bond resistance would be 917.2 psf. This was higher than the value of 750 psf assumed for design.

Proof Tests

Each of the production anchors was proof tested to 1.5 times the design load and locked off at 1.1 times the design load. Test loads were increased in increments of 25% deign load and held for 10 minutes each time. The anchors were evaluated for elastic behavior using the minimum and maximum apparent free length criteria as per FHWA guidelines. The minimum criterion requires the calculated apparent free length to be greater than 80% of the design free length plus the jack length (approximately 1.5 feet).

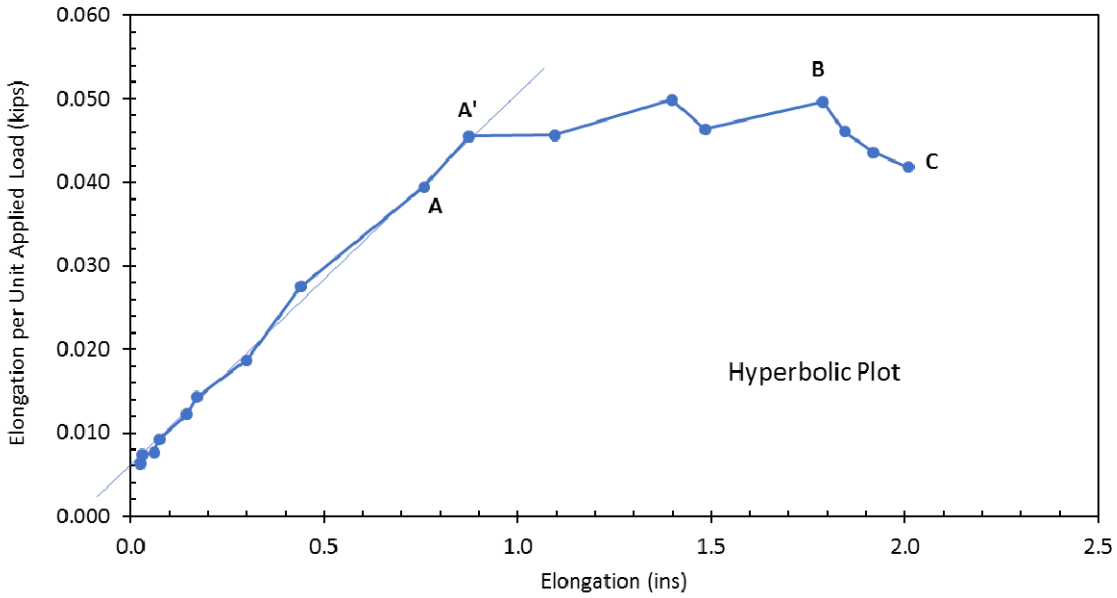


Fig. 10. Hyperbolic plot for trial test on Anchor SA-01

The maximum criterion requires the apparent free length to be less than the design free length plus 50% of the design bond length. Apparent free lengths for each anchor were calculated based on the observed total elongation at the respective proof loads (Table 2). The anchors can be classified into three categories based on their performance: Category A – Anchors with calculated apparent free length satisfying the minimum and maximum acceptance criteria; Category B – Anchors with calculated apparent free length less than the minimum criterion and Category C – Anchors with calculated apparent free length exceeding the maximum criterion. As can be seen, only nine anchors (SA-01, SA-02, SA-05, SA-08, SA-09, SA-11, SA-12, SA-17 and SA-20) satisfied both the minimum and maximum apparent free length criteria (Category A).

Nine anchors (SA-03, SA-04, SA-06, SA-07, SA-10 and SA-13 to SA-16) had apparent free lengths shorter than the minimum apparent free length criterion (Category B). The implication for these anchors was that additional movement of the retaining walls may occur due to additional extension of the anchor free lengths over time. The ratio of the calculated apparent free lengths to the acceptable minimum free length of 17.5ft was between 0.90 and 0.93 for SA-3 and SA-4, and between 0.54 and 0.63 for the remaining anchors. The estimated elongation to achieve the minimum free length criterion was 0.11 inches. Hence the additional elongation of the anchors would be small and would not be of consequence for the retaining wall application in this case.

Three anchors (SA-18, SA-19 and SA-21) exceeded the maximum acceptable apparent free length criterion (Category C). It is noted that the apparent free length calculated based on the total elongation overestimates the actual elastic deformation of the anchor and includes the plastic deformation of the soil. SA-21 only marginally exceeded the maximum free length criterion by 5% and can be considered to be acceptable within the margin of error of the elongation measurements. The calculated apparent free lengths for SA-18 and SA-19 were larger than the total anchor length of 45ft, suggesting that the method of assessment using total elongation was inappropriate in these cases. Figure 11 shows the load-displacement response of these anchors were reasonably linear during loading, implying acceptable elastic behavior. Hence, an anchor that exceeded the maximum apparent free length may be incorrectly considered to be unsafe even when it behaved elastically. The key evaluation is the elastic behavior of the anchor.

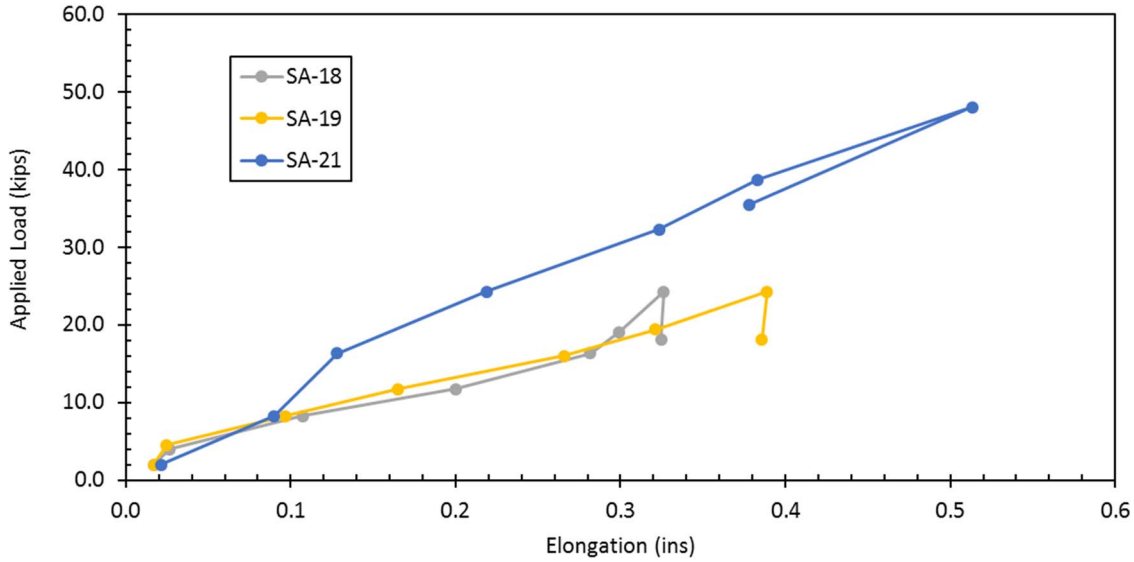


Fig. 11. Load-elongation plot for Anchors SA-18, SA-19 and SA-21

Table 2 shows that there was little difference between the lift off loads and lock off loads in the anchors. This indicated that loss of anchor load due to relaxation was not apparent. The loads in all anchors were maintained at the minimum lock off values of 17.6 kips (SA-01 to SA-20) and 35.2 kips (SA-21) respectively. An evaluation of the shear stress in the anchor bond lengths was also made to clarify the degree of mobilization of the available ultimate shear resistance of the anchor. It was conservatively assumed that all the load was resisted by the bond length alone without contribution from the free length. The calculated average shear stress mobilized at the grout-soil interface for Anchors SA-01 to SA-20 (25 feet bond length) ranged from 458 to 481 psf, with a mean of 466 psf and standard deviation of 5.1 psf. The corresponding mobilized shear stress for Anchor SA-21 (40 feet bond length) was 573 psf. These values were well below the maximum mobilized shearing resistance of 916.7 psf obtained from the preliminary trial test. The associated factors of safety were between 1.9 to 2.0 for SA-01 to SA-20 and 1.6 for SA-21, hence slippage at the grout-soil interface was not likely to have occurred at the level of loading for proof tests. The anchors were considered to be acceptable.

CONCLUSIONS

This paper presents the design of anchored double tier retaining walls constructed on a steep embankment for a waterfront development. Design requirements for sliding, overturning and bearing capacity were satisfied without the requirement for ground anchors. Ground anchors were only introduced to enhance global stability for a minimum factor of safety of 1.5 under permanent static loading conditions**.** A preliminary trial test was conducted on the first production anchor to confirm design assumptions. Trial results indicated that elastic elongation was small and plastic deformation will dominate anchor performance. Although proof tests indicated that three out of 21 anchors exceeded the maximum apparent free length criterion, lift off tests confirmed that the anchor loads were still maintained for the minimum lock off requirement of 1.1 times design load. This showed that the assessment of ground anchor acceptability based on total elongation which includes both elastic and plastic deformation components may be conservative. Mobilized shear stress on anchor bond lengths from proof tests indicated factors of safety achieved ranged from 1.7 to 2.0 based on the preliminary trial test results and were satisfactory.

Table 3: Anchor proof test results, lock off and lift off loads

Soil Anchor No.	Test Load (kips)	Elongation at Test Load (ins)	Apparent Free Length (ft)	Apparent Free Length Criteria (ft)		Lock Off /Lift Off Loads (kips)
				Minimum	Maximum	
SA-01	24.30	0.130	21.9	17.5	32.5	18.1/18.1
SA-02	25.19	0.192	31.2	17.5	32.5	18,1/18.1
SA-03	24.30	0.093	15.7	17.5	32.5	18,1/17.6
SA-04	24.30	0.096	16.3	17.5	32.5	18.4/18.4
SA-05	24.30	0.118	19.9	17.5	32.5	18.1/17.6
SA-06	24.30	0.056	9.4	17.5	32.5	18,1/18.4
SA-07	24.30	0.059	10.0	17.5	32.5	18.1/17.6
SA-08	24.59	0.120	20.0	17.5	32.5	18,1/17.6
SA-09	24.30	0.105	17.7	17.5	32.5	18.1/17.6
SA-10	24.89	0.064	10.6	17.5	32.5	18,1/19.3
SA-11	24.30	0.131	22.1	17.5	32.5	18.1/18.7
SA-12	24.30	0.104	17.7	17.5	32.5	18.0/18.4
SA-13	24.30	0.065	11.0	17.5	32.5	17.6/17.6
SA-14	24.30	0.065	11.0	17.5	32.5	18.1/17.6
SA-15	24.30	0.058	9.8	17.5	32.5	18.1/19.3
SA-16	24.89	0.061	10.1	17.5	32.5	18.1/18.4
SA-17	24.00	0.176	30.2	17.5	32.5	18.1/18.7
SA-18	24.30	0.326	55.2	17.5	32.5	18.1/18.4
SA-19	24.30	0.389	65.7	17.5	32.5	18.1/18.7
SA-20	24.30	0.132	22.3	17.5	32.5	18.1/18.4
SA-21	48	0.513	42.1	17.5	40.0	35.5/36.0

REFERENCES

Chin, F. K. (1970). "Estimation of the Ultimate Load of Piles Not Carried to Failure." Proc. 2nd Southeast Asian Conf. on Soil Engineering, pp. 81-90.

Federal Emergency Management Agency (1983). "Flood Insurance Maps".

Federal Highway Administration (1999). " Ground Anchors and Anchored Systems". FHWA-IF-99-015, Geotechnical Engineering Circular No.4.

Mononobe, N. and Matsuo, H. (1929) "On the Determination of Earth Pressure during Earthquakes", Proc. World Engineering. Conference, Vol.9, 176 p.

Morgenstern, N.R., and Price, V.E., 1965. "The Analysis of the Stability of General Slip Surfaces". Geotechnique, Vol.15, pp. 79-93.

Okabe, S. (1926) "General Theory of Earth Pressure", J. of the Japanese Society of Civil Engineers, Tokyo, Japan, 12(1).

New York City Buildings Department (2014), "New York City Building Code," New York, NY.

Post-Tensioning Institute (2014). "Recommendations for Prestressed Rock and Soil Anchors." PTI DC35.1-14, 5th Edition.

United States Geological Survey (1999). "Hydrologic Maps".

ASSESSMENT OF ANALYSIS TECHNIQUES FOR MULTI-PLATE ANCHORS IN SAND

Anastasia Nally, Northwestern University, Evanston, IL, USA, anastasia.nally@u.northwestern.edu
James P. Hambleton, Northwestern University, Evanston, IL, USA, jphambleton@northwestern.edu

ABSTRACT

This work focuses on the numerical simulation of multi-plate anchor systems (e.g., helical anchors) in sand subjected to vertical loading. In assessing the stiffness and capacity of these multi-plate anchor systems, full awareness of the abilities and limitations of the various analysis methods must be understood. This work first summarizes studies completed by others and then goes on to assess the failure mechanisms of multi-plate anchors in sand and the influence of (1) plate width-to-depth ratio, (2) number of plates, and (3) relative positioning of plates. The analysis makes use of (1) conventional limit analysis, (2) so-called modified limit analysis that employs reduced strength parameters to account for the influence of soil dilatancy, and (3) the displacement-based finite element method, which considers elastic as well as plastic deformation leading to failure. The work critically reflects on limitations in the current analysis methods for helical ground anchors.

Keywords: plate anchor, helical anchor, sand, numerical analysis, elastoplastic, limit analysis.

INTRODUCTION

Helical anchors are a relatively low cost foundation type, typically consisting of a steel rod and single or multiple plate attachments. In recent decades, they have seen rapid growth, and as outlined by Merifield and Sloan (2006) and Hambleton et al. (2014). Design techniques for helical anchors have previously been predominately empirical, as much of the past research in this field is experimentally based.

It is common practice for helical anchors to be modeled as horizontally oriented plate anchors in both numerical and experimental analysis. This work focuses on analysis based on the finite element method, including so-called finite element limit analysis and the conventional displacement-based finite element method, with some comparisons made to experimental studies. Numerical simulation of anchor pull-out capacity in cohesionless soils is stunted by the many difficulties faced when using numerical analysis with cohesionless soils. Additional variations can be seen when comparing the serviceability based load capacities to the ultimate load. In this work, both the force-displacement response (stiffness) and the ultimate anchor capacity are assessed, with more focus on the latter.

This work focuses only on analysis techniques for multi-plate anchors with vertical loading in cohesionless soils. Many studies have been completed in this area, some of which assume a rectangular plate in a plain strain model (Rowe & Davis, 1982; Merifield & Sloan, 2006; Cerfontaine et al., 2019). Whereas others use axisymmetric conditions (Baker and Kondner, 1966; Saeedy, 1987; Murray & Geddes, 1987; Ghaly & Hanna, 1994; Sakai & Tanaka, 1998; Merifield et al., 2006;) and minimal studies considered both axisymmetric and plane strain in the one study (Vesic, 1971; Tagaya et al., 1988; Murray & Geddes, 1987; Sarac, 1989).

A benchmarking study is first completed to compare the computed results to the break-out factors for circular plate anchors determined numerically by Merifield et al. (2006) and experimentally by Murray & Geddes (1987), Saeedy (1987) and Baker and Kondner (1966). This section of the study also investigates the plate width-to-depth ratio. The influence of the number of plates and the relative positioning of each of

© 2019 Deep Foundations Institute

these plates is then further investigated. In this investigation, particular consideration is given to assessing the ability of each analysis method to capture realistic failure mechanisms and well as the influence of some known errors within analysis techniques (e.g., mesh sensitivity).

PREVIOUS STUDIES AND CURRENT LIMITATIONS

Traditionally, theoretical studies in this area have been predominantly in the form of analytical approaches for single plate anchors. Notable studies include those by Meyerhof and Adams (1968), Murray and Geddes (1987), Basudhar and Singh (1994) and Smith (1998). For the case of analytical methods, many assume associated plastic flow, which results in unrealistic volume change and requires failure mechanisms to extend to the surface of the model. For the case of numerical analysis, both axisymmetric and plane strain analysis have been completed, with more detailed studies for plane strain. Rowe and Davis (1982), Vermeer and Sutjiadi (1985), Tagaya et al. (1988), Koutsabeloulis and Griffiths (1994) and Basudhar and Singh (1994) all conducted plane stain analysis on single-plate anchors. Tagaya et al. (1988), Koutsabeloulis and Griffiths (1994) and Merifield et al. (2006) presented the case of axisymmetric analysis. A more detailed summary of a wider range of studies in this area is provided by Merifield and Sloan (2006).

Studies of multiple plate anchor studies on granular material have predominantly been experimental, including publications from Baker and Kondner (1966), Ovesen (1981), Murray and Geddes (1987), Saeedy (1987), Dickin (1988), Tagaya et al. (1988), Ghaly et al. (1991), Ghaly and Clemence (1998), Ilamparuthi et al. (2002), Stanier (2011), Liu et al. (2012) and Tsuha et al. (2012). The major limitation of these studies is the lack of investigation into the interaction of multiple plates, which was experimentally assessed by Hao et al. (2018).

Finally, it should be noted that careful consideration should be given to the use of elastoplastic finite element analysis, and it should only be used by experienced professionals. In this study, the effect of mesh dependency on the elastoplastic finite element approach is addressed. Further analysis into other aspects of the abilities and difficulties of this technique is presented in Toh and Sloan (1980) and Sloan and Randolph (1982).

ANALYSIS METHODS

The three analysis techniques to be used in this work are (1) limit analysis (LA), (2) limit analysis with reduced parameters to account for the effects of a non-associated flow rule (Davis, 1968; Drescher and Detournay, 1993), denoted as modified limit analysis (MLA), and (3) elastoplastic finite element analysis (EP). These techniques are defined in subsequent sections. All three analysis techniques have been considered, as there is no perfect technique for the case of granular material. Assessing all three together highlights the possibilities and limitations of each. While an overview of each technique is provided below, the reader is referred to the detailed discussion and comparison of these methods by Sloan (2013) for more information.

Limit Analysis (LA)

Limit analysis considers a mode of failure expressed either in terms of an admissible stress field (lower bound limit analysis) or displacement field (upper bound limit analysis). Limit analysis cannot readily account for non-associative plastic flow, which is critical for the case of granular materials, nor can it capture the realistic failure mechanisms for multi-plate anchors. For this reason, the results can be expected to be somewhat inaccurate compared to the true results. Additionally, it is expected that the failure mechanism of limit analysis will not be capable of capturing the complex anchor geometry of multiple anchor plates. Both the upper and lower bound limits of a collapse load are utilized in this work to determine

the bounds of the collapse load for the given assumptions. All analysis completed here using the finite element limit analysis code OptumG2 incorporates mesh adaptivity with three steps and a target of 1000 elements. It should be noted that the number of elements specified following mesh adaptivity are generally well over this target.

Modified Limit Analysis (MLA)

This analysis incorporates all the same details outlined in Limit Analysis with the addition of material parameter factoring. In order to account for the non-associative behavior of sand, the reduced parameters approach first proposed by Davis (1968) and subsequently documented by Drescher and Detournay (1993) aim to capture the reduction in material strength caused by non-associative plastic flow. The general accuracy of the method is not well understood and cannot be assumed to provide comprehensive method to account for non-associative behavior. The material used in this study is cohesionless, and the friction angle is reduced according to the following equations (Drescher and Detournay, 1993):

$$\tan \varphi^* = \eta \tan \varphi \quad [1]$$

where $\varphi =$ friction angle, $\psi =$ dilation angle and η is given by

$$\eta = \frac{\cos \psi \cos \varphi}{1 - \sin \psi \sin \varphi} \quad [2]$$

Elastoplastic Finite Element Analysis (EP)

Elastoplastic finite element analysis was implemented through the multiplier technique provided in OptumG2, which progressively increases the applied load (in this case an upward orientated force) until a state of failure has occurred. A collapse load evaluated using this analysis technique in OptumG2 is determined using traditional displacement-based finite element analysis.

A major limitation of EP is mesh dependency, meaning that for a variation in mesh the resulting load will vary, with no convergence for an increasingly fine mesh. Although this limitation can be avoided by incorporating viscosity into the numerical model (Perzyna, 1966), this adds further complexities and OptumG2 does not offer this feature. A further assessment into the mesh dependency of this analysis is provided as part of the benchmarking and parametric studies. Finally, the EP has a significantly longer computational time when compared to LA. However, it is able to capture the effects of intricate anchor details LA cannot capture when assessing the failure mechanism.

PROPOSED MODEL AND BENCHMARKING STUDY

This work utilized OptumG2 for the analysis of a dense sand in order to determine the collapse load of different idealized ground anchors. The material properties for the dense sand were taken as the values presented in Table 1, which were selected in order for comparison to previous studies. An axisymmetric model was used, and boundaries were set sufficiently far so as to not influence the failure zones for an overall domain size of 40 m wide by 30 m high. In all cases plate elements were used to model the anchors and plates. These have frictionless interfaces and are treated as rigid elements in OptumG2. The load is applied above the surface to ensure no interaction with the surface material, with the load multiplier used to assess the collapse load applied to the full geometry. All plates are assumed to have zero thickness and sizes specific to each analysis are detailed in the subsequent sections.

In order to verify the analysis techniques used in this work, a benchmarking study was conducted wherein the pullout capacity of a single horizontal anchor was compared to previous axisymmetric studies. The

simplified horizontal plate anchor has numerous previous studies on granular material, with results from various numerical and experimental approaches. The axisymmetric results by Merifield et al. (2006), Murray & Geddes (1987), Saeedy (1987) and Baker and Kondner (1966) are compared here.

This analyses for this study were completed to assess the effect of the depth of embedment (H) to plate diameter (B) ratio (H/B) on the anchor pullout load, with the dimensions indicated in Fig. 1. The investigation included the three analysis techniques previously outlined in order to assess limitations and compute results for single-plate anchors as a basis for comparison with multi-plate anchors. For the single-plate anchor, the depth was kept at a constant of H = 20 m, and the plate diameter was such that the maximum H/B ratio was 10.

For this study, both upper and lower bounds were computed for LA and MLA, and the EP analysis with consideration of mesh sensitivity was also completed. In order to achieve the mesh sensitivity analysis for each H/B ratio computed, ten meshes were used to determine the collapse load. The meshes ranged from very fine to coarse with both uniform and non-uniform meshes incorporated into the analysis. Note that non-uniform meshes were achieved by specifying different areas of the same material, as shown in Fig. 2. It was determined that the break out factor (see Eq. [3] below) varied by an average of approximately $\pm 5\%$, and this is assumed to be the error caused by mesh dependency.

The results of the benchmarking study are presented in Fig. 3, where the break-out factors are calculated as

$$N_\gamma = \frac{q_u}{\gamma H} \qquad [3]$$

where q_u = average normal stress on the plate (kN/m^2), γ = soil unit weight (kN/m^3) and H = depth to the lowest plate (m). The average normal stress q_u is calculated as the ultimate force Q_u (Fig. 1) divided by the area of a single plate.

One can observe in Fig. 3 that the computed LA bounds produce the highest results, which is to be expected since associated plastic flow is assumed. MLA and EP both attempt to account for the non-associative behavior of sand, and thus produce lower estimates of the break-out factor. The LA data matches very closely with the numerical data reported by Merifield et al. (2006), denoted in the figure by SNAC. Additionally, the MLA and EP presented similar trends and fall within all of the previously published experimental data. From this is can be seen that all three analysis techniques give a reasonable approximation of the resisting loads for single horizontal plate anchors.

RESULTS OF PARAMETRIC STUDY

Following the benchmarking study, the influence of the number of plates and relative spacing of plates on the ultimate load was investigated. The break-out factor is no longer assessed as the normalization of the average stress over the area of a plate, which is less applicable with multi-plate anchors, but rather the normalized ultimate force $Q_u/\gamma H^3$. This was completed by assessing cases with varying plate numbers and spacing, where the anchor depth is kept constant at H = 20 m in order to better assess the capabilities and limitations of the analysis techniques. Each of the cases investigated were assessed using upper and lower bounds for both LA and MLA, as well as EP.

Number of plates

The influence of the number of plates on the break-out factor was assessed by using a constant length of B = 2 m and spacing of x = 2 m. From the previously assessed single plate anchor, additional plates were added, and the influence of these plates on the failure load and mechanism was assessed. As displayed in

Fig. 1, the plates are progressively included from the bottom, until a total of eight plates are added to the anchor and analyzed.

Both LA and MLA presented constant break-out factors and therefore the addition of multiple plates resulted in no benefit. This is due to the assumption of associativity embedded into the analysis technique and is a limitation, one which cannot be addressed within limit analysis. Limit analysis and elastoplastic analysis can be compared visually by assessing the failure mechanisms as presented in Fig. 4, where it can be seen that both variations of limit analysis predict similar failure mechanisms whilst the EP analysis predicts a significantly different failure mechanism. In Fig. 4, it can be seen that there are four plates and EP is able to capture the shear failure along the soil encompassing all plates. In contrast, LA selects a single failure surface, which extends from the bottom plate to the surface at an angle of approximately 45° and shows no failure along the upper three plates. Specifically for the case of EP, an increase in the number of plates resulted in a variation of the failure mechanism, as shown in Fig. 5. It can be seen that with a greater number of plates the failure plane is directed in a vertical orientation for an increasing distance towards the surface. This variation in the failure mechanism produces a variable collapse load and resulting break-out factor. As with the benchmarking study, mesh sensitivity is a limitation of EP and its influence on the results was assessed. For four plates, it was found that the error due to mesh sensitivity of this arrangement is approximately $\pm 10\%$.

The load-displacement curves for an increasing number of plates are presented in Fig. 6. These results suggest that increasing the number of plates may reduce the collapse load, whereas increasing the number of plates always results in a stiffer response. The decrease in capacity observed with an increasing number is plates is counterintuitive but nevertheless theoretically possible, and this requires further exploration. Furthermore, the reported displacements are unrealistically large given the expected anchor displacement required to mobilize the full load. Therefore, caution should be used when selecting the collapse load. This is a known limitation of elastoplastic displacement-based finite element methods, which were investigated by Sloan and Randolph (1982).

Relative positioning of plates

The influence of the relative positioning of plates on the break-out factor was assessed by using a constant length of $B = 2$ m and five anchor plates. The spacing was varied from $x = 0.25$ m up to $x = 3$ m. As displayed in Fig. 2, the plate spacing is progressively increased and each stage analyzed in a manner similar to the investigation previously completed.

As with the analysis completed for the influence of the number of plates, both LA and MLA presented constant break-out factors. This was due to the previously identified limitations of limit analysis. The EP analysis also produced very similar results to the previous analysis. The similarities can be seen in the failure mechanisms and load-displacement curves in Figs. 7 and 8, respectively.

CONCLUDING REMARKS

The work compiled in this paper utilized OptumG2 to complete a numerical study assessing analysis techniques for multi-plate anchors such as helical anchors. Three analysis techniques, LA, MLA and EP, were used to assess anchor capacity. A benchmarking study was first completed where break-out factors for single-plate anchors were compared to results from previous studies, hence verifying the numerical analysis techniques used. The benchmarking study confirmed that, for the case of a single horizontal plate anchor, all analysis techniques provided sensible results with explainable differences, with EP and MLA providing results closest to previously reported experimental data. This was followed by a parametric study examining the effects of the number of plates and plate spacing.

The results of the parametric study for multi-plate anchors presented a range of ultimate loads for all assessed limit analysis techniques, which did not encompass the results presented by EP. This difference can be attributed to the limitations of limit analysis—and in particular the assumption of associativity—and the significantly varying failure mechanisms presented by the two analysis techniques. In all cases of the parametric study, both LA and MLA presented constant ultimate loads, and this was determined to be a limitation of the analysis technique and a result of a constant failure surface.

Notably, for the case of EP, an increase in the number of plates resulted in a decrease in the ultimate capacity but an increase in stiffness. This would indicate that for a service load a larger number of plates would be desirable, whereas for ultimate load capacity a single plate is most desirable. While this counterintuitive result is theoretically possible, it requires further exploration in more detailed analyses and experimental investigations.

Both LA and MLA assume an associative flow rule, and as a result of volume change, the failure mechanisms in all cases unrealistically extended to the surface. LA was determined to be the least accurate due to its inability to capture the realistic soil behavior of multiple plates. For single plate anchors, MLA was determined to capture a more reasonable anchor capacity through the use of modified parameters. However, it was still limited in its ability to capture a realistic failure mechanism for multiple plates, which is further indicated by a constant ultimate load with a varying number of plates. Finally, EP was able to capture the intricate details of failure around multiple plates. Due to the assumption of non-associative plastic flow, the loading of anchors was able to cause elastic deformation and produce local failure mechanisms. The effect of mesh dependency was further assessed for elastoplastic analysis and found to produce variability in the predictions of ultimate capacity of up to 10%. There are still other potential sources or error in EP analysis, such as modeling assumptions relating to structural elements and contact, which are not addressed in this work. In all cases, caution should be used with all numerical analysis techniques.

ACKNOWLEDGEMENTS

This work could not have been completed without enabling financial support from the Australian Research Council (ARC) and the National Science Foundation (NSF), in particular through ARC award numbers DE160100328 and NSF award number CMMI 1846817.

REFERENCES

Baker, W.H., and Kondner, R.L. 1966. Pullout load capacity of a circular earth anchor buried in sand. Highway Research Record. No. 108: 1–10.

Basudhar, P.K. and Singh, D.N. 1994. A generalized procedure for predicting optimal lower bound break-out factors of strip anchors. Géotechnique, 44(2), 307-318.

Cerfontaine, B., Knappett, J. A., Brown, M. J. and Bradshaw, A. S. 2019. Effect of soil deformability on the failure mechanism of shallow plate or screw anchors in sand. Computers and Geotechnics. 109, 34-45.

Davis, E.H. 1968. Theories of plasticity and the failure of soil masses. In Soil mechanics: selected topics (ed.K. Lee), pp. 341-380. London: Butterworth.

Dickin, E.A. 1988. Uplift behavior of horizontal anchor plates in sand. J. of Geotech. Eng. 114(11), 1300–1317.

Drechser, A. and Detournay, E. 1993. Limit load in translational failure mechanisms for associative and non-associative materials. Géotechnique, 43(30), 443-456.

Ghaly, A.M., Hanna, A.M., and Hanna, M. 1991. Uplift behavior of screw anchors in sand. I: dry sand. J. of Geotech. Eng. 117(5), 773–793.

Ghaly, A.M., and Hanna, A. 1994. Ultimate pullout resistance of single vertical anchors. Can. Geotech. J., 31(5), 661-672.
Ghaly, A.M., and Clemence, S.P. 1998. Pullout performance of inclined helical screw anchors in sand. Journal of Geotechnical and Geoenvironmental Engineering, 124(7), 617–627.
Hambleton, J.P., Stanier, S.A., Gaudin, C. and Todeshkejoei, K. 2014. Analysis of installation forces for helical piles in clay. Australian Geomechanics, 49(4), 73–79.
Hao, D., Wang, D., O'Loughlin, C.D. and Gaudin, C. 2018. Tensile monotonic capacity of helical anchors in sand: interaction between helices. Can. Geotech. J., (in press).
Ilamparuthi, K., Dickin, E.A., and Muthukrisnaiah, K. 2002. Experimental investigation of the uplift behaviour of circular plate anchors embedded in Sand. Can. Geotech. J. 39(5), 648–664.
Koutsabeloulis, N.C. and Griffiths, D.V. 1989. Numerical modelling of the trap door problem Géotechnique, 39(1), 77-89.
Liu, J.Y., Liu, M.L., and Zhu, Z.D. 2012. Sand deformation around an uplift plate anchor. Journal of Geotechnical and Geoenvironmental Engineering, 138(6), 728–737.
Merifield, R.S., Lyamin, A.V. and Sloan, S.W. 2006. Three-dimensional lower bound solutions for the stability of plate anchors in sand. Géotechnique, 56(2), 123–132
Merifield, R.S. and Sloan, S.W. 2006. The ultimate pullout capacity of anchors in frictional soils. Can. Geotech. J. 43(8), 852–868.
Meyerhof, G.G. and Adams, J.I. 1968. The ultimate uplift capacity of foundations. Can. Geotech. J. 5(4), 225-244.
Murray, E.J. and Geddes, J.D. 1987. Uplift of anchor plates in sand. J. Geotech. Eng. ASCE 1 13, No. 3, 202-215.
Murray, E.J. and Geddes, J.D. 1989. Resistance of passive inclined anchors in cohesionless medium. Géotechnique, 39(3), 417-431.
Ovesen, N.K. 1981. Centrifuge tests of the uplift capacity of anchors. In Proceedings of the 10th International Conference on Soil Mechanics and Foundation Engineering, Stockholm. Vol. 1, pp. 717–722.
Pearce, A. 2000. Experimental investigation into the pullout capacity of plate anchors in sand. MSc thesis, University of Newcastle, Australia.
Perko, H. A. (2009). Helical Piles: practical guide to design and installation. John Wiley & Sons, Inc. Hoboken, New Jersey.
Perzyna, P. 1966. Fundamental problems in viscoplasticity. Adv Appl Mech. 9, 243–377
Rowe, R.K. and Davis, E.H. 1982. The behavior of anchor plates in sand. Géotechnique. 32(1), 25-41.
Saeedy, H.S. 1987. Stability of circular vertical anchors. Can. Geotech. J. 24(3), 452-456.
Sakai, T. and Tanaka, T. 1998. Scale effect of a shallow circular anchor in dense sand. Soils Found. 38, No. 2, 93-99.
Sarac, D.Z. 1989. Uplift capacity of shallow buried anchor slabs. Proc. 12th Int. Con Soil Mech. Found. Engng, Rio de Janeiro 2, 1213-1218.
Sloan, S. W. 2013. Geotechnical stability analysis. Géotechnique. 63(7), 531.
Sloan, S.W. and Randolph, M.F. 1982. Numerical prediction of collapse loads using finite element methods. International Journal for Numerical and Analytical Methods in Geomechanics. 6, 47-76.
Smith, C.S. 1998. Limit loads for an anchor/trapdoor embedded in an associated Coulomb soil. International Journal for Numerical and Analytical Methods in Geomechanics. 22, 855-865.
Stainer, S.A. 2011. Modelling the behavior of helical screw piles. Ph.D. thesis, University of Sheffield, England.
Tagaya, K., Scott, R.F. and Aboshi, H. 1988. Pullout resistance of buried anchor in sand. Soils Found. 28(3), 114-130.
Toh, C.T. and Sloan S.W. 1980. Finite element analysis of isotropic and anisotropic cohesive soils with a view to correctly predicting impeding collapse. International Journal of Numerical and Analytical Methods in Geomechanics. 4, 1-23.

Tsuha, C.H.C., Aoki, N., Rault, G., Thorel, L., and Garnier, J. 2012. Evaluation of the efficiencies of helical anchor plates in sand by centrifuge model tests. Can. Geotech. J. 49(8), 1102–1114.
Vermeer, P.A. and Sutjiadi, W. 1985. The uplift resistance of shallow embedded anchors. In Proceedings of the 11th International Conference on Soil Mechanics and Foundation Engineering, San Francisco, 12-16 August 1985. A.A. Balkema, Rotterfam, The Netherlands. 4, 1635-1638.
Vesic, A.S. 1971. Break-out resistance of objects embedded in ocean bottom. J Soil Mech. Found. Div ASCE 97, No. 9, 1183-1205.

TABLES

Table 1. Assumed Soil Properties

Parameter	Value
Friction Angle, φ (°)	40
Dilation Angle, ψ (°)	10
Cohesion, c (kPa)	0
Dry unit weight, γ (kN/m^3)	18
Young's Modulus, E (MPa)	50
Poisson's Ratio, v	0.3

FIGURES

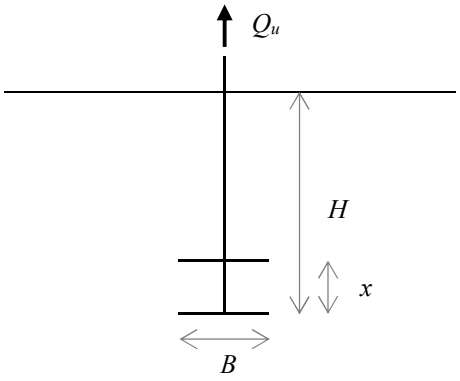


Fig. 1. Plate Anchor Dimensions

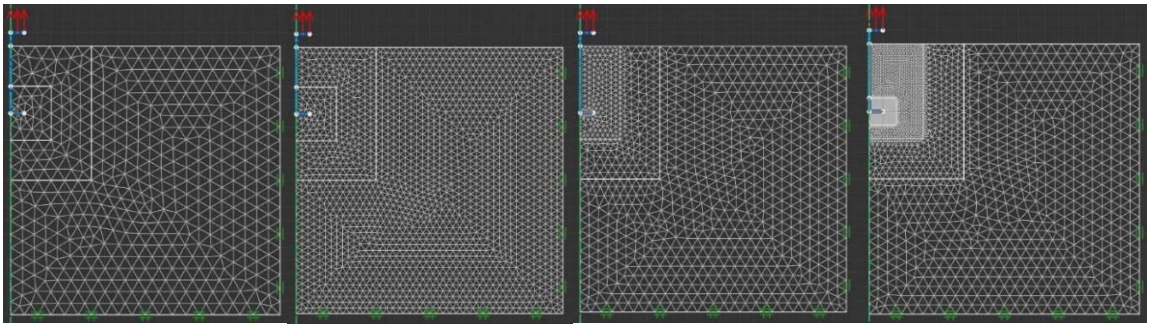


Fig. 2. Examples of meshes used in EP mesh sensitivity analysis

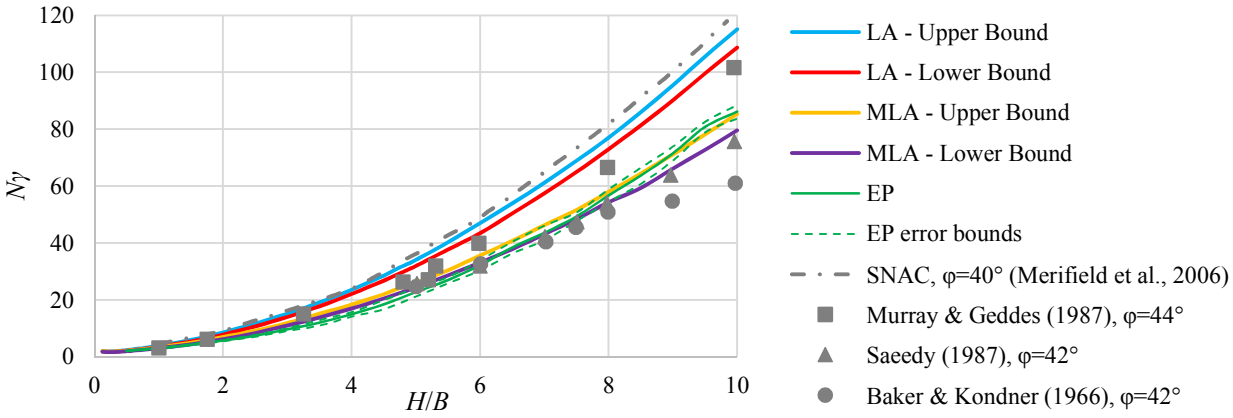


Fig. 3. Benchmarking study comparison (plot best viewed in color)

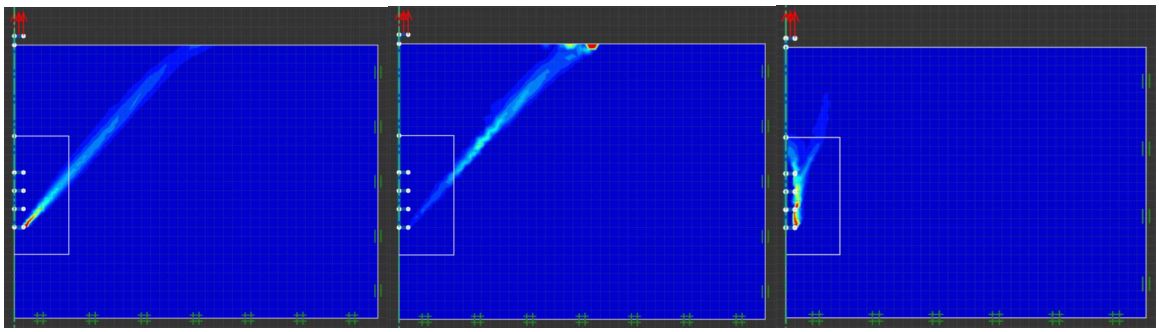


Fig. 4. Failure mechanisms for (left) upper bound limit analysis (middle) lower bound limit analysis (right) elastoplastic finite element analysis (contours show a representation of the deviatoric strain)

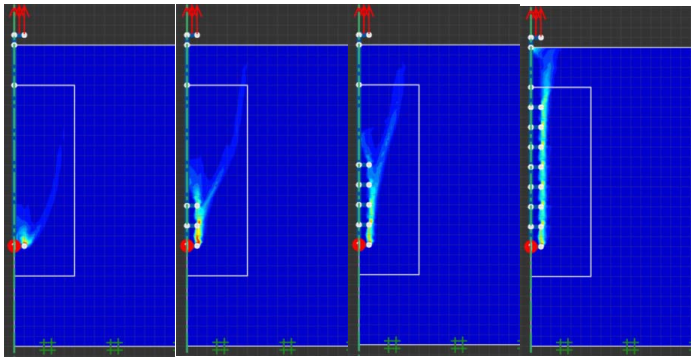


Fig. 5. Development of failure mechanism with increasing number of plates from elastoplastic finite element analysis (contours show a representation of the deviatoric strain)

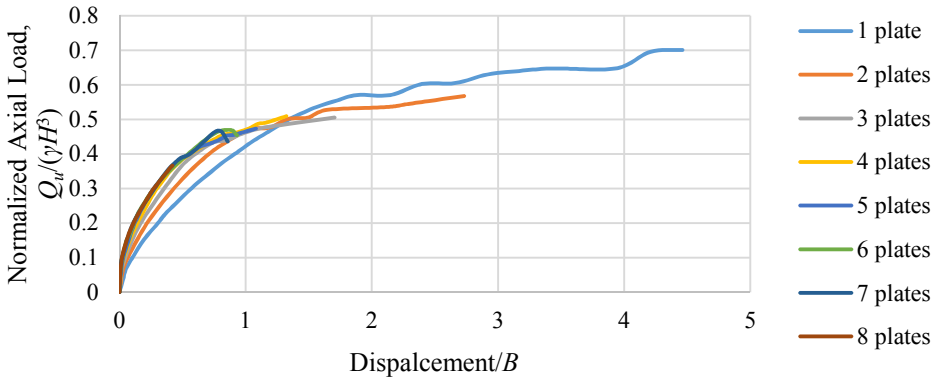


Fig. 6. Load-displacement curves for collapse loads for increasing number of plates (EP analysis; contours show a representation of the deviatoric strain; plot best viewed in color)

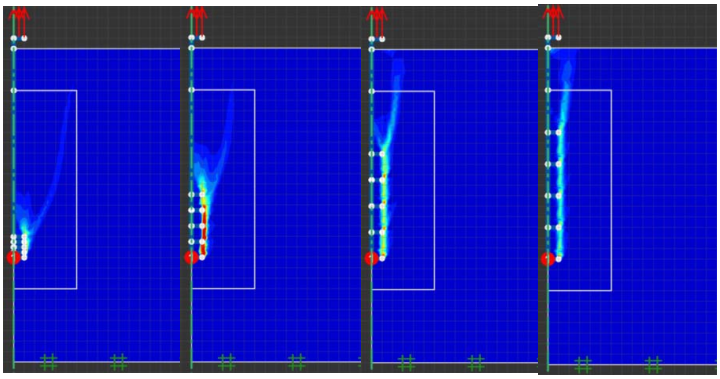


Fig. 7. Development of failure mechanism with increasing plate spacing (EP analysis; contours show a representation of the deviatoric strain)

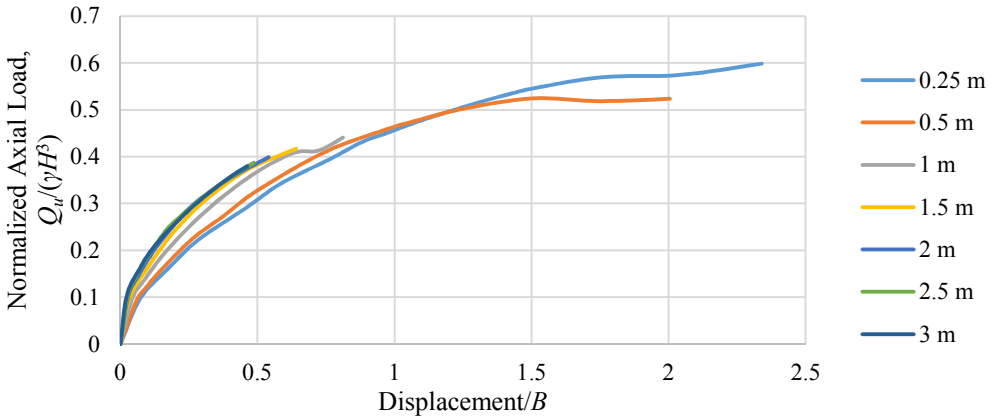


Fig. 8. Load-displacement curves for increasing plate spacing *x* (EP analysis; plot best viewed in color)

CASE HISTORIES OF CIRCULAR SECANT PILE ACCESS SHAFTS FOR TUNNELS

Stanley L. Worst, Schnabel Foundation Co., Cary, IL, USA, 847-639-8900, stanley@schnabel.com
Matthew J. Niermann, Schnabel Foundation Co., Sterling, VA, USA, 703-742-0020, matt@schnabel.com
Piotr Kozlowski, Schnabel Foundation Co., Cary, IL, USA, 847-639-8900, pkozlowski@schnabel.com

ABSTRACT

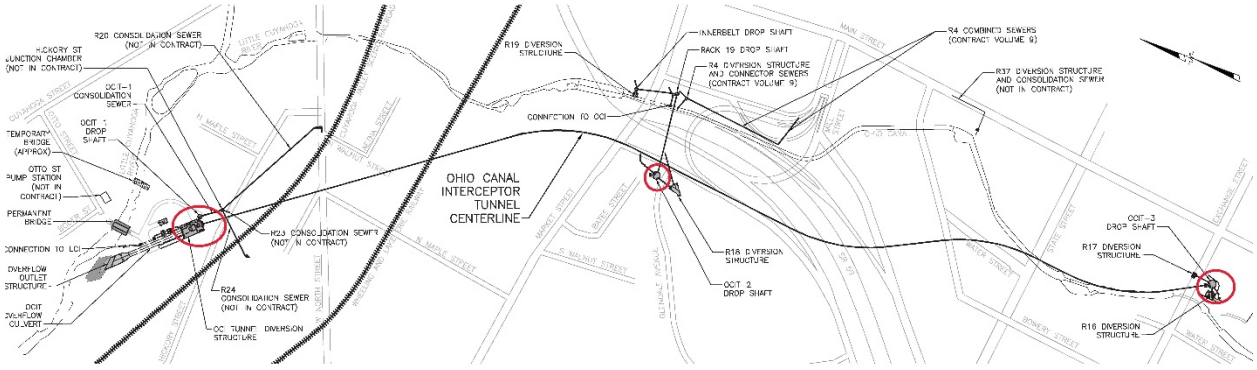
Circular secant pile shafts were installed along the tunnel alignments for both the Ohio Canal Interceptor Tunnel project in Akron, Ohio and the Ohio River Tunnel project in Louisville, Kentucky. The diameters ranged from 34 to 51 feet and the depths ranged from 49 to 107 feet. Verticality and concrete volumes were measured on all piles to verify compliance with the design, which for some shafts consisted of a finite element model with multiple openings using unreinforced concrete secant piles. All secant piles were drilled into rock to seal off the groundwater. This paper will discuss the design, construction and quality control of the secant piles for these projects.

INTRODUCTION

Many Midwest and Northeast cities have Combined Sewer Overflow (CSO) systems which discharge pollutants into waterways during wet weather events. One way to remedy this issue is to provide a temporary overflow tunnel. A temporary overflow tunnel connects to the combined sewer system and collects the overflow during wet weather events, storing the wastewater until the event has subsided. After the storm event, the stored wastewater can be pumped to the treatment facilities and processed as normal.

Project Background – Akron, OH

The Ohio Canal Interceptor Tunnel (OCIT) project was performed as a result of the Environmental Protection Agency's (EPA) Consent Decree with the City of Akron, Ohio. This Consent Decree required modification of the existing Combined Sewer Overflow system. The resulting project consisted of a 27-foot diameter tunnel with multiple points of entry to capture the sewer overflow and prevent it from entering waterways. The tunnel is over 6,000 feet long and is as deep as 150 feet below the ground surface; see Figure 1 below.



Source: City of Akron 2015.

Figure 1. OCIT Project layout

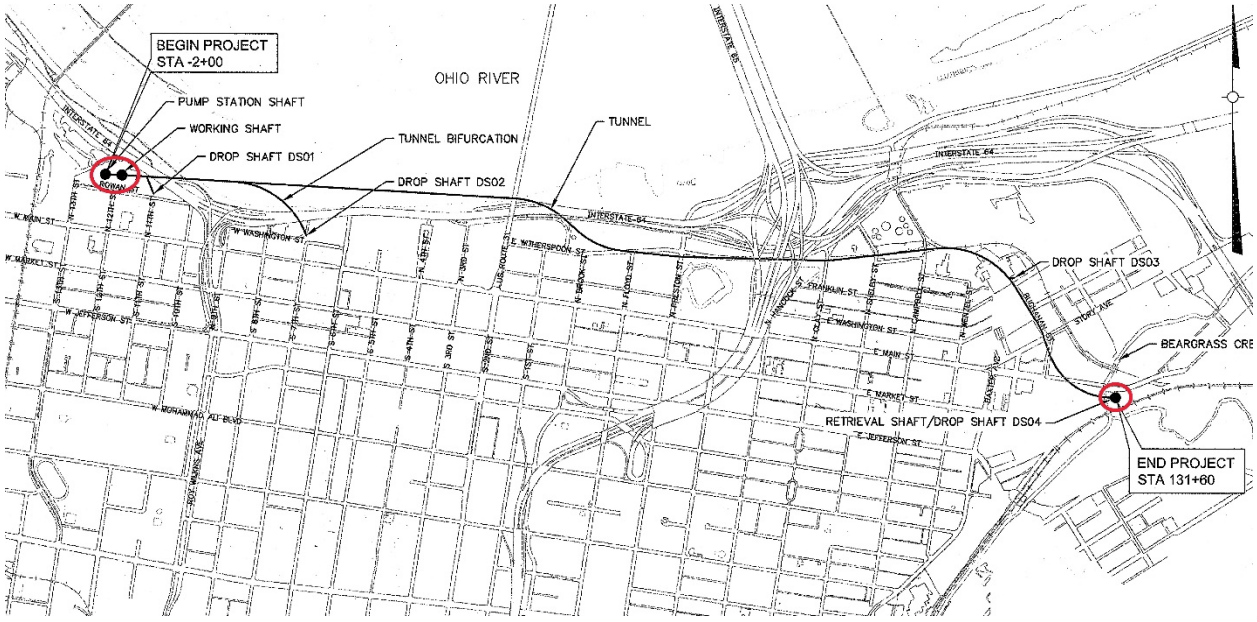
© 2019 Deep Foundations Institute

As part of the project, two circular secant pile access shafts were installed. One shaft, 46-foot inside diameter, was at OCIT-2, roughly the half-way point. The other shaft, 51-foot inside diameter, was at OCIT-3, one end of the tunnel. These were temporary Support of Excavation (SOE) structures to facilitate excavation and casting of the permanent drop structures.

Project Background – Louisville, KY

The Ohio River Tunnel (ORT) project was performed as a result of the EPA's Consent Decree with City of Louisville, KY in 2005. The resulting project consisted of a 20-foot diameter rock tunnel located below the downtown area. At a depth of up to 210 feet below the ground surface, the tunnel extends a maximum of 170 feet into rock and is over 13,000 feet long; see Figure 2 below.

Three circular secant pile access shafts were installed. Two shafts, the Working Shaft and Pump Station Shaft, were separated by only 150 feet. They were identical in diameter, 49 feet, and depth of secant piles, 58 feet. These two secant pile shafts were used as the starting point for the TBM. A hand-mined tunnel connected the two shafts in order to assemble the TBM trailing gear before mechanized tunneling began. The third shaft of secant piles, at the Retrieval Shaft, was 34 feet in diameter and 107 feet deep.



Source: City of Louisville 2017.

Figure 2. ORT Project layout

Geotechnical Information

Both Akron, Ohio and Louisville, Kentucky are midwestern cities which are underlain by a mixture of granular and cohesive soils overlying rock. The rock is sedimentary in nature, reflective of the depositional environment in which it was formed. Sandstone, shale, siltstone, limestone and dolomite are all typical sedimentary rocks found in the Midwest and were encountered on these projects. Much of the overlying soils were glacially derived and have many lenses of granular soils with perched water as well as cobbles and boulders of various origin.

At the OCIT-2 secant pile shaft location in Akron, Ohio, the upper 40 feet of soil was fill material which consisted of sandy silty clay along with silt and poorly graded sand. Blow counts varied between 10 and 27 blows per foot. Underlying the fill material was a layer of outwash and lacustrine medium dense silt with sand, which sat on top of shale bedrock. The shale contained laminations of sandstone and siltstone. The RQD of the shale was 83-99% and the unconfined compressive strength averaged approximately 11,000 psi. Groundwater was encountered above the top of rock. However, water infiltrating into the secant piles during drilling was sealed off by temporarily socketing the drill casing into the shale bedrock. Shale is a fine-grained, sedimentary rock which is drillable with conventional tooling.

At the OCIT-3 secant pile shaft location in Akron, Ohio, the upper 20 feet of soil was fill material which consisted of sandy clay and silty gravel with blow counts varying between 0 and 69 blows per foot. Underlying the fill material was a layer of very loose organic silt, medium dense silt and poorly graded sand all below the water table. Bedrock consisted of approximately six feet of sandstone underlain by shale. The sandstone had an 85% RQD and an average unconfined compressive strength of approximately 6,000 psi. The shale had an RQD of 47-53% and an average unconfined compressive strength of approximately 9,000 psi.

The Working Shaft and Pump Station Shaft in Louisville, Kentucky were close enough together to have the same geologic profile. Overburden consisted of up to 40' of alluvium and glacial outwash which consisted of silty clay, silty sand and gravel with blow counts ranging from 4 to 23. A layer of shale up to eight feet thick sat on top of the main rock unit which contained Limestone and Dolomite. The secant piles extended a minimum of five feet into the limestone and dolomite, which had an RQD of 78% and unconfined compressive strengths of approximately 12,000 psi.

The Retrieval Shaft in Louisville, Kentucky had varying soils to a depth of approximately 100 feet below the ground surface. These soils consisted of sandy clay, silty clay, sand, silty sand and gravelly sand with blow counts ranging from 3 to 24. Dolomite with an RQD of 91% and strength of up to 21,000 psi was encountered below the soils. The secant piles extended seven foot into this rock unit.

SECANT PILES

Design Basis and Concepts

The basic design concept for the circular secant pile access shafts is to analyze a vertical cylinder with horizontal hoop stresses. Overlapping secant piles laid out in a circular pattern form a cylinder of concrete which has an effective thickness. Figure 2 shows the concept of effective thickness, which is the dimension measured across the secant piles where two adjacent secant piles overlap. Vertical drilling is subject to minor deviation in the horizontal direction. Based on previous experiences of measuring this deviation, Schnabel Foundation Company chose a verticality tolerance of 0.5%, or 1 in 200, for the design of this project. Due to this verticality tolerance, there exists the possibility of a thinner effective thickness with depth. This theoretically thinner effective thickness is accounted for in the design by analyzing the pressure on the cylinder immediately above the top of rock, where the pressure is the greatest and the effective thickness can be the thinnest.

t_1 = Initial Effective Thickness at Top of Pile

t_2 = Final Effective Thickness at Bottom of Pile after Theoretical Deviation

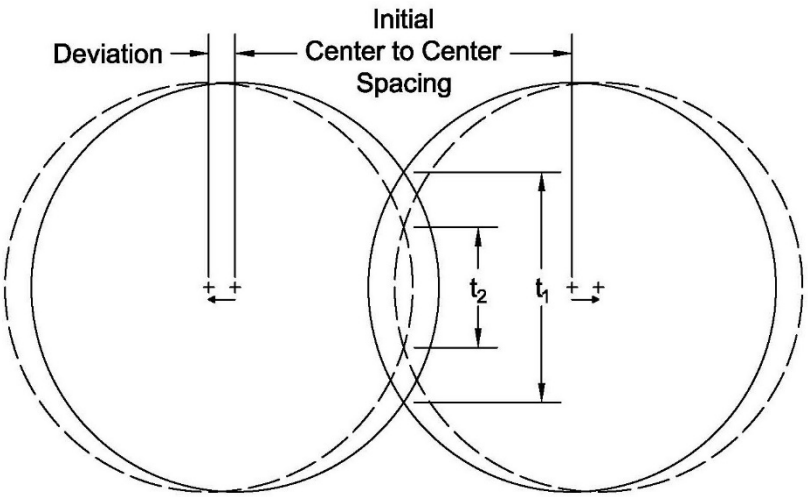


Figure 3. Secant pile deviation and effective thickness

Lateral forces on the cylinder are present in the form of Rankine earth pressures; linearly increasing with depth. Due to secant piles being very stiff and rigid, and that the cylinder is acting in compression, very little movement is allowed of the overall secant pile shaft. This lack of movement prevents active pressure from forming, resulting in a higher at-rest pressure. Therefore, K_o is used in the earth pressure calculations for this type of system. Hydrostatic water pressure is also added to the design and is a linearly increasing pressure with depth. Typically, for tunnel projects that take a few years to construct, the hydrostatic water pressure is designed at or above existing grade for 100-year flood conditions.

The critical case for Rankine earth pressure is where the pressure is the greatest, which is at the top of rock. For the temporary condition, rock is assumed to have a high friction angle and unconfined compressive strength, exerting a much lower lateral force on the cylinder at this elevation. The highest earth pressure at the top of rock also corresponds with the thinnest theoretical effective thickness of the overlapping secant piles due to verticality deviations. To account for this, the starting overlap of the secant piles at the ground surface (t_1 in Figure 3) is increased from what is required at depth (t_2 in Figure 3). Using the verticality tolerance of 0.5%, which Schnabel has confirmed it can achieve through experience, the amount that the overlap is increased can be calculated.

When viewed in plan-view, the lateral force that is exerted on the cylinder can be represented by a pressure, "P." As shown in Figure 3, that pressure is distributed over the diameter of the cylinder. It is resisted by the axial thrust in the internal hoop at that elevation. The thrust is represented as "T" on each side of the hoop. Therefore, Equation 1 represents force equilibrium.

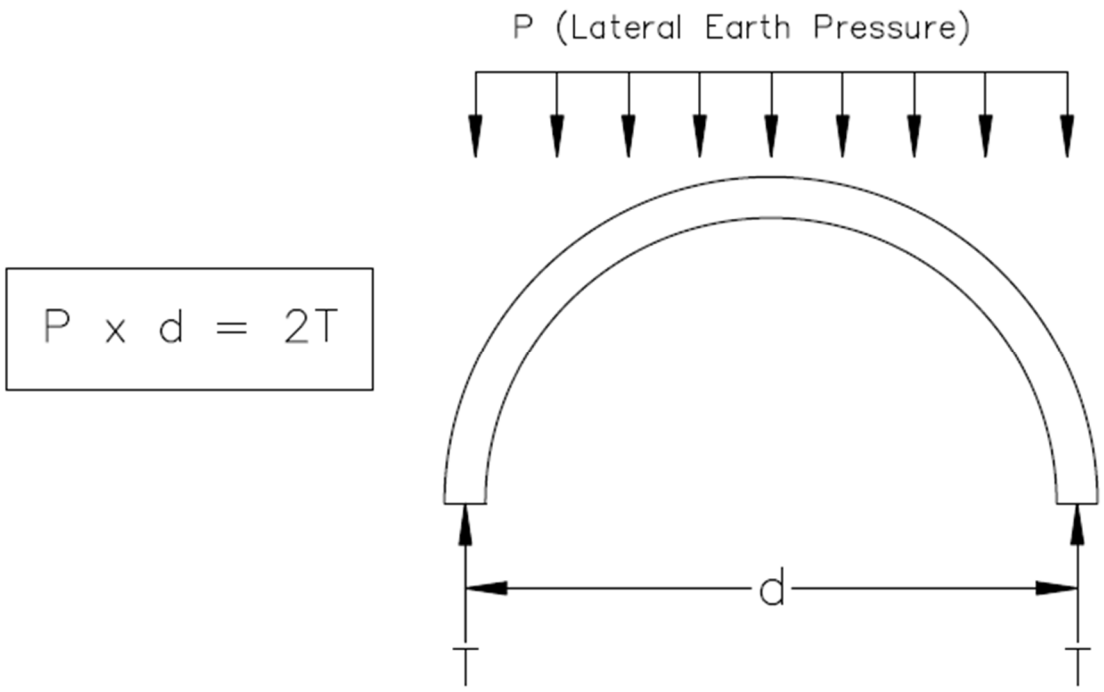
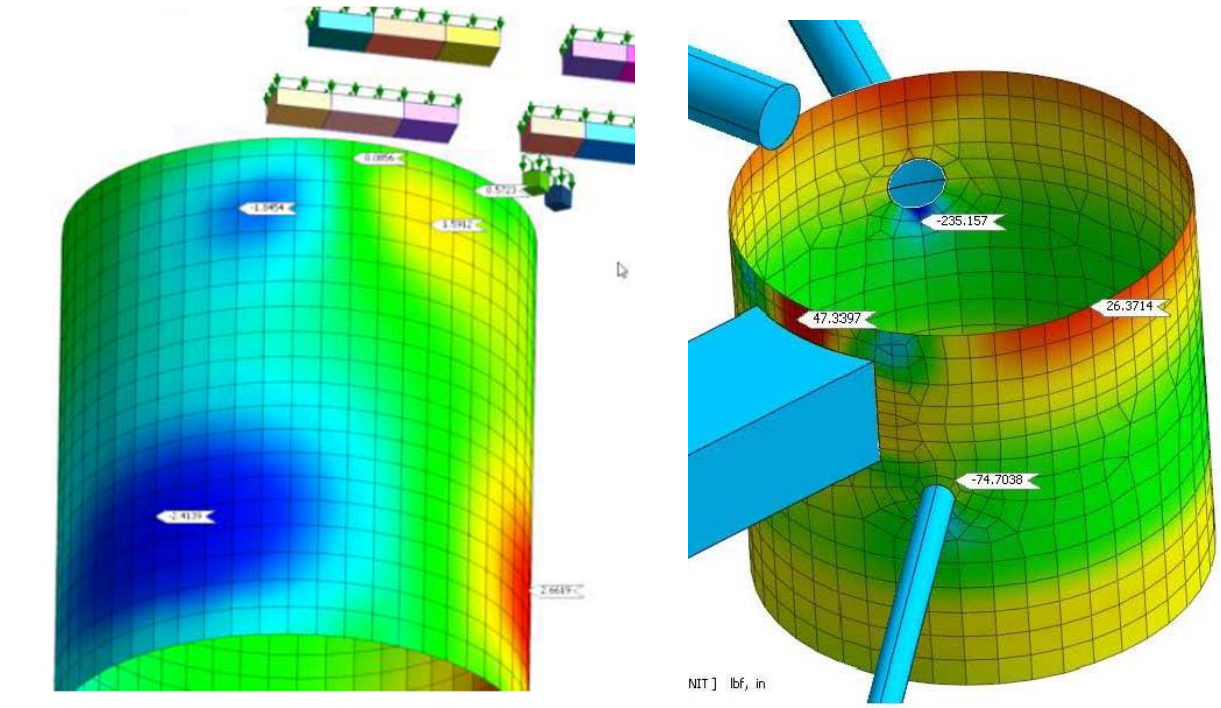


Figure 4. Force equilibrium on a vertical shaft

Equation 1: $2T = P \times d$.

The resulting thrust can be analyzed to determine the required compressive stresses in the concrete. For this project, unreinforced concrete secant piles were used to resolve these stresses. The secant piles were 1,180mm diameter above the top of bedrock and 1,060mm diameter in bedrock. These dimensions are the outside diameter of the temporary casing and the full diameter of the rock drill tooling used, respectively.

However, this simple form of analysis is only appropriate if the loading is symmetric. Unbalanced loading as a result of large crane surcharges or localized stresses from large openings in the cylinder present different design challenges. These situations can be analyzed using the Finite Element Method. Figures 4a and 4b show examples of how openings and large surcharges account for different levels of localized stresses which may or may not control the design. For the OCIT-3 shaft in Akron, Ohio, there were four different break-through openings within the secant pile shaft that were analyzed with finite element software. These openings were approximately 36 inches, 84 inches and 72 inches in diameter along with one rectangular opening that was 13 feet x 8 feet. For the Working Shaft in Louisville, Kentucky, heavily loaded spread footings were used on one side of the shaft to carry the weight of the conveyor and muck from the tunneling operations.



Source: Gamal 2016.

Figure 5. Finite element analysis of a) unbalanced loading on circular secant pile shaft; and b) openings in circular secant pile shaft

Quality Control and Construction

The verticality measurement of each individual secant pile is of utmost importance as the entire design concept is based on a certain effective thickness. Without having any redundancy or additional means of lateral support, the overlap of each secant pile must be met, and therefore it must be known prior to concreting the hole. There are a few different devices which can be used to measure the verticality. For this project, the Jean Lutz Prad system was used. This system consists of a wireless device which is mounted to the drill tooling. It is lowered to the bottom of the hole and raised back to the top of the hole with a controlled rotation and lift rate. This produces a deviation profile every few feet which can be seen by the operator in the cab of the drill rig. It also produces a printer-friendly version for submittal and documentation purposes. An example of the in-cab display is shown in Figure 5. Once each pile's deviation is known, the effective thickness at the top of rock can be calculated to check that it is equal to or greater than what was designed. This data can also be plotted to show the deviation and resulting effective thickness at various depths.



Figure 6. In-Cab display of verticality measurement

To achieve the tight 0.5% verticality tolerance, large, high-torque rotary drill rigs with flush-joint segmental casing are necessary. The casing is double-wall and very rigid, which makes it extremely difficult to deviate once it is in the ground. Advancing the casing along with the auger helps to maintain alignment. Also, a guidewall is used at the ground surface to act as a fixed point for the casing. The guidewall is constructed with lightly reinforced concrete and is poured to tight tolerances, which keep the casing from wandering off during the initial stages of drilling. The guidewall is typically a few feet thick and is poured a few feet on either side of the template. The template for the guidewall is generally constructed with either steel forms or foam blockouts.

The other factor that can affect the effective thickness of the secant pile shaft is the actual diameter of poured concrete in each pile. This can be indirectly measured by tracking the volume of concrete placed in the pile. If a volume lower than the theoretical volume is measured, there is likely a local cave-in of soil which prevented concrete from filling up the full pile diameter. This can be avoided by extending the temporary casing full depth down to the top of rock and using proper tremie concrete practices. Confirming the concrete mix design is fluid enough will also ensure that the concrete inside the temporary casing will fill the annular space left during casing extraction. Concrete volume measurement can also be an indicator of bulges which will need to be chipped away at later date during the shaft excavation. If volumes much higher than the theoretical volume of the pile are recorded, there exists the possibility of weak soils or voids in rock which allowed for extra concrete to be placed. On the project in Akron, Ohio, there was a layer of low blow-count organic silts below the water table which yielded takes of over 40% of the theoretical volume of concrete per pile on some piles. Extra concrete does not affect the design and can be removed during shaft excavation if it encroaches into the permanent structure.

CONCLUSION

Secant piles can be a very effective form of earth retention and water cutoff. They can be socketed into rock to seal off groundwater and can form self-supporting circular access shafts without any internal bracing or external tiebacks. Because secant piles are installed with very robust drill rigs and tooling, they are commonly used in ground where there are known to be boulders, rock or difficult drilling conditions. Secant piles can also be used to construct rectangular support of excavations to be either cantilevered or supported laterally with external tiebacks or internal bracing.

Secant piles cannot be immediately inspected first-hand, thus requiring indirect methods of sampling, testing and other quality control measurements during construction. These measures provide confidence that the secant piles were installed as intended and meet the design requirements. The secant piles can eventually be visually observed during the excavation of the shaft to confirm geometry and verify that there

are no voids or soil inclusions which might compromise the design. Secant piles were successfully used on the OCIT and ORT projects.

REFERENCES

Gamal, Mohamed. 2017. *Ohio River Tunnel Shafts Design*. Denver, Colorado. Prepared by Brierley Associates.

Louisville & Jefferson County Metropolitan Sewer District. 2017. *Ohio River Tunnel Contract Drawings*. Louisville, Kentucky. Prepared by Black & Veatch.

Steflik, Jonathan. 2017. *Ohio River Tunnel Geotechnical Baseline Report*. Louisville, Kentucky. Prepared by Black & Veatch.

COMPARISON OF 2D AND 3D ANCHOR ANALYSIS METHODOLOGIES

Murray Fredlund, SoilVision Systems Ltd., Saskatoon, SK, Canada
Gilson de F. N. Gitirana Jr., Universidade Federal de Goiás, Goiânia, GO, Brazil
Ruth McKeown, SoilVision Systems Ltd., Saskatoon, SK, Canada
HaiHua Lu, SoilVision Systems Ltd., Saskatoon, SK, Canada

ABSTRACT

The current design standards for the use of anchors in slopes is based on two-dimensional (2D) limit equilibrium analyses. Anchors are considered as discrete loads and the 2D anchor, factored based on the spacing distance, corresponds to extending anchors indefinitely in the third dimension. A three-dimensional (3D) analysis offers a more realistic representation of the problem, including the true discrete nature of the anchor point loads. This paper explores the typical differences between analyzing anchors in 2D and 3D, using four typical conceptual models. Slopes with constant cross sections were shown to be adequately represented by the traditional 2D approach. The maximum difference between 2D and 3D models was 21% and becomes negligible for lower anchor spacing values, as expected. A slope with an external load was analyzed to evaluate critical slip surfaces with lower aspect ratios. Slip surfaces with lower aspect ratios presented higher edge effects that contributed to the stability of the slope. The results indicate that optimum design requires the 3D evaluation of field conditions inducing low aspect ratios, such as concave and convex surfaces, weak layers, and external loads.

Keywords: anchor, limit equilibrium method, three-dimensional analysis

INTRODUCTION

Slopes may be stabilized using a variety of solutions, including anchors. When performing an analysis, geotechnical engineers often follow the traditional two-dimensional (2D), Limit Equilibrium Method (LEM). It is important to understand the consequences and limitations of the assumptions on which the 2D LEM is based. There are numerous studies on anchors that show the importance of considering the actual three-dimensional field conditions. Desai et al. (1986) proposed a three-dimensional procedure based on the Finite Element Method and considering elastoplastic behavior and interface elements, to account for stress and displacement distributions, the relative motion between the anchors and the soil mass, and nonlinear soil behavior. Several important stabilization mechanisms were explained. The role of grout injection was evaluated in terms of the produced normal stresses along the anchor-soil bounding surface. The approach was shown to reproduce adequately experimental tests on a sand, proving realistic stress distributions around the anchor. Nonlinear soil behavior influenced to a large extend relative interface motions. Michalowski (1989) applied an upper-bound limit analysis in 3D to slope stability analyses. Anchors were not specifically considered in this study, but the consideration of locally loaded conditions shed light on important modeling aspects. The manner how the slide mechanism becomes three-dimensional as the slope is locally loaded was demonstrated. This emphasizes the fact that anchors should produce field conditions that require 3D analysis approaches.

Briaud and Lim (1999) employed a 3D nonlinear (hyperbolic model) Finite Element analysis to evaluate design procedures for tieback walls. A combination of beam, spring, shell, and 3D elements were used to represent the several components of a soil-anchor systems. The construction method was reproduced,

© 2019 Deep Foundations Institute

including the excavation and anchor loading. The analysis of four case histories allowed several design recommendations regarding anchor position, spacing, unbounded length, among other variables. Anchors loads were shown to be the most importance design variable, affecting deflections and bending moments. Cai and Ugai (2003) discusses the limitations of the LEM in representing anchors in slope stability. The authors use an elastoplastic Finite Element analysis following the shear strength reduction technique, to evaluate anchors in three dimensions. Hypothetical scenarios were analyzed using the LEM (Bishop's simplified method) and the SSR approach, considering several anchor lengths, spacings, and orientations. The SSR was shown to represent the anchor-soil system in a more rigorous manner. However, the differences in Factor of Safety obtained using both methods were lower than 5%. Cai and Ugai (2000) also present the use of similar modeling approaches, for slopes reinforced with piles. Later, Yang et al. (2015) employed the shear strength reduction method to evaluate optimal anchor positioning. The author used a two-dimensional approach and did not evaluate 3D effects.

This brief background overview shows that there is significant evidence in the literature showing that three-dimensional approaches should be pursued when analyzing anchors. There are multiple methods of analysis, ranging from the standard Limit Equilibrium Methods of slices, to more advanced numerical analysis including elastoplastic analysis and the shear strength reduction method. There is some evidence indicating the LEM remains relevant as it provides reasonably accurate evaluations using relatively simple computations. There is, however, little evidence of what are the specific differences between applying the LEM in 2D and 3D. In this context, this paper presents the analysis of some slope scenarios that illustrate the differences between analyzing anchors in 2D and 3D. Simple and complex geometry conditions will be considered, along with various anchor placement conditions.

THEORY

Anchors may be represented in a 2D model as a single element, disregarding changes in the third dimension (Figure 1a). The implication is this modeling approach is that the applied 2D anchors correspond in 3D to plate elements, as shown in Figure 1b. The 2D approximation of anchor strength variables is based on the actual horizontal anchor spacing, as shown in Figure 2c. The tensile capacity of the tendons, the pullout resistance of the anchors, and the mobilized shear force are usually factored by the spacing between anchors and by reduction factors, as follows:

$$tr_d = \frac{tr}{wF_{tr}} \quad [1]$$

Where tr_d is the factored tendon resistance used in two-dimensional design (kN/m), tr is the tendon resistance (kN), w is the horizontal anchor spacing (m), and F_{tr} is a reduction factor.

$$pr_d = \frac{pr}{wF_{pr}} \quad [2]$$

Where pr_d is the factored pull-out resistance used in two-dimensional design (kN/m), pr is the resistance between the grout and the surrounding soils (kN), and F_{pr} is a reduction factor.

$$sr_d = \frac{sr}{wF_{sr}} \quad [3]$$

Where sr_d is the factored shear force used in two-dimensional design (kN/m), sr is the shear force (kN), and F_{sr} is a reduction factor. The minimum value between tr_d and pr_d determine the design quantity.

Rock masses may have anchors applied directly to the slope surface but may also be associated with shotcrete and other techniques. On the other hand, the use of anchors on slopes comprised of soil is generally accomplished by means of a tie-back wall. In this case, the anchor loads are applied to the wall and act on the slope surface as distributed loads and also along the anchor-soil bonding region. The actual shape of the load distribution on the soil surface depends on the ground movement and anchor positions. Within the scope of a LEM model, these distributed loads are reduced to point loads with a load position following the anchor placement and also distributed along the anchor length. The point load representing an anchor in a 2D model corresponds to a line load in 3D (Figure 1b). The actual anchor loading condition in the field may differ significantly from that of a line load when the anchor spacing is relatively large, compared to the size of the mobilized soil mass.

The application 3-D LEM analysis to anchor design requires the review of the effects of: i) anchor orientation, ii) anchor spacing, both lateral and vertical, and iii) the angle of the anchor. The effect of the third dimension introduces the point load nature of the supporting member. The introduction of the 3D effects and the primary differences affecting the critical 3D factor of safety (FOS) should also be reviewed. It is also important to understand the mechanisms producing differences between the FOS's. The primary differences for a 3D slope stability analysis (when compare to 2D) have been presented as resulting from i) the slip shape is more realistic, ii) the topology may vary in the 3rd dimension, iii) the geo-strata may vary, iv) the groundwater table may vary in the 3rd dimension, v) the pattern of slope supports may vary, and vi) the surface loading condition may vary spatially (Fredlund et al, 2017). Anchors have been likened to thin long plates when modelled in 2D. While in 3D, anchors are more representatively shown as point loads. So, we will take a staged approach in our proposed solution.

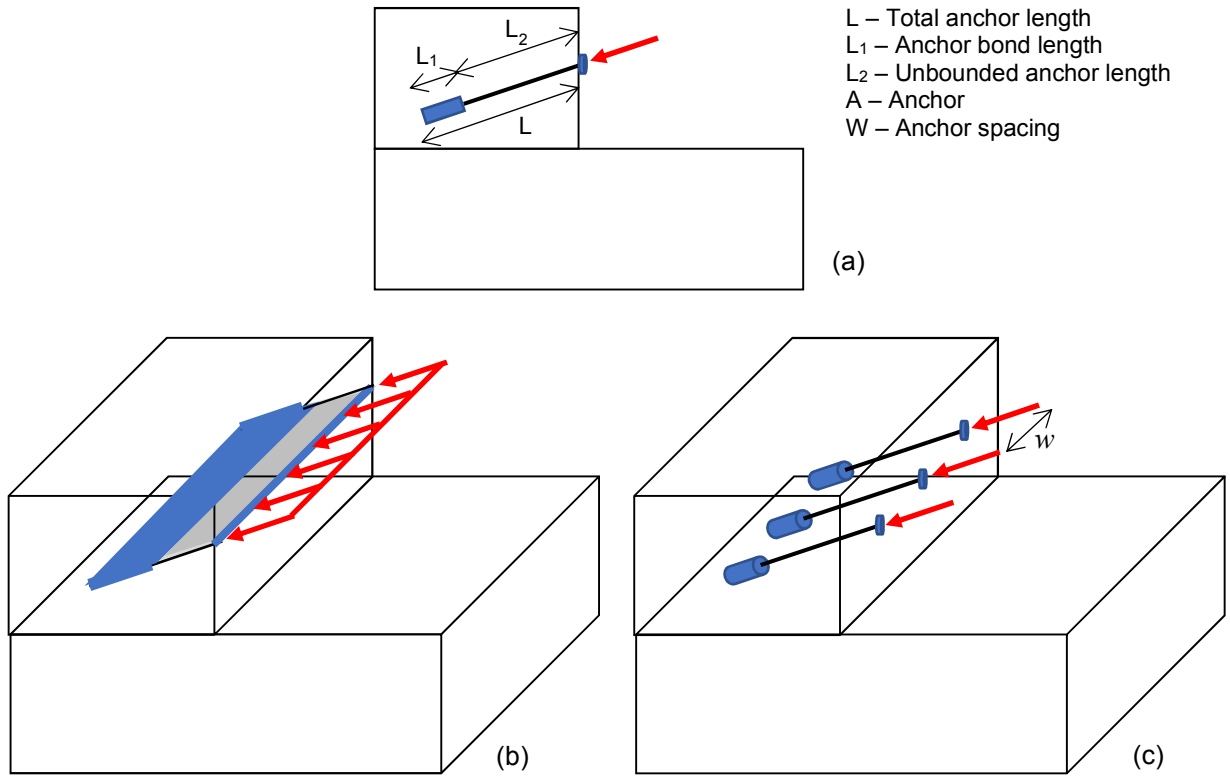


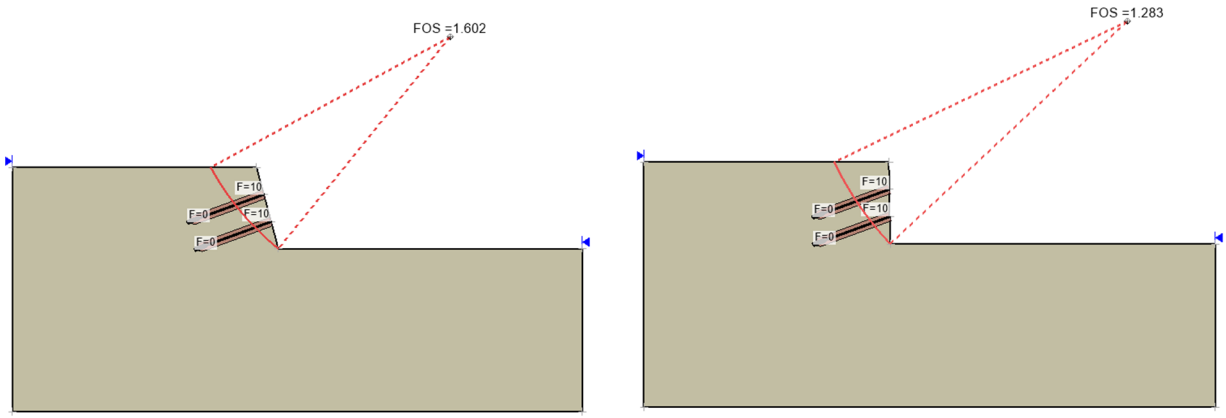
Fig. 1. A simple slope: (a) 2D representation; (b) equivalent 3D model; (c) actual 3D condtion.

EXAMPLE SCENARIOS

A number of example scenarios will be presented, with different geometries and stratigraphy conditions representing a wide range of typical field conditions. All analyses will be carried out with and without anchors and in 2D and 3D. Consistent spacing will be assumed between the actual 3D geometry and the 2D anchor spacing factors.

Example 1: a homogeneous slope

In the first example, two 5 m high slopes comprised of the same homogeneous material were considered, with surface slopes of 75 and 89°. The material was represented using the Mohr Coulomb shear strength envelope with undrained shear strength properties, presenting a cohesion of 15 kPa and a friction angle of 35°. The General Limit Equilibrium Method (Fredlund et al., 1981) was used in conjunction with the Cuckoo search method for locating the critical slip surface. Figure 2 shows the 2D representations of the reinforced slopes. Two anchor lines were placed, with the 5 m long tieback anchors placed 20 degrees down from the horizontal. The lateral spacing considered for anchor strength factoring was 2 m.



(a) (b)

Fig. 2. Cross-section of the reinforce homogeneous slopes: (a) 75o; (b) vertical.

The two 2D homogeneous slopes from Figure 2 were extruded to 3D models, as shown in Figure 3. The same material properties and calculation methods were used for the FOS and to search for the critical slip surface. In addition, the reinforcement parameters along with the tieback anchor angle and length were maintained from the 2D solutions, including now the actual anchor horizontal spacing of 2 m. The aspect ratio was searched for with a wide variety of values. For the 3D solutions, both models used multiple aspect ratios ranging from 1.0 – 5.0 in increments of 0.5; the ellipsoid curvature was kept constant at two. This was done to help minimize differences between the 3D models, so that the effect of the accurate representation of the point loads could be better isolated.

Table 1 summarizes the results of the 2D and 3D analyzes and the associated critical FOSs for the un-reinforced and reinforced slopes shown in Figures 2 and 3. The singular difference between the unsupported and reinforced models is the grouted tieback anchors, so it is reasonable to assume that the difference in the factor of safety is attributed to those anchors. Based on the 2D analysis, the critical FOS increased with the addition of the anchors by 15% for the 75° slope and by 7.2% for the 89° slope. The assessment of the effectiveness of the anchors was somewhat different considering the 3D analyses; the critical FOS increased

with the addition of the anchors by 9.8% for the 75º slope and by 21% for the 89º slope. The decreased in the assessed effect for the 75º slope may be attributed to the relatively shallow critical slip surface obtained for that condition. The 89º slope, on the other hand, presented significantly higher 3D effects, produced by the edges of the 3D slip surface. This behavior is typical of slip surfaces with relatively low aspect ratios. The differences between 2D and 3D design are summarized in the last column of Table 1. The relative differences between 2D and 3D FOS's ranges from 7.9 to 21.3%. This wide range is due to the varying degrees of 3D effects found in each case scenario. These results were based upon a very simplistic scenario with a single homogeneous material with no external loads and a consistent reinforcement pattern with only one support type. More complex conditions may produce different 3D effects.

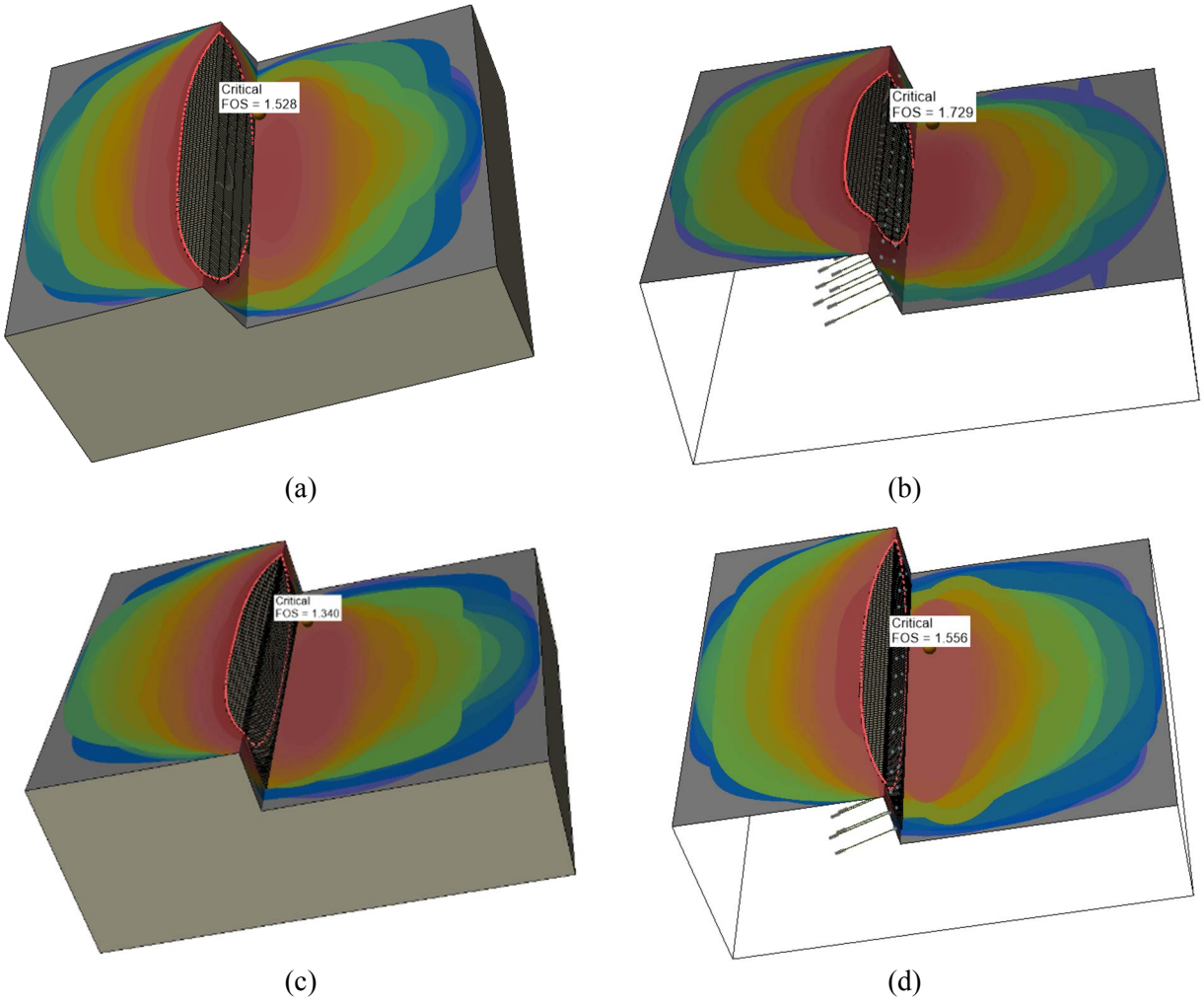


Fig. 3. Three-dimensional model for the homogeneous slopes: (a) 75º, base case; (b) 75º, reinforced slope; a) 89º, base case; (b) 89º, reinforced slope.

Table 1. Critical FOS for homogeneous unsupported and reinforced slopes in 2D and 3D.

Slope	2D Solution	3D Solution	Variation from 2D to 3D
Unsupported, 75º	1.414	1.528	8.1%
Reinforced, 75º	1.602	1.729	7.9%
Variation from	13.2%	13.1%	

unsupported to reinforced			
Unsupported, 89°	1.196	1.340	12.0%
Reinforced, 89°	1.283	1.556	21.3%
Variation from unsupported to reinforced	7.2%	16.1%	

Example 2: a complex stratified slope

The next example is a complex stratified slope. The Mohr Coulomb shear strength envelope was used for all materials. Two distributed loads of 360 lbf/ft^2 are placed along the top of the embankment to represent loads of vehicles on a highway. A water table is present, represented by a piezometric line. The GLE method and the Cuckoo Search were used for compute the FOS for the critical slip surface. Figure 4 shows the 2D solutions for the unsupported and supported scenarios. This complex slope was reinforced with 5 rows of end anchors and 3 rows of micropiles, as seen in Figure 4(b). The 120 ft long end anchors are placed at an angle of approximately 19 degrees from the horizontal. Micropiles are spaced 10 ft laterally with a row placed at the base of the embankment, another row 23 ft away, and a final row 90 ft away from the base of the embankment.

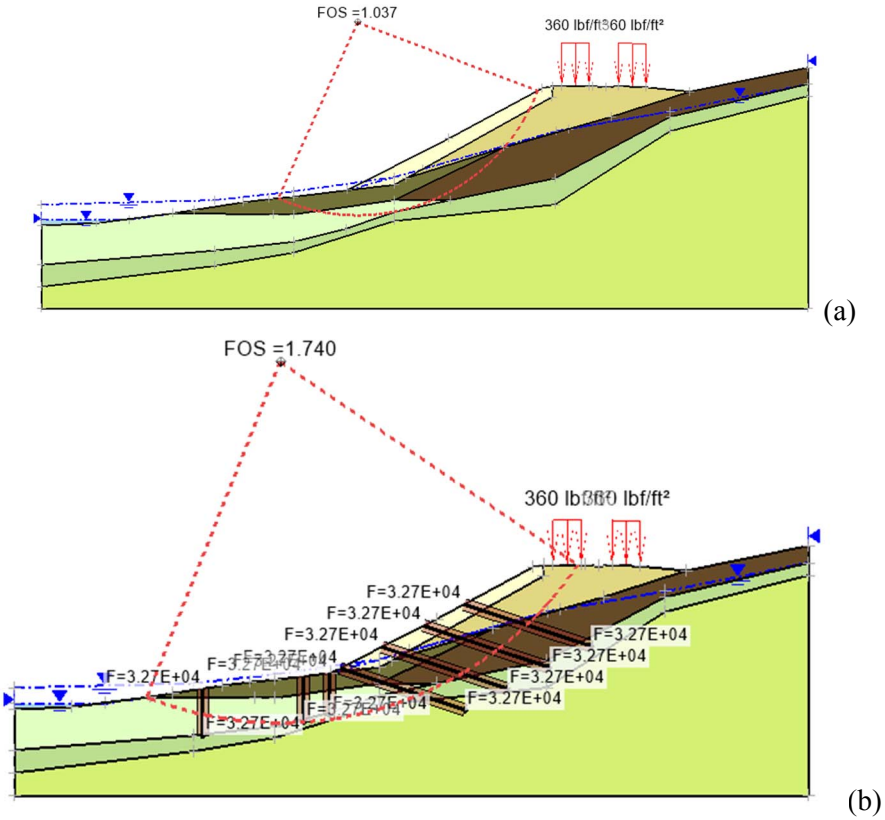


Fig. 4. Cross section of the complex slope:(a) base case; (b) reinforced slope.

The cross sections were extruded to assess the effect of the third dimension on the critical FOS for both the un-reinforced and reinforced slopes. The distributed loads along the top of the embankment were maintained as per the 2D complex model solution. Calculation methods and search methods were kept consistent to the 2D complex models as were the characteristics of anchors and micropiles. For both of the 3D complex slope solutions, multiple aspect ratios were used ranging from 0.5 – 6.0 in increments of 1.1

and the ellipsoid y-curvature was kept constant at two.

Figure 5 and Table 2 summarize the results obtained. Following the same reasoning provided in the simple homogeneous slope case, here too, gains in critical 3D FOS may be attributed to be a result of accounting for the effect of the point loads in the 3rd dimension. For the unsupported slope, the critical FOS increased by 4.6%, which could be attributed to the 3D ellipsoidal slip shape. The critical FOS for the 3D complex reinforced slope is 1.849 when compared to the critical FOS for the 2D solution of 1.740. This increase represents nearly a 6.2% increase. The effect of the 3rd dimension resulted in increases in the critical FOS of all examples shown. Regardless of whether the slope was stratified or not. When supports were accurately represented as point loads, the 3D FOS showed an even more marked increase compared to the 3D solutions where no reinforcement was included. From this, we could assume that accurately representing supports as point loads in 3D can have a significant effect on the critical 3D FOS for the supported solution.

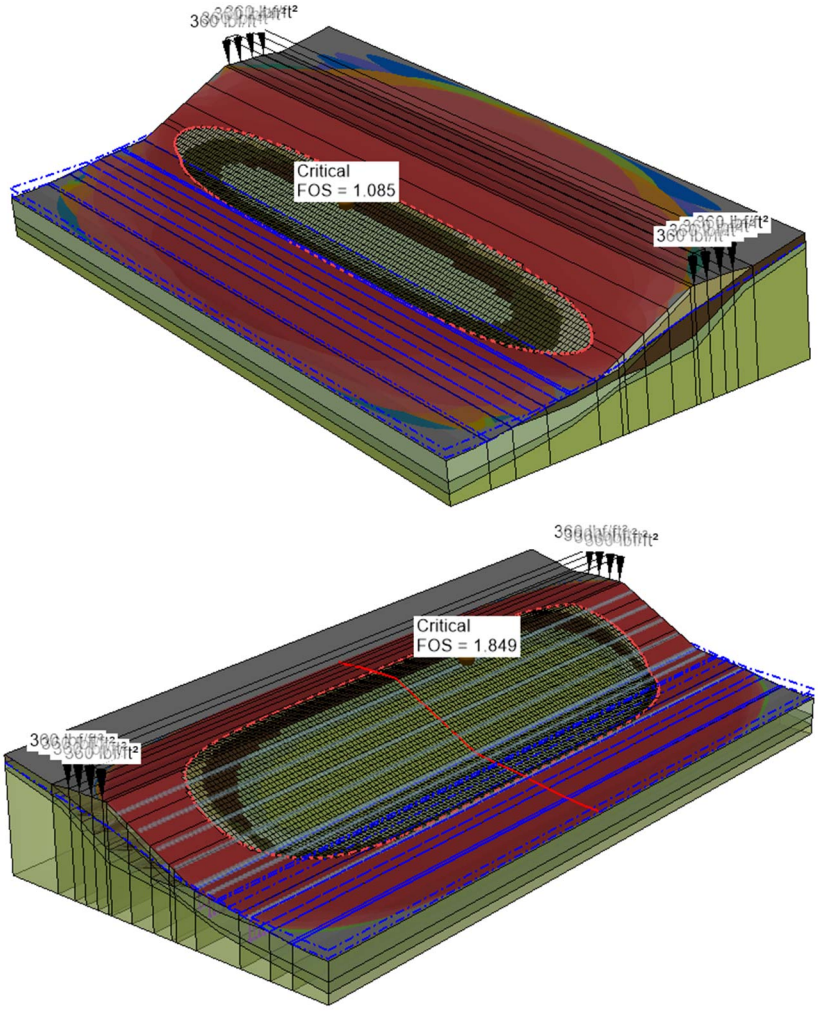


Fig. 5. Three-dimensional model for the complex slope:(a) base case; (b) reinforced slope.

Table 2. Critical FOS for complex unsupported and reinforced slopes in 2D and 3D.

Slope Description	2D Solution	3D Solution	Variation from 2D to 3D
Unsupported	1.037	1.085	4.6%
Reinforced	1.740	1.849	6.2%
Variation from unsupported to reinforced	68%	70%	

CONCLUSIONS

Two slopes, one homogeneous & one stratified were reviewed and critical FOSs were assessed for both 2D and 3D solutions. Each of these slopes was then reinforced in some manner to assess the effect of the 3rd dimension, and the effect of representing supports as point loads on the critical 3D FOS. From our investigation we observed:

- The critical 3D FOS was consistently higher than the critical 2D FOS regardless of stratigraphy, whether the slope was reinforced or not, and reinforcement type.
- Unreinforced slopes showed small increases in the critical FOS when moving from the 2D to 3D solution in the 1 – 2% range, and could be associated with the effect of the slip shape moving from circular to ellipsoidal.
- Reinforced slopes showed significant increases to the critical FOS when moving from the 2D to 3D solution, regardless of stratigraphy, and support type and with the critical 3D FOS ranging from 8 – 21% higher.
- The inclusion of 3D point loads to represent the various supports resulted in an increase in the calculated critical FOSs for the presented solutions ranging from 4.6-6.2%.

This paper has presented a step by step approach showing how the representation of anchors as thin plates in 2D, to point loads in 3D affects the resulting critical FOS. The effect on the critical 3D FOS, that could reasonably be attributed to the accurate representation of the supports as point loads, could be significant, and will vary with each project. This paper also presents a methodology of quantifying the effect of the supports on the critical FOS in both 2D and 3D analyses.

REFERENCES

Briaud, J.L. and Lim, Y., 1999. Tieback walls in sands: numerical simulations and design implications. ASCE Journal of Geotechnical and Geoenvironmental Engineering, 125(2) 101-110.

Cai, F. and Ugai, K., 2000. Numerical analysis of the stability of a slope reinforced with piles. Soils and Foundations, 40(1) 73-84.

Cai, F. and Ugai, K., 2003. Reinforcing mechanisms of anchors in slopes: a numerical comparison of results of LEM and FEM. International Journal for Numerical and Analytical Methods in Geomechanics, 27(7) 549-564.

Desai, S.S., Muqtadir, A., and Scheele, F., 1986. Interaction analysis of anchor-soil systems. ASCE Journal of Geotechnical Engineering, 112(5) 537-553.

Fredlund, M., Fredlund, D.G., and Zhang, L., 2017. Moving from 2D to a 3D Unsaturated Slope Stability

Analysis. 2nd PanAmerican Conference on Unsaturated Soil, 2017, Dallas, Texas. Proceedings of the 2nd PanAmerican Conference on Unsaturated Soils, 2017.

Fredlund. G., Krahn, J., and Pufahl, D.E., 1981. The relationship between limit equilibrium slope stability methods. Proceedings of the Tenth International Conference on Soil Mechanics and Foundation Engineering, Stockholm.

Michalowski R.L. 1986. Three-dimensional analysis of locally loaded slopes. Géotechnique, 39(1) 27-38.

Yang, G., Zhong, Z., Zhang, Y., and Fu, X., 2015. Optimal design of anchor cables for slope reinforcement based on stress and displacement fields. Journal of Rock Mechanics and Geotechnical Engineering, 7(4) 411-420.

DESIGN AND CONSTRUCTION BENEFITS OF PERFORMING A BI-DIRECTIONAL TEST ON A DRILLED SHAFT IN SAND, GRAVEL, AND COBBLE DEPOSITS

Van E. Komurka, P.E., D.GE, F.ASCE, GRL Engineers, Inc., Cleveland, Ohio, USA, 216.831.6131, vkomurka@grlengineers.com
Marco Fellin, P.E., Tetra Tech, Inc., Missoula, Montana, USA, 406.543.3045, marco.fellin@tetratech.com

ABSTRACT

Significant cost and construction benefits were obtained from performing a bi-directional static load test prior to construction on the Russell Street Bridge Replacement project in Missoula, Montana. The project utilized 24 drilled shafts to support two three-span bridges across the Clark Fork River. A bi-directional static load test ("BDSLT") was performed on a large-diameter production shaft to demonstrate construction methods and confirm design assumptions. Subsurface conditions consisted of gravel with sand to a depth of 20 feet (6.1 m), underlain by gravel with sand, silt, cobbles, and occasional boulders. The test shaft had a nominal diameter of 5.9 feet (1.8 m), and an embedded length of 75.5 feet (23.0 m). The geotechnical engineer of record and the BDSLT test engineer collaborated to optimize the BDSLT jack assembly location within the test shaft, determine appropriate instrumentation locations, and plan the test protocol. The maximum applied test load was 10,707 kips (47.6 kN). Significant benefits were obtained from performing the BDSLT test, including 1) reducing each production shaft's length by using a higher LRFD resistance factor allowed by having performed the testing, 2) using test-determined unit shaft resistances to evaluate and accept two production shafts that may have otherwise required remediation, and 3) providing the Montana Department of Transportation (and other designers) with increased presumptive unit resistance values in the gravel/cobble/boulder deposits.

PROJECT DESCRIPTION

The project was constructed in Missoula, Montana for the Montana Department of Transportation ("MDT"). The original bridge was approximately 60 years old, and consisted of a two-lane, 420-foot-long (128-m), four-span, riveted steel plate girder design spanning the Clark Fork River. The bridge was due for replacement owing to its deteriorated state, and the need for increased traffic volume capability afforded by a four-lane structure. HDR was the structural engineer. The preferred bridge alternate was a 459-foot-long (140-m), three-span, welded steel plate girder design. The new bridge was designed to meet current standards in accordance with MDT bridge design and AASHTO LRFD criteria. The new bridge was constructed in phases to keep traffic open during construction.

Based on early design type-size-location meetings, drilled shafts were the preferred foundation type for both abutments and the river piers, primarily due to environmental concerns related to the endangered bull trout population. Tetra Tech, Inc. of Missoula, Montana was the geotechnical engineer of record. Geotechnically, drilled shafts were the preferred foundation type due to the ability to advance through the anticipated cobbles and boulders.

The specific design methodologies used for the bridge foundation design were 1) LRFD Bridge Design Specifications (AASHTO, 2012), 2) Guide Specifications for LRFD Seismic Bridge Design (AASHTO, 2011), 3) the FHWA's drilled shaft design manual (FHWA, 2010), and 4) a Utah Department of Transportation ("UDOT") publication (Rollins, 1997). Hydraulic information provided by HDR indicates that the 100-year flood level would cause up to 15.0 feet (4.57 m) of pier scour, and no contraction scour.

Drilled shaft axial nominal resistances were calculated using the computer program SHAFT 6.0 (Ensoft, 2007). The SHAFT 6.0 program contains a gravel layer nominal resistance estimate based on the results of a UDOT study (Rollins, 2007). The analysis assumes that the gravel layer has greater than 50 percent

© 2019 Deep Foundations Institute

gravel content (which is the case for this project). The UDOT study proved through static tension load testing that soils with greater than 50 percent gravel content have a nominal resistance on the order of 170 to 300 percent greater than predicted by the FHWA 'sand' equation (Brown, et al., 2010). The gravel layer formula used by SHAFT 6.0 typically produces the same 170 to 300 percent increase over the FHWA formula, while still accounting for the load testing data scatter.

The project was designed to include a large number of drilled shafts ranging in diameter from 4 to 6 feet (1.2 to 1.8 m). Based on potential overall cost savings, as well as on obtaining valuable soil behavior information, a bi-directional static load test was specified to be performed during construction on the first production shaft. This allowed for the use of an increased geotechnical resistance factor for design, reducing required shaft lengths based on axial demands. Based on the LRFD design manual (AASHTO, 2012), and discussions and concurrence with the MDT Geotechnical Section, the LRFD resistance factor associated with performing a BDSLT was 0.70. The resulting design totaled 26 drilled shafts: eight 5.9-foot-diameter (1.8-m) river shafts (each with an embedded length of 65 feet (20 m), and 18 4.0- to 4.5-foot-diameter (1.2- to 1.4-m) abutment shafts (ranging in embedded length from 30 to 35 feet (9.1 to 11 m)). Construction on the test drilled shaft and northbound bridge started in March 2018, and the southbound drilled shafts are scheduled to be completed Spring 2020. Total construction cost is estimated to be $29M.

SUBSURFACE CONDITIONS

Four borings were drilled (one at each of the four bridge bent locations) during the geotechnical investigation, to depths on the order of 110 to 120 feet. In addition, samples were collected at 10-foot intervals during test shaft construction, and bulk samples were tested in the laboratory. In general, native poorly to well-graded gravel with sand, frequent cobbles, and occasional boulders were encountered during the geotechnical investigation and in the test shaft excavation. Occasional sand seams/layers, and gravel with higher percentages of sand, were encountered at all five explored locations. Native soils were predominantly subrounded to subangular quartzite, with a minor amount of argillite intermixed.

Subsurface Profile Used for Design

Figure 1 presents a generalized subsurface profile at the test shaft location based on conditions encountered in Boring BH-2 (located approximately 85 feet (26 m) from the test shaft), the estimated soil properties used for design, and for selecting the jack assembly location within the test shaft.

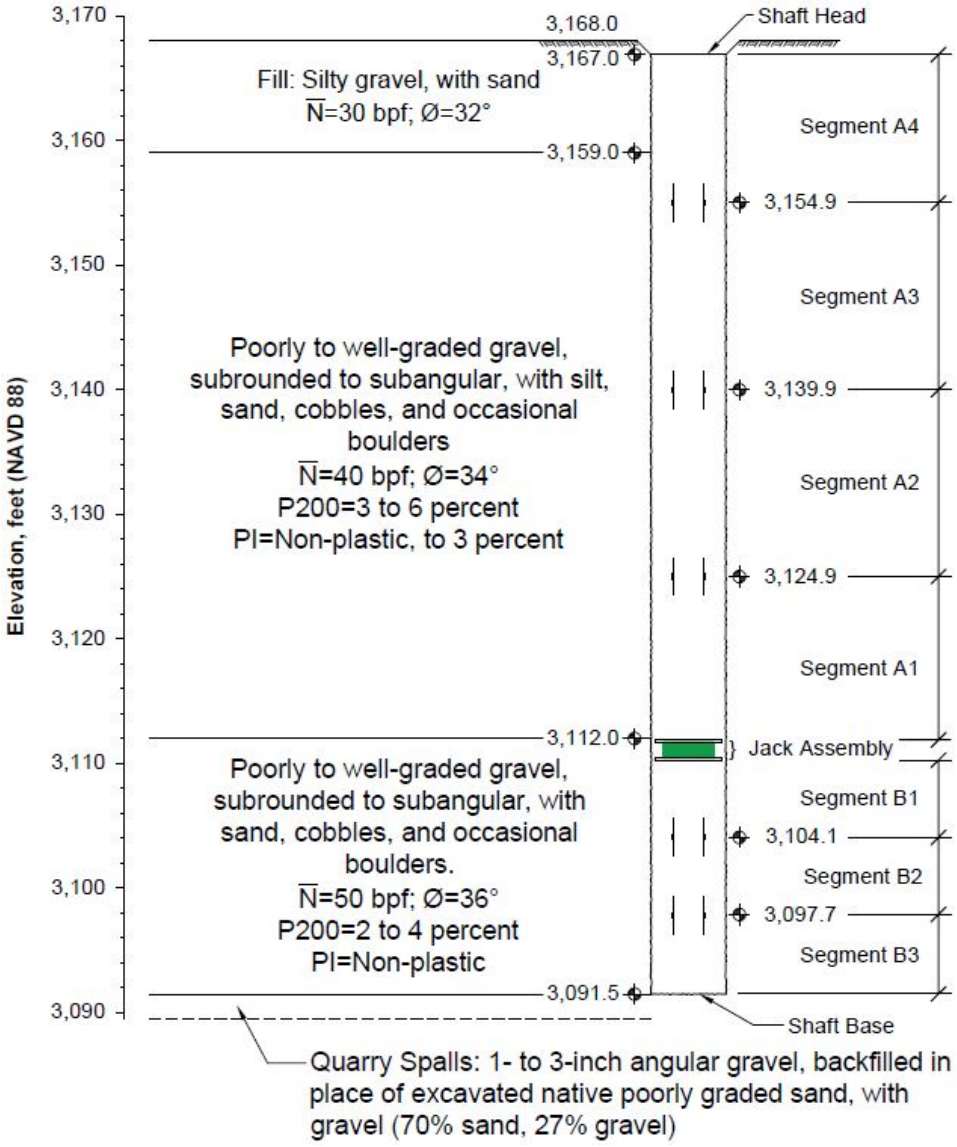
Subsurface Profile Encountered in Test Shaft Excavation

Table 1 presents laboratory testing results from test shaft excavation samples, which are similar to laboratory testing results from the geotechnical investigation. The table includes quarry spalls, which were placed in a zone two feet below the planned drilled shaft base to inhibit base softening following drilling.

TEST SHAFT DESIGN AND CONSTRUCTION

Design

Prior to the test, in an effort to optimize data obtained from the BDSLT, the jack assembly location (i.e., elevation) within the test shaft, and the minimum required test load and jack assembly capacity, were jointly decided upon. The jack assembly lower bearing plate was re-located to approximately 19 feet (5.8 m) above the shaft base (Fig. 1). Jack assembly capacity was increased to 6,600 kips (29,360 kN) with the use of three 2,200-kip (9,786 kN) **GRL-Cells** (Fig. 2), resulting in a maximum potential test load of 13,200 kips (58,716 kN) (6,600 kips (29,360 kN) upward, plus 6,600 kips (29,360 kN) downward). Instrumentation



"bpf" = blows per foot. 1 foot = 0.3048 m.

Fig. 1. Generalized subsurface and test drilled shaft profile.

included determination of jack assembly upper and lower bearing plate displacement, digital levels to monitor head displacement, base telltales, and five strain gage levels (Fig. 1).

Before the test, the estimated geotechnical nominal resistance above the jack assembly was approximately 125 percent of the geotechnical nominal resistance below the jack assembly: approximately 2,700 kips (12,010 kN) shaft resistance above the jack assembly, and 980 kips (4,360 kN) of shaft resistance and 1,180 kips (5,249 kN) of base resistance below the jack assembly, for a total estimated nominal resistance of 4,860 kips (21,620 kN). The jack assembly location was selected based on the assumption that as the base experienced displacement during the test, it would exhibit greater nominal resistance than estimated. The additional jack assembly capacity was intended to increase the likelihood of mobilizing all the resistance either above or below the jack assembly.

Table 1. Shaft Excavation Samples Laboratory Testing Results Summary

Depth, feet	Elevation, feet[A]	AASHTO Classification	ASTM Classification	P200[B]	Plasticity Index, PI
0-8	0-3,159	A-1	Fill: Poorly-Graded Gravel, with Sand	Not Tested	Not Tested
8-30	3,159-3,137	A-1	Well-Graded Gravel, with Sand	3	NP
30-40	3,137-3,127	A-1	Poorly Graded Gravel, with Silt and Sand	6	3
40-50	3,127-3,117	A-1	Well-Graded Gravel, with Sand	3	NP
50-60	3,117-3,107	A-1	Well-Graded Gravel, with Silt and Sand	4	NP
60-70	3,107-3,097	A-1	Poorly Graded Gravel, with Sand	4	NP
70-72	3,097-3,095	A-1	Poorly Graded Gravel, with Sand	2	NP
72-74	3,095-3,093	A-1	Well-Graded Gravel, with Sand	2	NP
74-75.5	3,093-3,091.5	A-1	Poorly-Graded Gravel, with Sand	3	NP
75.5-77.5	3,091.5-3,089.5	A-2	Poorly-Graded Sand, with Gravel	3	NP
75.5-77.5[C]	3,091.5-3,089.5	Quarry Spalls: 1- to 3-inch Gravel		0	NP

Notes:

A. NAVD 88.

B. "P200" denotes the percent (by weight) of material passing the #200 sieve size.

C. Native material was excavated, and quarry spalls were backfilled and compacted with 'flat-pan' on end of Kelly bar prior to reinforcing cage placement.

Construction

The test shaft was constructed in a production shaft location beneath a retaining wall. The retaining walls were founded on smaller-diameter drilled shafts than the river piers. To replicate river-shaft dimensions, the test shaft was constructed with the same diameter as the river shafts. However, to accommodate connection to the retaining wall it supported, the test shaft's reinforcing cage diameter was typical of a 4.5-foot-diameter (1.37-m) drilled shaft used to support the wall.

The project was awarded to Dick Anderson Construction of Missoula, Montana in February 2018, who subcontracted drilled shaft excavation to Inland Foundation Specialties of Boise, Idaho. GRL Engineers, Inc. of Cleveland, Ohio was contracted to perform the bi-directional static load test. The test shaft was the first production shaft constructed, was 70.9 inches (1,800 mm) in diameter, with and embedded length of 75.5 feet (23.0 m). Test shaft excavation was accomplished using a Casagrande B300SP drill rig with auger and cleanout bucket. Temporary casing was installed full-depth using a CMV casing oscillator connected to the drill rig. Fig. 3 illustrates typical drilling spoil.



Fig. 2. Jack assembly, showing upper and lower bearing plates, and three 2,200-kip GRL-Cells



Fig. 3. Typical subrounded to subangular poorly graded gravel, with sand, cobbles, and boulders (from 40 feet)

BI-DIRECTIONAL STATIC LOAD TEST RESULTS

The bi-directional static load test was performed on June 6th, 2018. Fifty-four test load increments of approximately 200 kips (890 kN) each were applied, with each load increment held for ten minutes, resulting in a maximum test load of 10,707 kips (47,627 kN). 200-kip (890-kN) test load increments were selected to provide a reasonable number of load increments based on the pre-test estimate of total nominal resistance. The large number of test load increments resulted from the mobilized nominal resistance exceeding pre-test estimates.

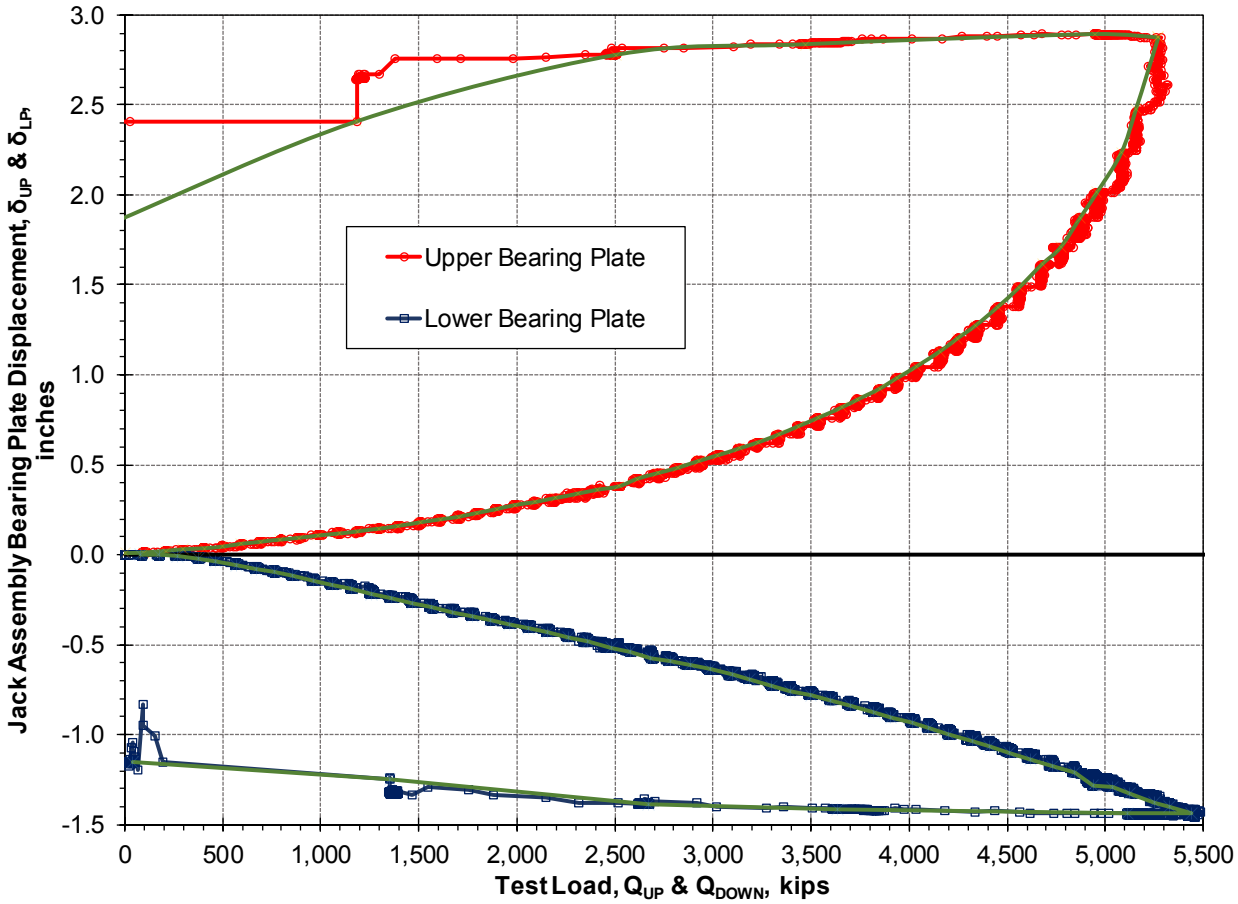
Bearing Plate Displacement

Upper and lower jack assembly bearing plate displacement as a function of test load is presented in Fig. 4. A review of Fig. 4 indicates that the test was limited by geotechnical "ascending" failure of the foundation portion above the jack assembly at an approximate upward test load of 5,270 kips (23,440 kN). Accordingly, shaft resistance was likely fully (or nearly fully) mobilized above the jack assembly, and likely not fully mobilized below the jack assembly.

Internal Force Profiles

Internal forces were known at three other locations in the test shaft: at the head (zero), and at the upper and lower bearing plates (upward and downward test loads, respectively). At each strain gage level, average measured strains were converted to internal force. Internal force at the base (equal to total base resistance, Q_{BASE}) was estimated by assuming that the lowest foundation segment (Segment B-3, Fig. 1) experiences the same average unit shaft resistance as the segment above it (Segment B-2, Fig. 1). The calculated internal force profiles are presented in Fig. 5. For clarity, results from every other load increment are plotted.

The average unit shaft resistance versus segmental midpoint displacement was calculated for each foundation segment. For each applied test load increment, the internal force profiles were used to calculate the average unit shaft resistance, t, for each segment by dividing the difference in boundary forces by the foundation segment's shaft surface area. Head displacement was measured using digital levels. Base displacement, z_{BASE}, was determined using base telltales. Segmental elastic compression was calculated using strain data. Segmental displacements, z, were calculated by summing elastic compression downward



1 inch = 25.4 mm; 1 kip = 4.448 kN

Fig. 4. Jack assembly upper and lower bearing plate displacement

from the head above the jack assembly, and upward from the base below the jack assembly. Unit base resistance, q_{BASE}, was calculated by dividing total base resistance by the base area.

The relationship between shaft displacement and unit shaft resistance is presented in Fig. 6. The relationship between base displacement and base resistance is presented in Fig. 7. The corresponding equivalent top-loading ("ETL") curves generated from the *t-z* and Q-z_{BASE} relationships, with differentiated shaft and base loads, are presented in Fig. 8.

A review of Fig. 1 indicates that for analysis, Segment A1's lower bound was established at the top of the jack assembly upper bearing plate. Establishing Segment A1's lower bound at the top of the jack assembly lower bearing plate decreases Segment A1's unit shaft resistance values presented in Fig. 6 by 10.5 percent.

BENEFITS OF BI-DIRECTIONAL STATIC LOAD TESTING

Increased Resistance Factor

As discussed previously, per LRFD design methodologies, a higher resistance factor can be used if top-loading or bi-directional static load testing is performed. Without static load testing, the LRFD resistance factors for drilled shafts in sand are 0.55 and 0.50 for shaft and base resistance, respectively. Because a BDSLT was performed, a resistance factor of 0.70 was used for this project.

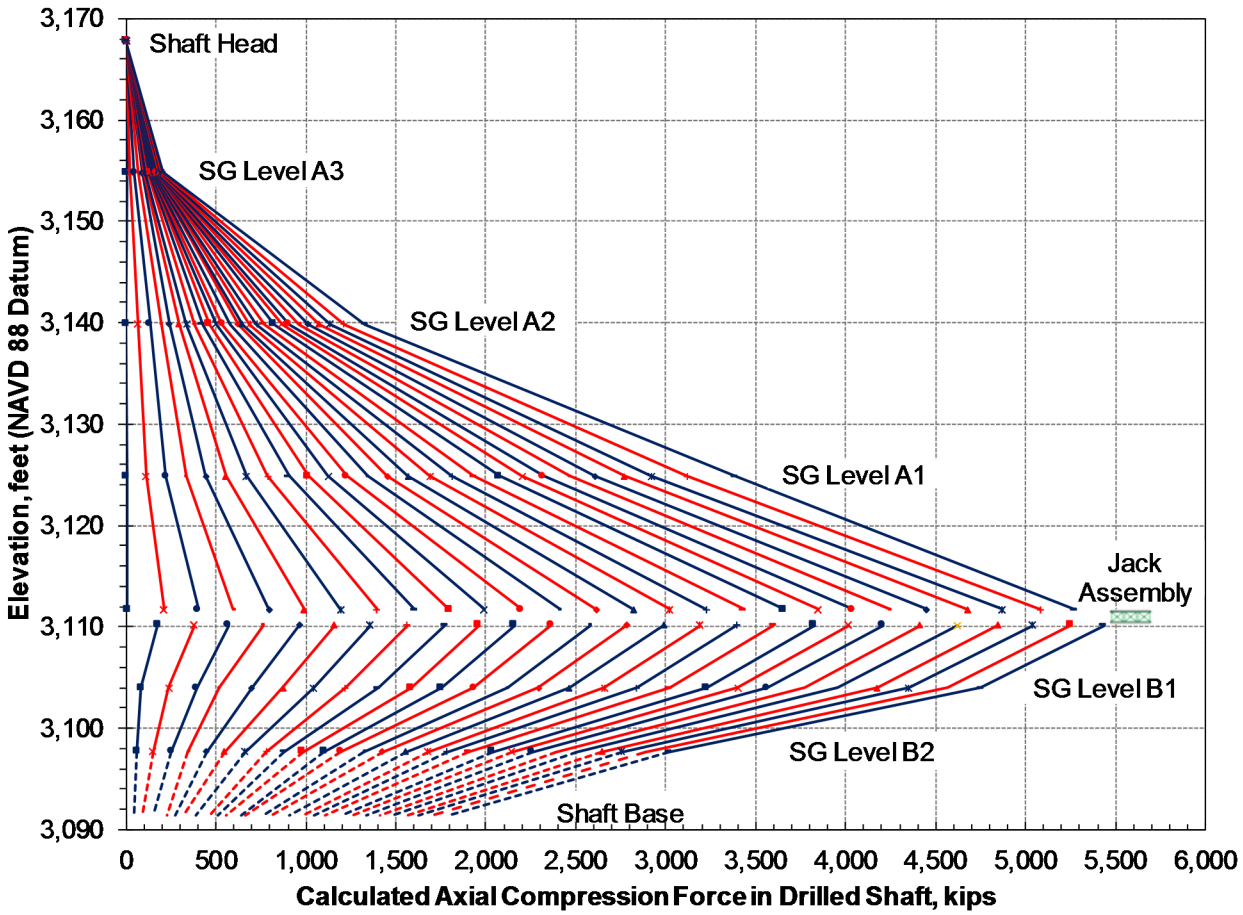


Fig. 5. Calculated Axial Internal Compression Force Profiles

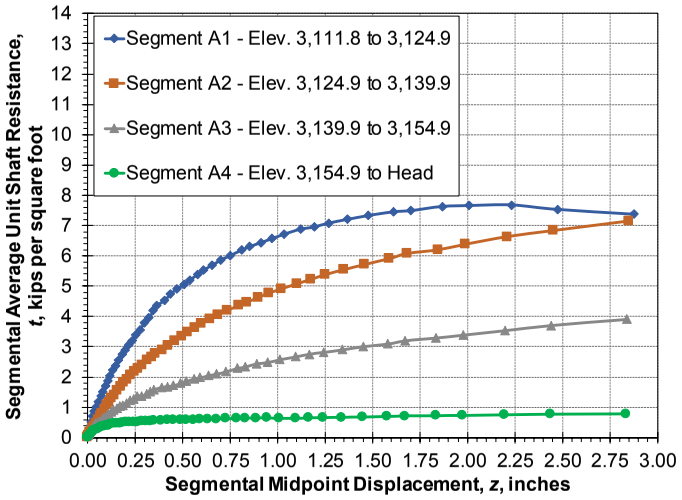
Foundation Displacement-Resistance Relationships – t-z, Q_{BASE}-z_{BASE}, q_{BASE}-z_{BASE}, and ETL Curves

The factored design load for each of the eight river piers was 2,370 kips (10,540 kN). Applying resistance factors of 0.55/0.50, the required embedment length for each 5.9-foot-diameter (1.8-m) drilled shaft was 66 feet (20 m) below bottom-of-scour elevation (81 feet (25 m) below river bottom to account for 15 feet (4.6 m) of scour). Applying a BDSLT-justified resistance factor of 0.70, required embedment lengths were reduced to 50 feet (15 m) below bottom-of-scour elevation, a length savings of 16 feet (4.9 m) per shaft. This resulted in a total savings of 128 feet (39.0 m) of constructed drilled shaft length. Applying a total BDSLT program cost of $172,500 to a reduction of $197,760 in drilled shaft construction cost results in a net savings of $25,260. The drilled shaft contractor estimates that the reduced shaft lengths saved a total of four days of construction schedule.

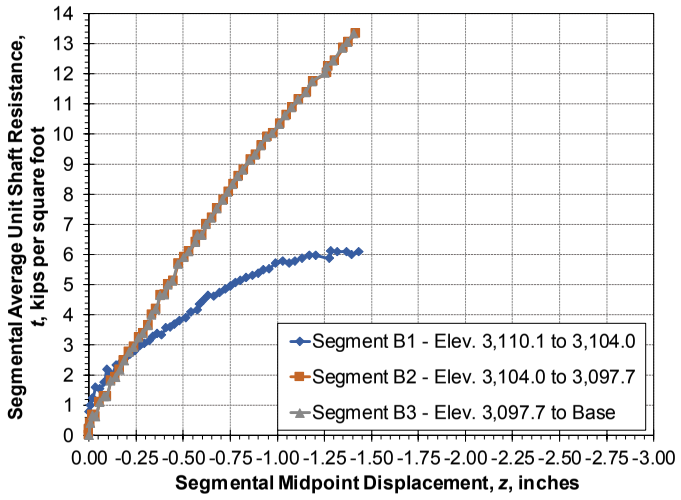
Minimum required embedment lengths to satisfy lateral resistance requirements precluded taking advantage of BDSLT results to additionally shorten the river shafts. For the 18 smaller-diameter abutment and retaining wall shafts, the minimum required embedment length to satisfy lateral resistance requirements controlled design compared to using resistance factors of 0.55/0.50 or 0.70 for resistance to axial demands.

Precluded Remediation

Crosshole sonic logging ("CSL") testing was performed on each of the northbound structure's four river shafts. Construction had not commenced on the southbound structure's four river shafts at the time of this writing; they will also receive CSL testing. CSL testing is performed on almost all large-diameter drilled



(a)



(b)

Fig. 6. Segmental Average Unit Shaft Resistance vs. Segmental Midpoint Displacement, *t-z* Curves (a) Above Jack Assembly; (b) Below Jack Assembly

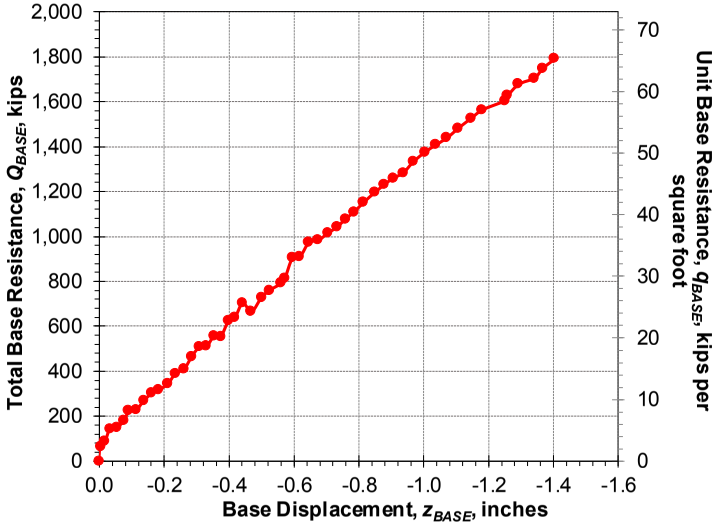


Fig. 7. Base Resistance vs. Base Displacement, Q-z_{BASE} and q-z_{BASE} Curve

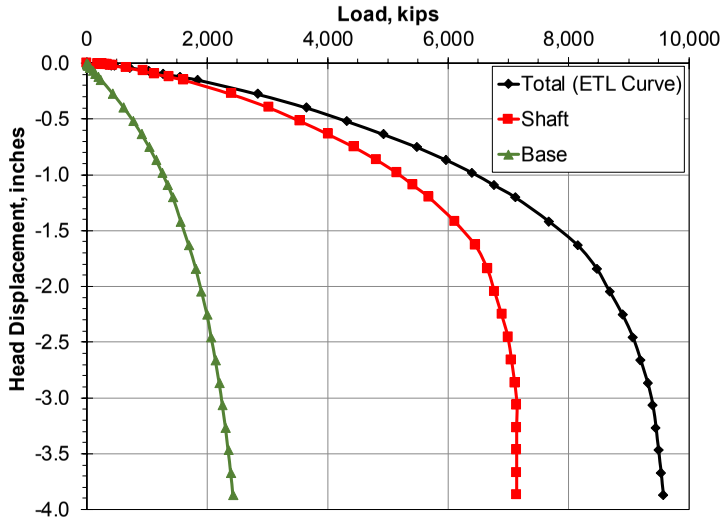


Fig. 8. Equivalent Top-Loading Curve

shafts on MDT projects to evaluate the structural integrity of the shaft concrete. When anomalies are detected, the anomalies are evaluated, and a determination is made as to whether or not the anomaly could affect long-term drilled shaft performance. If the anomaly is determined to be detrimental to shaft performance, the typical procedure is to core the shaft to better-characterize the anomaly. Once coring is performed and the cores and field data are evaluated, a course for remediation is determined. Remediation could include drilling a second core hole and grouting voids within the shaft, grouting or pressure-grouting poor soil zones at the bottom of the shaft through the CSL tubes, or constructing a new adjacent drilled shaft or shafts.

CSL results from the northbound structure's four river shafts indicated varying degrees of anomalies at the base of three shafts, characterized as the potential for weak or soft concrete. Following receipt of the CSL results from the first shaft with an indicated anomaly, the extent of the possible anomaly and its potential impact on the shaft's available base resistance to support design loads was evaluated. Since the apparent anomaly was at the base, it was decided as a first step to review the bi-directional static load test data to determine if shaft resistance alone (ignoring any base resistance) was sufficient to support design loads.

Based on the equivalent top-loading determinations (Fig. 8), the ultimate shaft resistance indicated by the bi-directional static load test was estimated. If base resistance is ignored, the shaft load curve in Fig. 8 can be taken as the equivalent top-loading curve. A number of approaches were used to estimate the ultimate shaft resistance based on BDSLT results, including the modified Davisson formula (slope-tangent) (Kulhawy and Hirany, 2009), the L2 method (Kulhawy and Hirany, 2009), and the FHWA 5% failure criteria (Brown et al., 2010).

The evaluation determined that the subject shaft (the first shaft for which CSL testing results indicated a potential anomaly) had sufficient factored shaft resistance alone to support the design load of 2,370 kips (10,542 kN), ignoring any contribution from base resistance. Similar analyses performed for the two subsequent river shafts for which CSL testing results indicated a potential anomaly also determined that factored shaft resistance alone was sufficient to support the design loads.

As discussed, drilled shafts that contain anomalies are usually remediated by the MDT, particularly when the anomaly is in the bottom several feet of the shaft where crucial base resistance is developed. For this project, base resistance was counted on in the original design. The remediation strategies can be time-consuming, and depending on the extent of coring and/or grouting, it can sometimes take several weeks or more to develop and approve a plan, and perform the remediation. Because a bi-directional static load test was performed at the beginning of this project, data were available to re-evaluate drilled shaft resistances and avoid having to potentially core and/or grout up to three large-diameter drilled shafts, which could have taken three to four weeks or more of project schedule to complete.

Geotechnical Unit Resistances Comparison

A comparison of unit resistance values was performed among 1) historical (published) results from two other bi-directional static load tests performed on drilled shafts with similar diameters and embedded lengths, subsurface conditions, and construction methods: one in Redding, California (Sorensen, 2010), and one in Thompson Falls, Montana (Murfitt, 2015), 2) values predicted for the gravel deposits by SHAFT 6.0 (used for design of the Russell Street Bridge), and 3) the results of the BDSLT performed for this project.

The SHAFT 6.0 model predicts nominal resistances. To compare similar results, an attempt was made to evaluate shaft and base unit resistances from BDSLT results at each of the three sites using the L2 and FHWA methodologies to estimate nominal unit resistances. For the Redding site, the data did not allow for evaluation using either the L2 or FHWA methodologies; the maximum mobilized unit resistance is reported, which underpredicts nominal unit resistances. For the Thompson Falls site, the L2 values were

based on the equivalent top-loading curve construction, and the base did not displace enough to apply the FHWA failure criteria. For the Missoula site, the L2 and FHWA values were based on the ETL curve construction (Fig. 8). The results of the comparison are summarized in Table 2.

Data from the Missoula test indicates shaft and base nominal unit resistance values on the order of twice the values predicted by SHAFT 6.0. It should be recognized that Table 2 presents generalized comparisons,

Table 2. Geotechnical Unit Resistance Values Comparison

Location / Source	Soil Deposit	Shaft Diameter, feet	Head Deflection at Maximum Mobilized Resistance, inches	Geotechnical Unit Resistance, ksf			
				L2		FHWA	
				Shaft	Base	Shaft	Base
Redding, CA BDSLT[1]	Very dense poorly graded gravel, with sand, cobbles, and boulders	8.2	0.4	5.3	N/A	5.3	N/A
Thompson Falls, MT BDSLT[2]	Medium dense poorly graded sand and gravel	8.0	1.3	2.99	35.65	N/A	N/A
SHAFT 6.0 Prediction for Missoula Site	Medium dense to dense poorly graded gravel, with sand	5.9	1.1 (L2); 3.2 (FHWA)	2.52	41.27	2.56	41.97
Missoula, MT BDSLT[3]	Medium dense to very dense poorly graded gravel, with sand, cobbles, and boulders	5.9	2.8 (L2); 3.2 (FHWA)	5.08	76.84	5.15	84.16

"ksf" = kips per square foot. 1 ksf = 47.88 kPa. "N/A" = Not Available.

Notes:

1. L2 unit shaft resistance values represent maximum mobilized unit resistances; nominal unit resistances are underpredicted.
2. L2 unit shaft and base resistance values based on ETL curve construction.
3. All unit shaft and base resistance values based on ETL curve construction.

and there are many factors that may contribute to differences in results, including the fractured nature of the deposits, groundwater table location, gradation, angularity, and density of the deposits, shaft instrumentation, test protocol, data evaluation and interpretation, construction procedures, etc.

CONCLUSIONS

Deep-foundation designers have many tools and data available to them, including numerous formulas, computer software, basic and sophisticated laboratory testing, and past experience. Often, several of these resources are used to estimate nominal resistances, to which a resistance (or safety) factor is applied to determine a factored resistance (or allowable load). Load testing provides the designer with an improved estimate of nominal resistances, and thus allows use of a higher resistance (or lower safety) factor. However, load testing can be perceived as expensive to some designers, clients, and agencies, viewed as not providing sufficient return on investment. This case history demonstrates that performing load testing on deep foundations can be money well-spent.

In the case history presented, bi-directional static load testing permitted the use of a higher resistance factor that than would have been used in the absence of testing. This resulted in saving 16 feet (4.9 m) of embedded length on each of eight river shafts for a new bridge structure. After accounting for the total cost of testing, a net savings of $25,260 in construction cost was realized, demonstrating that load testing can save more money than it costs (more savings would likely have been realized had the minimum required embedment length to satisfy lateral resistance requirements not controlled designs). Additionally, it is estimated that the decreased required footage saved four days of construction schedule.

More-difficult to quantify in terms of cost and time, but potentially even more-valuable, were the benefits realized from the bi-directional static load test results precluding remediation of three production shafts. When CSL testing indicated potential anomalies near their bases, BDSLT results were used to demonstrate that factored shaft resistance alone (ignoring base resistance) was sufficient to support design loads in three shafts, thereby precluding the need to core or remediate.

An additional benefit from the bi-directional static load testing is the resulting unit shaft and base nominal resistance values indicated by the test. These values can be included in a database of testing results for drilled shafts with similar diameters, soil deposits, and construction procedures. Used with prudence and judgment, such results may allow increased presumptive values to be used for future designs.

REFERENCES

American Association of State Highway and Transportation Officials, Washington, D.C. (AASHTO) (2011). Guide Specifications for LRFD Seismic Bridge Design, Second Edition, with 2012, 2014, and 2015 Interim Revisions.

American Association of State Highway and Transportation Officials, Washington, D.C. (AASHTO) (2014). AASHTO LRFD Bridge Design Specifications, US Customary Units, Seventh Edition, with 2015 Interim Revisions.

Brown, D.A., Turner, J.P., and Castelli, R.J. (2010). Drilled Shafts: Construction Procedures and LRFD Design Methods, FHWA-NHI-10-016, Geotechnical Engineering Circular (GEC) No. 10. U.S. Dept. of Transportation, Federal Highway Administration (FHWA).

Davisson, M.T. (1972). High Capacity Piles. Proceedings, Soil Mechanics Lecture Series on Innovations in Foundation Construction, American Society of Civil Engineers, ASCE, Illinois Section, Chicago, IL, pp. 81-112.

Ensoft, Inc. (2007). SHAFT – A Program for the Study of Drilled Shafts Under Axial Loading, Version 6.0 for Windows.

Kulhawy, F.H., and Hirany, A. (2009). Interpreted Failure Load for Drilled Shafts via Davisson and L1-L2. Geotechnical Special Publication. 127-134. 10.1061/41021(335)16.

Murfitt, T. (2015). Osterberg Cell Test Report, Thompson River – East. STPB-STPP-HSIP 6-1(106)56, Contract: 12514, Experimental Project MT-13-02.

Rollins, K.J., Clayton, R., Mikesell, R., and Blaise, B.C. (2005). Drilled Shaft Side Friction in Gravelly Soils. Journal of Geotechnical and Geoenvironmental Engineering – J GEOTECH GEOENVIRON ENG. 131. 10.1061/(ASCE)1090-0241(2005)131:8(987).

Sorensen, K. (2010). Effects of Gravels, Cobbles, and Boulders on Capacity of Large Diameter Shafts at the Cypress Avenue Bridge, Redding, California. Proceedings, Art of Foundation Engineering Practice Congress, 2010.

EFFECT OF ELECTROKINETICS ON PULLOUT RESISTANCE OF SHEET PILE WALLS

Antonio Kodsy, Teaching Assistant, Geotechnical Engineering, Civil and Urban Engineering Department, New York University, Brooklyn, New York, USA. Email: kodsy@nyu.edu

Lutful Khan, Associate Professor, Civil and Environmental Engineering Department, Cleveland State University, Cleveland, Ohio, USA. Email. L.Khan@csuohio.edu

ABSTRACT

A research was carried out to test the possibility of reducing the pullout resistance of metal sheet piles driven in clay soils using Electrokinetic (EK) conditioning. The hypothesis was applying an electric gradient for a certain period of time should reduce the adhesion between the clay soil and the sheet piles. Tests were conducted on bench scale thin stainless-steel metal plates embedded in pure kaolinite clay, and mixtures of kaolinite clay and sand. The pullout resistances were determined after 20, 40, and 60 minutes residence times of steel plates in the soils before and after EK conditioning under an electric gradient of 1500 V/m. In kaolinite clay, the pullout resistance showed linear reduction with the duration of EK conditioning and about 60 % reduction in pullout resistance was observed after 60 minutes EK conditioning. For the kaolinite-sand mixtures, the pullout resistances were reduced by about 70% and 80% for 20% and 30% sand contents respectively after 20 minutes EK conditioning and showed no significant improvement with the increase in conditioning duration. It was concluded that the proposed electrokinetic conditioning process could potentially reduce the pullout resistance of metal plates embedded in clay and clayey soils.

Keywords: Electrokinetics, Sheet pile walls, sheet piles, pullout, extraction

SHEET PILE WALLS

Sheet pile walls are typically used at waterfronts as retaining structures or during the construction phase to shore the soil and avoid collapse of the excavations. When used as permanent structures, sheet pile walls are not removed after the completion of the project. However, as temporary support, they are extracted after the completion of the project and reused. In pure clay soils the extraction processes often becomes a challenge requiring very large pullout forces which could damage the sheet piles. There is a research need for developing an efficient method of sheet pile extraction from clay soils addressing the issue of pullout force reduction. However, very few researches have been conducted regarding the extraction techniques of sheet piles and their economic effect on the cost of a project. In this study a novel method for reducing the pullout resistance of sheet piles in clayey soils using electrokinetic conditioning was explored.

The hypothesis of this research is that the electrokinetic process in soil/water system, specifically electrophoresis and electroosmosis, could be used to loosen the sheet pile walls embedded in cohesive soil and hence reduce the required force of extraction. The aim of this study was to test this hypothesis through laboratory tests carried out on steel plates embedded in cohesive soil samples. The pullout forces of the steel plates before and after varied duration of electrokinetic (EK) conditioning were evaluated and compared. The process was also investigated for clay-sand mixtures.

BACKGROUND

Clay particles are negatively charged primarily due to isomorphous substitutions and adsorb positive ions (cations) to balance this charge. In a clay-water system, the adsorbed cations are dislocated from the clay

© 2019 Deep Foundations Institute

surface due to the dipole action of the polar water molecules and produce a cation cloud. This results in a distribution of the positive ions over a region from the clay particle surface rather than a single layer, which is commonly referred to as electric double-layer. The characteristics of the electric double-layer in wet clay pores determines the electrokinetic properties of clay soil. The double layer concept was originally proposed by Helmholtz in 1947 [Helmholtz, 1879]. He proposed that the positive ions were attached to the negatively charged solid surface in a single layer. This concept was later modified by Gouy-Chapman and suggested that the positive ions were distributed in the liquid phase up to a certain distance from the charged surface [Gouy, 1910] [Chapman, 1913]. Stern later adjusted the double layer theory by proposing that the double layer contains a firmly attached layer on the solid surface as proposed by Helmholtz and a diffused layer as proposed by Gouy-Chapman [Stern, 1924].

Electrokinetic phenomena includes several different effects that occur in fluid filled charged porous matrix or when a fluid moves relative to a charged solid. These effects include electroosmosis, electrophoresis, streaming potential, and sedimentation potential. The electroosmosis and the electrophoresis phenomena are where, under the influence of an imposed electric gradient, the solid or the liquid phase move relative to the other. The streaming potential and the sedimentation potential, are electric potentials developed when the solid or liquid phase move relative to the other under the effect of a gravity or hydraulic force.

The two effects concerned with this study are electroosmosis and electrophoresis. Electroosmosis is the flow of liquid phase within a solid porous matrix under an electric gradient. In saturated clay soil, electroosmosis occurs when an electric gradient is applied and produces pore water flow towards the cathode. On the other hand, electrophoresis is considered to be the reverse of the process of electroosmosis. The electroosmotic process involves water movement through the pores of a charged solid matrix, while the electrophoresis process involves movement of charged colloids in a solid-liquid suspension under the influence of an electric gradient.

METHODOLOGY

The study was carried out on five samples labelled as K1 through K5. Samples K1 through K3 were pure kaolinite. Sample K4 was kaolinite mixed with sand with a ratio of 20% by weight of the kaolinite. K5 was kaolinite mixed with sand with a ratio of 30% by weight of the kaolinite. Stainless Steel rectangular plates (45.72cm x 7.62cm x 0.3175cm) were used to simulate sheet piles.

The test steel plates were driven in the compacted soil using a hammer and a right angle to ensure vertical alignment to a depth of 15cm as shown in Figure 1. The embedded sheets were allowed to rest for 60, 40, and 20 minutes and then the sheets were pulled out. The pullout resistance capacity was measured using a load frame equipped with a load cell and a strain transducer as shown in Figure 2. Failure was defined as the resistance decreasing with the increase in displacement. Peak value for each test was recorded as the maximum pullout resistance capacity. The values recorded served as datum values for comparison. All the control and test samples had identical boundary constraints. BC will be evaluated in future research.

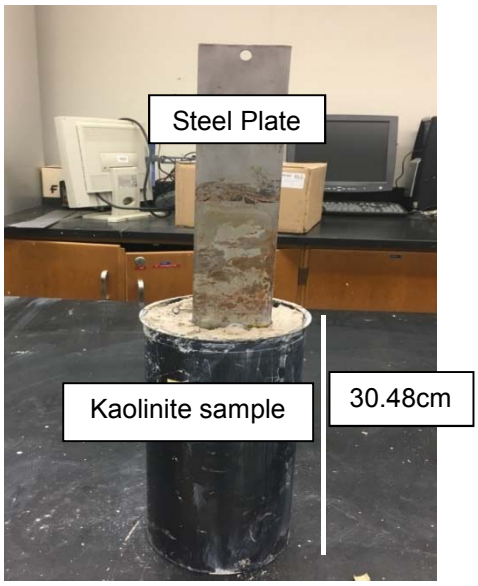


Figure 1. Steel Plate Installation in Compacted Sample

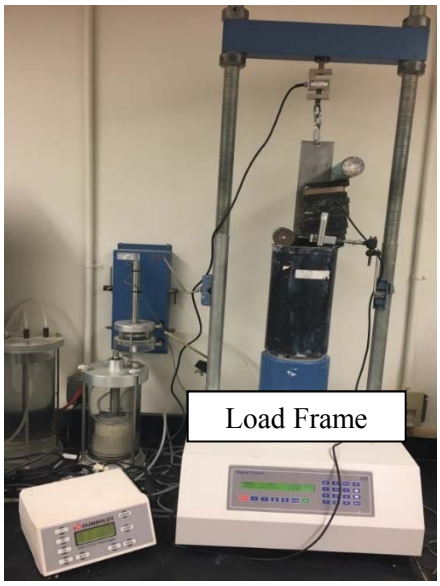


Figure 2. Pullout Resistance Capacity Test

To apply an electric gradient and evaluate its effect on the pullout resistance capacity of the steel sheets, four 35.56 cm long an 0.3 cm diameter stainless steel rods were driven on the sides of the steel sheet at a distance of 2 cm. The stainless steel rods were driven about 15 cm into the soil. A DC power supply was used to apply the desired voltage by attaching a wire to the steel sheet which acted as the cathode (negative electrode) while the stainless steel rods were the anode (positive electrode) in this procedure. The system was subjected to 30 volts continuously for 60, 40, and 20 minutes before pullout tests were performed. A voltmeter was used to measure the voltage between the steel sheet and the stainless steel roads throughout the procedure to ensure constant voltage. The setup is presented in Figure 3.

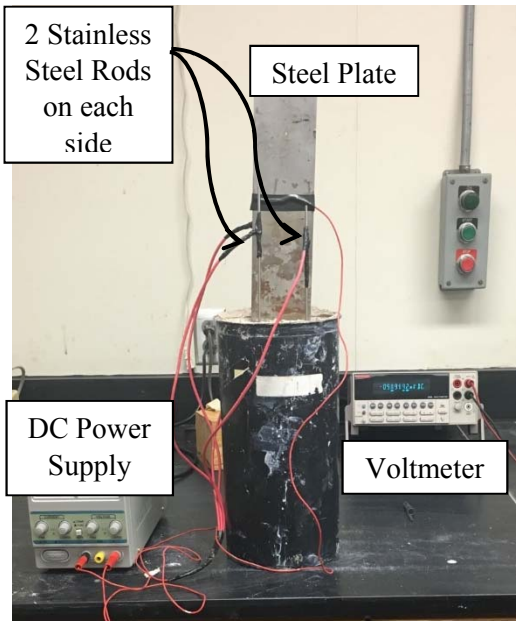


Figure 3. Electric Gradient Test

RESULTS

All samples were tested without EK conditioning and after applying the EK conditioning. For the pure kaolinite, a noticeable reduction was observed in the pullout resistance capacity of the embedded steel plates after the application of the electric gradient for 60, 40 and 20 minutes. For the 60 minutes exposure, the average pullout force for sample K1 decreased by 74%, while for sample K2 a 60% decrease was observed. Moreover, sample K3 experienced a reduction corresponding to 51%. The corresponding pullout resistance capacity for the 40 minutes exposure and the 20 minute exposures showed similar reduction level. Table 1 shows the percentage reduction in the pullout resistance for samples K1, K2, and K3 respectively after the application of the electric gradient.

Table 1. Effect of EK conditioning on Pullout Resistance of Test Sheet Piles in Pure Kaolinite clay

Sample	EK conditioning duration	Peak Value before EK conditioning (P_o)	Peak Value after EK conditioning (P)	Percentage Decrease
K1	60 Minutes	232 N	61 N	74 %
	40 Minutes	208 N	124 N	40%
	20 Minutes	119 N	95 N	20%
K2	60 Minutes	363 N	144 N	60%
	40 Minutes	330 N	124 N	62%
	20 Minutes	211 N	100 N	53%
K3	60 Minutes	219 N	107 N	51%
	40 Minutes	211 N	121 N	43%
	20 Minutes	148 N	94 N	36%

For the kaolinite mixed with 20% sand (K4), the results showed that the pullout resistance capacity of the steel plates decreased notably after EK conditioning for 20, 40 and the 60 minute durations. For the 20 minutes exposure, the average pullout resistance decreased by about 74%. For the 40 minutes and the 60 minutes exposure durations, no additional reduction was observed as shown in Table 2.

Table 2. Effect of EK conditioning on Pullout Resistance of Test Sheet Piles in Kaolinite Mixed with 20 Percent Sand

Sample	EK conditioning duration	Peak Value before EK conditioning (P_o)	Peak Value after EK conditioning (P)	Percentage Decrease
K4	60 Minutes	101 N	25 N	75 %
	40 Minutes	75 N	26 N	65%
	20 Minutes	102 N	27 N	74%

Finally, the kaolinite mixed with 30% sand (K5) experienced an 80% reduction in the pullout resistance capacity after applying the electric gradient for 20 minutes. Similar to sample K4, no additional reduction was observed for the 40 minutes and the 60 minutes exposure durations as shown in Table 3.

Table 3. Effect of EK conditioning on Pullout Resistance of Test Sheet Piles in Kaolinite Mixed with 30 Percent Sand

Sample	EK conditioning duration	Peak Value before EK conditioning (P_o)	Peak Value after EK conditioning (P)	Percentage Decrease
K5	60 Minutes	52 N	11 N	79 %
	40 Minutes	64 N	15 N	77%
	20 Minutes	58 N	9 N	84%

From the above results it was observed that the longer duration of EK conditioning was required to achieve the same level of reduction in the pullout resistance capacity as the kaolinite-sand mixture samples. Moreover, it was also observed that the level of reduction in the pullout resistance capacity in the kaolinite-sand mixture samples was nearly the same for all durations of EK conditioning. These results are presented in Figure 4.

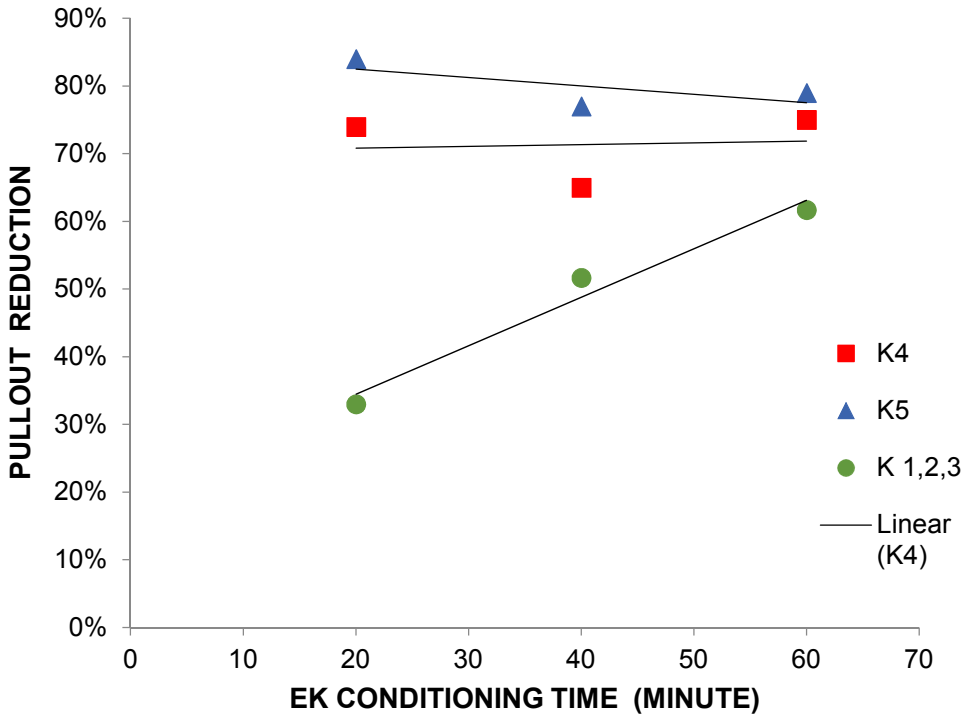


Figure 4. Comparison of EK conditioning duration on pure Kaolinite (avg. of K1, K2, and K3), Kaolinite mixed with 20% (K4) sand and Kaolinite mixed with 30% sand (K5)

Figure 5 shows the effect of steel plate embedment duration on the pullout resistance capacity. It is noticed in the graph that the pullout resistance capacity was maximum for the pure kaolinite sample and reduced as the sand percentage was increased in the mixture. The graph also clearly shows evidence of pullout resistance capacity reduction when the steel plates were subjected to EK conditioning.

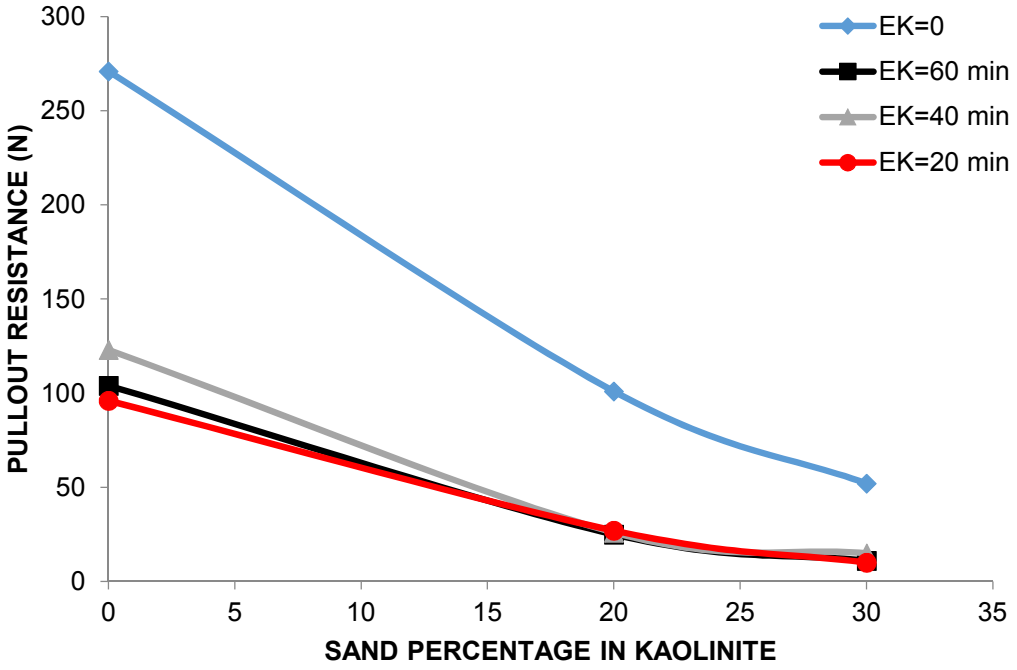


Figure 5. Effect of Steel Plate embedment duration on pullout resistance capacity

CONCLUSION

The results of the study confirmed the hypothesis that the proposed method of EK conditioning could reduce the adhesion between steel plates and clay soil. The following conclusions were drawn based on the results obtained.

- Electrokinetic conditioning as proposed in this research has notable effect on the pullout resistance of the steel plate embedded in clayey soils. It decreased the adhesion of the soil particles to the steel sheet which in turn, decreased the pullout resistance, making it easier to extract the plates.
- For pure kaolinite clay, the pullout resistance decreased significantly after the application of electricity for a period of 20 minutes. This pullout resistance further decreased linearly as the EK Conditioning time was increased to 40 and 60 minutes. The maximum reduction in pullout force was about 60 percent after 60 minutes of EK Conditioning.
- For kaolinite clay mixed with 20 percent sand, the pullout resistance of the steel plates reduced by about 70 percent for 20 minutes EK Conditioning and remained within that range for 40 and 60 minutes treatment duration.
- For kaolinite clay mixed with 30 percent sand, the pullout resistance of the steel plates reduced by about 80 percent for 20 minutes EK Conditioning and remained within that range for 40 and 60 minutes treatment duration.

- Increasing the sand percentage in the mixture composition of kaolinite and sand decreased the cohesion of the soil and therefore decreased the pullout resistance force required.
- The maximum reduction of pullout force was achieved for kaolinite mixed with 30 percent sand. Apparently, higher percentage of sand in clay produced higher pullout resistance reduction.
- The pullout resistances were the highest for pure kaolinite and decreased with the increase in sand content.
- Time dependent increase of pullout resistance of the steel plates was observed in the pure kaolinite during the 60 minutes residence time. Such effect was not observed during the 60 minutes time for the kaolinite mixed with sand samples.
- The results conclusively suggest the decrease in the pullout resistance. The effect of the duration of EK treatment, however, may not be conclusive.

REFERENCES

Chapman, D. L. 1913. A contribution to the theory of electrocapillarity, *Philosophical Magazine*, Vol. 25, No.6, pp. 475-481

Czech, K., & Gosk, W. (2016). Analysis of the Vibration Propagation Induced by Pulling out of Sheet Pile Wall in a Close Neighbourhood of Existing Buildings. *Procedia Engineering, 143*, 1460-1467. doi:10.1016/j.proeng.2016.06.172

Das, M. R., & Das, S. K. (2015). Optimal Design of Sheet Pile Wall Embedded in Clay. *Journal of The Institution of Engineers (India): Series A, 96*(3), 249-258. doi:10.1007/s40030-015-0128-9

Deckner, F., Viking, K., & Hintze, S. (2015). Vibration Transfer During Sheet Pile Driving – A Full-Scale Field Test. *6th International Conference on Earthquake Geotechnical Engineering*.

Finno, Richard J.; Atmatzidis, Dimitrios K.; and Nerby, Steven M., "Ground Response to Sheet Pile Installation in Clay" (1988). *International Conference on Case Histories in Geotechnical Engineering*. 34.

Gouy, G. 1910. Sur la constitution de la charge electrique a la surface d'un electrolyte, *Anniue Physique (Paris)*, Serie 4, Vol. 9, pp. 457-468

Helmholtz, H. 1879. *Wiedemanns Annalen d. Physik*, Vol. 7, p. 137

Jayasekera, S. (2015). Electrokinetics to Modify Strength Characteristics of Soft Clayey Soils: A Laboratory Based Investigation. *Electrochimica Acta, 181*, 39-47. doi:10.1016/j.electacta.2015.06.064

Kolwalkar, Susheel R., "Increasing Pile Capacity and Set-up in Clay by Electrokinetics" (2009). *ETD Archive.* Paper 167.

Lee, S., Kim, B., & Han, J. (2011). Prediction of penetration rate of sheet pile installed in sand by vibratory pile driver. *KSCE Journal of Civil Engineering, 16*(3), 316-324. doi:10.1007/s12205-012-1317-y

Massarsch, K. R., Fellenius, B. H., & Bodare, A. (2017). Fundamentals of the vibratory driving of piles and sheet piles. *Geotechnik, 40*(2), 126-141. doi:10.1002/gete.201600018

Micic, S., Shang, J. Q., & Lo, K. Y. (2003). Improvement of the load-carrying capacity of offshore skirted foundations by electrokinetics. *Canadian Geotechnical Journal, 40*(5), 949-963. doi:10.1139/t03-045

Mohamedelhassan, E. (2009). Electrokinetic strengthening of soft clay. *Proceedings of the Institution of Civil Engineers - Ground Improvement, 162*(4), 157-166. doi:10.1680/grim.2009.162.4.157

Paunescu, M. (1964). Resistance to vibration extraction of piles and sheet piles. *Soil Mechanics and Foundation Engineering, 1*(3), 191-194. doi:10.1007/bf01703674

Serbulea, M. (2013). Soil Improvement Using The Electro-Osmosis. *13th SGEM GeoConference on SCIENCE AND TECHNOLOGIES IN GEOLOGY, EXPLORATION AND MINING*. doi:10.5593/sgem2013/ba1.v2/s02.047

Smoulchowski, M. 1914. InL L. Graetz (ED.), *Handbuch der Eletrizitat und Magnetismus*. Vol. 2, J. A. Barth, Leipzig.

Stern, O. 1924, Zur Theorie der Elektrolytischen Doppelschriht, *Zeitschrift Electrochem*, Vol. 30, pp.508-516

Whenham, V., & Holeyman, A. (2012). Load Transfers During Vibratory Driving. *Geotechnical and Geological Engineering, 30*(5), 1119-1135. doi:10.1007/s10706-012-9527-0

White, D., Finlay, T., Bolton, M., & Bearss, G. (2002). Press-In Piling: Ground Vibration and Noise during Pile Installation. *Deep Foundations 2002*. doi:10.1061/40601(256)26

LEVEE REHABILITATION, LOWER WOOD RIVER PHASE II– EAST ALTON IL. DEEP CUTOFF WALL

Wesley Schmutzler, TREVIICOS, 38 Third Avenue, Charlestown, MA, 617-241-4800, wschmutzler@treviicos.com,

Matteo Bertoni, TREVIICOS, 38 Third Avenue, Charlestown, MA, 617-241-4800, mbertoni@treviicos.com,

Gene Bryant, Barr Engineering, 4300 Market Pointe Drive, Minneapolis, MN, 952-832-2833, gbryant@barr.com

ABSTRACT

The levees where the Mississippi River and the Lower Wood River meet near East Alton Illinois have been a problem area for years due to underseepage. The first phase of the deep cutoff wall was a 2,000-linear foot section that was completed in 2016 for the Illinois Flood Prevention District Council. This section was installed along the Wood River and the Mississippi river to depths of over 135', The United States Army Corps of Engineers was tasked with continuing the cutoff wall along the Mississippi river. The wall was a continuation of phase I with depths up to 140'. The 1,000' long cutoff wall was installed through fill, loose sands, cobbles, and sandy clay. The cutoff wall was terminated in either Glacial Till or sound rock. In order to provide wall permeability equal to or less than 1.0 X 10^{-6} cm/sec a self-hardening slurry (SHS) composed of ordinary Portland cement, slag cement, and water was utilized. The depths reached on this project using SHS is the deepest done to date in the United States. Along with the permeability requirements, a very narrow range for the unconfined compressive strength was specified at 50 – 180 PSI. In order to monitor the ground movement and water level fluctuations during the excavation of the panels with the Hydromill or Clamshell, 6 automated inclinometers were installed and monitored continuously during panel excavation in phase 1. Seven automated piezometers were monitored in phase 2. This paper will give an overview of the project with emphasis on the effect of the excavation on the instrumentation, specifically the reaction of the piezometers as the last panels were installed.

INTRODUCTION

The project is in Illinois, about 1000 feet downstream from where the Wood River Creek enters the Mississippi River between East Alton, IL and Wood River, IL adjacent to State Highway 143 (Fig. 1). The Wood River Lower Cutoff Wall Phase 2 Project (WR2) was awarded to TREVIICOS SOUTH (TIS) in September 2017. The Main Project features are: Construction of work platform, inclinometers installation and removal, cutoff wall construction by the Self-Hardening Slurry method (approx. 135,000 sf) up to 140' depth, clay cap installation, and site restoration. The levee system along this stretch of the Mississippi River has been plagued by under-seepage for several years. The phenomenon has worsened to varying degrees, depending on location, to the point that remediation was needed to ensure that Levee failure would not be an issue in the future.

The Specifications required that a test section comprised of two primary panels and one secondary panel be install before full production commenced. To perform the tasks required, the contractor utilized one Hydromill, one Clamshell, a de-sanding unit and a SHS grout plant. working two 12-hour shifts/day, 5days/week, excavating under SHS.

© 2019 Deep Foundations Institute

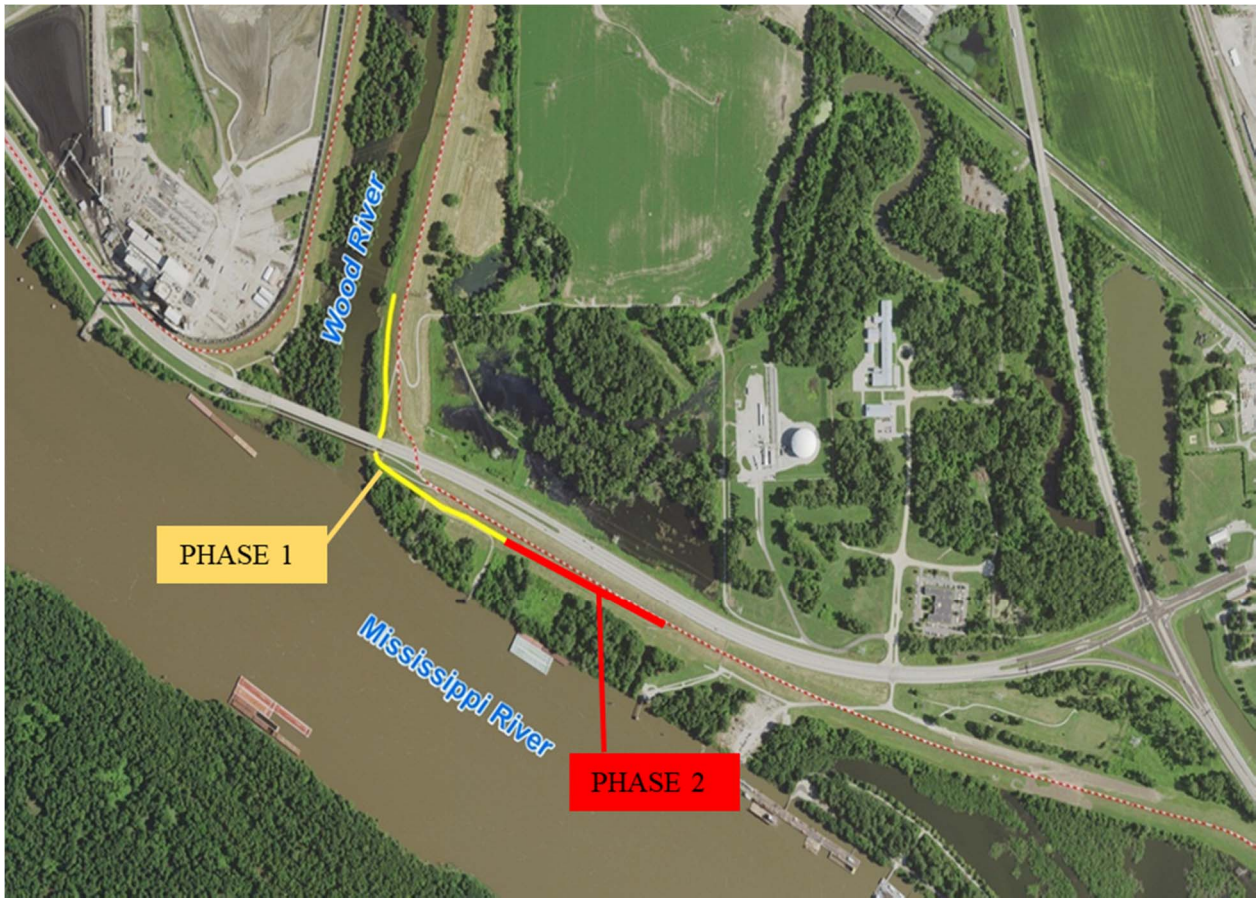


Fig. 1. Location of the Lower Wood River Cutoff Wall Project (Phase 2 in Red)

GEOLOGY

The LCW project is located in the Wood River Quadrangle, which is mostly contained within the alluvial valley of the Mississippi River known as the American Bottom. The ground level elevation of the area ranges from 420 to 440 feet (130 to 135 m) above sea level and is the result of processes of excavation and filling of the valley that likely occurred several times during the Quaternary Period.

The deposits of the Mississippi River valley consist of mixtures of water-laid clay, silt, sand, and gravel, up to 125 feet (38 m) thick above bedrock. These deposits are highly variable in the upper 50 feet due to former channels of the Mississippi River and its tributaries. There is a general coarsening trend with depth, with outwash (sand with gravel) typically comprising the lower one-third to one-half of the sediment volume. The underlying bedrock consists mainly of limestone or shale; locally the bedrock is covered by glacial till, preserved underneath thick alluvial sediments (Grimley and Lepley, 2005). There is a direct correlation between the alluvial deposits and the under-seepage occurrences of the area, as explained in the Technical Memorandum prepared in 1956 for the St. Louis District, Corps of Engineers by Waterways Experiment Station (WES TM 3-430, 1956). A typical soil profile along the cutoff wall centerline is in Fig 2. During construction, the top of the Glacial Till which had a zone of gravel and cobbles, was determined to be the greatest seepage path as could be seen by the reactions of the piezometers and the over consumption of SHS.

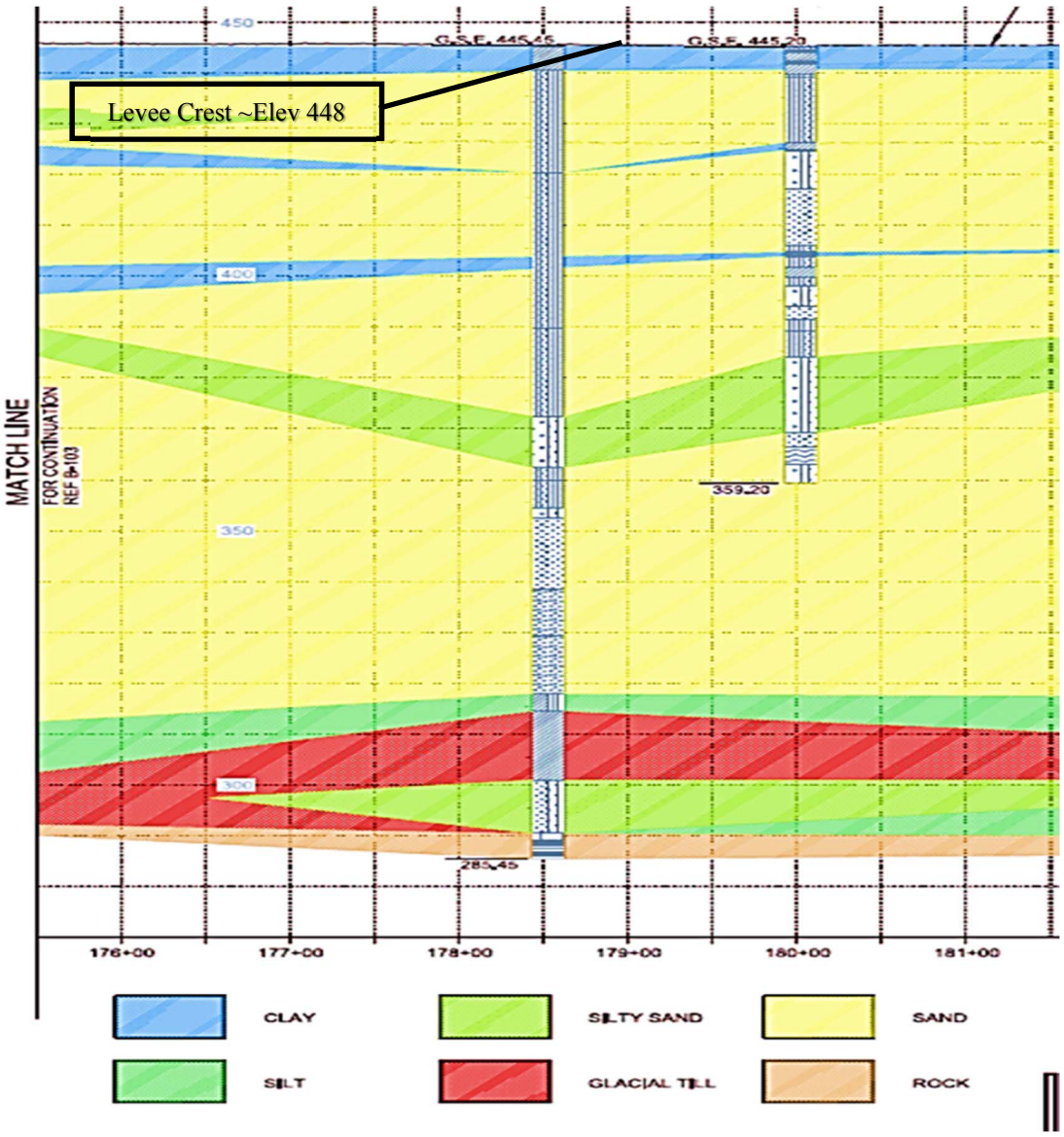


Fig. 2. Soil Profile

Scope of Work and Construction Methods

The project phase 2 design by USACE included a 1,000 foot long (305 m) cutoff wall installed adjacent to the river side toe of the levee along the Mississippi River.

The technical specifications required that the cutoff wall (COW) be homogeneous, a minimum 2-feet, and with a maximum hydraulic conductivity of 1 x 10^{-6} cm/s. The Unconfined Compressive Strength (UCS) at 28 days was to be between 50-180 psi with no individual specimen strength being lower than 30 psi or greater than 200 psi.

The cutoff wall was to be excavated through layers of granular soils, including dense sands, gravels, and cobbles, to depths of up to 140 feet (43 m), to be keyed a minimum of 5 feet (1.5 m) into till or, a minimum of 2 feet (0.3 m) into competent rock in those areas where the till was not present. The “panel method” (i.e.:

overlapping primary and secondary panels) was to be used, and a minimum overlap between primary and secondary panels of 20 inches (0.5 m) was required.
The geotechnical properties of the foundation soils constituted a reason of concern for the owner and the contractor. A collapse of the trench walls could have had catastrophic consequences: the possible scenarios included failure of the levee, serious damage to Berm Highway (Route 143). Six inclinometers were to be installed and continuously monitored for differential movements, a potential sign of an undergoing deformation of the trench walls.
The Contractor selected for the project a construction method consisting of using a combination of clamshell and hydromill (Fig. 3), under a self-hardening slurry (SHS). The method had been successfully used few years before for the rehabilitation of over 38,000 linear feet (11,850 linear meters) of the Herbert Hoover Dike in Florida (Granata et Al., 2016), a project with similar geotechnical properties.
The LCW project presented the Contractor with an additional and major challenge: never before had a cutoff wall installed using a hydromill under SHS reached such depths. The Herbert Hoover Dike project required a maximum depth of 84 feet, while the maximum depth of the cutoff wall at the LCW project was 140 feet.
The Contractor decided to limit the maximum length of the primary panels to 23 feet (7.0 m) and 9.2 feet (2.8 m) for the secondary panels. The width of the panels was set to 3 feet (0.9 m), to account for vertical deviations and guarantee the minimum required width.
A mixing plant was positioned at the toe of the land side of the levee for the preparation of the SHS. The equipment present included two high shear colloidal mixers supplied by vertical silos for cement and bentonite, one agitator, and baker tanks for bentonite slurry hydration and water storage.
The project specifications required that the installation of the full length of the cutoff wall be preceded by the construction of a test section, located on the Mississippi River side of the project, which was to be in compliance with the requirements set for the remainder of the cutoff wall.
The test section included, two 23 feet (7 m) primary panels, and one 9.2 feet long (2.8 m) secondary panels. Construction of the test section started on July 27, 2018 and was completed August 7, 2018. The construction method selected by the Contractor proved to be efficient and safe, and produced a wall in compliance with the specification requirements. Therefore, on September 24, 2018 the operations were resumed to complete the installation of the COW. The production phase consisted of installing 33 primary panels and 33 secondary panels and was completed 2.1 months later, on December 3, 2018. Completion was delayed by over 2 weeks due to the rising of the Mississippi River to historic levels for the season, which resulted in the flooding of the work platform.
Further details on the scope of work, construction method, and construction phases of the project can be found in the paper Construction of a Deep Cutoff Wall Along the Mississippi River at East Alton, IL (Granata et Al., 2017), which also discusses the SHS design phase.



Fig. 3 Hydromill

Quality Control/Quality Assurance Program

The project specifications provided comprehensive requirements for the execution of the work and the Quality Control/Quality Assurance (QC/QA) Program. The extensive test requirements resulted in almost 220 wet grab (WG) samples collected, over 3,000 specimens cast, and over 300 UCS tests (Fig.4) and over 50 permeability tests(Fig. 5) performed throughout the whole project. The test results were in compliance with the specification requirements. At the end of the project over 1,700 spare cylinders were discarded (Fig 6).

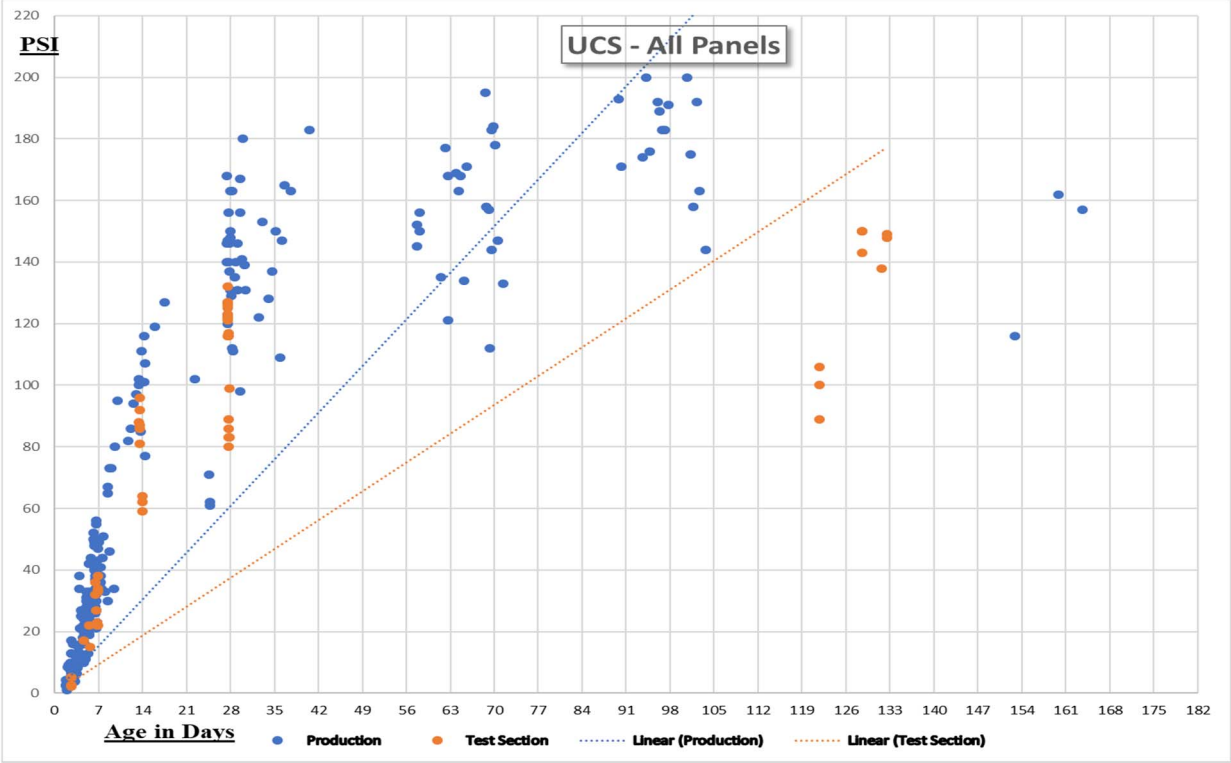


Figure 4: UCS of Wet Grab Samples

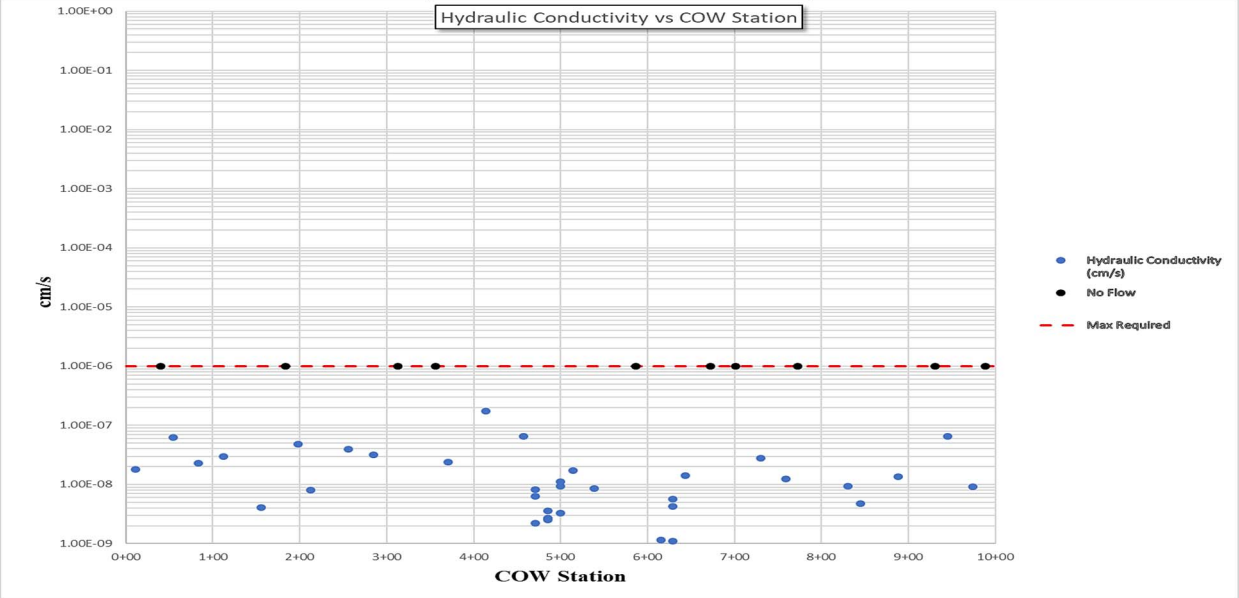


Fig. 5 Hydraulic Conductivity of Wet Grab Samples



Fig. 6 Discarded Cylinders

Instrumentation Monitoring

The location of the cutoff wall and the geotechnical properties of the foundation soils were of concern for the designer and the contractor. Therefore, the specifications required the installation of six inclinometers to be monitored in real time along the cutoff wall. The specifications also required that seven existing open-pipe piezometers be equipped with real time monitoring.
The Contractor selected Barr Engineering to install and monitor the instrumentation.

Instrumentation Overview

The primary objective for the instrumentation was to monitor lateral movement and pore-water pressures. The intent of the monitoring data was to allow design assumptions to be adjusted, and, if necessary, help to potentially mitigate excessive movements.
Three types of geotechnical instrumentation were installed and monitored during construction. These included six In-Place Inclinometers (IPIs), and 7 open-pipe piezometers with pressure transducers. A data acquisition system was installed, configured, and programmed to initiate, record and transmit measurements at specified intervals remotely. Instruments integrated into the data acquisition system include automated piezometers (pressure transducers), barometer, and in-place inclinometers. In addition to the installed instrumentation, online data from the USACE's nearby Mel Price L&D river gage was automatically polled and included in the monitoring results.
The piezometers monitored were located along the levee crest and landside, generally following the cutoff wall alignment. The IPIs were located 5-feet in both directions from the edge of the cutoff wall and at two cross sections. Another 2 inclinometers were placed centered between the cutoff wall and centerline of the levee, approximately 35 feet from the landside edge of the cutoff wall.
The instrumentation layout for the cutoff wall area is shown in Figure 7.

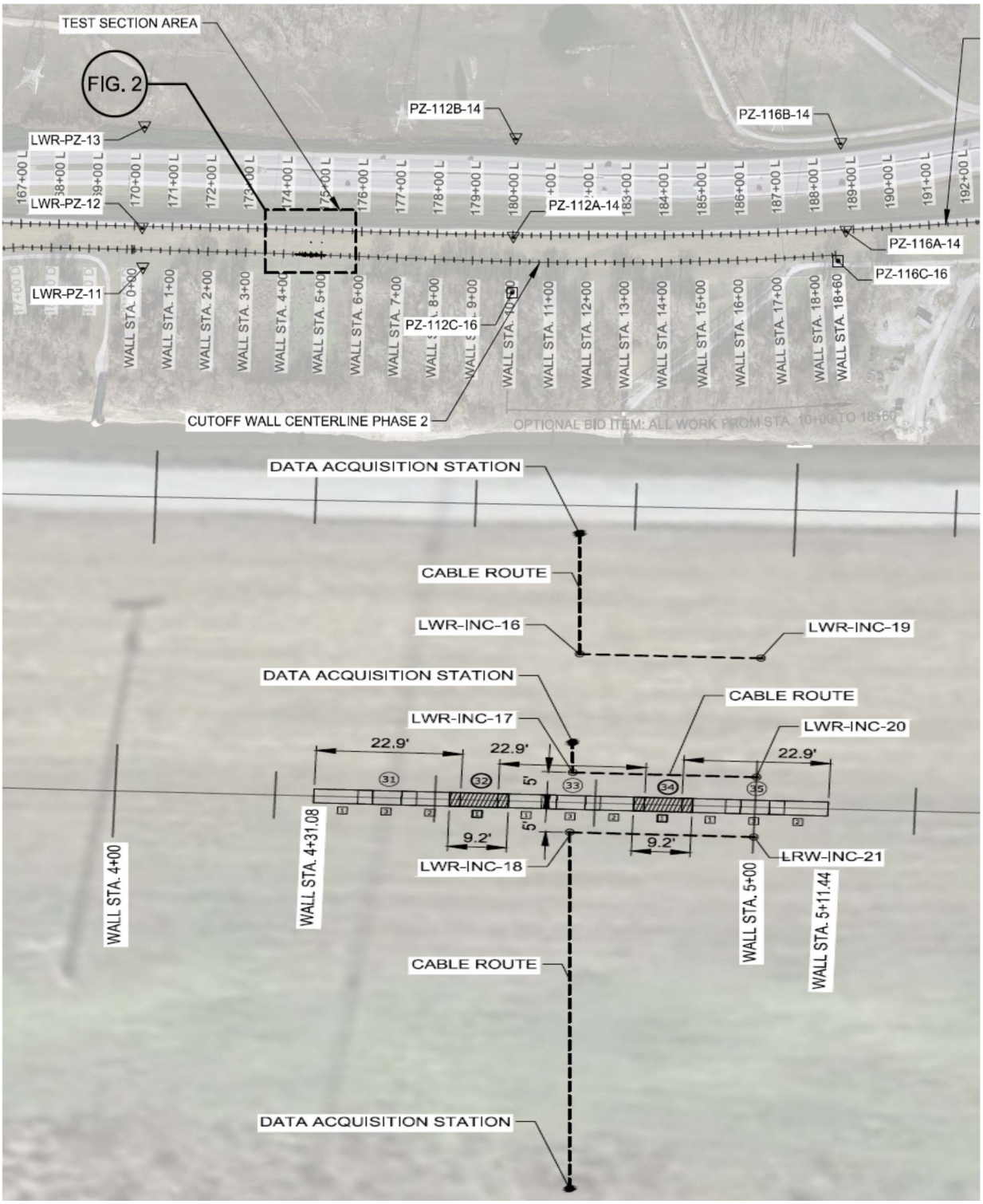


Figure 7: Instrumentation Layout

Monitoring Program

The minimum specified monitoring frequency during active construction, not including baseline, was once per shift for piezometers. For inclinometers, the frequency was weekly and then hourly once excavation began on adjacent cutoff wall panels.

For consistency and quality control purposes, all data was obtained at least on an hourly basis. Instrumentation monitoring data was provided in near real-time on an instrumentation monitoring website accessible to project stakeholders. Automated alerts for exceedance of instrumentation monitoring thresholds were incorporated into the monitoring program. The monitoring program was continued through completion of the cutoff wall.

Monitoring Results and Analyses

Piezometers

All piezometers were screened within the underlying sands. The results of the piezometer instrumentation monitoring indicate groundwater levels trending similarly to the elevation of the river (Mississippi River, Mel Price L&D TW).

Piezometer monitoring indicated measurements exceeding the threshold limit of elevation 417 feet due to an October river flood event and no panel excavation work was allowed for over 2 weeks.

During excavation of the panels a notable increase in the pore pressures was observed when the excavation of the panels reached a depth of about 90'-100' deep. Figure 8 below shows the reaction of the piezometers (PZs) while excavating primary panel number 5. The primary panels were comprised of three bites by the hydromill, a left bite, a right bite and a center bite. The increase in pore pressure was about 0.5 feet in this case. PZ 11 is 50' river side of the excavation and PZ 12 is 80' on the landside of the excavation. Also note that PZ 13 showed a slight increase in pore pressure and this PZ is 300' land side of the excavation. As can be seen by the reaction of the PZs, once the SHS permeated the area the pore pressures decreased to their static level almost immediately.

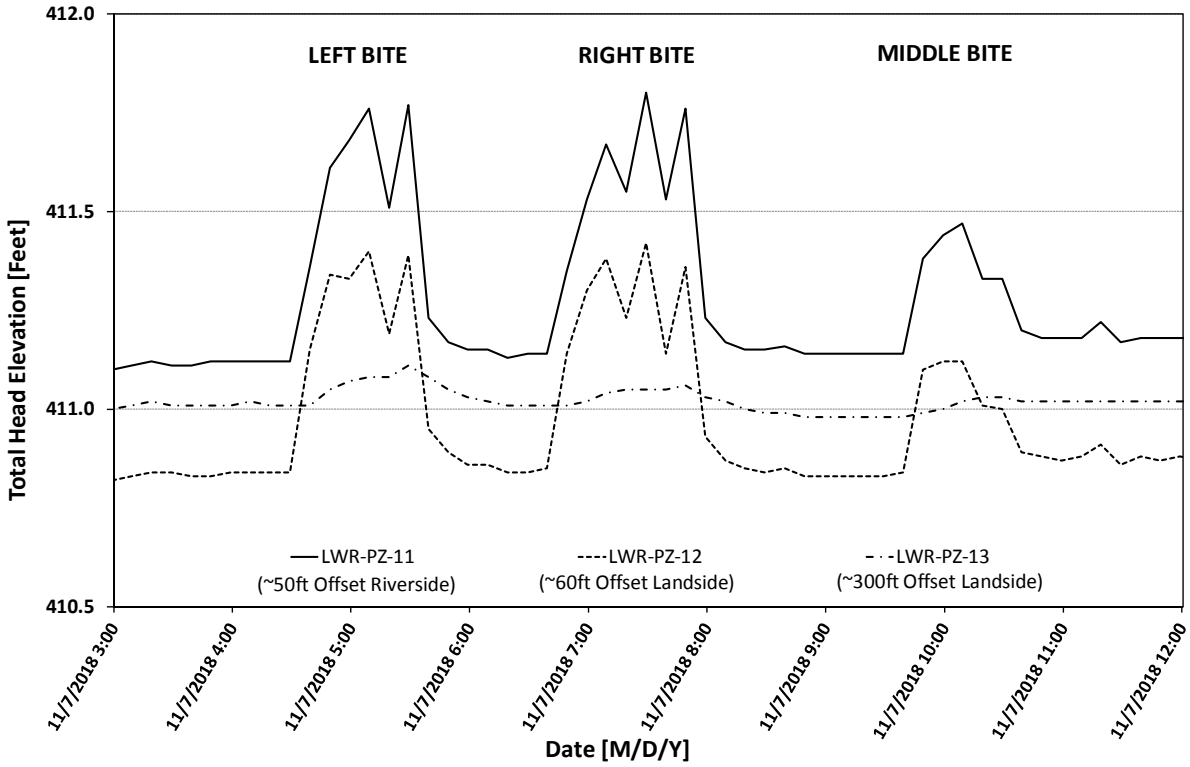


Figure 8: Piezometer Readings While Excavating

During the excavation of the last secondary panel on the project, the PZs reacted quite differently and did not return to their previous static level. As can be seen in Figure 9, PZ 11 that is on the river side of the cutoff wall, dropped below its pre-excavation level as the water no longer had a path to recharge the system. PZ 12, that is on the land side of the completed cutoff wall, showed an increase over the pre-excavation level as the ability of the system to discharge was cutoff. Even weeks after the completion of the cutoff wall, PZ 12 and 13, on the land side of the cutoff wall, that had previously reacted with the fluctuating levels of the Mississippi river no longer indicated this trend. The 2 land side PZs showed the impact of the functioning cutoff wall, however over a longer period of time, they eventually would mimic the rise and fall of the river due to the water path around the ends of the cutoff wall.

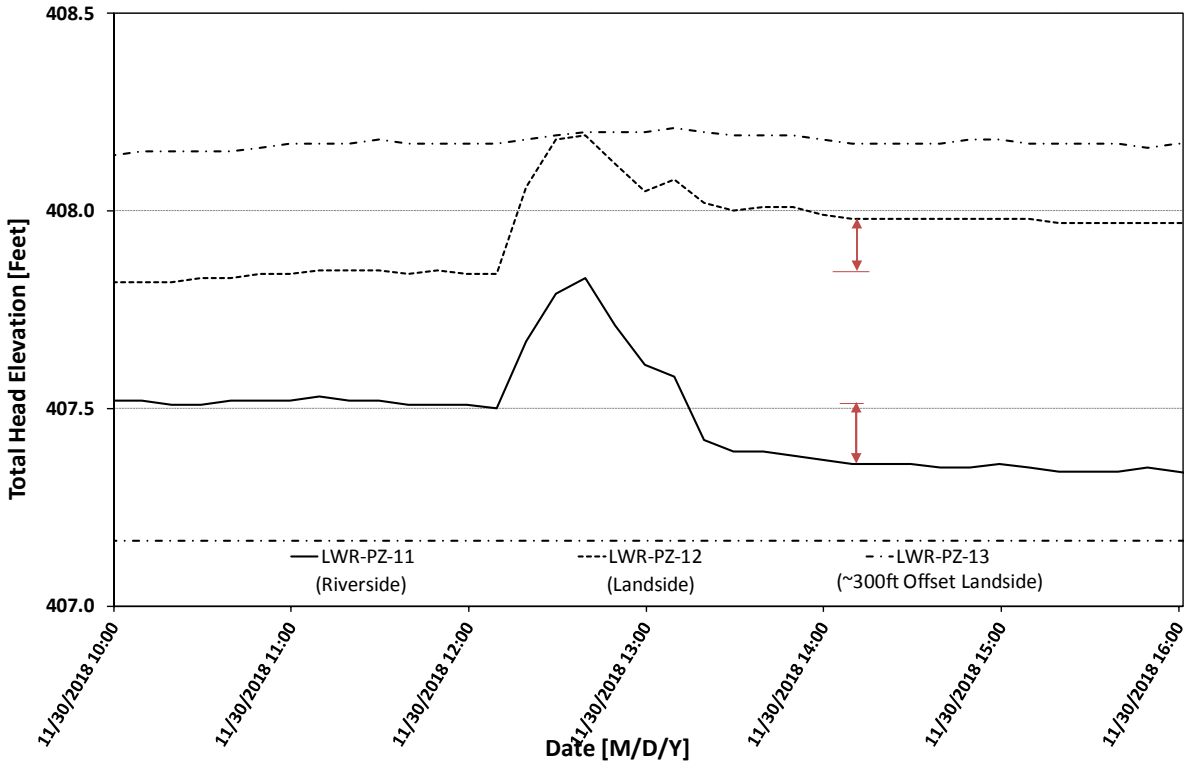


Figure 9: Piezometer Readings After Excavating the Last Panel

In-Place Inclinometers

Each IPI is comprised of a series of addressable, micro-electrical-mechanical-systems (MEMS) sensors. Two MEMS sensors within each tilt sensor allow for measurement in two directions (biaxial). All IPI's consisted of 15 or 16 biaxial sensors each, with gauge lengths varying from 5 to 10 feet. The A+ sensor direction was orientated towards the cutoff wall in all cases. Monitoring results include displacement like traditional inclinometer casing and probe systems. Temperature was also recorded on sensors at several locations, with results discussed later.

Displacement indicated by IPIs was generally limited, with movement most apparent into two discrete zones: Near surface displacement associated with local effects near the top of the inclinometer, and subsurface displacement associated with cobble layers. Near surface displacement was understood to be the result of construction traffic loading, surface disturbance, and deformation of fill placed as part of the work

platform. Potential movement of the guide wall or disturbance resulting from guide wall construction may also be a factor.

Cumulative lateral displacement near the top of inclinometer casing varied from negligible to as great as 2.0 inches depending on location. Inclinometers located in the work platform (flush mount vaults buried 1-foot below working grade) were subject to greatest disturbance and near surface displacement. An example from LWR-INC-18 is shown in Figure 10. The major concern with the inclinometer movement was in the cobble and loose sand zones at about 100' deep where the major seepage path was.

Some minor movement was noted in these areas as was expected from our experience on phase one of this project. However, given the high unit weight and the high viscosity of the SHS this zone did not present any problems.

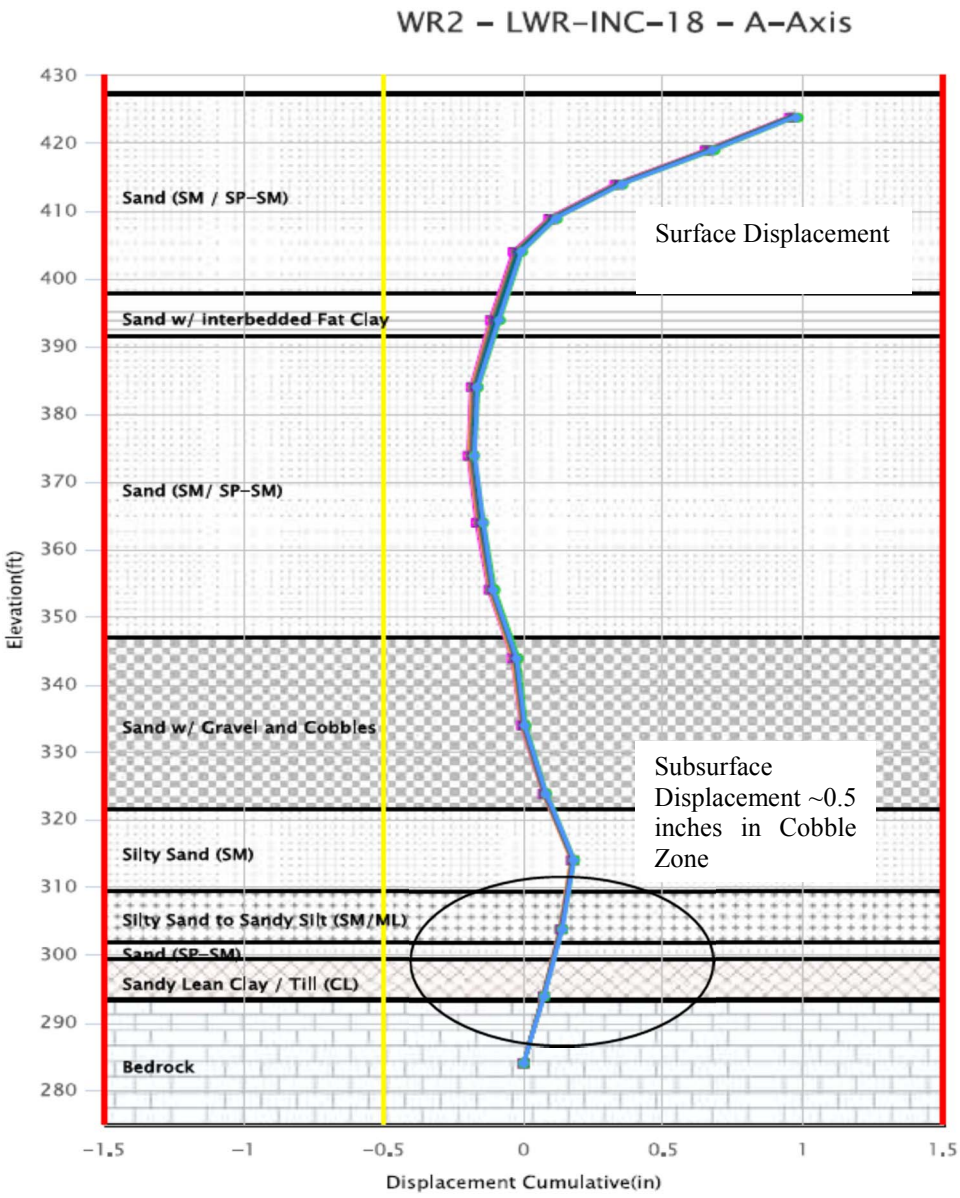


Figure 10: Inclinometer 18

Conclusions

The construction method produced a homogeneous and continuous cutoff wall meeting the required performance criteria.
The hydromill under SHS excavation method, was successfully used for the installation of a cutoff wall, through layers of loose soils, to depths of up to 140 feet.
The measured lateral deflections proved the cutoff wall method as a viable and safe option in proximity of numerous and vital infrastructures.
At the completion of the cutoff wall, the PZs confirmed that the seepage paths had been greatly reduced.

REFERENCES

Granata, R., Tucker, J., Bertoni, M., Schmutzler, W., (2017), *"Construction of a Deep Cutoff Wall Along the Mississippi River at East Alton, IL"*, American Society of Civil Engineers (ASCE) Grouting 2017 International Conference, July 2017, Honolulu, Hawaii.

Grimley D.A and Lepley S.W., (2005). *Surficial Geology of Wood River Quadrangle Madison County, Illinois*; Illinois Preliminary Geologic Map IPGM Wood River-SG; Department of Natural Resources Illinois State Geological Survey.

WES TM 3-430, (1956). *Investigation of Underseepage Mississippi River Levees, Alton to Gale, IL - technical memorandum* - Publisher: Waterways Experiment Station - Available Online: http://acwc.sdp.sirsi.net/client/en_US/search/asset/1004940.

EFFICIENT DEEP FOUNDATIONS, EARTH RETENTION SYSTEMS AND GROUND IMPROVEMENT – NEW SCHOOL TECHNIQUES FOR COLUMBIA MANHATTANVILLE'S SUBSURFACE CHALLENGES

Jeffrey Di Stasi[1], Frank Di Salvo, P.E.,[2], Justin Lukens[3]

[1]Moretrench American Corporation, 100 Stickle Avenue Rockaway NJ 07866; e-mail: JMDiStasi@HaywardBaker.com
[2]Moretrench American Corporation, 100 Stickle Avenue Rockaway NJ 07866; e-mail: fdisalvo@moretrench.com
[3]Case Foundation Company, 850 Cassatt Road Suite 100 Berwyn PA 19312; e-mail: JJLukens@casefoundation.com

ABSTRACT

Columbia University's Manhattanville Campus expansion includes the construction of two new business school buildings. The new buildings require development of an entire city block bound by 12th Avenue, W 131st Street, W 130th Street and Broadway in Upper Manhattan. A support of excavation (SOE) package was first released, followed by a foundation package. The SOE package consisted of approximately 100 soldier piles and 280 anchors, up to 215' long, to support a cut anywhere from 30'- 50' below street level. The foundation package alone included approximately 1600 drilled micropiles. Given the breadth of the work scope, Hayward Baker Inc and Moretrench joint ventured on these two projects to bring sufficient knowledge and work resources to complete the work in an efficient and timely manner. This included working with the Owner/Engineer to propose different means and methods for construction to significantly reduce the schedule while meeting the design intent, such as large diameter (36" diameter) augercast piles in place of conventionally drilled soldier piles and large hollow-bar micropiles (103/51 bars) in lieu of pressure-grouted micropiles. The anchors, ranging from 3 to 22 strands, were used for earth retention through both soldier pile and lagging walls and existing slurry walls. These anchors were complicated based not only on their size and length, but also the need to drill some of them under the historic Studebaker building. The overall magnitude of the project with considerations to resource management and material lead times will be addressed, highlighting critical strengths provided by the Contractor to ensure project success.

INTRODUCTION

The scope of work discussed in this paper was executed under two separate competitive bid contracts. The first contract included the support of excavation work and the second contract included the foundation package. The support of excavation comprised of drilled soldier piles (performed by Case Foundation as a subcontractor to the JV), driven soldier piles, driven sheet piles, hollow bar tiebacks, multi-strand tieback anchors and micropile soldier piles. The foundation package consisted of drilled micropiles. Due to the large scope of work and critical schedule requirements of the project, the JV had to think outside the box and present value engineered alternates to expedite installation durations.

SUBSURFACE CONDITIONS

The project site is located in a geological valley known as the "125th St Fault" (MRCE 2009). Bedrock depth varies greatly throughout the project site, in some areas being over 200ft deep, as a result of this valley being eroded by the force of glaciers and streams. The rock depth is deepest in the middle of the site and slopes up to about 50ft depth at the eastern side of the site, while only sloping up to about 150ft depth at the western side of the site. The soils above bedrock consist of varied arrangements of varved silts and clays, silty sand strata and glacial till strata. The water table ranges from about El +7 to El -1.

© 2019 Deep Foundations Institute

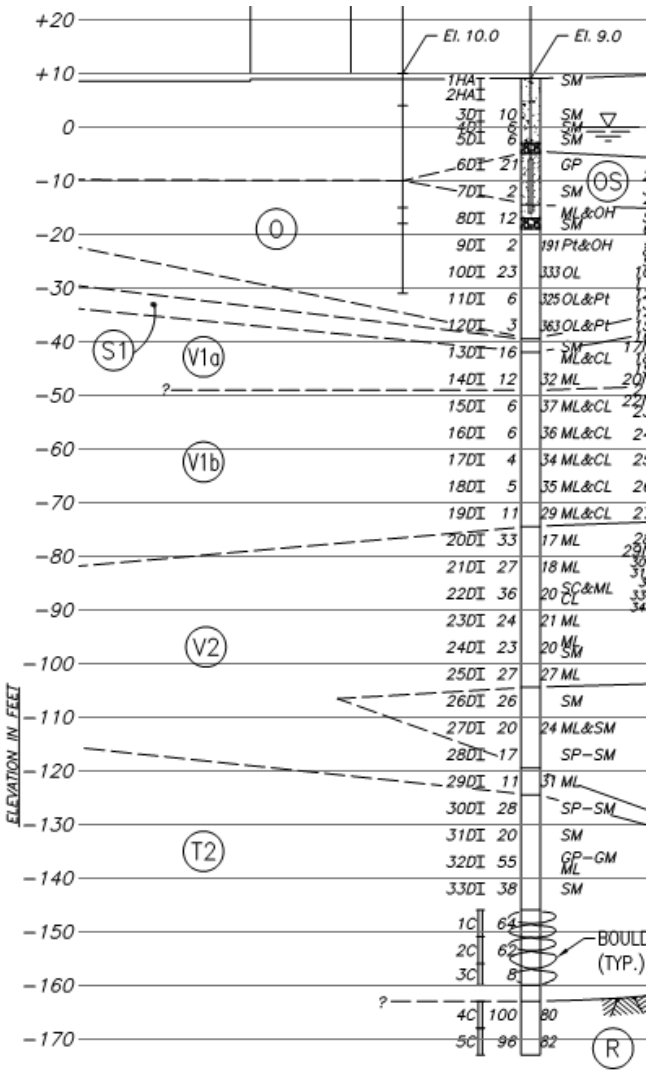


Fig. 1: Typical Geotechnical Boring

The variability of the subsurface profile required an assessment of which technology would be most suitable at various locations throughout the project. For those tieback anchors with high capacities, rock was necessary as the bonding stratum. Wherever soil was utilized as the bonding stratum, the variability of the soils' engineering properties, in particular their bond stress, was a consideration for the appropriate solution. Due to the comprehensive geotechnical investigation program provided in the contract documents, including prior pile load test results and soil/rock profiles that were well delineated across the site, the JV was confident in making well informed decisions in selecting best technology practices.

SUPPORT OF EXCAVATION (SOE)

The SOE had several concerns to consider in order to determine the ideal solutions across the site, so for this paper two scopes will be discussed, Soldier Piles and Tiebacks. The large quantity of 36" diameter soldier piles was a schedule concern if drilled in conventionally with double wall casing. The solution implemented for the soldier pile was an augered cast in place soldier pile. The quantity, capacity and length of the tieback anchors were also major considerations for constructability purposes. Tieback loads exceeded

700 kips with some lengths over 200ft. New equipment applications had to be utilized to handle those challenges.

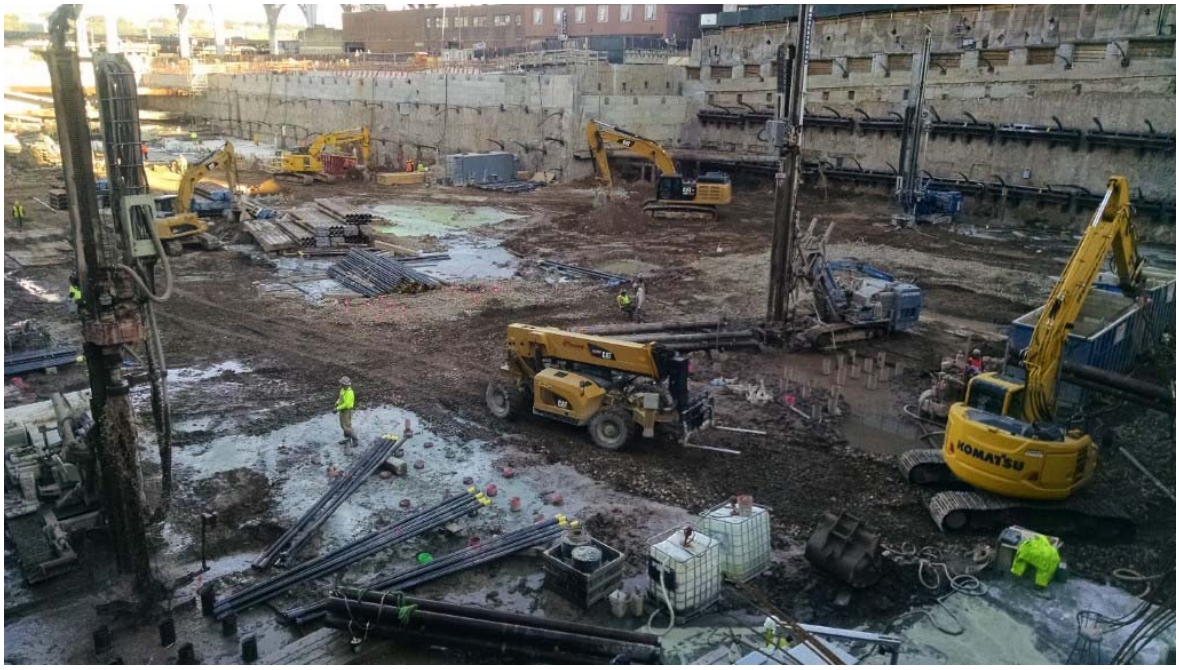


Fig. 2: Site Overview Photo

AUGER CAST SOLDIER PILES

The plans and specifications called for 52 soldier piles along a portion of the South Wall to depths up to 60ft, 41 piles along an Eastern Wall at depths up to 85ft and 8 pin piles at depths up to 100ft to support corner bracing on the Western side of the site. These piles were originally intended to be installed with temporary sectional casing utilizing water to maintain adequate head pressure.

After the SOE package was awarded, the JV reached out to Case for soldier pile pricing due to equipment availability. Case first envisioned using 880mm sectional casing and an oscillator to pull casing, which offered improved production without the need for multiple rigs. However, as the project progressed from bid stage to planning, the idea of a 36" diameter Continuous Flight Auger (CFA) pile gained traction.

The CFA pile option offered several benefits along with some inherent difficulties over the traditional temporarily cased pile. The identified benefits of the CFA pile included increased production, ease of spoils handling, and eliminating the need to handle pumped water during tremie pours. Alternatively, identified limitations for the CFA pile option included increased grout volume and cost versus traditional tremie placed concrete, difficulty of maintaining beam location tolerances, difficulty in drilling through natural or man-made obstructions, and difficulty in penetrating the CFA auger substantially into competent rock.

After thoroughly reviewing the extensive geotechnical information in the contract documents, and weighing the pros and cons of the CFA technique, it was decided to present this SOE pile alternate to the Owner/Engineer. As an added layer of assurance to these parties, the equipment used to install the CFA piles could be reconfigured reasonably quickly to drill caissons utilizing more traditional methods, should the CFA option need to be abandoned due to difficult ground conditions. Should any boulders be encountered, the rig would relocate to the next pile, revisiting skipped piles at the end of the project with

sectional casing methods to core through obstructions. This flexibility, along with potential schedule savings, helped convince the Owner/Engineer to accept the CFA pile option moving forward.

A heavy-duty 36" diameter CFA auger tipped with conical rock teeth for drilling to help penetrate the anticipated till layer was utilized. In order to plunge the soldier piles and maintain beam alignment, ring style spacers were tack welded to the flanges of the beams. These spacers were positioned to either center the pile or offset the pile as required for the SOE design. Proper pre-job planning involved performing extensive laboratory testing on the grout mix and selecting the correct additives. A third-party laboratory determined the best grout mix recipe, including admixtures, for the CFA piles. The mix design was validated when 100ft long beams were plunged into the fluid grout columns for the pin piles.

The end result of the soldier piles was successful installation of CFA piles at all locations within tolerance and ahead of schedule.



Fig. 3: Auger Cast Soldier Pile Installation

TIEBACK ANCHORS

The project included the installation of over 280 anchors. The anchors ranged from 100 kips to over 700 kips and depths ranged from 40 ft to over 200ft. The extreme variability in rock depth, coupled with the high anchor loads, was a challenge on the project. Since strand anchors were utilized, consideration had to be provided to determine anchor order lengths and lead times as the holes were drilled. For the majority of the holes, extra lengths were ordered on the tiebacks and cut to size once the hole was completed.

Permanent casing was installed for the rock anchors. The casing allowed the JV to optimize production and provided a means for sealing a hole into the rock. The crew did not have to expend time and effort extracting casing, which increased production and also increased quality of the anchor due to the relatively large lengths. On several occasions upon seating the casing and drilling out the rock socket, decomposed rock seams were encountered, and remediation measures had to be implemented to ensure the bond length was functional. One method utilized with success was to drill the anchor to completion, then grout the hole while extracting the drill rods and finally wet stick the anchor tendon. The drill rods acted as a tremie for the grout and allowed for no delay between drilling and grouting, thus reducing risk of compromising the bond zone with material inflows.

Given the large casing diameter and long threaded sections (up to 15'), the ability to handle the drill tooling by hand was not an option. Large tooling handlers and grapples were utilized to load the tooling onto the drill rigs. Also, due to the size and lengths of the larger anchors, the JV utilized a strand uncoiler to insert the tendons into the drill holes. For soil anchors, re-grout techniques were applied to increase bond stress and provide a means to mitigate the variable densities that the soils exhibited throughout the site.

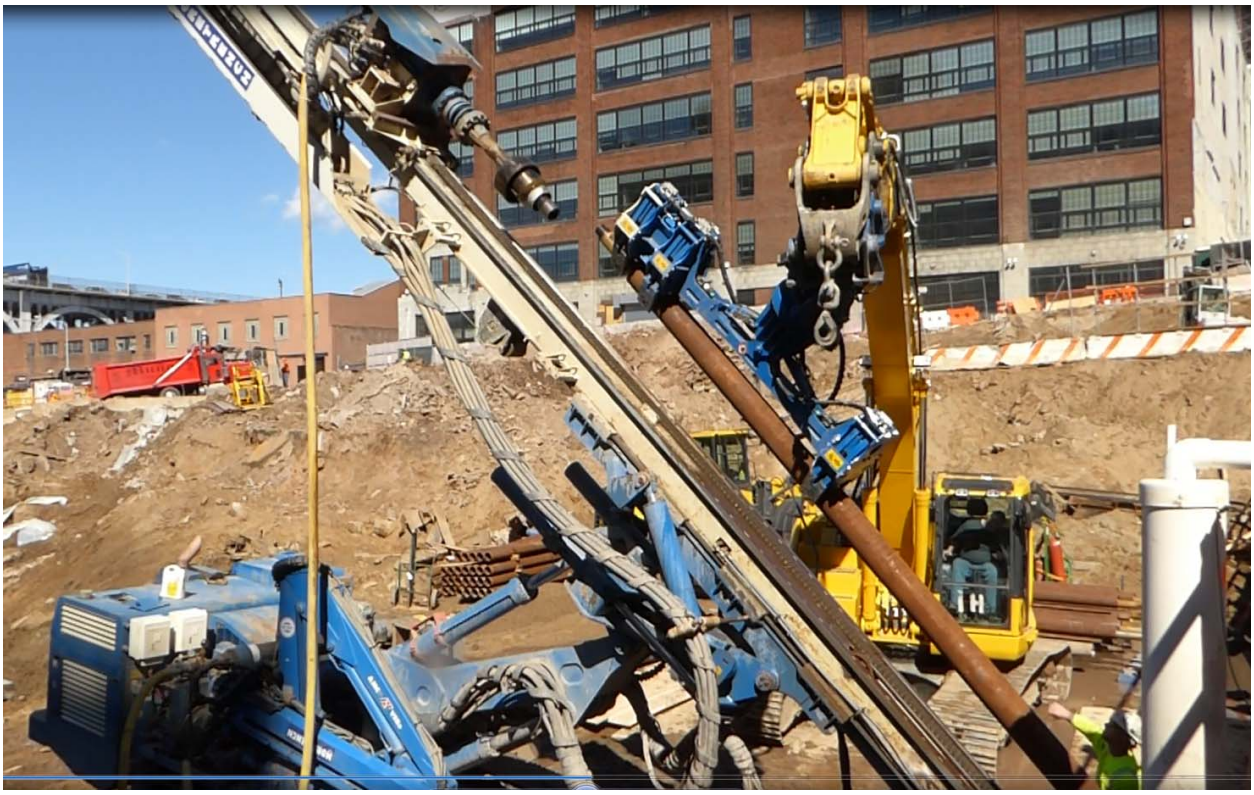


Fig. 4: Tieback Anchor Drilling with Handler

TIEBACK ANCHOR TESTING

The testing of the anchors required knowledgeable personnel to handle the challenges of testing 22 strand anchors. The proper setup of the testing apparatus was important to the efficiency of the testing process. For instance, time spent chipping the slurry wall opening to allow for the strands to spread properly into the wedge plate was warranted prior to setting up the jack assembly. On a few occasions where adequate chipping was not performed, the time and difficulty to perform the test increased greatly. During the setup phase, cutting back the anchor's sheathed length was a task that had to be done with care as well. Once the sheathing was stripped, the grease had to be removed and the strands had to be kept free of any soil or grout that would affect the wedge grip.

Due the larger anchor lengths and associated large elongations during the testing process, a depth gauge was utilized instead of a standard dial gauge to allow for easier measuring capabilities. A 500 ton jack with 24 inches of stroke had to be utilized to account for the large elongations in the strands during the testing process. The Engineer representative on site as an inspector was also knowledgeable in large anchor testing and the testing crew collaborated with the inspector to successfully complete the testing.



Fig. 5: Tieback Anchor Testing Setup

MICROPILE FOUNDATIONS

The original pile design was based on a drilled element with 150-ton compression, 80-ton tension capacity. The pile consisted of 9 5/8" OD x 0.545" wall Gr 35 casing with a full length #28 Gr 75 threadbar and 6,000 psi grout. Two pile details were provided: one for a drilled pile in rock, and the other for a drilled

pile in soil. The former had a min. 35’ cased length with min. 8’ rock socket length, while the latter had a min. 30’ cased length with min. 50’ soil socket length. The site geology dictated that the vast majority of the piles would derive their capacity in soil; approximately 50 piles in the northeast corner were anticipated to be founded in rock.

Eight (8) compression and eight (8) tension load tests were required as part of the QA/QC program. In accordance with NYC Building Code, piles socketed in rock would be video inspected in lieu of load testing.

The JV identified a number of concerns with this original design and detail. First, the compressive capacity was generally high for a pressure grouted pile founded in soil, particularly in some areas of the site where the presence of cohesive soils was more extensive or more variable. Pile creep was a concern during load testing, even if the total pile settlement was tolerable. Second, the work was resource intensive, requiring multiple crews and rigs to meet aggressive schedules. Traditional pressure grouted piles are inevitably slow as an entire pile must be drilled and grouted prior to moving to a new location. Third, the slurry wall surrounding the site did not extend fully to rock, which did not constitute an effective water cutoff, and there was some concern that the piles could be impacted by artesian conditions during their installation.

The JV ultimately proposed a hollow-bar pile as an alternate to the specified pile. This pile alternate, which was accepted by the Engineer and Owner, offered a number of advantages over the more traditional pile element. First, the hollow-bar pile had the potential for scouring the bond zone, creating a larger and rougher bond zone that could increase pile capacity per foot of bond zone. Second, hollow-bar piles can generally be installed at higher production rates than traditional pressure grouted piles, which would alleviate some constraints with regards to crew and equipment needs. Third, the positive fluid head needed when drilling a hollow-bar pile would also reduce the likelihood of any adverse effects from artesian conditions. The pile contractors’ experience on a prior project provided knowledge into the effectiveness of a hollow bar application to an artesian condition versus the detrimental effects an artesian condition could impact bond strength on a conventional duplex drilled bond length.

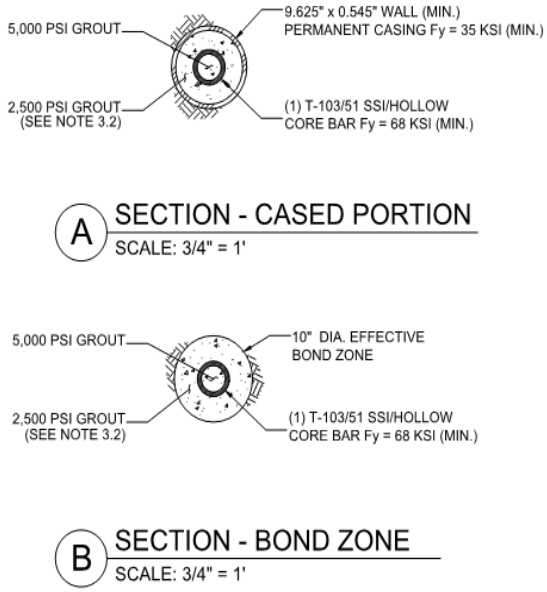


Fig. 6: Cross Section of Micropile

MICROPILE LOAD TESTING

Load testing was required on production piles, although the specific locations were left to be identified by the pile contractor. The pile contractor divided the site into eight (8) tributary areas, each containing approximately 200 piles, and then identified two separate test piles within each area (one for compression and one for tension). Generally, the test piles were installed with 38’ permanent casing and 47’ bond length. The exception was Area 1, where the soils were predominately cohesive throughout the bond zone profile. In this area, the contractor elected to extend the test pile to 59’ bond length based on review of the nearby borings.

The contract documents called for telltales to be installed in the compression test piles, but this was not constructible in the traditional sense since the telltales were not being lowered into a fully cased hole. The telltales would have been damaged or even destroyed as a result of them being affixed to the hollow-bar and drilled in-place. It was alternatively proposed that strain gages (Model 4911) be installed down the middle of the hollow-bar after pile installation (but before the grout had set). Instead of being affixed to the

threadbar, the strain gages had their bar ends machine threaded, so that multiple gages could be coupled in one series and placed at various depths within the pile.



Fig. 7: Strain Gauge Assembly

Each compression test was performed in accordance with ASTM D1143 and the NYCBC, where the maximum test load (200% design load) was maintained for minimum 12 hours. For an acceptable pile, net settlement had to be less than 0.75" and the creep rate during the maximum test load had to be held to less than 0.001" per hour average over a continuous 12-hr period. Seven of the eight compression load tests were successful in meeting the project requirements. The final compression test (Area 8) failed to achieve the design load and had its proven capacity downgraded. Using reliable extrapolation of the probable behavior of the pile based on the actual test result (as allowed by the Building Code), the pile contractor chose to extend the bond zone of all remaining production piles in this area by approximately 9' without the need for an additional load test.

Each tension test was performed in accordance with ASTM D3689, where the maximum test load (200% design load) was maintained for minimum 12 hours. For an acceptable pile, the load movement curve had to stay below the elastic lengthening plus 0.5" offset line and the creep rate during the 200% load hold had to be below 0.01" per hour. All eight tension load tests were successful in meeting the project requirements.

MICROPILE GROUTING

As the start of pile work approached, it became clear that grout service to the individual rigs was a potential choke point in the operation. The contract schedule was based on six rigs consistently working on the project site; two in low-headroom areas and four in open headroom areas. The potential grout demand to support six rigs was extremely high, particularly if all six were simultaneously grouting. Instead, three rigs

were typically allocated to casing installation, while the other three rigs were assigned to grouting tasks. This lessened the grout demand at any one time, and also offered flexibility if one task fell behind.

A large batch plant was erected, consisting of multiple bulk cement silos, agitator (storage) tanks, and pumps to facilitate the mixing and pumping of large grout volumes. The multiple setups within the plant provided equipment redundancy, as grout delivery was critical to the operation. Within the plant itself, one setup was dedicated to mixing an 'initial' or lean grout. This grout had a lower specific gravity and was used to facilitate drilling and maintain borehole stability prior to final pile grouting. Another setup was dedicated to mixing a 'final' or rich grout. This grout was introduced as the bond zone construction near completion, and was used to fully displace the lean grout within the pile. The setups were nearly similar in their erection and operation, and could be switched between making different grouts, if desired.

MICROPILE INSTALLATION CHALLENGES

One main challenge posed by this scope of work was procuring and delivering the materials to the jobsite in a timely fashion. With approximately 60,000 LF casing and 130,000 LF of hollow-bar, mostly procured from sources overseas, it was critical to sequence pile installation to remain productive throughout the work. The materials had several weeks of lead time, so the projections of productivity were made weeks in advance to stay ahead. As the job progressed, the JV found itself sourcing local materials as well to supplement the overseas material shipments so that schedule could be maintained and even accelerated.

Another challenge on the project was restricted headroom piles. The majority of piles were located in areas of unrestricted headroom, but a few hundred were impacted by overhead constraints. On the west side of the site, multiple levels of corner bracing were installed to support the slurry wall and soldier piles and lagging walls as excavation progressed to subgrade. These braces were installed prior to load testing and pile installation, the lowest being as close as 10' above subgrade. On the east side of the site, a number of piles were to be installed under W130th Street, which had been previously supported on caissons as part of an earlier contract. In both instances, the pile contractor needed both a casing and grouting rig capable of working in low headroom conditions. For the west side, a mini-rig was used for casing installation, while a larger rig with custom-built short mast was used for hollow-bar installation. The piles were purposely located clear of the bracing, so that once in position, the mast could be raised vertical and extend above the bracing (alongside of it). For the piles on the east side, mini-drills were used for both casing and grouting of piles.

In the northeast corner of the site near the Studebaker building, bedrock was encountered as shallow as 35' below subgrade before quickly dropping off to the south. The expectation was that multiple rock socketed piles could be drilled in this area prior to grouting them to gain some efficiency, so long as there was no communication between rock sockets. It was soon discovered during pile rock socket drilling that the rock quality was highly variable in this area. Frequent seams were encountered and communication was observed between the sockets of adjacent piles. This led the JV to either advance the casing deeper prior to construction of a new rock socket, or tremie fill the existing socket with neat cement grout (and without the pile reinforcement) and re-drilling it at a later date. In both scenarios, valuable time was lost within the construction schedule and ultimately the decision was made to convert several of these piles to 'soil' piles despite having their bond zone predominately constructed in rock. The bond lengths and drilling techniques for these converted piles matched those used for other soil piles within the same tributary area. Although the socket diameter was slightly smaller when drilling in rock, the Engineer concurred that the enhanced bond stress in rock offset this reduction. It still was a slower process than first anticipated with the presumed shallow rock piles, but provided a level of certainty in its construction.

Spoil handling and disposal were also integral yet challenging parts of the pile operation. The use of air and pneumatically driven down-the-hole hammers were not allowed as part of the pile drilling, so water flush

was used as the main drilling medium. This created large volumes of water, and thus a large effort was made to capture the drill fluid returning up the drill hole (during casing installation) and re-circulate it. Local ponds were excavated near the casing rigs across the site to handle these volumes. In the case of grout spoils, none of the spoils could be captured for re-use, either by the drill rigs or onsite as fill materials. The spoils were captured in large ponds excavated near each grouting rig and were allowed to (at least) harden overnight to be subsequently excavated and hauled offsite. However, in the easternmost areas of the site (Areas 7 and 8), the grout spoils also had the added benefit of being used to help construct a stable working platform. As the spoils overflowed the top of each pile casing, they mixed with the cohesive surface soils and coarse stone aggregate that was previously placed to help stabilize the ground, thus creating a solidified near-surface mass that provided adequate bearing for the drill rigs.

CONCLUSION

Overall, the flexibility that the foundation JV had with the combined experience and resources to handle multiple challenges was instrumental to the success of the overall project. Schedule was expressed as the primary concern for the project team at the early stages of the project and adjustments were made as the project moved along to continually reduce durations on scope items. The foundation schedule was completed 2 months ahead of schedule due to the innovative approaches, commitment of the project team to the schedule and active management of resources.

REFERENCES

Mueser Rutledge Consulting Engineers, MRCE (2009). LRFD Initial Geotechnical Report – Phase 1 Columbia University

FHWA NHI-05-039 (2015). Micropile Design and Construction: Chapter 5, Design for Structure Foundations, Section 5.18.3.

Geotechnical Control Procedure GCP 18 (2015). NY State Department of Transportation Geotechnical Engineering Bureau, Revision #4.

PTI DC35.1-14 Recommendations for Prestressed Rock and Soil Anchors (5th edition) (2014)

PERMANENT EARTH RETENTION FOR DEEP EXCAVATION INSTALLED WITHIN MINIMAL RIGHT OF WAY LIMITS

Christopher J. Ramsey, PE, Wood Environment & Infrastructure Solutions, Inc., Nashville, Tennessee, United States, 615-333-0630, chris.ramsey@woodplc.com

Thomas D. Humbert, PE, Wood Environment & Infrastructure Solutions, Inc., Nashville, Tennessee, United States, 615-333-0630, thomas.humbert@woodplc.com

ABSTRACT

Construction of a new underground parking structure in State College, Pennsylvania, is situated on a site constrained by limited ROW and required excavations ranging in depth from 25 ft to 40 ft. Additional complications included busy surface streets, an active intersection, and numerous underground utilities that could not be disrupted by construction activities. To combat these challenges, an innovative approach for earth retention was designed that combined multiple types of retention systems. The overall system included alternating sections of soil nail walls and a hybrid system of soldier pile walls (consisting of micropiles) that were partially restrained by a soil nail wall in the lower portions of the excavation. Further, due to the limited space within the property limits that inhibited the length of the permanent nails, the wall design team collaborated with the project designers to develop a solution such that the completed wall became an integral part of the final design/construction of the underground parking structure.

INTRODUCTION

HERE at State College is a mixed-use, high-rise building in State College, Pennsylvania. The 12-strory building has up to 3 levels of below-grade parking, with the above-grade levels consisting of residential and commercial/retail space. The existing property was a parking lot bound by the streets Calder Way to the north, Garner Street to the east, East Beaver Avenue to the south, and Heister Street to the west. The overall property sloped approximately 20 ft in elevation from southeast to northwest.

Excavation for the below-grade levels extended 21 ft to 36 ft (6.4 m to 11 m) below street level. During design-development phases of the project, it became evident that due to subsurface conditions and right-of-way limitations, conventional construction techniques would not be feasible. The full perimeter of the excavation would require earth retention including the weak shale bedrock along the bottom of the excavation. The project developer (CA Ventures) and general contractor (Brinkmann) coordinated with the specialty contractor and wall design engineer to find a solution. At this time, Coastal Drilling East (specialty contractor) and Wood Environment & Infrastructure Solutions (wall design engineer) became involved. The project developer and general contractor were aware they needed an earth retention system, but given the many variables the project faced, a single, straightforward solution would not work in this application.

SITE CONDITIONS

Soil depths across the site vary, but are generally shallow in comparison to the planned excavation depth. Sampling auger refusal was achieved between 6.5 ft and 14 ft (2 m to 4.25 m). The overburden consists of very soft to hard clay with varying amounts of gravel. Also cobbles and boulders were frequently noted throughout the overburden portion of the soil borings.

The project site is underlain by karstic dolomite, which is part of the Nittany Formation. The bedrock is notoriously difficult to excavate. Pinnacles present a special problem, and joint/solution channel openings are common. The geotechnical exploration indicated highly weathered zones and zones (typically less than

© 2019 Deep Foundations Institute

two feet in thickness) of more broken bedrock. Apparent open voids were encountered throughout the site, varying in thickness from 6 in to 30 in (150 mm to 760 mm). The voids were located between approximate depths of 16 ft to 37 ft (4.8 m to 11.2 m) below ground surface. Figure 1 depicts a typical soil profile for the project site.

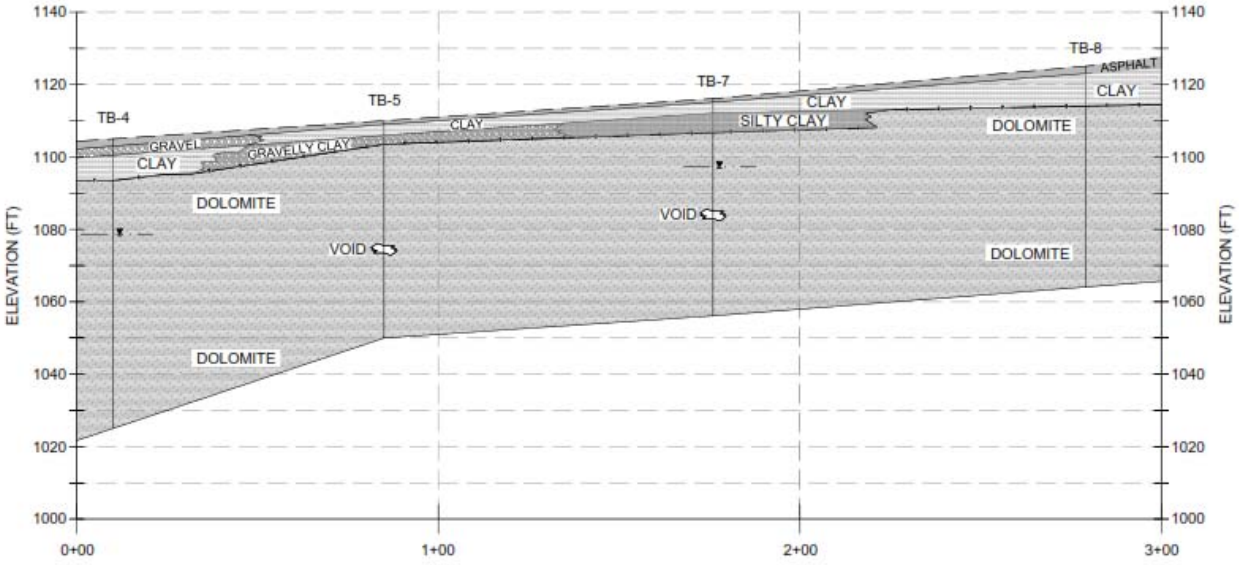


Figure 1 - Typical Soil Profile

The intact bedrock samples were typically hard to very hard, with unconfined compressive strengths ranging from 9,370 psi to 24,820 psi (64.6 MPa to 171.1 MPa).

Groundwater was not encountered at the time of exploration and groundwater was not anticipated to be encountered during construction.

SELECTION AND DESIGN OF EARTH RETENTION

The unique project constraints delegated a hybrid earth retention system for the final project solution. The primary hurdle was the property right-of-way (ROW) limitations. Most of the foundation walls for the project have an 8 ft to 12 ft (2.4 m to 3.6 m) buffer to the proximate ROW, except along STA 1+79 to STA 2+09 on Calder Way, where the ROW is only 5 ft (1.5 m) from the foundation wall.

An additional hurdle was the existing and proposed utilities. Existing utilities were prevalent along East Beaver Avenue and an existing, 66-inch (1675 mm) diameter storm sewer is under Calder Way. Several 60-inch (1524 mm) diameter storm basins were proposed around the site and were planned within 2 ft (0.6 m) of the foundation walls. Most of these conflicts were cleared within the upper 7 ft to 9 ft (2.1 m to 2.7 m). The ventilation shaft near the northwest corner of the building, along Heister Street, would also prove challenging. A site plan with earth retention layout is provided in Figure 2.

Finally, the developer wanted the earth retention system to be a permanent system. That is, the earth retention would serve as the permanent site walls in the final constructed phase of the project.

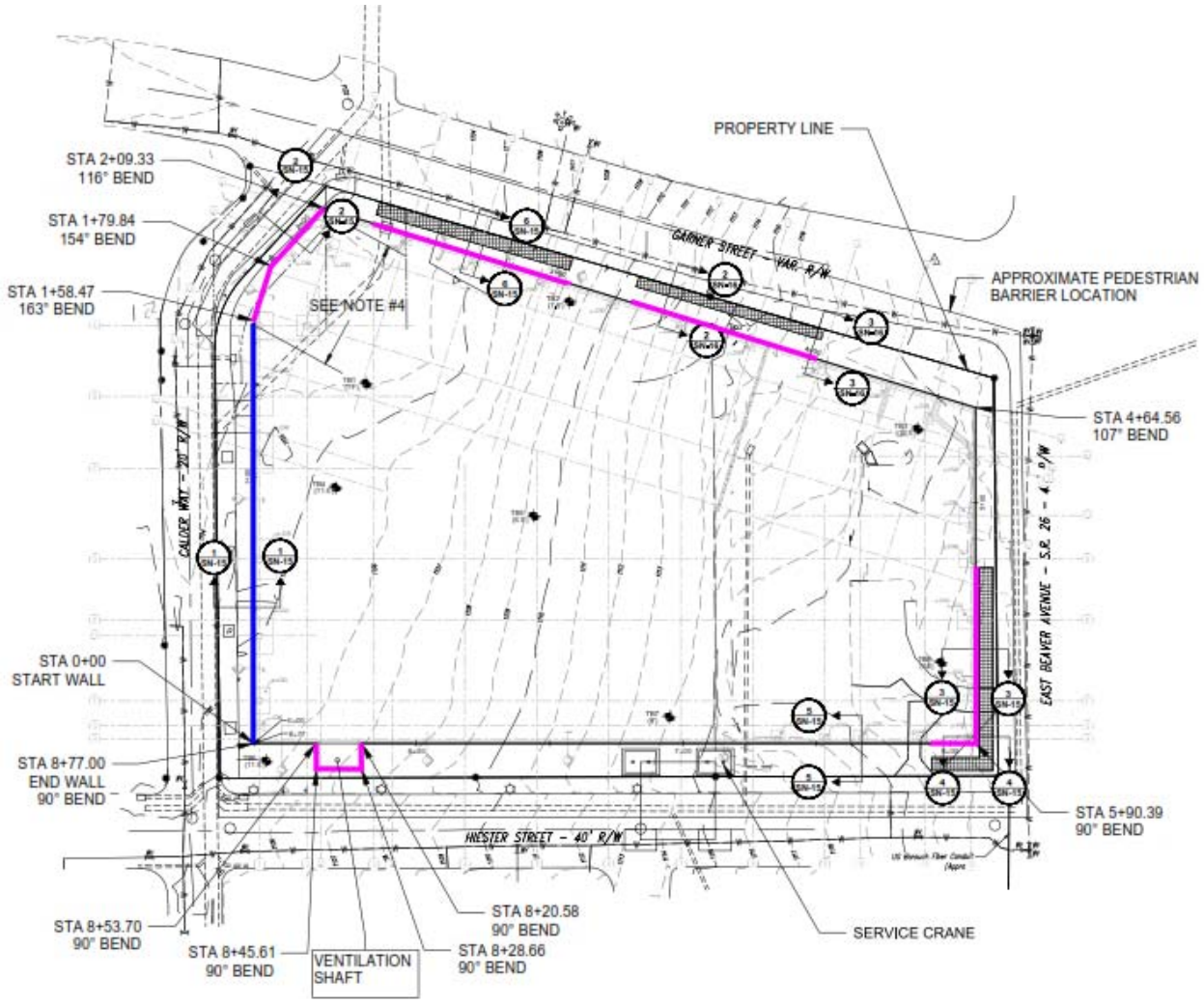


Figure 2 - Overall Site Plan

The initial selected earth retention system design was a soil nailing system with a shotcrete facing. After subsequent conversations with CA Ventures and Brinkmann, it became clear that a permanent system was desired, hence maintaining the soil nail elements within the ROW limits and clear of the utilities could not be achieved with a simple soil nailing approach. Other systems such as traditional soldier piles or secant pile walls were not considered because of potential high construction costs associated with drilling in larger, 24-in to 30-in (600 mm to 760 mm), diameter holes through the elevated rock surface.

Design

In the initial design phase, Wood analyzed several design sections in the full excavated (temporary) condition to determine approximate soil nail lengths. It was evident that soil nails would need to extend beyond the ROW in the temporary condition. The project team coordinated with local municipality to determine and later confirm that temporary nails could extend into the ROW for temporary support.

The final (permanent) condition would be analyzed using brace points from the planned garage floor structure on the inside of the excavation. The permanent condition was analyzed using a minimum continuous line load contribution from the reinforced concrete garage floors at elevations provided by the

building designer. This minimum continuous line load contribution from the planned garage floors allow the reduction of the permanent soil nails to within ROW limitations for the final condition.

In areas where utilities (proposed storm basins and existing storm sewers) or even ROW limitations precluded the use of soil nails, micropile-type soldier piles were designed full depth of excavation. Once excavation depths cleared the utility zone the upper ±10 ft (3 m), soil nails could be used again. This hybrid soldier pile system was also applied in the areas where ROW precluded the use of soil nails in upper layers. Once the excavation encountered rock, the local municipality allowed the use of permanent soil nails to extend beyond ROW, with the understanding that future utilities would not be installed in the bedrock.

The pink lines in Figure 2 indicate the areas that used micropile-type soldier piles due to existing or planned utilities, and near the corner of Heister Street and Calder Way (ventilation shaft). The blue line indicates an area where micropile-type soldier piles were used as part of a re-design due to field conditions encountered. The remaining areas were designed full height with temporary and permanent soil nails only. All areas received a permanent shotcrete facing.

The design included a generalized subsurface profile with material properties found in Table 1. The lean clay represents all the overburden, while the silty gravel represents the broken bedrock and highly weathered rock zone.

Table 1 - Material Properties

Material Description	Unit Weight	Static Strength		Ultimate Bond Strength (psi)
		Cohesion (psf)	Friction Angle (degrees)	
Lean Clay	125	100	20	10
Silty Gravel	130	0	30	40
Dolomite Bedrock	135	250	40	150

Soil Nails

All soil nails were designed and tested in general accordance with FHWA guidelines for soil nails. A 250-psf (12-kPa) surcharge was included atop the wall for a minimum distance of 25 ft (7.6 m) behind the wall, except along East Beaver Avenue (State Route 26), where PennDOT required a minimum surcharge of 350 psf (16.8 kPa) . Overall system stability was analyzed to a minimum safety factor of 1.35 in the temporary condition and 1.5 for the permanent condition. Typical design sections are depicted in Figure 3.

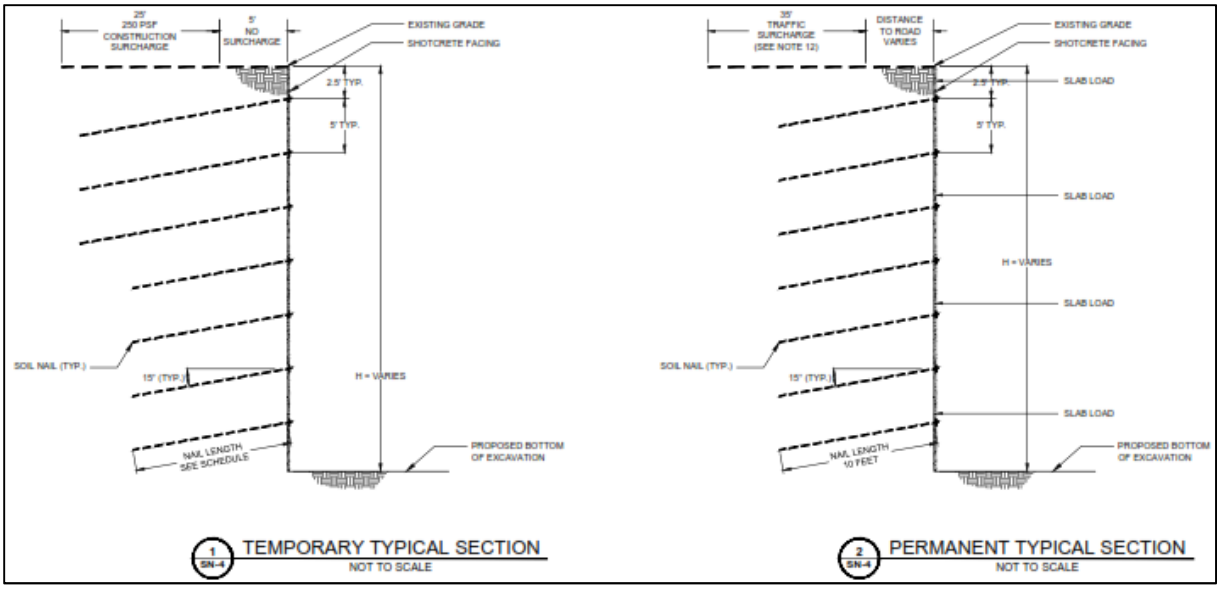


Figure 3 - Typical design sections

Global and internal stability of the soil nail system was check using SNAILZ, by the California Department of Transportation. The estimated nail loads and lengths were determined from analysis iterations for each section to find the critical failure surface.

Global stability was also evaluated using GeoStudio (Slope/W) by Geo-Slope. The reinforcing elements were modeled as "nail" reinforcing and assigned a design load determined during the SNAILZ analyses. The results of both Slope/W and SNAILZ models are compared and the appropriate nail lengths were selected for the final design section.

The relatively weaker overburden material was modeled separately to analyze nail lengths and for local stability, as a staged excavation. Then the overburden was included with the complete design section to determine minimum nail lengths. Temporary nail lengths ranged from 8 ft to 25 ft (2.4 m to 7.6 m) with loads approximately 14 kips to 32 kips (3.1 kN to 7.2 kN). The permanent nail lengths ranged from 8 ft to 10 ft (2.4 m to 3.0 m) with loads approximately 10 kips to 32 kips (2.2 kN to 7.2 kN). Shotcrete was designed with a four-inch initial facing with a seven-inch final facing

Soldier Piles

In areas with the utility and ROW restrictions, the temporary condition using micropile-type soldier piles was designed. The soldier piles were only needed to support the upper 10 ft (3 m). The remainder of the element, while drilled to below the bottom of the excavation, was supported with permanent nails and shotcrete. The upper portion of the wall was modeled as cantilevered to depths of 10 ft (3 m) below grade. At this depth, external loads were modeled where permanent soil nails would be installed, using soil nail loads determined from previous analyses. This design section was analyzed similarly in the permanent condition using external loads from the planned garage floor slabs. Figure 4 shows a typical section of an area that includes the use of the soldier piles and Figure 5 shows a schematic of the design used for the

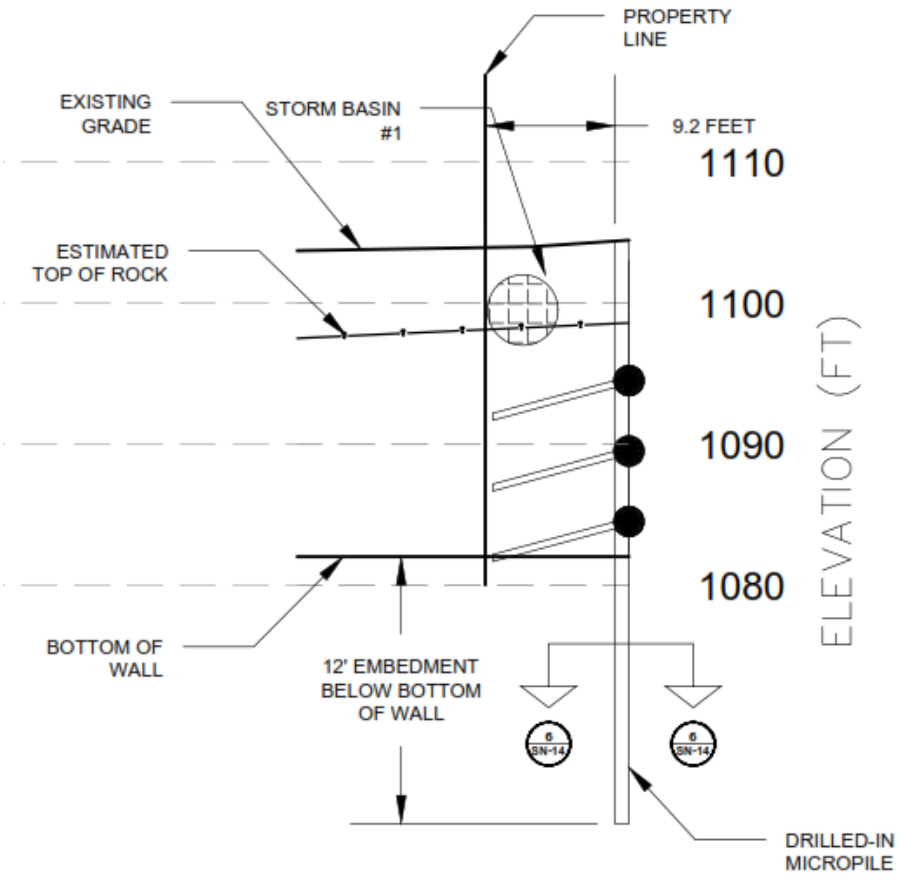


Figure 4 - Typical section with soldier piles

soldier pile system. The soldier pile analyses were performed using Shoring Suite, by CivilTech Software. Soldier piles were sized as 12-inch (300 mm) nominal diameter micropiles internally reinforced with a full-length 9.625-inch (244 mm) diameter casing to account for the threaded joints on the outer casing. All micropile material was 80 ksi (550 MPa) steel.

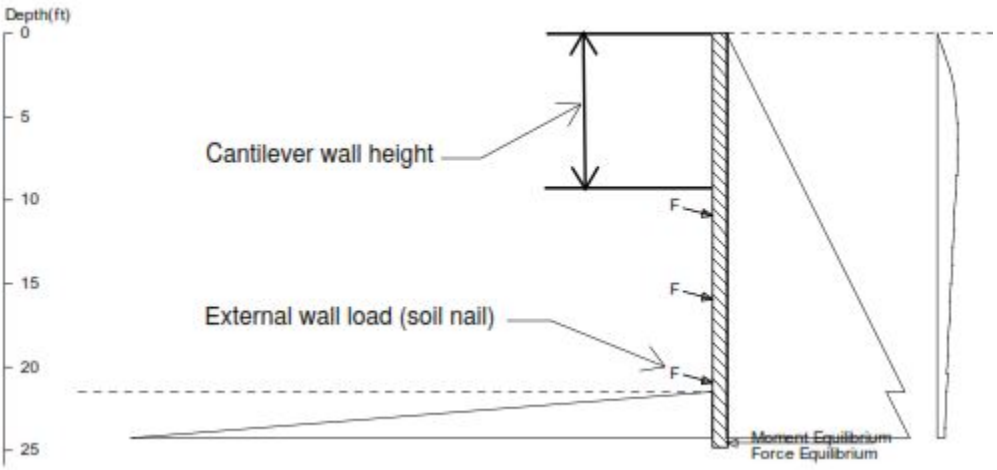


Figure 5 - Schematic loading diagram for soldier pile areas

An additional shotcrete wall facing design was performed to include the connection of the shotcrete to the soldier piles. The facing connection was achieved with shear studs welded to the face of the pile. The ½-inch (12mm) diameter shear studs extended full height of the wall and were 8-inches (203 mm) long, to engage both the initial and final shotcrete facings.

CONSTRUCTION



Figure 6 - Soil nail wall construction along Heister Street

Installation of the earth retention began along East Beaver Avenue. Excavation proceeded in 5-foot lifts to final grade. The excavated soil face was sprayed with a construction layer (initial facing) of shotcrete and then the soil nails were installed after initial set of the shotcrete. The final shotcrete facing was installed after final grade was achieved and placed in 10-foot lifts to allow the shotcrete to adhere to the initial layer while not sloughing. The final facing covers the soil nail anchorages and allows a clean, sprayed finish. Wall drainage was handled with a typical, full-height drain board, extending to weep hole at the base of the shotcrete. The weep hole will tie into a drain tile system under the base slab of the underground parking garage.

There were additional challenges during the construction phase. The cobbles and boulders noted in the borings presented adversities during the shotcrete placement throughout the overburden layer. The same difficulty was met during shotcrete placement within the bedrock layer due to the broken nature of the rock. The irregular excavated face to accept shotcrete placement tested the skills of the specialty contractor to

ensure proper installation with no large voids left behind the wall face. Bringing the wall face to a smooth finish and filling these voids led to overruns of shotcrete material.

Soil nail installation within the upper lifts included both temporary and permanent nails. The temporary nails extended beyond the ROW, while the permanent nails would be installed within ROW limits. Typically, within the bedrock the nails would dually serve in the temporary and permanent conditions. This is because they were only required to be 8 ft to 10 ft (2.4m 3.0 m) long and fit within the ROW. Figure 6 indicates a typical view of the drawing profile, providing the layout for temporary and permanent nails.

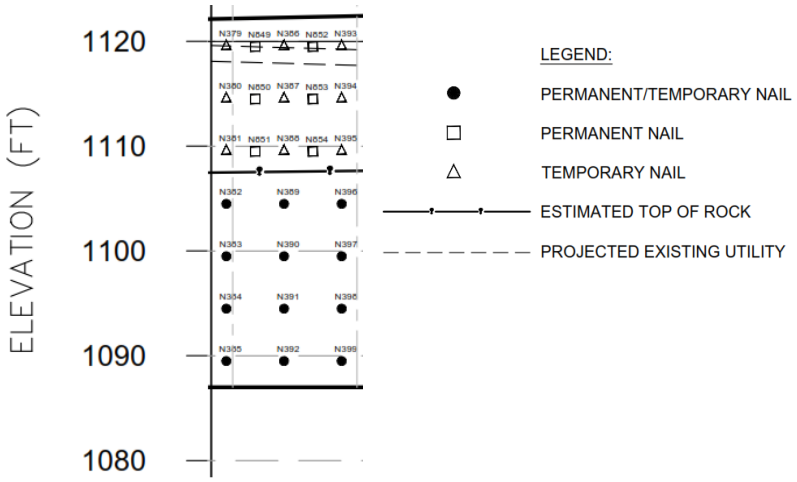


Figure 7 - Typical profile and legend

The boulders and cobbles previously mentioned did not adversely affect the soil nail installation. Nail drilling and grouting were observed and reported to be normal.

The ventilation shaft located on Heister Street near the southwest corner of the site, was situated such that it precluded the use of soil nails. In this area, internal bracing was designed and installed. The bracing coincided with the planned garage floor levels. The lateral support of the wall in this area was provided by the micropile-type soldier piles.

Three locations proximate to the planned foundation walls included the use of a proposed storm basin. In these areas, the storm basin would occupy the upper 10 ft (3 m) of the subsurface profile, thus precluding the use of soil nails. Micropiles were chosen to be used as soldier piles because of the similar equipment used to install the soil nails but also because the limited space that was becoming available along the wall profile.



Figure 8 - Soil nail wall with micropile soldier piles

The temporary and permanent nails were spaced at approximately 3 ft (1 m) centers. This left very little space for a conventional HP or W-section type soldier pile to be installed. The micropiles were selected as the soldier pile element and installed at 6 ft (1.8 m) centers.

The project received approximately 3-inches of rain that caused problematic ground conditions. Project phasing left the wall along Calder Way to be constructed last. The initial excavation in along Calder Way coincided within days of the rain. The specialty contractor discovered saturated ground and that the planned approach to use soil nailing was no longer viable. After attempting to install the first lift of soil nails noticeable movement within the soil nail wall and the sidewalk it was supporting had occurred. An alternate plan was quickly developed.

The alternate plan utilized the cantilevered soldier pile solution being used at locations throughout the project with ROW and utility challenges. Once the soil nail wall was temporarily stabilized by backfilling with an earthen berm, micropile soldier piles were installed immediately behind the shotcrete for the length of the affected area. The piles extended into bedrock, as it was assumed that the saturated overburden would be contained by the bedrock surface. After soldier pile installation, the earthen berm was slowly removed

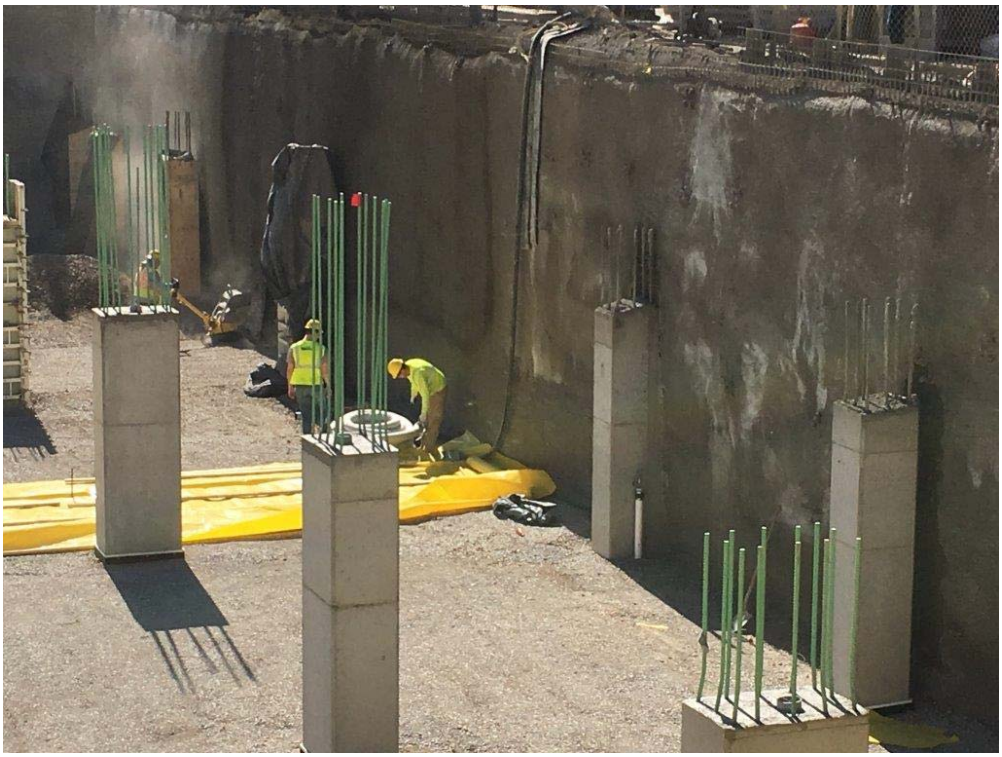


Figure 9 - Completed soil nail wall with building column construction in foreground

and any voids behind the wall were backfilled with low-strength, flowable fill prior to the complete removal of the earthen berm. After verifying the voids had been filled, the soil nail wall was constructed according to design plans.

CONCLUSIONS

The project included excavation depths requiring earth retention within tight ROW and utility easements for depths up to 36 feet. The project required careful coordination with the local municipality, property owners, project design team, and the specialty contractor to successfully implement the temporary and permanent earth retention elements. Given the ROW and utility constraints coupled with difficult subsurface conditions, a combination of conventional soil nail and hybrid soldier pile/soil nail walls were successfully implemented to meet and exceed the project developer's expectations. Cantilever micropile-type soldier piles in conjunction with a conventional soil nail wall allowed the excavation to proceed while staying within the project constraints. Additionally, collaboration between the wall designer and the building designer allowed for a successful design of a 36-ft excavation with permanent soil nails remaining within ROW.

Another takeaway from this project includes the need for open communication between the design teams and the constructors. Subsurface conditions including difficult soil and proximate utilities are hard enough design issues when implementing a single type of conventional earth retention. For this project, some existing utilities were unknown and some of the proposed utility locations changed during both the design and construction phase. All parties on the on the project benefited from the open channel of communication, because issues could be resolved in an efficient manner.

ACKNOWLEDGEMENTS

The authors would like to acknowledge the following organizations who were involved with the project and whose collaboration was invaluable throughout design and construction:

CA Ventures
Brinkmann
Coastal Drilling East

REFERENCES

Civiltech Software, *Shoring Suite, Version 8*, 2007

Geo-Slope International, Ltd., *GeoStudio 2016, Slope/W*, 2016

Lazarate, C.A., Elias, V., Espinoza, D. and Sabatini, P. *Geotechnical Engineering Circular No. 7, Soil Nail Walls*, Report No. FHWA 0-IF-03-017, Federal Highway Administration, March 2003

CASE HISTORY: COMPARISON OF CSL RESULTS TO PHYSICAL OBSERVATIONS

David S. Graham, P.E., Dan Brown and Associates, 205-427-0682, dgraham@dba.world
Paul J. Axtell, P.E., D.GE, Dan Brown and Associates, 913-744-4988, paxtell@dba.world

ABSTRACT

Crosshole Sonic Logging (CSL) non-destructive integrity testing identified anomalous readings near the base of a 6.5-foot diameter drilled shaft rock socket. The anomaly was confirmed to be a defect by subsequent coring and core hole camera inspection. A large void and exposed rebar were visually observed in one of the core hole camera inspections. The center of the shaft was then excavated initially with 3-foot diameter tooling and subsequently with 4-foot diameter tooling as part of the remedial actions to address the defect. While excavating with 3-foot diameter tooling, the shaft defect was not encountered. Excavation with 4-foot diameter tooling revealed the defect, a significant void around the majority of the shaft circumference. The void extended radially from the circumference of the 4-foot diameter excavation to beyond the reinforcement cage to the exposed wall of the rock socket around approximately 80 percent of the shaft circumference. CSL results and observations made during remedial shaft investigation and excavation are in good agreement. The shaft defect, located primarily outside of the reinforcement cage, was effectively identified by CSL testing. Although the defect was confirmed by investigative coring, the remedial excavation demonstrates how the investigative coring could have easily missed the defect. This paper shows how CSL results compare to physical observations made during a rare opportunity to characterize the full extent and nature of a drilled shaft defect originally identified as an anomaly by CSL testing.

Keywords: CSL, Anomaly, Core, Integrity, Remediation, Tremie, Drilled Shaft

INTRODUCTION

The case history presented here pertains to a drilled shaft for a multi-shaft bridge pier in the Midwestern United States. However, the observations presented in this paper are not a result of unique site conditions or the particulars of the project. The lessons learned from this case history are applicable to almost any drilled shaft constructed in the wet.

The overall length of the subject shaft is 22 feet including approximately 12 feet of permanently cased, 7-foot diameter shaft extending to bedrock and approximately 10 feet of uncased, 6.5-foot diameter rock socket. The shaft is designed to resist axial and lateral loads and considers the contributions of side and base resistance in the axial design. Six, 2-inch diameter steel Crosshole Sonic Logging (CSL) tubes are include in the shaft. The bedrock at the shaft location includes beds of sandstone, shale, and limestone. The shaft was drilled using conventional drilling equipment and tooling, and water was used as the drilling fluid. Conventional drilled shaft concrete appropriate for underwater tremie-placement was placed via a 10-inch diameter open hopper tremie.

CSL non-destructive integrity testing identified significant anomalous readings in the approximately bottom 4 feet of the rock socket. 13 of 15 CSL tube combinations tested indicated first arrival time (FAT) delays between 14 and 60 percent and energy reductions between 9.5 and 14.7 dB. An example of the CSL results is included in Figure 1. Tomography analysis of the CSL data was not performed at the discretion of the drilled shaft contractor.

Three core holes were advanced within the interior of the reinforcement cage to further investigate the anomaly. It was not practically possible to perform core drilling outside of the reinforcement cage. The core hole locations were selected by the drilled shaft contractor. Cores 1 and 2 were located with the intent

© 2019 Deep Foundations Institute

of intercepting the most anomalous readings encountered in the CSL. Core 3 was located on the opposite side of the shaft and was intended to intercept the least anomalous readings encountered in the CSL. The core locations are shown in Figure 2. Cores 1 and 2 confirmed a defect in the anomalous zone in the form of little to no drilling resistance, no concrete recovery, and recovery of sand. Core 3 did not encounter the defect. A submersible camera was inserted in Cores 1 and 2. Sand was observed in the bottom of Core 2. A significant void and exposed reinforcement were observed in Core 1. A screenshot from the Core 1 camera inspection video is included in Figure 3.

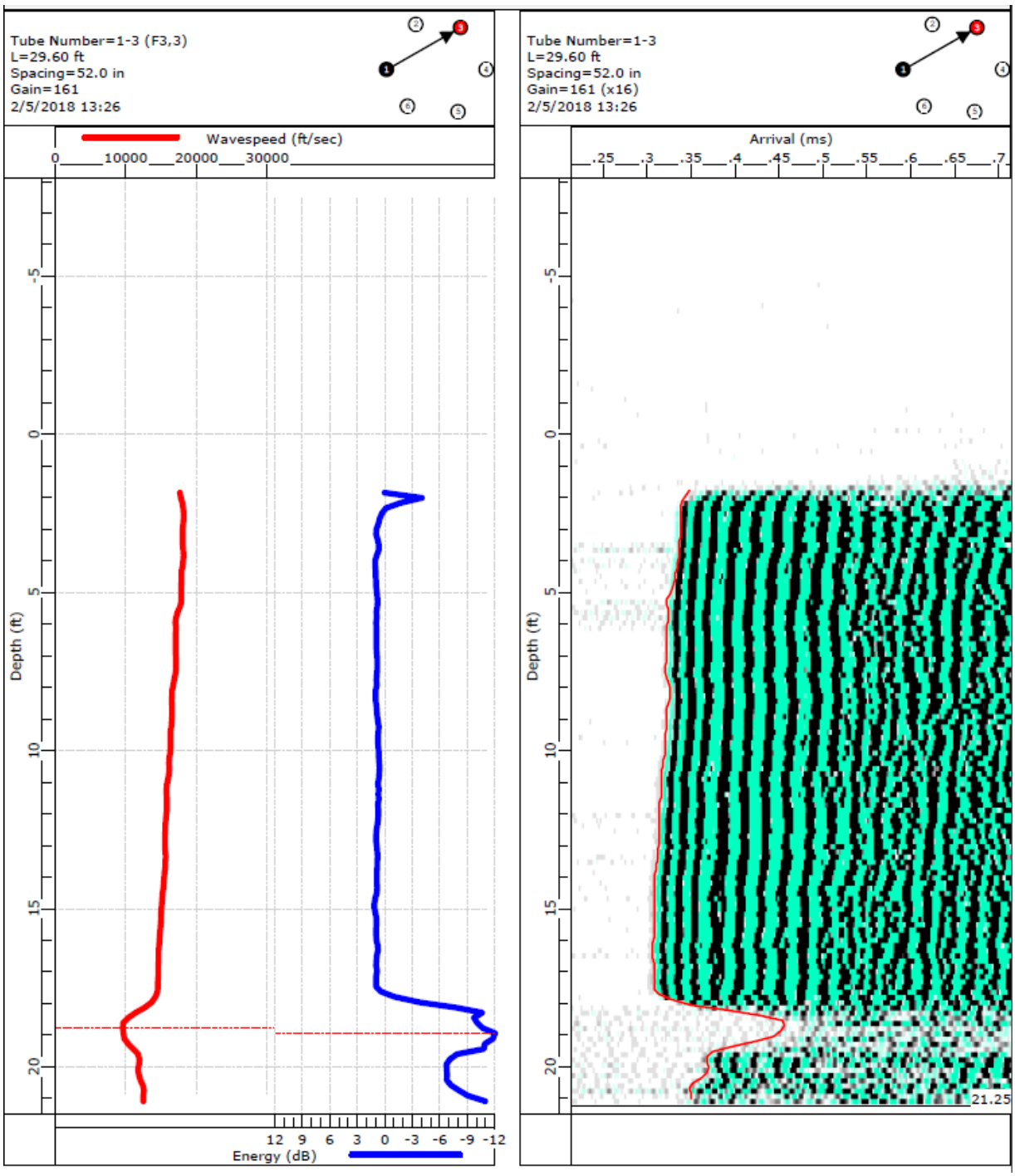


Figure 1. Example of typical CSL results.

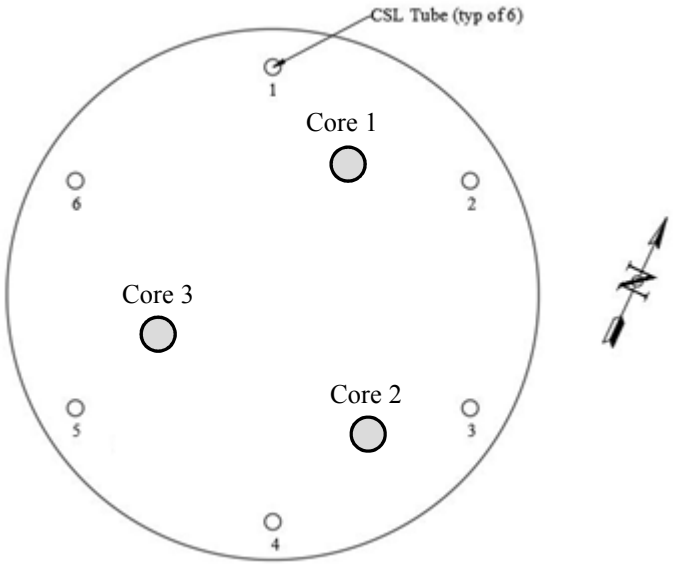


Figure 2. Core and CSL tube locations.

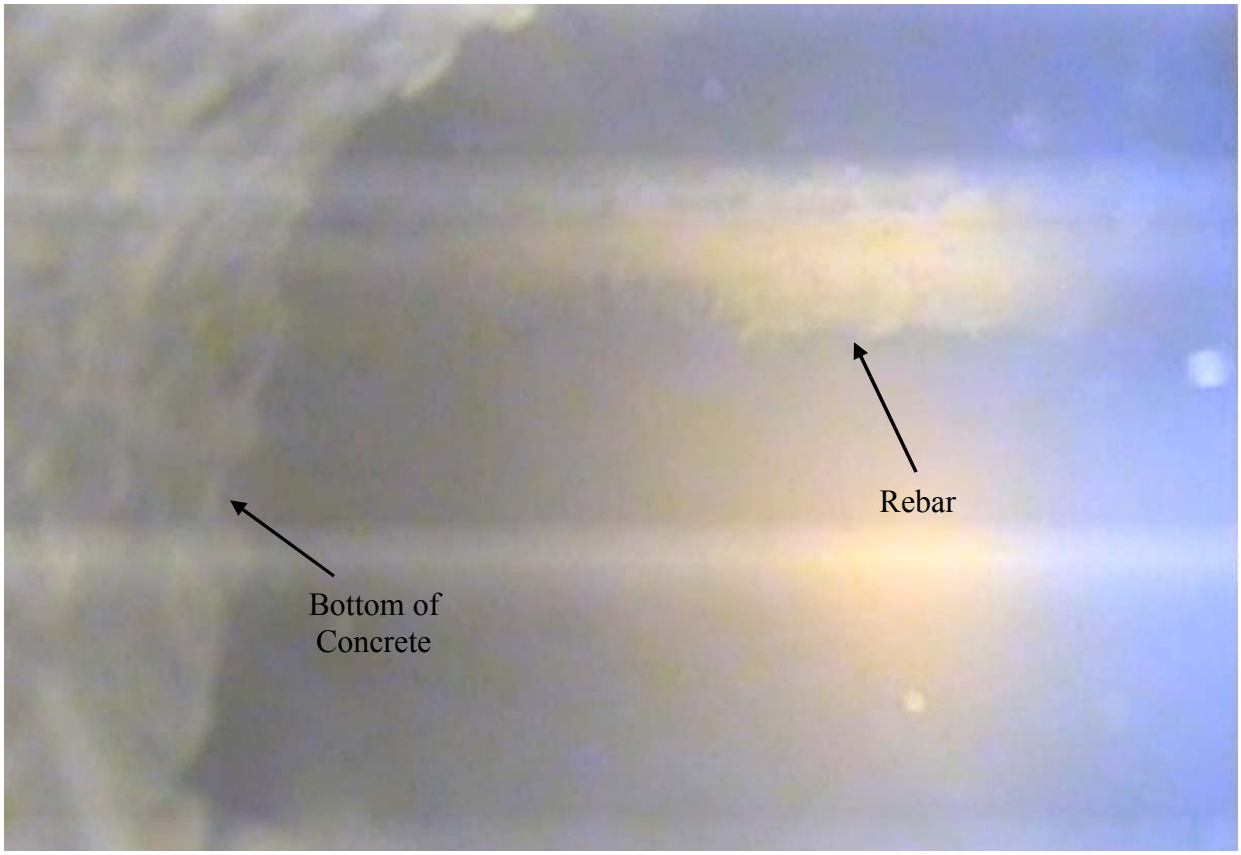


Figure 3. Screenshot from Core 1 camera inspection.

REMEDIAL ACTIONS

An observational method approach was employed during remediation of the shaft. The approach included excavating the center of the shaft to the depth of the anomalous zone and assessing the extent and nature of the defect. In addition to observations of the actual drilling behavior, assessment was to be made on a visual basis either directly under dry conditions or indirect by camera under wet conditions. Remedial actions were then to be determined based on the visual observations.

Initially, the center of the shaft was excavated using 3-foot diameter tooling. The hole was advanced to approximately 2 feet above the shaft tip. The hole was advanced in the dry through the upper approximately 12 feet of concrete. Then, the hole was flooded with water and advanced in the wet to prevent sudden hydraulic infiltration upon encountering the anticipated defect. After reaching the target depth, the hole was slowly dewatered in stages to check for hydraulic infiltration. No significant infiltration was observed and the hole was eventually fully dewatered, allowing for direct visual inspection. No defect was observed. A photograph of the dewatered 3-foot diameter hole is included in Figure 4. Note that there was some water seeping out of Core 1 just outside of the 3-ft diameter hole, as can be seen in Figure 4.

The 3-foot diameter hole was then enlarged using 4-foot diameter tooling in the dry. Upon completion of the diameter expansion, approximately 1.5 foot of water was present in the hole and the top of a void was visible around the circumference of the hole from approximately the 11 o'clock position to the 6 o'clock position, where CSL Tube 1 is the 12 o'clock position (Figure 5). The hole was dewatered as much as possible and visually inspected with a camera (Figure 6). On the basis of the visual observations, pieces of concrete of unknown quality were trapped between the reinforcement cage and wall of the rock socket. Vertically, the top of the void was approximately 4.1 feet above the base of the socket.

To remediate the shaft, a 30.5-foot long, 4-foot diameter socket was extended below the tip of the existing shaft. The new socket replaced the axial side and base resistance provided by the bottom 5-feet of existing 6.5-foot diameter socket, which was neglected for remedial design. The remedial socket included a reinforcing cage with 4 CSL tubes designed by the project's structural designer. The remedial socket was drilled and poured using typical procedures for the project's drilled shafts.



Figure 4. 3-ft diameter excavation.

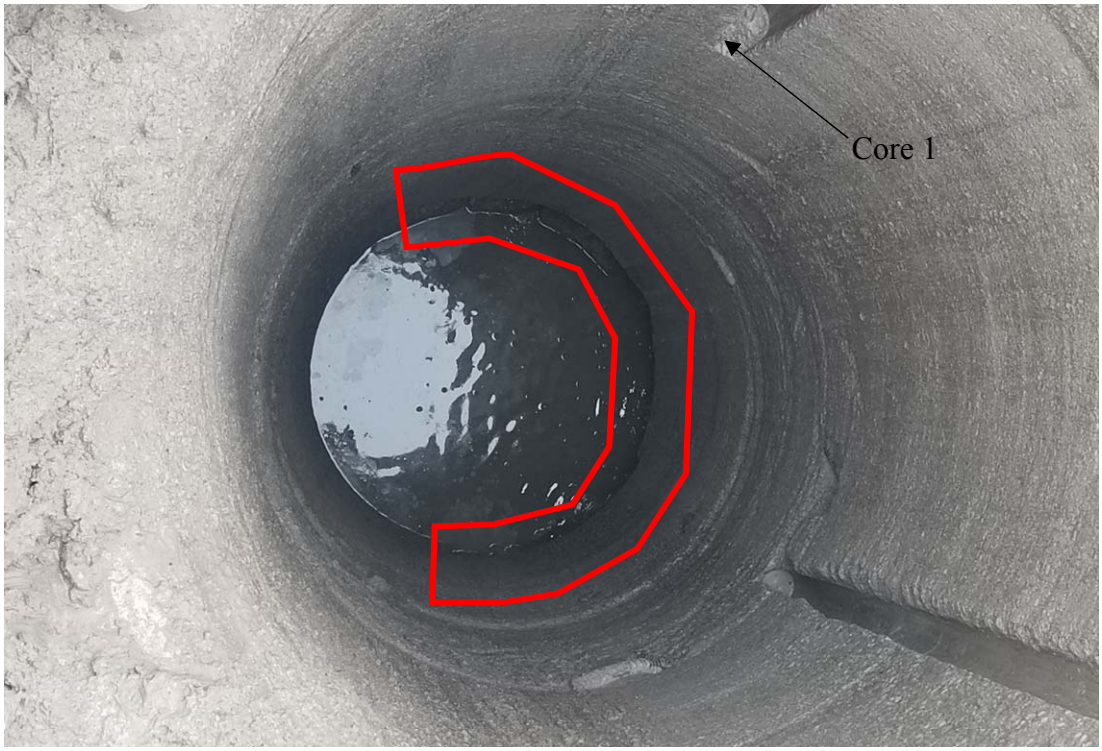


Figure 5. 4-ft diameter excavation, visible void outlined in red.



Figure 6. Camera inspection of side wall, exposed rebar visible.

DISCUSSION

Good agreement exists between the void observed in the 4-foot diameter excavation and the CSL results. This is shown in Figure 7 by comparing the maximum FAT delays between tube pairs and the observed void from Figure 5 super-imposed on the CSL results. Note that from the physical observations, the defect is primarily around outside of the shaft, as the 3-foot diameter excavation did not encounter the defect. Despite the defect being in the zone where CSL is often considered ineffective, CSL successfully detected the defect in this case. Although the results well match the physical observations, it was difficult to predict the nature and extent of the defect from CSL alone. Possibly, tomography analysis of the CSL data would have provided a better prediction of the extent and location of the defect. From the perspective of the drilling contractor, tomography analysis was unlikely to result in reduced remedial cost and was therefore not performed.

Cores 1 and 2 encountered the defect, while Core 3 did not, which also matches well to the physical observations. Had Cores 1 and 2 been performed slightly more towards the center of the shaft, it is unlikely the defect would not have been encountered by any of the cores.

The defect is believed to be the result of either a significant amount of loose material at the base at the onset of concrete placement or mixing of the first load of concrete with water in the shaft. There is no indication in the construction records as to the cause of the defect; however, the location of the defect around the outside of the shaft near the base suggests an issue at the onset of concrete placement based on documented fluid concrete flow patterns (Böhle and Pulsfort 2014 and Brown, Bailey, and Schindler 2005) and numerical modeling of concrete flow (Beckhaus et al 2018). The brown colored (1st batch) concrete in Figure 8 from Böhle and Pulsfort (2014) illustrates this point.

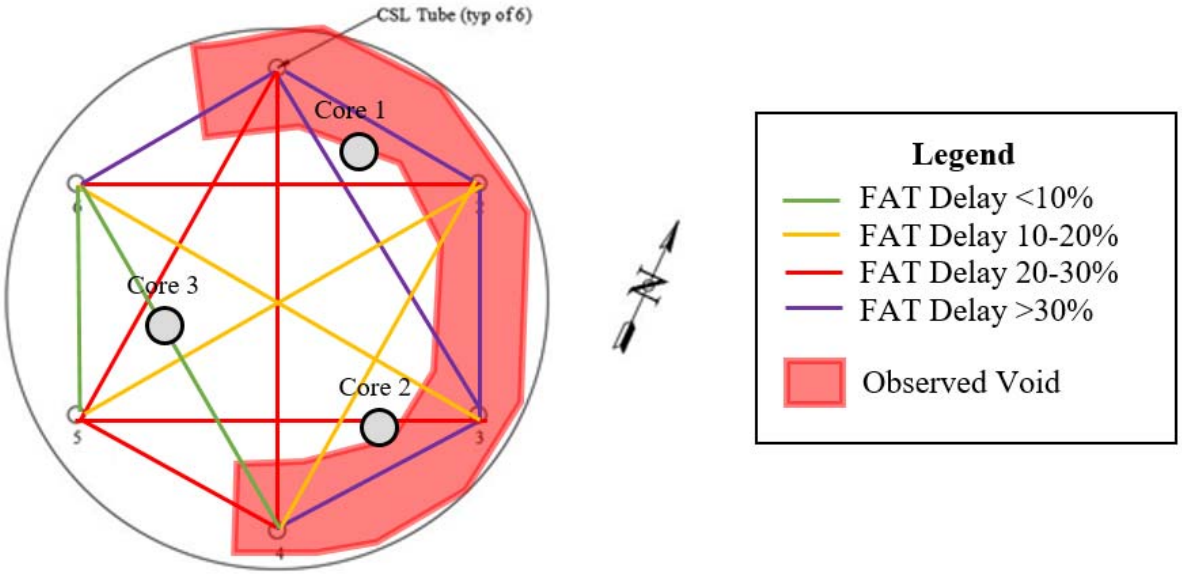


Figure 7. FAT delays with overlay of observed void from Figure 5.

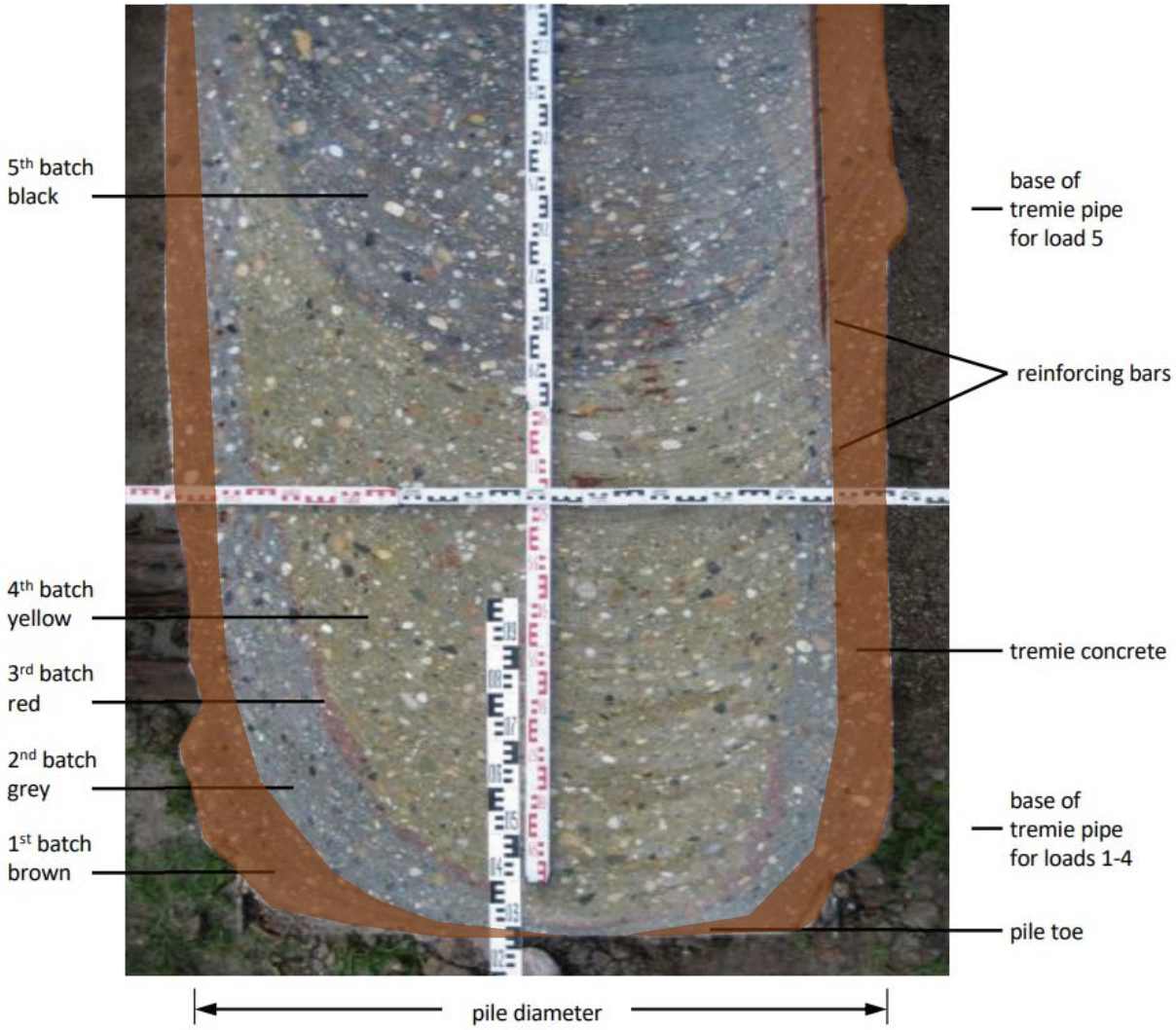


Figure 8. Cross section of a drilled shaft placed with dyed loads of concrete, first batch (highlighted in brown for clarity) approximately corresponded to the location of the defect observed at the case history shaft (Böhle and Pulsfort 2014).

SUMMARY AND CONCLUSIONS

This case history demonstrates that CSL is an effective non-destructive integrity test method for tremie placed concrete in drilled shafts. Based on the current industry understanding of the tremie placed concrete flow, the authors' believe many of the "false anomalies" commonly associated with CSL testing are likely not "false" but rather located around the outside of the shaft where it is difficult to confirm by coring. Additionally, when a poor quality concrete exists directly adjacent to multiple CSL tubes, the CSL results may appear to indicate a defect with a larger cross-sectional area than actually exists, as was the case with the shaft described here.

REFERENCES

Böhle, B. and Pulsfort, M. 2014 “Untersuchungen zum Fließ- und Ansteifverhalten von Beton bei der Herstellung von Beton bei der Herstellung von Bohrpfähle,” 33. Baugrundtagung, DGGT, Berlin, Germany. [English Title: “Fluid and casing supported Execution of bored Piles and their effects on Concrete Flow Behavior”]

Beckhaus, K. et al. 2018. “Guide to Tremie Concrete for Deep Foundations,” 2nd Ed., Joint EFFC and DFI Concrete Task Group, 83 p.

Brown, D., Bailey, J., and Schindler, A. 2005. “The Use of Self-Consolidating Concrete for Drilled Shaft Construction: Preliminary Observations from the Lumber River Bridge Field Trials”, Proc. of ADSC GEO3 QA/QC Conference, Dallas, Texas, 8 p.

COST AND TECHNICAL COMPARISON OF NON-DESTRUCTIVE TEST METHODS FOR DRILLED SHAFTS

Thomas Hyatt, P.E., GRL Engineers Inc., Cumming, GA, U.S.A, 678-371-491, thyatt@grlengineers.com
Daniel Belardo, GRL Engineers Inc., Cleveland, OH, U.S.A, 440-600-411, dbelardo@grlengineers.com
Ronnie Melker, Blythe Construction, Charlotte, NC, U.S.A, 704-375-8474, ronnie.melker@blytheconstruction.com
Joel Webster, E.I., GRL Engineers Inc., Harrisburg, NC, U.S.A, 704-456-7215, jwebster@grlengineers.com

ABSTRACT

Quality assurance of drilled shafts is highly dependent upon the construction practices used during the excavation and concrete placement process. When performed under slurry, challenges are presented in maintaining borehole stability and placing a uniform and continuous concrete column. An integral part of the construction operation is to evaluate the as-built integrity to verify the drilled shaft is capable of safely transferring the required loads to the subsurface. One such case is exemplified by a project involving the expansion of an existing public transit rail line. The expansion required the construction of a new bridge bent supported by seven 5-ft diameter drilled shafts of various lengths. The specifications for the project required both Cross-Hole Sonic Logging (CSL) and Thermal Integrity Profiling (TIP) for drilled shaft integrity evaluation. Both of these post-construction non-destructive tests (NDT) are designed to detect anomalies or the presence of regions with reduced concrete quality. However, the implementation and methodologies of performing each of these NDT methods are significantly different. Cross-Hole Sonic Logging uses ultrasonic signals emitted from a transmitter in one access tube to a receiver in another access tube. Thermal Integrity Profiling measures elevated concrete temperatures during the curing process using embedded thermal wires. Both test methods require different access details and therefore have different costs associated to the contractor or owner to perform. This paper provides a detailed comparison of these NDT methods as performed on these seven drilled shafts. The associated financial and time costs to perform each method are compared and the results are discussed in detail.

Keywords: Cross-Hole Sonic Logging, Thermal Integrity Profiling, cost analysis, quality control

INTRODUCTION

Drilled shafts are a fundamental deep foundation element that can be designed to resist large bending moments as well as to transfer large compressive axial loads through weaker upper soils to competent soils or rock below. Often times when the upper soils are very soft, lateral support by casing or slurry, or a combination of both, may be used to hold back the softer soils from collapsing into the hole before concrete has been placed. Due to the blind nature of drilled shaft construction and the qualities issues that may arise during the placement process, it is essential for design engineers to specify non-destructive testing (NDT) to assess the quality of the as-built drilled shaft. CSL and TIP testing are two NDT methods designed to detect areas of lower quality concrete or soil inclusions throughout the length of the drilled shaft and determine its overall quality. Each method uses different technologies and methods to achieve the results required to determine the as-built condition of the drilled shaft.

Both CSL and TIP test methods have unique monetary costs that are specific to each test. CSL testing requires the purchase and installation of access tubes to the reinforcing cage. After the testing is complete, it is generally required that each access tube be post-grouted. TIP testing requires the purchase and installation of Thermal Wire® cables onto the reinforcing cage. Time is another major factor in the

© 2019 Deep Foundations Institute

construction industry and both CSL and TIP require a specific amount of time after placement before the results of the test can be analyzed. CSL testing requires that the concrete in the drilled shaft has reached sufficient strength in order to transmit the ultra-sonic pulses from the transmitter to the receiver through the concrete as described by Webster, K. (2011). The time specified before a CSL test can be performed ranges from three to seven days after concrete placement. The time required for the concrete to obtain an acceptable strength is highly dependent on the cement content, aggregate, and the combination of admixtures in the concrete mix design. TIP testing also requires time after the concrete placement and for the hydration process between the cement and water to reach the peak temperature before the results can be analyzed. The window for TIP analyses is between the time of half peak temperature and peak temperature. The time required to reach the peak temperature is a function of the diameter of the shaft, cement content, aggregate, and admixtures in the concrete mix. The hydration process reaching peak temperature usually occurs between ten to forty-eight hours after concrete placement, although this time can be longer, especially in cases where retarders are used.

Different agencies have different acceptance criteria for both CSL and TIP that must be satisfied in order to categorize the drilled shaft acceptable. For this project the criterion for CSL testing is based on categories as described by Webster, K. (2011), with the categories of Good and Questionable concrete being acceptable, Poor/Flaw at the discretion of the engineer of record, and Poor/Defect requiring further methods of investigation. The TIP criterion for this project was based on the criteria discussed by Piscsalko, G. (2016) which states that if cover criteria is met and a 0% to 6% effective radius reduction is observed then the shaft is considered Satisfactory (S). If cover criteria is not met or if an effective average radius reduction of greater than 6% of the nominal radius is indicated the shaft is categorized as Anomaly (A) and requires further methods of investigation. During the testing on this project, multiple CSL and TIP analyses showed evidence of the presence of potential anomalies which will be discussed later in this paper.

FINANCIAL COST COMPARISON

CSL and TIP testing both have different requirements and methods for data acquisition. CSL requires multiple steel access tubes be installed along the length of the reinforcing cage and extending a reasonable distance above the top of the shaft. The number of tubes required is equal to the diameter of the shaft in feet. For this project the drilled shafts tested were five-foot diameter shafts that ranged in lengths from 60.8 to 75.6 feet of embedment. CSL tubes are typically purchased in 21 foot sections and spliced together using union couplings, which is included in the cost of the 21 foot section, to achieve the desired length of the reinforcing cage plus the required stick-up to ensure there is enough tube length extending above the top of the drilled shaft to properly run the test. Each tube also requires the installation of a cap on the tube at the base of the drilled shaft. After CSL testing is complete post grouting is generally required to fill the CSL tubes.

Similar to CSL, TIP requires that Thermal Wire® cables be installed along the length of the reinforcing cage. The same standard applies to Thermal Wire® cables as CSL tubes in which the number of cables required is equal to the diameter of the drilled shaft in feet. Table 1 below summarizes the consumables purchased for this project for each drilled shaft in order to perform both CSL and TIP testing.

Table 1. Total Quantities of Consumables Required to Perform CSL and TIP Testing.

Drilled Shaft Identification		Shaft 1	Shaft 2	Shaft 3	Shaft 4	Shaft 5	Shaft 6	Shaft 7
Length of Drilled Shaft	ft.	64.5	69.3	67.9	65.4	60.8	60.9	75.6
Number of 21ft CSL Tube Sections (each section includes coupler)	qty.	20	20	20	20	15	15	20
Number of Caps	qty.	5	5	5	5	5	5	5
Required No. of Thermal Wires	qty.	5	5	5	5	5	5	5
Total Linear Feet of Tube	ft.	420	420	420	420	315	315	420
Total Linear Feet of Cable	ft.	350	350	350	350	350	350	400

To estimate the total cost to the project for the installation of CSL and Thermal Wire® cables, a range of unit rates for this project have been provided for use in this paper. For the purposes of estimating the cost associated to both the consumables and labor to install the required access method the average of the unit rate was used. Table 2 below details the range of reported unit rates, the average unit rate used in the analysis, and associated cost per shaft.

Table 2. Summary of Consumable and Labor Costs Associated to Install CSL Tubes and TIP Cables

	Range of Unit Rate (U.S. Dollars)	Average Unit Rate (U.S. Dollars)	Shaft 1	Shaft 2	Shaft 3	Shaft 4	Shaft 5	Shaft 6	Shaft 7
CSL Tube Cost per LF	$6.00 - $7.00	$ 6.50	$2,730.00	$2,730.00	$2,730.00	$2,730.00	$2,047.50	$2,047.50	$2,730.00
CSL Cap cost	$9.50 - $10.00	$ 9.75	$ 48.75	$ 48.75	$ 48.75	$ 48.75	$ 48.75	$ 48.75	$ 48.75
CSL Install Cost per Tube (Labor)	$135.00 - $145.00	$ 140.00	$ 700.00	$ 700.00	$ 700.00	$ 700.00	$ 700.00	$ 700.00	$ 700.00
CSL Post Grouting per LF	$3.15 - $3.25	$ 3.20	$1,120.00	$1,184.00	$1,180.80	$1,184.00	$1,012.80	$1,011.20	$1,350.40
Total Cost per Shaft for CSL Tube	-	-	**$4,598.75**	**$4,662.75**	**$4,659.55**	**$4,662.75**	**$3,809.05**	**$3,807.45**	**$4,829.15**
TIP Wire Cost per Foot	$4.00 - $6.00	$ 5.00	$1,750.00	$1,750.00	$1,750.00	$1,750.00	$1,750.00	$1,750.00	$2,000.00
TIP Connector	$20.00 - $30.00	$ 25.00	$ 125.00	$ 125.00	$ 125.00	$ 125.00	$ 125.00	$ 125.00	$ 125.00
TIP Wire Install (Labor)	$115.00 - $125.00	$ 120.00	$ 600.00	$ 600.00	$ 600.00	$ 600.00	$ 600.00	$ 600.00	$ 600.00
Total Cost per Shaft for TIP Wire	-	-	**$2,475.00**	**$2,475.00**	**$2,475.00**	**$2,475.00**	**$2,475.00**	**$2,475.00**	**$2,725.00**

The respective total cost for the CSL and TIP consumables and labor is summarized in Table 3. Comparing the installation costs from CSL and TIP testing, there is a potential cost savings of approximately $13,454 U.S. Dollars if only Thermal Integrity Profiling would have been specified for this project. This potential cost savings could reduce the material cost of integrity testing of the drilled shafts by approximately 43% if only TIP testing is specified.

Table 3. Total Cost of Consumables and Labor for Project to Install CSL Tubes and Thermal Wires

	Cost in U.S. Dollars
Total Cost of Consumables and Labor for CSL Tubes	$ 31,029.45
Total Cost of Consumables and Labor for Thermal Wires	$ 17,575.00
Cost Difference	$ 13,454.45
Cost Percentage Difference	43%

ENGINEERING COST COMPARISON

Along with the material costs that are associated with both CSL and TIP testing, there is also the cost of equipment used to collect the data and perform the subsequent analyses. CSL and TIP data are collected in two separate manners. For CSL testing, a trained and qualified person is required to mobilize to the job site and physically collect each of the profiles to be analyzed for each drilled shaft needing testing. For TIP testing a qualified person must mobilize to the site for the first shaft to be tested in order to train onsite personnel, typically consisting of the driller or contractor's crew, on how to install the Thermal Wire® cables. During this initial training the equipment operation, required installation details, and recommended best practices are also covered. Once the data loggers are connected, they transmit the data via cellular connection to a cloud server. After the initial site visit and training, onsite personnel are able to independently install the cables and connect the data loggers so that the engineer can remotely download and analyze the data.

For this project there were a total of seven trips to the job site in order to collect the CSL data and one trip to the site in order to train the driller/contractor on how install the Thermal Cables and attach the data loggers. When including equipment costs, engineering time, travel expenses, and reporting fees for the seven drilled shafts tested the cost per shaft break down is shown in Table 4.

Table 4. Summary of Average Cost for Equipment, Engineering Time, Expenses, and Reports

Test Type	Average Cost per Shaft	Total Cost for 7 Shafts
CSL	$ 1,845.00	$ 12,845.00
TIP	$ 608.50	$ 4,260.00

TIME COST COMPARISON

Installation and data collection are not the only associated costs to a project with NDT testing. Another major factor to be considered when deciding to specify a preferred NDT method is the time impact to the project schedule. As mentioned previously, CSL and TIP both require a certain amount of time before each test can be performed and the results can be analyzed. For this project, CSL testing specifications required the contractor to wait 7 days before the CSL testing could be performed. TIP testing also requires a certain amount of time for the hydration process in the concrete to reach the peak temperature at which time the data is analyzed. Table 5 below summarizes the dates when the drilled shafts were placed as well as the dates when initial CSL testing and TIP testing were performed and analyzed.

Table 5. Summary of Dates for Installation, TIP Testing, and Initial CSL Testing

	Shaft 1	Shaft 2	Shaft 3	Shaft 4	Shaft 5	Shaft 6	Shaft 7
Date Drillled Shaft Installed	5/24/2018	5/22/2018	5/15/2018	5/10/2018	5/8/2018	5/1/2018	4/25/2018
Date of TIP Analysis	5/25/2018	5/23/2018	5/16/2018	5/11/2018	5/9/2018	5/2/2018	4/26/2018
Date of Initial CSL Analysis	5/30/2018	5/30/2018	5/23/2018	5/17/2018	5/17/2018	5/4/2018	5/2/2018

For this project the average time for the concrete mix design to reach the peak temperature was 20.1 hours after concrete placement. The average time at which point initial CSL testing could be performed for this project was 6.9 days or 164.6 hours after concrete placement. Table 6 below summarizes the time difference in hours and days for each of the drilled shafts tested with TIP and the initial CSL with regards to the dates in Table 5.

Table 6. Summary of Time Differences per Drilled Shaft Between TIP and CSL Results

	Time	Shaft 1	Shaft 2	Shaft 3	Shaft 4	Shaft 5	Shaft 6	Shaft 7	Average
Time difference between TIP and CSL Results	hrs	125.5	176	171	146.75	197.5	52	142.75	144.5
	days	5.2	7.3	7.1	6.1	8.2	2.2	5.9	6.0

The average time difference between shaft installation and when the results can be analyzed has a potential time savings for this project of approximately 6.0 days or 144.5 hours per shaft. Using TIP results solely to determine the acceptance or rejection of the drilled shafts for this project would allow the owner and contactor to move forward with the next project activity earlier than if using CSL either in conjunction with TIP or solely. For drilled shafts that do not meet the acceptance criteria this would allow both the owner and the contractor more time to plan for further investigation and or allow remediation efforts to begin sooner.

CSL AND TIP RESULTS COMPARISON

CSL uses ultra-sonic pulses transmitted from a transmitter probe through the concrete and picked up by a receiving probe. By measuring the distance between the CSL access tubes at the top of the drilled shaft and measuring the time at which the signal first arrives at the probe it is possible to calculate an average first arrival time (FAT) through the drilled shaft. By comparing the FAT at different locations to the overall average FAT it is then possible to find potential anomalies in the concrete. TIP testing measures the temperature increase from the hydration process of the cement and water reaction. Data loggers measure the temperature versus depth at 15 minute intervals until peak temperature is reach or until the data loggers are disconnected. The user selected thermal profile between half peak temperature and peak temperature is then used in the analysis along with the reported volume of concrete placed. The volume placed is an integral part of the analysis as it is used to calculate an effective radius. The effective average radius, effective local radii, and cage alignment are assessed in the analysis.

When CSL testing is performed before the concrete has reached a sufficient strength to pass the ultra-sonic pulse the results can be skewed and an inexperienced engineer can determine that the CSL results are unsatisfactory. In an attempt to try to speed up the time from when the concrete was placed and when CSL tests were performed Shaft 6 was tested with CSL after only 2.2 days of concrete curing. The results showed indications of anomalies due to the insufficient concrete strength required for CSL testing to be performed.

CSL testing was then performed again approximately 8 days after concrete placement. At this time, the concrete had sufficient time to gain strength and the CSL results showed no anomalies. Table 7 below presents a summary of CSL and TIP results indicating whether the test reported an anomalous zone or not. The table also shows which drilled shafts were re-tested with CSL testing and the conclusions of the re-test. Seven TIP tests were performed while ten CSL test were performed, including the retesting of Shafts 2, 3, and 6.

Table 7. Summary of Test Results for TIP and CSL

Type of Test	Initial Testing							Re-Test		
	Shaft 1	Shaft 2*	Shaft 3**	Shaft 4	Shaft 5	Shaft 6	Shaft 7	Shaft 2*	Shaft 3	Shaft 6
Anomaly Indicated by CSL Testing	No	Yes	Yes	Yes	No	Yes	No	Yes	No	No
Anomaly Indicated by TIP Testing	No	Yes	Yes	No	No	No	No	-	-	-

*Shaft 2 was required to have further investigation after CSL retest

**Shaft 3 had a reported volume that was 90% of the theoretical volume, later it was determined that the scales at the batch plant were incorrect. No further investigation was required for Shaft 3

The two most concerning results are those of Shafts 2 and Shaft 3. The CSL results for Shaft 2 and Shaft 3 indicated anomalies in the bottom 3.5 feet of the shafts. The TIP results for Shaft 2 indicated a reduction in the effective average radius greater than 6% in the bottom 2 feet. The TIP results for Shaft 3 indicated a reduction in the effective average radius greater than 6% from a depth of 23 feet to a depth of 50 feet below the top of shaft. While Shaft 3 was initially a concern, a CSL retest did not indicate FAT delays. It was determined that the recorded volume placed was incorrect due to an issue with a scale at the batch plant. With the concrete volume placed updated the TIP results did not show evidence of an effective average radius reduction. Thus, Shaft 3 was accepted as is with no further investigation required. The results for Shaft 2 and remediation efforts are further discussed in the following section.

SHAFT 2 - CSL AND TIP RESULTS

CSL results for Shaft 2 indicated FAT delays of 100% in six of the ten profile combinations and FAT delays greater than 30% in the remaining four profiles. The TIP results for Shaft 2 indicated that three of the five cables had a 6% reduction in the effective local radius from 2 to 4 feet above the drilled shaft base, while the remaining two wires had greater than a 6% reduction in effective local radius approximately 1 foot above the drilled shaft base. Part of the TIP analysis involves applying a bottom of shaft adjustment to account for the temperature roll-off to the soil or rock below a shaft. This adjustment is necessary as the base of the shaft represents an additional boundary for heat dissipation. A similar adjustment is applied to the temperature roll-off observed at the top of a shaft. After these adjustments were applied the TIP results indicated an effective average reduction of greater than 6% in the bottom 2 feet of the shaft. Figure 1 shows the reported TIP results in terms of effective radius versus depth. Figure 2 shows a representative sample of the initial CSL results obtained and reported. While the data in Figure 1 appears to be a typical roll-off heat signature the roll-off occurs earlier than what the theoretical model would suggest based adjustment parameters at the bottom of shaft. This early roll-off indicates a zone of lower quality concrete at the base of the shaft.

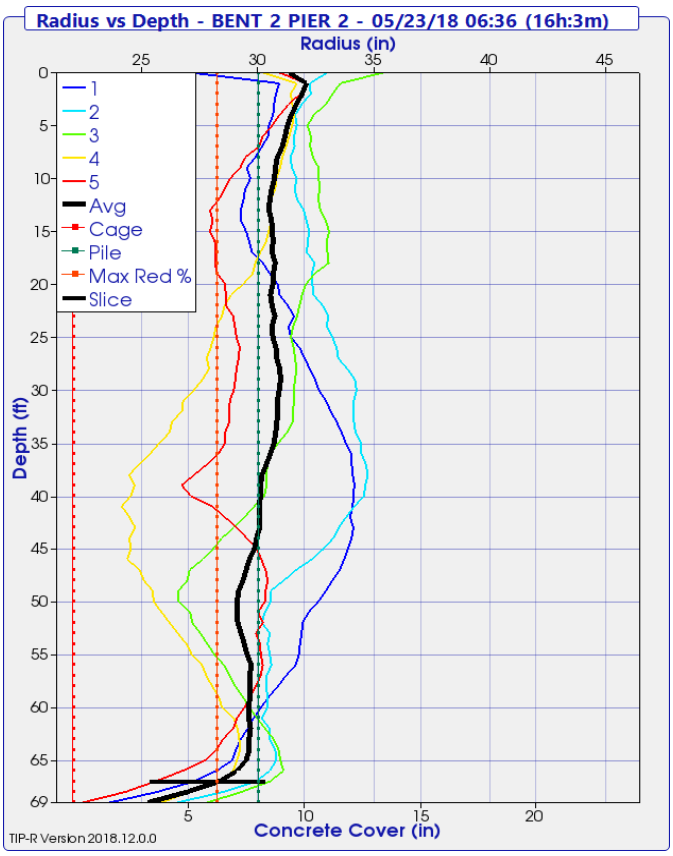


Figure 1. TIP Results Displaying Radius vs. Depth – Shaft 2

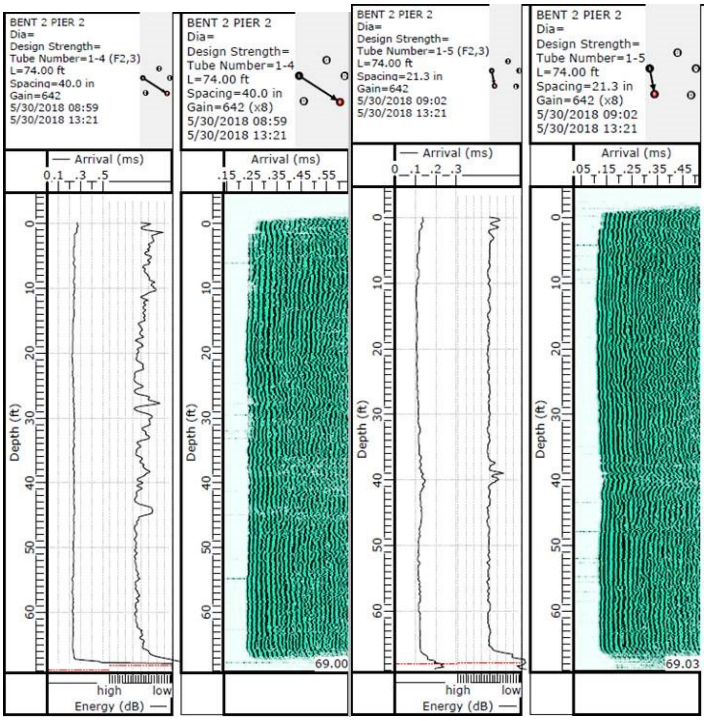


Figure 2. Representative Sample of CSL Results – Shaft 2

After reviewing the CSL and TIP results it was determined that further investigation was required for Shaft 2 in order to confirm the presence of the anomaly detected by both CSL and TIP near the shaft base. Coring was recommended and performed on June 12, 2018. The core results revealed honeycombing (voids and exposed aggregate) in the concrete beginning at a depth of 68 feet below the top of shaft. Lower quality concrete due to contamination was discovered from 68.5 to 70 feet below the top of shaft. Figure 3 presents the cores obtained in the field. Following the coring, the samples were taken back to a lab and tested to assess the compressive strength. Lab results indicated that the concrete in the bottom 2 feet of the drilled shaft had a compressive strength of approximately 1,140 psi. Comparatively, concrete samples tested at 65 feet below the top of shaft recorded unconfined compressive strength of greater than 7,000 psi. After the core results were presented to the Engineer, it was determined that hydro-blasting and pressure grouting was required to remediate the anomalous zone. Following the pressure grouting, additional CSL testing was performed to verify that the grout was able to flow in the bottom of the drilled shaft and remediate the issue. Table 8 compares the initial CSL results with the retest CSL results that were performed after hydro-blasting and pressure grouting was completed.



Core Samples NQ-13 to NQ-15: From left to right top core starting at a depth of 59.0 feet and bottom of core ending at 70.0 feet.

Figure 3. Pictures of the Cores Recovered from the Bottom of Drilled Shaft 2.

Table 8. Summary of Initial CSL and Post Grouting CSL Results

Profile	Max FAT Delay (%) 5/30/2018	Max FAT Delay (%) 6/15/2018
1-2	100	41
1-3	100	25
1-4	100	32
1-5	92	51
2-3	52	37
2-4	34	22
2-5	56	28
3-4	100	53
3-5	100	26
4-5	100	32

CONCLUSION

In summary for the project presented for this paper, seven drilled shafts were tested using both CSL and TIP. The results from the two different test methods were used in conjunction to determine the acceptance of the shaft or if further methods of evaluation were required. After the project had been completed a comparison study was performed for the financial costs, time impacts, and results associated with each of the test methods.

Overall, the findings from the data provided from this project show that Thermal Integrity Profiling can be a cost-effective alternative to traditional Cross Hole Sonic Logging. The material cost for CSL testing was calculated by including the cost of the access tubes, tube caps, labor to install CSL tubes, and the post grouting of CSL tubes. The material cost for TIP testing was calculated by including the cost of Thermal Wire® cables, TIP connection per wire, and the labor to install the wires. The material costs for CSL and TIP testing were calculated to be $31,029.45 and $17,575.00, respectively. This equates to a cost difference of $13,454.45 USD or a 43% cost difference. Additionally the cost comparison of collecting and interpreting the data revealed that for this project the cost of CSL and TIP testing was $12,845 and $4,260, respectively. This equates to a cost difference of $8,585 USD or a 67% cost difference. Therefore the total costs which includes the material cost, engineering cost, data collection, data analyses, and reporting fees for CSL and TIP testing are $43,874.45 and $21,835, respectively.

The data provided for this paper also shows that there is a potential for significant time savings or potential for an accelerated schedule. Both CSL and TIP testing requires a waiting period before the data can be obtained. In general CSL has a 7 day waiting period before the test can be performed while TIP data loggers collect data continuously from the end of concrete placement until the peak temperature is achieved. Peak temperature generally occurs between 10 to 48 hours after concrete placement. For this project TIP results were obtained on average approximately 24 hours after concrete placement, while CSL results could not be obtained until a minimum of 7 days after concrete placement. Therefore is TIP testing was the only specified

method of testing for this project the average time that could have been saved between results being obtained was 6 days.

Determining a potential flaw or anomaly in the concrete is the main objective of both CSL and TIP. Traditionally only one of the two test methods is generally specified for a given project. While this is industry standard, the limitations of either test can return false positives and therefore require expensive additional investigations to confirm the NDT results. For this project, the initial testing CSL results indicated that four of the seven drilled shafts could have potential anomalies. From the initial testing results from TIP testing two of the seven drilled shafts were reported to have potential anomalies. If only CSL testing was performed for this project, Shaft 6 could have been classified to have an anomalous zone after the first CSL test was performed. With the addition of TIP testing on this project, it was determined that an additional CSL test was required which confirmed the TIP results were correct. Without TIP testing, coring could have been required on Shaft 6. Shaft 2 was discussed in detail in this paper and both CSL and TIP results both indicated that there was a potential anomaly in the bottom two to three feet of the drilled shaft. After further investigation was completed, it was confirmed that both CSL and TIP detected an area of concrete that had lower compressive strength than desired. If only TIP testing was required for this project it would have been difficult to assess the success in post grouting. Without CSL being specified coring most likely would have been required to determine if the post grouting was successful or not. CSL offered the advantage of being able to run another CSL test after post grouting and verify that grout was able to flow between the grout access cores. As long as the Thermal Wire® cables have not been cut at the top or damaged due to the hydro blasting it is possible that the data loggers could be connected to the cable and temperature readings could be measured during the curing of the grout.

ACKNOWLEDGMENTS

We would like to thank all the individuals who helped to collect all the data that is presented in this paper. First we would like to thank Blythe Construction Company for providing data, assistance in the field while testing, and contributing review resources. We would also like to thank Lee and Sims Drilling Services, Inc. for their assistance and cooperation in the field during testing and F&ME for contributing data.

REFERENCES

Piscsalko, G., Likins, G., Mullins, G., (2016). "Drilled Shaft Acceptance Criteria Based Upon Thermal Integrity", *DFI 41st Annual Conference on Deep Foundations: New York, NY*, pp 1-10, October 2016.

Webster, K., Rausche, F., Webster, S., (2011). "Pile and Shaft Integrity Test Results, Classification, Acceptance and/or Rejection", *Compendium of Papers of the Transportation Research Board (TRB) 90th Annual Meeting: Washington, D.C.*

CROSSHOLE SONIC LOGGING VERSUS PERIMETER SONIC LOGGING: WHAT HAVE WE LEARNED?

Scott A. Jacobs, Case Foundation Company**,** Philadelphia, Pennsylvania, USA, Scott.Jacobs@CaseFoundation.com
Aaron Thomas, Case Foundation Company, Phoenix, Arizona, USA, ARThomas@CaseFoundation.com
Cory McElprang, Hoque and Associates, Phoenix, Arizona, USA, CMcElprang@HoqueandAssociates.com
Enamul Hoque, Hoque and Associates, Phoenix, Arizona, USA, EHoque@HoqueandAssociates.com

ABSTRACT

Crosshole Sonic Logging (CSL) only evaluates concrete on the inside of reinforcing cages leaving the outside unevaluated unless other types of testing are performed such as Perimeter Sonic Logging (PSL). While there have been some reports of PSL testing having accurately identified anomalies (e.g. Samtani et al 2005), experience by Case Foundation Company has indicated otherwise where false positives were determined with subsequent coring. Numerous cases of PSL false positives are presented as well as a study where a shaft was installed with both inside and outside tubes, and CSL and PSL data were compared.

To date, there is very limited data published on perimeter sonic logging, or Gamma-Gamma Logging (GGL) with tubes on the exterior of drilled shafts. Several cases will be presented where false positives were experienced where PSL testing was performed. In addition, a direct comparison will also be presented where a shaft was installed with both tubes on the inside and outside where CSL and PSL data is compared.

Keywords: Crosshole Sonic Testing, Crosshole Sonic Logging CSL, Perimeter Sonic Logging, Perimeter Sonic Logging, PSL, Integrity Testing, Drilled Shafts, False Positives, False Positives

BRIEF HISTORY – CSL TESTING AND TUBES ON INSIDE

The general procedure of Crosshole Sonic Logging (CSL) testing includes attaching tubes to the reinforcing cage to be able to send a transmitter in one tube and a receiver in another tube with which a sonic pulse is emitted from the transmitter and received in another tube. The time taken for the sonic pulse to travel between the tubes is measured and compared to expected values for the known distance between the tubes. Any increase in time from expected values indicates the sonic pulse traveled through a media other than homogeneous concrete such as objects in the path (spacer wheels, steel bracing, etc.), tube spacing, or soil inclusions. However, variations in arrival time can also result from differences in concrete density. The tubes have traditionally been placed on the interior of the reinforcing cage which protects them during hoisting and placement of the cage and reduces wave refraction caused by modulus of elasticity differences between steel and concrete. This allows the concrete within the interior of the reinforcing cage to be evaluated, but the concrete outside of the cage is excluded from traditional CSL testing. As a result, alternative integrity testing has been developed to not only provide different ways to evaluate the integrity of drilled shafts but to also address the issue of evaluating the concrete outside of the reinforcing cage. These alternative testing methods include Gamma-Gamma Logging (GGL), Thermal Integrity Profiling (TIP testing) and Perimeter Sonic Logging (PSL) which is similar to CSL testing but instead of the tubes placed inside the reinforcing cage, the tubes are placed on the outside of the reinforcing cage as shown in Fig. 1.

© 2019 Deep Foundations Institute

The unique concept of PSL testing is that since the tubes are placed on the outside of the cage, when testing adjacent tubes, some amount of concrete outside of the reinforcing cage can be evaluated. This technique has been implemented successfully in this regard as it adheres to the basic theory of CSL testing measuring sonic pulses through a homogenous material.

There have been cases of PSL where tubes placed on the outside have been used to evaluate the concrete between tubes where the sonic pulse crosses through the reinforcing cage. In this configuration, the sonic pulse potentially travels through sometimes numerous materials of varying density to be measured in the receiving tube (e.g the density of concrete and steel differs by a factor of 3.3). When various other materials such as spacer wheels (see Fig. 2) are present, this difference is only exacerbated (factor of 8). Differences in density alter the time taken for the sonic pulse to reach the receiver, creating noise which makes it difficult to differentiate between an anomalous zone within the concrete or the effect of traveling through the reinforcing cage.



Fig. 1. PSL tube placement on exterior of reinforcing cage



Fig. 2. Proximity of tube to items such as spacer wheels and reinforcing

The following case histories are presented where PSL testing was performed, anomalous zones were identified, and additional investigation was performed to evaluate the shaft concrete. In each case, it was determined that the concrete was of sufficient quality and the drilled shafts were accepted. Additionally, a case will be presented where CSL tubes were placed on both the inside and outside of a reinforcing cage to compare the results.

INA ROAD, MARANA, ARIZONA

The Ina Road project in Tucson, Arizona required PSL and GGL testing on all drilled shafts. This project had 76 drilled shaft foundations of which 35 (46 percent) indicated anomalous data with velocity reductions greater than 10 percent. The GGL testing indicated anomalies in 20 drilled shafts (26 percent).
The project designer and owner were concerned with the integrity of these foundations and required two drilled shaft foundations (EB DS-5 and WB DS-15) be cored which they selected as having the “worst” anomalies. Both of these shafts (and the majority of shafts on this project) were excavated under polymer drilling fluid support. Prior to cage and concrete placement, the shafts were sounded with a weighted tape and the polymer drilling fluid was tested for density, viscosity, pH and sand content. The drilled shaft specifications required the PVC access tubes to be extended to within 6 inches of the as-built shaft bottom

so the PSL length logged for DS-5 (see Table 1 and Fig. 3) was 78.30 feet and 78.55 feet for DS-15. The variance in PSL length tested is due to the clearance at the bottom of the shaft, the distance from the bottom of the probe to the signal source location and minor shifting of the PVC tubes due to reinforcing cage hoisting.

Table 1. Shaft DS-5 PSL Results (partial)

Pile	Profile	Start Feet	To Feet	Peak Feet	Energy Decrease	FAT Delay
17018	INA RD EB 5CRB D5-51-2	75.17	78.13	76.32	44.3dB	>100%
17018	INA RD EB SCRB DS-52-3	75.83	77.47	76.48	-	76%
17018	INA RD EB 5CRB D5-53-4	76.16	78.29	76.65	-	68%
17018	INA RD EB SCRB DS-56-1	75.83	78.13	76.81	-	29%
17018	INA RD EB 5CRB D5-51-3	75.34	78.13	76.81	43.1dB	>100%
17018	INA RD EB SCRB DS-52-6	75.50	78.13	76.81	43.0dB	>100%
17018	INA RD EB 5CRB D5-53-6	76.16	77.47	76.81	-	21%
17018	INA RD EB SCRB DS-52-5	75.66	78.13	76.98	-	24%
17018	INA RD EB 5CRB D5-53-5	76.32	78.29	76.98	-	33%
17018	INA RD EB SCRB DS-54-5	75.01	78.13	77.14	43.9dB	>100%
17018	INA RD EB 5CRB D5-52-4	75.66	78.13	77.14	43.7dB	>100%
17018	INA RD EB SCRB DS-54-6	75.50	78.13	77.14	44.1dB	>100%
17018	INA RD EB 5CRB D5-55-6	75.17	78.13	77.30	43.7dB	>100%
17018	INA RD EB SCRB DS-51-4	75.01	78.13	77.47	44.7dB	>100%
17018	INA RD EB 5CRB D5-51-5	76.65	78.13	77.47	-	26%

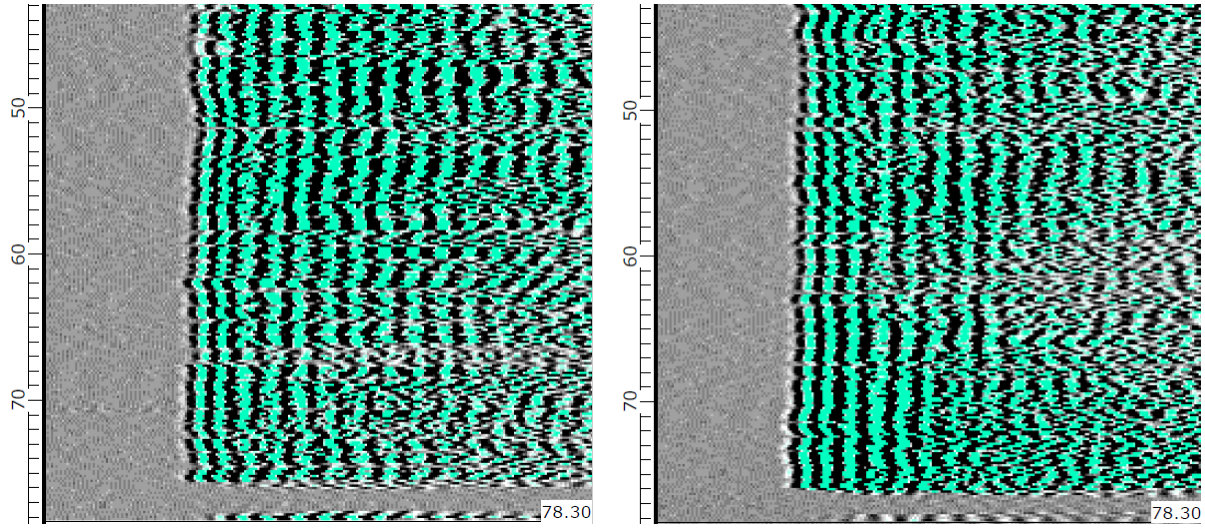


Fig. 3. Shaft DS-5 sample waterfall (bottom portion shown)

Cross sections indicated contaminated or poor-quality concrete from approximately 73.15 feet below top of concrete to the shaft tip.

To verify the PSL findings a four-inch diameter core was taken from DS-5 extending to the shaft tip. Due to the projected column extending above the top of the drilled shaft, a handheld coring unit was necessary

to perform coring operations. Additionally, the reinforcing tie "tails" that protruded into the center of the shaft required the location of the core to be 18 inches inside the cage from tube #1. The size of core taken was PQ or 3.35-inch diameter.

The coring operation took 60 hours to reach the shaft tip. Coring was completed 25 days after concrete was placed and compressive breaks were performed at 27 days after concrete placement (a day earlier than the standard 28 days). Compressive strengths indicated sound concrete with the break of the core from approximately 70 feet below top of concrete reaching 6,030 psi and the breaks at 75 feet and 79.5 feet below top of concrete reaching 5,170 psi and 5,460 psi compressive strength, respectively. Additionally, the concrete did not exhibit any visible signs of contamination or otherwise suspect concrete.
The PSL testing for DS-15 indicated contaminated or poor-quality concrete approximately from 69.38 feet to 78.39 feet below top of concrete in multiple tube combinations as depicted in Table 2 and Fig. 4. Offset PSL tomography for DS-15 was not obtainable due to PVC debonding when additional testing was requested.

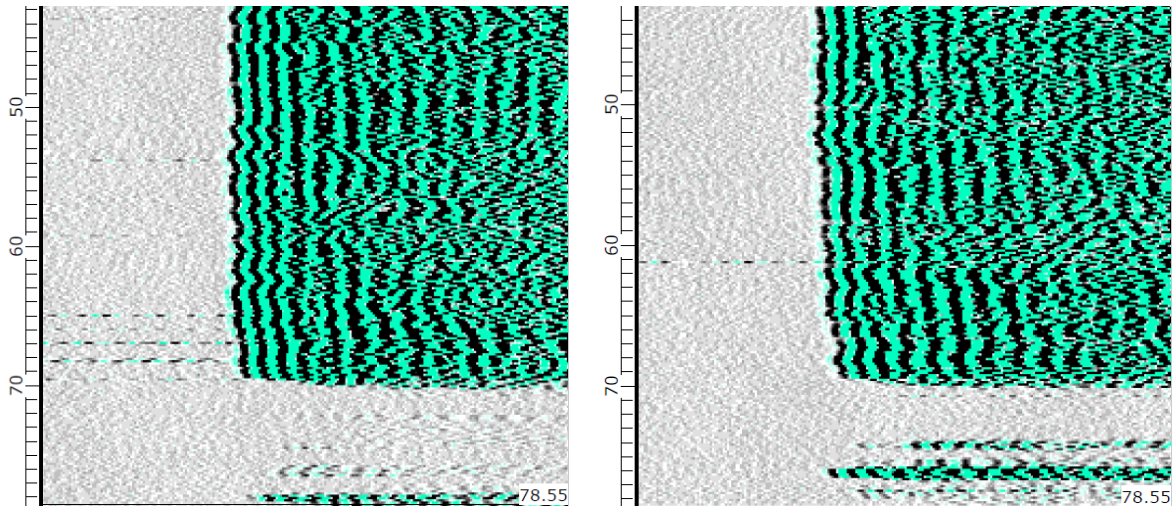


Fig. 4. Shaft DS-15 sample waterfall (bottom portion shown)

Another 4-inch diameter core was taken to the shaft tip elevation. DS-15 was similar to DS-5 in the reinforcing and, therefore, coring equipment was limited to a handheld coring unit.
The cores as pictured in Fig. 5 did not visually indicate concrete contamination or otherwise suspect concrete. Compressive strengths are also indicated in Figure 5.



Fig. 5. Concrete cores and compressive strength results from DS-15

None of the cores retrieved had compressive strengths below the required 3,500 psi. The average compressive strength of the six cores tested obtained from 71 feet 6 inches to 78 feet 6 inches below top of concrete was 6,433 psi, with a low value of 4,370 (77 feet to 77 feet 10 inches) and a high value of 7,350 psi (77 feet 10 inches to 78 feet 6 inches). A control sample from a depth of 60 feet was taken and had a compressive strength of 6,850 psi. Based on the results of the coring and compressive strength testing, all the drilled shafts for the Ina Road project were accepted.

SAN PEDRO RIVER BRIDGE, PALOMINAS, ARIZONA

The San Pedro river Bridge project drilled shafts (see Fig. 6) consisting of four 60-inch diameter shafts to 63 feet deep, four 60-inch diameter shafts to 76 feet deep, and four 96-inch diameter shafts to 94 feet deep (87.5 feet concrete length with a construction joint 7.5 feet below existing grade). All twelve shafts were constructed using polymer fluid drilling support. Similar to the Ina Road project, shafts were to be tested by PSL and GGL. Three of the twelve shafts tested exhibited PSL anomalies. Of those three shafts two also had GGL anomalies in the same areas as the PSL anomalies. The project owner directed the contractor to repair the anomalous zones or confirm the anomalies by coring. The first shaft cored was DS-4 which was a 60-inch diameter drilled shaft to a depth of 76 feet. PSL indicated 75.6 feet of PVC tube length was tested.

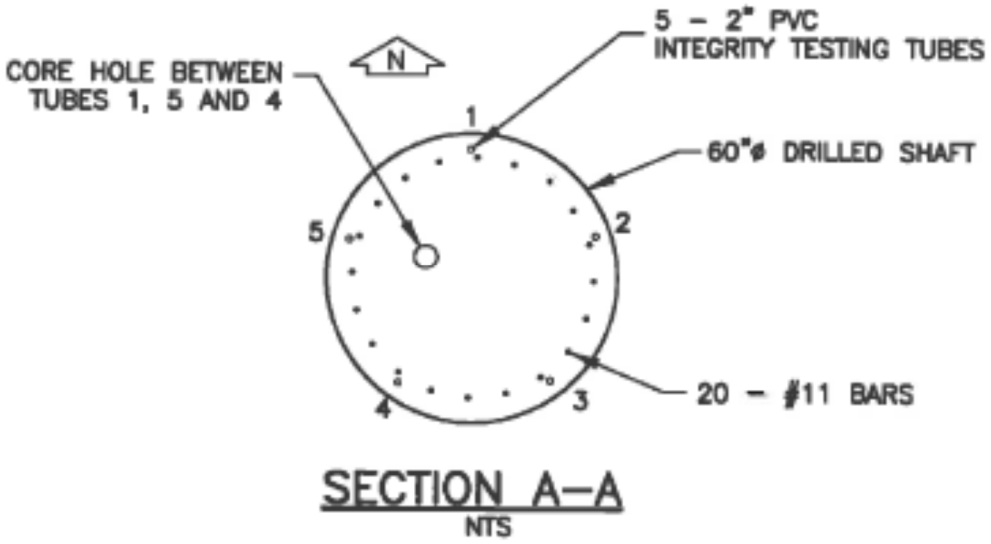


Fig. 6. Shaft section showing tube configuration

One of the tube combinations depicting PSL anomalies from the report is presented below (See Fig. 7) with correlating GGL results presented in Fig. 8. Both tests depict variations in data from 72 feet below top of concrete to tip of shaft.

Coring took multiple days to reach the anomalous zone with a 3.5inch diameter core retrieved. From the cores retrieved in the anomalous zone from 72feet to 76feet, seven 3.5inch x 7.1inch concrete cores were tested. Of the seven breaks the lowest compressive strength tested was 4,660 psi, the high of 8,500 psi and an average of 6,995 psi. Based on the results of the coring and compressive strength testing, the shafts were accepted.

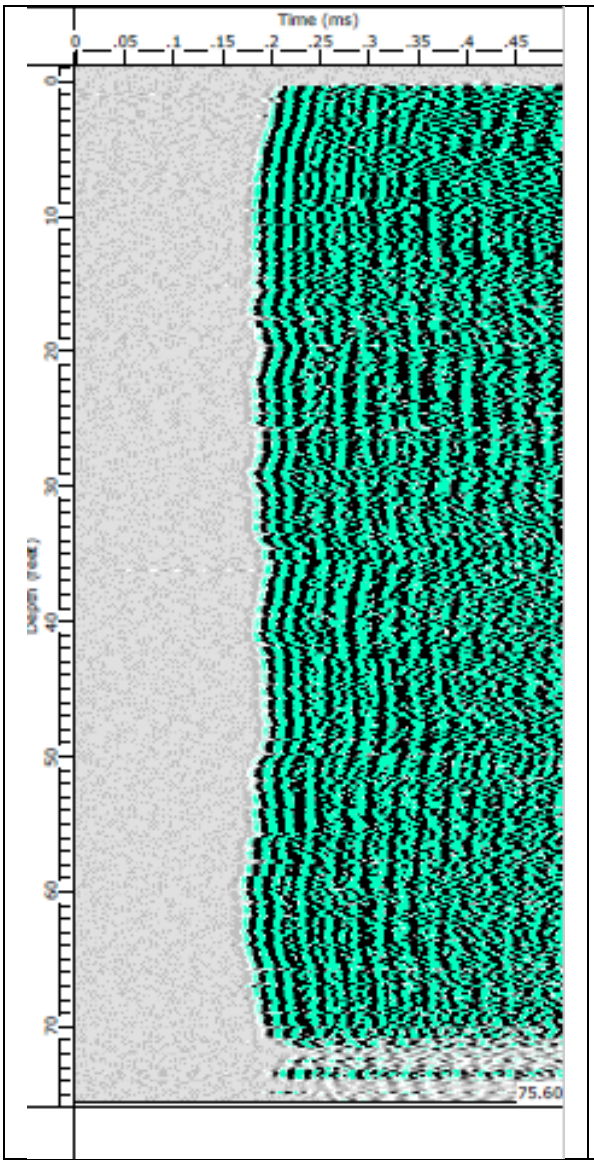


Fig. 7. Portion of PSL results from DS-4

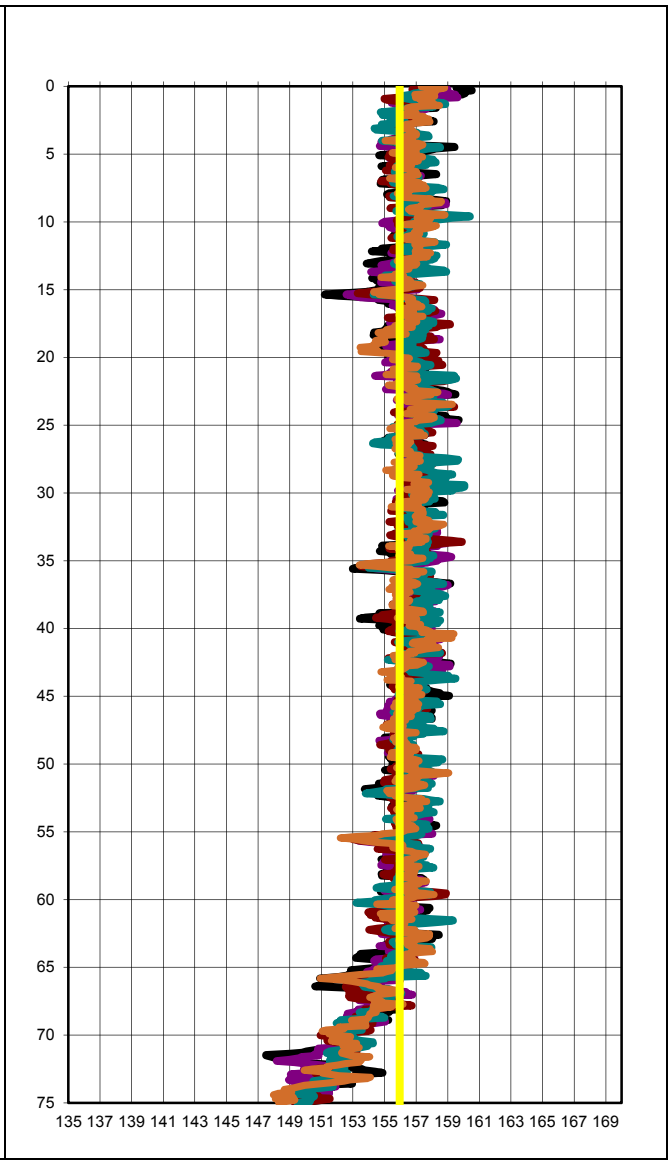


Fig. 8 GGL results from DS-4

SUNSET ROAD– STUDY OF TUBES ON OUTSIDE AND INSIDE

PSL and GGL testing was required on 21 drilled shafts of depths of 120 to 145 feet below the general site grade at the Sunset Bridge project in Tucson, Arizona. On this project nine of the shafts (43 percent) indicated anomalous readings within the bottom few feet of concrete. Drilling operations and concrete placement made no indication of excessive sediment at the tip of shaft before placement or suspended within the polymer used during drilling. Final measurements made using a weighted tape measure suggested the tip of shaft was firm. Additionally, final cleanout of the polymer displaced by the concrete showed little or no suspended sediment. Concrete placement curves calculated for each shaft showed no signs of necking within the depths of the anomalous readings. Considering the lack of correlation between the PSL and GGL and the observations made during construction, it was decided that two shafts would be selected to receive tubes on both the interior and exterior of the reinforcing cage.

Drilled shafts DS-8 and DS-11 were tested with both PSL and CSL methods along with GGL. These two shafts were 72 inches in diameter, 145 feet deep and as such, each of the shafts had a total of 12 access tubes installed. Six tubes were attached on the interior of the reinforcement cage and six were installed on the exterior of the cage. The access tube locations were alternated with a minimum distance of 9 inches to avoid any interference between GGL and CSL test data. The access tube configurations for exterior and interior positions are depicted in Figs 10-11. The intent of access tubes on both the exterior and interior of the rebar cage was to obtain comparative results to better determine the differences between tube placement locations.



Fig.10. Shaft tube placement and distances

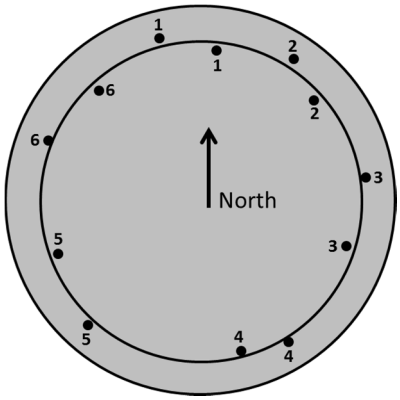


Fig. 11. Approximate Tube Locations DS-8

The testing requirements, test specification data analysis, and original report preparation including anomaly identification procedures were completed in accordance with Section 609-3.05 "Integrity Testing of the Special Provisions" of the Arizona Department of Transportation (ADOT). According to this specification, deficiencies are identified based on any combinations of the following criteria:

- CSL wave velocity reductions of at least 10 percent,
- CSL pulse energy reduction of 9.0 dB or more, and
- GDL data indicating concrete density reduction of 3 standard deviations below the average concrete density of the associated tube data.

Sunset Road DS-8 PSL and CSL data, both exterior and interior tubes, indicated similar variations in both PSL and CSL data within the top 10 feet of concrete that can be attributed to initial debonding, where the concrete delaminates from the PVC access tubes. It is notable that the PSL data within the upper 10 feet of depth indicated a pulse energy reduction of 12 dB and a velocity of 10,000 feet per second (fps). The average velocity of the entire length of shaft is about 13,000 fps indicating a reduction of approximately 23 percent in wave velocity. In the CSL test, within this depth, the reduction in pulse energy is also around 12 dB and the velocity is around 11,000 fps whereas the average pulse velocity is 14,000 fps. The CSL has depicted a reduction of approximately 21 percent, similar to PSL data. The plot of the PSL indicates energy loss to be scattered or "noisy" within the entire depth of the shaft in that tube combination. However, outside of the top and very bottom portions, no energy loss exceeded 9 dB. The CSL energy plot was straight and linear except for the upper 10 feet as discussed above. Although the energy plot of the PSL data indicated significant scatter or a noisy pattern, the values of the wave velocity fell within 10 percent variation except for the top portion as noted.

The PSL, energy also indicated loss of more than 9 dB at the bottom with no visible velocity drop. The CSL did not indicate any such reduction at the bottom. This increase in pulse energy loss as depicted in the PSL or exterior tube combinations, is attributed to interference by the higher modulus steel reinforcements with the pulse wave, creating additional variations particularly in adjacent tubes. DS-11 depicted similar differences in data for exterior and interior tube locations. Figures 12-13 depict DS-8 tube combinations 4-5 from exterior and interior tubes.

Data from these tube combinations, though not exactly parallel, depict the same general area of concrete within the drilled shaft. Figure 11 shows approximate tube locations for exterior and interior tubes of DS-8, which are similar to tube locations for DS-11. Wave refraction and interference as seen in Fig. 12 were common in adjacent tubes when attached to the exterior of the cage. Interior tubes, as seen in Figure 13, did not experience the same variations. In general, data for CSL did not experience the level of noise as the tubes on the exterior especially in adjacent tube combinations.

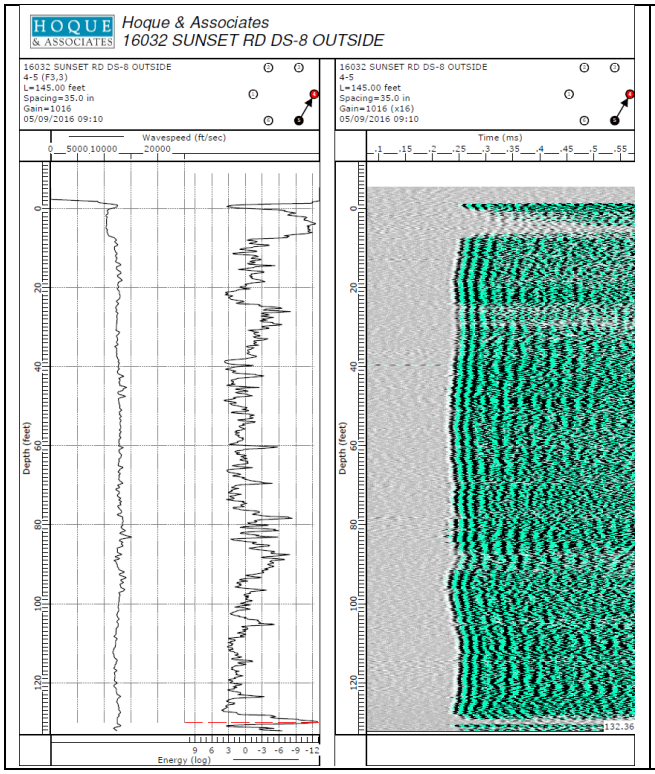


Fig. 12. Exterior Tube Combination 4-5

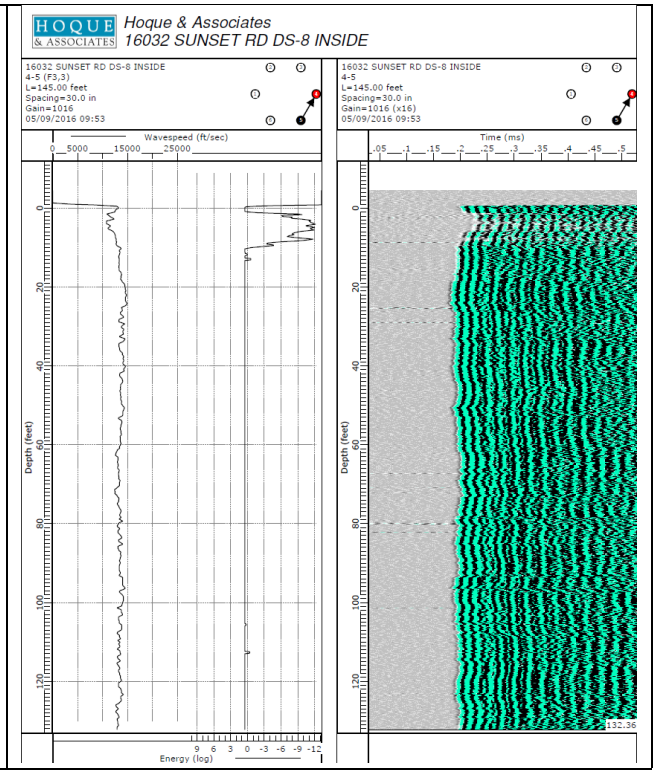


Fig. 13. Interior Tube Combination 4-5

As depicted in Figures 12 and 13, PSL data depicts increased variations in pulse energy and wave speed while CSL showed either no variation or a lesser degree of variation. DS-11 PSL data showed all tube combinations depicting reduction in wave speed of 10 percent or greater and pulse energy variations of at least 9 dB within the bottom 5 feet of concrete (120 to 125 feet below the top of the concrete). Data for CSL do not show variations in wave speed or pulse energy at the same depths. GGL data from DS-8 for both exterior and interior tubes did not indicate any variation in concrete density outside of some reduction within the specifications in the top 35 feet of concrete. However, minor inconsistencies in density data were observed in tubes placed on the exterior of the reinforcement cage. These inconsistencies can be attributed to minor deflections in the PVC tubes due to the pressure of concrete placed on, and variations in, the

sidewall inherent to auger drilling. DS-11 showed similar variations to those found in DS-8 in all but the bottom 5 feet of concrete. The bottom 5 feet of concrete for DS-11 showed reductions in concrete density which correlated with the CSL and PSL data for both sets of tubes. Figures 14 and 15 show a composite of exterior and interior GGL results.

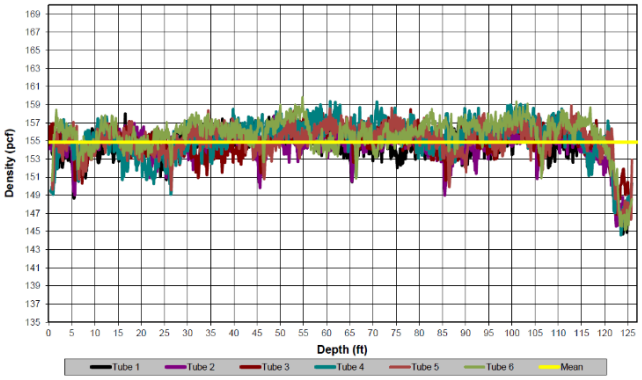


Fig. 14. Outside GGL results for DS-11

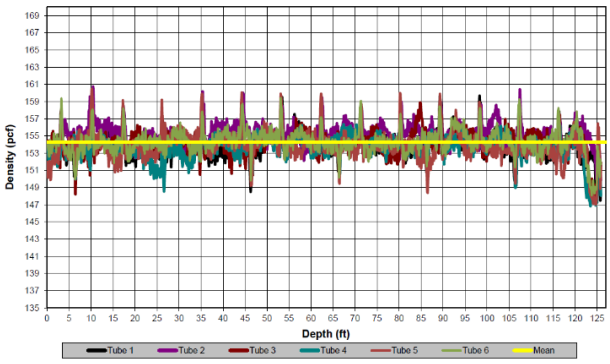


Fig. 15. Inside GGL results for DS-11

Results from tubes on the interior of the rebar cage clearly show more precise locations of both PVC couplers and interior crush rings. The same depiction for exterior tubes seems to be diffused for crush rings but decipherable for presence of couplers.Exterior and interior tubes indicated variations within the bottom 5 feet of concrete for DS-11. However, exterior tubes showed a decrease in density up to 3 pcf more than interior tubes.

SUMMARY AND CONCLUSIONS

As shown in the cases above, concrete cores taken from drilled shafts with anomalous PSL data did not correlate with the results of the integrity testing. The Sunset Road PSL testing indicated anomalies that did not show in the CSL testing. In general, the CSL has inherent limitations as the test tubes are attached to the reinforcing cage around the perimeter of the drilled shaft. By placing the test tubes on the outside of the reinforcing cage with PSL, the test method is further limited and an accurate evaluation of the concrete becomes increasingly difficult. PSL test tube location ensures the sonic wave travels through additional shaft areas that are not tested by CSL. Application of the CSL acceptance criteria with the variability of the PSL results, and the absence of confirmed anomalies have resulted in additional project costs for increased report data review time, false anomalies and destructive testing for shaft concrete evaluation. Based on the above observations, it is our recommendation that additional data would be required to replace CSL with PSL for evaluating drilled shaft concrete on the interior of the reinforcing cage.

ACKOWLEGEMENTS

The authors would like to acknowledge Pima County Department of Transportation and Arizona Department of Transportation for their involvement in the referenced projects.

REFERENCES

Samtani, N.C, Jalinoos F., Poland, D.M. 2005. Integrity Testing of Drilled Shafts – Existing and New Techniques. Proceedings, GEO Construction Quality Assurance/Quality Control Conference, ADSC, Dallas, TX, November 6-9, pp. 329-340.

FULL WAVEFORM INVERSION OF CROSS-HOLE STRESS WAVES FOR STRUCTURAL INTEGRITY TESTING OF DRILLED SHAFTS

Alireza Kordjazi, Temple University, Philadelphia, PA, USA, 267-774-0428, alireza.kordjazi@temple.edu
Joseph T. Coe, Temple University, Philadelphia, PA, USA, 215-204-6100, joseph.coe@temple.edu
Michael Afanasiev, Mondaic Ltd., Zurich, Switzerland, +41-767-470-715, michael.afanasiev@mondaic.com

ABSTRACT

Cross-hole sonic logging (CSL) is a common quality assurance measure for the evaluation of the structural integrity of drilled shafts. The results of CSL can be supplemented by a set of tomographic images generated by cross-hole tomography (CT). Although the same access tubes, sources and receivers are used in both methods, CT has the advantage of providing a higher quality image of the possible anomalies in drilled shafts. Nevertheless, it has been reported in literature that the CSL and CT miss anomalies with sizes of smaller than 10 percent of the cross sectional area of the drilled shaft. This implies poor resolution despite the high-frequency of the stress waves utilized in these methods. This issue with resolution can be at least partially attributable to the fact that CT relies entirely on the inversion of the first time of arrival and ignores the information embedded in the rest of the recorded traces. This study examines the application of full waveform inversion (FWI) to generate a higher resolution image of the possible defects in drilled shafts from the same data used for cross-hole tomography. FWI is a wave-field method that aims to directly match the recorded traces with traces obtained from a numerical model of the domain. This has the benefit of avoiding the selection of the first time of arrival, along with increasing the resolution of the final image due to extracting more information out of the traces. Through a series of numerical simulations, synthetic traces were generated from a drilled shaft with defects of known mechanical properties, dimensions, and location. These traces were then inverted to evaluate the performance of FWI for structural integrity testing of the drilled shafts.

Keywords: drilled shaft, structural integrity, cross-hole sonic tomography (CST), full waveform inversion (FWI)

INTRODUCTION

The presence of construction defects can compromise the structural integrity of drilled shafts and negatively affect their performance (O'Neil 1991; Sarhan et al. 2002; O'Neil et al. 2003; Poulos 2005). Several non-destructive testing (NDT) methods exist that are currently used for the evaluation of the structural integrity of drilled shafts. Cross-hole sonic logging (CSL), cross-hole sonic tomography (CT), and thermal integrity profiling (TIP) are well-established and documented in the industry and practical manuals (Brown et al. 2010). NDT methods prevent the need for coring and excavation and are relatively fast and cost effective. Successful implementation of these techniques has also been reported in the literature (Branagan et al. 2000; Iskander et al. 2001; Mullin 2010; Johnson 2016).

Hertlein et al. (2016) showed that CSL is the most popular NDT technique for structural integrity testing of drilled shafts in North America and Europe. The results of CSL can be supplemented by a set of tomographic images generated by cross-hole tomography (CT) to provide more information on the nature of the anomaly and its size (Brown et al. 2010). This benefit of CT comes at the cost of a more intensive data acquisition process where data is recorded by receivers at multiple depths for the same source. CT subsequently uses travel-time inversion of the numerous ray paths to generate a tomogram of the anomalous features. Despite the popularity of CSL and CT in the quality control and assurance (QC/QA) of drilled shafts, the success of these methods depends on the size and/or location of the anomaly in the drilled shaft

© 2019 Deep Foundations Institute

(Davis 1998; Sarhan et al. 2003; Samtani et al. 2005; Amir and Amir 2009). Multiple studies have demonstrated that CSL and CT are generally able to detect defects that are larger than 10% - 15% of the shaft cross-sectional area (Iskander et al. 2003; Sarhan et al. 2003).

The anomaly size limitations imply poor resolution of CSL/CT despite the high-frequency content of the stress waves utilized in these methods. This in part stems from reliance on the first time-of-arrival of signals between source and receiver, while the rest of the signal is practically ignored. Full waveform inversion (FWI) of stress waves instead attempts to match the entire signal based on results from forward modeling of the domain of interest. In this manner, as much information as possible is extracted from the recorded signals, leading to the construction of a high-resolution image of the domain. Though FWI is a relatively new technique in the field of NDT, FWI has shown promise in applications related to NDT evaluation of bridge abutments (Jalinoos et al. 2017) and conditions underneath drilled shaft excavations in karstic limestone (Kordjazi et al. 2018). FWI has also been successfully applied to resolve anomalies for non-destructive testing (NDT) of materials (Nguyen and Modrak 2018) and medical tomography (Vinard et al. 2018).

This study examines the application of FWI to generate a higher resolution image of the possible defects in drilled shafts from the same data used for cross-hole tomography. In the following sections, a brief introduction on the fundamentals of CT and FWI is provided followed by details regarding the numerical simulation of data acquisition and analysis in this study. The paper concludes with a discussion on the performance of each method and their advantages and disadvantages.

TRAVEL-TIME CROSS-HOLE TOMOGRAPHY (CT)

The goal of CT is to generate a tomographic image of the acoustic wave velocity of spatial variability in the model. The travel-times of the emitted waves from the sources (transmitters) to the receivers are measured first. In ray-based theory of wave propagation, the ray path can be assumed as a combination of numerous infinitesimal paths of length *dh* with a corresponding travel time of *dt*. In a domain with a spatial velocity distribution of V($\boldsymbol{x}$), where $\boldsymbol{x}$ is the location vector, the travel-time (t) of each ray can be written as (Santamarina and Fratta, 2005):

$$t = \int_{source}^{receiver} \frac{1}{\mathrm{V}(\boldsymbol{x})}\, dh \qquad [1]$$

By discretizing the domain into non-overlapping subdomains, the integral can be converted into summation. The inverse of the velocity (i.e., $1/V$) is also commonly referred to as slowness (s). For the travel-time measured for each pair of source and receiver, Eq. 1 can be developed in its discrete form. In a more general form, all of these equations can be summarized in the matrix form as:

$$[\mathbf{t}] = [\mathbf{h}] \cdot [\mathbf{s}] \qquad [2]$$

where, [**t**] is the vector of measured travel-times, [**h**] is the matrix of the travel length, and [**s**] is the vector of unknown slowness (Santamarina and Fratta, 2005). In CT, the slowness is inverted from the travel-time data. To solve this inversion problem, a ray-tracing scheme is required to determine the ray paths (Giroux and Larouche, 2013).

In this study, a shortest-path method was used to compute the travel-time along the travel path based on Fermat's principle. The type of discretization of the domain, however, can significantly affect the ray tracing process. To increase the accuracy of ray-tracing and provide adequate angular coverage, the domain was discretized using cells with primary nodes at their corners together with secondary nodes along the edges of each cell or element (Giroux and Larouche, 2013).

FULL WAVEFORM INVERSION (FWI)

FWI attempts to match the entire recorded waveforms to theoretical signals resulting from numerically solving the forward problem of wave propagation. Due to the inclusion of more realistic physics, FWI therefore has the potential to image more complex heterogeneous features that ray-based approaches may fail to capture. In FWI, comparisons between observed and synthetic data are used to infer the internal structure of the domain.

The forward problem of elastic wave propagation in the most general form can be represented by its partial differential equation of motion as below:

$$\rho(\mathbf{x})\,\ddot{\mathbf{u}}(\mathbf{x},t) - \nabla.\boldsymbol{\sigma}(\mathbf{x},t) = \mathbf{f}(\mathbf{x},t) \quad [3]$$

where, ρ is mass density, **u** is the displacement field in the domain at location **x** and time *t*. The stress tensor is denoted by $\boldsymbol{\sigma}$ and the **f** stands for the external force density. The operator ∇ denotes the gradient with respect to the position vector **x**. The solution to this partial differential equation is a displacement field, or waveforms. In order to implement FWI, a starting model based on the available knowledge of the domain is selected. This model, denoted by **m**, is often constructed from an estimate of the wave speed in the domain. The forward problem of wave propagation is then solved in this model and the results are compared with the real data.

Through a quantitative measure of misfit between observations and the computed synthetic signals, the inversion problem can be expressed as an optimization problem (Fichtner 2011; Modrak and Tromp 2016), where the objective is to minimize a measure of misfit $\chi(\mathbf{m})$. This misfit in a general representation can be written as :

$$\chi(\mathbf{m}) = \| (g(\mathbf{m}) - \mathbf{d}) \|_{L2} + \alpha\, \mathrm{R} \quad [4]$$

where, g is the forward modeling operator, **d** denotes a set of waveforms recorded at some receiver locations, and g(**m**) represents the synthetic data computed using a given realization of the model **m**. R is a general regularization term and α is a regularization weight. The ultimate goal is to minimize this misfit between the two sets of waveforms. Regularization allows to incorporate the a-priori knowledge of the domain in the inversion and improve the convergence of the inversion to physically meaningful results. A more detailed account of the implementation of regularization in this study is provided in the modeling section of this paper.

The misfit is systematically minimized through an iterative local minimization algorithm. The starting model is iteratively updated via a series of small perturbations. At the *i*-th iteration the current model $\mathbf{m}_i$ is updated to generate a new model $\mathbf{m}_{i+1}$. The difference between the models of the two consecutive iterations ($\delta\mathbf{m}$) is in fact the desired update. Obviously, the resulting model must explain data better than the previous iteration by having a smaller misfit; that is, $\chi(\mathbf{m}_{i+1}) < \chi(\mathbf{m}_i)$. The model update (i.e., $\delta\mathbf{m}$) can then be defined with respect to the misfit function $\chi(\mathbf{m}_i)$ using a descent direction $\mathbf{h}_i$ and a positive step length $\gamma_i > 0$. In the general descent method, the descent direction $\mathbf{h}_i$ is:

$$\mathbf{h}_i = -\mathbf{A}_i\,.\,\nabla_m\chi(\mathbf{m}_i) \quad [5]$$

where, $\mathbf{A}_i$ is a positive definite matrix that controls the magnitude of each iterative model perturbation. In Newton's method $\mathbf{A}_i$ is equal to the inverse of the second order gradient of the misfit, or the Hessian matrix. The gradient of the misfit function $\nabla_m\chi$ is computed using the adjoint method (Fichtner 2011), a process

which relies on the convolution of 1) the data-residuals back-propagated from the measurement locations, and 2) the time-reversed forward wavefield. In most applications of FWI a linesearch approach is adopted to estimate the optimum step length γ_i at each iteration. As an alternative to linesearch methods, a trust-region method was used in this study to solve the optimization problem of the FWI. In a trust-region method the direction and the step size of the update are simultaneously determined (Boehm et al. 2018). The model update can be calculated using a quasi-Newton approximation of the inverse Hessian. An L-BFGS approximation of the Hessian is used instead of the computationally intractable problem of determining the exact Hessian.

NUMERICAL SIMULATION (FORWARD MODELING)

This study used two-dimensional (2D) numerical simulations of wave propagation in drilled shafts to compare the capabilities of CT and FWI when evaluating anomalous shaft features. Although a 2D simulation represents a simplification of true three-dimensional (3D) conditions, it can provide an efficient way to evaluate the relative performances of CT and FWI. In fact, since the same waveforms are used for the FWI and CT, the focus is placed on how the two methods compare under similar circumstances.

A 1.0 m (3.3 ft) diameter drilled shaft was modeled in this study. The length of the shaft under investigation was also limited to 1.0 m (3.3 ft). Given the relatively large amount of data acquired during CT testing it is common to limit the data acquisition to the portions of the drilled shaft where the results of previous CSL testing indicate the presence of an anomaly. The velocity of the acoustic waves (V_P) in the sound concrete was set as 3900 m/s (Hollema and Olson, 2002). This value of acoustic wave velocity was selected to simulate practical conditions; however, any other reasonable value for wave velocity in concrete may be used. Moreover, instead of a constant background wave velocity, any random variations of wave velocity can also be simulated (Coe et al. 2019). This is also the case with assigning velocities to defects. In fact, the ability to assign relatively sharp velocity contrasts to the defect attests to the fact that the simulation can incorporate the variations in the wave velocity. Two anomalous zones were defined where there is a 25% drop in the concrete V_P (Fig. 1). The first anomaly is 0.1 m by 0.1 m in width and depth (i.e., lengths approximately 10 percent of the cross-sectional area of the shaft). The second anomaly is 0.2 m by 0.2 m and located in the top-right side of the domain (Fig. 1). The locations of all the transmitters and receivers are also illustrated in Fig. 1. The anomalies were intentionally located at locations where there is limited coverage of the waveforms. This increases the challenges involved with the inversion for both FWI and CT.

The first set of simulations was conducted using 9 transmitters and 17 receivers in forward modeling (Fig. 1). Source spacing was 0.1 m (4.0 in) and receiver spacing was 0.05 m (2.0 in). The array of sources and receivers were 0.8 m apart from each other. The sources were modeled with a 20 kHz Ricker wavelet. All boundaries were modeled as absorbing in this study to isolate the effects of any potential reflections. The resulting waveforms were subsequently used in FWI and travel-time inversions for CT analysis. For the acoustic FWI, a uniform velocity initial model was used. A constrained trust-region inversion algorithm (Boehm et al. 2018) was implemented through the inversion workflow in which a hybrid two-stage inversion with an L2 and cross-correlation misfit (Fichtner 2011) were employed. In fact, the choice of the misfit function plays an important role in the information extracted from the waveforms, and also on the stability of the inversion. Regularization was implemented via the solution of the heat equation, which acted on the model updates as a smoothing operator. The simulation of the ultrasonic waves and FWI were performed using Salvus software suite (Afanasiev et al. 2019). The waveforms generated during modeling of the forward problem were then also used to perform CT using pyGIMLi software package (Rücker et al. 2017).

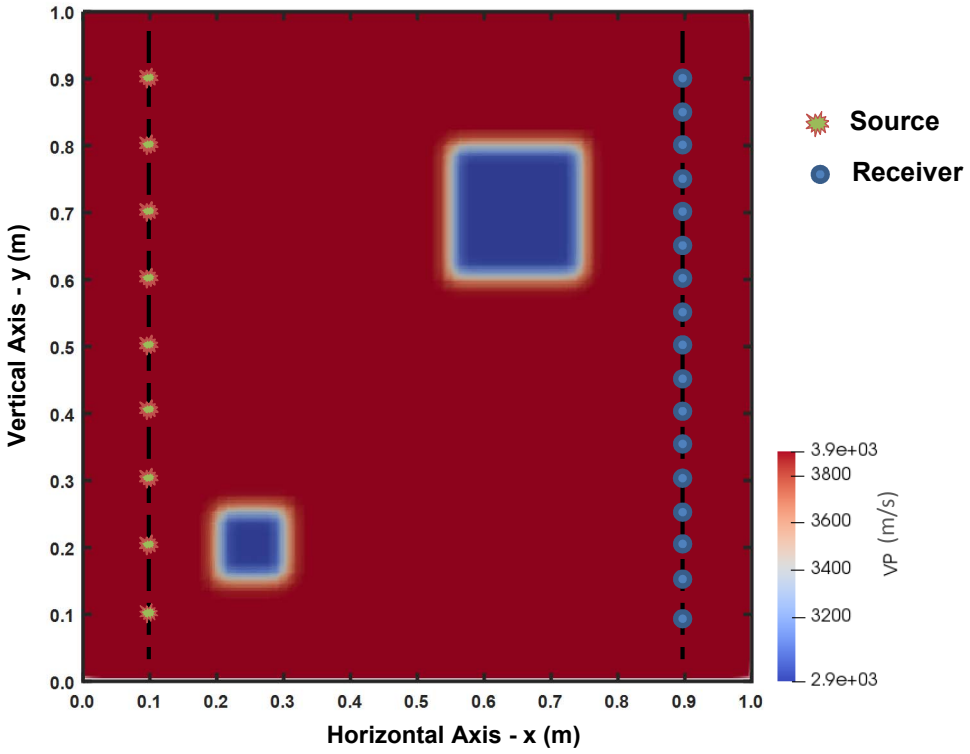


Figure 1. Two dimensional velocity model of in a cross-hole sonic testing setting.

RESULTS OF FWI AND CT AND DISCUSSION

The result of FWI is presented in Fig.2 as the distribution of inverted V_P in the model. Both anomalies are detected in the inverted model. However, the shape of both anomalies is much smoother than the true model, which results in oblong circular shapes instead of the squares in the true model. This can be attributed to the relatively large smoothing parameter for the regularization of the inversion and the finite aperture of the experiment. In the process of matching the two sets of waveforms through iterative optimization, attempting to get a complete fit generally leads to the failure of the optimization algorithm. In general, regularization is a tool used by users to prevent the inversion converging to a physically non-sensible solution. The smoothing parameter in this case controls the regularization. Due to the ill-posed nature of the inverse problem, a very small smoothing parameter increases the risk of converging to a model that is not physically meaningful or even failure of the inversion. Regulation, however, makes convergence of the inversion possible. A larger smoothing parameter makes the resulting model smoother with a faster convergence rate. Therefore the smoothing parameter controls the trade-off between the goodness of fit and quality of the model, so the increased tendency towards one usually means a decreased convergence rate towards the other. For a useful discussion on the choice of the smoothing parameter readers are referred to Modrak and Tromp (2016).

While the larger anomaly better approaches the anticipated shape and material properties, FWI overestimated both the size and V_P of the smaller anomaly. In both cases, the centroids of the anomalies compare favorably with the true locations in the model. The larger anomaly centroid was located at approximately 0.65 m along the x-axis and 0.7 m along the y-axis in the resulting FWI image, which is the same as the true model anomaly centroid location. The small anomaly was located at x = 0.23 m and y = 0.20 m in the FWI image, whereas it was located at x = 0.25 m and y = 0.20 m in the true model. Given the limited coverage of the waves on this anomaly, the inverted image is still satisfactory, as the presence of the small defect and its centroid was properly detected with only 0.03 cm (1 in) from the expected location

in the true model. These results would certainly provide useful information regarding the spatial extent and location of anomalies, which could be used to determine any negative effects on load-carry capacity and the degree to which remediation efforts would be necessary.

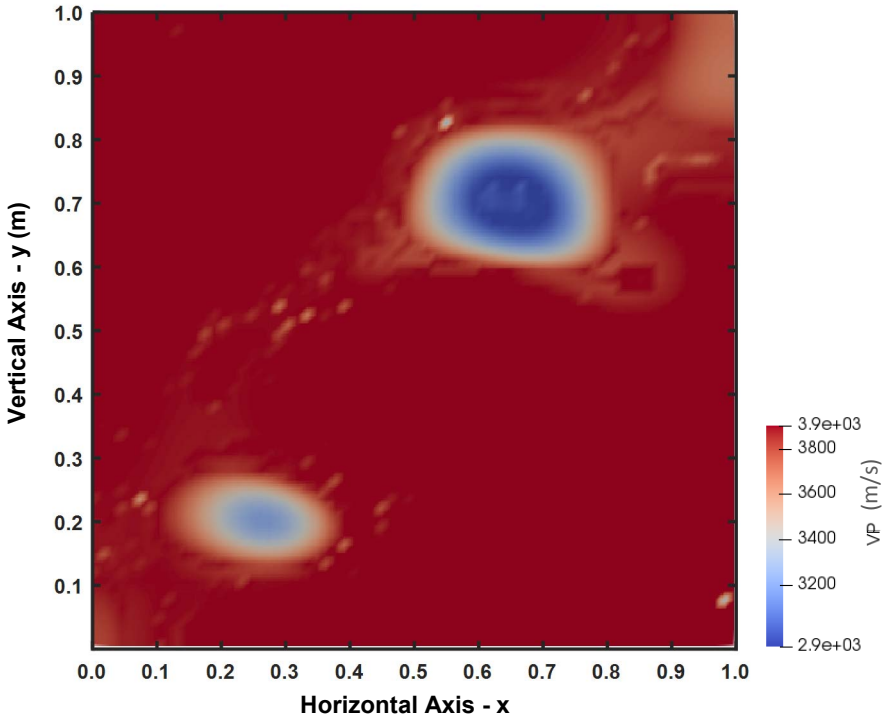


Figure 2. FWI results for V_P of the model.

It is also worth discussing how the image in FWI evolved. Figure 3(a) shows the starting model which is a uniform background speed model. Figure 3(b) presents how the anomalous features appear after 15 iterations of FWI with the cross correlation misfit function. It shows that the inversion is converging towards the true model; however, the inverted image is not still completely similar to the true model. This approach of using different misfit functions at different stages of inversion is in fact an effective way of preventing the inversion from failure. Using this results as the initial model for an L2 misfit, after a couple of iterations, more details on the wave speed and geometry of the features appear (Fig. 3.c).

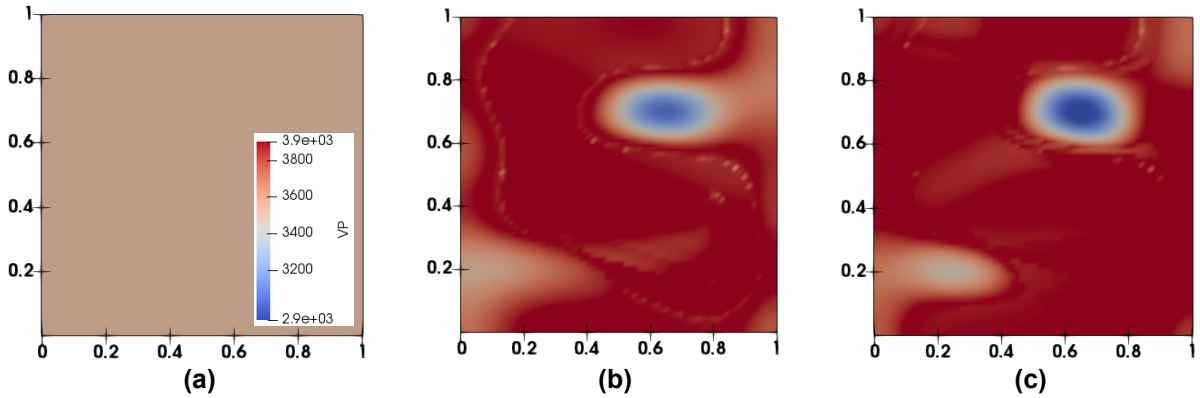


Figure 3. FWI results at different iterations, (a) starting model; (b) from Cross-correlation misfit; (c) from L2 misfit at the 10th iteration.

The picked travel-times from the waveforms were subsequently used for the CT travel-time inversion. A structured mesh with secondary nodes was first generated for the inversion. This domain was 1.0 m in depth and 0.8 m wide (which is the distance between the source and receiver arrays). The result of the CT analysis is presented in Fig. 4. Two regions of lower velocities are evident from the CT inverted image. The low velocity zone on the top-right hand side of Fig.4 is noticeably larger than the corresponding zone in the true model and in the FWI results. The shape is also much more incoherent than the squares in the true model and the oblong circular shapes in the FWI results. There is evidence of the smaller low-velocity zone on the lower left side of Fig. 4. However, this region is again oversized relative to the true conditions and much more difficult to assign a meaningful geometry. In both cases, the inverted CT image overestimates the V_P of the anomalies. With respect to location of the anomalies, the enlarged dimensions in the CT image create some difficulty in accurately assessing anomaly centroid locations. However, this location generally agrees well with the true model in the case of the larger anomaly [(0.7 m, 0.7 m) compared with (0.65 m, 0.7 m)]. The CT results imply though that this anomaly stretches as far over as x = 0.4 m compared to 0.5 m for the FWI image and 0.53 m in the true model. Given the irregular shape of the smaller anomaly and the enlarged zone over which V_P is observed to be lower than competent concrete (3900 m/s), it becomes impractical to asses a centroid location.

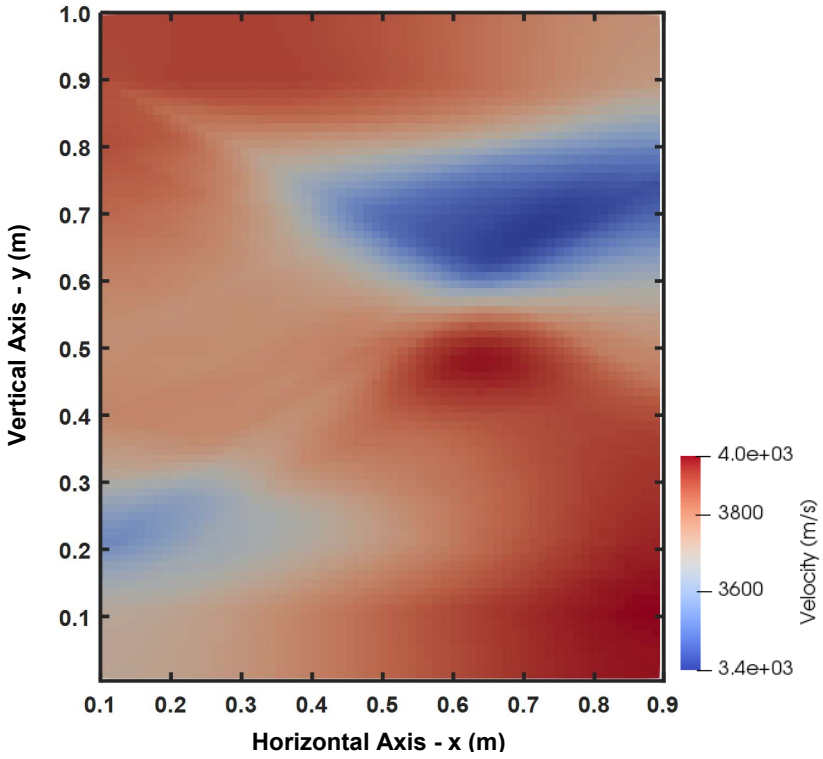


Figure 4. CT results for V_P based on travel-time of the simulated waveforms.

Although FWI yielded superior results, it took much higher computational effort and time. In fact, it took approximately 2.5 hours for the FWI to generate the present results, while the CT yielded the results in less than 10 minutes. Generally, the acquisition of redundant data is quite common in geophysical testing and NDT applications. In fact, some of the data acquired in the process contributes very limited information for constructing the image. The presence of such data, however, increases the computation time and efforts linearly. To investigate this issue, another numerical simulation was performed with 5 sources and 9 receivers using the same model domain as Fig. 1. In this simulation, every other source and receiver in Fig.1 was removed to model a reduced set of acquired data. The synthetic waveforms from this model were subsequently used to perform FWI and generate another image of the domain. CT analysis was not

performed given that FWI already proved superior for the case of an expanded set of acquired waveform data. The removal of sources and receivers would only serve to negatively affect the results of CT, which already was less capable than FWI in accurately assessing the anomalous regions.

The results of the second set of FWI analysis is presented in Fig. 5. Again, the inverted V_P model clearly distinguishes the zones of anomalous features from the competent concrete. A visual comparison of Fig. 2 and 5 demonstrates that the removal of sources and receivers in the data acquisition process did not overly affect the FWI results. In fact, the relative spatial extent, centroid locations, and estimated V_P of the anomalies are quite similar. More reductions in the number of sources and receivers and its impact on the quality of the results were not investigated, for the small defect started to appear with slightly higher velocity of the expected value. Given the similarities in the results between Fig. 2 and 5, it should be noted that any increase in computational efforts caused by an FWI approach can be at least partially offset by a reduction in efforts during the data acquisition phase.

Another important benefit of reducing the number of sources and receivers is reducing the computation time. In fact, the computation time in FWI is directly proportional to the number of sources. In this specific model, the reduction in the number of sources and receivers cut the computation time in half. It is also worth noting that as a results of this reduction in sources and receivers, the total number of waveforms went down from 153 to 45 traces, which means a 70-percent reduction in the amount of the acquired data. Putting this in the context of data acquisition in the field implies a meaningful reduction of acquisition time and efforts. This offset could help ensure that the improvements offered by FWI are indeed implemented in practice when anomalous features are detected in drilled shafts. Additionally, the spectral-element computations which contribute the bulk of the computational costs are almost perfectly scalable (Afanasiev et al. 2019) and significant efficiency gains can be realized by exploiting massively parallel (i.e. GPU-based) compute architectures (Komatitsch et al. 2010, Gokhberg and Fichtner, 2016). For these reasons we expect the computational cost of FWI to decrease significantly in the upcoming years.

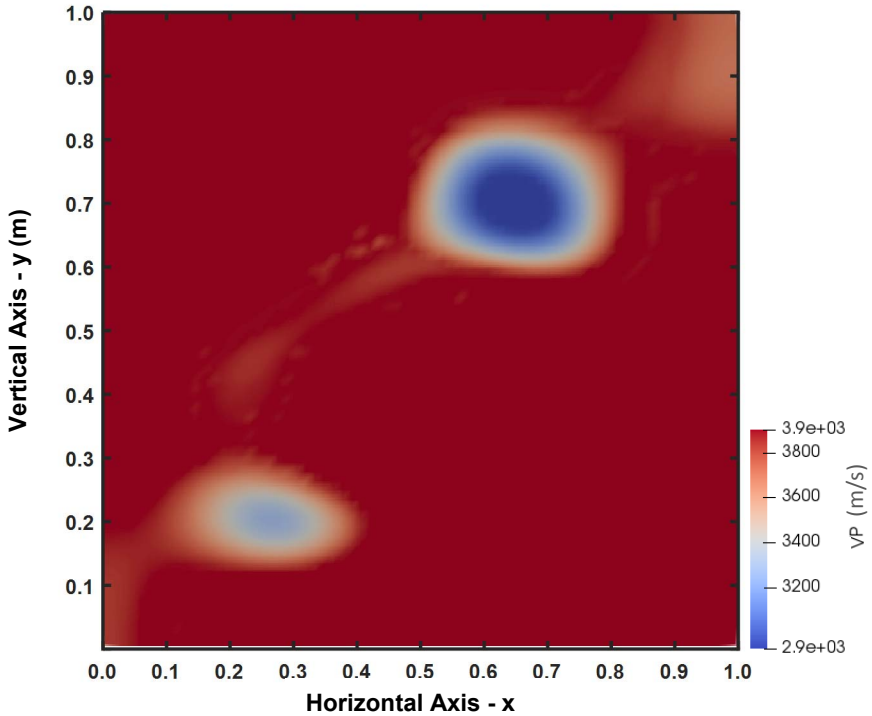


Figure 5. FWI results for V_P with a reduced array of 5 sources and 9 receivers.

CONCLUSIONS

In this study, the implementation of FWI to evaluate structural integrity of drilled shafts was numerically investigated. The main motivations behind this work are that FWI can generally yield high resolution images and CT has been shown to miss defects. The results of a direct comparison between the inverted model from FWI and CT showed that the former provides more accurate geometry and material properties of anomalies whose size was as small as 10% of the shaft cross-section. One of the key features of FWI in this application is that it avoids the need to select first-arrival times as is the case with CT. Generally, difficulties in picking travel-time can lead to errors in the CT inversion process. FWI is still in its development stage for geotechnical NDT purposes and research is continuing in this field to make it more accessible in practice. Despite the high-quality images resulting from FWI, the computational resources necessary for FWI are more extensive than CT. In order to mitigate this issue, FWI analysis was performed on the same domain with the number of sources and receivers reduced by almost half. The results were quite similar and highlighted that FWI was less dependent on redundancy in the data. CT data acquisition is generally very time-consuming as many combinations of source-receiver locations are tested. A reduction in the number of necessary measurements can significantly improve field data acquisition time and directly reduce the computational efforts of FWI to bring this approach closer in-line with CT and encourage the use of FWI in practice.

AKNOWLEDGEMENT

This research includes calculations carried out on Temple University's HPC resources and thus was supported in part by the National Science Foundation through major research instrumentation grant number 1625061 and by the US Army Research Laboratory under contract number W911NF-16-2-0189. The authors would like to thank Dr. Florian Wagner (University of Bonn, Germany) for his support with the pyGIMLi package.

REFERENCES

Afanasiev, M., Boehm, C., van Driel, M., Krischer, L., Rietmann, M., May, D.A., Knepley M.G., Fichtner, A. 2019. Modular and flexible spectral-element waveform modelling in two and three dimensions, Geophysical Journal International, Vol. 216(3), pp. 1675–1692.

Amir, J.M. and Amir, E.I. 2009. Capabilities and limitations of cross hole ultrasonic testing of piles. Proceeding of International Foundation Congress and Equipment Expo, Orlando, FL, pp. 536-544.

Boehm, C., Korta Martiartu, N., Vinard, N., Jovanovic Balic, I. and Fichtner, A. 2018. Time-domain spectral-element ultrasound waveform tomography using a stochastic quasi-Newton method, Proceeding SPIE 10580, Medical Imaging 2018: Ultrasonic Imaging and Tomography, 105800H.

Branagan, P., Vanderpool, W., Murvosh, H., and Klein, M. 2000. CSL defines CIDH defects; coring confirms results. Proceeding of Design Developments in Deep Found. Denver, CO., pp. 110-124.

Brown, D.A., Turner, J.P., Castelli, R.J. 2010. Drilled shafts: construction procedures and LRFD design methods. Publication No. FHWA-NHI-10-016, Washington, D.C., 970 p.

Coe, J.T., Mahvelati, S., and Kordjazi, A. 2019. Full waveform inversion to evaluate liquefaction triggering in soils exhibiting natural spatial stiffness variability. Proceeding of 7IECGE, Rome, Italy.

Davis, A.G. 1998. Assessing reliability of drilled shaft integrity testing. Transportation Research Record, 1633, pp. 108-116.

Fichtner, A. 2011. Full seismic waveform modeling and inversion. Springer-Verlag Berlin Heidelberg.

Giroux, B. and Larouche, B. 2013. Task-parallel implementation of 3D shortest path raytracing for geophysical applications. Computers &Geosciences, Vol. 54, pp. 30-141.

Gokhberg, A. and Fichtner, A. 2016. Full-waveform inversion on heterogeneous HPC systems. Computers & Geosciences, Vol. 89, pp. 260-268.

Hertlein, B., Verbeek, G., Fassett, R., and Arnold, M. 2016. A comparison of quality management for bored pile/drilled shaft (BP/DS) foundation construction and the implementation of recent technologies, DFI Journal, Vol. 10(2), pp. 87-94.

Hollema D.A. and Olson, L.D. 2002. Crosshole sonic logging and tomographic velocity imaging of a new drilled shaft bridge foundation. Proc. of International Symposium Non-Destructive Testing in Civil Engineering (NDT-CE), Berlin, Germany.

Iskander, M., Roy, D., Ealy, C., & Kelley, S. 2001. Class-A prediction of construction defects in drilled shafts. Transportation Research Record, Vol. 1772(1), pp. 73–83.

Iskander, M., Roy, D., Kelley, S., and Ealy, C. 2003. Drilled shaft defects: detection, and effects on capacity in varved clay. ASCE J. Geotech. Geoenviron. Eng., Vol. 129(12), pp. 1128-1137.

Jalinoos, F., Tran, K.T., Nguyen, T.D., and Agrawal, A.K. 2017. Evaluation of bridge abutments and bounded wall type structures with ultraseismic waveform tomography. ASCE J. Bridge Eng., Vol. 22(12), pp. 04017104-13.

Johnson, K.R. 2016. Analyzing thermal integrity profiling data for drilled shaft evaluation, DFI Journal, Vol. 10(1), pp. 25-33.

Komatitsch, D., Erlebarcher, G., Goddeke D., and Michea, D. 2010. High-order finite-element seismic wave propagation modeling with MPI on a large GPU cluster. J. Comp. Physics, Vol. 229, pp. 7692-7714.

Kordjazi, A., Coe, J.T., Mahvelati, S. 2018. Advances in stress-wave nondestructive testing methods for evaluation of deep foundations. DFI Journal, Vol. 12(2), pp. 108-121.

Modrak, R. and Tromp, J. 2016. Seismic waveform inversion best practices: regional, global and exploration test cases. Geophys. J. Int., Vol. 206, pp. 1864-1889.

Mullins, G. 2010. Thermal integrity profiling of drilled shafts. DFI Journal, Vol. 4(2), pp. 54-64.

Nguyen, L.T. and Modrak, R.T. 2018. Ultrasonic wavefield inversion and migration in complex heterogeneous structures: 2D numerical imaging and nondestructive testing experiments. Ultrasonics, Vol. 82, pp. 357-370.

O'Neil, M.W. 1991. Construction practices and defects in drilled shafts. Transportation Research Record, 1331, pp. 6-14.

O'Neill, M.W., Tabsh, S.W., and Sarhan, H. (2003). Response of drilled shafts with minor flaws to axial and lateral loads. Engineering Structures, Vol. 25, pp. 47-56.

Poulos, H.G. (2005). Pile behavior - consequences of geological and construction imperfections. ASCE J. Geotech. Geoenviron. Eng., Vol. 131(5), pp. 538-563.

Samtani, N.C., Jalinoos, F., and Poland, D.M. 2005. Integrity testing of drilled shafts - existing and new techniques. GEO Construction Quality Assurance/Quality Control Conference, Dallas, TX, pp. 596-608.

Santamarina, J.C. and Fratta, D. 2005. Discrete signals and inverse problems: an introduction for engineers and scientists. John Wiley & Sons Ltd, West Sussex, England.

Sarhan, H.A., O'Neil, M.W., and Hassan, K.M. 2002. Flexural performance of drilled shafts with minor flaws in stiff clay. J. Geotech. & GeoEnviron. Eng., 128(12), pp. 974-985.

Rücker, C., Günther, T., and Wagner, F.M. 2017. pyGIMLi: An open-source library for modelling and inversion in geophysics. Computers and Geosciences, Vol. 109, pp. 106-123.

Vinard, N., Martiartu, N.K., Boehm, C., Balic, I.J., and Fichtner, A. 2018. Optimized transducer configuration for ultrasound waveform tomography in breast cancer detection. Proc. SPIE Medical Imaging 2018: Ultrasonic Imaging and Tomography, pp. 105800I-1-15.

INNOVATIVE USE OF AN ACTIVE SOIL NAIL WALL IN LIEU OF PIT UNDERPINNING FOR A HISTORIC BUILDING

Yaser Taheri, P.E., Moretrench, Rockaway, New Jersey, USA, (976) 627-2100, ytaheri@moretrench.com
Maxim C. Schisler, P.E., Moretrench, Rockaway, New Jersey, USA, (976) 627-2100, mschisler@moretrench.com
Tai Luu, P.E., Moretrench, Rockaway, New Jersey, USA, (976) 627-2100, tluu@moretrench.com

ABSTRACT

The Stevens Gateway Project is an expansion of the Stevens Institute campus overlooking the Hudson River in Hoboken, NJ. The plans call for 90,000 ft^2 (8360 m^2) of new classroom, research, and student life facilities in new, 4-story buildings. The excavations for the building footprints were bounded by city streets and existing buildings, including the historic Carnegie Laboratory of Engineering, built in 1902. Pit underpinning was originally specified for the Carnegie building. However, given the depth of cut, construction time required for the 13 ft (4.9 m) deep pits would be substantial. The geotechnical contractor retained for the support of excavation work therefore offered an innovative active soil nail wall design that would meet project requirements in a shorter timeframe. Unlike the passive soil nail systems common in the industry that are chiefly used for soil slope stabilization, active soil nail walls contain pre-stressed anchor components to resist soil movement and limit settlement of soil and structures being contained. In addition to a discussion of the overall design approach of the active soil nail wall system, this paper will include a detailed description of its constructability and effectiveness. This project's use of a conventional slope stabilization technique for an unconventional purpose may have positive implications going forward.

Keywords: Soil Nail Wall, Active Soil Nail, Support of Excavation, Shoring, Shotcrete, Shotcrete Wall

INTRODUCTION

Stevens Institute of Technology is a private university in Hoboken, New Jersey that sits on the cliffs of the City of Hoboken overlooking the Hudson River and Manhattan Island to the east of the campus. In recent years, the university has executed numerous plans to expand and upgrade its campus academic, student life, and residential facilities. One such project is the Academic Gateway Complex. The plan adds 90,000 ft^2 (8360 m^2) of new classroom, research, and residential facilities while also enhancing community connections by building a park to serve as a green corridor for the city.

The proposed construction took place on the north and south side of 6th Street between Hudson Street and River Street. The project included the demolition of an existing university building followed by the construction of two, 4-story buildings on the north and south property lots. The north and south buildings will be connected by a second floor bridge spanning 6th Street. The buildings each contain a full basement extending from the proposed ground floor at approximately El. 41ft (12.5 m) to the basement subgrade at El. 26 ft (7.9 m). Each building will be constructed on respective mat foundations. Figure 1 presents an overview of the project area.

The north and south lots are bounded by city streets and residential and university properties with the Carnegie Building to the south and west of the south lot as seen in Figure 1. Due to the close proximity of existing buildings and city streets to the north and south lots of the Academic Gateway Complex, various support of excavation techniques were required to reach the mat foundation subgrades at El. 26 ft (7.9 m) The types of techniques implemented varied based on the site soil conditions detailed in the geotechnical report.

© 2019 Deep Foundations Institute

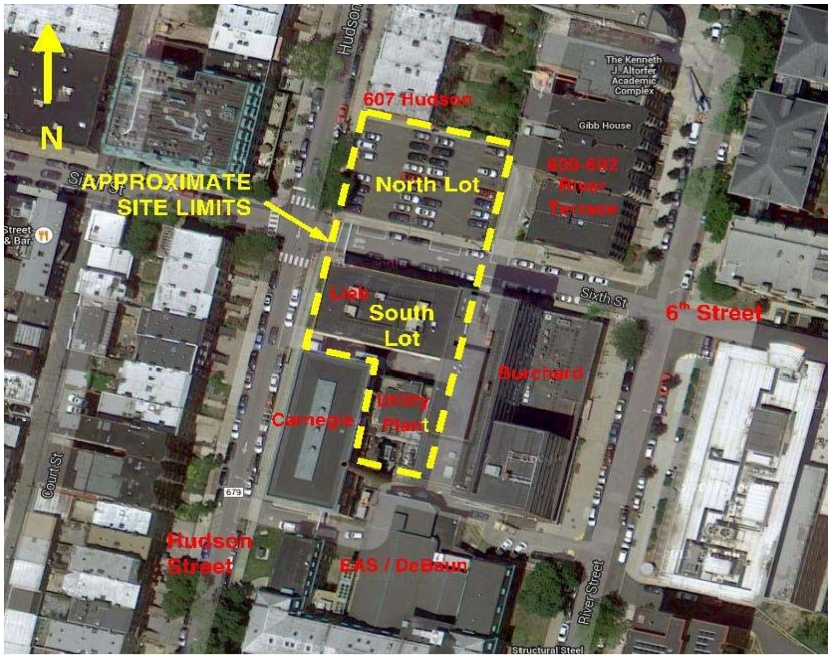


Fig. 1. Overall Site Plan of the Academic Gateway Complex

GEOTECHNICAL BACKGROUND AND RECOMMENDATIONS

Prior to construction, a geotechnical report was performed in February 2017 to better understand and identify the geological conditions expected to be encountered on site. The information from the geotechnical report was used by the engineer to recommend a design for the building foundations and the support of excavation.

The geotechnical investigation was comprised of 10 soil borings down to bedrock and nine test pits adjacent to the existing buildings to establish accurate building foundation subgrade elevations. The borings encountered a fill layer from the existing ground surface to a depth ranging from 4 ft to 12 ft (1.2 m to 3.6 m) below ground surface. Glacial soils were encountered in some borings below the fill from approximately 4 ft to 10 ft (1.2 m to 3.05 m) below ground surface and contained up to 35% of soil particles passing through the No. 200 sieve. The glacial soils also contained boulders up to 4 ft (1.2 m) in size that were discovered in some of the test pits. Some borings encountered cemented sand beneath the fill and glacial soils from approximately 7 ft to 20 ft (2.1 m to 6.1 m) below ground surface. A decomposed rock layer was encountered below the fill, glacial soils, and cemented sands. The decomposed rock was typically in the form of stiff to very stiff clay and sand with varying amounts of silt, gravel, and rock fragments. Rock underlaid the decomposed rock from El. 7 ft to El. -1ft (2.1m to -0.3 m) in the north lot and between El. 28 ft and El. 9 ft (8.5 and 2.7 m) in the south lot. The rock was classified as serpentinite with RQD values ranging from 27% to 75%.

The engineer's recommendation for the support of excavation was to use soldier pile and lagging walls with temporary anchors or rakers for soil retention, and pit underpinning techniques for the existing buildings that abut the proposed excavations. These buildings include 607 Hudson and the Carnegie building (Fig. 1). Conventional pit underpinning is accomplished using small wood-sheeted pits constructed beneath the foundation. Sheeted pits, typically 3 ft (1 m) wide, are hand-excavated below the footing to a competent bearing stratum. When the pit is completed, it is concreted to within several inches of the underside of the

existing footing and allowed to cure overnight. The gap is then dry-packed with stiff mortar to accomplish the load transfer. Pits are excavated and completed in a strategic order to form a continuous wall. Overall, the construction of pit underpinning is a time-consuming and labor-intensive process.

Figure 2 identifies the limits of the excavations required for the project as well as the locations of each type of support of excavation. The excavation limits marked in blue indicate where soldier pile-lagging walls may be used while the excavation limits marked in green indicate where the excavation abuts the existing buildings, requiring underpinning techniques.

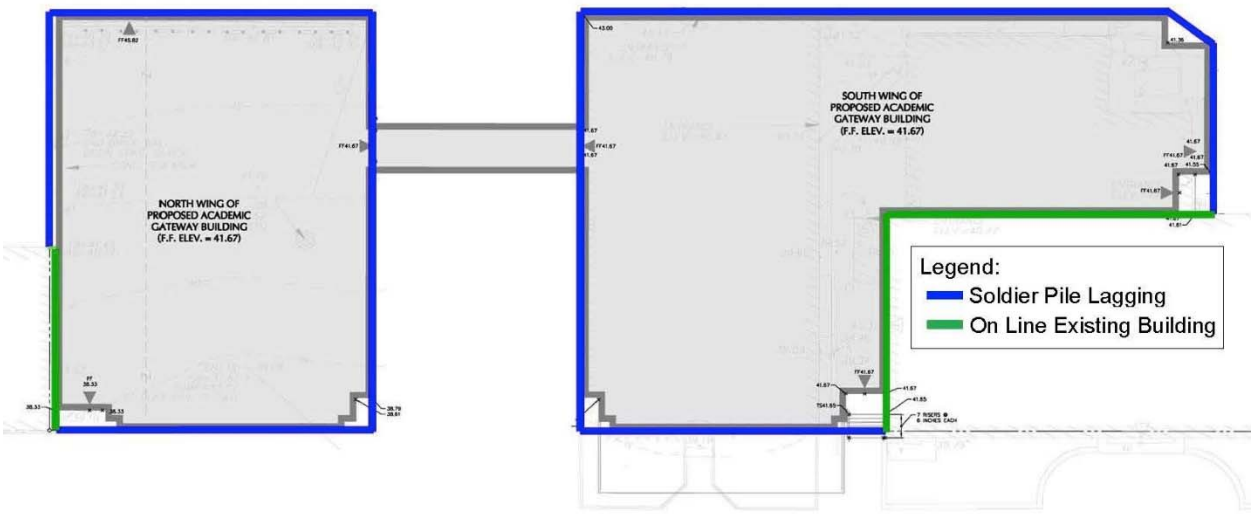


Fig. 2. Limits of Excavation for the North and South Lots

The underpinning for 607 Hudson building was required to extend from the bottom of existing footing at approximately El. 31 ft (9.4 m) to the subgrade of the Gateway building at EL. 26 ft (7.9 m). The bottom of the foundation for the Carnegie building was believed to be at approximately El. 39 ft to El. 37 ft (11.9 to 11.3 m). With the Gateway building foundations designed to be at El. 26, ft (7.9 m), the anticipated underpinning cut height needed to be approximately 11 ft to 13 ft (3.35 m to 3.96 m).

Upon reviewing the geotechnical information and evaluating of the existing foundations to be underpinned, 607 Hudson was found to rest on dense to very dense cementitious sands while the Carnegie building appeared to be underlain by glacial soils and decomposed rock. The geotechnical contractor came to the same conclusion as the engineer- that conventional pit underpinning would be an appropriate method to support 607 Hudson property. However, the contractor believed that a different technique should be utilized to support the Carnegie building to assist with the overall construction schedule.

The contractor offered an active soil nail wall design that would allow for excavation immediately adjacent to Carnegie building while meeting the project performance requirements. Unlike the passive soil nail systems common in the industry that are chiefly used for soil slope stabilization and earth retention, active soil nail walls contain pre-stressed anchor components to resist soil movement and effectively limit settlement of the soil and structures being contained.

ADVANTAGES OF AN ACTIVE SOIL NAIL WALL

Given the specific subsurface conditions under the Carnegie building, there were several drawbacks to the use of pit underpinning for this particular application that could be readily overcome by the use of an active soil nail wall.

Glacial soils with apparent cohesion and Decomposed Rock

As mentioned in the geotechnical report, the Carnegie building was known to rest on top of a dense soil layer with SPT N-values as high as 99 blows per foot and fine content ranging from 25% to 35%. More specifically, laboratory testing conducted on the samples retrieved from boring LB-7 found that the soils under the Carnegie building have a USCS soil classification of SM and have at least 25% of the soil grains passing through the No. 200 sieve. The apparent cohesion of the soil is expected to range from 100 psf to 200 psf (4.8 kPa to 9.6 kPa) for the soil layers under the Carnegie building (*FHWA Soil Nail Walls Reference Manual 2015)*. Figure 3 references the maximum values of apparent cohesion to be used for sandy soils. This temporary property of the soil provides sufficient standup ability to the ground during excavation.

Percent Passing No. 200 Sieve by Weight (%)	Maximum Apparent Cohesion, psf (kPa)
5-15	50 (2.4)
15-25	100 (4.8)
25-50	200 (9.6)

Fig. 3. FHWA Maximum Values of Apparent Cohesion

In addition, the boring logs also indicated the presence of decomposed rock under the Carnegie building. The decomposed rock was typically in the form of stiff to very stiff clay and sand with varying amounts of silt, gravel, and rock fragments. This is another suitable material for soil nailing. The fine content present in the soils as well as decomposed rock underlying the Carnegie building allowed the use of an active soil nail wall.

It must be noted that hand-excavation of these types of soils, especially in a confined space, is extremely difficult and is a time-consuming process. The presence of these materials under the Carnegie building would have made the excavation of pit underpinning an extremely slow and laborious construction method.

Bouldery Conditions

The presence of boulders under the Carnegie building would have been extremely consequential to the production of the pit underpinning pier installation procedures. The site contractor experienced a significant number of boulders in the overburden materials. If boulders were found to be fully or partially in the excavation path of an underpinning pier, the boulder would need to be removed manually in manageable pieces. This would have been a very time-consuming task for the workers to chip the rock with hand powered tools since there is no way of accessing such a deep pit with an excavator or other track-mounted

equipment. Figure 4 illustrates an example of the various sizes of some of the boulder found on site by the excavating contractor.



Fig. 4. A stockpile of boulders found on site during excavation efforts

During the removal process, there is a high risk of the boulder falling into the excavation area creating a large void directly under the building. This may result in differential building settlement. One such boulder was indeed encountered during the excavation to establish the shotcrete wall. The boulder was eventually shot in place in order to expedite construction. Figure 5 illustrates this situation.



Fig. 5. Boulder shot in place halfway under Carnegie

The use of an active soil nail wall as an excavation support technique significantly reduced the risk of excavating boulders by hand. All of the excavating was done by an excavator adjacent to the Carnegie building foundation footprint. The soils directly underneath the Carnegie building were minimally disturbed since the soil nail wall excavation limits remained outside of the Carnegie building foundation. This significantly limited the disturbance induced to the foundation.

Irregular Carnegie Foundations

The irregular foundations discovered under the Carnegie building in the test pit explorations performed during the geotechnical investigation would have further complicated the construction of a traditional pit underpinning system. Several test pits were dug adjacent to the Carnegie building that indicated that the foundation type varied along the limits of excavation. For example, TP-2 was performed on the northern facade of the Carnegie building and showed the foundation to be made up of cemented sand mixed with concrete and brick at approximately El. 37± ft (11.3 m). Alternatively, LTP-6 was performed on the western facade and discovered a concrete footing extending to El. 36± ft (10.9 m).

Based on the varying foundation types discovered, there would have been inherent potential risks in the construction of a pit underpinning system. Given that some of the foundations were composed of cemented stones, the foundation may have begun to disintegrate once undermined during underpinning efforts. The soil nail wall does not directly expose the soils underneath the foundation of the building. This minimized the risks described above.

Decomposed Rock

Decomposed rock discovered above the bottom of site excavation subgrade would have greatly limited the production of hand excavated pit underpinning piers. Figure 6 shows the excavation of the decomposed rock discovered within the last five feet (1.5 m) of excavation.

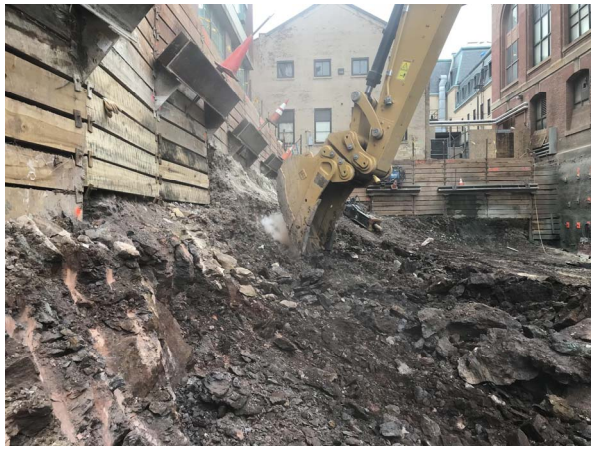


Fig. 6. Excavation of the decomposed bedrock found close to the subgrade of the south lot building foundation

It is evident in Figure 6 that the decomposed rock posed an issue for even the large excavator implemented for the bulk excavation work performed on site. The soil broke apart in flakey chunks that were scraped away from the virgin soil material by the bucket. Digging through this soil by hand underneath the Carnegie building would have proved to be a very slow and laborious process. The workers would have had to implement chipping hammers to break apart the soils and rock fragments. All of the excavation work for soil nailing could be performed by machines. this technique therefore proved much more efficient in supporting the Carnegie Building.

Overall Advantages

Based on the presence of glacial soil with apparent cohesion, the existence of boulders in the soils, the irregular foundations of the Carnegie building, and the presence of decomposed rock above the proposed construction subgrade, the use of an active soil nail wall in this application shortened the shoring construction schedule and improved safety during construction.

DESIGN CONSIDERATIONS FOR AN ACTIVE SOIL NAIL WALL

In a conventional approach, a soil nail wall is considered a passive type of earth retaining structure. Such a structure requires movement in order to mobilize resistance on the reinforcing elements. The project performance specifications limited the vertical movement of the building to 0.25 in. (6.35 mm) to prevent any damage to the existing Carnegie building. Normally, conventional soil nail walls would exceed this threshold in the process of generating resistance. However, in order to take advantage of the benefits provided by soil nailing construction technique discussed above, several key modifications in the design and implementation approach were needed to make the project successful.

First, the soil nail design was analyzed as an active earth retention system ,with surcharge of the building directly on top of the wall. The surcharge for the Carnegie building was estimated using the historical plan and data provided to the contractor. The surcharge was taken as a stiff wall element using Boussinesq's method for lateral earth pressure increase due to the vertical surcharge. The design section and stiffness of the shotcrete was considered to reduce the wall flexural movement during excavation. Active loading on the soil nails was considered similarly to anchors in a retention system. Prestressing loads for the soil nails were determined by the equilibrium force method. Flexural deflection of the reinforcement shotcrete section was designed to be minimal under full excavation conditions.

Secondly, the nails implemented in the field each had a free stressing length and bond length just like a tieback. Nails were bonded beyond the failure plane of the wedge. Nails on the first row and second row where movement was critical were tested and locked off. The implementation of these measures ensured the soil underneath the Carnegie foundation was retained with limited movement. This in turn helped the existing foundation to perform as it was intended prior to excavation.

FIELD CONSIDERATIONS AND WORK SEQUENCE

In addition to deviations the contractor made from traditional soil nail design, the contractor also made various constructability changes to the sequencing typically seen for soil nail wall installation. In soil nail construction, a vertical lift 4-5 ft deep (1.4-1.5 m), is excavated along the wall alignment, with the face of the cut fully stabilized before excavation of the next level. The horizontal length of the excavation is directly related to the area of soil face that can be completed in one working day. Closely spaced reinforcing bars (nails) are installed across the cut face that has already been shotcreted. The structural shotcrete fascia bridges the nails and supports the soil/rock between nails.

For the Stevens Gateway project, the constructability considerations implemented worked to minimized the risk of settlement on the Carnegie building. To meet that objective, the following procedures were adopted: A berm was placed in front of the wall on a 1:1 slope with a 3 ft (1 m) wide bench at the top. Next, the soil nails were installed through the berm and allowed to cure for a longer period of time. Finally, the berm was excavated to the finished slope and the shotcrete was installed. The berm is shown in cross section in Figure 7 from the contract drawings, and a photo taken prior to soil nail installation is shown in Figure 8.

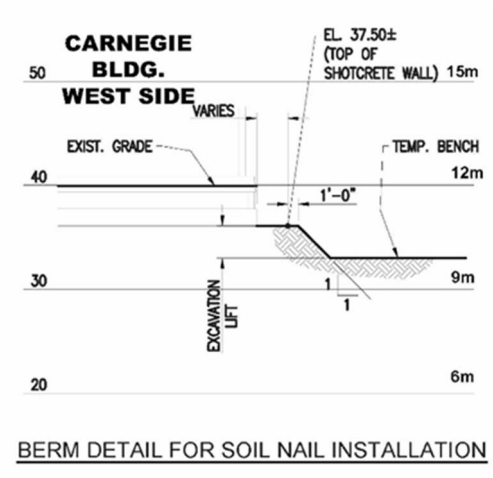




Fig. 7. Carnegie Building Soil Nail Wall Berm

Fig. 8. Carnegie Building Berm

This sequencing only exposed the finished slope for a maximum of 4 hours for each excavation lift. Each shotcrete lift was installed at a maximum plan linear foot length of 25 ft (7.6 m) at a time. The soil berm and the sequencing dimensions minimized the amount of time that the building was exposed to the most risk of settlement. This sequence alteration was crucial to the successful implementation of the active soil nail system under the Carnegie building. Figure 9 shows a photo of the soil nail wall prior to shooting the finished grade with shotcrete, and Figure 10 shows the shotcrete wall after tier 2 was shot. A boulder can be seen suspended halfway in the shotcrete wall.





Fig. 9. Shotcrete panel preparations

Fig. 10. Shotcrete wall section

The contractor drilled each soil nail using rotary duplex drilling techniques to ensure no unintended ground loss occurred during the soil nail drilling process. The casing and drill string were advanced simultaneously so that no soil caving could occur inside the holes. Despite the minor impact to the drilling production that duplex drilling inherently causes, this drilling method was still used and ultimately reduced the risk of settlement of the Carnegie Building's foundation.

CONCLUSIONS

Overall, active soil nailing proved to be the most efficient support of excavation technique, given the site real estate constraints and geological conditions. The system incorporated the constructability and productivity advantages of soil nailing with the design robustness of a conventional active earth retention system. If site real estate were not a concern for this area, perhaps traditional earth retention techniques would have been most efficient. Alternatively, if the underlain soils did not contain boulders or decomposed rock, traditional underpinning would have been an excellent shoring technique to pursue.

The unconventional use of a conventional soil nail wall ultimately allowed the contractor to complete the foundation work faster than was expected, which was beneficial for the project. By constructing a strong earth retention system through this method, the soil beneath the Carnegie building was retained in an effective manner. In addition, practicing this technique significantly expedited the construction schedule due to the risk of encountering boulders and other geotechnical impediments explored above. The benefits of this system in this situation are both of safety and productivity. For those reasons, cases where active soil nail walls could be implemented should be explored. Figure 11 shows the finished active soil nail wall.



Fig. 11. Finished Active Soil Nail Wall

ACKNOWLEDGEMENTS

The authors would like to recognize and thank Michael McNicholas, P.E. of Moretrench for his technical assistance and review during the project and the writing of this paper.

UNIQUE ALGORITHM WHICH TAKES INTO ACCOUNT SOURCE WAVE TRAVEL PATHS WHEN ESTIMATING ABSORPTION VALUES FROM DST DATA SETS

Erick Baziw
Baziw Consulting Engineers Ltd., Vancouver, Canada
Gerald Verbeek
Baziw Consulting Engineers Ltd., Vancouver, Canada

ABSTRACT:
Dynamic soil analysis (DSA) in geotechnical practice is intimately related to the capability of measuring the necessary soil properties of shear modulus and absorption. In DSA the methods of analysis are based upon the stress-deformation response of soils due to imposed shear strains. Typically the soil profile is numerically modeled as linear visco-elastic system. This technique is referred to as the Equivalent Linear (EL) method, and it requires the specification of the input parameters of low-strain ($<10^{-5}$) shear modulus, modulus reduction, and the equivalent viscous damping ratio, which is directly related to the soil absorption value. Downhole seismic testing (DST) has proven to be a very accurate tool for estimating low strain shear modulus values as long as source wave raypaths are taken into account, especially for near-surface investigations. DST has also been utilized to estimate low-strain interval absorption values. In these cases standard frequency domain absorption estimation algorithms (such as the spectral ratio technique) are utilized where it is assumed that the source waves are traveling along the same travel path, which is obviously not the case for near surface DST investigations. This paper outlines a unique DST absorption estimation methodology, which is carried out in the time domain and takes into account source wave travel paths.

1. INTRODUCTION

There is considerable interest in methods of geotechnical *in-situ* engineering that provide accurate estimates of the shear wave velocity and the associated absorption values in the ground, since these parameters form the core of mathematical theorems to describe the elasticity/plasticity of soils and they are used to predict the soil response (settlement, liquefaction or failure) to imposed loads (whether from foundations, heavy equipment, earthquakes or explosions).

In dynamic soil analysis the methods are based upon the stress-deformation response of soils due to imposed shear strains (Finn, 1984; Idriss, 1990; Idriss and Sun, 1992; Ishihara, 1982; Kramer and Paulsen, 2004; Seed and Idriss, 1970; Wilson and Clough, 1962). A fundamental assumption made in the majority of these techniques is that soil deformations are a result of vertically propagating shear waves. Seed and Idriss (1970) implemented the wave equation with the assumption of harmonic vertically propagating shear waves. In this case a 2nd order linear visco-elastic system (also termed spring-mass-dashpot system) is assumed when numerically modeling soil response characteristics to dynamic loading. This technique is referred to as the Equivalent Linear (EL) method, which is the most commonly utilized ground modeling technique in practice (Kramer and Paulsen, 2004). The important parameters required within the EL method are the low-strain shear modulus (G_0), the modulus reduction and the equivalent

© 2019 Deep Foundations Institute

viscous shear damping ratio (η_s), which is proportional to the energy loss from a single cycle of shear deformation.

Downhole Seismic Testing (DST) has proven to be a very effective tool for the estimation of low the strain shear modulus G_0 (ASTM, 2017; Baziw, 2002; Baziw and Verbeek, 2012 and 2014). In a DST configuration a seismic source is used to generate a seismic wave train at the ground surface. One or more downhole seismic receivers are used to record the seismic wave train at predefined depth increments. These downhole receiver(s) may be positioned at selected test depths in a borehole or advanced as part of an instrumentation package as in the case of Seismic Cone Penetration Testing (SCPT). When triggered by the seismic source a data recording system records the response of the downhole receiver(s).

DST is also utilized for low strain estimation of the shear damping ratio η_s, which is important when predicting and assessing ground amplification during earthquakes (Stewart and Campanella, 1993). The low strain shear damping ratio is also used as a reference point for laboratory test results, such as Resonant Column Test data. This paper outlines a new technique for estimating η_s values from DST seismic data: the Forward Modeling Downhill Simplex Method Absorption Analysis (FMDSMAA). This technique utilizes several estimated in-situ parameters (such interval velocities, source wave travel paths, angles of incidence and reflection, density, and source wave amplitudes) when estimating absorption values, and takes the soil structure into account as up to eight absorption values (eight layers) are estimated simultaneously along with the geometric spreading exponent. The FMDSMAA technique provides automatically an error estimate, which is equal to the residual between the synthetic and measured amplitude ratios for each depth increment.

2. ABSORPTION ANALYSIS

Attenuation of a seismic wave propagating in soils is the decay of the wave amplitude in space (Aki and Richards, 2002; Gibowicz and Kijko, 1994; Sheriff and Geldart, 1982). Total attenuation arises from geometric spreading (due to the change in wave front), apparent attenuation (due to mode conversion, reflection-refraction at an interface) and material losses (intrinsic attenuation or absorption). In general terms, the earth acts as both a low pass filter and an attenuator as a seismic wave travels through it. The signal amplitude A within a homogeneous medium at distance x from the source is related to the amplitude A_0 at distance x_0 by

$$A(x) = A_0(x_0/x)^n e^{-\alpha(x-x_0)} \tag{1}$$

In (1) it is assumed that the decay is due to only geometric spreading and absorption. The *Quality Factor*, Q, is related to the absorption coefficient as follows:

$$Q = \pi/\alpha\lambda \tag{2}$$

In eq. (2) λ is the source wave's wavelength. The *Quality Factor* is a desirable term to define the absorption of a medium because it is nondispersive. The *logarithmic decrement,* δ, and *fraction of critical damping or damping ratio*, η, are expressed as

$$\delta = ln\left(\frac{amplitude}{amplitude\ one\ cycle\ later}\right) = \alpha\lambda = \pi/Q \tag{3}$$

$$\eta = \frac{\delta}{2\pi} = \frac{1}{2Q} \tag{4}$$

Tables 1 and 2 outline estimates of soil damping ratios for laboratory and field measurements, respectively

The amplitude decay term in eq. (1) $(x_0/x)^n$ corresponds to geometric spreading where $n = 1$ based upon the conservation of the energy flux of a traveling seismic wave and spherical divergence. Some researchers have noted that the amplitude of the seismic wave generally does not decay as $1/r$ where r is the travel distance and this why the exponent n is incorporated into eq. (1).

The apparent attenuation due refraction at an interface is quantified by the transmission coefficient, which quantifies the loss of energy when transitioning from layer 1 to layer 2 as outlined below in eq. (5).

$$T_{12} = \frac{A_2}{A_1} = \frac{2G_1\eta_1}{G_1\eta_1 + G_2\eta_2} = \frac{2Z_1}{Z_1 + Z_2} = \frac{\boldsymbol{2\rho_1 V_1 cos\theta_1}}{\boldsymbol{\rho_1 V_1 cos\theta_1 + \rho_2 V_2 cos\theta_2}} \tag{5}$$

In eq. (5) T_{12} is the transmission coefficient for the source traveling moving from layer 1 to 2, A_1 is the amplitude of incident wave, A_2 the amplitude of refracted wave, ρ_i is the medium density of layer i, θ_1 denotes the incident angle, θ_2 is the refraction angle, V_1 is the medium velocity of layer 1, V_2 is the medium velocity layer 2 (note: $Z_i = \rho_i V_i$ is the *acoustic impedance)*, G_i the shear modulus of medium i (note $G = \rho V_s^2$), and η_i is the vertical slowness within medium i. Note that the fractions of energy reflected ($E_R = R^2$ (where is the reflection coefficient)) and transmitted ($E_T = \frac{Z_2}{Z_1} T^2$) must add to one (i.e., $E_R + E_T = 1$).

.

Table 1: Laboratory measurements of soil damping (after Stewart and Campanella, 1993)

Soil Type	Strain (%)	Damping η_s (% Np)	Q (1/Np)	Q (1/dB)	Reference
Cohesive	10^{-3}	3(1-5)	16.7(50-10)	1.92(5.76-1.15)	*Sun et al. 1988*
Clay	10^{-3}	0.9-2.4	55.6-20.8	6.4-2.4	*Zavoral 1990*
Sand	10^{-3}	1.5	33.3	3.8	*Ishihara 1982*
Cohesionless	10^{-4}-10^{-3}	0.5-2	100-25	11.5-2.9	*Seed et al. 1986*
Sand	10^{-3}	1	50	5.8	*Saxena and Reddy 1989*

3.0 SPECTRAL RATIO TECHNIQUE

The Spectral Ratio Technique (SRT) is the most widely used method for determining Q or damping ratio from P or S waves acquired in the field (e.g., Rebollar, 1984; Campillo *et al.*, 1985; Redpath and Lee, 1986; Blakeslee *et al.*, 1989; Kvamme and Havskov,, 1989).

Table 2: Field measurements of soil damping (after Stewart and Campanella, 1993)

Soil Type	Damping η_s (% Np)	Reference
Sand	6	Kudo and Shima 1981
Silt	2.5	Kudo and Shima 1981
Alluvium (sand and clay)	12(<25m);3.5 (>25m)	B.B. Redpath (private communication) (laboratory: 1.5-3.5%)
Sandy	5	Tonouchi *et al.* 1983
Clayey	1.7	Tonouchi *et al.* 1983
Fine Sand	1.7	Tonouchi *et al.* 1983
Bay mud	2.5	Tonouchi *et al.* 1983
	4	B.B. Redpath (private communication) (laboratory: 2.5%)
Clay	4-7	Mok *et al.* 1988
Sand	2-3	Mok *et al.* 1988 (laboratory: 0.7%)

But the implementation of the SRT in DST has two major limitations: inaccurate raypath assumptions and spectral ratio estimation sensitivities. Although it is not necessarily emphasized, SRT assumes that the source waves travel along the same path.. While this may very well be the case for crosshole seismic testing (as shown in Fig. 1), it is certainly not the case for DST. Source wave trajectories adhere to *Fermat's principle*, which means that the raypath travels along the trajectory that minimizes the travel time between points, and that means that every depth the raypath will be different as shown in Fig.2 (Baziw 2002; Baziw and Verbeek 2012 and 2014).



Figure 1: Assumed source wave travel paths when implementing SRT.

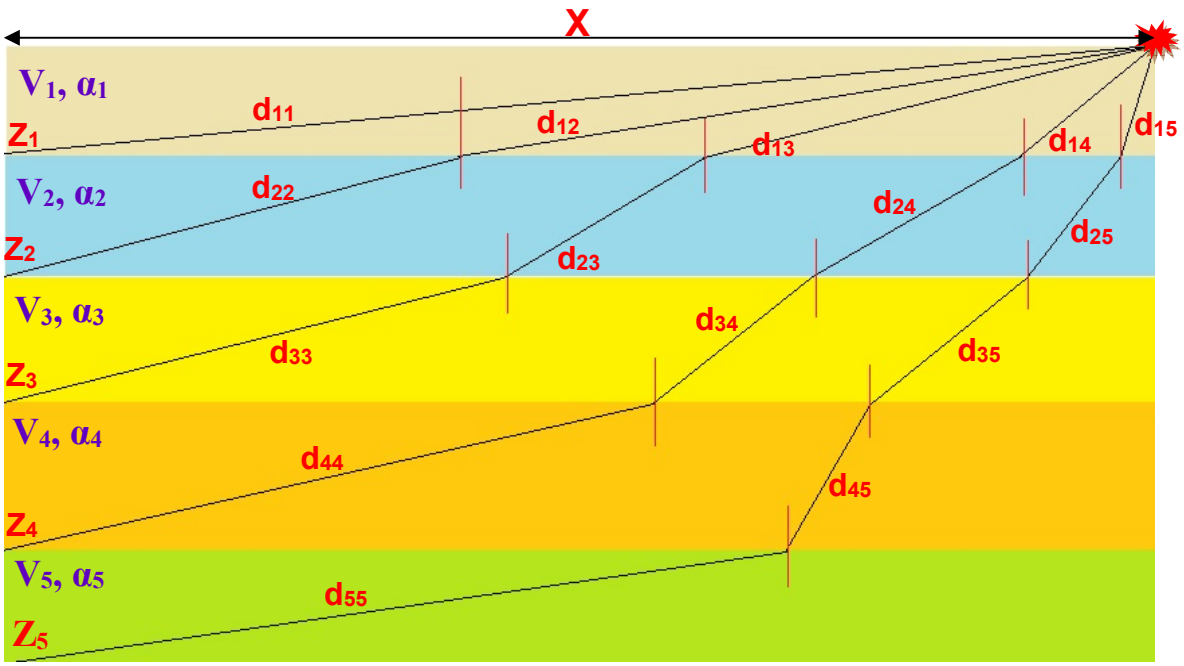


Figure 2: Near surface DST where SRT assumptions are not valid.

In addition SRT, just like any other frequency domain absorption estimation technique, can be highly susceptible to additive measurement noise or minor source wave distortions. This is best explained with an example. Figure 3 shows a wave (Wave 1) with a dominant frequency of 55 Hz that is assumed to be recorded at a vertical depth of 5m with a seismic source radial offset (X in Fig. 2) of 1.5m. Assuming that this wave travels through soil with a Q value of 30 Np^{-1} and a shear wave velocity of 153 m/s, the wave will reach a depth of 10 m 32 ms later (Wave 2). Figure 4 illustrates the output after applying the SRT on the traces illustrated in Fig. 3 and as is shown the derived Q value of 31.2 Np^{-1} is very close to the true value of 30 Np^{-1}. However, if a small amount of low frequency measurement noise is applied to Wave 1 and 2 (as illustrated in Fig. 5) the derived results change dramatically as shown in Fig 6: now the derived Q value of 6 Np^{-1} deviates significantly from the true Q value of 30 Np^{-1}.

Figures 7 and 8 illustrate a real data example of the challenges in applying the SRT. In this real data example SCPT seismic traces are acquired at depths of 3m and 15m as illustrated in Fig. 7. As is evident in Fig. 7, the maximum amplitude of the 3m traces is orders of magnitude greater than that of the 15m seismic trace. Figure 8 illustrates the results after applying the SRT on the traces illustrated in Fig. 7, generating a nonsensical estimate for Q of -66 Np^{-1}, implying that there was an increase in amplitude due to absorption as the source wave travelled to greater depths. In Fig. 7 rectangular time windows are applied to the full waveform seismic data under analysis so that spurious time series recordings and measurement noise are minimally incorporated into the spectral ratio analysis (Stewart & Campanella, 1993). The rectangular time window has an amplitude of 1.0 within a time span between t_1 and t_2. Start time t_1 is defined as the time location when moving back in time one zero crossing from the time index of the maximum pulse. End time t_2 is defined as the time location when moving forward in time two zero crossing from the time index of the maximum pulse.

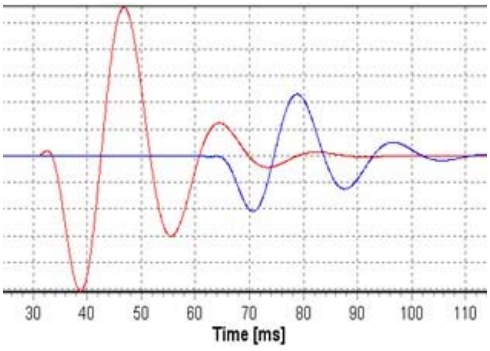


Figure 3. Source Wave 2 (in blue) superimposed on Source Wave 1 (in red) with 32 ms time offset.

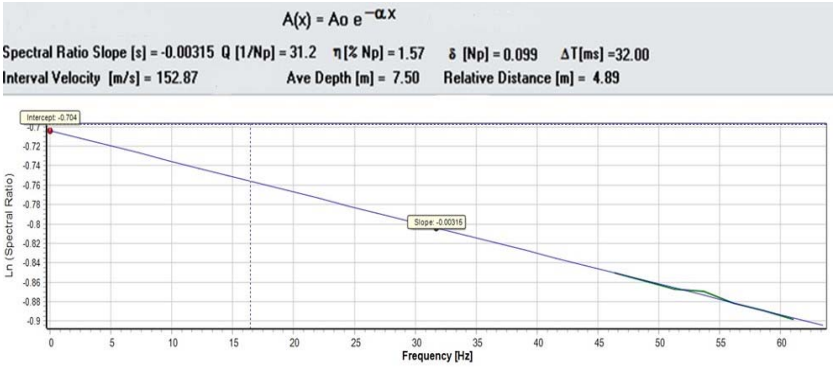


Figure 4: Output from SRT when processing the traces illustrated in Fig. 3. The estimated Q of 31.2 Np^{-1} is very close to the true Q value of 30 Np^{-1}.

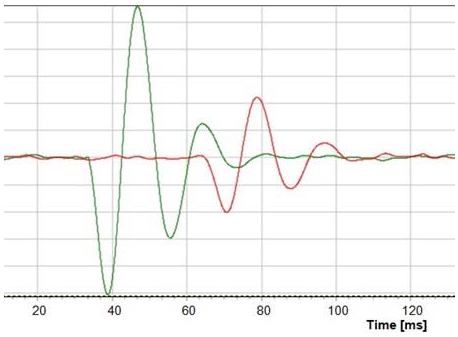


Figure 5. Traces illustrated in Fig. 3 with a small amount of additive measurement noise applied.

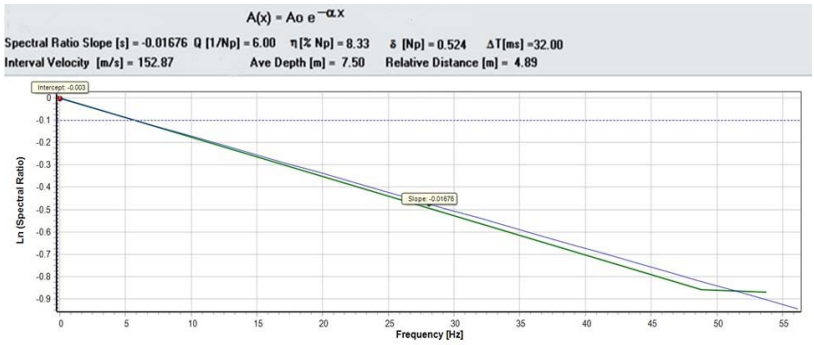


Figure 6. Output from SRT when processing the traces illustrated in Fig. 5. The estimated Q of 6 Np^{-1} deviates significantly from the true Q value of 30 Np.

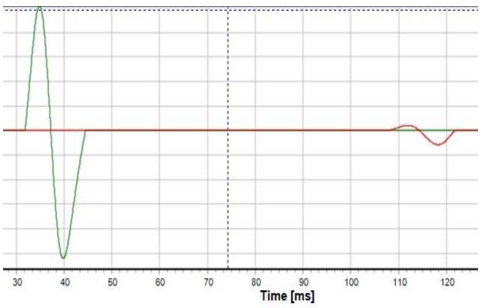


Figure 7. Real SCPT data with seismic traces acquired at 3m (green) and 15m (red).

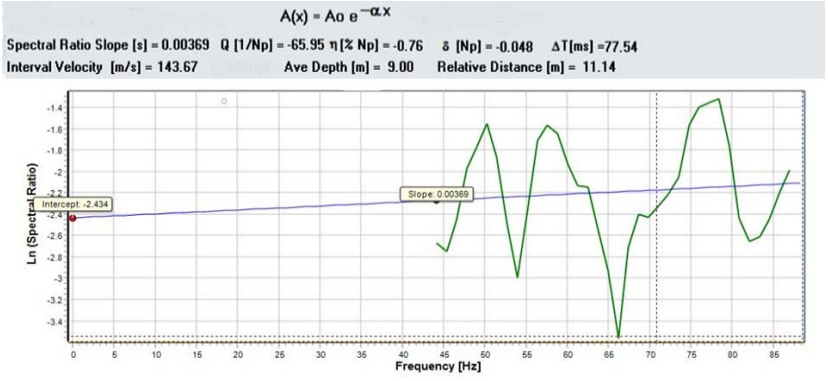


Figure 8. Output from SRT when processing the traces illustrated in Fig. 7. The SRT gives a nonsensical estimated Q of -66 Np^{-1}.

4.0 FMDSMAA TECHNIQUE

To address the SRT shortcomings a new algorithm was developed, which combines the Forward Modeling/Downhole Simplex Method (FMDSM) to ensure that the assumed raypaths are as accurate as possible with an Absorption Analysis (AA) that uses the absolute value of the full waveform amplitude as outlined in eq. (16).

$$|\rho(t)| = \sqrt{(X(t))^2 + (Y(t))^2 + (Z(t))^2} \tag{6}$$

where X(t), Y(t) and Z(t) are the orthogonal seismic sensor responses (where in case of an SH wave the Z(t) component can be ignored). The maximum $|\rho(t)|$ value is determined over the time window of the source wave responses, and it is obviously significantly simpler to obtain this full waveform maximum amplitude as opposed to rotating the X(t), Y(t) and Z(t) responses onto the full waveform, which is required for the SRT. Moreover, for low linearity traces source wave distortion can occur during rotation onto the full waveform, which can result in frequency distortion and poor SRT results as previously illustrated.

FMDMSAA technique utilizes several estimated in-situ parameters (such interval velocities, source wave travel paths, angles of incidence and reflection, density, and source wave amplitudes) when estimating absorption values, and it takes the soil structure into account as up to eight absorption values (eight layers) along with the geometric spreading exponent are estimated simultaneously. The FMDSMAA technique provides automatically an error estimate (i.e. the residual between the synthetic and measured amplitude ratios for each depth increment) and the algorithm allows for specification of minimum and maximum Q values to enhance the algorithm's performance.

4.1 FMDSMAA Algorithm Outline

The signal amplitudes for seismic traces recorded at various depths are defined utilizing eqs. (1) and (5) and the parameters illustrated in Fig. 2. In the subsequently outlined equations it assumed that there is an initial reference distance from the source of 0.1 m (i.e., $x_0 = 0.1m$ in eq. (1)). Equations (7), (8), (9), and (10) outlined below define the expected source amplitude for traces recorded at depths D_1, D_2, D_3, and D_4, respectively.

$$A_1 = A_0 \left(\frac{x_0}{d_{11}}\right)^n e^{-\alpha_1 (d_{11} - x_0)} \tag{7}$$

$$A_2 = T_{12} A_0 \left(\frac{x_0}{d_{12} + d_{22}}\right)^n e^{-(\alpha_1 (d_{12} - x_0) + \alpha_2 d_{22})} \tag{8}$$

$$A_3 = T_{23} T_{13} A_0 \left(\frac{x_0}{d_{13} + d_{23} + d_{33}}\right)^n e^{-(\alpha_1 (d_{13} - x_0) + \alpha_2 d_{23} + \alpha_3 d_{33})} \tag{9}$$

$$A_4 = T_{34} T_{24} T_{14} A_0 \left(\frac{x_0}{d_{14} + d_{24} + d_{34} + d_{44}}\right)^n e^{-(\alpha_1 (d_{14} - x_0) + \alpha_2 d_{24} + \alpha_3 d_{34} + \alpha_4 d_{44})} \tag{10}$$

In general terms, the amplitudes recorded at each subsequent DST depth of acquisition are mathematically expressed as follows:

$$A_i = A_0 \prod_{j=1}^{i-1} T_{ji} \left(x_0 / \sum_{j=1}^{i} d_{ji} \right)^n e^{-\left(\alpha_1 (d_{1i} - x_0) + \sum_{j=2}^{i} \alpha_j d_{ji}\right)}, \quad j \geq 1,\ i > 1 \tag{11}$$

If you then consider the ratio of the amplitudes, whether in absolute terms or globally normalized, the unknown amplitude A_0 drops out of the set of equations.

Based on the above the proposed FMDSM Absorption Algorithm (FMDSMAA) for estimating SH wave absorption coefficients can then be described as follows:

- Utilizing the standard interval velocity FMDSM technique (Baziw 2002; Baziw and Verbeek 2012 and 2014), obtain estimates of V_i, T_{ij}, and d_{ij}.

- For the depth increments under analysis determine the maximum amplitudes from the recorded amplitudes for each depth increment from the X and Y axes seismic recordings as follows:

$$A_i^m = max\left\{ \sum_{i=1}^{n} \sqrt{x^2(i) + y^2(i)} \right\} \tag{12}$$

- Specify the estimated densities for each depth interval based upon the CPTU recordings or known values. Typical density values are outlined below

Table 3: Approximate Material Properties (from ASTM D7128)

Material	*P*-Wave Velocity (m/s)	*S*-Wave Velocity (m/s)	Density (kg/m^3)
Dry sand/gravel	750	200	1800
Clay	900	300	2000
Saturated sand	1500	350	2100
Saturated clay	1800	400	2200
Shale	3500	1500	2500
Sandstone	2850	1400	2100
Limestone	4000	2200	2600
Granite	6000	3500	2600

- Implement FMDSMAA to calculate the synthesized amplitudes with eq. (11) based on assumed absorption coefficients, whereby the RMS difference between the measured and synthesizes amplitude ratios is minimized.

$$\min_{\alpha_i} \left\{ \sum_{i=1}^{n-1} \sqrt{\left(\frac{A_{i+1}}{A_i}\right)^2 - \left(\frac{A_{i+1}^m}{A_i^m}\right)^2} \right\} \tag{13}$$

In eq. (13) n is the number of layers or absorption coefficients to be estimated.

It should be noted that when utilizing the FMSDMAA it is mandatory that the seismic source has the same energy output throughout the seismic profile

4.2 FMDSMAA - Test Bed Example:

Table 4 below provides the working parameters for a test bed simulation of the FMDSM-Absorption Algorithm (FMDSMAA). For a seismic wave with a frequency (f) of 100 Hz arrival times are assumed for 1-m thick soil layers down to a depth of 12 m. In addition for each soil layer values for the density and absorption coefficient are assumed.

Using FMDSM interval velocities (V) are then calculated for each depth interval, and with the outcome the wavelength is calculated ($V = f \times \lambda$). In addition the Quality factor is calculated ($Q = \pi/(\alpha \times \lambda)$). The source wave raypath diagram shown in Fig. 9 is used to calculate the incident and refraction angles, after which the globally normalized maximum amplitude is calculated using eq. (1) to account for absorption and geometric spreading as the source wave travels within a specific layer and the terms of eq. (5) (shown in bold font) to account for the energy loss as the source wave transitions from one layer to the subsequent deeper layer.

Table 4: FMDSMAA Test Bed Example Parameters (f = 100 Hz)

	Assumed			Calculated			
Depth [m]	**Arrival Time** [ms]	**Density** ρ [kg/m^3]	**Absorption** α [1/m]	**Interval Velocity** v [m/s]	**Wavelength** λ [m]	**Quality factor** Q [1/ Np]	**Normalized Maximum Amplitude** [m/s^2]
1	17	1800	0.34129	131.5	1.32	7	1
2	25	1700	0.64708	97.1	0.97	5	0.45437
3	28	1600	0.162	176.3	1.76	11	0.341131
4	34	1400	0.275	142.8	1.43	8	0.235517
5	37	1500	0.05244	249.6	2.5	24	0.146707
6	41	1700	0.07431	222.5	2.23	19	0.111947
7	46	1600	0.1278	189.1	1.89	13	0.094043
8	49	1700	0.03701	303.2	3.05	28	0.061211
9	54	1800	0.10137	193.7	1.94	16	0.057829
10	58	1900	0.06177	242.2	2.42	21	0.042609
11	62	1500	0.05869	243.3	2.43	22	0.040829
12	65	1900	0.03048	322.1	3.23	32	0.027391

To validate the FMDSMAA the values shown in Table 4 for the arrival time, density, and the normalized maximum amplitudes are used as input data for the FMDSMAA. In addition the source wave raypath diagram shown in Fig. 9 was used to calculate the length and duration for each segment of the various raypaths. With these values the absorption was derived for each depth, after which the Quality Factor and the Damping Factor were determined as well. Table 5 outlines the output of the FMDSMAA where the calculated and assumed values for the absorption, the Quality Factor and the Damping Factor show very close agreement with the initial test bed values, which demonstrates the FMDSMAA's correctness.

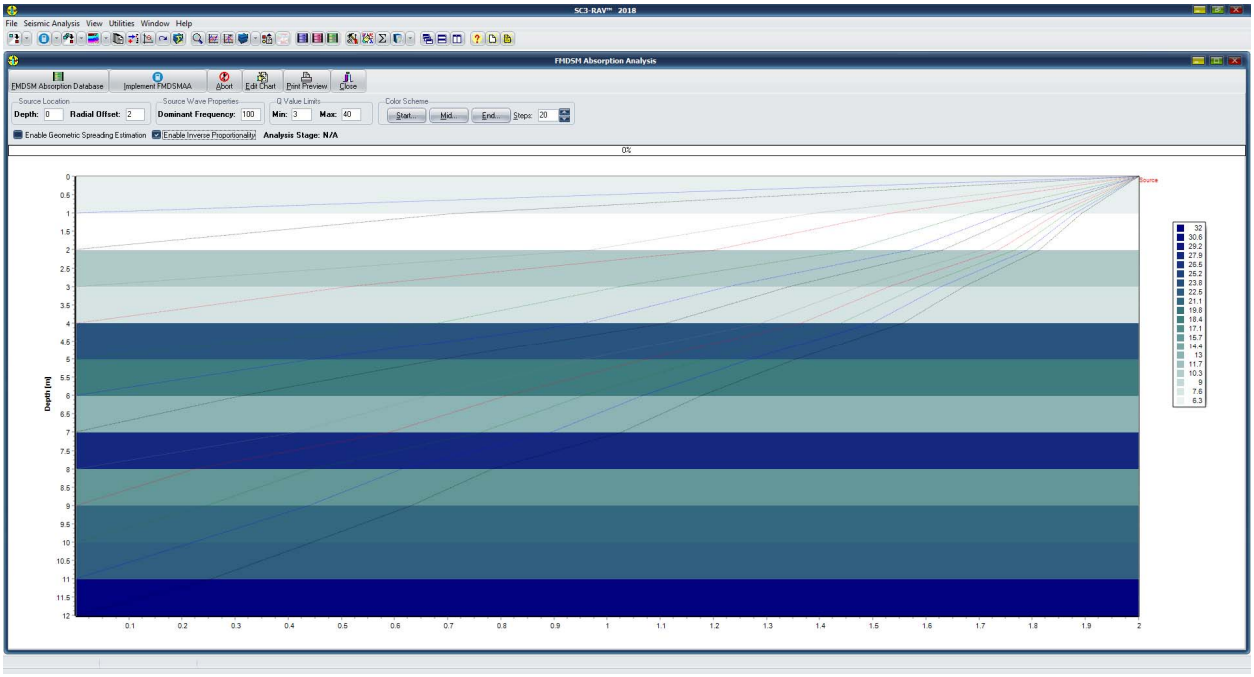


Figure 9: DST illustrating twelve simulated source waves as input into the FMDSMAA test bed analysis.

Table 5. FMDSMAA Test Bed Example Results

Depth [m]	Assumed Absorption α [1/m]	Calculated Absorption α* [1/m]	Q Based on α [1/ Np]	Q* Based on α* [1/ Np]	η* Damping Based on Q* [% Np]
1	0.34129	0.36115	7	6.6	7.59
2	0.64708	0.65681	5	4.9	10.14
3	0.162	0.16951	11	10.5	4.75
4	0.275	0.27762	8	7.9	6.32
5	0.05244	0.05449	24	23.1	2.17
6	0.07431	0.07514	19	18.8	2.66
7	0.1278	0.12823	13	13	3.86
8	0.03701	0.0374	28	27.7	1.8
9	0.10137	0.10154	16	16	3.13
10	0.06177	0.06191	21	21	2.38
11	0.05869	0.05879	22	22	2.27
12	0.03048	0.03054	32	32	1.56

CONCLUSIONS

This paper has outlined a unique DST absorption estimation methodology, which is carried out in the time domain and takes into account source wave travel paths. This new technique is referred to as the Forward Modeling Downhill Simplex Method Absorption Analysis (FMDSMAA), and it utilizes several estimated in-situ parameters (such interval velocities, source wave travel paths, angles of incidence and reflection, density, and source wave

amplitudes) when estimating absorption values. The FMDSMAA technique automatically provides for an error estimate, which is equal to the residual between the synthetic and measured source wave amplitudes for each depth increment. The implementation and performance of the FMDSMAA algorithm was demonstrated by considering a challenging test bed example. In a future paper the authors intend to demonstrate the algorithm with actual field data and compare it with the spectral ratio technique, which should further demonstrate the validity of this new technique.

REFERENCES

Aki, K. and Richards, P.G. (2002), Quantitative Seismology, 2nd edition, Sausalito, California: University Science Books.

ASTM (American Standards and Testing Methods). (2017). "D7400: Standard Test Methods for Downhole Seismic Testing." ASTM Vol. 4.09 Soil and Rock (II): D5877-latest.

ASTM (American Standards and Testing Methods). (2017). "D7128: Standard Guide for Using the Seismic-Reflection Method for Shallow Subsurface Investigation." ASTM Vol. 4.09 Soil and Rock (II): D5877-latest.

Baziw, E., and Verbeek, G. (2012). "Deriving Interval Velocities from Downhole Seismic Data", Geotechnical and Geophysical Site Characterization 4 – Mayne (eds), CRC Press, 1019–1024.

Baziw, E. (2002), "Derivation of Seismic Cone Interval Velocities Utilizing Forward Modeling and the Downhill Simplex Method", Can. Geotech. J., 39(5), pp.1181-1192.

Baziw, E. and Verbeek, G. (2014). "Identifying Critical Layers using SCPT and Seismic Source Moveout." In the Proceedings of the 3rd International Symposium on Cone Penetration Testing, CPT'14, May 12-14, 2014 - Las Vegas, Nevada, 357-364.

Blakeslee, S., Malin, P., and Alvarez, M. (1989), "Fault-zone attenuation of high-frequency seismic waves", Geophys. Res. Lett. 16, 1321-1324.

Capillo, M., Plantet, J.L., and Bouchon, M, (1985), "Frequency-dependent attenuation in the crust beneath central France Lg waves: Data analysis and numerical modeling", Bull. Seism. Soc. Am. 75, 1395-1411.

Finn, W.D.L. (1984). Dynamic response analysis of soils in engineering practice. In Mechanics of engineering materials. John Wiley & Sons Ltd., New York. Chapter 13.

Gibowicz, S.J. and Kijko, A. (1994), An Introduction to Mining Seismology, Academic Press Inc.

Idriss, I.M. (1990), "Response of soft soil sites during earthquakes," Proc. H. Bolton Seed Memorial Symposium, J.M. Duncan (ed.), Vol. 2, 273–290.

Idriss, I.M. and J.I. Sun (1992). SHAKE91: A computer program for conducting equivalent linear seismic response analyses of horizontally layered soil deposits, Center for Geotech. Modeling, Univ. of Calif., Davis.

Ishihara, K. (1982), "Evaluation of soil properties for use in earthquake response analysis", International Symposium on Numerical Models in Geomechanics, Zurich, pp. 237-259.

Kramer, S.L. and S.B. Paulsen (2004), "Practical use of geotechnical site response models", Proc. Int. Workshop on Uncertainties in Nonlinear Soil Properties and their Impact on Modeling Dynamic Soil Response, PEER Center Headquarters, Richmond, CA.

Kudo, K., and Shima, E. (1981), "Attenuation of shear waves in soil. In Seismic wave attenuation", edited by M.N. Toksoz and D.H. Johnston. Geophysics Reprint Series No. 2. Society of Exploration Geophysics, Tulsa, Okla., 325-338.

Kvamme, L.B., and Havskov, J. (1989), "Q in Southern Norway", Bull. Seism. Soc. Am. 79, 1575-1588.

Redpath, B.B., and Lee, R.C., 1986, In-situ Measurements of Shear Wave Attenuation at a Strong Motion Recording Site: Report Prepared for USGS Contract No. 14-08-001-21823.

Mok, Y.J., Sanchez-Salinero, I., Stokoe, K.H., and Roesset, J.M. (1988),."In situ damping measurements by crosshole seismic method", In Earthquake Engineering and Soil Dynamics 11. Proceedings, ASCE Specialty Conference, Park City, Utah. Geotechnical Special Publication No. 20, 305-320.

Rebollar, C. J. (1984), "Calculation of Qβ using spectral ratio method in Northern Baja California", Bull. Seism. Soc. Am. 74 , 1371-1382.

Saxena, S.K., and Reddy, K.R. (1989), "Dynamic moduli and damping ratios for Monterey No. 0 sand by resonant column method", Soils and Foundations, 29(2): 37-51.

Seed, H. B. & Idriss, I. M. (1970), "Soil moduli and damping factors for dynamic response analyses", Earthquake Engineering Research Center, College of Engineering, University of California - Berkeley California, Report No. EERC 70-10.

Seed, H.B., Wong, R.T., Idriss, I.M., and Tokimatsu, K. (1986), ”Moduli and damping factors for dynamic analyses of cohesionless soils”, ASCE Journal of the Geotechnical Engineering Division, 112: 1016-1032.
Sheriff, R.E. and Geldart, L.P. (1982), Exploration Seismology, Vol. 1, (2nd ed.) Cambridge, UK: Cambridge University Press.
Stewart, W.P., and Campanella, R.G. (1993), “Practical aspects of in-situ measurements of material damping with the seismic cone penetration test”, Can. Geotech. J. 30, 211 219.
Sun, J.I., Golesorkhi, R., and Seed, H.B. (1988), "Dynamic moduli and damping ratios for cohesive soils", Report UCB/EERC-88/ 15, University of California, Berkeley.
Toksoz, M.N., Johnston, D.H. and Timur, A. (1979), "Attenuation of seismic waves in dry and saturated rocks: I. Laboratory measurements", Geophysics Vol. 44, 681-690.
Tonouchi, K., Sakayama, T., and Imai, T. (1983), “ S wave velocity in the ground and the damping factor”, Bull. IAEG. No.26-27, pp.327-333. WOODS, R.D. and STOKOE, K.H.II. 1985. Shallow seismic exploration in soil dynamics. Richart Commemorative Lectures, ASCE. 120-156
White, J.E. (1965) Seismic waves. McGraw-Hill, New York.
Wilson, E.L. & Clough, R.W. (1962), “Dynamic response by step-by-step matrix analysis”, Symposium on the Use of Computers in Civil Engineering, Laboratorie Nacional de Engenharia Civil, Lisbon - Portugal, pp. 45.1 - 45.14.
Zavoral, D. (1990), Dynamic properties of an undisturbed clay from resonant column tests, M.A.Sc. thesis, Department of Civil Engineering, University of British Columbia, Vancouver.

A COMBINATION OF JET GROUTING AND MPSP GROUTING IN ISKAR RIVER CASCADE HYDROPOWER PLANT IN BULGARIA

Andrea M. R. Pettinaroli, StAP - Studio Ing. Andrea Pettinaroli S.r.l., Milan, Italy, a.pettinaroli@stap-engineering.eu
Mario Ruggiero, Sireg Geotech S.r.l., Arcore, Italy
Gabriele Balconi, Sireg Geotech S.r.l., Arcore, Italy
Massimo Poggio, Injectosond S.r.l., Arenzano, Italy
Riccardo Castellanza, University of Milano Bicocca, Milan, Italy

ABSTRACT

Grouting technologies are ground treatment techniques used for modifying the behaviour of a mass of soil or rock by injecting a mixture. The sleeved port pipes (also called Tube A Manchette) are highly diffused for grouting treatment of coarse soils and fissured rocks. This paper describes a combination of jet grouting and rock grouting with MPSP (multiple packer sleeve pipe) technique that has been used to realize waterproof curtains under fluvial structures for a cascade hydro-power plant. This is composed by five mini hydro-power plants, placed along the Iskar river, in Bulgaria, and composed by a penstock followed by the power house, a spillway, and an earth dam containing the reservoir. The geology of the site is characterized by an upper alluvial deposit lying over the bedrock. In each site, similar treatments were carried out: an impervious curtain along the plant section, obtained by executing jet-grouting columns in the surficial alluvial layers and grouting the underlying fractured rock by means of port pipes. The temporary embankment, built during the works for protecting each site from the possible river floods, has been waterproofed and stabilized by reinforced jet-grouting columns. The grouting processes have been controlled and monitored by a computerized system.

Keywords: rock grouting, MPSP, TAM pipes, tube à manchette, obturator bag, jet grouting, soil improvement, waterproofing.

INTRODUCTION

The Iskar river cascade hydropower plant is situated northern of Sofia, Bulgaria, and it is composed by nine plants. Actually five of them have been built and produce energy. Each plant is composed by a penstock followed by the turbine building, a spillway, and an earth dam that contains the reservoir.
The Iskar rivers runs in a narrow valley characterized by diorite or diabase rocks, with an upper deposit of alluvial soil, composed mainly by gravel and sand.
Each plant requires an impervious curtain under the structures and in correspondence of the earth dam: this has been obtained by means of a jet grouting treatment of the alluvial coarse soil, and a grouting treatment with cement mixtures of the underlying rock using the MPSP technology.
During the construction of the structures, the site has been shielded from the river water by a temporary earth embankment that has been statically improved and waterproofed by jet grouting columns reinforced with steel tubes; this allowed to work without interruption even in case of flood of the Iskar river.

© 2019 Deep Foundations Institute

THE DESIGN OF THE PLANTS

The design of each plant included a detailed campaign of geotechnical investigation, and a long term monitoring system for the control of the efficiency of the impervious curtain and of the stability of the earth dam.

Geotechnical investigation

The execution of several corings along the main cross section of each barrage allowed to reconstruct the bedrock surface covered by the surficial alluvial layer.
In each hole, permeability tests have been carried out at different depths: Lefranc test into the alluvial soil strata, Lugeon test in the rock. Usually the corings put in evidence that the upper part of the rock is rather fractured, being these information very often confirmed and better described by the Lugeon test results. The cross section in Fig. 1 concerns the plant of Lakatnik.

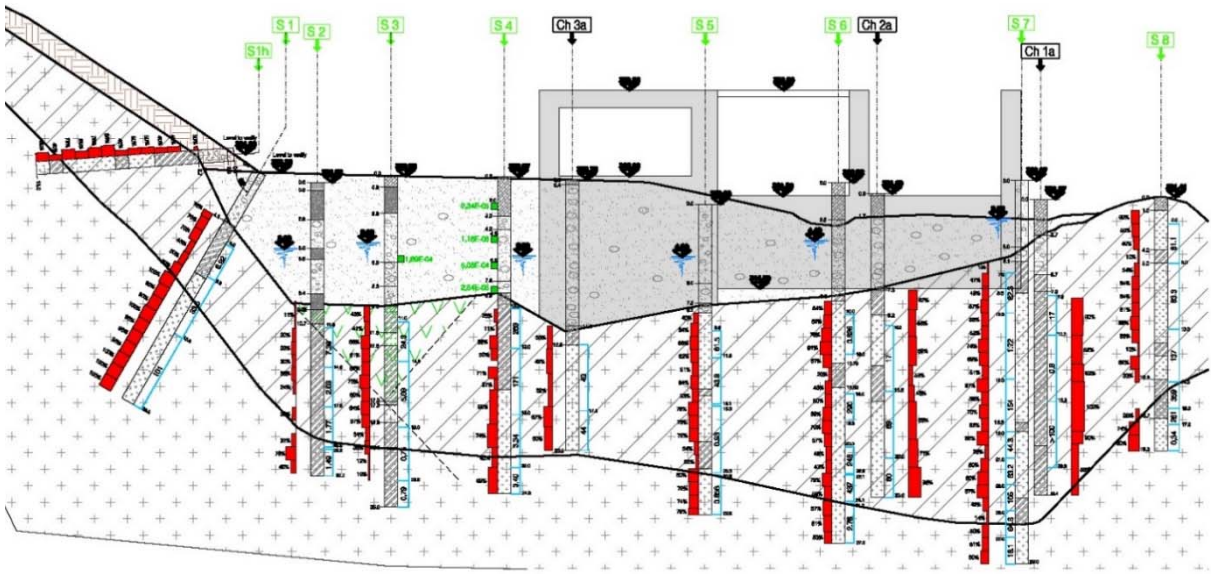


Fig. 1 Geotechnical investigation at the power plant of Lakatnik

Power plant design

Each plant is composed by: the main building that includes the intake channel, the turbine, the outlet channel, the control hall; the weir with the gates; the lateral earth dam (see fig. 2).



Fig. 2 Geotechnical investigation at the power plant of Lakatnik

During the plant construction, an earth embankment was built in order to protect the front, the back and a side site of the area from the river, as shown in the following figure 3. The embankment has been waterproofed by executing, down to the bedrock level, a line of jet grouting columns. This allowed to work for the execution of the concrete structures and the installation of the turbine and the electromechanical devices regardless of the variation of the flow rate of the river: no seasonal interruptions of the activities were necessary.

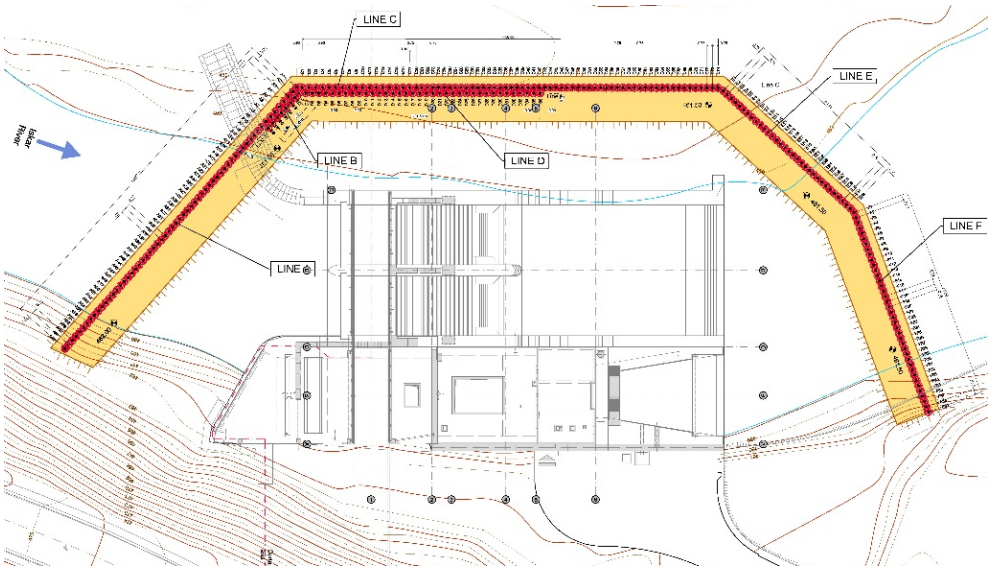


Fig. 3 Temporary embankment as protection of the site during the activities in case of river flood

In some sites the plant lies in correspondence of a narrow section of the valley, so in order to guarantee the necessary flowing section of the river, the embankment was placed beside the external alignment of the abutment wall of the plant. In this case the embankment has been considered as a gravity structure, with two lateral lines of jet grouting columns axially reinforced with a steel pipe anchored into the bedrock (see fig. 4).

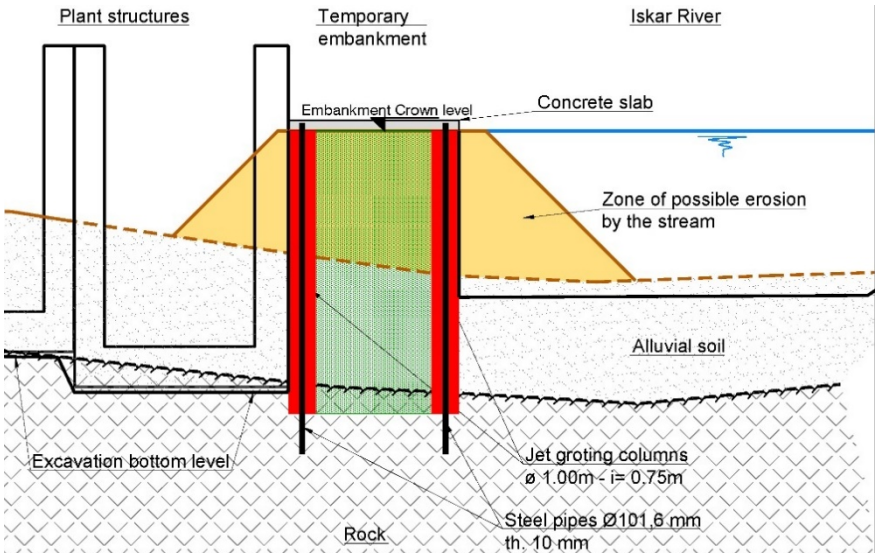


Fig. 4 Temporary embankment reinforced with jet grouting columns and steel pipes

The internal side of the embankment has been excavated up to uncover the jet grouting columns; during the works the grouted wall was protected with a mesh reinforced shot concrete, until the cast of the abutment wall finally covered the vertical surface. The reinforcements were designed taking into account that the water flow might remove the slope of the embankment, and considering the hydraulic effort applied to the remaining treated core with the deeper level reachable during the plant excavation. So the reinforced double jet grouting sheet has a double functions: to assure the equilibrium of the embankment; to protect it from the erosion by the river water.
For each plant a FEM analysis of the steady-state seepage process following the construction of the dam and hence the presence reservoir was carried out by applying a three-dimensional finite element code (Fig. 5).

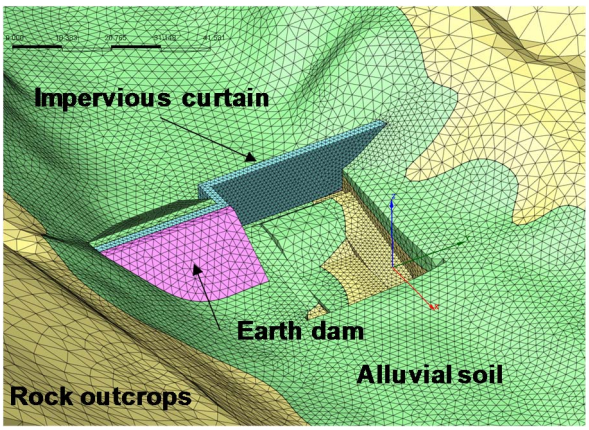


Fig. 5 The 3D model mesh

The setup of the geometry of the three-dimensional model was performed starting from the implementation of the 3-D DTM (Digital Terrain Model) model of the area and assembling the geometry of the dam structure according to the proper design. Then, based on the hydraulic properties of the rocks and the soils affected by the dam construction, which have been derived from the results of the investigations available, and the boundary conditions assigned to the model, the continuity equation governing the water seepage in the soil domain was integrated in order to derive the values of the hydraulic head for each node and the values of the pore water pressure accordingly. The

main features of the seepage regime consequent to the construction of the dam were calculated in order to design the impervious curtain under the weir and the dam foundation. A sensitivity analysis was carried out taking into account different values of the size of the impervious curtain to assess the optimal length of the same structure according to a cost-effective solution (fig. 6 and 7).

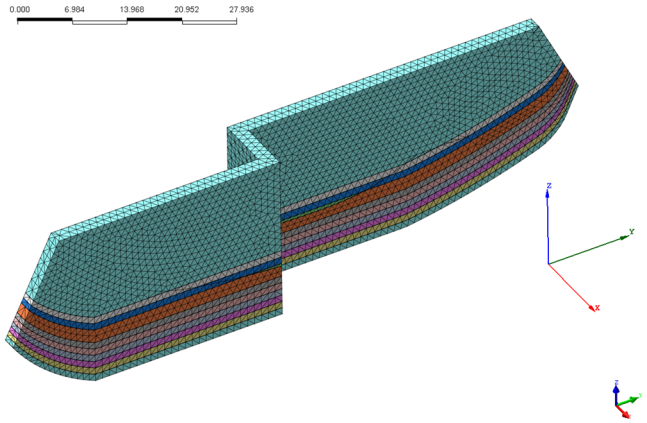


Fig. 6 A detail of the curtain elements (on the left)

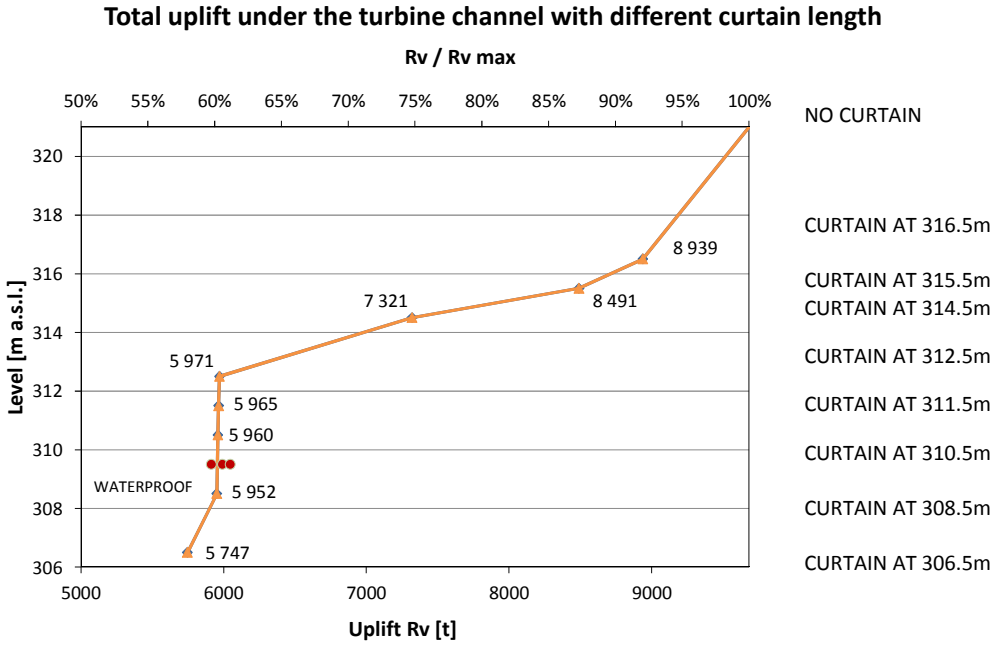


Fig. 7 Sensitivity analysis of the curtain depth

The impervious curtain

For all the plants the deepest excavation level is placed in the area of the power house, where the bedrock is always uncovered. Hence the impervious curtain required to treat the most surficial rock mass, all along the alignment, the coarse surficial deposit on the sides of the section, and the earth dam core.

The investigations showed that the upper part of the bedrock was normally cracked for a thickness variable from 2 m to 5-÷6 m, hanging from the local geological condition of each site, presenting very low RQD values; the

permeability values, measured with Lugeon test, vary normally between 3 and 50 UL, and in several cases they can rise up to 600 UL. According to the design model, the target of the treatment for the curtain was to not exceed 3 UL.
The alluvial formations were composed by gravel and sand, in some sites including 15-30% of silty fraction; boulders were detected in the zone of the current bed river and in the food plain side areas, but normally only in surficial position. The permeability, measured with Lefranc test, gave results included between $10^{-4} \div 10^{-6}$ m/s: the target after the soil treatment in those strata and in the earth dam core was fixed in $1 \div 5 * 10^{-7}$ m/s.
For the execution of the impervious curtain, it was decided to treat the soil with two lines of double fluid jet grouting columns Ø 1,30 m, and to grout the rock with cement mixes. The curtain was carried out after the execution of the earth dam, and, usually (but not always, due to the main works scheduling), after the cast of the weir and power house foundation plate.
The critical issues of this solution were hence:

- the locally highly fractured rock in the transition zone to the upper alluvial deposit
- the possible weakness of the jet grouting treatment at the bottom of the columns, in correspondence of the contact with the underlying rock
- the contact zone between the ground and the concrete foundations of the weir and the power house, because of the surficial disturb of the rock due to the excavation (made with blasting or with non-explosive agent) and of the discontinuity with the concrete casts that needs to be properly sealed.

In order to obtain a homogeneous treatment in all those critical zones, it was decided to perform the rock grouting by means of the MPSP (multiple packer sleeve pipes) placed into the holes that crossed the jet grouted soil or the concrete foundations.

THE GROUND TREATMENTS

Jet grouting

Jet grouting columns were executed as first, using air and a water/cement ratio W/C =1 for the grout, injected with a pressure of 40 MPa.
At the beginning of the activities, a trial field was executed in order to evaluate the result of treatment (see pictures in fig. 8) of the discovered columns) and to set up the operational parameters (flow rate and pressure of grout and air, uplift velocity, rotational speed) after the treatment energy procedure (Tornaghi et al. 2004).
In order to allow a more regular high pressure injection during the uplift phase, even in presence of boulders, each column execution was preceded by a predrilling, carried out 1 m down into the bedrock, by means of a dedicated drilling unit.
Some preliminary pre-drillings along the columns alignment (for the temporary embankment as well as for the impervious curtain) were initially made, in order to detect the bedrock level and hence to draw an accurate profile of the alluvial deposit base.
The geometry of the treatment involved the execution of inclined columns at the two ends of the curtain, with drillings made with angles up to 43° from the vertical.



Fig. 8 Jet grouting trial columns executed at the start of the works

During the treatment of the temporary embankment, the steel pipe reinforcement was usually inserted in the hole made for the jet grouting.
The effect of the treatment was successfully tested during the excavation for the plant construction. The picture in fig. 9 shows on the left the jet grouting wall that separates the bed river from the area of the site for the power house and the gates building. No significant water income from the waterproofed embankment occurred.



Fig. 9 On the left - Works in progress with the jet grouting wall protection from the river bed
On the right – The road on the crown of the embankment, used for the site traffic

This allowed to complete all the activities for the power plant construction (from the embankment construction to the test on the turbine) in 18 months without any interruption. In case of seasonal interruption (without the waterproofing of the temporary embankment), 6 additional months should have been considered. Until today, during the works for

the five plants made, only in one occasion the river has overflown the embankment crown, causing a flood that interrupted the works. The site was evacuated on time, thus limiting the damages. Two months were necessary for restoring the yard.

Rock grouting

The treatment of the rock for the impervious curtain was carried out using the MPSP (Multiple Packer Sleeve Pipe) system. After the hole drilling, a Ø 1”1/2 PVC TAM pipe (40/48 inner/ouer diameter) was installed, equipped, every 3÷5 meters, with several Heavy Duty Obturator Bags, made in polypropylene geotextile and mounted on one or two sleeves. The bags were initially folded and fixed to the pipe at the ends by a metallic tie (see fig. 10). The tube was centred by means of plastic collars.



Fig. 10 Folded and injected obturator bags mounted astride a manchette

Once the pipe was in place, the bags were filled with injecting cement grout (ratio W/C=0,6÷1) by a double packer lowered to one of the correspondent sleeves, and finally sealing the annular space between the plastic pipe and the borehole. Under the pressure of the injection, the cement of the grout separated from the water, being the latter ejected per seepage through the geotextile. As a result, the hole was divided into several sectors with predefined length by means of the tough sealings obtained injecting each obturator bag; a curing time of 18÷24 hours were sufficient for the aim (see fig. 11).

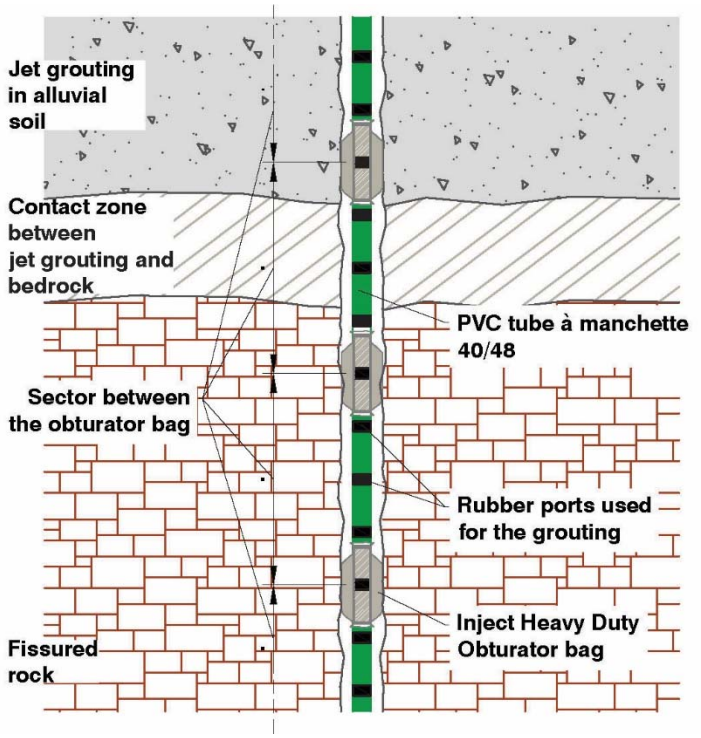


Fig. 11 Scheme of the MPSP system grouting

The grouting of each sector was then made after the usual TAM injection procedure: the double packer was placed astride one of the sleeves of the deeper sector, but in this case no plastic sheath was necessary. In fact, the grout filled initially the annular void space between the pipe and the borehole, and then it flushed into the fissures intercepted by the hole sector.

The injection was then carried out following the prescribed rules for the rock treatment.

The curtain was formed by two alignments of TAMs, spaced 1,50 m and with interaxis of 1,50 m between the boreholes. In a first phase primary pipes were drilled and injected; then the secondary pipes phase followed (fig. 12).

Along the earth dam axes the holes were drilled passing through the jet grouting columns.

The obturator bags were installed every 3÷5 m in the pipe stretch into the rock to be treated. Another bag was mounted about 1 m above the contact between rock and jet grouting, in order to treat this transition zone with a higher care.

In correspondence of the structures founded directly on the bedrock, the holes were drilled using as guides some plastic tubes previously embedded in the cast concrete.

The upper obturator bag was placed about 1 m under the foundation level, in order to obtain a sealed contact between rock and concrete. In this area a third alignment of pipes was executed, inclined towards the reservoir, in order guarantee a better treatment from the side of the hydraulic head.

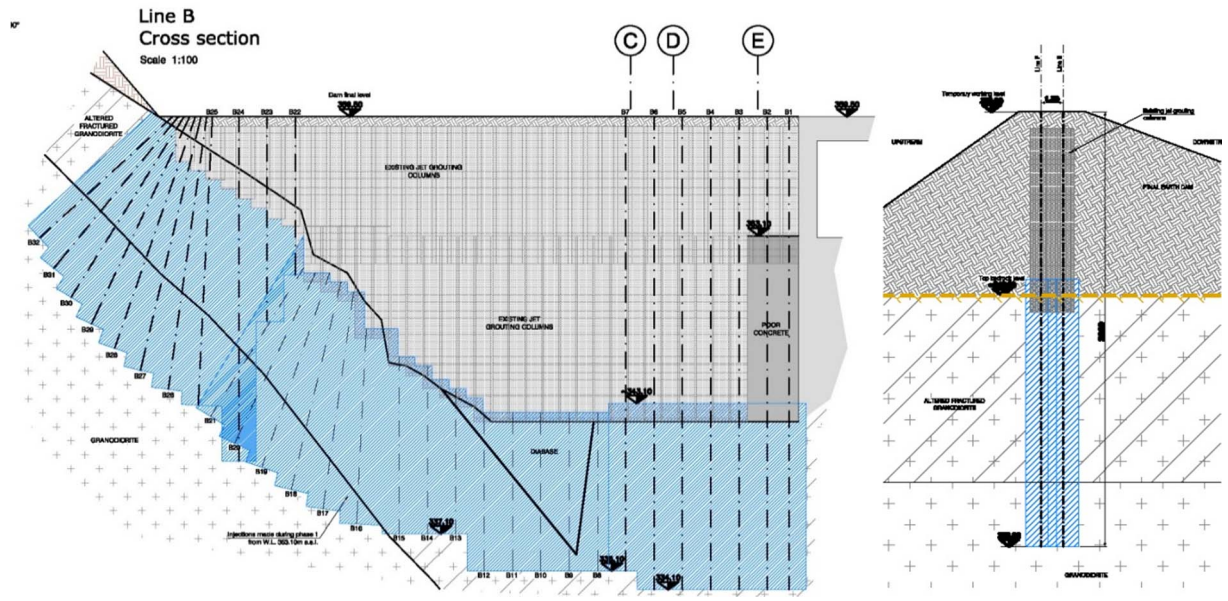


Fig. 12 Cross sections of the treatment for the impervious curtain along the earth dam

Final controls on the impervious curtain

After the completion of the jet grouting and rock grouting treatments, on each site a final investigation campaign was carried out, with execution of inclined corings along the impervious curtain and Lugeon and Lefranc tests at different depths in the holes, respectively in the rock and in the jet grouted soil.
The tests always showed the fulfilling of the prescribed permeability coefficient, as plotted in the following charts in fig. 13: the diagram on the left shows the permeability values before and after the jet grouting treatment in the soil, whereas on the right the permeability in Lugeon units before and after the rock grouting.

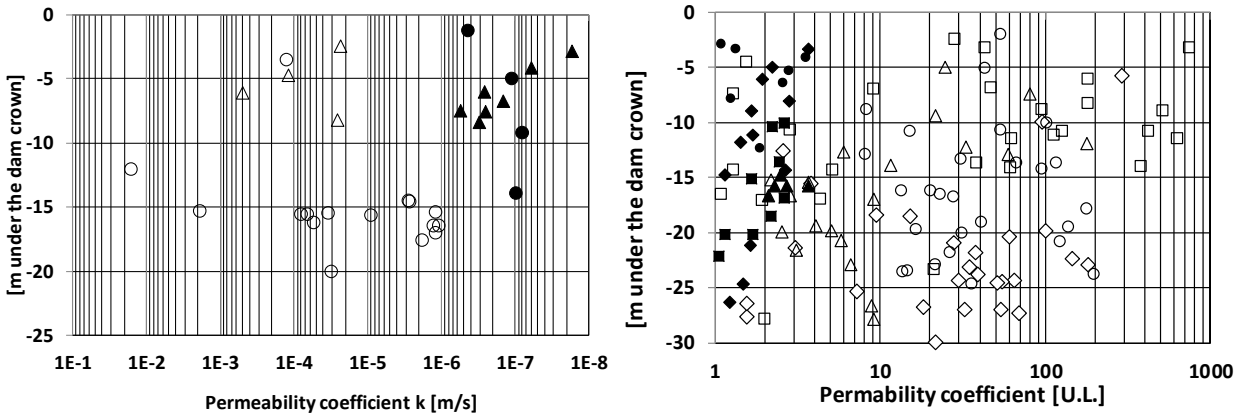


Fig. 13 Final controls on the impervious curtain: Lefranc test in soil (on left), Lugeon test in rock (on right) Permeability values after the treatment are plotted with full symbols

SUMMARY AND CONCLUSIONS

The cascade HPP of Iskar River, in Bulgaria, is composed by nine plants. For each of them, the design required the execution of a temporary embankment for protecting the power house excavation site from the river flow, and of an impervious curtain, along the earth dam and the structures section, against the water seepage in the ground, composed by rock basement underlying alluvial coarse soil. Until today, five plants are completed and regularly operating.
Jet grouting columns reinforced with steel pipes were executed along the provisional embankment in order to make it waterproofed and to work as gravity structure able to withstand the hydraulic effort of the water even in case of floods. This solution allowed to avoid any seasonal interruption during the works in the riverbed, gaining between 4 and 6 month in the execution schedule of each plant.
The impervious curtains have been executed by combining the use of jet grouting for the treatment of the coarse soil layers, and the MPSP system for the grouting of the underlying bedrock. The adoption of the MPSP allowed to save time during the treatment of crushed rock and to obtain a highly homogenous watertight treatment, particularly sealing some critical zones such as: the contact between the rock and the jet grouted soil; the upper part of the rock mass, weakened from the excavations (usually made by blasting); the contact between the rock and the concrete foundation structures of the power house and the weir. Final permeability controls on site into the curtains confirmed the good outcome of the treatments.

ACKNOWLEDGMENTS

A special acknowledgment to Plamen Dilkov, construction manager of Vez Svoghe OOD that owns and has built the plants, who directed the works with the support of Patrick Pauletto, to Achille Balossi Restelli and Elena Rovetto who have contributed to the develop and the design of part of the project, to Injectosond S.r.l., specialized company executor of the treatments.

REFERENCES

Balossi Restelli A., Rovetto E. and Fava A. R., 1993. La tratta Dinegro – Principe della Metropolitana di Genova. Atti del XVIII Convegno Nazionale di Geotecnica, Rimini (Italy), pp. 51-60.

Balossi Restelli A., Tornaghi R., Pettinaroli A: and Rovetto E., 2003. Reconstruction of La Fenice Theatre in Venice – Foundations problems. 13th European Conference on Soil Mechanics and Geotechnical Engineering, Prague, Vol.2, pp. 29-34

Bruce D. A., and Gallavresi F., 1988. The MPSP system: a new method of grouting difficult rock formations. ASCE Conference, Nashville, TN.

Manassero V., 1993. Different techniques for soil improvement and underpinning. Cambridge programme for industry, Magdalene College, Cambridge, Department Of Engineering.

Tornaghi R. and Pettinaroli A., 2004. Design and control criteria of jet grouting treatments. ASEP-GI Paris, pp 295-319.

ADAPTIVE DESIGN AND CONTRACTUAL APPROACHES TO ADDRESS GEOTECHNICAL UNCERTAINTIES IN A DESIGN-BUILD GROUND IMPROVEMENT PROJECT

Mark T. Howe, Hayward Baker, Inc., St. Louis, MO, USA, mthowe@HaywardBaker.com

Yan Zhang, Ph.D., P.E., Hayward Baker, Inc., Roselle, IL, USA yjzhang@haywardbaker.com

Mike Minton, P.E., Hayward Baker, Inc., Roselle, IL, USA mkminton@haywardbaker.com

Kalyani Devabhaktuni, P.E., McDermott International Inc., Plainfield, IL, USA
kalyani.devabhaktuni@mcdermott.com

ABSTRACT

During the procurement phase of a Design-Build (DB) project, design-build contractors must often commit to a fixed price based on limited or incomplete geotechnical information. This lack of information can result in an inaccurate assessment and allocation of project risk to either the contracting authority or the DB contractor. This paper presents a case study of an elevated water tank supported by mixed ground improvement techniques, including Vibro-Compaction (VC), Aggregate Piers (AP) and Compaction Grouting (CG) in East St. Louis, Illinois. An adaptive design and contracting approach provided the best value solution for a complicated set of geotechnical problems, including static bearing capacity and settlement concerns as well as liquefaction induced settlement. Close cooperation between the owner, the tank contractor, the geotechnical engineer and the ground improvement contractor was essential to produce an effective solution. Ground Improvement techniques resolved the geotechnical challenges at the site through adaptive design methods, utilizing progressive rounds of verification and real time data acquisition to achieve performance objectives. This paper details the evaluation of geotechnical criteria, the selection of ground improvement techniques, the adaptive design and implementation of ground improvements, as well as contracting methodologies used to ensure that the best value was provided.

Keywords: design-build, ground improvement, adaptive design, contracting methodology

PROJECT INFORMATION

In November, 2016, CB&I Storage Tank Solutions (McDermott) submitted a design/build proposal for an elevated water tank for Illinois American Water Company (IAW) in East St. Louis, Illinois. The purpose of this tank was to have backup water capacity for power generation. In the RFP, IAW requested two alternate styles of tank: Option 1, a 1250 Million Gallon (MG) Composite Elevated Tank or Option 2, a 1250 MG Waterspheroid tank. Option 1 consisted of a steel tank supported on a concrete tower. Option 2 consisted of a steel tank supported on a steel shaft. The height (determined by IAW) was 140 feet to the top capacity line measured from top of floor slab.

During the bid phase, McDermott submitted a proposal that included supporting the tank on auger cast pile foundations for the composite elevated tank (Option 1) and a shallow foundation with ground improvement for the Waterspheroid (Option 2). IAW selected Option 2, the all steel Waterspheroid, and post award, retained a geotechnical consulting firm to perform supplemental soil borings and prepare a site-specific seismic analysis.

© 2019 Deep Foundations Institute

The shaft of the tank was supported on a bell with a radius of 19.5 feet. A typical sketch of the tank is shown in Figure 1 below. The dead load of the tank was 810 kips and the product load was 10,799 kips. The earthquake shear and moment on the tank was 612 kips and 75,514 kip-ft respectively. Settlement tolerances were total uniform settlement of 2.5 inches or less and differential settlement in the form of tilt across the tank base diameter of 0.5 inches or less.

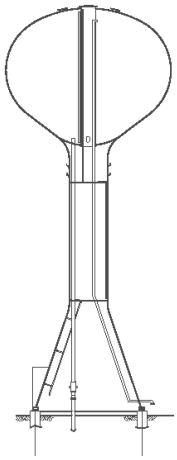


Fig. 1. Tank Sketch

SOIL AND SITE CONDITION

The original and supplemental geotechnical explorations consisted of performing 6 Standard Penetration Tests (SPT) borings and 5 Cone Penetrometer Tests (CPT) borings within the footprint and near the proposed tank. The geotechnical report identified the following subsurface conditions: Existing clay fill extended from the ground surface to a depth of about 5.5 feet. The fill was underlain by medium stiff lean clay that extended to a depth of about 12 feet. These soils were underlain by loose to very dense sands that extended to as deep as 107 feet. The fines content within the sand varied, with zones as low as 5% and as high as 20%+. Groundwater was encountered at a depth of 12 feet during drilling. The general soil profile is shown in Figure 2 below.

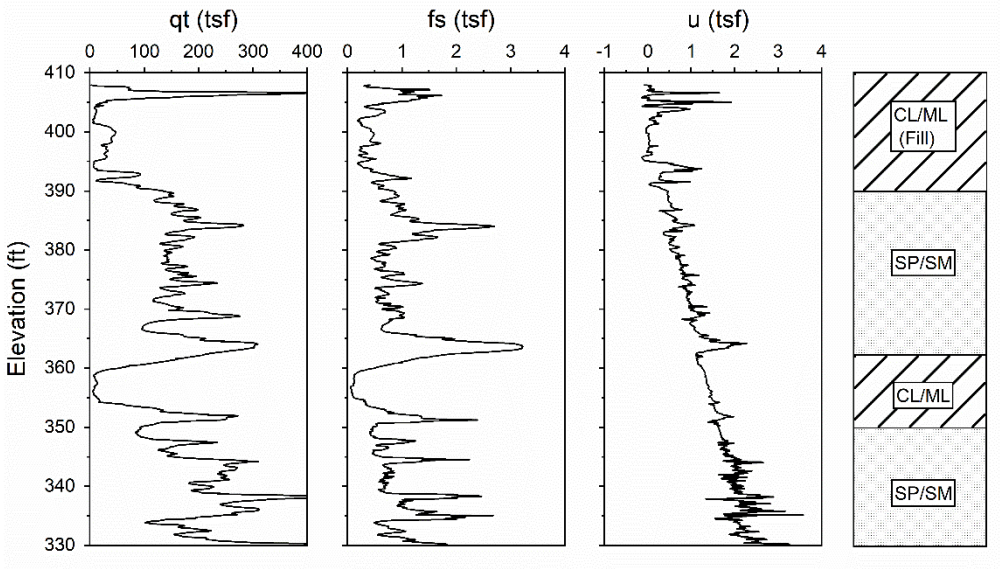


Fig. 2. Typical Subsurface Profile

The supplemental geotechnical evaluation and site-specific seismic analysis indicated that the loose sands encountered in the borings were susceptible to liquefaction and that the associated seismic settlement estimates ranged from about 6 to 18 inches during the design earthquake with differential settlements of about 6 inches. Due to the large amount of seismic settlement that was calculated, it was necessary to mitigate the liquefaction potential. Given the soil conditions encountered and the potential for liquefaction in the original and supplemental explorations, a site class "F" per ASCE 7 was selected for seismic design.

FOUNDATION DESIGN AND CONSIDERATION

In light of the initial and supplemental geotechnical evaluations, McDermott considered the following foundation options for support of the tank:

1) Deep Foundations (Driven piles, Auger-Cast-In-Place Piles (ACIP) and Displacement Piles, Drilled Shafts): Due to the deep liquefiable zones, the primary concern identified with driven piles was that the pile would be long and slender and would require multiple splices. The variable density of the in-situ sand with depth presented the problem of potential necking and over drilling for ACIP, and presented early refusal problems for Displacement Piles. Down-drag considerations presented additional problems for both driven and ACIP piles. Drilled shaft construction in this sandy, high water table profile would also have been difficult. Each of the deep foundation alternatives also encountered a design hurdle due to the thick liquefiable layers. Essentially, the deep foundations would be 'unbraced' during the design earthquake, so some method of improving lateral support would have been necessary with any of the deep foundation options.

2) Combination of Deep Foundations with Earthquake Drains (EQD): The purpose of the EQD in combination with deep foundation elements would be to relieve the excess pore water pressure that would build up during a seismic event, thereby mitigating liquefaction and eliminating concerns about "unbraced" lengths of the deep foundation elements. However, the interbedded dense sand layers at depth would have presented installation challenges for EQD. Furthermore, the cost of installation of EQD in combination with deep foundations difficulties (discussed above) were significantly higher when compared to the ground improvement option discussed below.

3) Shallow Foundation with Ground Improvement (GI): The primary objectives of GI were twofold: The first objective would be to reinforce and/or densify the on-site soils such that they would be capable of supporting the static loads applied by the tank foundation, while reducing settlement under static conditions to within acceptable tolerances. The second objective was to provide enough densification of the lower liquefiable sand layers such that their liquefaction potential was reduced. The GI scheme included a combination of AP and VC in the upper 30 feet of the soil profile, and CG from 30 to 60 feet.

After consideration and consultation with IAW, McDermott selected Option 3 because it provided the lowest overall cost and presented the least construction and design challenges. The final design of the

tank foundation consisted of a ring type footing, bearing at 11.5 below finished grade, with a 1.5-foot-thick leveling pad. A performance specification was issued to Hayward Baker which provided the foundation dimensions along with the structural loads and settlement criteria for the tank summarized above.

GROUND IMPROVEMENT DESIGN AND VALIDATION

The Ground Improvement (GI) system was designed and implemented to address the following primary geotechnical issues:

1. Insufficient allowable bearing capacity within the upper clay and sandy soils based on the tank foundation geometry and applied loads.
2. Settlement that exceeded tolerance due to the in-situ consistency of the native sands and a layer of compressible silty clay that was encountered between EL. 363 and 350.
3. The potential for liquefaction in the silty sand layer between EL. 368 and 343 under the design seismic event.

Figure 3 below shows the typical soil profile with the corresponding GI methods within the various layers. Generally, HBI performed Aggregate Piers (AP) within the upper 12 to 17 feet, Vibro-Compaction (VC) within the intermediate sand layer extending to about 30 feet, and Compaction Grouting (CG) within the deeper sandy and silty clay soils, extending to a depth of about 65 feet.

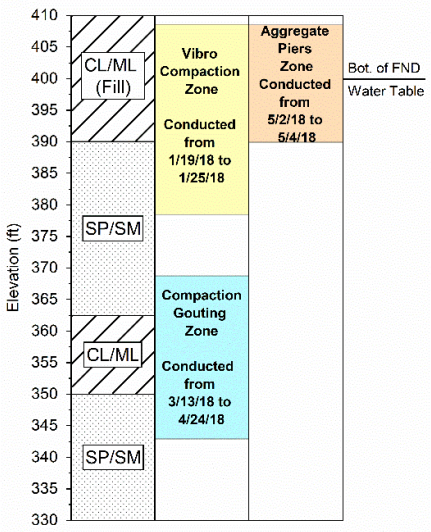


Fig. 3. Ground Improvement Configuration

Vibro-Compaction

The first GI technique that HBI installed at the site was Vibro-Compaction (VC). Figure 4 below displays the VC treatment pattern, along with the post VC CPT locations. The actual treatment depth varied from 22 to 30 feet. (approximate EL. 386 to 378).

VC is a process that uses a powerful depth vibrator to impart vibratory energy in a radial direction from the source to the surrounding soil matrix. The vibratory energy densifies granular soils that are relatively free of fines. The vibrator is lowered into the soil profile using water jets along with its own self-weight and vibratory energy to penetrate the soil.

The VC treatment extended one row outside of the planned foundation diameter, to ensure improvement of the edge condition. The VC treatment was designed to extend from the bottom of the foundation to refusal (within the medium dense to dense silty sand encountered approximately 30 feet) below the ground surface. Settlement estimates based on the pre-treatment CPT soundings indicated that settlement within the silty sand exceeded 1 inch. HBI choose a densification target of achieving an average CPT tip resistance (q_t) of 100 tsf within the VC zone, thereby reducing the predicted static settlement within the silty sand zone to about 0.4 inches.

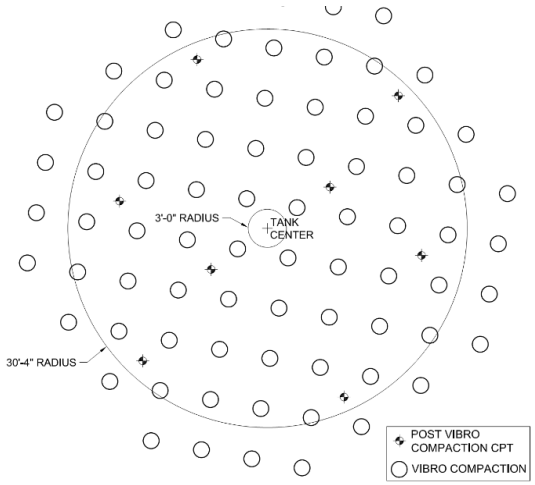


Fig. 4. Vibro Compaction Layout

The pre and post CPT tip resistances are displayed in Figure 5 below. Post VC CPT testing was performed within the foundation footprint which showed that the VC program resulted in an increase of the average q_t to 175 tsf between EL. 390 and 375. The corresponding static settlement predicted within the VC zone was reduced to as low as 0.2-inch.

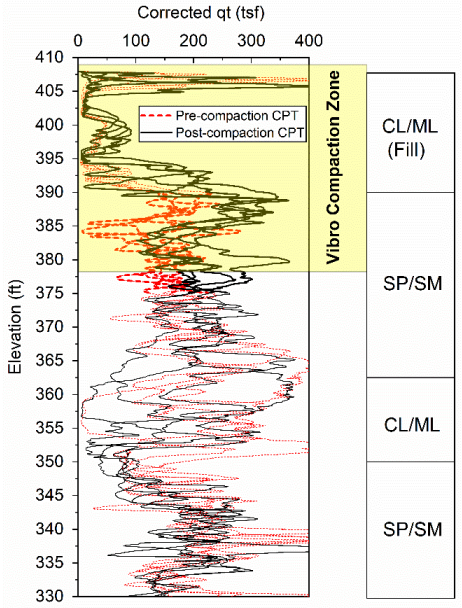


Fig. 5. Pre and Post-VC CPT Tip Resistance

Compaction Grouting

The second GI technique employed by HBI at the site was Compaction Grouting (CG). The VC program terminated in a dense sand layer that was encountered at a depth of approximately 30 feet, however, static settlement below that elevation still exceeded tolerance, and the site-specific analysis indicated a potential for liquefaction within those deeper soils under the design seismic event. CG involves drilling grout port casing pipes into the ground and pumping highly viscous grout under pressure and in stages to densify pre-determined zones within a soil profile. CG was performed below the VC zone from EL. 368 to 343 using a large drill and water flushing for reliable penetration through the dense granular materials where the VC terminated. Once the casing was installed to the bottom of the treatment zone (EL. 343), low mobility grout was injected through the casing into the soil strata being treated at various depths. HBI batched the grout on-site. During injection, various grouting parameters (depth, pulling rate, pumping pressure and grout volume) were continuously monitored, allowing HBI to make timely adjustments to the grout mix and process based on real-time feedback from the installation. Grout was injected at each stage until pre-established cutoff criteria was reached. This procedure was repeated over the length of the CG treatment zone.

Prior to installing the production CG program within the tank footprint, HBI performed several test sections at the edge of the tank footprint to establish the following: (1) to confirm whether the CG could effectively increase the CTP tip resistance between EL. 368 to 343 for the required reduction in static settlement and liquefaction potential and (2), to establish a cutoff criterion for the CG operation in terms of pumping pressure and grout volume. The test section layouts are displayed in Figure 6 below.

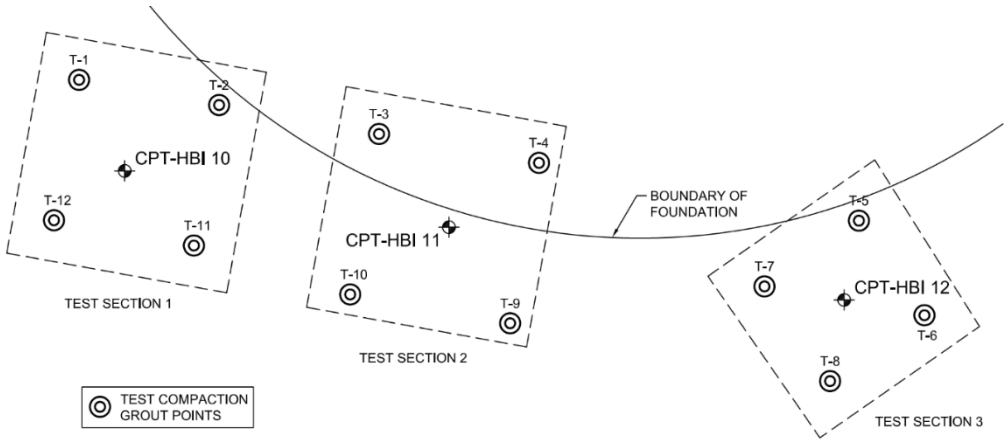


Fig. 6. Compaction Grouting Test Section

Figure 7 below shows the comparison between pre-CG CPT tip resistance (HBI-3 & 4) and post-CG CPT tip resistance (HBI-10 & 11) from within the test section area. The treatment zone shows significant improvement, particularly in the softer materials observed between EL. 363 to 350, with an average q_t of 200 tsf across the compaction grout zone measured in post-grouting CPTs.

The test section data allowed HBI to select appropriate primary and, if needed, secondary and tertiary grout point spacing and associated grout cutoff criteria. Based on the data from the test section, HBI selected a target improved average q_t of 80 tsf for the CG zone.

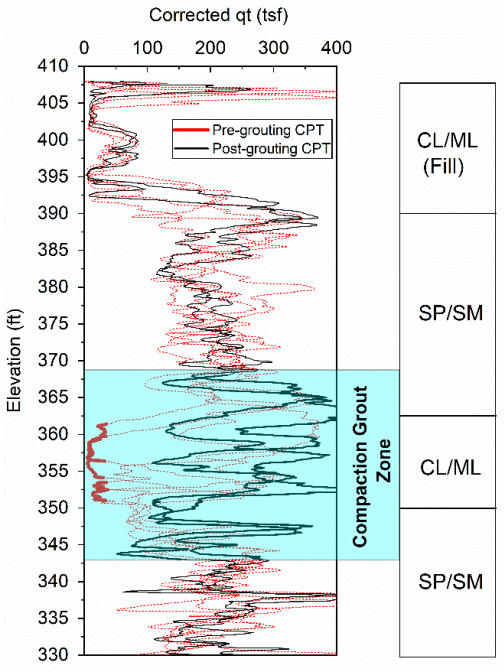


Fig. 7. Pre and Post-Test CG CPT Tip Resistance

Using the cutoff criterion in terms of pumping pressure and grout volume, determined from test sections, HBI performed the production CG program within the tank footprint. Figure 8 below summarizes the recorded grout volume and pressure at each grouting point across the site. The diameter of the grout column represents the injected grout volume while the color reflects the pumping pressure, with green being low pressure and red being refusal pressure.

As indicated in Figure 8, the grout volume and pumping pressure varied between grouting points, as well as at different elevations within the same grouting point. Generally, the softer or looser the soil within the grout stage, the lower the pumping pressure and therefore the higher the grout "take" before the cutoff criteria was achieved. The grouting record generally confirmed the findings of the subsurface exploration with regards to the intermittent deposition of soft and loose zones across the tank footprint at varying depths.

Figure 9 below shows the comparison between pre-CG CPT tip resistances (CPT-3, HBI-3, 4 and 5) and post-CG CPT tip resistances (HBI-20 to 24). As shown in the Figure, an average q_t greater than 200 tsf was measured in the post-CG CPTs within CG zone.

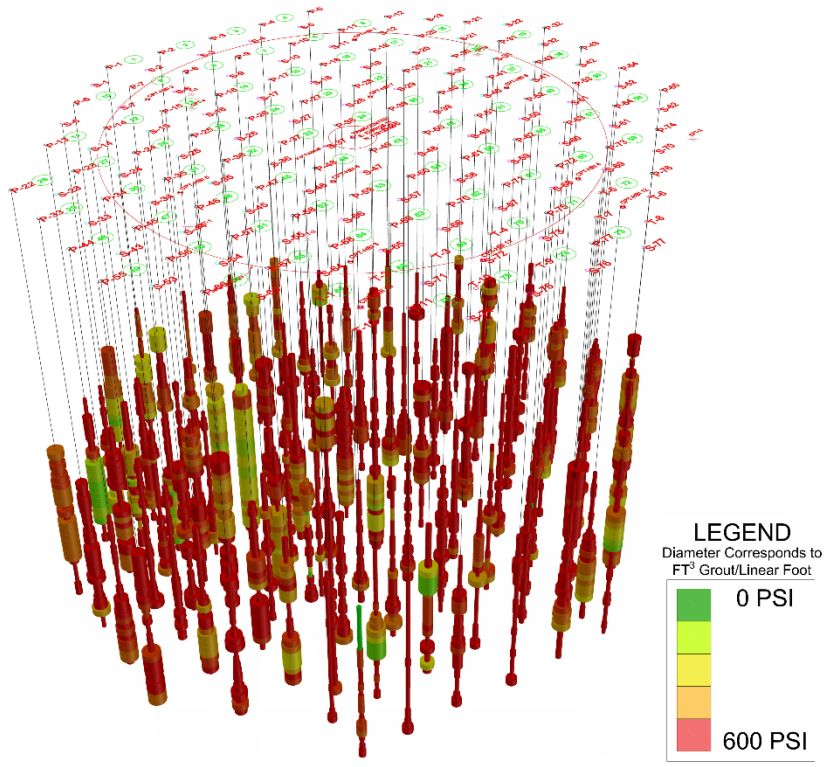


Fig. 8. Compaction Grout Injection Monitor

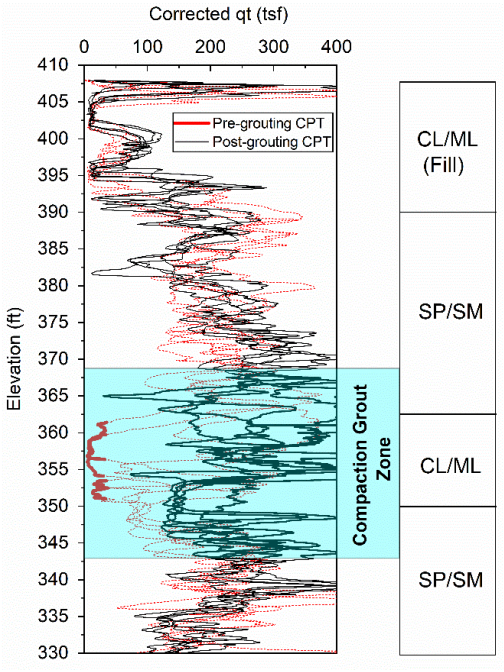


Fig. 9. Pre and Post-Production CG CPT Tip Resistance

Aggregate Piers

The final GI method employed to support the tank foundation was Aggregate Piers. Aggregate Piers (AP) are columns of highly densified stone that extend from the bottom of a foundation through zones of weaker soils and terminate either within a firm layer or at a point below significant vertical stress increase. The dense AP attract a high percentage of the stress applied to the foundation, with the remaining stress carried by the matrix soils. AP are reinforcing elements, and are used to improve soils with higher fines content that are not densifiable. The upper soils within the profile of the proposed tank were classified as silty clay fill and silty sand. After the VC and CG programs were completed, AP's were installed beneath the tank footprint to improve the shallow soils described above, thereby increasing the allowable bearing pressure and reducing expected settlement within those zones.

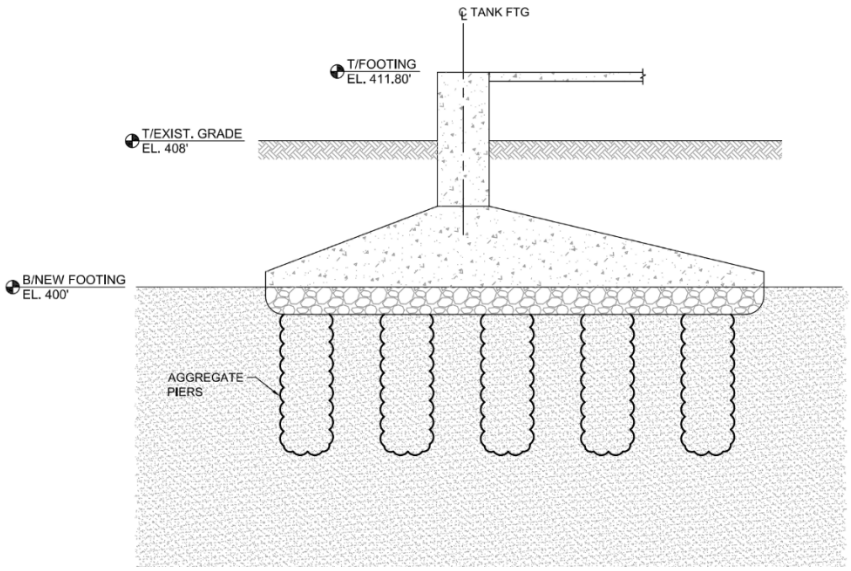


Fig. 10. Configuration of Aggregate Pier beneath Foundation

SUMMARY AND CONCLUSIONS

The involvement of the specialty geotechnical contractor (HBI) early in the process by McDermott on this project allowed the two parties to openly collaborate and agree upon the most effective project specific solution for the owner (IAW). The challenges presented by the site soils, with a heavily loaded critical structure, were not well suited to a typical lump sum contract approach. Proper design and construction relied on the collection of geotechnical data intermittently to confirm the effectiveness of ground improvement efforts and expand the understanding of the soils. The approach selected for this project, was lump sum pricing for known costs such as mobilization and general conditions, along with iterative pricing for discrete work items based on intermittent review of confirmatory data. Iterative pricing was based on time and material rates for much of the production work, and cost-plus base pricing for geotechnical investigation. This flexible contracting arrangement provided all parties (HBI, McDermott, and IAW) with an appropriate allocation of risk and cost. The collaborative approach avoided the need for significant change orders, and provided transparency to the contracting parties.

The inflexibility of strict lump sum pricing in light of the unknowns regarding the amenability of the soils to the various ground improvement techniques would have created an additional layer of risk to be

allocated. That risk would have been passed on to the Contractor, and ultimately the owner in the form of either inflated lump sum pricing to account for the risk, or in the form of contractual qualifications that may have resulted in a significant series of change orders to account for cost and schedule overruns.

This project serves as a case study for adaptive design by: (1) The Contractor engaging specialty geotechnical contractors early in the process and being open to investigating multiple potential solutions for a combination of challenging soil conditions and heavily loaded or settlement sensitive structure

(2) The owner agreeing to perform iterative geotechnical explorations during the project to optimize cost savings and lower risk. A one-size-fits-all approach is difficult for these types of projects, and requiring lump sum pricing despite unknowns regarding the soil conditions and/or structural needs creates additional risk. The collaboration between IAW, McDermott, and HBI allowed for an optimized, cost effective solution with the risk to be handled through thorough investigation and technical design, avoiding some of the costs associated with the ambiguities at bid phase.

REFERENCES

Hayward Baker, Inc., 2010, Vibro Systems.

Hayward Baker, Inc., 2011, Compaction Grouting.

Sehn, Allen L., and J. Tanner Blackburn. "Predicting performance of aggregate piers." In *Proceedings of the 23rd Central Pennsylvania Geotechnical Conference, Hershey, PA, USA*, pp. 28-30. 2008.

EFFECTIVENESS OF HEAD-ENLARGED CDM COLUMNS IN EVALUATIING SETTLEMENT OF IMPROVED GROUNDS

T.D. Nguyen, Vietnam Japan University & FECON Corp, Hanoi, Vietnam, Email: nt.dung@vju.ac.vn
Y.M. Ha & H.K. Choi, EXT Co. Ltd, Seoul, Korea, Email: haym@extpile.co.kr, & choihk@extpile.co.kr
D.T. Nguyen, Vietnam Japan University, Hanoi, Vietnam, Email: ductrungxd@gmail.com

ABSTRACT

Conventionally, cement deep mixing (CDM) columns are designed to have constant diameters over the improved depth as this facilitates the construction procedures. However, this design pattern may be inefficient in cases of spread footings or shallow foundations. This paper first briefly introduces principles of an improved CDM method that can create head-enlarged CDM (termed PF) columns. A simple analysis approach was introduced to obtain optimal shape of PF columns that results in minimum settlement. The effectiveness of this improved method over the conventional CDM method was then illustrated by settlement analysis for an actual footing in a case study using two recommended analytical methods in the literature. Analysis results from the case indicated that by using the same amount of soil-cement mixed volumes, settlement from a footing on PF columns can reduce up to 10 % compared with that from the same footing on CDM columns. In addition, a material quantity comparison for the case indicated that to have the same settlement values the volume of each PF column can be reduced of around 10% compared with that of the CDM column.

Keywords: CDM method, head-enlarged CDM columns, PF method, settlement

INTRODUCTION

The cement deep mixing (CDM) method is one of the most popular methods in ground improvement works. Details on the method such as construction procedures, necessary equipment and recommendations are described in many references or manuals (e.g. Bruce et al. 2013, BS EN 2015, Kitazume and Terashi 2013). Conventionally, CDM columns are designed to have constant diameters over the improved depth as this facilitates the construction procedures. However, this design pattern is found inefficient in cases of spread footings or shallow foundations as the upper soil layers are naturally weaker than the deeper ones but are subjected to larger amount of induced stress from the superstructures.

To improve such drawback of the conventional CDM columns, head-enlarged CDM column, named as Point Foundation (PF), has been recently introduced and implemented by EXT Co. Ltd. from S. Korea. In principle, as shown in Fig. 1, a PF column typically has three sections:

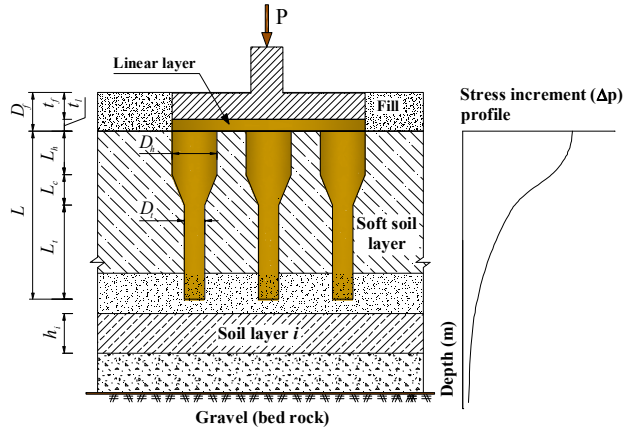


Fig. 1. Concept of PF in ground improvement



Fig. 2. An example of PF columns (EXT 2017)

© 2019 Deep Foundations Institute

the bigger head, the transitional cone, and the smaller tail. The larger head section of PF columns would provide a better reinforced stiffness in the upper weaker layers than the conventional CDM columns. Thus, proper designed dimensions of the columns would provide better stiffness profile with depth, resulting in larger bearing capacity or smaller settlement. Typical PF column excavated in the field are shown in Fig. 2.

Since its first introduction to the market (2012), the PF method has been extensively applied to more than 140 projects to improve grounds under car parking areas, industrial buildings, and shallow foundations of transportation structures in Korea. However, there have been no any quantitative reports on the effectiveness of the PF method over the conventional CDM method. This paper first briefly introduces principles of the PF method and then presents a quantitative evaluation of the effectiveness of the PF method compared with the conventional CDM method in term of settlement reduction. For the later, settlement of a shallow footing from an actual project is analysed and discussed.

BRIEF ON THE PF METHOD

The PF method was first introduced by EXT Co. Ltd in Korea in 2012 and has been then extensively applied in the country since 2014. The method has been patented in several countries including in the US. Similar to CDM, the PF method can be applied to reinforce grounds under roads, industrial buildings, storage yards, and especially can be used as pile foundation for lightweight transportation structures and low-rise buildings with a maximum applied pressure up to 350 kPa.



Fig. 3. Use of excavator (EXT 2017)



Fig. 4. Use of Drilling machine (EXT 2017)

The construction procedures and required equipment of the method are in principle similar to that of the CDM method. The key different points are the configuration of the mixing shaft and its flexibility to adapt to different base machines depending on the improved depth required. Typically, if the improved depth is less than around 15 m an excavator is often used as the base machine (Fig. 3). If the depth is larger, stronger drilling machines as often used in the CDM method (Fig. 4) are required. The mixing shaft consists of three sections assembled: the head, the tail, and the bit. The length of blades for the tail section is constant whereas that for the head section varies in the form of a truncated cone as schematically shown in Fig. 6. In actual projects, the length of the tail section is fabricated to be equal to that of the PF body and the screw-down of the mixing shaft until the design depth would form the head section as expected. The grout is injected (through some nozzles at the bit position of the shaft) and controlled through the whole mixing process until design volume of grout as well as the homogeneous condition of the mixed soil are reached.

Quality of the mixed soil columns is strictly controlled not only by soil sampling and mixing tests before construction but also by sampling during mixing at the sites as typically shown in Fig. 5. When the mixing steps are to be completed as design, special tube samplers are attached on the mixing shaft to collect the mixed soil samples at specific depths. The collected soil samples will be cured in the lab and tested at different curing time periods to check the strength of the mixed soil. Besides this sampling method, if



Fig. 5. Collecting mixed soil samples (EXT 2017)

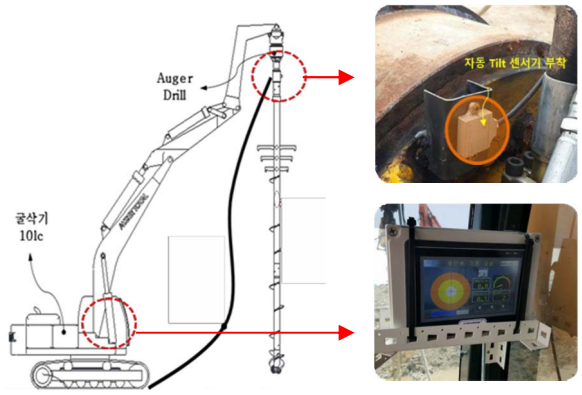


Fig. 6. Equipment for verticality control (EXT 2017)

required, coring method can also be used to collect continuous samples along the depth. For this, a PVC pipe is injected into the PD column right after the completion of mixing and it will be withdrawn after typically four to five hours. In addition to quality of mixed column, the verticality of the column is also strictly controlled during construction as typically illustrated in Fig. 6. As shown, a tilt sensor is attached on top of the agitation rod and it is wirelessly connected with digital controller attached near the operator. Thus during the construction, the machine operator can observe and control the verticality of the rod effectively.

SETTLEMENT ANALYSIS

Settlement evaluation methods

As the PF method has been mainly used to reinforce grounds under lightweight structures (rather than embankments and landfills), thus settlement of shallow footings is examined in this study. Two methods for estimating settlement of shallow foundations recommended in the literature are applied to the analysis: (*i*) three-dimensional (3D) elastic strain integration (CFEM 2006); (*ii*) Semi-empirical method of Schmertmann et al. (1978). For the first method, settlement of the deep mixed zone is calculated based on equal strains in the deep mixed ground and the adjacent untreated soil within the mixed zone area. This approach is therefore equivalent to using a composite modulus of the deep mixed ground and the adjacent soil (Bruce et al. 2013). Under 3D loading conditions, uncorrected settlement of a footing on an improved area can be estimated as follows (CFEM 2016):

$$S_{uncorr} = \sum_{i=1}^{n}\left[\Delta\varepsilon_{z,i}\Delta h_i\right] = \sum_{i=1}^{n}\left[\frac{1}{E_{comp,i}}\left(\Delta\sigma_{z,i} - \nu_i\left(\Delta\sigma_{x,i} + \Delta\sigma_{y,i}\right)\right)\Delta h_i\right] \quad [1]$$

where $E_{comp,i}$ is the (drain) composite modulus of sub-layer *i;* $\Delta\sigma_{x,i}$, $\Delta\sigma_{y,i}$, and $\Delta\sigma_{z,i}$ = (effective) stress increments in *x*, *y*, *z* directions at the center of sub-layer *i* under the estimated settlement point. The stress increments under a corner of a uniformly loaded rectangle can analytically be calculated by equations described in Poulos and Davis (1974) or in CFEM (2006) (Section 11.6.4); ν_i = Poisson's ratio of composite material of sub-layer *i*; Δh_i = thickness of sub-layer *i*. The composite modulus can be determined as follows,

$$E_{comp,i} = a_{PF,i}E_{PF,i} + (1 - a_{PF,i})E_{s,i} \quad [2]$$

where $E_{PF,i}$ and $E_{s,i}$ = equivalent (drained) elastic modulus of mixed soil-cement column (PF column) and of untreated soil of sub-layer *i*, respectively; $a_{PF,i}$ = improved area ratio by PF columns in sub-layer *i*.

The corrected settlement of the foundation is evaluated as:

$$S_{corr} = S_{uncorr} I_E I_F \quad [3]$$

where I_E and I_F are settlement correction factors for foundation embedment and foundation rigidity, respectively (CFEM 2006).

For the second method (Schmertmann et al. 1978), settlement of a rigid footing (S_{rigid}) on the improved ground is calculated as follows:

$$S_{rigid} = C_1 C_2 q_{net} \sum_{i=1}^{n} \left(\frac{I_{z,i}}{E_{comp,i}} \right) \Delta h_i \qquad [4]$$

where q_{net} = net applied pressure, C_1 = embedment correction factor, C_2 = correction factor for creep effect, I_z strain influence factor. Details of these factors are given in some manuals (e.g., Holtz 1991). Note that the Schmertmann et al. (1978) method was proposed based on experimental results of rigid steel plate load tests in the laboratory and extensive finite-element method (FEM) study on rigid shallow foundations. Thus, the settlement of an intermediate rigid foundation estimated by Schmertmann method should be corrected as: $S_{corr} = S_{rigid}\, I_F/I_{F,rigid}$, where $I_{F,rigid} \approx 0.786$ (for a perfectly rigid foundation).

For untreated sub-layers beneath the treated zone, the methods presented above are also applied, however the equivalent (drained) elastic modulus of the untreated soil (E_s) is used instead of E_{comp}. Note also that if an untreated sub-layer is clay layer, the approach of modifications to one-dimensional settlement (CFEM 2006) is applied.

A solution for the optimal shape of PF column

The effectiveness of the PF and CDM methods can be compared by examining the bearing capacity or settlement of the grounds reinforced by PF and CDM columns under equivalent conditions. In this study, the settlement of reinforced grounds is selected as a criterion to estimate the effectiveness of the methods. Following this approach, settlement of a shallow foundation under uniform applied pressure is examined for two cases: (1) reinforced by PF columns: (2) reinforced by conventional CDM columns. All input conditions for the two cases such as soil profile, foundation size and depth, applied pressure, number and stiffness of PF/CDM columns, and volume of each column type, are made equal.

Assuming that a cylindrical CDM column has a constant diameter of D and length L, the condition of equal volume of each column type gives:

$$\frac{\pi D_h^2 L_h}{4} + \frac{\pi}{3}\left(\frac{D_h^2}{4} + \frac{D_t^2}{4} + \frac{D_h D_t}{4} \right) L_c + \frac{\pi D_t^2 L_t}{4} = \frac{\pi D^2 L}{4} \qquad [5]$$

where D_h and D_t = diameters of head and tail of the PF column; L_h, L_c, and L_t = lengths of head, cone, and tail of the PF column ($L_h+L_c+L_t = L$) as shown in Fig. 1.

By setting $\alpha = L_h/L$, $\beta = D_h/D_t$, and θ = angle of cone face with horizontal plane (typically $\theta = 45^o$ - 60^o), Eq. (5) can be rearranged into the form of a cubic equation as follows.

$$aD_t^3 + bD_t^2 + c = 0 \qquad [6]$$

where $a = [\pi(\beta^3-3\beta+2)\tan\theta]/24$, $b = \pi L[(\beta^2-1)\alpha+1]/4$, $c = -\pi D^2 L/4$.

The roots of Eq. (6) (i.e. D_t) can be obtained as that of the general cubic equation (Zwillinger 2018). Note that, for a PF column, $\beta > 1$ and therefore $a > 0$, Eq. (6) always has only one positive root. Thus, with a set of given values of α, β, θ, D, and L, D_t is obtained as the positive root of the equation.

A CASE STUDY

General information of project

Among more than 140 projects that have been carried out in S. Korea, the use of PF method for ground improvement in construction of Jincheon Energy Factory (JEF) project is presented herein as a typical case study. The factory is located in Jincheon District, Chungcheongbuk Province, S. Korea. As shown in Fig. 7, the 19 ha factory includes 2 two main blocks (existing factory block and extended block), parking lots, waste water treatment, storages, etc. The PF method was adopted as the ground improvement method for

the extended construction area with a total improved area of 5.2 ha (158 m × 338 m). For this, a total number of 7,693 PF columns with a total length of 68,138 m were constructed. The foundation work of the project was carried out in nearly 208 days, lasting from August 1, 2016 to February 23, 2017. Some photos of foundation work are shown in Fig. 8.

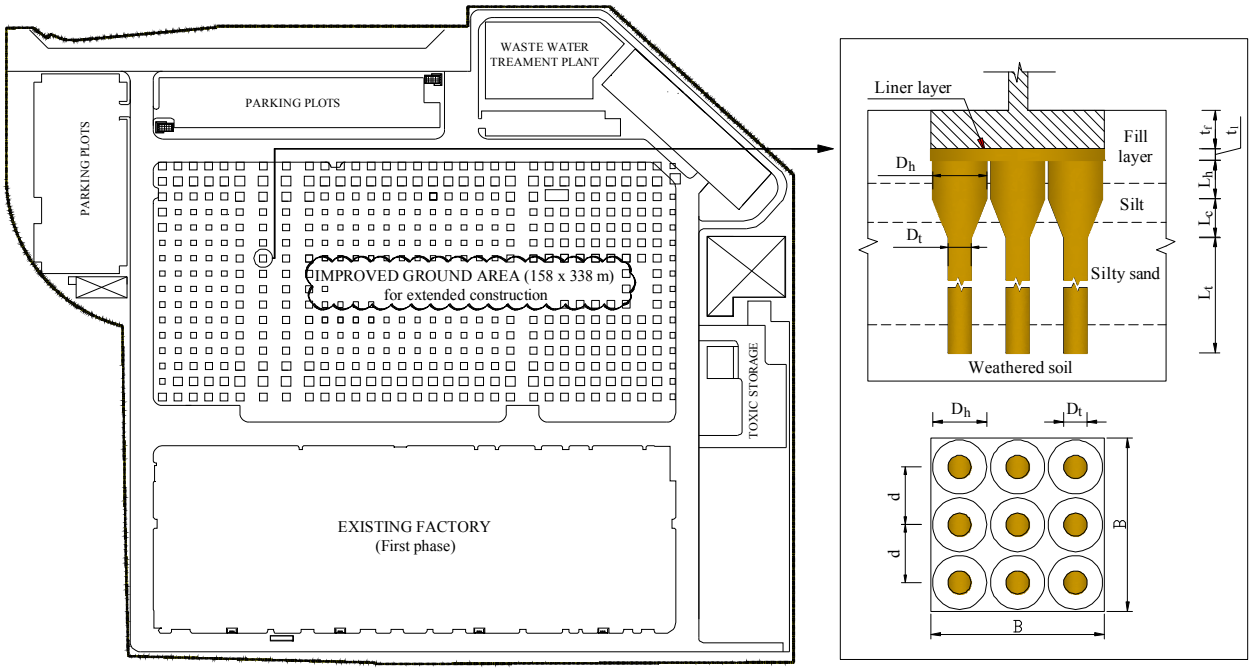


Fig. 7. Plan view of the JEF and views of a typical shallow foundation in the project



(a) (b)

Fig. 8. Typical photos during foundation work at JEF: (a) a section view; (b) an aerial view

Footing parameters

In the improved area, there were a total of 511 square footings and two rectangular footings. Depending on load intensity from structures, the size ($B \times L$) of the footings varied from 3.5 × 3.5 m to 7.2 × 15.0 m and the number of PF columns under each footing varied from 5 to 47. The improved depth (L) varied from 4.0 to 14.0 m depending on geological conditions in the improved zone. Under each footing slab (thickness = t_f), there was a liner layer (typical thickness t_l = 0.3 m) made of the same PF material. The linear layer was designed to ensure relatively uniformed pressure transferred to the PF columns in the group. Table 1 shows a summary of footing categories and associated parameters of each type.

Table 1 A summary of footing categories and parameters in the JEF project.

Footing Category	No. of footings	Dimensions: $B \times L \times t$ (m)	N. of PF columns	Improved depth (m)	D_f (m)
F1	160	3.5×3.5×1.1	5	6/8/10/12/14	1.4
F11	26	3.5×3.5×1.1	5	2/4/6/8/12	1.4
F2	92	4.5×4.5×1.1	9	6/8/10/12/14	1.4
F3	96	5.0×5.0×1.2	12	6/10/12/14	1.5
F13a	65	5.0×5.0×1.2	12	6/8/10/14	1.4
F4	60	5.7×5.7×1.3	14	6/8/10/12/14	1.5
F5	12	6.4×6.4×1.4	16	4/8/10	1.6
EF3	1	6.5×6.8×1.1	20	10	2.2
EF2	1	7.2×15.0×1.2	47	8	3.3

Soil profile

The soil profile below an F2 footing (circled and sketched in Fig. 7) is shown Fig. 9. The profile includes layers of fill materials (0 to 2.0 m), silt (2.0 to 3.0 m), loose to medium dense silty sand (3.0 to 9.0 m), medium dense to dense weathered soil (9.0 to 24.0 m) and weathered rock (24.0 m downward). The SPT N value in the upper three layers was significantly small (around 4 to 5). The value increased from 5 to 50 in the depths from 10. to 20.0 m and then above 50 in the last few meters of the weathered soil layers. The equivalent modulus of the soil (E_s) was evaluated as a simple function of the normalized corrected SPT N value (Sabatini et al. 2002): E_s (kPa) = $k(N_1)_{60}$, where k is a correlation coefficient and varies depending soil types. Following the suggestion in the manual, the coefficient was taken as: k = 400 for the first three layers, k = 700 for weathered soil layer from 10.0 m to 20.0 m, k = 1000 for the rest of the weathered soil layer.

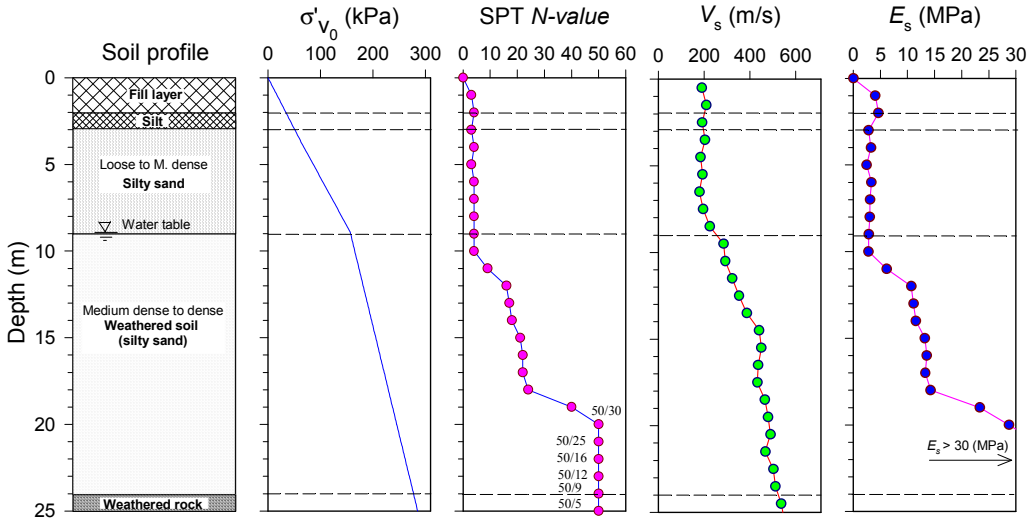


Fig. 9. Soil profile under an F2 footing in the JEF project

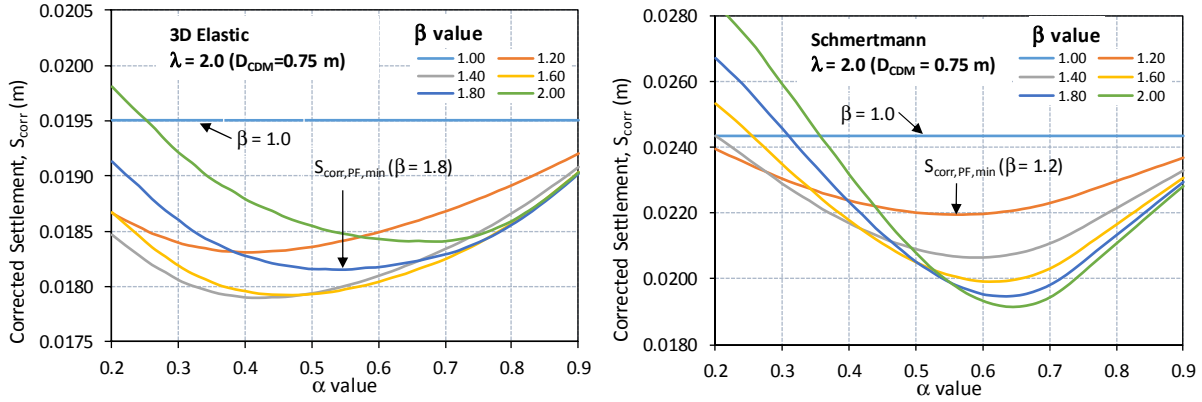
Settlement analysis

A comparative study on settlement of the F2 footing (4.5 m × 4.5 m × 1.1 m) placed on 9 PF columns (Fig. 7) and of the same footing on 9 CDM columns (assumed for comparison purpose) is presented to illustrate the effectiveness of the PF method. The toes of the PF columns in the project were designed to locate in compact silty sand (N = 10 to 30) of the weathered soil layer. For this F2 footing discussed herein, the toes were located at 13.4 m, resulting in a total PF column length of L = 12.0 m. Some key parameters used for settlement analysis are given in Table 2.

Table 2 Some key parameters used for settlement analysis

Parameter	Value	Unit	Parameter	Value	Unit
$B \times L \times t$	4.5× 4.5 × 1.1	m	$E_{s,avg}$	43400	kPa
D_f	1.4	m	E_{PF}	300.0	MPa
d	1.5	m	q/q_{net}	350.0/326.3	kPa
$E_{concrete}$	30,000	MPa	θ	60	Degree
I_F/I_E	0.788/0.940	-	ν	0.25	-

Settlement of the two footings was calculated using the analysis approach mentioned above. For this, all input parameters (i.e., soil and properties, footing size, number of PF/CDM columns, strength of mixed columns, loading conditions, etc.) were the same. Note, however, that any two CDM and PF columns were controlled to have the same volume. This condition is to make sure that both methods consume the same of amount of materials. For the 3D elastic method, the settlement evaluation was carried out until depth z = 24.0 m (end of the weathered soil layer) whereas for the Schmertmann method the evaluation was terminated at depth z = 10.4 m (i.e. 2B below the footing bottom).



(a) (b)

Fig. 10. Comparison of settlements from footings on CDM and PF columns: (a) 3D elastic method (up to z = 24.0 m); (b) Schmertmann method (up to z = 10.4 m)

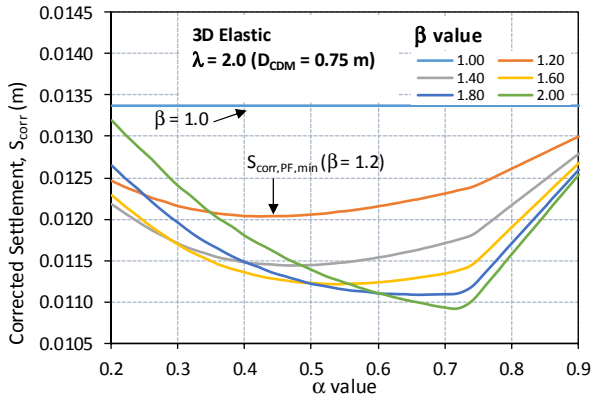


Fig. 11. S_{corr} by 3D elastic method (up to z = 10.4 m)

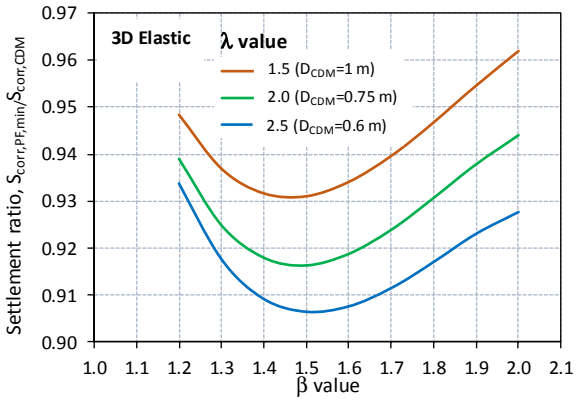


Fig. 12. Variation of $S_{corr,PF,min}/S_{corr,CDM}$

Under the confined conditions above, the α, β, and λ (λ=d/D_{CDM}, where d = distance between the centers of two columns (fixed value) and D_{CDM} = diameter of the CDM column (variable value)) were varied to examine the settlement behavior. The parameters were varied in the following manner: a pair of λ and β values was first set (e.g., λ = 2.0 and β = 1.8), and the α value was then varied from 0.2 to 0.9 for the given λ and β values. Figs. 10 (a) and 10(b) show settlement curves (S_{corr}) obtained from the 3D elastic and

Schmertmann methods, respectively, for λ = 2.0 and different β values. Note the horizontal line of β = 1.0 (i.e., $D_h = D_t$) in the figures corresponds to the settlement of the footing on CDM columns. It is clear from the figures that under some certain ranges of α (0.4 to 0.7) and β (1.2 to 2.0), settlement values of the footing on PF columns from the both methods are distinctively smaller than that on the CDM columns. This indicates that in general the configuration of PF columns improves the stiffness of the ground more effectively than the CDM columns. The different settlement values from the two methods are due to different strain distribution profiles.

It is also noted from Fig. 10 that the trend of settlement curves from the 3D elastic and Schmertmann methods are rather different, especially the variation of the minimum settlement value ($S_{corr,PF,min}$) with respect to β. That is, for the 3D elastic method (Fig. 10(a)), among five $S_{corr,PF,min}$ values from five β values, the smallest $S_{corr,PF,min}$ value (≈ 0.0178) from β = 1.4 reached at α of around 0.45, whereas, for the Schmertman method (Fig. 10(b)), the $S_{corr,PF,min}$ value continues to decrease with the increase in α value. This different trend is attributed to the different extension of stress/strain profile with depth. For a comparison purpose, Fig. 11 shows settlement curves from the 3D elastic method in which the evaluation was terminated at z = 10.4 m as done for the Schmertman method. As expected, the trends of settlement curves from Fig. 11 and Fig. 10(b) are now rather similar.

Fig. 12 shows the variation of $S_{corr,PF,min}/S_{corr,CDM}$ ratio obtained from the 3D elastic method with respect to β. It is interesting to note that, for three different typical λ values, the settlement ratios reached minimum values at relatively similar β values of 1.45 to 1.55. The figure also indicates that, for the λ values used, the optimal settlement (at β = 1.5) of the footing on PF columns is about 90.5% , 91.5 and 93% that of the footing on CDM columns, respectively.

The actual PF columns constructed in the project had α value varied from 0.2 to 0.4 and β value from 1.5 to 2.0 depending on the available agitation rods and ground conditions. All the footings were design to have settlements of less than 1.0 inch (25.4 mm).

A material quantity comparison

It is now clear that by using the same volume of improved (mixed) columns, the configuration of PF column is more effective than that of the conventional CDM column in term of settlement reduction. It might be interesting to check how much volume the PF column can be reduced (saved) to result in the same settlement values. A given value of CDM column (D_{CDM}) was first selected and the settlement of the footing on CDM columns was obtained ($S_{corr,CDM}$). Using the same analysis procedures discussed above, the settlement of the footing on PF columns was analyzed by gradually reducing volume of PF column until $S_{corr,PF,min} = S_{corr,CDM}$. Thus, for each β value, there exist an amount of volume decrease (ΔV) that satisfies this condition.

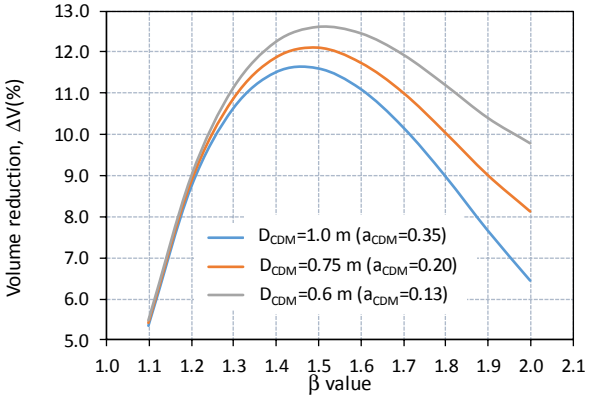


Fig. 13. Variation of volume reduction

Fig. 13 show the variation of ΔV (%) with respect to β value, in which $\Delta V = 100\times |V_{PF,final}-V_{CDM}|/V_{CDM}$, where $V_{PF,final}$ = final volume of the PF column that makes $S_{corr,PF,min} = S_{corr,CDM}$. Note from the figure that for D_{CDM} = 1.0 m, 0.75 m and 0.6 m, the maximum ΔV of about 11.5 %, 12.0 % and 12.5 % were obtained, respectively, at similar β values (1.45 to 1.55).

CONCLUSIONS

This paper first introduces an improved CDM method (named as Point Foundation (PF)). The PF method produces head-enlarged CDM columns that can improve the stiffness of natural soil profile more effectively than the conventional CDM method, especially for grounds under shallow footings. To quantitatively evaluate the effectiveness of PF method over the CDM method in term of settlement reduction, a simple approach to find the optimal shape PF column was introduced based on the condition that volumes of any two CDM and PF columns are equal. The effectiveness of the improved method was then illustrated by settlement analysis for an actual footing in a case study using 3D elastic and Schmertman et al. (1978) methods. The following are key conclusions drawn from the analysis for the footing analysed.

If stress/strain profiles are terminated at depth z = 2B (as recommended by Schmertmann method) both method resulted in rather similar trends of settlement curves as well as of the settlement values. However, if the full soil profile was taken into analysis, settlement from 3D elastic method was slightly larger than that from Schmertmann method.

Results from 3D elastic method indicated that for three typical ratios of center-to-center distance of two CDM columns over the column's diameter (λ = 2.5, 2.0, and 1.5), which correspond to the area improvement ratios of 0.126, 0.196 and 0.349, respectively, an optimal (minimum) settlement of the footing on the PF columns reached at relatively similar value of β = 1.5 (the ratio of diameter of the head to that of the tail of the PF column). These settlement predictions were about 90 to 93% of that from the same footing on CDM columns.

The material quantity comparison indicated that the volume of grout material used for the optimal PF columns would be less compared with that for the CDM columns (to have the same settlement amounts). For the analyzed case the material saving amount was around 10%, and for other actual projects the value may vary slightly depending on actual soil profiles and improved area ratio (*a*).

ACKNOWLEDGEMENT

This work was supported by VJU Research Grant No. VJU.CS.18.02 and by EXT Co. Ltd. The author would like to thank EXT very much for their kind permission to use information and some images of the PF method.

REFERENCES

Bruce, M.E.C., Berg, R.R., Collin, J.G., Filz, G.M., Terashi, M. and Yang, D.S. (2013). FHWA design manual: Deep mixing for embankment and foundation support, US Department of Transportation, Federal Highway Administration (FHWA), Publication No.: FHWA-HRT-13-046.

BS EN 14679 (2005). Execution of special geotechnical works – Deep Mixing, British Standards Institution.

CFEM (2006). Canadian Foundation Engineering Manual, 4th Edition, Canadian Geotechnical Society.

EXT (2017). Point Foundation - A foundation method for weak soil reinforcement using environmentally-friendly, highly functional binders, EXT's Brochure.

Holtz, R.D. (1991). Stress distribution and settlement of shallow foundation. Chapter 5 in Foundation Engineering Handbook, Fang H.S (eds), 2nd Edition.

Kitazume, M. and Terashi, M. (2013). The deep mixing method. CRC Press, 405 p.

Poulos, H.G. and Davis, E.H. (1974). Elastic solution for soil and rock mechanics, John Wiley & Son, Inc.

Sabatini, P.J., Bachus, R.C., Mayne, P.W., Schneider, J.A. and Zettler, T.E. (2002). Geotechnical engineering circular No. 5 – Evaluation of soil and rock properties. U.S. Department of Transportation, Federal Highway Administration, Report No. FHWA-IF-02-034.

Schmertmann J.H., Hartman, J.P. and Brown, P.R. (1978). Improved strain influence factors diagrams. Journal of the Geotechnical Engineering Division, ASCE 104(GT8): 1131-1135.

Zwillinger, D. (2018). CRC Standard mathematical stables and formulas. 33rd Edition, CRC Press, 858 p.

GROUND FREEZING: THE USE OF LIQUID NITROGEN SYSTEMS CONVERTED TO BRINE

Joseph A. Sopko, Moretrench, A Hayward Baker Company, Rockway, NJ, USA, 973-627-2100 x 231, jasopko@moretrench.com

ABSTRACT

There has been a trend in recent years in performing the initial formation freezing using liquid nitrogen (LIN) and then converting the system to circulating refrigerated brine. While proponents of this method state it decreases freezing time, it can also be considered an alternative to inadequate refrigeration capacity. This method was used on several small projects in the 1980s. Problems such as broken pipes, frozen brine, and unsafe work conditions caused contractors to re-think the method. This paper discusses these problems and also presents work schedules showing no schedule reduction. In fact, this method can lead to longer time as well as significantly higher costs.

Keywords: liquid, nitrogen, ground, freezing, brine

BACKGROUND

Ground freezing as a method to provide groundwater control and temporary earth support for excavations is completed using a relatively simple process: drilling and installing refrigeration pipes around the perimeter of the excavation and introducing a coolant into these pipes. The coolant extracts heat from the ground, converting the pore water to ice and forming a strong, impermeable material. A typical ground freezing system is illustrated in Fig. 1.

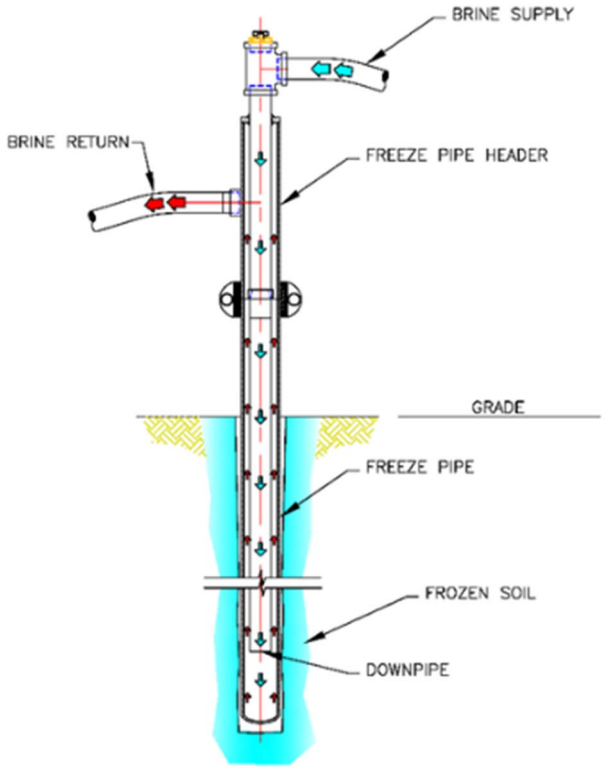


Fig. 1. Typical ground freezing system

© 2019 Deep Foundations Institute

SYSTEMS

There are two basic types of coolant systems: circulating and direct expansion. The circulating coolant system is made of two separate, closed systems. The medium circulating is the secondary coolant. It is cooled at a central refrigeration plant, circulated through the pipes, and warms as it extracts heat from the ground. It then circulates back to the plant where it is cooled. This coolant is chilled in a heat exchanger by the primary refrigeration system where a compressor system is charged with a refrigeration gas. The heat is ultimately extracted from the ground and expelled into the atmosphere by an evaporative condenser. Secondary coolants are usually a brine or glycol chemical while the primary refrigeration gas is anhydrous ammonia or another commercially available gas.

Direct expansion systems are much simpler. A cryogenic liquid such as nitrogen or CO_2 flows into the individual pipes and boils when in contact with the warmer soil. The gas then exits the pipe and is discharged into the atmosphere as shown in Fig. 2.

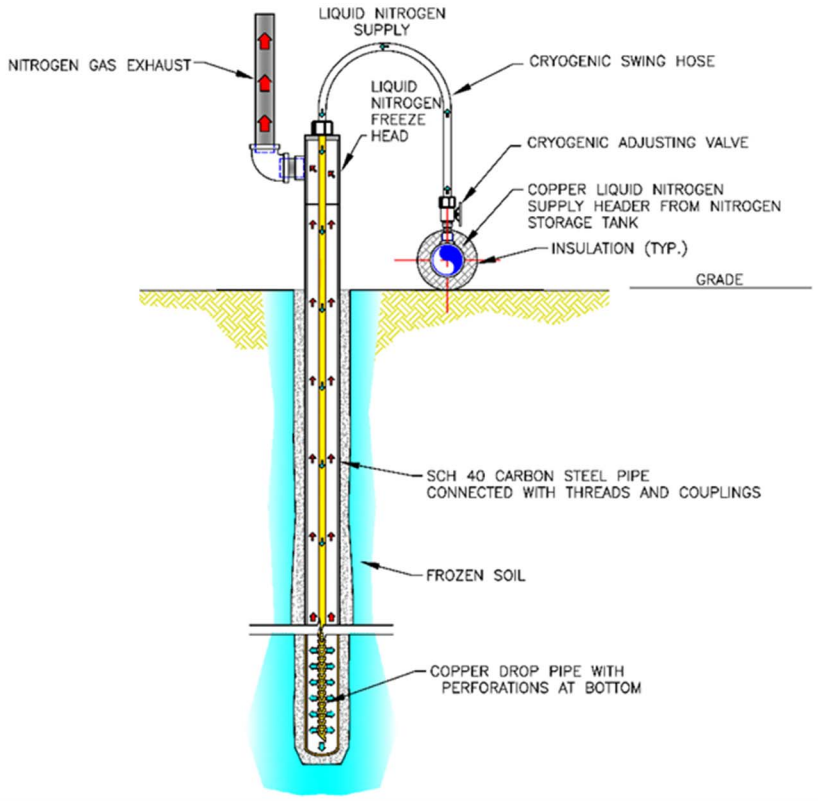


Fig. 2. LIN system

Both systems have a series of advantages and disadvantages, summarized in Tables 1a-b.

Table 1a. Circulating System

Advantages	Disadvantages
Lower cost	Longer freezing time
Location not a factor	Ammonia gas
Components readily available	Circulating calcium chloride
Adaptable for large projects	Electric power required

Table 1b. Direct Expansion

Advantages	Disadvantages
Reduced freezing time	Higher cost
Non-toxic to environment	Not always available in remote locations
Suitable for small project	Requires cryogenic components
Substantially colder and strong frozen soil	Asphyxiant

Technical comparisons

It is important to note the technical difference between the two methods prior to any economic evaluation. Most projects can be quickly evaluated relative to what method should be used. The circulating system is used for most ground freezing applications. The coolant can be pumped for long distances and is used in deep excavations exceeding 600 m. The pipe systems operate under relatively low pressures and present no dangerous situations. The frozen soil strengths range from 3.0 to 10.0+ MPa, which are suitable for most excavation support systems. A circulating system can be drilled and installed in any location that can be accessed and supported with diesel generators for electrical power.

With the direct expansion system, it is difficult to transport the LIN very long distances or flow into deep refrigeration pipes as it will boil off and become a gas. It should be emphasized that while the evaporated gas is very cold, it does not permit efficient heat transfer compared to the nitrogen in a liquid state. It can be very difficult to transport the LIN to remote places and in some cases also difficult to get the quantities necessary to freeze large projects. LIN plant capacity and location are key to considering its use prior to any detailed technical or economic evaluation. With the cryogenic temperature (T) of -196^{o}C, the frozen soil is considerably colder and stronger than with the circulating systems. While these Ts are usually not required for most excavation support systems, they are sometimes necessary to form a water tight frozen bond against the subsurface structure of a tunnel boring machine.

Economic comparisons

While an economic analysis of each method is beyond the scope of this paper, a few key points are warranted:

1) if the total length of refrigeration pipe for the project is greater than 1500 m, LIN is most likely more expensive than brine;
2) freight often charges due to long distances or traffic congestion through large metropolitan areas, making LIN technically unfeasible;
3) very small projects like sealing a breach in a slurry diaphragm or secant pile wall do not warrant the expense of installing a circulating coolant refrigeration plant and power supply, making LIN the primary choice;
4) if someone gives you an exact estimate of how much nitrogen is required to freeze a project, they are mistaken as it is very difficult to estimate LIN consumption as described in subsequent sections.

Refrigeration requirements

Initial steps in designing a frozen structure include evaluating the frozen soil's mechanical properties and then determining the frozen earth structure's size or thickness. A structural thickness also generally specifies the required T regime. Most specifications require either an average T of -10°C or the frozen zone to be considered at the zone between -2°C intrados and -2°C extrados; the latter is much easier to define. To determine the length of time required to form this frozen zone as well as the refrigeration load required, a thermal analysis is completed. A time-dependent heat transfer finite element model can be used to conduct such an analysis. In addition to the project geometry, using a simple tunnel or cross passage as illustrated in Fig. 3 is recommended for simplicity. The following parameters are required: unfrozen and frozen heat capacity, unfrozen and frozen thermal conductivity, volumetric water content, initial ground T, and coolant T.

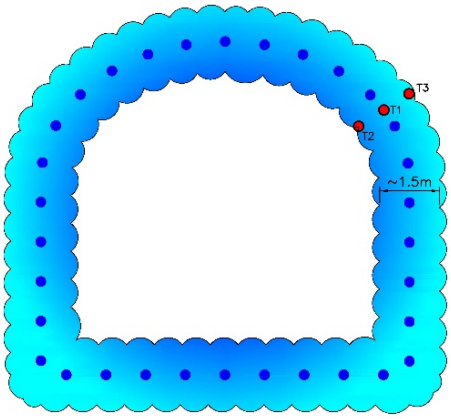


Fig. 3. Tunnel cross section

Using the geometry in Fig. 3 as the basis of the model, Ts at T_1, T_2, and T_3 are evaluated against time. Fig. 4a presents the time versus T plot when using a -25°C circulating brine while Fig. 4b sows the same plot but with -196°C expendable LIN.

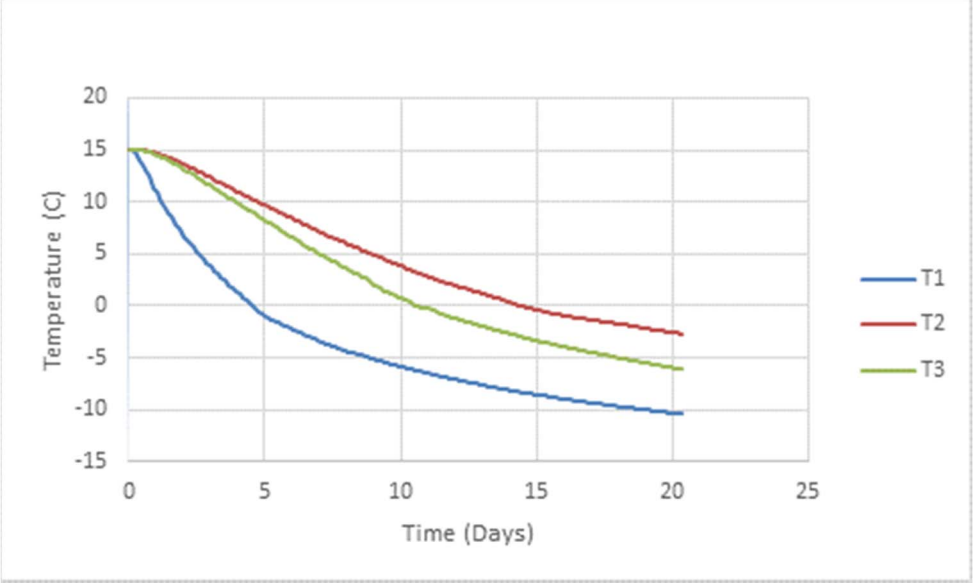


Fig. 4a. Time vs. T for circulating brine

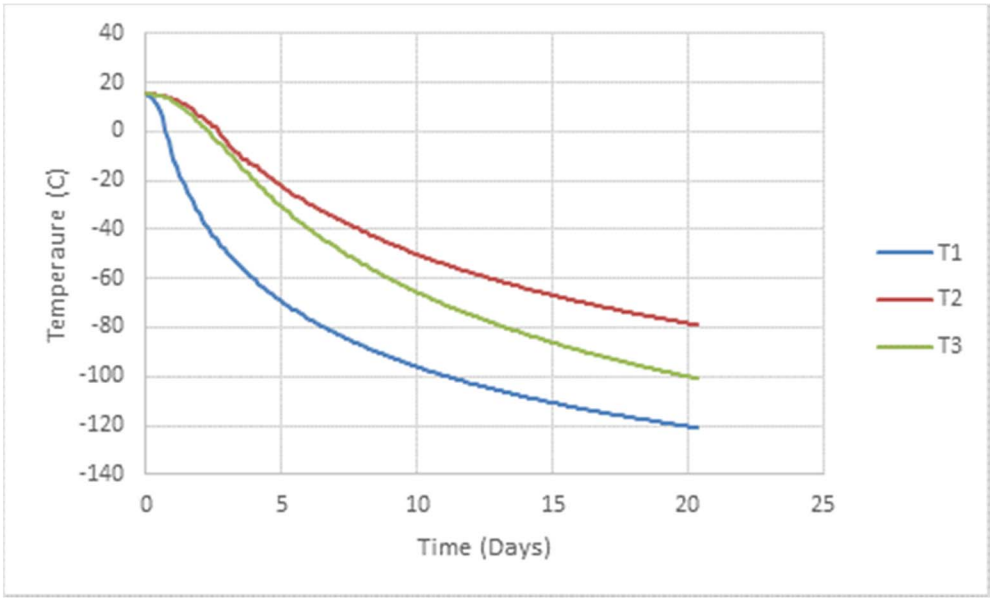


Fig. 4b. Time vs. T for expendable LIN

Interpretation of these two graphs is straightforward; T2 and T3 are both located 0.75 m off the centerline of refrigeration pipes, consistent with the 1.5-m-thick frozen zone determined in the structural analysis. With the brine system, the frozen structure is formed in 17 days, but only four days are required when using LIN. Before reaching the conclusion that faster is better, there are additional considerations.

Figs. 5a-b present the actual heat extracted (for one m of pipe) from an individual refrigeration pipe using each method.

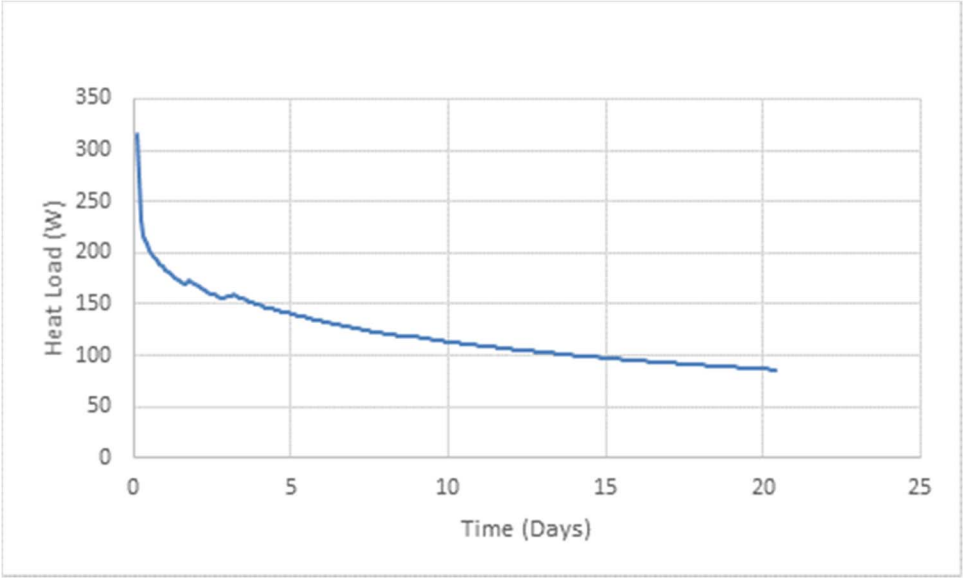


Fig. 5a. Time vs. heat load (per meter of pipe) for -25°c brine

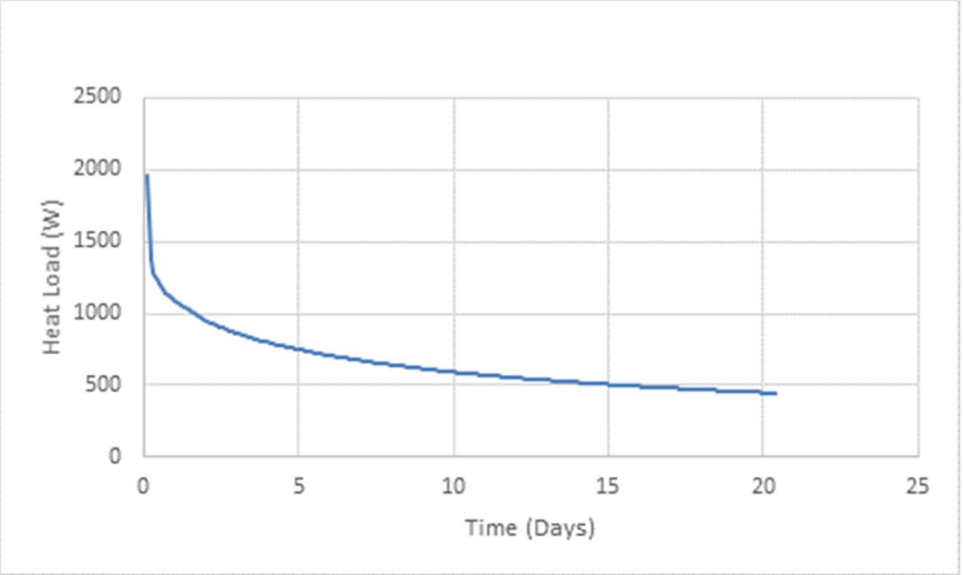


Fig. 5b. Time vs. heat load (per meter of pipe) for -196°c LIN

Using these graphs, it is possible to evaluate the total amount of heat removed during the formation freezing times. With the brine system, 1.82E+8 joules are extracted simultaneously with 3.26E+8 joules. Almost twice as much heat is extracted with LIN in about 25 percent of the time. This leads to considerable inefficiencies and additional costs.

LINDE, a producer of LIN, notes on its website that 1 kg of LIN has the capacity to extract approximately 200 kJ of heat from soil. This relationship has been used in the industry (including by the author) to evaluate the amount of LIN required to freeze the ground. Obviously, the computations are more complex and require the designer to evaluate the amount of soil to be frozen (obtained by the structural analysis) and soil T required. The soil T is the variable that can lead to inaccurate and underestimation of the quantity of LIN required.

As previously noted, it is necessary to evaluate the average T to be attained during freezing. Typically, -10°C is used. A simple way of evaluating this is to assume you have one m^3 of soil that you want to lower from 15°C to -10°C. Using the volume and a delta T of 25°C, one can compute the amount of heat extracted from the soil. However, referring to Fig. 6a, it can be readily observed that the delta T is significantly higher than 25°C.

Contrasting the contours in Fig. 6a with those in 6b, it can readily be observed that substantially more heat is extracted from the ground to form the required structural thickness of the frozen wall. At first glance, this may be seen as no consequence and perhaps even advantageous. The wall has been formed in less time and the lower Ts result in a significantly stronger (even though unnecessary) frozen mass. The problem with this is more logistic and economic.

Most engineers and contractors (including the author) have relied on 1 kg to extract 200 k estimate previously noted. As stated, this is based on a delta T of 25°C. Since the delta T is higher than 25°C, more LIN is required than estimated. Because of this, the author can state with confidence more LIN is always used than estimated using this relationship.

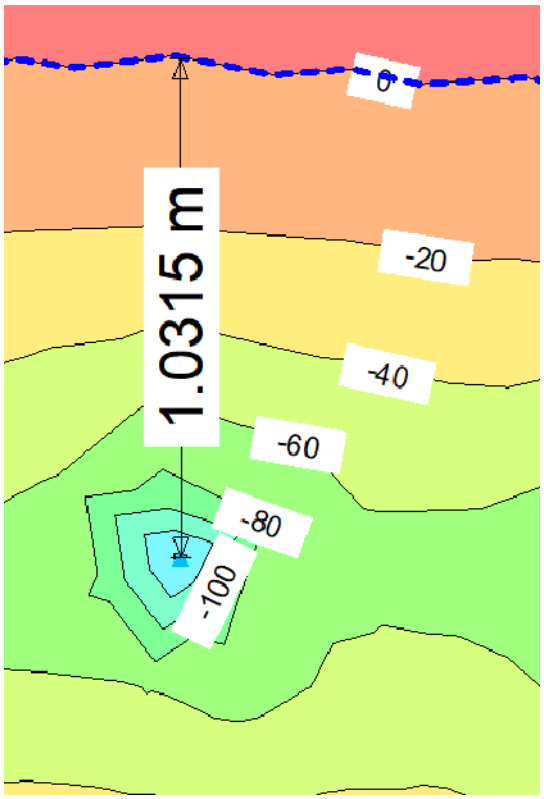


Fig. 6a. T contours (LIN)

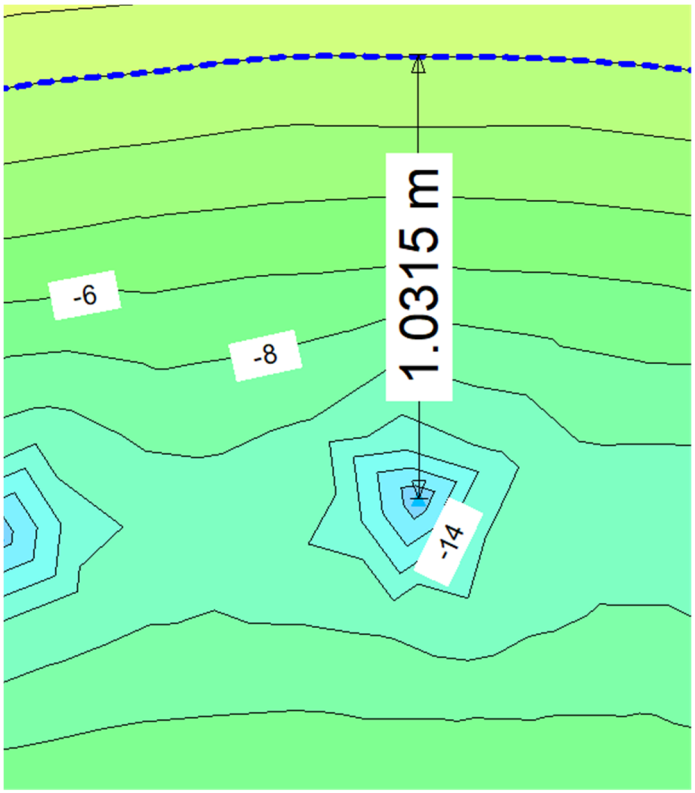


Fig. 6b. T contours (brine)

Experienced contractors have historical and proprietary methods of estimating LIN usage. Even with this knowledge, the fact remains that LIN is extremely inefficient compared with a brine system when evaluating the amount of heat to be extracted.

So why use LIN in place of brine in those cases where cryogenic Ts are not required? In these cases, the contractor does not have the appropriate refrigeration plants available and opts for a simpler and much more expensive approach with the LIN.

The heat load of approximately 300 w per m of freeze shown in Fig. 5a can be used to compute the required refrigeration plant size for a relatively short tunnel adit or cross passage. For example, a current tunnel adit has a length of 30 m. Multiplying 32 pipes by 30 m by 300 w indicates a refrigeration plant capacity of 288 kw is required. This is a refrigeration unit that does not indicate the electric power required. It should be noted this is the peak capacity required to form the frozen earth structure. Once formation has occurred (approximately 17 days), the required refrigeration load is decreased to approximately 100 w per m of refrigeration pipe.

There are two types of refrigeration plants used in civil tunnel projects, as shown in Figs. 7a and 7b. Fig. 7a shows a truck-mounted unit capable of producing 310 kw of refrigeration at -30ºC. It uses ammonia as a primary refrigerant and calcium chloride brine as the secondary circulating refrigerant. The unit shown in Fig. 7b is a smaller, portable unit capable of producing 100 kw of refrigeration at -30oC. Small units like this are used inside tunnels as they also offer the safety advantage of using refrigerant instead of ammonia.



Fig. 7a. 310 kw at -30ºC refrigeration plant



Fig. 7b. 100 kw at -30°C

It should be noted that a kilowatt of refrigeration does not indicate the amount of electric power required for the freezing. Additionally, a refrigeration plant's power rating is evaluated at specific coolant T. The 310 kw (at -30°C) has higher kw capacity at -20°C. Selection of refrigeration units also requires close evaluation of the coolant flow capacity through the system. A flow rate of at least 110 m^3 per day is required for efficient heat transfer.

COMBINING METHODS

Referring to the previous example cited, a recent project required 288 kw of refrigeration capacity during the initial formation freezing. A plant similar to the one shown in Fig. 7a would be used for that project. Referring to Fig. 5a, it can be observed the required load will decrease during maintenance freezing. This type of refrigeration plant is custom-made, often very expensive, and not readily available. As an alternative to using the appropriate equipment, attempts have been made to use LIN for the initially high load freezing and then convert to a circulating system for maintenance with a lower powered plant. This system is justified because it can get the initial freezing done in less time.

When referring to Fig. 4, it is readily apparent that LIN will freeze the ground faster, but in the scheme of the entire project, it will not necessarily save time or compress the schedule. Reasons for this include but are not limited to: two separate coolant distribution manifolds will have to be fabricated and installed; time will be required to change over from the LIN to the circulating coolant system; refrigeration pipes have a high probability of developing leaks during the LIN freezing and will require repair; the Ts resulting from the LIN freezing could result in freezing the brine after conversion; and two separate health, safety, and environmental protocols are required.

Using the two separate systems is certainly possible, but one must question the economic logic of doing this. As demonstrated, the LIN extracts more heat than required. The T will be lowered more than necessary

and then heated when the circulating system is implemented. As previously explained, estimates of LIN are frequently lower than estimated and more product is required; sometimes, more than twice as much. LIN can be very expensive depending on availability and transportation costs.

CONCLUSIONS

The author acknowledges any individual project is suited for either a circulating system or LIN for reasons cited. There may even be applications where a combination of the two methods is appropriate. However, combining methods because a contractor does not have the appropriate equipment will most likely have complications, require more time, and certainly cost more.

JET GROUT UNDERPINNING TO SUPPORT THE WATERMAN HOSPITAL

Stanley L. Worst, Schnabel Foundation Co., Cary, IL, USA, 847-639-8900, stanley@schnabel.com
Piotr Kozlowski, Schnabel Foundation Co., Cary, IL, USA, 847-639-8900, pkozlowski@schnabel.com
Matthew J. Niermann, Schnabel Foundation Co., Sterling, VA, USA, 703-742-0020, matt@schnabel.com

ABSTRACT
The Waterman Hospital in Tavares, Florida was undergoing an expansion and required a below-grade excavation immediately adjacent to the Emergency Department. This wing of the hospital was under high traffic and required uninterrupted access for ambulances as well as helicopter landings. The below-grade expansion was also next to a part of the hospital which did not have a basement. Tiedback soldier beams and wood lagging were used as the earth retention system where the shoring line was not immediately adjacent to the existing structure. Structural jet grout underpinning was used to support the existing building and to serve as the earth retention system in the more sensitive area. Jet grout underpinning was chosen to minimize movements, loss of ground and settlement of the structure which was bearing on clean sand deposits. This paper will discuss the design, quality control and construction of jet grouting and its application to this project.

Keywords: jet grouting, underpinning, earth retention system.

INTRODUCTION

Project Background
The expansion of the Waterman Hospital included an addition to the Emergency Department. This addition was located adjacent to the existing hospital building in a congested area with limited access. The north side of the addition was bordered by the ambulance drop-off area. The south side of the addition was bordered by the helipad landing area. Both areas had to remain open and fully accessible 24 hours a day, 7 days a week.

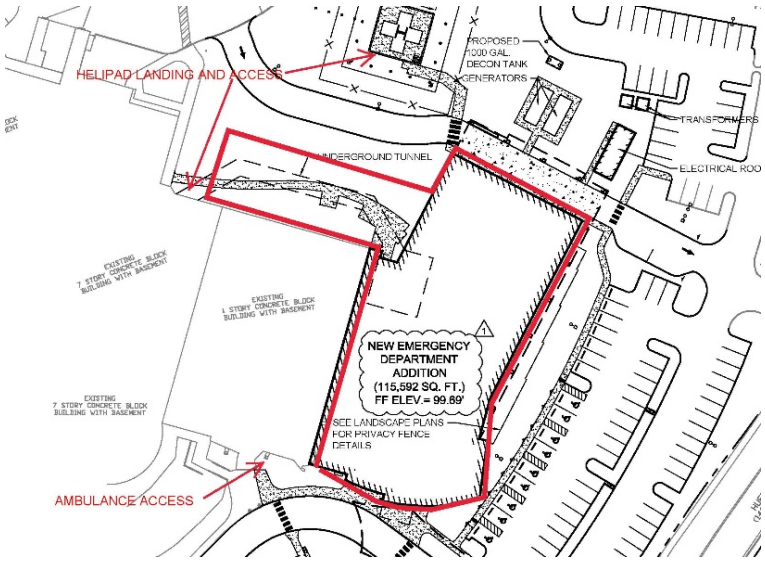


Figure 1 - Site Layout

The new addition to the Emergency Department required an approximately 20-foot excavation immediately next to the existing building. This building was resting on a slab on grade. The Earth Retention System (ERS) was required to support not only the ambulance drive-up and helipad access walkway, but the existing building itself. Figure 1 shows an overview of the project site with the new construction outlined in red. A soldier beam, lagging and tieback ERS was selected to support the ground away from the existing structure. A tiedback structural jet-grout underpinning ERS was chosen to support the existing building and the ground underneath.

© 2019 Deep Foundations Institute

Geotechnical Information

Tavares, Florida is located approximately 40 miles northwest of Orlando and is surrounded by multiple large lakes. The subsurface conditions are typical of central Florida and consist of loose to medium dense sand with occasional layers of silty sand to a depth greater than the proposed excavation. Groundwater was encountered approximately 25 feet below existing grade, which was below the bottom of excavation. Based on the soils report, the ground was very uniform throughout the depth of excavation. This deposit was broken up in a few places with backfill due to previous relatively shallow utility excavations.

The loose fine-grained sands with very little binder were of significant concern when evaluating how to support and underpin the existing structure. Excavation directly adjacent to existing shallow footings which bear on the loose sands run the risk of loss of ground and settlement of the structure. These sands are known for "running" during local excavations since there is little silt or clay content or cementation to hold the sand grains together.

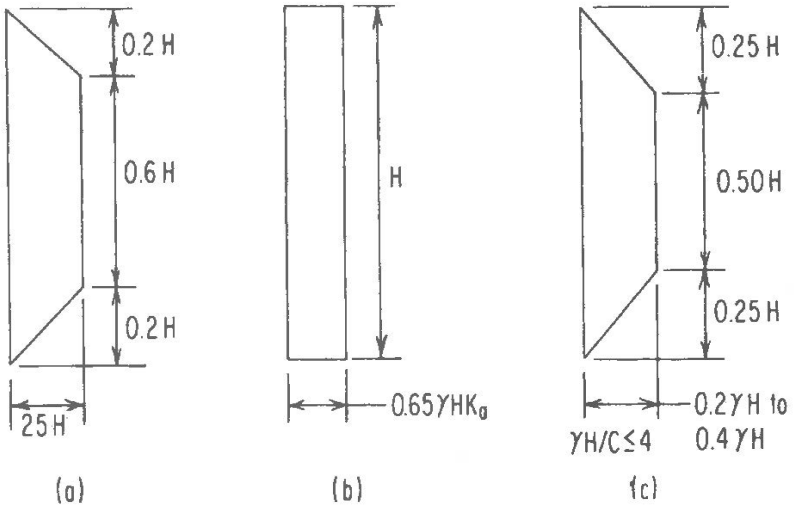
However, these types of sands are ideal for jet grouting. The low silt content and uniform grain size enable erosion, mixing, and jet penetration to occur during the jetting process. Sandy soils also yield a high rate of strength gain and high overall strength since the granular material acts as aggregate being mixed with cement.

CASE HISTORY

Design Basis

The purpose of installing jet grout columns underneath the existing footings was to achieve the following: 1 – serve as an earth retention system for the excavation; 2 – prevent ground loss and resulting settlement during the excavation process; 3 – structurally support the existing building by permanently transferring the load directly below subgrade.

Since no water was being retained, the earth retention part of the jet grout design could be analyzed with a simple Apparent Earth Pressure (AEP) diagram. Schnabel Foundation Company used an AEP diagram for this project that was developed from 60 years of experience. Figure 2 shows this pressure diagram and compares it to the original AEPdiagrams developed by Terzaghi & Peck. The main difference is the magnitude of overall load as well as the concentration of load around the tieback or strut. Experience of using the Schnabel AEP on thousands of projects has proven the Terzaghi & Peck diagrams to be slightly conservative in certain situations. The concept that the load is transferred to the stiffer parts of the structure has also been



Source: Schnabel, et al. 2002

Figure 2 - Apparent Earth Pressure Diagrams.
a) Schnabel; b) Terzaghi & Peck sand; c) Terzaghi & Peck clay

documented through monitoring of earth retention systems. Arching of the soils behind the wall allows for this to happen in relatively flexible systems. Also, as is typical with other AEP diagrams, a hinge was assumed at subgrade, resulting in zero moment below the bottom of the excavation.

The additional load of the existing structure was considered in the design of the jet grout wall. The surcharge of this structure was transferred directly to the jet grout columns. The columns were installed so that they extended underneath the footings and had intimate contact with the bottom of the footings. This transferred load directly into the jet grout columns, allowing for footing loads to be transferred below subgrade.

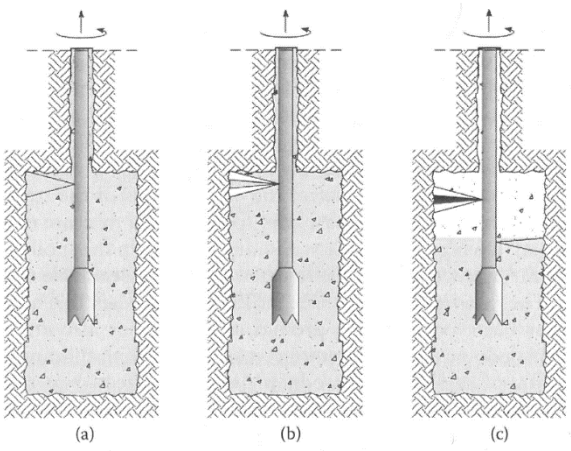
The application of load directly onto the jet grout columns required a combined bending and axial design analysis. Based on the magnitude of the earth pressure loading which exerted the bending stress, and the axial loading from the existing building, it was determined that the jet grout columns could be installed unreinforced. The internal stresses of the jet grout columns were analyzed per ACI-318 for unreinforced concrete given these conditions. The result of this analysis determined that the resulting jet grout columns required an unconfined compressive strength of at least 1,000 psi.

Jet grouting underneath an existing footing is a method of underpinning. As such, it requires careful sequencing since there is a temporary condition during which the jet grouting is still fluid and there is little to no support directly underneath part of the footing. Before the jet grout material sets up and hardens, there is a temporary reduction in the factor of safety on the bearing capacity. This reduction is managed by only undermining a small portion of the footing at a time. Jet grout underpinning was performed on this project under both continuous strip footings as well as isolated spread footings.

Jet Grouting Concept

The overlying concept of jet grouting is to inject fluid grout into the ground at high velocity so that it erodes and mixes with the in-situ soil, producing a column of jet grouted material which is stronger and less permeable than the original soil. As grout is injected, a mixture of excess soil, water, and cement (spoil) travels to the surface through the annulus around the drill rods created by the drill bit. The in-situ soil-cement strength, hydraulic conductivity, and column diameter resulting from jet grouting are functions of the rate and concentration of cement injected, in addition to the time spent jetting a certain area.

The concentration of cement is controlled by the mix design, which for neat cement grout is the water/cement ratio. This ratio is the amount of water divided by the amount of cement per unit volume, as measured by weight. A 1:1 w/c ratio has equal weights water and cement. Typical jet grout w/c ratios are in the range of 0.8 to 1.8.



Source: Croce et al. 2014

Figure 3- a) Single Fluid; b) Double Fluid; c) Triple Fluid

The amount of cement injected into the ground is controlled by two other factors; the flow rate and the lift rate. The flow rate is usually measured in gallons per minute and is a function of the pump capacity. The lift rate is usually measured in inches per minute and can be controlled at the drill rig. A zone of soil is treated for a longer time with a slower lift rate. This allows more cement to be injected as well as a potentially further radius of grout penetration into the soil.

The rotation rate during jetting is another variable which can be adjusted. To create cylindrical soil-cement columns, the rotation rate is generally calibrated to the lift rate to ensure the full circumference is treated. This can be achieved with a single nozzle and full rotation before lifting, or with two nozzles located 180 degrees apart and a half rotation before lifting.

Adjusting the w/c ratio, lift rate and flow rate will determine the amount of cement which is injected into the ground. Adjusting the lift rate, flow rate and jetting pressure will help determine the diameter of the soil-cement column. The selection of these parameters is based on the existing soil conditions and the experience of the specialty contractor. The fines content, the relative density of the soil and particle size are all factors which have an impact on the column diameter which can be achieved.

Single, double or triple fluid jetting can be performed (see Figure 3). Single fluid jetting injects a single fluid, cement grout, into the ground. Double fluid jetting adds a shroud of compressed air around the grout injection point. Triple fluid jetting utilizes double fluid injection of high-pressure water and compressed air, followed by injection of cement grout at lower pressure. Single fluid jetting was performed on this project. This method was selected because it provides the most control over column diameter and spoil return compared to methods utilizing compressed air.



Figure 4 - Exhumation of Three Test Columns

Quality Control and Construction

On almost every project a test program is performed prior to production work to verify the many different parameters to be used as well as to confirm the resulting soil-cement column diameter and strength. To confirm the column diameter, it is best to excavate around a test column and visually examine and measure the geometry first-hand. However, this is usually difficult if not impossible to do when dealing with limited space on a construction site and deep columns. One alternate method of checking the column diameter is to drill and retrieve samples from the centroid of a three-column layout. In this scenario, three individual test columns are installed in a triangular layout in which all three columns overlap slightly in the middle.

A borehole can be drilled in the centroid of this three-column layout, retrieving continuous split spoon samples. The blow counts from driving the split spoon can be compared with soil borings taken prior to jetting to confirm that the ground has been strengthened. Also, the retrieved samples, although disturbed, can be sprayed with a phenylthalene indicator, which turns a bright color in the presence of cement. This provides two ways of confirming that the column diameter has been achieved. Coring is also sometimes used to retrieve samples for lab testing. However, coring of relatively low strength material has proven to be unsuccessful in retrieving intact samples, especially in granular material containing gravel or cobbles. The rotary-wash action of the coring tends to erode low strength soil-cement; and, if any larger pieces of sand or gravel are present, they can get caught on the core barrel teeth, causing the sample to crumble. For shallow columns where exhumation is possible, visual examination is the best means of confirmation. Figure 4 shows exhumation of the three test columns on this project. Due to the consistent ground conditions with depth, it was determined that shallow exhumation and observation was adequate for this test program. Coring could have been performed but would have required a wait time of at least a week if not more in order to obtain intact samples.

Wet-grab samples are commonly used as a means of testing the soil-cement material for strength and hydraulic conductivity. These samples can be taken at depth in recently installed columns that are still fluid, or from spoils at the ground surface. To retrieve wet grab samples at specific depths, a device is needed to be lowered into the jet grout column. This can prove difficult if the jet grout column does not extend all the way up to the ground surface. For example, jet grouting may only be required for a 10' thick bottom plug which is 50' below the ground surface. The drill hole is typically around six inches in diameter, which makes it very difficult to insert a sampling device from the ground surface. Also, if a working slab

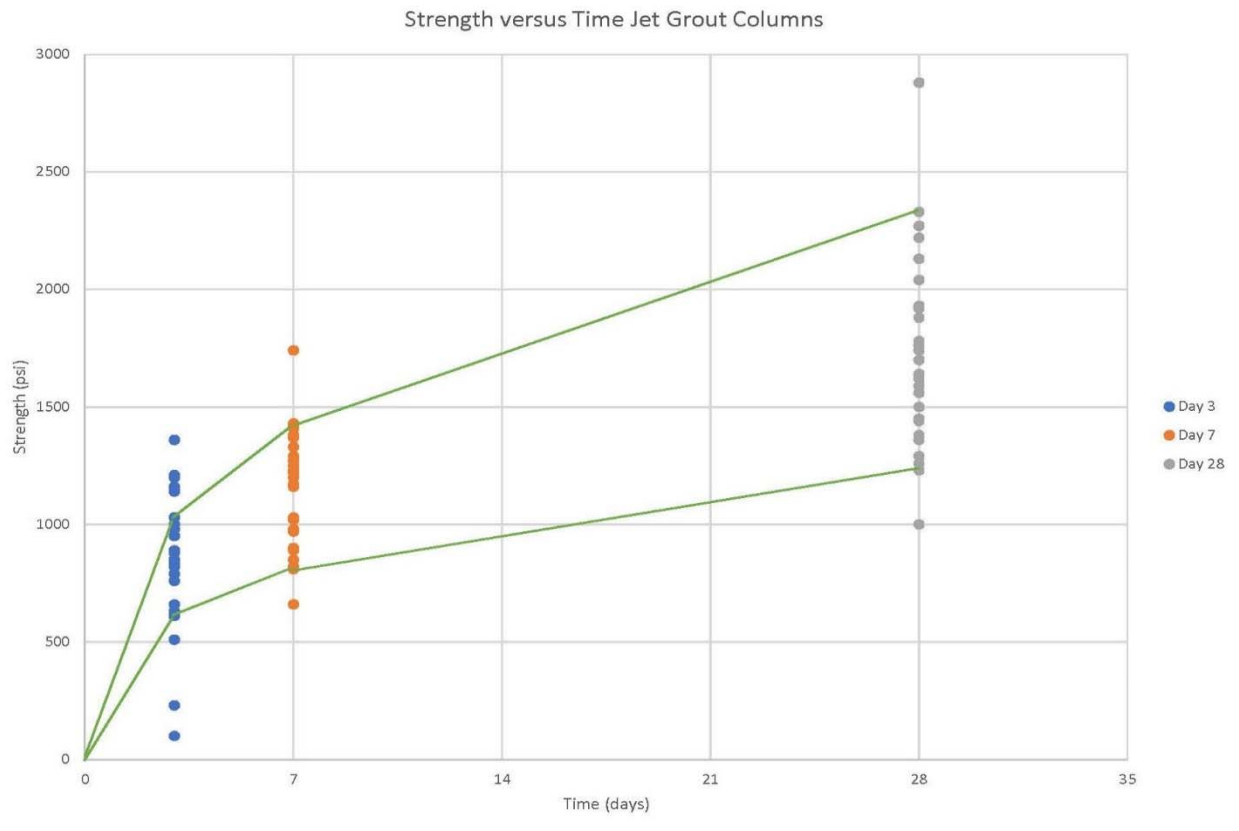


Figure 5. Soil-Cement strength vs. time - Waterman Hospital project

(concrete) is present, it may be impractical to insert a larger sampling device through the drill hole made in the working slab. In these instances, wet grab samples retrieved from the ground surface have proven to be sufficient for predicting strength and hydraulic conductivity. Cylinders are made from the spoils collected at the ground surface while jetting at specific depths. Since the in-situ soil is being turbulently mixed with the cement grout being injected, it is assumed that the return spoils are of similar consistency to the jet grouted material left in the ground. In general, comparisons have shown that wet grab samples achieve lower unconfined compressive strengths than cores taken post-production of in-situ columns. This is most likely a result of the enhanced in-situ curing environment as well as fluid head pressures that may facilitate pressure filtration and subsequent lowering of the in-situ water/cement ratio of the soil-cement.

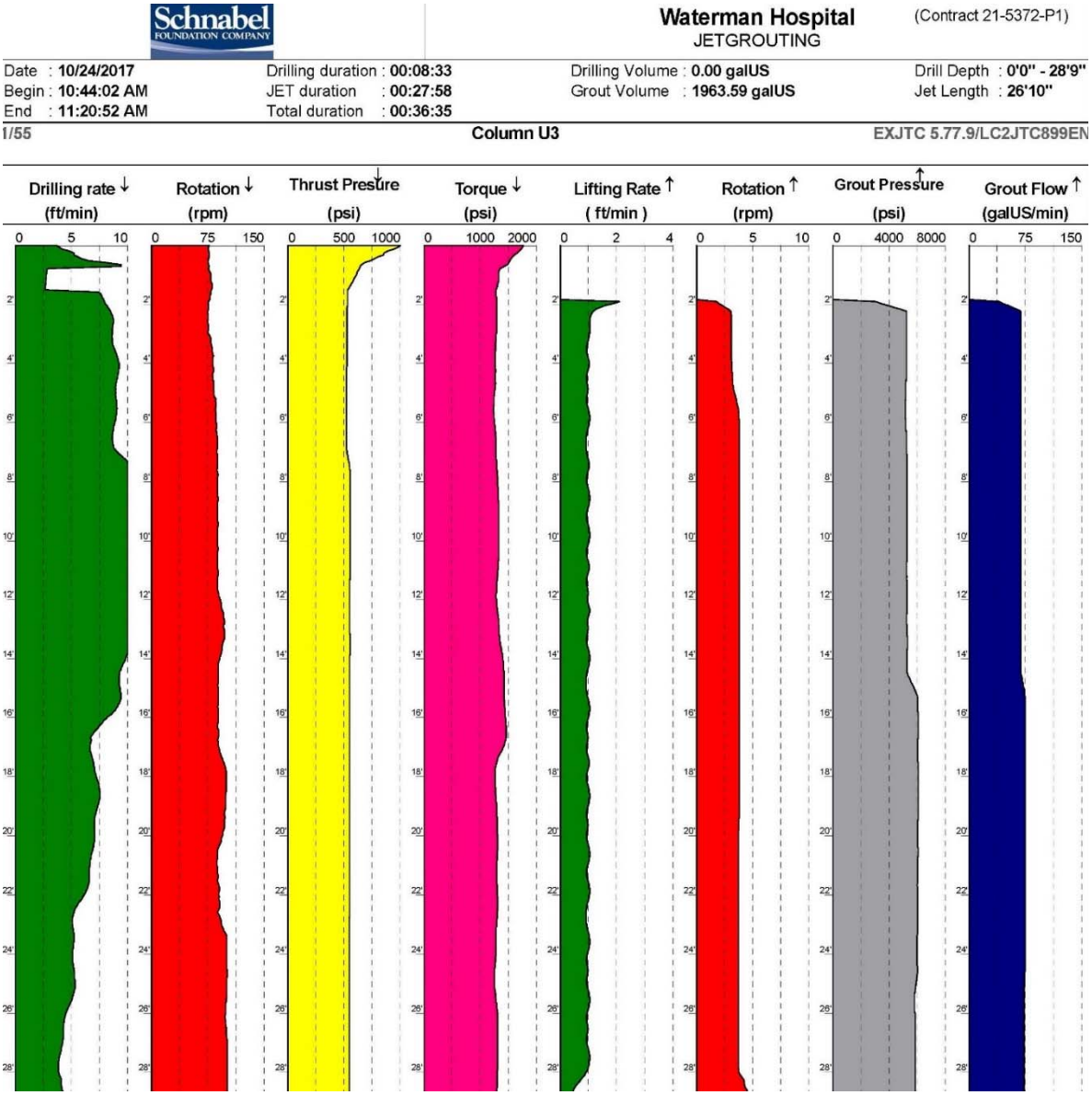


Figure 6. Jean Lutz record of measured jet grout parameters

The design of jet grout column strength is based on the 28-day strength of the soil-cement, similar to concrete design. Due to the heterogeneity of the ground, it is typical to get a wide range of strengths. As can be seen in Figure 5, the 28-day strengths ranged from 1,000psi to 2,800psi, with the majority falling between 1,200psi and 2,300psi. This wide of a range should be expected, especially as the target design strength is lower.

There are numerous input parameters that are measured for jet grouting. The following parameters are recorded with sensors and measuring devices that are mounted on the drill rig and automatically recorded for each column: lift rate, rotation speed, grout pressure, grout flow, air pressure, and air flow. These can be seen in graphical format in Figure 6. This gives an easy visual representation of the quality control for each jet grout column. Although the measurement of these parameters does not guarantee that the resulting column will be of sufficient diameter and strength, it verifies that the same parameters are being used which were shown to be effective in the pre-production test program.

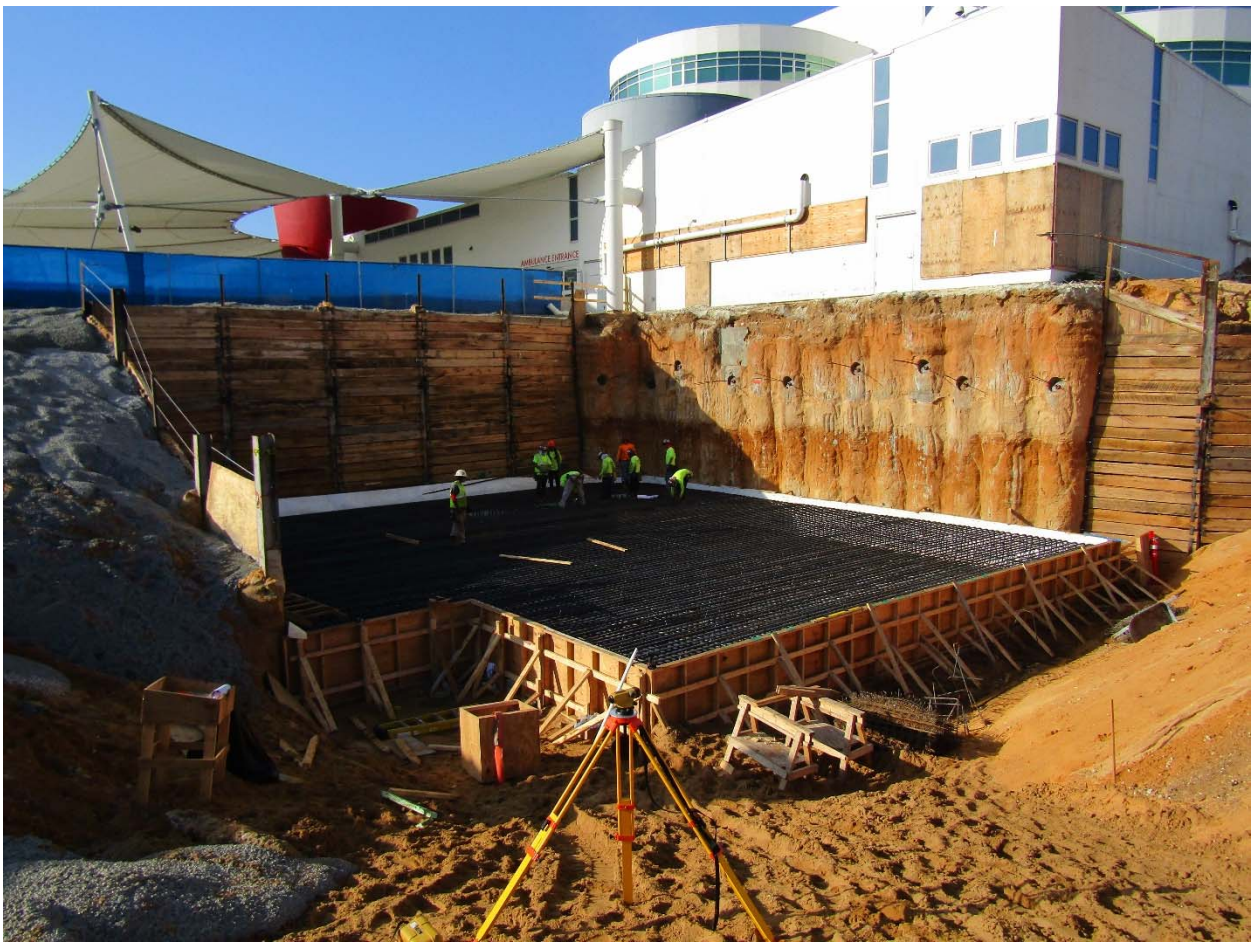


Figure 7. Exposed face of Jet Grout Underpinning Columns

For this project, the sequencing of jet grout underpinning columns proved adequate in both mitigating settlement as well as forming a continuous structural wall directly underneath the existing footing. To start, approximately every fourth column (1, 5, 9, 13…) was installed along the length of the wall to be underpinned. Next, the columns mid-span (3, 7, 11…) between the previously installed columns were

jetted. Finally, the remaining columns (2, 4, 6, 8…) were installed which had a previously installed jet grout column on either side, filling the gap and forming a continuous wall.

CONCLUSION

Jet grouting can be used as a form of structural underpinning as well as an earth retention system for building excavations. It is effective at controlling soil and building movement during excavation as well as building movement during installation. Structural jet grout underpinning can be analyzed using an unreinforced concrete design or a combined concrete-steel design. Both scenarios account for combined bending and axial loading due to the direct supporting of the existing structure.

Jet grouting cannot be immediately inspected first-hand. It requires indirect methods of sampling, testing and other quality control measurements to gain a level of confidence that the jet grout columns meet the design requirements. The jet grouting may or may not be exposed in the final condition for visual inspection. Variations in what is required for quality control can be adjusted based on the type of inspections and the direct or indirect testing that can be performed.

Due to the relatively low strengths that jet grouting can produce, as well as the depths at which jet grouting is performed, some forms of quality control and testing are not always appropriate. These include coring, in-situ water-pressure testing and at-depth wet grab sampling. These may be used on a job-by-job basis depending on the ground conditions, strength requirements and depths grouted. Although jet grouting is not always able to be directly inspected, there are ways of providing quality control which show conformance with the design intent.

Jet grouting was used successfully on the Waterman Hospital project as a means of supporting the existing building and retaining the soil adjacent to the excavation. There were no excess noise or vibration disturbances due to the jet grouting, which allowed for the hospital to remain in operation during construction. Wet-grab samples collected from the ground surface proved to be a conservative prediction of the strength of the in-situ jet grout columns.

Vertical movement of the existing structure was monitored before and during excavation where the jet grout columns were installed. The maximum recorded settlement was $1/16^{th}$ of an inch, which did not result in any cracking or distress of the structure.

REFERENCES

Croce, P., Flora, A., and Modoni, G. 2014. *Jet Grouting*. Boca Raton, FL: CRC Press.

Gresham Smith and Partners. 2017. *E.D. Addition and Renovation Drawings*. Tampa, Florida.

Schnabel, Harry; Schnabel, Harry, Jr. 2002. *Tiebacks in Foundation Engineering and Construction*. The Netherlands.

O'Brien, Brendan. 2017. *Florida Hospital Waterman ED Expansion - Geotechnical Engineering Report*. Winter Park, Florida. Prepared by Terracon Consultants, Inc.

SITE DEVELOPMENT AND FOUNDATION PLANNING FOR A WASTEWATER TREATMENT PLANT EXPANSION

Ali Ghandeharioon, Ph.D., P.Eng., Senior Geotechnical Engineer, Klohn Crippen Berger Ltd., Vancouver, BC, Canada, +1 604 669 3800, aghandeharioon@klohn.com
Steven R. Ahlfield, M.Sc., P.Eng., Principal Geotechnical Engineer Klohn Crippen Berger Ltd, Vancouver, BC, Canada, sahlfield@klohn.com

ABSTRACT

A wastewater treatment plant commissioned in 1978 is undergoing a major expansion. Planning various phases of the 8-hectare expansion at this site requires an understanding of the site response during and after construction, and the potential impact on adjacent properties and infrastructure. The expansion project requires nominally 5 m of site grading fill for flood protection. The site is underlain by loose to compact fine sand over firm to very stiff clay stratum that extends to great depths. Ground improvement is required to mitigate the liquefaction hazard in the fine sand stratum, and preloading is proposed to reduce post-construction settlements in the deep clay. Site development and foundation systems for the plant expansion project were evaluated by conducting settlement analyses which accounted for the historic and future site loading and 3-D modeling of soil layers with interpolation between borehole and cone penetration test (CPT) locations. The numerical model was calibrated to match short-term and long-term settlements measured at the plant site. The analyses were carried out to assess the effects of past loading, proposed preload and surcharge heights, lateral extents and durations as well as vibro-replacement ground improvement on post-construction settlements. Two design options were considered for the preload footprint across the site and foundation system for proposed facilities. It is shown that limiting the preload extent and founding some of the proposed structures on deep friction piles reduce the predicted settlements of adjacent infrastructure and result in reasonable performance for the proposed facilities.

Keywords: Infrastructure, Site Development, Ground Improvement, Pile Foundation, Settlement Analysis

INTRODUCTION

A wastewater treatment plant commissioned in 1978 will be replaced with a new plant on an undeveloped portion of the site to provide wastewater treatment for an expanded service area. The existing facilities must remain in operation until completion of the new plant. The site grade will be raised nominally 5 m for flood protection. The large areal extent of the site grading fill and plant structures will cause stress changes extending to great depths in the underlying soils and result in settlement of the existing and new structures. Historic settlement of the existing facilities has been tolerable for plant operations, but no settlement performance data was recorded during site development and post-construction from 1978 to 2007.

Development of the 8-hectare expansion at this site is planned in three phases to reduce the overall construction schedule. Planning for each phase requires evaluating the effects of various site development activities from start to completion of expansion and during the design life (i.e. post-construction period), and the potential impact on existing wastewater treatment facilities and adjacent properties and infrastructure including an adjacent viaduct structure. Figure 1 presents the site plan and three distinct site development phases considered for the plant expansion.

The original site grade is at nominally El. 2 m and the site is located immediately adjacent to a major river. The plant site is underlain by variable thickness of fill materials over a relatively thin soft to firm silty clay stratum underlain by loose to compact fine sand. The sand is underlain by a compressible clay stratum that extends to great depths. A liquefaction assessment indicated that the sand stratum was liquefiable under the

© 2019 Deep Foundations Institute



Fig. 1. Site plan and three phases of site preparation for the wastewater treatment plant

2,475-year return period design earthquake, and ground improvement (GI) was necessary to mitigate the liquefaction hazard and reduce seismic displacements. The required site grade is El. 7.6 m for flood protection. Preloading is commonly carried out in the site geographic area to reduce post-construction settlement in the deep, compressible clay layer. Surcharging is often used to accelerate construction settlement depending on the preload duration available in the construction schedule.

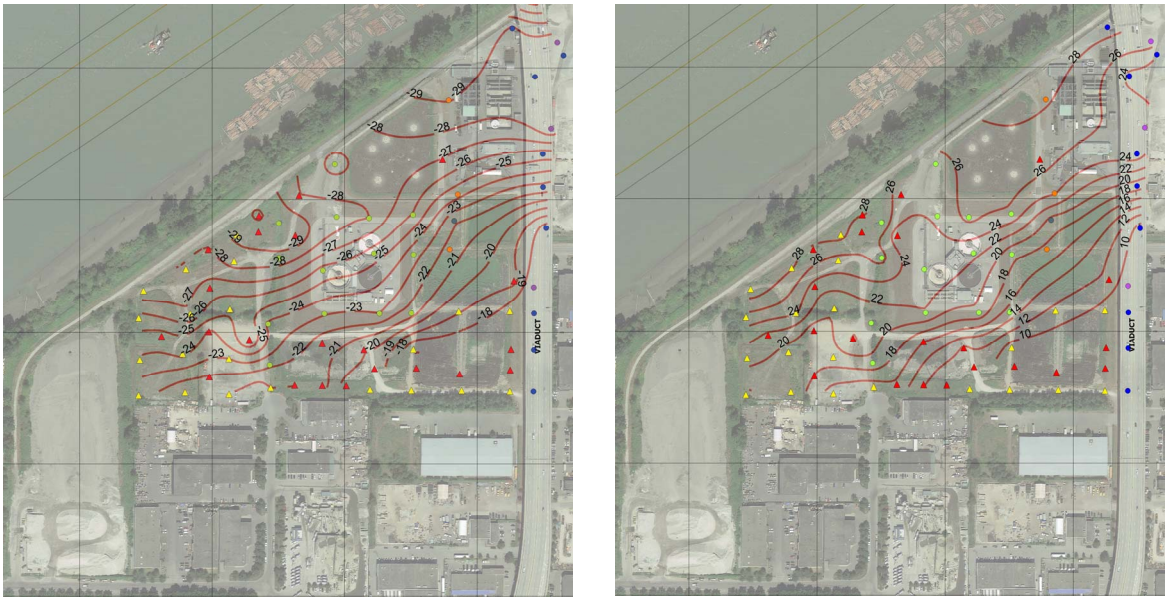
Site development and foundation systems for the plant expansion were assessed by conducting settlement analyses to evaluate the effects of historic loading, proposed preload and surcharge heights, lateral extents and durations on the new and existing facilities and adjacent structures. Two design options were considered for the preload extent and foundation system for the proposed facilities, and total and differential settlements of the adjacent infrastructure were assessed due to the expansion project.

SITE CHARACTERISTICS

The native surficial soil at the wastewater treatment plant site consists of a compressible, soft to firm, upper silt/clay stratum underlain by a sandy silt to silty sand layer. The silty sand grades to loose to compact fine sand followed by a thin layer of gravelly soil in some locations. A firm to very stiff lower clay stratum underlies the granular soils and extends to great depths. The groundwater level is generally located 1.3 m below the surface, i.e. at El. 0.7 m, but varies with river flood levels and seasonally. The upper soft to firm silt/clay stratum is interpreted to be an overbank floodplain deposit with a thickness of 2 m to 7 m over most of the site. At the southeast corner of the Phase 2 expansion area, i.e. the Lagoon D area, the thickness of the upper silt/clay increases rapidly to about 14 m to 16 m, and the sand stratum becomes thin. No data is currently available for the Phase 3 expansion area.

The sandy silt to silty sand, underlying fine sand and the discontinuous gravelly layer at the base of the fine sand are loose to compact fluvial soils. The geotechnical data indicates that the sand is a local-channel deposit that thins with distance inland from the current river banks. Figures 2(a) and 2(b) show contours of

the interpreted bottom elevation and thickness of the granular soil based on available drill hole logs and CPT data. The granular soils in the Phase 1 expansion area have a thickness of 20 m to 28 m. In the Phase 2 expansion area, the thickness of the granular deposits decreases rapidly to the southeast. In the Lagoon D area, the thickness of the granular soil decreases from about 12 m at the northwest corner to about 2 m at the southeast corner. Table 1 presents typical thickness of the soil layers across the plant site.



(a) **(b)**

Fig. 2. Contours of the interpreted (a) bottom elevation, and (b) thickness of the granular soils

Table 1. Typical thickness of soil layers across the site

Soil Layer	Typical Thickness of Layer at the Site excluding the Southeast Corner (m)	Thickness of Layer at the Southeast Corner of Site, i.e. Lagoon D (m)
Upper Silt/Clay	2 to 7	14 to 16
Sandy Silt to Silty Sand	2 to 7	1 to 5
Sand	13 to 26	2 to 4
Gravel	0 to 2	Not Present
Lower Clay		
Upper Layer	31 to 39	38 to 40
Mid Layer	20	20
Deep Layer	120	120

ANALYSES METHODOLOGY

A site response and liquefaction assessment indicated that the granular soils at the site were liquefiable under the design earthquake with a return period of 2,475 years. Seismic deformation analyses performed using FLAC (Itasca, 2011) and an effective stress-based soil model for a recent expansion project showed that stone columns installed to the bottom of granular soil were beneficial to mitigate the liquefaction hazard and reduce the seismic displacements of the facilities. Vibro-replacement ground improvement was modeled for all the expansion areas excluding the Lagoon D area as the thick upper silt layer renders ground improvement ineffective in that region of the Phase 2 area.

Planning for site development and foundation systems for the plant expansion was carried out by conducting settlement analyses using Settle3D software (Rocscience Inc., 2019) to assess the effect of area-wide site grading fill, structure and lagoon loads for the existing wastewater treatment plant and the proposed facilities. The 3-D vertical stress distribution in the soil stratum was calculated using the Boussinesq method. The Triangulated Irregular Network (TIN) technique, based on Delaunay triangulation method, was used in the Settle3D software to interpolate soil layers between drill hole and CPT locations. For areas outside the limits of the drill hole and CPT pattern, the software extrapolates the soil stratigraphy using the slope of the top and bottom of each stratigraphic layer at the boundary of the drill hole and CPT data. This technique was used at the boundaries of the wastewater treatment plant property and in the Phase 3 expansion area, where no drill hole or CPT data is currently available.

The drainage boundaries affect the rate of consolidation settlement with time, and were defined in this analysis at the bottom of the granular soil layer varying from El. -18 m to El. -30 m, at the bottom of a sand seam assumed to be continuous in the lower clay layer at El. -80 m, and at the bottom of the lower clay layer assumed to be at El. -200 m. No drainage path was defined at the bottom of upper silt/clay stratum as the underlying sand stratum provides relatively fast drainage.

Model Calibration for the Ground Improvement Zone and Upper Layer of Lower Clay Stratum

Vibro-replacement ground improvement changes the compressibility characteristics of the upper silt/clay and sand strata as the stone columns carry a significant portion of the load and provide drainage of pore pressures in the upper clay stratum. The densified sand in the ground improvement zone is also less compressible than the native sand. In this project, the ground improvement in Phase 1 and 3 areas was modeled as a single composite material replacing the thin upper silt/clay and deep sand strata once soil treatment was complete. However, the ground improvement in the Phase 2 area was modeled as two composite materials, one composite material replacing the upper silt/clay stratum with consolidation characteristics estimated based on the stone column area replacement ratio (Barksdale and Backus, 1983), and the other composite material replacing the lower densified silty sand and sand layers with only immediate (elastic) settlement characteristics. The thickness of the ground improvement zone was varied across the site to provide continuity of the drainage boundary at the bottom of the granular soil, as the bottom elevation of the granular soil changes across the site.

The properties of the composite material representing the ground improvement zone and properties of the upper portion of the lower clay stratum (from the base of the sand to El. -60 m) from laboratory testing were adjusted to approximately match measured settlements during preloading of an adjacent site during a 1.5-month period of preload/surcharge placement and a 4.5-month preload/surcharge monitoring period.

Model Calibration for the Middle and Deep Layers of Lower Clay Stratum

Historic settlement data was not available for the existing plant site during the initial 12-month preload period in 1975 and post-construction period of 1978 to 2007. However, settlement data was available for the period of 2007 to 2017. The numerical model was calibrated to the measured time-settlement data at the existing plant with a typical variation of approximately 10 mm to 20 mm during the 10-year monitoring period. The middle and deep portions of the lower clay stratum (i.e. El. -60 m to El. -80 m, and El. -80 m to El. -200 m, respectively) contribute to long-term settlements. The drainage assumptions used in the analysis (drainage at top and bottom of the deep layer of lower clay stratum) require many decades to achieve full primary consolidation in these strata. The coefficients of consolidation of the clay strata were varied to provide an approximate match to the measured long-term settlement at the original wastewater treatment plant. Table 2 presents properties of the native soil (i.e. outside ground improvement zones) and composite materials used to represent the ground improvement zones calibrated to approximately match the measured settlements at the wastewater treatment plant site.

Table 2. Calibrated soil parameters used in the settlement analysis

Material		Drained at Bottom	γ (kN/m^3)	E_s , E_{sur} (MPa)	C_c	C_r	e_0	OCR	C_v (m^2/yr)	C_{vr} (m^2/yr)	C_a (m^2/yr)	C_{ar} (m^2/yr)
Upper Silt/Clay		No	18.3	-	0.3	0.05	1.0	1.5	23	26	0.01	0.004
Sandy Silt to Silty Sand		Yes	19.1	-	0.1	0.03	0.87	1.5	270	270	-	-
Sand		Yes	19.8	15	-	-	-	-	-	-	-	-
Gravel		Yes	22	100	-	-	-	-	-	-	-	-
Composite Material for GI Zone in Phase 1&3 Areas	GI in Upper Silt/Clay	No	20.5	50	-	-	-	-	-	-	-	-
	GI in Sand	Yes	20.5	50	-	-	-	-	-	-	-	-
Composite Material for GI Zone in Phase 2 Area	GI in Upper Silt/Clay	No	20.5	-	0.21	0.035	1.0	1.0	2000	2000	-	-
	GI in Sand	Yes	20.5	50	-	-	-	-	-	-	-	-
Lower Clay												
Upper Layer		No	19.2	-	0.57	0.087	1.0	1.3	6	50	0.01	0.002
Mid Layer		Yes	19.9	-	0.57	0.087	1.0	1.2	6	50	0.01	0.002
Deep Layer		Yes	19.9	-	0.57	0.087	1.0	1.0	0.8	50	0.01	0.002

where:
γ = Bulk unit weight
E_s = Constrained modulus for initial loading
E_{sur} = Constrained modulus for reloading
C_c = Compression index
C_r = Re-compression index
e_0 = Initial void ratio
OCR = Overconsolidation ratio
C_v = Coefficient of consolidation
C_{vr} = Re-compression coefficient of consolidation
C_a = Secondary compression index
C_{ar} = Secondary re-compression index

Site Development and Loading Sequence

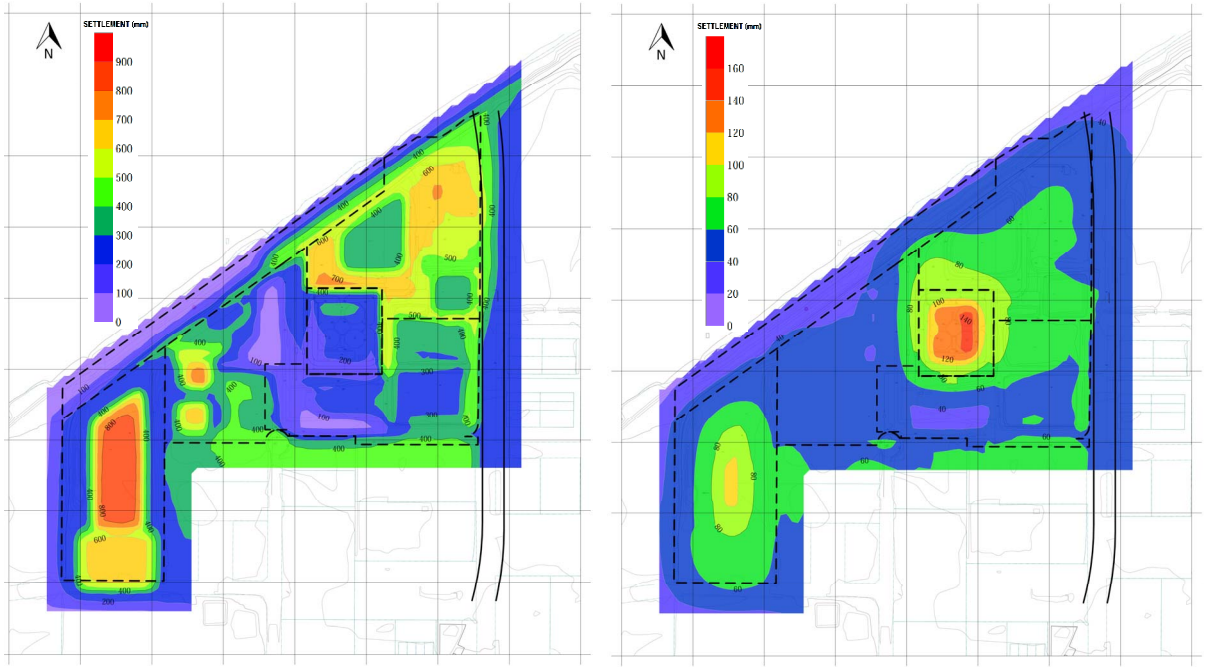
The site development sequence and loading during the original plant construction, operations and a recent expansion were modeled in the analysis. The Phase 3 expansion area has been used for stockpiling sand from local dredging operations and other aggregates for almost 20 years; therefore, preloading of this area will not be required for the expansion project. However, the stockpile loads were included in the model as they affect post-construction differential settlements between areas. The expansion project is simulated in the Settle3D model by including various site development activities at estimated dates from start of the expansion project in 2018 to completion of the expansion in 2026. Ground improvement and preloading of the various phases of the expansion will be conducted as an early works program while design of the wastewater treatment facilities is in progress. The Phase 1 and 2 ground improvement and preload was assumed to be completed in 2019 and 2020, respectively. Because the preload would remain until the start of construction in 2023, Phase 1 and 2 would have a 4-year and 3-year preload period, respectively. Post construction settlements of the facilities were predicted from the 2026 project completion to 2101 (i.e. 75-year design life).

ANALYSIS RESULTS AND DISCUSSIONS

Numerical analyses were conducted to estimate settlements across the plant site and adjacent properties. The analyses were performed for the base case, where no new construction or site development for the expansion project was modeled, and two design options considering different preload footprints across the site and foundation systems for the proposed facilities. Design Option 1 was carried out at the conceptual design stage and Design Option 2 was performed approximately 1 year later at the preliminary design stage.

Base Case Analysis

The analysis for the base case was performed to assess settlements from original plant construction in 1975 to start of expansion project in 2018, and subsequently until 2101 design life for the scheduled expansion assuming no new construction or site development. Figures 3(a) and 3(b) present settlement contours for the site from 1975 to 2018 and from 2018 to 2101, respectively. The results of the base case settlement analysis are summarized in Table 3. In the base case analysis, the minimum and maximum surface settlements for adjacent properties occur at the west side of the Phase 3 area and at the viaduct structure east of the original wastewater treatment plant, respectively.



(a) **(b)**

Fig. 3. Contours of surface settlements predicted from (a) 1975 to 2018, and (b) 2018 to 2101 for the base case analysis (i.e. no new construction or site development for the expansion project)

Table 3. Surface settlements predicted for the base case analysis

Location	General Range of Surface Settlements (mm)	
	1975 to 2018	2018 to 2101
Original Wastewater Treatment Plant	500 to 700	50 to 70
Lagoons A, C, and D	350 to 550	60 to 85
Secondary Clarifiers	150 to 350	85 to 140
Viaduct (east of treatment plant)	250 to 550	45 to 60
Private Properties – near south property line of the site	300 to 400	50 to 65
Phase 3 area – sand stockpile area in northern portion	200 to 850	45 to 105
Phase 3 area – aggregate stockpile area in southern portion	250 to 600	45 to 85

Design Option 1

Design Option 1 was based on Phase 1 and 2 ground improvement with preload to El. 8.3 m and El. 10.6 m, respectively. The Phase 3 area was modeled with ground improvement and site grading fill placed to El. 7.7 m. The analysis only considered site grading fill loads as structure loads had not been

determined at that time. Design Option 1 assumed that the toe of preload and site grading fills extended to the property boundaries, except in the Phase 2 area which had a clearance of 15 m to the eastern property line, and that the proposed facility in the Lagoon D area is founded on a raft foundation at the original site grade at El. 2 m.

Contours of predicted surface settlements in Design Option 1 for the expansion project are presented in Fig. 4(a) for the plant site from 2026 to 2101 (i.e. post-construction period) and in Fig. 4(b) for the viaduct area east of the plant site from 2018 to 2101. Figure 4(a) indicates that predicted post-construction settlements of the expansion project are moderate for the embedded wastewater treatment tanks and reasonably uniform. Hydraulic grade lines between structures are expected to be maintained by incorporating provisions for adjusting flow control weirs for plant operations. This is supported by the operation of the existing facilities over the last 40 years.

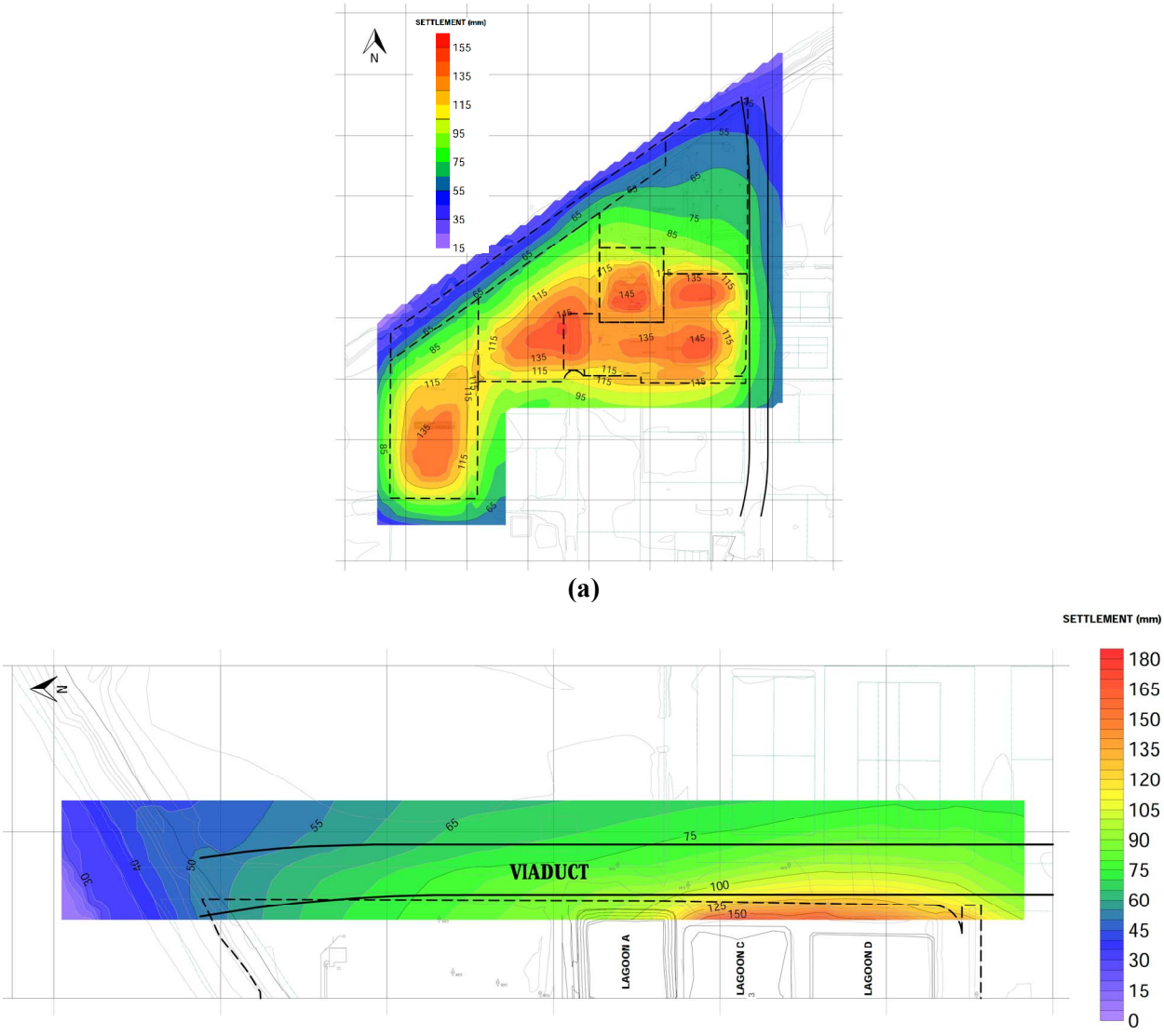


Fig. 4. Contours of surface settlements predicted in Design Option 1 for the (a) plant site from 2026 to 2101 (i.e. post-construction period), and (b) viaduct area from 2018 to 2101

The effects of the site development on adjacent properties and infrastructure, such as the elevated structure located at the east side of the site, were evaluated in this project. The viaduct piers are reportedly founded on 2.5 m diameter piles drilled nominally 40 m below grade through the liquefiable sand layer and into the top of the lower clay stratum. The loads from the Phase 2 area site grading fill adjacent to the viaduct spread laterally with depth, and the associated changes in vertical stress below the viaduct will cause settlement in the lower clay layer. The neutral plane of viaduct piles in the sand stratum will therefore undergo a settlement approximately equal to the predicted settlement at the ground surface.

Figure 4(b) shows that Design Option 1 for the expansion project would cause 75 mm to 125 mm of incremental settlement of the ground surface at the viaduct piers adjacent to Lagoons C and D. Incremental differential settlements between adjacent piers in the longitudinal and transverse direction are predicted to be up to 25 mm and 35 mm, respectively. Reduction of the incremental settlements of the viaduct piers due to the expansion project was desirable. Therefore, site development and foundation system alternatives for expansion structures adjacent to the viaduct were evaluated to reduce the predicted incremental settlements of the viaduct piers.

Design Option 2

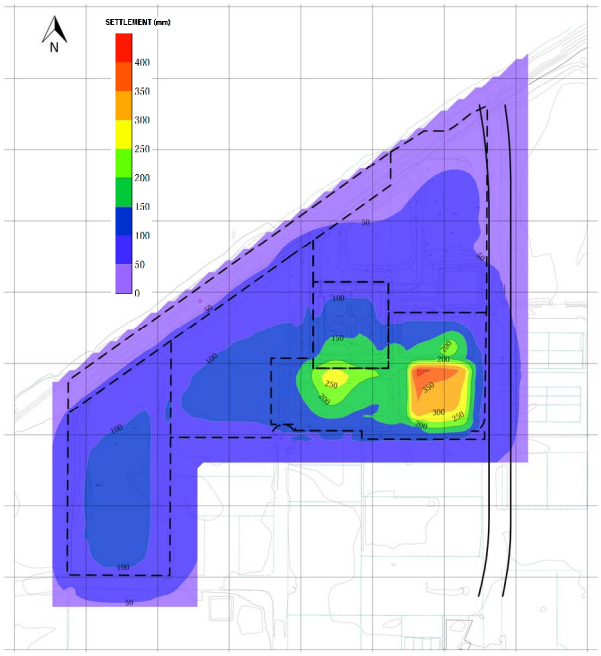
Design Option 2 was based on eliminating preload in the Phase 2 area at Lagoon D and founding the proposed facilities in that area on piled rafts with 40 m long friction piles to transfer the foundation loads to great depths, and hence reduce the lateral load spread below the adjacent infrastructure. In Design Option 2, the preload in the Phase 2 area had a clearance of 80 m and 40 m to the eastern property line in the Lagoon D and C areas, respectively, as opposed to a clearance of just 15 m in Design Option 1. The site stratigraphy was updated based on the borehole and CPT data obtained from recently completed exploration programs. Structure loads were included for facilities in the Phase 2 area, and ground improvement was assumed to exclude Lagoon D. Other aspects of the expansion project in Design Option 2, including ground improvement and preloading in Phase 1 and 3 areas, were maintained the same as Design Option 1.

Figure 5(a) presents contours of predicted settlements in Design Option 2 for the plant site from 2026 to 2101 and Fig. 5(b) presents settlements for the viaduct area east of the plant site from start of construction in 2018 to 2101. Figure 5(a) indicates that post-construction settlements for the plant facilities are similar to Design Option 1 except at Phase 2 and viaduct areas. The slight increase in estimated settlements in the Phase 2 area outside Lagoon D compared to Design Option 1 is due to including structure loads in that area.

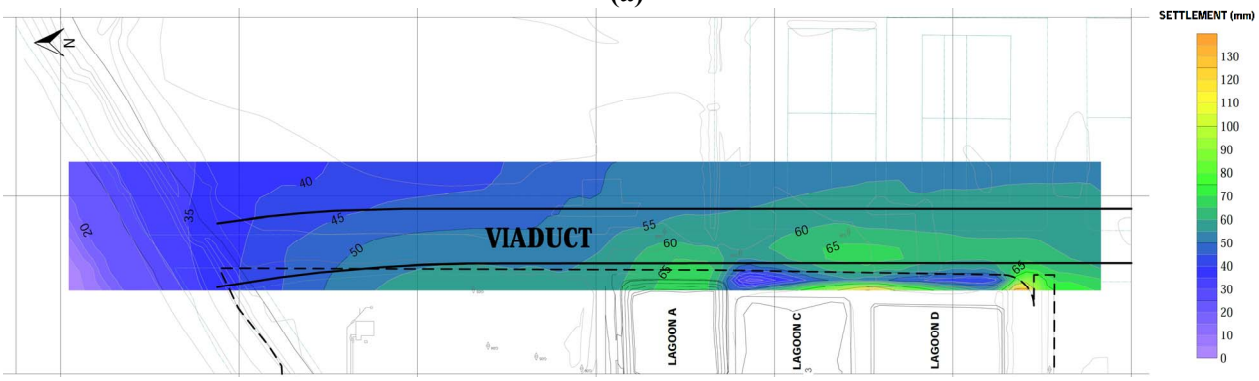
Figure 5(b) shows that limiting the preload and site grading fill footprint to outside Lagoon D and founding proposed facilities in that area on piled rafts reduce the lateral load spread below viaduct piles, and thereby decrease viaduct pier settlements compared to estimated settlements in Design Option 1. As shown in Fig. 5(b), the ground surface at viaduct piers adjacent to Lagoons C and D are predicted to settle 55 mm to 65 mm, similar to the base case analysis with no new construction. Incremental differential settlements between piers are predicted to be up to 5 mm in the longitudinal or transverse direction. Table 4 summarizes surface settlements predicted for Design Option 1 and 2 for the plant site and adjacent infrastructure.

The sensitivity of the proposed effluent treatment facilities founded on piled rafts in the Lagoon D area to the estimated total and/or differential post-construction settlements are not known at this stage. If the predicted post-construction settlements of those facilities are not acceptable, mitigation options exist to reduce the estimated settlements. The site grading fill north of Lagoon D could be eliminated, and the facility over Lagoon C could be founded at El. 2 m. Consequently, the sustained load applied north of the modeled piled rafts over Lagoon D would decrease compared to Design Option 2, and hence less post-construction settlements would occur at the northern edge of piled rafts. Alternatively, the proposed facilities at Lagoon D could be founded on longer piles than currently modeled in Design Option 2 (for example, on piles 60 m long). Lowering the pile group neutral plane to greater depths in the upper layer of

the lower clay would transfer the foundation loads deeper, and hence would result in lower total and differential post-construction settlements of the proposed facilities.



(a)



(b)

Fig. 5. Contours of surface settlements predicted in Design Option 2 for the (a) plant site from 2026 to 2101 (i.e. post-construction period), and (b) viaduct area from 2018 to 2101

Table 4. Surface settlements predicted for Design Option 1 and 2

Location	General Range of Surface Settlements (mm)	
	Design Option 1 Post-construction Period (2026 to 2101)	Design Option 2 Post-construction Period (2026 to 2101)
Phase 1 Expansion Area*	85 to 155	60 to 140
Phase 2 Expansion Area, excluding Lagoon D	105 to 145	80 to 260
Phase 2 Expansion Area at Lagoon D	95 to 145	260 to 400
Phase 3 Expansion Area*	65 to 135	60 to 120
Private Properties South of the Site	75 to 115	60 to 100
Viaduct	75^ to 125^	45^ to 65^

* Variations in settlement of these areas from Design Option 1 to 2 are due to updates in the geologic model.
^ Predicted settlements are for 2018 to 2101 period.

CONCLUSIONS

Planning for site development and foundation systems for a wastewater treatment plant expansion was performed by conducting settlement analyses to evaluate the potential impact of the expansion project on new and existing facilities at the site and adjacent infrastructure. The numerical model was calibrated to approximately match the short-term settlements measured for a previous expansion and the long-term settlements measured during the last decade.

Site preparation, including vibro-replacement ground improvement for liquefaction mitigation and preload/surcharging for reduction of post-construction settlement, will be carried out as an early works program to expedite the construction schedule. This allows unusually long preload durations of 4 and 3 years for the Phase 1 and 2 expansion areas at the site, respectively. Two design options were considered for preload extents across the site and foundation systems for proposed facilities. Design Option 1 assumed that the toe of preloading and site grading fill extended to property boundaries except in the Phase 2 area with a clearance of 15 m to the eastern property line, and that the proposed facilities in the Lagoon D area are to be founded on raft foundations at the original site. The predicted post-construction settlements of plant structures in Design Option 1 were reasonably uniform across the site with low differential settlement gradients. However, reduction of the incremental total and differential settlements of adjacent viaduct piers due to the expansion project was desirable.

Design Option 2 evaluated the effect of eliminating preload in the Phase 2 area over Lagoon D and founding the proposed facilities in that area on piled rafts with piles 40 m long in order to transfer the foundation loads to great depths, and hence reduce the lateral load spread below the adjacent infrastructure. The preload in the Phase 2 area had a clearance of 80 m and 40 m to the eastern property line in Lagoon D and C areas, respectively. It is shown that limiting the preload extents and founding some of the proposed structures on piled rafts with deep friction piles reduce the predicted total and differential settlements of adjacent infrastructure and results in reasonable performance for the proposed facilities.

ACKNOWLEDGEMENTS

The writers sincerely appreciate Mr. Lawrence Chiu from Klohn Crippen Berger for preparing figures for this paper.

REFERENCES

Barksdale, R.D. and Bachus, R.C. (1983). Design and Construction of Stone Columns, Report No. FHWA/RD-83-026, U.S. Department of Transportation, Federal Highway Administration, Turner Fairbank Highway Research Center, McLean, VA, USA.

Itasca, 2011. FLAC - Fast Langrangian Analysis of Continua User's Manuals. Itasca Consulting Group Inc., Minneapolis, MN, USA.

Rocscience Inc., 2019. Settle3D: Settlement and Consolidation Analysis Software, Toronto, ON, Canada.

STONE COLUMN GROUND IMPROVEMENT – A TRIAL IN SILTY SANDS

Ana Pereira, ENGEO Ltd, New Zealand Christchurch, apereira@engeo.co.nz
Donald Bruggers, ENGEO Ltd, New Zealand, Christchurch, dbruggers@engeo.co.nz
Naomi Norris, ENGEO Ltd, New Zealand, Christchurch, nnorris@engeo.co.nz

ABSTRACT

The city of Christchurch, New Zealand is predominantly founded on alluvial sediments consisting of interbedded layers of loose to medium dense sand, soft to stiff silt and clay mixtures, and pockets of organics. These soil deposits have high liquefaction potential. Following the 2010/2011 Canterbury Earthquake Sequence several ground improvement trials were undertaken within Christchurch to understand the effectiveness of different types of ground improvement in these silty sand geological conditions. This paper presents a discussion of a stone column ground improvement trial undertaken at a Christchurch site with high fines content soils. Stone columns were installed using two types of installation methods and a range of Area Replacement Ratios (ARR) to assess the effectiveness of these ground improvement methods in high fines content soils as well as the influence on the type of installation method. Pre- and post-column installation CPTs, seismic Dilatometer Tests (sDMTs), cross-hole shear wave velocity tests, and plate load tests have been undertaken to assess the effectiveness of the ground improvement. Results of the testing are presented in this paper.

Keywords: stone columns, liquefaction suppression, ground improvement.

INTRODUCTION

This paper presents the results of a stone column ground improvement trial undertaken in Christchurch, New Zealand (Fig.1).



Fig. 1 Location Plan

In 2010 and 2011, four large earthquakes (greater than magnitude 5.9) and thousands of smaller aftershocks occurred in the greater Christchurch region. These events are referred to as the Canterbury Earthquake Sequence (CES). Liquefaction occurred across large portions of the city during the stronger earthquakes,

© 2019 Deep Foundations Institute

particularly the February 2011 event. Following the CES a large amount of data was collected across the city including the location and volume of sand boils, and the location and magnitude of ground cracks. Additionally, data from thousands of ground investigations have been uploaded into a public database. As a result, there is clear evidence that silt and silty sands liquefy in addition clean sands.

The CES and resulting liquefaction motivated a series of studies and trials from different organisations aiming to better understand the available technologies for liquefaction mitigation.

The subject of this paper is a ground improvement trial undertaken by a local contractor specialising in deep foundations and ground improvement. They were interested in understanding the effectiveness of stone column ground improvement in high fines content (silty) soils using two different installation techniques, vibratory and non-vibratory. Different arrays and Area Replacement Ratios (ARRs) were used for each of the two methods of columns installation.

To assess the effectiveness of ground improvement, a series of *in situ* tests were undertaken pre- and post-column installation. These tests included Cone Penetrometer Tests (CPT), Plate Load Tests (PLT), Cross-hole shear wave velocity testing (CH) and sDMT.

SUBSURFACE GROUND CONDITIONS

The subject site is located in the St Albans suburb of Christchurch, which, based on nearby deep investigation, is typically underlain by alluvial deposits consisting of interbedded layers of loose to medium dense sand, soft to stiff silt and clay, and pockets of organics in the top 10m, followed by interbedded layers of medium dense to dense sand and gravel, and stiff sandy silt and clayey sand to a typical depth of 20m, where dense gravel of Riccarton formation occurs. It is estimated that bedrock in this area of the city is at approximately 300m depth.

A geotechnical investigation comprising several CPTs and s DMTs was undertaken at the site prior to column installation. CPT investigations were advanced to approximately 6m depth before refusing on dense soil. sDMT and measuring the horizontal stress and shear wave velocity (Vs) at regular depth increments were undertaken to a target depth of 5m.

The ground water table was measured between 0.4m and 0.9m below ground level (bgl).

The ground conditions inferred from the CPTs and sDMT are summarised in Table 1 and Fig. 2.

Table 1: Ground profile

Depth of top layer	Thickness of layer	Description	Qc (MPa)
0 m	2.5 m	Interbedded layers of soft silty clay and organic silty clay	0.1 to 1
2.5 m	0.6 m	Soft silt and silty clay	1 to 2
3.1 m	1.4 m	Loose silty sand	1 to 4
4.5 m	1.5 m	Loose to dense sand	4 to 40

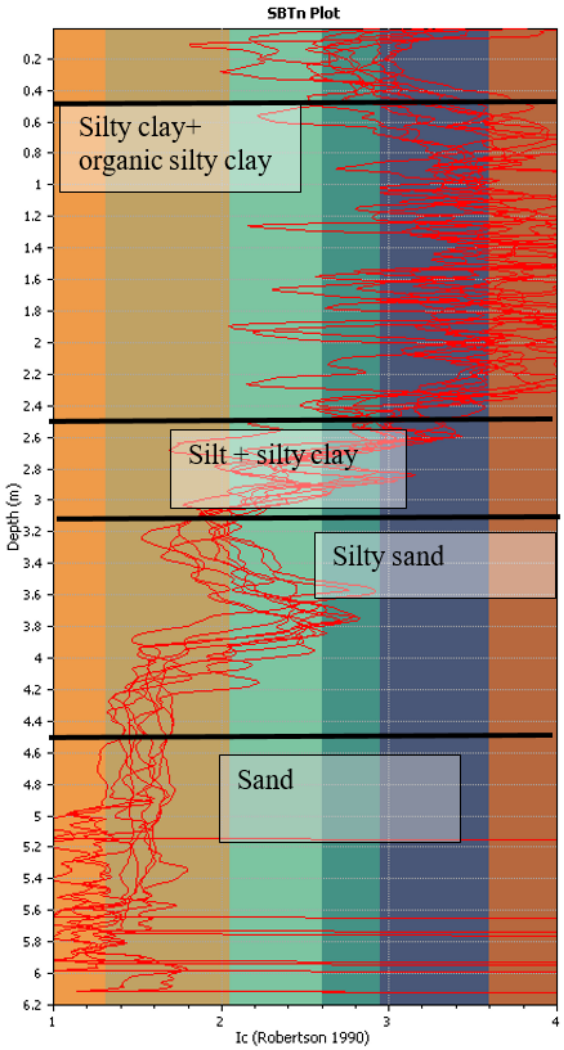


Fig.2 .Soil Behaviour chart

GROUND IMPROVEMENT

Motivation for ground improvement

Typically, the ground conditions across Christchurch consist of loose sands and silts and shallow water levels. As shown in the Canterbury Earthquake Sequence (CES), these conditions can cause significant land, infrastructure and structural damage as a result of liquefaction. One widely used technique to mitigate liquefaction effects is the stone column ground improvement. In this method, columns of dense gravel are installed to a target depth, displacing and densifying in situ sandy soils. There is a lack of understanding about how the installation method, and the fines content of the soil influences the effectiveness of the ground improvement. Accordingly, the purpose of this trial was to develop a better understanding of these issues.

Stone columns installed with a vibratory method

The ground improved area using a vibratory method consisted of 4m long and 550mm diameter columns in two different arrays, resulting in two different Area Replacement Ratio (ARR):

- Triangular layout with column spacing of 1.31 m , resulting in ARR=16.3%
- Quadrangular layout with column spacing of 1.85m, resulting in ARR=6.9%

The installation methodology is similar to a Rammed Aggregate Pier methodology. Initially it is opened a cavity (similar to excavating a pile), and then an excavator or tele handler continually loads stone into the hopper, feeding it down the mandrel and into the ground. The stone is compacted using a ramming and vibrating action to form a stiff, high-density, vertical aggregate pier within the ground. No water or air jetting is used in this method.

Stone columns installed with a NON-vibratory method

The ground improved area using a non-vibratory method consisted in 4m long and 930mm diameter columns in two different arrays, resulting in two different Area Replacement Ratio (ARR):

- Quadrangular layout with column spacing of 1.88 m, resulting in ARR=19%.
- Quadrangular layout with column spacing of 2.3 m, resulting in ARR=12.8%.

The non-vibratory method consists in a dual displacement tool inserted by rotational drilling displacement soil. The method of installation consists in inserting the displacing tool to the desired depth (similar to a Continuous Flight Auger, but with smaller helices and larger hollow). The stone is introduced into the hollow through an upper hopper and the top gearbox pushes an internal helical rod outside the tip of the soil displacement tool and the displacement of the stones start by hydraulically rotating counter clockwise the helical rod pushing the stones vertically and horizontally. After a certain hydraulic rotary pressure, the stones are full displaced in the diameter and the lifting of the tool starts, the lifting speeds is correlated to the pressure of the stone displacement to achieve the best improvement of the ground. No water or air jetting is used in this method.

POST INSTALLATION TESTING AND RESULTS

In Situ testing was conducted at the site following the installation of the stone columns. The testing was conducted several weeks after the installation of the columns to allow pore water pressure to dissipate.

The tests consisted of CPTs, sDMTs, plate load tests, and Cross-Hole shear wave velocity surveys. The CPTs and sDMTs were conducted at similar locations as the pre-installation tests to facilitate the comparison between non-improved and improved ground.

Cone penetrometer tests (CPT)

CPTs are commonly used to assess the effectiveness of a ground improvement technique to suppress liquefaction. This is done by comparing the results of CPT-based liquefaction assessments from pre-improvement and post-improvement CPTs. For this trial several CPTs were pushed both prior to, and following installation of the columns.

Some CPTs were pushed through the stone columns. This was unexpected as it was felt that a stone column should have a density that precluded penetration with a CPT cone.

Other CPTs were advanced between the stone columns within the improved ground.

The CPTs that were advanced through the columns achieved at most 20 MPa tip resistance. This indicates a lower than expected density, and quality of the columns themselves. Given that the columns achieved at the most a tip resistance (qc) of 20 MPa, improvement in density of the adjacent soil in between the columns is expected to be low with a limited increase in density as reflected in low qc values. Some of CPTs advanced between columns post ground improvement were pushed approximately at the same location as the ones advanced prior to column installation. Figures 3 and 4 show the CPT tip resistances and sleeve friction pre- and post- improvement for both methods.

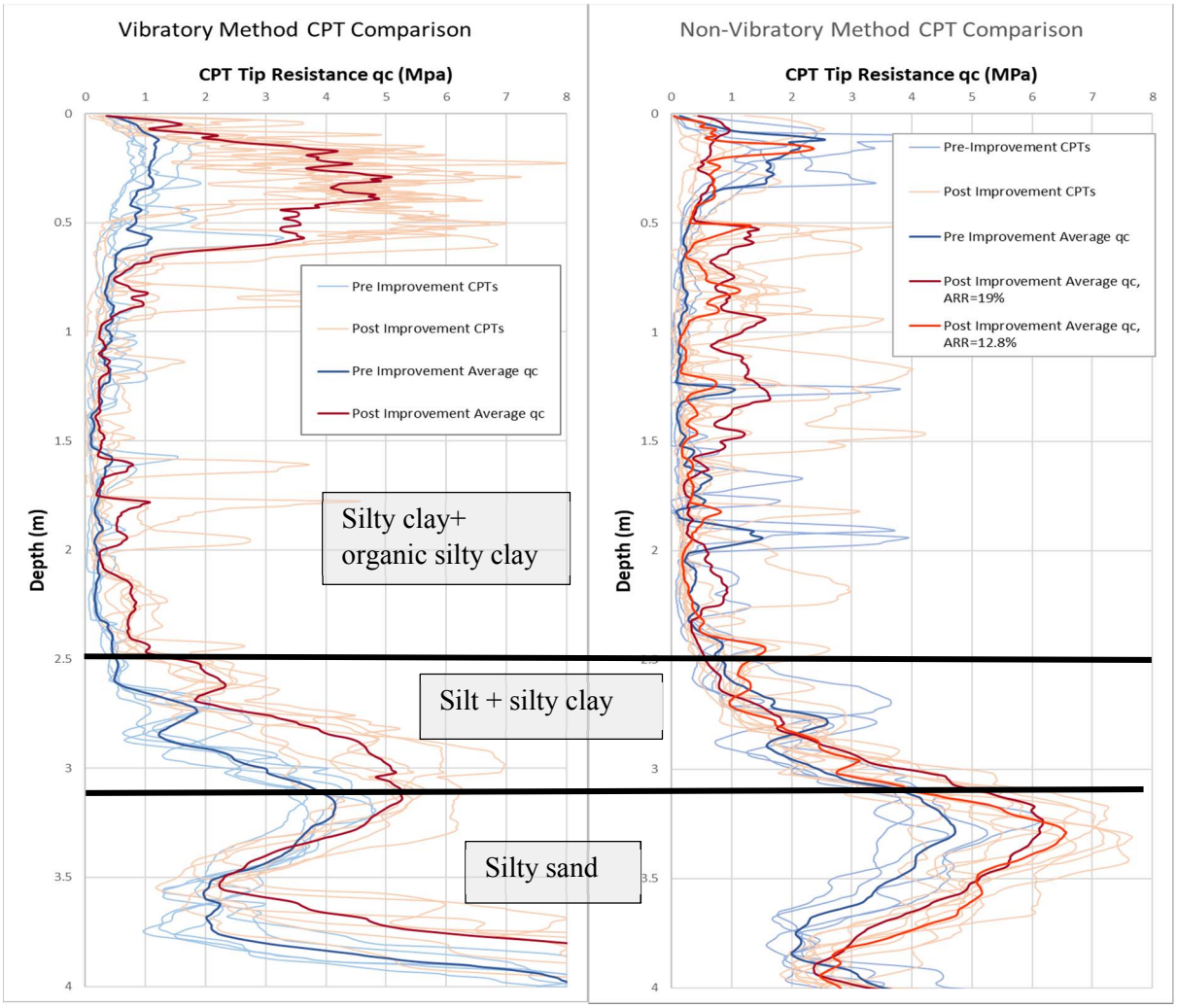


Fig. 3. Pre- and Post- Ground improvement CPT tip resistance between vibratory (left) and non-vibratory (right).

Based on the pre- and post- CPT testing data (refer to Fig.3), the effectiveness of the vibratory ground improvement methodology is not significantly noticeable within the clayey soils in the upper 2.5m of the ground profile.

However, for the non-vibratory ground improvement methodology, we provide the following observations based on the CPT testing:

- In fine grained soil, qc and fs increase as ARR increases from 12% to 19% (refer to Fig.3 and Fig.4).

- In granular soil, there is neither qc or fs change with an increase in ARR from 12% to 19%. We postulated that in medium dense silty sand, there may be a maximum threshold where limited, if any increase in density of the native ground will occur even with stone column ground improvement (Fig.3). This fact could be related to the presence of the silt in the sandy soil. Also, we note that the "cap" of clayey soil may have delayed the dissipation of pore water pressure following the columns installation, as a result the re-arrangement of the soil grains was slow as a slow alluvial deposit. It should be noted that even with significant shaking the sandy soils in Christchurch never densified following the CES and kept liquefying in every event.
- There is an increase in qc in the loose sandy layers but still not enough to suppress liquefaction as qc reaches at the most 8MPa (Fig. 3).

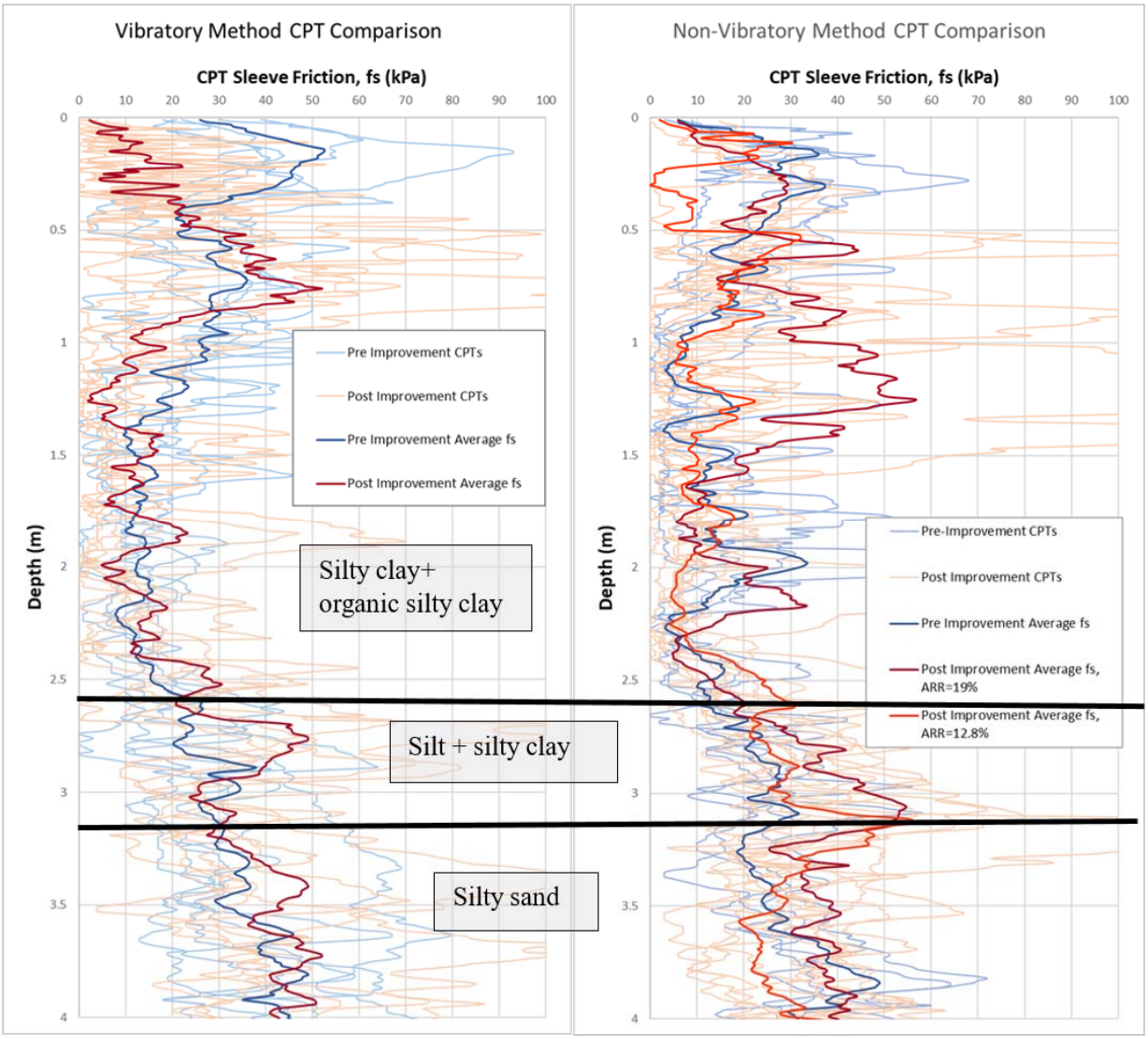


Fig. 4. Pre- and Post- Ground improvement CPT sleeve friction between vibratory (left) and non-vibratory (right).

Dilatometer test

A series of five sDMTs were undertaken to assess ground conditions pre- and post- ground improvement. The seismic component of this survey provided readings of shear wave velocity (Vs) at sDMT locations allowing for a better understanding on the behaviour of the silty layers.

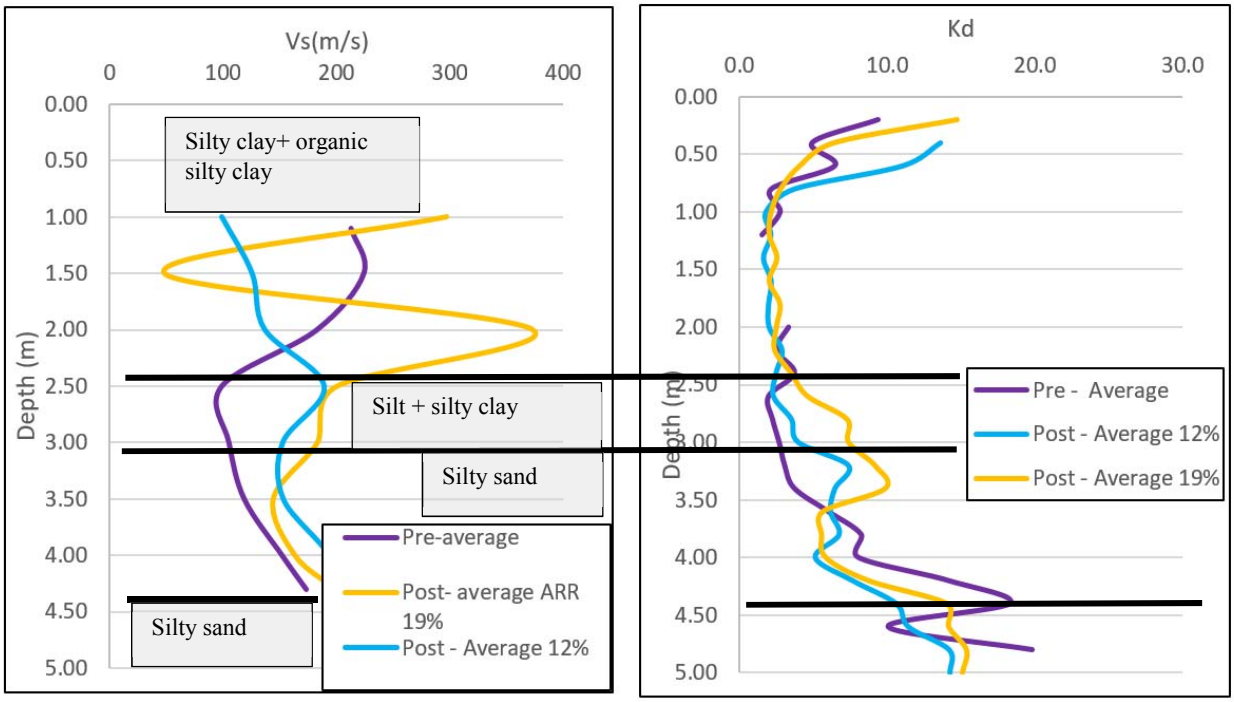


Fig.5: sDMT test profile pre-ground improvement, non- vibratory post ground improvement with ARR=12% and ARR=19%. Shear wave velocity (on left). Horizontal Stress Index (on right).

Based on the pre- and post- sDTM testing data, the effectiveness of the vibratory ground improvement methodology is not significantly noticeable. For the non-vibratory ground improvement methodology, we provide the following observations based on the sDMT and Vs profiles:

- Generally the horizontal stress index increases with increase of ARR from 12% to 19% in sandy soil (Fig.5 right).
- No evidence of change in horizontal stress index is noted in fine grained soil as a result of stone columns inclusions (Fig. 5 right).
- In fine grained soil, shear wave velocity (Vs) increases slightly with an increase in the ARR (Fig.5 left).
- In granular soil, Vs does not change with increase in the ARR (Fig.5 left).
- Overall increase in Vs in the improved profile compared to pre-improvement profile (Fig.5 left).

Both methods do not show significant improvement in the sDMT testing. Similar response of the soil profile in both methodologies

Static Plate Load Testing

Static plate load tests were conducted at the centre of nine stone columns. These tests indicate the stone columns have stiffnesses ranging from 4 kPa/mm to 11 kPa/mm for the vibratory method and 6kPa to 13kPa with non-vibratory method. Although the non-vibratory method show slightly higher stiffnesses it is not a significant difference to consider one method has better results than the other.

These stiffnesses are much less than anticipated as it was expected that the stone columns would have a stiffness of at least 30 kPa/mm, which is a typical stiffness for dense gravel. One explanation for the low stiffness could be the limited confinement provided by the soft clay and organic soil in the upper 2.5m of the soil profile surrounding soft near surface soil between the columns, resulting in bulging of the column when subjected to the plate load testing.

Cross-hole testing

Seismic cross-hole testing following stone columns installation was conducted. The purpose of this testing was to assess the changes in the ground stiffness through the shear wave velocity (Vs). Six tests were undertaken across the stone columns to assess column stiffness and four were undertaken between stone columns aiming to assess the increase in density in the improved soil profile between the columns as a result of stone column installation

It is generally agreed between geotechnical specialists that when Vs is greater than 200 m/s in saturated sandy layers, the liquefaction potential is very low. Accordingly, this criteria was used in our assessment to evaluate the effectiveness of the ground improvement to mitigate liquefaction.

Based on the seismic cross-hole testing results, the effectiveness of the vibratory ground improvement methodology is not significantly noticeable.

However, for the non-vibratory ground improvement methodology, we provide the following observations:

- Two Cross-Hole (CH) tests were undertaken between columns, and another two CH tests were undertaken across stone columns. The measured Vs across the stone columns and in between the columns can be read in charts of Fig.6.
- There is a clear increase in Vs due to the presence of the stone column, as expected. However, the Vs is still below 200m/s.
- We postulate that this could be related to damping effects in the surrounding soft soil, shear wave travelling through and either side of the column and then the arrival time is the average travelling time, or the stone column not be as dense as expected (dense gravel usually has Vs higher than 200m/s).

Note that tests were undertaken following column installation and it is only possible to compare the Vs across columns and ground between columns. There is no cross hole Vs testing prior to ground improvement to compare the Vs of Pre- and Post- ground improvement.

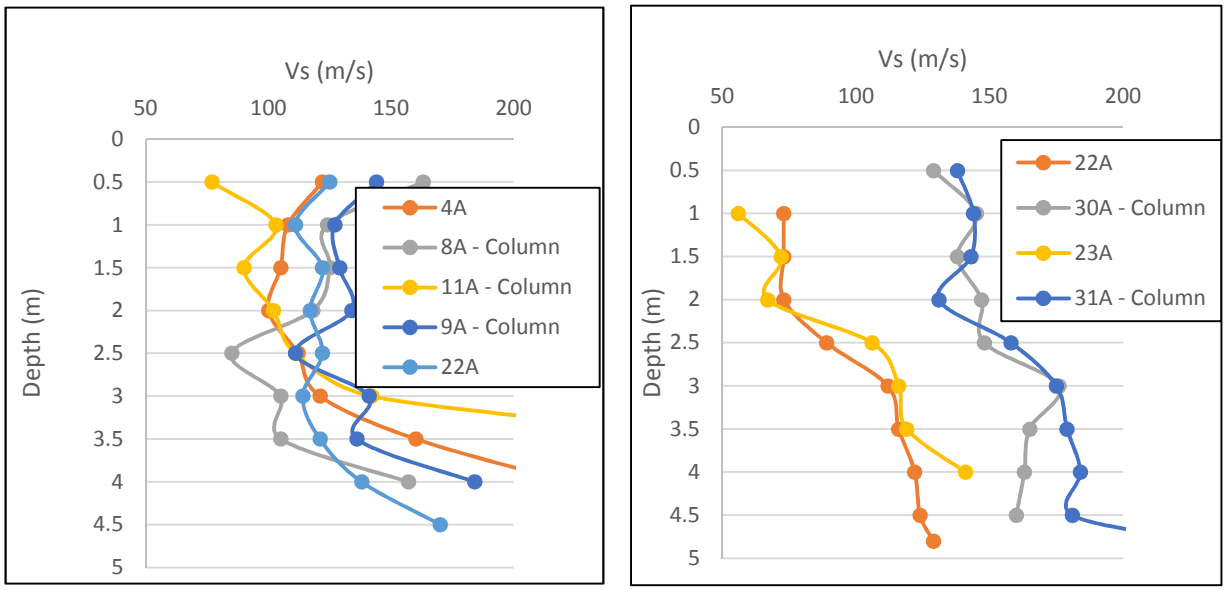


Fig. 6: cross hole testing results. Vibratory method (on left), non-vibratory method (on right). Tests 4A, 22A, 23A, in midpoint between columns. Tests 8A, 11A, 9A, 30A 31A across columns.

SUMMARY AND CONCLUSIONS

The case study presented in this paper intended to assess the influence of vibratory and non-vibratory methods to install stone columns in silty sands for liquefaction mitigation.

- The vibratory method has shown some improvement to the ground (on average less than 2MPa on CPT resistance between 2.5 and 4m) between pre- and post- columns installation are not evident.
- On the non-vibratory method an increase in tip resistance is more obvious in the fine-grained soils. Refer to fig.3 for 19% ARR. This could be due to lack of confinement in soft soil therefore more aggregate has been introduced to the ground causing increase in column diameter and resulting in reinforcement of the soil.
- Unexpectedly, CPTs pushed through the stone columns show a maximum tip resistance of 20 MPa following the non-vibratory columns installation. Therefore, this may indicate that the columns do not have a dense core. This may be caused by silty contamination of the stone column core during installation or lack of confinement within the clayey silty soils.
- The CPTs pushed between non-vibratory columns showed that an increase in ARR from 12% to 19% changes the behaviour of the fine grained soil as reflected by an increase in qc and fs.
- In sandy layers (from 2.5m to 4m depth, Fig. 3 and Fig. 4), there is clear evidence of improvement in density due to stone columns inclusions (both methods). However, no significant increase in *in situ* density associated with an increase of ARR from 12% to 19% was noted in the more granular deposits between 2.5 to 4m (refer to Fig. 3). We postulate that there is a threshold in density where sand reaches its maximum density due to the stone columns inclusions.
- Both methods show some improvement in the granular layers, and the non-vibratory method shows slightly more improvement in the fine-grained soil layers.
- Plate load tests were not undertaken between piles to verify the effective increase in bearing capacity of the top silt soils. However, the plate load tests on specific columns indicated low bearing for a

stone column, which we may be related to low lateral confinement provided by the clayey/organic soil surrounding the columns (both methods).

- Cross-hole tests performed across columns indicate an increase in Vs in the stone column profile when compared with cross-hole undertaken between columns.
- We suspect that the presence of soft soil above the granular material may influence the effectiveness of the stone column ground improvement, as the pore water pressure cannot dissipate quickly all the way to the surface as the clayey soil may act as a cap, and therefore the soil grains may settle slowly in a less dense arrangement.
- We conclude that neither improvement method shows great evidence of improvement to liquefaction susceptibility. We surmise that CPT is not the best test to assess the effectiveness of ground improvement in this type of silty soils, and therefore we recommend that future investigation should be undertaken to assess the effect to the stone columns in soft clayey sandy silt soils to mitigate liquefaction. We consider that geophysical testing across the entire improved block may be a methodology to assess the overall effectiveness of ground improvement in addition to the conventional pre- and post- CPT testing that assesses the effectiveness of a single column. This could be achieved with Multichannel Analysis of Surface Waves (MASW) survey undertaken pre- and post-improvement. Plate load tests could be also done in a group of columns rather than just a single column as the overall bearing capacity (BC) can be assessed rather than the BC of a single stone column.

ACKNOWLEDGEMENTS

The authors would like to acknowledge and thank McMillan Civil (NZ) for allowing them to present the above case study into ground improvement with stone columns.

REFERENCES

Brown, L.J. & Weeber, J.H. (1992). Geology of the Christchurch Urban Area 1:250,000. CGD5122. Institute of Geological and Nuclear Sciences.

Forsyth, P., Barrell, D. J., & Jongens, R. (2008). Sheet 16 - Geology of the Christchurch Area 1:250,000. Lower Hutt: Institute of Geological and Nuclear Sciences.

GNS Science, Earthquake Commission. (n.d.). Aftershocks. Retrieved 2019, from Geonet: www.geonet.org.nz/canterbury-quakes/aftershocks

Idriss and Boulanger. (2008). Soil Liquefaction during Earthquakes - EERI Monograph MNO12.

Youd, T. L. (2001). Liquefaction Resistance of Soils: Summary Report from the 1996 NCEER and 1998 NCEER/NSF Workshops on Evaluation of Liquefaction Resistance of Soils. ASCE Journal of Geotechnical and Geoenvironmental Engineering, 127(10), 817-833.

Zhang, G., Robertson, P. K., & Brachman, R. (2002). Estimating Liquefaction Induced Ground Settlements from the CPT. 39, 1168-1180.

Zhang, G., Robertson, P. K., & Brachman, R. W. (2004, August). Estimating Liquefaction-Induced Lateral Displacements using the Standard Penetration Test of Cone Penetration Test. ASCE Journal of Geotechnical and Geoenvironmental Engineering, 861-871

JET GROUTING FOR STRENGTH IN MARINE SEDIMENTS WITH HYDROCARBONS

Sharon G. Cranston, Simpson Gumpertz & Heger, Waltham, MA, 781-907-9419, sgcranston@sgh.com
Giuliana A. Zelada, Simpson Gumpertz & Heger, Waltham, MA, 781-907-9290, gazelada@sgh.com
Alessandro Bertero, Treviicos, Charlestown, MA, 617-413-2018, abertero@treviicos.com
Paul M. Schuman, Simpson Gumpertz & Heger, Waltham, MA, 781-907-9277, pmschuman@sgh.com

ABSTRACT

Many jet grouted columns were recently installed to create a jet grout-treated soil foundation for an earthen embankment used in a large shoreline stabilization project in the Mystic River in Charlestown, MA. A physical test program was used to determine whether the jet grouting parameters the Contractor selected would meet the design requirements given the local soil variability, including soft river sediments and organic soils. The presence of hydrocarbons encountered in the marine sediments during the test program caused concern that the design strength could not be achieved. The published literature discusses the environmental aspects of jet grouting with hydrocarbons. The literature did not include many studies of the effect on jet grout-treated soil strength for the types and concentration of hydrocarbons encountered on this project. The grout mix, air pressure, and number of passes of jet grouting were varied in a second field test program to determine jet grouting parameters needed to achieve the design strength of columns with hydrocarbons. A geo-probe study was performed to identify the type and concentration of hydrocarbons on the site. With few exceptions, the quality control core samples from the production columns met the design requirements with many strength values far exceeding the design strength. This paper presents the data, and reviews the lessons learned.

Keywords: jet grout, hydrocarbon, marine sediments, test programs

PROJECT BACKGROUND

The Charlestown Bus Garage, located in Cambridge, Massachusetts, is a Massachusetts Bay Transportation Authority (MBTA) bus maintenance facility located on the Mystic River. The site was home to a coal gasification facility before it was developed by the MBTA as a bus garage in 1978. A deadman-anchored steel sheet pile bulkhead wall installed along the Mystic river on the east side of the site supports the site grade at about El. 11 ft (NAVD 1988) (Figure 1).

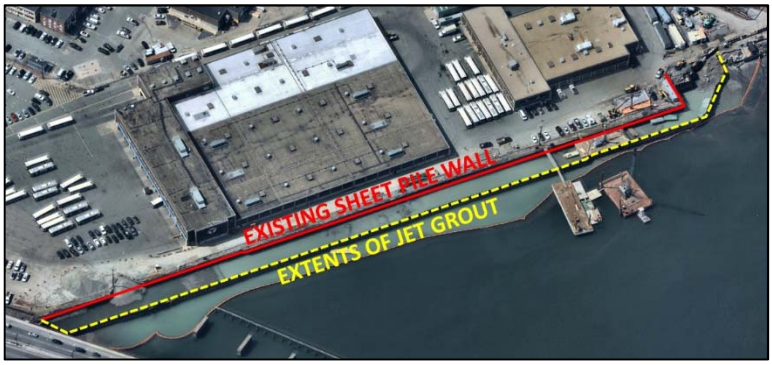


Figure 1. Project location plan showing the extents of the jet grouting.

In recent years, the MBTA observed ground settlement and large void formations in the landscaped areas and near drainage structures adjacent to the sheet pile bulkhead wall. It was determined that a portion of the soil loss was occurring through pitting holes in the sheet piles caused by corrosion. In addition, it was also determined that corrosion had advanced significantly in several portions of the sheet pile wall, reducing its effective section. Due to safety concerns related to both the remaining service life of the sheet pile bulkhead wall and the presence of ground

© 2019 Deep Foundations Institute

voids which could extend to the bus traffic areas of the facility, potentially undermining the pavement, the MBTA retained a designer to develop a remediation.

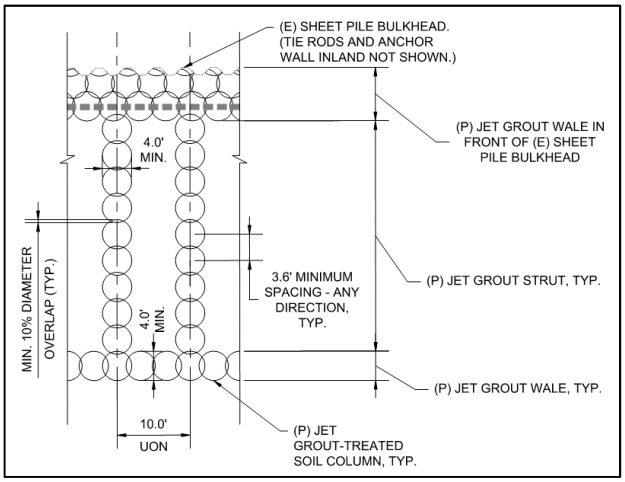


Figure 2. Jet grout column layout concept.

After evaluating several remediation options, the MBTA and the Designer elected to construct an earthen embankment in front of the bulkhead wall for lateral support. The upper portions of the embankment would be bio-stabilized with special plantings suitable for the specific site conditions, and a path at the crest would become part of a proposed circuit along the Mystic River intended to provide recreational bike and pedestrian connectivity to downtown Boston. Due to the presence of very soft marine sediments and compressible slightly organic soils overlying the marine sand and marine clay strata at the site, the earthen embankment was designed to be supported on a geogrid platform bearing on "strut" and "wale" embedded walls consisting of overlapping jet grout columns, as shown in Figure 2.

DESIGN AND SPECIFICATION OF EMBANKMENT JET GROUT FOUNDATION

The jet grouted foundation for the proposed embankment was designed to extend from Mean Low Water (MLW) to 5 ft of embedment into the medium stiff to stiff marine clay stratum underlying the site, along approximately 1200 linear ft of bulkhead wall. As shown in Figure 2, the strut and wale pattern of the jet grouted foundation consisted of an 8-ft to 12-ft wide continuous wale in front of the bulkhead wall with perpendicular 4-ft wide struts spaced at 10-ft center-to-center. The 4 ft diam. for the jet grout columns was based on consultations and research about what could be reasonably achieved in the site soils. Setting the top of the jet grouted foundation at MLW elevation required up to 7 ft of dumped stone fill placed in the wet over about half the length of the proposed embankment plus additional stone to provide a working platform for the jet grouting operations. Due to the in-the-wet placement of this stone fill, as well as the need for jet grouting of this material, the selection of the stone fill material gradation was left to the jet grouting specialty contractor.

Ground improvement by jet grouting is well known in underground construction. Grout is injected into a, typically, weak or compressible soil to form jet grout-treated soil columns; a mix of soil and grout that once hardened provides increased strength and stiffness to sustain the required applied loads. The degree of mixing of the soil and grout varies depending on the specific soil strata and jet grout installation parameters used (number of nozzles, fluid injection pressures, rotation and withdrawal rates of the drill rods and nozzles number and diameter). Performance specifications are typically indicated for jet grouting wherein the target strength, permeability, and/or size of jet grout-treated soil column is specified based on the design requirements, and the jet grout specialty contractor (herein referred to as the Contractor) is then responsible for selecting the installation procedures and grout mix that can best achieve those requirements.

With a surface area of about 1,200 ft long by 40 ft wide, and with required jet grout depths of up to 35 ft below final design grade, the MBTA Charlestown Bus Garage project is one of the largest jet grouting projects to be performed in a river, requiring about 714,500 cubic ft. of jet grout-treated soil for 1250 jet grout columns to be installed (without accounting for the actual soil-grout replacement ratios). Given the scale of the project, the known variability in subsurface stratigraphic conditions, and the potential variability

in soil strength and column diameters achieved, a pre-production field test program was specified for the jet grouting. The intent of the field test program was for the Contractor to prove their proposed installation procedures.

Based on the subsurface investigations performed at the site, the Designer required a minimum of two field test sites to evaluate the adequacy of the Contractor-proposed jet grouting installation parameters. The first test site was to be located in the central portion of the site where the stratigraphy consisted dumped stone fill over very loose/soft marine sediments over marine sand over medium stiff to stiff marine clay. This site was deemed representative of conditions between Sta 10+00 to Sta 18+50. The second test site was to be located in the north portion of the site (Sta. 18+50 to Sta. 21+00) where the stratigraphic column consisted of soft slightly organic marine clay over medium stiff to stiff marine clay.

The specifications required the test program to include at least three overlapping jet grout columns at each of the test sites. Once hardened, the Contractor needed to obtain full-depth cores at the center of each column and at each overlap region between columns. From each core, the Designer and the Contractor were to select four jet grout-treated soil samples from within the extent of each soil stratum for laboratory testing. The laboratory testing specified included two unconfined compressive tests and two triaxial shear strength tests for each soil stratum; one of each tested for 7-day strength and 28-day strength. The intent of the triaxial shear strength testing was to determine the correlation between shear strength and unconfined compressive strength to allow the use of only unconfined compressive strengths during production for quality control. In addition, the Contractor needed to propose a test method to confirm the required column diameter had been achieved. The specified minimum unconfined compressive strength for the jet grout-treated soil was 250 psi; the specified minimum shear strength for the jet grout-treated soil was 100 psi.

JET GROUT FIELD TEST PROGRAM IMPLEMENTATION

Once the contract was awarded, the Designer worked with the Contractor to lay out the jet grout field test program. The Contractor proposed modifying the design layout of the jet grout columns to use primarily 6 ft and 7 ft diam. columns, with 4 ft diam. columns in some areas. The as-designed clear spacing between jet grout column struts was maintained to prevent changes to the geogrid platform, which already included use of an imported very high-capacity geogrid. The use of larger diameter columns, which increased the center-to-center spacing of the jet grout struts from 10 ft to 14 ft, helped to reduce the number of jet grout set-ups required and thus, helped to control the schedule given that the jet grout column installation was in the critical path for timely project completion. In addition, the Contractor selected to use a ¾ in. uniformly graded stone for filling in areas where dumped stone fill was specified.

The Contractor selected as best option for the project the double-fluid technique, in which soil erosion and soil-grout mixing action are performed by a jet of grout that is assisted by an air shroud to improve its effectiveness and achieve larger columns diameter. Pre-washing (or pre-cutting) technique was implemented in presence of the stiff clay layer, where water is used to pre-erode the soil. Jetting energies and soil type and erodibility play a major role in determining the geometry; the column's size is directly proportional to the pressure and the flow of the injection fluids (grout, air, water) and inversely proportional to the rotation speed and to the withdrawal rate of the drilling rods. Target air pressures ranged from 8 to 10 bar and target grout pressures ranged from 430 to 440 bar. For the jet grout field test program the Contractor elected to install two sets of three columns in each required test site in order to test two different sets of jet grout parameters with different lifting speed and rotation speed, and two sets of grout mix with different water to cement ratio. One set of columns at each test site was to also include a pre-wash phase in the medium stiff to stiff clay stratum. For the southern two thirds of the site, the Contractor proposed installing three 6 ft diam. columns at each Sta. 15+59 and Sta. 15+85. For the northern portion of the site, where the slightly organic clay was present, the Contractor proposed installing two 6 ft diam. columns and

one 7 ft diam. column at each Sta. 19+49 and Sta. 19+77. Additionally, the Contractor installed 2 pairs of 4-ft diam. columns at Sta. 19+92 using no air.

The specifications required testing of the jet grout-treated soil strength at 7 days and 28 days curing. The purpose of the 7-day strength was to have an early confirmation that the jet grout-treated soil strength was developing as intended, based on a jet grout-treated soil strength gain curve vs. time for the design mix to be developed during the field testing. It was anticipated that the Contractor could install up to about 12-20 jet grout columns per day using two jet grout drill rigs (depending on depth and diameter). Waiting for 28-day strengths meant that about 500 jet grout columns could be installed before confirmation that the jet grout-treated soil had adequate strength; if any issues were identified the Contractor would need to install additional columns around the impacted area to make up for the deficiency, impacting the schedule. Because the Contractor indicated that coring the jet grout columns at 7 days of curing would be difficult and would more than likely impact the quality of the core samples obtained, the Designer requested the Contractor obtain wet grab samples of the in-place jet grout-treated soil during test column installation. The Contractor made several attempts to collect wet grab samples at various depths up to 15 ft below the top of the column, however the dumped stone fill on top of the native soils prevented the sampler from penetrating far into the column. The most successful wet grab sample was collected 5 ft below the top of the column. Given these difficulties, the Designer and the Contractor agreed that coring of the jet grout columns would be performed at 21 days from installation, the earliest that the Contractor deemed adequate for obtaining good core samples, and laboratory testing would be performed at 28 days. It was also agreed that coring would be performed at the center, overlap, 1 ft inside from the theoretical edge of the column and 1 ft outside from the theoretical edge of the column to confirm the column diameter, as shown in Figure 3.

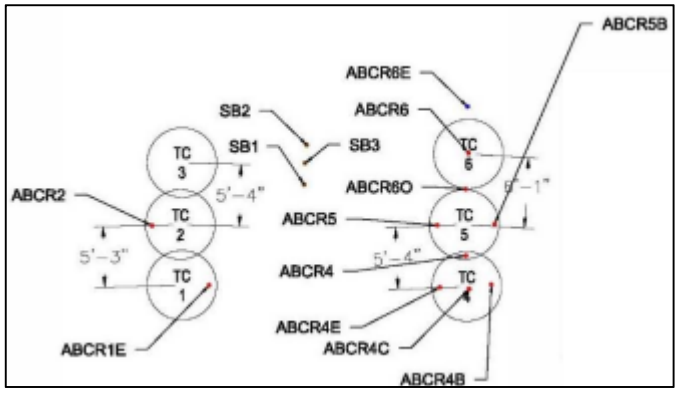


Figure 3. Jet grout test program coring layout.

In the north test section (Sta 19+49 to 19+77), all columns passed the field testing and the jet grouting parameters were approved for production.

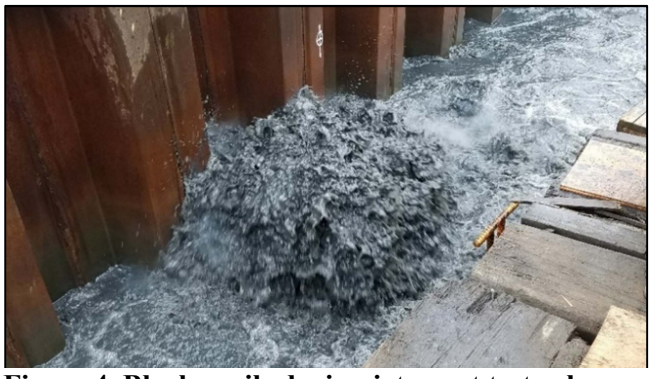


Figure 4. Black spoils during jet grout test column installation.

During the installation of the test columns in the southern test site (Sta 15+59 to Sta 15+85), the Contractor noted black spoils and a sheen in the water in the area immediately adjacent to where the jet grout columns were being installed (Figure 4); a hydrocarbon odor was also reported. The Contractor notified the project team of this condition, expressing a concern that the presence of hydrocarbons could adversely impact the strength of the cured jet grout-treated soil.

The Contractor started coring to obtain jet grout-treated soil samples for laboratory testing 21 days after installation. The first full-depth core performed on one of the columns at Sta 15+85 revealed a 1-ft zone of soft uncured marine sediment below the grouted ¾-in. dumped stone fill (Figure 5).

The sediment was black and with a distinct hydrocarbon odor. As a check for the presence of cement in this zone, the Contractor field-tested the sediment by applying Phenolphthalein to the uncured sediment; the Phenolphthalein turned magenta indicating cement was present. Although other full-depth cores performed at this test site did not encounter other extensive zones of uncured material, the results of the unconfined compression and shear strength testing on samples obtained from within the marine sediments were highly variable, with unconfined compressive strengths (UCS) ranging from 45 to 1010 psi.



Figure 5. Uncured marine sediment material with suspected hydrocarbon contamination.

Jet grout-treated soil samples from the test core program were sent to an environmental testing agency to test for Total Petroleum Hydrocarbons (TPH) content. The TPH concentration found in the initial test program jet grout-treated soil core samples ranged from undetected to 5,700 PPM. A chemical analysis of the jet grout-treated soil samples concluded that the hydrocarbons present in the cores likely consisted of Fuel Oil #6 and coal tar. Both of these contaminants are DNAPLs[1], which would tend to sink into loose or very soft soils. This could explain why during the pre-construction subsurface investigation performed, no hydrocarbons were encountered within the upper 3-ft of soils to be dredged.

A petrographic analysis of the uncured jet grout-treated soil samples encountered un-hydrated cement particles, but it also indicated that the amount of cement present was likely not sufficient to kick-start hydration and therefore it was not clear whether the hydrocarbons were impacting the hydration process or the uncuring was a result of poor mixing.

The project team was concerned that the hydrocarbons could impact the curing process and the strength of the jet grout-treated soil, as well as the mixing of the grout and soils. At the same time, the Designer considered the possibility that the reason for the uncured jet grout-treated soil zone encountered could be due to dispersion of the air pressure in the voids of the dumped stone fill above which could have reduced the efficiency of the mixing. It should be noted that during test column installations, air bubbles inside the water were sometimes observed around and up to 20 ft from a column installation location.

Because the unconfined compressive strength and shear strength of core samples with no or minimal TPH concentrations (undetected) met the specified minimum values, it was decided that an environmental geo-probe testing program would be undertaken to identify the extent of the hydrocarbons-contaminated area. In addition, based on the results at the northern test site, jet grouting production operations were allowed to proceed north of Sta 18+50. Jet grouting operations in hydrocarbon-contaminated areas would require a second test program after the design team and Contractor evaluated the available options to mitigate this condition.

EVALUATING THE IMPACT OF HYDROCARBONS ON JET GROUTING

To evaluate the potential impact of hydrocarbons on the jet grout embankment foundation, the project team researched published literature to help inform the decision making for development of a second field test program. At the same time, an environmental geo-probe testing program was developed and implemented

[1] Dense non-aqueous phase liquid.

to help define the areal extent and concentration of hydrocarbons on site. It should be noted that no hydrocarbons had been encountered during the water-side subsurface investigation performed during the design development phase of the project, and neither had hydrocarbons been identified in any of the available historical marine soil test boring logs provided.

Literature Review

Prior to selecting the second field testing parameters, the Designer and Contractor reviewed available literature to better assess the uncertainties regarding the impact of the hydrocarbons on the jet grout-treated soil strength and grout-soil mixing. Available literature on the specific topic of hydrocarbons and their impact on grout and/or grout-soil mixing was very limited. However, some general findings were useful to help guide the data evaluation and decision making, as follows:

- Petroleum oils were found to be, in general, compatible with Portland cement grouts. Although increases in set time were observed in some cases, there was no significant effect on the durability of the grout (Spooner et al. 1984).
- A site remediation project near the Monongahela River used 3-ft diam. jet grout columns as a support of excavation (SOE) system in soils containing petroleum hydrocarbons. The SOE design required a minimum compressive strength of 500 psi for the jet grout-treated soil at 28 days. Reportedly, all of the jet grout-treated soil samples achieved short term strengths in excess of 400 psi and long term strengths in excess of 500 psi with some values above 1,000 psi (Walker, undated).
- Crude oil can act as a compressive strength inhibitor and hinder the bond formation between the concrete constituent materials and can cause segregation. The higher the percentage of crude oil, the larger the decrease in strength. The study showed 13% to 22% strength loss of the concrete with 1% crude oil, 24% to 32% strength loss for 2% crude oil, and 52% to 64% strength loss with 5% crude oil (Osuji and Nwankwo 2015).
- A study of the strength of mortar containing oil-contaminated sand indicated that the highest compressive strength was obtained using sand with 1% oil contamination. At 10% oil contamination, there was an 18% decrease in the strength of the mortar compared to uncontaminated samples. The authors concluded that by increasing the crude oil content from 10% to 20%, the compressive strength decreased significantly and in this condition, the oil contamination in the mix hindered the hydration process of the cement (Abousnina et al. 2015).
- A report titled “Solidification/Stabilization of Soft River Sediments Using Deep Soil Mixing” concluded that the presence of concentrated organic material generally impedes the soil cement reaction by coating the cement particles, thereby preventing free combination of soil and cement particles. The authors indicated that this phenomenon could be overcome using higher doses of cement. The results of unconfined compressive strength tests indicated a detrimental effect on the jet grout-treated soil strength when the percentage of motor oil was greater than 10% by wet weight. At this concentration level, the oil had a pronounced coating effect that inhibited the hydration of the cement, and in turn resulted in a lower unconfined compressive strength (Maher et al. 2005).
- The impact of hydrocarbons on hardened concrete appears to vary and be affected by the type of hydrocarbons. Some authors indicate that hydrocarbons can reduce the long-term strength gain of concrete, sometimes by up to 25% (Wilson et al. 2001), while others indicate the effects on hardened concrete are not significant (Lea 1970 and Biczok 1964). In particular, Murdock et al. (1968) reported that petroleum oils and coal-tar distillates had no or very slight effect on hardened concrete strength and durability.

The published literature reviewed generally referred to low-density contaminants similar to the fuel oil found at the site. However, the majority of the hydrocarbons identified consisted of coal tar, a high-density

contaminant. The project team determined that the higher density contaminants were more likely to be encapsulated within the jet grout column and would not disperse during jet grouting.

Environmental Geo-probe Investigation

A geo-probe investigation plan was developed to determine the extent and concentration of hydrocarbons along the proposed embankment alignment. The test program extended from Sta. 10+20 to Sta. 19+00, with four geo-probes to be performed every 80 ft within the width of the proposed embankment. If hydrocarbons were encountered at a test station, additional geo-probes were performed in between test stations. The geo-probe investigation was completed within 3 weeks with a total of 54 geo-probes performed. Based on the environmental investigation, it was determined that hydrocarbons were present between about Sta 11+00 to Sta 18+00. In general, the concentration of hydrocarbons was well below 10,000 PPM (i.e. 1% by wet weight), with only three locations testing with hydrocarbons contents slightly greater than 10,000 PPM, as shown in Figure 6.

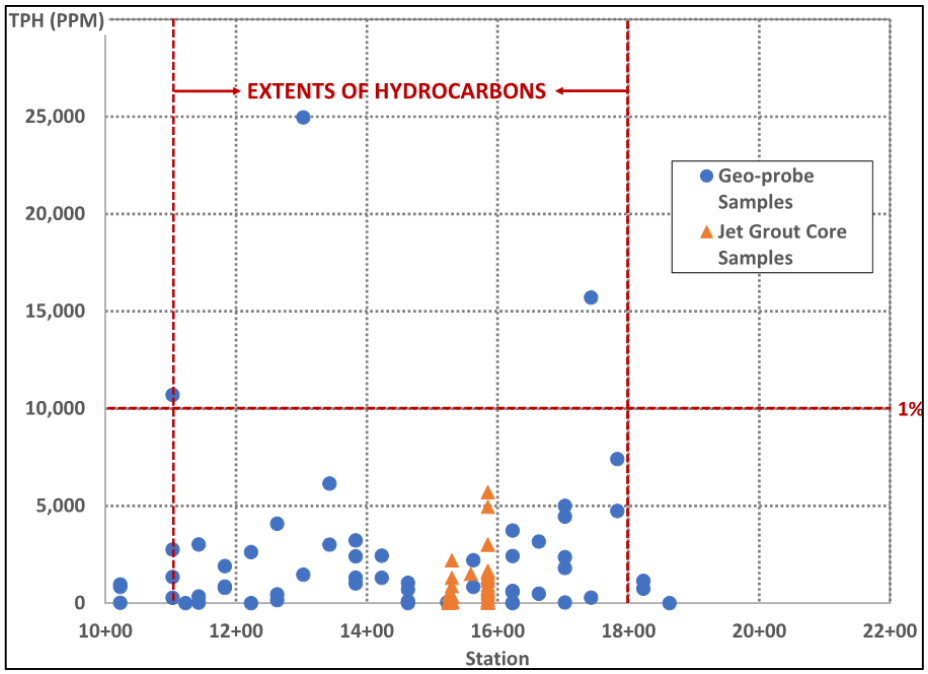


Figure 6. Geo-probe TPH test results by station.

Second Jet Grout Field Test Program

Using the information from the environmental geo-probe investigation and that found in the literature research, a second jet grout field test program was developed. Two test locations were selected. The first test area was located between Sta. 14+99 and Sta 15+50, close to the first field test site, an area with hydrocarbons. The second test area was located between Sta. 10+27 to Sta 10+51, in an area with no hydrocarbons. At each test location, a minimum of four pairs of jet grout columns were installed. Each pair of columns was installed with different jet grout parameters as follows: one pair of columns was installed using very low air pressure (0-2 bars); another pair of columns was installed using medium air pressure (3-5 bars); another pair of columns as installed using high air pressure (8-10 bars); and the last pair of columns was installed using double pass where the jet grout column was grouted, re-drilled, and re-grouted. In addition, two different grout mixes were used for each column in the pairs with one grout mix using 25% slag and 75% cement, and the second grout mix using 50% slag and 50% cement.

The results of the laboratory testing performed for this second test program indicated a general trend of increasing UCS with decreasing air pressure used during jet grouting. For jet grout-treated soil core samples obtained from jet grout columns installed with 0-2 bar air pressure, the minimum UCS was about 450 psi (Figure 7). Within the marine sediment stratum, the UCS values obtained from these jet grout columns

ranged from 465 to 1385 psi, whether or not hydrocarbons were present. For jet grout columns installed with medium to high air pressure UCS values as low as 85 psi were obtained. The columns installed using a re-stroke phase produced jet grout of a similar strength to typical columns, however they had better quality and homogeneity in the cores. Based on the results of the second test program, the project team opted to proceed with jet grout installation in both areas with and without hydrocarbons, using low air pressure during grout injection. If the contractor came across any areas where the hydrocarbons contents appeared to exceed values measured during the environmental geo-probe test program, double pass jet grout columns would be installed.

Additionally, the UCS and triaxial shear strength test results for both test areas were well correlated, which confirmed that relying on solely UCS testing during the production phase would provide sufficient quality control.

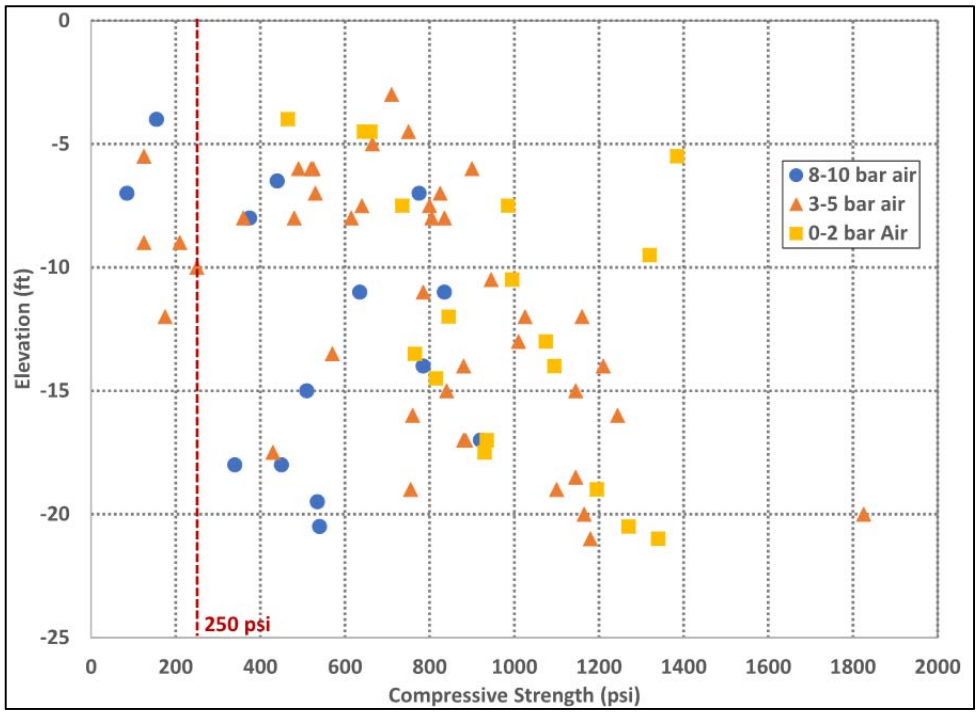


Figure 7. UCS vs. air pressure during jet grout test column installation for second test program.

PRODUCTION QUALITY CONTROL

The specifications required the Contractor to obtain full-depth cores from 2% of the total number of production jet grout columns, as selected by the Designer. Two core samples from within each soil stratum along the column would then be selected for UCS testing. Typically, production quality control cores were obtained from within 1 ft of the design column diameter or in the column overlap; this allowed to confirm the jet grout column diameter as well as provide UCS test data from the peripheral areas of the jet grout column where the UCS strength was most likely to be lower (in comparison to cores obtained from the center of the column).

Figure 8 illustrates the results of the jet grout production UCS test results spatially throughout the proposed embankment alignment. Figure 9 shows the relationship between TPH concentration observed during the geo-probe investigation and the UCS test results from the jet grout-treated soil cores. In general, the minimum 250 psi UCS design value specified was achieved within all soil strata, regardless of the hydrocarbons content. A few UCS tests indicated UCS lower than 250 psi; at these locations the Designer requested additional cores in the same column and it was determined that the lower strengths represented localized conditions with the average UCS over the full height of the column meeting the minimum requirements.

Jet grouting was completed successfully with all production jet grout columns accepted. No double pass jet grout columns were necessary.

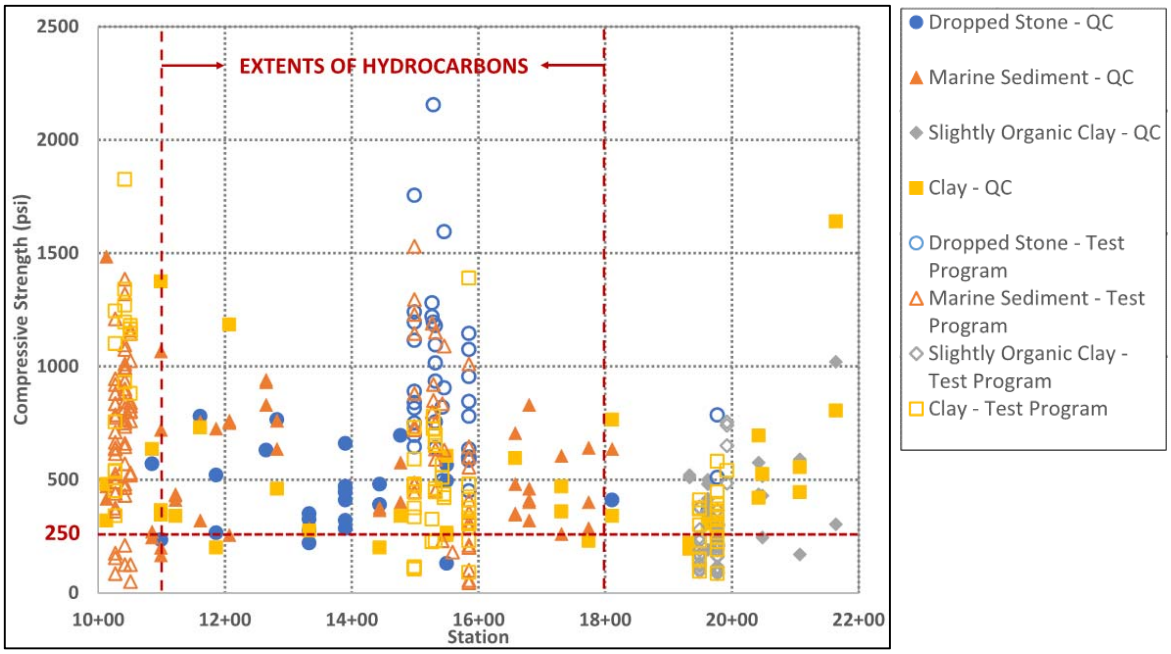


Figure 8. Pre-construction and quality control UCS test results by station.

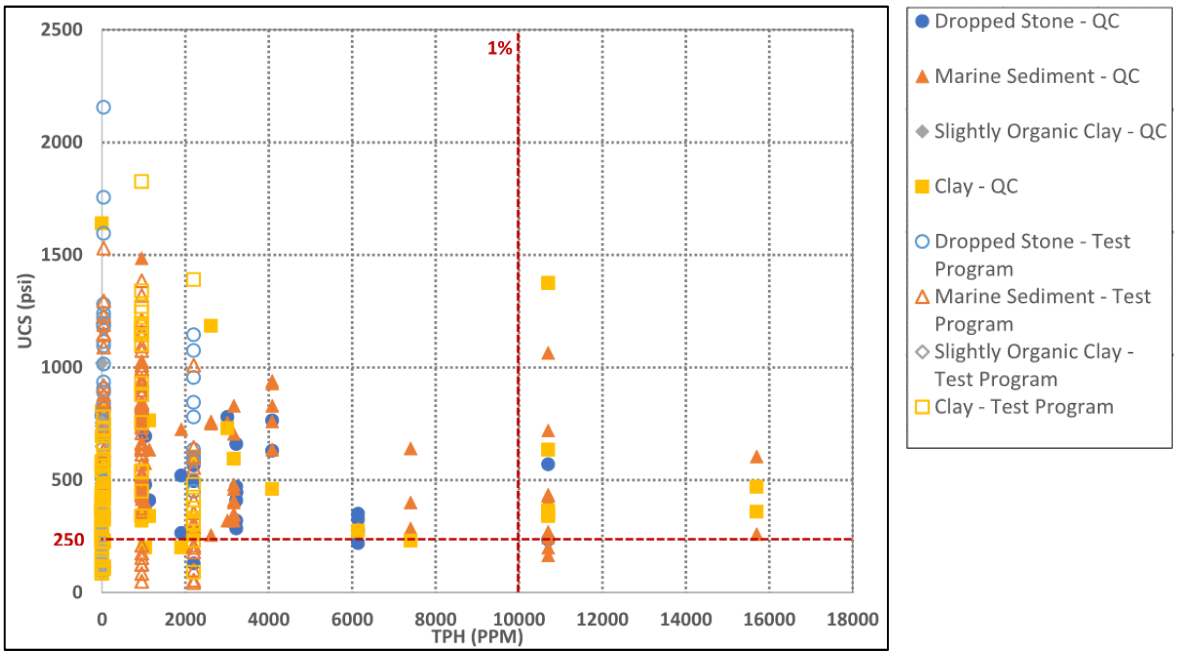


Figure 9. Pre-construction and quality control UCS test results correlated to maximum TPH value at nearest geo-probe test station.

LESSONS LEARNED

The challenges that the project team faced on this project were addressed in a collaborative approach. We summarize the following lessons learned when performing ground improvement using grouting methods in soils with hydrocarbons:

- Even though information that is found in a literature review does not directly correspond to the site conditions for a given project, it can be useful for informing decision making and manage expectations.
- The type and concentration of hydrocarbons combined with the design requirements impact the ability of the Contractor to achieve the project goals. While the hydrocarbons were noticeable during the jet grouting process, the level of hydrocarbons at the site was not high enough to impede the Contractor from achieving the target strength.
- The variable strength of the jet grout-treated soil formed during jet grouting, with or without hydrocarbons present, requires a comprehensive testing program to ensure that the design strength is sufficiently achieved throughout the project.
- The means and methods that the Contractor chose impacted the strength and size of the jet grout columns. It is important for the project team to rely on the expertise of the Contractor to select appropriate jet grout parameters for the site conditions. When the site conditions differ from what is expected, a collaborative effort that includes the unique expertise of the Designer, the Contractor, and the Owner will allow the project team to develop an optimal approach to problem solving.

REFERENCES

Abousnina, R.M., Manalo, A., Lokuge, W., and Shiau, J., 2015. Oil contaminated sand: an emerging and sustainable construction material. Procedia Engineering 118, 1119-1126.

Biczok, I., 1964. Concrete Corrosion and Concrete Protection. Publishing House of the Hungarian Academy of Sciences, Budapest, Hungary.

Lea, F. M., 1970. The Chemistry of Cement and Concrete, 3rd Ed. Edward Arnold (Publishers) Limited, London, England.

Maher, A., Najm, H., and Boile, M., 2005. Solidification/stabilization of soft river sediments using deep soil mixing (FHWA-NJ-2005-028). State of New Jersey Department of Transportation, NJ, 44 p.

Murdock, L. J. and Blackledge, G. F., 1968. Concrete Materials and Practice, 4th Ed. Edward Arnold Publishers Limited, London, England.

Osuji, S.O., and Nwankwo, E., 2015. Effect of crude oil contamination on the compressive strength of concrete. Nigerian Journal of Technology, 34(2), 259-265.

Spooner, P.A., Hunt, G.E., Hodge, V.E., and Wagner, P.M., 1984. Compatibility of grouts with hazardous wastes (EPA-600/2-84-015). JRB Associates, MacLean, VA and U.S. Environmental Protection Agency, Cincinnati, OH, 147 p.

United States Environmental Protection Agency, 2006. In situ treatment technologies for contaminated soil: engineering forum issue paper (EPA 542/F-06/013). 35 p.

Walker, A.D. Site remediation using soil mixing techniques on a hazardous waste site: a case history. Accessed 12 April 2019. https://pdfs.semanticscholar.org/ddb5/4e5faf1655fdc84d31b43b26170dbff3b672.pdf.

Wilson, A., Langdon, N.J., and Walden, P.J., 2001. The effects of hydrocarbon contamination on concrete strength. Geotechnical Engineering, 118(3), 189-193.

USE OF EPS FOR ROADWAY EMBANKMENTS ON SOFT SOILS

Mona B. Anwar, Associate Professor, Civil Engineering, Faculty of Engineering and Materials Science, German University in Cairo, Cairo, Egypt. Email: mona.anwar@guc.edu.eg

Sherif S. AbdelSalam, Associate Professor, Civil & Infrastructure Engineering & Management, Faculty of Engineering and Applied Science, Nile University, Giza, Egypt, 12588. Email: sabdelsalam@nu.edu.eg

Sylvia S. Eskander, Teaching Assistant, Civil Engineering, Faculty of Engineering and Materials Science, German University in Cairo, Cairo, Egypt. Email: sylvia.emil@guc.edu.eg

ABSTRACT

Expanded Polystyrene (EPS) geofoam has long been used in numerous geotechnical applications due to its lightweight and durability. Among these applications is the use of EPS as an alternative fill material to conventional roadway soil embankments. This study investigates the benefits of using EPS roadway embankments to reduce the induced stresses and strains on the underlying peat and soft clay. Firstly, mechanical and interface properties of the EPS were acquired from a companion study that also considered the cyclic loading and creep effects. In order to determine the actual stress-strain distribution within the EPS blocks, a physical prototype was developed in this study with overall dimensions of 1.2 x 1.0 x 0.5 m, with a density of 35 kg/m^3. The prototype EPS blocks were subjected to cyclic loading with intensities ranging from 10 to 50 kN. Then, a numerical model was developed to simulate the behavior of EPS roadway embankments. The numerical model outcomes were verified against the prototype measurements. A parametric design study was also conducted to develop a correlation between EPS embankment height and the stress-strain that occur in the underlying strata. Results showed that EPS embankments could reduce stress and settlement in the underlying soil by about 40% and 54%, respectively.

EPS APPLICATIONS AND BACKGROUND

Expanded Polystyrene (EPS) geofoam blocks have been effectively used during the past several decades in numerous geotechnical applications. EPS static and dynamic properties as well as interface behavior were extensively characterized in various published studies such as that conducted by Horvath, 1994; Stark et al., 2004; Zarnani and Bathurst, 2008; Trandafir et al., 2010; Athanasopoulos et al., 2012; AbdelSalam and Azzam, 2016; and others. However, to be able to use locally produced EPS blocks, its physical and mechanical properties must be thoroughly determined. The lightweight and compressible material of EPS geofoam makes it suitable both as a backfill and for absorbing pressure in both the vertical and horizontal directions. Kim et al. (2010) adopted EPS as an alternative for soil backfill around buried pipes; their model showed a reduction in the vertical stress acting on the pipes by up to 36%. Oshati et al. (2012) presented a case study of a field-instrumented box culvert with EPS blocks on top, which reduced vertical stress by 58%. Meguid et al. (2017) used an EPS inclusion to surround culverts and achieved up to 72% stress reduction, depending on the EPS density and the culvert depth to width ratio. AbdelSalam et al. (2017) used a relatively thin EPS inclusion behind flexible cantilever retaining walls, verifying that the lateral pressure can be significantly reduced by 25%; they also developed a design chart for this application. Moreover, AbdelSalam et al. (2019) investigated the use of EPS as a lightweight alternative for soil backfill above shallow tunnels. It was found that EPS had created a

© 2019 Deep Foundations Institute

differential movement between the wedge located above the tunnel and the neighboring soils, which accordingly reduced the vertical stress acting on the tunnel by 85%, due to the use of lightweight EPS material and positive soil arching.

Globally, the usage of EPS for roadway embankments is still occasional. According to Alfheim et al. (2011), EPS blocks were first used in 1972 for roadway construction in Norway, after assuring that these blocks can sustain repetitive stresses from road pavement and live loads, and after confirming durability. In 1972, EPS was selected due to its light load on the peat and soft clay sub-soils, which reduced the total settlement. Several other studies were conducted to assess the efficiency of using EPS under roadways. Aaboe (1985) created a prototype at the Norwegian Road Research Laboratory as part of the Lokkeberg Bridge project to test the creep behavior of EPS with 20 kg/m^3 density. Results provided by Aaboe (1993) indicated that the stress distribution in EPS blocks is 1 Horizontal (H):1.8 Vertical (V), and recommended using an optimum ratio of 1H:2V. Since that time, the use of EPS was adopted in a number of roadway and bridge abutment projects all over the world (Aaboe, 2011). Use of EPS was also featured in the Montana Department of Transportation design manual, which endorsed the use of EPS as backfill material for roadways because EPS can eliminate the bulk forces acting on the sub-soil strata, reduce stresses and settlement, and provide more stability to the embankment (MDT, 2008). MDT (2008) also recommended EPS use for projects with tight schedules. In 2016, Ozer carried out a study on the use of EPS blocks for roadway widening to enhance the performance of an earth embankment under seepage, and it was successful. However, it was found that to improve the stability of the EPS blocks, the minimum amount of earth fill was needed. In the Middle East and North Africa (MENA region), using EPS is still very limited, especially in applications related to roadways and bridge abutments (AbdelSalam et al., 2018).

In this study, the main goal was to adopt the locally manufactured EPS blocks of density 35 kg/m^3 as a replacement for conventional compacted soil embankments for roadways, especially those constructed on soft soils such as peat or soft clay. The study involved building a physical prototype in the laboratory to determine the stress-strain behavior of large EPS blocks under vehicular loads, and then developing a numerical model to match the prototype behavior using the hardening soil (HS) constitutive model of the software Plaxis 2D v.17 (Brinkgreve et al., 2015). The main outcomes of the prototype and numerical model give an idea of the expected amount of reduction in stress transmitted to the subsoil and the resulting settlement. Furthermore, a parametric study was carried out to determine the correlation between EPS embankment height and stresses in the underlying sub-soil.

EPS PROTOTYPE AND NUMERICAL MODEL

A laboratory prototype was prepared and tested in this study to observe the actual behavior of EPS blocks subjected to cyclic loads. This prototype was chosen in order to consider any possible effects in the material behaviors due to the block dimensions, as typically small EPS samples are used to determine the material's main properties. The prototype consists of two rectangular EPS blocks with density 35 kg/m^3, with dimensions 1.0 x 1.0 x 0.25 m for the upper block, 1.2 x 1.0 x 0.25 m for the lower block, and placed on a concrete slab. A rectangular steel plate 70 x 20 cm was placed on top of upper block to distribute the concentrated applied load. To investigate the stress distribution and the settlement of and within the blocks, two displacement gauges were placed at two different levels: displacement gauge 1 was placed on the upper block adjacent to the steel plate, and displacement gauge 2 was placed between the two blocks, as can be seen in Figure 1. Both displacement gauges

were totally disconnected from the loading frame and the EPS blocks. The instrumented block were placed under a steel loading frame that included a hydraulic jack and a pressure gauge with a maximum capacity of 250 kN. The EPS was loaded in increments from 10 kN to 50 kN (i.e., stress from 71 to 427 kPa). The loads of each increment was applied in stages, each represented 20% of the total load as recommended by ASTM D1196 (ASTM, 2016).

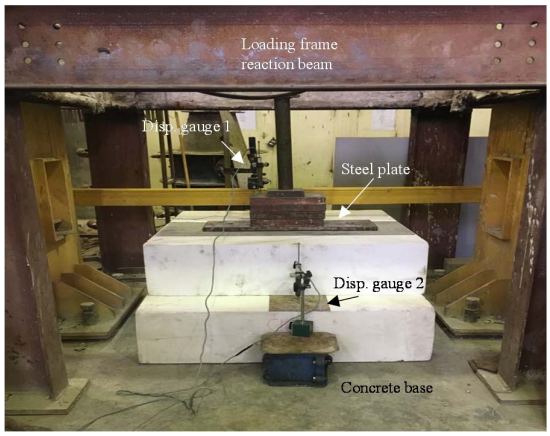


Figure 1. EPS laboratory prototype setup

The applied stress was measured through the pressure gauge. However, the strain induced in each block during each load increment was obtained by dividing the measured displacement with the initial thickness (t = 250 mm). The transferred stresses to the EPS blocks were calculated from multiplying the obtained strain by the modulus of elasticity of the material. The stress-strain behavior was plotted and presented in Figure 2 using a semi-log scale. These curves showed the applied stresses; the transferred stress to the upper block; and the transferred stress to the lower block. The results showed that a maximum strain in the upper and lower blocks were 5.65% and 0.7%, respectively, with an average value of about 3.18%. From the figure, it was noted that there is a difference between the applied and transferred stresses to the upper and lower blocks, which was around 35% and 90%, respectively. This could be due twofold: 1) load distribution on a larger area inside the upper EPS block; and 2) and possible localized crushing in the EPS beads under the steel plate.

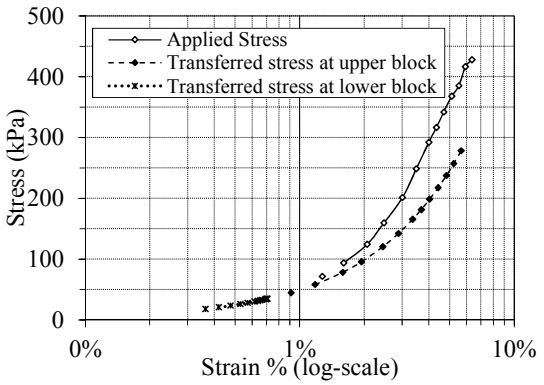


Figure 2. Difference between applied and transferred stresses in the EPS blocks

A numerical model was developed on Plaxis 2D v.17 for the EPS blocks using the same geometry, boundaries, and loading conditions of the prototype. The numerical model was conducted in an attempt to mimic the observed behavior from the laboratory prototype. The hardening soil (HS) constitutive model was used to simulate EPS behavior. The used EPS

properties for the HS model were based on measurements from other studies by AbdelSalam et al. (2018) and AbdelSalam et al. (2019) and after taking into consideration the size effects based on the EPS block dimensions. Accordingly, EPS initial modulus of elasticity, E_o, cohesion, c, and angle of internal friction, ϕ were determined as summarized in Table 1, which also includes Poisson's ratio, ν, and an interface reduction factor, R_{inter}.

Table 1. EPS properties used in the numerical model of prototype

Constitutive Model	Hardening Soil (HS)
γ (kN/m^3)	0.35
Cohesion, c (kPa)	84
Friction angle, ϕ (°)	35
Dilitancy angle, ψ(°)	6
Initial stiffness, E_0 (kPa)	4924
Secant stiffness, E_{50} (kPa)	4672
Poisson's ratio, ν	0.20
Interface reduction factor, R_{inter}	0.60

The numerical simulation was based on finite element (FE) analysis using a 2-dimentional (2D) plane strain model. The initial model is shown in Figure 3(a), where two EPS blocks, with dimensions 1.0 x 1.0 x 0.25 m for upper block and 1.2 x 1.0 x 0.25 m for the lower block, were used. The bottom boundary was fixed in both directions to simulate the concrete base; however, in the vertical direction the foam blocks were simulated to be able to settle vertically and expand horizontally. An unstructured 15-noded mesh was generated as shown in Figure 3(b), and load (A) was assigned on six phases starting from 10.5 to 60 kN/m to give stresses ranging from 70 to 400 kPa according to ASTM D1196 (ASTM, 2016), and to match test procedures adopted for the physical prototype. This was achieved by applying this load on a metal plate with a width of 0.15 m. It is worth noting that a 3-dimentional (3D) model would have been a better means to simulate EPS blocks; however, 3D was not available for this study. However, AbdelSalam et al. (2017) indicated for similar case studies that involved EPS that the difference between the 2D and 3D models is limited to around 5%.

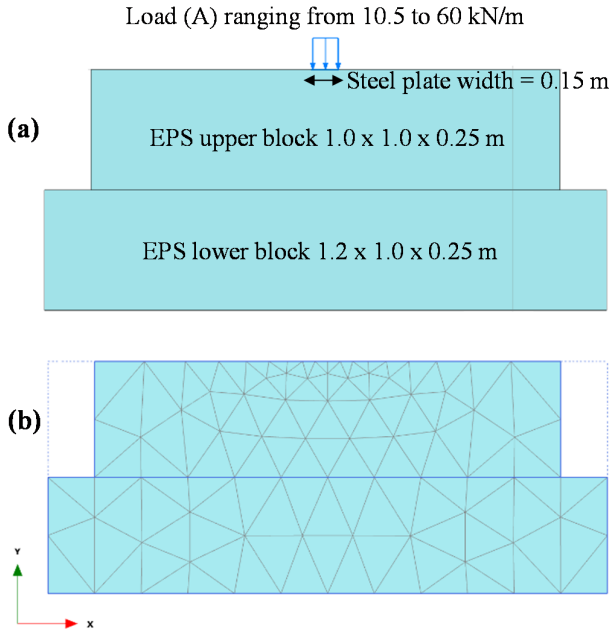


Figure 3. EPS blocks model: (a) geometery; and (b) unstructured undeformed mesh

Figure 4(a) shows displacement in the y-direction, Δ_{yy}, and it was found that the displacement was concentrated below the applied stress with a maximum value at the last loading phase (i.e., 400 kPa) of approximately 15.8 mm. The Δ_{yy} decreased with respect to EPS depth, which reached a value of around 2.0 mm at the interface between the EPS blocks. This was comparable to the measured displacements from the physical prototype at a maximum applied loading of 427 kPa. The measured displacement from the upper block of the prototype was 14.11 mm, and at the interface was 1.75 mm. Figure 4(b) shows the distribution of the effective normal stress, σ'_{yy}, induced in the EPS blocks during the last loading phase. The figure illustrates that the maximum transferred stress at the interface between the two blocks was 40 kPa, which is similar to that measured from the prototype.

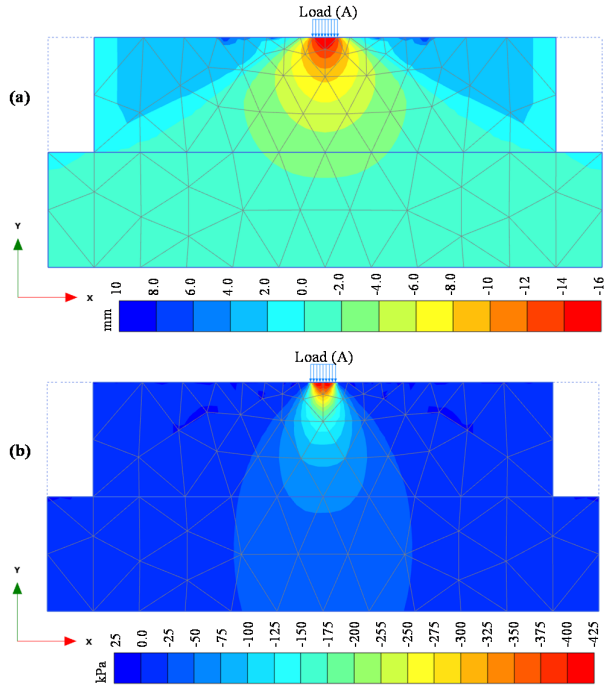


Figure 4. Numerical model outcomes: (a) displacement Δ_{yy}; and (b) stress σ'_{yy}

Figure 5(a) represents the stress-strain response of the EPS at two points, the first is located on top of the upper block (d = 0 m), and the second along the interface between blocks (d = 0.25 m). The stress-strain curves shown in the figure were based on measurements from the prototype and from the numerical model. For the response at d = 0 m, it can be seen that there is a similarity between the measured and the calculated curves, with a difference in the strains at the peak stress that ranged from 0.7% to 1.1%. At d = 0.25 m, there is a good match between the measured and calculated curves, especially along the initial portion of the curve until 2% strain, then the difference in the stresses did not exceed 15.7% at peak strain. Figure 5(b) represents the stain distribution along the EPS block depth (starting from 0 m at top, until 0.5 m at bottom), at various normal stress values. The curves shown in the figure were based on measurements from the prototype and from the numerical model.

From the curves, it is clear that the strain distribution decreases with respect to EPS depth, as expected. In addition, the differences between the measured and calculated curves are small, and they follow the same trend. Hence, the calculated outcomes of the numerical model can be considered acceptable at low strain ranges, limited to around 2%. This would mean that the HS constitutive model of Plaxis 2D was verified and considered appropriate for simulating EPS inclusions used in other geotechnical applications.

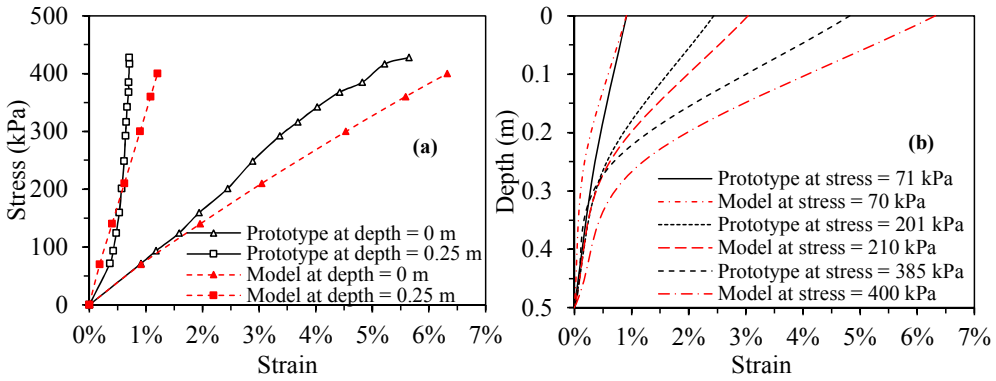


Figure 5: Numerical model outcomes: (a) displacement Δ_{yy}; and (b) stress σ'_{yy}

USE OF EPS FOR ROADWAY EMBANKMENT

A numerical study was conducted using Plaxis 2D v.17 to investigate the potential benefits of using EPS blocks as an alternative for conventional soil embankment of roadways. The study evaluated the change in the embankment height and the corresponding reduction in stresses and settlement in weak sub-soils consisting of peat and soft clay. Two types of fill materials were used as an embankment, the first was compacted well-graded sand, and the second was EPS blocks with density equal to 35 kg/m^3. The time required for the clay or peat sub-soil to consolidate was also calculated in order to estimate the total construction time required for each case. EPS was modeled using the HS material parameters given in Table 1. To simulate rigid pavement, a concrete slab was placed on top of the embankment and modeled using the linear elastic model. Table 2 summarizes all the material properties used.

Table 2: Soil parameters used in the roadway numerical model

Material	Embankment	Sand	Peat	Clay	Concrete
Model	Mohr Coulomb	Mohr Coulomb	Soft Soil	Soft Soil	Linear Elastic
γ_t (kN/m^3)	16	17	8	15	25
γ_{sat} (kN/m^3)	19	20	12	18	-
Initial void ratio	0.5	0.5	2	1	-
Modified comp. index	-	-	0.15	0.05	-
Cohesion, c (kPa)	1	0	23	25	-
Friction angle, ϕ (°)	30	33	2	1	-
Dilitancy angle, ψ (°)	0	3	0	0	-
Initial stiffness, E_{ref} (kPa)	2.5x10^4	3.5x10^4	-	-	3.0x10^7
Secant stiffness, E_{50} (kPa)	2.5x10^4	3.5x10^4	-	-	-
Permeability, k_x (m/day)	3.499	7.128	0.10	0.0475	-
Permeability, k_y (m/day)	3.499	7.128	0.05	0.0475	-

The main model is shown in Figure 6. The top soil layer consisted of peat from 0 to 3 m, followed by soft clay from 3 to 6 m, and sand down to 10 m, where the ground water level was -1.0 m from sub-soil surface. The roadway width was 16 m with side slopes of 3H:1V. The slope 3H:1V was selected based on typical values used in practice, which can be changed when using EPS embankments, as discussed later. The height of the embankment was the main variable in the parametric study, which ranged from 1 m to 10 m, and accordingly the

total width of the embankment base, B, varied as well from 14 m up to 38 m. This means that increasing the embankment height led to a significant increase in the base width, which should eventually reduce acting stresses on the underlying sub-soil but may increase the construction cost. As shown in Figure 6, a distributed stress of 50 kPa was applied to the top of the concrete slab to represent the roadway vehicular loads. The vertical boundary at the right side was released in y-direction, and the bottom boundary was fixed in both directions, knowing that the vertical boundary at the left side that represent the centerline of the roadway was totally released. An unstructured 15-noded mesh was generated, while the analysis was conducted using 12 stages as follows: 10 equal stages to increase the embankment height from H = 1 m to 10 m, one stage for the concrete slab, and the last stage for live load application. The sub-soil layers were left to consolidate in each stage until reaching the minimum pore water pressure of 1.0 kN/m^2. The model was evaluated first using a soil embankment, and again using EPS blocks as the embankment.

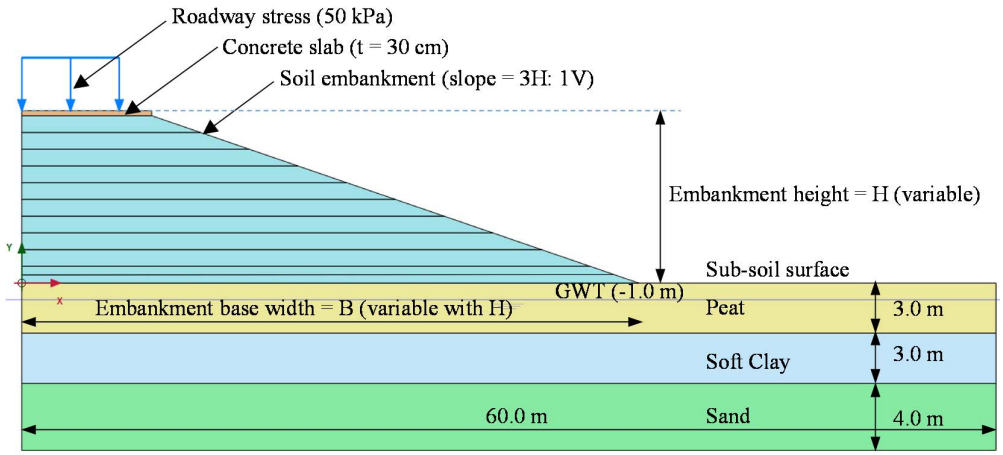


Figure 6: Numerical model geometry for the roadway embankment

Figure 7 represents outcomes of the roadway model where soil and EPS embankments were used at H = 10 m. For the soil embankment, Figure 7(a) shows vertical displacement in the y-direction, Δ_{yy}, which reached 1.80 m, corresponding to a consolidation time of 83 days. A slope 3H:1V was used to avoid general shear failure in the embankment and bottom soft soil, and to ensure the stability of the embankment. Figure 7(b) shows the distribution of the effective normal stress, σ'_{yy}, induced in the underlying soil due to the soil embankment and roadway loads, where the maximum stress reached 324.6 kPa. By replacing the soil embankment with lightweight EPS blocks, the model outcomes were totally changed. As can be seen in Figure 7(c), Δ_{yy} reached a maximum value of 0.84 m (i.e., 53.3% less than the previous case) and a consolidation time of 40 days. Figure 7(d) represents the induced σ'_{yy} in the underlying soil with a maximum value limited to 198 kPa, which is 39% less than the previous case. Another observation comparing Figures 7(a) with 7(c), the lateral stress spread within the roadway side slope was reduced by using EPS instead of soil embankment. This means that the side slopes can actually be reduced by using EPS, and this may result in changing the typical slope of the roadway embankment from 3H:1V to 2H:1V. However, a future parametric study may be considered to address this aspect in more detail.

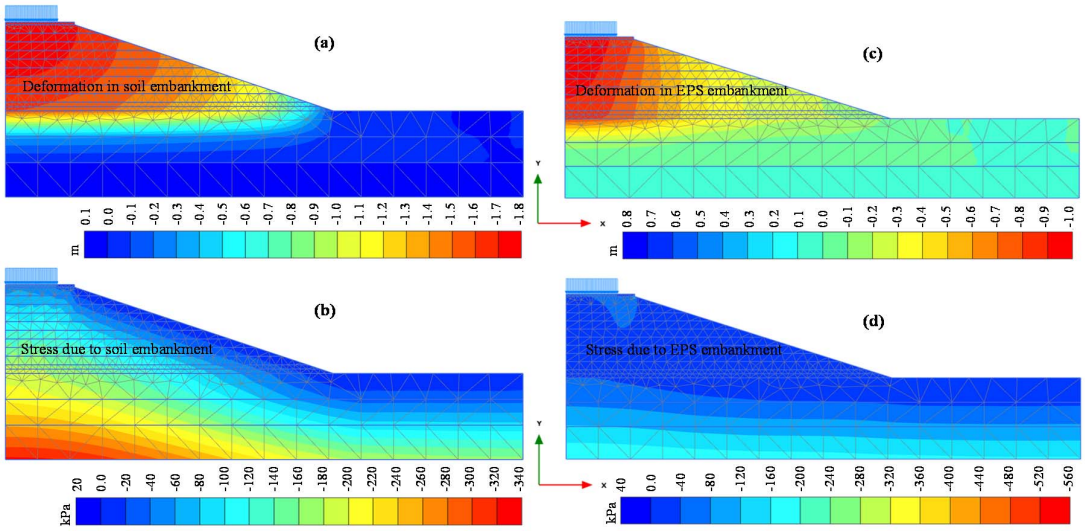


Figure 7: Roadway embankment model outcomes: using soil (a) disp. Δ_{yy}; (b) stress σ'_{yy}; using EPS (c) disp. Δ_{yy}; and (d) stress σ'_{yy}

Figures 8(a) and 8(b) illustrate vertical settlement, Δ, with increase in soil embankment height. The figures also show a similar correlation with the use of EPS blocks, and it was found that the settlement was almost constant with increasing EPS height. This is because the base-width (B) significantly enlarged by increasing the embankment high (3H:1V), which eliminated the EPS weight effect on increasing stress-settlement on the sub-soil. Accordingly, the correlation was normalized as presented in Figure 8(c) in order to remove the effect of the roadway base-width enlargement. Figure 8(d) shows the final consolidation time required for soil as well as EPS embankments.

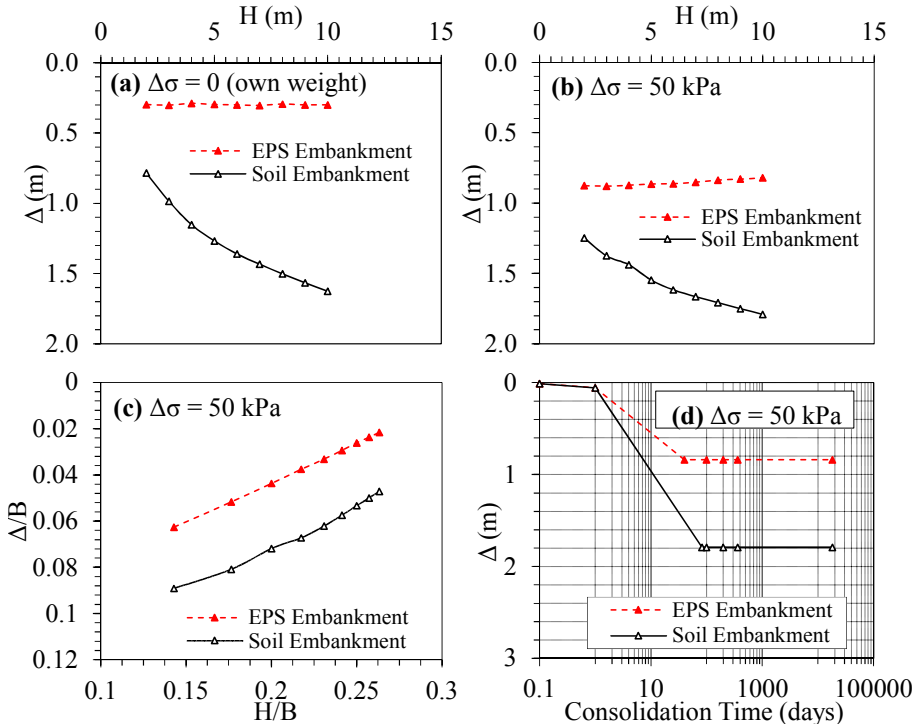


Figure 8. H vs. Δ (a) Δσ = 0; (b) Δσ = 50 kPa; (c) normalized; and (d) consolidation time

Figure 9(a) represents the expected increase in effective vertical stresses in the sub-soil under the roadway when using soil and EPS embankments. Outcomes from the figure are similar to the aforementioned, which indicates that using EPS did not cause any noticeable increase in the stresses even after increasing the embankment height to 10 m. It is also worth noting that the difference in the maximum stresses was reduced by about 39% when using EPS blocks. Figure 9(b) shows that using EPS embankments with soft soils reduced the construction time of the model roadway embankment by an average of 48%, which is depending on the required embankment height and reaching the minimum pore water pressure of 1.0 kN/m^2.

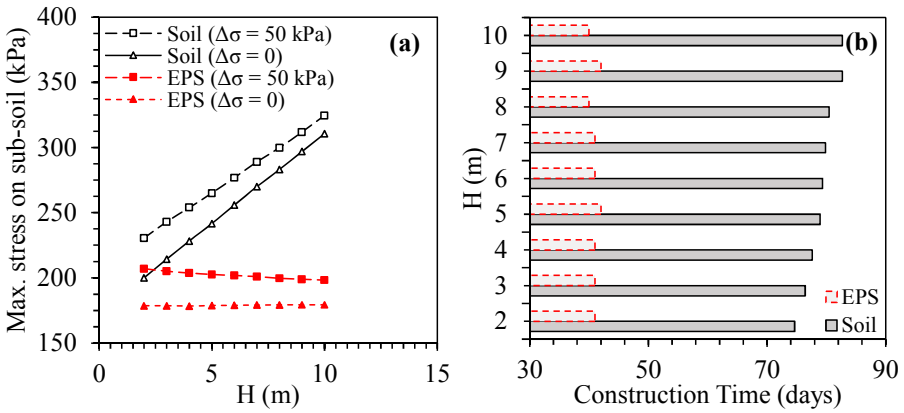


Figure 9. (a) Maximum Stress vs. Embankment Height; and (b) Construction Time

CONCLUSIONS

A prototype was assembled in the laboratory to measure the actual stress-strain behavior of EPS blocks at different depths within the blocks, when subjected to uniaxial cyclic loading. The hardening soil constitutive model was utilized to simulate the actual behavior of large EPS blocks at a low strain range limited to around 2%. Accordingly, a numerical model for a typical roadway embankment was established to investigate the advantages of using EPS blocks as an alternative for conventional soil embankments for roadways. The analysis was mainly concerned by the effect of change in the embankment height and the corresponding reduction in stresses and settlement in the underlying sub-soils of soft clay and peat. Major outcomes can be summarized as follows:

- Replacing the soil embankment by EPS blocks significantly reduced the vertical stress in the weak sub-soil by 39% and reduced the settlement by 53% with increasing the embankment height up to 10 m.
- Using EPS blocks reduced the consolidation time required for the weak sub-soil by 45% to 51%, for embankment heights ranging from 2 to 10 m, respectively.
- The roadway embankment side slope can be reduced from 3H:1V to 2H:1V by using EPS blocks instead of soil, which requires further investigation due to its significant effect on the construction cost.

REFERENCES

Aabøe R (1985). “13 years of experience with expanded polystyrene as a lightweight fill material in road embankments”. The 1st international conference on EPS geofoam blocks in construction applications, Oslo, Norway.

Aabøe R (2011). “40 years of experience with the use of EPS geofoam blocks in road construction”. The 4th international conference on geofoam blocks in construction

applications, EPS 2011, Lillestrøm, Norway.
AbdelSalam S. S., Jama, R. A., and Salah, M. A. (2019). "EPS inclusion to reduce vertical stresses on shallow tunnels". Geosynthetics International. DOI: 10.1680/jgein.18.00042.
AbdelSalam, S. S. and Azzam, S. A. (2016). "Reduction of lateral pressures on retaining walls using geofoam inclusion." Geosynthetics international, 23(6) pp. 395–407.
AbdelSalam, S. S., Anwar, M. B., and Eskander, S. S. (2018). "Long term behavior of EPS geofoam for road embankments". In: Meguid M., Guler E., Giroud J. (Eds), Advances in geosynthetics engineering. GeoMEast 2018. Sustainable civil infrastructures. Springer, Cham, https://doi.org/10.1007/978-3-030-01944-0_8.
AbdelSalam, S. S., Azzam, S. A., and Fakhry, B. M. (2017). "Reliability and 3D modelling of flexible walls with EPS inclusion." International journal of Geomechanics, 17(7), DOI: 10.1061/ (ASCE) GM.1943-5622.0000853.
Alfheim S, Flaate K, Refsdal, G (2011). "The first EPS geoblock road embankment –1972". The 4th international conference on geofoam blocks in construction applications, EPS 2011, Lillestrøm, Norway.
ASTM D-1196 (2016). "Standard test method for non-repetitive static plate load tests of soils and flexible pavement components for use in evaluation and design of airport and highway pavements". ASTM international, West Conshohocken, PA, USA.
Athanasopoulos, A. Z., Lamote, K., Athanasopoulos, G. A. (2012). "Use of EPS geofoam compressible inclusions for reducing the earthquake effects on yielding earth retaining structures". Soil dynamics and earthquake engineering, vol. 41, pp. 59–71.
Brinkgreve, R. B. J., Kumarswamy, S., Swolfs, W. M. (2015). "Plaxis 3D reference manual anniversary edition version 1". Plaxis, Delft. ISBN-13: 978-90-76016-19-2.
Horvath, J. S. (1994). "Expanded polystyrene (EPS) geofoam: an introduction to material behavior", Geotextiles and Geomembranes, vol. 13, no. 4, pp. 263–280.
Kim, H., Choi, B., and Kim, J. (2010). "Reduction of earth pressure on buried pipes by EPS geofoam inclusions." Geotechnical testing journal, 33(4) pp. 1–10.
MDT Geotechnical Manual (2008). Roadway slopes and embankments. Montana Department of Transportation (MDT) official website, accessed 4-April-2019.
Meguid, M. A., Hussein, M. G., Ahmed, M. R., Omeman, Z., and Whalen, J. (2017). "Investigation of soil-geosynthetic-structure interaction associated with induced trench installation." Geotextiles and Geomembranes, 45(4) pp. 320–330.
Oshati, O. S., Valsangkar, A. J., and Schriver, A. B. (2012). "Earth pressures exerted on an induced trench cast-in-place double-cell rectangular box culvert." Canadian geotechnical journal, 49(11), pp. 1267–1284.
Özer, A. T. (2016). "Laboratory study on the use of EPS-block Geofoam for embankment widening". Geosynthetics International, 23(2), pp. 71-85.
Stark, T. D., Arellano, D., Horvath, J. S., and Leshchinsky, D. (2004). "Geofoam applications in the design and construction of highway embankments." NCHRP project 24-11, transportation research board of the national academies, Washington D.C., USA.
Trandafir, A. C., Bartlett, S. F., and Lingwall, B. N. (2010). "Behavior of EPS geofoam in stress-controlled cyclic uniaxial tests." Geotextile and Geomembranes, 28(6) pp. 514–524.
Zarnani, S. and Bathurst, R. J. (2008). "Numerical modelling of EPS seismic buffer shaking table tests." Geotextiles and Geomembranes, 26(5) pp. 371–383.

AUGERED PILE WORLD RECORD DEPTH WITHIN A SOIL MIX BASEMENT

Andres M. Baquerizo, HJ Foundation Company, Miami, Florida, USA, (305) 592-8181, amb@hjfounation.com
Nicholas Feldt, HJ Foundation Company, Miami, Florida, USA, (305) 592-8181, nrf@hjfoundation.com
Jeremiah J. Filjones, Hayward Baker, Inc., Tampa, Florida, USA, (813) 884-3441, JJFiljones@haywardbaker.com

ABSTRACT

The Estates at Acqualina located in Sunny Isles Beach, FL, is comprised of two, ocean-front, 50-story, luxury towers with podiums and villas. With city regulations now requesting that above-grade floors be limited to commercial or residential units, parking facilities for the tower structures were situated within two levels of underground basement parking. However, ensuring dry excavation through south Florida's highly pervious limestone, immediately adjacent to the beach where the groundwater table is very shallow, can be extremely challenging and costly for developers. In recent years, significant advances have been made to overcome this challenge with the innovative use of deep soil mixing to create a "dry hole", assisting in the construction of foundations and underground usable space for parking, storage, etc. The "dry hole" system includes a soil mix bottom seal, with soil mix secant pile walls in combination with auger cast deep foundation elements to support the future structure. This approach enables groundwater control to greater depths than can be achieved by conventional sheetpiling and dewatering. For the Estates at Acqualina, a successful turnkey, design-build joint venture between two foundation and geotechnical contractors resulted in a dry excavation to 34 ft (10.4 m) below grade and to a record-breaking auger cast pile depth of 182.3ft (55.6 m), all within an aggressive 26-week schedule to deliver the "dry hole" excavation for the first tower. This presentation will discuss the logistics, quality control, design, and safety for the different techniques involved.

Keywords: deep soil mixing, auger cast piles, tie-back anchors, vibro replacement, excavation, dry basements

INTRODUCTION AND BACKGROUND

The Estates of Acqualina is a pair of 50-story luxury towers located on Sunny Isles Beach in Florida with a two-level underground basement for parking. The project's location just steps away from the Atlantic Ocean, geology, and high-water table created a challenging project.

The owner, Trump Group, contracted the joint venture of HJ Foundation and Hayward Baker (HJ/HB) to design-assist-build a system to control the groundwater, allowing the 2-story underground parking structure to be constructed. In order to accomplish this task, the JV utilized an installation technique known as deep soil mixing. This technique mixes the in situ material with a cement slurry to create a very impermeable material called "soilcrete".

A deep soil mix bottom seal area of approximately 130,000 ft^2 (120,77.4 m^2) was installed under the future parking structure, which had a maximum excavation depth of 34 ft (10.3 m) below existing grade, 30 ft (9.1 m) below the water table. The bottom seal was then surrounded by 2,300 LF (700 LM) of soil mix secant pile wall cantilevered shoring, reinforced with steel beams. The north wall of the North Tower included a layer of tieback anchors to further reinforce the shoring.

Additionally, HJ Foundation installed the auger cast piles supporting the structures. Each of the two towers was designed with approximately 200, 36-in. (1 m) piles; the 2-story underground garage was

© 2019 Deep Foundations Institute

designed with approximately 500, 16-in. (0.4 m) piles, and the surrounding podium areas was designed with around 650, 14-in. (0.35 m) piles.

After the installation of the deep soil mix and auger cast piles, vibrated aggregate stone columns were installed to densify and reinforce the soils to support the foundations at the entrance to the new towers. This method was chosen over foundation elements such as augercast piles as they would not conflict with the future utilities and drainage structures also located at the entrance.

Excavation of over 100,000 yd^3 (76,455 m^3) was performed for the tower mat foundations and underground parking structure.

GEOLOGIC CONDITIONS AND SITE CHARACTERIZATION

The site is located next to the Atlantic Ocean right on Sunny Isles Beach in south Florida (Fig. 1). Existing ground surface elevations varied between +7 to +10 ft (+2.1to +3 m) NGVD with groundwater at an approximate elevation of + 2 to +3 ft (+ 0.6 to +1 m) NGVD.

According to the Final Geotechnical Report by the geotechnical engineer Radise International (Radise, 2018), the site geology consists of relatively dense surficial sand above a layer of peat. Beneath the peat, the first layer of limestone was encountered overlaying a series of alternating layers of sand and limestone.

The deep soil mix bottom seal was located in the upper sands, extending through the peat and the first layer of limestone and the production auger cast piles were terminated into the deep limestone layers at approximately 170 ft (51.8 m).



Fig. 1. Site location.

GEOTECHNICAL ANALYSES AND DESIGN CONSIDERATIONS

The design of the “dry hole” deep soil mix system included initial analyses of the in situ soil. Borings from the geotechnical report were reviewed to determine the location of the soil mix plug. Depending on the material being mixed (e.g. peat), provision was made for additional measures such as predrilling to be implemented to homogenize the soil. Prior to installation, bench scale testing, including sampling of the in situ soil, was performed to determine the volume of cement slurry required to be injected into the soil to meet the design strength requirements.

The design of the auger cast piles was specified by the Structural engineer, CHM Structural Engineers, (CSM, 2018) and Radise. The 36-in (1-m) diameter piles supporting the two towers were designed with a compressive strength of 1,200 tons (1088 tonnes) and upon successful load testing were increased to 1,290 tons (1170 tonnes). The production piles were terminated in the deep layer limestone at approximately 170 ft (51.8 m) to provide settlement support.

DESIGN VERIFICATION

Multiple load test piles were conducted prior to the production work to verify the geotechnical design assumptions. ASTM D1143 was followed for the static axial compressive load tests and ASTM D3689 was followed for the static axial tensile load tests.

- Each of the two towers included a sacrificial, full-length, reinforced, dual-layer o-cell load test pile.
- The west parking garage included three sacrificial test piles; one compression test pile and two tension test piles.
- The podium area included four sacrificial test piles; two compression test piles and two tension test piles.

In addition to the sacrificial load test piles, one production pile in the South Tower was installed to a depth of 182.3 ft (55.6 m) with full-length reinforcing, which is a new record for the deepest single-pass augered pile installed to date.

OPERATIONAL LOGISTICS

The scope of the foundation work was required to be performed in a very aggressive 26-week schedule to deliver the South Tower excavation. In order to meet such a schedule, detailed planning was key.

Equipment was mobilized the day following the project award and preparations for the work begun. The existing site grade elevations varied from +7 to +10 ft (+2.1 to +3 m) NGVD consisting of beach sand. The site was cut down to a working grade of +5 ft (+1.5 m) NGVD and stabilized construction roads were built for equipment to traverse the site. Figure 2 shows initial site preparation by the JV. Within two weeks from project start, the soil mix batch plant, two soil mix rigs and a predrilling rig were mobilized.



Fig. 2. Initial site preparation.

PRODUCTION WORK

The 130,000 ft^2 (12077.4 m^2) of soil mix bottom seal was installed using two drill rigs supported by an onsite batch plant (Fig. 3) which produced the cement slurry. Installation began in the South Tower, the critical path. The soil mix bottom seal contoured to the different elevations of the future permanent foundation structure. The perimeter of the bottom seal was then surrounded by soil mix secant piles designed as the support of excavation. A total of approximately 2,300 LF (701 LM) of shoring wall was installed. Figure 4 illustrates the in-place bottom seal, shoring, and anchored north wall shoring. Different soil mixing colors represent different depths or thickness of soil mix columns.



Fig 3. Bottom seal soil mixing underway for the South Tower.

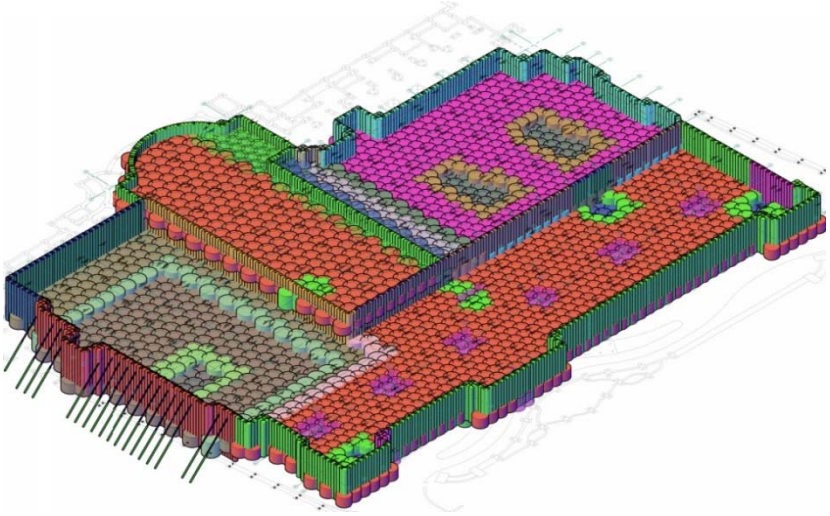


Fig 4. Bottom seal and shoring layout.

Following installation of the soil mix bottom seal and shoring, approximately 1,000 auger cast piles with diameters of 36 in., 16 in. and 14-in. (1m, 0.4m and 0.35 m) were installed through the bottom seal to serve as the foundation for the new towers and adjacent structures (Fig. 5). Additionally, the auger cast piles served as temporary uplift support for the soil mix bottom seal. The auger cast piles included production piles up to a depth of 170 ft (51.8 m) with full length reinforcing.

Subsequently, excavation of over 100,000 yd^3 (76,500 m^3) of soil mixing was performed by the JV for the tower mat foundations and underground parking structures. The soil mix secant pile shoring walls were shaved to within a 4-in (100-mm) tolerance, providing a flat interior face for the future concrete foundation. A layer of #57 stone was then installed on top of the soil mix bottom seal to act as a drainage layer below the water proofing and concrete foundations. Upon completion of the scope, water intrusion was measured to be less than 100 gal/min (378 l/min).

Figure 6 shows the south tower superstructure under construction while the earth support and foundation work was nearing completion for the north tower.



Fig 5. Arial photograph of installed North Tower auger cast pile foundation system.

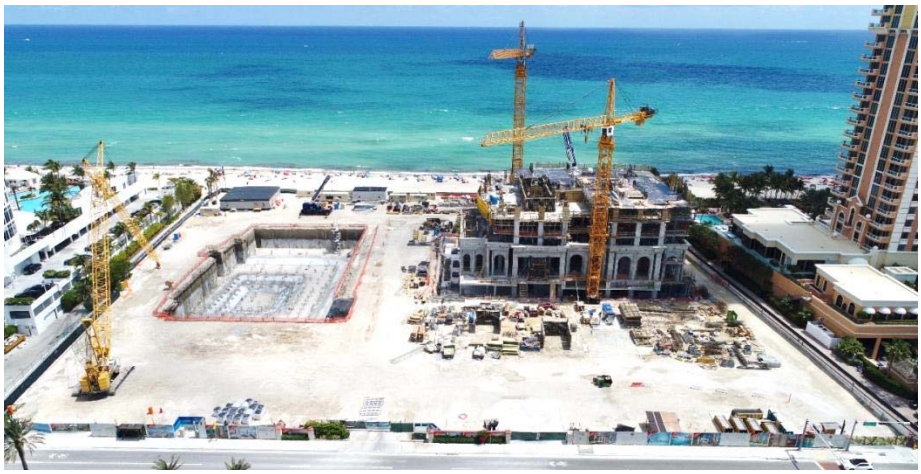


Fig 6. South Tower superstructure under construction while the earth support and foundation work was nearing completion for the north tower.

QUALITY CONTROL ASPECTS

Extensive QA/QC measures were taken throughout the soil mixing and auger cast work.

Soil Mixing

As with all foundation projects, quality control plays a key role in ensuring work installed meets the projects specifications. During the soil mix work, an extensive on-site quality control plan is performed. The drill rigs are fitted with on-board computers to monitor installation data such as depth, drilling rate, mixing energy (blade rotation number or BRN), and specific gravity of and volume of cement slurry injected. On-site field engineers review the installation reports daily and notify the design engineer of any out-of-spec work.

Sampling of material and testing of material is also performed on site by the field engineers. Soil mix material that is freshly mixed, known as "wet grabs", is sampled and screened to remove large debris and then cast into cylinders. The cylinders are stored in on on-site lab set up to ASTM specifications. After the samples are cured, the cylinders are tested in the onsite laboratory by a calibrated UCS machine. The results from the testing are immediately uploaded for the design engineer's review.

The constant monitoring of installation data and material testing allows potential problems to be identified early on, mitigating the need for remedial work.

Auger Cast

The auger cast pile installation was monitored by the 3rd party inspector, Radise, as well as the automated monitoring equipment on the piling rig. Grout from the installed piles was sampled at industry standard of every 50 yd^3 (38 m^3) and cast into brass cube molds. It was extremely important that the sampling, curing, and testing was performed per ASTM standards, since the specified strength of the grout was 9,500 psi (65,500 kPa).

SAFETY DURING CONSTRUCTION

Safety is always paramount, even more so when multiples operations with heavy equipment are occurring at once. It is imperative that each operation is aware of each day's sequence and schedule. To combat this, each day is started with a safety toolbox talk. The short safety meeting is used to discuss safety of the many day's activities, the schedule, and any other pertinent information the crews need in order to be successful.

Another proactive step in keeping a jobsite like this safe is to set clear boundaries around each operation, such as safety fencing or barricades to prevent people and equipment from entering danger zones.

SUMMARY AND CONCLUSIONS

Building a basement in south Florida is a quite challenging due to the geology and high-water table. The recent developments and advancements in soil mixing have created the ability to provide a "dry hole.

REFERENCES

Radise International (2018), Final Geotechnical Investigation and Report, 3.22.18
CHM (2018), Structural Drawing, 2.9.18

CASE STUDY ON THE FREDERICK DOUGLASS MEMORIAL BRIDGE AND THE USE OF LARGE DIAMETER OPEN END STEEL PIPE PILES, WASHINGTON, DC

Michael D. Venezia, P.E., ECS Mid-Atlantic, LLC, Chantilly, VA, (703) 995-6543, MVenezia@ecslimited.com
Karl A. Higgins III, P.E., D.GE, ECS Mid-Atlantic, LLC, Chantilly, VA, (571) 299-6026, KHiggins@ecslimited.com

ABSTRACT

The South Capitol Street Corridor Project is one of the District Department of Transportation's (DDOT) largest projects, and is currently under construction. This case study will focus on the design of the foundation piles for the main spans of the iconic Frederick Douglass Memorial (FDM) Bridge, and will include a discussion of the foundation design evolution from an originally designed alternative foundation system (i.e. coffer dams and drilled shafts), to the current use of driven Large Diameter Open End Pipe (LDOEP) Piles. The paper will provide a discussion of the design methodology used during preliminary engineering and final design, and will highlight insight gained from the extensive load testing program completed to date. The load testing program consists of a combination of high strain dynamic testing (PDA), as well as Statnamic Load Testing on select sacrificial, pre-production test piles. Specifically, data gathered during the nearly-completed load testing program suggests the development of significant internal shaft frictional resistance within the tested LDOEP Piles. This paper will also discuss limitations of currently accepted industry design methods for predicting the capacity of LDOEP piles, a subject that is also currently being researched by FHWA. The data from this test pile program will help design assumptions for future projects.

Keywords: driven piles, large diameter open end pipe piles

INTRODUCTION

The Frederick Douglass Memorial (FDM) Bridge carries South Capitol Street across the Anacostia River in Southeast/Southwest, Washington, DC, and is owned and maintained by the District Department of Transportation (DDOT). The existing FDM Bridge is nearly 70 years old, serves as a major artery into the city, and has been classified as functionally obsolete. As a result of the condition, age and limitations of the existing bridge structure, DDOT deemed it necessary for complete replacement of the bridge. The replacement project consists of the construction of a new bridge traversing the Anacostia River, as well as the reconfiguration of the Suitland Parkway and I-295 interchanges located at the eastern terminus of the FDM Bridge. Final design and construction services for the replacement project were procured by DDOT through a Design-Build contract.

This paper will focus on the driven Large Diameter Open End Pipe (LDOEP) Piles used for support of the main span of the new FDM Bridge which is currently under construction. Discussion regarding the LDOEP Pile design methodology has been included, along with commentary regarding currently available industry guidance related to design and construction of LDOEP Piles. Much insight has been gained during the mostly-completed and extensive load testing program which consists of a combination of high strain dynamic testing (PDA), as well as Statnamic Load Testing on select sacrificial, pre-production test piles. Specifically, data gathered during the mostly-completed load testing program suggests the development of significant internal shaft frictional resistance within the tested LDOEP Piles.

© 2019 Deep Foundations Institute

SUBSURFACE DATA

Sources of subsurface data consisted of a combination of historical geotechnical borings, together with project specific borings drilled within the alignment of the new FDM Bridge. The historical data included borings from the design/construction of the original FDM Bridge (1950's), as well as borings from various other sites in the general project vicinity. Preliminary geotechnical exploration and engineering services performed in connection with the RFP process included 12 borings generally along the proposed alignment between 2012 and 2014. Following contract award to the Design-Build team, a supplemental exploration was performed to include additional borings sited within the footprint of each of the major substructures of the selected FDM Bridge design; this included a total of 8 borings (2 per each of the 4 substructures). Figure 1 provides a graphical depiction of the RFP phase and supplemental borings in relation to the final FDM Bridge alignment and primary substructures. Substantial laboratory testing was included in both the RFP and supplemental explorations.

SE/SW WASHINGTON DC GEOLOGY

This portion of Washington, DC is sited within the Atlantic Coastal Plain Physiographic Province of Washington, DC; this Physiographic province is bounded to the east by the Continental Shelf and to the west by the Piedmont Province. "The Coastal Plain is separated from the Piedmont Province by the Fall Line (or Fall Line Zone), the topographic feature where major streams rapidly descend from the crystalline uplands into tidal rivers, estuaries, and embayments. The Coastal Plain is a wedge of continental and marine sediments that thicken from a few feet on the western boundary to many thousands of feet at the Atlantic Ocean. Potomac Formation deposits of Early Cretaceous age are the basal sediments throughout much of the Atlantic Coastal Plain", Obermeier (1984).

Based on the subsurface data collected during the subsurface explorations for the project, the subsurface profile, along the alignment of the FDM Bridge, can generally be subdivided into three distinct geologic units: 1) Quaternary Age Alluvial Deposits, 2) Pleistocene Age Terrace Deposits, and 3) Cretaceous Age Potomac Formation as detailed in the following. Figure 2 provides a representative cross section along the alignment of the FDM Bridge.

Quaternary Age Alluvium

The upper (natural) soils at the site generally consisted of Quaternary Age Alluvium. The upper Alluvium consists primarily of unconsolidated fine-grained sediments with accumulations or organics, and the lower Alluvium generally consists of sands and silty sands with occasional organics.

Pleistocene Age Terrace

Underlying the Quaternary Alluvium, Pleistocene Age Terrace deposits were encountered, which generally consist of fine-grained deposits, underlain by sands, silty and clayey sands and gravels. These Pleistocene Age geomaterials normally exhibit strength characteristics between those of the Quaternary Age and Cretaceous Age geologic units.

Cretaceous Age Potomac Formation

Cretaceous Age deposits of the Potomac Formation underlay the Terrace Deposits; the Potomac Formation is the oldest sedimentary deposit in the Washington, DC metro area. The upper portion of the Potomac Formation typically consists of highly over-consolidated clays (OCR 10 to 20), with the lower portion consisting of dense to very dense sands and gravels. Due to their strength characteristics, the

Potomac Formation soils are commonly the primary bearing stratum for many deep foundations in the local Washington, DC metro area.

FOUNDATION DESIGN EVOLUTION

In light of the typical geologic conditions and subsurface profile, mid-to-large commercial and transportation structures in the Southeast/Southwest, Washington, DC area are frequently founded on deep foundation systems. Common deep foundation options include the use of driven piles (precast prestressed concrete & steel H-piles), auger-cast-in-place (ACIP) piles, and drilled shafts. Driven, small diameter pipe piles have also been used for minor marine structures, such as for near-shore piers and docks.

Comparable Local Projects

Two comparable projects were completed within the past 10 years in the local Washington, DC metro market; these include the 11th Street Bridge (completed 2013) and the Woodrow Wilson Bridge (completed 2009).

The 11th Street Bridge project is located approximately 1 mile Northeast (up the Anacostia River) of the FDM Bridge, and carries I-695 across the Anacostia River in Southeast, Washington, DC. The foundations for the bridge superstructure included the use of driven Large Diameter Concrete Cylinder Piles, and driven steel H-piles for the landside abutments.

The Woodrow Wilson Bridge project is located approximately 5.5 miles South of the FDM Bridge, and carries I-495 across the Potomac River from Alexandria, Virginia to Prince George's County, Maryland. The foundations for the bride superstructure included the use of driven Large Diameter Open End Steel Pipe Piles, and prestressed concrete piles for the Virginia abutment, Brown and Thompson (2015).

Preliminary Design

A Preliminary Geotechnical Engineering Report (preliminary report) was prepared by an engineering consultant, on behalf of DDOT, during the RFP phase prior to the Design-Build bidding process. The preliminary bridge design included eight bridge piers; 2 land piers east of the river, 4 piers within the Anacostia River, and 2 piers west of the river. The potential use of shallow foundations for the main bridge structure was quickly discounted due to the adverse subsurface conditions at the project site. Several potential deep foundation options for support of the bridge superstructure were discussed in the preliminary geotechnical report. For the river piers, driven large diameter prestressed concrete cylinder piles, driven closed or open ended large diameter steel pipe piles, and drilled shafts were considered potential options. As for the 4 land piers, potential foundation options included driven prestressed square concrete piles, driven steel piles, and drilled shafts.

The preliminary report included a discussion related to the previously completed 11th Street Bridge and Woodrow Wilson Bridge projects. This contained a "Lessons Learned" component of the use of large diameter concrete cylinder and steel pipe piles, which concluded that significant challenges were not experienced during foundation construction for either of these two nearby projects.

Discussion of the varying foundation options for the FDM Bridge included potential concerns of challenges related to pile driving. The preliminary report went on to note "historical borings indicate that some of the underlying soils are very stiff to hard or very dense, and may pose challenges to pile driving. In some cases, blow counts over 100 blows per foot were indicated. Therefore, drilled shafts are proposed as the most suitable foundation option". The recommended preliminary drilled shaft design included shaft

diameters ranging from 4 to 8 feet, and lengths ranging from 95 to 110 feet for the land piers and 150 to 165 feet (below river level) for the river piers. The drilled shaft option may have required construction of an elaborate cofferdam around each river pier, particular if the drilled shaft cap was to be installed below the mud line as was assumed within the preliminary report.

Final Design

The selected Design-Build team's design proposed the use of LDOEP piles (spiral welded 60 in. OD, 1 in. wall) in lieu of the drilled shaft foundation system contained in the RFP preliminary design. Additionally, the number of bridge piers was reduced to 2 land piers (East & West Abutments), and 2 river piers (identified as V-Pier 1 & V-Pier 2). Initial LDOEP pile design was based on the RFP phase borings and local experience. Following contract award, additional borings were performed (within the footprint of each of the 4 substructures); pile lengths were continually re-evaluated during the design phase taking into consideration the updated subsurface data from the recent supplemental boring and evolving structural loading for the bridge superstructure.

In addition to the permanent bridge structure, the Design-Build team elected to erect a temporary trestle structure generally along the alignment of the new bridge, with the exception of a 150 ft. span between V-Pier 1 and V-Pier 2 to allow for a clear navigation channel during construction. The temporary trestle was constructed to facilitate crane access along the alignment during construction, including for use during pile driving. The trestle structure provides a 31 ft. wide deck and consists of 29 pile bents. For support of the trestle, driven 36 in. open end pipe piles were selected.

LDOEP DESIGN METHODOLOGY

Considerable research was performed during the design phase related to the behavior of LDOEP Piles, and the load transfer mechanism. Specifically, a substantial source of uncertainty was present with respect to whether the 60 in. or 36 in. LDOEP Piles would exhibit pile plugging behavior during or after driving, and/or the extent to which internal shaft friction may develop (in the event that plugging behavior did not occur). Pile plugging is the phenomenon by which a soil mass becomes lodged within the interior of an open-ended section resulting in behavior similar to that of a closed-ended section. A graphical example of pile plugging is shown in Figure 3 below, Brown and Thompson (2015).

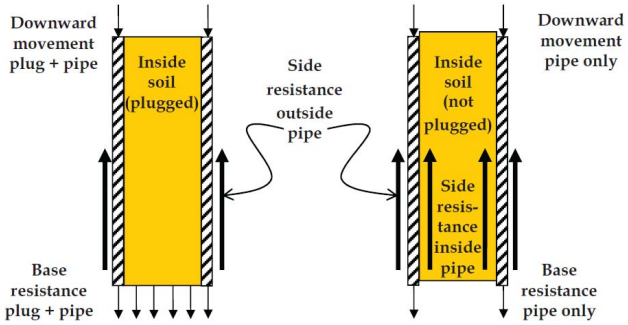


Figure 3: Representation of a soil plug with an open end pipe pile, Brown and Thompson (2015)

Extensive discussion regarding the inadequacies of industry guidance and research concerning the behavior of LDOEP Piles is highlighted within the NCHRP Synthesis publication by Brown and Thompson (2015). In this publication, LDOEP Piles were defined as 36 in. and larger; however, this is not necessarily a firmly defined definition consistent across industry. Contributing to the uncertainty with respect to plugging behavior, is the potential for differing behavior during pile driving and under static

loading conditions due to acceleration effects during pile driving. Frequently LDOEP Piles are subjected to High Strain Dynamic Testing in accordance with ASTM D4945-17 (i.e. Pile Driving Analyzer, PDA), rather than traditional static load tests, thus limiting available data on static LDOEP Pile behavior. Additionally, limited guidance with respect to the potential plugging of LDOEP Piles is provided in the FHWA GEC 12 publication, Hannigan et al. (2016); however, this publication does not provide definitive and/or concise recommendations concerning evaluation of potential LDOEP Pile behavior.

Selected Design Assumptions

The anticipated pile lengths for the 60 in. and 36 in. LDOEP Piles for the FDM Bridge, prior to the load testing program, were determined by static analysis. The primary method of static analysis, used to generate unit shaft friction and end bearing values for respective soil strata, was the Meyerhof method modified by Higgins for local geologic conditions, Higgins (2011). The adaptation of the original Meyerhof method by Higgins utilized load test data collected in the Washington, DC metro area to refine the empirical correlations, to SPT N-values, for unit shaft friction and end bearing.

A paper published on the *Design & Installation of Large Diameter Pipe Piles for LAXT Wharf*, Bhushan (2004), provided insight with regard to the behavior of 54 in. LDOEP Piles driven in comparable geologic conditions. Following load testing of these 54 in. LDOEP Piles at the LAXT project, the author of this paper noted pile capacity was generated by shaft friction on the outside and inside of the pile, plus end bearing on the steel rim area of the open end section.

To account for the uncertainty regarding the potential for pile plugging, static pile capacity analyses (prior to load testing) were performed using two assumptions regarding pile behavior. The first method assumed un-plugged conditions where axial pile capacity is generated by external shaft friction, internal shaft friction limited to 40% of the external unit value, plus end bearing acting on the rim of the steel section. The alternative analysis assumed partial-plugging where axial pile capacity is generated by external shaft friction, plus end bearing of a partial plug assumed to act on an area equivalent to 40% of the total cross section of the pile. Similar assumptions were utilized for design of the 60 in. permanent structure piles, as well as for the 36 in. temporarily trestle piles.

Peer Review

During the design/engineering phase following award of the Design-Build contract, but prior to the performance of the project specific load test program, the Design-Builder engaged a third party engineering consultant to peer review the anticipated pile lengths. This third party consultant provided a memorandum summarizing their analyses; however, detailed calculations were not made available for review. Based on the memorandum, the third party consultant utilized the similar assumption of external shaft friction, internal shaft friction limited to 40% of the external, plus end bearing limited to the steel rim of the pile. Additionally, the stated method of analysis used to generate unit shaft friction and end bearing values was the American Petroleum Institute (API) P2A Method – Mixed Soil Profiles.

The memorandum provided a summary table containing estimated pile tip elevations for the 60 in. piles at each of the 4 primary FDM Bridge substructures. The results of their analyses indicated estimated pile tip elevations that were substantially deeper than those calculated using the Meyerhof method (as modified by Higgins) for the 2 land substructures (East & West Abutments) and the 2 river substructures (V-Pier 1 & V-Pier 2) of 13 ft. to 17 ft. and 27 ft. to 30 ft., respectively.

LOAD TESTING PROGRAM

The load testing program performed under the Design-Build contract was conducted following much of the initial engineering analyses. The load testing program consists of a combination of high strain dynamic testing (i.e. PDA testing) performed in accordance with ASTM D4945-17, as well as Rapid Load Testing (i.e. Statnamic load testing) performed in accordance with ASTM D7383-08. The Statnamic load testing (performed by a specialty consultant) was used as a substitution for the bi-directional (i.e. O-cell) load test originally contemplated during preliminary design (within the RFP documents) due to the use of driven LDOEP Piles in lieu of drilled shafts. Load testing was performed on the 60 in. diameter sacrificial and permanent FDM Bridge piles, and the 36 in. diameter temporary trestle piles.

Sacrificial 60 in. Test Piles

The pre-production load testing consisted of the installation of 2 sacrificial test piles. Test pile SLT-1 was located offset from the West Abutment, and test pile SLT-2 was installed offset from V-Pier 1. Load testing of each of the 2 sacrificial test piles included PDA testing, as well as Statnamic load testing.

Test pile SLT-1 was partially installed with a vibratory hammer to an embedment of approximately 35 ft. Following the partial vibratory installation, the pile was driven to the plan tip elevation for the test pile (EL. -83 ft.) with a Pileco D180-32 diesel impact hammer. PDA monitoring was performed during the impact driving with the D180-32 during the initial drive. Following a set-up period (3 days after initial drive), PDA restrike testing was to be performed; however, due to mechanical issue with the Pileco D180-32 hammer, PDA restrike testing was postponed to 7 days following initial drive. Statnamic load testing was performed on SLT-1 10 days after the initial drive or 3 days following the final PDA restrike testing.

Test pile SLT-2 was driven with a Pileco D180-32 diesel impact hammer to the planned tip elevation for the test pile (EL. -105 ft.); due to soil conditions within the river, partial vibratory installation was not necessary, as the pile settled considerably under self-weight and weight of the hammer assembly. PDA monitoring was performed during the impact driving with the D180-32 during the initial drive. Following a set-up period of 3 days after initial drive, PDA restrike testing was performed. Statnamic load testing was performed on SLT-2 10 days after the initial drive or 7 days following the PDA restrike testing.

One additional non-planned sacrificial test pile was installed offset from the West Abutment to allow for the Design-Builder to evaluate structural consideration related to splicing of the 60 in. spiral welded piles. PDA monitoring was performed during the initial drive of this additional sacrificial test pile, as well as during a restrike conducted approximately 3.5 days following the initial drive. Similar to SLT-1, this pile was partially installed with a vibratory hammer, prior to driving with a Pileco D180-32 diesel impact hammer to a final tip elevation of EL. -90 ft.

Temporary Trestle Pile Load Testing

The planned load testing program for the 36 in. temporary trestle piles included 6 PDA load tests, during which PDA monitoring was performed during initial driving and restriking following a set-up period. Select trestle piles were partially installed with a vibratory hammer; impact driving was performed with a Junttan HHK 9S hydraulic hammer. The 6 planned PDA piles were split between the east and west portions of the trestle; for each the east and west, 1 PDA was performed for on the land, and 2 within the river. This PDA testing was performed on production piles, and was used to establish driving criteria for representative sections (bents) of the temporary trestle. The PDA testing of the trestle piles allowed for the comparison of their support characteristics to the larger, 60 in. FDM Bridge piles.

In addition to the 6 planned PDA tests, 2 additional PDA tests (restrike only) of 36 in. piles were performed due to inconsistencies during pile driving or for the case of a pile that did not meet the prior established driving criteria.

FDM Bridge Production Pile Load Testing

The planned production pile load testing program for the 60 in. FDM Bridge permanent piles included 8 PDA load tests, during which PDA monitoring was performed during initial driving and restriking following a set-up period. The 8 planned PDA piles were split between the 4 major substructures, and included 2 PDA tests per substructure. This PDA testing performed on the production piles, and was used to establish driving criteria and confirm tip elevation for each representative substructure. To date, production PDA load testing has been completed at each of the substructures, with the exception of the East Abutment. Production piles for the 3 substructures installed to date were driven with the same hammer (Pileco D180-32 diesel impact hammer) used to install the sacrificial test piles.

In addition to the 8 planned PDA tests, 2 additional PDA tests (restrike only) of 60 in. piles were performed due to inconsistencies during pile driving, or for the case of piles that did not meet the prior established driving criteria.

LOAD TESTING INSIGHT

Proportioning Shaft Friction vs. End Bearing

Figure 4 contains a breakdown and summary of the load testing (inclusive of the 60 in. sacrificial piles, 60 in. production piles & 36 in. trestle piles) performed to date; the only remaining planned load testing are 2 PDA tests to be performed on production piles at the East Abutment. This Figure details the total capacity measured during each respective load test, as well as the distribution of the measured resistance between shaft friction and end bearing.

The load test data indicated close agreement amongst the resistance proportioning between shaft friction and end bearing between the 60 in. and 36 in. LDOEP Piles. The average and median percentage of shaft friction/end bearing resistance distribution for the 60 in. piles is 88.3%/11.7% and 89.6%/10.4%, respectively. Likewise, for the 36 in. piles, the average and median percentage of shaft friction/end bearing resistance distribution is 89.4%/10.6% and 91.3%/8.7%, respectively.

Similarly, for the two sacrificial test piles subjected to the Statnamic load testing, test data indicated close agreement between the resistance proportioning between shaft friction and end bearing for the Statnamic and PDA load testing. The proportioning of measured shaft friction/end bearing resistance via the PDA and Statnamic Load Testing for SLT-1 is 90.1%/9.9% and 89.2%/10.8%, respectively and for SLT-2 84.0%/16.0% and 82.9%/17.1%, respectively.

In light of observed shaft friction to end bearing resistance proportioning, the authors found it evident that the 60 in. and 36 in. LDOEP Piles driven for this project did not exhibit indications of significant plugging during dynamic loading (i.e. pile driving and Statnamic Load Testing).

Development of Internal Shaft Friction

Figure 5 includes a summary of the comparison of unit shaft resistance, fs, determined by CAPWAP analyses using PDA data collected during restrike testing vs. the equivalent anticipated unit shaft resistance using the Meyerhof method as modified by Higgins. Within this comparison, the CAPWAP unit values measure total shaft friction (i.e. external + internal friction), whereas the Meyerhof/Higgins

method was used to calculate the equivalent external friction only. Therefore, when comparing the ratio between the CAPWAP unit shaft friction (CW fs) to that of the Meyerhof/Higgins unit shaft friction (MH fs), the internal shaft friction can be approximated as a percentage of the external shaft friction. While Figure 5 contains only the average and median values for each respective test pile, the authors' analyses evaluated each pile individually using 6.7 ft. (2 m) soil segments, which correspond to the soil segment length within the CAPWAP analyses, along the length of the embedded portion of the pile using the SPT N-values from the closest boring(s) to develop the individual soil segment Meyerhof/Higgins unit shaft friction. Additionally, to account for potential effects of partial-vibratory installation (which was used on a portion of the installed piles) and for potential effects within the pile lengths within soil strata where the pile sank under self-weight and/or weight of the hammer assembly, the authors have also provided the CW fs to MH fs comparison limited to the impact driven portion of the piles only (elevation at which impact driving commenced to final pile tip elevation). The impact driven portion of the pile was considered the primary source of long-term pile capacity.

For the 60 in. piles, the data suggests the development of internal shaft friction, as a percentage of external shaft friction, of 40% to 44% when considering the full pile length, or 48% to 64% when considering only the impact driven portion of the pile. As for the 36 in. piles, the data suggest the development of internal shaft friction, as a percentage of external shaft friction, of 60% to 90% when considering the full pile length, or 80% to 116% when considering only the impact driven portion of the pile. The authors note that for the 60 in. piles representative borings were generally sited in close proximity to the load tested piles; however, for the 36 in. trestle piles, interpolation between borings was necessary at times due to the location of available borings in relation to load tested piles.

SUMMARY AND CONCLUSIONS

Based on the substantial subsurface data and load testing, the 60 in. and 36 in. the LDOEP Piles did not exhibit apparent indications of plugging during dynamic loading (i.e. pile driving and Statnamic Load Testing) as exhibited by the proportioning of shaft resistant to end bearing. Load test data strongly indicated that significant internal shaft friction was developing along the shaft length of the driven LDOEP Piles, particularly below the elevation at which impact driving of the pile commenced. This is substantiated by the significantly higher than anticipated unit shaft friction values measured during the load testing program. As the load testing methods utilized do not differentiate between external and internal shaft friction in their measurements, the greater unit shaft friction values were attributed to the development of significant internal shaft friction. Interestingly, greater internal shaft friction was observed within the load test data for the 36 in. piles vs. that of the 60 in. piles, which points to size effects with respect to the extent to which internal shaft friction will develop. Moreover, the load test data substantiated the use of the Meyerhof method as modified by Higgins for use of developing unit shaft friction values, as well as the primary un-plugged analysis method with the development of proportioned internal shaft friction. The API P2A Method of static pile capacity prediction did not agree well with the load test data, and tended to under-predict pile capacity and over-predict required pile lengths.

REFERENCES

1. Bhushan, Ph.D., G.E., K. (2004). Design & Installation of Large Diameter Pipe Piles for LAXT Wharf. In GSP 125: Current Practices and Future Trends in Deep Foundations, Los Angeles, CA, July 27-31. American Society of Civil Engineers.

2. Brown, D.A., and Thompson III, W.R. (2015). Current Practices for Design and Load Testing of Large Diameter Open-End Driven Pipe Piles. Final Report. NCHRP Report 20-05, Topic 45-05, National Cooperative Highway Research Program, Washington, D.C.

3. Hannigan, P.E. PJ, Rausche, Ph.D, P.E. F, Likins, P.E. GE, et al (2016) Geotechnical Engineering Circular No. 12 – Volume I Design and Construction of Driven Pile Foundations, National Highway Institute, U.S. Department of Transportation, Federal Highway Administration, Washington, DC

4. Higgins, III, P.E. KA (2011) Evaluation of the Originally Published, Meyerhof Empirical Correlations of Shaft Friction and End Bearing Capacity For Driven Piles Using Dynamic Test Data. In: Proceedings of the 36th Annual Conference on Deep Foundations, Boston, MA, October 19-21. Deep Foundations Institute.

5. Obermeier, S.F. (1984). Engineering Geology of Potomac Formation Deposits in Fairfax County, Virginia, and Vicinity, with Emphasis on Landslides

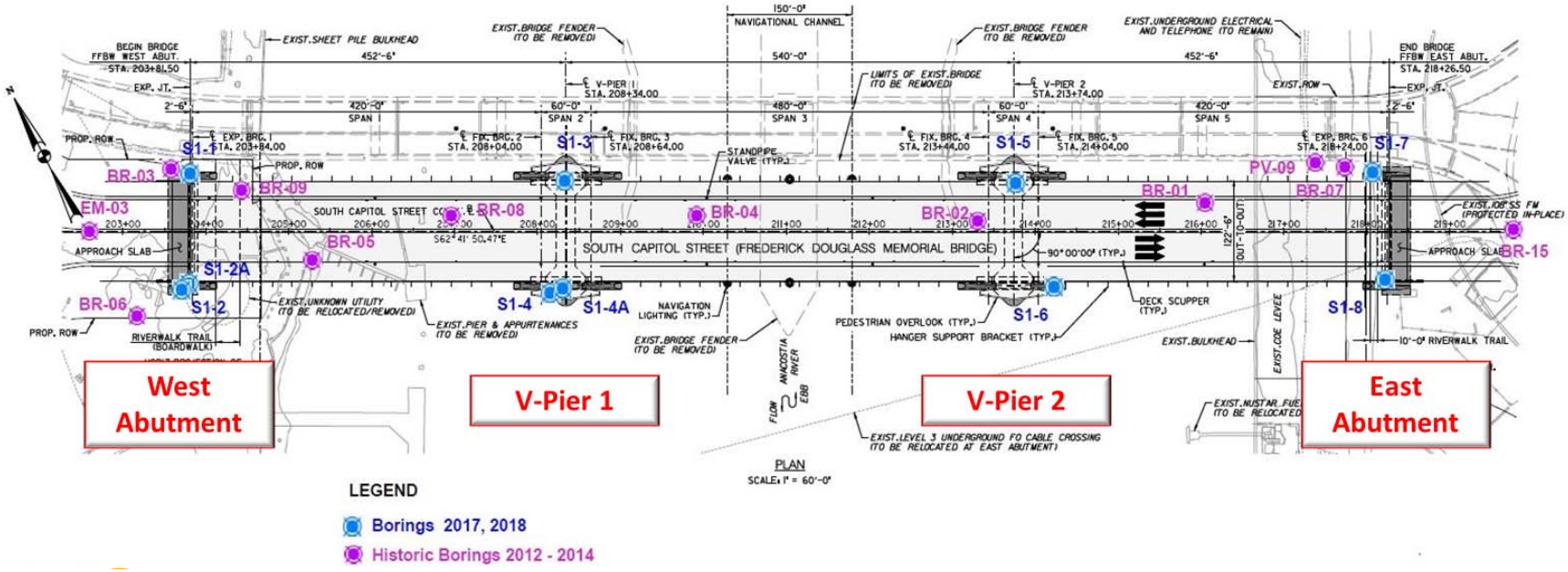


Figure 1. Boring Location Plan along the FDM Bridge alignment.

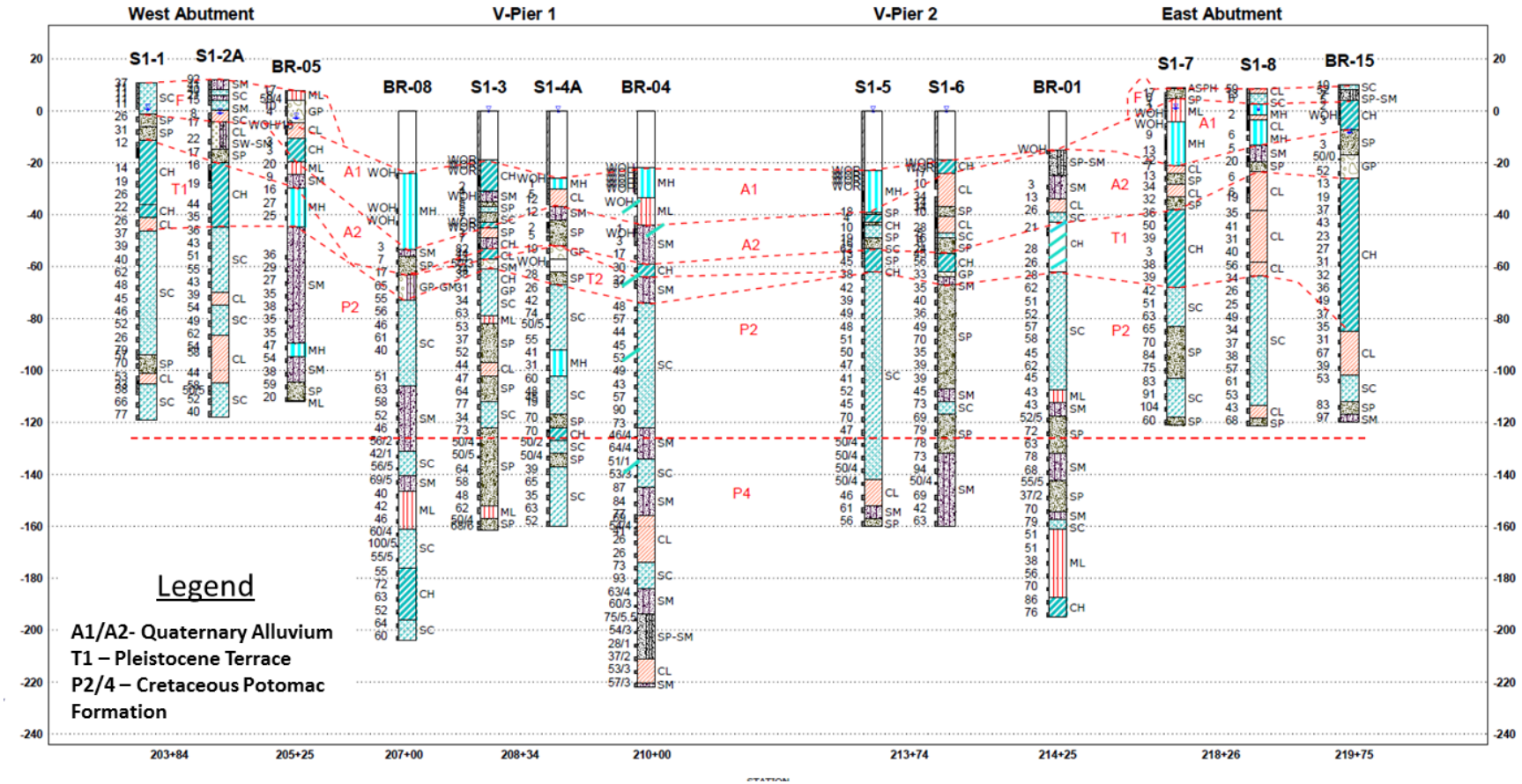


Figure 2. Subsurface Profile along the FDM Bridge alignment.

Structure	Location / Substructure	Pile No.	Pile Size / Type	Initial Drive Date	Restrike Date	Load Test Method	Capacity (PDA Restrike / Statnamic)				
							Ru, Total Capacity	SF, Shaft Friction		EB, End Bearing	
							kips	kips	%	kips	%
FDM (Permanent Structure)	West Abutment (Sacrificial Offset)	SLT-1	60-In. OEP	2/26/2018	3/5/2018	PDA	5511.0	4963.0	90.1%	548.0	9.9%
					3/8/2018	Statnamic	4921.0	4389.0	89.2%	532.0	10.8%
	V-Pier 1 (Sacrificial Offset)	SLT-2		7/2/2018	7/5/2018	PDA	4027.5	3384.4	84.0%	643.0	16.0%
					7/12/2018	Statnamic	5751.0	4769.0	82.9%	982.0	17.1%
	West Abutment (Sacrificial Offset)	Splice TP		11/1/2018	11/5/2018	PDA	5688.7	5294.1	93.1%	394.7	6.9%
	West Abutment	12		1/4/2019	1/7/2019	PDA	3469.5	3270.8	94.3%	198.7	5.7%
		33		1/2/2019	1/7/2019	PDA	3472.4	3238.7	93.3%	233.7	6.7%
		23		1/17/19 & 1/18/19	1/23/2019	PDA	4113.0	3900.8	94.8%	212.3	5.2%
		4		1/31/2019	2/5/2019	PDA	4737.3	3218.8	67.9%	1518.6	32.1%
	V-Pier 1	8		11/13/2018	11/16/2018	PDA	3801.0	3506.5	92.3%	294.5	7.7%
		29		11/13/2018	11/16/2018	PDA	3922.1	3314.0	84.5%	608.0	15.5%
	V-Pier 2	9		2/28/2019	3/4/2019	PDA	3601.3	3110.4	86.4%	490.9	13.6%
					3/13/2019	PDA	4019.8	3823.4	95.1%	196.4	4.9%
		28		2/14/2019	2/28/2019	PDA	4125.7	3634.9	88.1%	490.9	11.9%
	East Abutment	TBD		TBD	TBD	PDA					
		TBD		TBT	TBD	PDA					
	FDM Summary							Average	88.3%		11.7%
								Median	89.6%		10.4%
Temporary Trestle	Bent W2	Pile B	36-In. OEP	4/2/2018	4/5/2018	PDA	1868.4	1727.0	92.4%	141.4	7.6%
	Bent W6	Pile C		5/9/2018	5/11/2018	PDA	1358.0	1223.7	90.1%	134.3	9.9%
	Bent W6	Pile B		5/14/2018	5/16/2018	PDA	1450.7	1082.6	74.6%	368.1	25.4%
	Bent W11	Pile C		6/8/2018	6/12/2018	PDA	1924.0	1628.4	84.6%	295.6	15.4%
	Bent E3	Pile A		7/20/2018	7/23/2018	PDA	2077.3	1864.5	89.8%	212.8	10.2%
	Bent E6	Pile C		8/31/2018	9/4/2018	PDA	1814.7	1708.6	94.2%	106.0	5.8%
	Bent E10	Pile C		9/26/2018	9/28/2018	PDA	1636.9	1552.0	94.8%	84.8	5.2%
	Bent E12	Pile B		10/5/2018	10/9/2018	PDA	2033.3	1927.3	94.8%	106.0	5.2%
	Trestle Summary							Average	89.4%		10.6%
								Median	91.3%		8.7%
Combined Summary: FDM (60-In. OEP) and Trestle (36-In. OEP)								Average	88.7%		11.3%
								Median	90.1%		9.9%

Figure 4. Load Test Summary with resistance proportioning shaft friction vs. end bearing

Pile No.		Boring	CAPWAP f_s (CW fs) ÷ Meyerhof/Higgins f_s (MH fs) NOTE: f_s = Unit Shaft Resistance			
			All Data (Full Pile Length)		Impact Driving Length Only	
			Average	Median	Average	Median
FDM, 60-In. OEP (Permanent Structure)	SLT-1	S1-2A	1.55	1.16	1.74	1.63
	SLT-2	S1-4A	1.31	1.11	1.48	1.38
	Splice TP	S1-1	1.48	1.73	1.96	1.87
	Splice TP	BR-09	1.69	1.39	2.08	2.33
	WA P#33	S1-2A	0.99	1.39	1.36	1.46
	WA P#12	S1-1	1.25	1.50	1.46	1.53
	WA P#23	S1-2A	1.41	1.33	1.67	1.66
	WA P#4	S1-1	1.96	1.93	2.14	1.94
	VP-1, P#8	S1-3	1.50	1.30	1.43	1.27
	VP-1, P#29	S1-4A	1.38	1.45	1.46	1.45
	VP-2, P#28	S1-6	1.29	1.42	1.43	1.47
	VP-2, P#9	S1-5	1.40	1.51	1.47	1.51
	Summary	Avg	1.43	1.44	1.64	1.63
		Median	1.40	1.42	1.48	1.52
Temporary Trestle, 36-In. OEP	TR W2-B	BR-05	1.27	1.35	1.61	1.57
	TR W6-C	BR-08	2.18	1.51	2.18	1.51
	TR W6-B	BR-08	2.61	2.21	2.06	1.42
	TR W11-C	S1-4A	1.56	1.35	1.46	1.44
	TR E3-A	BR-07	1.30	1.30	1.76	1.80
	TR E6-C	BR-01	1.71	1.79	1.92	1.90
	TR E10-C	BR-01	2.33	2.50	2.67	2.78
	TR E10-C	S1-6	2.16	1.67	3.20	2.56
	TR E12-B	S1-6	1.96	1.60	2.53	1.92
	Summary	Avg	1.90	1.70	2.16	1.88
		Median	1.96	1.60	2.06	1.80
Combined Summary		Avg	1.63	1.55	1.86	1.73
		Median	1.50	1.45	1.74	1.57

Figure 5. Shaft Friction Summary with CAPWAP unit shaft friction to Meyerhof/Higgins unit shaft friction comparison

CASED CFA PILE – AN ALTERNATIVE PILING METHOD – A CHANCE FOR TECHNICAL AND ECONOMICAL SOLUTIONS

Franz-Werner Gerressen, BAUER Maschinen GmbH, Germany
Gordian Ulrich, Equipment Corporation of America, USA
John R. Grillo, P.E, M.ASCE, Moretrench, A Hayward Baker Company, USA

ABSTRACT

Most geotechnical construction professionals are aware of piling using hydraulic drill rigs and the so-called Kelly drill mode. Kelly drilling has many advantages as it can work with a wide range of tools facing almost all types of soil and rock conditions. Kelly drilling can also deal with diameters up to 10 ft (3.00 m) and bigger or depths of more than 330 ft (100 m). Nonetheless, there is a concern about Kelly drilling as it is a relatively slow installation process.

Therefore, an alternative piling method like Cased CFA (CCFA) Piles (Cased Auger Cast Piles) provides a significant advantage in terms of installation performance, schedule and cost saving potentials.

Major application for the Cased CFA system is the secant pile wall construction. Against the traditional secant pile wall systems like fully cased bored piles or CFA secant piling the Cased CFA secant pile wall system has the advantage in cost and time against the fully cased system and in quality against the standard CFA system. This paper will describe the methodology and installation process in general as well as first reference projects carried out in the United States. This paper will present the results in cost and schedule saving using this method. In addition, we will also describe the limitations of this method.

Keywords: CFA, Auger Cast Pile, Cased CFA, CCFA, Secant pile wall

INTRODUCTION

In the changing construction environment, companies are searching for new technologies or improvement of existing technologies to complete their projects in shorter time frames to provide a good economic solution. Especially with the focus of increasing urbanization, the aim of fast construction becomes more and more important. When thinking of piling, most people will have the same picture in mind: that of a hydraulic drill rig working in Kelly drilling mode; however, the perpetual drill rig development provides a number of options for the execution of specialist foundation projects, either for foundations or for pile walls when using single pass applications like CFA, Cased CFA and Full Displacement Piling (FDP).

Single pass means, in general, that the tool is pushed and rotated into the ground to the final depth in one stroke. After reaching the final depth, concreting is started and concrete is pumped continuously while the tool is withdrawn.

Significant progress has been made with systems for more and efficient quality control in combination with safe and quick pile installation. These alternative piling methods provide chances not only for technical and economical solutions, but moreover for time saving potentials. In the following, the focus will be on the Cased CFA method.

THE WORKING PRINCIPLE

The basic principle of a Cased CFA pile is that a continuous flight auger in combination with an outer casing is drilled simultaneously, but in opposite directions, into the ground to the required depth (Figure 1, Step 2). These characteristics led to the common term Cased Continuous Flight Auger Pile (CCFA). The

© 2019 Deep Foundations Institute

spoil is transported upwards by the auger flights surrounded by the casing and exits through openings at the top of the casing. Once the final depth is reached (Figure 1, Step 3) the concrete pump is activated and concrete is pumped through the hollow stem of the auger. After completion of concreting the drill string has to be cleaned (Figure 1, Step 4). The cleaning is done by rotating the casing and the auger in the opposite direction than during drilling to discharge the cuttings directly on the ground for removal by a support equipment. In some geology it can be beneficial to postpone the cleaning after reinforcement installation (Figure 1, Step 5).

This procedure requires double rotary drive systems to run an auger and casing at the same time. Different setups of double rotary drive systems are commercially available. One option is the use of two rotary drives, either working independent or dependent to each other. With a specific geometry this system is also known as Front-of-Wall (FoW) system. Another option is to use one rotary drive in combination with a torque multiplier. The torque multiplier is a mechanical unit attached to the Cardanic joint below the rotary drive. The ratio is fixed at 1:2, so that the torque multiplier doubles the incoming torque, halves the speed and inverts the direction of rotation of the casing.

Main application for CCFA piles is the use for pile walls, secant and tangent, as support for deep excavations. Of course, CCFA piles can be used for foundations as well.

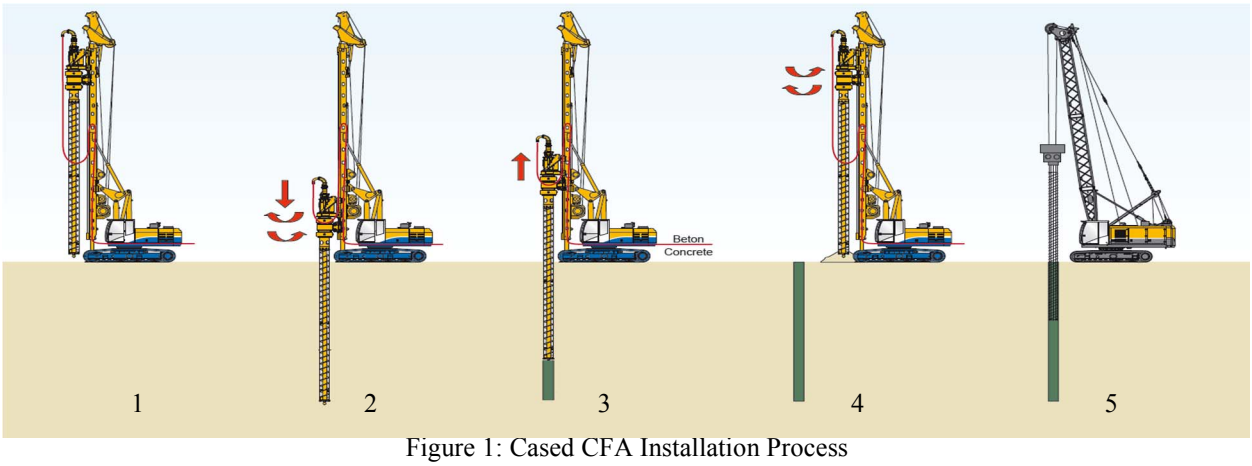


Figure 1: Cased CFA Installation Process

EQUIPMENT AND TOOLS

As described above, two major attachments can be utilized for the installation of CCFA piles.

The first is the Front-of-Wall (FoW) system as shown in Figure 2. The specific geometry of the double rotary drive system, allows working very close to adjacent structures, depending on the used system, in a range of 10.2″-22″ (260-660 mm). The FoW system is usually used for smaller diameter elements. Typical FoW drilling diameters are 16″, 20″, and 24″ (406 mm, 508 mm, and 610 mm).

The second is the CCFA system with a torque multiplier BTM (see Figure 3). To overcome the disadvantages of the two independent rotary drive units, further developments of the drilling method were investigated. The result was the torque multiplier in combination with a spoil discharge chute system.

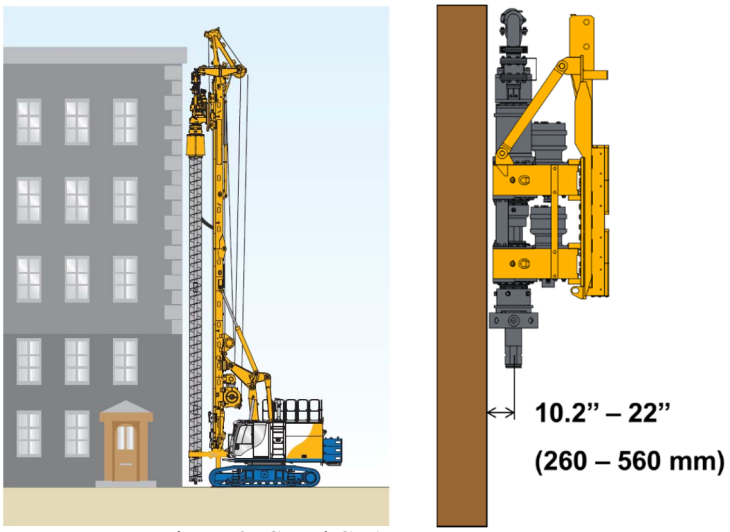
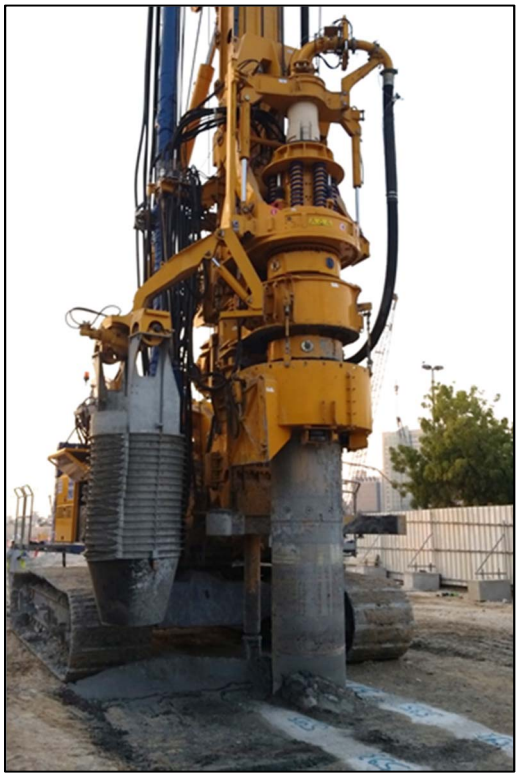


Figure 2: Cased CFA set up as FoW system

The Bauer Torque Multiplier (BTM) is a mechanical unit attached to the cardanic joint below the rotary drive. The ratio is fixed at gear ratio of 1:2, so that the BTM doubles the incoming torque, halves the speed and inverts the direction of rotation of the casing. The resultant torque has to be limited to remain within the structural capacity of the mast of the drilling rig.


Figure 3: BAUER BG 39 with torque multiplier BTM and spoil discharge chute system

As with other double rotary systems the spoil exits the top of the casing after drilling to a sufficient depth to fill the casing and auger string. To manage and reduce safety risk from spoil exiting the casing at high level, a spoil discharge chute system was developed. When the spoil reaches the top of the casing it enters an oversized collector. It is then swept round to an opening and then falls through a series of telescoping

chutes to the ground in a controlled manner. During the drilling process the chutes are raised or lowered to maintain a safe drop height for the spoil. To achieve the maximum drilling depth, the spoil discharge chute system needs to be temporarily moved. This is achieved by the use of a manipulator arm.

An additional improvement has been the introduction of air to the drilling process, via an air valve located on the concrete swivel. While drilling down air is pumped through the hollow stem to the tip of the auger. The air has several benefits - it prevents water or soil ingress from the base. Additionally, it has a drying effect on the spoil and assists the transportation of the spoil up the augers.

The conversion to this drilling mode is also relatively straightforward with any additional equipment being added without major alterations to the structure, hydraulics or electrics of a standard BG rig.

To be prepared for various soil conditions, different type of starter auger have been developed as shown in Figure 4.



Figure 4: Flat teeth for soft soils (clay) and sand (left) , Bullet teeth for gravel, cobbles and rock socketing (right)

ADVANTAGES, LIMITS AND CONSIDERATIONS

Verticality of CCFA when using for secant pile walls

The verticality of the pile is controlled and influenced by the outer casing. Attention must be paid to the accurate alignment of the casing. The relative stiffness of the combined drill string is significantly higher than that of a CFA auger alone. The counter rotation of the casing and auger also has a beneficial stabilizing effect. Therefore, the alignment of the pile wall reaches the same (or better) quality as known for the installation with cased Kelly drilling.

Suitable Soil Conditions

Similar to CFA, the CCFA method is suitable for cohesive soils and granular soils with sufficient cohesive content to allow soil transport on the auger. Undrained shear strength “cu” should be above 15 kN/m² and no boulders should be present. Rock socketing is possible to UCS values of approx. 3,000 psi (20 MPa).

Range of Application

Besides the limitations defined by the soil conditions mentioned earlier, the single pass methods are also limited in depth and diameter. The limiting factor on the one side is the mast height of the used equipment, and the required retraction force to get the tool, including the weight of the soil and the lateral friction, out of the ground on the other side. As guidance it can be said, that typical diameters of CCFA, mainly for secant pile walls, is in a range of up to 4′ (1,200 mm). Depth limit is 82′-98′ (25-30 m), very much dependent on the equipment. For sure these numbers are not fixed, as design of equipment and tools as well as project demands force further developments.

JOB SITE REFERENCES

In the last decade, secant pile wall piling projects changed from the traditional Kelly Drilling to the CCFA drilling frequently. Many piling projects using CCFA piles for secant pile walls have been completed with great success in the UK, Germany and Italy. The typical diameters for the piles have been 30″-35″ (750 mm - 880 mm). The tendency for bigger diameters can be seen. In the following, we will see two European examples showing the potentials in time saving due to the achievable performance.

First of all, a project reference in Bath, UK. It was expected to install 4 piles, 59′ (18 m) in length, for every single day. However, a peak performance of 14 piles per day was achieved with an average of 8 piles per day over the whole project. Figure 5 shows a BG 36 with BTM 400 during the operation, using the pile chute system for safe soil transport.



Figure 5: BG 36 with BTM 400, with pile chute system

In Naples, Italy, several excavation pits with secant pile walls were built during the new development of a new subway using CCFA. These pits are needed for the mechanical equipment of the air ventilation system of the tunnel. Exemplary, the following Table 1 shows the installation steps and required time for the installation comparing primary and secondary piles to a depth of 49′ (15 m).

	unreinforced	reinforced
Positioning	2 min	2 min
Drilling	8 min	16 min
Concreting	9 min	9 min
Installation of reinforcement		35 min
	1 min	
Total:	20 min	62 min

Table 1: Pile construction durations

As it can be seen in Table 1, the installation of the reinforcement cage took quite long. Reason for that was the fact, that due to the very confined jobsite situation, the cages were delivered in three sections and had to be connected two times during installation.

Although space on site was very limited (see Figure 6), the works were carried out without any problems. In this confined environment also the benefit of using flushed the air during drilling to dry the spoil meant no special facilities for the collection and control of water on the surface were needed.



Figure 6: BG 28 with BTM 400, 49′ (15 m) pile length, diameter 30″ (750 mm)

The spoil fell down through the soil discharge chute. The required length to keep the chute just above the ground surface is adjusted by a small winch. Therefore, it was possible to bypass the traffic directly along the adjacent street and pavements.

JOB SITE REFERENCE – USA

Recognizing the great success in European countries, the CCFA system made the first approaches to the US market as well. The following example shows one of the first approaches of using the CCFA system in the USA.

It was successfully carried out on a project in New York City in 2017. Hayward Baker, Inc. (HB), a Keller Group Company, was faced with the challenge to install 230 piles for a secant pile retaining wall for a healthcare facility in Brooklyn, NY. The depths averaged 50′-55′ (15.2m - 16.8m) and the design considered a 30″ (750 mm) diameter pile, with full length W-beam reinforcement in every other pile set through the wet grout.

From experience on other projects in this area Hayward Baker knew the biggest challenge will be the possible occurrence of cobbles and boulders based on the glacial geology of the site being at the terminal moraine. The soils report identified very dense sand with cobbles and the sporadic presence of boulders. Groundwater at the site was measured at about 80′ (24m) deep.

During the planning stage HB consulted with ECA to prepare for the worst-case scenario which was obviously what to do if they hit a large size boulder with the CCFA tooling. Will the equipment cut through the boulder or what does the procedure need to be in case the hole needs to be temporarily abandoned? The resulting decision was to have a second rig on site in regular Kelly Drilling configuration, which could be used to core through the boulder with core barrel and rock auger. This decision was also based on experience and recommendation which states rock or boulders are not suitable for CCFA.

While the HB rig was upgraded and the CCFA equipment installed on it, the excavation contractor started prepping the site and installed the guide wall. A large quantity of boulders were encountered immediately below previous building foundations. The surficial boulders were removed during excavation for the guide wall (see Figure 7).



Figure 7: Boulder removed for guide wall installation

After completion of rigging and training in the HB yard, the equipment was shipped to site and set up in March 2017 (Figure 8). Knowing production rates for the Kelly Drilling Application the question was how much faster will the CCFA application really be and of course what will happen when a boulder is encountered.



Figure 8: BG 30 with CCFA attachment

The drilling time to install the first 50′ (15.2m) long primary pile was 15 minutes, which is substantially faster than Kelly Drilling. Soon, thereafter, the crew was able to see how the equipment performed when hitting a boulder. On the second day of production a boulder was encountered. The operator reduced the penetration rate to start coring through the boulder utilizing the casing like a core barrel whereas the auger string was retracted using the relative movement feature which allows for 1′ (30 cm) advancement with the auger or 1′ (30 cm) advancement with the casing. Drilling time was about 15 to 20 minutes to cut through the boulder before the drill string could be advanced at regular speed of about 5 feet/min (1.5 m/min). Figure 9 shows exemplary "left overs" coming out of the spoil chute system after drilling through a boulder.



Figure 9: Left overs coming out of the spoil chute system after drilling through a boulder

The robust design of the heavy-duty solid wall casing shoe with exchangeable cutters in combination with double wall sectional casing and a rock auger allowed to cut through the boulders.

The backup rig in Kelly mode only had to be utilized twice to finish a piles which originally were started with the CCFA rig.

CCFA production averaged about 5 elements per day (250-275 LF (76-83 m)). The following excavation, as shown in Figure 10, revealed another huge advantage of the CCFA system which is the quality of the wall. Despite encountering boulders, every single pile remained vertical and well within tolerance.



Figure 10: Excavated wall

SUMMARY

Cased CFA piles, as seen herein, provide a lot of opportunities to the foundation market. Especially in terms of time saving potentials, the described method is a welcome alternative to the conventional piling methods. It could be seen, that this method provides high cost and schedule saving potentials, due to proven performance, design adjustments and material cost savings. Therefore, when the job site soil and boundary conditions will allow it, a single pass method like Cased CFA should be considered to provide schedule and cost savings.

Understanding newer technology and contractor capabilities, the Cased CFA piling method will become increasingly important with higher utilization. When evaluating a project site for the system use, the team needs to understand how to adjust the system to the soil conditions represented in the geotechnical investigation. The drilling rig must have sufficient torque, pull down, and extraction force to keep the drilling process steady at all times, even in difficult soil conditions. A consistent and reliable concrete supply must be organized as part of the work preparation to ensure a constant operating sequence. Good communication and coordination among the crew on site is important and changes in staff should be avoided.

These improvements and advances contribute to a better quality product. However, these will only be successful if used properly. Therefore, the importance of training, understanding and briefing to all personnel involved is vital to its success.

REFERENCES

Gerressen, F.-W., Platzek, P. 2010: OVERVIEW OF THE STATE OF THE ART OF DOUBLE ROTARY DRILLING METHODS, DFI and EFFC 11th International Conference - Geotechnical Challenges in Urban Regeneration, London, UK, 2010

Gerressen, F.-W., 2018: ALTERNATIVE PILING METHODS - CHANCES FOR TECHNICAL AND ECONOMICAL SOLUTIONS, DFI India, Gujarat, India November 2018

DYNAMIC AND STATIC LOAD TESTING: A COST SAVINGS APPROACH

Brandon Phetteplace, P.E., GRL Engineers, Inc., Houston, Texas, USA, 832-389-1156
bphetteplace@grlengineers.com
Thomas Hyatt, P.E., GRL Engineers, Inc., Atlanta, Georgia, USA, 216-470-1801
thyatt@grlengineers.com
Camilo Alvarez, P.E., GRL Engineers, Inc., Los Angeles, California, USA, 213-200-4956
calvarez@grlengineers.com

ABSTRACT

A test pile program was undertaken at a project site in Ain Sukhna, Egypt for an import/export oil jetty. Two 1219 mm diameter open ended steel pipe piles were evaluated at two separate test locations. Each test pile was dynamically tested during initial drive utilizing a Pile Driving Analyzer (PDA). Restrike testing was also performed to evaluate the time dependent soil setup. One static compression test and one static tension test was performed at each test location. A correlation of the static and dynamic load test results was established to develop a driving criteria for the piling across the two kilometer project. The constructability benefits of shorter piles will be discussed in more detail, given that the pile lengths were shortened by 9 to 10 meters on average. Lastly, the use of a four pile linear layout to perform both compression and tension tests will be covered.

Keywords: Pile Driving Analyzer (PDA), Static Load Testing (SLT), Soil Set-up, Pipe Piles

INTRODUCTION

With the increased number of Very Large Crude Carriers (VLCC) & Ultra Large Crude Carriers (ULCC) being used to transport oil products around the world, companies and/or nations are presented with the challenge of transferring these products to and from the carriers in deep water scenarios, typically 15 to 20 meter depths, to accommodate the vessels draft. One option for loading/unloading the oil products from a VLCC or ULCC would be to transfer to/from smaller vessels several miles offshore, whereas the most economical option is to unload directly to a pipeline via a berth/jetty platform near shore. These berth platforms must be designed to withstand multiple loading scenarios while these carriers are moored and transferring their products. The use of Large Diameter Open Ended Pipes (LDOEP) piles are a common foundation choice for this offshore application. One of the drawbacks of LDOEP piles, especially across a large project site, is that there can be extreme variability in the pile driving behavior. This can be caused by either a change in soil conditions or the performance of the soil plug. Due to this variability, it is important to verify throughout the duration of the project that the piling is being installed to the correct criteria as established during the load test program. A well designed driven pile load test program, preferably with the combination of Static Load Testing (SLT) and Pile Driving Analysis (PDA), should develop a driving criteria that can allow the contractor and owner to monitor any change in driving behavior.

PROJECT BACKGROUND

Egyptian Natural Gas Holding Company (EGAS) and Arab Petroleum Pipelines Company (SUMED) initiated the Ain Sukhna Product Hub (ASBH) project in Ain Sukhna, Egypt to further increase the nation's added value for its current and prospective clients. ASBH is located approximately 50 km south of the Suez Canal, on the north western edge of the Gulf of Suez. The facility is connected to the Sumed pipeline, which gives an alternative route for transporting oil from the Persian Gulf to the Mediterranean Sea if the Suez Canal is not passable. The ASBH project includes both onshore and offshore facilities for storage, loading, unloading and load out of Natural Gas, Fuel Oil and Liquefied Petroleum Gas (LPG). The onshore facilities include three 50000 LPG refrigerated tanks, three 35000 Fuel Oil tanks and one 20000 Gas Oil

© 2019 Deep Foundations Institute

flushing tank. The offshore facilities include one Floating Storage and Regasification Unit (FSRU)/Liquefied Natural Gas (LNG) berth for natural gas import via a 170000 cubic meter FSRU vessel and an export capacity of 14.1M cubic meters of gas per day. One combined LPG/product berth to accommodate LPG carriers in the range of 5000 to 82000 cubic meters and oil tankers in the range of 25000 to 160000 Deadweight Tonnage (DWT).

The two berths for this project extend approximately 2.2 km into the Gulf of Suez to reach the water depths required for the VLCC to safely access the unloading and loading platforms. A joint venture between Besix Group and Orascom Construction PLC (BO JV) was formed to execute the construction of the berths. The project required an accelerated timeline to meet the owner requirements with the first berth needing to be operational within six months of the start of the project and the second berth would be built while live gas was being conveyed to and from tankers.



Fig. 1: ASBH Marine Layout

SUBSURFACE

A soil investigation was performed in 2015 by Fugro Middle East, which consisted of 10 soil borings arranging in depth from 50 to 60 meters, 5 CPT Borings arranging in depth from 22 to 40 meters, In-situ vane shear tests and laboratory testing to further categorize the soil stratum. Based on this investigation, the upper 1 to 6 meters is a very weak layer, underlain by alternating layers of sand, silt and clay with a high proportion of secondary soil (ie. silty and clayey sand, sandy silt, sandy clay). Figures 2 & 3 give the soil profile for CPT06 and CPT10, which correspond to test location No. 1 and 2, respectively. These borings are approximately 390 meters apart. The sea bottom elevation is approximately -13.6 and -15.5 meters for CPT06 and CPT10 with a self-penetration depth of -14.1 and -16.5 meters, respectively. Overall,

the soil profile across the site cannot be generalized due to high variability in the stratum encountered during the investigation.

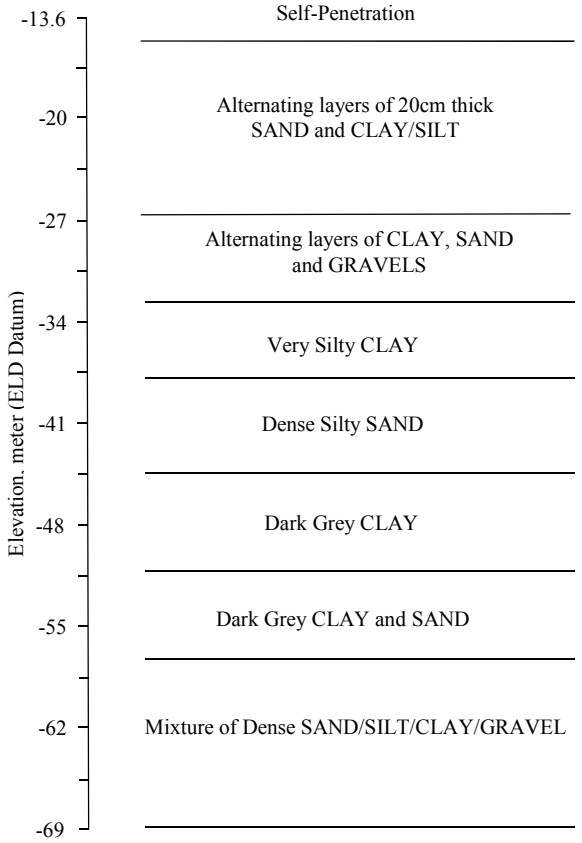


Fig. 2: Soil Profile – CPT06

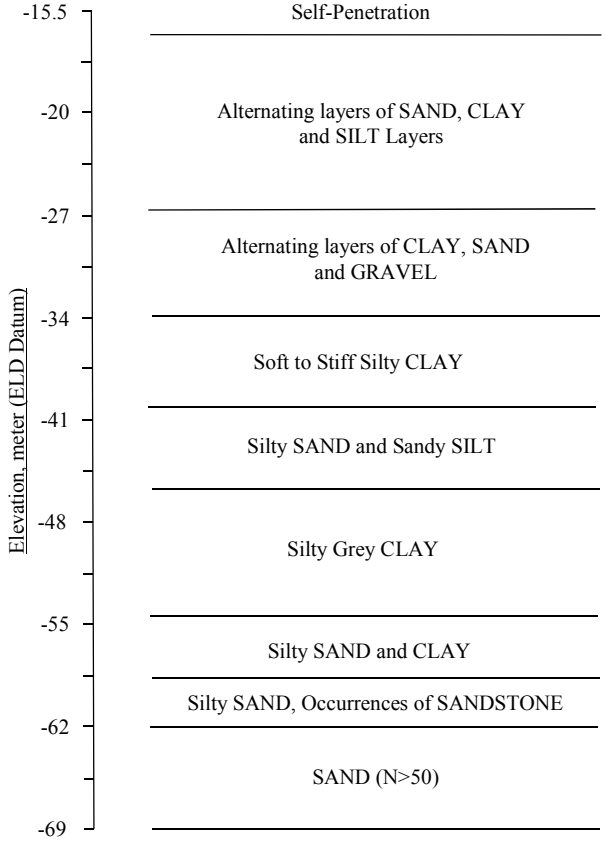


Fig. 3: Soil Profile – CPT10

PILE DESIGN

The soft upper layer indicated during the soil investigation has been neglected and the depth of the competent layer is summarized in Table 1.

Table 1: Depth of Competent Layer

CPT Boring	Test Location	Thickness of Very Soft Layer, m	Depth of Competent Layer (m, ELD)
6	1	1.5	-17.0
10	2	3.0	-23.0

The calculated undrained shear strength, c_u, was then utilized to calculate the ultimate bearing capacity in compression and tension with the API formula. A global safety factor of 2.0 and 2.5 were applied to the ultimate bearing capacity in compression and tension, respectively, for the operational conditions. Table 2 is the required penetration into the competent layer, as defined above, of a 1.2 meter outer diameter pile for varying ultimate bearing capacities in compression and tension.

Table 2: Required Penetrations for varying Ultimate Bearing Capacities

Ultimate Bearing Capacity, kN	Compression	Tension
	Required Penetration, m	Required Penetration, m
4000	-	30
6000	34	36
8000	40	42
10000	46	47
12000	50	-

The required allowable load was indicated to be 5000 and 4000 kN for compression and tension, respectively. With the above mentioned global safety factors, the required ultimate bearing capacity is 10000 kN for both compression and tension. Therefore, based on Table 2, 46 to 47 meters of penetration into the competent layer is required to achieve an ultimate bearing capacity of 10000 kN.

SOIL SET-UP

In certain soil types, driven piles can exhibit a higher capacity several hours, days or months later when compared to their capacity during initial installation (Fellenius et. al. 1989, Komurka 2004). Soil set-up is a phenomenon that is defined as an increase in shaft resistance that develops over a certain amount of time after installation. For the defined soil types on this project, this set-up is most likely caused by a combination of the remodeling of disturbed soil and an increase in soil strength as the excess pore water pressure dissipated. The rate of soil set-up can vary from site to site. Determining the EOD capacity along the set-up gain during a short-term (2 to 48 hours) and a long-term (5 to 50 days) restrike is helpful in evaluating the long term static capacity of the installed pile.

DYNAMIC LOAD TESTING

Dynamic Load Testing (DLT) using a Pile Driving Analyzer® (PDA) was performed on the compression and tension test piles at test location No. 1 and 2. The purpose of the DLT was to monitor hammer performance, assess pile structural integrity, calculate pile driving stresses, and evaluate bearing capacity. The bearing capacity for each testing scenario was further evaluated with CAPWAP®. CAPWAP allows for the computation of soil resistance forces and their distribution, ie. separation between the skin friction and end bearing. DLT measurements were taken using strain gages and accelerometers attached to diametrically opposite sides of the pile approximately 3 meters below the top of each pile under pile hammer impacts.

A total of 8 piles were installed: 4 reaction piles and 4 static load test piles. The test piles were 1219 mm O.D. x 22/18 mm open ended steel pipe test piles with a wall thickness of 22 mm in the upper 12 meters of the pile, reducing to 18 mm of thickness for the remainder of the pile. The total test pile lengths were 61 to 62 meters and were reported to have a minimum yield strength of 400 MPa. DLT was performed during initial drive (EOD) and during a short-term restrike (BOR) typically 24 to 48 hours after initial driving. Long-term restrikes were then conducted on the test piles 11 to 38 days after EOD. The piles were driven using either an IHC S150 or IHC S200. According to the manufacture's literature, the IHC S150 and S200 have a 74 and 98 kN ram and a maximum rated energy of 149 and 198 kN-m, respectively. Table 3 summarizes the calculated setup ratio based on the CAPWAP calculated EOD shaft resistance and subsequent shaft resistance values for short and long-term restrikes.

Table 3: Setup Ratio

Pile	Shaft Resistance (kN)		Time (days)	Setup Ratio	Embedment Depth* (m)
	EOD	BOR / BOR2			
Tension Pile 1	2200	7400 / 9500	0.9 / 11	3.4 / 4.3	38.25
Compression Pile 1	2100	8200 / 10000	1.8 / 12	3.9 / 4.8	38.25
Tension Pile 2	1700	7400 / NA	1.2 / NA	4.4 / NA	29.80
Compression Pile 2	1500	6800 / 8800	1.0 / 38	4.5 / 5.9	29.80

*Embedment Depth based on penetration into competent soil layer

STATIC LOAD TEST PROGRAM

Test location No. 1 was located approximately 800 meters from shore along the access trestle and test location No. 2 was located in the FSRU platform approximately 400 meters northeast of test location No. 1. For each of the test locations, four piles were driven in a linear configuration, two reaction piles, one compression test pile and one tension test pile. Each pile was installed with a spacing of approximately 4.5 meters. The load was applied with two 7000 kN jacks connected to a manifold. The applied load was monitored with two sets of bending compensated strain gages (three strain gages attached in a triangular pattern 120 degrees apart). The two sets were placed to assure accuracy and backup information in case of instrumentation problems. The applied load was also monitored via two manometers, however, the presented applied loads are based on the strain measurements. Four displacement measurement readers (LVDTS and Digital Dial Gages) were placed at 90 degrees to measure displacement on the test pile. Additional instrumentation was attached to the closest reaction pile to monitor the load and displacement.

Loading specifications required that the compression test piles be loaded to 10000 kN (200% of the design load) during the first cycle. After this load was achieved and failure had not occurred for compression test pile 1, the load was increased up to a target load 12500 kN (250%) during the second cycle. As shown in Figure 4 & 6, the maximum test load for compression pile 1 and 2 was 11600 and 8900 kN, respectively. At these points, the pile could not hold the load and geotechnical failure occurred. If using Davisson Criterion for failure load determination it is observed that the obtained failure load is 11600 and 8500 kN for compression test pile 1 & 2, respectively.

For the tension test piles, the first cycle had a target load of 10000 kN (250% of the design load). There was a contingency for a second cycle to 12500 kN (300%) if failure did not occur after the first cycle. As shown in Figure 5 & 7, the maximum test load for tension pile 1 and 2 was 9500 and 9200 kN, respectively. At these points, the pile could not hold the load and geotechnical failure occurred. If using a tangent criterion for failure load determination it is observed that the obtained failure load is 9500 and 8500 kN for tension test pile 1 & 2, respectively.

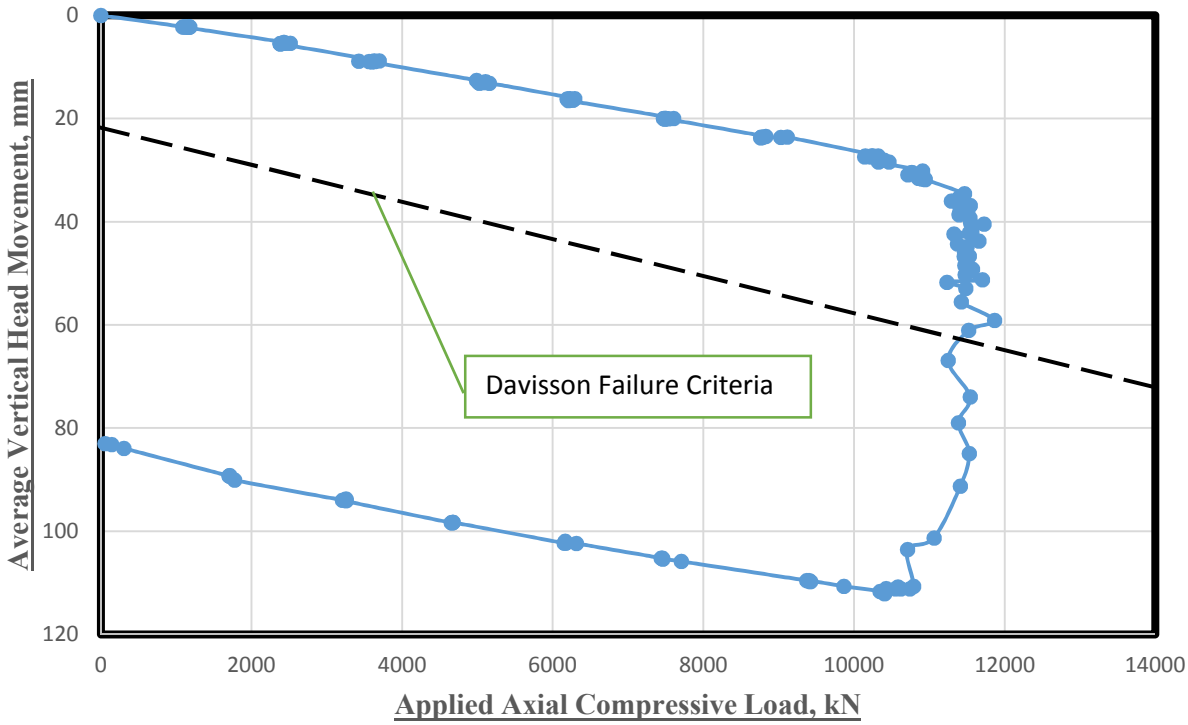


Figure 4: Compression Pile 1 – Load vs. Vertical Movement

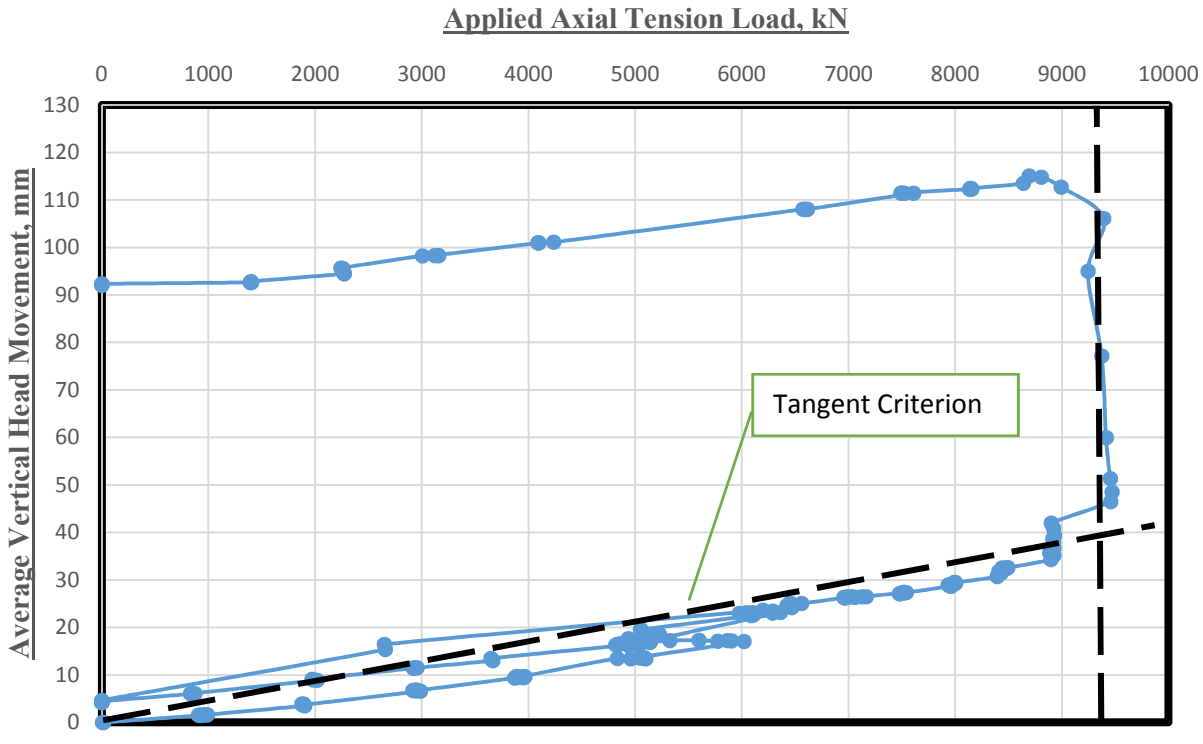


Figure 5: Tension Pile 1 – Load vs. Vertical Movement

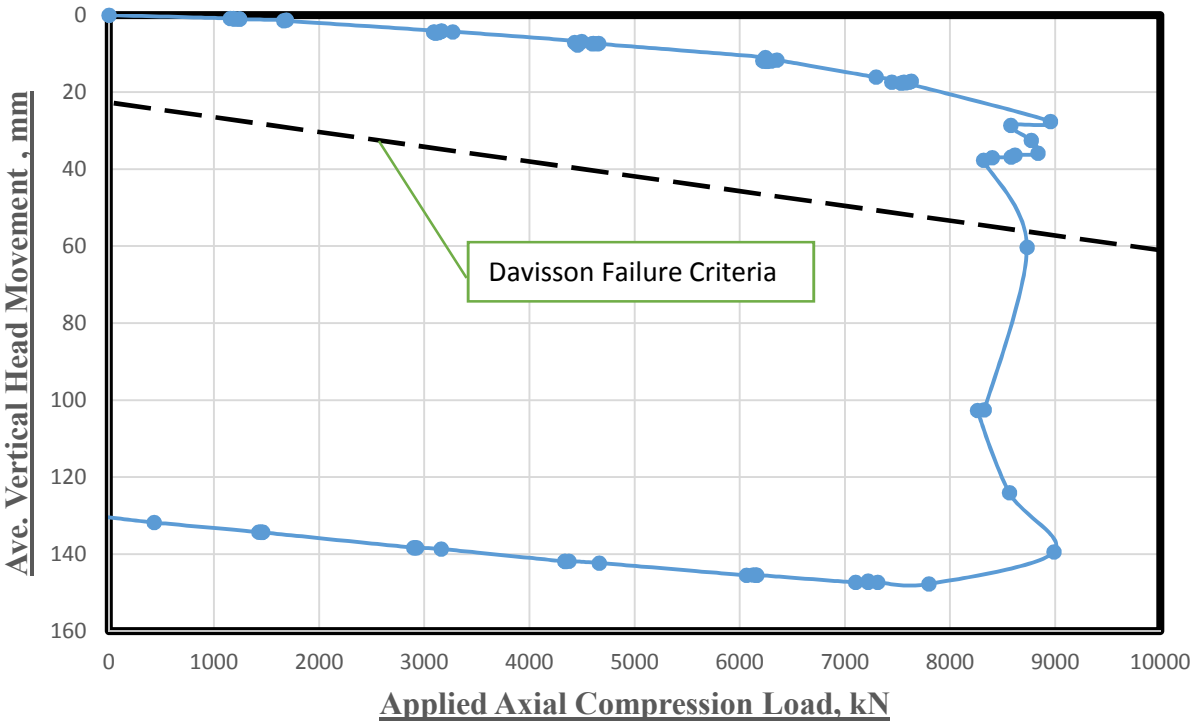


Figure 6: Compression Pile 2 – Load vs. Vertical Movement

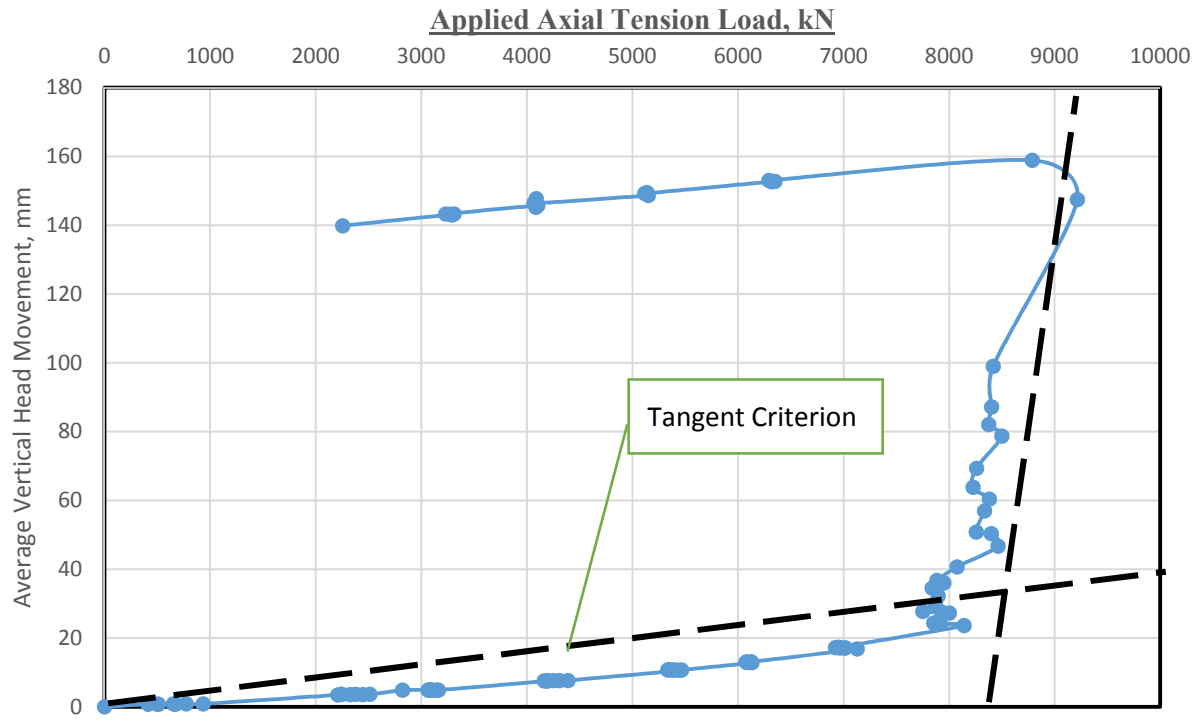


Figure 7: Tension Pile 2 – Load vs. Vertical Movement

CORRELATING DLT & SLT RESULTS

As evidenced for compression test pile 1, the shaft friction setup factor obtained when comparing the shaft friction at the end of initial drive (2100 kN) versus the shaft friction obtained during the static load test (10600 kN) generates a shaft friction setup factor of 5.0. The end bearing being was assumed to be 1000 kN, as was calculated during DLT testing. This implies an overall pile resistance setup factor (including end bearing) of 4.0 (11600kN/2900kN). Figure 8 presents on a log scale the estimated shaft friction vs elapsed time. The initial rate of shaft friction increase is considerably fast, but then slows down with time. A majority of the soil setup is gained in the first 10 days after initial pile installation. Both DLT and SLT results are consistent. The predicted failure load of compression test pile 1 during DLT was predicted to be 10500 kN after an elapsed time of 11 days after EOD, whereas the failure load during SLT was predicted to be 11600 kN after an elapsed time of 42 days after EOD. With this agreement, no adjustments are necessary to be performed to the DLT results to correlate with the SLT results. Based on Figure 8, a conservative estimate of the long term capacity is approximately 1000 kN higher than at the time of testing, however, it was decided to utilize this additional resistance as a conservative approach for the pile length determination.

Based on the tension test pile 1 results, the predicted failure load of 9500 kN was achieved after an elapsed time of 42 days after EOD. This implies that the uplift pile resistance is close to 90% of the measured compression shaft friction. Typically, a general assumption is that the compression shaft friction is reduced by 80% to calculate the uplift resistance. For these soil types in which most of the shaft friction is developed from cohesion, as evidenced by the large setup factor (5.0), a 90% reduction factor seems appropriate.

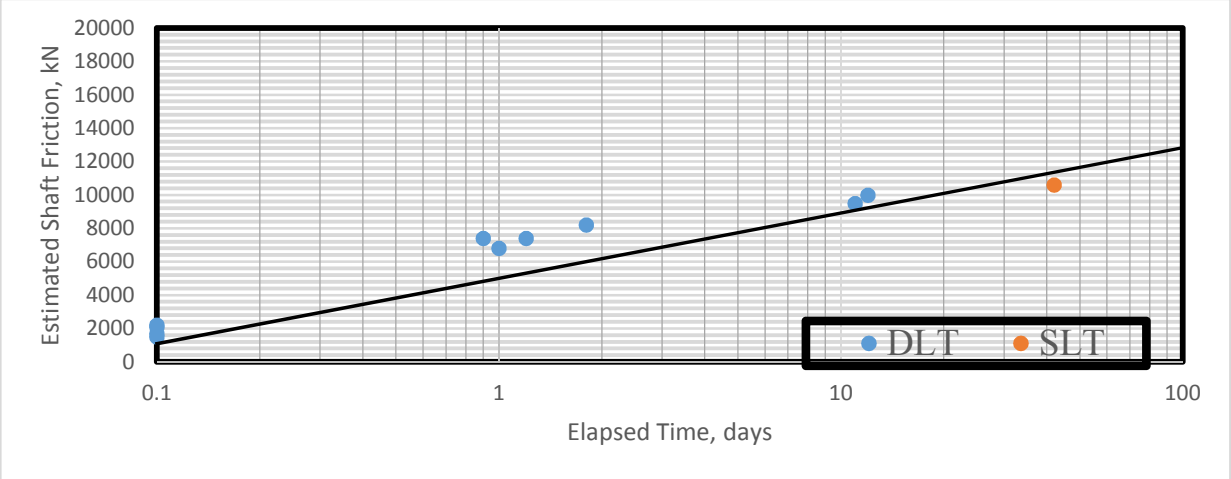


Figure 8: Shaft Friction vs. Log Scale Elapsed Time

DRIVING CRITERIA

Based on the obtained overall soil resistance setup factors from testing location No. 1 and 2, a driving criteria recommendation was established for the piles to be installed. The soil resistance setup factor was estimated to be 4.0 and thus the driving criteria was developed for EOD loads of 25% of the required ultimate load. The additional 75% of the resistance will develop with time after initial pile installation as soil setup occurs. The GRLWEAP® program was used to create a refined Wave Equation Analysis (WEAP) which creates a model that calibrates to the field testing that was performed. As shown in Table 4, the refined WEAP provides the required blow count for select ultimate bearing capacities for the IHC S150 at varying hammer energies. The driving criteria assumes a 62 meter long 1209 O.D. x 18 mm open ended pile with an embedment depth of 40 meters, without consideration of the competent layers as Table 1.

Three hammer settings were assumed; 100% (150 kJ) of the hammer, 80% (120 kJ) and 60% (90kJ) of the hammer. The driving criteria also considers that the piles will be installed in either a vertical orientation, or inclined on a 1:3 or 1:4 ratio. Driving criteria was also developed for the S90 and S200 hammers, but are not presented.

Table 4: Driving Criteria – S150 Hammer

Required Ultimate Capacity	Required BLC - Energy 60%	Required BLC - Energy 80%	Required BLC - Energy 100%
MN	blows/25cm	blows/25cm	blows/25cm
11	26	22	18
10	23	19	16
9	22	17	14
8	19	15	13
7	16	13	11
6	14	12	9
5	11	9	8
4	9	8	7
3	7	6	5

CONSTRUCTION BENEFITS

The pile driving operations were facilitated with jack-up barges and adjustable side mounted pile templates. Based on the initial design of the piling, it was assumed that a majority of the piles would be 71 to 72 meters in total length, however, after the load test program, the total pile length was optimized to 62 meters. The following benefits significantly aided in keeping the project ahead of the accelerated schedule, on budget, and avoiding costly delays with the potential for deadline penalties.

- The reduction in length was a significant cost savings when applied to 400+ piles (~3600 meters of piling length reduction)
- The contractor was able to mobilize a third jack-up barge to aid in installing piles. This third jack-up was not included in the initial construction plan because it did not have the configuration to handle piles over 70 meters.
- The decrease in total pile stick up, especially for the battered piles, reduced the bending and strain induced on the pile template during driving and thus saved down time that would have been required for maintenance and repairs.
- The jack-ups spent less time getting the platform to the proper elevations because of the reduced pile stick-up.
- The total number of blows required to install the piling was reduced.

FOUR PILE LINEAR LOAD TEST

Onshore static load testing generally uses a linear layout of test piles and reaction piles with the reference beams supported without the use of piles, but offshore testing typically relies on piling installed orthogonal to the test piles to support the reference beams. The setup for these static load tests utilized a four pile linear layout with the tension and compression test piles installed next to each other and the outer most piles acting as the reaction piles. The reference frame was then cantilevered from the non-test pile, as depicted in Figure 9. The reference frame was designed to be as stiff as possible, however, there was relative motion that was observed in the dial gage readings. This motion (~1 mm) was determined to be minute compared to the total displacement that was observed throughout testing.

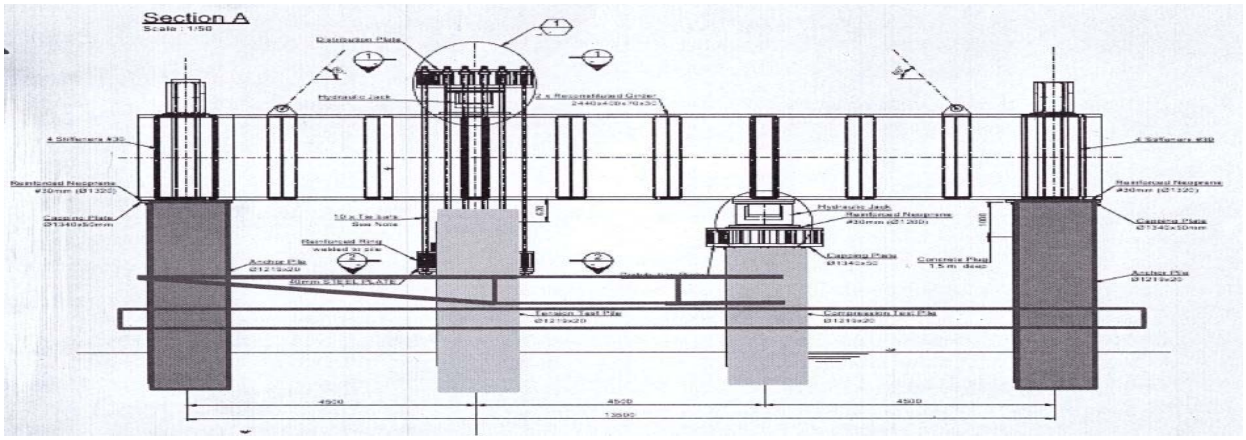


Figure 9: Four Pile Linear SLT Layout

CONCLUSIONS

Given the required accelerated timeline for this project, some may have foregone the load test program in favor of making progress. However, based on the benefits of shorter piles and additional equipment assisting in installing piles, the load test program was successful in providing significant cost savings to the project along with a quality control mechanism that increases the owner's confidence in the installed foundation. Furthermore, it was concluded that the dynamic load testing and static load testing results were very comparable for this site. The tension load tests indicated the pile uplift resistance can be assessed as 90% of the measured compression resistance obtained from the dynamic testing. A friction setup factor of 5.0 was obtained a combination of testing, yielding an overall setup factor (including end bearing) of 4.0.

ACKNOWLEDGEMENTS

The authors gratefully acknowledge Besix Group for the release of the design documents, load test program results and production pile DLT results presented in this paper.

REFERENCES

Besix Orascom Joint Venture (2016). Preliminary Geotechnical and Pile Capacity Report, Document No. ASPH-BD-GE-DN-07901_Rev00.

Fellenius, B.H., Riker, R.E., O'Brien, A.J., and Tracy, G.R. (1989). Dynamic and Static Testing in a Soil Exhibiting Set-up. ASCE Journal of Geotechnical Engineering, 115(7) 984-1001.

Komurka, V.E., Wagner, A.B., and Edil, T.B. (2003). Estimating Soil/Pile Set-up, Wisconsin Highway Research Program, Contract No 0092-00-14, Report No. 03-05.

Komurka, V.E. (2004). Incorporating Set-up and Support Cost Distributions into driven Pile Design, Current Practices and Future trends in Deep Foundations, ASCE/Geo-Institute, Geotechnical Special Publication, GSP125, pp. 16-49.

Rausche, F. (2018). Combining Static And Dynamic Loading Test Results Of Piles, Symposium: 10th Int. Conf. on Stress Wave Theory and Testing of Deep Foundations, San Diego, CA.

Solly, Raymond (2007). Tanker: The History and Development of Crude Oil Tankers.

EFFECT OF INSTALLATION METHOD ON THE RATIO OF TENSILE TO COMPRESSIVE UNIT SHAFT RESISTANCE OF PILES IN DENSE SAND

Galvis-Castro, A. C.[1], Ganju, E.[2], Tovar-Valencia, R. D[3], Prezzi, M.[4] and Salgado, R.[5]

ABSTRACT

It is generally accepted that the unit shaft resistance of piles in sands is lower for tensile loading than for compressive loading. So far, very little attention has been paid to the influence of the installation method on the tensile-to-compressive unit shaft resistance ratio. The objective of this paper is to analyze the effect of installation method on the ratio of unit shaft resistance in tension to that in compression for a model pile installed in a dense silica sand. To study installation effects, load tests on model piles were carried out in a half-cylindrical calibration chamber with digital image correlation (DIC) capability. The model piles were either jacked in one stroke using a constant rate of advance, or pre-installed into the dense sand samples. Digital images of the model pile and sand were taken during the load test and processed using DIC to obtain the displacement field in the sand. It was found that unit shaft resistance was essentially the same in tension and compression for the pre-installed pile, however for the jacked pile, the unit shaft resistance in tension was approximately half of that in compression. DIC analysis revealed that: (1) during the load test, more displacement occurs in the soil domain for the pre-installed pile compared to the jacked pile, (2) for the jacked pile, the magnitude of displacement in the soil domain is greater in tension than in compression and (3) for the pre-installed pile, the magnitudes of displacement in tension and compression are similar.

Keywords: Displacement and non-displacement piles; Digital Image Correlation (DIC); Calibration chamber; Model piles; Sand.

[1] PhD. Candidate, Lyles School of Civil Engineering, Purdue Univ., West Lafayette, IN, USA (corresponding author) E-mail: agalvisc@purdue.edu

[2]PhD. Candidate, Lyles School of Civil Engineering, Purdue Univ., West Lafayette, IN, USA E-mail: eganju@purdue.edu

[3]Assistant Professor. Civil and Environmental Department, Universidad del Norte, Barranquilla, Atlántico, Colombia E-mail: rubent@uninorte.edu.co

[4] Professor of Civil Engineering, Lyles School of Civil Engineering, Purdue Univ., West Lafayette, IN, USA. E-mail: mprezzi@ecn.purdue.edu

[5] Charles Pankow Professor in Civil Engineering, Lyles School of Civil Engineering, Purdue Univ., West Lafayette, IN, USA. E-mail: rodrigo@ecn.purdue.edu

© 2019 Deep Foundations Institute

INTRODUCTION

Pile foundations can be categorized into two main types depending on the method of installation: displacement piles (e.g., jacked or driven piles) and non-displacement piles (e.g., bored piles or drilled shafts) (Basu et al. 2010; Salgado 2008). The response of these piles to loading can be studied in the laboratory by means of calibration chamber experiments on model piles that are either jacked into the samples, representing displacement piles (Jardine et al. 2005; Lee et al. 2011; Tovar-Valencia et al. 2018), or pre-installed in the sand sample, representing non-displacement piles(Galvis-Castro et al. 2019a; Le Kouby et al. 2013; Tehrani et al. 2016)

It is generally accepted in research and practice that the unit shaft resistance of displacement piles in sands is lower for tensile loading than for compressive loading (Beringen et al. 1979; Chow et al. 1997; De Nicola and Randolph 1993, 1999; O'Neill and Reese 1999). Various experimental studies of the loading response of non-displacement piles in sand in the field and in the laboratory have shown that the shaft capacity of fresh non-displacement piles is similar for tensile and compressive loading (Chen and Kulhawy 2002; Galvis-Castro et al. 2019a; Ismael 2001; Le Kouby et al. 2013; Kulhawy 2004; Kulhawy and Hirany 1989). According to Galvis-Castro et al. (2019), the negligible effect of loading direction on the shaft resistance of non-displacement piles could be attributed to the installation method, which does not preload the soil in any way. Despite experimental evidence, in practice a reduction factor is often applied to the shaft resistance of non-displacement piles in compression to compute the shaft resistance in tension (Brown et al. 2010; O'Neill and Reese 1999).

The objective of this paper is to study the effect of installation method on the unit shaft resistance of displacement and non-displacement piles under tensile and compressive loading. Static load tests on model piles are carried out in a calibration chamber with Digital Image Correlation (DIC) capabilities. The use of DIC allows to accurately measure the displacements of the soil surrounding the pile shaft during loading, which give insights into the mechanism of mobilization of shaft resistance.

MATERIALS AND EXPERIMENTAL SET-UP

Load tests on model piles are performed in a half-cylindrical calibration chamber, 1.2 m in height and 1.68 m in diameter, with three observation windows on the front wall of the chamber. To load the pile in tension and compression, a jacking system is positioned above the calibration chamber, aligned with its flat edge. Prior to load test, three CMOS cameras (one for each observation window) and multiple lighting systems are positioned in front of the calibration chamber. Figure 2 shows a schematic of the setup, further details of the setup have been described by Arshad et al. (2014).

The sand used for this study is a silica sand, known as Ohio Gold Frac. Table 1 shows its index properties. The sample is prepared by raining down the sand into the calibration chamber using a pluviator with diffuser sieves, which ensure sample homogeneity. The relative density D_R of the sand, dense ($D_R \approx 90\%$) or medium-dense ($D_R \approx 65\%$), is controlled by the drop height. Multiple samplers are placed inside the calibration chamber at different stages of sample preparation to get a measure of sample density along the depth. Further details of the sample preparation method have been described by Arshad (2014) and Lee (2008).

The model piles used in this research are half-cylindrical, closed-ended piles with a diameter of 31.75 mm. The pile installed by jacking has a conical base with an apex angle of 60° and the pre-installed pile has a flat base. It was found that the shape of the base does not affect the unit shaft resistance significantly, especially for pre-installed piles (Galvis-Castro et al. 2019a). The pile base in both the piles is instrumented with a miniature load cell of 10 kN capacity which captures the tip resistance in compression. The pile head is connected to a tension/compression load cell with a capacity of +/- 20 kN.

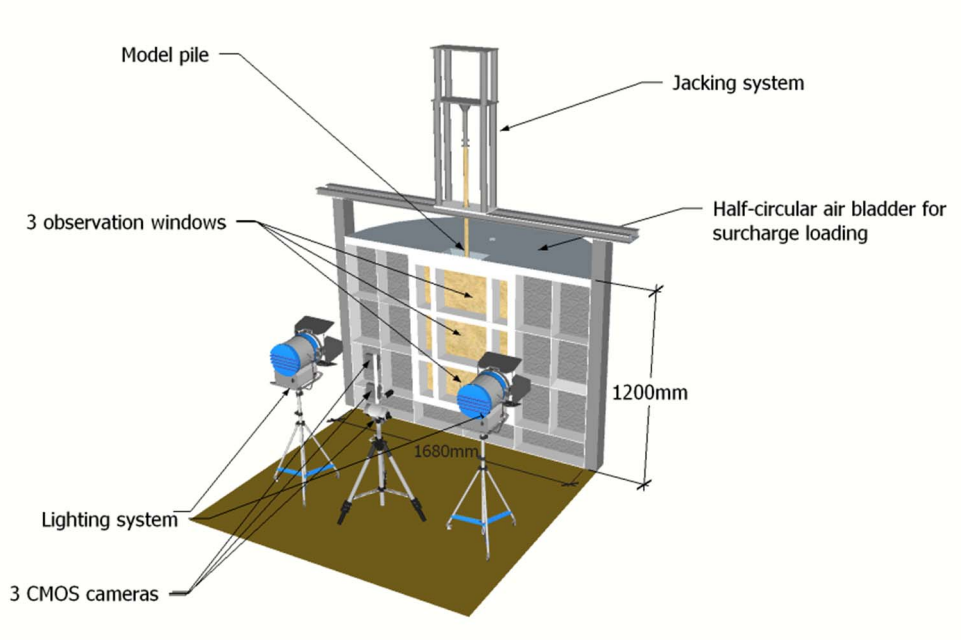


Figure 1. Experimental equipment for model pile testing (Doreau-Malioche et al. 2019)

Table 1 Index properties of Ohio Gold Frac sand (Modified after Galvis-Castro et al. (2019b); Han et al. (2018b)**)**

D_{50} (mm)	C_u	C_c	e_{max}	e_{min}	G_s	R^a	S^b	$USCS^c$
0.62	1.44	0.94	0.81	0.59	2.65	0.43	0.83	SP

[a] Roundness (Wadell 1932); [b] Sphericity (Wadell 1932); [c] United Soil Classification System

The total shaft resistance is computed as the difference of the load cells at the pile base and head. The shaft of the model pile is covered with sand paper (Brand 3M, Grit #120) to simulate the roughness of production piles (Tovar-Valencia et al. 2017). The shaft roughness is quantified using the normalized roughness parameter R_n (= 0.131) computed according to the procedure outlined by Tovar-Valencia et al. (2018). The computed R_n, according to the findings of Han et al. (2018), correspond to a very rough surface. Therefore, the shearing is expected to take place internally in the sand.

It is known that if the relative size of the model pile to the chamber is too large, it can lead to boundary effects and distort the resistance measurements (Salgado et al. 1998). Additionally, if the size of the model pile is too small in comparison to the sand particle, it can lead to scale effects and an over estimation of resistances. The ratio of the diameter of the calibration chamber (1680 mm) to the diameter of the pile (31.75 mm) is 52.9, reducing any effect of the rigid boundary of the calibration chamber on the pile resistance. With respect to the scale effect, the ratio of the D_{50} of sand particle (0.62 mm) to the diameter of the pile (31.75 mm) is 51, ensuring that scale effects are also negligible (Gui and Bolton 1998; Salgado 2013)

Slightly different sample preparation procedures were followed for the jacked and pre-installed piles. For the jacked pile, the sand sample was prepared by raining the sand into an empty calibration chamber. In the case of the pre-installed pile, first the model pile was positioned inside the calibration chamber (with the base positioned at the center of the second window) using spacers and then the sand was rained down using the pluviator. After the sand sample was prepared, a surcharge of 70 kPa was applied on its top surface

using a surcharge bladder and maintained for the duration of the test. For the case of the jacked pile, installation was carried out monotonically at a rate of 0.8 mm/s.

After the piles were installed, load test was carried out by pushing the installed pile at a rate of 0.1 mm/s, simulating quasi-static conditions. The minimum displacement achieved during the load test was approximately 31.75 mm (1.0*B*). During the load test, the model pile's base load Q_b and the head load Q_t were recorded at a frequency of 2 readings per second. Each of the three digital CMOS cameras were set to take images at a rate of 2 frames per second (fps).

Table 2 shows the load test program followed for the study. In the table, the test code describes if the pile was jacked monotonically (JM) or pre-installed (PI) and subsequently if the load test was carried out in compression (C) or in tension (T). The commercial software VIC-2D (Correlated Solutions 2009) was used to analyze the digital images captured during load test using the Digital Image Correlation (DIC) technique. Details of DIC fundamentals and camera calibration can be found in Pan et al. (2009) and Arshad et al. (2014).

Table 2 Loading test program for model pile to study effect of installation method on unit shaft resistance in tension and compression

Test code	Installation	Static load test	Base geometry
JM-C	Jacked monotonically	Compressive	conical
JM-T		Tensile	
PI-C	Preinstalled	Compressive	flat
PI-T		Tensile	

All model piles had the same surface roughness (R_n= 0.131), all tests were performed in dense sand samples. JM: jacked monotonically, PI: preinstalled, T: tension test, C: Compression test

RESULTS

Unit shaft resistance during pile load test

The unit shaft resistance was calculated as the difference between the loads at the pile head and pile base, divided by the surface area of pile in contact with the sand. Figure 2 (a) shows the absolute value of the unit shaft resistance $|q_{s,avg}|$ versus absolute value of the pile head displacement $|w|$ of tensile and compressive static load tests performed on pre-installed model piles. A peak in shaft resistance q_{sP} is clearly observed in the tensile (test PI-T) and compressive (Test PI-C) loading tests. The magnitudes of the peak resistance $|q_{sP}|$ measured from the compressive loading test (i.e., $|q_{sP}|$ = 90.8 kPa in test PI-C) is comparable to the $|q_{sP}|$ from the tensile loading test (i.e., $|q_{sP}|$ = 91.1 kPa in test PI-T). After the peak, $|q_{s,avg}|$ decreases and tends to stabilize at the limit unit shaft resistance q_{sL} (= 70 kPa) as $|w|$ increases. Similar values of $|q_{sL}|$ measured in the compressive and tensile loading tests indicate a negligible effect of the loading direction on the peak shaft resistance measured in virgin pre-installed piles, as also observed in field and laboratory experiments by Ismael (2001), Le Kouby et al. (2013), Kulhawy (2004), and Kulhawy and Hirany (1989).

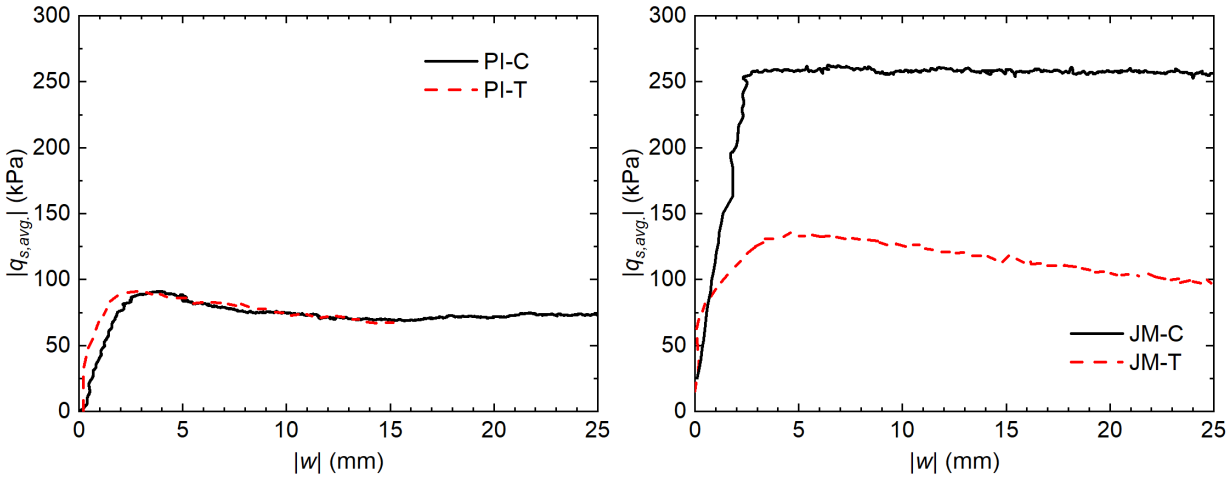


Figure 2. Absolute value of the unit shaft resistance $|q_{s,avg}|$ vs. absolute value of pile head displacement $|w|$ for (a) pre-installed model piles tested in tension (test PI-T) and compression (test PI-C) and (b) monotonically jacked model piles tested in tension (test JM-T) and compression (test JM-C)

Figure 2 (b) shows the absolute value of the unit shaft resistance $|q_{s,avg}|$ versus the absolute value of the pile head displacement $|w|$ for the static loading test performed on model piles installed by monotonic jacking. In Figure 2 (b), it is clear that greater magnitude of $q_{s,avg}$ is developed when the pile is loaded in compression than when it is loaded in tension. No peak in shaft resistance is observed in the load-settlement curves during the compressive load test (i.e., test MJ-C): after the $q_{s,avg}$ reaches a maximum value, it stabilizes to its limit unit shaft resistance.

In these experiments, the maximum absolute value of $q_{s,avg}$ (peak unit shaft resistance) develops at a magnitude $|w|$ of the pile head displacement equal or less than 3.6 mm = $0.1B$ = $5.8D_{50}$. Given the load on the head and base of the pile, and its axial stiffness, we can reasonably assume that 3.6 mm is the shear displacement of the soil elements next to the pile shaft. This is generally true for short and rigid piles or pile sections, such as those tested in calibration chamber experiments. This is not the case for longer and compressible piles.

The peak is observed at the approximately the same shear displacement for compressive and tensile loading, which is similar to what was observed by Le Kouby et al. (2013). Table 3 presents the data from literature concerning the shear displacement required to mobilize maximum unit shaft resistance in non-displacement piles with rough interface. For these, the displacement needed appears to be in the range of 4-10D_{50}. The displacement needed to mobilize the peak shaft resistance appears to be independent of the pile diameter.

Table 3 Pile-head displacement required to mobilize the peak unit shaft resistance during static loading for non-displacement piles

Reference	$\|w_p\|$ (mm)	B (mm)	D_{50} (mm)	$\|w_p\|/D_{50}$	$\|w_p\|/B$
Fioravante (2002) (*)	1.5	10	0.22	6.8	0.15
Lehane et al. (2005) (*)	1.1-1.9	3-18	0.19	5.4-9.7	0.1-0.6
Le Kouby et al. (2013) (+)	0.75	20	0.20	3.75	0.038

(*) test in centrifuge; (+) test in calibration chamber

Table 4 presents the ratio of the limit unit shaft resistance in tension and compression for the pre-installed and jacked piles. Results show that, for the jacked piles, the tension-to-compression shaft resistance ratio SRR is 0.5; whereas for the pre-installed piles, the ratio is 1. From Table 4, the limit unit shaft resistance in compression for the pre-installed pile is 28% of that for the jacked pile. While in tension, the unit shaft resistance for the pre-installed pile is 56% of that for the jacked pile. Although the unit shaft resistance from model pile tests cannot be directly applied to a prototype pile due to scale effects (Foray et al. 1998; Loukidis and Salgado 2008) the study of the processes that take place next to a model pile during loading in either tension or compression are relevant to the understanding of the fundamental behavior of full-scale displacement and non-displacement piles.

Table 4. Absolute value of unit shaft resistances $|q_{s,L}|$ from tensile and compressive loading and tensile-to-compressive unit shaft resistance ratio *SRR*

Test code	Static loading	$\|q_{s,L}\|$(kPa)	*SRR**
PI-C	Compressive	70	1.0
PI-T	Tensile	70	
JM-C	Compressive	250	0.5
JM-T	Tensile	125	

**SRR*= tension-to-compression limit shaft resistance ratio calculated as the maximum value of the unit shaft resistance from the tensile loading divided by the unit shaft resistance at w=15mm from the compressive loading, both measured from static loading tests from piles of the same installation method.
JM: jacked monotonically, PI: preinstalled, T: tension test, C: Compression test

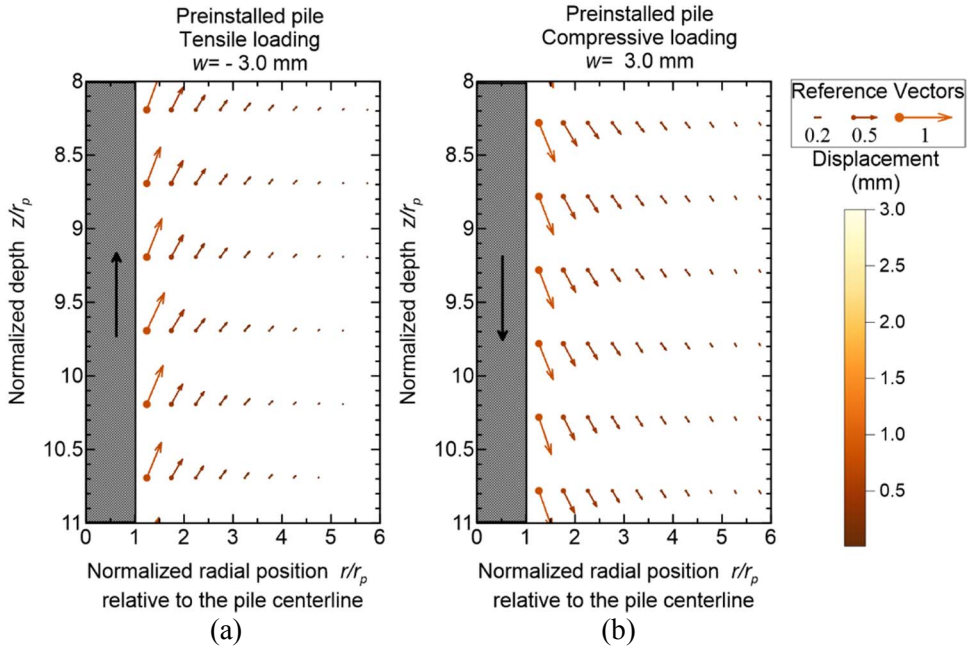
Soil displacements from Digital Image Correlation

Figure 3 (a)-(d) show the soil displacement vectors for pre-installed and jacked pile, under tensile and compressive loading. The displacement vectors correspond to a pile head movement $|w|$ of 3 mm. The vectors are obtained from the DIC analysis of the images collected during the load tests. The displacement vectors are plotted in the z/r_p versus r/r_p plane, where z is the vertical distance from the sample surface, r is the radial distance relative to the pile axis, and r_p is the radius of the model pile.

From Figure 3 (a) and (b) it can be seen that for the pre-installed piles, the magnitude of displacement during tensile or compressive loading is maximum near the shaft and reduces with increasing radial distance. The magnitude of the displacement vectors for tensile loading is comparable to that for compressive loading of displacement piles. Additionally, the orientation of the displacement vectors in tensile loading is the mirror image of that in compressive loading. The radial component of the displacement vectors for both loading direction, tensile and compressive loading, show that the soil is moving radially

away from the pile, indicating a dilative behavior of the soil. These observations provide an explanation of why the unit shaft resistance measured in tension is similar in magnitude to that measured in compression for pre-installed piles.

Figure 3 (c) and (d) show that for jacked piles, the magnitude of displacement during tensile or compressive loading is highly localized. This may be attributed to the densification caused by cavity expansion and formation of a crushed band of material next the shaft during jacking. The orientation of the displacement vectors during compressive loading shows that the soil is moving away from the pile, indicating a dilative response of the soil. However, in the case of tensile loading, the displacement vectors show that the soil is moving towards the pile indicating a contractive response of the soil. These results may explain why the measured unit shaft resistance in tension is significantly less than that in compression for jacked piles.



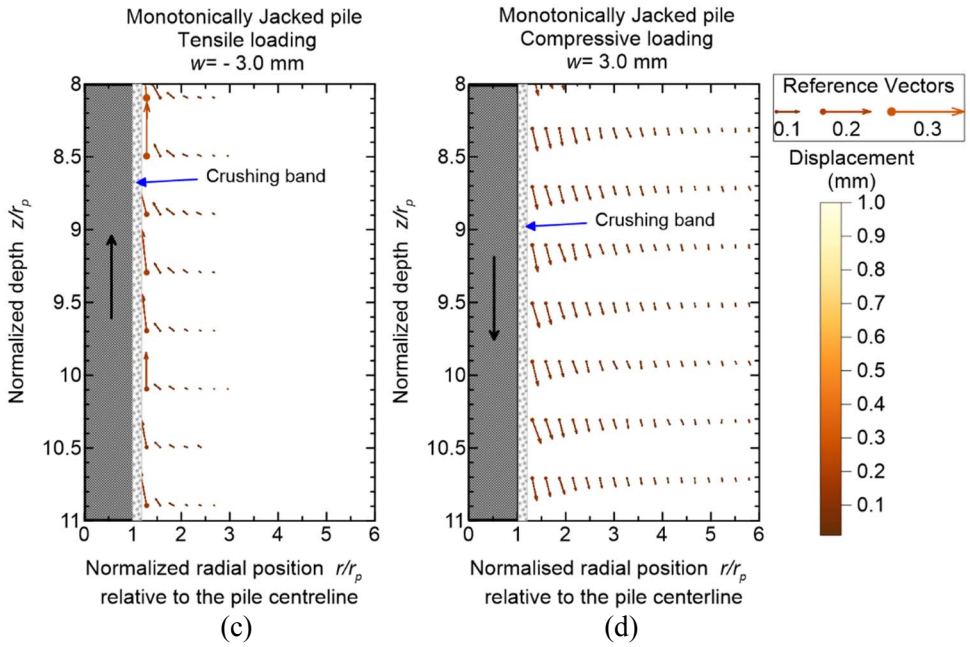


Figure 3 Soil displacement vectors after 3 mm of pile head displacement for (a) pre-installed pile loaded in tension, (b) pre-installed pile loaded in compression, (c) monotonically piles loaded in tension and (d) monotonically jacked pile loaded in compression

CONCLUSION

Capacity of pile under tensile and compressive loading is significantly affected by the installation method. In this study, the effect of installation method on the unit shaft resistance of model pile was studied by means of load test carried out in a calibration chamber with DIC capabilities. Four static load tests, two in tension and two in compression, were carried out on model piles which were either pre-installed (representing non-displacement piles) or monotonically jacked (representing displacement piles) in dense sand samples. During the static load test, the load at the pile head and base were recorded and images of the model pile and sand were captured and analyzed using DIC techniques to obtain the displacement vectors in the sand.

Results showed that the unit shaft resistance for pre-installed piles is lower than that for jacked pile in both tension and compression. It was also found that for the pre-installed model piles, the magnitude of unit shaft resistance was similar in tension and compression. DIC analysis revealed that the soil response is dilative, with similar magnitude, for both loading directions, which agreed with the measured $SRR = 1$. For jacked piles, the limit unit shaft resistance in tension was half of that in compression ($SRR = 0.5$); this is supported by the contractive behavior of the soil observed from DIC analysis next to shaft of the pile loaded in tension.

REFERENCES

Arshad, M. I. (2014). "Experimental study of the displacements caused by cone penetration in sand." Purdue University, West lafayette, IN.

Arshad, M. I., Tehrani, F. S., Prezzi, M., and Salgado, R. (2014). "Experimental study of cone penetration in silica sand using digital image correlation." *Géotechnique*, 64(7), 551–569.

Basu, P., Prezzi, M., and Basu, D. (2010). "Drilled Displacement Piles – Current Practice and Design." *DFI Journal - The Journal of the Deep Foundations Institute*, 4(1), 3–20.

Beringen, F. L., Wind, D., and Van Hooydonk, W. R. (1979). "Results of loading tests on driven piles in sand." *Recent developments in the design and construction of piles. Proceedings of the Conference Held at the Institution of Electrical Engineers*, A. M. Burt, ed., Institution of Civil Engineers, London, UK, 213–225.

Brown, D. A., Turner, J. P., and Castelli, R. J. (2010). *Drilled shafts: Construction Procedures and LRFD Design Methods FHWA NHI-10-016*. *National Highway Institute U.S. Department of Transportation Federal Highway Administration*.

Chen, Y.-J., and Kulhawy, F. H. (2002). "Evaluation of drained axial capacity for drilled shafts." *Deep Foundations 2002 An International Perspective on Theory, Design, Construction, and Performance*, M. W. O'Neill and F. C. Townsend, eds., American Society of Civil Engineers, Reston, VA, United States, 1200–1214.

Chow, F. C., Jardine, R. J., Nauroy, J.-F., and Brucy, F. (1997). "Time-related increases in the shaft capacities of driven piles in sand." *Geotechnique 47*, (5), 353–361.

Doreau-Malioche, J., Galvis-Castro, A., Tovar-Valencia, R., Viggiani, G., Combe, G., Prezzi, M., and Salgado, R. (2019). "Characterising processes at sand-pile interface using digital image analysis and X-ray CT." *Géotechnique Letters*, 0, 1–9.

Fioravante, V. (2002). "On the shaft friction modeling of non-displacement piles in sand." *Soils and Foundations*, 42(2), 23–33.

Foray, P., Balachowski, L., and Rault, G. (1998). "Scale effect in shaft friction due to the localisation of deformations." *Centtifuge 98*, (September 1998), 211–216.

Galvis-Castro, A. C., Tovar-Valencia, R. D., Salgado, R., and Prezzi, M. (2019a). "Compressive and tensile shaft resistance of non-displacement piles in sand." *Journal of Geotechnical and Geoenvironmental Engineering*, 145(9), 0401041.

Galvis-Castro, A. C., Tovar, R. D., Salgado, R., and Prezzi, M. (2019b). "Effect of loading direction on the shaft resistance of jacked piles in dense sands." *Geotechnique*, 69(1), 16–28.

Gui, M. W., and Bolton, M. D. (1998). "Geometry and scale effects in CPT and pile design." *Proc. 1st Int. Conf. Site Characterization*, Balkema, Rotterdam, 1063–1068.

Han, F., Ganju, E., Salgado, R., and Prezzi, M. (2018). "Effects of Interface Roughness, Particle Geometry, and Gradation on the Sand-Steel Interface Friction Angle." *Journal of Geotechnical and Geoenvironmental Engineering Effects*, 144(12), 04018096.

Ismael, N. F. (2001). "Axial Load Tests on Bored Piles and Pile Groups in Cemented Sands." *Journal of Geotechnical and Geoenvironmental Engineering*, 127(9), 766–773.

Jardine, R. J., Chow, F., Overy, R., and Standing, J. (2005). *ICP design methods for driven piles in sand and clays*. Thomas Telford, UK.

Le Kouby, A., Dupla, J. C., Canou, J., and Francis, R. (2013). "Pile response in sand: experimental development and study." *International Journal of Physical Modelling in Geotechnics*, 13(4), 122–137.

Kulhawy, F. H. (2004). "On the axial behavior of drilled foundations." *Geosupport 2004*, J. P. Turner and P. W. Mayne, eds., American Society of Civil Engineers, ASCE, USA, 34–51.

Kulhawy, F. H., and Hirany, A. (1989). "Interpretation of load tests on drilled shafts—Part 2: Axial uplift." *Foundation engineering: current principles and practices*, F. H. Kulhawy, ed., ASCE, New York, NY, United States, 1150-1159.

Lee, J. (2008). "Experimental Investigation of the load response of model piles in sand." *Purdue University*, Purdue University.

Lee, J., Prezzi, M., and Salgado, R. (2011). "Experimental investigation of the combined load response of model piles driven in sand." *Geotechnical Testing Journal*, 34(6), 103269.

Lehane, B. M., Gaudin, C., and Schneider, J. A. (2005). "Scale effects on tension capacity for rough piles buried in dense sand." *Géotechnique*, 55(10), 709–719.

Loukidis, D., and Salgado, R. (2008). "Analysis of the shaft resistance of non-displacement piles in sand." *Géotechnique*, 58(4), 283–296.

Martinez, A., and Frost, J. (2016). "The influence of surface roughness form on the strength of sand-structure interface." *Geotechnique Letters*, 00(00), 1–8.

De Nicola, A., and Randolph, M. F. (1993). "Tensile and compressive shaft capacity of piles in sand." *Journal of Geotechnical Engineering*, 119(12), 1952–1973.

De Nicola, A., and Randolph, M. F. (1999). "Centrifuge modelling of pipe piles in sand under axial loads." *Géotechnique*, 49(3), 295–318.

O'Neill, M. W., and Reese, L. C. (1999). *Drilled shafts: Construction procedures and design methods. Report No. FHWA-IF-99-025*.

Pan, B., Qian, K., Xie, H., and Asundi, A. (2009). "Two-dimensional digital image correlation for in-plane displacement and strain measurement: a review." *Measurement Science and Technology*, IOP Publishing.

Salgado, R. (2008). *The Engineering of Foundations*. McGraw-Hill.

Salgado, R. (2013). "The mechanics of cone penetration : Contributions from experimental and theoretical studies." *Proceedings of the 4th International Conference on Site Characterization 4, ISC-4*, R. Q. Coutinho and P. W. Mayne, eds., Taylor & Francis, London, UK, 131–153.

Salgado, R., Mitchell, J. K., and Jamiolkowski, M. (1998). "Calibration Chamber Size Effects on Penetration Resistance in Sand." *Journal of Geotechnical and Geoenvironmental Engineering*, 124(9), 878–888.

Tehrani, F. S., Han, F., Salgado, R., Prezzi, M., Tovar, R. D., and Castro, A. G. (2016). "Effect of surface roughness on the shaft resistance of non-displacement piles embedded in sand." *Géotechnique*, 66(5), 386–400.

Tovar-Valencia, R. D., Galvis-Castro, A. C., Salgado, R., and Prezzi, M. (2017). "Effect of surface roughness on the shaft resistance of model piles in sand." *Journal of Geotechnical and Geoenvironmental Engineering*, Accepted(144), 3.

Tovar-Valencia, R. D., Galvis-Castro, A. C., Salgado, R., and Prezzi, M. (2018). "Effect of surface roughness on the shaft resistance of displacement model piles in sand." *Journal of Geotechnical and Geoenviromental Engineering*, 144(3), 04017120.

Wadell, H. (1932). "Volume, shape, and roundness of rock particles." *The Journal of Geology*, 40(5), 443–451.

EFFICIENT TORQUE-INSTALLED PILE USE IN SOUTHERN CALIFORNIA

Molly Winston, P.E., Shannon & Wilson, Glendale, California, USA, (720) 258-4109 mam@shanwil.com
Jason Buenker, P.E., Shannon & Wilson, Glendale, California, USA, (818) 539-8425 jzb@shanwil.com

ABSTRACT

Torque-installed piles are gaining popularity in Southern California as the go-to deep foundation element for small- to medium-capacity loads in urban environments. The torque-installed pile is a displacement-based screwed pipe pile with a closed-end conical tip welded to the bottom of the pipe. Torque-installed piles are most efficient in loose to medium dense soils with high liquefaction potential. Where used properly, torque-installed piles can be installed faster, require less clean-up, and create less onsite vibration/disturbance than other pile alternatives. However, torque-installed piles are not applicable in all soil conditions and care must be used to apply the pile effectively in the correct subsurface environment. This paper will review current Southern California state-of-the-practice for torque-installed pile design and construction, potential roadblocks to successful installation, and available capacities from load tests.

Keywords: piles, torque-installed piles, deep foundation, load test

INTRODUCTION

Torque-installed piles are a type of full-displacement screwed pipe pile originally developed in Southern California circa 2001 by Substructure Support, Inc. The pile is unique for its proprietary closed-end conical tip shown in **Fig. 1**. The tip has a welded steel-helix plate and cutter teeth that allow the pile to be advanced efficiently under applied torque and down pressure (crowd). Since original development of the pile, several contractors or manufacturers have proposed similar proprietary screw-type piles with comparable conical tips. Pile installation is relatively quiet, vibration-free, does not generate spoils, and faster than comparable pile types. The pile was originally developed as an alternative to driven pile foundations and remains a critical substitute to driven foundations in urban environments.

Torque-installed piles are conventionally specified as 12 ¾-inch outside diameter (OD) steel pipes with a ⅜-inch-thick wall, although larger sizes with alternative dimensions have been used outside Southern California. Pile installation lengths generally range from 30 to 50 feet but may reach 80 feet or greater where soil conditions permit. The pile is generally backfilled with concrete following installation to increase lateral pile stiffness and may incorporate rebar cages or other reinforcing steel to facilitate connections to structural elements. The pile is frequently specified using performance-based specifications that encourage contractor innovation and use of proprietary installation means and methods.

Torque-installed piles are adaptable to a variety of soil conditions but are most efficient in loose to medium dense soils with high liquefaction potential. These conditions facilitate rapid penetration of the pile through potentially liquefiable soil and into an underlying bearing stratum. Limited pile penetration into hard/dense bearing strata is typical, which may include dense sand, hard clay, or weathered bedrock. Torque-installed piles are not typically suitable in soils that include cobbles or boulders.

PILE INSTALLATION METHODOLOGY

Torque-installed piles are “screwed” into the ground by a drill rig that simultaneously applies torque and

© 2019 Deep Foundations Institute

crowd at the pile head as shown in **Fig. 2**. Drill rigs used to install the piles range in size and capacity but are typically equipped with hydraulic motors that provide up to 200,000 foot-pounds (ft-lbs) torque and main winches that provide up to 30 tons crowd for installation of the conventional 12 ¾-inch OD piles. Piles are typically installed to site-specific refusal criteria that incorporate maximum levels of torque, crowd, or pile advance rates. Torque and crowd-based refusal criteria are frequently equal to the maximum capacity of the drill rig. Piles may be predrilled to facilitate deeper pile installations or penetrate shallow layers of hard/dense strata.



Fig. 1: Torque-Installed Pile Tip

Torque-installed pile capacity is influenced by installation means and methods, and excessive soil disturbance or pile damage during installation may dramatically reduce the mobilized pile resistance. Soil disturbance may result from excessive predrilling, pile removal and reinstallation, or excessive freedom of movement in the drill rig head during installation. Inexperienced rig operators frequently attempt to increase pile penetration depth by withdrawing and readvancing the pile or spinning piles in place without advancement for long durations. These techniques rarely deepen finished pile installations, but instead generate heat from friction at the pile tip and may melt the tip, as shown in **Fig. 3,** or cause puncturing of the tip. To mitigate the risk of pile capacity loss due to soil disturbance or pile damage, torque-installed piles should be installed in a single continuous motion that consists of a controlled gradual increase in applied torque and crowd commensurate with the mobilized soil resistance. Pile installation by high-quality, experienced contractors using skilled drill rig operators is key to long-term pile performance.



Fig. 2: Pile Installation

PILE CAPACITY EVALUATION

Torque-installed pile capacities may be evaluated using empirical displacement pile methods during project design; however, nearly all torque-installed pile projects incorporate load testing to evaluate ultimate pile capacity. Load testing is common because the proprietary nature of pile tip design and installation methodology makes pile capacities estimated using static design methods uncertain. **Figure 4** presents a typical load test configuration.

Torque-installed pile load testing typically consists of compression and tension load tests performed in accordance with ASTM International D1143 Standard Test Methods for Deep Foundations under Static Axial Compressive Load - Quick Test and

ASTM International D3689 Standard Test Methods for Deep Foundations under Static Axial Tensile Load, respectively. The pile head is typically instrumented with at least two displacement dial gauges and two linear variable displacement traducers (LVDTs). LVDT values can be monitored using a data acquisition system while the dial gauges are monitored manually as backup. Strain gages may also be installed to evaluate mobilized pile resistance with depth Strain gage depths are selected to measure pile resistance at soil interfaces and at the bottom of the pile to evaluate mobilized end bearing.



Fig. 3: Melted Pile Tip



Fig. 4: Pile Load Test Configuration

CASE HISTORIES

The authors recent experience with torque-installed pile projects in Southern California that incorporated load testing provide a basis for installation methodologies and capacity evaluations discussed here. The load tested piles were installed in a range of subsurface conditions and encountered various challenges during pile installation. The following case histories provide pile capacities and highlight roadblocks to successful design and installation of torque-installed piles. Each load test was administered by GRL Engineers, Inc. (GRL) on behalf of the respective project contractors. Data presented here is based on the GRL load test summary reports.

Case History #1 - Los Angeles International Airport South Terminals

The redevelopment of two Los Angeles International Airport (LAX) south terminals consisted of a seismic retrofit and expansion while the terminals maintained air traffic service with intermittent gate closures during construction. New or expanded structures for the project were founded on torque-installed pile foundations. Project designers selected torque-installed piles as the preferred foundation alternative because the pile could be installed efficiently at irregular intervals, with minimal noise or vibration disturbance at the ground surface. The project incorporated three torque-installed pile load tests.

Subsurface conditions at the terminal consisted of fill underlain by layers of sandy clay and dense to very dense dune sand. The 15-foot-thick fill ranged from medium dense to dense silty sand with pockets of loose silty sand. The 5- to 10-foot-thick sandy clay was low-plasticity, stiff to hard clay with fine sand and numerous sand lenses. The underlying dune sand had low silt content and transitioned from dense to very dense within the upper 5 feet of the stratum. N_{60} values in the dune sand were greater than 50 blows per foot and cone penetration test (CPT) tip resistance ranged from 300 to 600 tons per square foot (tsf).

The first torque-installed pile load test consisted of one compression pile and one tension pile performed on a single pile. The load tested pile was installed to 28 to 29 feet below ground surface and predrilled the full 30 feet. Pile refusal criteria was based on maximum torque capacity of the drill rig, which was 150,000 ft-lbs. The contractor attempted to deepen the pile installation by repeatedly withdrawing and readvancing the pile. Based on ASTM D1143 and ASTM D3689 criteria for the compression and tension test, respectively, each load test failed. The compression load test was terminated at 220 kips or 55 percent of the required ultimate compression load of 400 kips due to approximately 2 inches of deflection at the pile head. The tension load test was terminated at 115 kips or 90 percent of the ultimate tensile load of 130 kips, because of continuous progressive displacement. Pile head deflection prior to application of the final tension load stage was ¾-inch.

The second torque-installed pile load test consisted of one compression and one tension pile performed on a single pile, with the pile installed about 25 feet away from the first load test. The test pile was predrilled to 18 feet depth to penetrate surficial fill layers and installed to 32 ½ feet depth using a drill rig capable of applying a maximum torque of 200,000 ft-lbs and maximum crowd of 30 tons. Pile refusal criteria consisted of zero advance rate at the maximum torque capacity of the drill rig under maximum crowd. The compression load test was terminated at 440 kips or 110 percent of the required ultimate compression load of 400 kips because of accelerating pile creep (plunging). Pile head deflection prior to plunging was 1 inch. The tension load test was terminated at the ultimate tension load of 130 kips at a deflection of <¼ inch. **Figure 5** presents the results of this load test. Based on ASTM D1143 and ASTM D3689 criteria for the compression and tension test, respectively, each load test passed.

The third torque-installed pile load test consisted of one compression and one tension pile performed on a single pile, with the pile installed about 300 feet from the first load test. The piles was installed without predrilling to 33 feet below ground surface using a drill rig capable of applying a maximum torque of 200,000 ft-lbs and maximum crowd of 30 tons. Pile refusal criteria consisted of zero advance rate at the maximum torque capacity of the drill rig under maximum crowd. The compression test was terminated at 440 kips or 110 percent of the ultimate compression load due to plunging; pile head deflection prior to plunging was ½-inch. The tension test was terminated at 220 kips or 170 percent of the ultimate tension load of 130 kips with a pile head deflection of ½-inch. Based on ASTM D1143 and ASTM D3689 criteria for the compression and tension test, respectively, each load test passed.

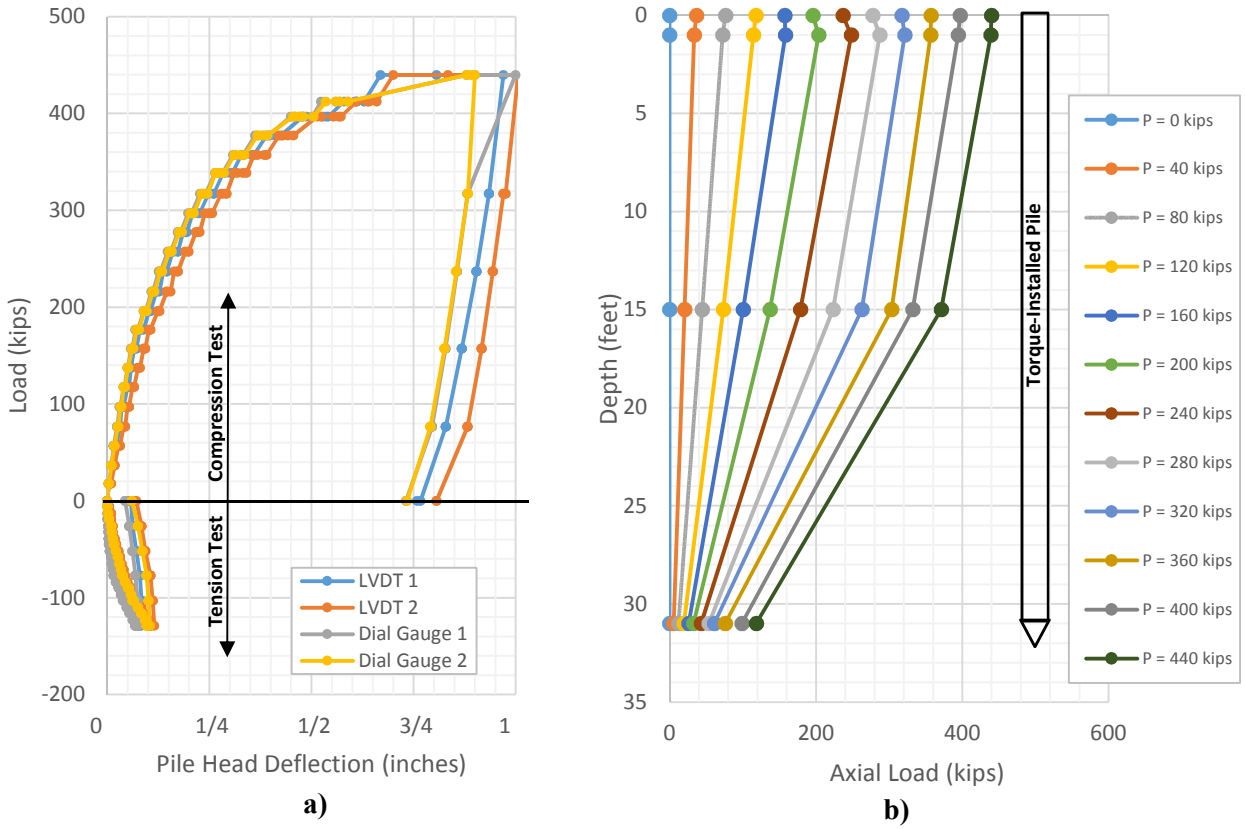


Fig. 5: LAX Terminals 7 and 8 Pile Load Test Data, Second Pile Load Test – a) Pile Load v. Head Deflection and b) Compression Pile Resistance v. Depth

The first and second pile load tests highlight the impact of pile installation means and methods on mobilized pile capacity. The first load test piles were predrilled beyond the full pile depth, which likely diminished mobilized skin friction resistance throughout the pile length and transferred most of the load to the irregularly shaped pile tip. Because of the concentration in load at the pile tip, pile head deflection increased rapidly under even low loads. Repeated attempts to advance the pile may have also damaged the tip during installation, which would create additional difficultly mobilizing end bearing resistance. In contrast, the second load test piles were predrilled only through fill layers, installed in a continuous motion, and installed using a drill rig capable of applying 200,000 ft-lbs of torque. The second load test piles consequently performed well in similar subsurface conditions as the first load test. The third pile load test highlights the repeatability and consistency of torque-installed pile load tests when piles are installed correctly, as the third load test results closely match the second load test in similar subsurface conditions and with piles installed using identical means and methods.

Case History #2 - Los Angeles International Airport North Terminals

The redevelopment of two LAX north terminals consisted of installation of new jet boarding bridges and various structures for the terminal, which maintained service with intermittent gate closures during construction. Project designers selected torque-installed piles as the preferred foundation element because the pile could be installed efficiently at irregular intervals, with minimal noise or vibration disturbance at the ground surface. The project incorporated one torque-installed pile load test and two high-strain dynamic pile capacity tests. The dynamic pile capacity tests were performed on production piles.

Subsurface conditions at the terminal consisted of variably thick fill deposits underlain by layers of silty sand, fine-grained soil, and dense to very dense dune sand. Fill was 10 to 12 feet in thickness and varied from medium dense to dense silty sand. Silty sand underlying the fill consisted of medium dense to dense fine sand. A thin, variable layer of fine-grained clay, sandy clay, and silt underlies the silty sand. The underlying dune sand is approximately 25 to 30 feet below ground surface and consists of dense to very dense poorly graded sand with low silt content. The CPT tip resistance in the dune sand ranged from 400 to 700 tsf.

The first torque-installed pile load test consisted of compression and tension load tests on a single pile. Prior to pile installation, the pile location was potholed to 12 feet below ground surface to a diameter of 10 inches. The pothole was backfilled with 1-sack sand slurry before being predrilled to a depth of 12 feet below ground surface. The test pile was then installed using a drill rig capable of applying a maximum torque of 200,000 ft-lbs and maximum crowd of 30 tons until reaching refusal at 30 feet below ground surface. Pile refusal criteria consisted of zero pile rotation at the maximum torque capacity of the drill rig under maximum crowd. The compression test was terminated at 460 kips or 115 percent of the ultimate compression load of 400 kips due to pile plunging; pile head deflection prior to plunging was less than ½-inch. The tension test was terminated at an ultimate tension load of 310 kips or 130 percent of the ultimate tension load of 240 kips with a pile head deflection of ½-inch. Based on ASTM D1143 and ASTM D3689 criteria for the compression and tension pile, respectively, the load test passed.

Based on the load test results, torque-installed piles were permitted for the project with the qualifier that piles must be installed to a minimum of 30 feet below ground surface, which was the depth of the load test pile. Production piles were required to meet the minimum depth requirement in addition to pile installation refusal criteria developed using the load test results. Pile refusal criteria for the test piles consisted of zero pile rotation at the 200,000 ft-lbs torque under 30 tons crowd. During construction, two production piles were installed to refusal at 26.5 and 28.5 feet below ground surface. To comply with permit requirements, high-strain dynamic pile tests were performed to confirm capacities of these shallow piles. Dynamic tests were analyzed using Case Pile Wave Analysis Program (CAPWAP), which indicated pile capacities of 680 and 540 kips for the 28.5 and 26.5 foot-long piles, respectively. The CAPWAP capacities exceeded capacities achieved by the pile load tests.

This case history highlights potential issues in permitting approval of torque-installed piles. Due to variability in soil deposits, torque and crowd administered to the pile during installation are a better proxy of installation capacity than pile depth. However, pile construction permits may include minimum depth requirements that negate pile refusal criteria for shallow piles. This limitation is problematic for torque-installed piles, which cannot readily be deepened with greater effort from a drill rig that has likely already installed the pile to its maximum capacity. As demonstrated in the previous section, greater effort to deepen pile installations at the maximum drill rig capacity may actually result in pile damage that leads to pile capacity loss. Further substantiation of pile capacity using dynamic testing may be necessary to satisfy permitting requirements. Close coordination with reviewing agencies may be necessary to permit torque-installed piles in a fashion that is suitable for the installation method. To avoid potential issues associated with pile installation depth, test piles should be installed where the anticipated bearing stratum is the shallowest. Multiple test piles may also help showcase the difference in the possible installation depth and illustrate pile refusal criteria as a better indicator of capacity than installation depth.

Case History #3 – Mid-Rise Construction on Alluvium Site in the San Fernando Valley

The site is located within the San Fernando Valley, on the northern flank of the Santa Monica Mountains at the northerly base of the Cahuenga Pass. Subsurface conditions consist of 45 to 50 feet of alluvial soil overlying weathered siltstone bedrock of the Upper Topanga Formation (Dibblee, 1991). Unconfined

compressive strength of Upper Topanga Formation siltstone typically ranges from 100 to 200 pounds per square inch, with CPT tip resistance of approximately 400 tsf. The overlying alluvium consists of silty clay, sandy silt, silty sand, and sand deposits. Sand and silt deposits were classified as potentially liquefiable during a design earthquake, resulting in over 30 feet of potential liquefaction and liquefaction-induced downdrag on foundation elements. Due to the loose, potentially liquefiable overburden with relatively shallow underlying bedrock, designers selected torque-installed piles for building foundations.

Torque-installed pile load testing consisted of two compression tests and one tension test. The first compression pile and tension pile were installed continuously to 57 feet below ground surface, approximately 5 feet into bedrock. Pile refusal criteria consisted of zero pile advance rate under the maximum torque and crowd capacity of the drill rig. The second compression pile was installed to 65 feet below ground surface with a pile that was previously used in an aborted attempt to install the first compression pile. The aborted pile installation included multiple efforts by the contractor to deepen the pile by withdrawing and readvancing the pile and spinning the pile in place for about 20 minutes. The contractor withdrew the pile when they realized that the pile could not be advanced deeper under these efforts. The withdrawn pile tip was damaged, as shown in **Fig. 3**. The contractor subsequently cut off the damaged pile tip, welded a new tip on the pile, and installed the refurbished pile as the second compression pile.

The first compression pile load test was terminated at 500 kips or 100 percent of ultimate compression load, as presented in **Fig. 6**, because the pile met the project design criteria. Based on ASTM D1143 criteria, the load test passed. The tension pile load test was terminated at 600 kips or 120 percent of the ultimate tension load of 500 kips because the test had reached the maximum capacity of the hydraulic jack and the design capacity of the reaction frame. Based on ASTM D3689 criteria, the load test passed. The second compression pile load test was terminated at approximately 375 kips or 75 percent of the ultimate compression load of 500 kips due to pile plunging, as show in **Fig. 7**. Based on ASTM D1143 criteria, the load test failed. Strain gage data indicated that the failed pile mobilized little end bearing and that most available resistance was provided in skin friction.

Project designers concluded the second compression pile likely experienced structural failure due to weakness from fatigue loading in the refurbished pile fabricated from used steel. To substantiate this conclusion, two additional borings were drilled at the pile load test location. The borings did not encounter soft rock that might contribute to pile plunging, which reinforced the conclusion that structural failure likely generated the observed pile behavior. Further, experienced contractors consulted for the project indicated that structural failure of used pile steel is common and recommended that piles withdrawn after installation be discarded and not reused.

The first and second compression pile load tests highlight the impact of pile installation procedures on pile capacity, and particularly emphasize the need to avoid fatigue overloading of the pile structure. Piles installed and subsequently withdrawn should be discarded and not be reused as production piles unless structural integrity testing is performed to demonstrate the pile meets required project specifications. Further, because torque-installed piles are proprietary, pile-specific installation methodology will always be required for successful pile installation and commonly-used approaches to install similar piles may not be applicable. Torque-installed piles require a learning curve and owners or designers should anticipate potential pile capacity issues with inexperienced contractors.

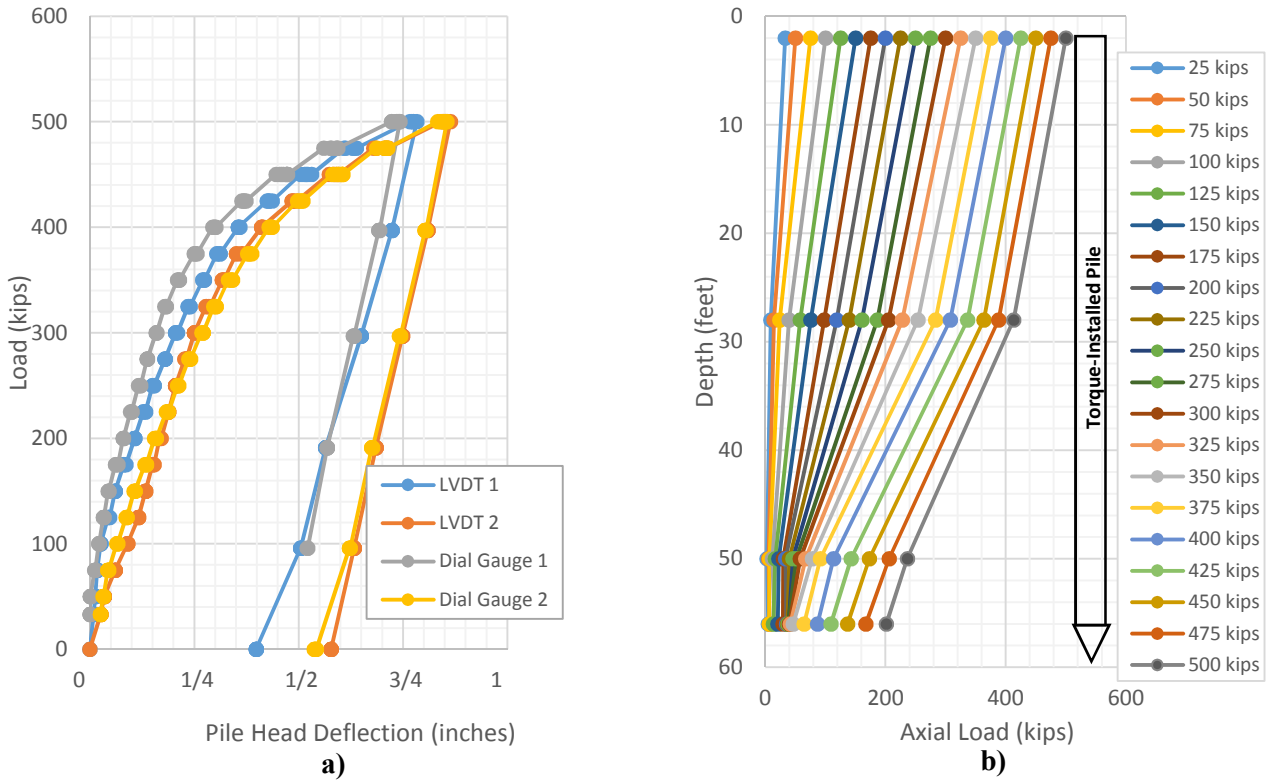


Fig. 6: Alluvium Site in the San Fernando Valley Load Test Data, First Compression Pile Load Test – a) Pile Load v. Head Deflection and b) Pile Resistance v. Depth

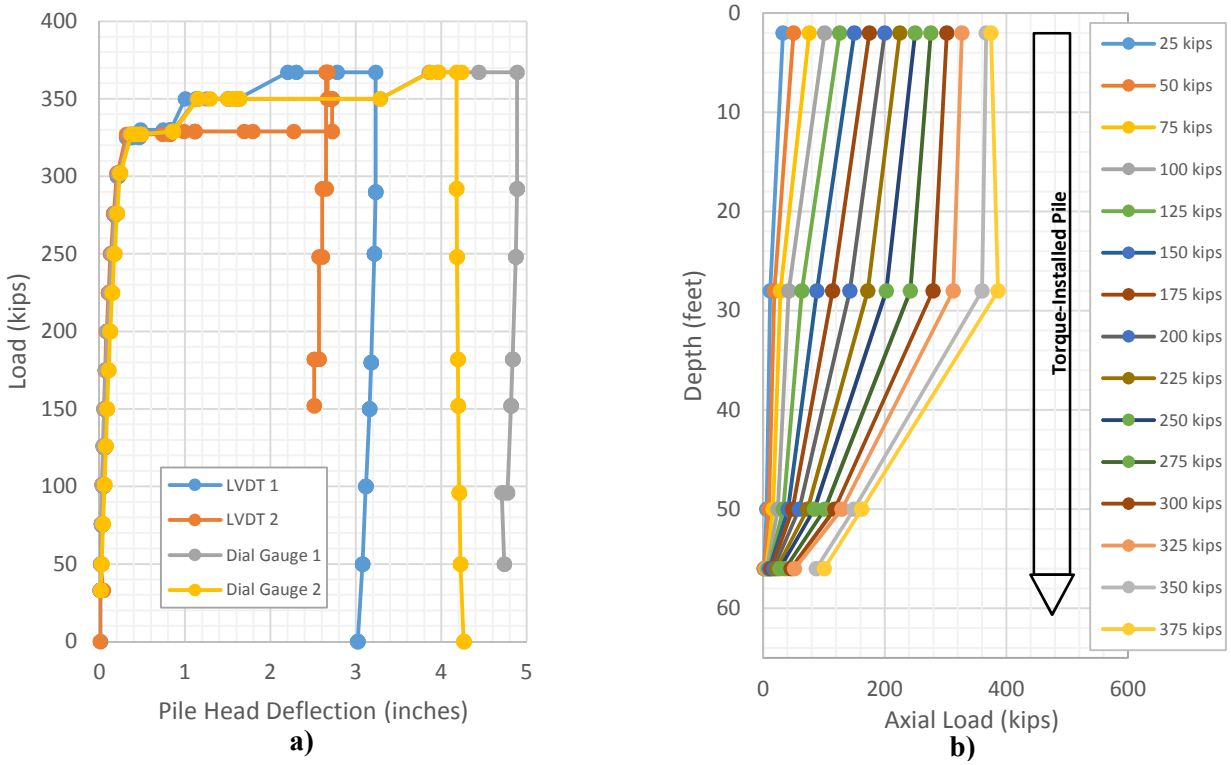


Fig. 7: Alluvium Site in the San Fernando Valley Load Test Data, Second Compression Pile Load Test – a) Pile Load v. Head Deflection and b) Pile Resistance v. Depth

SUMMARY AND CONCLUSIONS

Torque-installed piles are an important and valuable option for deep foundation support. Where used properly, torque-installed piles can be installed faster, require less clean-up, and create less onsite vibration or disturbance than other pile alternatives. However, torque-installed piles are not applicable in all subsurface conditions and the nascent nature of the technology means that standards of practices vary among designers and contractors, leading to potential issues during construction. These issues include soil disturbance, pile damage, or difficulties meeting pile installation criteria linked to minimum pile depths. Each of these issues were highlighted in case histories presented in this paper, including solutions to mitigate the impact of these issues. Southern California load tests on 12 ¾-inch diameter piles indicate that ultimate compressive capacities ranged from 400 to 500 kips and a similar range of ultimate tension capacities. The case histories highlight the repeatability and consistency of torque-installed pile load tests when piles are installed correctly. Experience in Southern California has demonstrated that, when used correctly, torque-installed piles are an effective deep foundation pile alternative.

REFERENCES

ASTM D1143 / D1143M-07(2013)e1, Standard Test Methods for Deep Foundations Under Static Axial Compressive Load, ASTM International, West Conshohocken, PA, 2013.

ASTM D3689 / D3689M-07(2013)e1, Standard Test Methods for Deep Foundations Under Static Axial Tensile Load, ASTM International, West Conshohocken, PA, 2013.

Davisson, M.T., 1973, High capacity piles, in Lecture Series, Innovations in Foundation Construction, American Society of Civil Engineers (ASCE), Illinois Section, Proceedings: Illinois, ASCE, 52 p.

Dibblee, Thomas W., 1991, Geologic Map of the Hollywood and Burbank (South ½) Quadrangles, Los Angeles County, California: Dibblee Foundation Map No. DF-30, scale 1:24,000.

GEOTECHNICAL INSTRUMENTATION OF PILE FOUNDATIONS EMBEDDED IN MOLASSE OF A HIGH-RISE BUILDING

R. Milane, Univ Lyon, INSA-Lyon, GEOMAS, F-69621, France, rosy.milane@insa-lyon.fr

L. Briançon, Univ Lyon, INSA-Lyon, GEOMAS, F-69621, France, laurent.briancon@insa-lyon.fr

A. Daouadji, Univ Lyon, INSA-Lyon, GEOMAS, F-69621, France, ali.daouadji@insa-lyon.fr

S. Grange, Univ Lyon, INSA-Lyon, GEOMAS, F-69621, France, stephane.grange@insa-lyon.fr

P. Cazes, Antea Group, Lyon, France, pierre.cazes@anteagroup.com

ABSTRACT

Construction in congested urban areas is often accompanied by geotechnical problems due to high loads and the impact caused by nearby buildings. For this reason, it is important to understand the behavior of the soil and the structure without forgetting the essential role of the interaction between them. Experiments, instrumentation and numerical modeling are the main methods used to study this behavior. To this end, pressure cell, strain gages, vibrating wire extensometers and optical fiber sensors are installed on the reinforcement steel of pile and raft foundations to monitor stresses and induced deformation in these elements during and after construction. A fiberglass rod extensometer is placed in the soil to help measuring the displacement due to excess loading, knowing that the pile foundations are embedded in the Rhône's alluviums and reach the molasse, a particular and challenging soil with properties that are not yet well understood. The objective of this paper is to present the geotechnical instrumentation program carried out for the tower Silex2 in Lyon, France, and to describe the types of sensors used and their installation on site.

Keywords: deep foundations, field instrumentation, soil-structure interaction, monotonic and cyclic loading, high-rise building.

INTRODUCTION

The complexity of geotechnical structures like dams, bridges or high-rise buildings requires a sound understanding of the behavior of the soil, the structure itself and the interface. Therefore, a geotechnical instrumentation program can be essential in many ways. During the site investigation stage, it can help determine the initial conditions experienced by the soil in the field by measuring parameters such as the compressibility index or the permeability. During the construction stage, real time measurements can protect the structure from premature failure, help validate and optimize the design if needed. In addition, sensors measuring pore-water pressure, loads, deformations and settlements allow for monitoring the performance of the structure. This is called the observational method. Finally, during the operating phase, instrumentation aims to study the long-term behavior of the structure (Nicholson et al., 1999).

"Fondasilex" is a collaborative research project funded by Région Auvergne-Rhone-Alpes in France between a research unit GEOMAS at INSA Lyon and a company named Antea Group. The project Silex2, located in Lyon-France, consists in rehabilitating the existing EDF tower built in 1977, and constructing a new high-rise building of 135 m high with two small buildings. The main reason for instrumenting in Silex2's foundations is to study their behavior and that of the soil present at the site location, since geotechnical issues may occur due to high loads and nearby structures (i.e. Silex1, EDF tower, RTE

© 2019 Deep Foundations Institute

building). In this framework, geotechnical instrumentation was planned and executed during the construction of this new tower. This has required installation of sensors within the piles, soil and raft foundation without affecting any of the work conditions. Even though many instrumentation results are presented in the bibliography, only few papers describe clearly the instrumentation procedure. Therefore, this paper is primarily concerned with the *in-situ* monitoring program and the soil characterization.

FOUNDATION PLAN

The new high-rise building is founded on 10 points of supports, each relying on a pair of 1.2 m diameter piles via a concrete transfer structure. The foundation plan is presented in Fig.1, showing the six monitored piles in red (17A/B, 18A/B and 20A/B). Reaching up to 17.5 m depth, the twenty piles are all anchored in the molasse layer. They are casted using continuous flight auger (CFA) techniques. To design the piles, load transfer from the superstructure to the foundation was calculated for ULS load combination, as shown in Table 1. The concrete specified for the piles has a compression strength of 50 MPa.

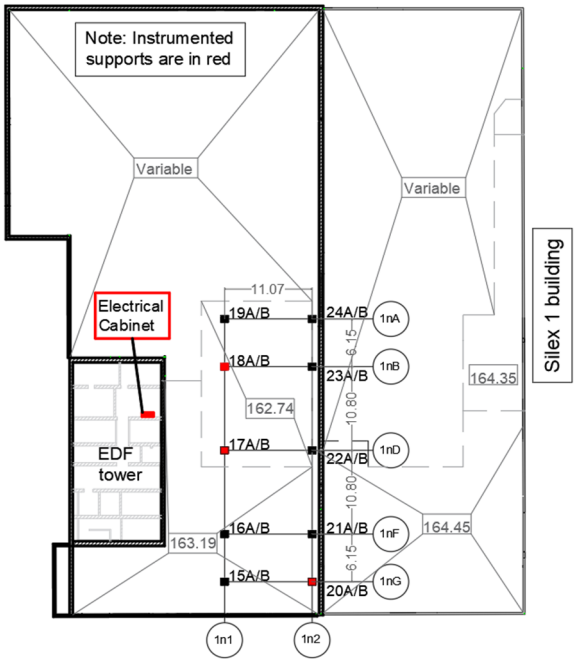


Fig.1. Foundation Plan for Silex[2]

Table 1. Load Transfer from the Superstructure to the Instrumented Foundations Calculated for ULS Load Combination

Pile Number	Maximum Normal Force (kN)	Minimum Normal Force (kN)	Maximum Horizontal Force (kN)	Bending Moment (kN.m)
Pi17A	11292.3	0	224.1	174.9
Pi17B	11292.3	0	224.1	172
Pi18A	9911.4	0	316.9	258.8
Pi18B	9911.4	0	316.9	250.5
Pi20A	10904.2	-1161.5	580.7	596.7
Pi20B	10904.2	-1161.5	580.7	604.2

SOIL FORMATION AND CHARACTERISTICS

The site is located on the left bank of the Rhône River in France at 168 m NGF. The NGF is a vertical datum used in France by an ordnance survey as the basis for deriving altitudes. Beneath a few meters of embankments, is a hidden 15m-layer of Rhône's alluviums. They consist of sand, gravels and sandy gravels of medium denseness with a maximum particle diameter ranging between 30 and 100 mm. They contain 1 to 4 meter- layer of sand with silt content at different depths. A thick layer of molasse dating from the Miocene period underlies the alluviums extending to 96 m NGF. The molasse is a silty sand soil that present greasy indurated clayey layers. Under the molasse, there is a clay formation dating from the Oligocene period.

Due to its proximity to the Rhône, a shallow ground water table characterizes the city of Lyon. The average level is 162.5 m NGF, 0.8 meters below the working platform. The presence of water in superficial layers of alluviums made the design and the construction more challenging.

The characteristics of the soil layers are presented in table 2, knowing that the pressuremeter modulus E_M and the limit pressure p_{l*} are harmonic mean values and the density γ is estimated as $20kN/m^3$.

Table 2. Soil layers geotechnical characteristics

	Thickness (m)	**Top of Layer (NGF)**	**Pressuremeter modulus E_M (MPa)**	**Deformation modulus E (MPa)**	**Limite pressure p_l* (MPa)**	**α**
Embankment	3.5	168	4.3		0.4	0.33
Alluviums 1	6.75	164.5	62	135	4.5	0.33
Alluviums 2	4	157.75	8	20	1.4	0.33
Alluviums 3	5.75	153.75	67	150	4.7	0.33
Molasse	>10m	148	95	300	4.8	0.5

INSTRUMENTATION SCHEDULE

Sensors are tools that transform a physical quantity into a parameter that can be measured. Briançon et al. (2016) classified the measured parameters into four main categories: i) mechanical (Stress, force), ii) hydraulic (Water level, pore water pressure), iii) geometric (deformation, displacement, inclination) and iv) environmental (temperature). According to Paikowsky and Hajduk (2004), the main steps needed to set up an instrumentation schedule are i) define the project conditions, ii) define the purpose of the instrumentation, iii) select the parameters to be monitored, iv) predict magnitudes of change, v) select instruments, and finally vi) select instrument locations.

Accordingly, and based on previous experience, five types of instruments were selected for installation in this project. They are easy to be installed, simple to manipulate and most importantly adequate for concrete and soil. Finally, since long-term measurements are needed, sensors with a lifespan of at least 10 years were chosen. In addition, they are able to provide real time monitoring through the Data logger or the optical interrogator. All the used instruments, except optical fibers, are analog. Meaning they provide an electrical quantity as an output (voltage, current, resistance, etc.) as oppposed to numerical or logical sensors.

Pile deformation was measured using three types of sensors: vibrating-wire strain gages, electrical resistance strain gages and strain optical fiber cables described hereafter.

Vibrating Wire Strain Gages (VWSG)

Measuring the strain through the frequency variation is advantageous since voltage drops caused by weather changes do not affect the frequency output (Hayes and Simmonds, 2002). Vibrating wire strain gages (VWSG) were chosen because of their i) small size, ii) moisture resistance, iii) long term stability under static loading and iv) possibility of using long instrument cables without significant loss of accuracy (Bica et al., 2013). Fourteen arc-weldable vibrating-wire strain gages (Model 0VK4000VS00 from SISGEO) were distributed on five of the instrumented piles. They have a built-in thermistor that can measure the temperature of the concrete.

Electrical Resistance Strain Gages (ERSG)

Electrical resistance strain gages (ERSG) were chosen to provide redundancy in case of failure of VWSG. Electrical strain gage have a resistance that changes when subjected to strain. They are small and easy to be installed. However, they are not stable for long term and are generally more sensitive to humidity (Bica et al., 2013). Thirty-six strain gages (Model KFGS-5-120-C1-11 provided by KYOWA) were used in total. This particular model of gages is moisture proof and has excellent flexibility.

Both types of strain gages (VWSG and ERSG) were installed at different depths: 5 m, 12 m and 15.5 m, measured from the top of the reinforcing cage.

Optical Fibers (OF)

In addition to strain gages, the deformation of the piles and raft foundation in both directions was measured using distributed optical fiber sensors (DOFS) and optical frequency domain reflectometry (OFDR) technology. This system is based on Rayleigh scattering arising due to the random density distributions of fiber materials. Developed by Eickhoff (1981), the OFDR technique has high sensitivity and high spatial resolution up to 1mm. Instead of reading the intensity of the Rayleigh backscattered signal, OFDR measures the interference fringes of the Rayleigh scattered light from a tunable laser source and a static reference fiber in frequency domain. By means of the inverse Fourier transformation, the amplitude and phase in frequency domain are converted to the time/spatial domain (Leung et al., 2013). The installation of optical fibers needs care, but it gives more accurate results than a traditional profilometer. In this context, 8 optical fibers provided by Dimione, the French distributor of LUNA products, were used. Table 3 presents their length and location.

Table 3. Location and Dimensions of the Optical Fibers

Optical Fiber Number	Length (m)	Extension Length (m)	Location
1	30	20	Raft foundation North-South
2	50	-	Pile 20B + Raft foundation East-West
3	30	20	Pile 20A
4/5	30	20	Pile 17B/17A
6/7	30	20	Pile 18B/18A

Concrete Pressure Cells (CPC)

Concrete pressure cells (CPC) are sensors used to measure the pressure on the pile head, transferred from superstructure to the piles. With an output signal (4-20mA), this instrument consists of two rigid disks filled with a hydraulic fluid (oil). The hydraulic pressure is converted to an electrical signal. The length of the cable does not affect current sensors (4-20mA) as the current is very insensitive to electromagnetic

disturbances and in this case, two cables are sufficient. A zero value indicates the breakdown of the sensor. Three CPC's (Model E Φ 30 AI 50 and E Φ 30 AI 150, provided by GLOTZL), were installed on the head of each of the piles 17A/B, 18A/B and 20A/B, to measure the pressure induced by the load combinations. Four instruments have a range 0-150 bars to measure high pressures in late stages of construction, on the top of 20A/B and 18A/B.

All the measuring instruments used in this study are easy to be installed and they can be easily connected to the data logger system. Some examples are shown in Fig.2. Tables 4-5 provide a summary of the selected instruments and their characteristics. The soil profile and instrument layout are presented in Figs. 3-4.

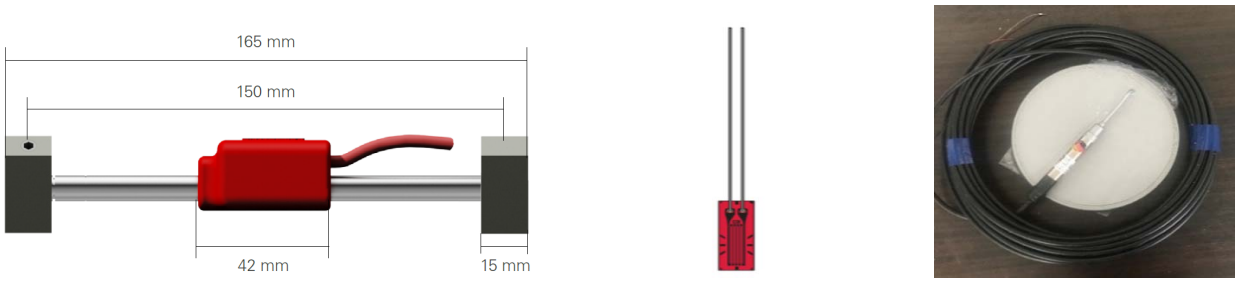


Fig.2. Examples of Measuring Instruments Used in Silex^2: VWSG from SISGEO (left), ERSG from KYOWA (middle) and concrete pressure cell from GLOTZL (right)

Table 4. Summary of pile instrumentation

Pile Number	Concrete Pressure Cell (CPC)	Electrical Resistance Strain Gages (ERSG)	Vibrating wire Strain Gages (VWSG)	Optical Fibers (OF)
17B	3	6	1	1
17A	3	6	1	1
18A	3	6	6	1
18B	3	6	-	1
20B	3	6	5	1
20A	3	6	1	1

Fiber Glass Rod Extensometer

Given the pressuremeter moduli E_M of the soil layers, and by doing a retro-analysis with the tower "Oxygene" built in 2007 in the same neighborhood, the settlement of the soil beneath Silex2 was estimated at 25 mm during the design stage. Soil displacement is measured using a multipoint borehole extensometer that can detect the relative movement between an anchor point and measuring head. It consists of anchors, rods and a reference head.

Therefore, a fiberglass rod extensometer (Model GKTE from GLOTZL) is used. The head is equipped with six measuring points at different depths (2, 8, 14, 20, 27 and 35 meters from its top), to measure the displacement in both the alluviums and the molasse layers. Fiberglass rods transfer this displacement from the anchors to the head of the extensometer. Since access to the reference head is difficult, displacement sensors, called potentiometers, are installed inside the reference head. They have an internal resistance strip that gives different values with displacement. Accordingly, six displacement sensors with open casing with 60 mm maximum displacement (Model GWLO 22/60 from GLOTZL) were used.

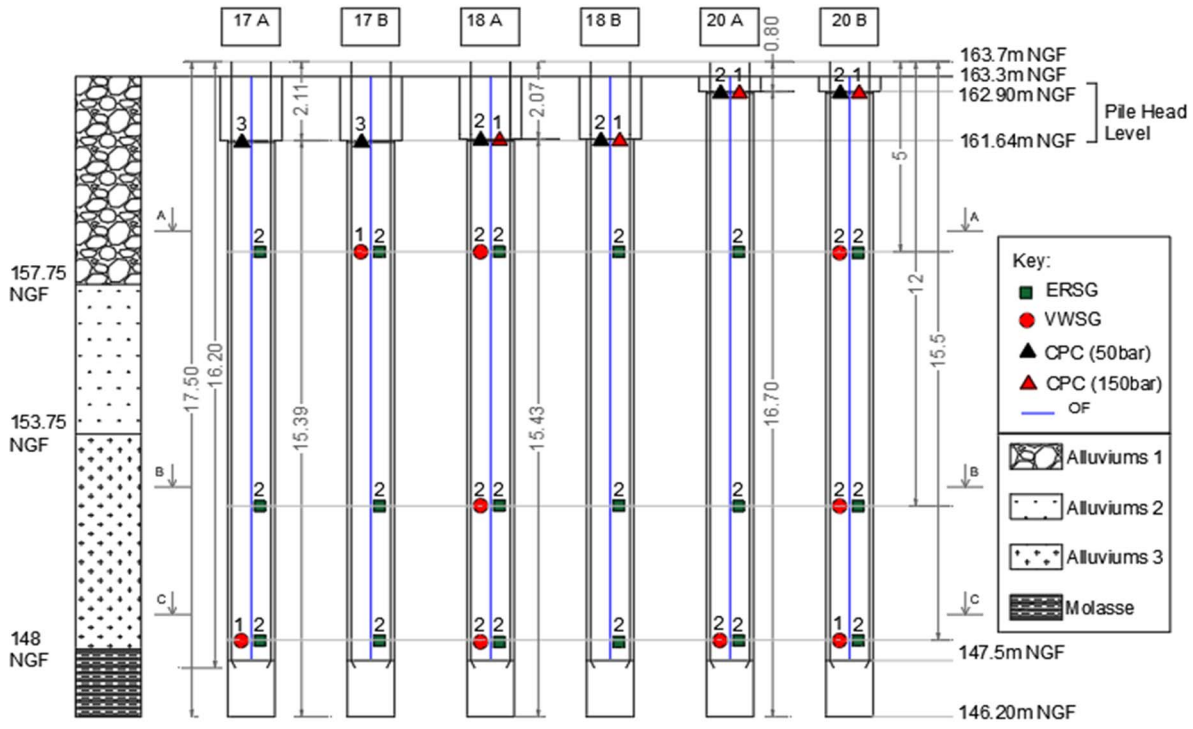


Fig.3. General Soil Profile and Pile Instrumentation Layouts

INSTRUMENTS INSTALLATION

The instruments were installed according to the following procedure:

1. To install the vibrating-wire strain gages, mounting blocks were welded on the steel bars using a mounting jig as a reference. Gages were then fixed on them to allow their compression or tension
2. The electrical resistance strain gages were glued, coated and protected on a 1-m steel bar that was welded on site on the reinforcing cage
3. The optical fibers were taped along the steel bars
4. The cables were fixed to the reinforcement cage using plastic cable fastener. A steel tube served as channel to take them out as shown in Fig. 5.
5. After pile breaking, a thin layer of sealing mortar was applied on the top of the pile on which where CPC were installed.
6. All the cables were pulled in the raft foundation until an electrical cabinet, equipped with the data logging systems and located in a room in EDF building.
7. The Optical fibers in the raft foundation were pulled progressively in the raft foundation.

Following the sonic drilling, rods and anchors were installed at the corresponding depths. The head of the extensometer was fixed on the drill head. A specific grout for stiff clayey soil was used to fill the drill hole with the following composition: 15% cement, 80% Kaolin and 5% Bentonite (NF P 94-156, 1995). The installed six displacement sensors were connected to an 18-wire cable until the electric cabinet.

A measurement was taken right after the installation of the sensors to ensure they were working properly. Zero values correspond to those measured after the casting of the raft foundation.

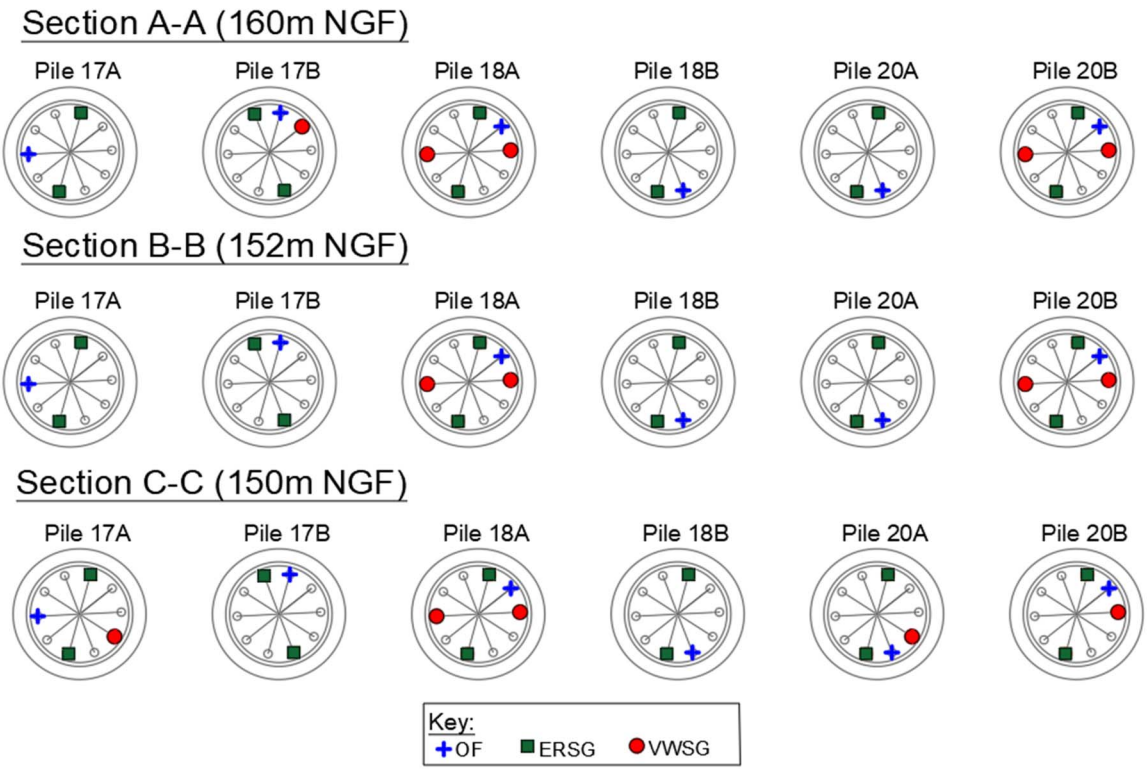


Fig.4. Pile sections at three different levels

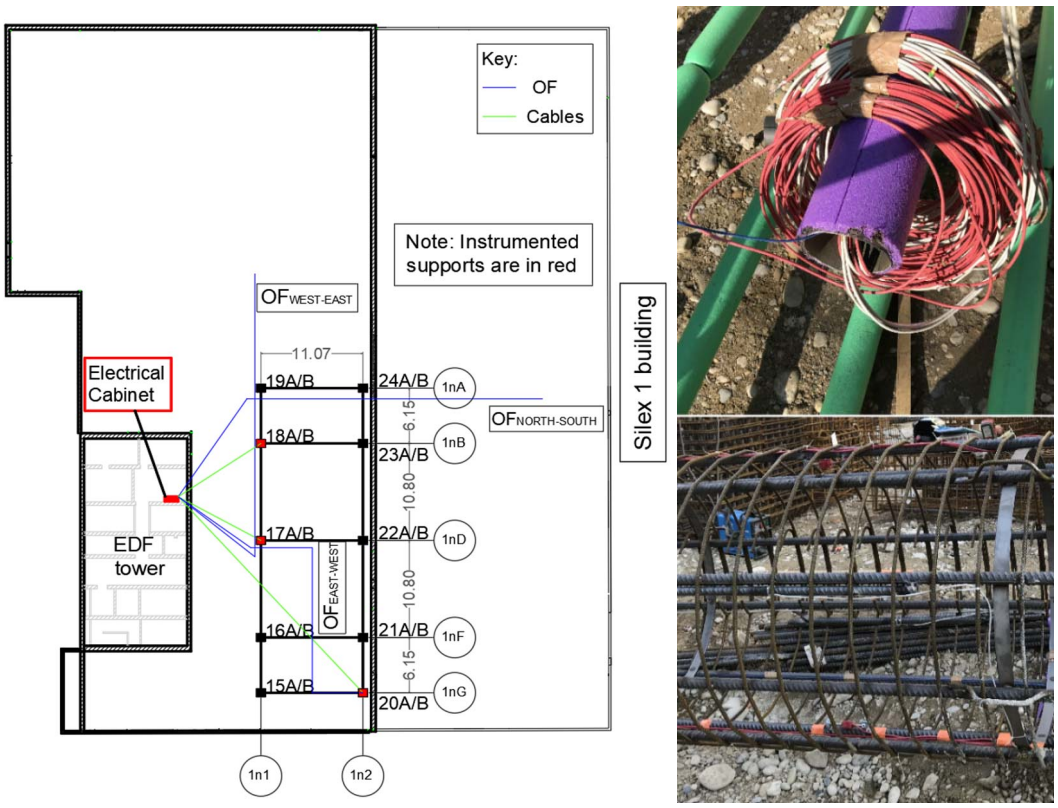


Fig.5. Cables and Optical Fibers: layout (left) and installation on site (right)

LOST SENSORS DURING INSTALLATION

It is highly probable to lose a number of sensors during one of the installation stages, especially when it is done in the field. However, all the sensors have survived during the casting of the piles, even though the CFA technique was used, in which the sensors were fixed on the steel cage before this latter was introduced in the concrete. Whereas, during the construction of the transfer concrete structure, one optical was cut and one sensor from each type (ERSG, VWSG and CPC) failed to survive due to slippage of cables. It is also expected to see some malfunctions during the data collection.

Table 5. Summary of Instruments Characteristics by Type

	CPC		VWSG	ERSG	Potentiometer
Supplier	GLOTZL	GLOTZL	SISGEO	KYOWA	GLOTZL
Model	E Φ 30 AI 50	E Φ 30 AI 150	0VK4000VS00	KFGS-5-120-C1-11	GWLO 22/60
Number	14	4	14	36	6
Diameter/ Length	ϕ 300 mm	ϕ 300 mm	150 mm	5 mm	
Measuring range	0-50 bar	0-150 bar	3000 με (±1500 με) 520-1020 Hz		0 - 60 mm
Operating Temperature	-25°C … + 80°C	5°C … + 60°C	-20 °C …+ 80°C		-30°C …+ 70°C
Calibration factor	0.32mA/bar	0.10667mA/bar	-	-	
Resolution	< à ± 1% f.s.	< à ± 1% f.s.	± 0.5% f.s.	-	< à ± 1% f.s.
Other	Overload protection: 20% Initialization time: 6 s Output signal: 4-20 mA		Coil resistance: 150 Ω Max cable length: 1000 m	Resistance : 119.8 Ω ±0.2%	Resistance 4.7 kΩ

DATA LOGGING SYSTEMS AND DATA PROCESSING

In addition to instrument calibration and installation, data collection, processing and interpretation are also of high importance. Measurements for CPC's, VWSG's and displacement sensors were retrieved using a data logger DATATAKER DT85GLM3-4, located in the electrical cabinet. It has 16 analog channels and can be connected to two additional channel expansion modules (CEM) with 20 additional channels each. Optical fibers were connected to an Optical Distributed Sensor Interrogator (LUNA ODiSI 6100) which is configured to measure Rayleigh High Definition Fiber Optic Sensors. ERSG's measurements were taken via an Integrated Measurement & Control (IMC). The three machines are shown in Fig 6.

The frequency of readings generally depends on the construction activities. It should be moderate to avoid missing events or overloading the data processing (Dunnicliff, 1994). During the first stages of construction, readings has to be taken every two hours. After the values had stabilized, two measurements per day will be enough. Additionally, long-term monitoring of the behavior of the structure for ten years of service was planned. Table 6 shows the list of instruments with the corresponding data logging system, the parameter they measure and the physical parameter needed.



Fig.6. Data Logging Systems: DATATAKER (left), optical machine (middle) and IMC (right)

Table 6. List of All Instruments with the Parameter They Measure

Instrument	Data Logging System	Parameter Measured	Physical Parameter
VWSG	DATATAKER	Frequency	Strain
ERSG	IMC	Strain	Strain
CPC	DATATAKER	Current	Pressure
Potentiometer	DATATAKER	Resistance	Displacement
Optical fiber	ODiSI 6	Optical frequency	Strain

SUMMARY AND CONCLUSIONS

In the framework of the FONDASILEX collaborative project, the behavior of the tower Silex^2's deep foundation was investigated. Six out of twenty piles were instrumented to monitor geotechnical properties. In total, 14 VWSG's and 36 ERSG's were installed to measure the deformation along the piles, and 18 CPC's to evaluate the pressure on the piles heads. Optical fibers helped to measure to deformation of the piles and the raft foundation. In addition, a fiberglass extensometer, equipped with six anchors for different depths, was embedded to measure the settlement of the soil.

Based on the above, the most important stages of instrumentation are the following:

1. Selection of the instruments based on the parameters to be measured, the budget and the instruments characteristics
2. Instrumentation installation that should be done with extreme care, especially when it comes to deep foundations and 35-m sonic drilling.
3. Data collection, processing and interpretation

Since the tower Silex2 is under construction, readings are still in process and the measurements will be analysed as constructions progresses, especially when the piles will be subjected to the full load of the tower. The instrumentation of Silex^2 is only the first step of a major project that aims at the subsequent steps to calibrate a numerical model made with FLAC3D, using an advanced constitutive model.

ACKNOWLEDGMENTS
This work is funded by the Auvergne-Rhône-Alpes region (AURA) in the framework of the project Pack Ambition 2017. The authors would like to acknowledge "Covivio", the owner of the tower Silex^2, who agreed to instrument the foundations, Eiffage Construction Confluences (ECC) and Société Générale de Confortement (SGC) for the help they provided during the works.

REFERENCES
Bica A., Prezzi M., Seo H., Salgado R. and Kim D., 2013. Instrumentation and Axial Load Testing of Displacement Piles. Lyles School of Civil Engineering Faculty Publications. Paper 6.

Briançon L., Cazeaudumec B. and Pincent B., 2016. Auscultation Géotechnique. Techniques de l'ingénieur Géotechnique, base documentaire : TIB238DUO., no. ref. article : c229.

Dunnicliff J., 1994. Geotechnical instrumentation for monitored field performance. John Wiley & Sons. ISBN 978-0-471-00546-9

Eickhoff W. and Ulrich R., 1981. Optical frequency-domain reflectometry in single-mode fibers. Appl. Phys. Lett. 39(9), 693–695.

Hayes J. and Simmonds T., 2002. Interpreting strain measurements from load tests in bored piles. Proceedings of the ninth international conference on piling and deep foundation, 2002, 3-5

Leung C.K.Y., Wan K.T. Inaudi D., Bao X., Habel W., Zhou Z., Ou J., Ghandehari M., Wu H.C. and Imai M., 2013. Review: Optical fiber sensors for civil engineering applications. Mater. Struct., 48, 871

Nicholson D., Tse C. and Penny C., 1999. The Observational Method in ground engineering – principles and applications. Report 185, CIRIA, London

NF P94-156 (octobre 1995) Sols : reconnaissance et essais – Mesures à l'inclinomètre

Paikowsky S. and Hajduk E., 2004. Design and Construction of Three Instrumented Test Piles to Examine Time Dependent Pile Capacity Gain. 27.6 (2004), 1–17

LINKING THE INSTALLATION RESPONSE OF SCREW PILES TO SOIL STRENGTH AND ULTIMATE CAPACITY

James P. Hambleton, Northwestern University, Evanston, IL, USA, jphambleton@northwestern.edu
Sam A. Stanier, University of Cambridge, Cambridge, UK, sas229@cam.ac.tuk

ABSTRACT

A perceived advantage of screw-type foundations is the ability infer aspects of foundation performance from quantities measured or observed during installation, especially the installation torque. A particular concept widely used in practice is to correlate installation torque to ultimate capacity. This notion has proven useful as a field verification technique despite the absence of validated models that relate key variables of interest, such as installation torque, axial (crowd) force, geometrical parameters, and soil strength. This paper considers previous work by the co-authors and collaborators on analytical, numerical, and physical modelling of screw piles to relate the quantities measured or controlled during installation (e.g., installation torque) to the ultimate capacity and soil strength. Attention is given to saturated clay as a particular soil type amenable to simplified analysis. An analytical model for a single-helix pile is considered as a means of directly relating the ultimate capacity and undrained shear strength to the installation torque, crowd force, plate pitch, plate diameter, shaft diameter, installation depth, and surface roughness. The connection between the installation variables and ultimate capacity—and the sensitivity to crowd force in particular, a quantity that is typically not measured during field installations—is also discussed. The theoretical predictions are compared against data obtained from small-scale laboratory experiments that suggest the installation torque relates to the remolded strength of the soil.

Keywords: screw piles, helical anchors, installation, torque-capacity correlation, modeling, experiments

INTRODUCTION

Screw piles are deep foundations that are twisted into the ground through an applied torque. Advantages over driven piles or drilled foundations include the relative silence of the installation, with low ground vibrations, and the possibility of being easily decommissioned by reversing the direction of twisting. Screw piles are now routinely encountered as a flexible, low-cost solution for numerous applications (Figs. 1 and 2), and they are also being considered for applications in offshore energy production due to limitations being imposed with respect to decommissioning and underwater noise.

Also known as “screw anchors,” “helical piles”, or “helical anchors,” screw piles consist of helices or helical plate elements attached to a central shaft. Figure 3a shows the components of a single-helix pile and key variables. The diameters of the shaft and helix are denoted by d and D, respectively, and p is the pitch of the helix. Variable H denotes depth of the helical plate, and T and N denote the torque and axial (crowd) force applied during installation. In typical applications, the pile includes multiple helical plates, and the shaft is composed of segments that allow for it to extend to large depths into the soil.

© 2019 Deep Foundations Institute

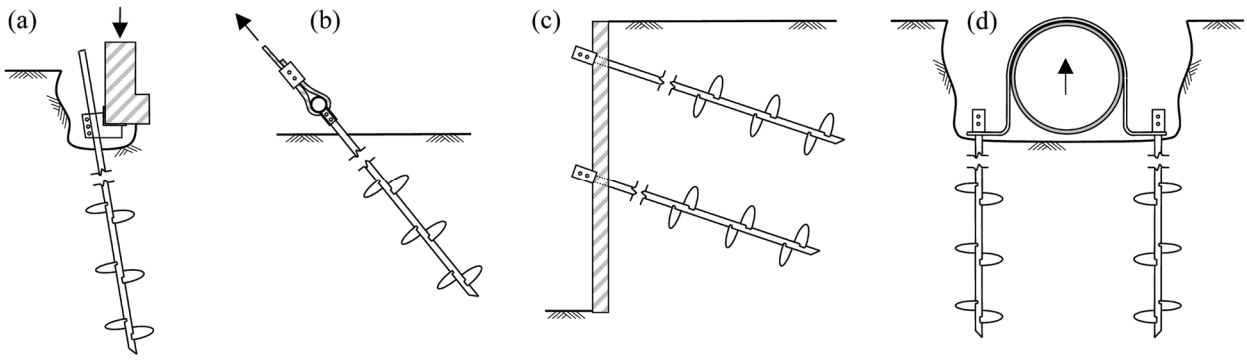


Fig. 1. Selected applications for helical anchors: (a) underpinning of shallow foundations; (b); ground anchorage; (c) tiebacks; (d) control of buoyancy for buried and underwater pipelines (Hambleton et al. 2014; reproduced with permission from the Australian Geomechanics Society)



Fig. 2. Installation of screw piles (helical anchors) to be used as tiebacks in a slope stabilization project

A compelling concept utilized widely in practice is that the installation torque should, in principle, relate to the ultimate capacity of the pile. In other words, a larger installation torque implies a larger capacity. This concept of "torque-capacity correlation" is embodied in the following formula (Hoyt and Clemence 1989):

$$F_{\max} = KT \qquad [1]$$

where $F_{\max}$ is the ultimate axial capacity of the pile in tension or compression and K is the "capacity-to-torque ratio." Perko (2009) ascertained the following empirical expression for K based on numerous field measurements:

$$K = 1433 d^{-0.92} \qquad [2]$$

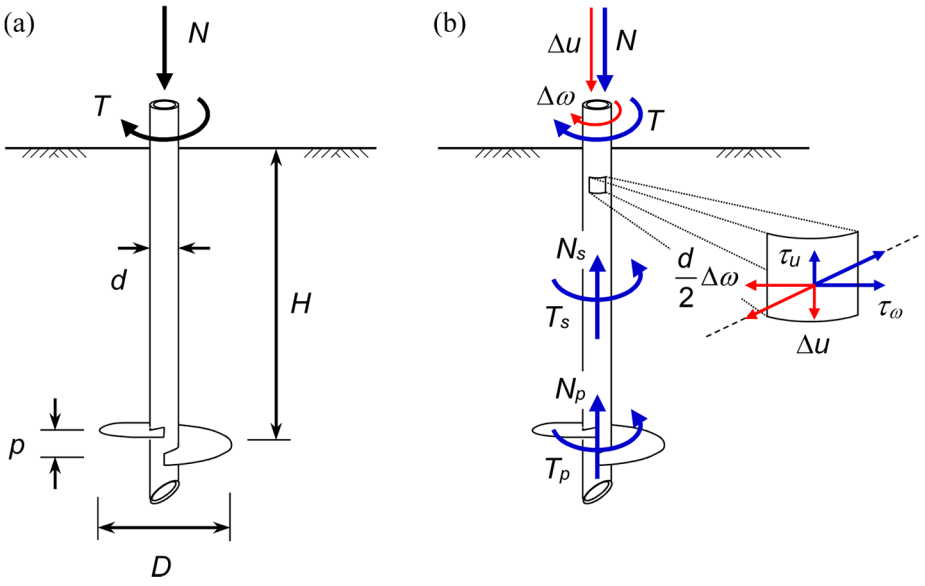


Fig. 3. Schematic of a single-helix screw pile: (a) key variables; (b) stresses and resultant forces generated on the shaft and helical plate during installation (Hambleton et al. 2014; reproduced with permission from the Australian Geomechanics Society)

In Eq. [2], K and d have units of m^{-1} and mm, respectively, such that F_{max} and T in Eq. [1] have units of N and N·m. Standard practice is to assume that Eqs. [1] and [2] apply to the ultimate capacity in both tension and compression, and this is supported by data showing that K is only slightly higher in compression compared to tension (Perko 2009). The equations above are assumed to hold regardless of the soil type.

A concept explored in this paper specifically is that the installation torque should relate to the strength of the soil. This concept has not received prior attention in large part due to the absence of theoretical or empirical models that involve soil strength as a variable, as evidenced by Eqs. [1] and [2]. Provided installation torque can be related to soil strength, a record of installation torque with depth could potentially be interpreted to determine a soil strength profile in much the same way as a cone penetration test is used to infer soil strength from tip resistance.

This paper considers the theoretical model proposed by Hambleton et al. (2014) as a means of understanding the merits and limitations of torque-capacity correlation and, by relating the installation response to soil strength, the possibility of regarding the installation process as a form of *in situ* testing. Attention is limited to the case of installation and ultimate loading under undrained conditions (e.g., saturated clay), and focus is exclusively on the single-helix configuration shown in Figure 3. The analysis highlights the fact that the capacity-to-torque ratio in Eq. [1] depends on not only the shaft diameter but also the crowd force and undrained shear strength of the soil among other variables.

ANALYTICAL MODEL FOR SCREW PILE INSTALLATION IN CLAY

Hambleton et al. (2014) developed a theoretical formula that predicts the installation torque for a single-helix pile installed in undrained conditions (e.g., saturated clay). As illustrated in Fig. 3b, the underlying analysis considers the total installation torque T as the torque mobilized along the shaft (T_s) and at the helical plate (T_p). Similarly, the axial (crowd) force N is the summation of resistance along the shaft (N_s) and the plate (N_p).

Upon assuming that the displacement rate Δu and rotation rate $\Delta\omega$ are determined by the helix pitch p (so-called neutral rotation with $\Delta\omega/\Delta u = 2\pi/p$), T_s and N_s are determined by assuming that the shear stresses mobilized along the shaft are co-axial with the incremental axial displacement and rotation of the pile, as shown in Fig. 3b. The shear stresses are assumed to be uniform along the shaft and given by $\tau = \alpha s_u$, where α is the so-called adhesion coefficient ($0 \le \alpha \le 1$) and $\tau = (\tau_\omega^2 + \tau_u^2)^{1/2}$. The case $\alpha = 0$ corresponds to a perfectly smooth (frictionless) shaft or no contact, and the case $\alpha = 1$ corresponds to perfect adhesion between the shaft and the soil, such that the undrained shear strength s_u is fully mobilized along the interface.

The torque and axial force at the plate, T_p and N_p, are determined based on the following yield envelope, determined from a large number of finite element simulations for a single deeply embedded helical plate subjected to combined torque and axial force (Todeshkejoei et al. 2014):

$$\left(\frac{N_p}{N_{p,\max}}\right)^q + \left(\frac{T_p}{T_{p,\max}}\right)^r = 1 \qquad [3]$$

where

$$q = 1.07, \quad r = 5.16 - 8.02\frac{p}{D}$$
$$N_{p,\max} = 10.82 s_u D^2 \left[1 - \left(\frac{d}{D}\right)^2\right]\left[1 + \left(\frac{p}{D}\right)^2\right]^{-\frac{1}{2}}, \quad T_{p,\max} = s_u D^3 \left[0.74 + 0.33\frac{p}{D}\right] \qquad [4]$$

The relationships given in Eq. [4] are valid for $0.16 \le p/D \le 0.48$ and $0 \le d/D \le 0.4$, and they are based on the assumptions of perfect adhesion between the shaft and soil, as well as plate thickness $t = 0.05D$. In Eqs. [3] and [4], $N_{p,\max}$ is the ultimately capacity of the plate under pure axial loading ($T_p = 0$), which for all values of p/D and d/D remains close to the theoretical capacity of $12.42 s_u D^2$ for a deeply embedded circular plate (Martin and Randolph 2001).

The final formula derived by Hambleton et al. (2014) can be expressed as

$$T = \frac{\pi^2 \alpha s_u d^3 H}{2\sqrt{p^2 + \pi^2 d^2}} + T_{p,\max}\left\{1 - \operatorname{sign}\left(N - \frac{\pi\alpha s_u dHp}{\sqrt{p^2 + \pi^2 d^2}}\right)\left[\frac{1}{N_{p,\max}}\left|N - \frac{\pi\alpha s_u dHp}{\sqrt{p^2 + \pi^2 d^2}}\right|\right]^q\right\}^{\frac{1}{r}} \qquad [5]$$

where q, r, $N_{p,\max}$ and $T_{p,\max}$ are given by Eq. [4]. Equation [5] is slightly adapted from the original expression given by Hambleton et al. (2014) to allow for the case when crowd N is insufficient to overcome the resistance along the shaft, such that the force generated on the pile by the soil must be directed downward ($N_p < 0$). In Eq. [5], the function sign(x) assumes values of sign(x) = 0 for $x \leq 0$ and sign(x) = 1 for $x > 0$, and the function $|x|$ gives the absolute value of x.

Despite its apparent complexity, Eq. [5] provides a straightforward way of relating the torque T, crowd force N, undrained shear strength s_u, shaft roughness α, embedment depth H, and the parameters that define the pile configuration (d, D, and p). The formula can be easily programmed into a spreadsheet, which can then also be used to solve for any variable as a function of the others. The Appendix shows an example completed with an Excel spreadsheet available for download on the first author's website: https://sites.northwestern.edu/hambleton/resources/.

Figure 4 plots the torque T computed using Eq. [5] for a typical set of parameters: d = 50 mm, D = 250 mm, p = 70 mm, H = 1.5 m, s_u = 40 kPa, and α = 1 (full shaft adhesion). The torque is plotted as a function of the crowd force N to highlight two particularly important features. First and foremost, it can be observed that Eq. [5] directly provides a prediction of the pile's axial capacity by considering the particular case T = 0 and solving for the axial force N. This point corresponding to the maximum axial force is indicated as "pile capacity" in Fig. 4. This value is somewhat larger than the capacity of the plate alone due to resistance generated along the shaft, which is also responsible for reversing the direction of the axial force on the plate ($N_p < 0$) at low values of the crowd force, as indicated in the plot. The second important feature to recognize is that the installation torque T is a function of the crowd force N, a fact that is notable due to the absence of any consideration for the crowd force in empirical torque-capacity correlations such as Eqs. [1] and [2]. Indeed, guidance pertaining to how much crowd force should be applied during installation is limited (Perko 2009), and unlike installation torque, crowd force is typically not measured during construction.

Figure 4 includes the value of torque obtained from the empirical torque-capacity correlation given by Perko (2009) and encapsulated in Eqs. [1] and [2], assuming $F_{\max}$ is given by the plate capacity $N_{p,\max}$. This value of 638 N·m determined using the empirical formulas agrees surprisingly well with the value of 611 N·m predicted for zero crowd force using Eq. [5]. However, the discrepancy between the constant value obtained using the empirical formula and the values obtained using the theoretical model grows as the crowd force increases.

RELATIONSHIP BETWEEN TORQUE AND ULTIMATE CAPACITY

The analytical model presented in the previous section suggests that the installation torque is indeed directly related to ultimate capacity. However, the model also suggests that the capacity-to-torque ratio K commonly used in torque-capacity correlation is not in fact a constant that depends only on the shaft diameter but rather a function that depends on crowd force, soil strength, shaft roughness, embedment depth, and other parameters defining the pile configuration. The simplest means of obtaining a theoretical prediction of K is to assume, as commonly done in practice, that the ultimate capacity of the pile $F_{\max}$ is identical to the plate capacity, which is given in Eq. [5] by the variable $N_{p,\max}$. Upon equating $F_{\max} = N_{p,\max}$, Eq. [5] can be used to compute the capacity-to-torque ratio K directly.

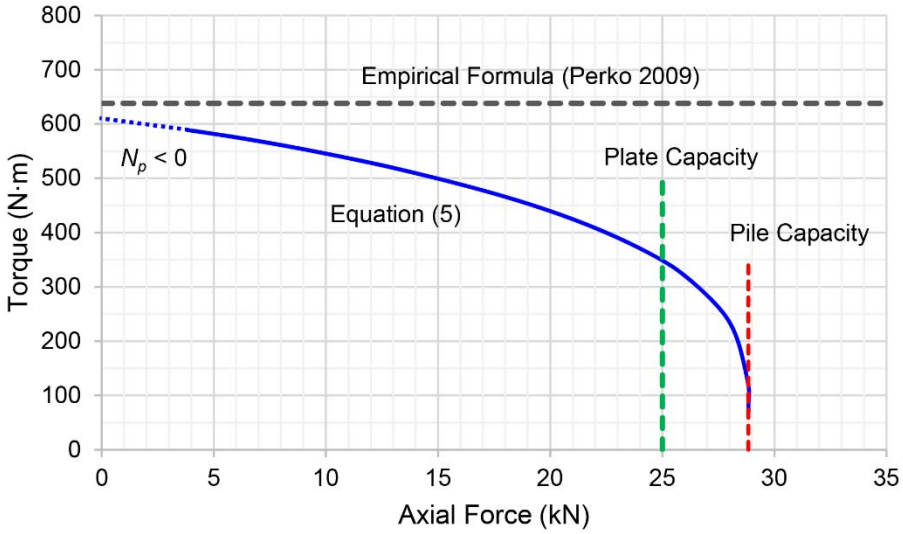


Fig. 4. Predictions of installation torque *T* from Eq. [5], plotted against axial (crowd) force *N*, for assumed parameters *d* = 50 mm, *D* = 250 mm, *p* = 70 mm, *H* = 1.5 m, s_u = 40 kPa, and α = 1 (rough shaft)

Figure 5 shows theoretically predicted values of the capacity-to-torque ratio K in comparison to the empirical values obtained using Eq. [2]. The theoretical predictions, totaling roughly 100 in Fig. 5, are obtained using Eq. [5] with randomized parameters that fall into the following ranges: 50 mm $\leq d \leq$ 400 mm, 250 mm $\leq D \leq$ 750 mm, 30 mm $\leq p \leq$ 140 mm, 1 m $\leq H \leq$ 4 m, and 10 kPa $\leq s_u \leq$ 100 kPa. The adhesion coefficient α was set to $\alpha = 1$ for all calculations. The figure shows that the theory tends to follow the empirical relationship overall but that significant deviations are present as a result of variations in the capacity-to-torque ration produced by changes in individual parameters. It must be emphasized that these deviations are not random but rather variations that are predicted by the theoretical model of Eq. [5]. This scatter is rather remarkable in comparison to the deviations evident in the data compiled by Perko (2009) and reproduced in Fig. 5, which has been heretofore tacitly attributed to random error and unattributed to the effects of any particular parameters.

RELATIONSHIP BETWEEN TORQUE AND SOIL STRENGTH

An overlooked feature of screw piles is the possibility of inferring soil strength from the measured response during installation. This is directly reflected in Eq. [5], which in principle can be solved to determine the undrained shear strength s_u as a function of all other variables. While the equation does not lend itself being solved with respect to s_u explicitly, s_u can be computed numerically. A spreadsheet for computing s_u, when all other quantities are known, can be downloaded from the first author's website: https://sites.northwestern.edu/hambleton/resources/ (see also Appendix).

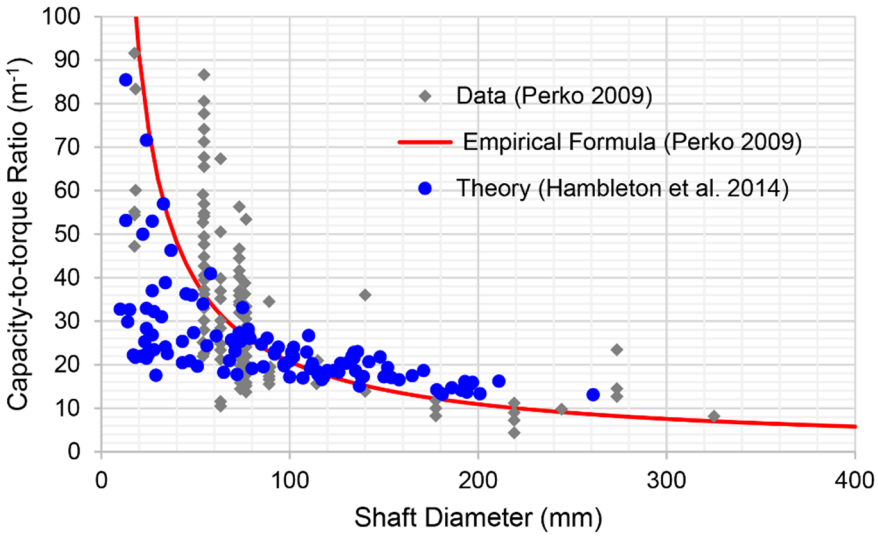


Fig. 5. Relationship between the capacity-torque ratio *K* and the shaft diameter *d* as predicted by the theoretical model of Eq. [5] for randomized inputs compared against the values obtained using the empirical formula of Eq. (2) (Perko 2009)

Data obtained by Todeshkejoei (2019) from small-scale laboratory tests is used to illustrate how soil strength can be assessed from measured torque and axial (crowd) force. Todeshkejoei's tests were completed on kaolin samples using a model screw pile with shaft diameter d = 10 mm, plate diameter D = 40 mm, and pitch p = 8.5 mm. Piles were tested in various configurations and under a range of loading protocols, but here only the data corresponding to neutral installation of a single-helix pile is considered. While the pile was instrumented with strain gauges to measure torque and axial force at various locations along the shaft, only the measurements corresponding to the top of the shaft, which correspond to the total installation torque and total axial (crowd) force, as might be measured during a field installation, are presented and discussed here. The clay samples were prepared by mixing kaolin with a high water content to form a slurry, and then consolidating the mixture in a press. The reader is referred to the thesis by Todeshkejoei (2019) for additional details.

Figure 6 shows the data collected by Todeshkejoei (2019) for the two tests completed by installing the pile through "neutral rotation," such that the advance rate of the pile per revolution is equal to the pitch ($\Delta\omega/\Delta u = 2\pi/p$). It should be emphasized that the smooth curves plotted in Fig. 6 were obtained by digitizing and replotting the data from Todeshkejoei's thesis, which results effectively in some filtering that does not in any substantive way obfuscate the trends in the original data. The curves were slightly adjusted, using some degree of judgement, such that all curves originate from the origin. The two tests plotted in Fig. 6 correspond to the same test completed at different locations across the clay sample, indicating a high degree of repeatability.

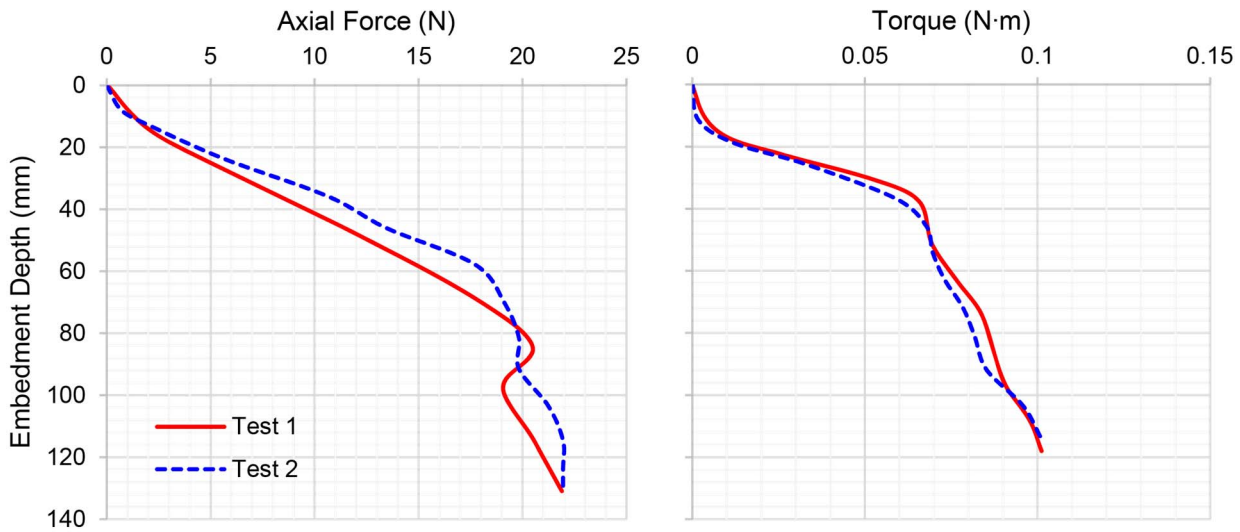


Fig. 6. Axial (crowd) force and torque measured by Todeshkejoei (2019) for a single-helix pile installed in clay

Figure 7 shows the values of undrained shear strength s_u back-calculated from the data plotted in Fig. 6 using Eq. [5]. Only the data for "Test 1" is considered in the back-calculation. An adhesion coefficient of $\alpha = 1$ is assumed, but all other parameters are measured or otherwise known quantities. Figure 7 also shows the intact strength measured using a T-bar, as well as the remolded strength obtained by dividing the intact strength by the measured sensitivity of $s_{u,intact}/s_{u,remolded} = 3$ (Todeshkejoei 2019). It can be observed that the back-calculated values of the undrained shear strength deviate from the remolded strength at small embedment depth but match the remolded strength closely as the embedment depth increases. The source of the discrepancy at small embedment depth is unknown but not unexpected given the complex deformation induced as the screw pile first comes into contact with the soil. Similarly, the strong correlation between the measured installation response and the remolded strength is as one might expect, given the large shear deformations produced as the screw pile is twisted into the ground.

CONCLUDING REMARKS

The analysis considered in this paper casts new light on the concept of torque-capacity correlation and provides some evidence to suggest that soil strength can be inferred by measuring the installation response of screw piles in much the same way that strength is inferred from other types of *in situ* tests (e.g., cone penetration or T-bar). The paper shows that the theoretical relationship derived by Hambleton et al. (2014) for a single-helix pile in clay can be used as the basis for computing capacity-to-torque ratios that include dependence on key parameters such as crowd force, soil strength, shaft roughness, embedment depth, shaft diameter, plate diameter, and helix pitch. Moreover, the analysis reveals that the capacity-to-torque ratio should not be considered a constant but rather a function of the numerous parameters involved. The analysis presented in this paper considering experimental data from small-scale testing on saturated clay further suggests that one can potentially infer the remolded strength of fine-grained soil from measured installation torque and axial (crowd) force. These conclusions require validation from carefully completed full-scale testing.

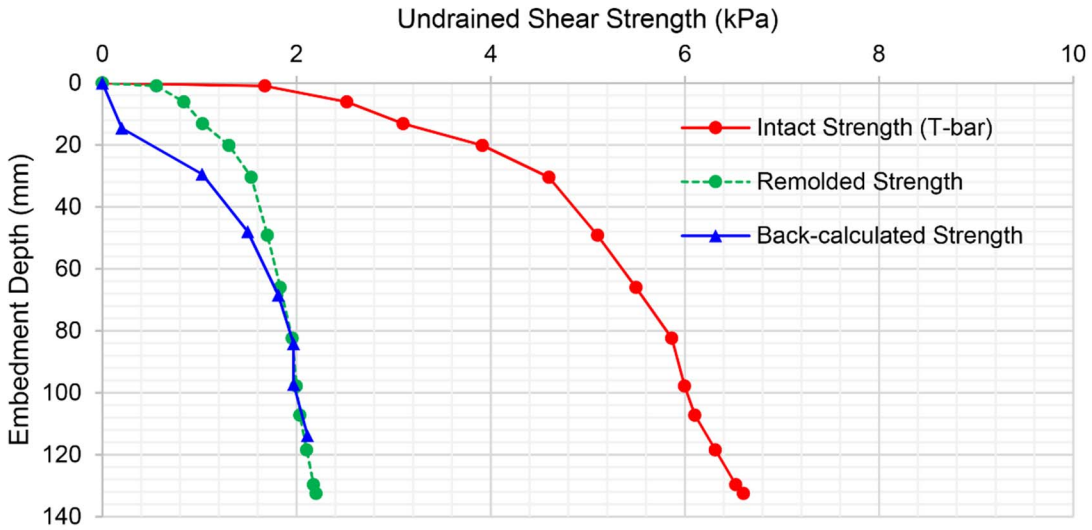


Fig. 7. Comparison of back-calculated and measured strengths from installation data collected by Todeshkejoei (2019) for a single-helix pile installed in clay ("Test 1" only)

This paper considers only a limited subset of the possible configurations and soil types encountered in applications. In addition to validating and refining the model described in this paper, extensions to multi-helix systems and other soils types, particularly sand, represents areas of future work.

APPENDIX: SPREADSHEETS

Spreadsheets for computing torque and shear strength using the theory described in this paper can be downloaded on the first author's website: https://sites.northwestern.edu/hambleton/resources/. Figure 8 shows an example calculation of installation torque.

ACKNOWLEDGEMENTS

The content of this paper was first presented at the 1st International Symposium on Screw Piles for Energy Applications in Dundee, Scotland on May 27-28, 2019, the proceedings of which include an extended abstract that reproduces a small portion of this work (Hambleton and Stanier 2019). This work could not have been completed without enabling financial support from the Australian Research Council (ARC) and the National Science Foundation (NSF), in particular through ARC award numbers CE110001009 and DE160100328 and NSF award number CMMI 1846817.

	A	B	C	D	E	F	G	H	I	J
1	Calculator for single-helix screw piles in clay									
2	Reference: Hambleton, J. P., Stanier, S. A., Gaudin, C., & Todeshkejoei, K. (2014). Analysis of installation forces for helical piles in clay. Australian Geomechanics, 49(4), 73-79.									
3										
4	**Variable**	**Value**	**Units**	**Description**						
5	***Primary Inputs***									
6	s_u	50000	N/m^2	Undrained shear strength						
7	α	1	-	Coefficient of adhesion for shaft (varies from 0 for smooth to 1 to rough)						
8	D	0.25	m	Helix diameter						
9	p	0.07	m	Helix pitch						
10	d	0.05	m	Shaft diameter						
11	H	1.5	m	Embedment depth						
12	N	15628.91	N	Axial (crowd) force						
13	***Calculated Inputs and Secondary Inputs***									
14	q	1.07	-	Exponent in Eq. (4) of Hambleton et al. (2014)						
15	r	2.9144	-	Exponent in Eq. (4) of Hambleton et al. (2014)						
16	$T_{p,max}$	650.3125	N·m	Ultimate torque computed for plate						
17	$N_{p,max}$	31257.81	N	Ultimate force computed based on bearing capacity of plate						
18	***Computed Torque***									
19	T	654.8191	N·m	Installation torque computed from Eq. (9) in Hambleton et al. (2014)						

Fig. 8. Spreadsheet for computing installation torque *T* for specified values of undrained shear strength s_u, adhesion factor *α*, helix diameter *D*, helix pitch *p*, shaft diameter *d*, embedment depth *H*, and axial (crowd) force *N* based on Eq. [5]

REFERENCES

Hambleton, J.P., and Stanier, S.A., 2019. Linking the installation response of screw piles to soil strength and ultimate capacity. *Proceedings of the 1st International Symposium on Screw Piles for Energy Applications*, Dundee, May 27-28, pp. 57-58. https://doi.org/10.20933/100001123

Hambleton, J.P., Stanier, S.A., Gaudin, C., and Todeshkejoei, K., 2014. Analysis of installation forces for helical piles in clay. *Australian Geomechanics*, 49(4), 73-79.

Hoyt, R.M., and Clemence, S.P., 1989. Uplift capacity of helical anchors in soil. *Proceedings of the 12th International Conference on Soil Mechanics and Foundation Engineering*, Rio de Janeiro, August 17, Vol. 2, pp. 1019-1022.

Martin, C.M., and Randolph, M.F., 2001. Applications of the lower and upper bound theorems of plasticity to collapse of circular foundations. *Proceedings of the 10th International Conference of the International Association for Computer Methods and Advances in Geomechanics*, Vol. 2, pp. 1417-1428.

Perko, H.A., 2009. *Helical piles: A practical guide to design and installation*. John Wiley and Sons, Hoboken.

Todeshkejoei, K., 2019. *The mechanics of screw piles in clay*. PhD thesis. University of Newcastle, Australia.

Todeshkejoei, C,. Hambleton, J.P., Stanier, S.A., and Gaudin, C., 2014. Modelling installation of helical anchors in clay. *Proceedings of the 14th International Conference of the International Association for Computer Methods and Advances in Geomechanics*, Kyoto, Sept. 22-25, pp. 917-922.

OBSERVED DRIVING PERFORMANCE OF OPEN-ENDED STEEL PIPE PILES WITH AND WITHOUT PLUGGED TOES

Chu E. Ho, Arup, New York, USA, Tel: 1-917-4388029, Email: chu.ho@arup.com
Paul Napoli, Arup, New York, USA, Tel: 1-212-8963269, Email: paul.napoli@arup.com

ABSTRACT

This paper presents the performance of nineteen open-ended steel pipe piles driven through highly variable overburden soils into glacial till and schist bedrock. The piles were 16 inches in diameter and 0.656 inches thick, with yield strength of 50 ksi. The piles were designed for a service capacity of 250 kips and were driven to achieve an ultimate geotechnical capacity of at least 500 kips. Due to the large variation in the ground conditions, installed pile lengths ranged from 25 to 66 feet. Some piles were driven to refusal on the bedrock while others were terminated at final driving resistance of 2 to 7 blows/in. Two piles were suspected to be plugged during driving while others did not. Each pile was instrumented with strain gages and accelerometers near the pile top, and observed using a Pile Driving Analyzer (PDA) to provide preliminary guidance on pile capacity achieved at end of initial drive (EOID). The influence of plugged and unplugged pile toe conditions on the interpretation of pile capacity was investigated using Case Pile Wave Analysis Program (CAPWAP). Characteristics of driving energy, compressive and tensile stresses developed in the steel pipe piles, and the resulting pile deformation behavior are discussed.

Keywords: steel pipe pile, drivability, dynamic pile testing, CAPWAP analysis, soil plug

INTRODUCTION

The Hunters Point South redevelopment in Long Island City, Queens is one of New York City's major efforts to transform former manufacturing zones into mixed developments for the middle-income community. The site is located along the eastern shoreline of the East River and Newtown Creek. The development included low to high-rise residential buildings, a public school and retail structures. Open spaces were created along the East River and Newtown Creek waterfronts in the form of a continuous park providing for recreational and community related activities. Waterfront structures included small park buildings, walkways and viewing platforms with the shoreline protected by revetments as part of the City's flood mitigation strategy. The project was implemented in two phases, with completion of construction for Phase 1 in 2013 and Phase 2 in 2019.

Based on available historical information, extensive reclamation took place between 1855 and 1898. After 1951, changes to the shoreline were made along the East River, including the removal of reclaimed land along the northern portion of the project site to allow for docking facilities. By 1977, these facilities had been demolished and backfilled to form the current shoreline configuration. The present site was temporarily used as a parking lot with stockpiles of fill mixed with construction demolition rubble, rip-rap and boulders of varying heights across the site. The existing ground surface varied significantly up to approximately 25 feet difference in elevation. The stockpiles were removed and the site was re-graded during final development of the project. This paper discusses the foundation design challenges due to the loose overburden soils and potential obstructions within the fill material, in particular, the issues relating to installation of open-ended steel pipe piles through the ground conditions encountered on site.

FOUNDATION DESIGN CONSIDERATIONS

The subsurface profile at the project site consisted of miscellaneous fill overlying soft organic clay, medium dense silty/clayey sand, glacial till, decomposed rock and schist bedrock. The fill material was the most difficult to quantify. Standard penetration tests (SPT) in the fill indicated N_{60} ranging from 0 to greater than 50

© 2019 Deep Foundations Institute

blows/6ins (refusal). The refusals were attributed to presence of demolition debris in the fill and not indicative of the relative density of the fill material itself. Most of the refusals occurred in the upper 10 feet of the fill layer. Disregarding the refusal values, the SPT blow count averaged about 24 blows/ft overall. It was observed however, that lower penetration resistance (averaging 14 blows/ft) was indicated between the elevations of around EL+0 ft and EL-12 ft (NAVD88), suggesting the material within this zone was in a looser state. Observation wells had indicated the groundwater table was influenced by tidal action, and fluctuated between EL+2.5 and -2.6 ft. It would appear that the fluctuating groundwater level may have influenced the state of compactness of the fill material below the mean tidal elevation of EL+0 ft. Table 1 summarizes the characteristics of the geologic materials identified.

Table 1. Geotechnical parameters of soil and rock units

Stratum	Thickness	SPT N_{60} (average)	Unit weight	Friction angle	Cohesion	Undrained shear strength
	ft	blows/ft	pcf	degree	psf	psf
Fill	14 to 65	0 to refusal[a] (24)	110	34 (above EL+0 ft) 30 (below EL+0 ft)	0	-
Organic Clays and Silts	2.5 to 22	0 to 24 (6)	106	-	-	700
Silty or Clayey Sands	4 to 25	2 to 55 (23)	120	31	0	-
Silty Clays	4 to 25	3 to 61 (19)	120	-	-	800
Glacial Till	3 to 51	16 to refusal[a] (55)	130	35	0	-
Decomposed Rock	4 to 7	40 to refusal[a] (refusal[a])	130	38	0	-
Bedrock	-	-	171	-	-	(UCS[b] 9 ksi)

Notes:
a. SPT blow count > 50 blows/6ins; b. Uniaxial compressive strength of rock

Design of park structures were based on New York City Building Code (NYCBC, 2014). Retaining walls and various light structures were founded on shallow foundations bearing on the ground or compacted engineered fill. Where soft compressible organics and clay layers were present, the shallow foundations were limited only to areas previously improved by surcharge preloading. For more significant construction such as new pedestrian bridges and overlook structures, deep foundations were adopted to mitigate settlements arising from long term consolidation of underlying soft soils and potential seismic settlements. The deep foundations were required to resist both vertical and lateral loading, including imposed structural moments. Sewers, drainage pipes and manholes were supported on standard 40ton timber piles based on New York City Department of Environmental Protection (NYCDEP) specifications.

To avoid difficulty with handling loose soils and potential obstructions within the highly variable fill material, driven piles were considered more appropriate for the site conditions. Steel pipe piles were considered more robust than H-piles due to their circular cross-sections and more capable of handling piling deviation in any direction. Compaction of the loose soils within the fill during driving would provide increased load carrying capacity in both side and end bearing resistance. Close-ended pipe piles however have a higher chance of reaching premature refusal on obstructions within the fill. In the final analysis, open-ended steel pipe piles were adopted as they have the greatest flexibility in handling the different site

conditions, both for penetration through loose soils and the ability to drill through obstructions from within the pipe section if encountered. The interior of the pipe section could be filled with concrete to enhance the pile capacity if necessary. As a prudent precautionary measure, predrilling was specified within the upper 15 feet to avoid driving refusal on embedded boulders and man-made obstructions.

INSTALLATION OF OPEN-ENDED STEEL PIPE PILES

Nineteen open-ended steel pipe piles were installed at several overlook structures and bridges. Piles 101 to 109 and 118 to 119 were single isolated piles supporting pedestrian bridges and minor overlook structures. Piles 110 to 112 and 113 to 117 were installed in two pile groups of three and five piles respectively, which supported a major overlook structure. The piles consisted of 16 inches outer diameter steel pipes 0.656 inches thick, with a yield stress (F_y) of 50 ksi. The piles were designed for a service capacity of 250 kips based on the American Association of State Highway and Transportation Officials Load and Resistance Factor Design Method (AASHTO, 2014). The piles were assumed in the design to carry load entirely in end bearing and were required to be driven to bedrock to achieve a minimum ultimate capacity of 500 kips. Piles were driven in three sets of single lengths: 50, 70 and 73 feet. A Junttan HHK-5S single-acting hydraulic impact hammer was used to drive the piles. The hammer ram weight was 11,027 lbs with a variable drop height of up to 4 feet, capable of delivering a maximum rated energy of 44.108 kips-ft. In general pile driving was executed with the hammer drop height at 3 feet to provide a rated energy of 33.081 kips-ft, except during re-driving when the drop height was raised to achieve increased penetration. Pile penetration lengths varied significantly across the site, ranging from 25 to 66 feet. Only ten piles achieved refusal on the bedrock (Pile Nos. 101 to 109 and 117). The remaining piles were driven to final resistances of between 2 and 8.5 blows/in, terminating within the glacial till.

DYNAMIC MEASUREMENTS

All nineteen piles were instrumented and monitored using a Pile Driving Analyzer (PDA) to provide preliminary guidance on pile capacity achieved at the end of initial drive (EOID). Two sets of gages were fixed at about 2 feet from the pile top, each comprising a piezo-resistive accelerometer and a strain transducer. Continuous monitoring was made for the complete driving process for Piles 110 to 114 and 118 to 119. For piles 101 to 109 and 115 to 117, dynamic measurements were made only after a driving resistance of at least 10 blows/in had been achieved. Table 2 summarizes the driving performance achieved. All piles attained the required minimum capacity of 500 kips at initial drive, except for 118 and 119. Piles 118 and 119 were subsequently re-driven after a waiting period of 17 hours and further extended by 13 feet and 2 feet respectively in order to meet the specified capacity. Based on PDA measurements, the efficiency of the hammer system in terms of energy transfer (EMX) ranged from 78 to 95%. The maximum measured compressive stresses in the pile section at the level of the gages (CSX) during driving ranged from 24.8 to 37.6 ksi. The compressive stresses at the pile toe (CSB) ranged from 13.9 to 42.2 ksi. These values were less than the $0.9F_y$ limit (45 ksi) recommended by FHWA (2016a). Force and velocity traces indicated no evidence of pile damage. Figure 1a shows that for piles driven to a hard refusal, the compressive stresses at the pile toe were always higher or equal to that at the pile top, while those that terminated in a soft toe registered lower compressive stresses at the pile toe in comparison to the pile top. Pile capacities (RX7 and RX9) were calculated using the CASE Method assuming damping factors $j_c = 0.7$ and 0.9 respectively to account for the variability of soil types (FHWA, 2016b). Figure 1b shows that the CASE capacity based on $j_c = 0.7$ and 0.9 do not differ significantly.

Figures 2 to 5 compare the continuous driving characteristics for piles of similar lengths installed through the upper sandy fill and soft organic clays into underling silty/clayey sands and silty clays, terminating in the glacial till. In the case of Piles 110 and 111, the driving resistance (RX) increased steadily as the pile penetrated the ground. The transferred driving energy (EMX) was more efficient at the deeper penetrations within the stronger soils. The compressive stress at the pile top (CSX) was proportional to the transferred

energy (EMX). The compressive stresses developed at the pile toe (CSB) followed closely to the trend of the driving resistance (RX) and approached the stress level at the pile top at final termination depth. The strong reflection in the force signal traces at elapsed time t = 2L/c, where L = pile length below monitoring gages and c = wave speed in pile material (16,807.9 ft/s), indicated evidence of dominant end bearing resistance. The strength of the secondary reflection was about 78% and 75% of the initial peak magnitude for Piles 110 and 111 respectively. Separation between the post-peak force and velocity traces was not very large, suggesting contribution of frictional resistance along the pile shaft was moderately significant.

Table 2. Pile driving performance parameters from dynamic measurements.

Pile No.	Total pile length	Penetration Length (Toe Elevation)	Final Driving Resistance [c]	Maximum Transferred Energy (EMX)	Compressive Stress at Pile Top (CSX)	Compressive Stress at Pile Bottom (CSB)	Maximum CASE Capacity (j_c =0.7)	Maximum CASE Capacity (j_c = 0.9)
	ft	ft	blows/in	kip-ft	ksi	ksi	kips	kips
101	70	31 (-24)	refusal (7/0in)	29.9	28.2	39.5	1128	1099
102	70	25 (-22)	refusal (6/0in)	23.6	28.8	40.6	1219	1205
103	50	31 (-29)	refusal (6/0in)	26.4	37.6	37.6	1220	1220
104	50	34 (-31)	refusal (6/0in)	27.7	32.3	38.6	1138	1119
105	70	50 (-47)	refusal (7/0in)	28.4	28.4	41.1	1194	1160
106	73	52 (-49)	refusal (6/0in)	30.9	27.5	38.6	1106	1069
107	50	48 (-42)	refusal (8/0in)	27.2	36.0	42.1	1267	1244
108	50	45 (-39.5)	refusal (6/0in)	28.3	28.2	31.6	815	799
109	50	43 (-37.5)	refusal (6/0in)	31.1	34.4	42.2	1247	1213
110	70	63 (-43)	4.83 (29/6ins)	31.3	25.6	25.7	731	709
111	70	66 (-46)	7	31.8	25.7	23.1	729	697
112	70	66 (-46)	6	32.8	26.4	30.9	803	739
113	70	47.5 (-42)	4.4 (22/5ins)	27.9	27.0	34.7	965	943
114	70	51 (-45.5)	2.75 (33/12ins)	30.4	25.7	26.1	731	716
115	70	46 (-40.5)	2 (20/10ins)	27.2	28.1	32.6	968	950
116	70	47 (-41.5)	3 (27/9ims)	31.1	26.6	24.2	759	737
117	70	47 (-41.5)	Refusal (7/0in)	28.1	26.3	35.8	1071	1035
118	70	53 (-50)	8.5 (34/4ins)	29.7	24.8	13.9	368	344
118R[a,b]	70	66 (-63)	3.7 (26/7ins)	38.5	27.6	14.9	547	521
119	70	64 (-61)	4.5 (54/12ins)	31.6	26.3	17.4	476	461
119R[a,b]	70	66 (-63)	6	30.4	25.4	17.0	571	542

Notes:-

a. Pile Nos. 118 and 119 were re-driven approximately 17 hours after initial drive.
b. PDA measurements taken at end of re-drive.
c. Bracketed values indicate the actual number of blows achieved for the respective penetration shown.

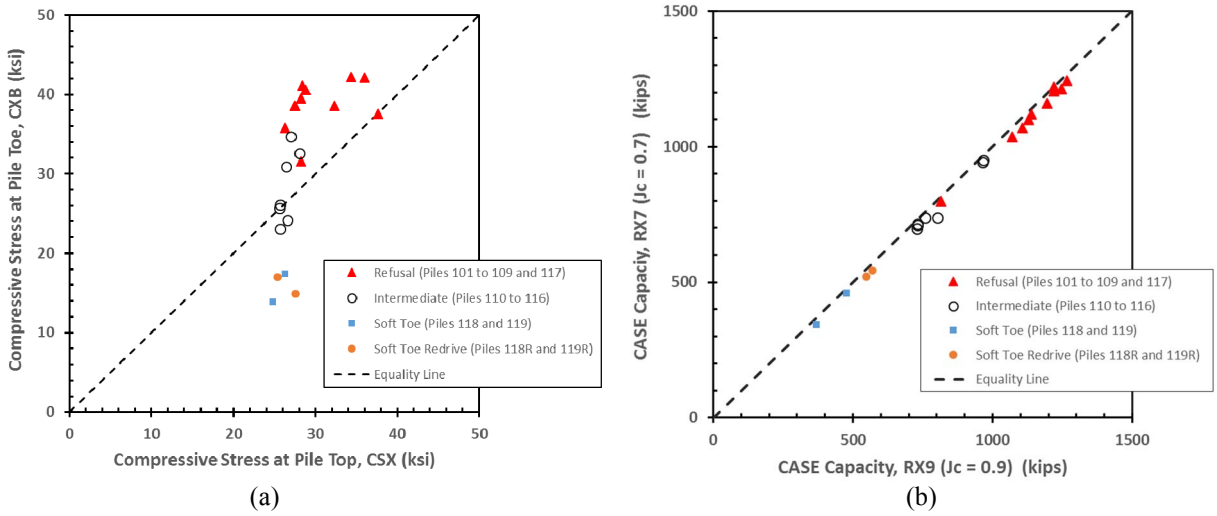


Fig. 1. Compressive stress and CASE capacity from PDA measurements

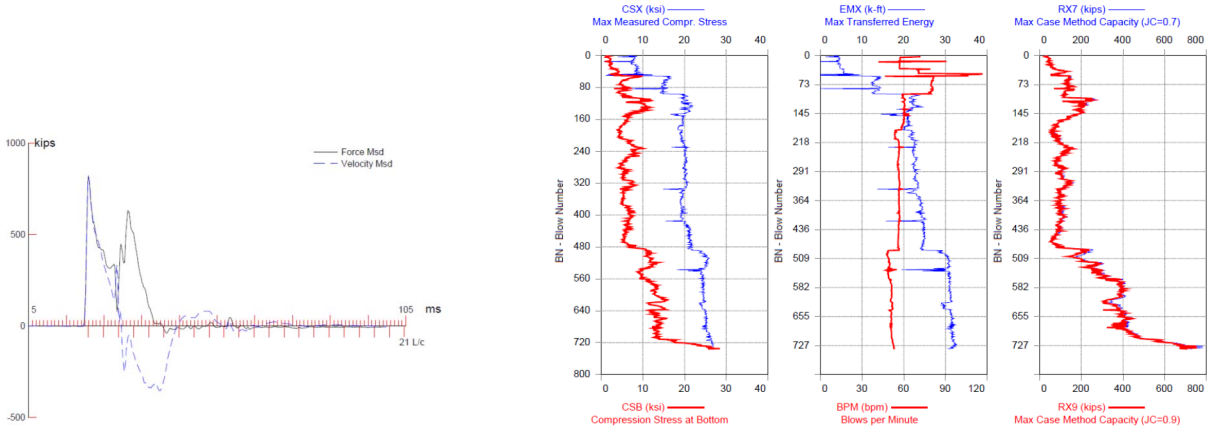


Fig. 2. Driving characteristics for Pile 110 (63 feet penetration length)

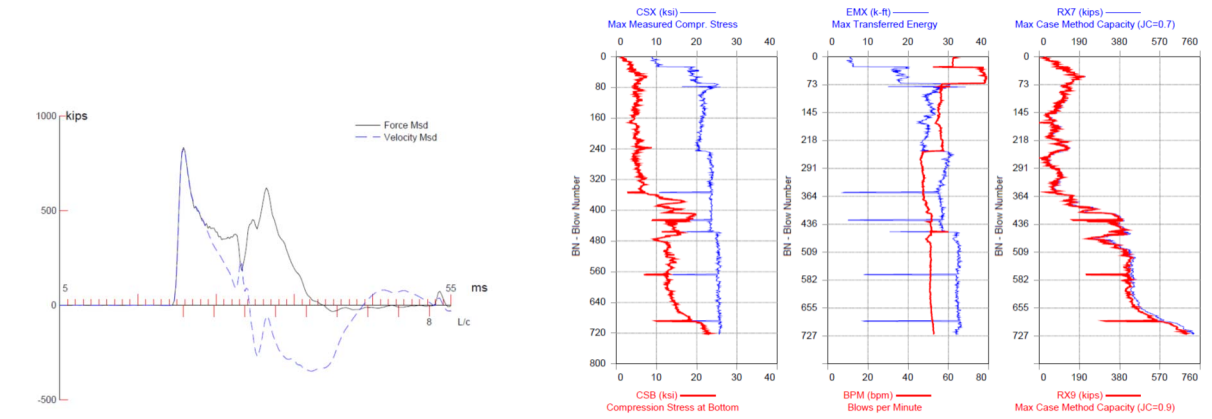
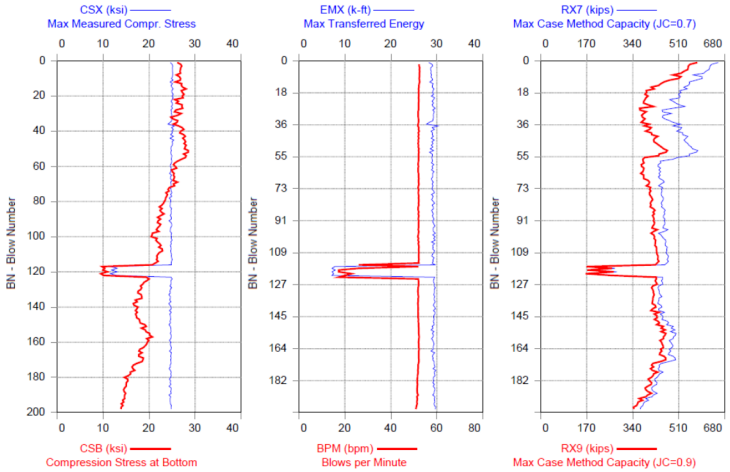
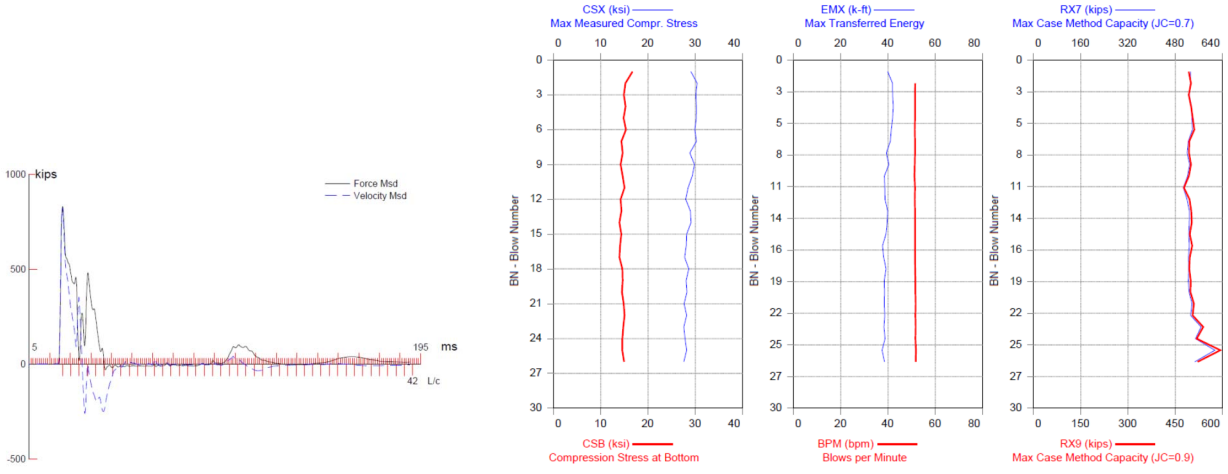


Fig. 3. Driving characteristics for Pile 111 (66 feet penetration length)

Figure 4 demonstrates the case for Pile 118 where very large and consistent driving resistance (RX) was experienced right from the commencement of pile driving. The energy transfer was highly efficient and was practically constant throughout the entire period of driving. This same trend was reflected in the compressive stress at the pile top (CSX). It was noted that the compressive stress at the pile toe (CSB) reduced steadily as the pile penetrated the ground, suggesting less energy was being transferred to the pile toe due to progressive increase in shaft resistance. The pile was re-driven after 17 hours waiting period using a higher energy input. All parameters remained reasonably constant for the next 13 feet up to final termination depth. The compressive stress at the pile toe (CSB) was well below that at the pile top (CSX) and difference between them was approximately constant. The force signal trace at final termination depth indicated a smaller secondary reflection at the pile toe (about 58% of initial peak value) suggesting a softer toe response. The clear separation between the post-peak force and velocity traces indicated that the side resistance was likely to be more significant. It would appear that a soil plug may have developed during the re-drive due to set up in the silty soils after the waiting period.



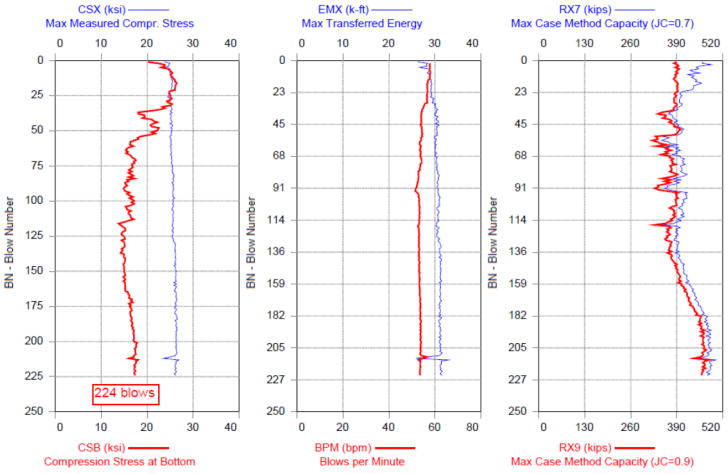
(a) Initial drive (53 feet penetration length)



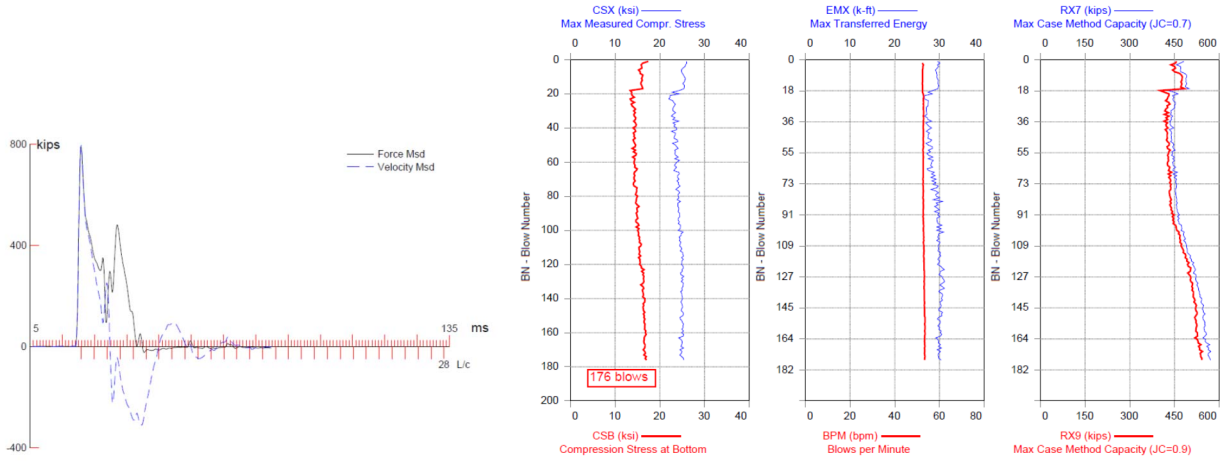
(b) Re-drive after 17 hours (66 feet penetration length)

Fig. 4. Driving characteristics for Pile 118

A similar behavior was observed for Pile 119 (Figure 5). Pile 119 was re-driven another 2 feet after a waiting period of 17 hours. The consistent pattern of a constant difference between the compressive stress at the pile top and pile toe was obvious. The secondary reflection at the pile toe was about 60% of the initial peak value. These observations suggest that a soil plug may have similarly formed in this pile during subsequent re-drive. The separation between the post-peak force and velocity traces was less clear in this case, implying contribution of the shaft friction was expected to be smaller.



(a) Initial drive (64 feet penetration length)



(b) Re-drive after 17 hours waiting period (66 feet penetration length)

Fig. 5. Driving characteristics for Pile 119

CAPWAP ANALYSIS

The measured force and velocity data for each pile was further analyzed using the Case Pile Wave Analysis Program (CAPWAP) using an iterative signal matching procedure to obtain the total pile capacity and soil resistance distribution along the pile, based on assumptions of soil quake and damping characteristics (Rausche et.al. 2002). The influence of plugged and unplugged pile toe conditions can be input as a variable for the prediction of pile driving resistance. The piling conditions can be grouped into three categories: Type 1 - Unplugged (driven to refusal); Type 2 - Unplugged (driven to between 2 and 7 blows/in); Type 3 - Plugged (driven to between 3.7 and 6 blows/in). Table 3 summarizes the CAPWAP analysis results.

Table 3. Pile driving performance parameters from CAPWAP analysis.

Pile No.	Piling Condition	Maximum Transferred Energy (EMX)	Maximum Pile Top Displacement (DMX)	Maximum Compressive Stress (Location below Gage)	Maximum Tensile Stress (Location below Gage)	Total Static Resistance (R_u)	Side Resistance (R_s)	Toe Resistance (R_b)
		kip-ft	in	ksi	ksi	kips	kips	kips
101	Type 1	25.13	0.57	38.3 (35ft)	9.23 (3.5ft)	975	40	935
102	Type 1	21.51	0.50	39.1 (29ft)	6.01 (14.5ft)	1015	25	990
103	Type 1	25.58	0.64	36.6 (36ft)	7.10 (28.8ft)	1022	63.6	958.4
104	Type 1	26.83	0.60	35.6 (37ft)	6.82 (13.5ft)	1120	55	1065
105	Type 1	28.11	0.68	39.2 (53ft)	9.75 (9.9ft)	1090	75	1015
106	Type 1	29.14	0.68	34.4 (55ft)	9.84 (10.3ft)	1049.6	119.6	930
107	Type 1	26.59	0.63	39.0 (47.5ft)	5.68 (20.4ft)	1195	50	1145
108	Type 1	27.59	0.76	29.5 (47ft)	7.32 (23.5ft)	825	25	800
109	Type 1	30.26	0.65	38.9 (46ft)	6.90 (26.3ft)	1200.1	65	1135.1
110	Type 2	30.79	0.76	25.9 (13.4ft)	5.21 (33.5ft)	749.9	139.9	610
111	Type 2	30.61	0.71	26.5 (13.2ft)	6.17 (39.6ft)	714.9	169.9	545
112	Type 2	32.12	0.75	26.9 (33ft)	6.99 (33ft)	720.1	170.1	550
113	Type 2	27.46	0.72	32.3 (54.5ft)	9.79 (17ft)	935	105	830
114	Type 2	29.54	0.76	26.7 (34.4ft)	5.82 (34.4ft)	689.9	84.9	605
115	Type 2	26.84	0.72	30.8 (49ft)	12.28 (10.5ft)	950	100	850
116	Type 2	28.77	0.70	33.0 (51ft)	10.43 (13.6ft)	899.9	149.9	750
117	Type 1	26.71	0.64	35.0 (51ft)	8.57 (13.6ft)	1104.2	230.2	874
118R	Type 3[a]	37.50	0.85	26.7 (6.8ft)	2.46 (3.4ft)	550	160.9	389.1
119R	Type 3[b]	29.92	0.76	26.9 (47.3ft)	5.0 (47.3ft)	545	114.9	430.1

Notes:-

a. Soil plug weight = 0.17 kips
b. Soil plug weight = 0.21 kips

Figure 6 shows the comparison between the maximum compressive and tensile stresses developed in the pile section at EOID. The location of the stress occurrence is referenced to the gage position and designated as relative location (RL), where RL is the ratio of the distance of stress occurrence to the distance of pile toe below the gage. As can be seen, the maximum compressive stress in Type 1 piles almost always occur at the pile toe (RL = 1.0), while that for Types 2 and 3 may occur within the pile shaft. However, the maximum tensile stress may occur anywhere within the pile for all pile types.

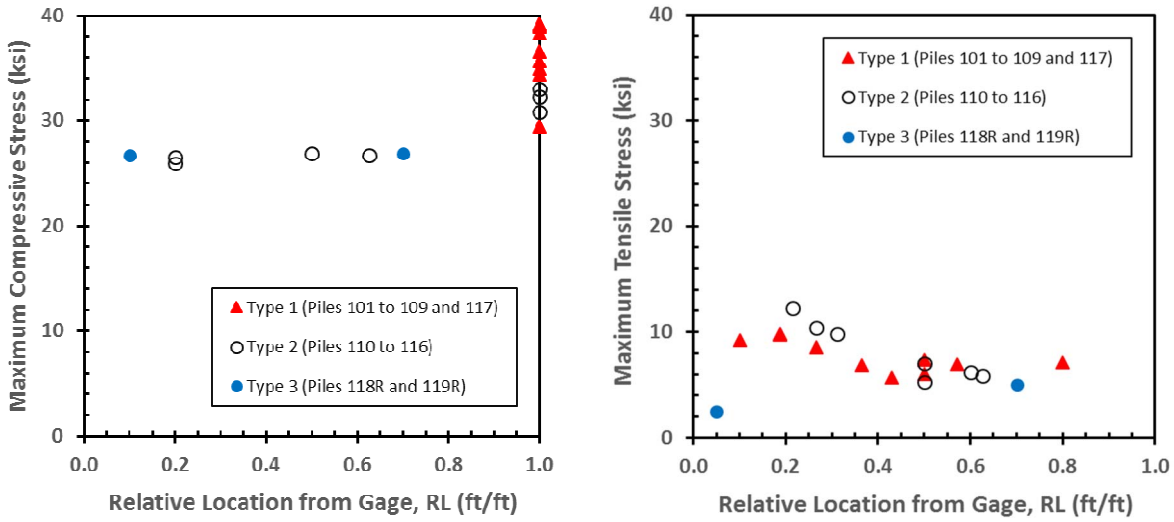


Fig. 6. Maximum compressive and tensile stresses

Figure 7a shows the maximum pile top displacement (DMX) was reasonably proportional to the maximum input energy (EMX). This implies that the pile system behaved elastically and no damage to the pile was noticeable from the stress wave measurements. The static side resistance (R_s) and toe resistance (R_b) derived from CAPWAP is shown in Figure 7b. As can be seen, the toe resistance overwhelmingly dominated the pile capcities in all cases. From Table 3, the proportion of total static capacity (R_u) carried by toe resistance (R_b) averaged 93% for Type 1, 83% for Type 2, and 75% for Type 3 piles. It was noted that toe resistances of Type 3 piles were very low even though they were plugged. Using Meyerhof's equation for ultimate toe resistance in granular soil, q_{bu} (tsf) = $4N_{60}$ (Meyerhof, 1976), it was estimated that N_{60} would be about 34 and 38 blows/ft to match the R_b values for Piles 118R and 119R respectively. It was likely the piles achieved limited penetration in the glacial till.

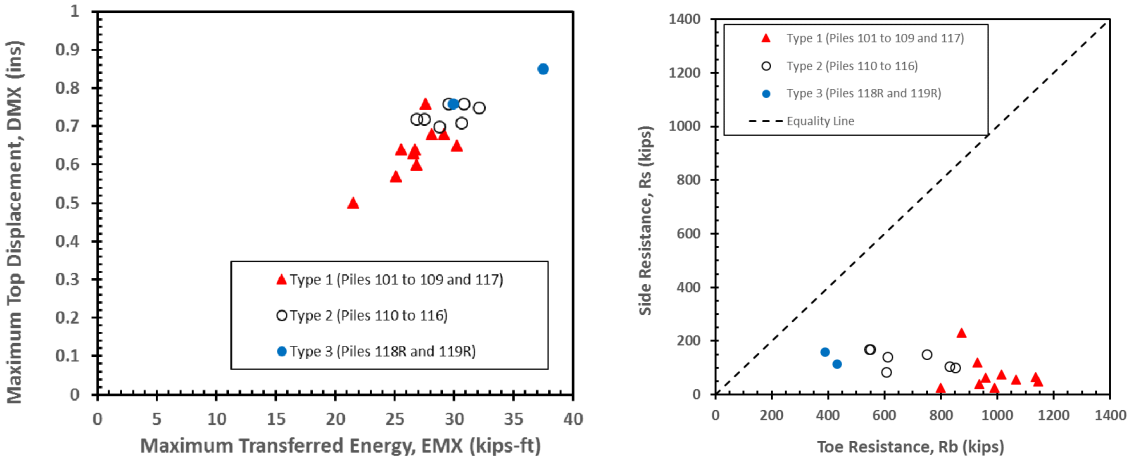


Fig. 7. Maximum pile top displacement and derived static pile capacities

Figure 8 compares the pile capacities given by CASE Method with that computed by CAPWAP. It appears that RX9 (based on jc = 0.9) correlated slightly better with CAPWAP capacities than RX7 (based on jc = 0.7). It was noted that in both cases, CASE Method overpredicted the capacities for piles that were driven to refusal (Type 1). Where the piles were terminated over a final penetration distance (Types 2 and 3), CASE Method seemed to provide reasonable predictions.

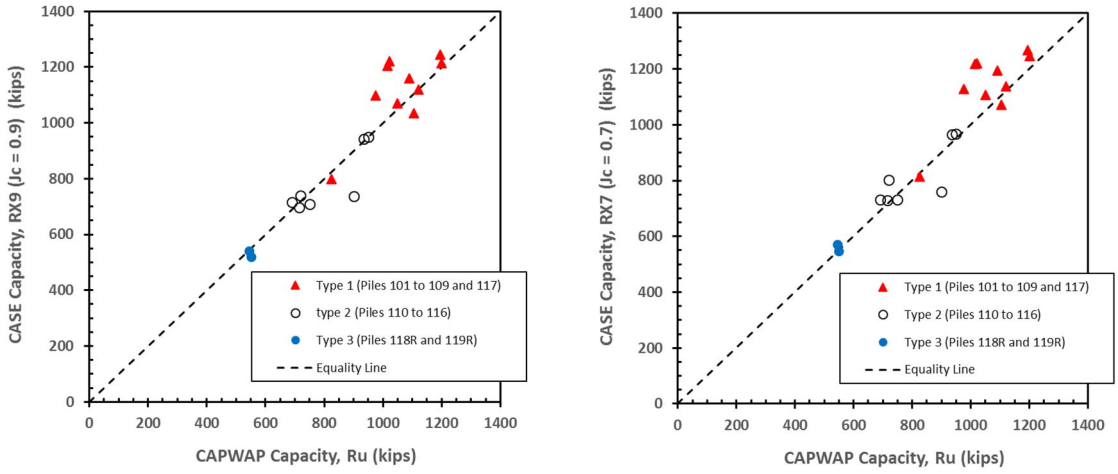


Fig. 8. Comparison of pile capacities using CASE Method and CAPWAP

Figures 9 to 12 present representative examples of the typical force and velocity signal traces used for CAPWAP analysis and the corresponding predicted load-deformation response of the piles under various piling conditions. As can be seen, pile deformation behavior was highly influenced by the stiffness of the material at the pile toe. From Figure 9, the toe response was very stiff because the pile terminated on the rock, and the majority of the pile top displacement was likely due to elastic shortening of the pile shaft, since the mobilized side resistance was relatively small. Where the piles terminated over a penetration distance (Types 2 and 3), the overall pile behavior was more significantly influenced by the toe response (Figures 10 to 12). The softest toe response was indicated for plugged piles (Type 3). The movement of the pile toe also allowed greater mobilization of the side resistance. Based on the soil plug self weight modeled in CAPWAP, it was estimated plug lengths of 13.3 and 16.5 inches had formed in Piles 118R and 119R respectively, assuming the unit weight of soil plug to be 130pcf (similar to glacial till). This representted about 0.91 and 1.12 times the internal diameter of the pipe section respectively.

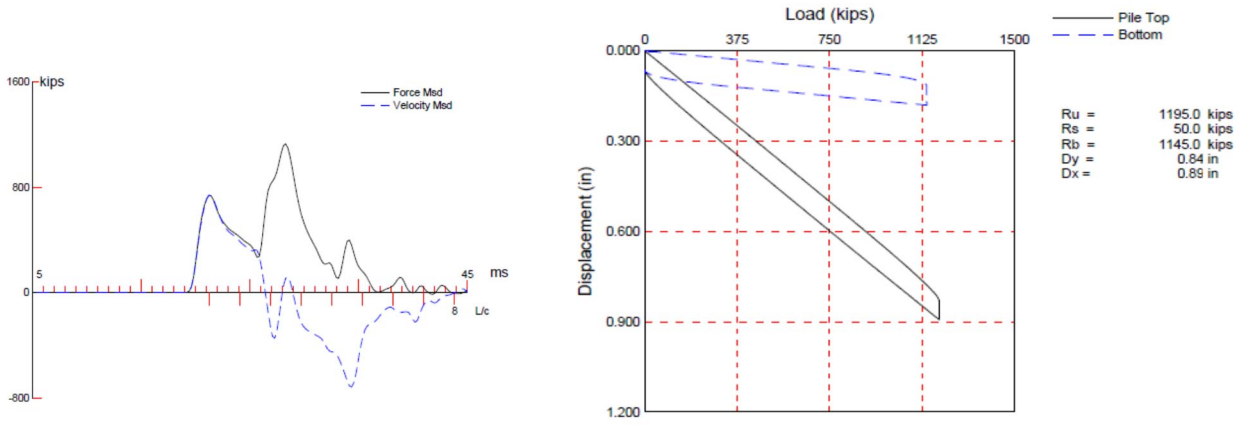


Fig. 9. Load-deformation characteristics of Pile 107 (TYPE1)

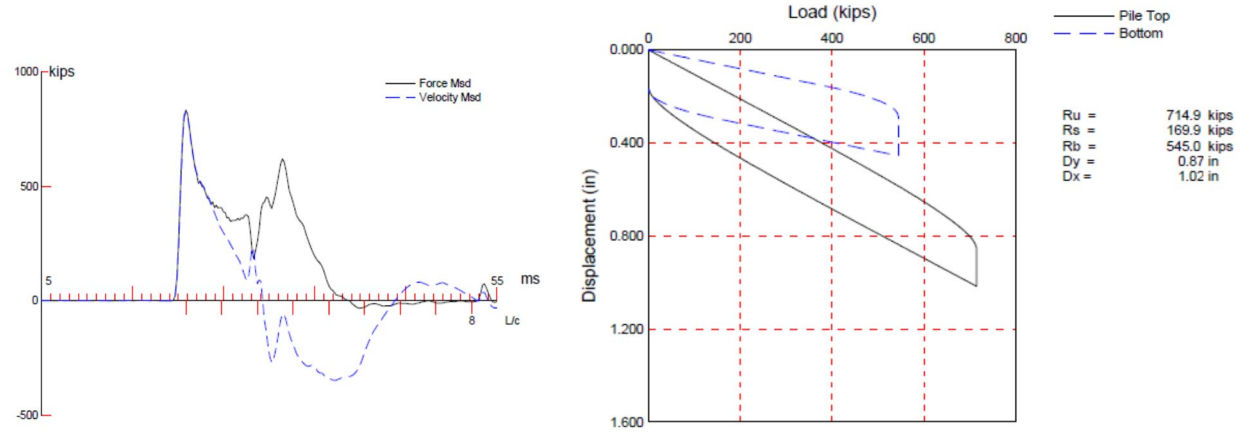


Fig. 10. Load-deformation characteristics of Pile 111 (TYPE 2)

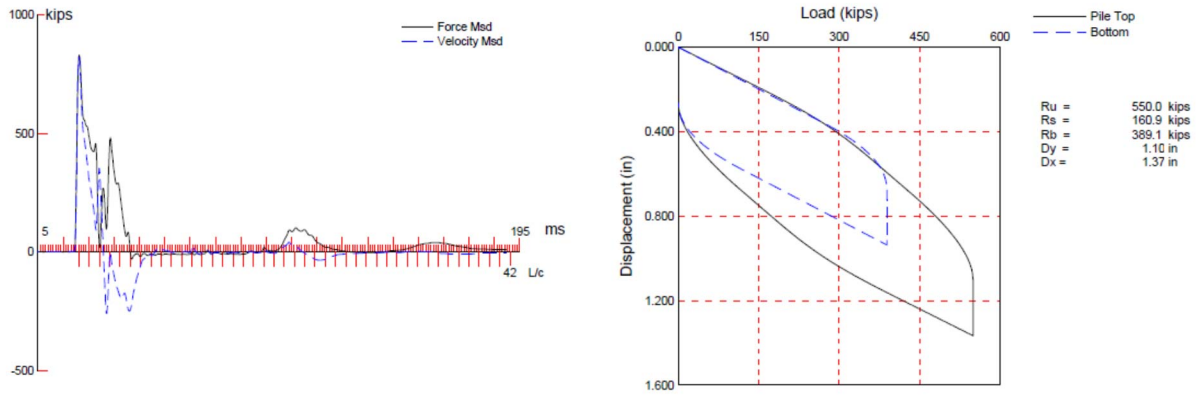


Fig. 11. Load-deformation characteristics of Pile 118R (TYPE 3)

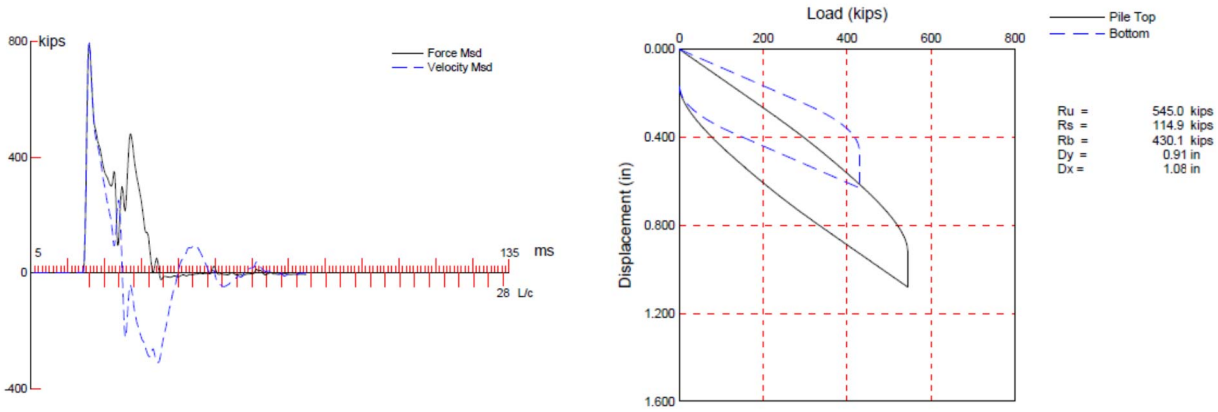


Fig. 12. Load-deformation characteristics of Pile 119R (TYPE 3)

CONCLUSIONS

This paper discusses the observed driving characteristics of open-ended steel pipe piles as indicated by PDA and CAPWAP analyses. Nineteen piles were driven through miscellaneous fill and soft organic soils into competent clayey sands, silty clays, glacial till and schist bedrock. PDA measurements at end-of-initial-drive (EOID) provided guidance for termination of the piles based on CASE capacities. Ten piles achieved refusal on the bedrock. The remaining piles were driven to final driving resistance of between 2 and 7 blows/in within the glacial till. Pile penetrations varied significantly across the site, ranging from 25 to 66 feet. Continuous PDA monitoring of selected piles revealed possible soil plugging when driving through sandy soil layers at depth. CAPWAP analysis using signal matching technique confirmed that soil plugs needed to be included in the model for proper prediction of pile capacity. The proportion of total static load carried by toe resistance was on the order of 93% for unplugged piles driven to a hard refusal (Type 1), 83% for unplugged piles driven to final drives of 2 and 7 blows/in (Type 2), and 75% for plugged piles driven to final drives of 3.7 to 6 blows/in (Type 3). CAPWAP analysis indicated overall pile deformation behavior was greatly influenced by the response of the material at the pile toe. For piles driven to a hard refusal, pile deformation was dictated by elastic shortening of the pile shaft. For piles terminating over a penetration distance, overall pile behavior was governed by the deformation of the pile toe. Plugged piles

resulted in softer toe response under static loading than unplugged piles. Estimated plug lengths were on the order of 0.91 to 1.12 times the internal diameter of the pipe section.

REFERENCES

AASHTO (2014). AASHTO LRFD Bridge Design Specifications, American Association of State Highway and Transportation Officials, Washington, D.C.

FHWA (2016a). Design and Construction of Driven Pile Foundations – Volume 1, US Department of Transportation Federal Highway Administration, Washington D.C.

FHWA (2016b). Design and Construction of Driven Pile Foundations – Volume II, US Department of Transportation Federal Highway Administration, Washington D.C.

Meyerhof G.G. (1976). "Bearing Capacity and Settlement of Pile Foundations". Journal of Geotechnical Division, ASCE, Vol. 102, No. GT3, 197-228.

NYCBC (2014), "New York City Building Code". New York City Buildings Department, New York, NY.

Rausche, F, Goble, G.G. and Likins, G. E. (2002). "Dynamic Determination of Pile Capacity". Current Practices and Future Trends in Deep Foundations, Geotechnical Special Publication No.125, ASCE, 398-417.

ACCURACY OF LOW-STRAIN PILE INTEGRITY TEST RESULTS

Mahesh Hingorani, *Pilex India, Vadodara, Gujarat, India, +91-7698016319, pilex.india@gmail.com*

ABSTRACT

Integrity issues for bored cast-in-situ piles have raised the need for the use of non-destructive tests to verify pile integrity and detect possible anomalies in installed pile sections that could adversely affect their serviceability. Integrity inspections performed after installations are often the most reasonable alternative available to assess the shaft quality. The two most common methods are pulse-echo from a small hand held hammer at the pile top, and cross-hole ultrasonic transmissions along the shaft between parallel sonic pipes. While different in technique, each method has its advantages and limitations. This paper emphasizes more on the degree of accuracy of low-strain pile integrity test by comparing the results with cross-hole sonic logging. Reliable data collection and interpretation by an experienced test engineer will reveal the integrity of the pile.

Cross-hole sonic logging and low-strain pile integrity testing were both specified as quality control measures for a metro rail project in India. Both cross-hole sonic logging and low-strain pile integrity testing indicated defects in several bored piles. Also minor imperfections recorded by cross-hole sonic logging were observed in low-strain results. The observations of the two test methods are presented and compared for a better understanding of the importance of low-strain test results for any project.

Keywords: pulse-echo; low-strain integrity testing; cross-hole sonic logging; non-destructive test

INTRODUCTION

Cast-in-situ concrete piles are often chosen as a deep foundation alternative where challenging soil conditions exist. Although quality control measures are almost always taken during the installation of the piles, it is often difficult or impossible to confirm the integrity of the pile at this stage, particularly in wet conditions. Because of the relatively high probability of bored piles having anomalies, quality assurance of each bored pile is essential for each project.

Non-destructive test (NDT) has become the standard in quality assurance for deep foundations. Several methods are available to perform this testing. Among the most common methods of NDT testing are cross-hole sonic logging and low-strain integrity testing. Individually, each test method has its own advantages and limitations inherent in the test method. When both test methods are used in conjunction, certain characteristics of a potential defect may be clarified. This paper presents a case history where anomalies are indicated by both test methods. The results of the two test methods are compared.

LOW STRAIN INTEGRITY TESTING

Low-strain integrity testing, also known as Pulse Echo Method (PEM) or Pile Integrity Testing (PIT), is a NDT based on wave propagation theory. The pile top is impacted with a hand held hammer and the resulting pile top motion is measured with an accelerometer attached to the pile top. The hammer impact creates a low strain compression stress wave that propagates down the pile. The wave is reflected when a change in ‘‘impedance’’, the pile toe, or soil resistance effects are encountered. Impedance is related to a pile’s cross sectional area, elastic modulus, and stress wave propagation speed. An impedance reduction causes a reflected tensile wave (an increase in the velocity curve) and an increase in impedance causes a reflected compressive wave (a decrease in the velocity curve). High soil resistance can also cause compressive reflections which can sometimes be minimized through filtering techniques.

© 2019 Deep Foundations Institute

The test method is described in ASTM D5882. Figure 1 shows a typical field test using the pile integrity tester. Low strain integrity testing has many potential applications. The most typical application is to evaluate newly constructed shafts as a quality control measure.

Low Strain Integrity Testing Result Interpretation

In order to fully evaluate the pile integrity using low strain integrity testing results, a clear toe reflection in the velocity record must be observed. When the length of the pile is known, the appropriate material wave speed can be applied to the record. Tensile reflections that occur prior to the toe reflection can be investigated to determine if any impedance reductions occur in the pile.



Fig. 1 Low-Strain Integrity Testing

Several factors can deplete the strain wave and therefore diminish any observable toe reflection. These factors include high soil resistance, several minor or one major impedance change, and excessive length. Piles with length to diameter ratios above 30 often have excessive damping due to soil resistance and/or pile material properties which deplete the strain wave and cause no observable toe reflection, although this rule can sometimes be deviated and piles with a greater ratio can be reasonably tested under special circumstances (Massoudi and Teferra, 2004).

Low Strain Integrity Testing Advantages

- Minimal pile preparation required
- Relatively quick and inexpensive; allowing the possibility for every pile to be evaluated
- Can provide depth and severity information regarding major defects
- Can potentially evaluate length and quality of existing foundations
- Test shafts can be selected after installation

Low Strain Integrity Testing Disadvantages

- Inconclusive results or complicated signals can be caused by several factors
- Records require experienced interpretation

- L/D limitations
- Horizontal extent of a defect often cannot be evaluated
- Accuracy of length or depth to defect is dependent on an assumed wave speed

CROSS-HOLE SONIC LOGGING

Cross-hole sonic logging (CSL) is a NDT method which involves ultrasonic signal transmission through the pile between two parallel water filled sonic tubes. The sonic tubes are often tied to the rebar cage and cast permanently into the pile. The total number of sonic tubes typically depends on the pile diameter. A transmitter probe and a receiver probe are lowered to the bottom of the pile in separate sonic tubes. Measurements of the signal transmission are collected approximately every 5cm as both the probes are raised together to the top of the pile. The cables attached to the probes are pulled through calibrated encoder wheels which can accurately determine the depth of the probe during testing. A collection of measurements from one sonic tube to another is called a profile. Profiles are collected from all combinations of sonic tubes. The test method is described in ASTM D6760. Figure 2 shows a typical configuration for collecting CSL data.



Fig. 2 Cross-Hole Sonic Logging

CSL Result interpretation

The interpretation of CSL result requires experience and understanding of the capabilities and limitations of the method. Quality assessment of pile from CSL is primarily based on the first arrival time (FAT) of the signal. The concrete wave speed can be estimated by dividing the distance between the sonic tubes by the recorded FAT. The wave speed of concrete can be used as a judgment of the overall concrete quality. However, during placement of the rebar cage or concrete, the sonic tubes often move slightly out of parallel and ultimately the distance between the tubes is not always constant with depth. Therefore, it is more practical to evaluate the FAT as a relative measurement for each individual pile, comparing signal delays to a ‘‘running’’ average of data from the same shaft. Often a running average of approximately 75 consecutive data points, which would represent approximately the surrounding 3.75 m, are averaged for comparison to evaluate a local defect.

Signal strength is another important measurement for evaluation of CSL data. The signal strength is converted to signal ‘‘energy’’ by integrating the signal over a defined time. Relatively low energy can indicate poor quality concrete or a defect in the pile. Often a major defect will cause both a significant FAT delay and decrease in relative energy. Interpretation of a major defect from CSL is often intuitive, however, evaluating a relatively minor FAT delay or energy decrease requires engineering judgment. Likins et al. (2007) suggested the CSL results scale shown in Table 1. New CSL criterion for the interpretation of the CSL results may be proposed soon by others.

Table 1. Suggested CSL Results Scale

Concrete Quality	FAT Increase (%)		Energy Reduction (dB)
Good	0 to 10	and	<6
Questionable	10 to 20	and	<9
Poor / Flaw	20 to 30	or	9 to 12
Poor / Defect	>30	or	>12

Flaws and Defects should be addressed if they are indicated in more than 50% of the profiles. Defects or flaws indicated over the whole cross-section usually require repair or replacement.

CSL Advantages

- Relatively simple interpretation when a major defect is present
- No pile length limitation
- Can determine the depth of an anomaly with reasonable accuracy
- Can estimate horizontal extent of a defect if enough access tubes are present

CSL Disadvantages

- Sonic tubes must be installed during pile construction (Test pile must be preselected)
- Several factors can influence results (uncured concrete, debonding, etc.) however, the cause for the FAT delay and/or energy decrease often cannot be determined
- Only concrete between sonic tubes can be assessed
- Evaluation often requires experience and engineering judgment when results are complicated or not outwardly conclusive

TEST METHOD COMPARISONS

Both of these NDT methods are effective tools in quality assurance and foundation evaluation. The advantages and disadvantages of each individual test method have been discussed. The two test methods also inherently have similarities and differences in their application and results.

Test Method Similarities

- Non- destructive and repeatable
- Time dependent – results depend on concrete curing (with respect to wave speed)
- Evaluate concrete quality and overall shaft acceptability, however often cannot determine the cause or material properties of a defect, only that it is present
- Require experienced interpretation of results and engineering judgment in presenting results
- Can reasonably be performed on all production piles

Test Method Differences

- CSL can only evaluate the concrete between sonic tubes while PIT can evaluate the full cross section as well as profile of the shaft
- CSL can estimate depth, horizontal position, and extent of a defect, PIT only indicates the depth and only a very rough estimate of the extent
- CSL is effective in identifying a ‘‘soft toe’’ condition while PIT cannot be always reliable for this application
- PIT can evaluate the outer profile of the pile by Profile Analysis, while CSL can also give an internal view of the shaft by Tomography Analysis.

Both of these test methods can be used on the same shaft. In conjunction, the combined test results sometimes provide a more comprehensive evaluation of the shaft than either single test alone. For example, if PIT testing indicates an impedance decrease at a certain depth however CSL results do not indicate FAT delays or energy decreases at the corresponding depth, it is likely that the impedance decrease indicated from PIT results is from a reduction in cross section and not from a material quality issue.

CASE HISTORY

Pile foundation was proposed for a Metro Rail Project in one of the fast growing cities in India. The project had groups of 4 piles and 6 piles for Viaduct and Station Area respectively. Both cross-hole sonic logging and low-strain integrity testing were specified. Four sonic tubes were cast in the piles of 1200mm diameter to facilitate CSL testing. All piles in the project were supposed to be tested for low-strain integrity test and only 20% of piles for CSL test in each pile group.

Piles with major defect

Figure 3a and 3b show the results from low-strain integrity testing and the sonic profiles from CSL testing respectively on a 21m deep bored pile. The ‘waterfall diagram’ from CSL shows quite clearly a delay in first arrival time (FAT) and energy losses at 13.5m. The defect was indicated in all sonic profiles. FAT delays were more than 30% and energy decrease was also more than 12dB. The pile top velocity curve from the low-strain integrity testing indicated a very strong tensile reflection (major reduction in impedance) at approximately 13.5m. Both testing methods clearly indicated a defect in the pile.

Figure 4 shows PIT and CSL results from another pile with major defect. The CSL results indicated FAT delays of more than 30% and total energy decrease of more than 12dB, which would classify it as a defect. The flaw was indicated in all CSL profiles at approximately 26m depth. In Figure 4, the diagonal sonic profile (center) indicates complete loss of signals beyond 26m. The pile top velocity curve from PIT indicates a clear tensile reflection as the low strain wave could not propagate beyond 26m. This could be evaluated as a signal of early toe reflection.

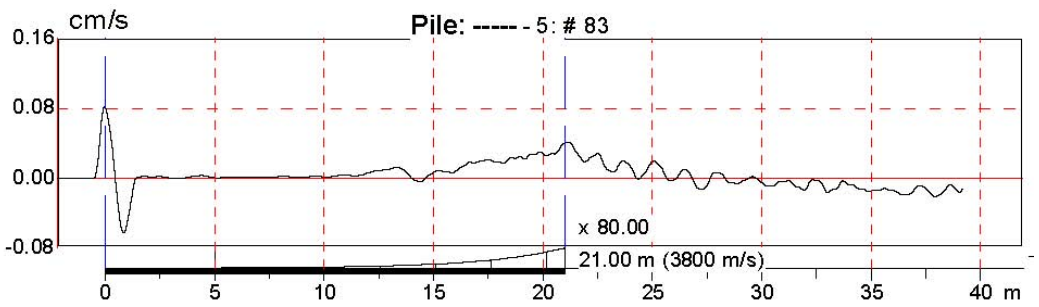


Fig. 3a PIT Result on a pile with major defect

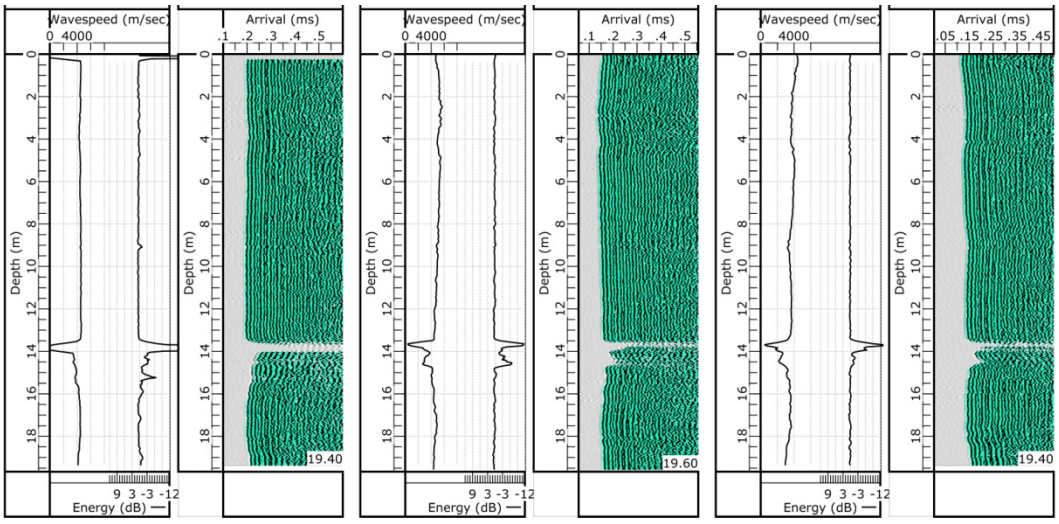


Fig. 3b CHSL Result on a pile with major defect

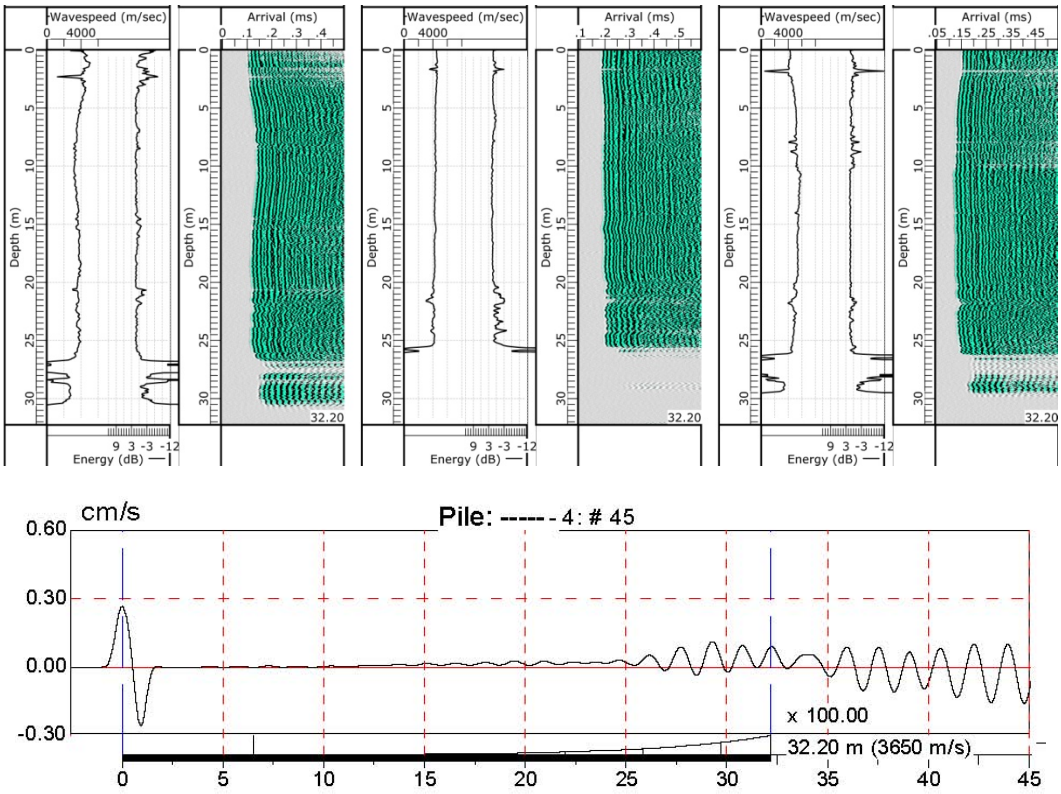


Fig. 4 CSL Result (Top) and PIT Result (Bottom) from a pile with major defect

Uniform Pile free of flaws or defects

Figure 5 shows typical CSL & PIT record from a uniform pile free of flaws or defects. The CSL results indicate a consistent FAT and energy measurement. The PIT record is relatively flat throughout the length of the pile (no impedance changes) with a clear reflection from the pile toe.

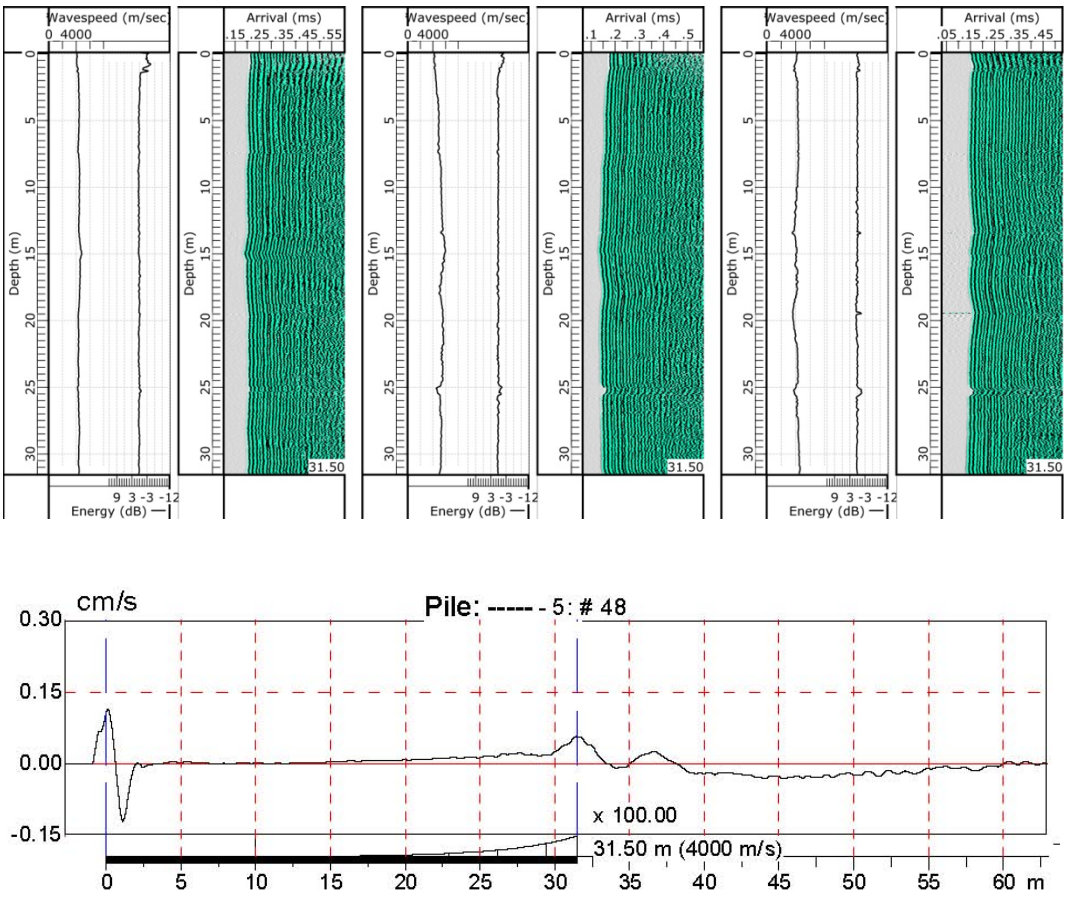


Fig. 5 CSL Result (Top) and PIT Result (Bottom) from a uniform pile free of flaws or defects

Uniform Pile with minor imperfections

Figure 6a and 6b present PIT and CSL results respectively from another uniform pile but with minor imperfections. The 'waterfall diagram' from the CSL test indicates minor variation in FAT around 30m till pile toe. The PIT record also shows few spikes after 30m to the pile toe, indicating minor imperfections due to change in the pile concrete density.

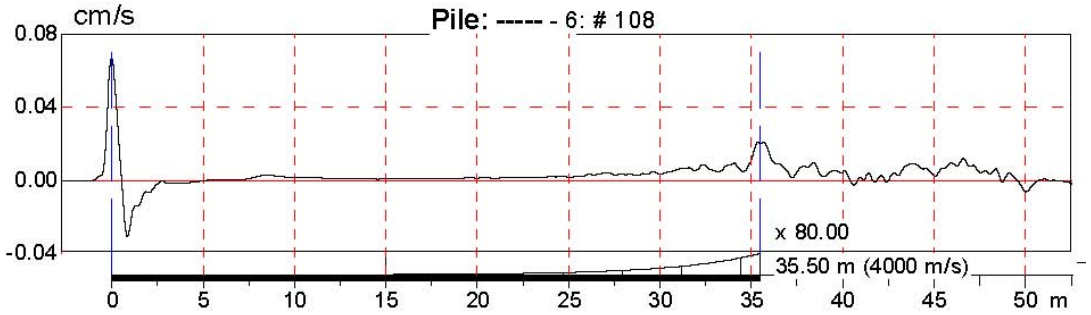


Fig. 6a PIT Result from an uniform pile with minor imperfections

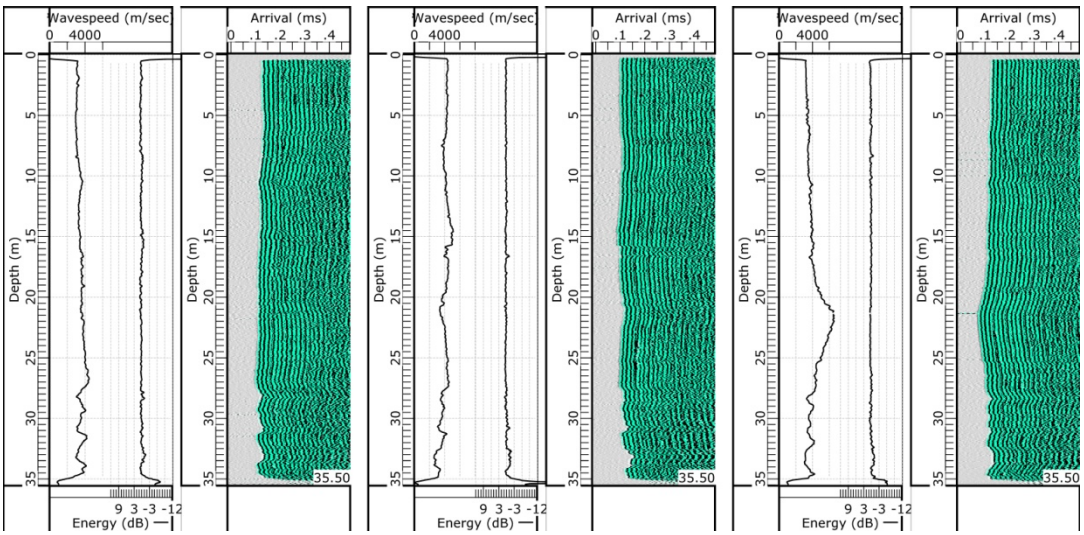


Fig. 6b CSL Result from an uniform pile with minor imperfections

Pile with possible Soft Toe

Figure 7a and 7b show PIT and CSL results respectively from a pile with possible soft toe condition. The 'waterfall diagram' of CSL record indicates reduction in FAT for more than 30% after 33m till pile toe. However the energy reduction of significant amount is not observed so as to classify it as a defect, but an indication of low density concrete. The PIT record shows tensile reflection at 33m indicating major impedance reduction. However toe reflection from 35.5m is not observed due to low density concrete.

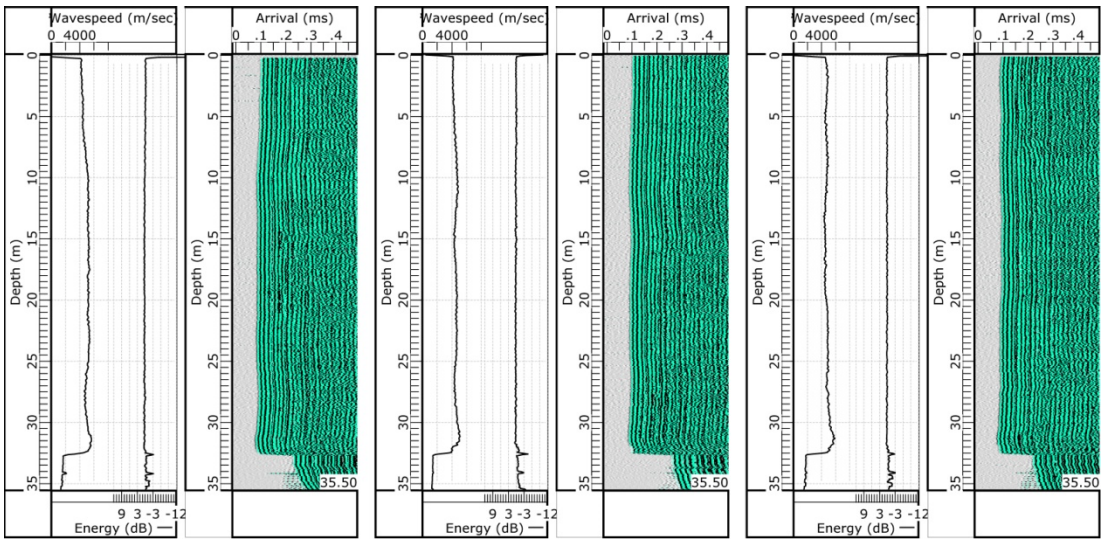


Fig. 7a CSL Result from a pile with possible soft toe

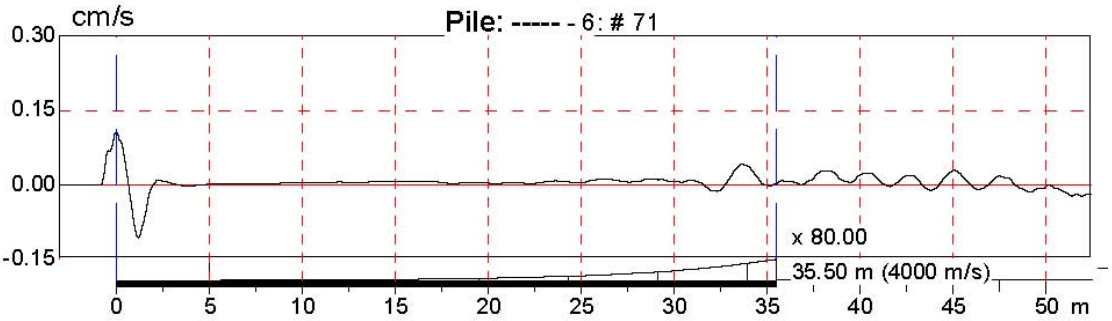


Fig. 7b PIT Result from a pile with possible soft toe

CONCLUSIONS

Low-Strain Integrity testing and Cross-Hole Sonic Logging are both effective tools in quality control and quality assurance of deep pile foundations. However, a clear result from either test requires experienced interpretation as well as an understanding of the test methods and their limitations.

As more preparation is required (casting sonic pipes into the pile) for CSL testing, it is sometimes expensive to perform testing on all working piles. CSL provides a more reliable method to detect a defect in the pile and allows for accurate determination of shaft quality and integrity below a major defect, but is limited to evaluation of the concrete within the sonic tubes.

Low strain integrity testing is relatively inexpensive and with only minimal pile preparation, can reasonably be performed on all working piles. The case history presented in this paper demonstrate cases in which both type of testing present similar results, be it a defect or uniformity of pile. Also minor imperfections recorded by CSL testing were revealed by the PIT curves. Hence, if reliable test data is collected from the site and interpretation is carried out by an experienced engineer, a very effective pile health condition equivalent to CSL result can be obtained with the low-strain integrity test.

When either of these testing methods is utilized, individually or in combination, the limitations should be understood when interpreting the results.

REFERENCES

ASTM Standard D 5882 (2007) “Standard Test Method for Low Strain Pile Integrity Testing of Deep Foundations” ASTM International, www.astm.org

ASTM Standard D 6760 (2002) “Standard Test Method for Integrity Testing of Concrete Deep Foundations by Ultrasonic Cross-Hole Testing” ASTM International, www.astm.org

Linkins, G.E., Rausche, F., Webster, K. and Klesney, A. 2007 “Defect Analysis for CSL Testing”. Geo-Denver 2007 New Peaks in Geotechnics: Denver, CO

Massoudi, N. and Teferra, W. 2004 “Non-Destructive Testing of Piles using the Low-Strain Integrity Method”. Proceedings of the Fifth International Conference on Case Histories in Geotechnical Engineering: New York, NY; 1-6.

EFFECTS OF ATMOSPHERIC CONDITIONS ON ENERGY PILE PERFORMANCE

Randall A. Pietersen, United States Air Force Academy, Colorado Springs, CO, USA, 719-333-4485, C20randall.pietersen@usafa.edu
Melissa S. Beauregard, PhD, United States Air Force Academy, Colorado Springs, CO, USA, 720-527-9029, melissa.beauregard@usafa.edu

ABSTRACT

This study focuses on quantifying the effects of water infiltration on a full-scale energy pile system's ability to meet the thermal demand of an HVAC system. Theoretically, an energy pile system should increase its thermal capacity after a rain event due to increased moisture content creating an increase in thermal conductivity of the surrounding soil matrix. The United States Air Force Academy has an energy pile research site consisting of 8 full-scale energy piles located below a shower facility. The local colluvium surrounding the piles allows for relatively high water infiltration during rain events. This study uses an 11kW Precision Geothermal Geocube to apply a thermal load on two single-loop piles. A weather station located south of the structure records atmospheric conditions. Results indicate that moderate rain events can caused up to a 23% increase in the system's thermal exchange capacity. This change is due to the increase in moisture content near the surface, which penetrates to deeper soil layers with time. The time required for moisture to penetrate to greater depths and then dissipate in the soil matrix, explains why increased system performance is seen for over a week following the passing of a singular rain event.

Keywords: energy piles, ground source heat exchange, thermally active geotechnical systems

1 INTRODUCTION

With a "future-forward" focus, there is an ever-pressing economic and environmental need to use sustainable sources to meet growing energy needs. HVAC is typically responsible for 34% of the overall energy required by commercial buildings and 48% of the energy required by residential buildings (USEIA, 2009; USEIA, 2012). Energy piles are a low cost, sustainable technology that have been used to offset this energy demand incurred by a building's space heating and air conditioning requirements.

An energy pile consists of heat exchanging elements in a closed loop system integrated into a building foundation and connected to a ground source heat pump (GSHP). It is most common for these heat-exchanging elements to be constructed within a drilled shaft foundation due to both construction practices and geometric considerations. This system operates based on the principle that at a certain depth below ground (typically 4 meters) subterranean temperature remains constant at a value equal to the mean annual air temperature at a given location (Kavanaugh et al., 1997). This allows the soil to function as a heat sink for cooling operations and a heat source for heating operations when exchanged within this zone of relatively constant temperature. For the past 25 years, the implementation of energy pile technology in public, residential, and even large-scale architectural complexes has slowly expanded which has created an increase in research into the topic as a result (Brandl, 2006; Hamada, 2007; Sekine et al., 2007; Gao, 2008; Bourne-Webb, 2009; Stewart and McCartney, 2013; Murphy et al., 2014). When pile construction takes place beneath the groundwater table, soil is under fully saturated conditions, maximizing thermal exchange for a GSHP system. Under unsaturated conditions, however, changing moisture contents change thermal conductivity values in a soil, which affect a GSHP system's ability to meet a thermal demand. The observational data presented in this paper apply to GSHP systems in unsaturated soil conditions.

© 2019 Deep Foundations Institute

There have been many studies on the thermo and thermo-mechanical response of energy foundations to heating, cooling, and multiple cycles of both (Brandl, 2006; Bourne-Webb, 2009; Stewart and McCartney, 2013; Murphy et al., 2014; Murphy et al., 2015; Murphy 2013). There have also been several studies linking atmospheric conditions to building HVAC performance for renewable technologies, although these studies largely focused on integrating ground source heat pump technology with other renewable technologies to increase system efficiency (Arteconi et al., 2013; Thygesen and Karlsson, 2016). This paper follows those previous studies, but shifts its focus to system performance coupled with meteorological considerations. The goal of this investigation is to quantify to what degree atmospheric changes may increase thermal exchange between energy piles and the surrounding unsaturated soil.

2015 saw the completion of a single-story Energy Pile Education and Research Facility (ePERF), intended to also function as a shower-shave washroom, at the United States Air Force Academy (USAFA). The facility is heavily instrumented to measure the performance of the building, the building foundation, and the surrounding soil under service HVAC loading conditions. Previous research was completed at this site (Murphy, 2013; Murphy et al., 2014a; Murphy et al., 2014b) focusing on thermo-mechanical response of each of the 8 energy piles under artificially induced thermal loads. A conclusion from this previous study was that thermally induced strains were well within reasonable structural limits. As these studies established the structural viability of exchanging building heat with the ground via the foundation, the next logical step was to observe how the piles perform under service loads. This paper presents the meteorological data and energy piles' inlet/outlet temperature data, to identify, quantify, and explain any observed correlation between the two data sets. Data collected during this timeframe includes flow rate through the foundations, inlet/outlet temperatures for each foundation, soil temperature, soil volumetric water content, wind direction, wind speed, rain gauge, and soil moisture sensors. Conclusions drawn from this investigation are most directly applicable to energy pile systems installed in silty sand intermediate geomaterials, however, soils sharing similar hydraulic conductivity and thermal conductivity characteristics could see trends similar to those reported in this study.

2 Background

2.1 Meteorological Consideration

As global weather patterns fluctuate and change, building resilient systems that can respond and optimize in relation to these changes will be increasingly necessary. At the USAFA ePERF site, ground temperatures near the surface fluctuate between 5 and 16 ^{o}C but begin convergence around 4m in depth (Murphy et al. 2015). This temperature converges to 9 ^{o}C around 10m in depth as displayed in **Fig. 1** (Murphy 2013).

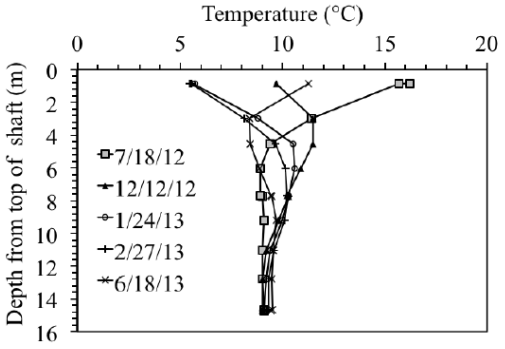


Fig. 1. Season temperature profile of Foundation 4 (Murphy 2013).

Though seasonal temperature changes at the ground surface can partially account for this variation, precipitation and subsequent water infiltration also affect ground temperature, and therefore the energy pile system. Performance of energy pile systems is heavily dependent on thermal conductivity of the surround soil. As a soil's moisture content increases, liquid water fills the voids previously occupied by gaseous air, increasing continuity within the soil mass, which results in increased thermal conduction (Jumikis 1977), as shown in **Fig 2**.

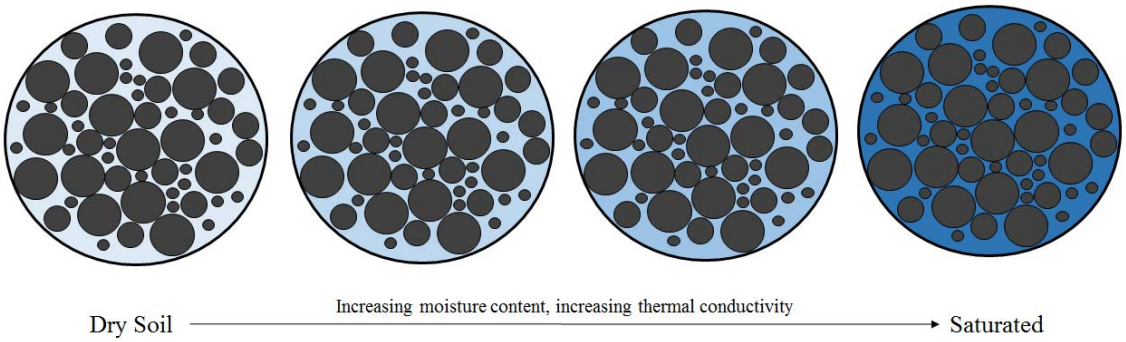


Fig. 2. Schematic depicting moisture-dependent thermal behavior in soils

It is common at USAFA, and in the surrounding area, for afternoon rainstorms to move through in the late summer months. These storms typically occur in the July and August timeframe when average afternoon temperatures approach 30 ^{o}C. This rain infiltrates the soil, causing both a sudden decrease in temperature and more prolonged increase in thermal conductivity. Understanding what kind of meteorological changes affect energy pile performance, and by how much, is a focus of this investigation.
For this investigation, rain event classification follows the guidelines summarized in **Table 1.**

Table 1. Rain event classification values

Rain Event Classification	Rate of Rainfall
Light Rainfall	$I \leq 2$mm/h
Moderate Rainfall	$2 < I \leq 15$ mm/h
Heavy Rainfall	$15 < I \leq 30$ mm/h
Very Heavy Rainfall	$30 < I \leq 60$ mm/h
Torrential Rainfall	$I > 60$ mm/h

2.2 Infiltration and Fluid Flow through Unsaturated Soil

The soil at ePERF is a well-graded sand with silt and gravel. According to the United States Department of Agriculture, the typical range of hydraulic conductivity for this type of soil is 0.914m/day to 9.14×10^{-4} m/day. This range of hydraulic conductivity suggests that, even for a heavy rain event, it could take days or even weeks for moisture infiltration to reach a significant enough depth to cause a measurable change in energy pile performance.

3 Project Description

3.1 ePERF Site Description

The Energy Pile Education and Research Facility (ePERF) is a one story 334m^2 restroom, shower, and laundry facility built to service the training needs of the United States Air Force. Constructed on eight, 15.2m deep by 0.61m diameter energy piles, the facility began construction in 2012 to evaluate the sustainable energy technologies, a mission in line with Department of Defense "net-zero" development initiative for energy. **Figure 3** presents a dimensioned schematic of the overall building footprint, including locations of each of the 8 energy piles.

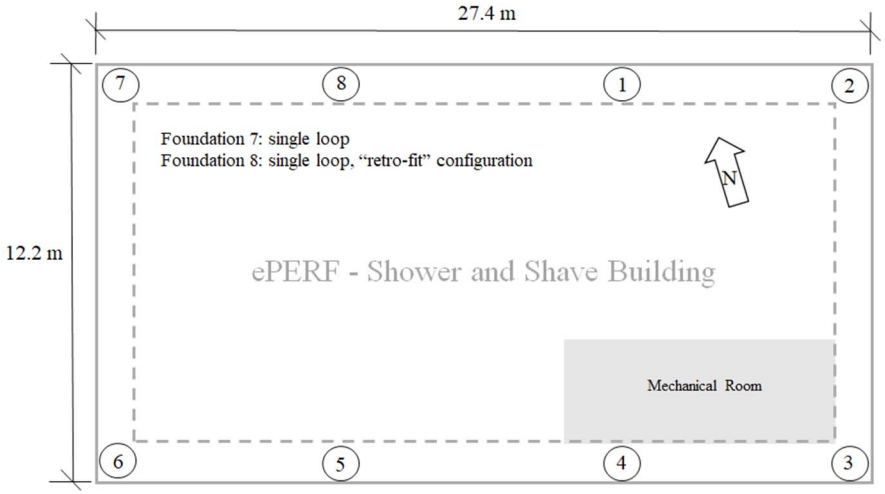


Fig. 3. ePERF Dimensions with Energy Pile Foundation Locations

In September 2011, Hernandez performed two 102mm-diameter borings to a depth of 14 meters. **Figure 4** summarizes the results from this study. At no point during site investigation, nor construction and installation, was groundwater found, leading researchers and engineers on site to estimate groundwater at depths of 16m or greater.

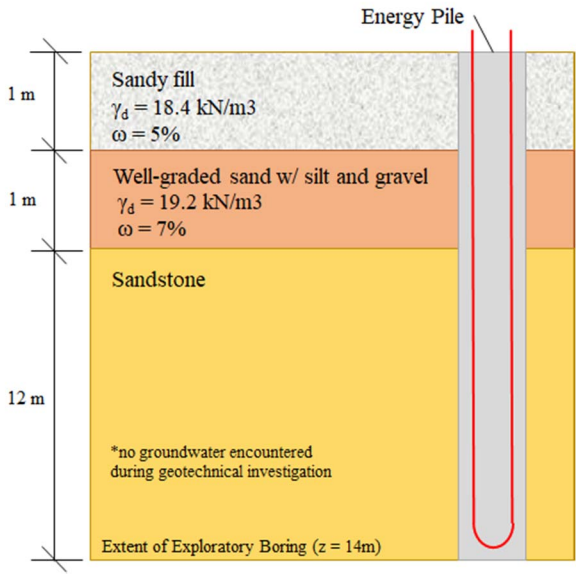


Fig. 4. Summary of stratigraphy encountered during subsurface exploration at ePERF

3.2 GSHP Shower-Shave Facility Instrumentation

The instrumentation used in this study is integrated into the GSHP at the FERL Energy Pile Research Facility. The array of sensors installed at ePERF measure energy pile performance metrics, the surrounding soil under service HVAC loading conditions, and the building foundation. This array includes a set of 10 IFM SM7x01 Magnetic-inductive flow meters that capture the volumetric flow and consumed quantity, and Geokon pipe-plug thermocouples to measure inlet/outlet temperatures of the fluids pumped through each of the energy piles. **Figure 5** shows the labeling of the flowmeters corresponding to foundations 7 and 8. This data will allow for the analysis of system efficiency and capacity.

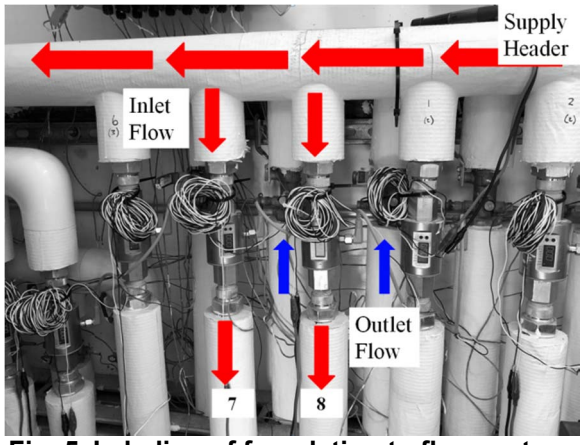


Fig. 5. Labeling of foundation to flow-meter piping layout

4 Methodology

The focus of this study lies in the comparison of meteorological precipitation and energy pile performance data. The meteorological data used for this analysis was obtained through a United States Air Force Academy Meteorology Department weather station located approximately a half mile south of ePERF. The energy pile performance data comes from pipe-plug thermocouples measuring inlet and outlet temperature of the heat exchange solution being pumped through each individual energy pile.

Proof of concept for this analysis comes in the form of the lab test data quantifying the change in thermal conductivity with respect to changes in soil moisture content. Soil gathered for these tests was from the energy pile site and compacted to the in-situ dry density, as determined during the initial site investigation. A potential range of moisture contents for compacting the soil to the field dry density was determined by developing a proctor curve. This moisture content range was from 5 to 11 percent. A KD2 Pro thermal conductivity probe was used on samples with various moisture contents within that predetermined range, all compacted to the same dry density, to generate a plot of thermal conductivity values with respect to moisture content.

To identify and quantify significant corollary trends between meteorological changes and inlet-outlet temperatures, a relatively steady supply of heat, at a constant flow rate, was provided to the heat exchange solution via an 11kW Precision Geothermal Geocube. During periods without precipitation, data was obtained to ensure steady heat exchange was occurring and a relatively constant inlet-outlet temperature differential was observed. Then, after periods of moderate rainfall, the inlet-outlet temperature data was continually monitored for approximately one week, to account for response delays predicted by the rate at which moisture infiltrates the soil.

Both foundations are evaluated independently for differences in inlet-outlet temperatures, using time periods lacking precipitation as the control values that can be compared to periods of precipitation and other major meteorological variations. The Geocube effectively maintained steady-state heat exchange and flow rate through the entire duration of both these periods. This ensures ambient ground temperature heating or cooling does not cause any fluctuations, which would be a result of heat buildup or dissipation in the soil after inconsistent usage patterns.

With all other variables held constant, should there be an inlet-outlet temperature differential change observed within approximately a week of a moderate rain event, we can conclude that meteorological phenomenon are having a significant impact on system performance.

RESULTS AND ANALYSIS

Laboratory tests were conducted to quantify thermal conductivity on samples of soil from the site at various moisture contents at in-situ dry density **(Fig. 6)**. Within the bounds of typical moisture content values for this site, the change in thermal conductivity with respect to moisture content was found to be exceptionally linear. Testing shows a 30% increase in thermal conductivity between the lower and upper bounds tested for moisture content. This evidence suggests a sufficiently penetrating rain event could have the potential to change a GSHP system's capacity for heat exchange.

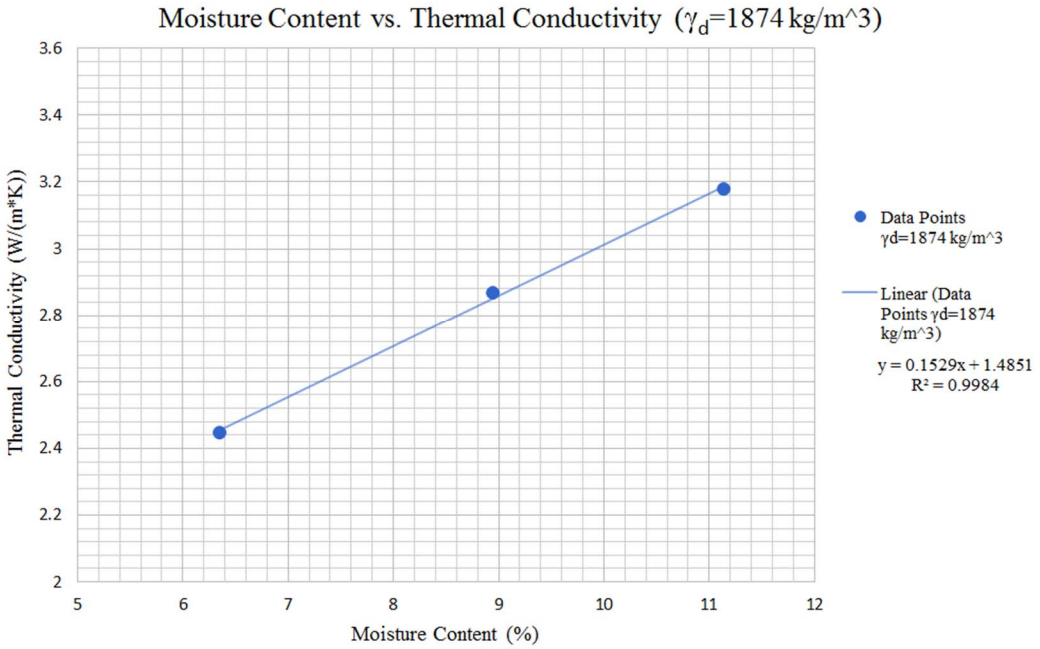


Fig. 6. Laboratory data quantifying the change in thermal conductivity with respect to changes in soil moisture content. Soil gathered for these tests was from the energy pile site and compacted to the in-situ dry density.

The inlet and outlet temperatures for foundation 7 and 8 over the two-week investigation are found in **Fig. 7** and **Fig. 8**, respectively. Inlet flow temperature is identical between both foundations, due to the shared supply header connection used by the system. The outlet flow temperatures for both foundations follow the same general trends as those exhibited by the inlet flow, but vary based on the thermal conductivity of the soil and the temperature gradient present for heat exchange. Cyclical diurnal fluctuations in both inlet and outlet temperatures appear throughout the two-week investigation. These same fluctuations exist in foundations without any heated fluid pumped through the system and are therefore assumed to be caused by fluctuations in mechanical room temperatures.

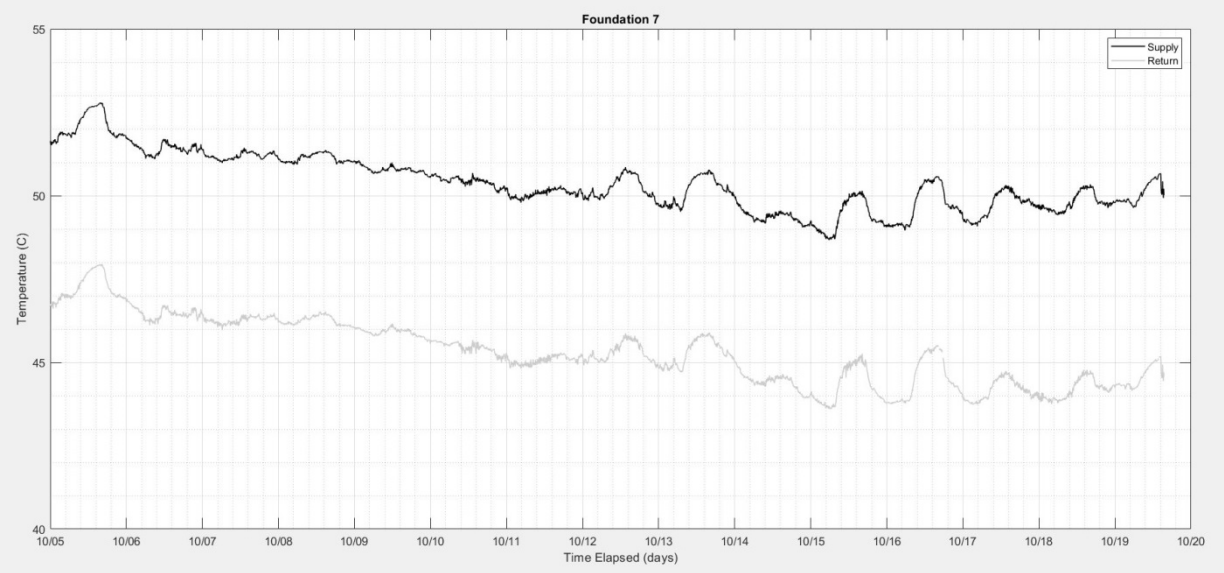


Fig. 7. Foundation 7 Inlet and Outlet Flow Temperature data over time

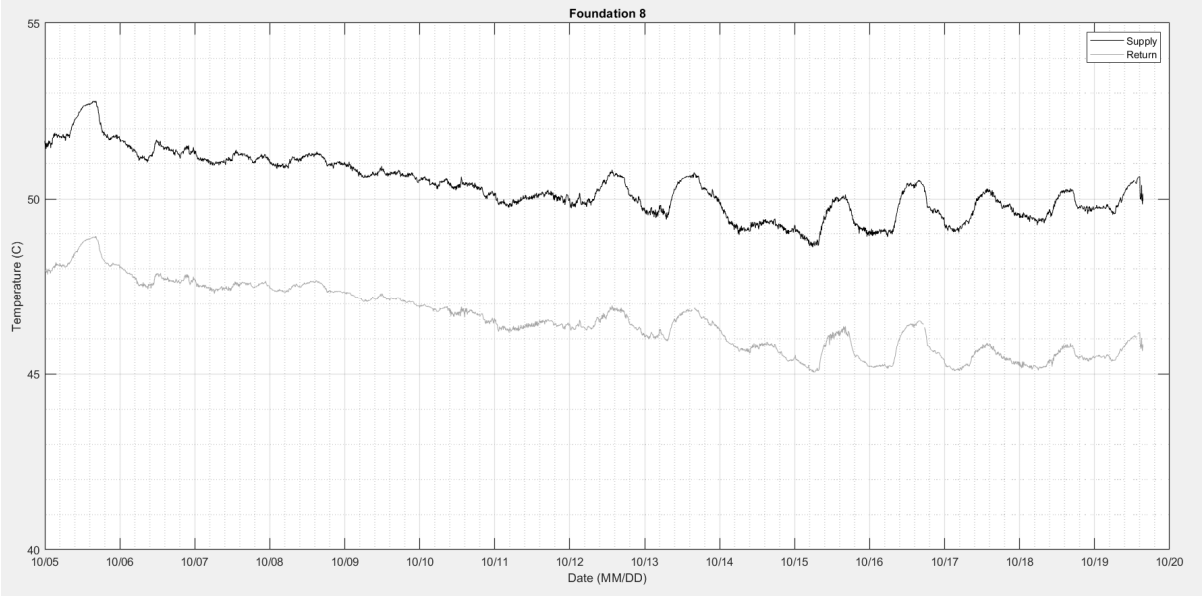


Fig. 8. Foundation 8 Inlet and Outlet Flow Temperature data over time

The change in outlet-inlet temperature is graphed against time in **Fig. 9**. From 05 Oct 2018 to 12 Oct 2018, heat exchange occurring in foundation 7 and 8 is around 4.8^{o}C and 3.7 ^{o}C, respectively. After the rain event, from 14 Oct 2018 to 20 Oct 2018, the difference between outlet and inlet temperature in foundations 7 and 8 reaches a maximum value of 5.87 ^{o}C and 4.54 ^{o}C, respectively. This results in a maximum difference between outlet and inlet temperatures of 1.07 ^{o}C and 0.84 ^{o}C for Foundations 7 and 8, respectively.

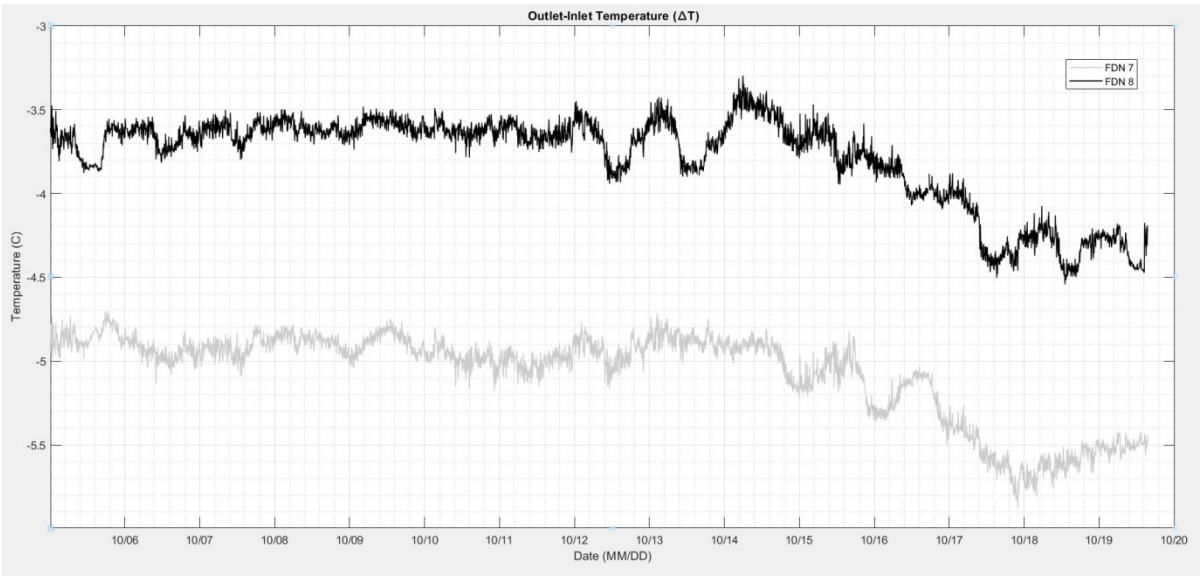


Fig. 9. Change in temperature (outlet-inlet temp) for foundations 7 and 8 with respect to time.

Figure 10 presents the precipitation data during the 2-week period of observation. Based on the previously stated approach for categorizing rain events, the rain events observed during this investigation are considered light to moderate. The maximum rate of 9.14mm/hr was observed on 08 Oct 2018. Moderate to light rain events continued intermittently from 08 Oct 2018 to 12 Oct 2018.

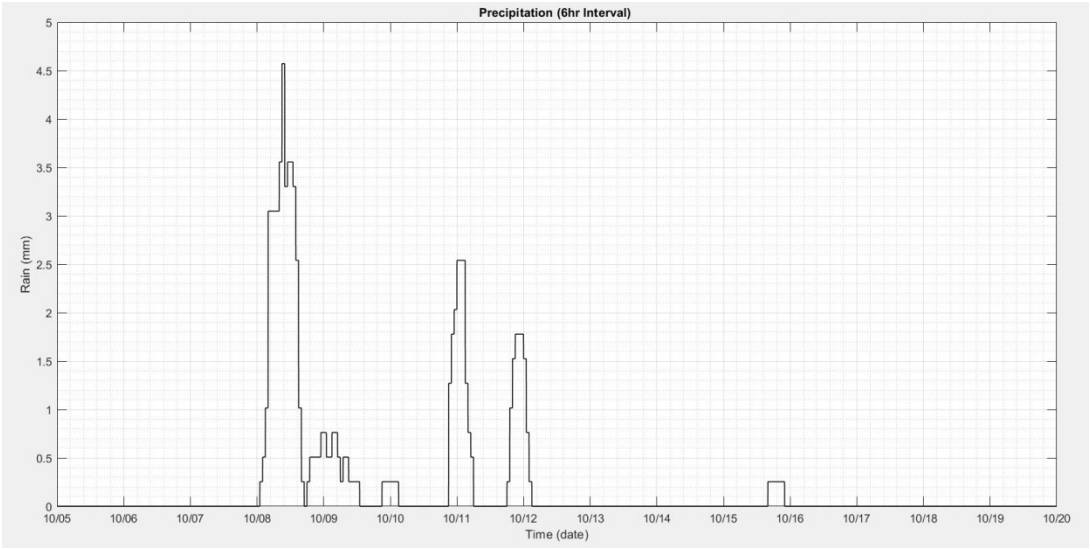


Fig. 10. Precipitation data taken on 6 hour intervals out at a weather station a half mile south of ePERF

Though theoretically possible, the full-scale system data provides confirmation of this initial assessment. Moderate to light rain events experienced over the period of four days (08-12 October 2018), would take several days to infiltrate soil to a sufficient depth, as to see changes in thermal exchange as seen. This is indeed what occurs as shown in **Fig. 11**. Prior to any significant meteorological variation, outlet-inlet temperature differential holds relatively constant in foundations 7 and 8 at 4.8C and 3.7C, respectively. On 15 Oct, there begins an identifiable increase in the magnitude of each foundation's heat exchange. Over the course of several days the maximum magnitudes for outlet-inlet temperature differential are reached, peaking at a 22% increase in foundation 7 and a 23% increases in foundation 8.

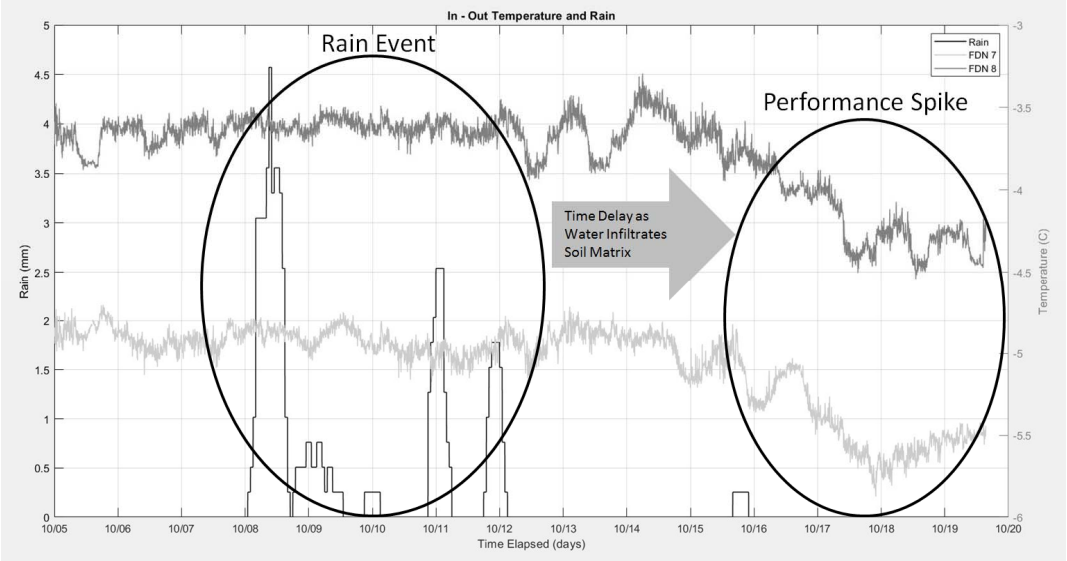


Fig. 11. Corresponding precipitation and inlet-outlet temperature data from ePERF

7 Discussion

Although this correlation may not extend to sites with relatively low permeable soils, there are numerous locations beyond ePERF where highly permeable soils and seasonally strong rain events coincide. In these areas, this study has shown that there could be potential to harness atmospheric fluctuations to work in favor of renewable geothermal energy sources. The light to moderate rain systems investigated in this examination provide a realistic condition for this system response. It will not take a 50-year storm to see an improvement of GSHP system performance.

Additionally, this data suggests that the effects of a single storm system have lasting impacts on the GSHP system performance long after the system has passed. Due to the slow nature of water infiltration, the increased performance benefits may be able to be capitalized on for days or even weeks after a storm has passed, depending on the soil characteristics. Future research done on this topic will focus on coupling unsaturated flow and heat exchange models to quantify and predict the increase in thermal exchange and the duration of this increased capacity, given the size of a certain rain event.

References

Arteconi, A., Hewitt, N.J. and Polonara, F., 2013. Domestic demand-side management (DSM): Role of heat pumps and thermal energy storage (TES) systems. Applied thermal engineering, 51(1-2), pp.155-165.

Bourne-Webb, P., 2013. An overview of observed thermal and thermo-mechanical response of piled energy foundations. In European Geothermal Congress. Pisa, Italy (pp. 1-8).

Brandl, H., 2006. Energy foundations and other thermo-active ground structures. Géotechnique, 56(2), pp.81-122.

Gao, J., Zhang, X., Liu, J., Li, K. and Yang, J., 2008. Numerical and experimental assessment of thermal performance of vertical energy piles: an application. *Applied Energy*, *85*(10), pp.901-910.

Hamada, Y., Saitoh, H., Nakamura, M., Kubota, H. and Ochifuji, K., 2007. Field performance of an energy pile system for space heating. Energy and Buildings, 39(5), pp.517-524.

Hernandez, R., 2011. Geotechnical investigation report. Construct shower/shave facility. United States Air Force Academy, Colorado. Terracon Consultants Inc, 34 p

Kavanaugh S, Rafferty K, Geshwiler M., 1997. Ground-source heat pumps—design of geothermal systems for commercial and industrial buildings. ASHRAE. 167 p

Kjellsson, E., Hellström, G. and Perers, B., 2010. Optimization of systems with the combination of ground-source heat pump and solar collectors in dwellings. *Energy*, *35*(6), pp.2667-2673.

Leong, W.H., Tarnawski, V.R. and Aittomäki, A., 1998. Effect of soil type and moisture content on ground heat pump performance: Effet du type et de l'humidité du sol sur la performance des pompes à chaleur à capteurs enterrés. *International Journal of Refrigeration*, *21*(8), pp.595-606.

Murphy, K.D., McCartney, J.S. and Henry, K.S., 2014. Thermo-mechanical characterization of a full-scale energy foundation. In *From Soil Behavior Fundamentals to Innovations in Geotechnical Engineering: Honoring Roy E. Olson* (pp. 617-628).

Murphy, K.D., McCartney, J.S. and Henry, K.H., 2014. Thermo-mechanical response tests on energy foundations with different heat exchanger configurations. *Acta Geotechnica*, *1*, p.17.

Sarbu, I. and Sebarchievici, C., 2014. General review of ground-source heat pump systems for heating and cooling of buildings. *Energy and buildings*, *70*, pp.441-454.

Sekine, K., Ooka, R., Yokoi, M., Shiba, Y. and Hwang, S., 2007. Development of a Ground-Source Heat Pump System with Ground Heat Exchanger Utilizing the Cast-in-Place Concrete Pile Foundations of Buildings. Ashrae Transactions, 113(1).

Stewart, M.A. and McCartney, J.S., 2013. Centrifuge modeling of energy foundations under cyclic heating and cooling. ASCE J Geotechn Geoenviron Eng.

Thygesen, R. and Karlsson, B., 2016. Simulation of a proposed novel weather forecast control for ground source heat pumps as a mean to evaluate the feasibility of forecast controls' influence on the photovoltaic electricity self-consumption. *Applied energy*, *164*, pp.579-589.

United States Department of Agriculture, https://directives.sc.egov.usda.gov/, Accessed on 22 March 2019.

United States Energy Information Administration, 2011. Annual energy review. Report No. DOE/EIA-0035(2019/2)

United States Energy Information Administration, 2009. https://www.eia.gov/energyexplained/. Accessed on 22 March 2019.https://rmets.onlinelibrary.wiley.com/doi/pdf/10.1002/joc.692

ELIMINATION OF ENVIRONMENTAL FOOTPRINT: LVCC EXPANSION - FOUNDATION INSTALLATION

Zachary Q. Maassen, BOS Solutions, 10343 Sam Houston Park Drive, Houston, TX, USA
Zachary.Maassen@bos-solutions.com #281-477-5313

ABSTRACT

Upon approval from the Las Vegas Convention and Visitors Authority (LVCVA), Turner/Martin Harris, A Joint Venture began construction on the estimated $860 million expansion for the Las Vegas Convention Center District Plan. Totaling around 600 shafts (60 feet depth and 3-foot diameter), the foundation installation completed via uncased drilled shaft operation, spanned from October to December of 2018. During this installation, flowback water from the water table was encountered that contained various solids ranging from cobbles to clays to silts, as well as trace amounts of contaminants of concern (COCs) left behind as a result of previous business that used to occupy the same real estate as the current expansion; more specifically, Perchloroethylene (PCE), an organic chemical widely used as a solvent and degreaser. With over 2.5 million gallons of waste slurry to be treated, technologies were deployed to reclassify the waste from liquid to solid waste as well as recover and treat the water for reuse in land spraying applications. Utilizing these technologies, it is estimated that 1.2 million gallons of water was able to be reclaimed along with over 6,400 tons of solids; resulting in hundreds of thousands of dollars in cost and environmental savings.

Keywords: Slurry, Waste, Dewatering, Reclamation

PROJECT OVERVIEW

Amidst its famous attractions from gambling to world class entertainment, Las Vegas has long been highlighted as the "No. 1 trade show destination in North America for 24 consecutive years" (LVCVA, 2018). Each year, Las Vegas hosts approximately 22,000 meetings, conventions and trade shows, which support an estimated 65,000 jobs paying $2.7 billion in wages and salaries. In 2017, the Las Vegas Convention Center hosted 21 percent of convention attendees traveling to southern Nevada, which supported approximately 13,800 jobs, paying more than $576 million in wages and salaries. Including indirect and induced impacts, the Las Vegas Convention Center's attendees generated $2.1 billion in economic impact for the local economy (LVCVA, 2018) . This substantial economic impact of course due in part to the attractions Las Vegas offers to its trade show attendees, along with Las Vegas' easy accessibility to major metropolises along the West Coast and reasonable travel prices offered if coming in from the East, allows for a very attractive venue. And while being a famous destination is great for business, the city wants to further distinguish itself by offering the best venue as well. For this reason, the Las Vegas Convention and Visitors Authority (LVCVA) approved a three-phase expansion plan for the Las Vegas Convention Center District totaling well over a billion dollars, slated for completion by 2023.

Foundation Operations

Phase Two operations are currently underway and have been since September of 2018, after LVCVA awarded the work to Turner Martin-Harris JV. During the initial operations of Phase Two, the installation of 600 foundation shafts were required. These shafts were designed to total a depth of 60 feet with a 36-

© 2019 Deep Foundations Institute

inch diameter and were to be installed as uncased shafts. This method was utilized due to the soil conditions being stable enough to support the hole without the risk of caving the borehole.

During the excavation of the shafts, groundwater was encountered during the last 20 feet of the boreholes which led to the generation of over 2.5 million gallons of waste slurry. This waste slurry presented a unique disposal issue as initial geology and sampling, completed prior to shaft excavations, noted the presence of trace amounts of metals as well as a PCEs (Tetrachloroethene/Perchloroethylene), an organic chemical widely used as a solvent and degreaser; commonly used in the dry-cleaning industry. It was assumed that the presence of this chemical was due to the previous business occupations over the previous decades. Due to this chemical presence, it was required that the slurry be treated prior to disposal.

Slurry Treatment Issues

Initially, large mobile storage tanks, capable of holding over 21,000 gallons of slurry were deployed to store the waste slurry as it was generated from the shaft installations. Paired with these storage tanks, was a series of sock filters and carbon filters whose operation was meant to remove the solids and chemical contaminants residing within the waste slurry. While using this means of treatment, operators onsite continued to note the slow processing rates of the filters and were constantly requiring the deployment of several more storage tanks to keep up with the waste slurry displacement from the shaft excavations. After completing approximately half of the uncased shafts, operators decided to employ a different means of treating the waste slurry, as the current treatment process was dampening the shaft installation operation, resulting in project delays and exceeding budgets allocated to the treatment.

BOS Solutions Employment

After a preliminary site assessment of the current slurry treatment system by a BOS Technical Advisor, it was determined that the solids content in the stored slurry was too great to be pumped through the series of filters. This overload of solids in the filters instantly caused the filters to plug off and cease further treatment. To alleviate this problem, a process needed to be implemented that would separate out all the suspended and dissolved solids out of the waste liquid phase, before passing through the series of filters.

To meet this need of a mobile, continuously operated liquid/solid separation solution, the drilling operator opted to deploy a known technology in the deep foundation industry used to clean and dewater drilling fluids and waste slurries; the BOS Closed Loop System. Utilizing a Combination Flocculation and Centrifuge (CFC) Tank, BOS tied into the existing manifold connecting the series of storage tanks on location containing the waste slurry. Through this manifold connection, the BOS System could then utilize their pumps to pull slurry from any of the storage tanks to feed the centrifuge. Upon entering the centrifuge, the waste slurry was met with a simultaneous feed of flocculant that combined with the waste slurry to generate large, easy settleable colloidals that were both suspended and dissolved in solution.

Additional Equipment Deployed:

- BOS IV CFC Tank
- BOS 20 Centrifuge
- (3) 3” Centrifugal Pumps

Modified Waste Slurry Treatment Process:

1. Waste slurry is generated from uncased shaft excavation.
2. Waste slurry is pumped from the shaft and displaced into the large storage tanks.
3. Waste slurry is pumped through the storage tank manifold to the BOS CFC Tank.

4. Flocculant is made within the BOS CFC Tank Chemical mixing tanks and simultaneously injected into the BOS 20 Centrifuge with the waste slurry. Over 2000 G's of force is applied to the waste slurry, resulting in a clean, clear reclaimed water and dry, stackable, paint filter pass solids; the process known as dewatering.
5. Reclaimed water is pumped back to the large storage tanks where it awaits to be processed through the Sock and Carbon Filters.
6. Dried solids are piled and hauled off to solids stockpile on location.
7. Sock and Carbon Filters perform final treatment on reclaimed water to further reduce any contaminants remaining in the water.
8. Filtered water is tested, passes all discharge criteria and is land sprayed on location as dust control.

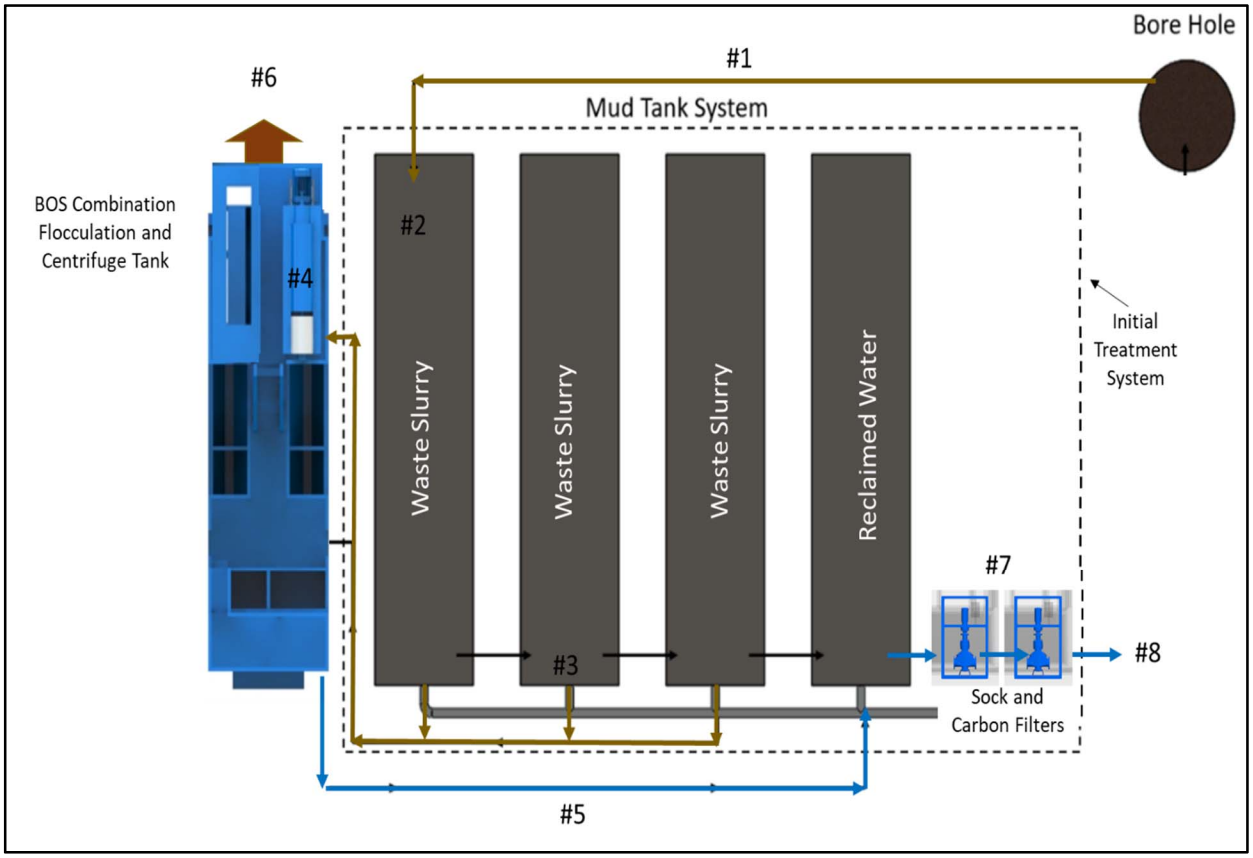


Figure 2. Site Layout and Flow Diagram



Figure 2. Photo of Waste Slurry (Left), Reclaimed Water (Middle) and Dried Solids (Right) produced via the BOS Solutions System

Slurry Properties

During treatment operations, field testing and extensive laboratory testing of the waste slurry and reclaimed water was conducted to monitor the effectiveness of the new waste treatment process. The results of that testing are outlined below.

Table 1. Field Testing Data (Average Values)

Field Testing Parameters		Waste Slurry Average Value	Reclaimed Water Average Value
pH		9.2	8.7
Hardness	(mg/l)	800+	800+
Density	(lb/gal)	8.9	8.3
Funnel Viscosity	(sec/qt)	31	26
Sand Content	(%)	6.4	0.0
Solids Content by Volume	(%)	9.45	0.23
			Dried Solids to Disposal
Solids Content by Volume	(%)		58.4

Table 2. Water Quality Analysis Completed by Tomson Technologies – Composite

Water Quality Analysis		Waste Slurry	Reclaimed Water
Temperature	°F	72	72
pH		9.79	8.74
Hydroxide Alkalinity	mg/L	44.2	0
Bicarbonate Alkalinity	mg/L	0	32.94
Carbonate Alkalinity	mg/L	36.6	0
TDS	mg/L	2368.00	2144
TSS	mg/L	100100.00	66
COD	mg/L	30.00	75
Conductivity	us/cm	194.60	3350
Turbidity	NTU	>1100	0
Hardness as CaCO3	mg/L	1636.20	1523.5
Ba	mg/L	< 1	< 1
Sr	mg/L	6.82	6.12
Ca	mg/L	655.27	610.14
Mg	mg/L	< 1	22.8
K	mg/L	40.50	33.11
Na	mg/L	229.88	244.34
Fe	mg/L	3.30	3.29
B	mg/L	1.36	1.47
Cl	mg/L	213.27	266.78
Br	mg/L	2.05	< 1
SO4 2	mg/L	1511.94	1592.78
ΣCations	meq/L	44.00	44.05
ΣAnions	meq/L	41.08	41.24
Cation/Anion Charge Balance	%	3.44%	3.3

Table 3. Water Quality Analysis Completed by Tomson Technologies – Metals & PCE

Water Quality Analysis		Waste Slurry	Reclaimed Water
As	mg/L	1.96	<0.00200
Cd	mg/L	<0.463	<0.00200
Cr	mg/L	6.75	0.0217
Cu	mg/L	2.53	<0.00200
Pb	mg/L	2.96	<0.00200
Hg	mg/L	4.92	<0.00200
Ni	mg/L	3.09	<0.00200
Ag	mg/L	<0.463	<0.00200
Zn	mg/L	9.70	0.00734
Tetrachloroethylene	ug/kg	<2.1	ND

As seen in the above results, the water produced from the newly implemented treatment process removed all heavy metals and the PCE contamination without even requiring the use of the Sock and Carbon Filters. However, to ensure the quality of the reclaimed water and as an added fail safe, all reclaimed water was still processed through both filters.

SUMMARY

The original treatment solution of utilizing large storage tanks paired with Sock and Carbon Filters proved to be ineffective due to the solids content of the produced waste slurry. Upon deployment of the BOS Closed Loop System, a continuous process of dewatering was able to remove all the suspended and dissolved solids within the waste slurry, producing a dry waste cake and clean, clear reclaimed water. With the deployment of these technologies it is estimated that over 1.2 million gallons of water was reclaimed and avoided disposal offsite. This reduction of waste volume (~48%) accounted for over $500,000 dollars in disposal cost savings as well as significant environmental savings due to the reduction landfill volume required and greenhouse gas eliminated from the additional hauling of waste.

REFERENCES

LVCVA. (2018, September 11). *LVCCD Articles - Construction Set to Begin on Highly Anticipated Las Vegas Convention Center Expansion*. Retrieved from Las Vegas Convention and Visitors Authority: https://www.lvcva.com/convention-center-district/news-updates/post/construction-set-to-begin-on-highly-anticipated-las-vegas-convention-center-expansion/

EXPERIMENTAL P-Y CURVES FROM CENTRIFUGE TESTS ON PILE FOUNDATIONS SUBJECTED TO LIQUEFACTION AND LATERAL SPREADING

Milad Souri, Graduate Student Researcher, Department of Civil and Environmental Engineering, Portland State University, Portland, OR; msouri@pdx.edu
Arash Khosravifar, Assistant Professor, Department of Civil and Environmental Engineering, Portland State University, Portland, OR; karash@pdx.edu
Scott Schlechter, Principal, GRI, Beaverton, OR; SSchlechter@gri.com
Nason McCullough, Principal Geotechnical Engineer, Jacobs, Corvallis, OR; Nason.McCullough@jacobs.com
Stephen, E. Dickenson, Principal Engineer, New Albion Geotechnical, Inc., Reno, NV; sed@newalbiongeotechnical.com

ABSTRACT

The results of five centrifuge models were used to evaluate the response of pile-supported wharves subjected to inertial and liquefaction-induced lateral spreading loads. The centrifuge models contained pile groups that were embedded in rockfill dikes over layers of loose to dense sand and were shaken by a series of ground motions. The p-y curves were back-calculated for both dynamic and static loading from centrifuge data and were compared against commonly used API p-y relationships. It was found that a significant reduction in ultimate soil resistance occurred in dynamic p-y curves in partially/fully liquefied soils as compared to static p-y curves. It was also found that incorporating *p*-multipliers that are proportional to the pore water pressure ratio in granular materials is adequate for estimating pile demands in pseudo static analysis.

Keywords: Pile foundations, Liquefaction, Lateral spreading, Centrifuge models, p-y curves.

1. INTRODUCTION

Liquefaction-induced ground deformations can cause severe damage to pile-supported wharves and other waterfront structures. A common approach in analyzing the lateral behavior of piles against seismic loads is using the beam on nonlinear Winkler foundation (BNWF) or p-y spring analysis. One common p-y relationship for sand is the one proposed by the American Petroleum Institute, also known as the API sand model (API 1993). While the API sand model was originally developed for the static loading conditions, it is common to modify the API sand curves for the effects of cyclic loading. However, there is no consensus on how to modify the static p-y curves for the effects of liquefaction and pore water pressure generation in loose granular soils. In previous studies, p-y springs of piles in liquefying soils were back-calculated from case histories, centrifuge model studies (e.g., Wilson et al. 2000; Brandenberg et al. 2005; Abdoun et al. 2003), full-scale tests (e.g., Rollins et al. 2005; Chang and Hutchinson 2013), and numerical analyses (e.g., McGann et al. 2011). In general, these studies found the softening effects of soil liquefaction on p-y curves, as well as a hardening behavior attributed to the dilative response of the liquefied soil around the pile. However, these studies provide varying recommendations on how to modify the static p-y curves to capture this complex behavior. Some design guidelines propose softening the static p-y curves using *p*-multipliers (e.g., Caltrans 2012). Other studies propose an upward concave shape for p-y curves in liquefied soils (e.g., Franke and Rollins 2013; Chang and Hutchinson 2013).

The focus of this study is to evaluate the effectiveness of the *p*-multiplier approach in modifying p-y springs in partially/fully liquefied soils to predict the lateral response of piles. This was done by using the results of five centrifuge tests simulating pile-supported wharves in sloping ground (McCullough et al., 2001). The p-y curves were back-calculated in loose sands, dense sands and sloping rockfill dikes. The p-y curves were back-calculated for both static piles subjected to push/pull forces at pile head, as well as dynamic piles subjected to earthquake shaking. The static p-y curves were approximated using API relationships for sands

© 2019 Deep Foundations Institute

and the input parameters for API curves were back-calculated. The dynamic p-y curves were compared against the static p-y curves to provide insights on the applicability of the *p*-multiplier approach in developing p-y curves for liquefied zones. To evaluate the effectiveness of using *p*-multipliers on API sand curves, the piles in centrifuge tests were modeled using pseudo-static analysis in *LPILE* (Ensoft 2014) and the predicted maximum bending moments in each pile were compared against the measured values in centrifuge tests. It will be shown that the maximum bending demands in piles were reasonably captured using p-multipliers that are proportional to the pore water pressure ratio in partially/fully liquefied zones.

2. DESCRIPTION OF CENTRIFUGE TESTS

2.1. Centrifuge models and cross sections

Data from a series of five centrifuge tests were analyzed to back-calculate pile lateral behavior (i.e. p-y springs) for static and dynamic loading conditions. These tests were performed on pile-supported wharves by Dickenson, McCullough, Schlechter, and coworkers at the UC Davis Center for Geotechnical Modeling (McCullough et al. 2001). These centrifuge models represent the typical layout of major port facilities in California, and the findings can be used to represent other similar pile-supported wharves embedded in rock dikes over native, potentially liquefiable soils. The cross sections of all models and key soil properties are shown in Figure 1.

2.2. Dynamic piles

The wharf deck was supported by three rows of seven piles (for a total of 21 piles). The pile diameters ranged from 0.38 m to 0.68 m. Each centrifuge model was subjected to a sequence of scaled input motions with the peak base acceleration ranging from 0.15 g to 0.82 g. The piles were subjected to the combined effects of inertial and liquefaction-induced kinematic demands during earthquake shaking (these piles are referred to as *dynamic piles*). The dimensions discussed in this paper are all in prototype scale unless noted otherwise.

2.3. Static piles

Two of the five tests (SMS02 and JCB01) included two single piles that were statically pushed by two to seven cycles of loads using actuators attached to their pile heads (these piles are referred to as *static piles*). The static loads, which were applied prior to earthquake shaking, provided key data for comparing the p-y springs under static and dynamic loading conditions. In these two tests, the static pile at the back was placed in dense sand with no slope; the static pile at the front was placed in sloping rockfill in SMS02 and in a sloping rock face overlying loose sand in JCB01. The layout for the static piles is shown in Figure 1. The properties of the static piles were the same as those for the dynamic piles.

2.4. Sensors and instruments

Measurements for all centrifuge tests conducted in this study were obtained using the following sensors and instrumentation. Linear volt displacement transducers (LVDT) mounted on the wharf deck, ground surface and the shear box container were used to measure the horizontal and vertical displacements. Pore pressure transducers (PPT) were embedded within the soil model at various depths. Accelerometers were embedded within the soil model and attached to the wharf deck and the shear box. Strain gauges were attached to static and dynamic piles to measure the bending moments.

3. PROCEDURES TO BACK-CALCULATE P-Y CURVES

3.1. *Lateral soil reactions*

Bending moments were measured at discrete locations along the pile where strain gauges were attached. The bending moments were interpolated along the pile length using the cubic spline fitting method before being numerically double-differentiated to back-calculate the lateral soil reactions, *p* (Haiderali and Madabhushi 2016; Brandenberg et al. 2010). For the piles where the bending moment at the pile head was

not measured, the bending moments were extrapolated assuming a constant shear force above the ground surface. The bending moments and shear forces at the pile tips were assumed to be zero.

3.2. Horizontal pile displacements

The horizontal pile displacements were estimated by double-integrating the bending moments along the pile and dividing them by the pile flexural stiffness (*EI*). The rotations at the pile head were assumed to be zero as the piles were rigidly connected to a relatively rigid wharf deck.

3.3. Horizontal soil displacements

Total horizontal soil displacements were calculated by combining the transient (high-frequency) and permanent (low-frequency) components of displacement following methods described by Wilson et al. (2000). The transient soil displacements were calculated by double-integrating the recorded accelerations. A high-pass Butterworth filter was applied to remove the low-frequency motions from the recorded accelerations. The permanent soil displacements were calculated based on the displacements recorded using LVDTs at the ground surface after applying a low-pass Butterworth filter. The pattern of distributing the permanent component of the soil displacement with depth was a major source of uncertainty in our analyses. The estimated pile bending moments in our consecutive pseudo-static analyses were also found to be very sensitive to the assumptions made regarding the pattern of permanent soil displacements with depth, which warranted investigating this issue methodically. After considering various patterns of permanent soil displacement with depth and investigating their effects on the estimated bending moments, we used the normalized shape of the maximum transient displacements with depth as a guide to determine where the subsurface shear failure zones formed as well as to distribute the permanent component of the soil displacement from the ground surface down to the shear failure plane. No permanent soil displacement was considered below the shear failure plane.

3.4. Back-calculated p-y curves

Lateral pile behavior is commonly characterized using p-y curves extracted at various depths along the pile. The p in these relationships corresponds to the lateral soil reaction, and the y corresponds to the relative displacement between the soil and pile (i.e. y = horizontal pile displacement – horizontal soil displacement). As described earlier, there is some uncertainty in estimating the horizontal soil displacements and pile displacements for dynamic piles. Therefore, the dynamic p-y curves were used primarily for estimating ultimate lateral soil reaction, and the relative soil–pile displacement (i.e. y) was only used qualitatively.

4. RESULTS

4.1. Experimental p-y curves from static piles

Experimental p-y curves were extracted from the results for statically loaded piles in SMS02 (penetrating dense sand and rockfill) and JCB01 (penetrating dense sand, loose sand and a thin rockfill) prior to shaking. Given that these soil and rockfill units are made from granular materials, the back-calculated p-y curves were approximated using API sand relationships. The API sand model recommends a hyperbolic tangent function to characterize the ultimate soil reaction (p_{ult}) and the initial stiffness (k_T).

In the API sand model, the ultimate lateral reaction (p_{ult}) increases with depth, pile diameter and internal friction angle. Internal friction angles of 33°, 37° and 45° were used to develop API curves for loose sand (D_R = 30%), dense sand (D_R = 70% to 80%) and rockfill, respectively. Comparing the ultimate resistances of the API curves with those of the back-calculated p-y curves at shallow depths, where the ultimate soil reaction was mobilized, confirmed that the API relationships estimated the ultimate resistance of the p-y curves reasonably well. As an example, a comparison between the experimental p-y curve and the API relationship for loose sand is shown in Figure 2a for the front pile in JCB01 at a depth of 3.05 m (~5D). This static pile was subjected to seven cycles of static loading. Different loading cycles are plotted with different colors on this figure to help understand the evolvement of p and y in the experimental p-y curve.

As can be noticed from this figure, the API sand curve using a friction angle of 33° captures the ultimate resistance of the experimental p-y curve reasonably well. Additionally, the sand p-y curve proposed by Reese et al. (1974) was plotted in Figure 2a which aligned reasonably well with the experimental p-y curve. Figure 2b shows the 6th cycle of the same experimental p-y curve compared against the same API curve manually shifted to the left for plotting purposes. This figure clearly shows that the reduced modulus of subgrade reaction better captures the stiffness of the experimental p-y curves at larger displacements. Similar conclusions could be made for dense sand and rockfill units.

The initial stiffness in the API sand curve (k_T) is the product of the depth below the ground surface and the modulus of the subgrade reaction (k). The initial stiffness was back-calculated from the experimental p-y curves at various depths and within different soil units. These initial stiffness values were divided by the corresponding depth to obtain the modulus of subgrade reaction (k) for loose sand, dense sand and rockfill. It was found that the moduli of subgrade reaction calculated from experimental p-y curves were significantly smaller than the values recommended by API. For example, the modulus of subgrade reaction for loose sand was calculated as 3500 kN/m^3, while API suggests a value of 16000 kN/m^3. This might be attributed to the limitations of centrifuge tests in simulating the in situ soil stiffness (i.e. freshly deposited sands in the centrifuge vs. aged sands in the field) and the pile driving conditions. This highlights the need to incorporate lower- and upper-bound multipliers in developing soil springs in design as recommended by standard ASCE COPRI 61-41.

Table 1 lists the input parameters to use for API sand curves based on the experimental p-y curves obtained from static piles. No significant difference was observed in the back-calculated subgrade reaction moduli between loose and dense sands; therefore, the same modulus is recommended for simplicity.

Table 1. Back-calculated input parameters for API sand p-y curves

Soil unit	Friction angle	Initial modulus of subgrade reaction, k (kN/m^3)
Loose sand (D_R = 30% to 40%)	33°	3500
Dense sand (D_R = 70% to 85%)	37°	3500
Rockfill	45°	5200

4.2. Experimental p-y curves from dynamic piles

Experimental p-y curves were also derived from centrifuge tests for piles supporting the wharf deck. These piles were subjected to wharf inertia during shaking, combined with varying magnitudes of ground deformation induced by partial/full liquefaction. These dynamic p-y curves were then compared to the static p-y curves to investigate the effects of excess pore water pressure in liquefiable soils on the lateral response of piles and p-y curves.

Figure 3a presents a comparison of static versus dynamic p-y curves for loose sand (D_R = 40%). The static p-y curve shown in this figure was derived from the front static pile in JCB01 (same as Figure 2.) The dynamic p-y curve was derived for Pile #3 in JCB01 during the first earthquake motion. Both static and dynamic p-y curves are extracted at the same depth (3.05 m below the ground surface) and normalized by the same pile diameter (0.64 m). For clarity, the dynamic p-y curve is plotted only for the time window shown in the time histories in Figures 3b and 3c. These time histories illustrate the lateral soil resistance (p), relative lateral displacement between soil and pile (y), and pore water pressure ratio (R_u) in the loose sand. It can be observed that as the excess pore water pressure ratio increases in the loose sand in sloping ground, lateral spreading occurs that exerts lateral loads on the pile. It is also observed that the lateral soil reaction (p) in liquefied soil exhibits sudden spikes in the downslope direction. Careful examination of the spikes in p reveals that they follow transient drops in R_u implying that they might be attributed to the dilative

response of sand combined with an increase in the relative displacement between the soil and pile driven by the inertial demand from the wharf deck. However, the magnitude of spikes in p are not very large (i.e. less than 20% of P_{ult} of the static p-y curve) suggesting that a simple p-multiplier approach could be an effective choice to modify the static p-y curve to envelope the complex behavior of dynamic p-y curve in liquefied soil.

Overlapped on Figure 3a are two API sand curves that approximate the p-y responses under static and dynamic conditions. The API sand curve for the static condition is developed using the input parameters in Table 1. The experimental dynamic p-y behavior is complex and is affected by contraction and dilation of loose sand and the inertial demand from the superstructure during the earthquake loading. To fit within the envelope of the dynamic experimental p-y curve, the API sand curve was softened using p-multipliers (P_m) to account for the first-order effects of liquefaction. Other researchers have shown that P_m depends on the pore water pressure ratio (R_u) generated during shaking (e.g., Wilson et al. 2000; Brandenberg 2005). For simplicity, the p-multipliers in this study were calculated using $P_m = 1 - R_u$. It is observed from Figure 3c that an R_u of approximately 0.8 was developed in the loose sand. Therefore, a P_m of 0.2 was used to soften the API curve, as shown in Figure 3a.

5. VALIDATION AGAINST PILE DEMANDS

The effectiveness of the back-calculated input parameters for API sand curves and the R_u-proportional p-multipliers in liquefiable soils is investigated by comparing the pile bending moment profiles measured in the centrifuge tests to those estimated using p-y models in *LPILE* (Ensoft 2014). The *LPILE* models considered combined kinematic and inertial effects, in which the soil displacements were imposed to the end nodes of p-y springs and wharf inertia was imposed by a shear force at the pile head. The kinematic demands (i.e. soil displacements) and inertial demands (i.e. pile head shear) were directly calculated from the centrifuge tests at the exact time when the bending moments are at their peak values. The p-y curves were developed for each soil unit based on the API relationships with the input parameters reported in Table 1. The p-y curves were then softened using p-multipliers proportional to the pore water pressure ratio (R_u) using the equation $P_m = 1 - R_u$. The R_u values were extracted from the pore pressure transducers (PPT) in the corresponding unit.

Figure 4a shows a snapshot of soil displacement profiles along two instrumented piles in JCB01 along with the pile displacement estimated from *LPILE*. Figure 4b shows a comparison of the bending moments obtained from centrifuge tests to those estimated from the *LPILE* analyses. The reasonable agreement between the measured and predicted pile bending moments validates the effectiveness of the API sand curves with the input parameters recommended in Table 1 and modified by p-multipliers that are proportional to the pore water pressure ratio (R_u) in granular materials. In this test, the recorded R_u values ranged between 0.9 and 0.5 at various depths in the loose sand and was approximately 0.4 in the dense sand. This corresponded to P_m values of 0.1 to 0.5 for the loose sand and 0.6 for the dense sand.

In order to further investigate the applicability of the modified API curves, similar analyses were repeated for the piles in all other centrifuge tests. Figure 5 compares the peak bending moments in each instrumented pile from the centrifuge tests to the corresponding bending moments estimated using *LPILE*. It can be observed that bending moments can be reasonably predicted in piles subjected to liquefaction and lateral spreading loads using the modification made to the API sand curves. The majority of the peak banding moments from centrifuge tests occurred when the wharf deck was moving in the downslope direction. The bending moments below the mudline are plotted in blue and the bending moments above the mudline (at

pile head) are plotted in red, showing that the p-y models were more accurate in estimating the bending moments at pile head.

6. CONCLUSIONS

The results of five centrifuge tests on pile-supported wharves in saturated sands were used to back-calculate representative static and dynamic p-y curves for laterally loaded piles. Two types of piles were used in this study: 1) static piles loaded with various cycles of shear loads applied at the pile head prior to shaking, and 2) dynamic piles that supported the wharf deck and were subjected to deck inertia and liquefaction-induced lateral spreading during earthquake shaking. The primary conclusions of the analyses are summarized as follows:

- Back-calculated p-y curves from static piles were approximated using API sand curves. The friction angles of 33°, 37° and 45° were used for loose sand (D_R = 30% to 40%), dense sand (D_R = 70% to 85%) and rockfill, respectively. These friction angles appeared to be adequate in estimating the ultimate lateral resistance (P_{ult}) of the experimental p-y curves and no modifications were necessary. However, the stiffness values of the p-y curves that were back-calculated from the centrifuge tests were softer than those recommended by API. The back-calculated moduli of subgrade reaction were 3500 kN/m^3, 3500 kN/m^3, and 5200 kN/m^3 for loose sand, dense sand and rockfill, respectively. These values are smaller than the values recommended by API (1993) by a factor ranging from 5 to 14, which might be attributed to the limitations of centrifuge tests in simulating the in situ soil stiffness and pile driving conditions.
- The *p*-multipliers (P_m) in fully/partially liquefied zones, which were calculated based on the pore water pressure ratio (R_u) generated during dynamic loading using $P_m = 1 - R_u$, were applied to account for the softer response in liquefied zones.
- The comparison of the recorded pile bending moments and those estimated from *LPILE* demonstrates that the recommended modification on API sand curves can reasonably predict the maximum bending moments along the piles due to liquefaction-induced lateral spreading.

ACKNOWLEDGEMENTS

Support for conducting the centrifuge tests was provided by Grant No. CMS-9702744 from the National Science Foundation (NSF) and Grant No. SA2394JB from the Pacific Earthquake Engineering Research Center. Support for performing recent analyses on the centrifuge test results was provided by Grant No. CMMI-1761712 from NSF and Grant No. 171126 from the Deep Foundations Institute.

REFERENCES

Abdoun, T., Dobry, R., O'Rourke, T. D., and Goh, S. H. 2003. Pile response to lateral spreads: Centrifuge modeling. J. Geotech. Geoenviron. Eng., 129(10), 869–878.

American Petroleum Institute, API, 1993. Recommended practice for planning, design, and constructing fixed offshore platforms. API RP 2A–WSD, 20th Ed., API, Washington, D.C.

Brandenberg, S. J., Boulanger, R. W., Kutter, B. L., and Chang, D. 2005. Behavior of pile foundations in laterally spreading ground during centrifuge tests. ASCE J. Geo. and Geoen. Eng. 131(11), 1378–1391.

Brandenberg, S.J., Wilson, D.W., and Rashid, M.M., 2010. A Weighted Residual Numerical Differentiation Algorithm Applied to Experimental Bending Moment Data. Journal of Geotechnical and Geoenvironmental Engineering, 136(6), 854–863.

California Department of Transportation (Caltrans). 2012. Guidelines for foundation loading and deformation due to liquefaction induced lateral spreading. Sacramento, CA: California Dept. of Trans.

Chang, B.J. and Hutchinson, T.C., 2013. Experimental evaluation of p-y curves considering development of liquefaction. Journal of Geotechnical and Geoenvironmental Engineering, 139(4), pp.577-586.

Ensoft, 2014. User's Technical Manual for LPILE.

Franke, K.W. and Rollins, K.M., 2013. Simplified hybrid p-y spring model for liquefied soils. Journal of Geotechnical and Geoenvironmental Engineering, 139(4), pp.564-576.

Haiderali, A. E., and Madabhushi, G., 2016. Evaluation of Curve Fitting Techniques in Deriving p--y Curves for Laterally Loaded Piles. Geotech. and Geological Engineering, Springer, 34(5), 1453–1473.
McCullough, N. J., Dickenson, S. E., & Schlechter, S. M., 2001. The seismic performance of piles in waterfront applications. In Ports' 01: America's Ports: Gateway to the Global Economy (pp. 1–10).
McGann R, Arduino P, Mackenzie-Helnwein P., 2011. Applicability of conventional p–y relations to the analysis of piles in laterally spreading soil. J Geotech Geoenviron Eng ASCE; 137(6):557–567.
Reese, L. C., Cox, W. R., and Koop, F. D., 1974. Analysis of Laterally Loaded Piles in Sand, Proceedings, 6th Offshore Technology Conference, Vol. II, pp. 473-484.
Rollins, K. M., Hales, L. J., Ashford, S. A., and Camp, W. M. 2005. "P-Y curves for large diameter shafts in liquefied sand from blast liquefaction tests." ASCE Special Publication: Seismic Performance and Simulation of Pile Foundations in Liquefied and Laterally Spreading Ground, 145, 11–23.
Wilson, D. W., Boulanger, R. W., and Kutter, B. L. 2000. Observed seismic lateral resistance of liquefying sand. J. Geotech. Geoenviron. Eng., 126-10, 898–906.

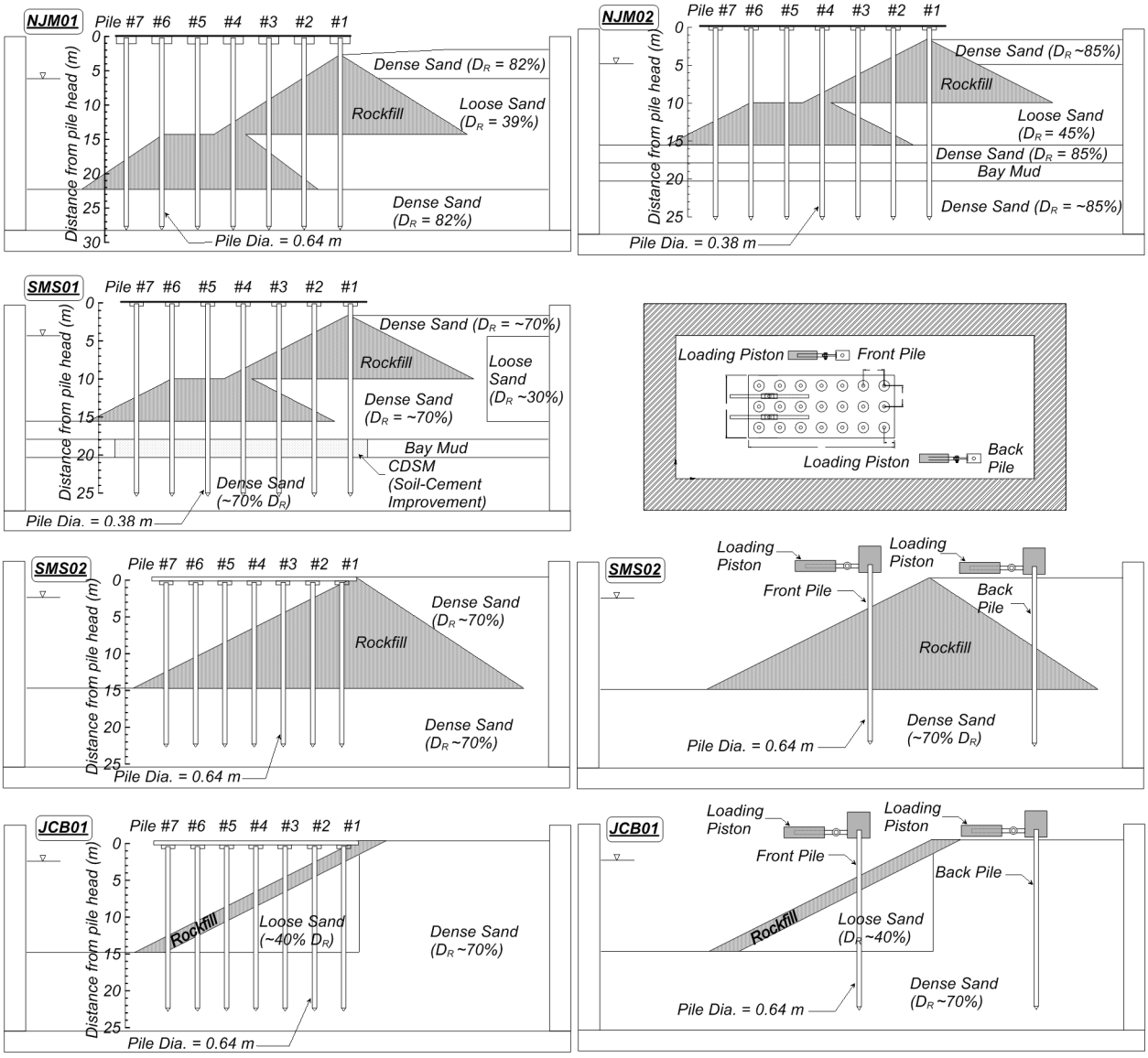


Fig. 1. Cross sections and plan view of five centrifuge tests on pile-supported wharves.

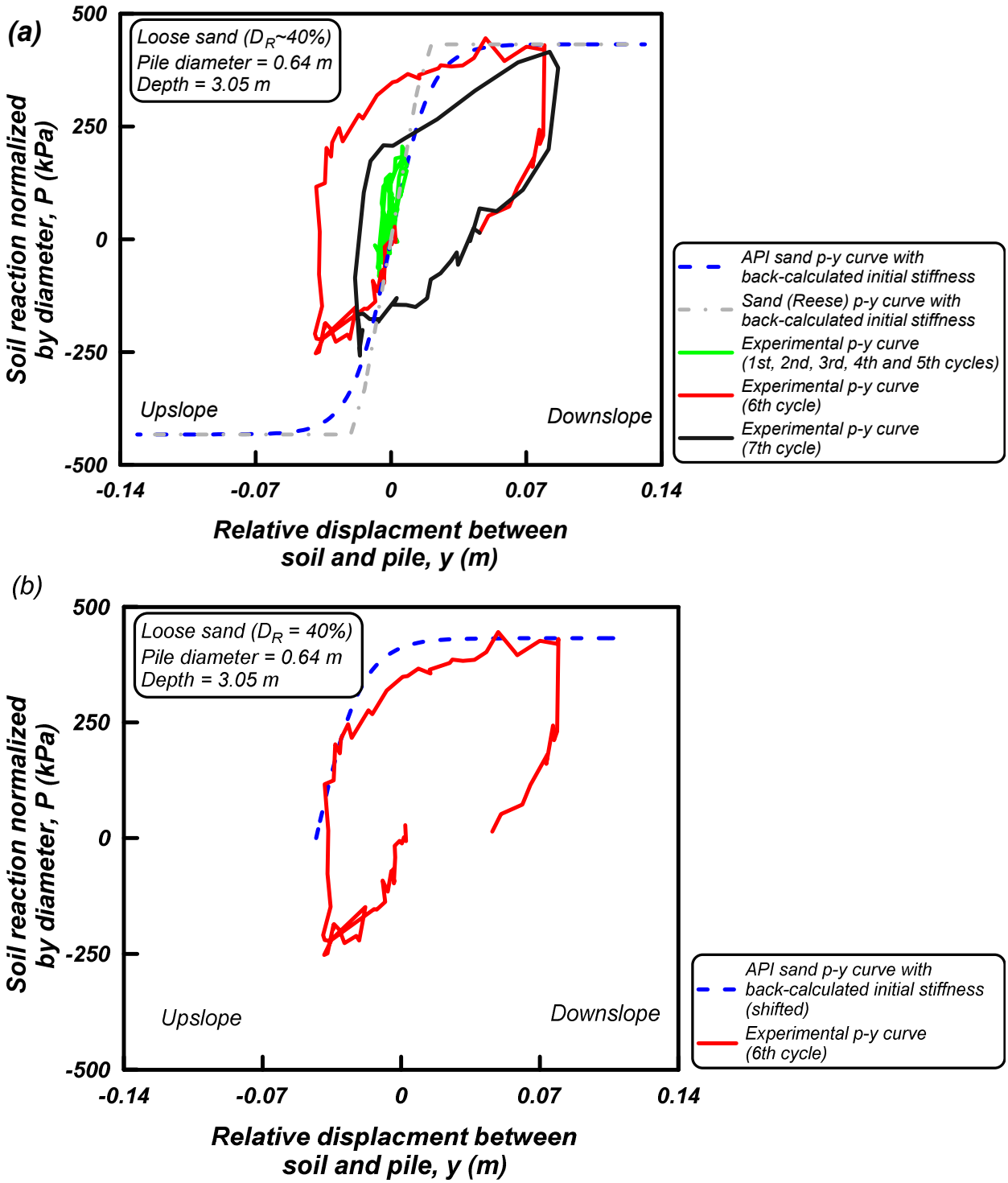


Fig. 2. Comparison of experimental p-y curves for loose sand (D_R = 40%) from the front static pile in JCB01, API sand and sand (Reese et al. 1974) using back-calculated input parameters.

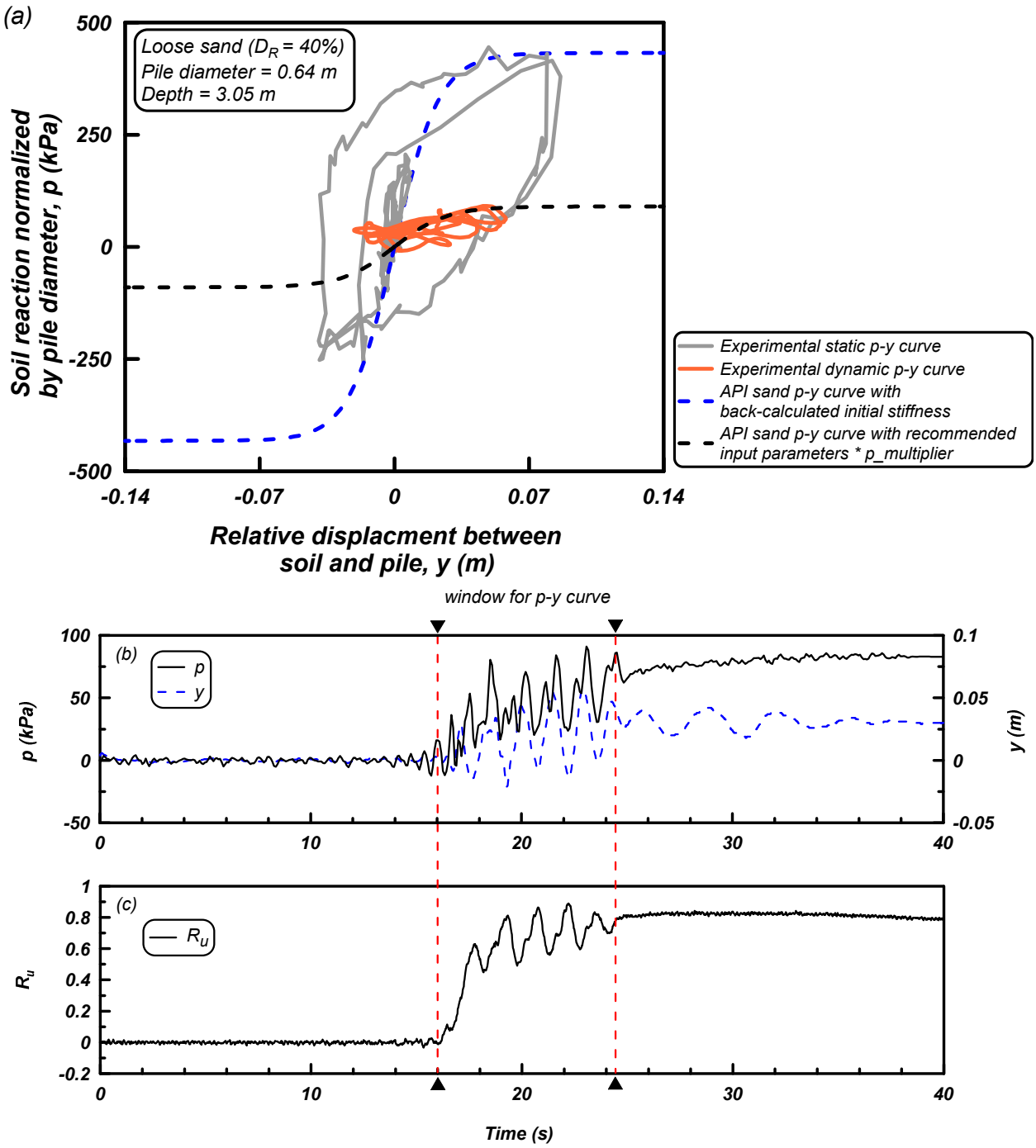


Fig. 3. (a) Comparison of static versus dynamic p-y curves in loose sand; (b) Time histories of back-calculated soil reaction and pile displacement relative to adjacent soil; (c) Excess pore water pressure ratio measured in loose sand in JCB01.

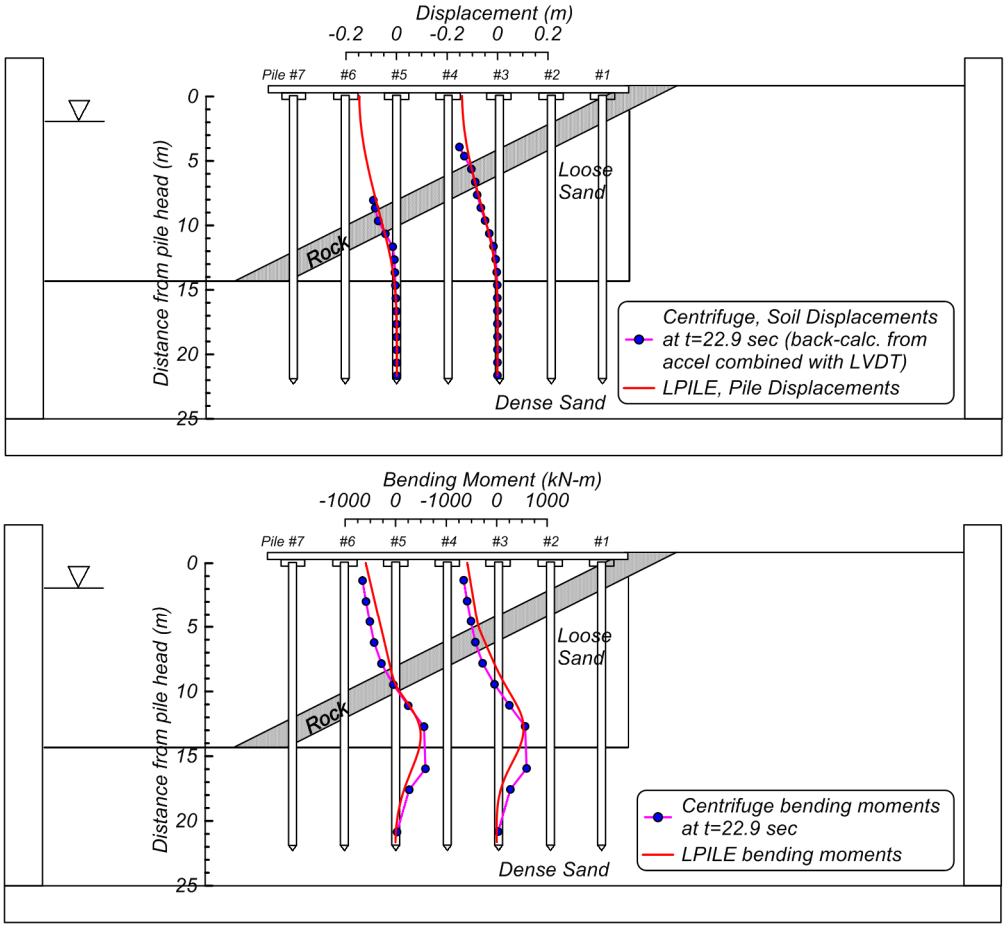


Fig. 4. (a) Back-calculated soil displacement profiles at the pile locations from centrifuge tests with estimated pile displacement profiles from *LPILE;* (b) Comparison of bending moments from centrifuge tests to the estimated moments from the *LPILE* analyses for JCB01.

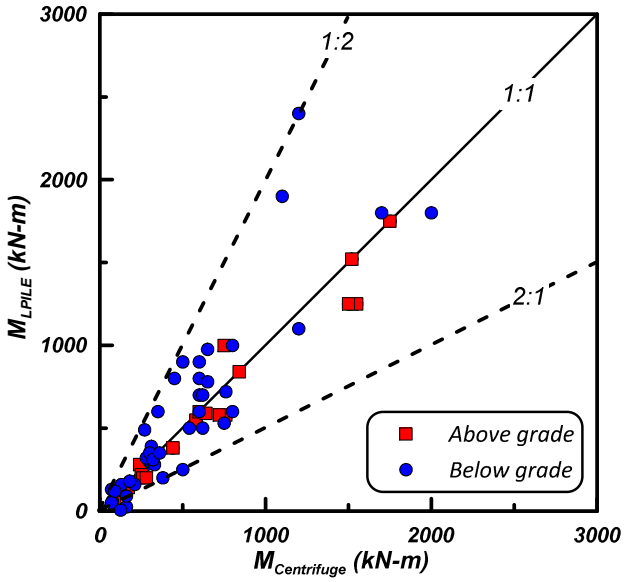


Fig. 5. Comparison of bending moments recorded from centrifuge and estimated from the *LPILE* analyses for all five centrifuge tests.

FUNDAMENTALS FIRST

Daniel P. Dietzler, P.E., CEO, Patrick Engineering Inc. and President, Dietzler Construction Corp., 4970 Varsity Drive, Lisle, Illinois, USA, 630.795.7200, ddietzler@patrickco.com

Jeffrey C. Schuh, P.E., President, Patrick Engineering Inc., 4970 Varsity Drive, Lisle, Illinois, USA, 630.795.7200, jschuh@patrickco.com

Logan Bloemer, P.E., Project Manager, Dietzler Construction Corp., 5027 County Road 37, Yoder, Wyoming, USA, 970.673.2217, lbloemer@dietzlerconstruction.com

ABSTRACT

Over the past 30 years, the authors have encountered numerous projects where recognizing the geology, soil properties and groundwater conditions, and considering alternative construction techniques have promoted efficient and cost-saving construction. The construction documents for these projects, produced by various engineering firms, provided basic information on geotechnical conditions. The authors became involved in each project either because there was a problem during design or construction or, as a contractor, won the project because they saw a value engineering opportunity to take advantage of the geologic setting of the project to design and build alternatives to what the designer depicted. Understanding the geologic setting is critical before planning and designing begins. Being able to work with the geology and the materials on site is preferred before specifying more costly and complex solutions, which often require the importing of materials and adherence to unnecessary and/or inappropriate specifications. Failing to understand the geology or not knowing all the techniques available for construction can lead designers to develop solutions that could be inappropriate. This paper presents several examples of value engineering and project performance enhancements developed through knowledge of basic soil mechanics and implementing innovative solutions.

Keywords: geologic setting, soil mechanics, design-build, innovative solutions

History and Background

Most people attend DFI meetings, present their experiences, listen to others, and read articles and papers with the hope they can learn from others. Geotechnical engineers and contractors often interface with others in the execution of projects who have, at best, a rudimentary knowledge of geology and soil mechanics. Of course, there is a need for architects, bankers, and regulators, etc., but they typically do not have much interest in the nuances of geotechnical engineering, which relies on both art and science. Thus, significant time is spent educating counterparts in the need for comprehensive subsurface investigation programs and the intricacies of construction in the "dirt," as they typically refer to soil and rock.

Until Karl Terzaghi began his first scientific studies of soil classification and soil structure interaction about 100 years ago (1926), this branch of civil engineering did not exist. Until that time, the design and construction of retaining walls, dams, tunnels, and foundations were based on empirical observations. That is, what worked previously was thus deemed to be appropriate at any location regardless of the geologic setting and differences in soil properties. The evolution of Terzaghi's work, which was then greatly expanded by Arthur Casagrande, Dr. Ralph Peck, et al. is worthwhile reading. The 1999 publication, *"Karl Terzaghi: The Engineer as Artist,"* authored by Richard E. Goodman, (1999) is entertaining and informative about the evolution of soil mechanics.

© 2019 Deep Foundations Institute

Noteworthy is that several fundamentals accepted then (100 years ago) as providing guidance were subsequently proven to be misleading. For example, years ago, geology was viewed as a science that was predominantly academic. It was not viewed prior to Terzaghi as an important site-specific precursor to measuring and predicting the behavior of bedrock, soil, and groundwater at a construction site. Today, the geotechnical engineer generally begins a site investigation with some level of description of the local geology as it could impact the design, construction, and performance of the project. In the last 50 years, additional emphasis has been placed on the potential for seismic effects on structures. Standards have been set and are now widely practiced.

Similarly, investigations of foundation conditions have advanced in recent decades to include in-situ testing methods, such as pressuremeter tests, packer tests, etc., that are more informative than just SPT values. However, it is still not uncommon to see geotechnical recommendations and predictions based on meager field data and, occasionally, on improperly run tests. The same goes for laboratory tests that are sometimes erroneous. There are, as most of us have learned, good drillers and accurate boring and/or coring logs, and labs. And there are others… Virtually everyone in this business of constructing foundations and earth structures is aware of case histories and claims linked to poor, missing, or misleading data. Changed conditions, defective specifications, and violations of the Spearin Doctrine (1918) are all too familiar on projects that involve underground construction.

This paper presents five case studies where it was apparent to the authors that a clear comprehension of the fundamentals of site geotechnical conditions were probably not understood by the designers or contractors. Contractors, engineers, and suppliers in this industry have similar experiences and often trade war stories, both for entertainment and in the spirit of sharing the dangers on the trails ahead. Many contractors and engineers have a secret, or not so secret, list of owners for whom many would refuse to contract with again, or at least proceed with a great deal of trepidation, because of rock, soil, and/or groundwater issues encountered on a prior project and how those issues were resolved.

On the other hand, outstanding and valuable client relationships have been established by providing value with innovative, "value-engineered" solutions. Some of the most profitable projects have emerged from situations where understanding of the site conditions provided an advantage over the competition. Most contractors, engineers, and suppliers who thrive in this industry are comfortable with managed risk and the potential to make a fair profit based on their knowledge.

The Fundamental Tools

The publication, "*Soil Mechanics in Engineering Practice*," by Karl Terzaghi and Ralph B. Peck, was and still is, in its updated version with Gholamreza Mesri, (1996), a widely used textbook in geotechnical engineering. Most engineers in the profession today have been exposed to this publication and it was, and still is, used as the core of the curriculum at major universities that offer a master's degree in geotechnical engineering. However, there are many colleges and universities that graduate engineers who do not go through a curriculum based on this publication. Many of those engineers are now practicing geotechnical engineering and have a PE.

There are, of course, other text books that go into more detail on specific topics, such as, "*Seepage, Drainage and Flow Nets,"* by Cedergren et al. (1989), *"Foundation Engineering,"* edited by G.A. Leonards (1962), *"Pile Foundation Analysis and Design,"* by Poulos and Davis (1980), and many others. Government agencies have published technical guidelines for specific topics such as the *FHWA on Drilled Shafts*, etc. (2006). A lot of information is available, some proven and some simply found on the internet without having a good foundation for use. The profession and industry continue to evolve. This is both an art and a science.

Interestingly, whether the project is large and has a big budget for geotechnical investigations and analysis or is small and has a meager budget, the need for understanding the fundamentals is still important. The authors have seen examples of both large, well-funded projects that experienced problems and small projects that had obstacles. The idea that each project has someone or a team of true experts making the critical geotechnical decisions is altruistic. Frustrating delays, cost overruns, and ugly claims can result on both small and large projects. Similarly, creative solutions based on highly perceptive designers' or contractors' knowledge of geotechnical practices can lead to outstanding outcomes, regardless of project size.

It is an observation that many general and civil contractors, and some subcontractors, do not appreciate the value of geotechnical investigations. It is not uncommon to see contract packages out for bid that do not include geotechnical data. Often, the exploratory data is summarized on the civil drawings, and key pertinent information is omitted. Asking for the full geotechnical report is sometimes perceived by the designer as offensive and intrusive, or even threatening. Yet, without the information that is contained in those reports, a contractor is taking greater risk than necessary. In addition, those owners and designers that state that the contractor should make his own or supplementary geotechnical investigations prior to bidding are unrealistic.

What constitutes a thorough geotechnical investigation? Interestingly, some of the best geotechnical engineers collaborated in the 1990's and developed the ASCE Publication, *Geotechnical Baseline Reports for Construction, Suggested Guidelines."* This publication was upgraded in 2007 and serves as a valuable guide for owners, designers, geotechnical consultants, contractors, and legal professionals. Today, it serves as the best publication to help all stakeholders avoid or resolve claims related to geotechnical issues.

Bidders raising questions during the pre-bid period involving geotechnical conditions run the risk of losing any insight or hunches the bidder may have or remove a strategic advantage in the bidding process. However, not asking for geotechnical information adds risk to the project. Smart, experienced contractors either have competent geotechnical engineers on staff or they have a geotechnical engineer they trust to decipher and understand the critical geotechnical data that is supplied. When the project is large enough, it is prudent to invest in such counsel versus assuming anything. The consequences of a bad assumption can lead to significant losses and/or claims.

Some owners try to shift as much risk as possible to the contractor. Geotechnical engineers, because investigations may be limited due to owner-imposed budget constraints and because of the inherent risk in characterizing site conditions with a limited number of borings, have been trained to qualify data interpretation and corresponding recommendations. For some, it also limits or hopes to shift the responsibility to the contractor. However, the contractor needs data, reliable data, to provide a fair price; and the owner is well advised to recognize that if the data is incomplete, erroneous, or the work cannot be built per the information provided, a good construction lawyer will make the owner pay for such inadequate or erroneous work product.

Every engineer and contractor should be familiar with the Spearin Doctrine (1918). Yes, it is typically not a topic that is taught either in the engineering curriculum or emphasized during training by an employer. Most issues get resolved before a dispute escalates into a costly claim. However, once burned, whether as a designer or a contractor, people embrace the fundamentals critical to their industry.

In summary, the designer and/or the contractor need to:

- Understand the site geology, soil properties, groundwater conditions and what is practical to construct, regardless of the project budget.
- Read the geotechnical report and understand the data or hire someone who can interpret the information.

- Provide the contractor with sufficient geotechnical data to result in fair pricing.
- Be respectful. The designer needs to answer questions and be open to alternative solutions. Assigning all risk to the contractor is unlikely to result in a positive project outcome.
- Avoid making assumptions that are based on misunderstandings or lack of geotechnical data. Have a backup plan if the basic assumption, such as groundwater control, does not work.

This is an interesting and challenging yet rewarding industry. One must subscribe to continuous learning to stay abreast of the changes. Supporting a professional means for dialogue prior to and during construction with all stakeholders is paramount to the success of a project.

In the following case studies, the importance of the fundamentals will be stressed.

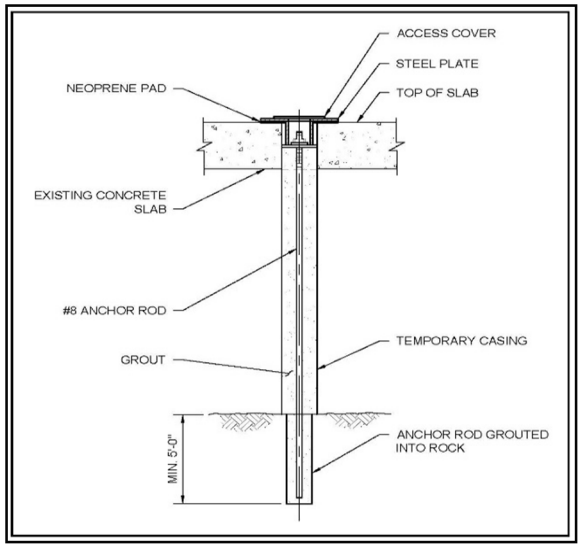


Fig. 1. Detail of Anchor Assembly

Case Study Number 1

The case involved a small dam and spillway constructed in a remote area of Wyoming. The project was built without issue and put into service in the Fall of 2016. In January 2017, the design engineer, for some unknown reason, checked his calculations and became concerned that under high flows, the approach apron to the spillway could fail due to uplift. The engineer and owner asked the contractor to remobilize to the site and pour a 14 in. (0.4 m) thick reinforced concrete slab on top of the apron and dowel it into the existing slab. This work needed to be done before snowmelt and high flows in April. Because the spillway was in service and there was no means for a bypass, placing the additional concrete would involve cordoning off discrete areas and pouring concrete in cold weather with the attendant issues.



Fig. 2. Anchor installation

The contractor asked the engineer for the hydrostatic uplift pressures and proposed an alternative to thickening the slab. The alternative was to core through the existing slab, avoiding rebar, and anchor the slab into the competent bedrock 15 ft. (4.6 m) below with steel anchors. The spacing of the tie downs and size and thickness of the steel plates were determined, working collaboratively with the engineer. A detail of the Anchor Assembly is shown in Fig. # 1. Anchor installation is shown in Figs. # 2 – # 3.

The engineer, no doubt, suffered some economic consequences. Furthermore, had the apron failed, the entire spillway would have been damaged, and an embarrassing claim would have resulted. Safety is always a concern. The tie down work was completed in far less time and with less exposure to workers in water than adding concrete would have entailed. It took some convincing to get the

engineer, who had no prior experience with anchors, to agree with this solution. All parties worked together, and there was a mutual professional respect between the contractor and the designer.



Fig. 3. Anchor Plate installation

Case Study Number 2

This project was a flood control reservoir in the Denver area. The design plans included excavating 400,000 CY to build a normally dry water channel, building a mile long homogeneous, earth fill dam with this excavated material, and constructing a large concrete outlet structure. When the bids were opened, the project was significantly over budget.

The contractor proposed a change to the embankment dam geometry to lower costs. The dam cross-section, designed by others, called for blending the highly variable soils from required excavation from the channel construction to produce a low permeability, homogeneous soil embankment. The contractor proposed a revised "central core" cross-section for the dam. This enabled the granular soils to be placed and compacted in the outer zone. A smaller fill zone of low permeability soil could be achieved using on-site soils without mixing. In addition, with the granular shell, the side slopes could be steepened, reducing fill volume, increasing reservoir storage, and reducing project cost. The revised embankment cross-section is shown in Fig. # 4.

The State Engineer's Office signed off on the contractor's redesign supported with stability and seepage calculations. This change enabled the excavated material to be placed in either the central core or shoulder zone as it was excavated in a progressive manner. That reduced material handling and improved earthwork efficiency.

Another issue arose during excavation for the outlet structure. Borings had not been made along the outlet structure alignment due to access issues during design. The foundation conditions were thus "inferred."

During excavation, it was determined the bottom of this outlet structure would be a foot or two into claystone. The contractor asked if the claystone could be susceptible to swelling. If so, that could this impact construction of the formed concrete outlet structure.

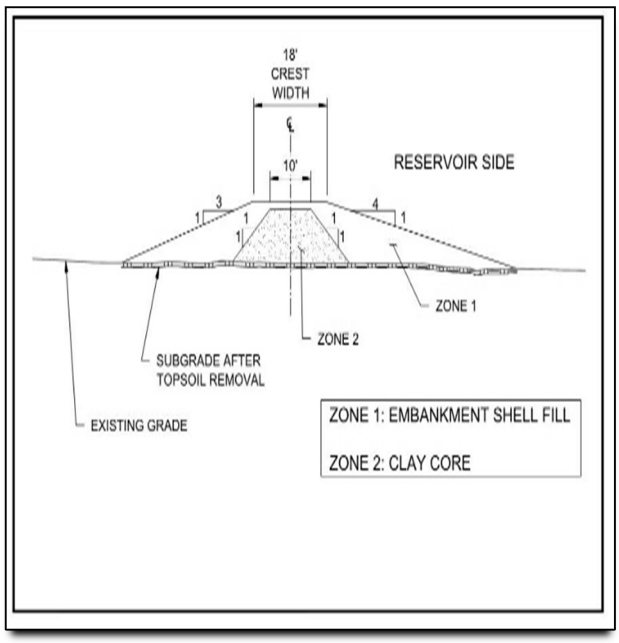


Fig. 4. Revised embankment cross-section

- Thoroughly exploring and classifying the soils resulting from required excavation is valuable to the contractor, who must meet moisture density and, in this case, permeability specifications to build a fill with such soils.
- Checking for swelling soils and swelling bedrock (claystone) that would be exposed is an important consideration during exploration. Concrete construction requires a stable subgrade or serious problems will result due to subgrade movements.

Interestingly, owners may be told by the engineer that all soil and foundation issues are the responsibility of the contractor. In the end, if what the engineer has depicted on the plans and specifications cannot be built by standard means and methods, the Spearin Doctrine (1918) comes into play. Knowing and reporting the engineering soil properties and making sure what is designed can be built per the plans and specifications is fundamental.

The engineer obtained samples, tested them, and concluded the claystone would be susceptible to expansion; and, therefore, remedial efforts were needed. The engineer directed the contractor to excavate 5 additional ft. (1.5 m) of the claystone and replace it with compacted low permeability cohesive soil, refer to Fig. # 5. Figure # 6 shows the formed structure prior to wall and roof structure construction.

The excavation and replacement of the claystone added cost and schedule but did not result in a claim. Setting formwork on swelling soils would have been a big problem. Fortunately, the issue was caught in advance and resolved amicably.

Lessons learned from this project were:

Mixing soils is not an efficient contractor activity, yet some engineers fail to realize that reality.



Figs.5. Excavation of swelling claystone and replacement with cohesive soil

Case Study Number 3

This project was a wind farm in Northern Illinois. The plans specified the turbine foundations were to be massive concrete founded at a shallow depth with over excavation performed if the soils at bearing elevation did not meet the required bearing pressure. The designer, for whatever reason, had not made borings at all foundations. The few borings that were made indicated silt soils could be present. Almost immediately, excavations encountered high groundwater levels, and excavations encountered silt soil that "ran" into the excavation, resulting in an almost endless excavation quantity. An acceptable bearing level could not be reached. Earthwork operations were stopped, and a geotechnical engineer was contacted to assist the owner in determining a reasonable path forward to control foundation costs.



Fig. 6. Formed structure prior to wall and top concrete placement

The first step was to obtain USDA soil survey maps to gain an understanding of the near-surface soils at each foundation location and identify those foundations likely to be located in problem areas (high groundwater table with silt soils). Borings were then made at the locations deemed to have potential for foundation installation issues. Upon determining the stratigraphy at each foundation, alternative foundations were considered. Foundations needed to be repetitive with low cost. Because acceptable bearing soils were generally located at less than a depth of 20 ft. (6.1 m), the alternative of rammed aggregate piers was selected. This system could be used to avoid over excavation of silt soils, could be installed on short notice; and was cost-effective.

A specialty contractor was contracted to finalize the design at the selected foundation locations. Work progressed with cooperation between the original contractor and the specialty contractor and the project was completed without issue.

The foundation installation problem could have been avoided with an adequate geotechnical investigation during the design phase and discussion with the contractor on its means and methods for foundation excavation before any earthwork was performed. Once the excavation is open and groundwater is found to be high (which is especially true in the Spring), it is too late to start developing a contingency plan.

Case Study Number 4

This project, located in Northwest Indiana, involved the unanticipated settlement of railroad tracks along an expanded rail siding in an active industrial facility. The expansion was completed without a detailed geotechnical investigation and included placing up to 15 ft. (4.6 m) of fill with a wire-faced retaining wall. After fill placement and track installation, the tracks settled; and the retaining wall rotated, showing obvious signs of slope failure.

The owner needed the track "fixed." A geotechnical engineer was retained to complete a subsurface investigation. It was determined the imported embankment soil was granular (good), but a 4 ± ft. (1.2 m) thick layer of organic soil was located below this fill. This organic layer was the cause of the settlement and the rotation of the retaining structure. A Remedial treatment was required.

Various alternatives were evaluated, from consolidation grouting to auger-cast piles. It was determined that stone columns using crushed stone as the replacement soil would provide the needed shear strength to protect the slope from failure and consolidate the soils to arrest settlement. The geotechnical engineer worked with a specialty contractor under contract with the owner to design the spacing and depth of the stone columns, and the project was completed without further issue.

The costs for the remedial treatment were considerable and could have been avoided with adequate subsurface investigation and design. Site reconnaissance, provided by the appropriate professional, would have suggested the potential for the organic soils to be present. A few strategically placed borings would have added minimal cost and would have identified the need for excavation/treatment of the organic soil. If identified during the design phase, the organic soils could have been addressed before fill was placed, saving hundreds of thousands of dollars in construction cost as well as costs associated with loss of production at the facility.

Case Study Number 5

This project, located in Illinois, was for the installation of a rail loop for a unit coal train at a power plant. Figure # 7 is an aerial photograph of the facility. The loop was planned to cross an existing pond, two inlet channels, and two outlet channels. The site is located partially within the floodplain of the Illinois River and, thus, the surficial soils at the site are primarily alluvial. The original design-builder had planned on conventional fill placement for the new embankment. The fill was over one mile in length and up to 30 feet (9.1 m) high, including placing fill in the pond and the channels. The plan was to import all soil for construction. The design-builder had no soil boring or bathymetry information regarding these features. They had also contracted with the owner for all design and construction for a lump sum fee.

Separate from the design-builder, an engineer was engaged by the owner to assist in permitting the project with the U.S. Army Corps of Engineers and with state agencies. During one project meeting, the design-builder was asked to quantify the amount of material it would take to construct the embankment across the pond, as the fill foot print area is important for permitting. The response was, "Keep filling until it is up to the final grade." Obviously, this was not acceptable to the owner who requested the engineer perform a bathymetric survey and a comprehensive geotechnical investigation to define site conditions.

Drilling was performed from a barge, and supplemental borings were made on land. Shear strength and consolidation tests were performed. It was determined the foundation soils were extremely soft (unconfined compressive strength 0.1 tsf) and compressible.



Fig. 7. Aerial of the site

Predicted settlements were 2 ft. (0.60 m) for the new embankment in the pond. Stability analyses indicated the embankment would fail if foundation strength was not increased. The project was on an expedited schedule and, therefore, proactive foundation treatment was required.

The owner then assigned the engineer to serve as the design-builder for the rail loop project. The engineer designed a comprehensive treatment plan for the portion of the embankment across the pond and the old intake and discharge channels. This work included wick drains (as seen in Fig. # 8) to force consolidation of the compressible alluvial soils, jet grouting to provide stability to soils in the outlet channel, and over excavation of unstable soils.

Using soil survey maps, the engineer identified the potential for granular deposits on property adjacent to the site. He encouraged the owner to perform a subsurface investigation to verify the quantity and quality of the deposit. Upon verification, the owner purchased the site for use as a borrow source, providing over 300,000 tons of gravel at a cost of less than $1 per ton. The embankment was designed with buttressing using otherwise unsuitable soil from undercutting operations. Staged construction was implemented to allow foundation strength to increase before subsequent embankment lifts were placed. In all, the embankment settled 2 ft. (0.6 m) in 30 days with no further settlement. The track has been in service for 8 years with no issue.

Embankment could not be used in the intake channel as head losses, even with large diameter conduits, would impact the delivery of cooling water. Soil borings indicated this portion of the site consisted of granular soil over bedrock near a depth of 50 feet. A deep foundation system of single drilled piers socketed into bedrock with hammerhead bents was selected to support the bridge across the intake channel to minimize head losses. The drilled piers were installed using portable barge segments, as seen in Fig. # 9.

The geotechnical conditions at the project site needed to be fully understood to design and construct the project components. The existence of the problem soils in the pond and the old intake and discharge channels influenced the design and impacted the means and methods used to construct the embankment in those areas. The design criteria for the intake channel necessitated a deep foundation system that would minimize head losses in the channel. The owner had relied on the original design-builder to do what was needed to reduce risk and develop a design that could be implemented at a reasonable cost; but without a geotechnical appreciation, the geotechnical aspects of the project were shoved aside. Fortunately, questions were asked, and adequate investigations were completed to finalize the design before construction began. The project was completed by the engineer on a design-build basis and under the owner's budget.



Fig. 8. Wick drain



Fig. 9. Portable barge segments and pier installation

Conclusions/Lessons Learned

Design and structural engineers rely on other professionals, such as geotechnical engineers, owners, and contractors to build projects. All must have an appreciation for the impact geologic conditions have on a project. Subsurface investigations are critical to addressing risk on most projects. Such work needs to be performed by professionals that understand fundamental design and construction means and methods. Design teams need to depict the geologic, soil, groundwater and bedrock conditions in a manner that enables a contractor to anticipate such conditions with reliability. All parties need to be open to alternatives and practical construction methods. There are a few parties outside the industry that recognize that the behavior of soil, as Karl Terzaghi (1996) recognized, can be predicted. What is considered to be fundamental to some is mysterious to others. The value of geotechnical investigations is often unappreciated. Often parties without subsurface investigation and specialty construction experience or those marginally knowledgeable ignore the fundamentals. Occasionally, people and companies suffer from such ignorance; and some occasionally profit from knowing and practicing these fundamentals. It pays to know the fundamentals.

REFERENCES

Cedegren, H.R., 1989. Seepage, Drainage and Flow Nets. John Wiley & Sons.

Essex, R.J., 2007. Geotechnical Baseline Reports for Construction. ASCE Press.

Goodman, R.E., 1999. The Engineer as Artist, ASCE Press.

Leonards, G.A., 1962. Foundation Engineering, McGraw Hill Book Company

Poulos, H.G. & Davis, E.H., 1980. Pile Foundation Analysis and Design, Rainbow Bridge Book Co.

Terzaghi, K. B., Peck, R, and Mesri, G., 1996. Soil Mechanics in Engineering Practice. New York, J. Wiley.

United States Department of Transportation, FHWA, Publication, Dec., 2006, No. FHWA NHI-06-089.

IDENTIFICATION AND QUANTIFICATION OF PILE RELAXATION

Patrick J. Hannigan, P.E.[1], Alex Ryberg, P.E.[2], and Rozbeh B. Moghaddam, Ph.D., P.E.[3]

[1] GRL Engineers Inc., Cleveland, OH, U.S.A, 216-831-6131, phannigan@grlengineers.com
[2] GRL Engineers Inc., Holmes, PA, U.S.A, 610-459-0278, aryberg@grlengineers.com
[3] GRL Engineers Inc., Cleveland, OH, U.S.A, 216-831-6131, rmoghaddam@grlengineers.com

ABTRACT

Driven piles are widely used for foundation support. In the vast majority of cases, an increase in pile capacity occurs with time which is referred to as "set-up." However, in a very limited number of cases, a decrease in capacity with time can occur. This phenomenon is referred to as "relaxation." This paper will provide a brief review of the relaxation phenomenon, as well as pile driving information and dynamic test data on cases where relaxation has occurred.

The pile types in the presented relaxation cases include H-piles, open-end and closed-end pipe piles, prestressed concrete piles, and prestressed concrete piles with H-pile stingers. The soil conditions where relaxation occurred includes dense to very dense fine sands, heavily over consolidated clays, and weak laminated rocks. Relaxation information from 36 piles at 26 sites is assessed. The collected data will assist foundation designers by identifying the subsurface conditions where relaxation has occurred, as well as by documenting the corresponding relaxation magnitude.

One method of addressing relaxation when it is encountered is to drive the foundation piles to a greater end of initial driving capacity than required long-term. Hence, the identification and quantification of the relaxation magnitude will be beneficial to foundation designers installing similar pile types in similar subsurface conditions. The paper will also present pertinent observations and recommendations on mitigating relaxation when encountered.

INTRODUCTION

One of the earliest observations of a decrease in redriving resistance following initial driving was reported by Miller (1937). He reported that piles driven into a saturated, coarse grained soil could lose 40 to 50% of their resistance when redriven 24 hours after initial driving. Yang (1956) similarly reported that after a break in driving, a decrease in driving resistance could be encountered for piles driven in dense fine sand, inorganic silt, or stiff fissured clay. Parsons (1966) in his paper that described piling difficulties in the New York City metropolitan area termed this phenomenon "relaxation". In this time period, pile capacity was most often evaluated from a pile driving formula frequently checked by a static load test. Hence, the true magnitude of the capacity decrease on a given pile was often poorly quantified. Furthermore, dynamic measurements that could determine what influence driving system performance variation had on the observed redriving resistance were not yet readily available.

The consequences of relaxation can be significant if not identified and addressed during construction. As a result of relaxation, the installed piles will have less than the desired ultimate capacity or nominal resistance yielding a lower factor of safety than targeted. In severe relaxation cases, foundation performance can be compromised and excessive settlements may occur. Morgano and White (2004) presented two case histories where relaxation occurred, one where the piles were driven into shale, and the other where the piles were terminated in sand. Test results indicated a reduction in ultimate capacity of 29% at the shale site and of 30% at the sand site. Both cases required the piles to be driven deeper to mitigate relaxation.

© 2019 Deep Foundations Institute

RELAXATION MECHNAISMS

Thompson and Thompson (1985) reviewed end of driving and restrike blow count data from eight sites where the decrease in the observed blow count at the beginning of restrike, relative to the end of driving blow count, suggested relaxation had occurred. Fortunately, these sites also had dynamic measurement data which allowed the authors to differentiate between real relaxation, which occurred at only two of the eight sites, and apparent relaxation, where the decrease in restrike blow count was due to improved hammer performance. The pile types in the two real relaxation cases were an H-pile and a closed-end pipe pile. The two projects were located near each other. In both cases, the bearing layer was a weathered shale bedrock with thin limestone layers and clay seams. The H-piles typically penetrated two to four feet into the shale whereas the heavier loaded closed-end pipe piles penetrated up to 10 feet into the shale and were restruck as many as five times. Possible relaxation mechanisms were shale softening from water migration to the pile toe in the peripheral opening created by the pile driving shoe or closure plate, as well as shale shattering beneath the toe of an already driven pile caused by driving adjacent piles to a deeper final penetration depth. Relaxation of locked-in horizontal rock stresses following pile driving was theorized as another potential relaxation mechanism.

York et al., (1994) reported on a case at JFK International Airport in New York where both setup along the pile shaft and relaxation at the pile toe were encountered in a medium dense, medium to fine glacial sand. Relaxation happened in some larger displacement pile groups when densification of the sand occurred as a result of pile driving. The dense sand dilated and developed negative pore pressures as later piles in the group were driven into the dense material. The negative pore pressure resulted in temporarily elevated effective stresses that required a few hours or several days to return to normal. Once the effective stresses had normalized, piles could be driven past the densified sand layer.

Herrera (2015) reviewed pile relaxation cases in Florida granular soils. He recommended that potential relaxation zones, identified by Standard Penetration Test (SPT) resistance values, be assessed using cone penetration tests with shoulder pore pressure measurements, CPT-u. SPT N values in silty and shelly sands greater than 24 with an automatic hammer, or greater than 30 with a safety hammer were of particular concern. Soil layers where negative pore pressures are encountered in the CPT-u data should then be evaluated with pore pressure dissipation tests. He recommended these results be used as a guide in identifying soils where restrike tests should be performed to check for relaxation.

DYNAMIC MEASUREMENT RECORDS

Figure 1 presents dynamic measurement data for a typical relaxation case. The data is from an H-pile driven into a shale bedrock with a single acting diesel hammer. Force and velocity records versus time are presented for the end of initial driving (EOID) in the top half of the figure and at the beginning of restrike (BOR) in the bottom half. The time of impact is indicated by the dotted vertical line on the left, and the toe response, time 2L/c, is indicated by the dotted vertical line on the right. Selected Case Method output quantities are identified by their three letter code along the left margin.

In the end of initial driving records, the impact force, FT1, is 353 kips. This is also the maximum force at the gage location, FMX. The force reflected from the pile toe is 350 kips, slightly less than the impact force. The velocity record at that time is negative resulting in a mobilized resistance of 400 kips as quantified by RX9, the Maximum Case Method resistance with a damping factor of 0.90. The mobilized resistance exceeds the impact force. The ratio of the resistance over the impact force, ROF, is 1.13. For the record presented, the calculated hammer stroke, STK, is 7.03 ft and the energy transferred to the pile head is 9.9 ft-kips. CSX, the calculated compression stress at the gage location, is 22.8 ksi and CSB, the calculated compression stress at the pile toe, is 27.8 ksi. The equivalent penetration resistance over the final inch of driving was 28 blows per inch as the pile terminated in a hard shale bedrock.

Records from the beginning of restrike, clearly indicate a weaker toe resistance and relaxation. The impact force, FT1, is 372 kips, the calculated hammer stroke, STK, is 7.31 ft, and the energy transferred to the pile head is 10.9 ft-kips. However, the reflected maximum force from the pile toe of 253 kips is significantly less than the 350 at the end of initial driving. The penetration resistance over the first inch of restrike was 8 blows per inch. The pile was restruck with an equivalent to slightly greater impact force and transferred energy, and moved substantially easier due to the lower toe resistance. This is also indicted by the lower ratio of the resistance over the impact force, ROF, of 0.73.

End of Initial Driving		
FT1	353	kips
FMX	353	kips
RX9	400	kips
ROF	1.13	%
STK	7.03	ft
EMX	9.9	ft-kips
CSX	22.8	ksi
CSB	27.8	ksi

Beginning of Restrike		
FT1	372	kips
FMX	372	kips
RX9	271	kips
ROF	0.73	%
STK	7.31	ft
EMX	10.9	ft-kips
CSX	24.0	ksi
CSB	20.9	ksi

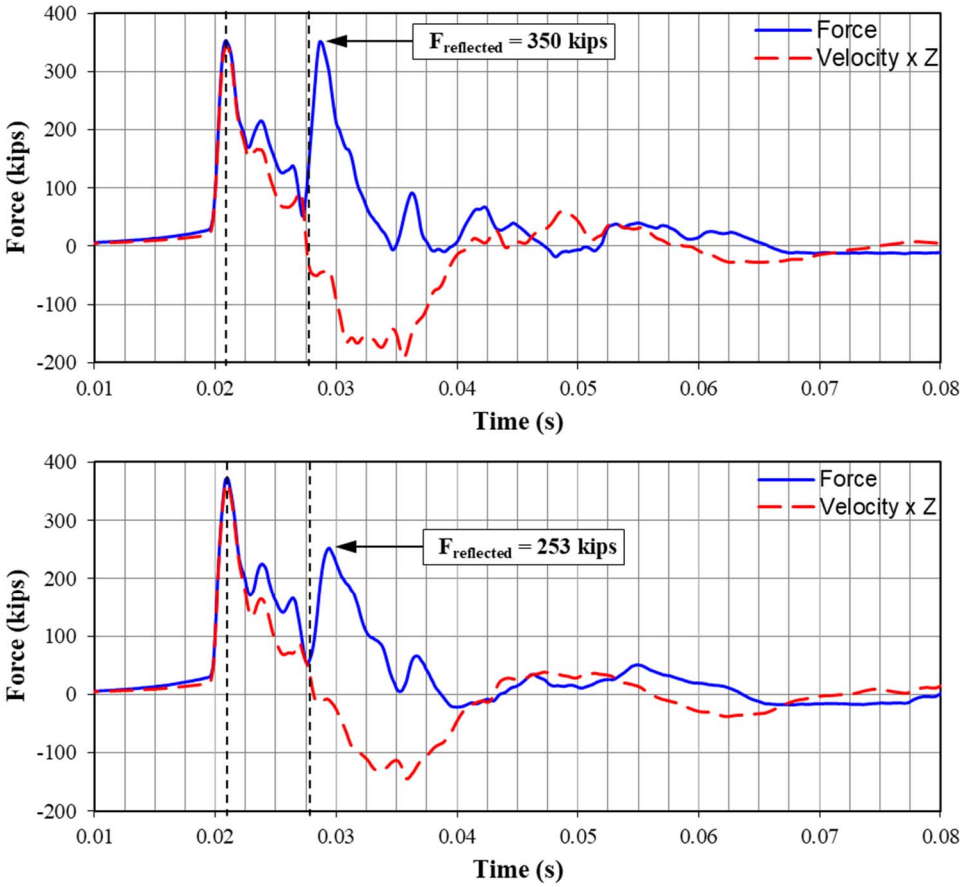


Fig. 1. Dynamic measurement data for a pile driven into a shale bedrock

The ratio of the mobilized resistance over the impact force is very useful in assessing relaxation particularly when the hammer performance often increases from blow to blow such as with a single acting diesel hammer. If the ROF ratio is the same or greater than it was at the end of driving and yet the mobilized resistance is less, this is an indication of the limited impact force mobilizing less capacity. If the ROF ratio is less at the beginning of restrike yet the impact force is equivalent or greater than it was at the end of driving, relaxation has likely occurred. However, an increase in the dynamic soil resistance between the end of driving and beginning of restrike could also be a contributing factor.

RELAXATION DATABASE

Relaxation data from 36 piles at 26 sites were compiled and reviewed. The pile types included 23 H-piles, two open-end pipe piles, five closed-end pipe piles, four prestressed concrete piles, and two prestressed concrete piles with H-pile stingers. The soil or rock materials at the pile toe included 13 cases in dense to very dense sands, one case in heavily over consolidated silty clay till, and 21 cases in weak laminated rocks. The rock cases consisted of 18 cases in shale, three cases in limestone, and one case in siltstone.

Table 1 presents a summary of the pile type and end bearing material for the 36 cases. This table includes the magnitude of the toe resistance loss as well as the percentage loss in toe resistance. The table also summarizes the restrike pile penetration required to re-obtain the geotechnical resistances equivalent to the design load, the ultimate capacity, and the signal matching determined end of initial driving capacity.

Relaxation is quantified by the decrease in capacity that occurs between the beginning of restrike and the end of initial driving. In some cases, an increase in shaft resistance may occur at the same time that a decrease in toe resistance occurs. When this happens, the soil setup will mask the full magnitude of the toe relaxation. Therefore, signal matching analysis is the best dynamic analysis method to assess the change in soil resistance and its distribution on the pile. The dynamic measurements reported in this paper were analyzed with the CAPWAP signal matching program, Rausche at al., (2010).

A key item in determination of the relaxation magnitude is selecting the appropriate hammer blow for signal matching analysis to evaluate the shaft and toe resistance. In general, the dynamic measurements acquired near the end of initial driving are similar from one blow to another. Hence, impact force and data quality are the key factors in selecting the blow for signal matching analysis. For restrike situations, the blow selected for signal matching analysis is again chosen based on the data quality, impact force, as well as the ratio of the mobilized resistance divided by the impact force, ROF. In cases where the ROF value decreases over the initial restrike blows and then increases, the blow with or close to the lowest ROF is generally the blow for signal matching analysis contingent upon data quality and impact force magnitude.

Figure 2 presents a summary of several calculated quantities from each hammer blow over the first inch of restrike. The lowest ROF ratio of 0.85 occurred for blow 2 in conjunction with a somewhat lower impact force, FT1, of 775 kips. Blow 3 had a marginally higher ROF ratio of 0.87, with an impact force of 866 kips. This impact force is also closer to the impact force at the end of initial driving of 880 kips.

Driving Status	Blow Number	Impact Force FTI (kips)	Signal Matching Capacity (kips)	Case Method Capacity (kips)	Transferred Energy EMX (ft-kips)	Hammer Stroke STK (ft)	Resistance / Force ROF (%)
EOID	125	880	963	959	57.9	8.88	1.09
BOR	1	529	- - -	445	21.9	Trip Blow	0.88
	2	775	- - -	627	46.9	7.72	0.85
	3	866	713	717	55.4	7.17	0.87
	4	872	- - -	751	57.3	8.75	0.91
	5	880	- - -	791	57.2	8.91	0.95
	6	884	- - -	808	57.5	8.97	0.96
	7	903	- - -	842	60.0	9.26	0.98
	8	911	- - -	863	60.0	9.30	1.00

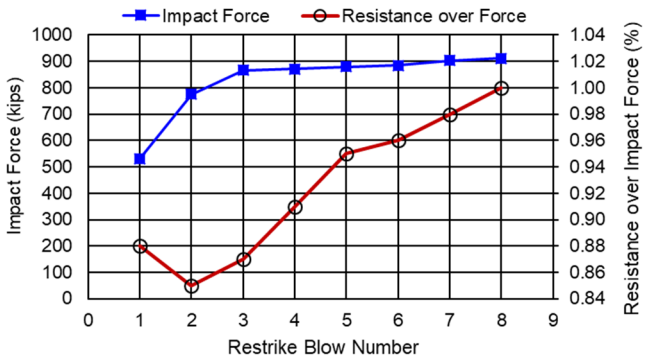


Fig. 2. Example of the restrike blow selection process for relaxation assessment

Blow 3 was therefore chosen for signal matching analysis and assessment of the relaxation magnitude. The increase in ROF ratio with subsequent blows indicates the pile was being redriven into the shale to regain the additional capacity noted for those subsequent blows. This process was used for the restrike cases in Table 1 to select the blow to analyze for the toe relaxation magnitude.

Figure 3 presents the loss in toe resistance between the end of initial driving and the beginning of restrike for the piles driven into dense granular soils. As noted in Table 1, the Unified Soil Classification System designations for the materials at the pile toe included SP, SM, SP-SM, SM-SC, and SW-SM. In all cases, these sand materials were dense to very dense with uncorrected Standard Penetration Test (SPT) resistance values ranging from 31 blows per foot with an unreported SPT hammer type to 50 blows / 0.1 inches with an automatic SPT hammer. For the 13 sand cases, the restrike toe resistance ranged from 12% to 89% of the toe resistance at the end of driving and averaged 62%. The magnitude of relaxation for the two low displacement H-piles was less than that encountered by the 11 displacement piles in the dense granular materials.

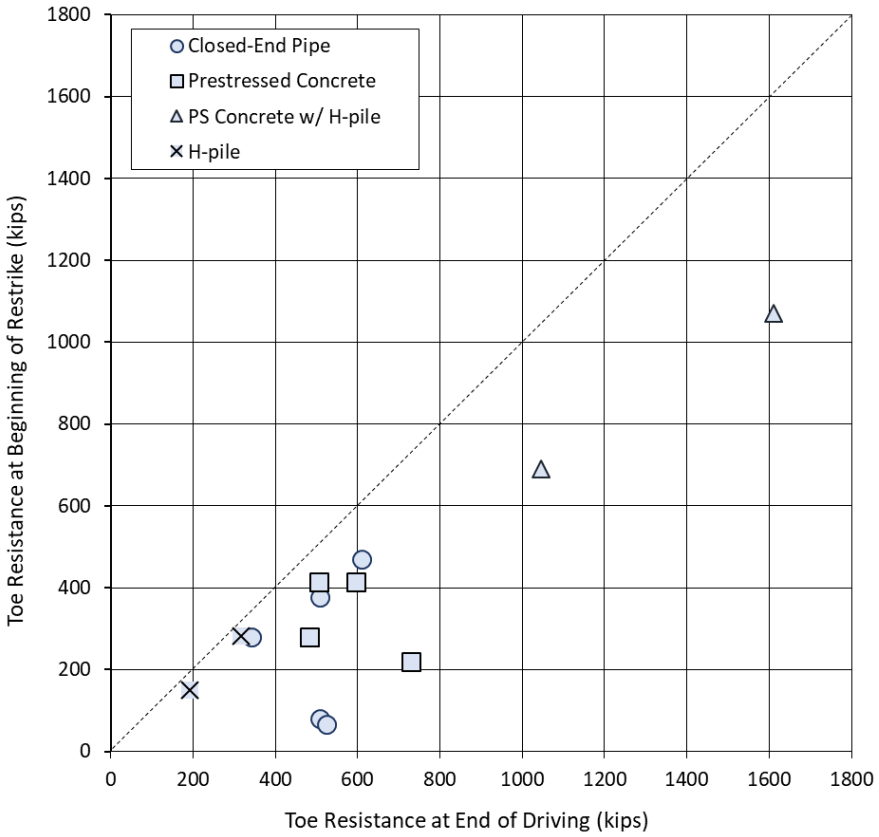


Fig. 3. Change in Toe Resistance in Sands

Table 1 includes the restrike pile penetration required to re-obtain the geotechnical resistances equivalent to the design load, the ultimate capacity, and the signal matching determined end of initial driving capacity. The pile penetration required to re-acquire these resistances was determined from the number of hammer blows applied before re-acquiring that resistance and the associated pile movement from the recorded blows per inch or fraction thereof. Piles having a restrike geotechnical resistance less than the design load would experience settlement under that applied load. Therefore, the pile penetration required to re-achieve the design load is presented solely as an indicator of the maximum potential settlement magnitude if relaxation had not been identified and addressed.

For the restrike event, 0.0 to 0.5 inches of movement was needed to re-achieve the geotechnical resistance equal to the design load with an overall average of 0.05 inches. The penetration required to regain the required ultimate capacity varied from no movement in four cases to in excess of 22 inches in three cases. One pile was driven 104 feet without achieving the ultimate capacity. Piles that required no movement to regain the ultimate capacity had initially been overdriven to satisfy minimum penetration requirements.

The loss in toe resistance between the end of driving and the beginning of restrike for piles driven into shale bedrock is presented in Figure 4. The piles in 16 of the cases were H-piles with driving shoes and in the other two cases the piles were open-end pipe piles with driving shoes. The shale material properties were characterized by either Rock Quality Designation (RQD) values or SPT resistance values. Where the shale was cored, the RQD values ranged from 0 to 90%. Many sites had an RQD of 0% so the average RQD was only 14%. Where the shale was sampled using a split-spoon sampler, uncorrected SPT resistance values ranged from 50 for 5 inches to 100 for 0.1 inches, both with an unreported SPT hammer type. For the 18 shale cases, the restrike toe resistance ranged from 27% to 82% of the toe resistance at the end of driving and averaged 65%.

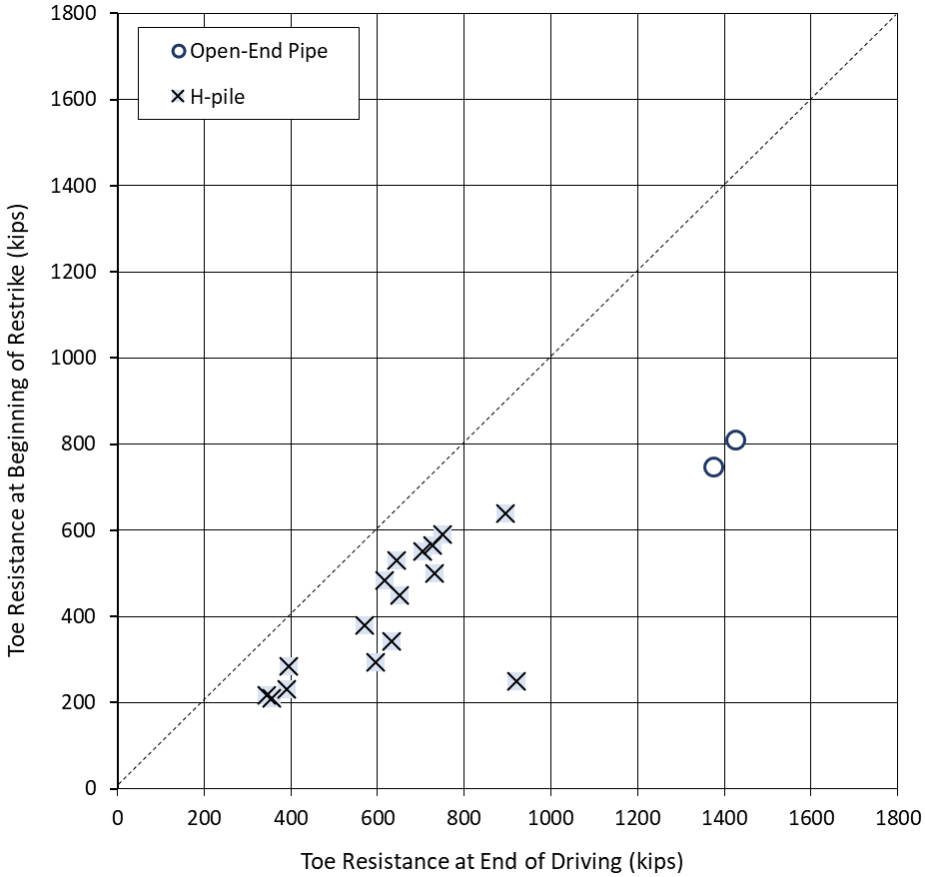


Fig. 4. Change in Toe Resistance in Shales

When piles driven into shale exhibit relaxation, a common question is whether they will relax again after being redriven. In the shale data sets presented herein, the same pile was redriven and restruck a second time in five cases, and redriven and restruck a third time in two cases. The reduction in toe resistance for the five, second restrike cases ranged from 14% to 71% and averaged 36%. The toe resistance for the two, third restrike cases ranged from 32% to 46%. The second and third restrike data is not presented in Figure 4 but it is included in Table 1.

For the first restrike event, no movement to 7.0 inches of movement was needed to re-achieve the geotechnical resistance equal to the design load with an overall average of 0.47 inches. It should be noted that 17 of the 18 cases required 0.33 inches of penetration or less to achieve the design load. To regain the ultimate capacity, no movement to 84 inches of penetration were required with five cases needing 1.3 inches or greater penetration. Piles that required no movement to regain the ultimate capacity had initially been driven to a capacity greater than the ultimate capacity because relaxation had been anticipated.

For piles subject to a second restrike, four of the five piles required no movement to re-achieve the design load with the fifth pile requiring 1.33 inches of movement. To regain the required ultimate capacity in the second restrike, 0.44 to 7.75 inches of additional pile penetration was required.

Figure 5 summarizes the loss in toe resistance between the end of driving and the beginning of restrike for piles driven in other materials including limestone, siltstone, and silty clay till. In all five cases, the pile type was an H-pile with a driving shoe. The database in these materials is too limited for further analysis. However, the change in toe resistance for the H-piles driven into the limestone and siltstone materials is not dissimilar to the shale bedrock. In the limestone cases, the rock description included the terms "severely fractured", "containing a steep fracture plane", or "containing thin shale seams". These features likely explain why a limestone bearing material which is not generally associated with relaxation problems exhibited relaxation. Heave was also not reported for this pile which, if observed, would be another reason for the reduced capacity upon restrike.

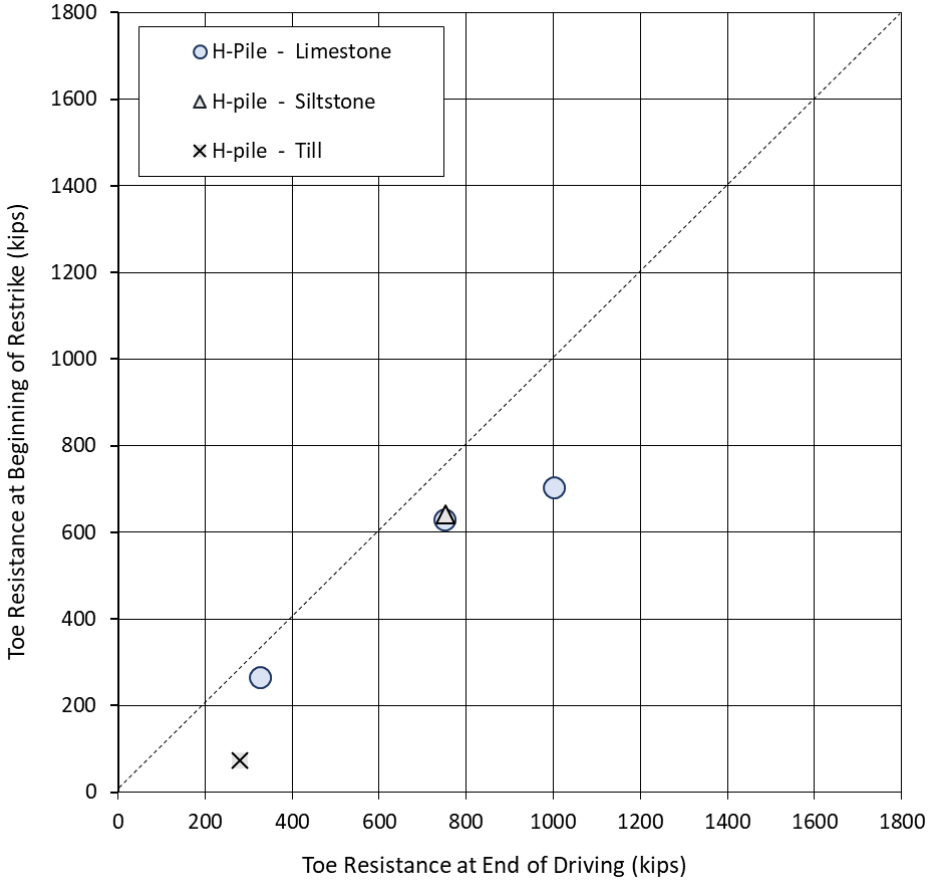


Fig. 5. Change in Toe Resistance in Limestone, Siltstone, and Silty Clay Till

RELAXATION VERSUS TIME

The change in toe resistance was also evaluated as a function of the elapsed time since initial driving with consideration of the end bearing material and pile type. Plots of the percentage toe resistance loss as a function of log time are presented in Figure 6 for sands and shale bearing materials. Only data for the initial restrike is presented in the figure. It should not be construed that long term restrikes are required in sands, as the same magnitude of relaxation would like have been apparent if the initial restrike had been performed at an earlier time. Shales however have been known to exhibit a greater magnitude of relaxation with time. Regardless, no clear trend in relaxation magnitude as a function of time is indicated by the sand or shale data other than restrike tests should be performed in materials prone to relaxation.

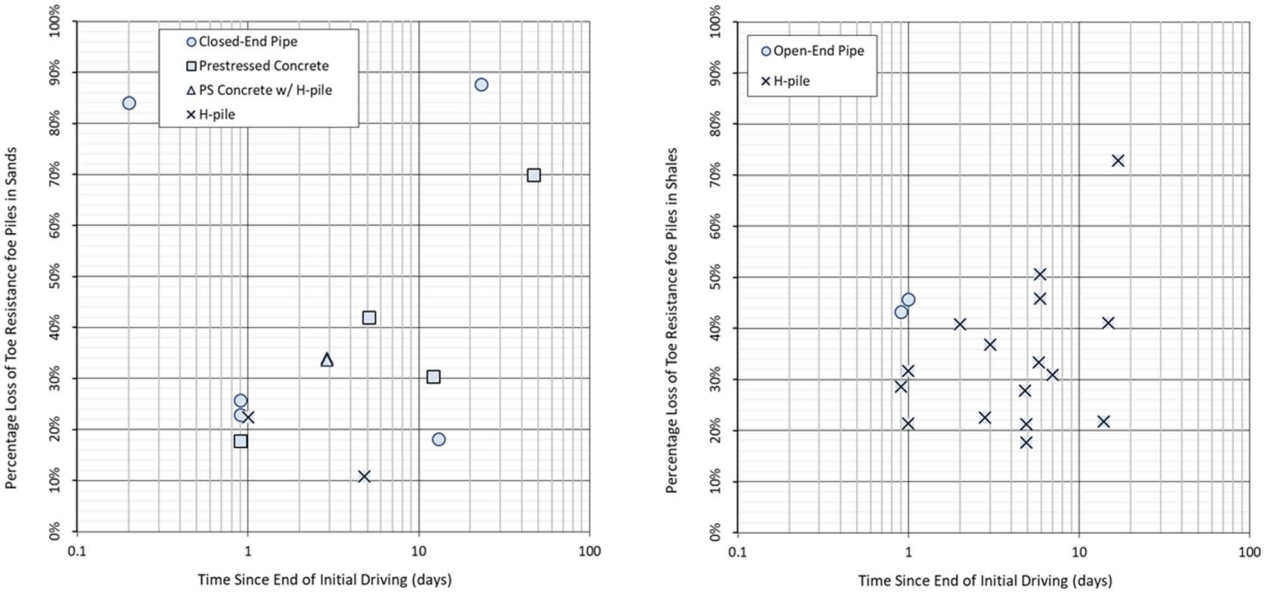


Fig. 6. Percentage Toe Resistance Loss in Sands (left) and Shales (right) Versus Time

DISCUSSION

Many of the piles in the database were driven to bedrock. In these situations, a low set per blow is often encountered at final driving and dynamic test methods can underestimate the ultimate capacity. Several potential data sets were not included in this database, such as the example data presented in Figure 1, due to high end of drive or restrike blow counts. However, a few of the end of driving cases with high final blow counts were retained (ID-7, ID-10, ID-11, and ID-18) if the restrike blow count was less than 11 blows per inch. A similarly high end of driving blow count occurred for ID-6 which was terminated in sand. In actuality, the loss in toe resistance for data sets with high final driving resistance including the above noted cases would be underestimated due to the end of initial driving toe resistance being underestimated.

In many of the cases, relaxation was anticipated based on the end bearing material and those piles were driven in excess of the required ultimate capacity to accommodate some later magnitude of relaxation. In other cases, satisfying minimum penetration requirements resulted in overdriving. For the database piles in sand, the piles were driven on average to a capacity 59% greater than the required ultimate capacity with a range of 6% to 202%. Database piles driven into rock were driven on average to a capacity 28% greater than the required ultimate capacity with a range of 2% to 86%. This may have resulted in the rock piles terminating in less weathered material.

While pile penetration into the rock is not quantified in this paper, experience has indicated that piles terminating in more weathered materials generally tend to have a greater magnitude of relaxation than pile driven deeper into less weathered material. Hence, the toe resistance loss for the rock database piles may have been greater if pile driving had been terminated at only the required ultimate capacity.

In two cases, the pile was hammer changed or the pile was concrete filled between the end of driving and beginning of restrike. This caused inconsistency in the ROF values between the end of drive and the beginning of restrike noted for ID-2, and ID-6 in Table 1.

CONCLUSIONS AND RECOMENDATIONS

Piles driven into dense to very dense sands with Unified Soil Classification System designations of SM, SP, SP-SM, SM-SC, and SW-SM can have a significant loss in toe resistance over time. The limited number of cases presented herein suggest the average magnitude of toe relaxation loss is 38% in these materials and is greater for the 11 displacement piles (33%) than for the two low-displacement H-piles (17%). Piles driven into shales had an average toe relaxation loss of 35%. The average toe resistance loss was greater for the two open-end pipe piles (44%) than for the 16 H-piles (34%). Additional data is needed for all pile types in these end bearing materials.

The data sets indicate that overdriving is beneficial to limit the detrimental effects of relaxation. Piles were overdriven to some magnitude to accommodate future relaxation in all but three of the 36 data sets. The average toe resistance loss was 32% for the overdriven pile data sets compared to an average toe resistance loss of 46% for the three data sets not overdriven. Additional data is again needed to bolster this conclusion.

Based on the data sets reviewed, driving to a capacity in excess of the required ultimate capacity is recommended when piles are terminated in relaxation prone materials. The average magnitude of toe resistance loss in sands was 244 kips or 38% of the end of initial driving toe resistance. In shales, the average magnitude of toe resistance loss was 258 kips or 35% of the end of initial driving toe resistance. For fractured limestones, the average magnitude of toe resistance loss was 160 kips or 22% of the end of initial driving toe resistance, and for the one case in siltstone, the magnitude of toe resistance loss was 114 kips or 14% of the end of initial driving toe resistance. All of these relaxation magnitudes are based on the pile sizes noted in Table 1.

Pile designs and wave equation drivability analyses should consider the potential magnitude of relaxation and the pile-hammer system be designed accordingly. Depending on the end bearing material and pile type, most of the data presented herein suggests that driving to an ultimate capacity that includes a 20 to 45% loss in toe resistance would compensate for the relaxation magnitude in 83% of the database cases. However, the database indicates a greater loss in toe resistance in six cases. Therefore, restrike dynamic load tests with signal matching analysis or static load tests should also be performed to quantify relaxation magnitudes on site specific materials and pile types where relaxation is a design concern.

REFERNCES

Herrera, R. (2015) Relaxation of Driven Pile Resistance in Granular Soils, PowerPoint Presentation, Geotechnical and Materials Engineers Committee Conference, Cocoa Beach, Florida.

Miller, R.M. (1937). Soil Reactions in Relation to Foundations on Piles, Proceedings of the American Society of Civil Engineers, New York, NY; pp 1057-1080.

Morgano, C.M. and White, B.A. (2004) Identifying Soil Relaxation from Dynamic Testing. Proceedings of the Seventh International Conference on the Application of Stress Wave Theory to Piles, The Institution of Engineers Malaysia; pp 415-421.

Parsons J.D. (1966). Piling Difficulties in the New York Area. American Society of Civil Engineers, Journal of the Soil Mechanics and Foundation Division, Vol. 92, No. SM1, New York, NY; pp 43-64.

Rausche, F., Likins, G.E., Liang, L., Hussein, M.H. (2010). Static and Dynamic Models for CAPWAP Signal Matching. The Art of Foundation Engineering Practice, Geotechnical Special Publication No. 198, American Society of Civil Engineers, Reston, VA; pp 534-553.

Thompson, C.D. and Thompson, D.E. (1985). and Apparent Relaxation of Driven Piles. American Society of Civil Engineers, Journal of Geotechnical Engineering, Vol. 111, No. 2, New York, NY; pp 225-237.

Yang, N.C. (1956). Redriving Characteristics of Piles. Proceedings of the American Society of Civil Engineers, Vol 82., No. SM3. New York, NY.

York, D.L., Brusey, W.G., Clémente, F.M., and Law, S.K. (1994). Setup and Relaxation in Glacial Sand. American Society of Civil Engineers, Journal of Geotechnical Engineering, Vol. 120, No. 9, New York, NY; pp 1498-1513.

Table 1. Summary of Pile Type, Bearing Material, and Resistance

Case ID	Pile Type	Boring Distance to Pile	Toe Bearing Material Description	Toe Bearing Material Classification	Toe Bearing Material Strength	Design Load or *Factored Load*	Ultimate Capacity or *Nominal Resistance*	Test Status	Pen	Time Since EOID	Reported Blows per Inch	Impact Force	Blow No. to EOID or From BOR	Signal Matching Analysis (SM) Total Capacity	Shaft Resistance	Toe Resistance	Total Capacity / Impact Force	Signal Matching Toe Resistance Loss		Signal Matching Total Resistance Loss		Penetration Required to Regain Prior SM Capacity	Design Load	Ultimate Capacity
		(ft)				(kips)	(kips)		(ft)	(days)		(kips)		(kips)	(kips)	(kips)	(%)	(kips)	(%)	(kips)	(%)	(in)	(in)	(in)
1	14 in O.D. x 0.50 in CEP	10	M Dense to V Dense Fine Sand, Trace Silt	SP, SP-SM	N=40[a]	TBD	TBD	EOID	64.7	- - -	3	747	4	644	137	507	0.86	- - -	- - -	- - -	- - -	- - -	- - -	- - -
						"	"	BOR	64.7	0.2	1	580	2	211	130	81	0.36	426	84%	433	67%	> 841 in	n.a.	n.a.
2	14 in O.D. x 0.50 in CEP	44	M Dense to V Dense Fine Sand, Trace Silt	SP, SP-SM	N=79[s]	TBD	TBD	EOID	65.7	- - -	3	747	2	737	212	525	0.99	- - -	- - -	- - -	- - -	- - -	- - -	- - -
						"	"	BOR	65.7	23.1	4	334*	2	425	360	65	1.27	460	88%	312	42%	n.a.	n.a.	n.a.
3	HP 12x53 w/shoe	50	V Dense Sand and Gravel with Cobbles	- - -	N=50/5 in[u]	*270*	*386*	EOID	53.3	- - -	4	446	5	447	131	316	1.00	- - -	- - -	- - -	- - -	- - -	- - -	- - -
						"	"	BOR	53.3	4.8	3	432	4	350	68	282	0.81	34	11%	97	22%	> 1244 in	None	> 1244 in
4	14 in O.D. x 0.375 in CEP	135	Medium Dense Sand	SP-SM	N=31[u]	180	360	EOID	25.1	- - -	3	654	4	568	60	508	0.87	- - -	- - -	- - -	- - -	- - -	- - -	- - -
						"	"	BOR	25.1	0.9	4	614	3	504	127	377	0.82	131	26%	64	11%	6 in	None	0.25 in
5	HP 12 x74 w/shoe	16	Loam (Sandy Silty Clay)	CL-ML	N=87/11 in[u]	*265*	*379*	EOID	34.0	- - -	2	738	4	493	214	279	0.67	- - -	- - -	- - -	- - -	- - -	- - -	- - -
						"	"	BOR	34.0	2.9	3	646	3	350	276	74	0.54	205	73%	143	29%	> 6 in	None	5.5 in
6	14 in O.D. x 0.375 in CEP	unknown	M Dense to V Dense Sand	SM	N=75/10 in[u]	180	360	EOID	30.6	- - -	15	604	5	458	117	341	0.76	- - -	- - -	- - -	- - -	- - -	- - -	- - -
								BOR	30.6	13.0	11	204*	10	402	123	279	1.97	62	18%	56	12%	n.a.	n.a.	n.a.
7	HP 12x53 w/shoe	unknown	Gray Shale	Shale	No RQD	160	320	EOID	30.1	- - -	28	360	4	388	33	355	1.08	- - -	- - -	- - -	- - -	- - -	- - -	- - -
						"	"	BOR	30.1	2.0	8	373	2	271	61	210	0.73	145	41%	117	30%	1.25 in	0.25 in	0.50 in
8	HP 14x117	unknown	Shale	Shale	No RQD	744	1488	EOID	30.1	- - -	7	1490	3	1140	220	920	0.77	- - -	- - -	- - -	- - -	- - -	- - -	- - -
						"	"	BOR #1	30.1	16.9	3	1165	3	503	253	250	0.43	670	73%	637	56%	85 in	7.0 in	84 in
						"	"	EOR #1	37.2	- - -	9	1463	4	1335	335	1000	0.91	- - -	- - -	- - -	- - -	- - -		- - -
8	HP 14x117	unknown	Shale	Shale	No RQD	744	1488	BOR #2	37.2	37.7	3	1204	2	635	347	288	0.53	712	71%	700	52%	9 in	1.33 in	7.75 in
						"	"	EOR #2	37.95	- - -	14	1446	2	1530	400	1130	1.06	- - -	- - -	- - -	- - -	9 in	1.33 in	7.75 in
9	HP 12x63 w/shoe	unknown	Red Shale	Shale	No RQD	200	400	EOID	22.6	- - -	13	383	1	600	210	390	1.57	- - -	- - -	- - -	- - -	- - -	- - -	- - -
						"	"	BOR	22.6	14.8	6	361	3	470	240	230	1.30	160	41%	130	22%	3.3 in	None	0.33 in
10	HP 14x89 w/shoe	60	Weathered Gray Shale, broken, wthrd joints	Shale	RQD = 0	450	900	EOID	81.2	- - -	13	880	4	963	67	896	1.09	- - -	- - -	- - -	- - -	- - -	- - -	- - -
						"	"	BOR #1	81.2	0.9	8	867	3	713	73	640	0.82	256	29%	250	26%	1.8 in	0.25 in	1.3 in
10	HP 14x89 w/shoe	60	Weathered Gray Shale, broken, wthrd joints	Shale	RQD = 0	450	900	EOR #1	81.5	- - -	20	860	2	855	75	780	0.99	- - -	- - -	- - -	- - -	- - -	- - -	- - -
						"	"	BOR #2	81.5	13.7	10	893	2	754	94	660	0.84	120	15%	101	12%	0.75 in	None	0.80 in
11	HP 14x89 w/shoe	120	Highly Weathered and Broken Gray Shale	Shale	RQD = 35	450	900	EOID	95.33	- - -	28	880	2	819	87	732	0.93	- - -	- - -	- - -	- - -	- - -	- - -	- - -
						"	"	BOR #1	95.33	1.0	11	796	4	668	168	500	0.84	232	32%	151	18%	1.8 in	0.27 in	2.1 in
11	HP 14x89 w/shoe	120	Highly Weathered and Broken Gray Shale	Shale	RQD = 35	450	900	EOR #1	95.58	- - -	23	821	1	910	190	720	1.11	- - -	- - -	- - -	- - -	- - -	- - -	- - -
						"	"	BOR #2	95.58	13.2	43 / .5	795	2	805	185	620	1.01	100	14%	105	12%	0.18 in.	None	1.1 in
12	24 in x 0.5 in OEP w/shoe	65	Thickly Bedded, Weathered Sound Gray Shale	Shale	RQD = 90	600	1200	EOID	100.25	- - -	9	1289	4	1522	95	1427	1.18	- - -	- - -	- - -	- - -	- - -	- - -	- - -
						"	"	BOR #1	100.25	0.9	6	1267	2	958	148	810	0.76	617	43%	564	37%	> 2 in	0.17 in	0.67 in
12	24 in x 0.5 in OEP w/shoe	65	Thickly Bedded, Weathered to Sound Gray Shale	Shale	RQD = 90	600	1200	EOR #1	100.41	0.9	14	1367	4	1445	125	1320	1.06	- - -	- - -	- - -	- - -	- - -	- - -	- - -
						"	"	BOR #2	100.41	13.1	16	1277	1	804	331	473	0.63	847	64%	641	44%	1.25 in	None	0.69 in
12	24 in x 0.5 in OEP w/shoe	65	Thickly Bedded, Weathered to Sound Gray Shale	Shale	RQD = 90	600	1200	EOR #2	100.54	13.1	10 / 0.5	1373	2	1511	191	1320	1.10	- - -	- - -	- - -	- - -	- - -	- - -	- - -
						"	"	BOR #3	100.54	23.9	6	1296	1	911	291	620	0.70	700	53%	600	40%	> 1 in	None	0.67 in
13	24 in x 0.5 in OEP w/shoe	40	Weathered Gray Shale, Broken, Weathered Joints	Shale	RQD = 0	600	1200	EOID	88.66	- - -	9	1326	2	1456	81	1375	1.10	- - -	- - -	- - -	- - -	- - -	- - -	- - -
						"	"	BOR #1	88.66	1.0	6	1113	2	877	131	746	0.79	629	46%	579	40%	> 6 in	0.33 in	3.2 in
13	24 in x 0.5 in OEP w/shoe	40	Weathered Gray Shale, Broken, Weathered Joints	Shale	RQD = 0	600	1200	EOR #1	89.16	- - -	9	1287	2	1265	125	1140	0.98	- - -	- - -	- - -	- - -	- - -	- - -	- - -
						"	"	BOR #2	89.16	13.1	9	1411	2	1123	153	970	0.80	170	15%	142	11%	0.67 in	None	0.44 in
13	24 in x 0.5 in OEP w/shoe	40	Weathered Gray Shale, Broken, Weathered Joints	Shale	RQD = 0	600	1200	EOR #2	89.33	- - -	9	1410	5	1416	166	1250	1.00	- - -	- - -	- - -	- - -	- - -	- - -	- - -
						"	"	BOR #3	89.33	24.1	7	1323	1	1044	194	850	0.79	400	32%	372	26%	> 3 in	None	0.71 in
14	HP 12 x 63 w/shoe	66	Moderately Weathered Gray Shale, Thinly Bedded	Shale	RQD = 0	*300*	*430*	EOID	15.2	- - -	8	579	1	662	67	595	1.14	- - -	- - -	- - -	- - -	- - -	- - -	- - -
						"	*Rndr = 505*	BOR #1	15.2	5.9	9	479	1	365	71	294	0.76	301	51%	297	45%	> 4 in	None	0.55 in
						"	"	BOR #1	15.2	5.9	9	540	4	525	63	462	0.97	133	22%	137	21%	> 4 in	None	0.55 in

Notes: EOID = End of Intital Driving, BOR = Beginning of Restrike, TBD = To Be Determined, a = automatic SPT hammer, s = SPT safety hammer, u = unreported SPT hammer type, Pen = embedded depth in ground, * = concrete filled pipe

Table 1. Summary of Pile Type, Bearing Material, and Resistance (continued)

Case ID	Pile Type	Boring Distance to Pile (ft)	Toe Bearing Material Description	Toe Bearing Material Classification	Toe Bearing Material Strength	Design Load or *Factored Load* (kips)	Ultimate Capacity or *Nominal Resistance* (kips)	Test Status	Pen (ft)	Time Since EOID (days)	Reported Blows per Inch	Impact Force (kips)	Blow No. to EOID or From BOR	Signal Matching Analysis (SM) Total Capacity (kips)	Shaft Resistance (kips)	Toe Resistance (kips)	Total Capacity / Impact Force (%)	Signal Matching Toe Resistance Loss (kips)	(%)	Signal Matching Total Resistance Loss (kips)	(%)	Penetration Required to Regain Prior SM Capacity (in)	Design Load (in)	Ultimate Capacity (in)
15	HP 12 x 63 w/shoe	54	Moderately Weathered	Shale	RQD = 0	*300*	*430*	EOID	20.2	- - -	8	582	2	665	33	632	1.14	- - -	- - -	- - -	- - -	- - -	- - -	- - -
			Gray Shale, Thinly Bedded			"	*Rndr = 520*	BOR #1	20.2	5.9	9	481	1	407	65	342	0.85	290	46%	258	39%	1.7 in	None	0.46 in
						"	"	BOR #1	20.2	5.9	9	528	4	520	53	467	0.98	165	26%	145	22%	1.7 in	None	0.46 in
16	HP 12 x 63 w/shoe	47	Dark Gray, Slightly	Shale	RQD = 0	*295*	*425*	EOID	13.8	- - -	11	547	3	664	94	570	1.21	- - -	- - -	- - -	- - -	- - -	- - -	- - -
			Weathered Shale			"	*Rndr = 500*	BOR #1	13.8	5.8	6	483	2	474	94	380	0.98	190	33%	190	29%	5.2 in	None	0.50 in
17	HP 12 x 63 w/shoe	67	Dark Gray, Slightly	Shale	RQD = 0	*295*	*425*	EOID	17.0	- - -	12	614	3	725	75	650	1.18	- - -	- - -	- - -	- - -	- - -	- - -	- - -
			Weathered Shale			"	*Rndr = 500*	BOR #1	17.0	7.0	9	563	2	560	111	449	0.99	201	31%	165	23%	> 4 in	None	0.22 in
18	HP 14 x 73 w/shoe	75	Severly Fractured	Limestone	No RQD	*425*	*703*	EOID	42.5	- - -	15	732	2	853	103	750	1.17	- - -	- - -	- - -	- - -	- - -	- - -	- - -
			Light Gray Limestone			"	*Rndr = 751*	BOR #1	42.5	1.0	10	738	2	738	108	630	1.00	120	16%	115	13%	> 2 in	None	0.20 in
19	HP 12 x 74 w/shoe	25	Highly Weathered	Shale	No RQD	*284*	*472*	EOID	54.0	- - -	6	785	3	712	96	616	0.91	- - -	- - -	- - -	- - -	- - -	- - -	- - -
			Gray Shale			"	*Rndr = 505*	BOR #1	54.0	1.0	5	850	3	591	107	484	0.70	132	21%	121	17%	> 6 in	None	0.40 in
20	HP 12 x 53 w/shoe	32	Highly Weathered	Shale	√=100/0.10 in	*134*	*191*	EOID	37.6	- - -	10	404	3	409	64	345	1.01	- - -	- - -	- - -	- - -	- - -	- - -	- - -
			Black Shale			"	*Rndr = 266*	BOR #1	37.6	3.0	6	401	2	316	98	218	0.79	127	37%	93	23%	6.1 in	None	None
21	HP 12 x 84 w/shoe	46	Weathered Hard Black Shale,	Shale	RQD = 0	*307*	*439*	EOID	22.8	- - -	7	838	1	743	40	703	0.89	- - -	- - -	- - -	- - -	- - -	- - -	- - -
			Thinly Bedded			"	*Rndr = 539*	BOR #1	22.8	13.9	7	733	2	597	47	550	0.81	153	22%	146	20%	4.4 in	None	0.28 in
22	HP 12 x 84 w/shoe	11	Weathered Black Shale	Shale	N=50/3 in[a]	*307*	*439*	EOID	22.6	- - -	10	831	3	795	45	750	0.96	- - -	- - -	- - -	- - -	- - -	- - -	- - -
						"	*Rndr = 539*	BOR #1	22.6	4.9	6	885	2	635	45	590	0.72	160	21%	160	20%	1.2 in	None	0.28 in
23	HP 14 x 89 w/shoe	42	Weathered Interbedded	Shale	- - -	*410*	*586*	EOID	71.0	- - -	8	964	4	660	265	395	0.68	- - -	- - -	- - -	- - -	- - -	- - -	- - -
			Sandstone and Shale			"	*Rndr = 686*	BOR #1	71.0	4.8	8	852	4	560	275	285	0.66	110	28%	100	15%	0.75 in	0.25 in	> 6.0 in
24	24 in. PS Concrete	13	Very Dense Clayey	SP-SC	N=48[s]	*280*	*374*	EOID	38.0	- - -	10	787	3	658	176	482	0.84	- - -	- - -	- - -	- - -	- - -	- - -	- - -
			Fine Sand			"	"	BOR #1	38.0	5.1	5	1051	1	460	180	280	0.44	202	42%	198	30%	> 3.75 in	None	None
25	18 in. PS Concrete	33	V Dense Fine Sand to	SP, SP-SM	N=52[a]	*200*	*268*	EOID	26.0	- - -	10	1056	3	810	214	596	0.77	- - -	- - -	- - -	- - -	- - -	- - -	- - -
			Fine Sand with Silt			"	"	BOR #1	26.0	12.1	10 / 1.5	1159	2	660	245	415	0.57	181	30%	150	19%	> 1.5 in	None	None
26	18 in. PS Concrete	57	V Dense Fine Sand to	SP, SP-SM	N=35[a]	*340*	*454*	EOID	33.0	- - -	7	992	3	640	135	505	0.65	- - -	- - -	- - -	- - -	- - -	- - -	- - -
			Fine Sand with Silt			"	"	BOR #1	33.0	0.9	4	1383	2	586	171	415	0.42	90	18%	54	8%	> 1.75 in	None	None
27	24 in. PS Concrete	8	V Dense, Light Gray,	SP	N=56[s]	*320*	*428*	EOID	32.0	- - -	20	1259	2	935	205	730	0.74	- - -	- - -	- - -	- - -	- - -	- - -	- - -
			Fine Sand with Trace Clay			"	"	BOR #1	32.0	47.0	3	1317	2	420	200	220	0.32	510	70%	515	55%	> 3.25 in	None	1.6 in.
28	HP 14 x 73 w/shoe	45	Hard Limestone with	Limestone	N=50/1 in[a]	220	480	EOID	33.0	- - -	7	672	2	490	163	327	0.73	- - -	- - -	- - -	- - -	- - -	- - -	- - -
			Thin Shale Seams			"	"	BOR #1	33.0	2.8	3	816	2	425	160	265	0.52	62	19%	65	13%	8.3 in	None	8.3 in.
29	HP 14 x 84 w/shoe	13	Weathered Gray Siltstone	Siltstone	N=50/1 in[a]	*435*	*622*	EOID	26.4	- - -	6	902	3	799	45	754	0.89	- - -	- - -	- - -	- - -	- - -	- - -	- - -
						"	*Rndr = 722*	BOR #1	26.4	3.8	5	841	3	686	46	640	0.82	114	15%	113	14%	6.5 in	0.40 in	1.2 in
30	HP 14x89 w/shoe	108	Severely Weathered	Shale	N=50/5 in[u]	280	644	EOID	80.8	- - -	8	921	7	818	90	728	0.89	- - -	- - -	- - -	- - -	- - -	- - -	- - -
			Gray Shale			"	"	BOR #1	80.8	2.8	6	926	2	666	102	564	0.72	164	23%	152	19%	> 7.0 in	None	0.17 in
31	HP 12x74 w/shoe	5	Hard, Gray, Sandy Loam Till	SC-SM	N=50/4 in[a]	280	370	EOID	101.0	- - -	6	743	2	415	223	192	0.56	- - -	- - -	- - -	- - -	- - -	- - -	- - -
			with Gravel			"	"	BOR #1	101.0	1.0	4	842	2	385	236	149	0.46	43	22%	30	7%	> 4 in	None	0.50 in
32	HP 12x84 w/shoe	6	Weathered Gray Shale	Shale	N=50/1 in[a]	*210*	*364*	EOID	26.0	- - -	10	979	3	831	187	644	0.85	- - -	- - -	- - -	- - -	- - -	- - -	- - -
						"	*Rndr = 446*	BOR #1	26.0	4.9	10	944	4	727	197	530	0.77	114	18%	104	13%	> 2 in	None	None
33	HP 14x89 w/shoe	8	Hly Wthrd Soft Limestone	Limestone	N=50/5 in[a]	*435*	*625*	EOID	36.5	- - -	10	1036	3	1067	67	1000	1.03	- - -	- - -	- - -	- - -	- - -	- - -	- - -
			w/Steep Fracture Plane			"	"	BOR #1	36.5	1.0	8	908	4	782	79	703	0.86	297	30%	285	27%	> 2 in	None	0.12 in
34	16 in x 0.5 in CEP	6	V Dense Gravelly Sand	SM	N=50/0 in[a]	*318*	*454*	EOID	16.0	- - -	9	840	2	661	51	610	0.79	- - -	- - -	- - -	- - -	- - -	- - -	- - -
			with Cobbles			"	"	BOR #1	16.0	0.9	8	796	3	550	80	470	0.69	140	23%	111	17%	> 4 in	None	0.25 in
35	24 in PSC, HP12x53 Toe	55	V Dense, CMF Sand,	SW-SM	N=86[a]	500	1000	EOID	47.6	- - -	4	1830	2	1110	65	1045	0.61	- - -	- - -	- - -	- - -	- - -	- - -	- - -
			Little Gravel, Trace Silt			"	"	BOR #1	47.6	2.9	4	2133	4	875	185	690	0.41	355	34%	235	21%	> 299 in	0.5 in	> 299 in
36	24 in PSC, HP12x53 Toe	141	V Dense, CMF Sand,	SW-SM	N=74[a]	850	1700	EOID	57.8	- - -	11	2029	8	1800	190	1610	0.89	- - -	- - -	- - -	- - -	- - -	- - -	- - -
			Trace Silt			"	"	BOR #1	57.8	2.9	4	2897	5	1490	420	1070	0.51	540	34%	310	17%	> 22.8 in	None	22.5 in

Notes: EOID = End of Intital Driving, BOR = Beginning of Restrike, TBD = To Be Determined, a = automatic SPT hammer, s = SPT safety hammer, u = unreported SPT hammer type, Pen = embedded depth in ground, * = concrete filled pipe

INFERENCE IN THE DETECTION OF PILE INTEGRITY DEFECTS USING CURRENT QUALITY CONTROL METHODS

M. Ansriou, Franki Foundations Belgium, Saintes, Belgium, mohamed.ansriou@ffgb.be
T. Wulleman, Franki Foundations Belgium, Saintes, Belgium, thomas.wulleman@ffgb.be

ABSTRACT

Integrity testing is a primary quality control check on a product that is for the most part not accessible to visual examination. Their cost can be expensive when using direct methods of inspection (like coring a pile) or more economical when using indirect methods (e.g. acoustic testing). All indirect methods operate by "inference" which means that they do not directly measure the defect of integrity. Indirect methods measure the variation of physical values (temperature, impedance, speed, ect.) correlated to the integrity of the pile allowing the detection of integrity defects, although these methods do not allow for the characterization of the defect.

Keywords: geotechnics, piles, quality control, anomalies, performance.

1. INTRODUCTION

Cast-in-place piles are particularly prone to integrity defects. The reasons for this are multiple, including lack of high quality of contractor workmanship, experience and supervision necessary in construction, variable soil and groundwater conditions on site, etc. Furthermore, visual inspection of the finalized pile is usually impossible. Therefore, special care has to be taken both during the execution process and during the subsequent quality control campaign to detect any defects of executed piles.

Today, a lot of methods do exist to assess pile integrity. It is thus essential to understand the mechanism governing those devices to both make an engineering choice of the pile integrity testing method and to interpret correctly the provided results.

2. QUALITY IN PILE FOUNDATIONS

2.1 Pile anomalies

A pile having an anomaly is a pile which has a different behavior from what is normally expected. The presence of a pile anomaly does not necessarily imply that a pile cannot be used for its intended purpose (Gordon & Chapman 2004). An anomaly can be considered as a defect, or a "performance" depending on the ability of the pile to fulfil the following three criteria (3C):

C1 - Meet the Service Limit State (SLS) requirement and support the proposed working load without settling more than admissible by the superstructure ;
C2 - Meet the Ultimate Limit State (ULS) requirement and carry a specified load with an adequate factor of safety against failure ;
C3 - Remain durable throughout the design life of the structure such that the pile is not affected by time dependent activities (chemical attack, corrosion of steel reinforcement, ect.), which would jeopardize its ability to maintain its compliance with the first two criteria.

The non-compliance of the first two conditions induces inadequate performance of the pile where non-compliance of the third condition implies inadequate pile integrity (Fig. 1).

© 2019 Deep Foundations Institute

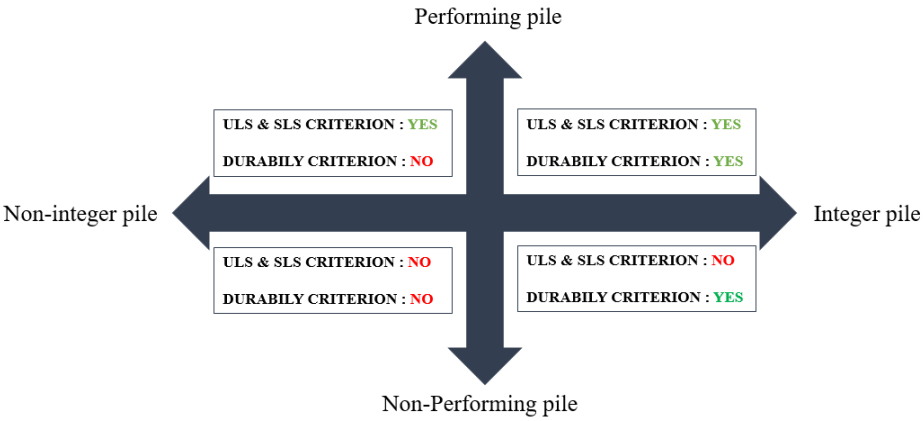


Figure 1 – Integrity and performance of piles

2.2 Evaluation of pile integrity and pile performance

A clear difference has to be made between the evaluation of pile integrity and the evaluation of pile performance. Indeed, those aspects are often confused in the piling industry. Pile integrity evaluation is measuring, through inspection tests the pile geometry, its length and material homogeneity while pile performance evaluation is evaluating the capacity of the pile to withstand its SLS & ULS loads. A pile may be unsuitable because of its lack of integrity while having superior performance. Therefore the measurement of the pile integrity does not always reflect the pile performance. We define the notion of "integer pile" as the ability of a pile to fulfil its geometry, length and material criteria. In the same way, a non-integer pile is pile which do not conform to one of the three above mentioned criterion.

Knowing this, two kinds of quality control measurements can be differentiated : integrity tests and performance tests. Integrity tests can be further subdivided into two types: direct methods and indirect methods. The difference between the two is related to the method of assessing the integrity defect. Indirect methods utilize inference which means that they do not directly measure the defect of integrity. Instead, they measure the variation of physical values (temperature, impedance, speed, etc.) correlated to the integrity of the pile. Direct methods (such as coring) extract a sample of the pile allowing direct examination. At the same time, there are two types of performance tests: destructive and non-destructive test. The non-destructive performance tests allow the reutilization of the pile after testing while the destructive pile tests result in the geotechnical and/or structural rupture of the test pile without any possibility for further use as a bearing pile, see Fig. 2.

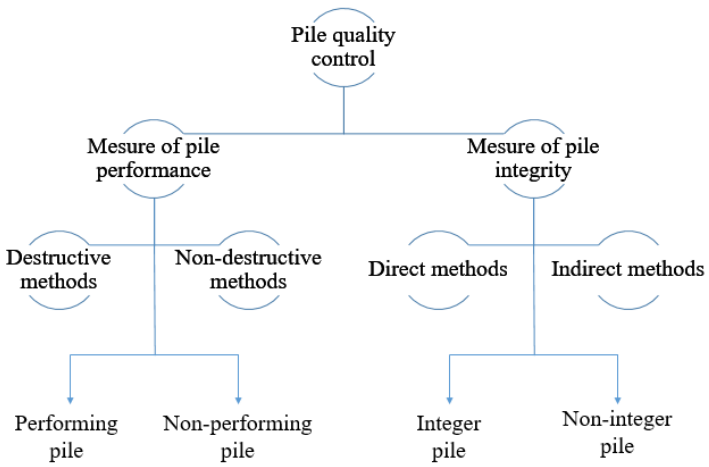


Figure 2. Classification of quality control methods

3. PILE DEFECT CLASSIFICATION

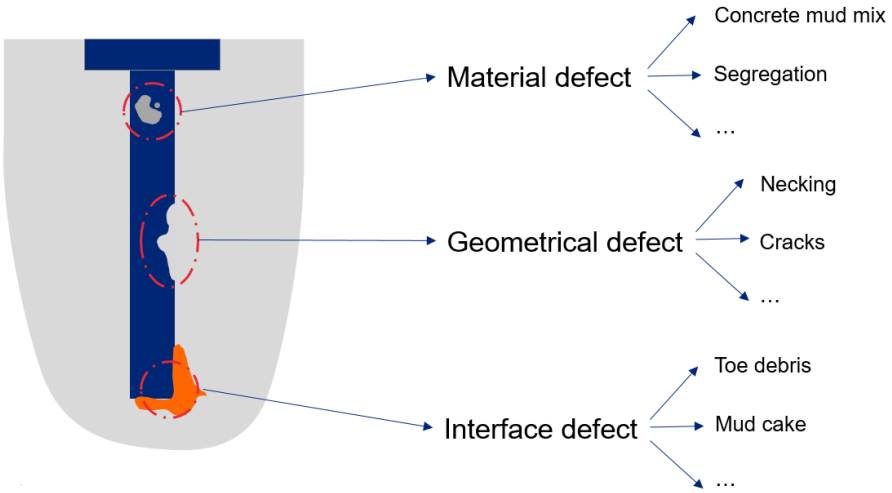


Figure 3. Pile integrity defect classification

Pile defects can be categorized into three types : material, geometrical and interface defects. Material defects are related to weakening the concrete due to various causes such as concrete-mud mix, concrete washout, gravel nests, etc. Geometrical defects are related to deviation from the standard pile geometry along its length (cracks, necking, ect.). Interface defects refer to disruption in the pile/surrounding soil contact area (toe debris, mud cake, ect.) see Fig. 3.

Material and geometrical defects affect the pile integrity whereas interface defects affect the pile performance.

4. QUALITY CONTROL METHODS IN PILE FOUNDATIONS

4.1 Sonic Integrity Testing - SIT

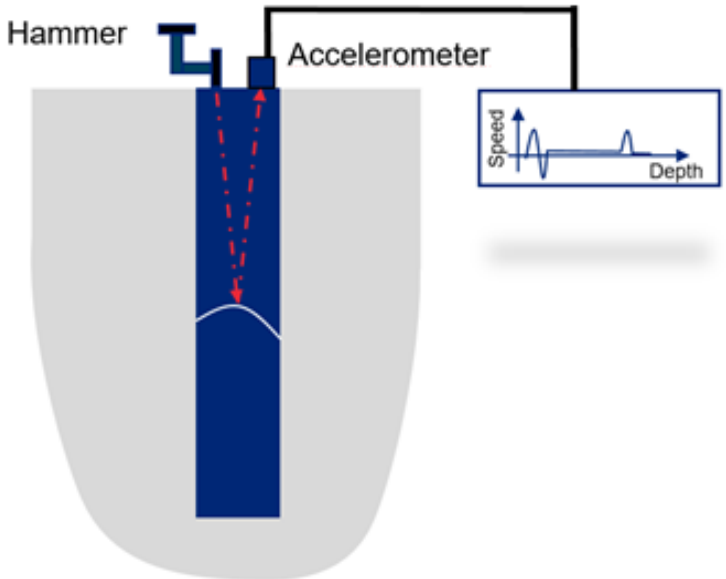


Figure 4. Sonic Integrity Testing

4.1.1 Test principle

A mechanical wave is generated in the pile with a hammer blow. The wave will be reflected if it either, meets a variation of impedance Z or travels to the base of the pile and is reflected. The returning waves travel back to the pile head and are picked up by an accelerometer, see Fig. 4. Impedance variation can be due to :

- Area variation (cracks, necking, etc.) ;
- Young's modulus variation ;
- Density variation ;
- Pile tip ;
- Soil friction

$$Z = A\sqrt{E\rho}$$

A : cross section

E : Young modulus

ρ : density

4.1.2 Test results and interpretation

To interpret results of SIT, it is first of all necessary to identify the soil signature by comparing the signals with the soil data. Then the interpretation of an individual signal with respect to the soil signature can be conducted. Increasing of the medium impedance (higher cross section, higher Young's modulus, etc.) creates a change in velocity of opposite sign compared to the input. Reduction of the medium impedance creates a reflection causing a change in velocity of the same sign as the input.

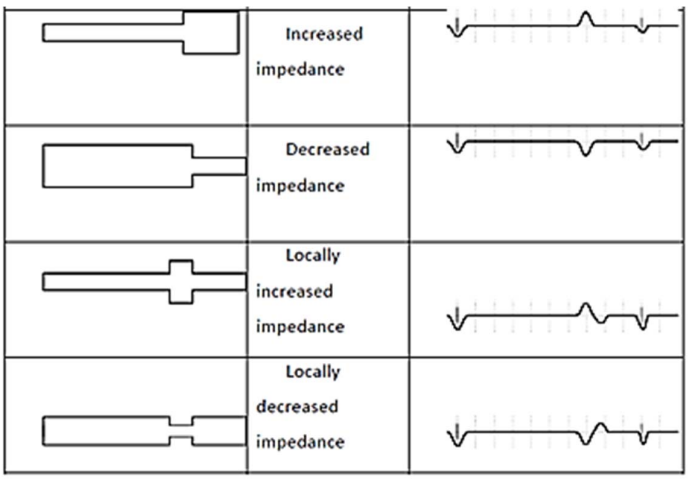


Figure 5. Signal results depending on the pile profile (Amir, 2012)

Results of SIT are presented in the time domain as shown in Fig. 5 or in the frequency domain as shown in Fig. 6. The collected pile response data used in both methods of presentation is identical. To eliminate the hammer/pile blow response from the plot, it is necessary to record additionally the hammer force in the frequency domain.

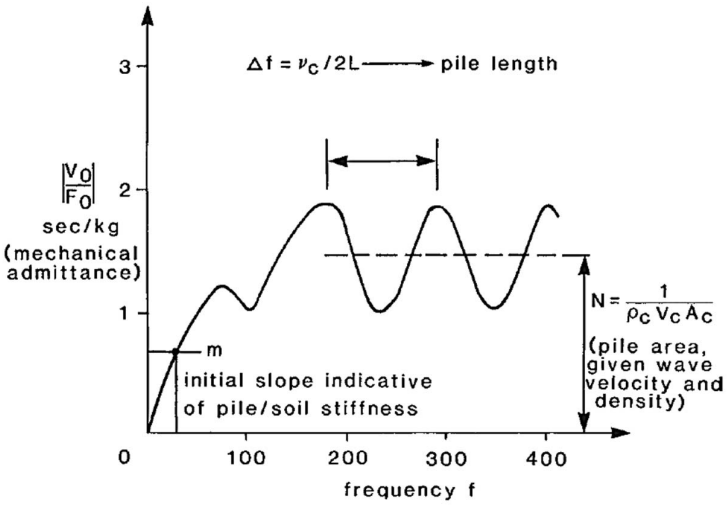


Figure 6. Idealized response curve in the frequency domain (Fleming, 2012)

4.1.3 Limitations

- Difficult to determine of the exact nature of the anomaly and its location trough the section ;
- Uncertainty about the pile length due to uncertainty of 10 % of concrete speed (Amir, 2015);
- Difficult interpretation when the noise due to friction effects becomes important ;
- Ratio *L*/*D* must be less than 30 to avoid the damping effect on the signal ;
- Gradual changes in the cross section are not detected ;
- Defect detection occurs when the area variation exceeds 25 % (Amir, 2015) ;
- Especially suitable for tubed or driven piles for which the section is regular along most of the pile length.

4.2 Cross/Single Hole Sonic Logging – CSL/SSL

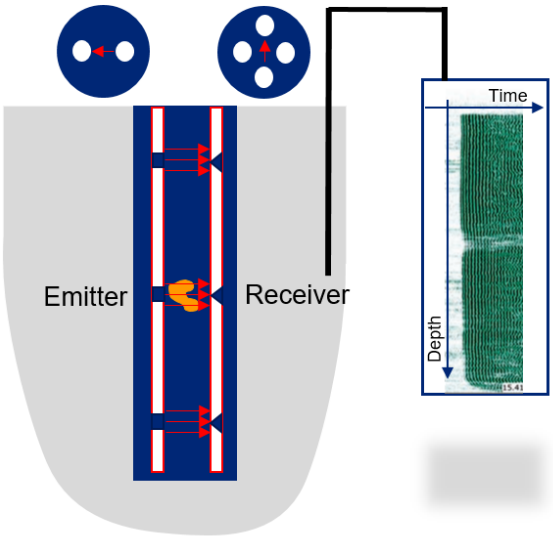


Figure 7. Cross Hole Sonic Logging Test

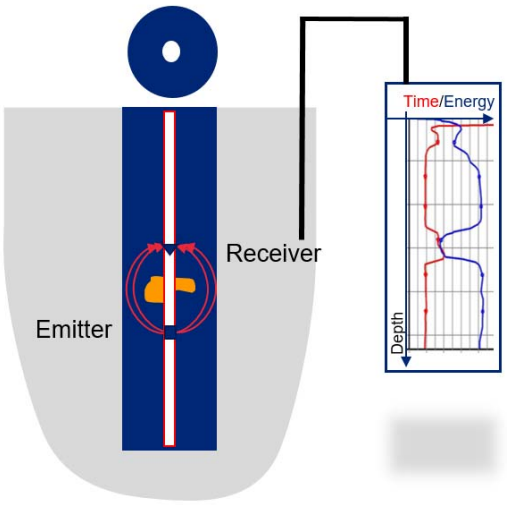


Figure 8. Single Hole Sonic Logging Test

4.2.1 Test principle

Pulses are generated by an emitter and picked up by a receiver. The time for the pulse to travel from the emitter to the receiver is measured. From the "First Arrival Time" (FAT) of the signal and the spacing between access tubes, the wave speed can be calculated. Any abnormal delay in FAT observed would indicate a potential defect in the concrete. The test can be conducted with two tubes (Fig. 7) or with one tube containing the emitter and the receiver (Fig. 8). In the case of SSL, detection of anomalies is only possible at 5 to 10 cm from the outside surface of the tubes (Amir, 2002).

$$t = \frac{L}{c_{medium}}$$

t : time to go from emitter to receiver
L : length between the emitter and the receiver
c_{medium} : wave speed in the medium

The signal picked up by the receiver can also be converted to relative energy, which is used to interpret the signal. A decreasing of the relative energy indicates an integrity defect in the pile area.

4.2.2 Test results and interpretation

Medium properties change leads to affected pulse propagation and signal attenuation. A delay of FAT, as compared to the vicinity, suggests the existence of suspected anomalies at the depths shown in the printout results of Fig. 7 and 8.

4.2.3 Limitations

- Not applicable to piles with diameters less than 600 mm because of the high cost of the test compared to cost the pile (Turner, 1994) ;
- Perimetral defects are not detected ;
- Difficult characterization of the nature of the anomaly since material and geometrical defects give the same CSL profiles ;
- Quality of the bonding between tubes and concrete : poor bonding would be regarded as a defect on the transmission path ;

- Differential curing rate of concrete within the pile may lead to different strength development and produce false impression on concrete quality (Paikowsky et al. 2000).

4.3 Gamma Ray Scattering – GRS

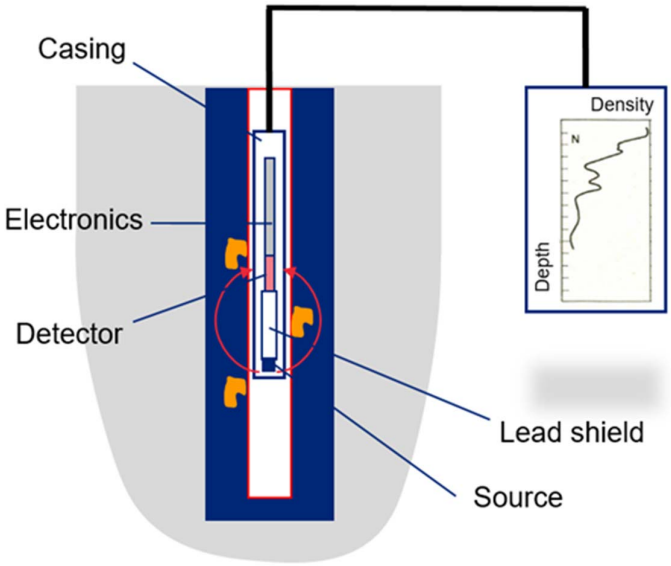


Figure 9. Gamma Ray Scattering

4.3.1 Test principle

A radioactive source at the bottom of the probe emits Gamma rays into the material surrounding the access tube. These Gamma rays collide with electrons in the surrounding material, which reduces their energy and changes their direction in what is called Compton Scattering. Finally, some of those particles are scattered into a detector located in the probe (Fig. 9).

4.3.2 Test results and interpretation

The number of interactions are directly related to the number of electrons in the surrounding material. The electron density of the surrounding material is measured (Fig. 9 & 10).

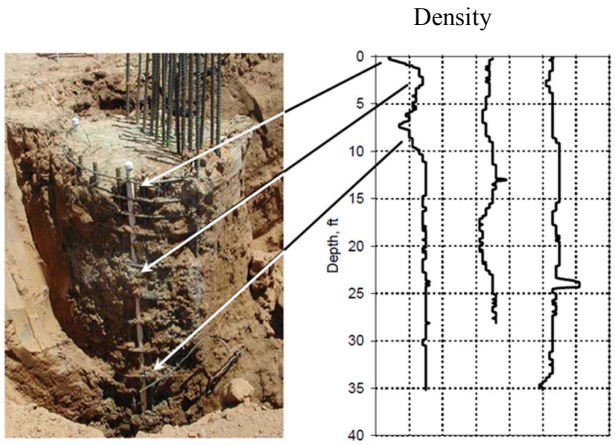


Figure 10. Results of a GRS (Rucker, 2002)

4.3.3 Limitations

- Unrepresentative results as the volume seen by the probe is approximately 50 cm to 75 cm radial (Amir, 2015) ;
- A scatter is observed on the results for a sound foundation, due to the non-homogeneity of in-situ concrete.

4.4 Coring

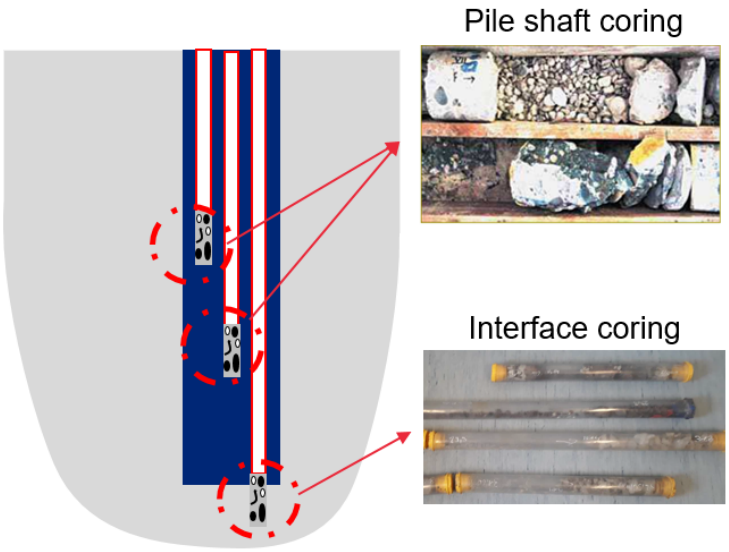


Figure 11. Shaft and interface coring's

4.4.1 Test principle

Coring consists of accessing the pile body by drilling. Two objectives can be pursued, see Fig. 11 :

- Assess the integrity of the pile shaft ;
- Assess the bonding between the pile toe and the soil at their interface.

4.4.2 Test results and interpretation

The main objective of this test is to extract a sample of concrete from the pile for :

- examination of the concrete quality and strength (shaft coring);
- visual examination of the quality of the contact surface between the pile concrete of the pile and the underlying rock mass (interface coring).

4.4.3 Limitations

- Unrepresentative results since only 1 to 3 % of the pile's cross section is analyzed and positive results may cause misinterpretation ;
- Method highly sensitive to the quality and the methodology of the boring.

4.5 Thermal Integrity Profiling – TIP

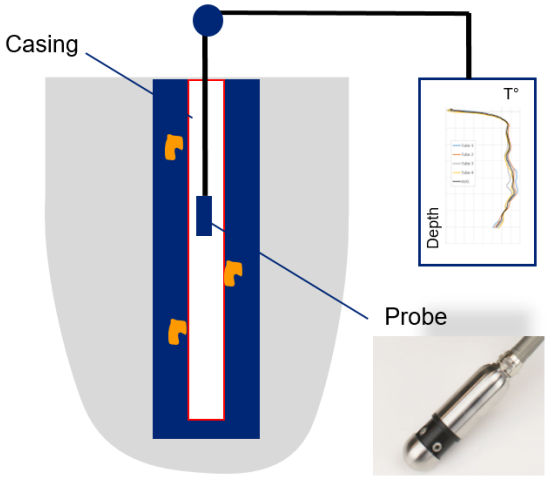


Figure 12. Thermal Integrity Profiling – Probe Method

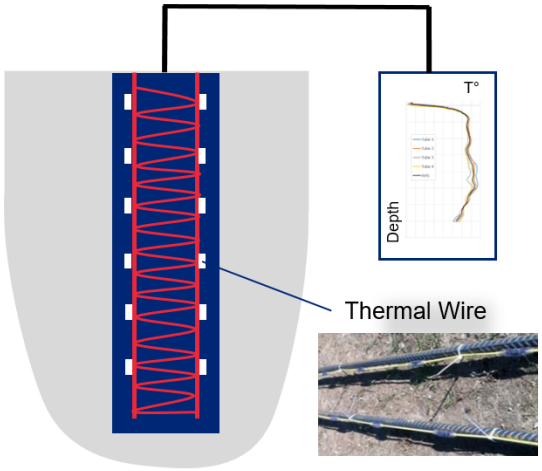


Figure 13. Thermal Integrity Profiling – Wire Method

4.5.1 Test principle

Two methods are possible using the thermal integrity profiling : the probe method or the wire method.

4.5.1.1 Probe method

By using the probe option, TIP is performed by lowering a thermal probe equipped with radially oriented infrared sensors in 4 orthogonal direction. The probe measures the internal temperature of the shaft which is increased due to the cement hydration after curing. The measured temperatures and the depth of the probe are monitored and recorded (Fig. 12).

4.5.1.2 Wire methods

Thermal wires are tied into the reinforcement cage with discrete temperature sensors along their lengths. Each wire is connected to a dedicated data collection box and temperatures are continuously collected at user's defined intervals, mostly every 15 minutes.

4.5.2 Test results and interpretation

Two levels of interpretation exist, the first consists of the observation of the raw thermal profiles. A decreased temperature may indicate an integrity defect (necking, soils inclusions, ect.) but may also be associated with cage eccentricity as the measured temperature is sensitive to the eccentricity of the cage. When the cage is centric, the temperature should be equal on each wire. However, a cage located slightly closer to one side of the excavation will exhibit reduced temperatures compared to tubes closer to the soil wall and higher temperatures from tube closer to the center of the shaft. Therefore a perfectly formed cylindrical shaft can exhibit differential temperatures between tubes on opposite sides of the cage when the cage is not centered correctly. By comparing both the highest and lowest tube temperatures from opposite sides of the cage with the average temperature at a given depth, cage offset can be differentiated from unwanted changes in cross section integrity.

The second level of interpretation consists of superimposing construction logs and concrete information to confirm first level observations and to convert temperature measurements into the shape of the shaft as shown on Fig. 14. The authors refers to the report of Mullins G. & Johnson K. (2017) for further information.

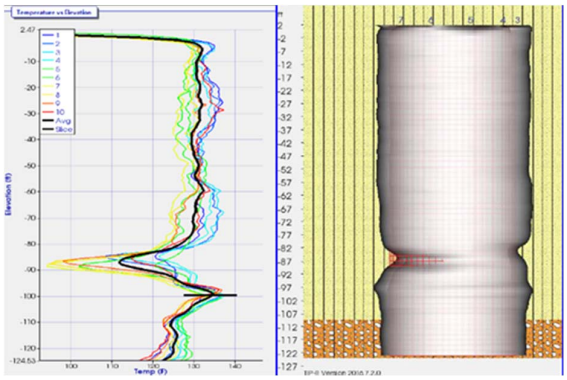


Figure 14. TIP results and pile modelling (Bixler, 2016)

4.5.3 Limitations

- Influence of water table and soil thermal conductivity on the pile temperature profile are not known;
- The probe method is time-sensitive since the maximum concrete temperature is not reached at the same time at each level. This results in a variation in temperature along the pile length without necessarily indicating an integrity defect;
- TIP does not allow for the detection of cracks since the measurements are made during pile curing.

5. CONCLUSION

Many methods to assess pile integrity are currently used in the industrial practice. Except for coring, all methods are indirect which means that they do not directly measure the defect of integrity. Instead, they measure the variation of physical values (temperature, impedance, speed, etc.) correlated by inference to the integrity of the pile.

The consequence of the indirect nature of those methods is that they do not allow for the exact identification of the integrity defect. Material or geometrical defects will have the same effect on the physical values such as a decrease of impedance, temperature or density. Furthermore, the impedance methods (SIT and S/CSL) and the GRS method do not allow for the definition of the transversal position and the size of the defect on the cross section. In addition, it is incorrect to suggest that modern integrity tests will highlight every defect that may exist in the pile. Small zones of segregated concrete or inclusions may be difficult to detect but most of the systems can, depending on their sensibilities, provide an indication on the presence of any significant integrity damage of the pile.

Finally, it is yet unknown how an integrity defect affects the pile performance. Indeed, measured pile integrity defects such as necking or segregation of the concrete do not explain how SLS, ULS or durability criteria are affected. Engineering judgement plays a crucial role to decide if performance tests are required to assess the pile performance.

ACKNOWLEDGMENTS

The authors thank Prof. Alain Holeyman and Ir. Thomas Marpels for their advices on this study.

REFERENCES

Amir J, 2015, https://www.piletest.com/show.asp?id=Engineer , Pile Testing, 1-100.

ASTM D5882, 2016, *Standard Test Method for Low Strain Impact Integrity Testing of Deep Foundations*, ASTM International, West Conshohocken, PA, 2016, www.astm.org

Bixler M, Belardo D., Piscsalko P. , 2016, Geotechnical Engineering Conference, *Case Histories Utilizing Thermal Integrity Profiling for Foundation Quality Assurance*, September 2016, Vancouver, Canada.

Fleming K, Weltman A, Randolph M, Elson K, Taylor & Francis, *Piling Engineering*, 2008; 294-295.

Gordon C. & Chapman, 2004. Ground Engineering, *Quality assurance of bored pile foundations*.

Likins G, 2015. Seminar on Special Foundations Engineering and Geotechnics, *Pile testing – State-of-the-Art*. June 2018

Holeyman, A. E. , Proceedings of the fourth international conference on the application of stress waves theory to piles, *Keynote lecture: Technology of pile dynamic testing*, The Hague, The Netherlands. 1992

Mullins G. 2010. DFI Journal, *Thermal Integrity Profiling of Drilled Shafts*. December 2010 53-64.

Mullins G. & Johnson K. 2017, USF University of South Florida, *Thermal integrity profiling for augered cast-in-place piles,* August 2017, 43-47.

Mullins G. & Piscsalko 2012. Deep Foundations Magazine, *Thermal Integrity Profiling: An Innovative Technique for Drilled Shafts*. May/June 2012; 51-54.

Paikowsky S.G. & Charnauskas, L.R, 2000, Application of Stress Wave Theory to Pile, *Examination of a New Cross-hole Sonic Logging System for Integrity Testing of Drilled Shafts*, September 2000, Brazil.

Rucker M. & Verquer M, 2002, 2nd International Conference on the Application of Geophysical and NDT Methodologies to Transportation Facilities and Infrastructure, *Gamma density logging of drilled shafts – some observations and interpretations*, April 2002, Los Angeles, California.

Sellountou, E.A. & Rausche, F., 2013, Seminar on the "Evolution of Experimentation in Construction, Crete; 329-346.

Turner, 1994, CIRIA Funders Report/CPT/28, *The Role of Integrity and Other Non-Destructive Testing in the Evaluation of Piled Foundations*, CIRIA, London.

WONG Yi-wai E, 2004. Master Thesis, *Behaviour of large-diameter Bored Pile Groups with Defects*. September 2004.

INNOVATIVE DRIVEN PILE SOLUTION FOR THE RHODE ISLAND ROUTE 6/10 INTERCHANGE PROJECT

Seth H. Hamblin P.E., Geosciences Testing and Research, Inc., 55 Middlesex St # 225 No. Chelmsford, MA 01863, shamblin@gtrinc.net
Leo J. Hart, Geosciences Testing and Research, Inc., 55 Middlesex St # 225 No. Chelmsford, MA 01863, leo@gtrinc.net
John E. Regan P.E., Geosciences Testing and Research, Inc., 55 Middlesex St # 225 No. Chelmsford, MA 01863, john@gtrinc.net

ABSTRACT

The Route 6 /10 10 Interchange Design/Build project, located in Providence, Rhode Island, involves the design and construction of five (5) new elevated bridge structures to replace and reconfigure the existing interchange and to provide a link between Route 10 northbound and Route 6 westbound. Due to site logistics, headroom restrictions, and depth to bedrock, 50 ton drilled micropiles installed in the deep medium dense sand strata were initially proposed as the deep foundation solution. Post project award, Geosciences Testing and Research, Inc. (GTR) performed various analyses and developed an alternate driven pile solution using steel Tapertube. The results of these analyses indicated that driven steel taper tube and steel pipe piles could develop greater capacities than the drilled micropiles in the granular soil layer, thereby reducing the number of foundation elements, decreasing construction schedule and providing a more cost effective foundation alternative.

A comprehensive driven pile load test program was subsequently executed by GTR and the Design Build Team led by Barletta Heavy Division of Canton, Massachusetts, to assess the performance of Tapertube and steel pipe piles, including pile drivability, load-deformation characteristics under static and dynamic loading, and to develop site-specific design parameters in two (2) distinct test areas. The test pile program included dynamic, static compression, tension and lateral load tests on each test pile. Load test measurements were automated with embedded Vibrating Wire Strain Gages (VWSG) to measure load transfer with depth. The execution and results of the successful pile load test program are presented and offer unique case study and valuable data for the use of Tapertube piles on deep foundation projects in the New England region

INTRODUCTION

The Rhode Island Department of Transportation (RIDOT) Route 6 / Route 10 Interchange is located west of downtown Providence. Originally constructed in the 1950's as a highway bypass around the historic Olneyville neighborhood, the interchange consists of a series of nine (9) bridges and ramps that serve as a vital east-west link between Interstate 295, 95 and 195. Based on recent bridge rating assessments, seven of the nine bridge structures are rated "*structurally deficient*". With many bridge structures shored with temporary supports as many as 15 years ago, the interchange is in critical need of replacement.

In 2018, RIDOT awarded the Route 6/10 Reconstruction Design-Build Project to 6/10 Constructors, Joint Venture. Led by Barletta Heavy Division of Canton, Massachusetts, the Design Build team includes O&G Industries, DW White Construction, Aetna Bridge Co. and AECOM. The scope of work includes the replacement of the bridges and ramps, and will provide direct access from Route 10 northbound to Route 6 westbound. Valued at over $400M (US), this is currently the largest project awarded in RIDOT history.

BACKGROUND AND SITE CONDITIONS

The Route 6 / Route 10 Interchange project consists of five (5) superstructures: Viaduct, Ramp B, Ramp C, Ramp D, and a Flyover with 19 specified substructures. Given the narrow corridor available for the project it was necessary to replace the existing structures within the limits of the current right-of-way. Due to site logistics, soil conditions, headroom restrictions and depth to bedrock, drilled micropiles were initially proposed to provide deep foundation support of various structures. The originally proposed construction

© 2019 Deep Foundations Institute

and demolition sequence dictated that many of the drilled foundations would be installed under the existing viaduct, thus restricting headroom access for pile driving rigs.

Prior experience by Hart et al. (2004) from a test pile program performed for a RIDOT interstate highway project in Providence lead to the concept of potentially using a driven pile alternative for this project. GTR reviewed the load test results of that project, performed various static pile analyses, and completed drivability analyses for select types of driven piles. The results of all the analyses indicated that driven steel taper tube and steel pipe piles could provide cost effective alternatives to the drilled micropile foundations.

Subsurface Conditions

Supplemental borings performed as part of the design phase of the project indicated a soil profile generally consisting of fill overlying peat overlying loose to medium dense sand that densifies with depth. Based on the project team's review of the subsurface conditions, two representative test areas with different soil profiles, denoted East of Amtrak (EOA) and West of Amtrak (WOA), were chosen as evaluate the potential driven pile foundation solution. Note that the available subsurface information from this project and other adjacent areas indicates that bedrock is located greater than 200 ft. below existing grade.

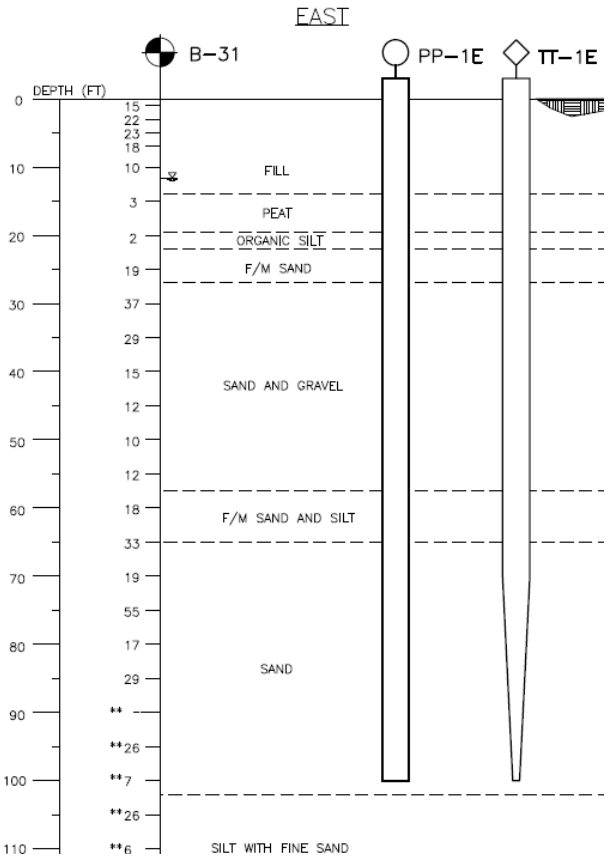


Fig. 1. East of Amtrak Soil Profile

The borings reported adjacent to the East of Amtrak Test Area indicate the following subsurface conditions; approximately 15 feet of granular Fill consisting of medium dense fine to coarse grain sand, with some gravel and traces of ash, gravel, brick, and fines overlying 3 to 5 feet of soft peat, with some medium to fine grained sand. Below the peat is approximately 3 feet of soft organic silt with observable fibers, overlying 7 feet of medium dense, fine to medium Sand, trace fines were encountered below organics. 30 feet of medium dense, well graded, fine to coarse Sand and Gravel, with few fines underlies this layer, below which was observed 7 feet of medium dense, fine to medium Sand, with silt, and 40 feet of medium dense to dense, fine to coarse Sand, trace Gravel, Trace Silt. A subsurface profile is depicted in Fig. 1.

The borings reported adjacent to the West of Amtrak Test Area indicate the following subsurface conditions; approximately 20 feet of medium dense granular Fill consisting of medium dense, fine to coarse Sand, with Silt, and traces of ash, gravel, brick, and glass; overlying, 17 feet of soft peat; several samples were fibrous and contained some fines. Below that 20 feet of loose, poorly graded fine Sand was encountered, overlying 15 feet of loose to medium dense, fine grained Silty Sand and 40 feet of interbedded layers of medium dense Gravel and medium dense Silty Sand. The information summarized above was presented in the load test data report by Hamblin et al. (2018).

PILE LOAD TEST PROGRAM

The test pile program included instrumenting and executing static compression, tension and lateral load tests for one (1) 16-inch Tapertube test pile and one (1) 16-inch steel pipe pile at both the East of Amtrak and West of Amtrak test sites. The test piles were driven using a Junttan HHK5A hydraulic hammer and dynamically monitored during driving using a Pile Driving Analyzer (PDA). Subsequently, four (4) static

compression load tests, three (3) tension load tests, and two (2) lateral load tests were performed. All load testing was performed in general accordance with applicable ASTM standards and RIDOT requirements. The project team also performed vibration, noise, and ground deformation monitoring during pile installation to evaluate potential environmental impacts to neighbors and adjacent infrastructure.

Test Pile Summary

Two (2) test piles were driven at both the EOA and WOA test sites. At each test site one (1) 16-inch diameter, 0.375 wall thickness, close-ended steel pipe pile and one (1) steel Tapertube pile having a 16-inch diameter, 0.375 wall thickness top section, and a 16"x8"x25' taper section at the bottom were installed.

The target ultimate compression capacity for the test pile program was 400 kips (200 tons). The assumed steel yield strength for each pile was 50 ksi and the design 28-day compressive strength for the neat cement grout placed in the piles after installation was specified to be a minimum of 4000 psi.

Steel Pipe Piles (Test Piles PP-1 & PP-2)

Test pile PP-1, installed at the WOA test site, was initially 120 feet long and consisted of two 60-foot long sections. Test pile PP-2, installed at the EOA test site, was also initially 120 feet long and consisted of two 60-foot long sections. The two pile sections were spliced together in the field using a full penetration weld. Flat, one (1) inch thick steel tip plates were welded to the ends of the piles by the pile manufacturer prior to arrival onsite.

Steel Tapertube Piles (TTP-1 & TTP-2)

Test pile TTP-1, installed at the WOA test site, was initially 120 feet long and consisted of one 25-foot long Tapertube section, and 35-foot long and 60-foot long pipe pile sections. Test pile TTP-2, installed at the EOA test site, was initially 60 feet long and consisted of one 25-foot taper tube section and a 35-foot long pipe pile section. The pipe pile sections were spliced together in the field using a full penetration weld. The Taper tube sections were spliced to the 35-foot pipe pile sections in the shop by the pile manufacturer prior to their arrival onsite. Each Taper tube section included an 8-inch diameter conical point at the bottom.

After driving, a center bar and rebar cage equipped with Geokon vibrating wire strain gages was placed into each test pile. A 2.75-inch O.D. inclinometer casing was strapped to the center bar. The cross sectional area of the 16"x0.375" pipe section of the pile was 18.41 square inches. The cross sectional area of the top of the Tapertube section was 14.8 square inches. The cross sectional area at the tip of the Tapertube section was 7.5 square inches. The maximum allowable compressive and tensile driving stress for this pile type were 45 ksi, based on AASHTO guidelines of 90% of the assumed steel yield strength for of 50 ksi.

Test Pile Instrumentation

The internal geotechnical instrumentation for the test piles included Geokon model 4911 vibrating wire strain gage 'sister bars' (VWSG), and a 2.75-inch O.D. ABS plastic inclinometer casing. All test piles were instrumented with ten (10) strain gages to measure load transfer and strain during each static test, and the inclinometer casing was used to evaluate lateral deflection in the pile during the lateral load test. The upper three pairs of strain gages were attached to an internal steel reinforcing age and the lower two pairs were affixed directly to the centerbar. The as-built VWSG locations for each pile can be seen in Table 1. Load was calculated at each gage by multiplying the observed micro strain reading by the cross-sectional area of the pile and the composite pile modulus (E).

Table 1. Strain Gage Locations

WOA		EOA	
Distance from Pile Tip (ft)			
PP-1	TTP-1	PP-2	TTP-2
1.6	1.6	1.6	1.6
36	36	25	23
86	86	45	29
101	101	58	42
111	111	68	52

Test Pile Installation

All four test piles were installed using a Junttan HHK5A hydraulic impact hammer, having a ram weight of 11.02 kips and a maximum equivalent stroke of 3.94 feet, thus producing a maximum rated energy of 43.4 kip-ft.

The test piles at the WOA and EOA test sites were installed in May 2018. Restrike testing to evaluate time dependent pile capacity was performed 5 days after installation at each test site.

East of Amtrak Test Piles

Test pile locations PP-2 and TTP-2 were pre-augured to a depth of ~23 feet below ground surface. Test pile PP-2 was driven to a penetration of 70 feet and a blow count of 3-3-4 blows per inch for the final three inches of pile penetration. Test pile TTP-2 was initially installed to a subgrade penetration of 51 feet and a blow count of 3-3-3 blows per inch for the final three inches of pile penetration. Both piles were installed with the Junttan HHK5A operating at an approximate 3-foot stroke and providing between 22 kip-ft. and 27 kip-ft.

Restrikes were performed five (5) days after the end of initial drive (EOD). The hammer was operated at an approximate 3-foot stroke during restrike testing to provide similar transferred energy as EOD. Based on the results of restrike testing at pile TPP-2, the pile was advanced an additional four feet to a subgrade penetration of 55 feet and a blow count of 26 blows per foot for the final one foot of pile penetration.

West of Amtrak Test Piles

Test pile locations PP-1 and TTP-1 were pre-augered to a depth of 23 feet below ground surface. Test pile PP-1 was driven to a penetration of 113 feet and a blow count of 16 blows per foot for the final one foot of pile penetration. Test pile TTP-1 was installed to a penetration of 113 feet and a blow count of 41 blows per foot for the final one foot of pile penetration. Both piles were installed with the Junttan HHK5A operating at an approximate 3-foot stroke and providing between 24 kip-ft. and 25 kip-ft.

Restrikes were performed five (5) days after the end of initial drive (EOD). The hammer was operated at an approximate 3.5-foot stroke during restrike testing to provide greater than or equal transferred energy as EOD.

DYNAMIC PILE TESTING

Dynamic pile testing was performed on all test piles to evaluate driving stresses, capacity, pile integrity and hammer performance using the Pile Driving Analyzer™ (PDA) Model 8G, manufactured by Pile Dynamics, Inc. (PDI). The PDA records, digitizes, and processes the force and acceleration signals for use in calculating the Case Method and CAPWAP ultimate pile capacity. The dynamic testing was carried out in general accordance with ASTM D4945, "Standard Test Method for High Strain Dynamic Testing of Piles".

Dynamic testing was performed during initial drive after the lower pile section was installed and the upper and lower pile sections were spliced. Restrike testing was then performed after a set-up period of 5 days to evaluate time-dependent changes in pile capacity.

The results of the dynamic testing performed to date are summarized in Tables 2 below. This table include information on date of driving, the driven depth, blow count, maximum transferred energy, stroke, maximum pile top displacement, and maximum compressive stress at the pile top and tip and CAPWAP results. The transferred energy, maximum pile top displacement, and maximum compressive stress at the pile top are determined by the PDA at the gage locations. The maximum compressive stress at the pile tip is estimated by the PDA.

Also included in Table 2 is the pile bearing capacity as determined by the Case Method in the field and CAPWAP analysis. The Case Method capacity is representative of the blow(s) indicated at EOD and BOR. CAPWAP analyses were performed on selected piles from EOD and BOR data.

Table 2 presents BOR data from both early (blow 2 and 3) and later impacts (blows 6-8) to demonstrate the sensitivity of the soil resistance during restrike testing. Blows 1-3 generally produced higher total capacities than blows 6 through 8, thus demonstrating how quickly the skin friction was 'broken' and the pile tip was remobilized.

Hammer Performance and Pile Integrity

The test piles were installed with the Junttan HHK5A operating at a 3 to 3.5-foot stroke and providing between 22 kip-ft. and 27 kip-ft. of energy transfer, measured at the PDA gages. When compared to the theoretical energy transfer of 33.1 kip-ft. for that stroke height, the calculated efficiency of approximately 65% to 85% is within the expected range for this hammer type.

The maximum compressive and tensile driving stresses for all test piles were below the allowable limit (45 ksi) throughout testing and the dynamic test data did not indicate any signs of pile damage during pile installation.

East of Amtrak Dynamic Pile Testing Results

Test Pile PP-2 was driven to 70 feet below existing grade, a blow count of 3 to 4 blows per inch (bpi) and an average Case Method field capacity (RX7) of 325 kips. Subsequent CAPWAP analysis performed on data from EOD indicated a capacity of 330 kips, with 140 kips in skin friction and 190 kips in end bearing.

Restrike testing performed five (5) days after installation showed similar capacities within 5% of those calculated at EOD. Specifically, the BOR CAPWAP capacity of blow numbers 2 and 7 were 355 and 310 kips, respectively; with approximately 50% of the capacity developed in end bearing.

Test Pile TPP-2 was driven to 51 feet below existing grade, a blow count of 3 to 4 blows per inch (bpi) and an average Case Method field capacity (RX7) of 400 kips. Subsequent CAPWAP analysis performed on data from EOD indicated a capacity of 390 kips, with 220 kips in skin friction and 170 kips in end bearing.

Restrike testing performed five (5) days after installation showed similar capacities within 10% of those calculated at EOD. Specifically, the BOR CAPWAP capacity of blow numbers 2 and 8 were 447 and 397 kips, respectively; with approximately 40% of the capacity developed in end bearing.

Based on the results of restrike testing at pile TPP-2, the pile was advanced an additional four (4) feet to a subgrade penetration of 55 feet and a blow count of 26 blows per foot for the final one foot of pile penetration. The Case Method capacity at the EORD was 368 kips and a CAPWAP analysis performed this data indicated a capacity of 360 kips, with 180 kips in skin friction and 180 kips in end bearing.

West of Amtrak Dynamic Pile Testing Results

Test Pile PP-1 was driven to 113 feet below existing grade, a blow count of 16 blows per foot (bpf) and an average Case Method field capacity (RX7) of 235 kips. Subsequent CAPWAP analysis performed on data from EOD indicated a capacity of 220 kips, with 90 kips in skin friction and 130 kips in end bearing.

Restrike testing performed five (5) days after installation showed approximate increases of 110% and 70% in capacity when compared to the EOD capacity. Specifically, the BOR CAPWAP capacity of blow numbers 2 and 6 were 465 kips and 370 kips, respectively; with approximately 25% of the capacity developed in end bearing.

Test pile TTP-1 was driven to 113 feet below existing grade, a blow count of 41 blows per foot (bpf), and an average Case Method field capacity (RX7) of 340 kips. Subsequent CAPWAP analysis performed on data from EOD indicated a capacity of 340 kips, with 210 kips in skin friction and 130 kips in end bearing.

Restrike testing performed five (5) days after installation showed approximate increases of 35%, 25%, and 15% in capacity when compared to the EOD capacity. Specifically, the BOR CAPWAP capacity of blow numbers 2, 4, and 6 were 455, 425, and 395 kips, respectively; with approximately 16% of the capacity developed in end bearing.

Table 2. Summary of Dynamic Load Testing Data

Test Site	Test Pile	Time of[1] Driving	Date	Driven[2] Depth (feet)	Stroke[3] (feet)	Maximum[4] Transferred Energy (kip-ft)	Maximum[4] Comp. Stress Pile Top (ksi)	Maximum[5] Comp. Stress Pile Tip (ksi)	Case Metho Capacity RX7 (kips)	CAPWAP Capacity (kips)
WOA	PP-1	EOD	5/16/18	113.0	3	24.8	27.9	16.7	235	220
		BOR	5/21/18		3.5	28.2	29.1	28.2	487	465
		BOR	5/21/18		3	24.8	28.4	26.8	415	370
	TTP-1	EOD	5/16/18	113.0	3	25.1	26.4	22.0	343	340
		BOR	5/21/18		3.5	33.6	32.1	28.2	438	455
		BOR	5/21/18		3.5	28.5	29.5	26.4	421	425
		BOR	5/21/18		3.5	28.7	29.4	26.3	412	395
EOA	PP-2	EOD	5/30/18	70.0	3	27.1	29.8	20.8	326	330
		BOR	6/4/18			25.2	30.4	21.3	358	355
		BOR	6/4/18			21.4	27.3	18.9	325	310
	TTP-2	EOD	5/30/18	51.0	3	22.8	26.3	21.0	404	390
		BOR	6/4/18			22.2	30.5	19.5	447	420
		BOR	6/4/18			20.6	29.7	19.6	397	395
		EORD	6/4/18	55.0		21.8	27.2	20.0	368	360

1. EOD Indicates that the data was obtained at the end of drive
2. Depth is referenced from tip grade next to pile.
3. The blow count and stroke were reported by others.
4. The maximum transferred energy, maximum pile top displacement, and maximum pile top compressive stress are determined by the PDA at the gage locations. These values represent an average over the blow(s) indicated.
5. The maximum pile tip compressive stress is estimated by the PDA. These values represent an average over the blow(s) indicated.
6. The Case Method capacity was determined using the RMX method (JC value of 0.7 and 0.9). These values represent an average over the

Table 3. Summary of Static Load Test Results

								Static		Dynamic
Test Site	Test Pile	Driven Date	Driven Depth (ft)	Observed Blow Count (bpf)	Measured Energy (k-ft)	Lateral Load at Measured Deflections		Nominal Tension Capacity (kips)	Nominal Comp. Capacity (kips)	Nominal Resist. Capacity (kips)
						1" (kips)	1.5" (kips)			
WOA	PP-1	5/16/2018	113	16	24.8	57	65	165	350	465
	TTP-1	5/16/2018	113	41	25.1	39	50	255	430	455
EOA	PP-2	6/4/2018	70	5,5,5,4 bpi	21.4	48	58	N/A	280	355
	TTP-2	6/4/2018	55	26 bpf	21.8	54	70	270	560	420

COMPRESSION LOAD TESTING

Four (4) compression static load tests were performed for this program. Two load tests were performed at both the East of Amtrak and West of Amtrak test sites. The compression load tests were performed 10 days after pile installation.

Compression load tests were performed in general accordance with ASTM D1143 – "Piles Under Static Axial Compressive Load", using Procedure A: Quick Test. During each load test the imbedded VWSGs were monitored by an automated data acquisition system (ADAS) to evaluate load transfer along the length of the piles. The ADAS collected readings at 60-second intervals throughout the test.

All test piles were tested to failure to evaluate overall pile capacity and soil resistance distribution. Select Load vs. Displacement plots are show in Fig. 2 and 3.

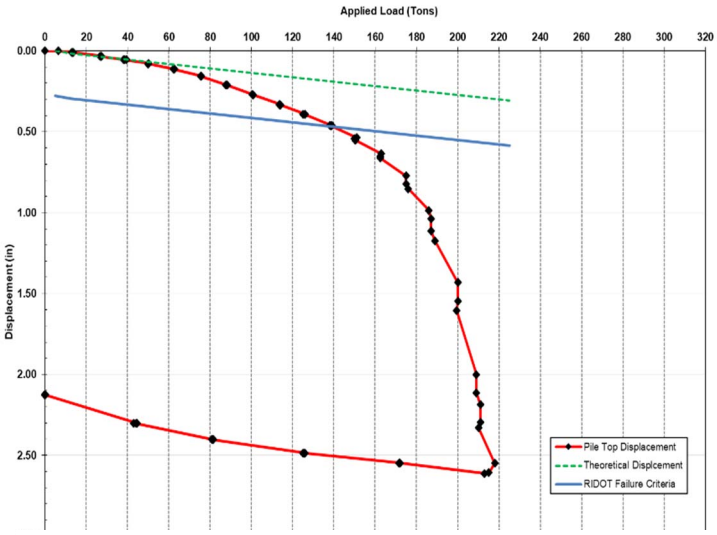


Fig. 2. Pipe Pile Comp. Load vs. Disp.

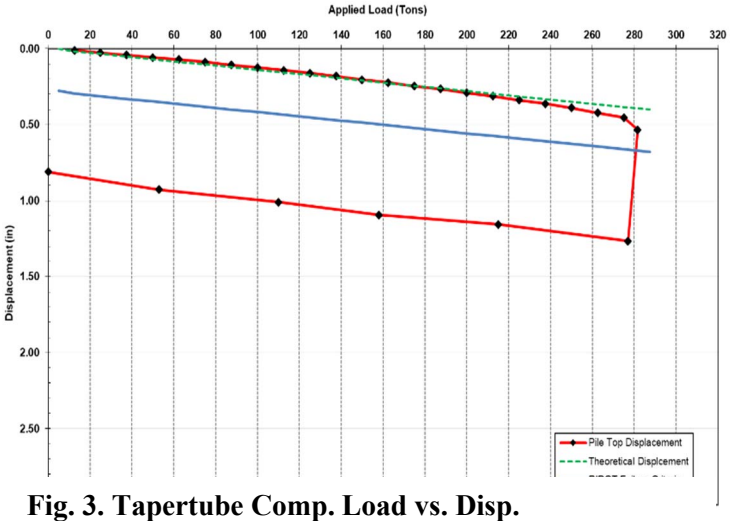


Fig. 3. Tapertube Comp. Load vs. Disp.

TENSION LOAD TESTING

Three (3) tension static load tests were performed for this program. Two load tests were performed at the West of Amtrak test sites and one (1) was performed at the East of Amtrak test site. The tension load tests were performed following a minimum of 72-hour period after the compression load tests. The project initially intended to perform a tension load test on the EOA pipe pile, however, that test was eliminated for convenience based on the superior performance of the EOA tapertube during the compression load test. Additionally, after observing similar ultimate tension capacities from the load tests of both tapertube piles, we made the determination that testing the 2nd pipe pile was unnecessary.

The test piles were tested to failure to evaluate overall pile capacity and soil resistance distribution, and to determine parameters for us in future pile design. Failure/Stopping Criteria was defined as continuous and excessive deflection under constant loading. Select Load vs. Displacement plots are show in Fig. 4 and 5.

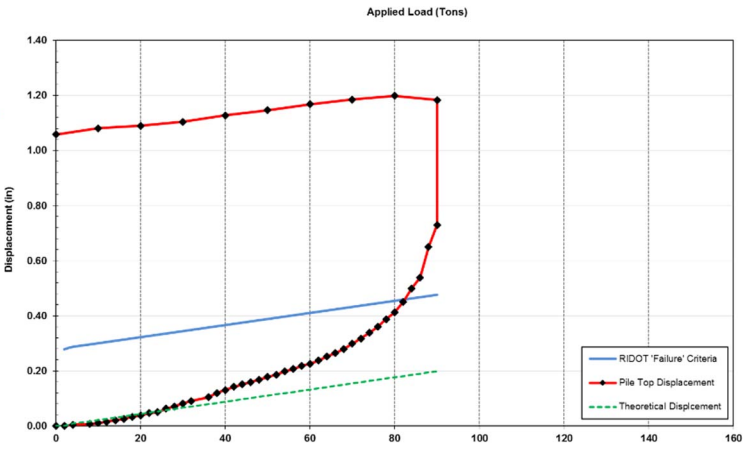


Fig. 4. Pipe Pile Tension Load vs. Disp.

LATERAL LOAD TESTING

Two lateral load test were performed, one on the East of Amtrak test site, and the other on the West of Amtrak test site. The Lateral load test were performed to evaluate the applied load that

produced both 1-inch and 1.5-inches of maximum deflection. The VWSGs were monitored at all 4 test piles to evaluate moment vs. depth and the inclinometer casings were monitored to evaluate lateral displacement with depth. A select Load vs. Displacement plot is show in Fig. 6.

The results of the static load test program are presented above in Table 3.

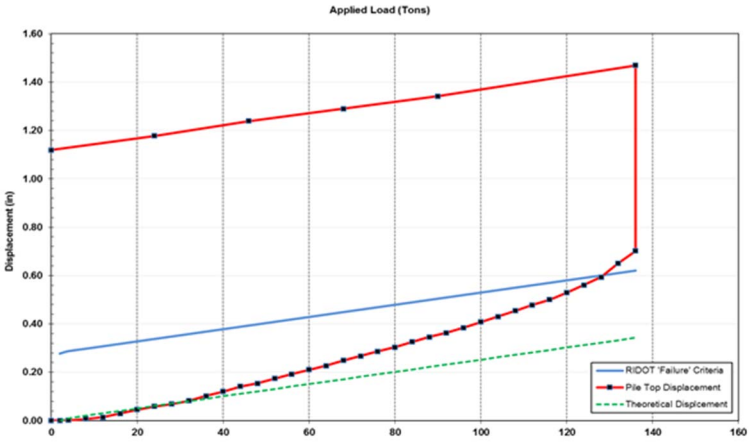


Fig. 5. Tapertube Tension Load vs. Disp.

Vibration, Noise, & Deformation Monitoring

Soil settlement monitoring was performed at both test sites to evaluate the relationship between pile driving activities and potential displacement of the surrounding ground. Surface Monitoring Points (SMPs) were installed radially around each test pile at 15 foot, 25 foot, and 50-foot offsets. The SMP's were monitored before, during and after pile driving activities using an automatic level and leveling rod.

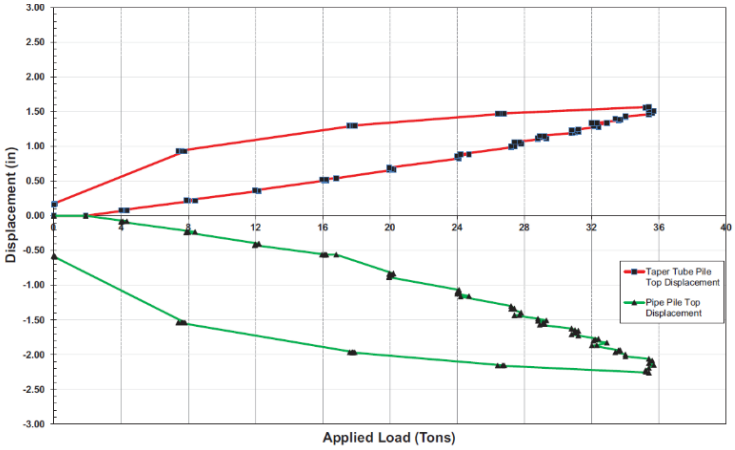


Fig. 6. Tapertube & Pipe Pile Lateral Load vs. Disp.

Vibration and noise monitoring was performed at both test sites to measure ground vibration and noise emissions during pile driving and evaluate the relationship between the two test pile types. Data was collected with tri-axial geophones and 'A' weighted microphones connected to an Instantel brand Minimate Plus Seismograph. Background readings were monitored for a minimum of one (1) day prior to test pile installation to document pre-construction noise levels and noise monitoring was performed during installation of all test piles.

CONCLUSIONS

The data collected confirm that the Tapertubes out-performed the steel pipe piles. The primary conclusion isthat at similar penetration lengths, and when driven to similar penetration resistances (blow counts), the tapertube piles exhibited greater ultimate pile capacities than pipe piles of identical diameter.

The results of the compression load tests showed that the two tapertube test piles achieved an ultimate pile capacity of 430 kips and 560 kips while the corresponding pipe piles achieved 350 kips and 280 kips. This equates to tapertube ultimate capacities of 22% and 100% greater than the pipe piles. The load vs. displacements plots for both pile types were also dissimilar. The data from the pipe piles showed generally more displacement per load increment than the tapertubes and more creep per interval. The tapertube data

indicated minor deviation from the approximated theoretical compression at most load increments, until reaching the ultimate pile capacity, where a plunging failure was observed.

The strain gage data collected during each compression load test revealed differences between the load transfer profiles of two pile types. At the maximum test load for each pile type, the pipe piles exhibited much greater load resistance at the pile tip than the tapertubes. As shown in Fig. 7 & 8, approximately 50% of the pile resistance in the pipe pile is at the tip, compared to less than 1% with the tapertube pile. The tapertube pile strain gage data indicates that approximately 66% of the load is shed along the 25-foot-long tapered section, with minimal load reaching the tip of the pile. The load transfer data from the upper sections of each pile type displays similar frictional capacities.

The results of the static tension load tests were similar, with the tapertubes exhibiting greater ultimate tensile capacities than the pipe piles. The data indicated that the Tapertubes developed ultimate tension capacities that were 50% greater than the pipe piles. The load vs. displacements plots for both pile types were similar as the applied load was increased for 0 to 80 kips, however after that load increment the slopes of the load vs. displacement curves diverge.

Load transfer calculations based on the strain gage data from the tension tests showed that the majority of the resistance occurred in the upper section of the pipe pile and had minimal resistance in the lower 25 ft. of the pile. Data from the tapertubes show that a significant component of the uplift resistance occurred along the lower tapered section of the pile. Load transfer plots from the tension tests are presented in Fig. 9 & 10.

Data collected during the lateral load tests indicated that the tapertube and pipe piles performed very similarly. The applied lateral load at 1" of measured deflection was 39 kips and 54 kips for the tapertube piles and 57 kips and 48 kips for the pipe piles. It was our expectation that there would not be a significant difference between the performances of each pile type as they upper sections were both 16-inch diameter pipe piles.

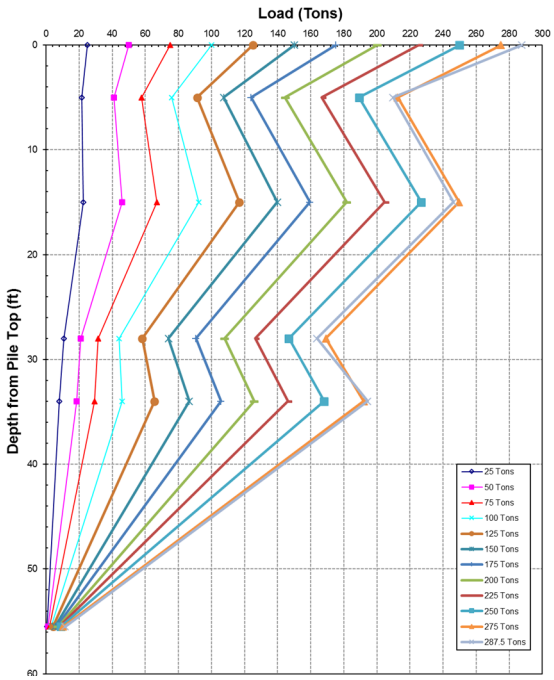


Fig. 7. Tapertube Pile Compression Load Test Load Transfer vs. Depth

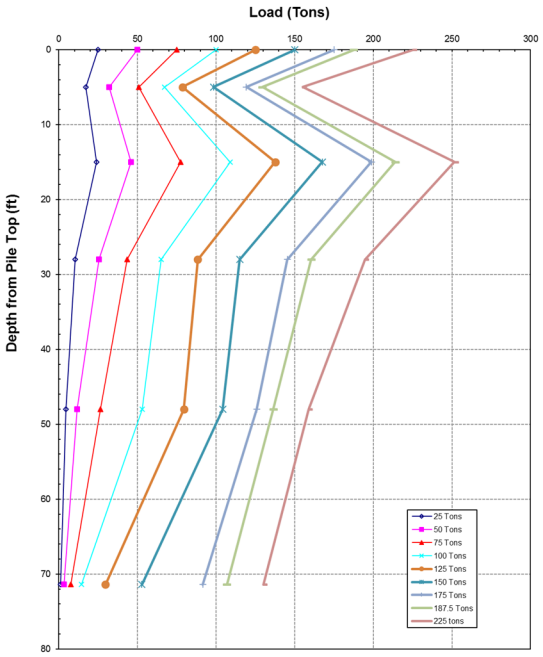


Fig. 8. Pipe Pile Compression Load Test Load Transfer vs. Depth

The results for the settlement monitoring indicated that ground displacement at the EOA test site due to pile driving ranged between 0.01 feet of heave to 0.03 feet of settlement. No soil heaving was observed in the SMP data from the EOA site. Ground settlement at the WOA test site due to pile driving ranged between 0.000 feet and 0.120 feet. The maximum settlement was observed 15 feet from both test piles. Settlement

at SMP's located 25 feet from the test piles indicated approximately 0.02 feet of settlement and SMP's at 50 foot offsets indicated less than 0.01 feet of displacement.

The background noise/sound levels observed at both test sites prior to pile driving ranged between 95 dB(A) and 101 dB(A). Noise levels obtained during pile driving ranged from 100 dB(A) to 108.5 dB(A), which indicates an approximate 5% to 8% increase above ambient levels. Noise level measurements at the 25-foot and 50-foot offset distances were approximately the same and the noise level and range did not appear to be influenced by the pile type. Ground vibrations from pile driving were also very low, measured at less than 0.25 in/sec. at offset distances of 25 feet.

In comparison to the originally proposed drilled micropile foundation solution, the results of the tapertube load test program produced ultimate foundation capacities that were 400% greater than the proposed loads for drilled micropile to be installed in the same soil conditions. Additionally the tapertubes were superior to the micropiles in resisting the critical and stringent uplift and lateral loading conditions imposed on the foundations.

The use of tapertubes reduced the number of foundation elements per pier from 60-80 drilled micropiles to 20-30 driven piles. Overall, the driven pile substructures were installed in 2-4 days each, compared with the 25-30 days each budgeted for the micropiles. The reduction in the quantity of foundation elements decreased schedule needed for foundation installation, which permitted the first phase of superstructure and pier demolition to be performed first. By demolishing, the existing structures prior to pile driving, headroom restrictions were eliminated and standard pile driving equipment could be used to drive the piles.

Our research has determined that this project was the first large scale infrastructure project to use tapertubes in the New England region. The data collected during this load test program suggests that this foundation type is an appropriate and effective solution for projects with deep bedrock and overlying medium dense granular soils. This subsurface profile is common across southern New England, from Cape Cod to Connecticut, thus suggesting that tapertubes may be a more efficient pile type than other steel and concrete piles.

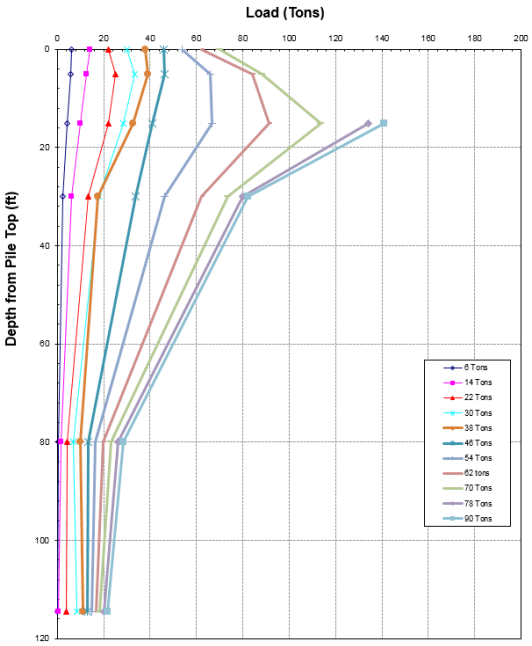


Fig. 9. Pipe Pile Tension Load Test Load Transfer vs. Depth

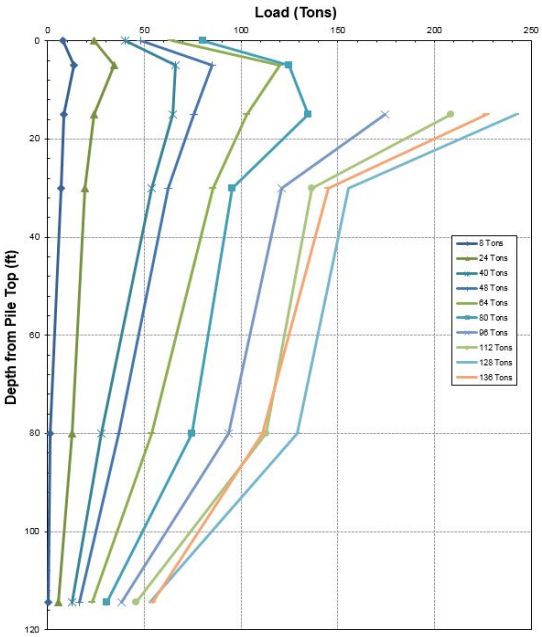


Fig. 10. Tapertube Tension Load Test Load Transfer vs. Depth

REFERENCES

Hart, L.J., Chernauskas, L.R., Paikowsky, S.G., 2004, Design Phase Pile Load Testing Program Report, Improvements to Interstate Route I-195, Providence, RI

Hamblin, S.H., Regan, J.E., Hart, L.J., 2018, Design Phase Pile Load Testing Program Report, RIDOT Reconstruction of the Route 6 / Route 10 Interchange, Providence, RI

INSTALLATION AND EFFICIENCY OF COMMON HELICAL PILE COUPLINGS

Jason Herron, Hubbell Power Systems, Inc., Centralia, MO, USA, 573-682-8630, jwherron@hubbell.com
Joseph Brown, Hubbell Power Systems, Inc., Centralia, MO, USA, 573-682-8378, jrbrown@hubbell.com

ABSTRACT

The common couplings for joining sections of helical piles with an outside diameter of 6.625 inches and 8.625 inches are square on square, flange to flange, external pipe sleeve, internal pipe sleeve, and welded joint. Each coupling type has advantages and disadvantages in efficiency, capacity, installation, and economics of the installed pile. All these coupling types have been used in the helical pile market in North America for various applications and designs. Many of these applications require on-site testing, but test records are not typically shared with the helical pile industry. Due to the lack of information available for square on square and flange to flange couplings, testing was done to compare the efficiency of installation, load to deflection response, and torque to capacity ratios of external pipe sleeve, square on square, and flange to flange couplings. Field installations and tension tests were performed in non-cohesive (sand type) soil near Caseyville, IL and in cohesive (clay type) soil in Centralia, MO. The data collected during these tests included rotations per foot during installation, installation torque, applied pressure, and deflection. The results of this testing are analyzed and discussed within this paper. The results indicate that the square to square coupling is the most efficient of the designs tested, but this conclusion cannot be fully justified without further testing due to the variability in the data gathered and the small number of piles tested.

INTRODUCTION

A helical pile is typically assumed to be a medium-displacement pile when its outside diameter is between 4.5 inches and 8 inches and a high-displacement pile when its outside diameter is greater than 8 inches. A helical pile designer has multiple options when selecting a coupling type for medium- to high-displacement helical piles. Each type of coupling has advantages and disadvantages and must be analyzed on the bases of efficiency, capacity, installation, and economics of a project. Typical couplings that are chosen by designers include square on square, flange to flange, external pipe sleeve, internal pipe sleeve, and welded joint. A helical pile must transfer axial, lateral, bending moment, and torsional loads, and the coupling must be designed to effectively and efficiently transfer each type of load.

During the installation of a helical pile, the rate of penetration and the disturbance of soil layers play a critical role in the efficiency and torque to capacity ratio (K_t) of the pile. It is common for a coupling to protrude beyond the outside diameter of the pipe section being used. This is necessary for the function of certain coupling types and can facilitate the connection of couplings. However, it causes increased soil disturbance and reduce the rate of penetration due to soil bearing against the protruding portion of the coupling. A helical pile designer typically will work to minimize the coupling protrusion and create a pile with optimal installation efficiency but may choose a design with lower installation efficiency if it offers sufficient economic advantage.

Many helical pile applications require on-site testing, but test records are not typically shared with the helical pile industry. Testing information generally remains with the installing contractor, manufacturer, or end user. Field test results have been presented to provide recommendations for torque to capacity ratios for medium- and high-displacement helical piles with pipe sleeve and welded joint couplings. For design of square on square and flange to flange couplings, design assumptions are typically made based on proprietary testing performed by installers or manufacturers. Due to the lack of information available for square on square and flange to flange couplings, field installations and tension tests were done to compare the efficiency of installation, load to deflection response, and torque to capacity ratios of external pipe sleeve, square on square, and flange to flange couplings.

© 2019 Deep Foundations Institute

The test piles were twelve medium-displacement piles made from 6-inch nominal diameter schedule 40 pipe (6.625 inch OD) and twelve high-displacement piles made from 8-inch nominal diameter schedule 20 pipe (8.625 inch OD). Equal numbers of each pile size were fitted with each of the three coupling types. The testing was performed for non-cohesive (sand type) soil near Caseyville, IL and for cohesive (clay type) soil in Centralia, MO, resulting in a total of twenty-four installations and tension tests. The data collected during these tests included rotations per foot during installation, installation torque, applied pressure, and deflection. The test data was used to compare performance of the three coupling types with respect to each other and to standard torque to capacity ratios based on Equation 10 in section 3.13.1.1 of the International Code Council Evaluation Service (ICC-ES) report AC358, Acceptance Criteria for Helical Foundation Systems and Devices.

COUPLING TYPES

Square on Square

A square on square coupling consists of two square sections of different size that fit closely one inside the other to create a positive connection that can transfer torque via the bearing of the two square sections against one another. This coupling type has advantages in ease and efficiency of installation and load transference. The square design enables the rapid connection of sections and reduces alignment time typical to other coupling types. In applications where reversing axial loads are required, this coupling has a disadvantage due to coupling slack in each joint that can vary from 1/16 inch to 1/8 inch depending on the manufacturing tolerances of the bolt holes. Coupling slack increases the gross deflection when the load direction reverses.

Flange to Flange

A flange to flange coupling consists of a flange welded to each connecting end of the helical pile sections. Sections are then coupled by clamping or bolting the flanges together. A common design utilizes a bolt hole pattern in the flanges and a set of bolts and nuts for connecting the flanges. The number and size of bolts can vary depending on the loads that are transferred. This coupling has advantages in ease of installation and pile rigidity. There is no coupling slack and performance is good for all axial loads including reversing loads. The disadvantage is reduced pile efficiency due to a large amount of coupling protrusion that adversely affects pile advancement and increases soil disturbance around the pile.

External Sleeve

An external sleeve is a coupling type consisting of a pipe sleeve or a formed upset applied to the end of a pipe section to create a bolted connection that fits over the outside diameter of another pipe section. This type of coupling is typically welded to extension sections that are bolted to previously installed sections. An external sleeve can also be free of weld and be bolted to each pile section at both ends of the coupling. This coupling type is one of the most common in the helical piling industry and has advantages in efficiency and ease of installation. It has a disadvantage in applications with reversing axial loads due to coupling slack that yields increased gross deflection when the load direction reverses.

Internal Sleeve

A pipe sleeve or a formed extrusion can be applied to the end of a pipe section to create a bolted connection that fits within the inside diameter of another pipe section. The fitting methods, advantages, and disadvantage stated for external sleeve couplings above also apply to the internal sleeve coupling. It also eliminates the protrusion beyond the outside diameter of the pipe section. This coupling type has additional disadvantages in manufacturing and relative cost. It is one of the more difficult to manufacture due to material availability of applicable sleeve diameters, and the much thicker wall required for the internal sleeve to match the torque and bending capacity of the pipe section adds to the material cost.

Welded Joint

A welded joint couples two sections of helical pile via a groove weld applied to the ends of the pipe sections. This coupling has advantages in installation efficiency and load transference. The welded joint eliminates coupling slack and creates a stiff load to deflection response. It has disadvantages during installation because crews must have equipment, training, and permits necessary to perform hot work in the field. An experienced and well-trained crew is typically required for successful application of welded joints.

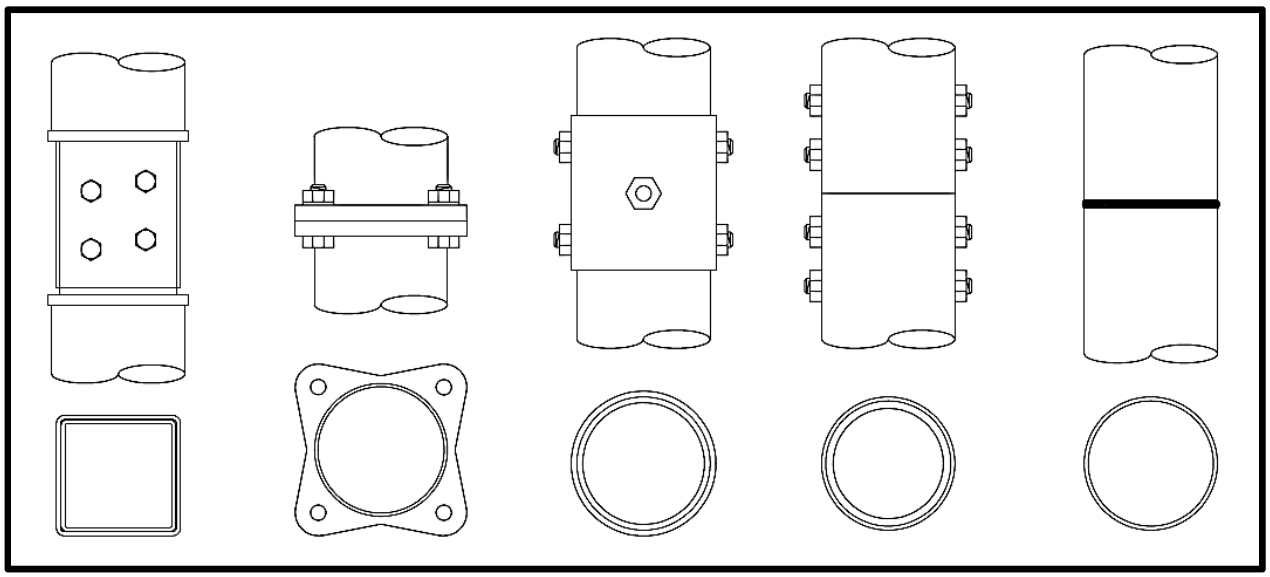


Fig. 1. Coupling Types from Left to Right: Square on Square, Flange to Flange, External Sleeve, Internal Sleeve, Welded Joint

TESTING AND SITE INFORMATION

Test Material

For these tests, 6-inch nominal diameter schedule 40 (6.625 inch OD) and 8-inch nominal diameter schedule 20 (8.625 inch OD) pipes were selected as the shafts for the helical piles. The coupling types chosen for testing were external sleeve, square on square, and flange to flange. These three types were chosen due to their availability and their prevalence in the helical piling industry.

For all the test piles, the lead section was 7 feet long with two helices. The helical configuration of all 6-inch lead sections was a 14-inch helix and a 16-inch helix spaced 42 inches apart, and for all 8-inch lead sections it was a 16-inch helix and an 18-inch helix spaced 48 inches apart. All extension sections had an effective length of 5 feet.

Description of Testing

Twenty-four helical piles were installed in two different locations (twelve piles in each location) to test in both non-cohesive and cohesive type soils. At each location, two installations and tension tests were performed for each coupling type for both the 6-inch and 8-inch piles.

Installation Equipment

A 1989 Ford L8000 equipped with an Altec D1000 digger derrick and a 20,000 ft·lb, two-speed Eskridge 74 Series drive head was used with CHANCE® installation tooling to install the helical piles. A calibrated CHANCE® digital torque indicator was used to monitor torque during installation.

Installation Procedure

The helical pile sections were laid out in their order of installation and marked in 1-foot intervals so torque and rotations could be recorded at each foot during installation. The pile sections were first connected to the tool string of the digger derrick and then moved to the installation location. Groups of piles were installed at a uniform extension of the digger derrick to minimize variation in the downward force applied during installation, and one operator performed all installations with consistent practices and installation rates. Plumbness of the pile sections was continually monitored visually and checked with a carpenter's level as needed. Two ground crew members were employed to monitor plumbness and record torque and rotations at each foot. For the 6-inch piles, a lead section and two extension sections were installed. Due to the limitation of the drive head torque output, the 8-inch piles were limited to the lead section and one extension section.

Test Equipment

A Power Team hydraulic pump was used with a load to pressure calibrated hydraulic cylinder and gauge combination consisting of an Enerpac RCH606 60-ton hollow plunger cylinder and an Enerpac G4088L 10,000-psi gauge to apply load to the piles via a 1-inch diameter section of DYWIDAG threaded bar. Two calibrated Mitutoyo ABSOLUTE Digimatic indicators were used to monitor deflection of the pile under load. The test frame consisted of 6-inch square wood cribbing supporting a 100-kip-rated aluminum test beam, and miscellaneous lengths of angle iron were used to build an independent reference beam to support the digital indicators. An adapter was made for each coupling type to connect the DYWIDAG bar to the helical pile.

Test Preparation

The test frame was centered about the vertical axis of the pile. The DYWIDAG bar was attached with a nut inside the coupling tension adapter and extended through the center hole of the test beam. The hollow plunger hydraulic cylinder was lowered over the DYWIDAG bar and placed atop the test beam. A bearing plate was positioned over the cylinder plunger and a nut was used to attach the DYWIDAG bar to the bearing plate. The hydraulic pump and gauge were then connected to the cylinder. The independent reference beam was constructed and the digital indicators were mounted in magnetic bases attached to the reference beam. The indicators were positioned equidistant from the pile center on either side.

Test Procedure

Once preparation was complete, load was applied to the helical pile in 600-psi increments via the hydraulic pump. The hold interval was 4 minutes at each load per the requirements of ASTM D3689, Standard Test Methods for Deep Foundations Under Static Axial Tensile Load. The spacing of wood cribbing did not follow the requirements for reaction spacing of ASTM D3689 due to constraints of the test frame size. This was considered acceptable since the load tests were used strictly for comparison of the effects the various coupling types had on axial capacity and not for the value of the axial capacity obtained. The test setup was the same for all piles, and it was assumed that any downward bearing pressure effects from the test frame were uniform for all piles.

Indicator readings were recorded for each load at the beginning and end of the hold interval. The load was increased until the pile was sufficiently loaded to determine ultimate geotechnical capacity. Once ultimate geotechnical capacity was exceeded, the pile was rebounded in three to four decrements with 1-minute hold intervals. The final rebound deflection was recorded with all load removed to determine net pile deflection.



Fig. 2. Test Setup

Non-Cohesive Test Site

A site with a fill layer of loose to medium-dense, well-graded sand at the approximate intersection of Interstate 255 and Bunkum Road near Caseyville, Illinois was selected for the non-cohesive test site. Borings of the area were not taken; however, the site was known to be a fill of uniform sand that was well-graded to a depth adequate for testing. Figure 3 below shows a sample of the soil from the test site. The water table at the site was estimated to be 5 to 10 feet below the surface based on the inspection of test piles following their removal and considering the site's proximity to a small lake and its location within the Mississippi River plain. Testing was completed at this location from November 6, 2018 through November 9, 2018.



Fig. 3. Typical Soil Sample from Caseyville, IL Site

Cohesive Test Site

Testing in cohesive soil was done in Centralia, Missouri at the intersection of Brick and North Howard Burton Streets. The soil in the area is a medium-stiff clay that transitions to very stiff with depth. During the period of testing, the ground was estimated to be fully saturated to an approximate depth of 5 feet below the surface due to snow melt and recent rains. Testing was completed at this site from February 11, 2019 through March 17, 2019. Table 1 is a representative boring that was performed on July 27, 2004.

Table 1. Centralia, MO Soil Boring Near Brick Street Test Site

BORING CME 55		
LOCATION: NE CORNER OF PRATT AND BRICK ST. CENTRALIA, MO		
DEPTH (ft)	**SOIL DESCRIPTION**	**SPT N**
0	MEDIUM STIFF CLAY (CL)	11
5	MEDIUM STIFF CLAY (CL)	5
10	STIFF CLAY, SOME SAND (CH)	7
15	STIFF CLAY, SOME SAND (CH)	12
20	SANDY CLAY (CL)	8
25	SANDY SILTY CLAY (CL)	21
30	VERY STIFF CLAY (CL)	14
NOTES: WATER TABLE AT 21 FEET		

TEST DATA AND RESULTS

Figures 4 and 5, respectively, are examples of rotations versus depth and torque versus depth charts of data that were recorded during installation. Figure 6 is a chart of the results from a tension test. Each reading from the two indicators was averaged to yield the deflection of the pile center, and the official calibration record of the cylinder and gauge was used to yield load values from the recorded pressure data. These plotted results are shown with the graphical representation of the ultimate capacity determination methodology used. The theoretical ultimate deflection of a helical pile was determined by the following equation:

$$D_{ULT} = PL/AE + 10\% D_{AVE} \quad [1]$$

Where D_{ULT} = ultimate deflection, P = applied load, L = total length of the pile, A = cross sectional area of the pile, E = elastic modulus of the pile shaft, and D_{AVE} = average diameter of the helices. (Seider, G., 2019) The PL/AE portion of this equation is the elastic deformation of the pile under load.

The ultimate capacity (P_{ULT}) of the pile was determined from the intersection of the Equation 1 line and the plotted deflection versus load results from the pile test. The P_{ULT} value is represented by the vertical red line in Fig. 6. This method yielded an ultimate capacity of 75.3 kip for the pile in this example.

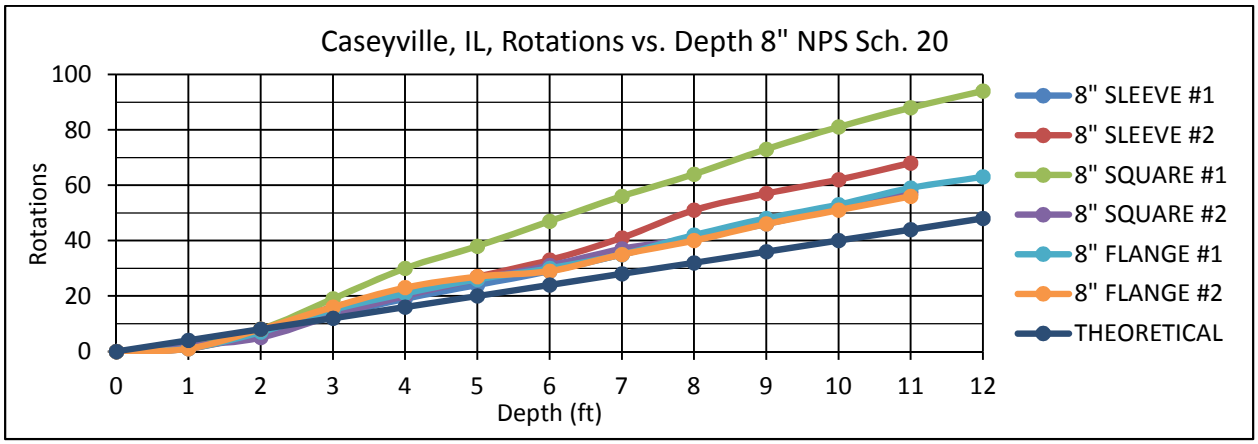


Fig. 4. Rotations vs. Depth Chart Example

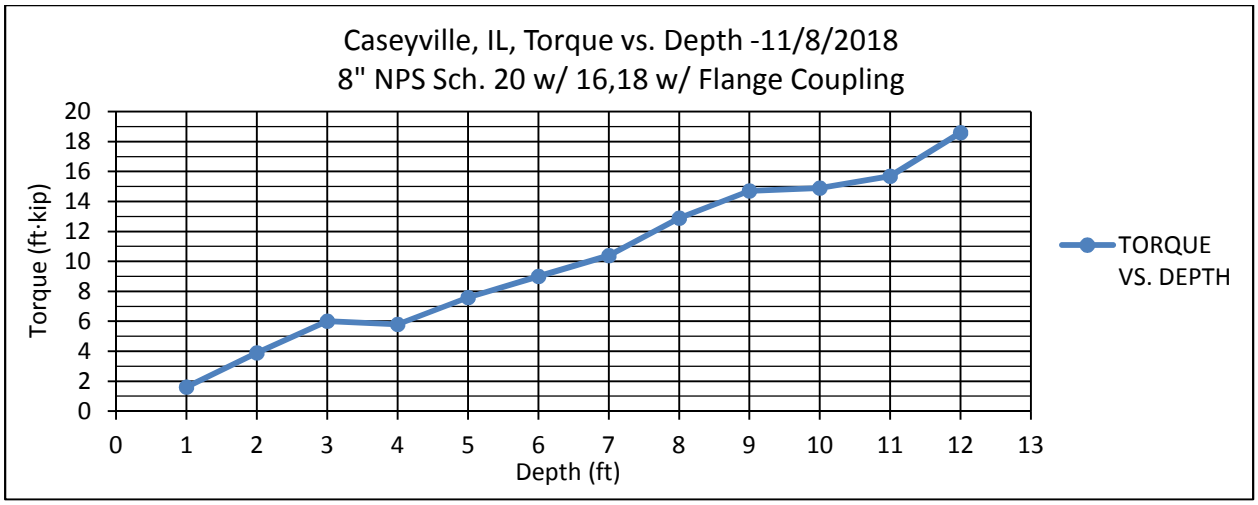


Fig. 5. Torque vs. Depth Chart Example

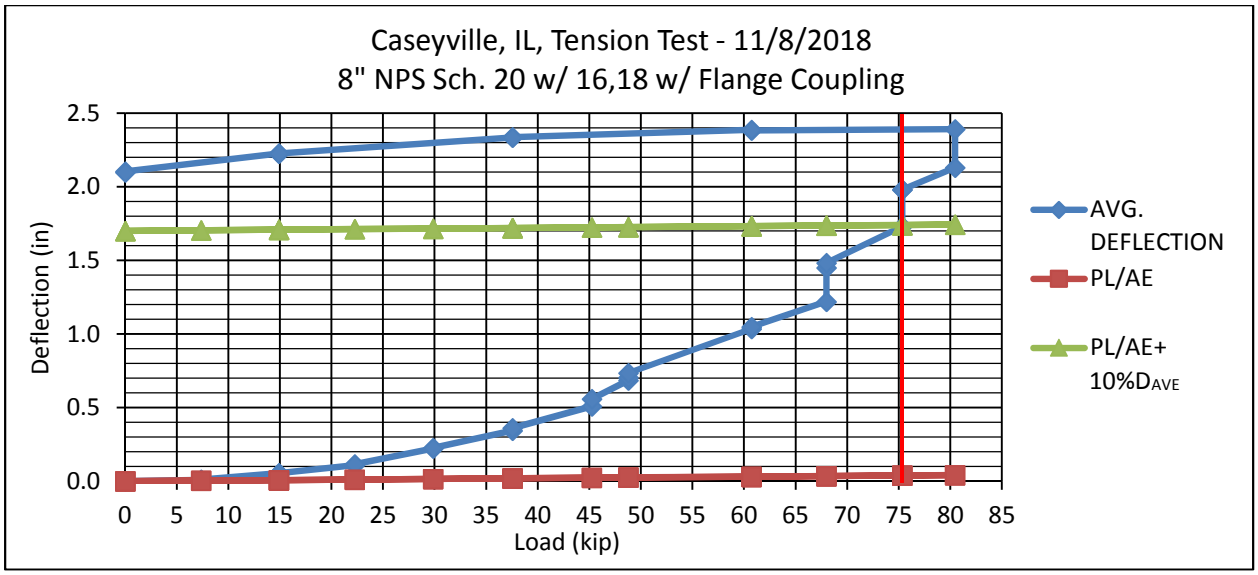


Fig. 6. Deflection vs. Load Chart Example with Ultimate Capacity Determination Criteria

Tables 2 and 3 summarize the averaged data and results for each pile configuration (each unique combination of pile size and coupling type) at the Caseyville, IL and Centralia, MO test sites, respectively. Two piles of each configuration were tested at each location.

The average rotations per foot values were determined by first calculating the rotations between each depth increment from the cumulative rotations data recorded during installation. All of the rotations per foot values for each pile configuration were then averaged.

Effective torque is the average of the final three torque readings recorded during a pile installation. The two effective torque values for each pile configuration were averaged to yield the average effective torque.

The average ultimate capacity of each pile configuration was calculated by averaging the ultimate capacity (P_{ULT}) values that were determined as explained above.

The torque to capacity ratio (K_t) of each pile was calculated by dividing the ultimate capacity by the effective torque, and the K_t values were then averaged to yield the average K_t for each pile configuration.

Table 2. Caseyville, IL Results Summary

HELICAL PILE SIZE	COUPLING TYPE	AVERAGE ROTATIONS PER FOOT	AVERAGE EFFECTIVE TORQUE (ft·lb)	AVERAGE ULTIMATE CAPACITY (kip)	AVERAGE TORQUE TO CAPACITY RATIO (K_t)
6" NPS Sch. 40	Sleeve	6.68	7,788	44.5	5.71
6" NPS Sch. 40	Square	8.16	9,417	35.2	3.71
6" NPS Sch. 40	Flange	11.38	8,483	41.1	4.95
8" NPS Sch. 20	Sleeve	5.73	15,450	70.0	4.53
8" NPS Sch. 20	Square	5.28	11,483	66.8	5.91
8" NPS Sch. 20	Flange	4.98	16,383	75.3	4.60

Table 3. Centralia, MO Results Summary

HELICAL PILE SIZE	COUPLING TYPE	AVERAGE ROTATIONS PER FOOT	AVERAGE EFFECTIVE TORQUE (ft·lb)	AVERAGE ULTIMATE CAPACITY (kip)	AVERAGE TORQUE TO CAPACITY RATIO (K_t)
6" NPS Sch. 40	Sleeve	4.68	11,333	57.1	5.06
6" NPS Sch. 40	Square	4.63	9,983	51.6	5.17
6" NPS Sch. 40	Flange	5.35	11,633	58.2	5.00
8" NPS Sch. 20	Sleeve	4.95	9,250	31.2	3.39
8" NPS Sch. 20	Square	4.45	8,217	31.4	3.82
8" NPS Sch. 20	Flange	4.83	9,517	39.5	4.15

ANALYSIS OF RESULTS

Tables 4 and 5 show the average torque to capacity ratio (K_t) and average rotations per foot results taken from Tables 2 and 3 with the three configurations of each pile size ranked from 1 (green; best performance) to 3 (red; worst performance). The K_t and rotations per foot were weighted based on relative importance with factors of 0.75 and 0.25, respectively. The rank numbers of each configuration were multiplied by their associated weight factor to yield weighted rankings which were then added to yield the weighted coupling score. With only two parameters being weighted, the specific factor values were unimportant to determine the relative rank of the weighted coupling scores, and the values of 0.75 and 0.25 were chosen to enlarge the spread of the weighted coupling scores. The choice of the parameter that was weighted more was significant, and it was considered that the torque to capacity ratio had a greater importance and was a superior indicator of the overall performance of the pile in service.

The weighted coupling scores from Tables 4 and 5 for each pile configuration at both test locations were averaged to yield the average coupling score for each pile configuration shown in Table 6.

The average coupling scores of both pile sizes for each coupling type were then averaged to yield the overall coupling scores shown in Table 7.

Table 4. Caseyville, IL Ranked Results and Weighted Coupling Scores

HELICAL PILE SIZE	COUPLING TYPE	AVERAGE TORQUE TO CAPACITY RATIO (K_t)	AVERAGE ROTATIONS PER FOOT	WEIGHTED COUPLING SCORE
6" NPS Sch. 40	Sleeve	5.71 (1)	6.68 (1)	1.00
6" NPS Sch. 40	Square	3.71 (3)	8.16 (2)	2.75
6" NPS Sch. 40	Flange	4.95 (2)	11.38 (3)	2.25
8" NPS Sch. 20	Sleeve	4.53 (3)	5.73 (3)	3.00
8" NPS Sch. 20	Square	5.91 (1)	5.28 (2)	1.25
8" NPS Sch. 20	Flange	4.60 (2)	4.98 (1)	1.75

Table 5. Centralia, MO Ranked Results and Weighted Coupling Scores

HELICAL PILE SIZE	COUPLING TYPE	AVERAGE TORQUE TO CAPACITY RATIO (K_t)	AVERAGE ROTATIONS PER FOOT	WEIGHTED COUPLING SCORE
6" NPS Sch. 40	Sleeve	5.06 (2)	4.68 (2)	2.00
6" NPS Sch. 40	Square	5.17 (1)	4.63 (1)	1.00
6" NPS Sch. 40	Flange	5.00 (3)	5.35 (3)	3.00
8" NPS Sch. 20	Sleeve	3.39 (3)	4.95 (3)	3.00
8" NPS Sch. 20	Square	3.82 (2)	4.45 (1)	1.75
8" NPS Sch. 20	Flange	4.15 (1)	4.83 (2)	1.25

Table 6. Average Coupling Scores for Pile Configurations

HELICAL PILE SIZE	COUPLING TYPE	AVERAGE COUPLING SCORE
6" NPS Sch. 40	Sleeve	1.50
6" NPS Sch. 40	Square	1.88
6" NPS Sch. 40	Flange	2.63
8" NPS Sch. 20	Sleeve	3.00
8" NPS Sch. 20	Square	1.50
8" NPS Sch. 20	Flange	1.50

Table 7. Overall Scores for Coupling Types

COUPLING TYPE	OVERALL COUPLING SCORE
Sleeve	2.25
Square	1.69
Flange	2.06

Among the 6-inch piles, the external sleeve coupling had the best weighted coupling score at Caseyville and the second-best score at Centralia. The sleeve coupling had the worst score and the worst values for K_t and rotations per foot among the 8-inch piles at both Caseyville and Centralia. The overall score of the external sleeve coupling was the worst at 2.25.

The square to square coupling scored best among the 8-inch piles at Caseyville and the 6-inch piles at Centralia. It had the second-best score for 8-inch piles at Centralia and the worst score for 6-inch piles at Caseyville. The 6-inch square coupling at Caseyville had the worst K_t and the second-best rotations per foot among the 6-inch piles at that location. The square to square coupling had the best overall score of 1.69.

The flange to flange coupling scored best for the 8-inch piles at Centralia and second-best for the 6-inch and 8-inch piles at Caseyville. The flange had the worst score, K_t, and rotations per foot among the 6-inch piles at Centralia. The overall score was second-best at 2.06.

To compare the torque to capacity ratios obtained from testing to standard theoretical values, the following equation from ICC-ES report AC358 section 3.13.1.1 was used:

$$K_t = 22.285\left(d_{eff}\right)^{-0.9195} \quad [2]$$

Where K_t = torque to capacity ratio and d_{eff} = effective shaft diameter. (ICC Evaluation Service, 2103)

From Equation 2, the theoretical K_t value for an 8-inch-diameter helical pile is 3.073 and for a 6-inch-diameter helical pile is 3.917. All the test piles except for one exceeded these theoretical K_t values. The Number 2 pile of the 6-inch, square coupling configuration at the Caseyville site yielded a K_t of 3.25, which is lower than the theoretical value of 3.917.

CONCLUSION

The ranked results in Tables 4 through 7 indicate that the square to square coupling is the most efficient design for axial loads when compared with flange to flange and external sleeve couplings. However, this conclusion cannot be fully justified without further testing due to the variability in the data gathered and the small number of piles tested. All coupling types are ranked highest among their size group in at least one test location, but the rankings for K_t and rotations per foot vary widely. The ranking system chosen also assumes that the torque to capacity ratio has a greater importance than the rotations per foot in determining the relative efficiencies of the coupling types.

The data suggests that most pile installations will meet or exceed the theoretical K_t recommendation from Equation 2 and that there is a possibility that flange to flange couplings could affect installation rates more than other coupling types. The tests discussed within this report were limited in depth and torque due to the constraints of the digger derrick used. Future tests that are installed to greater depths and at higher torque values may yield more discernable differences in the test data.

REFERENCES

Herron, J., and Brown, J. (Spring 2019). “Pile Installation” Personal.

Seider, G. (2019). Technical Design Manual, 4rd Edition.

ICC-ES Evaluation Services (2013.) AC358 Acceptance Criteria for Helical Foundation Systems and Devices

American Society for Testing Materials (2013). ASTM D3689 / D3689M - 07 Static Load Test Method for Pile under Static Axial Tension Load, 2013 Edition 1.

LARGE DIAMETER OPEN-END PIPE PILE DRIVEABILITY ANALYSIS INCLUDING GEOTECHNICAL FRICTION FATIGUE

Rozbeh B. Moghaddam, GRL Engineers, Inc., Cleveland, OH, USA, 216-831-6131, rmoghaddam@grlengineers.com

Patrick J. Hannigan, GRL Engineers, Inc., Cleveland, OH, USA, 216-831-6131, phannigan@grlengineers.com

Frank Rausche, GRL Engineers, Inc., Cleveland, OH, USA, 216-831-6131, frausche@grlengineers.com

ABSTRACT

Large diameter open-end pipe piles are increasingly used as deep foundations to support heavy onshore and offshore structures. During the driving process, several factors such as subsurface conditions, hammer type, hammer efficiency, pile type, plug conditions, temporarily increased base resistance, and loss of shaft resistance have direct impact on the driveability of large diameter open-end pipe piles. In a uniform subsurface condition, the unit shaft resistance increases with depth. Consequently, more resistance is accumulated as piles penetrate to greater depths which results in higher driving resistance. However, according to the friction fatigue analysis, the greater the number of shearing cycles occurring on a soil segment along the pile shaft, the greater the reduction of its shear resistance. As a consequence, since upper soil layers are subjected to a greater number of blows than those at greater depths, they have a relatively lower resistance compared to what would be calculated with standard geotechnical analysis methods. As a result of this progressive and nonuniform loss of shaft resistance with driving, blowcounts tend to increase at a lower rate than expected from traditional analyses.

This paper discusses one of the approaches to the driveability analysis with the geotechnical friction fatigue consideration. It also shows comparisons between predicted driveability obtained from wave equation analysis and field driving records. All analyses were performed for a 2.134 m (7.0 ft) diameter open-end pipe pile installed at a total depth of 192.90 m (554 ft). Two separate static resistance and wave equation analyses were completed for the case study presented in this paper: 1) Friction Fatigue analysis based on the recommendations of Alm and Hamre (2001), subsequently referred to as the FF model, and 2) Standard Driveability analysis based on soil set-up factors, hereafter referred to as the SD model in this paper. Results from analyses included the shaft resistance distributions compared to the result of the signal matching analyses determined from the pile dynamic measurement. Furthermore, predicted blowcounts were compared to observed blowcounts during the pile driving. The comparison analyses indicated a 54.4 percent resistance loss of the Static Resistance during Driving (SRD) due to the geotechnical friction fatigue corresponding to a 46 percent reduction in total resistance. The analyses also showed that average predicted blowcounts using the friction fatigue were 6.4 percent lower than measured blowcounts, whereas, the standard driveability approach showed 42.1 percent higher blowcounts compared to the blowcounts shown in the driving log values.

© 2019 Deep Foundations Institute

Introduction

Because of uncertainties associated with specific project site conditions and/or foundation type, measured data provides a better understanding of the soil resistance and its distribution throughout the embedded length of the pile. Back-analysis from a pile driving process based on a series of measured data could yield more accurate models for a better prediction. One of the analysis regarding pile driving during the design phase is the “driveability analysis” where capacity, blowcounts, maximum stresses in the pile element, and transferred energy from the hammer to the pile element are predicted using mathematical models. Such analysis requires relevant information regarding soil, pile, and hammer properties combined with a good understanding of their impact on the driveability analyses. Two widely discussed topics regarding installation and analysis of large diameter open-end pipe piles are the geotechnical fatigue or the “friction fatigue”, and the soil plug development during the driving process.

The friction fatigue concept relates to the soil resistance reduction along the pile shaft as the pile is driven deeper into the soil layers. Traditionally, instead of the friction fatigue approach, driveability analyses were performed assuming an empirical soil set-up factor for each soil layer. Therefore, it was assumed that during driving, regardless of the number of hammer blows, the SRD would be the long-term static resistance (LTSR) divided by the soil set-up factor. For example, if the soil set-up factor was 2 then the SRD was assumed to be 50% of the long-term resistance. This approach has been satisfactory for onshore piles with moderate penetration lengths. In case of the offshore piles, representative set-up factors were not as well defined for marine soils, in particular, marine clays. In some instances, the set-up factors ranged between 2 and 10.

Open-end pipe piles are susceptible to soil plugs formed during the driving process due to the side resistance build-up between the pile inner wall and the inner soil mass. Once the plug is formed, the foundation base resistance will be acting on the foundation full base area. In contrast, when the soil plug is not developed then the entire foundation base resistance will be acting on the pile annulus. Each one of these conditions will impact differently the driveability analysis.

This paper presents a background and review of previous work completed relevant to the geotechnical friction fatigue. The driveability analysis and its associated parameters are discussed. A geotechnical friction fatigue assessment model based on the Alm and Hamre (2001) recommendations is used to analyze the driveability of an open-end pipe pile pertaining to the foundation system supporting an offshore structure. As part of the results of analyses, comparisons between FF model-based SRD and SD model-based SRD and further between results of dynamic measurements are presented. The total shaft resistance for models are determined and discussed. Finally, predicted blowcounts are compared to blowcounts reported during the driving process. This case study, however, only addresses the pile driving caused shaft resistance reduction and not the plugging problem.

Friction Fatigue

In theory, the unit shaft resistance for a pile driven into a uniform soil deposit increases as the penetration depth is increased. Therefore, more resistance to driving is encountered at greater penetration depths (i.e., higher blowcounts with depth increase). However, for long piles undergoing thousands of hammer blows, it has been demonstrated that the unit shaft resistance decreases as the depth of penetration increases, (Moghaddam et al., 2017). The reduction of the shaft resistance was primarily attributed to the cyclic shearing process that the soil surrounding the pile undergoes during the driving. This event was introduced by Heerema (1979) as the friction fatigue concept, Figure 1.

In addition to observations made at a pile driving project, Heerema (1980) developed a laboratory device to further analyze the friction fatigue, and simulate the interaction between the steel wall of the pipe pile and the soil material. Results from the laboratory tests showed that the initial shear strength of the soil was decreasing as the number of oscillations were increasing which further confirmed the observations reported by Heerema (1979). After these results, other studies have evaluated several correlations regarding the friction fatigue concept and its impact on the design process; Randolph et al. (1991), Alm and Hamre, (2001), White et al. (2004), White (2005), Gavin et al. (2007), Schneider et al. (2010), and Moriyasu et al. (2018).

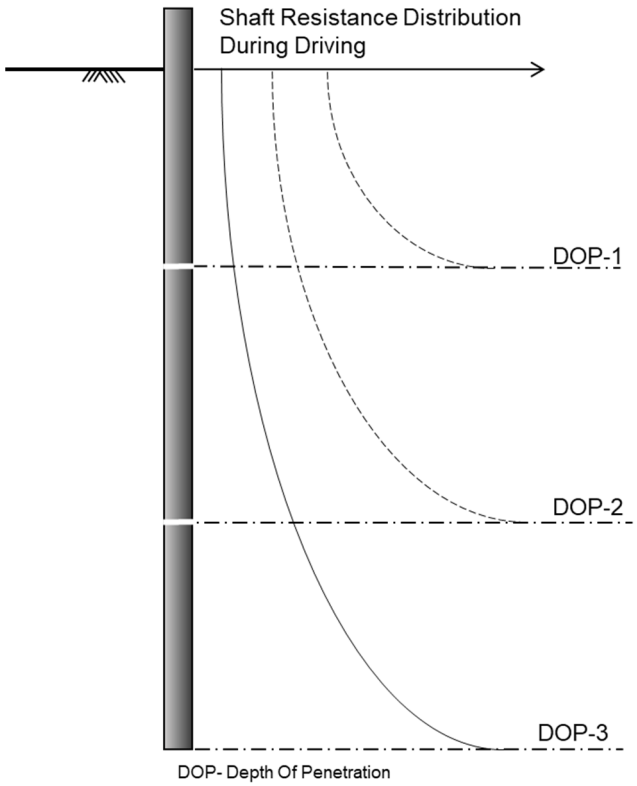


Figure 1. Shaft resistance distribution at different driving depth (Moghaddam, 2017)

The driveability analysis has a direct impact on the installation method, and the construction equipment selection including the driving hammer. Driveability analyses are commonly performed by wave equation analysis, using the E.A.L. Smith (1960) model. Also, other parameters such as soil conditions, pile material properties, pile dimensions, the friction fatigue concept, and in the case of open-ended pipe piles the plugging conditions have notable impact on the pile driveability predictions. Alm and Hamre (2001) presented a fitted model (A&H model) based on driveability studies of large diameter pipe piles installed in the North Sea. In order to reduce uncertainties associated with the selection of soil parameters, the strength parameters used for the determination of pile predicted capacities were determined using the cone penetration test results, and both unit shaft resistance, f_s, and unit base resistance, q_b, were correlated to the cone penetration test tip, q_t, and sleeve friction, q_s, resistances. From field logs and driving records, A&H concluded that the unit shaft resistance of a pile driven into soil layers will decrease exponentially from an initial unit shaft resistance, $f_{s\text{-}i}$, (i.e., long-term unit shaft resistance) to a residual value, $f_{s\text{-}res}$, (i.e. unit shaft resistance during driving). The mathematical model properly fitted to the measured data is presented by equations (1a and 1b). A&H model used expressions presented in Table 1 to determine $f_{s\text{-}res}$ and $f_{s\text{-}i}$. These expressions are classified based on soil type, CPT parameters, and effective vertical stress.

$$f_s = f_{s\text{-}res} + (f_{s\text{-}i} - f_{s\text{-}res})\, e^{-kh} \quad (1a)$$

$$k = \frac{1}{80}\sqrt{\frac{q_t}{\sigma'_0}} \quad (1b)$$

Where f_s is the unit shaft resistance, $f_{s\text{-}res}$ is the unit shaft resistance during driving, $f_{s\text{-}i}$ is the initial unit shaft resistance, h is the distance of a soil particle above the pile tip, k is the exponential function's shape factor determined from equation 1b, q_t is the CPT tip resistance, and σ'_0 is the effective vertical stress at the CPT depth.

Table 1. Expressions derived for $f_{s\text{-}i}$ and $f_{s\text{-}res}$ (Alm & Hamre 2001)

Soil Type	$f_{s\text{-}i}$	$f_{s\text{-}res}$
CLAY	Recorded CPT Sleeve Friction (q_{sf})	$0.004q_t(1 - 0.0025\frac{q_t}{\sigma'_0})$
SAND	$0.0132q_t(\frac{\sigma'_0}{P_a})^{0.13}\tan(\delta)$	$0.20f_{s\text{-}i}$

Analyzed Dataset

Geotechnical information and driving records for a four-legged offshore jacket were compiled and used for the comparison analysis presented in this manuscript. The foundation piles consisted of 2133.6-millimeter (84-inch) dimeter steel pipe piles with wall thickness varying from 25.0

millimeter (1.0 inch) to 38.1millimeter (1.5 inches) along the pile length. The piles were driven on a 1:8 batter, in four sections to a maximum depth of 110.5 m (363 feet) below the mudline.

Boring logs associated with this project indicated that the predominant subsurface conditions consisted of medium to coarse sand layers with interbedded soft to stiff clay layers varying between 3 meters (10 ft) to 11 meters (36 feet) in thickness. In addition to the borings, one CPT was completed at the project site to a maximum depth of 120-m (394-ft) below the mudline. Results from the CPT was used to determine A&H model parameters.

Hammer and Driving System

The driving systems used to install the main foundation steel pipe piles to the desired pile penetration depth consisted of a double acting hydraulic hammer (Menck MHU 800S) with a ram weight of approximately 445 kN (100 Kips). The maximum equivalent stroke is approximately 1.87-m (6.15-ft) resulting in a maximum manufacturer's rated energy of 820 kJ (605 ft-kips). This Menck hammer does not use a hammer cushion, resulting in steel on steel impact, and the helmet weight was assumed to be 104.8 kN (24 kips). According to the manufacturer, the total weight of the hammer is approximately 828 kN (186 kips).

Driveability Analysis

To evaluate the predicted blowcounts associated with the pile driving process, driveability analyses were performed using a Wave Equation Analysis Program, GRLWEAP Version 2010-8-Offshore. Input data including pile length, final penetration depth, location of splices, pile inclination, hammer stroke (energy level), hammer efficiency, unit shaft resistance, unit base resistance, quake and damping values, set-up factors, and base area were determined from relevant project information and the geotechnical report. As recommended by Alm and Hamre (2001), all driveability analyses were completed modeling a fully coring condition during driving with 100% external and zero internal friction. Also, for both analyses, the base resistance was only considered acting against the pile steel area, which would yield conservative driveability results.

Two driveability analyses were completed. The first analysis included the A&H friction fatigue model ("FF") where the static unit shaft and base resistances were determined using results from the Cone Penetration Test (CPT) completed at the project location and the equations shown in Table 1, Figure 2. The second analysis consisted of a standard driveability analysis ("SD") where the unit shaft and base resistances were determined using the American Petroleum Institute (2011) approach, Figure 3.

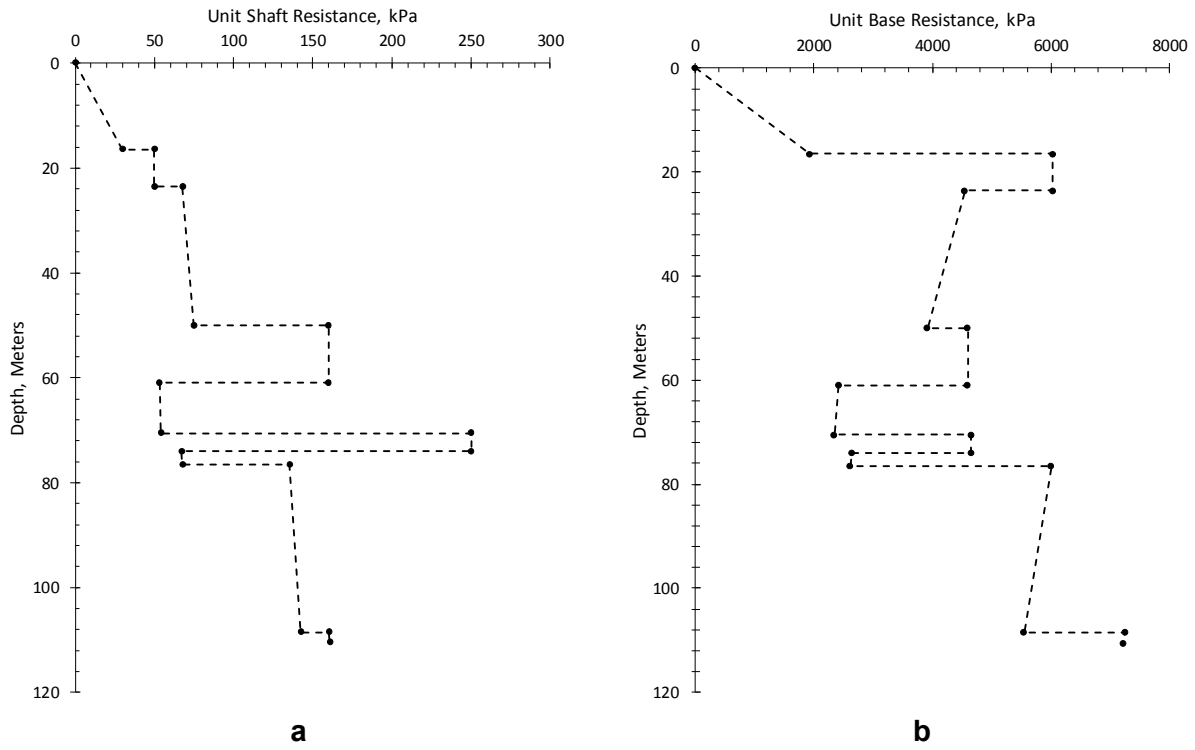


Figure 2. CPT and A&H based values for a) Unit Shaft Resistance and b) Unit Base Resistance

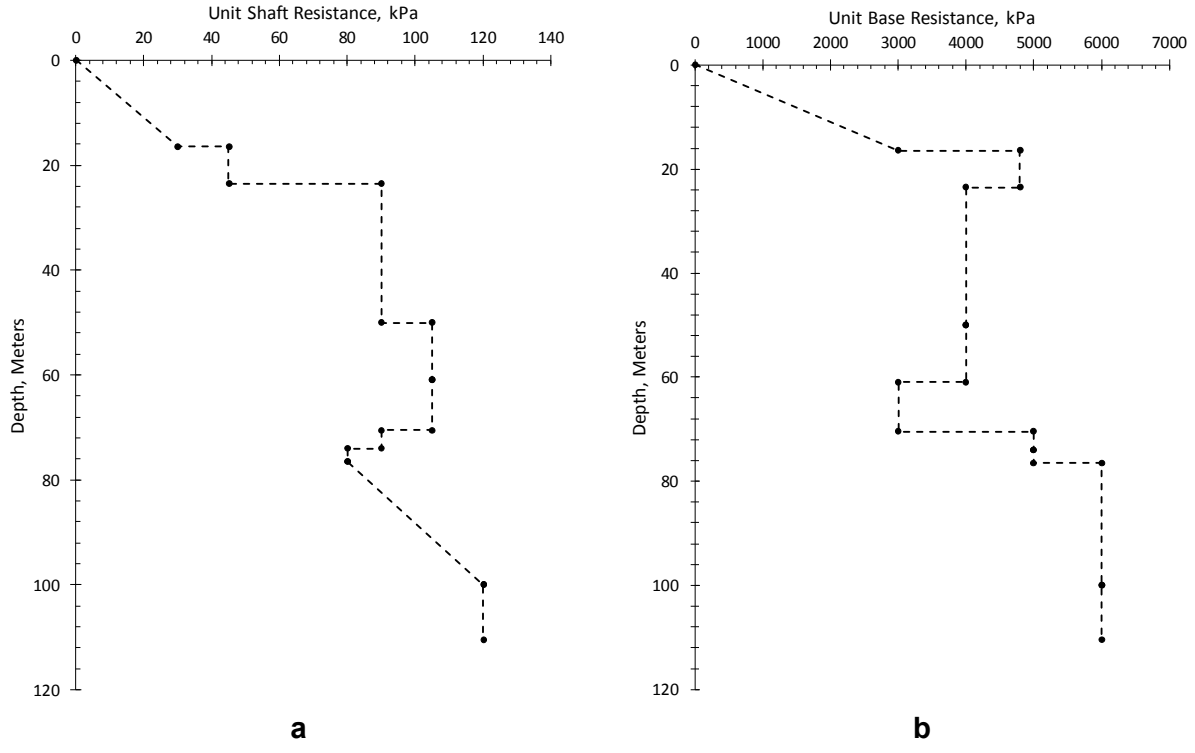


Figure 3. API based values for a) Unit Shaft Resistance and b) Unit Base Resistance

Standard Driveability Analysis

For the SD analysis, the unit shaft and base resistances were determined from Figures 3a and 3b, respectively. Since the driveability analysis was based on a fully coring model during driving, i.e., only the steel cross-sectional area used as the pile base area, a relatively high shaft and base quake values of 2.5-mm (0.1 inch) were used. For damping factors, values recommended by Smith (1960), studied by Rausche et al. (1992 and 2010), and further recommended by GRLWEAP-Offshore (2010) were used. Pile shaft damping factors of 0.16 s/m (0.05 s/ft) for sands and 0.65 s/m (0.2 s/ft) for clays were considered for the analysis; base damping factors were input as 0.50 s/m (0.15 s/ft) for all soil layers. Also, for the SD analysis, soil set-up factors of 1.20 and 2, and set-up times of 24 and 368 hours were considered for clays and sands, respectively. It should be mentioned that the set-up factors were average values observed for a variety of onshore pile driving sites. Also, the set-up time input allowed for modeling soil set-up gains during driving interruptions.

Friction Fatigue Driveability Analysis

For the FF model, the same dynamic parameters used in the SD model were selected. Unit shaft and base resistances, the set-up factors, i.e., the ratios of initial to residual shaft resistance values (see Table 1), and A&H model shape factors were determined using equations 1a and 1b.

Results

Calculated SRD distributions for the FF model and SD model were plotted and compared to the resistance distribution obtained from the dynamic measurements, Figure 4. For the comparison, the last blow where the pile reached the final penetration depth was considered and analyzed using CAPWAP® following the procedure presented by Rausche et al. (2010). Values determined and presented in Figure 4 correspond to the shaft resistance per 1-meter (3-feet) segment of the pile. The SRD corresponding to the FF model illustrates the expected decrease in the shaft resistance for a long pile where the soil layers undergo large shearing cycles. Results from the FF model showed approximately 54.4 percent decrease of the SRD when the pile reached the final depth of penetration. The main difference as far as driveability was concerned was a much higher anticipated shaft resistance in the standard approach at depths between 45 meters (148 feet) and 55 meters (180 feet) when compared to both FF model and CAPWAP results.

Comparing predicted resistance values to those measured using dynamic monitoring shows that measured values are on average 11.4 percent less than those obtained from the FF model and approximately 72.4 percent less than the results of the SD model. Understandably, these differences could be attributed to many variables associated with the pile driving process of a large diameter open-end pipe pile. In comparing the three plots shown in Figure 4, a gradual reduction in the shaft resistance is noted indicating the loss due to the friction fatigue concept. Furthermore, it is observed that between depths of 48 meters (158 feet) to 80 meters (263 feet) two noticeable resistance increase are present which could indicate a presence of a stiffer soil layer.

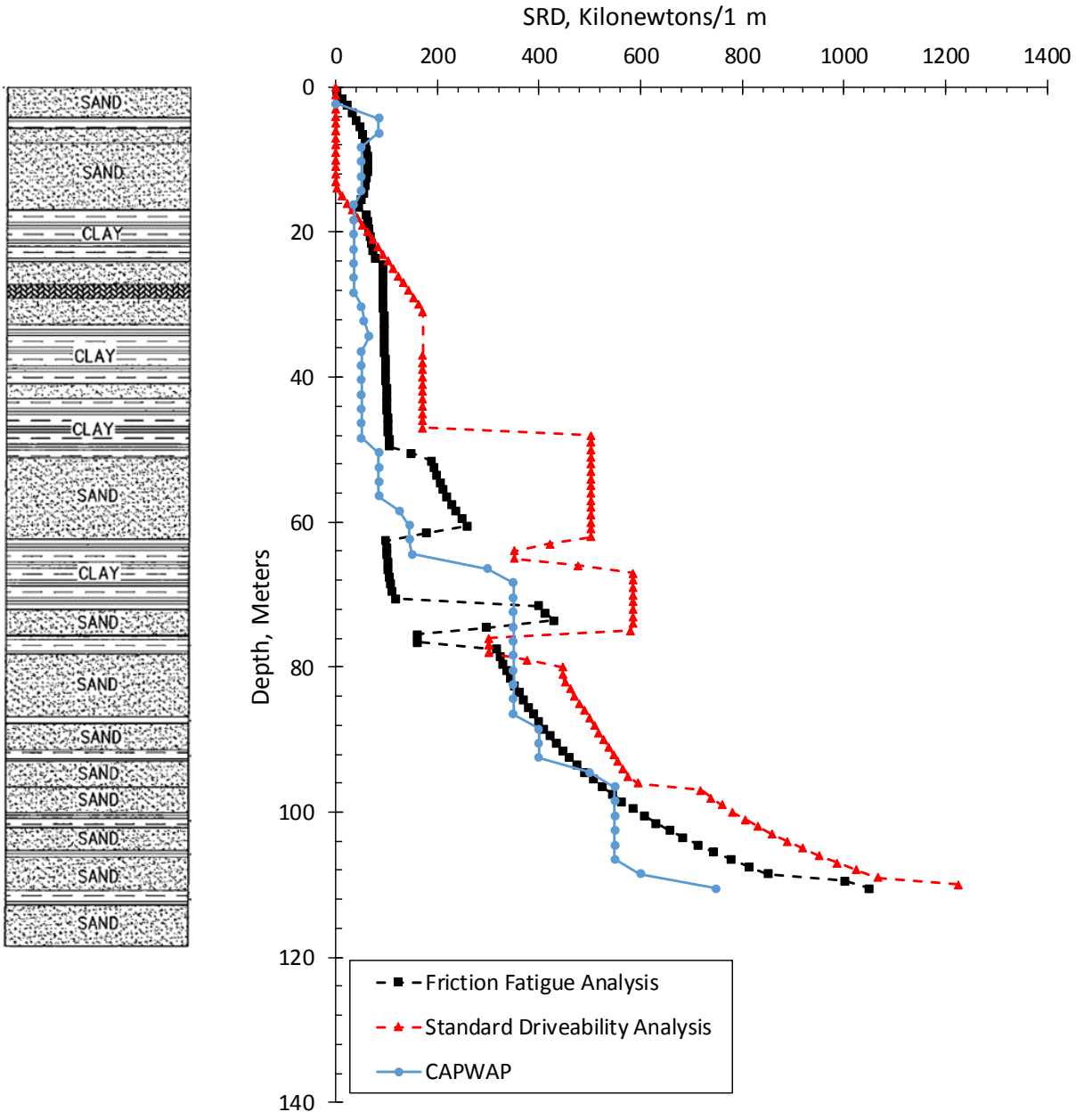


Figure 4. Shaft resistance distribution from predictive driveability analysis and measured dynamic monitoring

In addition to the SRD comparison, the friction fatigue effect was also demonstrated by plotting the total shaft resistance determined for each depth analyzed for the FF and SD models, Figure 5. The difference between the SD model and the FF model at the very end of driving is about 84%. It should be mentioned that for clarity, the soil profile was greatly simplified by ignoring thin soil layers. Also, the spikes in the SD shaft resistance plot near 40 meters (131 feet) and 76 meters (250 feet) depth could be attributed to soil set-up during pile splicing operations.

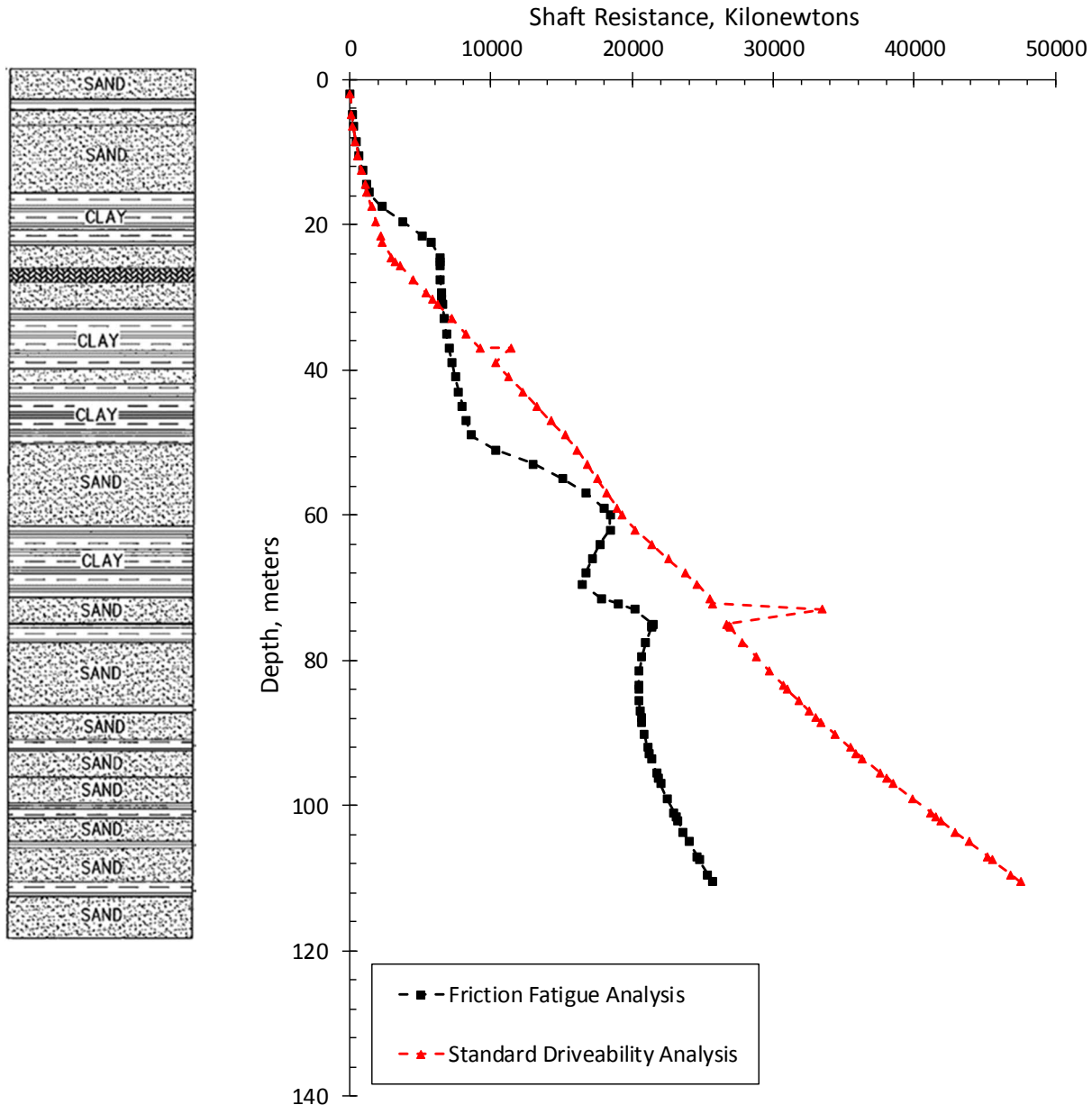


Figure 5. Comparison of FF Model and SD Model Total SRD

Finally, blowcounts resulting from the SD model, FF models, and observed blowcounts during installation are shown in Figure 6. It should be mentioned that all relevant analyses were completed using a constant hammer efficiency value of 95% at full energy setting. In reality, the energy settings were somewhat lower during the early part of the driving. However, the characteristic differences between the analyses become apparent in Figure 6; the FF model approximates the more or less constant blowcount behavior at the deeper penetrations while the SD model shows an exponential increase which would quickly lead to a refusal prediction. The observed blow count showed a number of spikes two of which were caused by soil set-up during

driving interruptions at 40 meters (131 feet) and 76 meters (250 feet) while other may have been due to variations in end bearing which either analysis failed to predict. Another difference between observed and calculated blowcounts are 0 blows (pile would be expected to penetrate under its own weight) down to approximately 20 meters (65 feet) in depth while the actual blow counts were fluctuating typically at values less than 5 blows per 250 mm (1 inch) at very low energy levels. No effort has been made to match those parts of the driving log by more appropriate energy levels since the main concern was the blowcount behavior at greater depths.

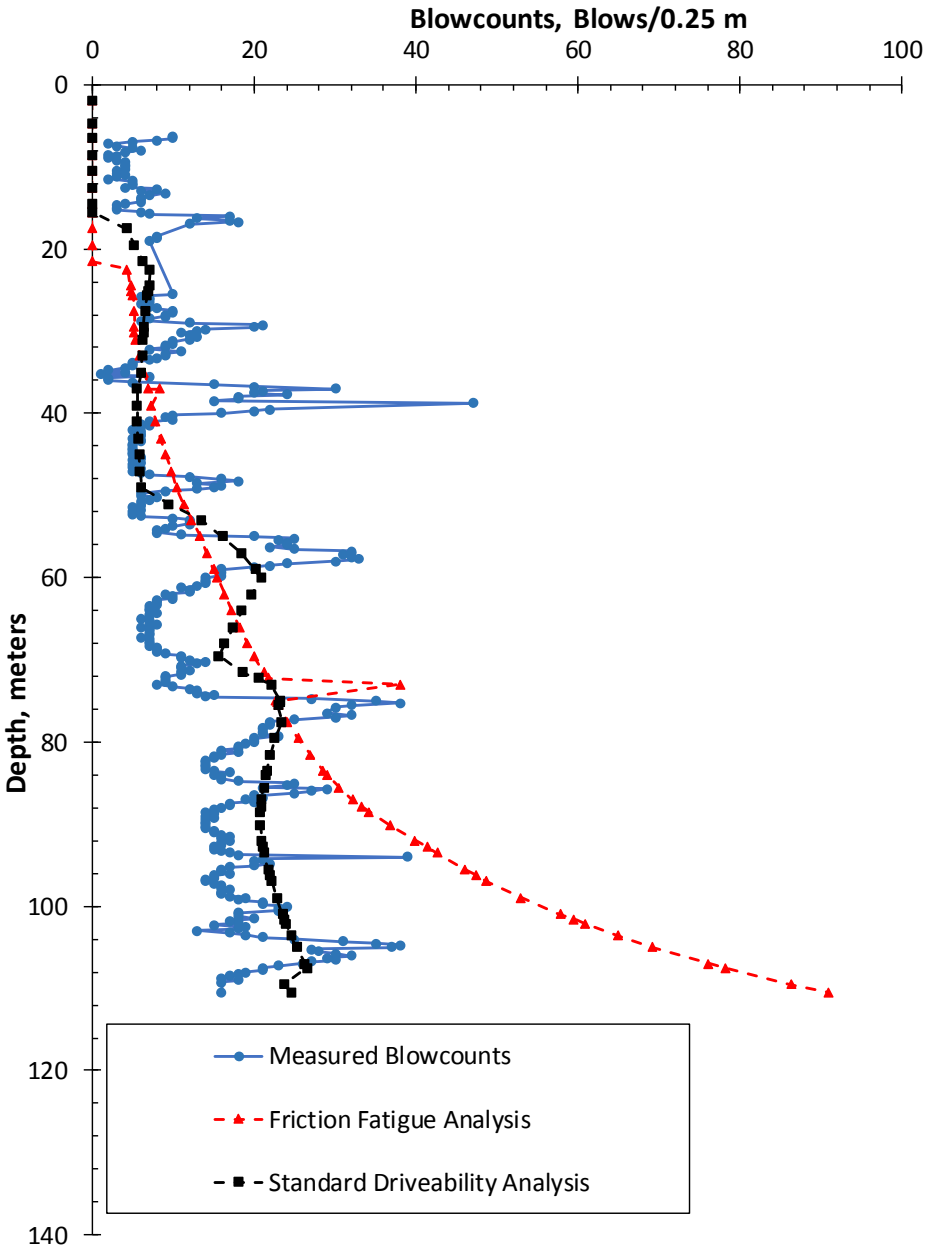


Figure 6. FF and SD model based Predicted blowcounts compared to observed blowcounts

Conclusions

This paper presented discussions regarding one of the approaches to the driveability analysis with the geotechnical friction fatigue consideration. It also shows comparisons between predicted driveability obtained from wave equation analysis and field driving records. All analyses were performed for a 2.134 m (7.0 ft) dimeter with wall thicknesses varying from 25.0 millimeter (1.0 inch) to 38.1millimeter (1.5 inches) along the pile length. The piles were driven on a 1:8 batter, in four sections, and to a maximum depth of 110.5 meters (363 feet) below the mudline. Two separate static resistance and wave equation analyses were completed for the case study presented in this paper: 1) Friction Fatigue analysis (FF Model), and 2) Standard Driveability analysis (SD Model).

Results from analyses, indicated an average of 54.4 percent loss of the Static Resistance during Driving (SRD) due to the geotechnical friction fatigue which represents 84 percent reduction in total shaft resistance. Furthermore, average predicted blowcounts using the friction fatigue were 6.4 percent lower than measured blowcounts, whereas, the standard driveability approach showed 42.1 percent higher blowcounts compared to the blowcounts shown in the driving logs.

For the FF model the high mid-length shaft resistance was practically “worn out”, whereas, For the SD model, the mid-length high shaft resistance was one of the main reasons for the high calculated blowcounts. Another reason could be that the standard soil set-up factors derived from relatively short onshore piles were not appropriate for the marine soil conditions.

All analyses were performed under the assumption of fully coring condition. The overall predicted blowcount behavior supports this assumption when it is compared to observed blowcounts during the driving process. A prediction under a fully plugged condition would have led to refusal blowcounts significantly prior to reaching the final penetration depth. From the measured data it was also noted that at least a partial soil plug is formed with noticeably short duration.

Friction fatigue and/or other reasons for an SRD less than expected values from standard static soil analysis based on soil borings or in-situ tests greatly impacts the shaft resistance and the pile driveability with deep penetrations For the case presented in this paper, the friction fatigue approach explains why the blowcounts do not increase in an exponential fashion as a constant increase in unit shaft resistance with depth would suggest. Therefore, it is recommended to use the friction fatigue approach with fully coring condition when large diameter open-end pipe piles are analyzed and are planned to be driven to greater depths. As the A&H model suggests, CPT data are required to perform a friction fatigue-based analysis. Therefore, if CPT data are not available, perhaps modifications of the A&H equations and model would be needed.

References

Alm, T., & Hamre, L. (2001). Soil model for pile driveability predictions based on CPT interpretations. In Proceedings of The International Conference On Soil Mechanics And Geotechnical Engineering (Vol. 2, Pp. 1297-1302). Aa Balkema Publishers

American Petroleum Institute. (2011). Geotechnical and Foundation Design Considerations, API
Basu, P., Loukidis, D., Prezzi, M., & Salgado, R. (2014, February). The mechanics of friction fatigue in jacked piles installed in sand. In Geo-Congress 2014American Society of Civil Engineers

Gavin, K. G. and Lehane, B. M., 2007, "Base Load-Displacement Response of Piles in Sand," Can. Geotech. J., No. 44, pp. 1053–1063

Heerema, E. P. (1979) Relationships between wall friction, displacement velocity and horizontal stress in clay and in sand, for pile driveability analysis. Ground engineering, 12(1)

Heerema, E. P. (1980) Predicting pile driveability: Heather as an illustration of the" friction fatigue" theory. In SPE European Petroleum Conference. Society of Petroleum Engineers

Moghaddam, R.B., Rausche, F., Webster, S.D. (2017) Friction Fatigue and Driveability Analysis of Open Ended Pipe Piles Based On Cone Penetration Testing Results, Proceedings of 43rd Annual Deep Foundation Institute, New Orleans, LA

Moriyasu, S., Kobayashi, S. I., & Matsumoto, T. (2018). Experimental study on friction fatigue of vibratory driven piles by in situ model tests. Soils and foundations, 58(4), 853-865
Offshore Pile Plugging." Marine Geotechnology, 8(3), pp. 213-230

Randolph, M. F., Leong, E. C., & Houlsby, G. T. (1991). One-dimensional analysis of soil plugs in pipe piles. Geotechnique, 41(4), 587-598, RP GEO, American Petroleum Institute, Washington, DC.

Rausche, F., Likins, G., Liang, L., Hussein, M., 2010.The Art of Foundation Engineering Practice, Geotechnical Special Publication No. 198, American Society of Civil Engineers: Reston, VA; 534-553.

Rausche, F., Goble, G. G., & Likins, G. E. (1992). Investigation of dynamic soil resistance on piles using GRLWEAP. In Proceedings of the Fourth International Conference on the Application of the Stress-Wave Theory to Piles, AA Balkema, Netherlands (pp. 137-142)

Schneider, J. A., & Harmon, I. A. (2010). Analyzing Drivability of Open Ended Piles in Very Dense Sands. DFI Journal-The Journal of the Deep Foundations Institute, 4(1), 32-44

Smith, E.A.L. (1960), "Pile Driving Analysis by the Wave Equation", Journal of Soil Mechanics and Foundation Division, ASCE, Vol. 86, No. SM4, 35-61.

Stevens, R. F. (1988) The effect of a soil plug on pile drivability in clay, Proc., III Int. Conf. on Applications of Stress Wave Theory to Piles, Ottawa, Balkema, Rotterdam, 861–868

White, D. J. (2005, September). A general framework for shaft resistance on displacement piles in sand. In Proceedings of the 1st International Symposium on Frontiers in Offshore Geotechnics, ISFOG 2005 (pp. 697-704). Taylor and Francis

White, D. J., & Lehane, B. M. (2004). Friction fatigue on displacement piles in sand. Géotechnique, 54(10), 645-658

p-y CURVES FOR ANALYZING MICROPILES IN SANDY SOILS USING LATERAL LOAD TEST DATA

Akhter Hossain, Ph.D., P.E., Geotechnical Engineer II, AECOM, 1255 Broad Street Suite 201, Clifton, New Jersey, 07013, USA, e-mail: akhter.hossain@aecom.com
Mahdi Soudkhah, Ph.D., P.E., Senior Geotechnical Engineer, AECOM, 250 Apollo Drive, Chelmsford, Massachusetts, 01824, USA, e-mail: mahdi.soudkhah@aecom.com

ABSTRACT

Vertical micropiles are generally considered to be low in lateral resistance. Therefore, battered micropiles are often used when additional lateral load carrying capacity is required. However, battering of micropiles can sometimes be restricted due to existing adjacent structures or utilities, especially in highly urbanized areas. For example, presented in this paper are lateral load test data from a 43-story building project in New York City where vertical micropiles were used due to proximity to adjacent structures. Three static lateral load tests were conducted on micropiles consisting of 13.375-in-outside diameter and 25- to 51-ft-long casings, and socketed 10 to 12.6 ft into the bedrock (gneissic schist). The subsurface profile above the bedrock consists of loose to very dense, mostly sandy and silty soils. The design load for the three test piles was 14,000 lb and the maximum load applied during the tests was 200% of the design load. Lateral load-displacement behavior of the free pile heads from the load tests are compared with the results of p-y analyses based on a widely used p-y method for sandy soils and using a lower and an upper bound estimates of soil index properties and strength parameters. Since the existing p-y curves were formulated for larger diameter driven piles at a specific geographic location, major differences are observed between the results of the load tests and the p-y analyses. In general, the lateral displacements estimated based on the p-y analyses using upper bound soil parameters are relatively closer to the results of the field load testing. Modified p-y curves specific to the sandy and silty soils representative of the general subsurface conditions of New York City matched with the lateral load tests are presented in this paper.

Keywords: micropile, lateral load test, p-y curves, New York City

INTRODUCTION

Micropiles generally are limited in lateral load carrying capacities due to their relatively higher slenderness ratios (ratio of depth to diameter) compared to more conventional deep foundation alternatives, such as driven piles and drilled shafts. So, micropiles are not typically considered as deep foundation solutions when significantly high lateral loads are expected on the substructures. Various means to increase the lateral resistance of micropiles include battering and installing an oversized casing in the top portion of the piles (FHWA 2005; and Richard and Rothbauer 2004). However, it is often not possible to install micropiles in a battered position in highly urbanized areas due to existing adjacent structures or utilities. Installation of oversized casing is often restricted by limited space availability and concerns of losing lateral capacities due to closely spaced group of piles. Thus, estimation of lateral resistance of vertical micropiles can become highly important for geotechnical engineering projects in urban areas when a small to moderate amount of lateral resistances are expected from the substructures, often to withstand seismic and wind loads.

The current state of the practice for estimating lateral resistance of piles involves the p-y analysis method contained within computer programs, such as LPile (Ensoft 2017). The p-y curves developed by Reese et al. (1974) are widely used for piles in sandy soils although they were not developed specifically for micropiles. The Reese et al. p-y curves were developed based on lateral load tests on 24-inch-outside diameter (OD) driven pipe piles installed in a predominantly clean fine sand to silty sand site on Mustang Island in Texas. As stated by Reese et al., "*Evidence in geotechnical literature amply declares that each sand deposit is distinctive, with characteristics depending not only on the nature of the grains and their*

© 2019 Deep Foundations Institute

arrangements but also on the history of the deposit." Thus, a certain amount of variability is expected while using the p-y curves by Reese et al. to estimate lateral resistances of micropiles at sandy soil sites in other areas of the world.

In the last fifteen years, many researchers have investigated the lateral resistance of vertical micropiles installed in various silty and sandy soil sites located in USA, Canada, Germany and Italy by performing static monotonic (Anderson and Babalola 2011; Abd Elaziz and El Naggar 2015; Ischebeck and Ischebeck 2014; Long et al. 2004; Richard and Rothbauer 2004; Wright et al. 2014), static cyclic (Abd Elaziz and El Naggar 2015) and dynamic (Capatti et al. 2016) lateral load tests. Comparisons were made between the results of load tests and p-y analyses in some of these studies, which showed that the static load tests provided consistently higher capacities than the values estimated based on the p-y method. One of the main reasons for the lower estimates of lateral resistances by the p-y method can be attributed to overly conservative assumptions regarding soil shear strength, especially near the ground surface (Richard and Rothbauer 2004).

Presented in this paper are the results of three static lateral load tests on micropiles from a predominantly sandy/silty soil site in New York City. Lateral load-displacement behavior of the pile heads from the load tests are compared to the results of LPile analyses based on p-y curves by Reese et al., and using a lower and an upper bound estimates of soil index properties and shear strength parameters. Modified site specific p-y curves matched with the load test results are also presented in this paper.

SITE LOCATION AND SUBSURFACE CONDITIONS

Results of the three pile load tests presented in this study were obtained from a 43-story building (with one cellar level) project. The project site is located near the Queens Plaza Subway Station in the borough of Queens in New York City. A total of 14 Standard Penetration Test (SPT) borings were drilled at the project site in December 2013 and January 2015. All split-spoon samples collected from the borings were visually classified, and grain size analyses and Atterberg limits tests were performed on some selected samples in a geotechnical laboratory.

Generalized subsurface profiles at the locations of the three test piles (Test Piles TP-1, TP-2 and TP-3) along with the three nearest SPT borings (Borings B-1, B-2 and B-3, respectively) are presented in Figure 1. Based on these three borings, the top soil layer (Stratum 1) at the test locations generally consists of loose to medium dense, medium to fine sand with thickness varying between 13 and 23 ft. Stratum 1 is underlain by a loose to medium dense silty sand layer (Stratum 2) with thickness ranging from 14 to 20 ft. Underlying Stratum 2 is a stiff to very stiff, low plasticity sandy silt to silt layer (Stratum3) with thickness ranging from 5 to 20 ft. Stratum 3 is underlain by a very dense layer (Stratum 4) of glacially deposited till material comprising mostly of sand with occasional clay and rock fragments. Thickness of Stratum 4 vary from 5 to 10 feet at the test locations. Bedrock comprising of medium hard to hard sound (Rock Quality Designation, RQD, of 73% or higher) gneissic schist of the Hartland Formation (Baskerville 1994) was encountered at depths of 44 to 67 feet below the original ground surface. As shown in Figure 1, the top 15 to 21 feet of soil were excavated prior to installation of the piles.

Groundwater observation wells were installed upon completion of two of the borings. In addition, five observation wells were installed just outside of the project boundary to monitor the fluctuation in groundwater table throughout the project duration. As shown in Figure 1, the groundwater table was very close to the ground surface after excavation. Sump pits and pumps were used for dewatering.

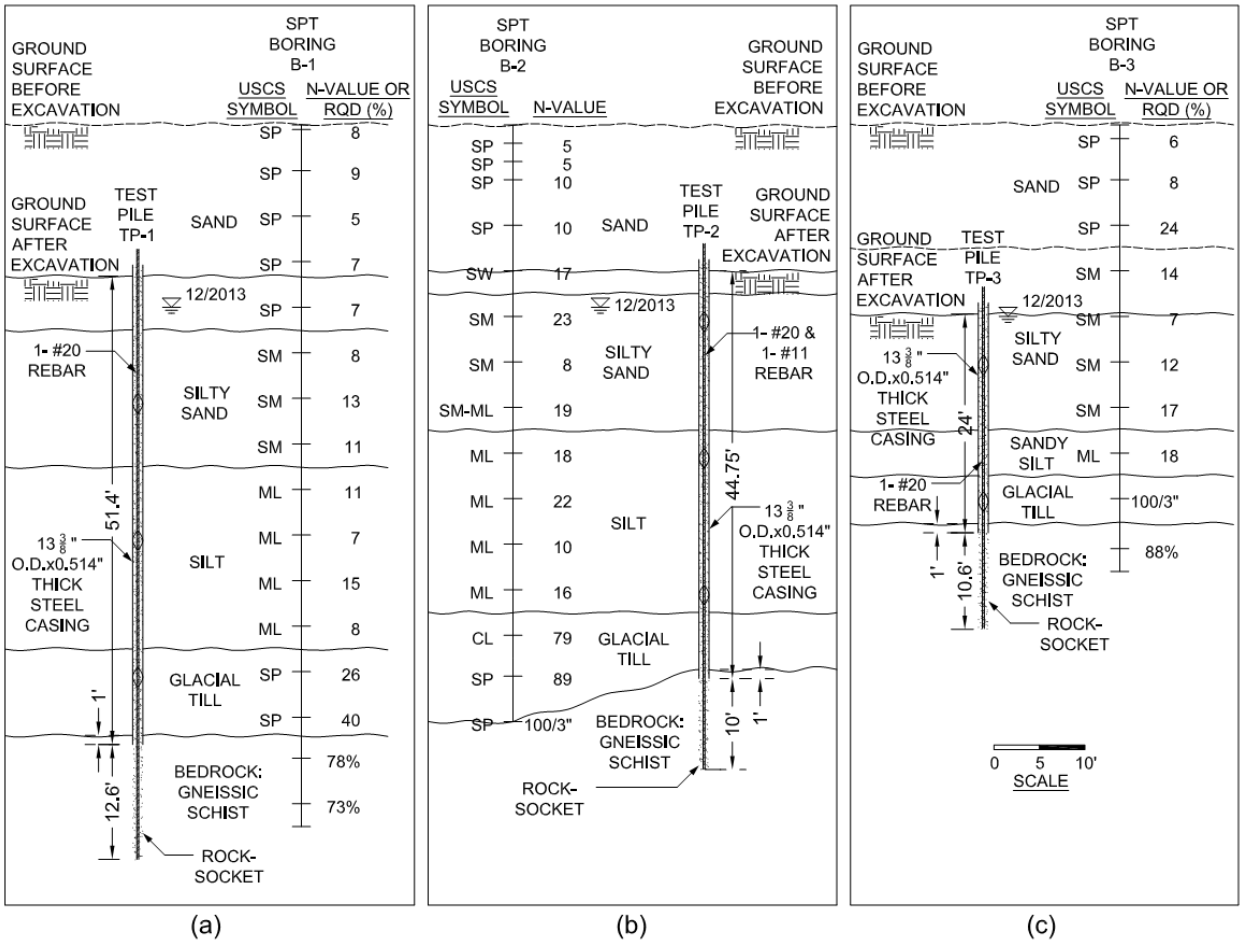


Fig. 1. Details of the three test piles and subsurface profiles at the pile locations - (a) Test Pile TP-1 and Boring B-1, (b) Test Pile TP-2 and Boring B-2, and (c) Test Pile TP-3 and Boring B-3

PILE INSTALLATION

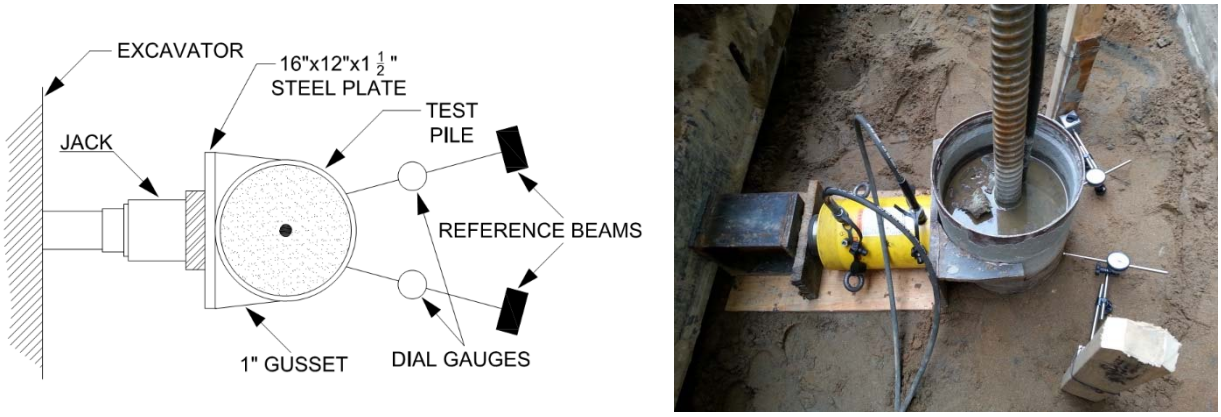
The three test piles were installed in August 2015 in general accordance with the New York City Building Code (2014) requirements. 13.375 in-OD and 0.514 in-thickness steel casings with yield strength of 80,000 lb/in^2 were drilled through the four soil strata overlying the bedrock using a down-the-hole hammer and air flush. The casings were drilled into the bedrock to achieve 1 ft of embedment. As shown in Figure 1, the total lengths of the casings below the ground surface after excavation were approximately 51, 45 and 24 ft for Test Piles TP-1, TP-2 and TP-3, respectively.

After the casings were advanced to the specified embedment depths, rock sockets were drilled and the inside of the casings were cleaned of all spoils by flushing with water. Video inspections were performed using a down-the-hole camera to verify the competence of rock in the sockets. Grade 150 threaded reinforcing bars were placed with spacers to the bottom of the sockets. Lengths of the rock sockets were approximately 13, 10 and 11 ft for Test Piles TP-1, TP-2 and TP-3, respectively.

Tremie-grouting operations were conducted by placing a PVC tube to the bottom of the socket until good grout exited the top of the casings. Compressive strengths of four cylindrical (diameter of 3 in and height of 6 in) grout specimens cast from the grout pours used for Test Piles TP-1 and TP-3 were tested in a concrete laboratory. The compressive strengths ranged from 4,022 to 5,931 lb/in^2 at the age of 4 and 7 days.

PILE LOAD TESTING

All lateral load tests were performed on production piles in October and November 2015 following the general procedures outlined in ASTM D3966/D3966M (ASTM 2013). A schematic diagram of the load test set up and a photograph of the load testing of Test Pile TP-1 are presented in Figures 2a and 2b, respectively. Timber cribbing was used to provide stable support to the test frame components. All elements of the test frame were tack welded together. An excavator with an operating weight of 42,770 lb was used for providing reaction during application of the test loads. The loading plate, hydraulic jack, reference beams and dial gauges were installed in the arrangement shown in Figure 2. Two additional dial gauges with reference beams were positioned on the excavator body in order to detect and remove the effects of any possible movement of the excavator.



(a) (b)

Fig. 2. (a) Schematic of pile load test set up, and (b) photograph of lateral load test on Test Pile 1

As shown in Figure 2, the lateral load tests were performed on the piles at free (pinned) head condition (i.e., the pile head was free to rotate). Load was applied in ten 1,400 to 3,500 lb increments to two times the design load (DL) (28,000 lb), followed by unloading in four 7,000 lb increments. The loading increments and the hold times for each increment are listed in Table1. For each loading increment, the load and deflection were recorded immediately after the application of load and then at an interval of 5 to 20 minute until the end of the hold time.

Table 1. Loading increments and hold times

Increment	Load (lb)	Hold Time (minute)	Increment	Load (lb)	Hold Time (minute)
0	0	--	8	1.8DL = 25,200	20
1	0.25DL = 3,500	10	9	1.9DL = 26,600	20
2	0.5DL = 7,000	10	10	2DL = 28,000	60
3	0.75DL = 10,500	15	11	1.5DL = 21,000	10
4	DL = 14,000	20	12	DL = 14,000	10
5	1.25DL = 17,500	20	13	0.5DL = 7,000	10
6	1.5DL = 21,000	20	14	0	--
7	1.7DL = 23,800	20			

Note: DL = design load.

TEST RESULTS

Presented in Figure 3 are plots of lateral loads applied to the three test piles versus lateral displacements of the pile heads. Test Piles TP-1 and TP-3 showed almost the same load-displacement behavior with a maximum lateral displacement of 0.66 and 0.67 in, respectively. However, Test Pile TP-2 exhibited a much softer response with a maximum lateral displacement of 1.28 in. One likely reason for this softer response is that the top soil around Test Pile TP-2 may have been disturbed by over-excavation followed by backfilling without proper compaction.

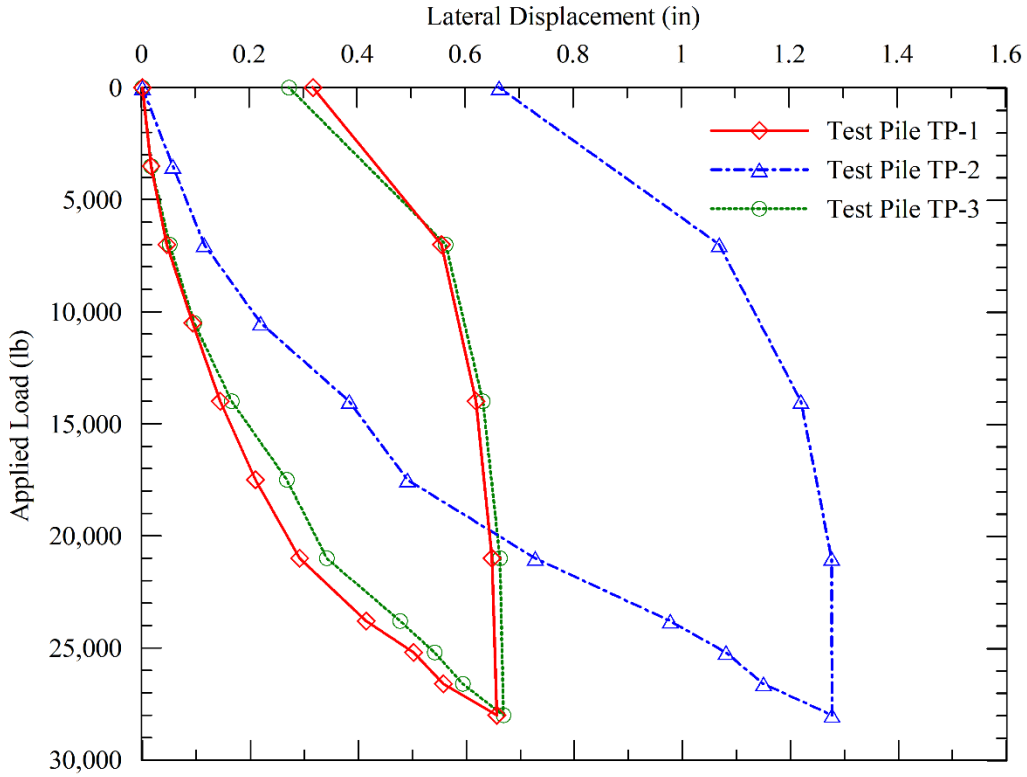


Fig. 3. Results of lateral load tests on the three test piles

p-y ANALYSES

Lateral displacements of the three test piles at the maximum load of 28,000 lb were estimated using the computer program LPile. The p-y curves for sandy soils developed by Reese et al. (1974) contained within LPile were used for the top four soil strata. For the bedrock stratum, p-y curves for the "Strong Rock" model within LPile were used. Analyses were performed using a lower bound (LB) and an upper bound (UB) sets of soil index properties and strength parameters (i.e., unit weight, friction angle and p-y modulus) based on the SPT boring and laboratory test results, which are presented in Table 2. Values of ϕ for various soil strata were estimated using the following correlation based on the stress-normalized and energy corrected N-value, $(N_1)_{60}$ (NCHRP 2019):

$$\phi = 20° + \sqrt{15.4\,(N_1)_{60}} \qquad [1]$$

Table 2. Soil index properties and strength parameters used for the LPile analyses

Stratum No.	Stratum Description	Total Unit Weight, γ (lb/ft^3)		Friction Angle, ϕ (°)		p-y Modulus (lb/in^3)	
		LB	UB	LB	UB	LB	UB
1	Sand	112	119	34	42	60	90
2	Silty Sand	113	121	34	44	60	125
3	Silt/Sandy Silt	112	121	34	45	60	125
4	Glacial Till	122	131	41	45	90	125

Note: LB = lower bound; and UB = upper bound.

Lateral displacements of the pile heads from LPile analyses of the three test piles are presented in Table 3. As shown, the p-y curves by Reese et al. predicts much higher lateral displacements for all three test piles when the LB soil parameters of the sandy/silty soils are used. For Test Piles TP-1 and TP-3, even with the UB soil parameters, the p-y curves by Reese et al. predict higher (although to a lesser extent) lateral displacements of the piles. However, for Test Pile TP-2, the p-y curves by Reese et al. predict a smaller lateral displacement based on the UB soil parameters.

Also presented in Table 3 are the required modification factors (MF) for the p-y curves by Reese et al. to match the lateral displacements of the pile heads from LPile analyses to the results of the load tests. As can be expected, the values of MF are greater than 1 for all cases except for Test Pile TP-2 with the UB soil parameters.

Table 3. Comparison between lateral displacements of pile heads from lateral load tests and LPile analyses

Test Pile	Lateral Displacement from Load Tests (in)	Lateral Displacement from LPile Analyses (in)		Modification Factor for p-y Curves to Match Displacements from LPile Analyses with Load Test Results	
		LB Soil Parameters	UB Soil Parameters	LB Soil Parameters	UB Soil Parameters
TP-1	0.66	1.69	0.86	3.1	1.4
TP-2	1.28	1.68	0.81	1.4	0.56
TP-3	0.67	1.66	0.75	2.9	1.15

Note: LB = lower bound; and UB = upper bound.

Comparison of p-y curves by Reese et al. based on the LB and UB soil parameters for the top three sandy/silty soil stratums are presented in Figures 4(a), 4(b) and 4(c), respectively. Also presented in these figures are the modified p-y curves after applying the respective MF listed in Table 3. The lower and upper p-y curves in each range represent the p-y curves near the top and bottom of each soil stratum, respectively. As shown in Figure 4, ranges of the modified p-y curves for each soil stratum are generally stiffer compared to the p-y curves by Reese et al. estimated using the LB and UB soil parameters.

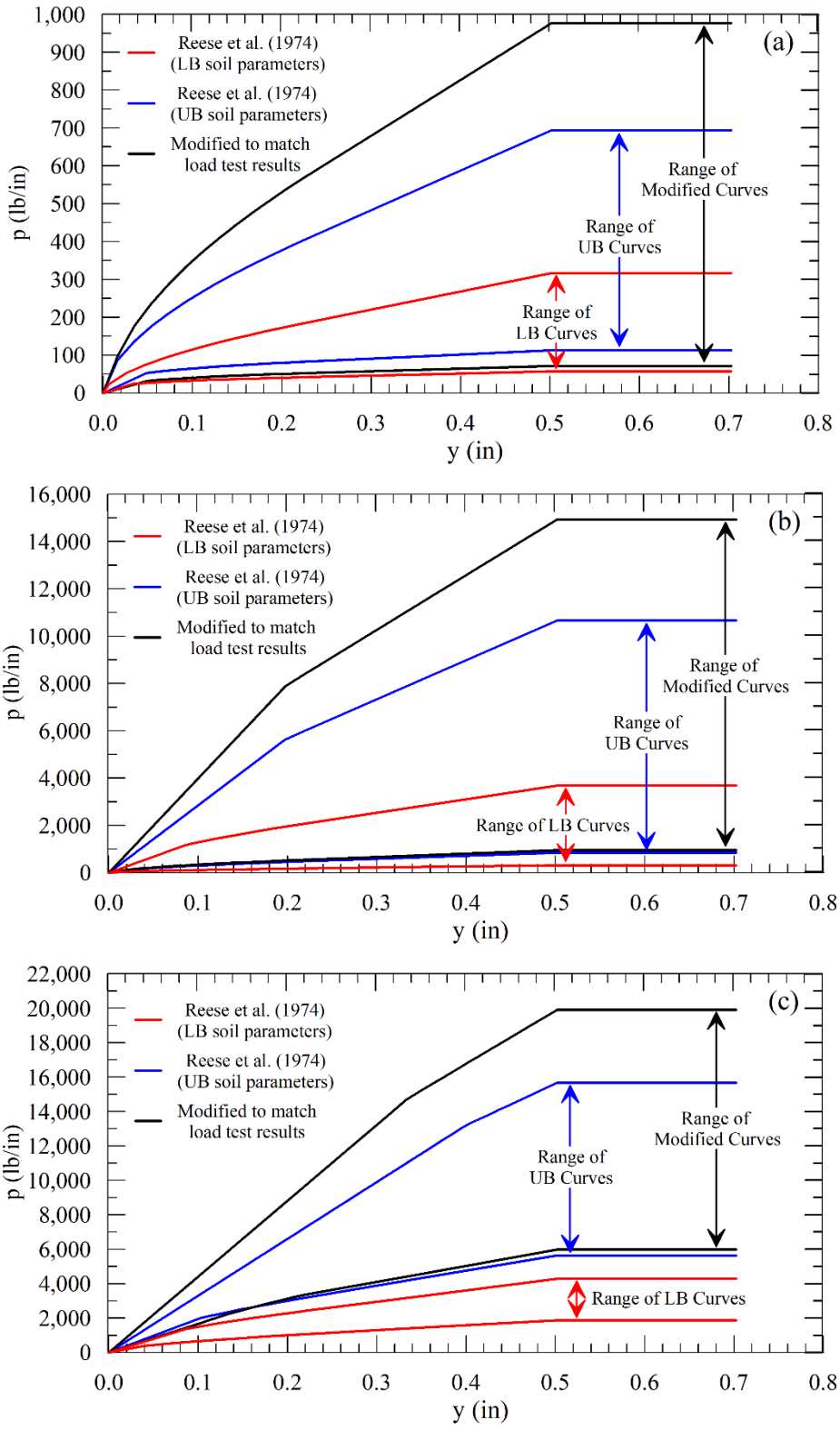


Fig. 4. Reese et al. p-y curves using the lower bound (LB) and upper bound (UB) soil index properties and strength parameters and the modified p-y curves to match the lateral load test results for - (a) Stratum 1: sand, (b) Stratum 2: silty sand, and (c) Stratum 3: silt/sandy silt

Based on the results presented in this section, one may conclude that for estimating lateral resistances of micropiles using computer programs, such as LPile, the UB soil parameters may generate more realistic p-y curves than those using the LB soil parameters. Although the use of LB soil parameters is generally preferable in geotechnical engineering practices, softer p-y curves estimated from the LB soil parameters do not always represent a conservative approach, especially in the design of deep foundations under lateral loads. For example, if battered piles are subject to downdrag or liquefaction induced settlements, bending moments imposed on the piles will be higher when stiffer p-y curves (i.e., UB soil parameters) are used in the analysis. Therefore, in addition to the generally preferable conservative approach, an alternative analysis for a case with realistic or stiffer p-y curves is recommended, especially when piles are subject to soil movements or settlements.

CONCLUSIONS

Results of three static lateral load tests on vertical micropiles from a 43-story building project site located in the borough of Queens in New York City were presented in this paper. The design load for the three piles was 14,000 lb and the maximum lateral load applied during the load testing was 28,000 lb. Lateral displacements of the pile heads at the maximum applied load were 0.66, 1.28 and 0.67 in for the three test piles. A comparison between the lateral load-displacement behavior from the load tests and the results of p-y analyses based on the widely used Reese et al. p-y curves for sandy soils indicated that the Reese et al. curves generally yields a lower lateral resistance of micropiles. The p-y analyses were conducted using a lower and an upped bound estimates of soil index properties and strength parameters. The lateral load-displacement behavior of micropiles based on the p-y analyses using the upper bound soil parameters was relatively closer to the load test data. Modification factors were applied to the Reese et al. p-y curves to match the load test data. Ranges of modified p-y curves specific to the sandy/silty soils at the project site are presented in this paper. A more comprehensive study involving lateral load tests on instrumented micropiles with measurements of bending moments and lateral displacements throughout the entire length of the piles is required to formulate and generate a more reliable set of p-y curves specific to the sandy/silty soils in New York City.

REFERENCES

Abd Elaziz, A.Y., and El Naggar, M.H., 2015. Performance of hollow bar micropiles under monotonic and cyclic lateral Loads. Journal of Geotechnical and Geoenvironmental Engineering, 141(5), 04015010.

American Society for Testing and Materials, ASTM, 2013. Annual book of ASTM standards, West Conshohocken, Pennsylvania, Vol. 4.08, D3966/D3966M.

Anderson, J.B., and Babalola, M.R., 2011. Lateral load testing micropiles to evaluate the impact of threaded joints and casing embedment on short micropiles in shallow rock. DFI Journal - The Journal of the Deep Foundations Institute, 5(2) 23-34.

Baskerville C.A., 1994. Bedrock and engineering geologic maps of New York County and parts of Kings and Queens Counties, New York, and parts of Bergen and Hudson Counties, New Jersey. United States Geological Survey Open-File Report 89-462, scale 1:24,000.

Capatti, M.C., Dezi, F., and Morici, M., 2016. Field tests on micropiles under dynamic lateral loading. Procedia Engineering, Vol. 158, 236-241.

Ensoft, Inc., 2017. Technical manual for LPile 2018 (using data format version 10), a program for the analysis of deep foundations under lateral loading. Ensoft, Inc., Austin, Texas, 238 p.

Federal Highway Administration, FHWA, 2005. Micropile design and construction reference manual. United States Department of Transportation, Washington, D.C., Publication No. FHWA-NHI-05-039, 456 p.

Ischebeck, E.F., and Ischebeck, B., 2014. Micropile foundations for vertical and horizontal loads – design examples and load test results. Proceedings of the 12th International Workshop on Micropiles, Krakow, Poland, June 11-14, International Society of Micropiles, Eighty Four, Pennsylvania, pp. 1-20.

Long, J., Maniaci, M., Menezes, G., and Rory, B., 2004. Results of lateral load tests on micropiles. Proceeding of the GeoSupport Conference, Orlando, Florida, December 29-31, American Society of Civil Engineers, ASCE GSP 24, pp. 122-133.

National Cooperative Highway Research Program, NCHRP, 2019. Manual on subsurface investigations. National Academics of Sciences, Engineering, and Medicine, The National Academic Press, Washington, D.C., Final Report for NCHRP Project 21-10, 372 p.

New York City Building Code, 2014. International Code Council, Inc. Publications, Country Club Hills, Illinois, 916 p.

Reese, L.C., Cox, W.R., and Koop, F.D., 1974. Analysis of laterally loaded piles in sand. Proceedings of the Sixth Offshore Technology Conference, Houston, Texas, May 6-8, Vol. 2, Paper No. OTC 2080, pp 473-483.

Richards, Jr, T.D., and Rothbauer, M.J., 2004. Lateral loads on pin piles (micropiles). Proceeding of the GeoSupport Conference, Orlando, Florida, December 29-31, American Society of Civil Engineers, ASCE GSP 24, pp. 158-174.

Wright, W.B., Padgett, T.G., Shiver, B., Zur, K., and Snow, W.L., 2013. Micropile lateral load testing in Charleston, South Carolina, USA. Proceedings of the 12th International Workshop on Micropiles, Krakow, Poland, June 11-14, International Society of Micropiles, Eighty Four, Pennsylvania, pp. 1-20.

THE USE OF VIBRATORY DRIVING OF FOUNDATION PILES FOR OFFSHORE APPLICATIONS - STATE OF THE PRACTICE

Rob van Dorp
Allnamics Geotechnical Experts
Nicolas Moscoso
Allnamics Geotechnical Experts
Marcel Bielefeld
Allnamics Geotechnical Experts
Gerald Verbeek
Allnamics USA

ABSTRACT
Upon recently, most offshore foundations were based on a number of driven piles that were installed with an impact hammer. With the increase in offshore windfarms two major developments have occurred: the shift from jackets to monopiles, leading to increase of the diameter of the foundation piles, and a shift from impact hammers to vibro hammers.
As the use of vibratory hammers is becoming more and more common practice, the need for accurate vibro-driving simulation software has increased, which requires that the soil modelling is enhanced to address soil fatigue during pile driving and to predict reliably the soil behavior and resistance during pile driving. In addition pile driving monitoring, which is routine for piles driven with an impact hammer, needs to become common practice.
This paper addresses advances in soil modelling that allows more accurate pile driving simulation as well as the application of Vibro Driving Analysis (VDA) or Monitoring (VDM) to validate the simulation results. This is illustrated by a case study of the test pile for the Delft Offshore Turbine project, a 28 m long monopile with a diameter of 4 m that was driven 15 m into dense sand layers using a vibro hammer. After some 6 months the pile was extracted, and pile driving simulations and VDA were done both for the installation and extraction phase.

1. INTRODUCTION

At the end of 2017, the total worldwide offshore wind power capacity was 18.8 GW [1]. The vast majority of offshore wind farms are currently in Northern Europe, which together account for over two thirds of the total offshore wind power installed worldwide, followed by East Asia, while developments in North America are still in very early stages.

Since the construction of the first offshore wind turbine (Vindeby, being installed in Denmark in 1991) the construction and installation of offshore wind farms and turbines has become more efficient. Not only the (electrical) efficiency of the turbines has improved substantially, the substructure and foundations have developed as well. As windfarms are preferable installed in relatively shallow water (to limit the foundation costs) and near shore (to limit the costs of electrical connections to shore), more and more monopiles are applied. Especially in water depths up to 30 m (100 ft) monopiles are clearly preferred over tripods or jacket structures, and even in less shallow water (depths up to 60-80 m (200 – 260 ft)) this development is beginning to occur. Due to the increased capacity of equipment (vessels, cranes, pile driving hammers, etc.) larger piles can be installed and project developers are taking full advantage of this increase,

© 2019 Deep Foundations Institute

which in turn encourages the development of even larger equipment Nowadays in the North Sea monopiles with a diameter of 8 m (26 ft) and a length of 60 to 70 m (200-230 ft) are installed routinely, and in the near future it is expected that pile diameters of 10 to 11 m (30-40 ft) and lengths up to maybe 80 m will be become common.

2. VIBRATORY DRIVING

Offshore piles are generally driven to depth using impact hammers, while vibratory hammers are used to stab the pile [12] [13]. However, with the growing availability of high(er) capacity vibratory hammers [4] and sophisticated upending tools, the use of vibratory hammers in the offshore industry is increasing rapidly as together they allow for a more efficient piling process: reduction of tool changes, avoiding the need for a template, and easy retraction when the location or position of the pile works out to be erroneous (Figures 1-4). Other advantages are the high penetration speed, reduction in the total installation time, reduction of steel fatigue damage during installation (due to substantially lower driving stresses) and the reduction in absolute noise levels, which becomes more important for environmental friendly installation of offshore foundation piles, although according to some interpretations and standards this may be offset by longer duration [4] [11].

There are, however, geotechnical issues associated with the installation of piles with vibratory hammers. One of these is the need for accurate means of predicting whether the target penetration depth can be reached with a given pile and vibratory hammer combination to ensure that premature refusal is avoided. A major milestone in this effort was the Hong Kong – Zhuhai – Macau Bridge project in 2011 (Figure 5), where a total of 8 (!) massive vibratory hammers (with a total capacity of 8 x 240 kgm = 1920 kgm, rotating together at a speed of 1400 rpm (23 Hz), leading to a dynamics force of F_{dyn} 41150 kN) were combined in order to install very large monopiles (diameter 22 m (72 ft) diameter, length 49 m (160 ft)) [2] [3] [4]. The soil profile consisted mainly of silty clay, clay and moderate dense sand with SPT N-values ranging from 8 to 40. Vibratory Driving Predictions (VDP) executed by the engineering consultant responsible for the drivability studies (that were performed with simulation software developed by the same firm) played a key role in convincing the client that vibrating these gigantic piles into the bottom of the South China Sea to the required depth was indeed possible. On May 15, 2011 the world's largest vibratory hammer drove the world's largest pile at that time in 7½ minutes, just as the driveability studies had predicted.

3. PREDICTION OF VIBRATORY DRIVING OF PILES

The success of the Hong Kong – Zhuhai – Macau Bridge project was one of main reasons for the companies involved in the 2012 Riffgat Offshore Wind Farm project in the German North Sea to use a vibratory hammer setup to install the monopiles for 30 wind turbines [3] [4]. The monopiles are between 53 and 70 m long (175-230 ft), with a diameter of 4.7 m (15 ft) at the top of the pile and between 5.7 and 6.5 m (18 – 21 ft) at the pile tip. The same engineering consultant was used for the VDPs, and also for vibratory pile monitoring (VDM) during the initial field test at sea to enhance the predictions at locations with stiff clay.



Figure 1. Installation of foundation piles for offshore wind farms



Figure 2. Big, bigger, biggest: all offshore equipment increases in time:. an upending tool combined with a 920 kgm vibratory hammer



Figure 3. Upending a monopile with a vibro hammer using an advanced upnding tool



Figure 4. Positioning and stabbing a monopile without template using the dynamic positioning of the vessel

The original project execution plan called for a vibrator setup whereby the piles would be stabbed as deep as possible before the start of impact driving. However, based on the VDP it was concluded that the impact hammer would not have been needed for the piles at locations with a sandy soil profile. Nevertheless, the client required that the final 10 m (32 ft) of penetration had to be achieved with an impact hammer to ensure adequate bearing capacity (as it was assumed by some that vibratory driving would result in a permanent loss in soil strength, which is in fact not the case). Installation of the monopiles at Riffgat was a successful operation, with net driving times to the allowed penetration (mostly 20-30 m below seabed) in less than 15 minutes. The VDP results were supported during actual driving by the fact that the pile at the start of driving with the impact hammer showed a blow count of 100 blows/25cm with an impact energy of 1,200 kJ (885,075 ft-lbs), which clearly demonstrated a strong recovery of the soil strength after vibratory driving.

The Riffgat project extended to locations with very stiff clay and glacial till in the soil profile, and the initial PDP for these locations implied that the monopiles might not be stabbed deep enough to remain stable when mouniting the impact hammer. Therefore at two of these locations field tests were done by driving down and extracting a scaled pile with a scaled vibro, all with VDM. The VDM results obtained during the field test were then used to improve the VDP for the piles that had to be installed in stiff clay. This required adjustments to the Beta factor (the soil resistance reduction because of soil fatigue) and the quake factor, after which the VDP fairly accurately predicted the stabbing of the piles in these clay soil profiles.

Around the same time as the installation of the monopiles at Riffgat took place, a test with a vibratory hammer setup was done for the Anholt offshore windfarm in the Kattegat Sea in Denmark [5] [18]. The same engineering firm that was involved in the Hong Kong – Zhuhai – Macau Bridge project was once again engaged to perform VDP. The monopoles for this project had a length ranging from 39 to 40 m (128 to 131 ft), a diameter ranging from 4.9 m in the conical part at the top to 5.3 m (16 to 17.4 ft), a wall thickness varying from 45 to 65 mm (1.75 to 2.6 in) and a weight of 270 to 280 metric tons (298 to 309 US tons). The piles had to penetrate 17 to 19 m (56 to 62 ft) into the seabed, into a soil profile that mainly consisted of dense, calcareous sand. The test results confirmed once again that vibratory hammers are suitable for the installation of monopiles, at least in sandy soil conditions similar to the Anholt project and that this process can be accurately simulated through VDP.

4. PREDICTION MODELS

Driveability studies for impact driving have a much longer history than those for vibratory driving [6]. As soon as pile driving got started there has been this quest for that ultimate, universal impact driving formula, which is applicable and reliable in all conditions (soil, pile, hammer, etc.) and that is superior to all other existing driving formulas, and this quest even continues today, but there has never been a satisfactory result. Instead, large numbers of different driving formulas have been developed, with a (very) wide spread in results, applicability and reliability [7] (Figure 6). This wide spread of formulas is one of the main reasons why in the early 1970 s companies involved in (offshore) piling started developing and applying methods for driving predictions that were based on the stress wave theory. This approach is now generally considered state of the art for driveability studies [4][5][6][7], although driving formulas and simplified models are still used, but mostly only for first quick assessments, not for design calculations.



Figure 5. Project OctaKong in Macau: 8 simultaneous operating, synchronized vibratory hammers installed this 22 x 45 m (72 x 160 ft) monopile easily. Note the two engineers working in the crew basket, top right of the pile, to get a feeling for the scale of this operation

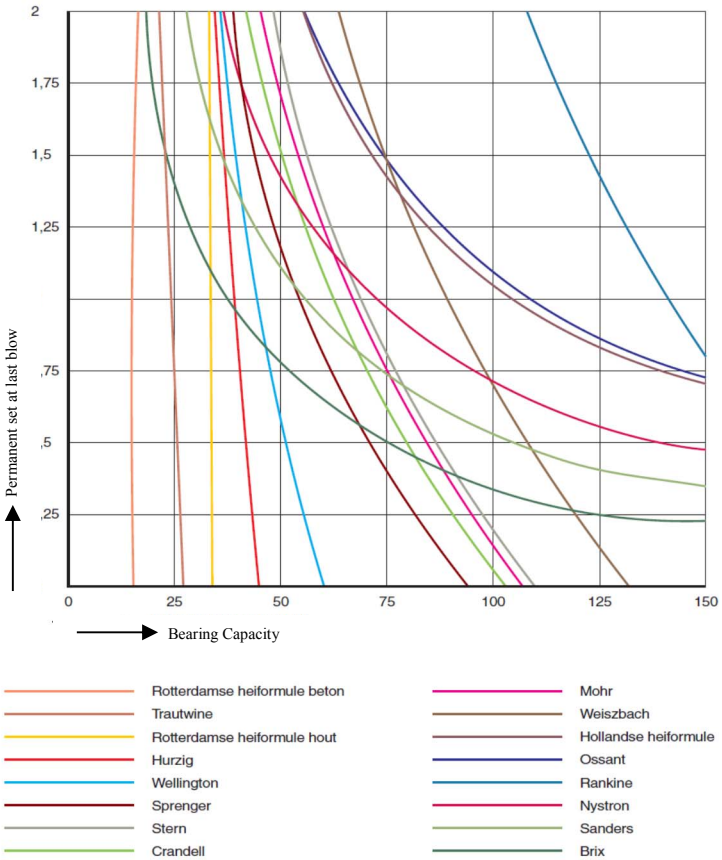


Figure 6. Typical driving formulas (here presented for driven precast concrete piles) show a wide spread. Using these formulas a blow count of 25 (blows per 25 cm), which equates to a permanent set of 1 cm per blow, can imply a bearing capacity between 15 and 140 tf [8]

These stress wave methods were never specifically designed for pile driving, let alone for impact driving. In the 1860s a Frenchman, A.J.C Barre de Saint Venant [14], applied the principles of conservation of mass and momentum to the water flow in an open channel. The application resulted in two quasi-linear differential equations, for which de Saint Venant produced a theoretical solution, the so-called method of characteristics. This method was then used for a variety of hydrology related issues, such as to predict the propagation of tidal waves. Starting in the 1930s Saint Venant's equations were applied to pile driving around the world, more specifically to model stress wave propagation in a pile [15] [16] [17]. Therefore these methods can be applied not only for impact pile driving, but also for vibratory driving [5] [9]. In both cases stress waves patterns are introduced into the pile that are affected by the hammer, pile length, actual penetration depth and the soil profile, albeit that there are fundamental differences depending on the driving method. During impact driving the wave energy of each single blow gets dissipated before the next blow is applied, so the pile is more or less (back) at rest at the start of each blow. The wave length is normally shorter than, or in the range of, the pile length, and the soil resistance is only excitated during the passage of the wave. Vibratory driving, on the other hand, is a continuous process with oscillating forces on the pile top and a continuous supply of power. All soil resistance along the pile is continuously excitated by a wave pattern that depends on the frequency of the oscillating forces and the pile length. Irrespective of the driving, the determination of the proper wave (oscillation) pattern of the pile and the corresponding displacements, velocities and acceleration at each pile segment are essential for the proper calculation of the soil resistance during driving. For impact driving these predictions have a long history with applications all around the world in all kinds of soil profiles. In turn the feedback from actual piling results was used to gain a better understanding which parameters really affected the impact driving process and also to determine realistic values for the dynamic soil properties based on the static soil properties obtained from a soil investigation. All these experiences, or better completions of the learning loop shown in Figure 7 below, have led to an increased reliability of the Pile Driving Predictions as the dynamic behavior of various soil types during impact driving could be predicted ever more accurately. [10].

A similar large database, including different relevant parameters (like soil fatigue, toe gap, etc.) is not yet complete for vibro driveability studies, because the general experience worldwide is still limited, especially with large offshore (mono)piles. It is therefore essential that the industry should perform consistent and proper monitoring of projects with vibro driven piles in order to complete this learning loop of prediction, monitoring, post analysis of results and feedback on predictions, to enhance this database. At the same time it is fair to say that the experience in this decade (as highlighted earlier in this paper) has demonstrated that for non-cohesive, granular soil profiles accurate VDPs can be generated based on soil investigations (i.e. that realistic values for the dynamic soil properties can be selected based on the static soil properties obtained from a soil investigation), and that for more challenging (stiff, cohesive) soil profiles accurate VDPs can still be produced when calibrated using the results of VDM of a test pile. This obviously assumes that the pile does not encounter boulders or other larger obstacles, which would lead to immediate refusal.

5. VIBRO DRIVING PREDICTION MODEL

Although the exact mechanisms that take place in the soil during vibro driving are not yet completely understood, a simplified description of the main mechanism of the effect of vibro

driving on the soil is that the soil is disturbed by the vibrations, making it temporarily and locally (in the immediate vicinity of the pile) lose a substantial part of its strength (especially the friction between pile and soil), which allows the pile to penetrate the soil under the net weight (i.e. the weight of the pile and hammer minus the actual hook load in the crane. For this reason the weight of pile and hammer are important factors contributing to the penetration in the soil layers. This is an important difference compared to impact driving, where this weight is not an important factor.

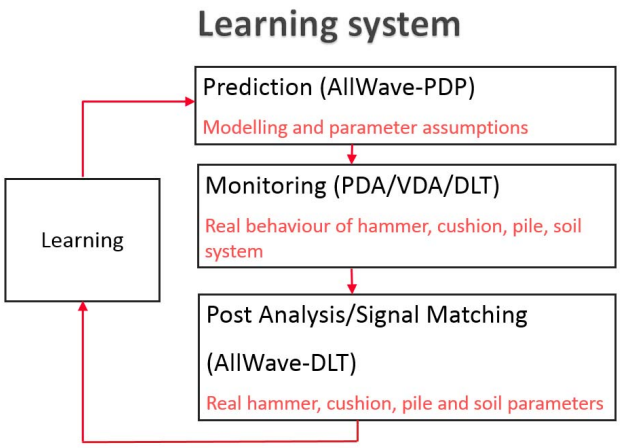


Figure 7. The closed learning loop that over time has led to an increased reliability of the Pile Driving Predictions.

Vibratory driving generates continuously static and dynamic soil resistances that are regrouped in standing wave patterns. In the vibrodriving prediction model the dynamic resistances are modeled through dampers, defined by a damping factor. This factor is more or less linked to the sand/clay content of a soil, characterizing its fluid/viscous state, respectively. Static resistances are modeled through springs, defined by quakes values and the yield stress that is based on soil investigation results. On top of those resistances, vibratory driving has to take into account soil fatigue/liquefaction, defined by the Beta Factor, that decrease the static resistance when vibrodriving. After termination of driving, the soil then regains (most of) its original strength, and in case of granular soils the soil strength after driving may even exceed the original strength due to densification as a result of the vibrations. While this is the basic principle behind vibro compaction, a well recognized and widely used ground improvement method that densifies loose granular soils, it is somehow assumed by some that vibrodriving achieves the very opposite: that it would result in a permanent loss in soil strength, which is clearly not the case. As Riffgat project showed, after vibrodriving, high energy and high blowcounts were in place at the start of impact driving. However, presently the densification aspect is not yet incorporated in any VDP software.

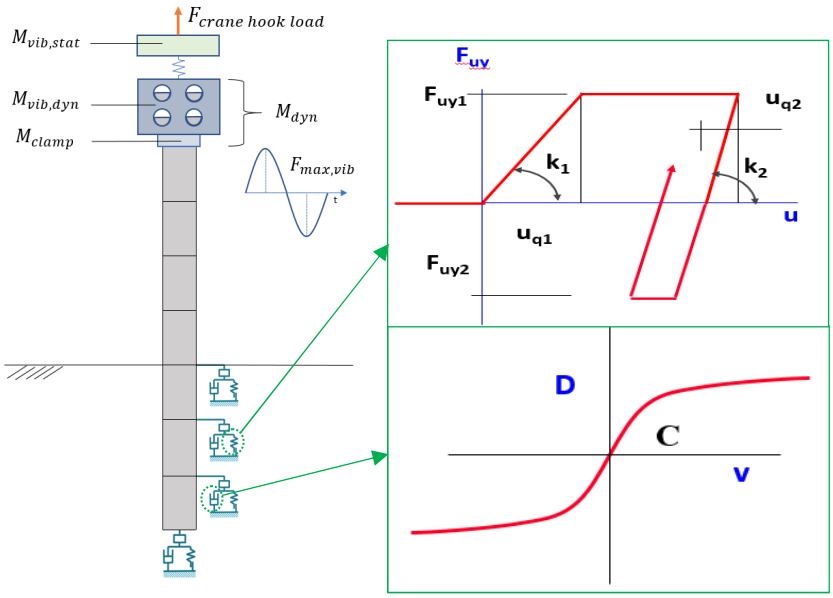


Figure 8. Left, full vibrodriving model, right, spring and dampers soil models

6. MEASURING DURING VDM

The method of evaluating the driveability with a vibratory hammer is by the application of back-calculations using the monitoring results of previously installed piles. It is therefore essential that during VDM all information during installation is monitored and recorded, including performance and behavior of the pile and the vibratory hammer. Monitoring of pile stresses (and their contribution to fatigue of the pile material), pile penetration (both in absolute terms and as a function of time) and hammer frequency and efficiency are just a few of the parameters to ensure quality control for piles installed with a vibratory hammer. Another important parameter is the applied hook load in the crane as this affects the pile penetration. The measured signals are then post-analyzed with simulation software, where simulated results (using a soil model with dynamic soil parameters based on the static soil parameters) are compared with measured results. The parameters in the soil model are then adjusted to such that the simulated parameters match (as closely as possible) the measured results, similar to the signal matching that is done for piles driven with an impact hammer. In addition the results of each post-analysis can be used to gain better insights which parameters really affected the vibratory driving process and also to determine realistic values for the dynamic soil properties based on the static soil properties obtained from a soil investigation.

It should be noted, however, that unlike for piles driven by an impact hammer where the main performance parameter is the blow count and transferred energy, there is not an unambiguous performance parameter for vibratory driving, which at least at the present leaves the open question regarding which factors need to be monitored during vibratory pile installation. The corresponding performance parameters for vibratory driving are penetration speed and eccenters rotating frequency. However the penetration speed is capped by the releasing speed of the crane, and while the eccenters rotating frequency should be able to define the transmitted energy in the pile, it too is affected by the hook crane load, absorbing part of it, and by the interaction with the static mass of the vibrator. Those interactions generate some losses in the transmitted energy to the pile that are currently not accounted for, especially if the transmitted energy is merely based

on the oil flow rate and the hydraulic pressure in the power pack that drives the vibratory hammer.

Given the fact that for non-cohesive granular soils the dynamic soil properties associated with vibratory driving can be predicted accurately based on the static soil properties from soil investigations, the VDM results can be used to generate fairly reliable predictions for the static bearing capacity for vibratory driven piles. The VDM results allow determination of the actual dynamic soil properties, which can then be used to adjust the static soil properties from the soil investigation, which in turn allows the calculation of the static bearing capacity (in the same manner that the results of dynamic testing of piles with an impact hammer are routinely used to predict the static bearing capacity). However, given the limited experience with vibro driving the safety factor applied to these predictions should be (somewhat) higher than those used for the results of dynamic testing with an impact hammer. impact driven piles. For cohesive soils this is not the case, and it will require substantial efforts to reach the same level of confidence that currently exists for granular soils, although major progress is being made.



Figure 9. With accelerometers and strain gauges mounted on the pile, VDM (Vibro Driving Monitoring) can monitor all important parameters during installation

7. CASE EXAMPLE

Delft Offshore Turbine (DOT) concerns the development of a new concept for wind turbine generators (WTG), whereby the rotor on top of the mast directly drives a hydraulic pump, which pumps oil to a hydraulic motor on the seabed that is coupled to a (sea water) pump. This pump sends the water to a central power generator, where the electricity is generated.

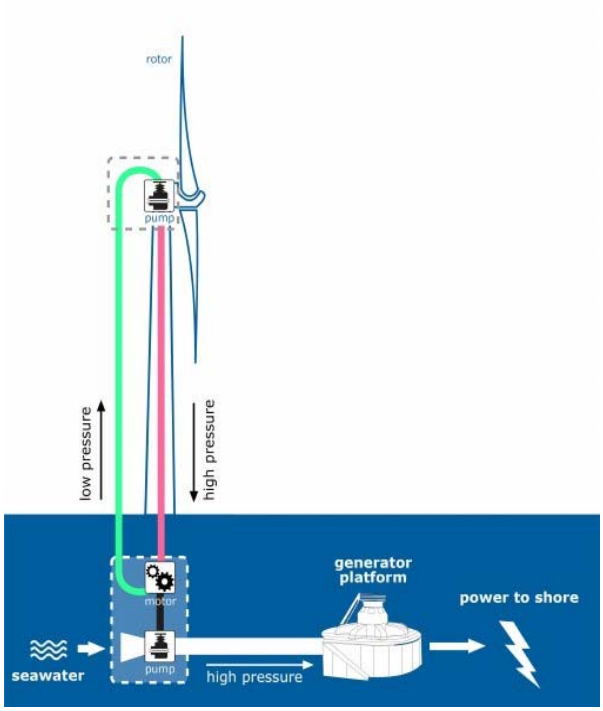


Figure 10. Delft Offshore Turbine Concept.

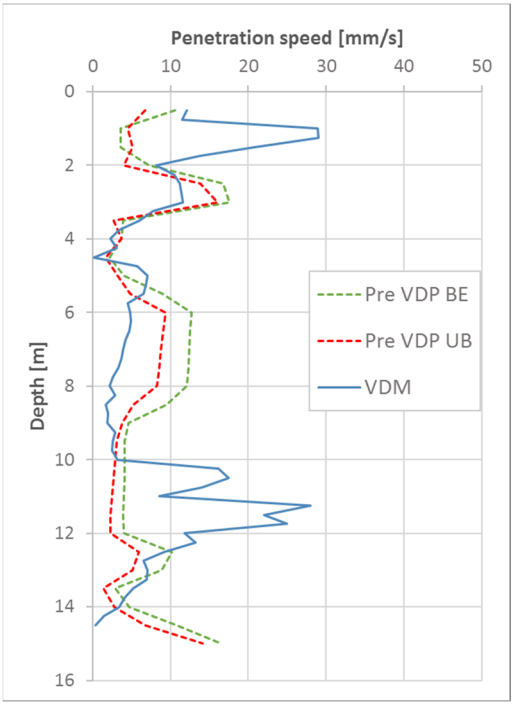


Figure 11: Penetration Speed for 1st Test Phase (blue: actual; green: original prediction (best estimate); red: (conservative estimate)

This development involved a first test phase onshore (2016-2017) and a second offshore test phase (2018-2019/2020). Both test phases involved a monopile being installed with a vibratory hammer and then getting extracted with a vibrohammer at the end of each test phase. Various engineering firms were involved in both test phases to perform VDP, VDM and post-analysis of the monitoring results.

Table 1: Overview main DOT project values

Project	Pile weight	Pile length	Vibrator dyn. Mass	Eccentric moment	Operating frequencies	Cone Resistances	Friction Resistances	Soil type
[stage]	[tons]	[m]	[tons]	[kg.m]	[Hz]	[MPa]	[kPa]	[-]
1st	126	27.2	54	320	17.9 - 21.8	4.8 - 31	24 - 155	Sand
2nd	300	56.6	119	640	14.9 - 16.4	7 - 31	36 - 155	Sand

The first test phase was an onshore trial on reclaimed land in Rotterdam harbor in the Netherlands, where a monopole was driven 15 m (49 ft) deep into the soil (for pile and hammer details see Table 1 and Figure 12). Initial predictions showed a difficult vibrodriving in the dense, partially dry sand, but it was expected that it would be possible to achieve target depth, although with low penetration speeds. During installation this prediction was confirmed: the monopile reached target depth, with a near refusal at the initial 4 m (13 ft), just like the predictions had indicated. This near refusal, as can be seen from the CPT data in Figure 12, corresponds to a peak in soil resistance in the dry sand layer, where liquefaction is limited and thus vibrodriving efficiency reduced. Other variables, such as force, velocity, accelerations and displacements (at sensor level), were deviating from predictions, esspecially close to the depth

where the near refusal occurred, where a dry sand behavior and a peak soil resistance were generating some instabilities in the vibrodriveability simulations. Figure 13 shows the initial predictions (in red), the recorded values (in blue) and the revised predictions after post analysis, and these figures clearly show the challenges that still exist when trying to predict the vibratory driving process. During post-analysis the main objective is to match the refusal as closely as possible, followed by the other parameters. The outcome, however, is frequently that a parameter is accurately predicted over a certain depth interval, but not for other depth intervals and that other parameters good matches are achieved for a completely different interval or, in some cases, not at all. In this particular case there was an excellent match for the top acceleration between 3 m and 8 m (10 and 26 ft), but at 4 m (13 ft) all other parameters showed substantial deviations.

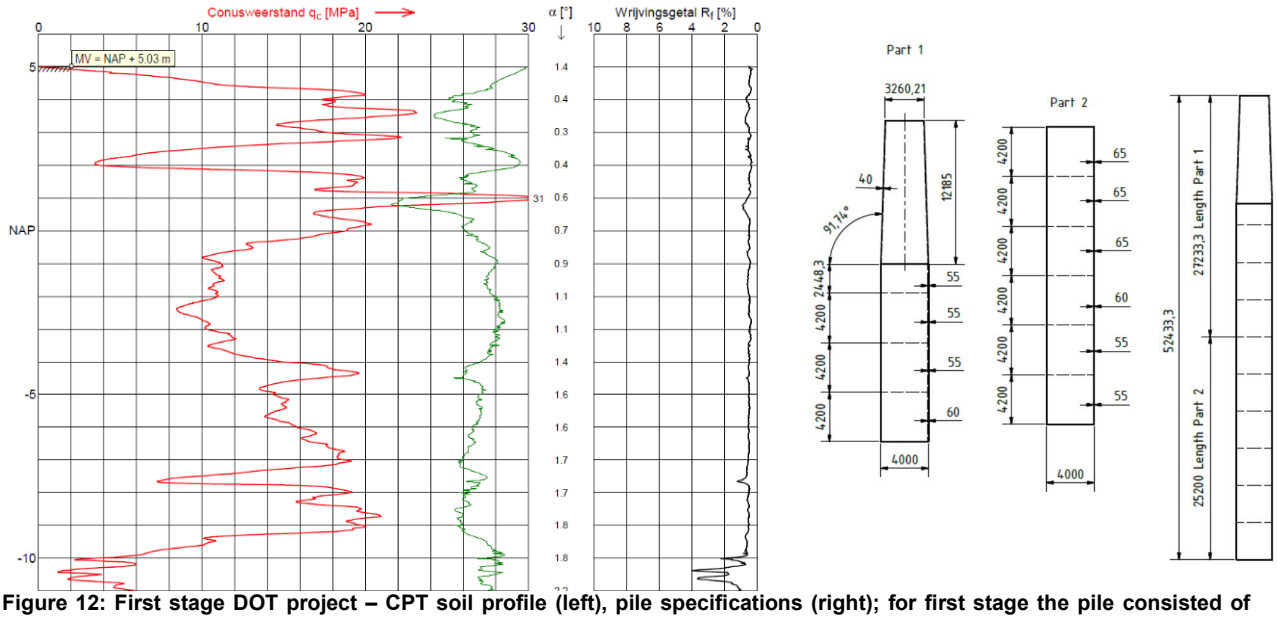


Figure 12: First stage DOT project – CPT soil profile (left), pile specifications (right); for first stage the pile consisted of part 1 only, while for the second stage it consisted of part 1 and 2.

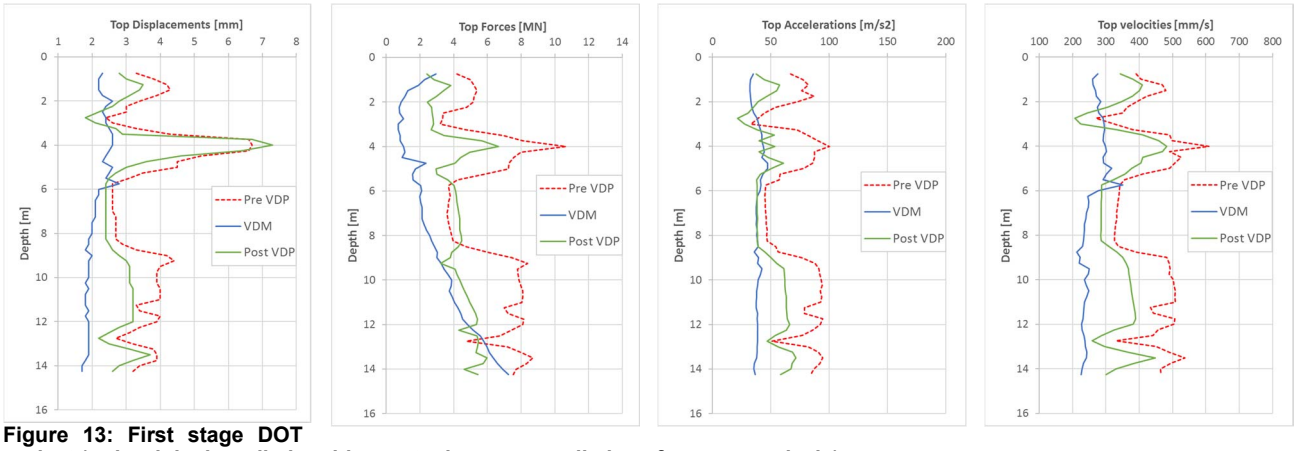


Figure 13: First stage DOT project (red: original prediction; blue: actual; green: prediction after post-analysis)

To extract the pile a floating shearleg crane was used that would be positioned as close to the pile as possible. The VDP prediction was that without disturbing the soil by water jetting extraction would require a hook load of 500 metric tons (550 US tons). At first this caused some concern, because the crane vessel company indicated that based on the planned postioning of the

vessel the maximum hook load was 300 metric tons (330 US tons). However, as the extraction was performed during high tide the vessel could come a lot closer to the pile and apply hook load between 400 and 500 metric tons (440 and 550 US tons), which was more than enough to extract the pile.

The second stage consisted of vibrodriving a similar size, but longer monopile into the seabed at the location of an already operational Offshore Wind Farm in the Dutch North Sea (for pile and hammer details see Table 1 and Figure 12). As part of the research the pile was installed and extracted twice (at locations close to each other), before getting installed at its final position. According to the project planning the pile will be extracted again after the second test phase is completed in 2019 or 2020.



Figure 14. First Stage DOT project – pile extraction

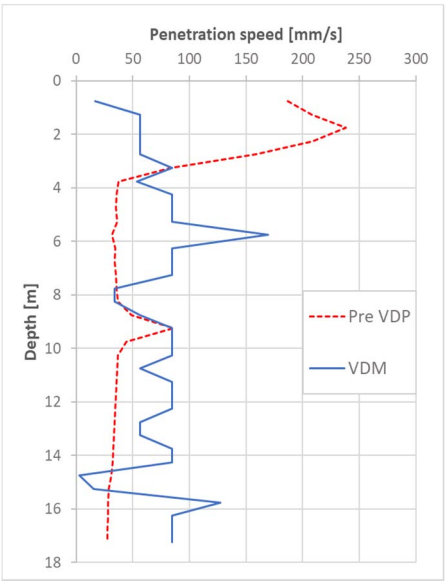


Figure 15: Penetration Speed for 2nd Test Phase (red: original prediction; blue: actual)

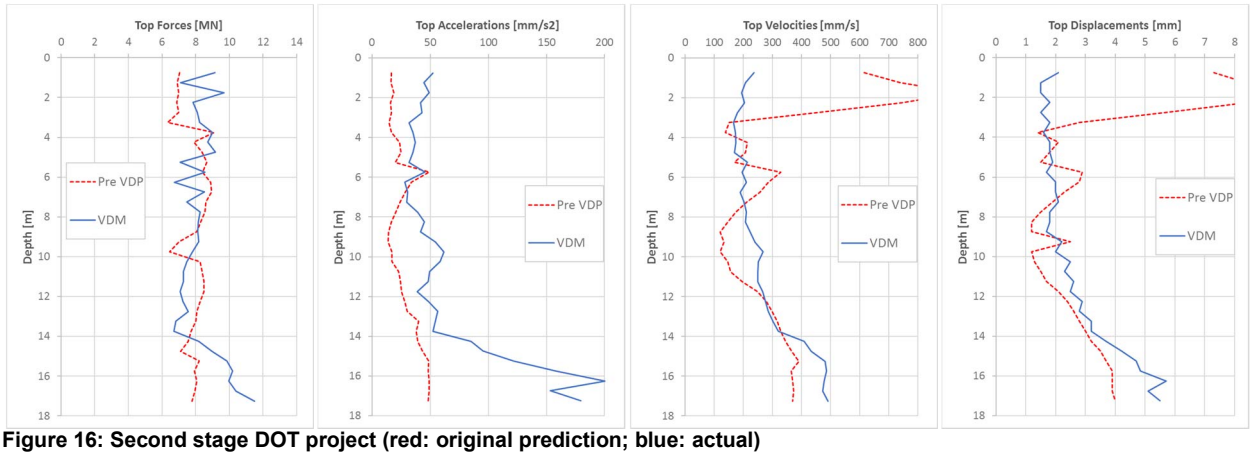


Figure 16: Second stage DOT project (red: original prediction; blue: actual)

For this second stage the VDP was performed after the first stage had been completed and at the time this paper is written only the VDP for the first installation and the comparison with the VDM results for that installation can be, as the results for the remainder of the second stage are still being analysed.

As can be seen from

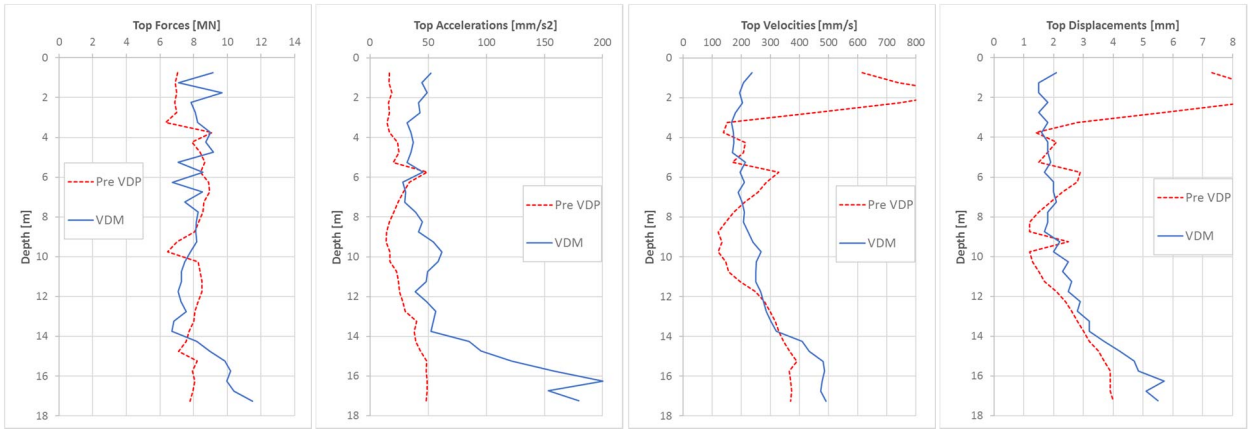


Figure 15 and 16, for this second phase the VDP results matched the VDM results more closely, and it VDP accurately predicted that the pile could be driven 17 m into the seabed using the vibratory hammer. At the same time it should be noticed that while the VDP results for the parameters at the pile top as shown in Figure 16 are generally fairly accurate predictions, the actual penetration speed was generally higher than predicted. This should not be surprising as it is standard practice for driveability predictions to overestimate soil resistance and underestimate hammer efficiency, since because of a safe approach. Nevertheless the deviations are a clear indication that there is real need for more data and most post-analysis of that data to allow the generation of more accurate predictions.

8. CONLUSION

The use of vibratory hammers instead of impact hammers for installing foundations for offshore windfarms is becoming more and more common practice. As a result the need for accurate vibro-driving simulation software has increased. This requires that the soil modelling is enhanced to address soil fatigue during pile driving and to predict reliably the soil behavior and resistance during pile driving.

One way to achieve this is to use actual piling results to gain a better understanding which parameters really affected the impact driving process and also to determine realistic values for the dynamic soil properties based on the static soil properties obtained from a soil investigation. All these experiences have led to an increased reliability of the Vibratory Driving Predictions (VDPs) as the dynamic behavior of various soil types during vibratory driving could be predicted ever more accurately.

At this time it is fair to say that for non-cohesive, granular soil profiles, accurate VDPs can be generated based on soil investigations (i.e. that realistic values for the dynamic soil properties can be selected based on the static soil properties obtained from a soil investigation), and that for stiff, cohesive soil profiles, which are more challenging for vibro driving since the cohesion in these soils reduce or even prevent local liquefaction, accurate VDPs can still be produced when calibrated using the results of Vibratory Driving Monitoring (VDM) of a test pile.

To enhance the prediction capabilities even further it is essential that not only VDM pile becomes common practice, just as it is for piles driven with an impact hammer, but also that during pile driving all essential parameters are monitored and recorded, incl. the crane hook load and accelerations of the static mass.

Finally, whilet for non-cohesive granular soils the VDM results can be used to generate fairly reliable predictions for the static bearing capacity for vibratory driven piles, for cohesive soils this is not the case, and it will require substantial efforts to reach the same level of confidence that currently exists for granular soils, although major progress is being made.

REFERENCES

[1] "Offshore Wind" (PDF). gwec.net. GWEC. May 2018.

[2] Middendorp,P., Dorp van, R., From Mini- till Giga-piles (Van Mini- tot Giga-palen), Dutch, Geotechniek, Funderingsdag 2012 Special, Netherlands, 2012.

[3] Middendorp, P., Verbeek, G. (2012). At the cutting edge of pile driving and pile testing, 9th International Conference on Testing and Design methods for Deep Foundations; Kanasawa, Japan

[4] De Neef, L.; Middendorp, P.; Bakker, J. (2013). "Installation of Monopiles by Vibrohammers for the Riffgat Project", Pfahlsymposium Proceedings of the Institute for Soil Mechanics and Foundation Engineering, Technische Universität Braunschweig, Germany

[5] H. van Koten, P. Middendorp and P. van Brederode, "An Analysis of Dissipative Wave Propagation in a pile", Proceedings of the International Seminar on the Application of Stress Wave Theory on Piles, Stockholm, 1980

[6] P. Middendorp and P. van Brederode, "Skin Friction Models for Sand from Static and Dynamic Laboratory Load Tests", Second International Conference on the Application of Stress Wave Theory on Piles, Stockholm, 1984.

[7] P. Middendorp and A.F. van Weele, "Application of Characteristic Stress Wave Method in Offshore Practice", 3rd International Conference on Numerical Methods in Offshore Piling, additional contributions and discussion, Nantes, 1986

[8] Foundations based on precast concrete piles, Handboek Funderingstechnologie (in Dutch), Prepal, 1998

[9] Bielefeld, M.W., Middendorp P. (1992). Improved pile driving prediction for impact hammer and vibratory hammers, 4th International Conference on Stress Waves, The Hague, , Balkema.

[10] Fischer, J., Sychla, H., Bakker, J., Neef de, L., Stahlmann, J., A comparison between impact driven and vibratory driven steel piles in the German North Sea, Conference on Maritime Energy, Hamburg, 2013.

[11] Jonker, G., Middendorp, P., Subsea installations using vibratory piling hammers, 20th OTC, Houston, Texas, 1988

[12] Middendorp.P. (2004). Thirty years of experience with the wave equation solution based on the method of characteristics: 2004, Seventh International Conference on the Application of Stress Wave Theory to Piles, Kuala Lumpur, P95,

[13] A. Ligterink, C. van Zandwijk and P. Middendorp, "Accurate Vertical Pile Installation by using a Hydraulic Vibratory Hammer on the Arbroath Project", 22nd annual Offshore Technology Conference, Houston 1990.

[14] Saint-Venant. B. de, 1867, Memoire sur le doc longitudinal de deux barres elastiques, Journal de Mathematique, 2, ser XII, pp 237-376.

[15] Voitus van Hamme, G.E.J.S.L., Jansz, J.W., Bomer, H. Arentsen, D. "Hydroblok and improved pileddriving analysis", De Ingenieur, 1974

[16] De Josselin De Jong, G. 1956, "Wat gebeurt er in de grond tijdens het heien" (What happens in the soil during pile driving) De Ingenieur, No. 25, Breda, The Netherlands

[17] Massau. J., 1914 ,Mémoire sur l'intégration graphique des équations aux dérivées partielles. (Note on the graphical integration of partial differential equations). Mons

[18] LeBlanc Thilsted, C., "Vibro-Driving Monopiles—A Feasible Installation Concept for the Future?" presented at the Danish Geotechnical Society Seminar, Gentofte, Denmark, April 1, 2014, https://danskgeotekniskforening.dk/sites/default/files/pdf/pdf2014/Moede%202/Session%204%20-%20Presentation%203%20-%20C%20LeBlanc%20-%20DONG%20Energy%20-%20Vibro-driving%20of%20monopiles%20-%20DGF%20Seminar%202014-04-01.pdf

A FULLY CONNECTED JOBSITE IS A MUST FOR THE FUTURE

Jochen Maurer, CEO - fielddata.io GmbH, Munich, Bavaria, Germany, +49 89 20 70 42 669, jochen.maurer@fielddata.io

Christian Hoyme, Product manager - fielddata.io GmbH, Munich, Bavaria, Germany, +49 89 26 20 57 903, christian.hoyme@fielddata.io

ABSTRACT

Most of the current foundation projects are suffering from disconnected information silos. In the first silo there is the planning of the project with corresponding data, presented by paper or digital drawings. Here will Building Information Modeling (BIM) be one of the trends for the future. We will see more and more projects leaving the "old way" of 2D drawings and moving into 3D planning including metadata of the foundations. But even with a perfect BIM model of a jobsite, we are not at final end of digitalization.

While execution of the project at the jobsite, a second data silo is evolving. Data collected directly from construction equipment and manual measurements is currently undervalued in most projects. Paper is passed to the equipment operator and major data from measurements on site are noted on paper and digitized afterwards. Automatically collected data is not be used to create site progress reports or similar report. So, the real "data" just flows around without connection to any other data already existing in projects.

And then the third silo arises: The documentation of the project. Data collected on paper es reentered to create some basic documentation of the work handed over to the client. Spreadsheet software is still the "tool-to-be-used" to create at least some documentation. Finally, the documentation is not connected to the data created while planning and not connected to the automatically collected data from the jobsite.

A connected jobsite in the foundation industry must link these information silos and have to create a full data-workflow from the design through the execution to the as-built documentation.

INTRODUCTION

Building information modelling (BIM) is currently the most popular term of construction business in Germany and probably all over the world. But as often there are many different definitions out there and everyone has his own definition or at least understanding what BIM is about. But for sure it is the most relevant for the construction industry in the near future.

Most popular is the digital twin for the upper structure of a building. In most cases the BIM models just shows the building itself, but there is more to be implemented. For example: projects where a special foundation is needed, BIM should include also the foundation elements with meta data. There are several advantages. Not only the clash detection of anchors, but also the possibilities to check the interaction with neighbor constructions, power lines and so on are a use case. For sure most of the special foundation elements are not relevant for the whole lifecycle of a building. But during construction and later the demolition the information about the hidden elements is important and gives a benefit to all stakeholders. In the future there will be not the question: "What is already in the ground?". The risk for following construction projects on the same ground will be minimized.

The information from the tendering phase, construction phase and the usage period need to be made available for the future and handed over to the relevant stakeholders throughout the lifecycle of the building. But here are difficulties in regards of the different information silos, which are usually not yet connected. Even if some projects are working with 4D-Models, they are commonly reduced back to 2D drawing and

© 2019 Deep Foundations Institute

tables on paper. This happens in each transmission of a project from one phase to another. This is shown in Fig. 1.

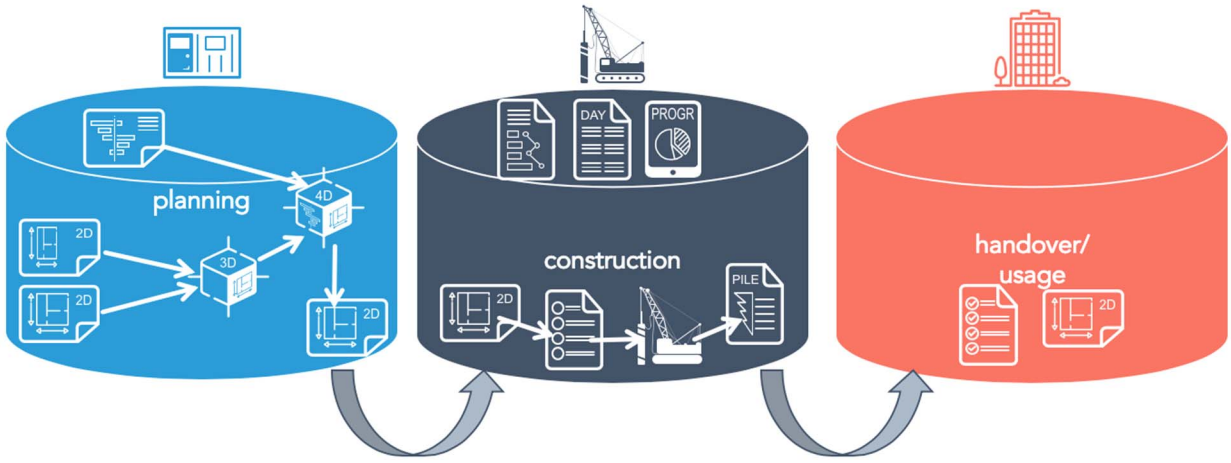


Fig. 1: Todays "flow" of information and data in a construction site with data silos

Besides the future benefit of BIM and a perfect digital twin, there are some hurdles on the path to a digital construction process. The experience with the implementation of new tools to special foundation projects is that the stakeholders (client, project management, site personnel) are not ready yet. And there are many doubts and even fears out there.

SPECIAL FOUNDATION CONSTRUCTION BUSINESS FROM THE PAST TO THE FUTURE

In the past the special foundation companies used different forms to collect information in regards of quality documentation, inspections, health and safety and more. Most of them have been important and are still relevant for several reasons. Some documents are issued to the client and others are for internal use only, but all contain information about the construction project.

Usually the forms are printed and filled by persons in charge for a certain task. Then the document is filed, some paperwork is copied, and the copies are sent to the office, checked, double-checked and combined for passing them to the client. Each folder on a project contains important information but is usually only relevant for fulfilling contractual requirements.

Later (in the last decade) with the rise of "digitalization" the companies insisted to transfer the paper records to a digital copy. So, in most cases the engineers had to type in the field records to a file. This causes up to now a high time consumption by this task. Due to many other duties in the daily work on site, the risk of mistakes, simple misspelling when transferring the paper to a digital copy is very common.

Another main task of site engineers is the documentation of the progress. For example, it is necessary to record the activities on site like drilled pile length per day, time of concrete delivery, works carried out by subcontractors and so on. A lot of this information the site engineer needs to collect on an old-fashioned way (Fig. 2).

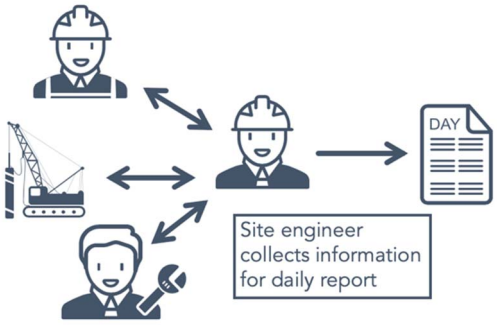


Fig. 2: Old-fashioned way of collecting the information for the daily report

Usually the site engineer asks for example the superintendent or the drilling rig operator. Sometimes it is like a question and answer game between stakeholders. The engineer needs a lot of time for collecting the data. On this data he is doing the quality documentation, reports and performance analysis. How wonderful it would be, if the required information comes to the site office on the fly.

Citation:

"Digitalisation means accessing information to gain insights and leveraging the "power of information" that stems from the collection, analysis and management of data to provide new solutions with a higher value added. "CECE 2019 p.11. This is exactly what the base line is in special foundation projects. There is a lot of data available, but the effort to gain additional benefit out of it is high and in most current cases only achievable with lot of manpower.

Besides the paper work, there are a lot of data around a site. Starting with manual measurements, pictures taken by the personnel, surveying data, and also the equipment is producing every second data. Additionally there is monitoring of geotechnical sensors out there. But focusing on construction data: Some machines are able to send these sets to a server of a manufacturer, where the data can be at least viewed. Imagine a typical special foundation company with a fleet of different equipment types. They usually have drilling rigs from different manufacturers, wheel loaders from others, cranes supplied again from another manufacturer or even rental companies. All of these machines are spreading out some data, which is more or less relevant for the documentation. Unfortunately, there is not an easy way for construction companies to access their data at a single point.

But the various points where certain data is stored is not the only challenge to come to a fully connected site. On a site there are also time sheets of the employees, delivery notes, and many more. So providing applications to smartphones for example could cope every single topic. For example recording the working hours of the personnel on site. The supervisor can approve the data sets and send it to the server. Also the concrete quantity, comments can be collected by different appllications and also sent to the site office. Here the data is connected and combined to pre-defined reports. Additionally there is the advantage, that the information are available not only for a daily report and can be displayed for example at the management dashboard in the head office. The data should be collected by all relevant site "participants", this includes besides the personnel also the equipment. If the machines are not able to send their data, it is necessary to identify at least the relevant ones and equip them with data collecting devices. These devices should be able to send the data to a server.



Fig. 3: Future way of data collection and reporting

Current reasons for being "old fashioned"

At the moment construction business is following to the next step of evolution and trying to establish the digitalization in their organizations. Therefore, everywhere single solutions are presented, commonly by using tools like spreadsheet programs.

This is caused by two reasons; one is for sure the complexity of each single special foundation project. Each is unique and one spreadsheet based tool which has been "developed" for one construction site does not suit the requirements of the other project. The other reason is, that site engineers are civil engineers and not IT-specialists. Usually they are able to set up a solution or adopt existing spreadsheet program based tools to their specific issue, but are unable to connect the issues in a complete environment. This results in many information pools, which are not connected and not available for complex analyses.

Additionally, there is no time and no man power assigned in the projects for the digital tasks. If the management requests the projects to use digital tools, there should be the capacity and resources to deal with it. For big companies it might be reasonable to have an expert team or set-up a digital taskforce for large project, but many small and medium sized companies cannot afford additional personnel to deal just with data.

Summarizing the above mentioned reasons there is one conclusion: The tools which the construction companies and especially the sites need, must be simple. The involved persons on the projects have a lot of tasks and do not have the expertise to go deep into programming and complex digital tools. What they require is a simple user experience which is able to cope with complex relationships in the backend.

Tender and Planning Stage

Two main catalysators can be identified. The first is the client. He can ask for example via the contract for digital tools and 3D-Models of his project. Nowadays the number of requests by the clients is rising and of course a nice 3D-Model can impress the client. Furthermore a 3D or 4D model is improving the communication with third parties. And the second catalysator are the construction companies themselves. The construction industry is keen in getting information on the fly. Key-Performance-Indicators (KPI) allow a rough but quick assessment of the project status. Besides that, there are other KPIs for several purpose.

One reason is to have a basis for tendering. Everyone who is trying to calculate a new project needs numbers such as drilling speed, wear and tear rate, and so on. Here comes the first point of a project, where an

advantage by collecting data can be achieved. But for this, the tendering person needs access to a filled database from completed projects with a high grade of detail information. Collecting project data, even down to the machine data for example, the companies can rely on a big database. Which leads by the time to a huge knowledge about KPIs, wear and tear, diesel consumption and so on. Of course there is the difficulty to find out the best matching project, which had similar conditions, but this can be solved by having a well-documented and maintained database. Out of the documented projects, there should be as many as possible similar projects. This ensures a reliable acquisition of estimated KPIs. So there is a need to collect data from construction sites to get the base data for future projects.

Construction stage

In most of the cases the contractors do not need to evaluate all of the collected data and do not have a real interest in analyzing it yet. This is caused by the high effort if any evaluation or analysis besides the normal scope is requested. It needs a lot of manual working hours to evaluate for example the machine data as there is currently no system/ software for easy-to-use analytics and the data coming from the construction machinery is not normalized.

During construction, the companies are producing and collecting data. Not only paper records, also equipment is providing a lot of data. And each company has different machines from various manufacturers. A typical small site in Germany with piling works has a drilling rig, a wheel loader, generators, a small excavator and some small machines, tools and containers. The leading machine is the drilling rig, this provides data for example data for the quality and the performance while drilling. But also, the wheel loader can provide data such as On-off times, operation mode and others. Similar information can be provided by generators. Hereby every manufacturer provides different formats, interfaces and web based platforms. For construction companies it is not easy to collect them and do analyses. The data from all machines need to be normalized and in the next step they can be connected and analyzed. But therefore, the industry has to work out interfaces according to standards such as AEMP. As soon as the machines are providing the data according to the standard, the construction companies with a mixed machinery park are able to go the next step in towards a consistent data flow on their sites. Having that in place, the first and maybe the most important hurdle is taken.

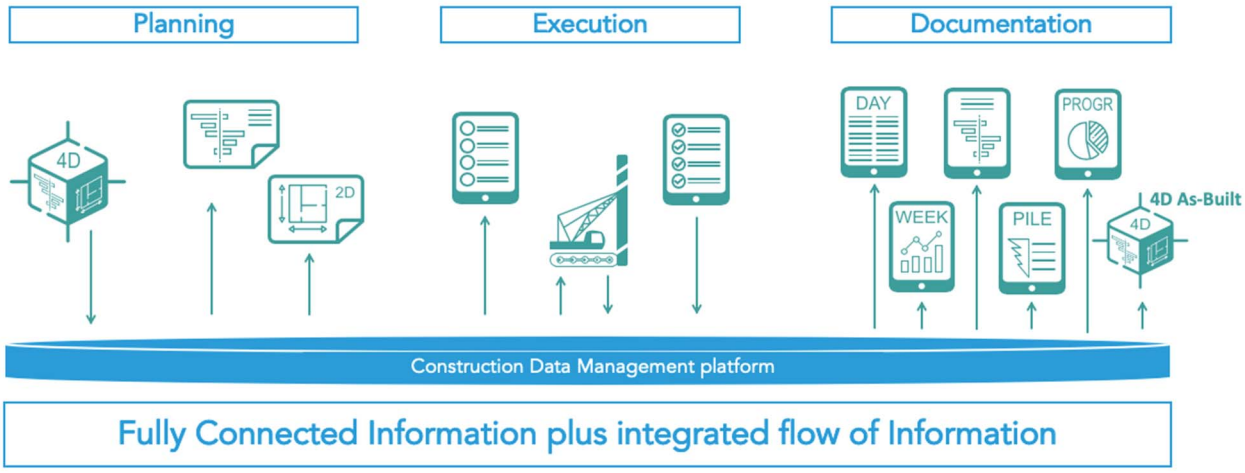


Fig. 4: Ideal process of information flow assisted by a construction data management platform

Operational stage (using the construction/ building)

Information which have been collected during project execution might be interesting for the owner of the construction. More and more projects request a long-term monitoring during usage. For example, monitoring of the pile head forces, vibrations at bridge bearings, stress in the reinforcement. Therefore, the construction industry in Germany is slowly developing solutions to meet the client requirements. Even here is the requirement to provide consistent data, available as contractual agreed and in a format, which can be processed to suit the clients needs. The sets of data can be implemented into the BIM-Model, which at this stage is an as-built-model, but also handed over as raw data for other purpose.

CONCEPTS AND SOLUTIONS OF ACTUAL MACHINE DATA ANALYTICS

Predictive maintenance is something what every machine related stakeholder knows and there is a broad interest in it. For everyone it is obvious that there is a benefit to maintain the machine prior a breakdown is occurring.

But there is an additional perspective to use the machine data. In combination of soil data constructions companies are enabled to calculate much better the performance and predict the progress. Coming from the machine data view it is simple to estimate the excavated material and get numbers at least for a double check. But also, it is obvious, that data measured by sensors is valid and we can trust them probably more than the information provided on a handwritten piece of paper.

Furthermore, in large projects it is very convenient to collect data automatically, get quality records on the fly and to have a system which is providing summaries of the production. In combination with a checking routine, the site engineers are able to minimize the effort to have a perfect quality documentation and control in place.

Typical experiences made at a special foundation project:

One site with six rigs which were executing vibro stone columns. Each rig did up to 120 pieces per day. Each column was recorded by a data logging software on the machine, with several data channels. The software recorded depth, some pressures, the time and the name of the element. In the end of a working day the quality engineer had collect all sets of data, print them and check each of the up to 720 reports. This took him in average seven hours and even trying his best, he still missed some mistakes in the report. Which caused some follow-up questions and correction works. The project management decided to establish a database which was connected to an open GIS system, equipped with some logical modules for checking single channels and providing tables which showed summaries of the relevant parameters. Elements which did not meet the quality requirements were highlighted. With this system the effort for the quality engineer was reduced to 1,5 hours and he was able to do reduce his working time to normal working hours. This has been a demonstration how digital tools are improving the work on sites. A second benefit was, that the quality documentation improved to error rate almost to zero.

Investigations on site showed that the experienced operators are more open to new systems than the unexperienced. Obviously this relates to the “boring” daily routine and the experienced like new tools which help them to do the documentation. During the implementation of a tracking system, which was used for getting additional information about time consumption of the drilling rigs, the first reaction was “Big Brother is watching you”. Some were afraid that someone could monitor their work, but once the advantages are obvious the operator starts to love new systems. Quote: “You know, I like this new system, because I can now easily report to the office what I am doing the whole day”.

CONCLUSIONS (OUTLOOK)

In case the construction companies and the equipment manufacturers are able to establish a consistent flow of data from the machines to the site office the first step is made. Construction companies then need to use instruments which allow a simple reporting, which is based on complex relationships between data sources. This will enhance the quality of the documentation by simultaneously decreasing the effort of creating for example reports.

Furthermore, the advantage of using digital instruments like connected work flow management systems or automatically generated reports will improve the documentation. The risk of missing reports, reports containing errors and so on are things of the past. All stakeholders are on the same level of information. The clients can be enabled to have a transparent "live" view to the works currently running. This will change the relationship of all participants and increase the transparency, not only in regards of the cost estimation.

In special foundation business the need of analyzing the data will also be more relevant. The big chance is to understand how the interaction between soils and machine output works. An additional benefit of collecting data is to get the chance of gaining relevant information just on-the-fly. Having a good concept of data recording in combination of analyses, the construction companies can provide BIM-relevant data to the client or even hand-over the as-built-model. Important is the basic workflow. The existing information silos of tools must be specially designed for the foundation industry to fulfil the needs of these highly technical projects. The Goal is to collect data, normalize and analyze it and create interpreted reports for daily usage.

As above pointed out the current situation is not very convenient. Companies and clients are moving towards a BIM world and a digital twin, but still there are high hurdles to a smooth digital workflow. Especially the transformation of data from one phase to the following is currently still challenging. Construction sites need in the first place easy tools which enable the work life as easy as possible. These tools need to be linked to a database to get all relevant information in place. Once the information is stored, it can easily be accessed. Having an excellent database in the backend, reporting will be much easier than in the past. Furthermore, the quality of all reports will increase significantly.

Based on a database, which is containing all datasets of a single project, the handover procedure will also improve. The construction company can create a complete 4D model for example with all necessary and contractual agreed data of the project. This is just on the fly and ideally just made in the future by "one click".

There are certain tasks to work on to get to a connected jobsite. But once having this in place the information silos are transferred between all stakeholders in all phases. The information is not lost anymore and ensures a consistent way from the tender phase to the handover with all documents of the as-built.

In Germany the automobile industry is evolving the first self-driving cars. There are certain parts of the Autobahn, where the companies can test their new models, equipped with a lot of sensors, computer performance, cameras and whatever is necessary for achieving the autonomous vehicle for the transportation of people. In opencast mines the transformation process to autonomous vehicles is ongoing since a couple of years and we will for sure see an equivalent development on special foundation construction sites. In the future, there might be a fence around the site, the contractor comes and leaves a bunch of machines, and the rigs are working by themselves. Engineers will have then constructed the digital twin in 4D, which is then sent to the equipment 4.0 and the equipment provides the data and all necessary recording to automatically generate the 4D as-built-model.

LITERATURE :

CECE 2019 : Digitalising the Construction Sector – Unlocking the potential of data with a value chain approach, January 2019.

DEFINITION OF DRILLING-ACTIVITY PATTERNS BASED ON PRODUCTION DATA PROFILES

Diego Bellato, Ph.D. P.E.
Head of Digitalisation and Process Management, Technical Services Department, Züblin Spezialtiefbau GmbH; Albstadtweg, 3, Germany; e-mail: diego.bellato@zueblin.de

ABSTRACT

Production data recorded by special foundation rigs during construction activities at the site are commonly used for quality assurance / quality control procedures and, in particular, to prove that the installed foundation elements comply with the geometrical and quality requirements defined in the design specifications. Parameters such as crowd force, penetration/withdrawal rate, rotational speed etc. are usually presented in reports in the form of depth and/or time profiles. This type of protocols are already standard QA/QC solutions for ground improvement methods like deep soil mixing or jet-grouting, but they are quite rarely applied in combination with other techniques like diaphragm walls or Kelly drilling. In the latter cases, one of the main reasons behind this lack of site documentation is related to the difficulty in interpreting huge amount of data collected during the creation of single elements, which, in some cases, can last several days (not always in a row). In addition, the building sequence is often characterized by many alternated operations involving different movements of the rig and the use of different tools. In this context, the identification of specific construction activities based only on the mere exam of the time profiles of the recorded production parameters is extremely difficult. In this paper, the time profiles of production parameters obtained from a fully-cased Kelly drilling rig employed on a site in Karlsruhe (Germany) have been investigated and compared with a detailed series of activities deduced from a video filmed during installation. Typical time profile patterns associated to specific procedures have been identified by combining the different information available. The outcome of this study helped project engineers to automatize the recognition of activities directly from production data and led to an overall understanding and optimization of the construction process.

KEYWORDS: fully-cased Kelly piles, production data, construction phases

INTRODUCTION

The special foundation industry is characterized by the use of highly sophisticated machinery for the realization of geotechnical systems such as piled rafts, retaining walls and slabs for excavation pits, cut-off walls for levees and embankments or ground improvement solutions. Rigs can vary in size, weight, and power and can be provided with several drilling tools to cope with the different soil conditions (e.g. clay, sand, rock) and the different geometries of the elements to be built at the site (e.g. micro-piles, large-diameter bored piles, diaphragm walls, anchors). Due to the challenging construction procedures, various types of sensors have started to be mounted on the equipment in the last decades to monitor the behavior of some important machine parameters and to inform rig operators about the on-going process and the status of their devices.

Production and machine data are typically transferred to a server of the manufacturer by a modem directly placed in the cabin and additionally saved as text files on the on-board computer. A file is initially generated

© 2019 Deep Foundations Institute

after the rig operator introduces some essential features related to the next element to be created (e.g. name of the jobsite and of the element) and presses a start-recording button on the main control touch-screen display. The logging ends once the element is finalized and another stop-recording button is pressed. The records can be subsequently retrieved with a USB-stick/CF-card or possibly downloaded from the server of the manufacturer.

Information such as depth, start and end installation times, crowd force, hydraulic pressure, temperature and many other details are nowadays available for most of the existing special foundation techniques. Ground improvement, for instance, is one of the fields where production data represent a crucial factor in the interpretation and evaluation of the activities carried out at the site, due to the need to estimate the effects of the treatment performed on the natural soil (e.g. Bellato et al. 2015; Dreese et al 2003; Park and Oh 2018; Ochmański et al. 2015). The importance of data logging in this context is also confirmed by norms, which for methods like compaction grouting (ASCE/G-I 53-10) or deep soil mixing (EN 14679:2005) define the reaching of a certain threshold level for a predefined set of parameters as a standard criterion to assess the success of the works or to identify hindrances or obstacles.

Machine data are also monitored during customary drilling operations. However, circumstances frequently occur where the review of the recorded values turns into an extremely time-consuming process, which requires unexpected efforts due to the complexity of the building sequence. The creation of bored piles is one of these situations, the continuous alternating of several movements of the rig and drilling tools being the most difficult aspects to be distinguished from a first look at the behavior of the production parameters. A clear example is reported in Fig. 1, which shows the time profiles of depth, rotation speed, drilling pressure and crowd-force during the installation of a single bored pile in weak to hard rock conditions over a period of three days. In such projects, the digital documentation is generally required at the jobsite to comply with contractual obligations. Nevertheless, a proper interpretation including gross and net performances or quantitative and qualitative analyses are typically not derived from the monitored parameters, which, in the best case, are visualized on demand as profiles plotted over time and/or over depth like those illustrated in Fig. 1.

It is worth mentioning that the available international literature has been mainly focusing on small-diameter drilling for mining, energy or oil industry applications (e.g. Chen et al. 2016; Hegde and Gray 2017), where the need to elaborate operational information is directly associated with the characterization of rock strength and the optimization of performance in hard formations (e.g. Babaei Khorzoughi and Hall 2016; Kalantari et al. 2018). On the other hand, comprehensive studies on production data obtained during drilling of large-diameter piles in cohesive and/or granular soils do not seem very common in the international literature. This research aims at providing a proper understanding of the interaction between different parameters collected from a big diameter piling rig employed on a site for the construction of fully-cased Kelly piles. In addition, it discusses in details the series of events identifiable from the time profiles of depth, drilling pressure, crowd force and rotational speed of the rotary drive and establishes the bases for the development of future algorithms for the automatic recognition of the several phases involved in the piling process. The possibility to gain a clear and easy approach for the interpretation of production data is considered as a significant step forward for a more accurate determination of performances whenever claims or discussions with other stakeholders arise.

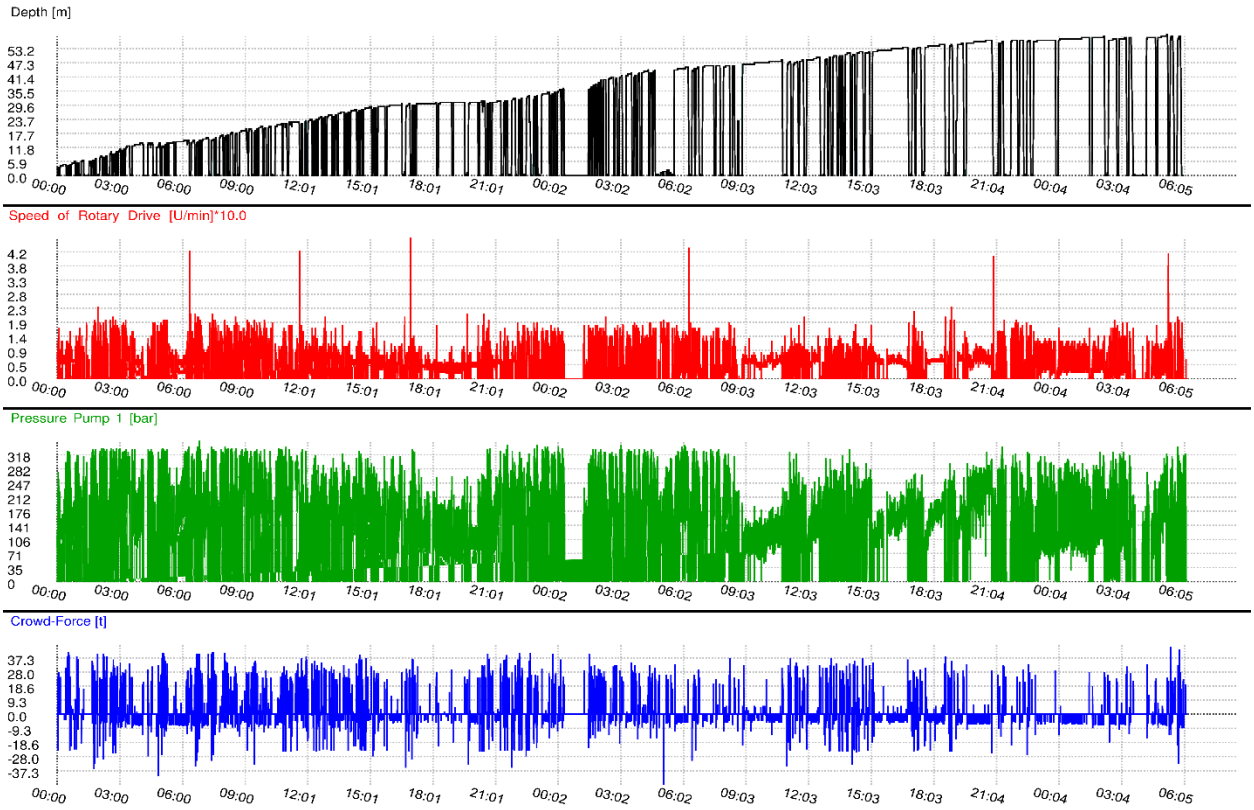


Fig. 1. Production parameters recorded during the construction of a bored pile in rock conditions.

PROJECT DESCRIPTION

The project selected for this study is the Kombilösung project in Karlsruhe (KASIG), which is an ongoing jobsite intended to further develop the public transportation network of the city by 2021. In this context, a new cut-and-cover tunnel for motor vehicles with a length of approximately 1850 m (1.15 mi) is currently under construction by Züblin Spezialtiefbau GmbH. The tunnel is conceived as a watertight rectangular frame composed of several concrete blocks located within an excavation pit supported by impermeable diaphragm walls and secant pile walls retained by 3 to 4 layers of tie-back anchors. The bottom of the excavation pit is sealed by means of a slab obtained by deep injections of soft gel with a deepest treated level of 21 m (68.9 ft) below ground level.

After the surface layer composed of vegetation or asphalt pavement, man-made sandy gravelly fillings could be found until a max depth of 5 m (16.4 ft) below the ground level (b.g.l.), locally interlayered with silty lenses of up to 2 m (6.6 ft) in thickness. Occasionally, slag, metal or wood residues were also encountered in the backfill. Underneath, the natural soil consisting of a sequence of heterogeneous quaternary deposits characterized by different grain size distributions was met until the max exploration depth (30 m (98.4 ft) b.g.l.). The alternation of prevalently sandy and gravelly layers with a thickness ranging from a few decimeters to several meters was not even across the site and included cobbles with a size of about 0.15 m (0.5 ft). Sporadically, traces of cohesive soil (mainly silt) were also observed in the granular mixtures and thin clayey-silty lenses between the sandy gravelly horizons were detected.

During site operations, the groundwater level originally comprised between 3.20 m (10.5 ft) and 5.40 m (17.7 ft) b.g.l. is deepened by means of wells situated along the perimeter of the tunnel, which are then converted into dewatering wells once the bottom of the excavation is reached.

The secant pile wall is produced in accordance with the pilgrim step system (primary – secondary piles) by using two Liebherr LB36 drilling rigs. The piles have a diameter of 1.2 m (47.2 in) and a depth comprised between 15.0 m (49.2 ft) and 23.0 m (75.5 ft) with a center-to-center distance of 0.90 m (3 ft). Due to the granular nature of the soil, the support of the wall is guaranteed by casings for the whole length of the drilled hole. Water is used as drilling fluid. In order to avoid possible filtration effects at the pile toe, the fluid level inside the casings is always maintained higher than the outside groundwater level. A double-cut rock drilling bucket is mainly adopted to achieve a high performance in the dense sandy and gravelly soil layers.

COLLECTION OF PRODUCTION DATA

Production data have been collected from one of the two Liebherr rigs employed in KASIG (Fig. 2a). Both rigs were equipped with the Liebherr proprietary software PDE (Prozessdatenerfassung), which allows the logging of several parameters on a text file during the installation of the bored piles. The recording frequency was set to 1 Hz. Among the different information stored in the log-files, particular consideration has been given to:

- depth (from a predefined zero-level – in m):
- drilling pressure (oil pressure of the hydraulic engine at the rotary drive – in bar);
- crowd force (force applied by the crowd winch to the sledge where the rotary drive is placed – in kN);
- torque (torque applied by the rotary drive – in kNm);
- rotation speed (rotation speed of the rotary drive – in rpm).

Despite the possibility to record the data in the form of depth profiles (values assigned and grouped in predefined depth intervals), a time representation was chosen in this case since it generally provides a more unbiased and meaningful understanding of the working activities. Moreover, misinterpretations or false assumptions are less likely to occur. Time diagrams gave the opportunity to study in detail (second per second) the status of the rig throughout the construction process and to deduct automatically the corresponding phases based on the behavior of several properties within a predetermined time interval. This kind of interpretation is directly linked to performance issues and, in particular, to the overall dependences of performance from soil conditions, excavation tools, rig operators, and other external factors.

The log files referred to each pile (containing general information and production data) were downloaded at the end of the working day manually from the Liebherr server or, alternatively, by reading the CF-card of the on-board PDE computer mounted in the cabin. While in the first circumstance a Liebherr proprietary software is required, no supplementary programs are necessary when the files are directly copied from the card.

INTERPRETATION OF PRODUCTION DATA

The first stage of the research was directed at the definition of the main phases for the construction of a fully-cased pile at KASIG. To this purpose, a video was filmed throughout the whole installation procedure of pile B2008 (Fig. 2b).



a) b)

Fig. 2. a) Liebherr LB36 operating in KASIG (Karlsruhe) and b) video-recording equipment

The video had the objective to support initially the interpretation of the production parameters by synchronizing the stream of data generated by the rig with the sequence of frames recorded by the camera. In addition, the images could provide explanations whenever apparent breaks in the drilling and casting processes could be observed in the time diagrams.

The operations were classified in five main groups as follows:

C1. movement of the rig (positioning, swinging, movement of Kelly bar, emptying of drilling bucket etc.);
C2. handling of casing (introduction or extraction of casing in/from the soil, connection/disconnection of casing parts etc.);
C3. drilling (penetration of drilling tool into the soil);
C4. other activities related to the rig or tools (refueling, increase of level of drilling fluid inside the casing, cleaning of tools, standstill);
C5. other activities unrelated to the rig or tools (introduction of reinforcement in the hole and concreting).

A clear visualization of the sequence of operations is reported in Fig. 3b, which shows the profile of depth over time superimposed to the alternating series of activities grouped according to the categories mentioned above. A general description of the main stages of production is also presented in Fig. 3a.

The experimental graphs of depth, drilling pressure, crowd force and rotational speed could be then simultaneously analyzed in detail and compared with the previous subdivisions of the time axis to define the algorithm for the final automatic recognition of construction phases and their respective start and end.

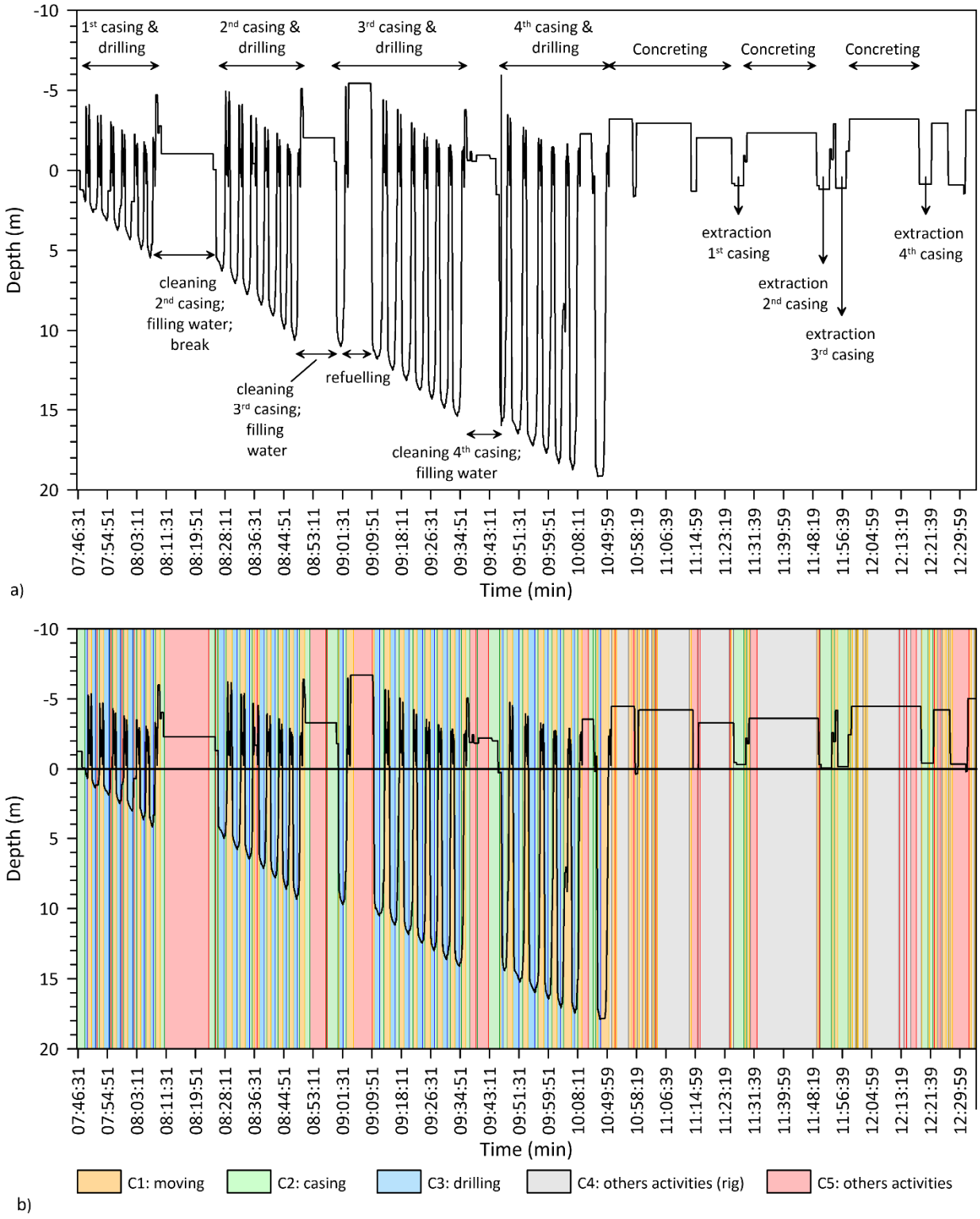


Fig 3. Identification of construction operations based on the video recorded at the site; a) depth profile with main stages of production; b) detailed sequence of operations based on the predefined groups of activities: Yellow: C1; Green C2; Blue: C3; Grey: C4, and Red: C5

It is worth mentioning that the Liebherr monitoring system does not currently track variations in torque for gears different than the first (high-torque gear), which was used at the site particularly for the introduction or extraction of casing parts into or from the ground. An attempt to estimate the torque during the whole installation process was conducted based on the effective relationship between torque and rotational speed provided in the technical documentation of the rotary drive mounted on the rig. The outcomes, unfortunately, did not yield to the expected level of reliability and, therefore, they were not included in the following investigations.

Criteria have been programmatically specified in terms of rules and limit values for the following construction activities:

- drilling (A1);
- introduction of casing into the ground (A2);
- extraction of casing from the ground (A3);
- fast downward movement (A4);
- fast upward movement (A5);
- movement of the rig or short break (A6);
- emptying of drilling bucket (A7);
- closing of drilling bucket (A8);
- break (A9).

The most important indicator for the automatic detection of such phases was certainly depth, initially adjusted to refer to the actual jobsite zero level, i.e. the platform level. Penetration and withdrawal rates were further used to distinguish among fast/slow downward (positive gradient) or upward (negative gradient) movements of the Kelly bar. In order to determine the possible status of the rig for each recorded event (t_i, with i varying from 0 to the total number of measurements taken throughout the recording process), a look-ahead analysis was carried out assuming an observation time interval (t_a) equal to 10 seconds. During t_a, the following values of depth were compared with the one at time i (d_i) and, if found deeper (beyond a certain predefined tolerance, Δd, assumed here equal to 0.01 m (0.4 in)), the rate was calculated. A rate lower than 5 m/min (3.3 ft/min) (r_t) has been associated with slow downward movement of the Kelly bar while a rate higher than that has been linked to a fast-downward movement. No variations of depth (within Δd) over t_a were considered a symptom of interruptions. However, approximately constant depth profiles for a period of 5 s (t_m) were related to rig movements. When depths lower than d_i were reached in the observation period, the threshold rate r_t was applied to discern between slow or fast withdrawal of the Kelly bar. Negative values of depth clearly indicated operations occurring above the ground surface (movement of rigs or actions with the drilling bucket or casing parts). Breaks and surface movement of the rig were identified by means of the same rules described above.

To confirm the previous considerations and, moreover, to differentiate slow penetration from drilling and emptying from closing of drilling bucket etc., the behavior of other data such as drilling pressure, crowd force and rotational speed of the rotary drive needed to be simultaneously evaluated. For instance, drilling was accepted only for slow downward movement characterized by a drilling pressure constantly above 100 bar (1450 psi) and a rotational speed continually higher than 10 rpm for at least 70% (efficiency rate, e) of t_a. A drop of pressure and rotational speed was regarded as an indication of the forthcoming conclusion of a drilling step. Pressure values below 35 bar (508 psi) or rotational speed equal to 0 rpm for for a duration

of at least 70% of t_a were attributed to movements of rig or of the Kelly bar. Emptying of bucket was defined by negative depths with a fast downstroke followed by a fast upstroke of the Kelly bar and by a pressure higher than 35 bar (508 psi) and a rotational speed different than 0 rpm for the duration of the transition (change in sign of the depth rate) period. The closing of the drilling bucket differed from the emptying procedure for the reduced pressure (lower than 35 bar (508 psi)) and for a deeper level of the transition (less than 1 m (3.3 ft) above the ground surface). It is interesting to note that a phase like the introduction and extraction of casing parts could not be directly detected from the trend of the depth profile. The introduction, in particular, was recognized because of the high values of drilling pressure and crowd force (above 150 bar (2176 psi) and higher than -50 kN (-11.2 kip), respectively) and rotational speed concurrently beyond 5 rpm for at least 70% of t_a.

The crowd force profile was found in general very variable during the installation of the pile and, for this reason, could be used only when an evident match with a certain activity was observed. An additional detail that could be deduced from the crowd force was the weight of the tools attached to the mast (rotary, Kelly bar and drilling tool) during movement of the rig above the ground level.

An excerpt (10 minutes) of the results obtained from the implementation of the algorithms for the recognition of the construction phases for pile B2008 at KASIG is reported in Fig. 4. The figure shows a combined representation of normalized depth, drilling pressure, crowd force and rotational speed profiles over time superimposed to the automatic classification of activities, which proved its capability to interpret correctly the main operations occurring during production. The same method of analysis was applied with a satisfactory degree of accuracy also to the log files referring to other piles created at the site.

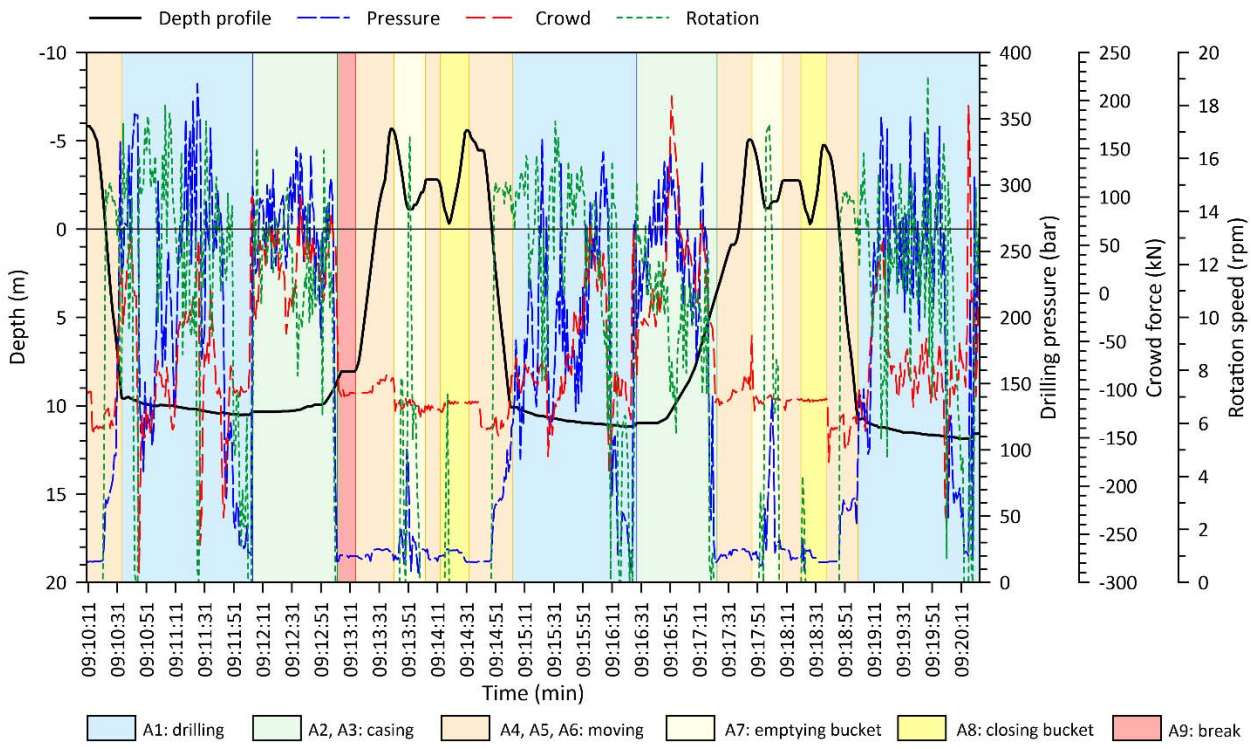


Fig. 4. results of the automatic phase recognition algorithm: Blue: A1; Green: A2 and A3; Orange: A4, A5 and A6; Pale Yellow: A7; Yellow: A8; Red: A9.

Project engineers could manage the outcomes of this intelligent approach to assess the efficiency of the installation process in a more comprehensive way and to highlight anomalies in productivity or in the workflow.

Complementary studies are required to confirm the validity of the criteria individuated in this research for fully-cased piles and to extend the field of applications to further special foundation methodologies (e.g. direct or indirect circulation drilling). It is expected that a precise definition of the activities to be recognized along with a suitable calibration of the parameters affecting the algorithms can provide results similar to those presented in this paper.

Finally, it is worth mentioning that the consideration of supplementary machine data (e.g. torque, position, RFI sensors mounted on tools etc.) are believed to refine and support in the future the interpretation procedure in an extremely wide range of conditions.

CONCLUSION AND WAY FORWARD

Production and rig data collected during the works represent an essential information for a more comprehensive understanding of drilling processes. These details can be used to automate the recognition of the sequence of rig activities carried out at the jobsite. This paper presents the results of such interpretation technique applied to a fully-cased pile installed at the KASIG project in Karlsruhe (Germany). Criteria were determined based on depth, drilling pressure, crowd force and rotation speed of the rotary drive to classify construction operations with the help of method parameters calibrated for the case under consideration.

The automatic recognition of phases supported engineers by providing a quick overview about net and gross performance along with the duration of standstill periods. Analyses of production rates associated to different piles created with the same/different equipment or by the same/different crews were also possible.

Data can also be utilized to determine correlations between in-situ test measurements obtained from initial geotechnical investigations and the specific energy required to drill 1 m³ of soil. When combined with performance, consumptions and wear & tear, relationships between specific drilling energy and soil type can be applied by tender engineers to prepare more accurate and reliable cost estimations of incoming projects. Additionally, by comparing curves referring to different tools in similar ground conditions, the most efficient drilling tool to be used in particular soils can be reasonably identified.

The research conducted so far has taken into consideration only one construction project where fully-cased piles were installed into medium to high dense granular soils. However, the promising results observed until now encourage further extensive implementation of such methods of analysis on other sites. The eventual introduction of additional machine data in the algorithms is expected to provide a suitable solution also for other special foundation applications.

REFERENCES

Bellato, D., Spagnoli, G., and Wiedenmann, U., 2015. Engineering and environmental aspects of offshore soil mixing. Proc. ICE – Geotechnical Engineering, 168(3) 267-278.

Babaei Khorzoughi, M., and Hall, R., 2016. Processing of measurement while drilling data for rock mass characterization (2016). International Journal of Mining Science and Technology, 26(6), 989-994.

Chen X, Gao D, Guo B and Feng Y (2016). Real-time optimization of drilling parameters based on mechanical specific energy for rotating drilling with positive displacement motor in the hard formation. Journal of Natural Gas Science and Engineering, 35 686-694.

Dreese, T. L., Wilson, D. B., Heenan, D. M., and Cockburn, J., 2003. State of the art in computer monitoring and analysis of grouting. Third International Conference on Grouting and Ground Treatment – ASCE, February 10-12, 2003, New Orleans, Louisiana, US.

Hegde, C., and Gray, K. E., 2017. Use of machine learning and data analytics to increase drilling efficiency for nearby wells. Journal of Natural Gas Science and Engineering, 40 327-335.

Kalantari, S., Hashemolhosseini, H., and Baghbanan, A., 2018) Estimating rock strength parameters using drilling data. International Journal of Rock Mechanics and Mining Sciences, 104 45-52.

Ochmański, M., Modoni, G., and Bzówka, J., 2015. Prediction of the diameter of jet grouting columns with artificial neural networks. Soils and Foundations, 55(2) 425-436.

Park, D., and Oh, J., 2018. Permeation grouting for remediation of dam cores. Engineering Geology, 233 63-75.

DESIGN AND DELIVERY OF MICROPILE INSTALLATION LEVERAGING AUGMENTED AND VIRTUAL REALITY

Zachary T. Fleming, GEI Consultants Inc., Madison, WI, USA, zfleming@geiconsultants.com
Guilherme L. M. G. Carvalho, GEI Consultants Inc., Rio de Janeiro, Brazil, gcarvalho@geiconsultants.com

ABSTRACT

In a world of 2-dimensional design documents, envisioning and understanding 3-dimensional interferences for complex foundation construction scenarios can be challenging. Videos and computer models serve as 3-dimensional spatial aids but have drawbacks related to a fixed perspective. Augmented and virtual reality (AR/VR) provide new tools to communicate design challenges and improve construction planning. This paper provides a practical look at the basics of AR/VR systems and the tools available to the foundation design and construction industry by giving a high-level example of the technologies' use in the design and delivery phases of a complex micropile installation project for the remediation of a dam foundation. Using these technologies, GEI was able to design and deliver a complex foundation remediation solution. AR/VR benefited regulators, and the client, to help understand the design concept, construction sequencing, and approach to overcoming installation challenges. Due to its user-friendly nature and less rigorous programming and hardware requirements, AR proved to be more useful than VR for this scenario. AR/VR will likely not replace videos and computer models; however, it can be a useful 3-dimensional visualization aid that complements the project delivery process and offers benefits that traditional methods cannot.

Keywords: augmented reality, virtual reality, visualization

INTRODUCTION

Augmented and virtual reality is a promising and rapidly developing technology within the engineering and construction world. Like any rapidly developing new technology, the language describing it can be confusing and dynamic. To eliminate the confusion some definitions must be made.

AR/ VR definitions

The definitions of virtual reality (VR) and augmented reality (AR) for the purposes of this paper are as follows: VR is a computer-generated immersive environment that the user experiences within a digital 3-dimensional space (Satava, 1993)AR is a composite view created by superimposing digital objects into the user's real-world view (Azuma, 1997). Often, VR is used in an office environment and allows the user to "visit" the digital site to review site planning, construction sequences, and interference geometry. AR can be utilized in both the office and onsite environments. Like VR, the in-office application for AR is commonly site planning. AR also can be utilized in the field for applications such as seeing through the ground to locate known existing obstructions like utilities, gas tanks, etc.

3 and 6 Degrees of Freedom

The definition of 3 Degrees of Freedom (3DF) for the purposes of this paper is as follows:

© 2019 Deep Foundations Institute

The user has control of the three axial angles (pitch [up and down], yaw [left and right], and roll [side to side]) (Paul, 1981). 3DF systems have a wide range of accessibility. For instance, most smart phones today can achieve 3DF AR/VR.

The definition of 6 Degrees of Freedom (6DF) for the purposes of this paper is as follows:
The user has control of the pitch, yaw, roll as well as the x, y, z position (Paul, 1981). This allows the user to have full control over their position and point of view in the simulation. 6DF systems are not as widely accessible as 3DF; however, they provide the user with a much deeper experience.

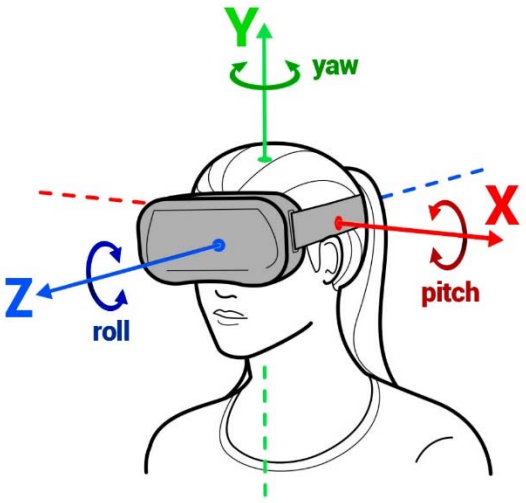


Fig. 1. Diagram explaining the three axial angles (pitch, yaw, roll). (dSky, 2015)

Project Introduction
The project that utilized this technology was a complex foundation remediation design for a large dam. Due to a non-disclosure agreement the specifics of the project have been intentionally kept vague. The project required the proposed foundation piles to be drilled from the top of the dam deck, through the rollway, and through an open gallery containing utilities and structural objects. Due to the large number of obstacles to avoid while advancing the casing (Fig. 2), success of the project was directly related to a clear, 3-dimensional understanding of the drilling path. The idea to use AR/VR to help demonstrate the construction sequence and drill path came late in the design phase resulting in a tight budget. Since the 3D model was developed in the design phase, and the target device was a smartphone, the cost of implementing an AR/VR application depended solely on the software development effort.

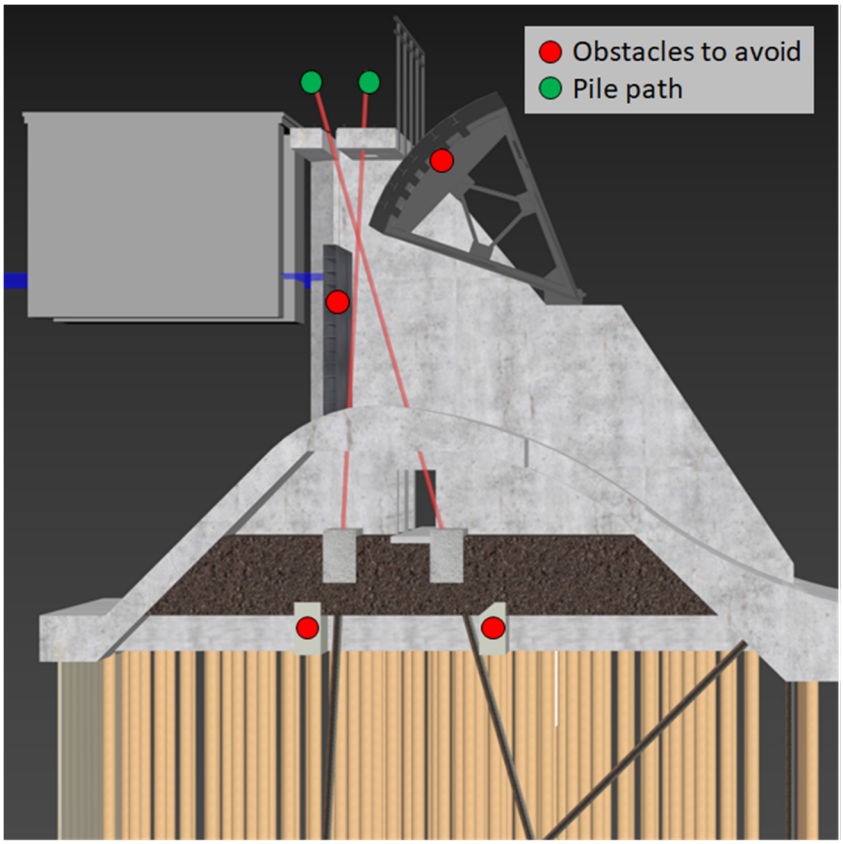


Fig. 2. Section of dam gate with micropile drill path highlighted and obstacles to avoid marked

METHODS

How VR Works and Common Uses

VR was first popularized in the Architecture, Engineering, Construction, and Owner (AECO) industry around 2015 (Jarvinen, 2018). This paper's definition of VR was used before 2010 in the form of digital models and interactive walkthroughs, mostly when the user controlled a camera to navigate a space with a keyboard and mouse. However, in today's context, the use of VR often implies the utilization of a headset. A VR headset works by placing two high definition screens on the inside of the lenses, close to the user's eyes, and by blocking out all external light. Drawing, also called rendering, (Eck, 2018) the model twice (one for each eye) allows the simulation to achieve stereoscopic VR. Stereoscopic VR gives the user a sense of depth and helps to achieve what is essentially fooling the user's brains to create a realistic immersive experience. Accelerometers within the headset measure the pitch, yaw, and roll of the user's head, and more advanced systems will also measure the x, y, z position of the headset using a local coordinate system created by sensors. When the pitch, yaw, roll, x, y, or z changes, the model is updated within the simulation. A new frame (what the user sees on the screen) is drawn with each angle or position update. The speed in which frames are drawn is measured in frames per second (FPS). The industry standard for high quality VR is typically 90 FPS. Rendering photorealistic models at 90 FPS requires a large amount of computing power, but a FPS below this threshold causes a lag in the update of what the user sees and can result in unpleasant physical side effects, like nausea (Mullis, 2016).

3DF systems have a wide range of accessibility. For instance, most smartphones today can achieve 3DF VR. Couple this with a cheap headset mount for mobile phones (such as Google Cardboard) and a decent stereoscopic 3DF VR experience can be achieved. This method has some limitations. Smartphones are restricted by the rendering power they can provide; therefore, the image quality of the model will suffer and likely will not be photorealistic. This limitation results in a "cartoony" style for most phone VR experiences. Creating a monoscopic view is an approach to help reduce the required amount of rendering power. This effectively halves the rendering cost at the expense of the sense of depth, which diminishes the VR experience, and doesn't work well with headsets. Photorealistic VR on phones is often referred to as a 360 panorama. These panoramas are created by placing the user in the center of a sphere where the images are projected, allowing the user to see one framed portion of the sphere at a time, and providing the ability to interact with that view. With the help of capable hardware, more advanced 3DF systems can render photorealistic models above 90 FPS. The most advanced VR setups give the user control of the pitch, yaw, roll and the x, y, z position. 6DF VR allows the user to both look around and move around. This is usually achieved by positioning sensors in the corners of a room and then the user can move within the model, limited to the extents of the real-life room. For obvious reasons, this works best if the real-life room is empty, but there is a warning system if the user is close to a real-life wall. This form of VR can be so believable that users will attempt to lean on digital objects but will fall because the objects don't exist in real life. To help with safety, rooms can also be set up with some of these objects, like furniture, to allow the user to touch real objects. 6DF VR is commonly used in the architecture and interior design industry to visualize what a space will look and feel like before it has been constructed.

How AR works and Common Uses

AR became commonplace in the AECO industry by about 2015 (Augment, 2016). AR has both headset and mobile phone uses, with the mobile phone AR the more popular of the two. Like VR, AR has all the same prefixes that describe the quality of the simulation, or in this case the augmentation. The simplest form of AR is 3DF non-interactive AR. This type of AR is a live video feed from a mobile phone with a digital object augmented over it. This augmentation does not provide any depth or interaction, so the user is unable to walk closer to, or further from, the object, and would not be able to interact with a real-world object (sit on a table for instance). For the AECO industry, interaction with the real world is critical. With that in mind there are two main methods to achieve the desired interaction: 3DF interactive AR and 6DF interactive AR. 3DF and 6DF have almost the same pros and cons as they did with VR, however safety is a lot more critical. Like before, 6DF allows the user to freely move around, however there is a lot more danger in AR because the user is simultaneously interacting with both virtual and real worlds. Having a disconnect between what is and isn't a real object can have hazardous consequences. For example, imagine the danger posed when augmenting a virtual manhole cover over areal manhole. Both 3DF and 6DF AR can be experienced with monoscopic (phones, tablets) or stereoscopic (Headsets) hardware. The main difference, as far as AECO is concerned, is the accuracy of the placement of the augmentation for georeferenced models. Currently GPS capabilities of smartphones are not enough to accurately place an augmentation working on satellites alone, which requires secondary correction. Usually this correction comes in the form of manual user alignment of the model via the touch screen or attaching an external GPS antenna to the mobile device. The array of sensors within a headset offers more accuracy and for this reason is often the first choice for georeferenced AR in the field. In a non-georeferenced scenario (like placing a 3D diorama on a table) the mobile device builds a local coordinate system using its camera. This allows the mobile device to achieve 6DF AR entirely on its own. This can be done in two ways. The traditional way is using an image target. An image target is

a complex image that the camera can recognize and can differentiate points of high contrast. It then tracks these points when the camera moves and then moves the model accordingly. The second approach to a non-georeferenced AR experience are two relatively new systems called ARcore (Google) and ARkit (Apple). These both work by allowing the camera on a mobile device to gather information about the environment within view. Much in the same way that the image target works, the camera picks up points of high contrast in the environment and then builds surfaces for the placement of augmented objects. The success of this system relies upon high-end cameras, so it is limited to certain newer devices (Vieyra Software, 2018).

PROJECT IMPLEMENTATION

Deciding the Best Use Case for the Scenario

The first, and arguably the most vital, step in project implementation is deciding on whether the project truly benefits from the use of AR/VR. If AR/VR is used in a situation that it is ill suited or sub-par compared to other visualization solutions, it can come off as feeling like a gimmick. The AECO industry offers a vast array of AR/VR technology, so it is important to compare the needs of the project with the capabilities of the various systems. A good place to start this evaluation is to consider the hardware either accessible or acquirable by the end user. While headsets are not available on the shelf of every AECO firm, smartphones are likely in the possession of each person, thus mobile hardware is often the easy choice for many projects. For VR, it is important to consider the resolution and texture quality of the model. If the intent is to show a construction sequence, then most effective approach is to only show the "big picture" aspects from a specific, carefully selected, vantage points locked into 3DF. These large scope vantage points don't rely upon high definition texture quality and often a cartoony or solid color look can even help highlight the important steps and motions of the construction sequence. If the presentation of the final building is important, it may be more appropriate to consider a headset with photorealistic rendering capabilities, which will create the effect of fooling the user's brain into seeing a virtual model as if it were real. Since the aesthetics of deep foundations is not a critical factor, photorealistic VR is not required. The power of AR/VR for the deep foundations industry is rooted in its ability to communicate and visualize 3D information, so for construction sequencing, drilling path, highlighting difficult geometry, etc. the solid color vantage point approach is appropriate.

Both AR and VR were implemented on the micropile project that is the example for this paper. A custom AR/VR software solution was developed since there was not already a software that fit the specific needs of the project. For the reasons mentioned above, among others, a mobile-based hardware platform was selected. The goal was to show a complex construction sequence and complicated drilling path, so, for clarity, a 3D model with only the essential parts and simple textures was used. This benefitted the hardware selection because nothing more powerful than a phone/tablet was required to render the model. The ubiquity of mobile devices eliminated the cost of hardware altogether, which would have been substantial if a headset and computing rig were required for the low-budget project. Considering the audience for the AR system was a large group of clients and regulators, the most reasonable approach to illustrate the construction sequence was to have a digital animated scaled down model augmented onto a conference room table. This approach required the creation of an image target-based 6DF AR solution. This approach allowed for a group of people to simultaneously watch the construction sequence together, from any position and angle they choose. The VR solution was chosen to help the designer choose a drill angle, but a benefit was also to reassure the end users that the drill casing would not collide with any critical existing elements. The VR

solution developed was a 3DF system that allowed the user to see the drill casing advancing as if they were on site (Fig. 3).

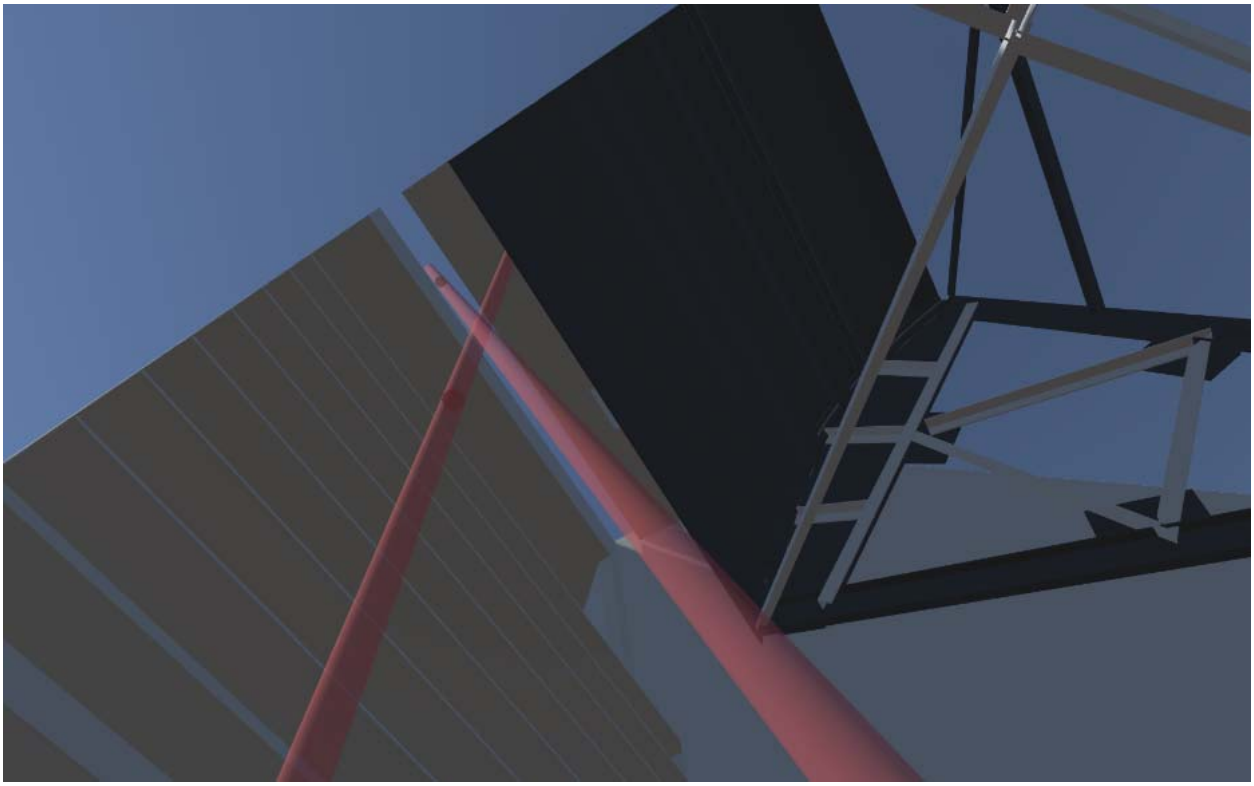


Fig. 3. Drill path highlighted red in VR, standing on the rollway looking up. First-person perspective of tight drilling angle tolerances.

Building the AR/VR Experience

After determining what type of AR/VR would best fit the project, the next step was to build the models. A section of the dam spillway was modeled in Revit, based on record drawings, and a model of the entire spillway was captured using drone photogrammetry. Animations for the construction sequence and advancing the drill casing were then completed in a post processing step. The AR/VR solution was built in the videogame software Unity3D (Unity Technologies, 2019). A plugin called Vuforia facilitated the creation of an image target and a model that would be augmented when a user's mobile device camera recognized the target (Fig. 3). To more clearly visualize smaller portions of the construction sequence, scalability of the model was incorporated. Most phones could track the target and render the model at around 30 FPS. Upgrading to a tablet allowed for a higher FPS count of around 50-60. A Google cardboard plugin for Unity then achieved 3DF VR. The vantage point chosen was one where the user would be able to see the most treacherous part of advancing the casing. The vantage point selection was critical to help assure the owner and regulators that the casing would not intersect critical existing objects. This vantage point also better informed the engineer in choosing a drill angle since they did not previously have access to this perspective. An inexpensive headset was also incorporated into this VR experience. This allowed for a stereoscopic view, which was important since depth was a primary factor in achieving a complete understanding of the drill angle. The phone screen was split down the middle and the view was rendered

twice at slightly different angles, then inserted into the headset. This process exhausted the phone's computing power and was unable to achieve 90 FPS. Testing across multiple phones revealed results of 20-60 FPS.

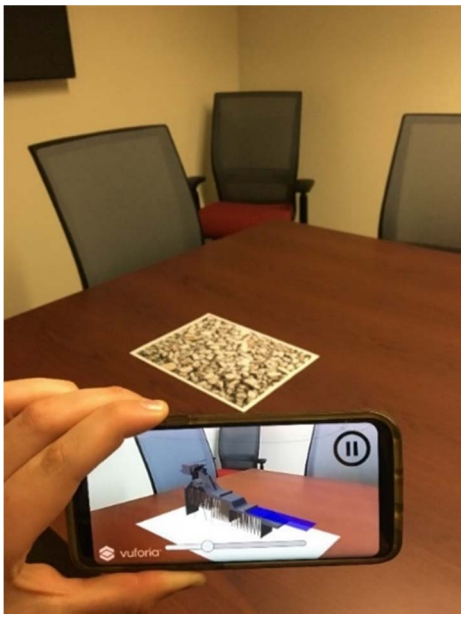


Fig. 4. Augmented micropile construction sequence model rendered with mobile phone and image target.

Final Product and Uses

The final product was used in meetings with designers, clients, contractors, and regulatory agencies. One of the design engineers used the VR application to confirm and reassure that the correct drilling angle was chosen and then to evaluate the tolerances of the critical obstacles. The AR solution was used in larger meetings with the client, contractors, and regulators to demonstrate the proposed construction sequence. This allowed for the group to visualize construction difficulties and confirm the difficult drilling geometry.

CONCLUSION

AR/VR Pros/Cons from the Project

The final AR/VR experience overall benefited the project. The application of VR was most helpful in the design phase. It allowed for the design engineer to gain a sense of depth and aided in deciding on a drilling angle. Due to the VR experience requiring a headset to hold the phone, and a limited number of available headsets, it was hard to supply the meetings with the proper amount of equipment. This meant that only a few people were able to experience this part of the project through VR. Also due to the rendering power required, the model had to be limited to only its most essential elements. Even with limited models 90 FPS was impossible. This led to the possibility of discomfort when viewing the model with the VR headset. The amount of discomfort varied between users but most felt none to slight discomfort (after no longer than 15 minutes).

The utilization of AR was most useful in presentations of the design to federal regulators, contractors, and clients. The AR method was more widely used due to the only hardware requirement being a mobile device with a camera. It facilitated the explanation of a complicated 3D micropile installation process in a 3D environment. This alleviated the difficult task of conveying a difficult 3D process with only 2D documentation. The user experience was smooth, and a tablet was preferable due to its larger viewing screen and improved FPS (due to higher computing power). Had there been a larger budget, it would have been useful to explore targetless AR. The image target worked well until the user wanted to look at the model from an angle were the target wasn't visible (from the side). A targetless method was attempted for this configuration, however it was prone to errors in the transition from the target and back again. Doing a full targetless AR solution would have alleviated this limitation and may have been an improvement overall. Also, with a larger budget it would have been beneficial to utilize AR in the field. The ability to visualize a digital starter casing advanced through the structure in the field could have been a significant advantage.

AR/VR Compared to Traditional Methods

When compared to traditional 3D methods, these AR/VR solutions had advantages. Videos are often used to explain construction sequences; however, they suffer from a fixed perspective. This means that the video will always be from the perspective of the filming angle. Therefore, if the video was shot from a bad perspective, the model will forever be viewed through a less than ideal lens. Further complicating this idea is the notion that a good and bad perspective is subjective and varies based on the user. It would be impossible to allow for every end user's preferences with a video that is only capable of showing one perspective. AR/VR had an advantage in this project since the perspective was free. The 6DF AR solution for example, allowed the user to view the model at any stage in the sequence from any angle. This provided reassurance to the owner and regulators as it allowed them to answer a lot of their own questions by simply looking for themselves. With the reduced need for clarification, this method moved technical meetings along faster. Giving the power to the end user to clarify some of their own questions by looking is unique to AR/VR and could not be recreated with videos and pictures due to their fixed perspective. Another traditional way of viewing a 3D model is using a computer and orbiting around the model with a mouse and keyboard, giving the user a free perspective. One could argue that this is a form of VR given the definition stated at the beginning of this paper. This method can be clunky and awkward to navigate and doesn't offer a real-world feel, especially related to depth perception. Headset and mobile AR/VR has an advantage over this method since the perspective is controlled by naturally looking and moving around, which is intuitive.

Cost of Development

The cost of including AR/VR in the project was relatively low. This was due to the fact that mobile phones, provided by the end users, were the target device. The software Unity3D was used to make the application for the project. Unity3D came with a $131.88 monthly price tag (free for entities that have less than $100k per year in revenue). The application was developed quickly allowing GEI to pay for a single month. It took roughly 24 hours of development time to put together both the AR and VR applications. The 3D modeling time was not considered since the models were already made as part of the design workflow.

There is a wide variance of cost when it comes to implementing AR/VR into projects. The development software is cheap and accessible, reducing the barrier of entry to developing AR/VR applications by the day. As second and third generations of headsets are released, the hardware costs are starting to come down

from their currently high buy in. The average smartphone however, comes with augmented and virtual reality capabilities. The highest cost to the project will likely be the development time for the application. This too is being reduced by private developers and easy to use software. Overall, if AR/VR is applied to the project correctly, the benefit it can provide outweighs the cost. This is especially so if the goals can be achieved with cheap hardware (mobile phones) and a simple concept.

AR/VR Future Outlook and Current Uses for Foundation Design

The future of AR/VR in the engineering and construction world is promising. Communicating 3D information is much more effective when the need for translating 2D information is eliminated. For the deep foundations industry, AR is more promising than VR. VR will have uses in planning, however it is most applicable in construction scenarios. AR will be an advantageous tool when deployed in the field. With the ever-growing wealth of subsurface spatial data, AR will be primed for most projects. The risk associated with installing foundation systems around existing subsurface elements (utilities, older foundations, possible obstructions etc.) will decrease when the operator is able to "x-ray" through the ground and utilize the spatial data of those elements. In the far future, it is likely that AR will be used by every person on site as 3D information is communicated in real time from the office. With that being said, the current form of AR/VR can benefit projects today. Today's VR/AR will likely not replace videos and computer models; however, it can be a useful 3-dimensional visualization tool that complements the project delivery process and offers benefits that traditional methods cannot.

ACKNOWLEDGMENT

The authors gratefully acknowledge the contributions of G. Meister and D. Mackey for their review efforts.

REFERENCES

Augment. (2016, May May 12th). *Infographic: The History of Augmented Reality*. Retrieved from Augment: https://www.augment.com/blog/infographic-lengthy-history-augmented-reality/

Azuma, R. T. (1997, August). A Survey of Augmented Reality. *Presence: Teleoperators and Virtual Environments 6*, pp. 355-385.

dSky. (2015, May 14). *VR tech 411 : 6DoF, XYZ + YPR, position + orientation in 3space*. Retrieved from dSky : VRFAQ: http://dsky9.com/rift/vr-tech-6dof/

Eck, D. J. (2018). Introduction To Computer Graphics. Geneva: Department of Mathematics and Computer Science Hobart and William Smith Colleges.

Jarvinen, T. (2018). Presentation about Virtual Reality in Clean Room Design. *R3* (p. 31). Naantali: Granlund.

Mullis, A. (2016, July 15). *How does virtual reality work?* Retrieved from andriodauthority.com: https://www.androidauthority.com/virtual-reality-work-702049/

Paul. (1981). *Robot Manipulators: Mathematics, Programming, and Control.* Boston: MIT Press.

Satava, R. M. (1993). Virtual reality surgical simulator. *Surgical Endoscopy*, 203-205.

Unity Technologies. (2019). *Unity Real-Time Development Platform*. Retrieved from https://unity.com/

Vieyra Software. (2018, September 24). *Comparing Google ARCore and Apple ARKit*. Retrieved from Medium.com: https://medium.com/@vieyrasoftware/comparing-google-arcore-and-apple-arkit-81b4727132ad

DIGGS DOES DEEP FOUNDATIONS

Robert Bachus, Ph.D., P.E., D.GE[1], Nikolaos Machairas[2], and Allen Cadden, P.E., D.GE[3]

[1]Geosyntec Consultants, 1255 Roberts Blvd., Suite 200, Kennesaw, GA, 30144; rbachus@geosyntec.com
[2]New York University, Tandon School of Engineering, 6 Metro Tech Center, Brooklyn, NY, 11201; machairas@nyu.edu
[3]Schnabel Engineering, 1380 Wilmington Pike, Suite 100, West Chester, PA 19382; acadden@schnabel-eng.com

ABSTRACT

Data Interchange for Geotechnical and Geoenvironmental Specialists (DIGGS) is a data transfer standard that is gaining widespread acceptance in the geotechnical and geoenvironmental communities. Originally developed using funding from the Federal Highway Administration (FHWA) to efficiently capture data related to geotechnical boring logs, cone penetration test (CPT) soundings, and lab testing results, the data transfer protocol is rapidly gaining traction. It has been shown to have beneficial impacts in other allied areas where disparate parties (i.e., consultants, contractors, vendors, etc.) routinely publish/submit data as part of project deliverables. The historic problem is that many of these submissions use paper copies (i.e., .pdf images) to transmit valuable data for the project… data that may extend beyond the "technical" aspects of the project (e.g., equipment operating conditions, construction production rates, project costs, etc.). These data could be used by multiple parties to assess project performance and safety, as well as to track productivity, etc. Currently, in the limited situations when actual data are compiled and transmitted, the data often are submitted as an author-specific (and often proprietary) software application and must then be re-entered into other software applications (e.g., analysis software, database, etc.) for use beyond simple data collection. An initiative undertaken by the Geo-Institute (G-I) of the American Society of Civil Engineers (ASCE) focuses on exploiting the full potential of DIGGS to geoprofessionals both within and outside of the transportation community. The deep foundations industry represents one community that could benefit significantly from using DIGGS. Data of interest to DFI members include production records, quality assurance information (e.g., verticality and alignment, concrete strength), and, importantly, load test results. When adopting DIGGS, users need not modify how they capture data, but rather will use DIGGS as a vehicle to transfer data to other applications in a standard format where it can be shared, used, stored, and retrieved. This paper and associated presentation will describe DIGGS and demonstrate how DIGGS can be used effectively within the deep foundations community.

INTRODUCTION

In virtually all aspects of life today, we are inundated with data and asked/forced to provide, manage, and/or use data. In some cases, we are asked to *provide* these data, while in other cases we *request* data. For example, to attend this conference, each person in attendance likely needed to make on-line airline, hotel, and rental car reservations as well as submit information for the

© 2019 Deep Foundations Institute

conference registration. In other cases, we request that data/information be provided to us (e.g., credit card payments, bank statements, Google search requests, etc.). We essentially take these data exchanges as a way of life and readily comply with the requirements of the specific organization requesting/managing the data, not realizing that the data request utilizes a standardized online template to allow efficient transmission and storage of the data. If we now transition from personal to professional interests, we certainly realize that to address our numerous professional obligations, we need data/information to perform calculations, conduct analyses, and prepare reports. However, when we consider the data collection process, we consistently tailor our processes to a specific project and often will balk whenever anybody asks us to submit the "data" in a standard format. Moreover, our "data" transmittals are often in the form of a .pdf file and/or Excel table or plot that do not conform to any standard reporting format. For those that use "standard" or "accepted" electronic platforms or computer programs (e.g., gINT, HoleBase, etc.), they are required to adopt a specific format defined by the vendor. To later access these data, it may be necessary to use proprietary programs provided/sold by the vendors. Should anybody want to re-use this information in the absence of the "accepted" program, they will need to either cut-and-paste or manually re-enter the information to suit their own purposes. Why we, as a profession, continue to operate this way remains an enigma, particularly when we realize the benefits of (and comply with) standardized data and facilitated data transfer procedures in our non-professional lives. The purpose of this paper is to: (i) highlight the numerous advantages of effective data management; (ii) introduce a relatively recent tried-and-true data management strategy that can help virtually all professions; and (iii) demonstrate how the strategy can be used effectively in the deep foundations industry.

HISTORICAL DATA MANAGEMENT STRATEGIES

There is little history to speak of regarding data management strategies in civil engineering practice. Engineers and professionals have always recognized the need to collect and manage information for a given project, if for no other reason than to comply with the reporting and submittal requirements imposed by owners, regulators, etc. However, most professionals have historically preferred to: (i) structure data in the way that is convenient, familiar, and/or logically to the user; (ii) manage and use the collected data in a user-preferred format; and (iii) allowed modifications "on the fly" as selected by the user to maintain maximum flexibility. This historical practice leads to the following processes and potential drawbacks:

- ***Data Completeness*:** If one is collecting data in the field, there is the potential that they leave the field with incomplete data. Therefore, to avoid a potential catastrophe of missing key data, development of a "checklist" can help minimize this problem. However, one must give forethought to the development of the project- or task-specific checklist to be sure that the collected data are complete. The user must then be sure to train potential data collectors to be sure that they understand the process of data collection and the importance of data completeness.
- ***Data Integrity as a Result of Manual Entry*:** When data are collected manually and then re-entered into a table or used for a graph/plot, it is all-to-easy to inadvertently make a transcription error that can get introduced into the project database. Rigorous quality

control is needed at all phases of data management where data entry/re-entry is involved. Without this check, one may be driving piles in downtown Chicago, only to find out that because of a transposition error involving local GPS coordinates during manual entry, the data are recorded for a site in Maryland. Other data-integrity errors can be (and usually are) much more subtle. Despite having a checklist, it is necessary to have a verification system to be sure the data are internally consistent and correct.

- ***Data Re-use*:** Consider a case in which two different inspection organizations working along two different interchanges for a State Department of Transportation (DOT) are required by the owner (i.e., the State DOT) to compile their field results. They need to adopt one of the two (or agree upon a standard) data collection/recording systems or else transfer the data into another centralized system. They may even opt to manually re-enter the field-collected data into another format preferred by the State. Alternatively, suppose that the State requires the inspecting organization to report the data on a MicroStation-generated drawing that does not recognize the format in which the original data were collected, because the inspecting organization typically utilized AutoCAD. In both cases, it will be necessary to cut-and-paste and possibly modify fields of data from a spreadsheet or re-type the previously collected information before it can be successfully re-used. This is an inefficient process and can lead to numerous errors. Historically, professionals give little thought to how others may need and/or use collected data beyond the initial intended use.
- ***Data Ownership*:** When a consultant works for a client to perform field data collection, the consultant often thinks that the data belongs to the collecting entity, when in reality, the data belongs to the project/client/owner. The authors have experienced cases where consultants essentially hold data "hostage" because of this perception of ownership. Given this reality, it would seem incumbent on the owner, not the consultant, to: (i) dictate the format in which the data are collected and communicated, and (ii) demand that data be provided in compliance with the owner-specified format.
- ***Data Transfer*:** When the client/owner requests a copy of the data or if the data are to be communicated to another consultant, it is not unheard of that a .pdf copy or a "data dump" in some unique (and often proprietary) format is provided. Either of these are of little use to the client/owner unless they again re-enter the data into yet another spreadsheet. This is an inefficient and unnecessary step that is prone to the errors described above.
- ***Data Management*:** Engineers and professionals generally have little sense (or training) in proper "data management". As mentioned previously, "data" to many professionals is often synonymous with a .pdf or paper copy of information collected in the field or generated in a laboratory. While this is valuable information about the project, it does not qualify as "data" that can be seamlessly collected, compiled, manipulated, and transferred. In cases when "data" are collected by different parties, they often use different formats and/or do not utilize the same software. Therefore, (i) "information" can be "data" if managed appropriately, and (ii) data would be most useful if it were managed in such a way that it could be easily transferred for use.

The net result of this historical view of data collection and management is that current practices are inefficient, ineffective, and prone to errors. With the proliferation of data in current professional practices, the authors note that the current state-of-the-practice regarding data management is simply not sustainable. There is a need today (in fact the need existed years ago) to change the practice, lest we be left drowning in data (or information). While few professionals

will likely disagree with these observations, a key question remains: "*How do we change the state of practice?*" Like the captain of a loaded barge on a crowded river, the change must be planned and will require a series of slow and steady implementable steps. DIGGS offers such a strategy for this needed change, as will be shown in the remainder of this paper.

DATA MANAGEMENT, XML, AND DIGGS

The authors acknowledge that they are not the first to observe the need to translate project information to useful data. In fact, over the past several years the geotechnical community in general and the State DOTs in specific have recognized this value, prompting state and federal agencies to migrate critical agency functions to databases and to subsequently fund database development for geotechnical data. While the primary focus has been directed to obtaining timely and high-quality data that can be used and shared *internally* by the agency/organization, it is important to also look into the means and methods that this information can be stored and subsequently shared *externally*.

In understanding the similarities between databases (formally referenced as Relational Database Management Systems, RDBMS, that include Access, SQL Server, SAP, Oracle, etc.) and other data file formats, it is important to understand their respective properties, advantages, and disadvantages. Proper database design follows strict rules that are needed to create a structure (aka "schema") which can facilitate efficient data storage and retrieval. Information/data are stored in tables that are "linked" with each other, ensuring data integrity. Although each database system may rely on different schema rules, there is one thing to remember about databases, that is: "*they result in a complex, yet highly efficient structure*." Internally, this represents a significant advantage because once an agency adopts a specific (and usually proprietary) database system, the rules regarding the structure become well-known and can be implemented internally by multiple parties. However, should the agency decide to switch database systems or software programs, or if the agency desires to communicate with others who utilize the same of different systems or software, the complexities of the adopted data structure can pose significant challenges. Since most agencies and organizations adopt different programs that utilize different schemas, we are faced with a good news-bad news situation. The good news is that we now have captured "data"; the bad news is that it is relatively difficult to share these data outside of the specific organization and virtually impossible to think of some type of "universal" file/table sharing algorithm.

The problem identified above could be resolved if every organization utilized the same RDBMS. While this may be a noble goal, it does not reflect reality. An alternative to a conventional database for storing or transferring data is the eXtensible Markup Language (XML), which defines a set of rules so that information may be stored easily in files. Unlike the more typical RDBMS, the structure of XML files is not complex. Information is stored in plain text format within "tags" that are labeled according to the details that are contained between them. For instance, an XML file storing the diameter and length of a steel pipe pile could be as simple as:

```
<pile>
  <type>Steel Pipe</type>
  <diameter>12 inches</diameter>
  <length>20 feet</length>
</pile>
```

As long as two parties agree on the file structure, i.e. that pile diameter will always be stored within tags named "diameter" and that pile length will always be stored within tags named "length", then information storage and transport can become highly efficient for all parties desiring to share this information/data. Furthermore, data from XML files can easily be ported to a large-scale RDBMS by matching XML tags to database attributes. The advantage of the XML file transfer concept is that it is "agnostic" to a specific RDBMS, so it addresses one of the major obstacles regarding the external sharing of data described above. The disadvantage is that someone has to define the schema and tags for the XML files. This is precisely the role and intention that led to the development of DIGGS. So just what is DIGGS?

DIGGS is the acronym for Data Interchange for Geotechnical and Geoenvironmental Specialists (DIGGS). DIGGS was originally envisioned in 2002 and was later developed by a coalition of government agencies, universities, and industry partners with a goal of becoming an international data transfer standard for geotechnical and geoenvironmental data routinely needed for transportation-related projects. The coalition was coordinated by the Federal Highway Administration (FHWA) and became the Transportation Pooled Fund project TPF-5(111) titled "*Development of Standards for Geotechnical Management Systems*." The final report, released by the Ohio Department of Transportation (ODOT), and the release of DIGGS v 2.0.b are available on http://www.diggsml.org, a website managed by the Geo-Institute (G-I) of the American Society of Civil Engineers (ASCE). By design and intention, DIGGS is open-source, freely available, and requires no proprietary software to use.

In the early days of the pooled fund study, the DIGGS developers adopted XML for the development standard. While not necessarily being well understood by geoprofessionals, XML is the most_common language adopted by the computer science profession for storing and transferring structured data. Because most of the data of interest to geoprofessionals has a spatial and/or geometric component (i.e., coordinate location and elevation and/or structures/features that can be modeled with geometric shapes such as lines or polygons), DIGGS adopted a Geographic Markup Language (GML) application schema, meaning that it extends GML, which is a standardized XML grammar for encoding geospatial information. The user can think of the link between "XML and geotechnical data" in the same spirit as the link between "HTML and the internet." In this spirit, we all recognize that we do not need to understand HTML to be able to browse the internet, because we know that the developers of HTML were tasked to just make sure that it works! Under the leadership of the G-I, the mission of the DIGGS Development Team is to simply "*make it work*." This effort has leveraged existing ASTM geotechnical standards, and the collective experience and expertise of the team's contributors, along with tools for querying and transforming XML data files to make DIGGS work as a user-friendly model where the user

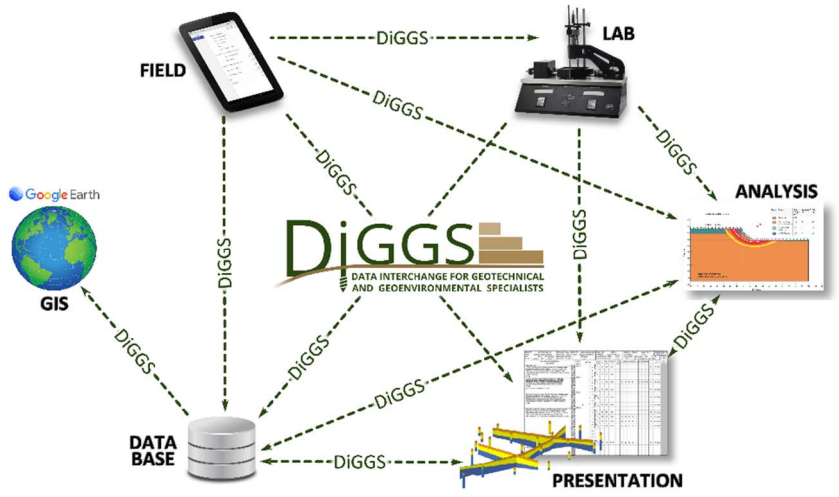
does not need to "get under the hood" of the XML/GML computer code to become an effective user of the technology.

WHY XML AND DIGGS?

As summarized previously in this paper, the geotechnical profession (hopefully) recognizes that we need to start managing geotechnical (and deep foundations) data. We also know that most organizations have adopted a RDBMS that works for the organization, whether the organization is a State DOT, FHWA, a consultant, or a deep foundations contractor. Therefore, in thinking of a long-term, sustainable data management solution, a logical question is "*why not just establish a standard database and/or database schema and instruct the user on how to use the database?*" This is a fair question and one that has been asked by the geotechnical, materials, and pavement sections at 50 State DOTs (recall that DIGGS has the FHWA and State DOTs at its roots). The answer to the question involves three critically important observations/facts:

- Virtually every State DOT has at least one database system that it uses and to the best of the authors' knowledge no two of the State's systems are similar.
- By prescribing a specific database and database schema, it would likely require that the DOTs purchase additional (potentially proprietary) software or change their current practices. Requiring an agency to change established systems is inviting disaster.
- Currently, the geotechnical sections at most DOTs do not use the available database resources to manage data and/or their systems are not readily extensible and available for new data objects.

Therefore, if the goal is to start managing data, what is needed is NOT a specific database, but rather a specific set of "instructions" to organize and represent data such that the data can be transferred or shared by any number of software applications, including established databases. This is explicitly the DIGGS concept, as depicted graphically in **Figure 1**.



(after http://www.diggsml.org)

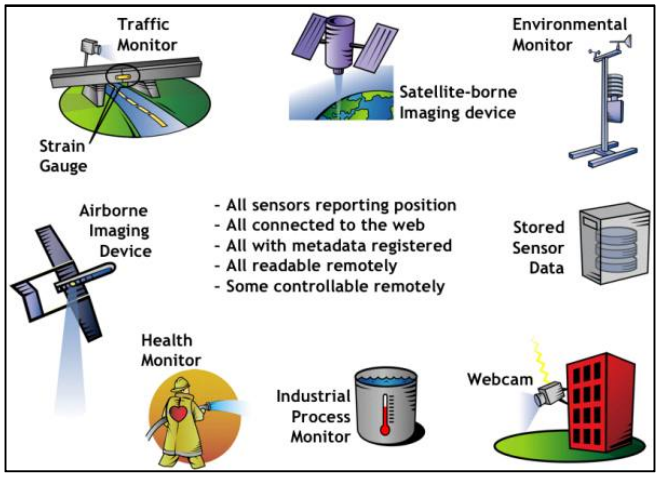
Figure 1. Schematic of DIGGS Utility

As shown, DIGGS becomes the common language that facilitates communication among any number of software applications. It is important to recognize the relationship between DIGGS and

data; explicitly, DIGGS is *not* a database, but rather DIGGS is a standardized representation of data using XML that can be imported into, or exported from, a database (or other computer software applications).

XML and GML provide the rules for communicating data across the internet and between software systems, regardless of how the data are generated. The DIGGS Development Team continued the work of the initial pooled-fund study primarily because within the IT community and among software vendors, these languages are as common as drill rigs and pile driving hammers are to the deep foundations community. By selecting XML and GML as the language-of-choice for developing the DIGGS schema, the following two significant hurdles for acceptance and adoption are addressed:

- ***Data Export***: Data are often generated in the field as millivolt signals, amperage readings, and frequency measurements on data collection and recording equipment (e.g., survey total stations, piezometers, load cells, flow meters, slope inclinometers, pressure transducers, etc.), some of which are attached to the drill rigs to provide instant feedback to the operator. After signal processing, these analog or digital signals can be converted to engineering units and stored for eventual transmission/transfer to a readout unit, text file, data storage device, etc. At this point, the equipment vendor could simply elect to generate a DIGGS XML file that contains the collected results. As reported by the Open Geospatial Consortium (OGC) and shown in **Figure 2**, …*"The OGC's Sensor Web Enablement (SWE) standards enable developers to make all types of sensors, transducers and sensor data repositories discoverable, accessible and useable via the Web."* Therefore, using industry-accepted protocols, equipment vendors will be able to easily export GML-compliant DIGGS data files from their equipment. Data that are not generated using sensors are often collected manually and recorded electronically. These data can similarly generate GML-compliant DIGGS data files for electronic transfer.



(after http://www.opengeospatial.org/ogc/markets-technologies/swe)

Figure 2. Example of Open Geospatial Consortium (OGC) Sensor Web Enablement (SWE) Functionality

- ***Data Import***: Once data are collected, they need to be processed, viewed, stored, and managed. Typically, professionals utilize proprietary spreadsheet formats, local databases, or customized computer software programs for these activities. If these software products can "accept" DIGGS files for import and similarly export data in a DIGGS format from its software, then the data can be seamlessly transferred without manual re-entry into a vendor-specific format. In this way, the data becomes "software agnostic" and users need not change their current software of choice. Another major advantage of this import function is that owners can simply require that all consultants submit valid DIGGS files as part of project delivery so that the owner now has all data from all projects from numerous consultants in a consistent format. Not only is this a significantly more efficient way of doing business, it addresses many of the problems identified previously with the current/historical data management strategies.

The selection of XML/GML for DIGGS was carefully considered. The DIGGS Development Team adopted an open-source, industry-standard that would be available to a wide range of users. The authors believe that DIGGS adoption can significantly benefit the entire profession. That being said, there is a "full disclosure" component that is noted best by the good news-bad news cliché. The bad news is that while XML/GML may be considered "standard," much like HTML is a standard for internet data exchange, the authors do not mean to imply that DIGGS is considered "user-friendly" by itself to the geotechnical or deep foundations communities. At some point, the authors recognize that someone has to "get under the hood" and actually develop user-friendly applications to work with and display the data in the underlying DIGGS format. The good news, however, is that this has been done (and will continue to be advanced) to a limited degree by the DIGGS Development Team. You (i.e., the deep foundations user community) need to know how DIGGS can best be used in your practice.

USE AND BENEFITS OF DIGGS TO THE DEEP FOUNDATIONS COMMUNITY

The authors have been working on the implementation of DIGGS for several years, and clearly see the benefits of adopting this as *the* data standard for geoprofessionals. The following three examples highlight benefits of adoption by the deep foundations community: (i) real-time control systems; (ii) subsurface characterization data; and (iii) load test database opportunities. While these examples were selected to demonstrate the benefit for those working with deep foundations, the benefits of DIGGS extend to a wide range of geotechnical and construction application that include dams, earthwork, ground improvement, performance monitoring, etc. Rosen, et al (2012) and Bachus, et al (2014) provide detailed examples regarding the information management system (IMS) concept for construction projects that rely and benefit from properly managed data.

Real-time Control Systems: Most contractors have included automated control and monitoring equipment in parts of their construction practice. These systems include instrumentation that provides in-cab or at-plant monitors for verticality, crowd, energy, flow, load, etc. Most of these systems are custom designed by specific hardware/software vendors and have proprietary systems for data collection, processing, and reporting. These systems provide a level of quality control that was unheard of just ten years ago. However, should the contractor wish to integrate data from different systems, it is extremely difficult because of the proprietary nature of the software. Should a DIGGS format be adopted and with a DIGGS-export option included by the vendor, then the

contractor would be able to readily output data from the vendor's system and integrate these data into the contractor's system, which could then store and data from various equipment, processes, and vendors in a single contractor-selected system.

Subsurface Characterization Data: When responding to project opportunities, contractors need information regarding subsurface conditions at the project site. As part of bid packages, owners typically provide results of subsurface drilling activities, as well and results from insitu and laboratory tests. In most cases, these results are provided as paper copies or, if transmitted electronically, as .pdf documents. Should the contractor (or its consultant) desire to graphically present results, develop cross sections, or summarize for its bid/proposal/presentation, they have to manually re-enter the information into a proprietary software package or a generic spreadsheet preferred/selected by the contractor. This is an inefficient and time-consuming activity that is prone to transcription errors. If geotechnical data were transmitted electronically is a DIGGS format and if software vendors had a DIGGS-import function, then significant time and energy could be saved on the owner's side because they do not have to compile specific project documents and on the contractors/consultants side because they now have readily available "data" for use. The DIGGS functionality offers untold benefits to both communities.

Pile Load Test Database: Many contractors and geotechnical engineers recognize the benefits for deep foundation databases to provide a "data archival" functionality. Unfortunately, their practical value is currently limited to basic information retrieval, despite the numerous attempts in the past to address this unfortunate situation. The second author and his colleagues have spent the better part of the past three years to rectify this problem and not surprising, has concluded that a standard data transfer protocol (like DIGGS) is a valuable and necessary component of any go-forward effort. Widespread adoption of DIGGS and its expansion to accommodate pile data can upgrade existing and future pile load test databases. DIGGS can be used to import and export information from pile load test databases. For reasons identified previously, because of the diversity and proprietary nature of non-standardized databases, the seemingly simple task of data transfer is actually a time-consuming and complicated task. Furthermore, with support from software vendors, these data could be loaded on popular foundation design and analysis software as well as in-house design algorithms. DIGGS could also facilitate automated and highly reproducible processes allowing for analyzing pile data in batches. As a result, workflow efficiency can be dramatically increased while reducing errors from manual entry. The batch analysis process opens opportunities for a high-level evaluation of the performance of foundations by statistical analyses over a large volume of results. Because of the unique opportunity that DIGGS presents regarding pile load test data management, additional discussion and demonstration are provided.

These benefits notwithstanding, the authors note that there are disadvantages with standardized data and DIGGS. First, the authors recognize that adoption or development of a *data* management strategy may require a change to current practice by the contractor and consultant. Change is difficult and requires additional dedicated time, training, and expense to facilitate development and adoption. Additionally, the authors recognize that to the geotechnical and construction community, data in XML and project databases are new concepts that are fundamentally different

than data in Excel spreadsheets. Therefore, it will take time to see and appreciate the benefits of full integration. These are recognized disadvantages specific to DIGGS. Two other disadvantages of "standardized" data management warrant discussion. There is a tendency to think that since the data are now in a database, the data must be correct and can be relied upon without critical review and assessment. Data "management" is critical and measures for data quality assurance, security, and review must be developed and adopted by all parties. In addition, one must avoid the tendency to overly rely on the compiled data by reducing investigations in critical areas because "I have data regarding that stratum" in the database. Standardized data will allow the profession to do its job better and more efficiently, but it does not reduce the need to critically assess and analyze these data and recognize when additional data are needed.

DEMONSTRATION OF DIGGS AND PILE LOAD TEST DATA

For the past 30+ years, engineers and researchers have been independently collecting pile load test and relevant subsurface data while organizing this information into structurally dissimilar repositories. Despite their competent efforts, the overall result is highly fragmented with very little benefit to the greater geotechnical community. Meanwhile, scientists aided by state-of-the-art data analytics have been transforming their respective industries, producing remarkable predictions and insights. The unstructured and decentralized current scheme of this valuable pile load test data is a hindrance to the geotechnical community at large.

Geotechnical engineers working with deep foundations do not have to look further than the current methods commonly used (and still being taught) for designing deep foundations to understand the importance and potential benefits of efficient data management. Many of the methods currently in use for pile design are empirical (or at least semi-empirical), based on small databases of interpreted load test data, with empirical formulas that required gross overgeneralization to develop. Specifically:

- Granular Soils: Nordlund (1963) developed a method of calculating bearing capacity of driven piles in cohesionless soils from as few as 41 load tests from 8 different test sites. The piles represented by these data range in diameter from 12 to 16 inches in diameter.
- Cohesive Soils: Tomlinson (1957) employed a small data set of 56 piles to develop his popular α-method. Again, the piles considered by Tomlinson varied from 6 to 30 inches in diameter. And the clays varied from soft to very stiff over-consolidated clays.

Consider that in the age of modern pile driving and a full suite of energy-feedback capabilities and load tests, the authors estimate that the profession has designed and installed >1,000,000 driven piles. Similarly, the authors anticipate that more than 100,000 load tests have been conducted worldwide, yet the most commonly cited design approaches are >60 years old and rely on <100 load test records. We can and should do better! The inherit generalization of these methods could be improved dramatically by allowing contractors, researchers, and other interested parties the ability to analyze the vast number of high-quality load test and production data that pile driving/testing specialists are currently producing. Based on the authors' experience, the main hindrance in doing so is finding a convenient way to share deep foundation performance-related information. A standard XML file structure could solve this problem. A pile foundation load test

is a project that requires and generates a significant amount of complex data. An engineer working on such a project would have multiple files, of varying formats, spread across several folders in their computer along with pages of notes and other reports. Sharing the relevant geotechnical, pile property, and load test data is far from a straightforward process. However, it is a process that we should address and facilitate. It seems to the authors that DIGGS is an ideal framework for accomplishing this goal.

Figure 3 shows a typical work flow that is anticipated if someone were to tackle the problem with developing and managing a pile load test database for widespread public use. Given the diversity and quantity of existing data, experience has shown that collecting, compiling, and simply handling the data comprises approximately 60 to 80 percent of the total effort. This entails extracting relevant information from the original sources and transforming it in a format that is consistent for input into the database. Traditionally, this a dominantly a manual process that often requires entering the same data in multiple applications, at different times, by different people. Once the data are available in a consistent format (i.e., once in a consistent and complete database), the remaining approximately 30 percent of total effort is spent extracting the data for analysis. This latter effort is, in fact, the objective of the entire process, but it would take considerable resources to achieve this objective. As shown in **Figure 3**, if the data were available in a DIGGS-compliant XML file format, this error-prone and inefficient process of moving data around could be eliminated.

The premise of this paper is that although DIGGS was originally developed for geotechnical and transportation projects, the authors envision a much wider range of applicability. The range includes the deep foundations community where vast amounts of valuable data are generated and could be beneficially utilized by the industry, its practitioners and academicians. All of this "information" actually qualifies as "data" that can be appropriately managed and should be available to the owner/operator regardless of the entity that performs/monitors the installation. DIGGS is a logical and ideal protocol for these efforts. **Figure 4** shows how DIGGS as it exists today can be relatively easily expanded to pile and load test data. The forms identified in this figure could be completed from an existing paper copy or an Excel spreadsheet. In the future, data could be captured at the source using a field-deployed tablet, and/or a web-enabled form on a tablet or smart phone.

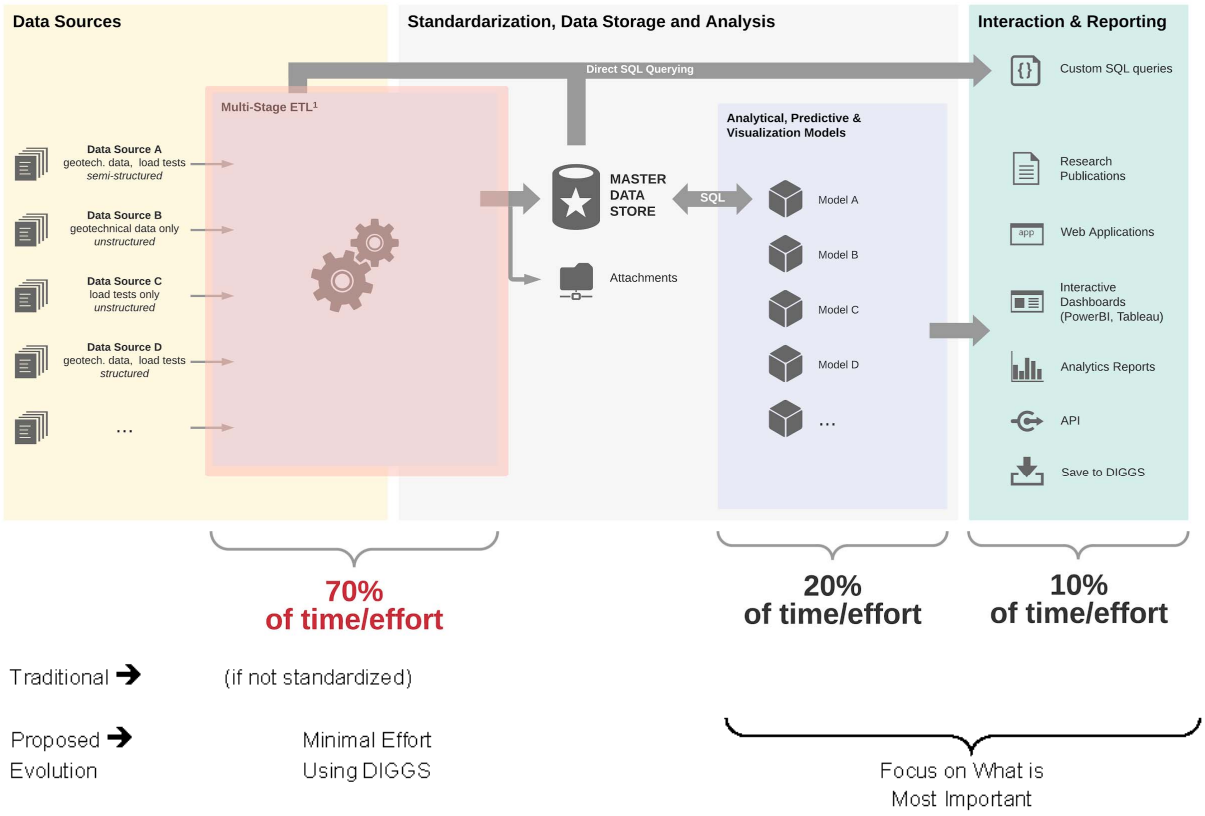


Figure 3. Example New York University Load Test Data Work Flow

Once the form is populated, a DIGGS file will be automatically generated and can be transferred to a database. In some cases, the inspection may require the collection of data from sensors (i.e., pressure, temperature, flow, etc.). These data, too, can be collected in the field on a form similar to that shown in **Figure 4**.

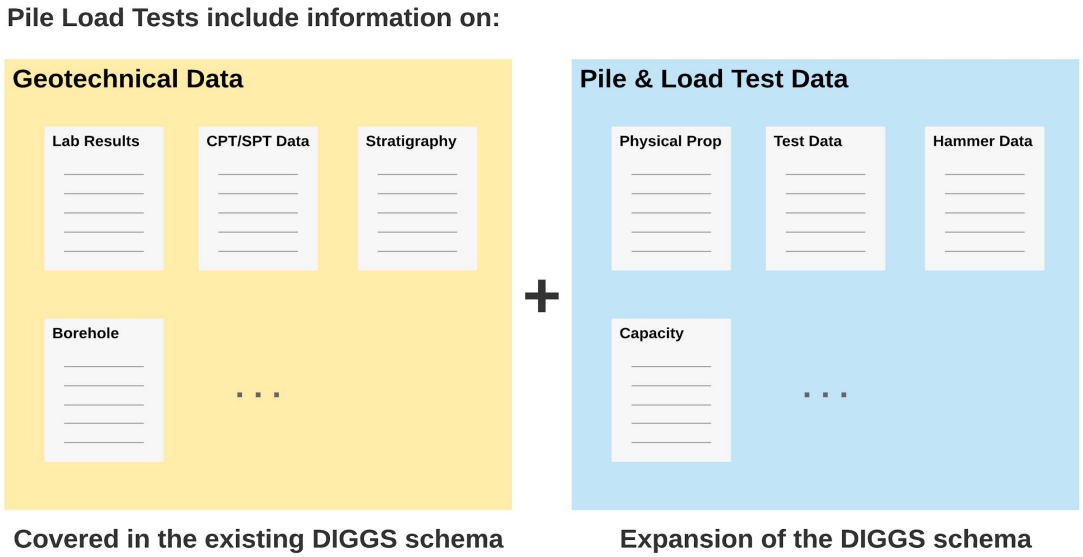


Figure 4. Expansion of DIGGS to Include Pile and Load Test Data

Once data are entered into the forms identified in **Figure 4**, a DIGGS file can be generated and transferred to the database shown in **Figure 3**. The authors believe that future expansion of the DIGGS structure would we well suited to record load test data and performance data that are collected during operation. The benefits would be quickly recognized.

MOVING FORWARD

DIGGS is now ready for general use. On the previously referenced DIGGS website, instructions help the user become familiar with the DIGGS data structure (i.e., the schema) and provide a "data dictionary" to identify the "rules" for the specific data elements. The website also provides the user with access to tools (i.e., DIGGS Feedback Tool and DIGGS Toolbox) to allow users to generate DIGGS (i.e., XML) files that can be used to populate tables, generate plots, and/or interface with software that will accept DIGGS/XML structured data. During the development process, the G-I committed to host the DIGGS website and to provide web-based tools for generating and using DIGGS files. The DIGGS Development Team has committed to: (i) support development of user friendly interfaces, (ii) provide recommendations for data management, (iii) provide training for developing and using DIGGS files, (iv) work with software developers to include DIGGS formatted data as acceptable imports to (and exports from) their programs, and (v) establish a sustainable business model to allow the future growth and adoption of DIGGS. This offer of support extends to the deep foundations community.

The G-I and the DIGGS Development Team are committed to its success and have developed plans for ongoing technical assistance, development, and training to encourage/support the use of DIGGS. The authors recognize that the ultimate goal is to have software vendors fully support the import and export of GML-compliant DIGGS files, so that geoprofessionals do not have to become "closet programmers" for DIGGS to be successful. For this to happen, the geotechnical profession needs a groundswell of support and demand from the user/owner community. This is one way for the deep foundations community to contribute. Until this happens, however, the authors realize the need to provide ongoing support and assistance to the potential users. The following provides a strategic plan for advancing the cause.

- The DIGGS website (http://diggsml.org) will be continuously updated with information for the user and development community. A current version of a DIGGS schema (version 2.0.b) is available on this website with a new release (i.e., version 2.5) soon to come. For those interested in the specific development activities, a GitHub site (https://github.com/DIGGSml/diggs-schema) has been developed and users interested in development and "getting into the weeds" are encouraged to contribute.
- To help users understand DIGGS and to facilitate its use, the DIGGS website will include open-source and freely available development tools that will generate valid, GML-compliant DIGGS files from user-specified tables, spreadsheets, and forms. Currently, the DIGGS Feedback Tool (developed by Keynetix) can generate valid DIGGS files from user-specified spreadsheets, Keynetix data files, or gINT datafiles. The DIGGS Toolbox (developed by New York University) allows the user to generate DIGGS files "on-the-fly."
- Examples of DIGGS output options are presented on the DIGGS website and GitHub, specifically to show how a DIGGS file can be uploaded into a RDBMS and used to generate summary tables and plots.

- The DIGGS Development Team is preparing a series of training sessions via short videos and webinars to demonstrate the utility of DIGGS. These will be free and available to all interested parties.
- The DIGGS Development Team is working with the American Association of State Highway Officials (AASHTO) to develop a procedure that will allow delivery of data to the DOTs in a DIGGS format.

So, this is what DIGGS will do for you… the deep foundations community… and the authors solicit your interest and support. This can commence with a meeting/teleconference that includes interested parties within the deep foundations community to better understand industry needs and current practices. The DIGGS Development Team welcomes review comments regarding the DIGGS and GitHub websites. Finally, the authors solicit feedback from the entire deep foundations community (e.g., contractors, owners, consultants, vendors, trade organizations, etc.) regarding: (i) the proposal outlined in this paper, (ii) suggestions as to how DIGGS can better service the deep foundations industry, and (iii) how the DIGGS Development Team can potentially enlist hardware/software vendors to support this initiative.

ACKNOWLEDGEMENTS

The authors are appreciative of members of the DIGGS Development Team who have devoted untold hours on the development and promotion of DIGGS. Special thanks to Tom Cadden (Temple University), Roger Chandler (Keynetix), Scott Deaton (Dataforensics), Chris Merklin (Ohio DOT), Peter Narsavage (E.L. Robinson), Dan Ponti (USGS), Ben Rivers (FHWA), Stephen Taliaferro (Ohio DOT), and Loren Turner (Caltrans). Ongoing support for the DIGGS development efforts is being provided by the Geo-Institute of ASCE, under the leadership of Brad Keelor. The authors also acknowledge the encouragement of Mary Ellen Large from DFI who has encouraged the preparation of this paper. Support of these individuals is appreciated.

REFERENCES

LINKVIT (2018), http://www.linkvit.eu/training-modules/basic-concepts-xml-gml

http://www.diggsml.org

https://github.com/DIGGSml/diggs-schema

Machairas, N., Highley, G. A., and Iskander, M. G. (2018). "Evaluation of FHWA Pile Design Method Against the FHWA Deep Foundation Load Test Database Version 2.0." *Transportation research record*, SAGE Publications Ltd.

Bachus, R.C., A. Cadden, and N. Machairas, "DIGGS Does Pipelines," Proceedings of Pipelines 2018, American Society of Civil Engineers, Toronto.

Rosen, J.B., Bachus, R.C., Siebenmann, R., Carr, P. and Rathburn, C., "Using GIS to Track, Visualize, Analyze and Report Grouting Data," Proc. *Grout 2012*, GeoInstitute of ASCE, New Orleans, LA, February, 2012.

Bachus, R.C., Rosen, J., Roff, R., Bateman, V., and Zoccola, M., "Data Management System and Construction Monitoring Results from Wolf Creek Dam Rehabilitation," Geostrata, September/October, 2014.

NUMERICAL EVALUATION OF TOP OF ROCK PROFILE, ROCK STRENGTH AND CONDUCTIVITY.

L. John Endicott, AECOM, Hong Kong, phone +852 94014418, email john.endicott@aecom.com

Zhang Wengang, School of Civil Engineering, Chongqing University, Chongqing, China, email zhangwg@cqu.edu.cn

ABSTRACT

The properties of many geological materials are variable. This is especially true for variations in elevation of the top of rock profile, strength of weathered rock, and conductivity of rock masses. Often the site investigation stage is completed by site specific ground investigation utilizing boring, sampling, and testing. Statistically this is a sampling procedure, but the borings are often widely spaced, and ground conditions between borings are deduced by interpolation. Often budgets are a limiting restraint and the information that is obtained may be less than desired. Sampling and testing is often biased. If claims for unforeseen ground conditions are to be avoided, the properties of the ground should be adequately identified. This paper describes how data can be used to evaluate the subsurface top of rock profiles, and can give insight into representative, maximum, and minimum strengths, and variation in conductivity relating to inflow of water into excavations, that can assist in planning the works and also in resolution, or avoidance, of disputes about unforeseen ground conditions.

KEYWORDS: Rock, Strength, Conductivity, Granite, Metamorphosed Rock, Top of Rock Profile

INTRODUCTION

The mechanical properties of the ground are naturally variable. The work of Geologists, Engineering Geologists and Geotechnical Engineers is fundamentally investigative. Frequently, budgets for ground investigation are squeezed, resulting in widely spaced boreholes, with conditions between them determined by interpolation. Profiling can be adopted but the measurement, such as seismic velocity, is used as an indirect means of computing in-situ profiles and mass properties. Often a lot of test data are generated on large projects or by many projects in the same vicinity. Published data enlarge the database for a given project, and databases can be interrogated to gain insight into different categories of ground. Integration with geological studies can then lead to more reliable characterization of the ground in terms of identifying the materials present, their extent and their range of properties.

This paper focuses on properties of rocks that are generally required for ground engineering, namely the top of rock profile, the unconfined strength of rock materials, and the mass conductivity. Data are obtained from Granodiorite and Granite in Hong Kong, and from Granite and the Jurong Series of weakly metamorphosed sedimentary rocks in Singapore. All four rock types have been tropically weathered, resulting in widely varying top of rock profiles, material strengths and mass conductivity. With a wide range in values for these parameters, project specific ground investigation conducted within a limited budget may run the risk of falling short of obtaining sufficiently reliable data sets, resulting in risk that unforeseen ground conditions may be encountered.

TOP OF ROCK PROFILE

Very often, before construction, top of rock profile is determined by widely spaced boreholes, and elevations of top of rock profile between the boreholes remain to be estimated. The depth to top of rock profile often affects the depths of piles and diaphragm wall panels. When diaphragm wall panels are required to be excavated to a pre-determined level, estimating the top of rock profile is very important

© 2019 Deep Foundations Institute

because, if rock is encountered at a higher level, excavating in rock is time-consuming and expensive, and the amount of rock that is excavated can be the subject of a large claim for unforeseen ground conditions.

Tropical weathering can result in very rugged top of rock profiles. For example, tenders for bored piles for a viaduct may be made on the basis of one borehole per column, say at 35 m spacing, and during construction boring for adjacent piles may encounter top of rock at elevations differing by up to 15 m. Because of such variations, geological profiles that are interpolated between widely spaced boreholes and shown on tender drawings are often annotated with a warning note that elevations of top of rock profile may vary between the elevations determined at the borehole locations.

What is required of a tenderer is to determine as accurately as possible the elevations of top of rock profile at pile locations around and between boreholes. From statistics, there is a method of interpretation derived from fractal analysis that can be adopted. The method is valid if the data points are from the same set. In other words, the approach should be valid within a single geological structural domain. The method is to compute the difference in elevation of top of rock between pairs of boreholes and to plot the difference versus the spacing of the boreholes. In the case of 20 boreholes there are only 19 adjacent pairs. However, if one considers all possible combinations of pairs, the number of pairs increases from 19 to become $2C_{20}$ ($20 \times 19/2=190$) combinations, which is 190 points for 20 boreholes.

The question is: can the method be used reliably? In order to examine this question, data for a site in Hong Kong that is underlain by Granodiorite have been used. Figure 1 shows the data from widely spaced boreholes carried out before tender as a plot of difference in elevation of top of rock at the borehole locations versus the distance between pairs of boreholes. The red line on Fig. 1 shows the 90 percentile and indicates that overall along the length of the site there is a 90% occurrence of differences in elevation of top of rock profile of about 20 m to 28 m. At closer spacing, say less than 30 m, the difference in elevation is smaller. At a spacing of 6 m, typical for the spacing of pre-drilling for diaphragm wall panels, the data are very sparse but the difference in elevation of top of rock profile is estimated to be 0 m to 5 m at 90% probability.

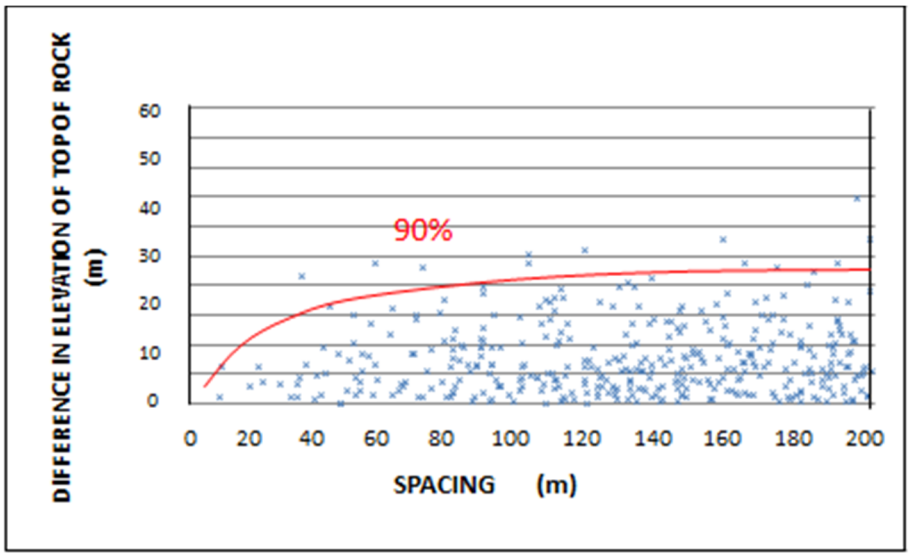


Fig. 1. Borehole data before construction

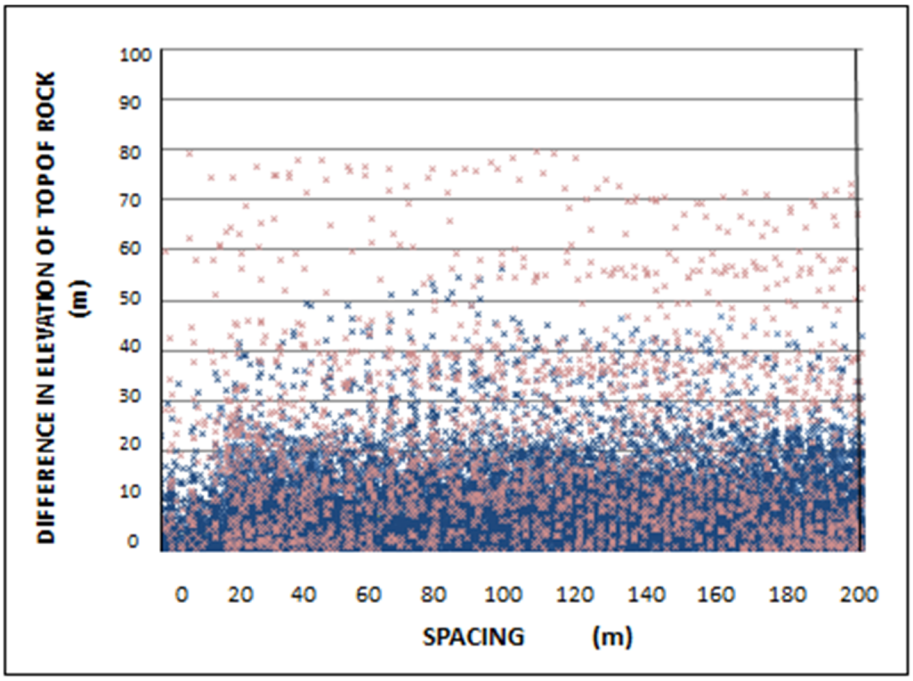


Fig. 2. All boreholes and pre-drilling

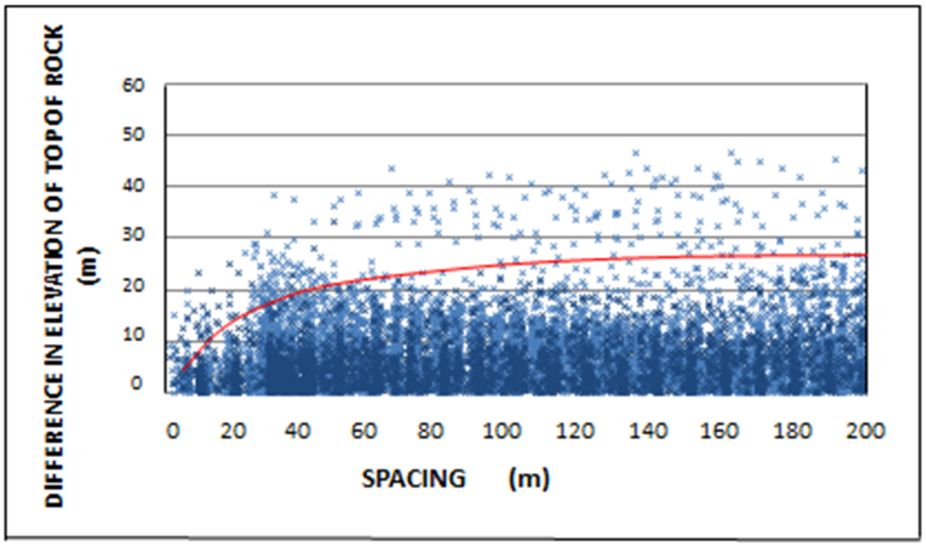


Fig. 3. Pre-drilling data omitting the fault zones

During construction, pre-drilling was carried out for individual wall panels, at about 6 m spacing. A plot of difference in elevation of top of rock at borehole locations and pre-drilling locations versus spacing of all boreholes and pre-drilling is shown in Fig. 2. In this plot, differences in elevation of up to 80 m are shown. This is due to the presence of a deeply weathered fault crossing the site where tender boreholes did not reach rock. The data from pre-drilling, omitting data from within the faulted zone, are plotted in Fig. 3 and show less extreme differences in elevation. The red line is 90% probability for this set of data. The result is similar to the pre-tender data shown in Fig. 1 and indicates that the estimate for variations in elevation of top of rock between adjacent wall panels based on widely spaced boreholes is similar to the actual data from more closely spaced pre-drilling when using this method. Comparison between Fig.1 and Fig. 3 demonstrates that, by excluding the faulted zone, the results are similar, and in this case the method

appears to be reliable. Comparison between Fig. 1 and Fig. 2 shows that the presence of the faulted zone results in a large difference, indicating that the combined results from different structural domains are not reliable.

MATERIAL STRENGTH

Determining the strength of rock material is important in foundation engineering, for example for determining the bearing capacity, and the effort required to excavate rock. Often, knowing the range of strength and the proportion of rock that is stronger than a given value, or the probability of occurrence of rock that is weaker than a given value, is more important than knowing the average strength. By quoting average strength, the range in strength may not be appreciated or, by relying on a small number of tests, the range and maximum strength might not be fully represented, and claims from unforeseen ground conditions could arise. Tropical climate can result in extensive chemical decomposition of rock materials. In Hong Kong and Singapore, material decomposition of rock is classified into six Grades that are similar in the two regions. Grade I is Fresh Rock with no decomposition, Grade II is Slightly Decomposed Rock and Grade III is Moderately Decomposed Rock. Grade V and Grade IV are both classified as soils, being crushable by hand in hand specimens. The term "weathering" is generally applied to rock masses, but some authors also use the term "weathering" to refer to material decomposition. The process of decomposition results in weakening of the rock material. For example, Zhou et al (2001) assessed the average uniaxial compressive strength (UCS) of Bukit Timah Granite in Singapore to range from 79.27 MPa for Grade 1, to 61.97 MPa for Grade III. However, recent data from over 200 tests by Zhang et al. (2018) cover a range of strengths from 230 MPa to 4 MPa. It is clear that reporting a maximum strength of 79.27 MPa does not reflect the maximum strength of 230 MPa that can be obtained by testing Bukit Timah Granite, and the average values do not reflect that about 15% of the total data lie above 100 MPa.

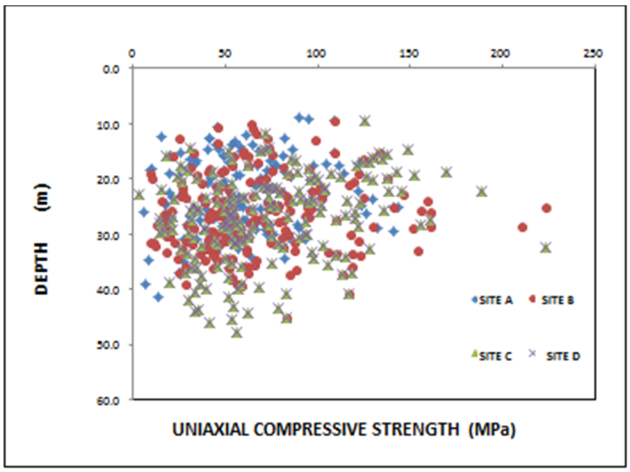


Fig. 4. U.C.S. for Bukit Timah Granite

The Jurong Series in Singapore comprises a weakly metamorphosed sedimentary rock. It includes mainly Sandstone, Siltstone and Mudstone, with some Limestone. Recognition of degree of decomposition by eye is difficult, and very often Grades I and II, and sometimes Grades I to III, are classified as one type. Values of UCS for rock samples can range from 4 MPa to over 200 MPa depending on the lithology and the degree of decomposition.

Figure 5 shows the data separated according to lithology and indicates that Sandstone is generally stronger than the other types of rock in the Series. UCS values for Mudstone, Siltstone and Limestone are on average about 45MPa and are generally less than 100 MPa, tending to increase with depth. Sandstone

has an average UCS value of about 60 MPa, with two values over 200 MPa with little observable trend with depth.

With such a wide range of strengths for different types of rock material, quoting an average strength does not reflect the range in strengths that can be expected. Conducting only a small number of tests runs a high risk of not representing the whole range of strength.

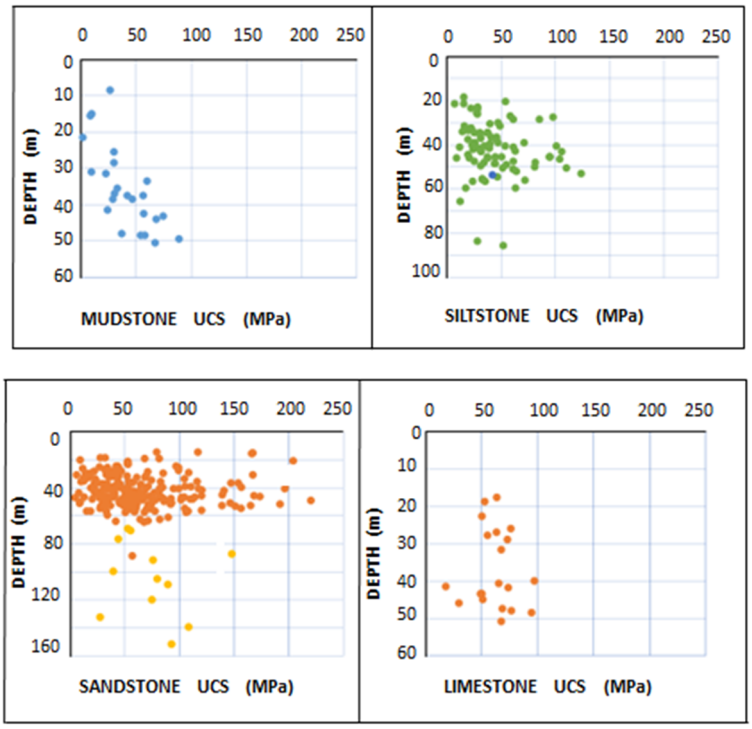


Fig. 5. Strength v depth for Mudstone, Siltstone, Sandstone, and Limestone of the Jurong Series

MASS CONDUCTIVITY

The material permeability of the plutonic igneous rocks such as Granite is extremely low, whereas the mass conductivity can be much higher, depending on the frequency and aperture of fractures, and the extent of their interconnection. The frequency of occurrence and aperture of fractures are primarily controlled by the geological structure and are not very dependent upon the lithology. Packer tests in boreholes are commonly used to measure conductivity of rock. The range of packer test results is usually very scattered, over several orders of magnitude, and the results of a small number of packer tests may not be very representative of the mass conductivity. Examination of a large number of tests within the same formations assists in determining the mass characteristics, and especially extremely high values that can cause problems during construction. Publication of a lot of data assists in understanding the properties of the rock masses and can reduce the opportunities for claims of unforeseen ground conditions.

Forsythe et al. (2014) reported a wide range of conductivity determined by in-situ tests in Bukit Timah Granite in Singapore with values widely ranging from 6.0×10^{-10} m/sec to $1.0E\times10^{-5}$ m/sec. Figure 6 shows the values of conductivity sorted according to the grade of mass weathering.

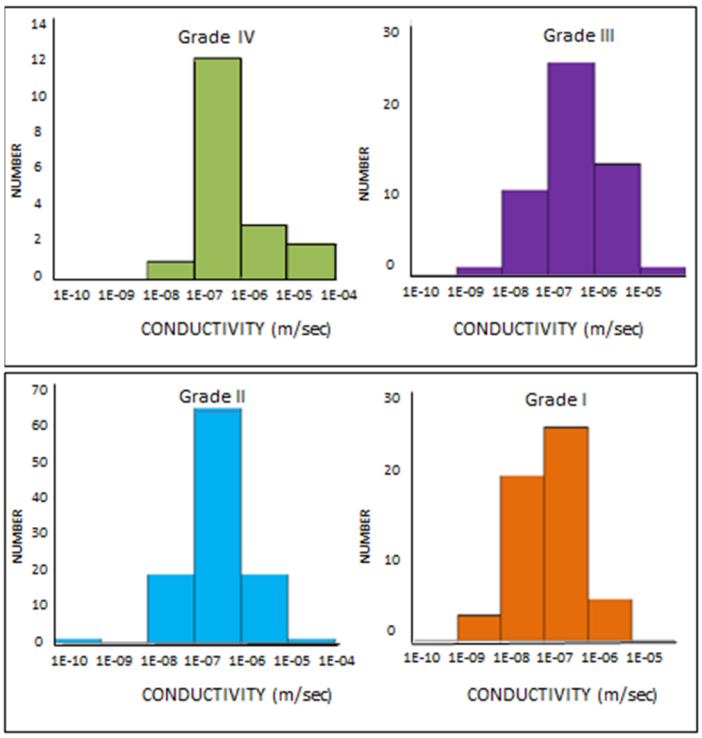


Fig. 6. Conductivity test results for Grades I to IV Bukit Timah Granite (source Forsyte et al)

The median values of conductivity are 1.5×10^{-7} m/sec for Grade IV, 1.0×10^{-7} m/sec for Grade III, 5.0×10^{-8} m/sec for Grade II and 3.0×10^{-8} m/sec for Grade I and generally increase with grade of weathering. Given that there is such a wide range in conductivity, determination an average value may not be helpful, and by conducting only a few tests, the range in conductivity might not be captured.

Figure 7 shows a plot of values of conductivity from 1189 packer test results, colored black, collected from several sites located in the Kowloon Granite Pluton in Hong Kong,. The range is from 0.0001 Lu to 700 Lu. The median value is about 0.4 Lu (about 4.5×10^{-8} m/sec). About 1.2% of the values are greater than 100 Lu. More than 10% of the values are greater than 10 Lu, which indicates that there can be zones of relatively high conductivity, and rates of flow into deep tunnels could be unacceptably high.

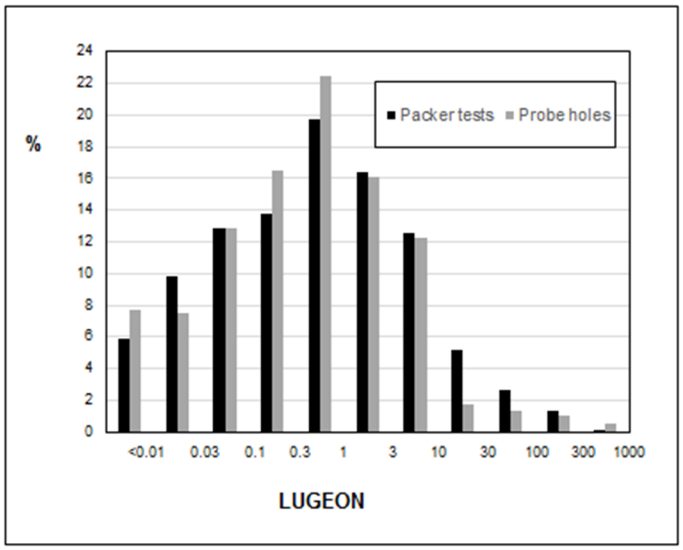


Fig. 7. Conductivity of Kowloon Granite determined from 20m long probe holes compared with packer tests

The question is: does this large data set proportionally represent the mass conductivity of Kowloon Granite? Packer tests are generally conducted in boreholes with test lengths of one meter or only a few meters in length, and not often continuously. Packer tests are often conducted at selected locations to investigate specific features, and usually the tests are conducted in suspected conductive zones. In seemingly solid rock, packer tests in rock with very low material permeability might not be conducted. With selective sampling of locations for testing, the sampling is likely to be biased. When testing is continuous, the results are not selective. Probe holes driven continuously ahead of tunnels are not selective. Probe holes are generally longer than packer tests, typically 20m long at a time. Records of rates of inflow of ground water encountered by continuous probing horizontally ahead for a tunnel excavated in Kowloon Granite were used to determine mass conductivity. Data on rates of inflow from 762 probe holes driven ahead of more than 3.5 km of tunnel are also shown plotted as Lugeon values in grey in Fig. 7. The median value is about 0.5 Lu, which is comparable with the median value of 0.4 Lu for the shorter length packer tests. It can be seen that the results are broadly similar, saving that Lugeon values are reported per meter length and therefore discrete large inflows are reduced in magnitude for 20 m probes, whereas frequently occurring minor inflows are not affected by the length. For example, a single inflow of 1,000 liters per minute at 10 bar is recorded as 1000 Lu in a packer test, but within a probe hole the Lu value would be reduced to 50 Lu on account of the test length being 20m. Whereas more than 10% of the packer test results are greater than 10 Lu, 4.2% of the results from probe holes are greater than 10 Lu. This result indicates that large Lugeon values are associated with discrete conductive features. On the other hand, three probe holes encountered rates of inflow greater than 6000 l/sec from discrete features, shown plotted as >300 Lu. None of the packer tests report Lugeon values as high as this. 5.6% of the packer test results lie below 0.01 Lu, whereas 7.7% of the probe results lie below 0.01 Lu. This could have resulted from bias in conducting fewer packer tests in more solid rock.

Data from 170 packer tests in the Jurong Series in Singapore also show a wide range of conductivity from 1.0×10^{-9} m/sec to 5.5×10^{-5} m/sec. The median value is about 9.0×10^{-8} m/sec. Figure 8 shows the values for conductivity separated into the types of rock: Siltstone in blue, Sandstone in grey, Mudstone in brown and Limestone in yellow, present at the test location. There are limited data from each rock type, and the results for Siltstone, Sandstone and Mudstone are broadly similar. This observation is probably because the strata are relatively thin, faulted and folded, and during a test the conductivity is measured over a zone extending several meters. Therefore tested zones are likely to include a mixture of the respective types of

rocks. Based on these results, the mass conductivity is probably independent of the different types of rock at the locations of these tests.

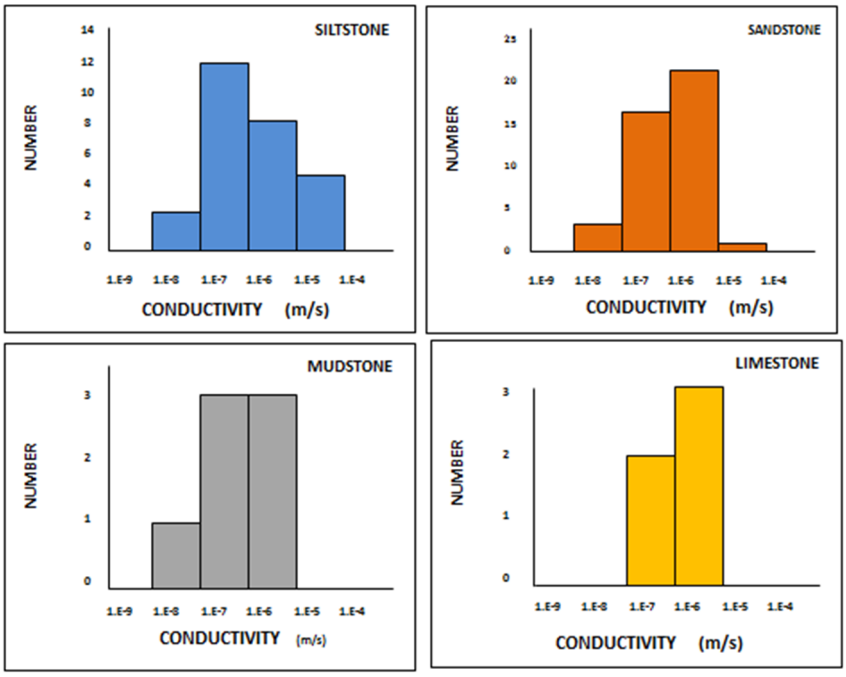


Fig. 8. Conductivity of different types of rocks of the Jurong Series

The data for four types of rock of the Jurong Series in Fig. 8 show a wide range of conductivity. Although the median value for these tests collectively is about 0.8 Lu, about 5% of the data have values more than 1.0×10^{-5} m/sec indicating that the Jurong Series at the depths of these tests, which were generally less than 30m below top of rock, are relatively permeable. With such a wide range of test results and many high values, quoting the median value or conducting only a limited number of tests might not represent the range and high values obtained, and published data can assist in appreciation of the range of mass properties and potential problems in highly conductive locations.

As a general practice, many packer tests are conducted in vertical boreholes, and few packer tests are conducted in inclined boreholes. The tests in 20m long probe holes reported here were conducted in horizontal holes. Recently, packer tests were carried out in vertical boreholes alongside inclined boreholes. The results are shown in Fig. 9. For vertical boreholes, shown in red, the median value is 0.15 Lu. For inclined boreholes, shown in green, the median value is about 1.05 Lu. These data come from boreholes located on a steep slope, where the preferred drainage path is expected to be downslope. The results from this project indicate that boreholes inclined normal to the slope and therefore intercepting many downslope-orientated fractures are more conductive than vertical boreholes which intercept downslope fractures less frequently.

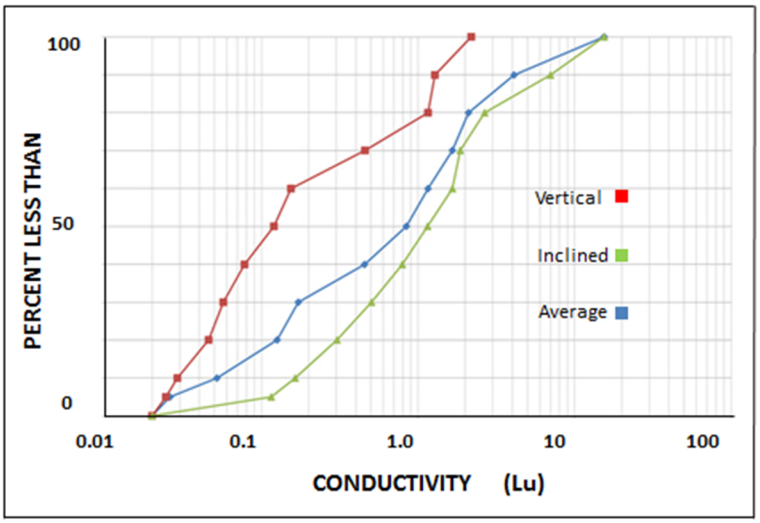


Fig. 9. Conductivity measured in vertical and inclined boreholes

Another observation of anisotropy of mass conductivity was made when tunneling in Kowloon Granite in Hong Kong. Dewatering was detected more than 1,000 m ahead of the tunnel drive, indicating a high conductivity along the alignment of the tunnel whereas, after completion of the tunneling, dewatering was not detected further than 200 m on either side of the tunnel. Site staff reported that sub-longitudinal joints yielded a lot of water whereas transverse joints were less obviously wet (personal communication). Geological studies in the vicinity observed that the in-situ lateral stress roughly along the alignment was relatively high and transverse to the alignment was almost zero. It can be considered that compression on transverse joints reduced their aperture and lowered their conductivity, whereas lack of pressure on longitudinal joints allowed the joints to flow with water.

SUMMARY AND CONCLUSIONS

Interpolating top of rock profile between widely spaced boreholes is a common problem and can be unreliable. The statistical method of Fractals provides a means of interpolation between widely spaced boreholes. A trail was carried out for a site underlain by Granodiorite in Hong Kong. A comparison is made between an estimate based on a few widely spaced boreholes and the detailed results from pre-drilling for diaphragm wall panels at about 6 m spacing. The method is shown to be useful for estimating the variation in profile of top of rock in the same structural domain and where domains are mixed with zones of deep weathering, such as resulting from faults, the presence of the zones of deep weathering can be recognized.

Material strength of rock is affected by tropical weathering and can vary considerably over a wide range. The results from only a few tests might not reflect the range and this can lead to inadequate characterization and a risk of inappropriate designs, inappropriate choice of equipment and methods of working, and claims for unforeseen ground conditions. Whereas limited site specific data might not represent the range of properties of rock, collections of data for the same type of rock that are published can be helpful for designing, planning the work methods, and in resolution of claims. Data are presented for two rock types/series in Singapore. The variations in strength are shown in relation to depth below the top of rock, the lithology and the degree of weathering.

Because many intact rock materials have very low permeability, the mass conductivity is determined by the frequency of occurrence of fractures, the openness of the fractures and their connectivity. Data are presented from packer tests conducted in boreholes in Bukit Timah Granite and in Jurong Series in Singapore and in Kowloon Granite in Hong Kong. The median values are between 0.3 Lu and 1.0 Lu but

the data range over several orders of magnitude. Individual tests have recorded up to 700 Lu. With such a wide range in values of conductivity, by conducting only a few tests, there is a high risk that the properties of the ground are not adequately characterized.

The data for Bukit Timah Granite are sorted according to material weathering, Grade I to Grade III, and show a small dependence on degree of weathering.

Data for Kowloon Granite have been collected from many projects and comprises 1189 packer test results. Packer tests are often conducted with a bias. For example, tests are sometimes located at specific features, and seemingly solid rock might not be tested. There is a possibility that such a bias would affect the proportional representativeness of collections of test results as presented in this paper. By comparison, continuous probing ahead of tunneling has no such bias, and data from 762 number 20 m long probe holes are also presented in this paper. The test length for packer tests conducted in boreholes is usually only one or two meters. Continuous probing 20 m ahead of tunneling has no bias, and rates of inflow can be compared with the packer test results. The results are broadly similar, saving that Lugeons are reported per meter length, and therefore discrete large inflows are reduced in magnitude for 20 m probes, whereas frequently occurring minor inflows are not affected by the length.

The data on conductivity for Jurong Series rocks is sorted according to the types of rock, namely Mudstone, Siltstone, Sandstone and Limestone. The results are fairly similar, and based on these results the mass conductivity is probably independent of the different types of rock at the locations of these tests.

Recent experience indicates that conductivity can be anisotropic. Packer tests in vertical holes and in inclined holes in a slope have shown anisotropy consistent with preferred downslope drainage paths. Observations of dewatering ahead and to either side of a tunnel indicated anisotropy in mass conductivity that is consistent with anisotropy of in-situ stress, whereby joints under high compression are less conductive than orthogonal fractures orientated under lower compression.

REFERENCES

Endicott, L.J., Zhou Y. X., Ong H. L., Teo T. Y. 2018. Mechanical Properties of Rocks of the Jurong Series. Proc. of ARMS 10, 10th Asian Rock Mechanics Symposium and ISRM International Symposium 2018, Singapore.

Forsythe, A., Pearse-Hawkins, N. 2014. Assessment of Hydraulic Conductivity and Groundwater Flow Models in the Bukit Timah Granite. Proc. Underground Singapore

Zhou Y., 2001. Engineering geology and rock mass properties of the Bukit Timah Granite. Proc. Of Conference Underground Singapore. 308-314.

Zhang W., Han L., Yang C., Zhou X., Wu C., Goh A. T. C. 2018. Variability of Mechanical and Physical Properties of Singapore Bukit Timah Granite Rocks and Residual Soils. Proc. of ARMS 10, 10th Asian Rock Mechanics Symposium and ISRM International Symposium 2018, Singapore.

DIVING UNDERGROUND - THROUGH A HOLOGRAM - TO BETTER UNDERSTAND FOUNDATION RISK

Scott A. Anderson. Ph.D., P.E., BGC Engineering, Inc., Golden CO, 720-598-5982, scanderson@bgcengineering.com

Benjamin S. Rivers, P.E., Federal Highway Administration, Atlanta GA, Benjamin.Rivers@dot.gov

Silas Nichols, P.E., Federal Highway Administration, Washington DC, Silas.Nichols@dot.gov

Derrick D. Dasenbrock, P.E., D.GE, Minnesota Department of Transportation, Maplewood, MN, Derrick.dasenbrock@state.mn.us

ABSTRACT

Unknown geotechnical conditions are a major source of risk. Unexplored places vastly outnumber the sampled and tested ones, and widely spaced boreholes with intermittent tests and samples are the norm. Sometimes site-specific planning and thought goes into locating these special, tested places, such as basing them on the geologic understanding or anticipated key locations for the structure; more often they are simply evenly distributed. We demonstrate a holographic model that allows viewers to see real data in real space, scaled or not, and to visualize where measurements are taken, what those values are indicating, and where there exists more unknown and more risk. The holographic model shows in an intuitive way, values from Standard Penetration and Cone Penetration tests, and surface geophysics. The mixed reality of this future is that a wide audience – owners, designers, project managers, contractors, and stakeholders interact together in a real space where they see and talk to each other, while at the same time are individually looking all around below or above ground, like a gopher, in a virtual one. Risk in the future will be better managed through more thoughtfully designed investigations and better communication of 3D data in a world of augmented reality.

Keywords: risk, exploration, investigation, mixed reality, augmented reality, visualization

INTRODUCTION

This paper explores the use of augmented reality to convey understanding of the subsurface conditions of a bridge site. This is in contrast with the current state of practice where this information is contained in a geotechnical report, and the ideas are also applicable to other structures, earthworks, and excavations. "Augmented reality" describes a situation where a 3D holographic model is displayed for users in such a way that the users experience both the model and the real environment of their setting- such as at a desk, in a meeting room, or in an open space at a project site (Figure 1).

The 3D holographic model is used to directly visualize underground features, to see through the earth to the actual locations where explorations are made, samples are obtained, or measurements are taken, design values are assigned, or construction is planned. An immersive model provides the following three powerful functions for users:

- Revealing how little of the subsurface is actually characterized in typical investigations, and how much more could be done to improve site characterization.
- Facilitating shared and common understanding of complex 3D data in a short amount of time. These data may include the ground surface, phreatic surfaces, stratigraphy, sampling locations, material

© 2019 Deep Foundations Institute

property variations, failure surfaces, sensor measurements, previous, existing, and proposed structures and foundations, and boundaries or delineations of various types.

- Presenting design alternatives in 3D space while using step-wise progressions of images or overlapping semi-transparent volumes. This can enhance the review and decision-making process, especially in a collaborative setting.



Fig. 1. A hologram in a meeting room with viewers sharing their interpretations.

FOUNDATION RISK

For many transportation and civil projects, foundation construction and ground stability during construction or service, represent primary sources of risk. This risk may relate to cost, schedule, safety, or combinations of these or other factors. Geotechnical project risks may evolve throughout project life-cycle phases of scoping, preliminary planning, design, procurement, construction, and maintenance for long-term performance.

Geotechnical risks during planning might be related to making broad project direction, scheduling or alternative selection based on very preliminary information – information that might later be shown to be incorrect. In the investigation and design phase of the project, more detailed information is available, but the same risk exists: design assumptions may turn out to be incorrect. In the procurement stage, new team members are brought into the delivery process, and additional risk is in miscommunicating understanding or expectations. In the construction phase of a foundation project, the amount of knowledge about ground conditions can quickly exceed anything known prior because exploration samples and tests represent only a very small fraction of a project. Construction processes reveal more project information as the works impact larger volumes of material.

The risk in construction below ground lies in discovering unforeseen conditions or discovering the planned means and methods are not effective or desirable. From the owner's perspective, this is the risk of schedule delays, claims and contract cost escalation. From the contractor's perspective, this is the risk of unprofitable work, or in some cases safety. Each phase of the project adds new foundation risks.

MITIGATING FOUNDATION RISK

Being a combination of the probability of outcomes and the consequences of those outcomes, risks are mitigated by reducing the likelihood of a given threat occurring, by reducing the consequence if that threat occurs, or both. Geotechnical threats are often thought of as mischaracterized physical conditions such as low quality samples, erroneous measurements, or poor interpretations of the available information. Important information such as boundary locations, material types and properties, spatial variability, or temporal variability may not have been well defined across the site. Conversely, the original data may be of high quality, but interpretations and assessments could be inappropriate due to oversimplification, overlooking critical factors, or having a basis on accurate but incomplete data.

Two studies cited in the NCHRP Synthesis 484, *Influence of Geotechnical Investigation and Subsurface Conditions on Claims, Change Orders, and Overruns*, concluded large geotechnical project risks are attributable to the human interpretation and decision-making aspects of the geotechnical design process. As reported in the Synthesis, (Baynes 2010), the collective evaluation of several studies of geotechnical risks concluded that "available information suggests that the ground conditions and the project staff responsible for the geo-engineering process are both significant sources of geotechnical risk and that the project staff may actually be the largest source." Clayton (2001) described this "human" aspect of geotechnical risk as follows:

> "There are numerous ways in which the ground can cause problems for construction, for example due to chemical attack, heave, subsidence, groundwater flow, slope failure, excessive foundation settlement, and so on. Because of the considerable range of risks the ground can pose, it is relatively easy for an inexperienced or non-specialist designer, perhaps using routine procedures, to fail to recognise a critical mechanism of damage or failure that may threaten either the financial viability or health and safety of a project. If a mechanism of damage (a limit state) is not foreseen then it cannot be designed for, and it is often for this reason that ground-related problems occur."

Whether due to original information quality or subsequent evaluation, low quality information often leads to inappropriate design decisions, insufficient final designs, and future construction problems. Transportation projects often are developed by multidisciplinary groups where the risks in one discipline, such as geotechnical engineering, can often propagate to other functional areas such as hydraulics, pavement, structures, and construction.

Additional risk can also be introduced during the execution of the project and associated contractual process. Each party often obtains all or limited portions of a project's geotechnical data separately, at different times, in different sequences, with different focus, resulting in different conclusions about what the data showed or what it implied about the site character or behavior. Parties enter into an agreement with one another unaware of each other's interpretations as they may relate to methods, sequencing, equipment, labor, schedule, cost, and safety.

Regardless of accuracy, precision, or quality, incomplete subsurface information or the ineffective communication of subsurface conditions often results in risks being realized. Improved communication and clear comprehensive presentation of geotechnical project information to internal and external stakeholders mitigates risk in general.

Conservatism

A common design approach to address geotechnical risk is to counter a small investigation scope with project requirements or elements which are thought to be conservative in nature- "overdesigning" project elements to compensate for the geotechnical unknowns. The concept that foundation risk can be mitigated by a conservative approach through subsequent design overlooks the reality that this is risk transfer, not risk reduction. Non-conservative (minimal) geotechnical exploration effort transfers risk to both the design and construction phases of a project.

While minimal geotechnical effort can be thought to accelerate the project schedule or simplify contracting effort, a de-emphasis on the importance of this information usually results in performing exploration work to the absolute minimum standard of care on a limited budget: the fewest holes, least sampling and testing, and often an avoidance of newer technologies and techniques. This approach leads to the minimum possible knowledge of the subsurface. Codes and standards may be relied on more heavily in the absence of good quality site information. Planners may make assumptions to manage the risk of unknowns and provide guidance to designers. Designers may add their own conservatism in the foundation designs and in specification requirements and acceptance language, leading to larger and more numerous foundation elements, excavations or anchors, introducing risk tied to their construction. The likelihood of encountering obstructions, surprises or equipment malfunction increases with the increased subsurface effort. More construction work imparts more project construction cost and construction risk.

Codes and Standards

While codes and standards provide uniform and successful risk mitigation for above-ground aspects of design and construction, this is less frequently the case for underground works. Work below ground is often challenging for a variety of reasons:

- Even for relatively small project sites there could be considerable variability in the subsurface stratigraphy. Larger, linear, project sites such as roadways, pipelines, transmission lines, and railroads often have more variability due to the larger site footprint.
- Material properties are generally not uniform across a project resulting in changes in strength or settlement behavior, which could require adaptation in the field compared to initial designs.
- Groundwater behavior may differ from design assumptions; it can vary seasonally or by the influence of unplanned weather events (rain and flood) or nearby landowners or 3rd party impacts.
- Foundation performance is often influenced by construction means and methods, typically unknown (unless specified) at the time of the foundation design.

Nevertheless, many owners and agencies rely on language in codes and standards to provide guidance for a minimum standard of practice. For complex projects, these minimums may be insufficient to provide the owner with enough information to make informed decisions with respect to foundation selection, design, construction means and methods, contractor qualifications and selection, procurement types, and both construction and long-term performance risks.

It is frequently the case that "minimum" requirements for exploration are adopted as standards for all projects even when projects are known to be more complex in nature, usually due to a lack of project specific risk assessment, and the effort associated with developing a site specific set of requirements. As an example, in Minnesota Department of Transportation (MnDOT) practice, it is relatively uncommon to specify project-specific consultant drilling requirements that deviate from the standardized (minimum) requirements established in the MnDOT Geotechnical Manual [available on-line]. There is perhaps

perceived efficiency or economy in this approach: contractors are familiar with the requirements, the deliverables are consistent, and the level of effort in prescribing and administering the work is minimal.

Most highway transportation geotechnical investigations, when not performed by the owner's staff, are procured using a "low bid price" model to perform the specified work. Using this model, the requirements are usually standardized and there is no easy way to adapt the work to changes in the field discovered during the progress of the exploration. As with other aspect of the work- "You get what you pay for" applies.

Even when using owner's staff, the project development process often does not provide geotechnical engineers an opportunity to revise or amend a site investigation plan or proposal due to perceived adverse impacts to the timeline and budget. This provides the owner with the challenge of developing an adequate scope of geotechnical work prior to the investigation process- and making sure this is defined and conveyed to the project partners when developing the project schedule and cost estimate. Here too, good communication and understanding of the project scope and needs can mitigate several potential risk factors.

Advanced Exploration Methods

The Federal Highway Administration (FHWA) has recognized that one way to improve the process of geotechnical site characterization is to promote and advocate for the use of newer and more technically advanced exploration methods. These investigation methods are often safer, faster, and more repeatable, providing improved data quality at a lower price point than traditional investigations. By using newer techniques, the minimum standard of practice can be improved while potentially also adding value to the project cost and timeline. FHWA, through the American Association of State Highway and Transportation Officials (AASHTO) and its state partners, has recognized the need to actively engage State Departments' of Transpiration (DOTs) and promote underutilized existing and emerging exploration technologies. A new FHWA Every Day Counts (EDC) initiative "Advanced Geotechnical Exploration Methods highlights several proven, but generally underused, technologies, including 1) Exploration geophysical methods; 2) Cone Penetration Testing (CPT); 3) Measurement while drilling, (MWD); and 4) Acoustic and Optical tele-viewers. The EDC program provides resources to State DOTs to become more familiar with and potentially adopt some of these techniques on a project, potentially opening the door to regular programmatic use.

By introducing these newer techniques and explicitly considering project risks and site variability, the minimum standard of care can be improved. High quality and reproducible CPT soundings can be advanced to supplement traditional SPT borings. To further increase CPT testing value, additional sensors can be used to provide soil resistivity or seismic wave speed. MWD can be added to traditional SPT drill rigs and provide continuous drilling records in terms of penetration rate, torque, down-pressure, rotation speed and fluid-pressure that can be correlated to material differences, engineering properties and drilling performance. As new or different techniques with new information are being introduced to owners and consultants, it is a convenient time to assess how the measurements are stored, transmitted, displayed, and used for analysis so that the value of these techniques is maximized by geotechnical engineers and their project partners. Much of the value of the newer techniques comes from automated data collection, processing, and presentation.

ACHIEVING COMMON UNDERSTANDING OF THE SUBSURFACE ENVIRONMENT

Even if risks are reduced by improved technology and processes, the value is greater if geotechnical conditions and associated uncertainty are also effectively communicated to all the users and stakeholders who need to fully understand and appreciate it for sound decision-making. This is where the newer technology of augmented reality adds value. Geotechnical data are inherently three-dimensional, as each measurement generally represents a quantity associated with a particular location in a project's surface or

subsurface space. Geotechnical investigation content is often still presented in a very traditional format using a paper report, black and white printed logs as in Figures 2 and 3, and sometimes cross sections showing simplified boring logs as in Figure 4. In some cases, the geotechnical information is entirely separate from the project plans, except for locations or representative elements. For many years now, it has been possible to generate 3D models using CAD or other software, but these models have been viewed as 2D images on paper or on a computer monitor and are frequently only used internally and not made available to contractors bidding on the work (they are often not a part of the contract documents).

There is a trend toward 3D design and visualization, but usually only for large specialty projects. Building Information Models (BIM) are becoming more common, particularly in the building design and construction community. When viewing models, there is usually a "driver" controlling the model viewing, zooming, and rotation, and "passengers", who are passively viewing the information. Their experiences are different, and it is likely their project perception and understanding are also different and therefore their interpretation of risk is also different, perhaps much like the driver and passenger in a car when driving. Perception of risk is also effected by external factors such as education, background, project role, and familiarity with the risks associated with a particular project. Not all project participants will have an understanding of staged or temporary construction, extreme events, adjacent landowner and utility considerations, and the nature of different types of design solutions (shallow or deep foundations, lightweight fills, ground improvement, etc.) and how these factors alone or in combination influence risk.

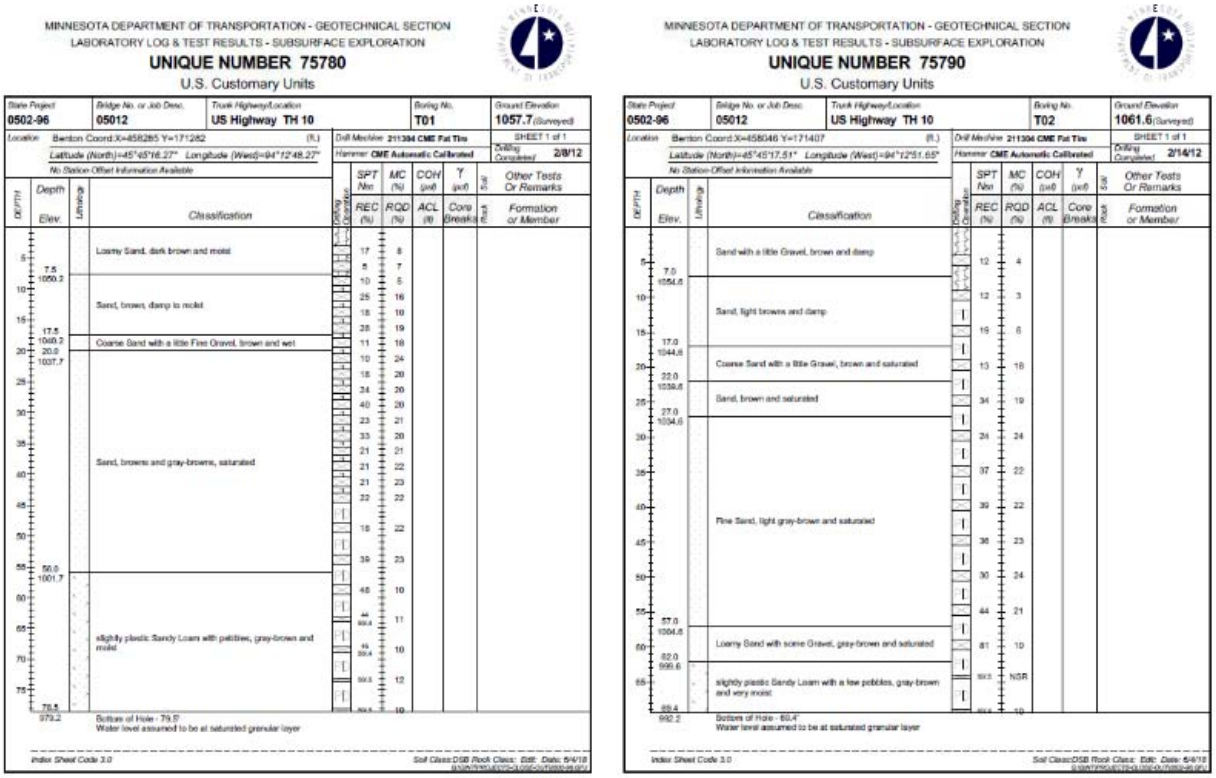


Fig. 2. MnDOT boring logs showing subsurface information as would typically be included in a geotechnical data report or design memorandum. Sample intervals are typically 2.5 feet in the upper 50 feet of the boring, and 5 foot intervals from 50 to 100 foot of depth.

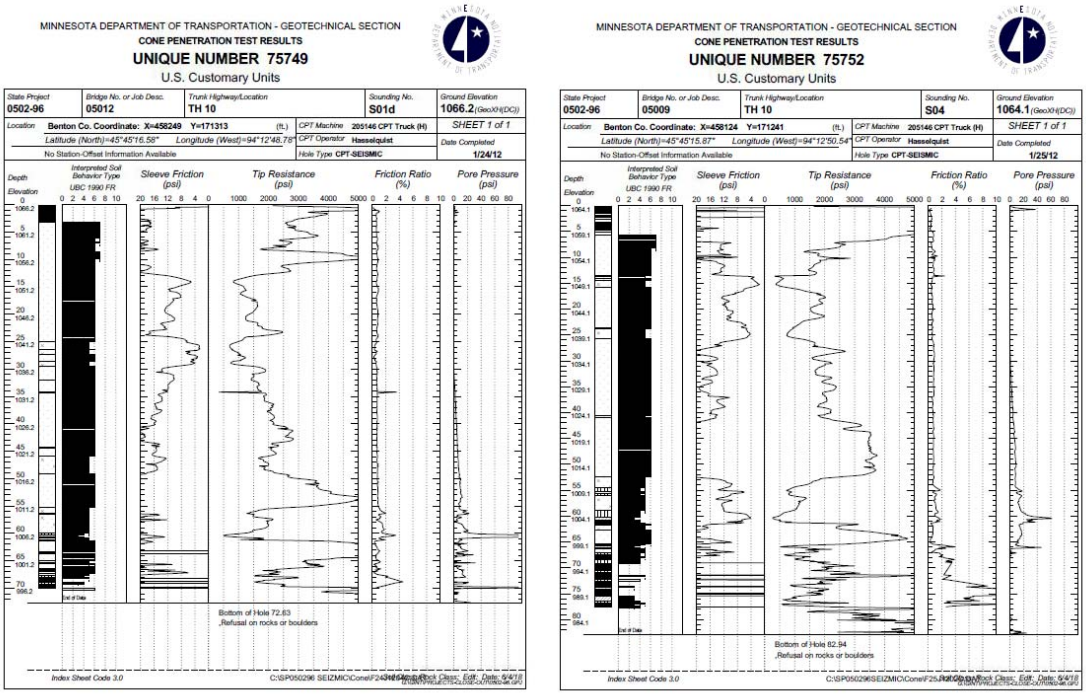


Fig. 3. MnDOT CPT Sounding Logs showing subsurface measurements obtained using that testing system. Measurements are obtained every 20mm of advance of the CPT instruments.

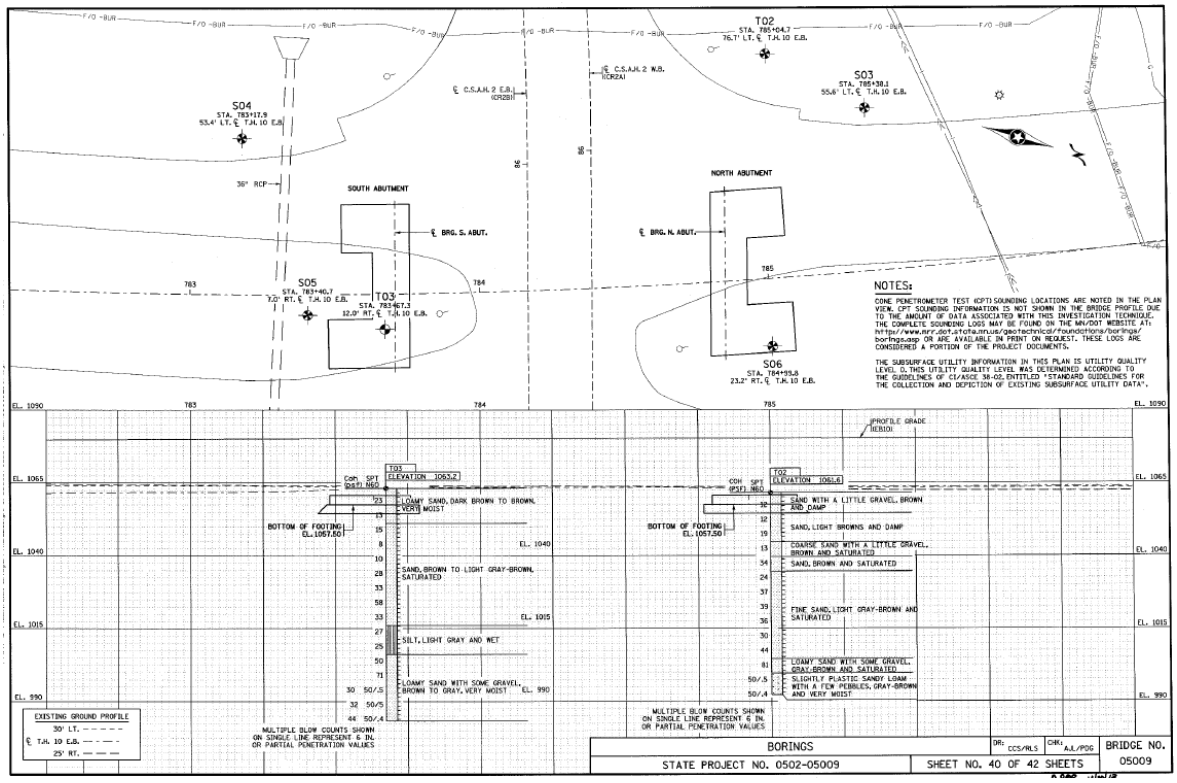


Fig. 4. Project plan sheets showing two of the soil borings with respect to the proposed footings for MnDOT Bridge 05009 at Rice, MN.

New ways of better visualizing a 3D environment, particularly using holograms and 3D spatial tools, are resulting from developments in computer animation and the gaming industry. Virtual reality is the name given to an experience where a user is completely immersed. It is powerful, but often individual or solitary (even to some extent in so-called "multi-player" environments), and for many, unsettling. Augmented reality is different in that the reality of a user's immediate environment is not lost; it is modified with additional content. The user does not need to let go of their real experience to participate and comparatively few people find this added element uncomfortable. A 3D holographic environment is usually immersive but less passive than 3D movies as users generally move around the environment and can interact in the 3D space from different vantage points by moving themselves around in the room or other setting.

Users can participate in an augmented reality setting individually or within a collaborative group. When in group, the common setting lends itself to interaction and, in the authors' experience, invariably a discussion ensues, wherein people are gesturing and interacting (to the extent they can) with the hologram. This interaction is a shared experience and fosters different impressions than a solitary experience otherwise would, depending on the participant interaction with the 3D holographic images and the other participants in the group. This observation comes from experience with an environment described in the next section.

A SIMPLE BRIDGE EXPLORATION VIEWED IN 3D

MnDOT has been routinely using SPT testing and borehole drilling since the Foundations Unit was created by the former Minnesota Department of highways in the middle of the last century. Cone Penetration Testing (CPT) was added as an in-house geotechnical service in 2001, and geophysical exploration was added in 2006. Both SPT borings and seismic CPT soundings were advanced at a project site for a new set of bridges at a proposed grade separation project in Rice, MN. Electronic project information, subsurface information, and construction photos were readily available for this project, making it easy to adapt to a case-history for the FHWA EDC initiative. A holographic model was created, and loaded into the Microsoft HoloLens (see Figure 1) using the Ada Platform™ mixed reality software. The Rice, MN bridge holographic model displays engineering values from Standard Penetration borings (SPT), seismic Cone Penetration tests (SCPTu), and electrical resistivity geophysical methods using graphical symbols and color (For the case study presentation a geophysical survey from a different MnDOT project was included as a conceptual example use-case).

The mixed reality was demonstrated to a wide audience of DOT and related transportation agency professionals at five FHWA EDC summits in 2018. With one or two guides, 3 or 4 additional users interacted together in conference rooms, foyers, and other space to intuitively experience the value of subsurface site characterization using the Rice, MN bridge model. Users in the mixed reality environment were able to see and talk to the guides, each other, and looking around the 3D model below or above ground. The model stepped through the investigation types, so users could see the depth, location, and measurements associated with the 3 SPT borings (Figure 5), 6 SCPTu soundings (Figure 6), and 2 planar representations of electrical resistivity surveys (Figure 7).

Users could walk around and through the fixed 3D model creating a rich shared experience. The guides discussed the types of data, their data density and accuracy, as well as the time and cost associated with the investigation techniques. The setting allowed users to appreciate how the investigation measurement locations compared to the proposed foundation system for the bridge in a volumetric setting (as opposed to looking at plans, profiles, and cross sections). Through feedback gained at the summits and other subsequent A-GaME outreach efforts, it was immediately recognized that participants viewed the 3D spatial visualization, in this augmented reality world as a significant and meaningful departure from traditional project plans and reports.

Nearly all participants expressed creative ideas on how they could leverage the augmented reality setting to convey spatially related concepts for their own work – from public interest forums relating visual aesthetics and impacts of proposed construction to conveying complex orientations, multi-dimensional conditions and project sequencing for excavation and utility work. Geotechnical engineers and geologists often saw great advantage in communicating complex ground conditions and the relative sparsity of geotechnical in-situ or lab testing data points. In all cases, the authors observed a recognition within participants of a tool that can greatly improve communication and understanding. These observations suggest that we have barely "scratched the surface" on the visualization potential of this technology.

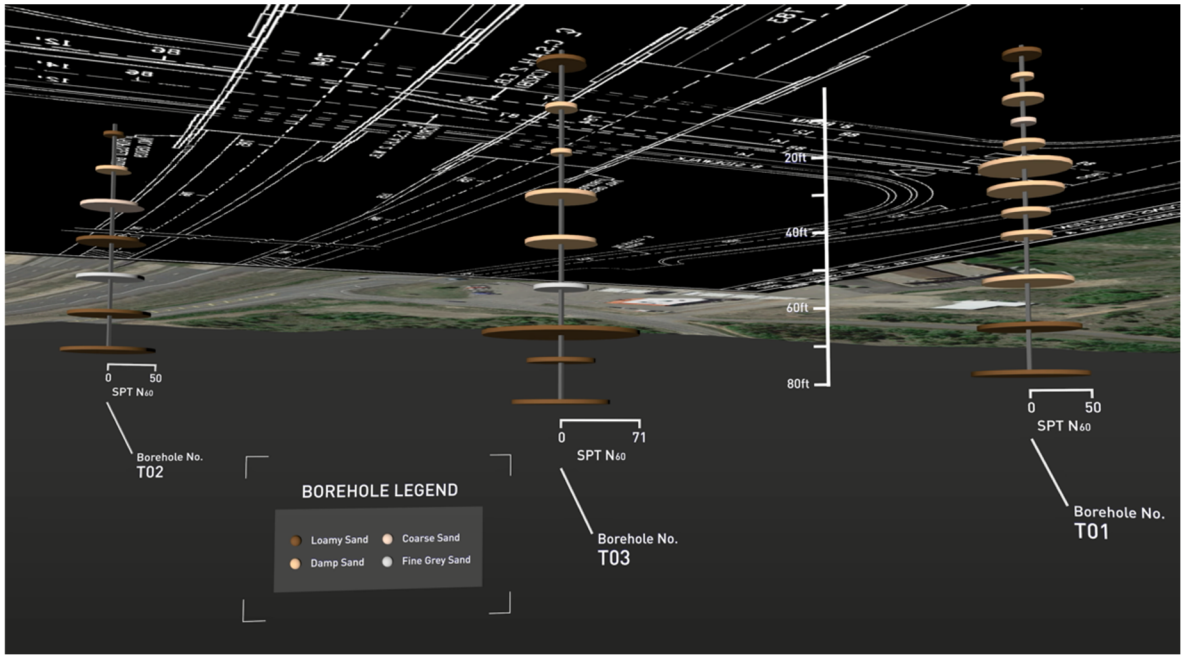


Fig. 5. SPT boring information as shown in the 3D model.

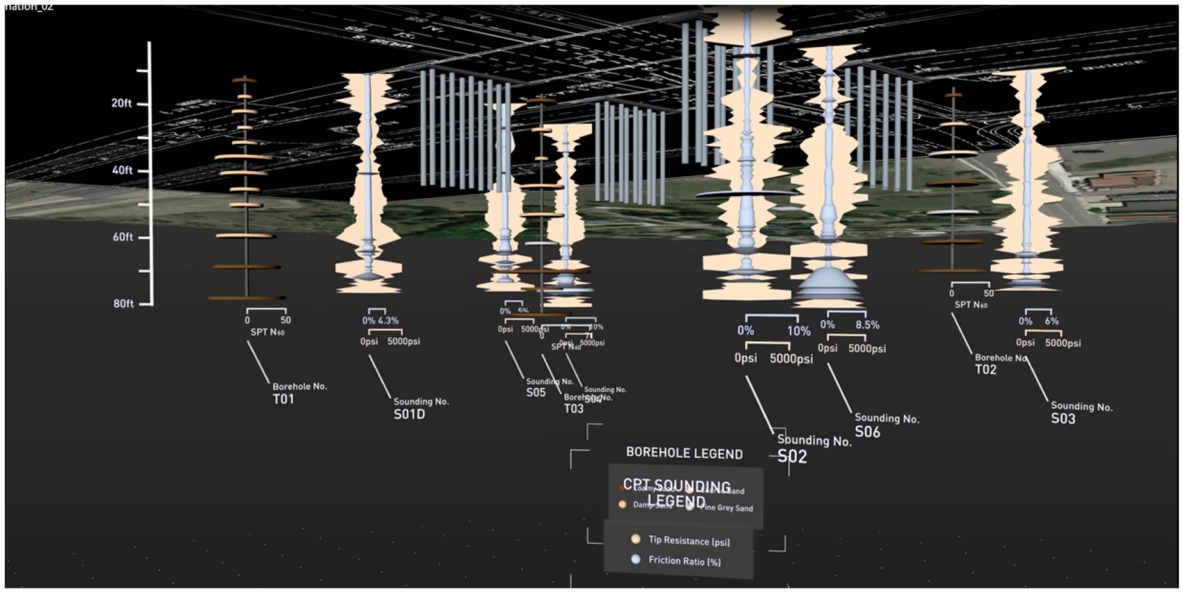


Fig. 6. SPT boring and SCPTu sounding information shown in the 3D model. Also seen are pile elements associated with one foundation option considered for the proposed bridges.

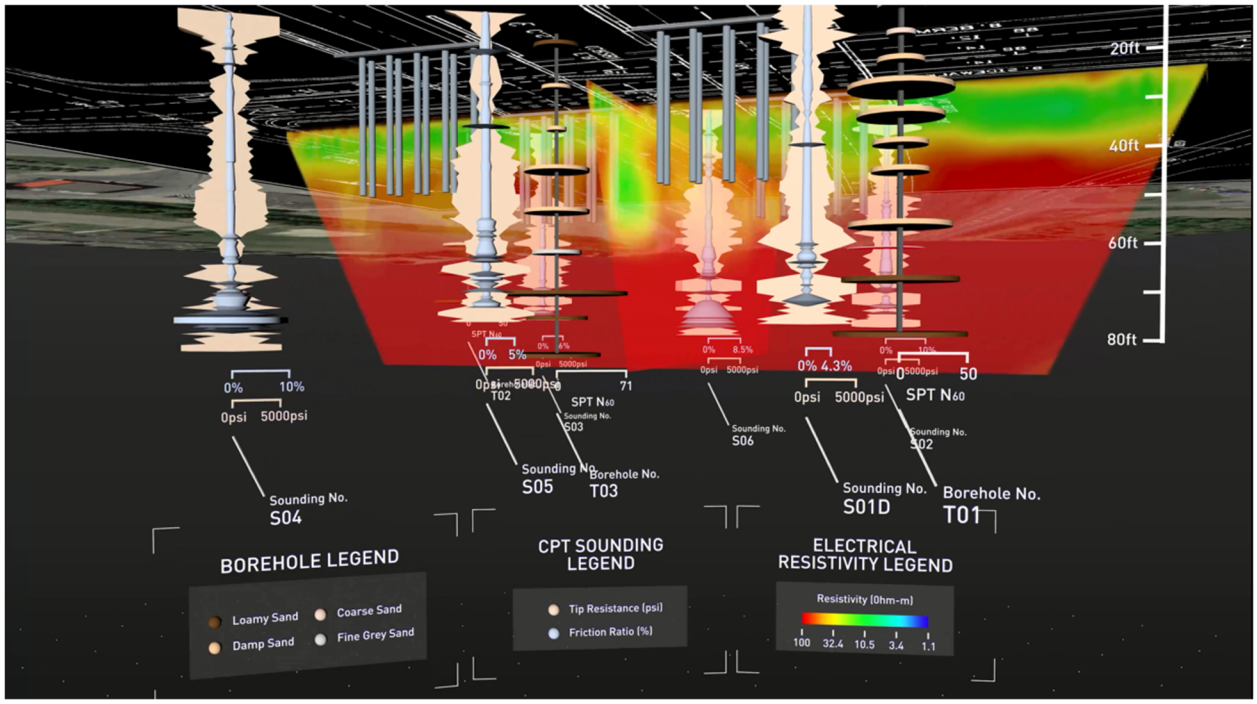


Figure 7. The same model, adding two vertical planes of electrical resistivity geophysical data.

CONCLUSION

A major source of project risk relates to subsurface conditions. Geotechnical investigations are often limited by time and budget considerations. Soil and rock material properties and behavior are frequently variable enough across a project site that risks from variability need to be considered in design. As relatively small portions of project sites are investigated extrapolation and interpretation are a necessary element of geotechnical work. Traditional two-dimensional plans and boring logs have served as standard practice for decades, but new and emerging technologies developed in the computer gaming industry are suddenly providing game-changing opportunities for data presentation and collaborative experiences to help transportation project participants better understand risk and uncertainty associated with the underground environment and potential design options. Representing a significantly different experience in data presentation and collaboration than current practice, a 3D holographic model, using a HoloLens and the Ada mixed reality platform allows viewers to see real data at its location in real scaled or full size project space. The example holographic model displays values from multiple subsurface investigation techniques, with respect to the project setting- conveying the relationship of the geotechnical data to the in-situ environment and the proposed construction. Future models, which can be created with current technology can show additional information such as that from in-situ sensors (pore water pressure, inclination, etc.).

The use of augmented reality to convey understanding of the subsurface conditions of a bridge site has been contrasted with the current state of practice where this information is contained in print documents. The 3D environment, with its spatial nature, is a useful tool to establish the locations where measurements were made and convey the scale, proportion, and relationships of tested and un-tested materials in typical and robust site characterization programs. The authors suggest that both geotechnical information and the associated risks in the 3D environment can be better visualized, appreciated, and comprehended and therefore be better managed, resulting in a less uncertainty. More efficient and tailored designs can result

in project economy through better project definition, contractor prequalification (if appropriate), bid pricing, and scheduling. While the example provided focuses on transportation geotechnics, the 3D environment is wholly applicable to use on other structure types and in related engineering disciplines.

The technology may be employed by an individual user, but is more meaningfully applied in a collaborative environment. When used collaboratively, complex 3D data can be presented and (more importantly) shared in a short amount of time. In addition to static geotechnical information the system can also show progression of measurements or site characteristics in time, as well as conceptual design alternatives. Augmented reality (Microsoft calls this Mixed Reality) is a promising tool to display 3D data and to share the experience. In deploying the technique as part of the FHWA EDC initiative the authors have found that despite being partly in the virtual world, the augmented reality shared experience is a "real" user experience.

The 3D holographic space and the collaborative nature of the Hololens and Ada tools, allow project geotechnical risks to be better perceived, identified, quantified, managed, and mitigated. Improved project design and better solutions are achievable more quickly and with greater potential value from early design adaptation based on better understanding of project sites and subsurface properties, variability, susceptibility, and predicted performance based on anticipated conditions and stresses during the project design life.

REFERENCES

Baynes, F.J., "Sources of Geotechnical Risk," Quarterly Journal of Engineering Geology, Vol. 43, 2010, pp. 321–331.

Clayton, C.R.I., "Managing Geotechnical Risk: Time for a Change?" Geotechnical Engineering, Proceedings of the Institution of Civil Engineers, Vol. 149, No. 1, 2001, pp. 3–11.

Federal Highway Administration (FHWA) Every Day Counts (EDC) Advanced Geotechnical Methods in Exploration (A-GaME) website accessed on April 19, 2019: https://www.fhwa.dot.gov/innovation/everydaycounts/edc_5/geotech_methods.cfm

NCHRP SYNTHESIS 484, TRANSPORTATION RESEARCH BOARD, WASHINGTON, D.C., 2016, www.TRB.org, Influence of Geotechnical Investigation and Subsurface Conditions on Claims, Change Orders, and Overruns, A Synthesis of Highway Practice; Consultants Andrew Z. Boeckmann and J. Erik Loehr, University of Missouri–Columbia.

ELECTRONIC INSTRUMENTATION IN SUPPORT OF INSTALLATION OF SPECIAL FOUNDATION PROJECTS AS PART OF THE DIGITAL FUTURE - Ensuring Safe Production and Improving Quality Control

Franz-Werner Gerressen, Bauer Maschinen GmbH, Germany, franz-werner.gerressen@bauer.de

ABSTRACT

New developments are required each day as our industry becomes more competitive. To improve performance, continue and to ensure future demands can be met. This requires the development of technical support systems that enable a more constant delivery and quality of installation of pile foundations and other applications. For example: assistance systems capable of relieving the machine operator of automating monotonous or repetitive operations. Real time installation control of the production process to manage quality control, or data transfer and reporting systems capable of keeping pace with the digital future. This paper will describe these new approaches and considerations required for these new developments. The paper also describes the equipment which is needed to execute the work under the various conditions and provides references herein.

Keywords: Electronic, Assistant Systems, Continuous flight auger (CFA), Piling, Piling data, Rig instrumentation

INTRODUCTION

The success of a construction site is influenced by a number of factors. Selecting the most efficient and economic methods during the planning phase to defining the right direction. This means having multifunctional equipment available. To ease the usage of this equipment by the operator, uniform operation and control systems are essential. Systems like this can provide uniform handling procedure for more than 20 different installation techniques.
Experienced operators are not always available. Therefore, to ease the start for beginners and to support training, numerous assistance systems were developed. This ranges from simple information for controls shown on the monitor avoiding misuse to systems which can partly automate the construction process.
Regardless, the best equipment is not enough when the construction is not running smooth. The control system not only helps to organize and coordinate service of the equipment; moreover, it allows the operator to control the quality during the installation process reacting if needed. It allows process optimization as well as documentation which might be required for later negotiations.

THE MACHINE UNDER CONTROL

General

The actual electronic systems (e.g. the B-Tronic) enables you to efficiently **operate, assist** and **manage** individual machines (e.g. piling equipment, cranes etc.) as well as entire fleets. The highly efficient systems are based on dozens of small sensors, such as heat, pressure and level sensors, placed at all critical locations on the machines, which continuously collect data. This data is logged centrally and processed. High-resolution touch- screens with a range of different display modes inform the machine operator instantly and comprehensively about the status of his machine and provide him with valuable information for the optimal use of the machine. This helps to securely monitor and precisely evaluate your projects and work processes. Data transmission systems, such as W-LAN, USB and DTR (a BAUER specific communications unit), facilitate the transmission of machine operating and production data both locally and globally.

© 2019 Deep Foundations Institute

In addition to the basic operational data described above, general machine operating parameters (e.g. engine data) can be acquired and monitored. The display of current machine operating status and error messages serve as a valuable aid for targeted and effective fault finding by service personnel on-site, as well as specialists based out of offices as data can be transferred real time via internet connection. This not only allows the control of equipment and installation process including relevant reporting, but also "virtual reality" and "reality"; hence, planned and actual execution, which enables the project manager to control the schedule and budget.

Operating Control Systems

With the increasing variety of equipment and applications it is important for the operator that the interface is as recognizable as possible. Of course, specific information for specific applications must be readily available, e.g. rotation and penetration speed, concrete consumption and pressure for single pass piling applications. Conversely, periodic required information or functions should be available in a secondary manner. This leads to a requirement that the interface for each application have a similar appearance (refer to Figure 1 below).



Figure 1: Various B-Tronic Displays

Simulators are available to improve operator preparation and training (refer to Figure 2 below). Simulators allow training on basic procedures without risking damages to the equipment.



Figure 2: Foundation Simulator, BFS In-cabin (Left), BFS-T Table Version (Right)

Assistance System

In a growing global market for the specialist foundation industry it is becoming more difficult to find experienced operators or to recruit and train new operators educated to the level required to meet the quality standards required of the installed product while maintaining high productivity and keeping costs competitive. As a result, it becomes more important to equip the machines with "intelligence" to assist the operator in optimized use and help reduce errors. For instance, drilling parameters for an optimized process in the complex interaction between ground conditions, machine regulations and operator intuition are difficult to define.

Recalling from prior experience, a special focus was placed on development of practice-oriented and process-specific support systems intended to aid the machine operator in the execution of his/her routine tasks, such as: crowd and torque control during drilling with the Drilling Assistant, or volume and pressure control during concreting with the Extraction Assistant, both hands-free operations. These systems relieve the operator by automating repetitive operations with a system like the B-Tronic system. They help to prevent faulty operation of the machine thereby protecting both person and machine. Automatic, fast control processes increase the drilling performance and reduce wear of both, equipment and tools. Assistance systems thereby ensure a consistently high production quality. There are more than 20 different assistant systems are available for various applications. All assistant systems are integrated into the general electronic monitoring and control system. All relevant data is displayed on the operator's monitor (refer to Figure 3).



Figure 3: Exemplary B-Tronic Display During the Concreting Process in Automatic Extraction Mode

Satellite-based Navigation System for Positioning and Documentation

With the Assistant Positioning System, the machine operator can utilize the advantages of a satellite based navigation system for positioning the drilling rig. The system guides the rig operator simply, quickly and accurately to the next pile position (refer to Figure 4).

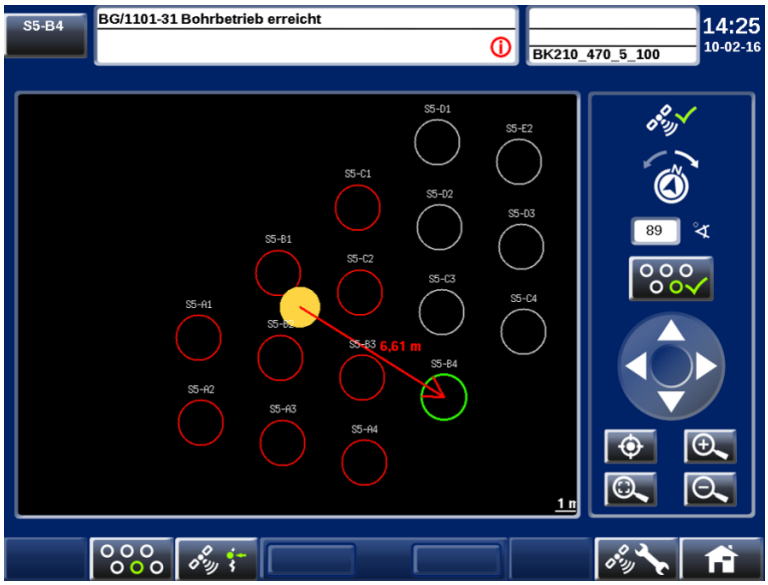


Figure 4: Operating Screen for Satellite Based Positioning

Nominal and actual coordinates of each pile are logged after completion and can be used to verify that all piles have been installed to specified tolerances. In addition to the benefit of quality control, time and cost saving for single piles, manual setting-out of pick-up points can be achieved.

Controlling the installation process, e.g. by using a "Drilling" and "Concreting Assistant"

Most rigs can be equipped with electronic software for use with the "Drilling Assistant", a program that modulates the optimum rate of penetration and crowd force during the drilling process for an optimal speed of rotation of the drilling tool. The drilling assistant is effective when working in single pass methods like continuous flight auger (CFA), full displacement piles (FDP) and cased CFA. The desired initial parameters can be input by the rig operator with the help of onscreen menus.

The benefits of the drilling assistant are two-fold. Relieving the operator from duties that requires full concentration over a long time, and increasing the drilling performance compared to manual working.

In addition, the system avoids two un-wanted situations for CFA. The first known as "over-flighting" (refer to Figure 5) which means the penetration speed is too low compared with rotation speed. This leads to a situation, where the surrounding soil becomes disturbed and the load capacity of the pile is reduced as a result. In addition to the increased amount of spoil overconsumption of concrete can be observed. Both lead to increased costs for the pile installation. Moreover, as a worst case scenario, this can cause ground around the tool to become unstable and including ground settlement induced.

The second situation to be avoided is the so called "corkscrew effect". Here the situation is reversed. Penetration speed is too fast and rotation speed is too low in relation. In this case the tool can get stuck and removal can damage the tool or the machine.

Both scenarios can be avoided by using the "Drilling Assistant".

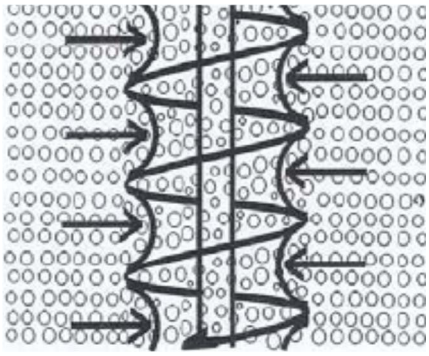


Figure 5: Principle of “Over-Flighting” [3]

While the “Drilling Assistant” is focused on performance, the “Concreting Assistant”, especially for the single pass methods, focuses on the pile quality.

By using the "Concreting Assistant", the speed of extraction and volume of concrete can be adjusted. This involves measuring concrete volume continuously during the concreting process and automatically regulating the speed of extraction based on the concrete flow rate. The concrete pressure is also monitored and controlled during the concreting process. As control over these parameters takes place, concrete overconsumption can be reduced and blockages can be avoided.

Concrete Link

The Concrete Link is a bi-directional remote-control link between the machine and the concrete pump (see Figure 6). The drilling rig operator can control the concrete pump direct from his/her cabin. All relevant data for both the concrete pump and the concreting process are available via the operator screen. The extraction speed of the rig is automatically adjusted with the concrete volume. The rig operator can set the optimum speed and intervene in the process at any time. Incorrect concrete volumes and blockages can be prevented by full control and high degree of process automation. All information from the concrete pump is displayed on the operator screen.

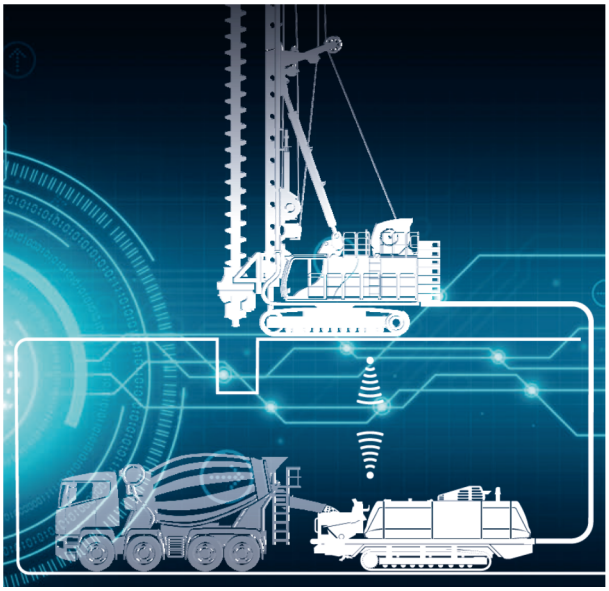


Figure 6: Principle of Concrete Link

Advancements for CFA Drilling - iCFA

The iCFA system is a development intended to fulfill the growing demand in quality assurance for the installation of CFA piles. The ability to monitor a higher concrete pressure than earth pressure is required. Per typical practice, the concrete pressure is measured at the top of the drill string, the pressures below grade are oftentimes higher than measured and can cause unnecessary concrete overconsumption and in some cases blockages of the concrete line. The iCFA system is now equipped with a pressure sensor at the bottom of the drill string that allows more accurate pressure measurements, thereby potentially saving costs realized in concrete overconsumption. In addition, the iCFA drilling rod measures the inclination of the pile at the bottom of the drilling string. The components of the iCFA-equipped drilling rod are illustrated in Figure 6 below.

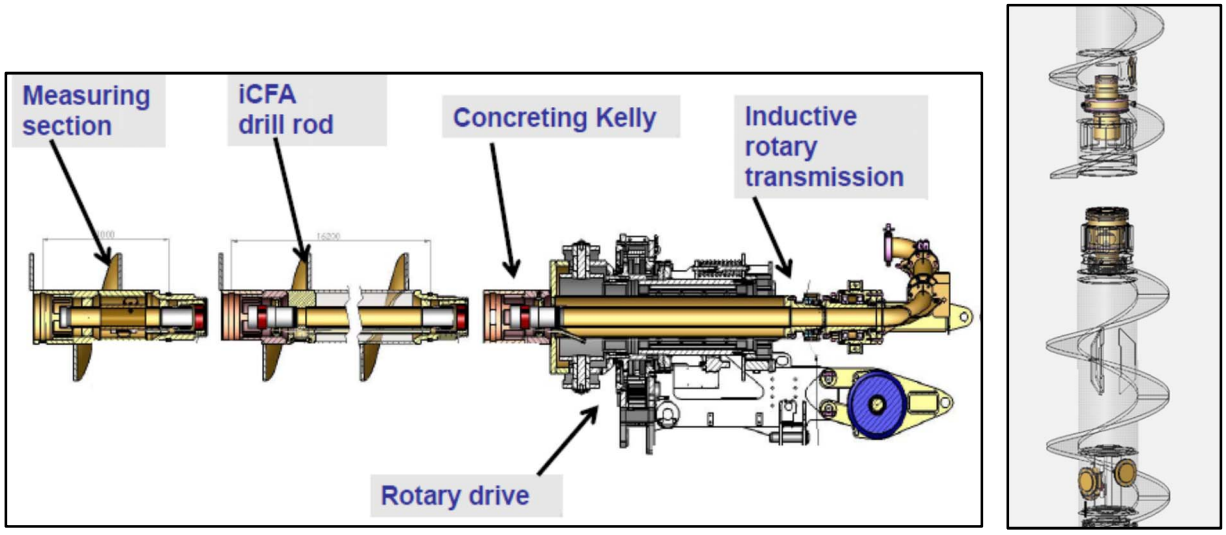


Figure 6: Configuration of iCFA-equipped Drilling Rod

As measurement at the bottom of the piles is logistically complicated, a special drill string was developed. A unique feature is the data transmission method, completed by inductive data transmission through the auger joints as opposed to through a wire, thus the acronym “i” in the name.

As expected, this iCFA drill string is two to three times more expensive than a standard drill string. Mainly, due to the couplers and additional sensors. Those who have made this investment agree it will be recovered over a reasonable time by the potential savings in unnecessary material waste.

The system has been proven on a number of sites, where the concrete pressure was measured parallel at the top and bottom in parallel (refer to Figure 7).

The graph shows a significant difference in pressures measured at top and bottom sensors.

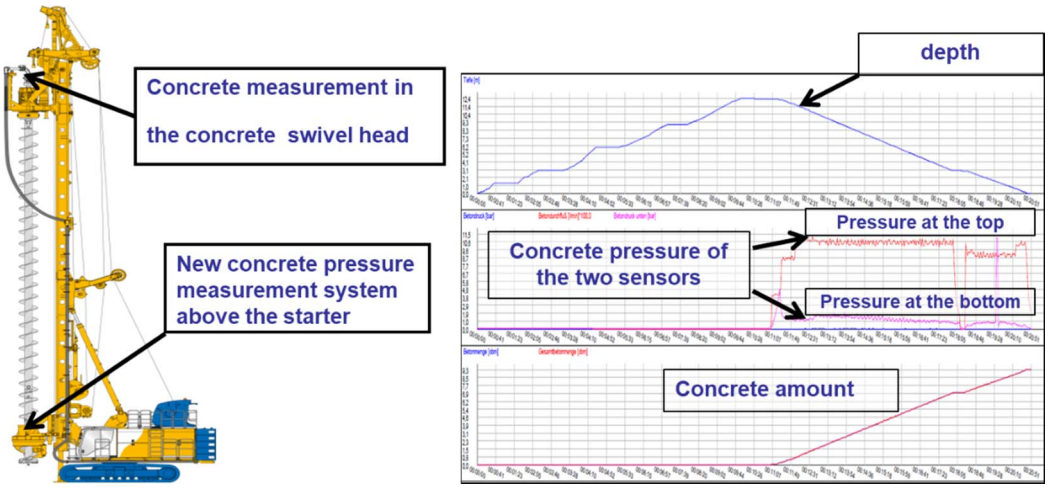


Figure 7: Positions of Pressure Sensors (Left), Pile Report with Both Pressure Measurements (right)

As both values are provided real time (refer to Figure 8), the operator can immediately react as required.

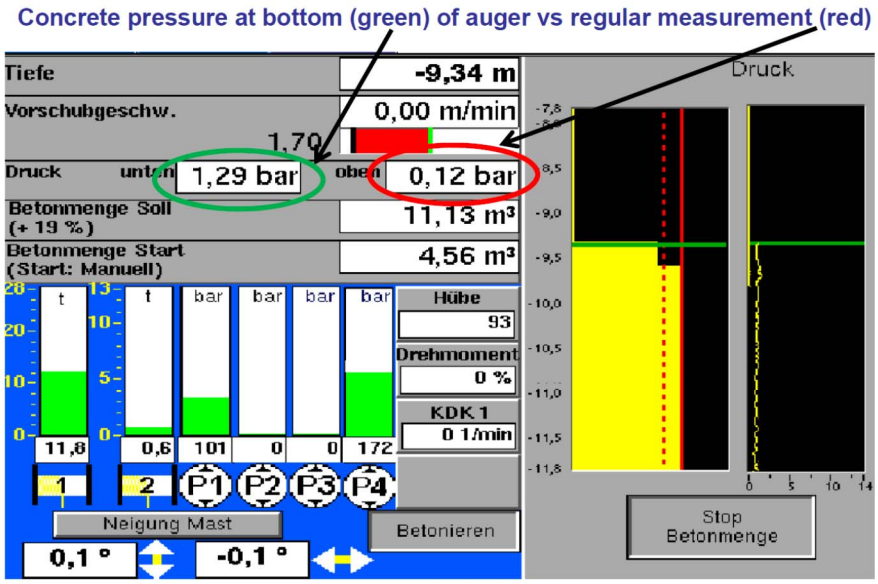


Figure 8: B-Tronic Screen with Both Concrete Pressures in Real Time

Reference Projects for iCFA

Several projects have been carried out using the iCFA system. Two projects in southern of Germany can be serve as examples.

For the first project, the main criterion was to control the concrete pressure. Due to cavities in the weathered lime stone, concrete pressure was restricted to protect nearby water wells.



Figure 9: Installation of CFA Piles Using the iCFA Auger

The use of the iCFA auger was instrumental to completing the job as no real alternative existed. Figure 9 shows the installation of CFA pile on the site. A total length of approx. 10.500 ft (3.200 m) of CFA piles were installed successfully.

The second project required a high demand of verticality control. The installation of a secant pile wall with CFA piles can become difficult and costly if the verticality is not properly maintained. Because the results are not exposed until the excavation begins, CFA pile walls carry some risk that an error will not be discovers until it is too late. With the use of iCFA the verticality can be controlled during the installation process and the operator has the opportunity to adjust earlier if needed. This leads to a reduced risk for leakage due to unacceptable installation tolerances for CFA piles for secant pile walls. A positive result is illustrated in Figure 10, showing a partially excavated secant pile wall.



Figure 10: Partially Excavated Secant Pile Wall Using the iCFA

REMOTE MANAGEMENT: AN EYE ON PROJECTS AND COSTS

The best machine will not help the piling crew if the production on the jobsite is not running smooth. It is essential, to optimize and coordinate the use of people and material. Various people have differing functions. For instance, the operator runs the equipment, the service technician takes care of service and repair, the foreman overseas the production process and maybe takes care of the QA/QC, the site engineer is busy in the jobsite office and the controller is busy with administrative tasks in the main office.

Verification of the production output and quality is essential for establishing an organization's ability to qualitatively and competitively bid and execute construction projects. While today's installed control systems record relevant measured data from both the machine and the production process, the recorded data should be accessible from practically any location.

This is now possible. Anytime, anywhere you can have access via internet to the status of your equipment or the production process via live online display of the operator's screen. A communication overview is shown in Figure 11.

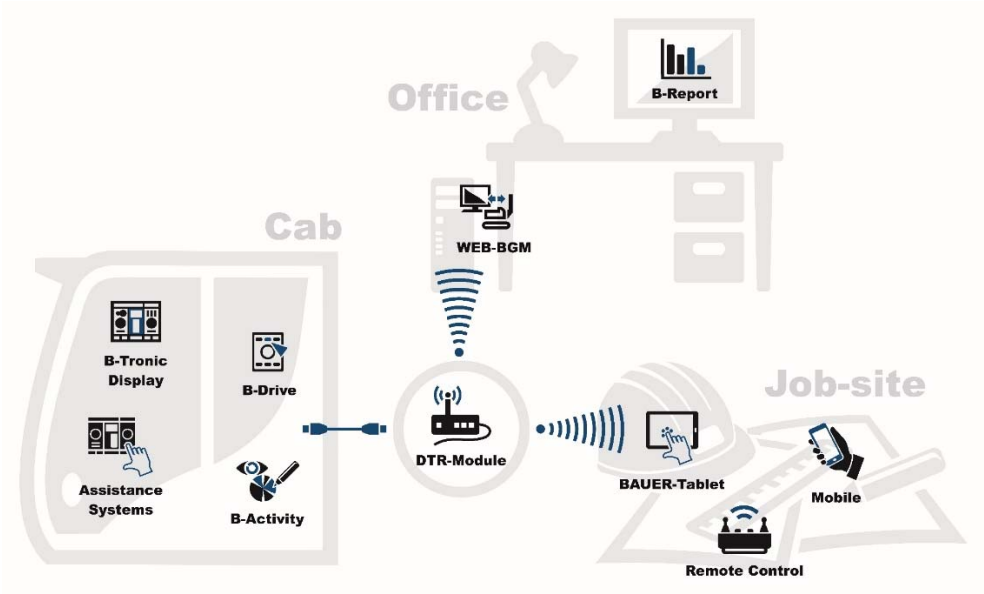


Figure 11: Communication Overview

Because the data is accessible anywhere a reliable internet connection exists, necessary evaluations can be performed locally at the site office as well as at the company's headquarters.

For instance, the user can individually select data and map the entire work process by selecting the correct reporting tools. All machine and production data are documented to illustrate the progress for subsequent verification. The data can be processed into texts, charts, or presentations and the reports can be customized to your design requirements, corporate identity standards, logos and so on.

The online analysis of the machine status outputs warning messages and trouble reports from machines being operated in different locations. Downtimes and problems are immediately detected, thus significantly reducing reaction times. Via the online connection to the operator's screen, experienced staff members can provide remote support.

The analysis is based both on the automatically recorded machine and production data and the data input by the machine operator. This aids overall construction site planning and process optimization and facilitates the timely supply of wear parts. A target-performance comparison of current data provides a more accurate basis for predictions on future projects.

SUMMARY

Real time installation control, data transfer and reporting systems become more important and will serve future demand ensuring the five dimensions of a jobsite. That means not only the three dimensions are covered, but also the dimension of time and money.

The assistant systems will relieve the operator and help to ensure consistent quality. Of course, operator training is required, but the effort to train these additional features is low as these are small add-ons to the general required training to operate such equipment.

In addition, they will provide cost savings potential in form of reduced wear and tear on the equipment as well as a reduction in materials consumption (e.g. concrete). These will, after a reasonable time recover the investment cost that accompany the implementation of these features.

Aside from the assistant systems, developments like iCFA offer opportunities for additional quality assurance and cost savings. References demonstrate the successful implementation of this feature.

The examples shared in this publication represent some of the recent advances in technology available to rising demand for quality control, documentation and competition (in the form of both productivity and reduced labor and material costs). As these demands continue to drive our industry, additional technologic advances and new features will undoubtedly be introduced to the market.

REFERENCES

[1] Sebastian Bauer, Elektronik auf Baugeräten, BauPortal 7/2015

[2] BAUER Maschinen GmbH, BAUER B-Tronic System, 03/2017

[3] Fleming, W. G. K. (1995), The understanding of continuous flight auger piling, its monitoring and control. Proceedings of the Institution of Civil Engineers - Geotechnical Engineering: 157 - 165..

[4] DIN EN 1536, Execution of special geotechnical work –Bored piles

GEO-FOUNDATIONS PROJECT INFORMATION MANAGEMENT SYSTEMS ON A BUDGET

Jamey B. Rosen, P.Geo. Geosyntec Consultants, 130 Stone Road W., Guelph, Ont. Canada, jrosen@geosyntec.com

Keywords: PIMS, verticality, tolerance, koden, database, GIS, visualization

ABSTRACT. As Project Information Management Systems (PIMS) technologies develop, the range of projects to which one can apply these technologies grows while the cost to apply them shrinks. In recent years, technologies previously limited to large "megaprojects" (e.g., major dam rehabilitations) owned by major entities (e.g., the United States Army Corps of Engineers) with large budgets have been applied to smaller projects with less stringent specifications and more modest budgets. This paper will describe applications of PIMS technologies to small projects with limited budgets, including examples from levee construction, small-scale grout curtain installation, and diaphragm and secant pile cut-off walls. We will include a demonstration of how PIMS technologies can effectively analyze verticality data from koden and hydromill data streams to automatically generate models and as-built drawings showing overlap and deviation along the depth of the foundation.

INTRODUCTION

This paper discusses the application of Project Information Management Systems (PIMS) technologies to geo-foundations projects, with a focus on technologies and examples that are in a lower cost range. PIMS technologies allow contractors and other stakeholders to perform efficient quality control on their data, generate quick or automatic reports and as-built drawings, perform analyses to better understand their construction, and ultimately use their data to increase the quality of their construction.

As PIMS technologies are relatively new to the deep foundations industry, and owner specifications on their use are generally viewed as complex and limited to large scale projects, PIMS technologies are frequently viewed as an expensive component that is beyond the scope of a smaller or simpler project. However, the same principles and techniques generally associated with large projects can be applied to projects at smaller scale. Furthermore, as these technologies develop both in the deep foundations and other industries, the cost of application is decreasing quickly making them even more affordable for smaller projects.

The remainder of this paper provides some justification for applying PIMS technologies, describes some scalable data management concepts and workflows and then provides some examples of "low cost" applications of these technologies.

THE NEED FOR A PIMS

Information Management includes the use of databases to store, validate, and organize data; tools to populate the database (e.g., forms and instrument file transfer tools); tools to analyze the data (e.g., statistical and spatial analysis); tools to visualize data (e.g., maps and graphics); and tools to access the data (e.g., interactive websites). Foundation projects require some or all of these tools, and they are frequently applied when there is a specific need driven by one or more factors:

© 2019 Deep Foundations Institute

- Field decision making, including the need for a specific analysis of existing data to determine how to proceed with the next phase of work. For example, analysis of grout take trends across a grout curtain determine where to drill additional grout holes;
- Specification compliance, including the need to quickly to and transparently generate reports and as-built drawings for submission to the owner; and
- Contractual obligation, including the requirement for a contractor to submit organized data in a specific format to the owner.

DATA MANAGEMENT WORKFLOWS

The above principles are generally applied through the design and development of basic workflows that allow data to be collected into a database and then served from the database to models, analyses, visualizations, CAD, and mapping systems. A generic workflow (**Figure 1**) contains three basic categories of activities or objects:

Inputs – data sources either typed into a spreadsheet or form (hand entry); generated from an instrument; or produced from some existing process.

Storage – the database and its components. This consists of a database ("enterprise" if the database is accessible over an intranet or the internet), the Database Management System (DBMS) (which contains the "tools and rules" and automation to facilitate populating the database and serving the data to the outputs), and potentially a document library, which can be a separate database optimized for handling documents.

Access and Outputs – tools to analyze, visualize, and interact with the data in the database.

The following case studies apply each of these items in a basic low-cost manner.

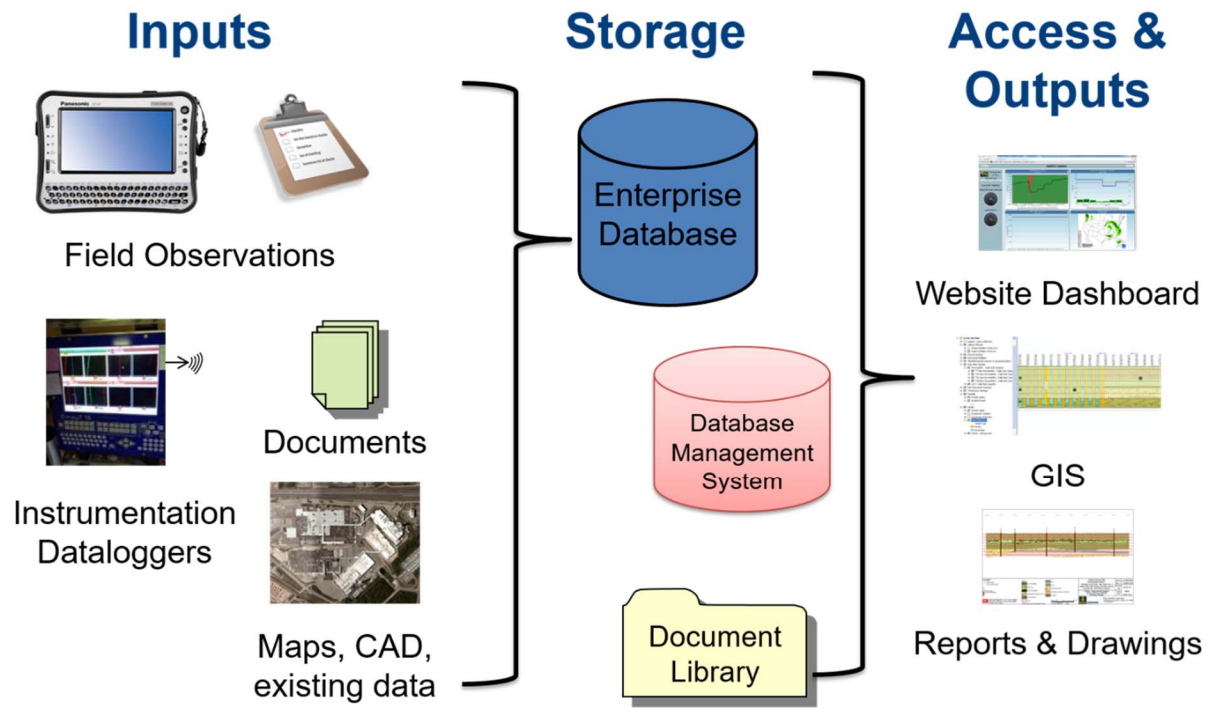


Fig. 1. Generic Data Management Workflow

EXAMPLES AND CASE STUDIES

Slurry Wall – Compression Ring

In this case study, Malcolm Drilling installed an 85 foot deep, 60 foot diameter access shaft the Airport Access Shaft – Gravity Pipeline Project). This reinforced concrete slurry wall consists of 8 slurry wall panels (3 bites per panel), each excavated under bentonite slurry and connected to the next panel with watertight construction joints. The verticality was confirmed using 3 ultrasonic (koden™) surveys per panel.

A small PIMS was developed to capture the as-built excavation data, and quickly generate reports (**Figure 2**) and as-built drawings (**Figure 3**) at multiple depths. In this very simple system, the text files generated by the koden surveys were uploaded to a shared web-based folder (using Dropbox™), from which they were imported into a database that also contained spatial details on the layout and proposed koden survey position. This way as soon as the koden data were imported to the database, a panel report in PDF format was automatically generated and downloaded by the Contractor; and an as-built drawing was automatically exported in AutoCAD format.

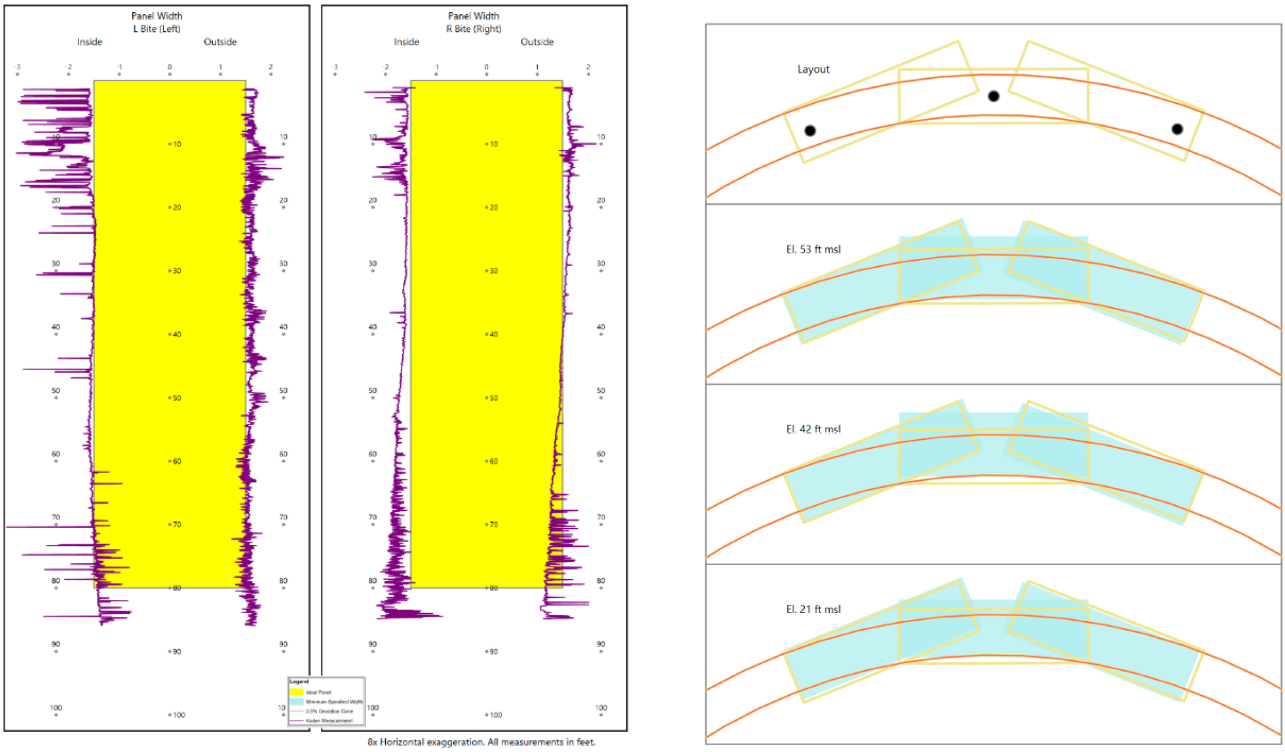


Fig. 2. Excerpts from "Panel Report" showing ultrasonic verticality data in profile and calculated plan view excavation footprints at key elevations

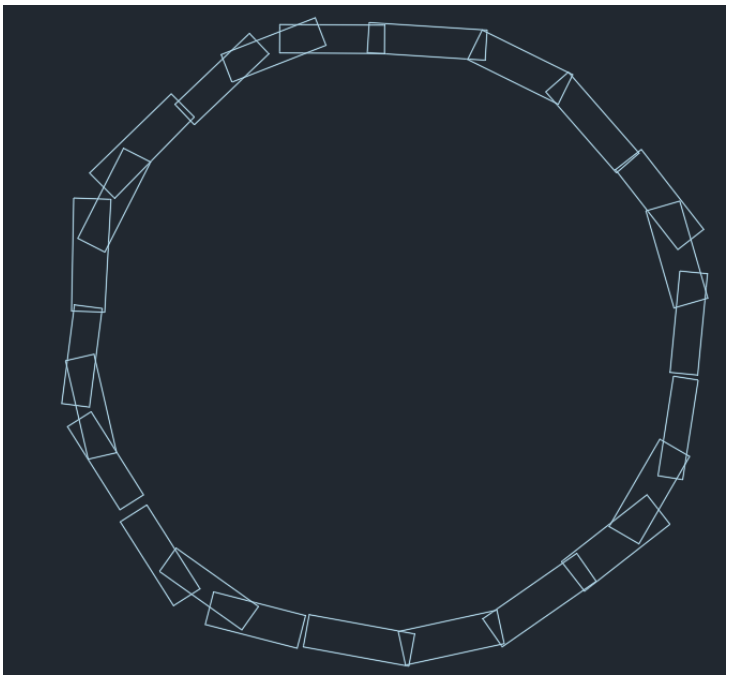


Fig. 3. As-Built Excavation in AutoCAD

Cut-Off Wall with Hydromill Telemetry

In this case study, Treviicos South (TIS) is installing a diaphragm wall as part of the government-owned Herbert Hoover Dike Gap closure project at Lake Okeechobee, Florida. This wall consists of 3-bite primary panels overlapping 1-bite secondary panels that reach depths of up to 80 feet. Bites are excavated with a clamshell and Hydromill rig. Following each bite excavation, TIS personnel export tables containing the X and Y deviation of the Hydromill at several depth intervals, and then upload this file to a web-based PIMS dashboard. TIS also enters some basic data (excavation date, comments, etc) into a web-based table. These Hydromill data and the hand-entered tabular data are then combined into a printable report that TIS uses in their QC process and ultimately submits to the owner. Additionally, the Hydromill data are used to automatically populate a simple interactive webmap, and to generate As-Built CAD files in plan, profile and 3D views.

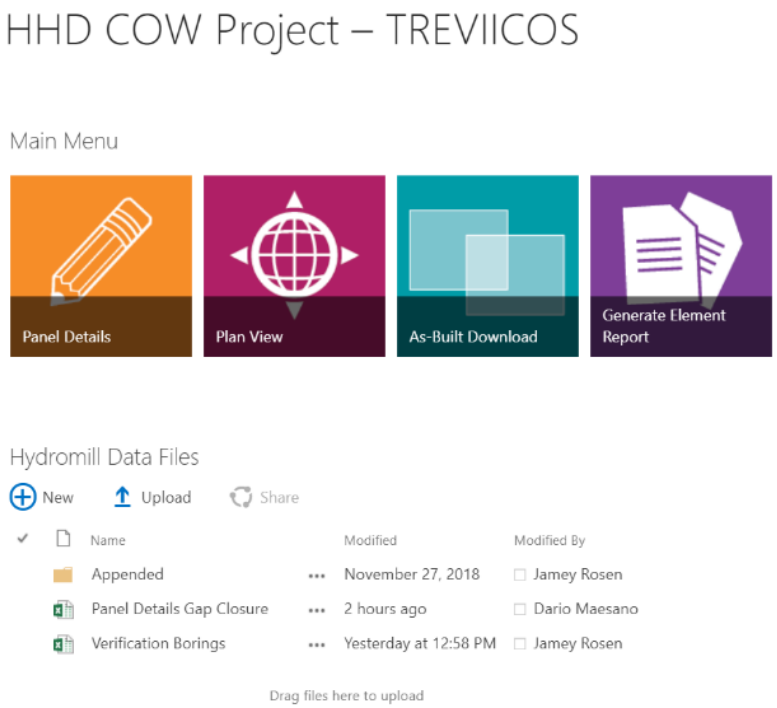


Fig. 4. Website used by Contractor to quickly enter/upload data and generate reports. Hydromill rig position (verticality) files are "dragged" into the website.

Activities on this site follow a simple workflow in which operators export a file generated by the Hydromill on-board rig position software, name the file following a naming convention that includes the panel and bite name, and "drag" it into a website to upload the data to the PIMS database. Following this, the operator enters basic panel information into a web-accessible Excel file (e.g., the first button in the website shown in **Figure 4**), including the date of excavation and any other information desired to show in the panel report (**Figure 5**). Once both these data sources are available, operators can click a button to immediately download a panel report in PDF format and an as-built CAD file showing panel positions at multiple depths in plan and profile views (**Figure 6**). This same information is accessible in an interactive web-based mapping tool (**Figure 7**).

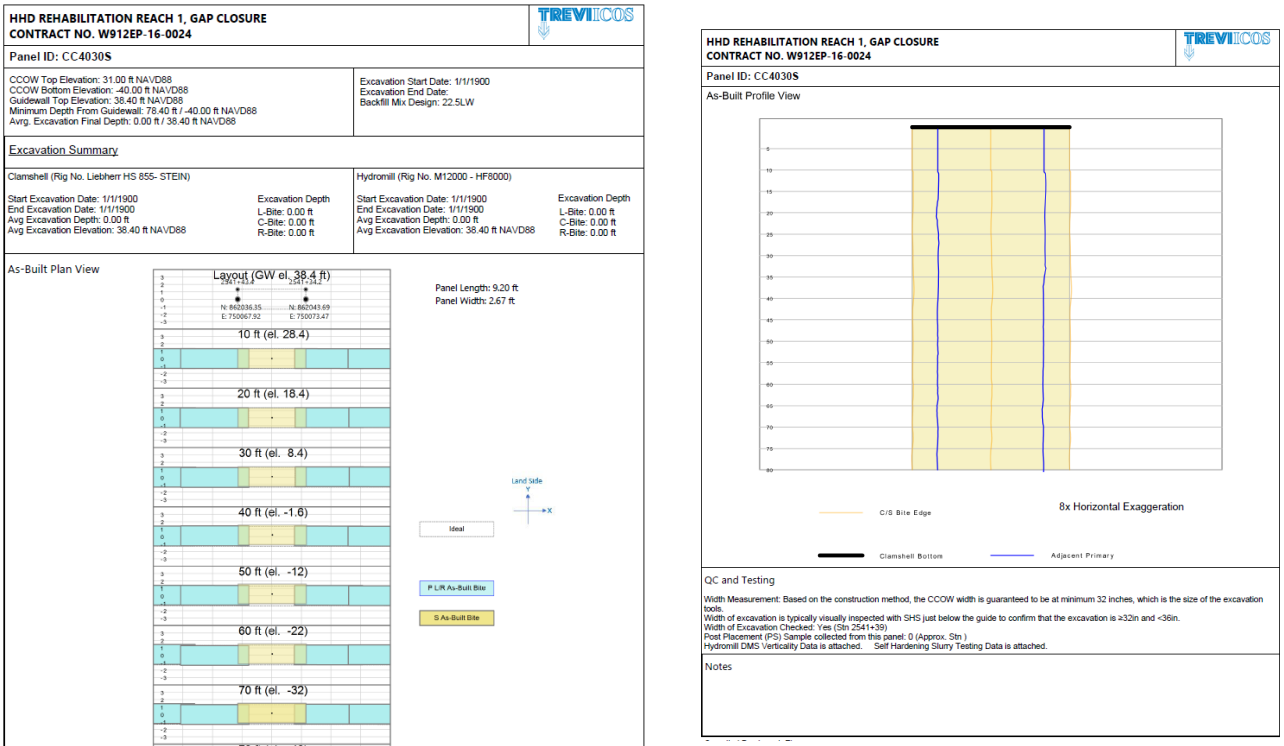


Fig. 5. Example "Panel Report" generated via the website

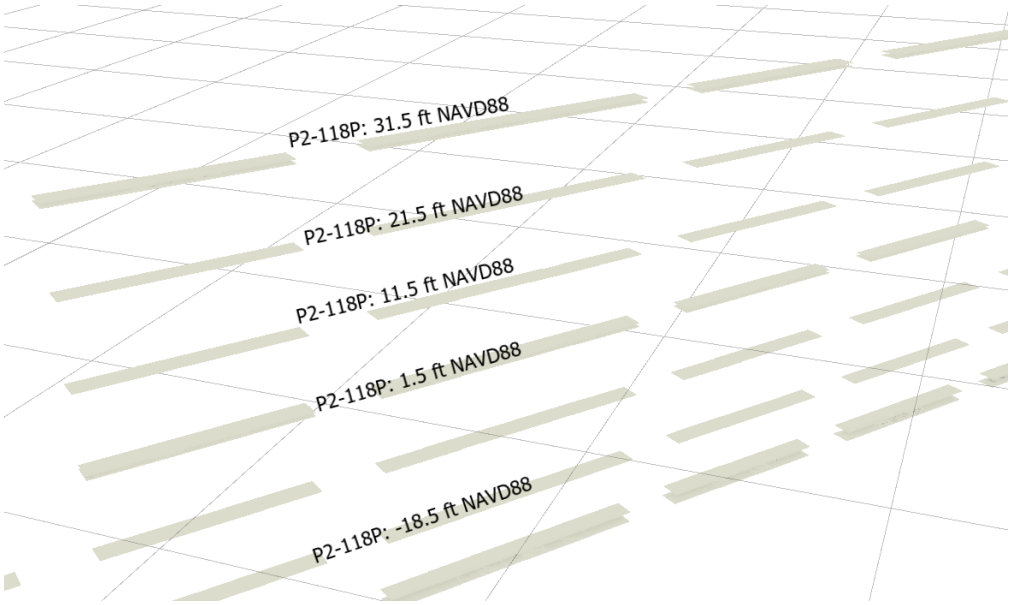


Fig. 6. 3D CAD File produced from Depth "cuts" calculated from Hydromill rig data

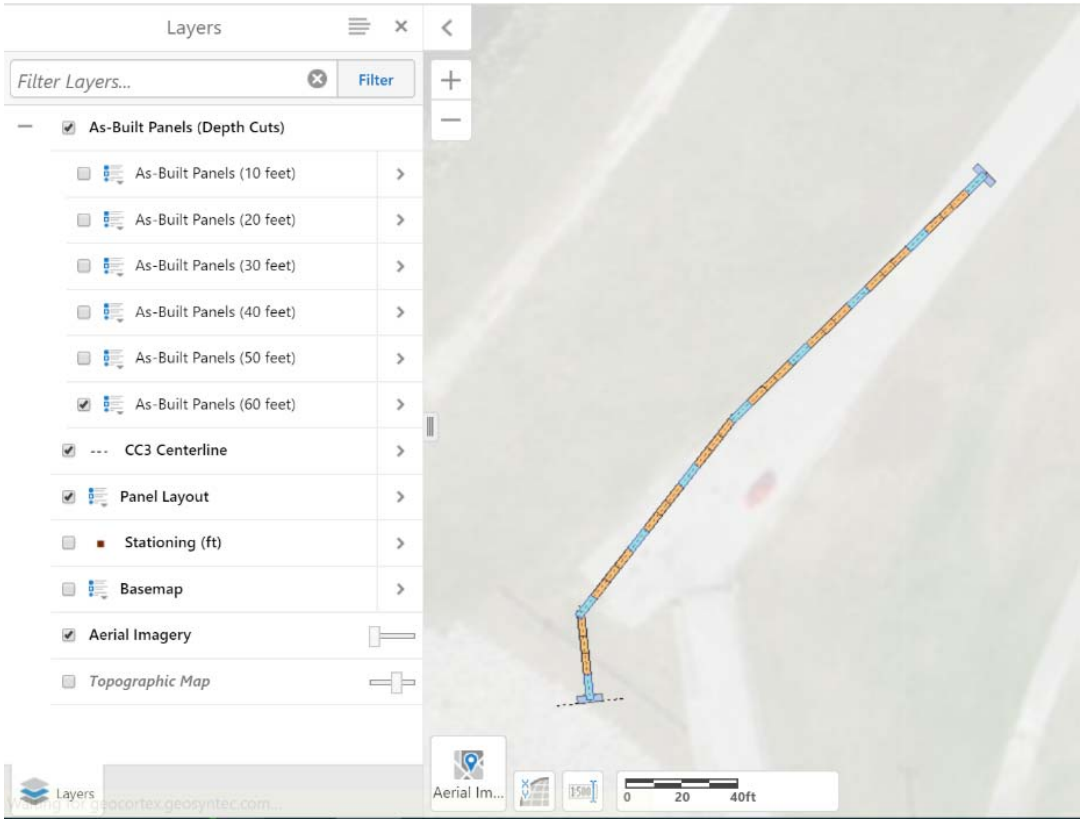


Fig. 7. Interactive web-based map showing depth "cuts" in the context of other site features

Small Grout Curtain

In this case study (based on a 1,200 foot long grout curtain), PIMS principles are applied to compilation and visualization of grout take data read off of a grout monitoring device. For larger projects or when the technology is available, data from grout monitoring devices are generally streamed directly into a database for reporting, however for this example this task is reduced to some simple data entry.

Operators of this site followed a simple PIMS workflow, shown in stages below:

1. Electronic Data Entry of Drilling Details

PointID	HoleDepth	Boring Type	Elevation	Plunge	Bearing	Station	Offset	North	East
S210U	70.7		985.21	-60		212.96		359,940.823	2,264,525.08
S230D	70.8		985.33	-60		226.93		359,947.892	2,264,509.46
S230U	70.6		985.1	-60		232.95		359,936.896	2,264,505.479
S250D	68.4		984.33	-60		248.14		359,943.706	2,264,488.636
S250U	67.4		982.47	-60		251.38		359,933.275	2,264,487.42
S270D	66.7		981.85	-60		268.99		359,939.639	2,264,468.223
S270U	66.6		981.68	-60		270.95		359,929.45	2,264,468.225
S290D	66.3		981.58	-60		289.2		359,935.675	2,264,448.391
S290U	65.9		981.22	-60		290.61		359,925.595	2,264,448.947
S301F20U	59.3		979.85	-70		300.88		359,923.089	2,264,438.965
S301F-20U	59.4		980.03	-70		301.05		359,924.028	2,264,438.618
S301F-40D	73.6		980.87	-50		300.69		359,932.939	2,264,437.218

Fig. 8. Interactive web-based table allowing entry of borehole details

In this stage users populate a simple web-based form (**Figure 8**) with data sufficient to define the geometry of grouting boreholes in a profile dimension. These details generally consist of the borehole

name, location coordinates or station/offset, surface elevation, direction and batter of hole (for inclined holes, common in grout curtains), and total depth.

2. Electronic Data Entry of Grout Takes by Stage

Following the grouting of each borehole stage, the field personnel populate a similar web-based form (**Figure 9**) by selecting the borehole (i.e., from the list linked from the above table), entering the top and bottom depth, and inputting the total grout take for that stage (as well as the associated grout mix design, date/time of grouting, and any other applicable details):

BoreholeID	Top_depth_ft	Bottom_depth_ft	Injected_Volume_gal
P000D	15.8	34.3	1.07
P000D	34.3	64.4	1,078.72
P000U	12.5	23.3	2,021.11
P020D	15.5	32.8	429.82
P020D	15.5	37.7	1.25
P020D	23	35.9	0
P020D	32.8	46	1,654.3
P020D	37.7	67.7	33.36
P020U	13.8	30	2,180.1

Fig. 9. Interactive web-based table allowing entry of grout stage details

As with other examples of web-based forms discussed above, any data entered into these forms are immediately sent to a database which, in turn, immediately serves the data to the tools and reports described below.

3. Visualization of Grout Takes in Profile View

Given the geometry calculated from the first table and the grout takes by stage entered into the second, the above information is sufficient to immediately visualize grout takes in profile view (a common way of assessing a grout curtain). A web-based interactive Geographical Information System (GIS), or simply GIS-produced PDFs sent to an owner, can be used for this visualization (**Figure 10**):

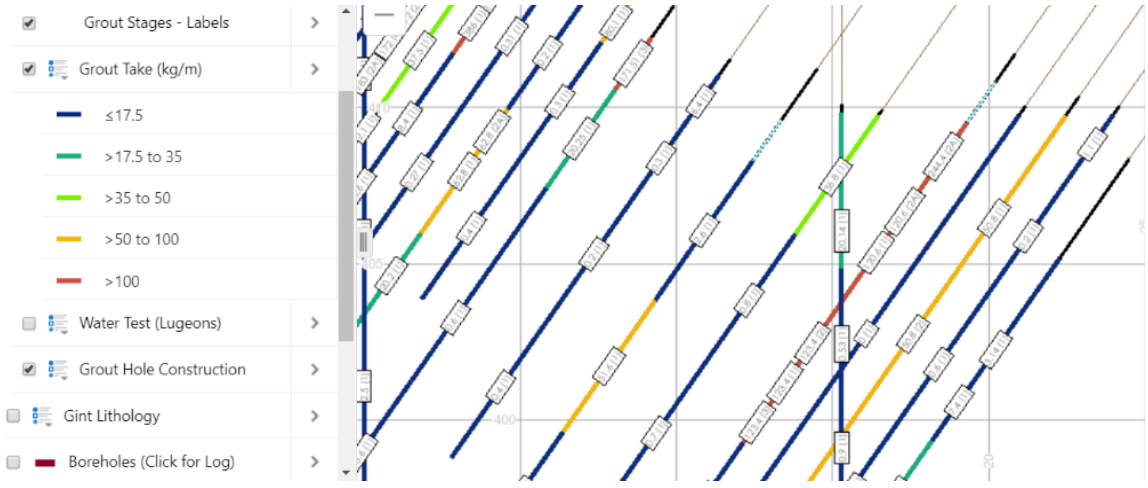


Fig. 10. Interactive web-based profile showing grout stage data

4. Automatic Generation of Grouting As-Built

Once in the GIS, these data (i.e., the grout stage geometry and grout take values) are automatically and routinely printed to paper/PDF or exported to CAD (or MicroStation) format for submission as As-Built or Progress Drawings.

5. Reporting of Grout Closure and Pay Items

Frequently grout curtain data are reported in terms of "grout closure" (total grout take by hole series); progress (number of stages grouted as a function of the total proposed) and total grout placed. These (and any other metrics calculable from the entered data) are generally available as a database report (**Figure 11**) on a website and/or electronically transmitted on a routine basis to the contractor and owner:

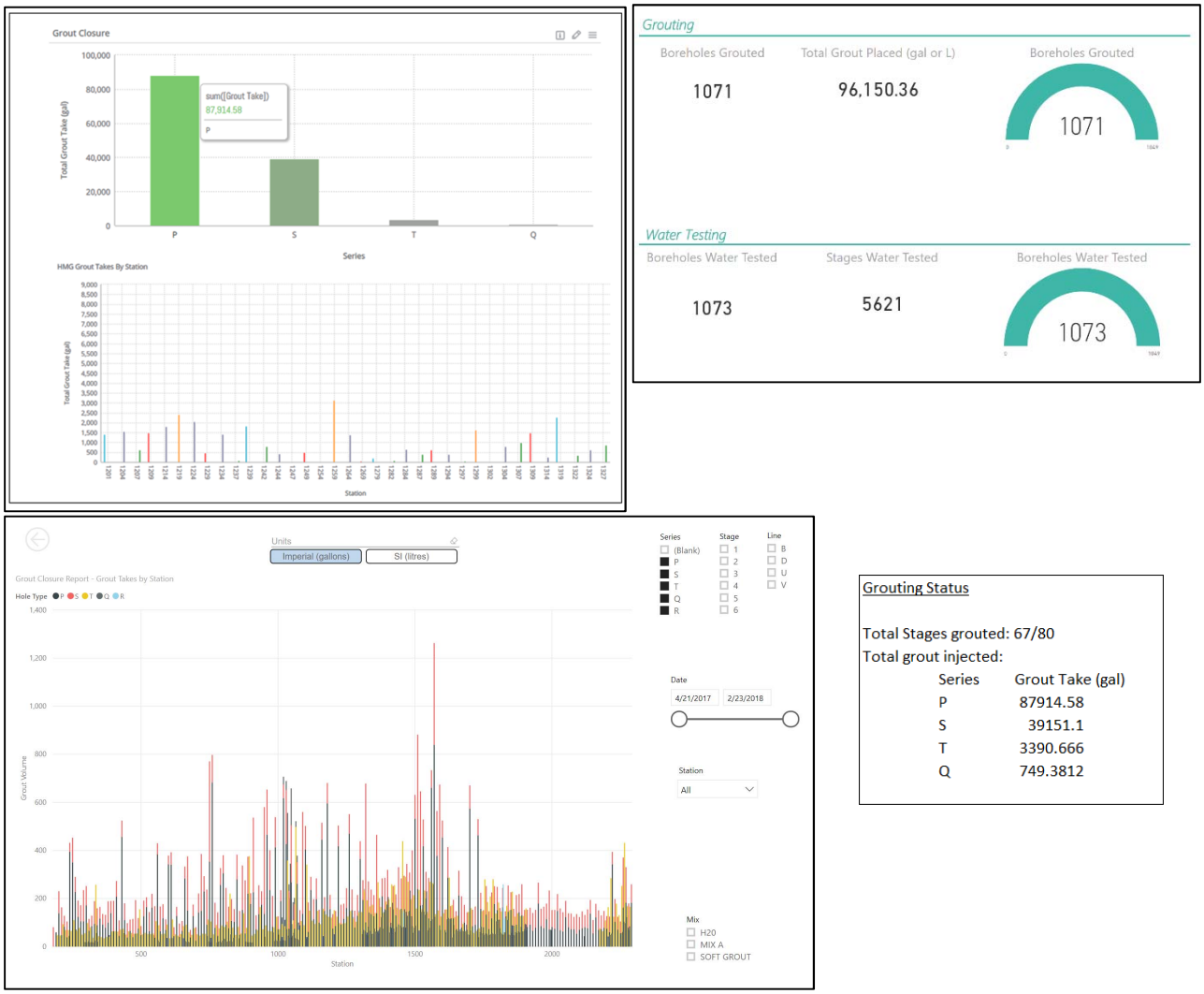


Fig. 11. Interactive web-based reports showing grout information in real time

PIMS PROCUREMENT AND COST

PIMSs like those described above are predominately services as opposed to software, in that they generally can not be purchased "off the shelf", but rather are developed and maintained by one or more data management professionals with sufficient background in geospatial database technology and the particular deep foundations concepts applicable to the given project. These professionals can be hired "in house" or retained as contractors. Several geotechnical contractors are currently providing these services to the industry.

Although these technologies require specialized skills to develop and manage, the computer (software) technologies used are generally inexpensive (e.g., an enterprise database can be rented from a cloud computing provider for only a few dollars per month) or open source (i.e., not requiring any software licensing fees). These systems can usually be developed using industry-standard or non-proprietary software, allowing significant sharing and reuse by contractors. Importantly, where possible these systems can be "transparent" in their data sources and calculations, facilitating peer review or audit by owners.

The cost of a PIMS is entirely dependent on the number of data sources ("streams") involved (e.g., a single grout monitoring device vs. a series of disparate field forms and instruments), the duration of construction (as PIMSs often require a monthly or weekly maintenance fee), and the nature of any associated specifications (i.e., some projects require a Data Management Plan or other submittals). The projects described above range in cost from US$15,000 to $40,000, including a development/deployment fee of about 80% with the remainder as the ongoing maintenance fee.

CONCLUSIONS

Project Information Management Systems are a crucial component of the analysis, documentation, and quality control components of a construction project. Today's PIMS technologies include field data entry forms, geospatial visualization tools, interactive data query tools, automated report and as-built drawing generators, and interactive web-based dashboards. PIMSs operate by facilitating field data entry (e.g., via a mobile device, spreadsheet, or web-based form) and combining these data with data downloaded or streamed from instruments, drill rig monitors, etc.; visualizing all data in a common context, often including a planimetric, profile, or three-dimensional geospatial view; and serving these data to formatted reports, interactive tools, and CAD-based drawings.

Historically these technologies were primarily used on, or even limited to, large-scale projects with significant owner oversight. However, the data management principles that drive a PIMS apply to data at any scale, including small or inexpensive foundation work. The web, database, and geospatial technologies described in this paper have matured to the point that they can be cost-effectively applied to small projects. With good data management tools and templates borrowed from larger projects, these smaller projects can benefit from the same efficiency and quality improvements required by owners at the larger scale.

TODAY'S CONNECTIVITY: USING HISTORICAL DATA TO ANTICIPATE FUTURE RISK

Michael Frawley
Terracon Consultants, Inc., Raleigh, North Carolina
(919) 436-2987
michael.frawley@terracon.com

Jessica Turner
Terracon Consultants, Inc., Salt Lake City, Utah
(719) 572-7698
jessica.turner@terracon.com

Deana Ruud
Terracon Consultants, Inc., Olathe, Kansas
(913) 202-7546
deana.ruud@terracon.com

ABSTRACT

Technology is allowing for new ways to mitigate risk associated with subsurface exploration and unanticipated subsurface conditions during construction. Unanticipated subsurface conditions have the potential to force delays and cost overruns on even the best-managed and well-executed projects. For more than a century, geotechnical professionals have documented the location and conditions encountered in hundreds of thousands of subsurface borings. Utilizing processes for compiling and managing data, owners can streamline site selection and receive access to a conceptual geotechnical model before field exploration takes place. Digitizing historical subsurface information allows for creation of an interactive, web-based platform combining publicly available information and culminating with the opinion of a local, experienced geotechnical engineer. This connectivity aids in the reduction of risks associated with unknown conditions on prospective project sites. Through this conceptual project study, we demonstrate how a project owner would be able to use a comprehensive desktop study to review the expected conditions prior to making a purchasing decision. Following the purchase, the expected conditions would be confirmed through traditional methods, confirming potentially problematic site conditions and the associated risks.

Keywords: Subsurface, Site Conditions, Geotechnical, Site Selection, Risk Mitigation, Innovation, Big Data, GIS, Methods Consulting

© 2019 Deep Foundations Institute

INTRODUCTION

Preliminary project planning is often based on assumptions made by the design team with regards to site suitability. After due diligence, site development is traditionally initiated by the owner or the owner's representative when engaging a geotechnical engineer to perform a thorough subsurface exploration at a site. The data generated by the geotechnical engineer's analysis of the site is required to design foundations, pavements and earth retaining structures and move the project from concept into design. This necessary, subsurface exploration can be time consuming, intrusive, and require significant resources, often when resources during construction seasons when resources are most limited.

By leveraging historical data generated from previous subsurface exploration, a more thorough analysis of project risk can be developed prior to mobilizing a drill rig. Ultimately, preliminary budgets and designs are more accurate and geotechnical field exploration is more strategic. The geotechnical engineer's role transforms from raw exploration and analysis to confirmation of anticipated conditions.

For this conceptual project study, we refer to a hypothetical commercial development in Colorado with significant variability in potential site conditions and the escalated potential costs associated with that variability. In our scenario, project planning will be assisted by identifying potentially problematic zones within the site and the implications those zones will have on project completion. During the analysis for our hypothetical project, conceptual geotechnical models will be generated based on historical geotechnical data in the area, publicly available GIS data and the experience of local professional engineers. These conceptual geotechnical models will be the basis for site selection and the subsequent tailored site exploration strategy.

INITIAL CONCEPT

Our hypothetical project includes a six-story structure with basement which will serve as the anchor of a larger master-planned development. Additional site development associated with the initial phase of construction includes retaining walls and a five-story parking deck designed to accommodate a future sixth-level of parking. Successive phases of construction include multiple additional parking decks, multi-story commercial development, and low-rise retail development.

The project will be initiated by the site selection process and our utilization of historic data to aid the client in site selection. An integrative plan will be developed to manage the site selection process and tailor a program of site characterization that would build on the preceding site exploration to avoid repeating exploration for subsequent phases of construction.

DESKTOP STUDY

Due to the high likely variability of subsurface conditions underlying the various parcels, a report of expected conditions would be prepared that referenced historical geotechnical data, publicly available Geographic Information System (GIS) data and the experience of local professional engineers. The intent of this desktop study would be to conceptually model the subsurface conditions across the site and discuss the implications that those anticipated subsurface conditions would likely have on future site development.

For our hypothetical project, data was compiled from 14 historical geotechnical projects within one-mile of the site. Due to the quantity and quality of previous geotechnical investigations near the potential site (Figure 1. Nearby Historical Geotechnical Data), Terracon is able to anticipate subsurface conditions, and the associated impacts that those conditions would have on eventual development of the site, with a high level of confidence.

The historical geotechnical data in the vicinity of the site and possessed by Terracon was produced over a span of about 30 years and contained multiple projects and the associated boring logs, Standard Penetration Test (SPT) N-Values, various modulus values, soil classifications, laboratory test results and other geotechnical considerations. These data were reviewed by the local geotechnical engineer and summarized in the creation of conceptual geotechnical models for the hypothetical project parcel(s).

A Conceptual Geotechnical Model (Figure 2. Conceptual Geotechnical Model) was prepared to estimate anticipated lithology at the site and provide initial insight for foundation design concepts and potential subsurface condition challenges associated with development.

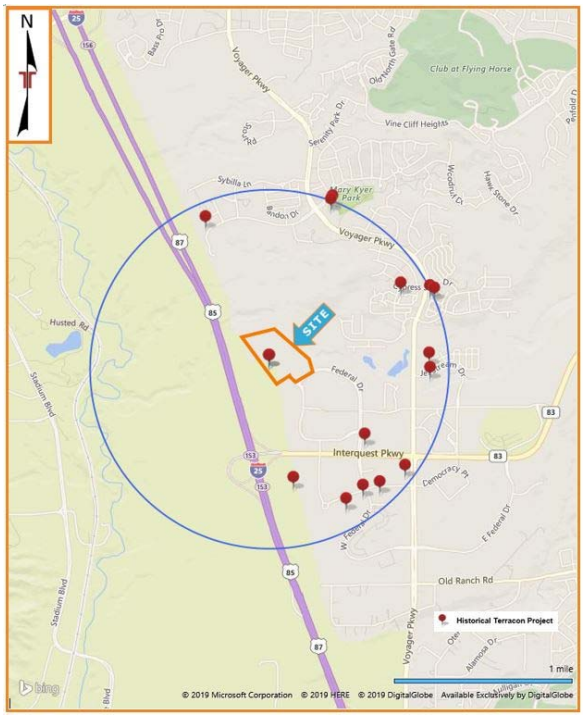


Figure 1. Nearby Historical Geotechnical Data

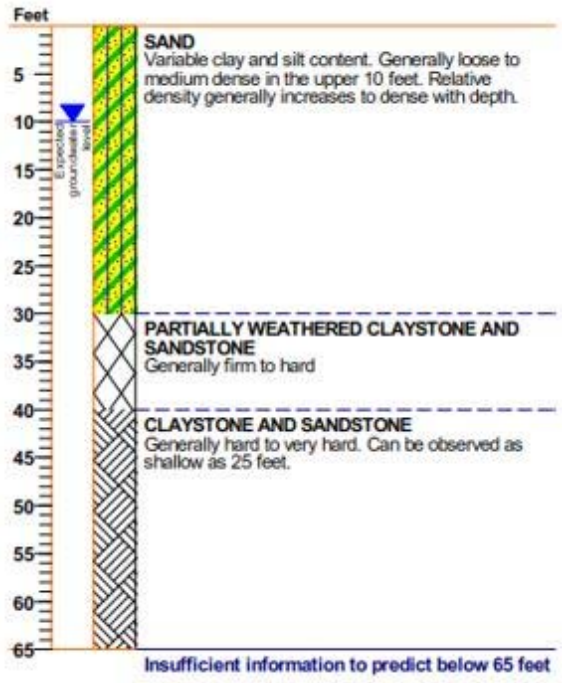


Figure 2. Conceptual Geotechnical Model

FOUNDATION DESIGN CONCEPTS

Based on anticipated subsurface conditions, it was apparent that shallow foundations would not provide adequate support of the hypothetical structural loads if bearing on conventional structural fill. Furthermore, extending shallow foundations to bear directly on the Partially Weathered Claystone and Sandstone was not considered feasible based on the anticipated depth of rock. Conceptual design information for our hypothetical project generated downward structural loads of up to 1,250 kips. For structural loads of this magnitude and the anticipated subsurface conditions, a deep foundation system would be appropriate.

With an initial design assumption made to support the structure on a deep foundation system, attention turned to the integrity of the Partially Weathered Claystone and Sandstone materials presumed to underly the site. Our recommendation would be to perform core and pressuremeter testing within the bedrock formation to better delineate rock integrity and support characteristics.

Pressuremeter testing would provide in-situ data that may allow for an increase in allowable bearing capacity and skin friction compared to conventional drilling and SPT; thereby potentially reducing the length and diameter of deep foundations and thus the costs associated with a deep foundation system.

Because hypothetical future development of the site included multiple buildings and loading scenarios, shallow foundation support on modified ground improvement (such as rammed aggregate piers) was not eliminated from consideration. Subsequent exploration of the site was tailored to obtain the necessary design data should ground improvement be warranted for future phases of development.

Our hypothetical site is situated in an area that typically produces as Seismic Site Class C or D. Based on the local geotechnical professional's knowledge of the area, conventional soil drilling and sampling might not provide adequate information to confirm a Seismic Site Class C. Seismic refraction testing would be recommended to obtain the necessary shear wave data to evaluate the potential to increase the seismic site class from a Site Class D to a Site Class C.

CONCEPTUAL CONSTRUCTION CONSIDERATIONS

Based on the expected conditions report, groundwater would be anticipated at a depth of approximately 10 feet below existing site grades. Furthermore, the residual soils would be anticipated to consist of generally loose to medium dense sands. Potentially difficult excavation and dewatering would likely impact site development. Historical aerial imagery of the selected parcel(s) indicated that remedial site grading had been previously performed within portions of the site. Specifically, the site contained an existing detention pond that would be of concern due to the presence of loose, saturated soils. Of particular concern would be areas where the proposed building(s) and site development elements would be oriented directly above the former pond. Subsequent specialized exploration of the pond area would be recommended to evaluate the potential for excessive settlement associated with the wet, loose soils.

For our hypothetical project, a preliminary site grading plan was prepared to indicate fills between 10 to 18 feet in thickness. The settlement of deep fill zones, in addition to settlement of underlying on-site soils would need to be considered. Settlement monitoring pins would be recommended after placement of fill materials and prior to construction of foundations and slabs, placement of ancillary structures and flatwork.

DESKTOP STUDY CONCLUSION

The expected conditions report would be able to anticipate potential development challenges in the subsurface conditions prior to the owner purchasing the property. After deliberation and negotiation, the owner would be able to proceed with purchase of the property and implementation of the recommended exploration plan, consisting of:

- SPT borings to depths ranging from 30 to 65 ft within the proposed buildings and parking garages and to depths ranging from 5 to 10 ft within the proposed parking lots.

- Geophysical study: A geophysical field survey will include Seismic Refraction testing by Refraction Microtremor (ReMi) methods using 24 geophone arrays to measure S wave velocity. At least one energy source location off each end of the spread will be utilized. The geophysical survey would be performed at the location of the proposed six-story Building and Parking Garage.

- Pressuremeter Testing: Based upon the proposed construction and relatively high structural loads, pressuremeter testing was recommended to better define the engineering strength characteristics of the underlying rock. These consisted of three tests in the recommended 65-ft deep borings in the proposed building and parking garage.

The desktop study would be concluded in three days' time, with initial site data reported to the project owner within one day. The delivery timetable and level of confidence estimate would allow the project owner to move forward with site acquisition and project planning transitioning into traditional site exploration with an increased level of confidence.

TRANSITION TO TRADITIONAL GEO

With the desktop study having identified potential site challenges and problematic portion(s) of the site, full-scale site exploration commenced. Exploratory drilling would consist of SPT borings advanced to depths ranging from 5 to 65-ft below site grades in addition to Seismic Refraction testing and pressuremeter testing of the underlying rock.

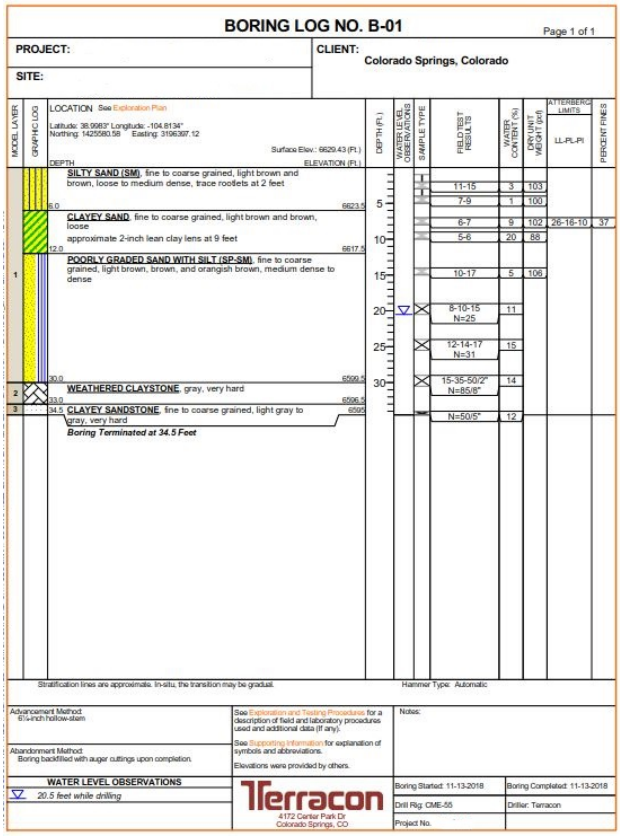


Figure 3. Boring Log B-01

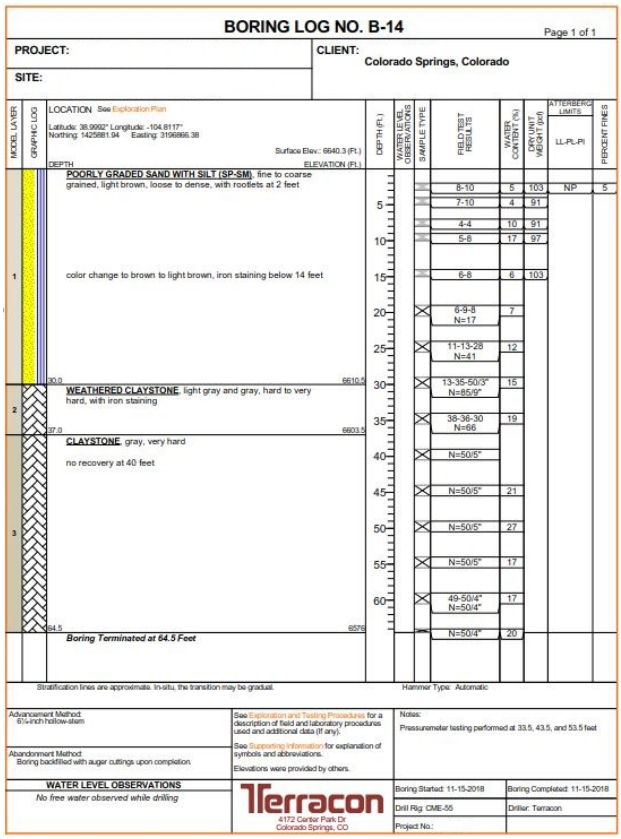


Figure 4. Boring Log B-14

The results of the geotechnical exploration would then be compared to the anticipated lithology generated by the Conceptual Geotechnical Model (See Figure 2. Conceptual Geotechnical Model).

Pressuremeter testing would be performed at three locations to better define the engineering strength characteristics of the underlying bedrock. Pressuremeter testing would be performed using a TEXAM Pressuremeter (Figure 5. Pressuremeter Test Results).

Based on the selected structural loads and results of exploratory borings, shallow foundations would not be recommended when bearing on site soils or conventional structural fill.

Support of structures on deep foundations bearing within the underlying bedrock formation would be recommended. Options for deep foundation systems include: drilled shafts; auger cast-in-place; H-piles, and helical piers. Preliminary design recommendations would be provided for helical piers based on conversations with specialty designers.

Exploratory borings for our hypothetical project did not encounter existing fill soils; however, based on historical site imagery, it appears that remedial site grading has been performed at this site in the past, particularly within the existing detention pond.

In addition to the SPT borings, a geophysical field survey would be performed using Seismic Refraction testing by Refraction Microtremor (ReMi) methods for Seismic Site Classification (See Figure 6. Shear Wave Profile).

The results of the Seismic Refraction testing indicate an average shear wave velocity of 1,310 feet per second to 100 feet. The resultant average shear wave velocity indicated a Seismic site classification of C was appropriate for the site. Seismic site classification was based in general accordance with the 2018 International Building code, which refers to ASCE 7-16.

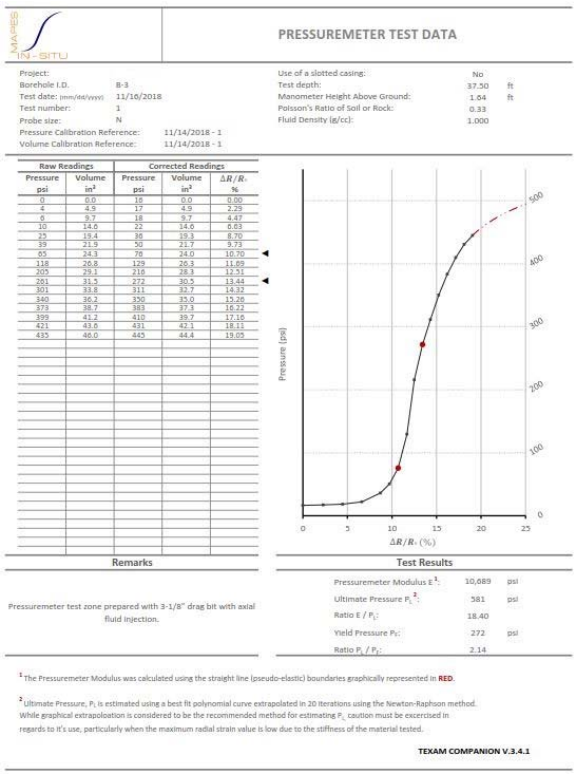


Figure 5. Pressuremeter Test Results

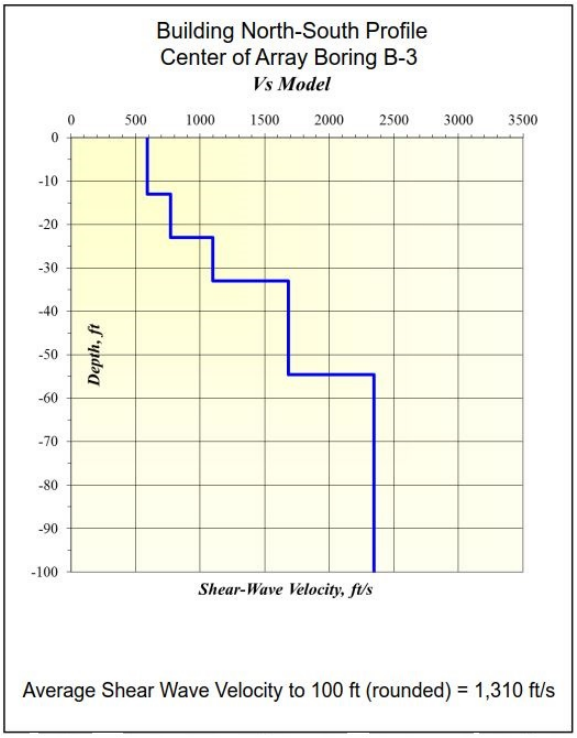


Figure 6. Shear Wave Profile

GROUND IMPROVEMENT

As an alternative to supporting the future phases of construction on deep foundations bearing within the underlying bedrock formation, consideration would be given to ground modification/improvement techniques to improve strength and compressibility characteristics of the foundation soils and to allow for support of the structures on shallow foundations.

Based on our analysis of the parcels, maximum allowable bearing capacities of 6,000 to 7,000 pounds per square foot (psf) are deemed possible with the installation of properly installed aggregate piers. Aggregate piers extending to depths up to 20 ft below foundation bearing elevation would likely be necessary to achieve these allowable bearing capacities. Further detailed analysis and design would be performed by specialty foundation contractors based on the results of the subsurface exploration.

We would also recommended discussions include the potential for adding the sixth level to the parking garage at a future date, and that the addition of this level will not cause unsatisfactory differential movement of the structure as a whole.

DEEP FOUNDATIONS

Although ground improvement was deemed a viable alternative for future phases of construction for our hypothetical project, a deep foundation system extending to rock was selected for support of the six-story structure and five-story parking deck. Based on the provided loading, deep drilled shaft or auger cast pile foundations would be recommended.

Soil design parameters would be provided for the design of deep foundations. The values presented for allowable side friction and end bearing include a factor of safety (Figure 7. Drilled Shaft Parameters). We recommend neglecting skin friction for the upper 30 inches of foundations because of the effects of frost penetration and potential for disturbance.

Drilled Shaft and Auger Cast Pile Design Summary [1]

Stratigraphy [2]		Allowable Skin Friction (psf) [3]	Allowable End Bearing Pressure (psf) [4]
GeoModel No.	Material		
1a	Sand (compacted structural fill)	150	End Bearing within Sand Soils Not Recommended
1b	Sand (upper 10 feet of native profile)	100	End Bearing within Sand Soils Not Recommended
1c	Sand (native profile below upper 10 feet)	130	End Bearing within Sand Soils Not Recommended
2	Weathered Claystone and Sandstone Bedrock	1,500	35,000
3	Claystone and Sandstone Bedrock	2,000	50,000

1. Design capacities are dependent upon the method of installation, and quality control parameters. Skin friction values should not be used within the soil profile if slurry or other "wet" shaft techniques are used for installation.
2. See **Subsurface Profile** in Geotechnical Characterization for more details on stratigraphy.
3. Applicable for compressive loading only. Reduce to 2/3 of values shown for uplift loading. Effective weight of pile/shaft can be added to uplift load capacity.
4. Piles/shafts should extend at least 5 feet into the bearing stratum for end bearing to be considered.

Figure 7. Drilled Shaft parameters

Parameters would also be provided for lateral loading evaluation in LPILE (Figure 8. LPILE Parameters). The provided lateral parameter design values do not include a factor-of-safety, which should be applied. We recommend neglecting lateral resistance for the upper 30 inches of foundations because of the effects of frost penetration and potential for disturbance.

Stratigraphy [1] GeoModel No.		L-Pile Soil Model	S_u (psf) [2]	ϕ [2]	γ (pcf) [2]	ε_{50} [2]	K (pci) [2]	
							Static	Cyclic
1a	Sand (compacted structural fill)	Sand	---	32°	125	Allow L-Pile to choose these parameters based on the undrained shear strength or friction angle provided in this table.		
1b	Sand (upper 10 feet of native profile)	Sand	---	32°	120[3]			
1c	Sand (native profile below upper 10 feet)	Sand	---	34°	120[3]			
2	Weathered Bedrock	Stiff Clay w/o Free Water	4,000	---	125			
3	Bedrock	Stiff Clay w/o Free Water	5,500	---	130			

1. See **Subsurface Profile** in Geotechnical Characterization for more details on Stratigraphy.
2. Definition of Terms:
   S_u: Undrained shear strength
   ϕ: Internal friction angle,
   γ: Moist unit weight (above groundwater), Saturated unit weight (below groundwater)
   ε_{50}: E50 strain
   K: Horizontal modulus of subgrade reaction
3. Saturated unit weight value of 57 pcf should be used below water table for sand soils.

Figure 8. LPILE Parameters

ALTERNATE FOUNDATION TYPES

Steel H-piles driven into the bedrock to virtual refusal would be considered an acceptable alternative to drilled piers or auger cast piles. Virtual refusal criteria, as defined by the Colorado Department of Transportation Standard Specifications for Road and Bridge Construction, is no more than one inch of penetration for the final ten blows. This virtual refusal criteria would need to be specified for construction. Because of driving the piles to virtual refusal, we did not recommend using skin friction values in combination with end bearing capacity.

A helical pier foundation system would be considered suitable for support of select structures depending on final axial, lateral, and uplift loads. For multiple helix plates, the plates should be spaced no closer than three (3) times the diameter of the upper helical plate.

Vertical capacity of helical piers is typically based on torque achieved during installation, helical plate size, and shaft type. The pile capacity was to be determined through the results of the load tests correlated to helical pier installation torque.

To develop adequate capacity, helical piers would need to bear on or within the claystone and sandstone bedrock identified near depths of 20 to 30 ft. Based on the observed site conditions, there is a potential for the helical piers to "spin-off" at the top of the bedrock and may not fully penetrate the bearing stratum. When "spin-off occurs", torque correlation can no longer be used to estimate or verify pier capacity. "Spin-off" on competent bedrock may be an acceptable termination criterion; however, full-scale, on-site load tests would be required to verify capacity.

Helical piers are a proprietary product and should be designed and installed in accordance with the manufacturer's recommended procedures by a contractor with experience in pier installation. We would recommend that pile load testing be performed on test piers be used to verify proper torque for anticipated structural loading conditions will be achieved prior to full scale installation.

CONCLUSIONS

Can predicting subsurface conditions with vast public domain data, historical geotechnical data, and local experience eliminate the risks that are inherent in development? No. But bringing this information and expert opinion to the design team earlier provides a major step forward in the development of realistic conceptual designs for more precise (and less conservative) budget estimates. Furthermore, technological advances are creating an industry environment where project team members can access valuable information in seconds via internet-based knowledge sharing services. The time it takes to obtain preliminary geotechnical information via traditional methods is unsustainable by comparison.

The method employed by this conceptual project case study is an evolution of an engineer's local experience being relied upon to predict subsurface conditions at sites yet unexplored. Engineers have utilized this method out of necessity for decades with varying degrees of success. The approach outlined in this paper represents a shift in the geotechnical engineer's role on a project. No longer are subsurface conditions completely unknown prior to performing subsurface exploration. By creating and utilizing an expected condition report the exploration schedule is shortened and provides a preliminary understanding of site conditions not previously available to the owner, ultimately reducing the unknown risk of subsurface conditions.

UTILIZING DRONES TO IMPROVE PROJECT WORKFLOWS

Barritt Lovelace, PE
Collins Engineers, Inc.
blovelace@collinsengr.com
651-341-4039

Abstract

Collins Engineers has been researching and implementing the use of drones on Civil Engineering Projects since 2015. Applications include bridge inspection, asset management, mapping, construction site management and emergency response. Recently this technology was used to map and model construction sites with deep foundations to verify and quantify designs.
The ability to collect and use large amounts of data is transforming our world. Drone hardware and software is being used to capture and digitally replicate assets, giving owners unprecedented ability to visualize and manage their projects. Our teams help owners collect and process drone data into deliverables to be analyzed, annotated, stored, and shared. The use of drones can transform the way projects are managed and can improve project workflows. Data collected with drones can be processed into a digital twin of any project site or asset. This digital twin provides owners with a three-dimensional geometrically and geospatially accurate model. These models can be annotated and tagged with information that can be stored and shared locally or on cloud-based platforms. The data can be exported and used in a wide variety of CAD and GIS platforms.

Goals

When considering the use of UAS for several items need to be considered when establishing project goals.

Safety

Drones can be used to reduce job site safety risks in two ways. The first is that use of the drone can remove personnel from harm's way. Surveyors and other project staff will traditionally walk the site to collect survey and other site information. These efforts can be replaced with the use of a drone eliminating much of the need for personnel to be on the job site itself which improves safety. The other way safety can be improved is that a digital model of a job site can be created on a daily or weekly basis that can be quickly analyzed for safety hazards. This analysis could be done remotely by safety officers to identify job site hazards which can then be corrected before injuries happen.

Improved Deliverables

Perhaps the most important reason to incorporate drones into project workflows it the ability to improve the project deliverables. Drones have the ability to quickly collect large amounts of high quality data which can be processed into orthomosaics, point clouds and 3D models that give engineers and project managers the information they need to make better decisions on design or project management.

Cost Savings

Drones are a form of automation which has the potential to reduce project costs. By eliminating or reducing the need for personnel to visit the site to collect data cost savings are realized. More importantly cost savings can be realized in the ability of engineers and project managers to make better decisions and avoid costly errors. For instance, a project manager can use the 3D site models to measure distances to help choose what equipment fits on the site and what equipment is best suited for the site conditions. An example

© 2019 Deep Foundations Institute

would be the ability to choose a crane location and verify crane reach to ensure the correct crane is used on site.

Equipment

Utilizing commercial quality hardware to collect data is critical to the success of projects. Utilizing professional high-quality hardware is important and has the following advantages:

- Improved reliability
- Improved data quality
- Advanced mission planning features
- Integration with post processing software

TOOLS

Our drone teams employ a variety of purpose-built commercial drones **and hardware to meet the specific needs of each asset and location.**



senseFly Albris
- Inspection
- Mapping
- High resolution imaging
- Infrared images and video
- Ultrasonic object sensing



Intel Falcon 8+
- Inspection
- Mapping
- High resolution imaging
- Infrared images and video
- Ultrasonic object sensing
- Interchangeable payloads



Flyability Elios
- Inspection
- High resolution video
- Infrared video
- Collision tolerant



Propeller Aeropoints
- Automatic GCPs
- Enable survey grade geospatial accuracy
- Locate assets and defects accurately

In order to achieve a good relative accuracy (local) and absolute accuracy that corresponds directly to GPS coordinates, our team uses automatic Ground Control Points (GCP). The Propeller Aeropoints have built in GPS, solar panel, battery and WiFi. Each unit collects GPS data while fieldwork is being performed and the data is automatically uploaded to a server where it is adjusted via a correction network to attain up to 2 cm accuracy. A report is generated which gives each GCP's survey grade location and the accuracy that can be expected for each point.

Case Studies

Case Study 1 - Wabasha Avenue Rock Slide

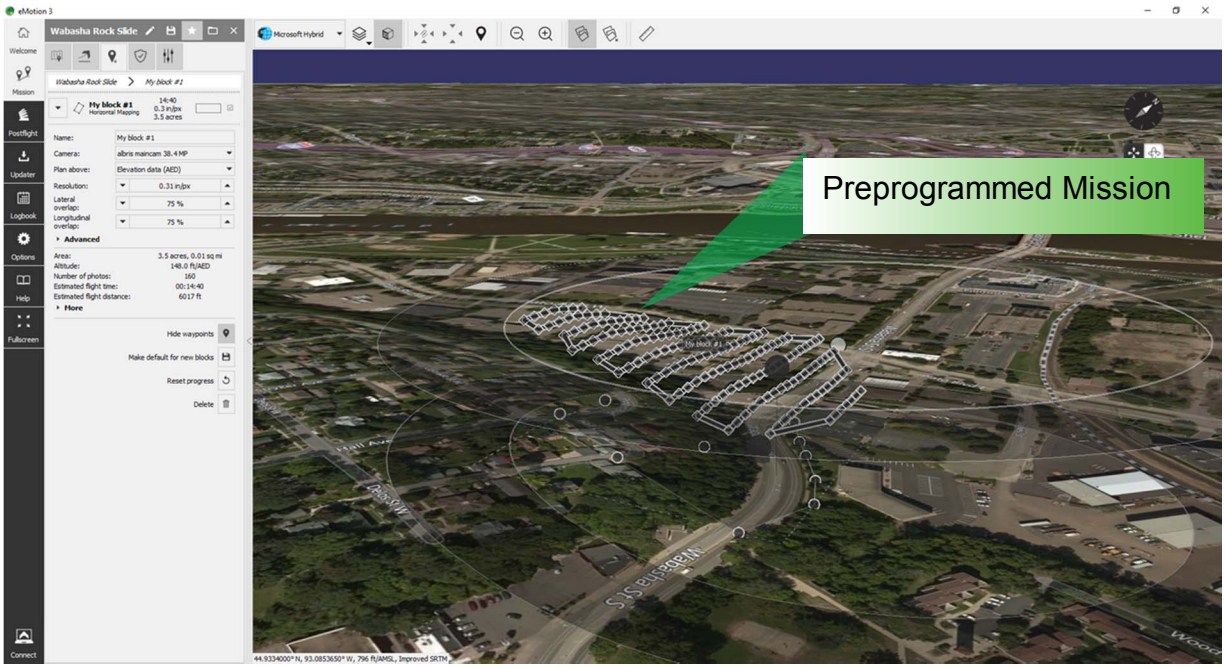
On Saturday April 28th, 2018 at approximately 3:30 pm, a rock slide occurred without warning and closed Wabasha Street in St. Paul. Despite happening in the middle of the afternoon in a dense urban environment, there were no injuries. The area was deemed unsafe and closed to the public until the site could be assessed by engineers and a plan to clean up and stabilize the bluff could be prepared. The City of St. Paul contacted Collins Engineers to map the site with an Unmanned Aircraft System (UAS) to gather information needed to start the remediation effort.

Fieldwork

The City of St. Paul contacted our team on May 2nd in the afternoon and a field crew was mobilized and on site the following morning. The City of St. Paul communicated with nearby property owners to inform them of the planned work. The field crew consisted of two professional engineers certified as small UAS pilots. One field member flew the drone while the other acted as a visual observer. Fieldwork consisted of distributing ten Aeropoint Ground Control Points throughout the site. The City of St. Paul surveyors also set ground control points to ensure the resulting location data was correct. The points were well distributed to ensure accuracy with half being placed on the upper part of the bluff and half being placed near the bottom of the site by Wabasha Street.

Although the area is near Homan Field and is considered restricted airspace, our team had an FAA airspace waiver in place that allowed inspection work to be performed under the FAA's Part 107 Small UAS Rule. The project area was flown from two locations, one at the top of the bluff and one near the bottom of the bluff. High-resolution images were collected using a preprogrammed autonomous mapping mission, and interactive flights where the pilot was manually flying the drone. The interactive flights utilized the drone's cruise control and image auto-trigger feature to collect images of the face of the bluff and slide area.

The site is challenging due to the large elevation change and the need to map not only the horizontal surfaces but also the vertical surfaces of the face. Moderate wind at the site was accelerated at the top of the bluff and approached 25 miles per hour. The drone was able to handle the wind but the vegetation became hard to process because it was moving during the flights. Even with the challenges the data was successfully collected in less than four hours including setup.

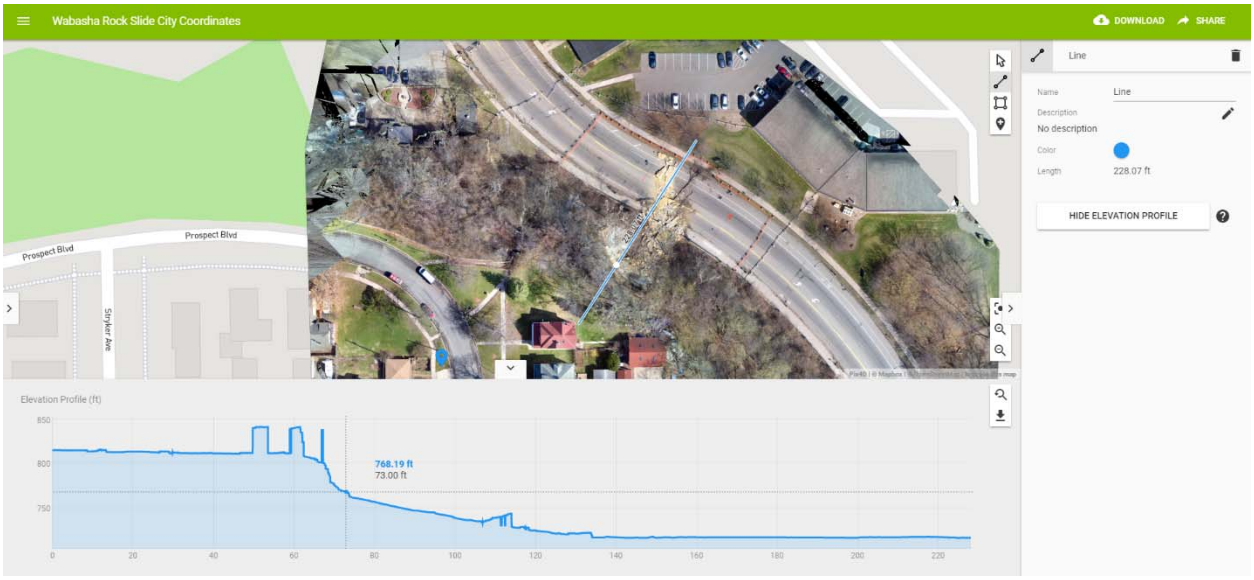


Data Processing

The high-resolution images were post processed using Pix4D Software to create the project deliverables. The Aeropoint GCP's and the City surveyor GCP's were incorporated into the model to ensure both relative and absolute accuracy. Deliverables included an orthomosaic map of the area, a point cloud and a triangular mesh model of the site. The processing was performed locally on a high-end computer and also on Pix4D's cloud processing service.

Results

The field investigation proved to be an efficient and safe way to collect and process a large amount of data efficiently and cost effectively. The entire data collection effort was accomplished without any staff having to enter areas that were considered unsafe or unstable. The resulting maps and models of the area were useful to engineers involved in the project in several ways. The profile of the bluff was easily determined at various locations without the need for any manual surveying of the slide area.



Elevation Profile of Wabasha Street Rock Slide

The 3D model and point cloud was used by the geotechnical engineer to determine the geometry of the slide area. It was also used by City Staff to communicate the extent and impact of the rock slide.



3D Point Cloud of Wabasha Street Rock Slide

The orthomosaic map of the area was used to compare the extents of the slide to property lines to determine if private property was affected by the slide. The map is dimensionally correct and was used to measure distances and convey the extents of the slide.



Orthomosaic Map of Wabasha Street Rock Slide

Pix4D includes a cloud version which enables the sharing of the map and models without the need to transfer large amounts of data and without the need for the end user to have Pix4D software. The cloud version has virtual inspector tool which serves as a three-dimensional photo log of the inspection. Once the model is created from the images, the photos are linked to the model. If a particular area of the project site needs to be reviewed, the user can click on that point on the model and all of the photos will be displayed of that particular element being inspected. The cloud version also includes annotation tools to communicate results more effectively.



Virtual Inspector Tool

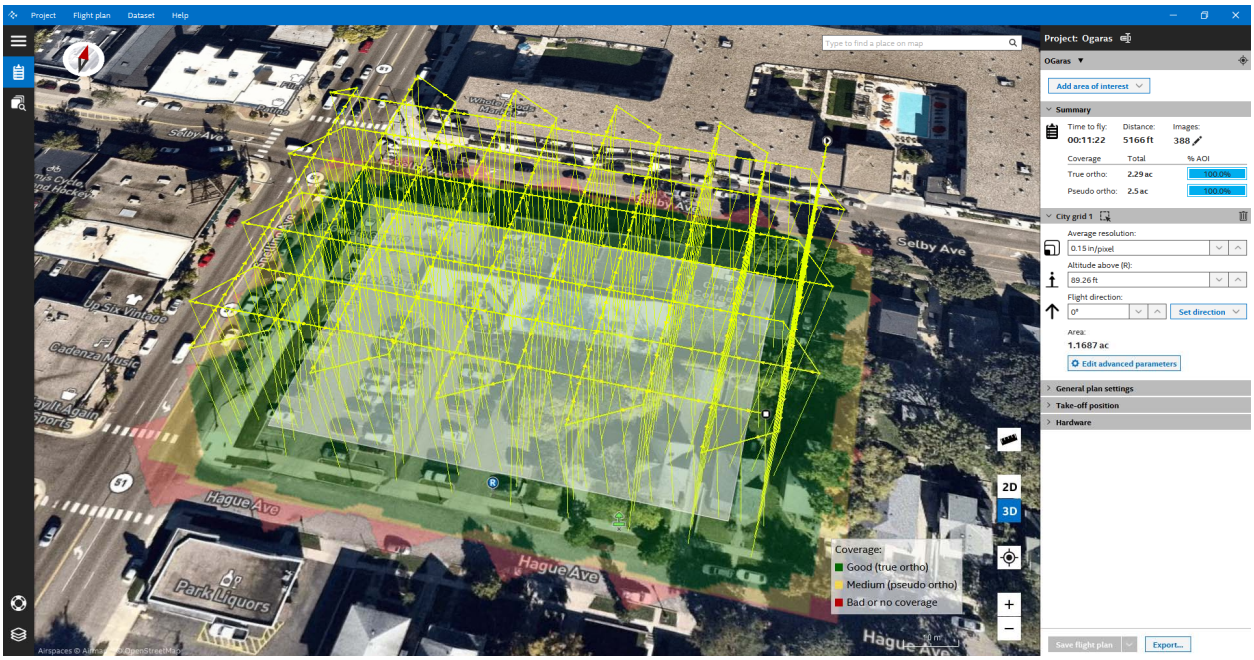
Wabasha Rock Slide Cloud Model:
https://cloud.pix4d.com/pro/project/304433/3d?shareToken=4548e50ce69f494cbf2b7e96d7dad6f6

Case Study 2 – Deep Foundation Construction Site

The redevelopment of the O'Garas Site in St. Paul MN is currently underway with construction activities ongoing. Ryan Companies is the General Contractor and Bolander is performing the deep foundation work. The project encompasses the existing restaurant and parking lot, as well as three single family homes. The proposed design includes 163 apartment units, 205 parking stalls, an integrated co-working space, apartment amenity spaces, and of retail space for the new O'Gara's. The project is located in an urban area and deep foundation shoring is being utilized during construction.

Fieldwork

Drone fieldwork was completed on January 3rd, 2019. Aeropoints were placed throughout the project site so that the final deliverables would be survey quality for both relative and absolute accuracy. Two autonomous flights were conducted collecting 298 high resolution images. The flights were conducted from the job site and the entire effort lasted less than 90 minutes and did not disrupt ongoing construction activities. The actual flight time less than 20 minutes.



Preplanned Autonomous Flight Mission

Data Processing

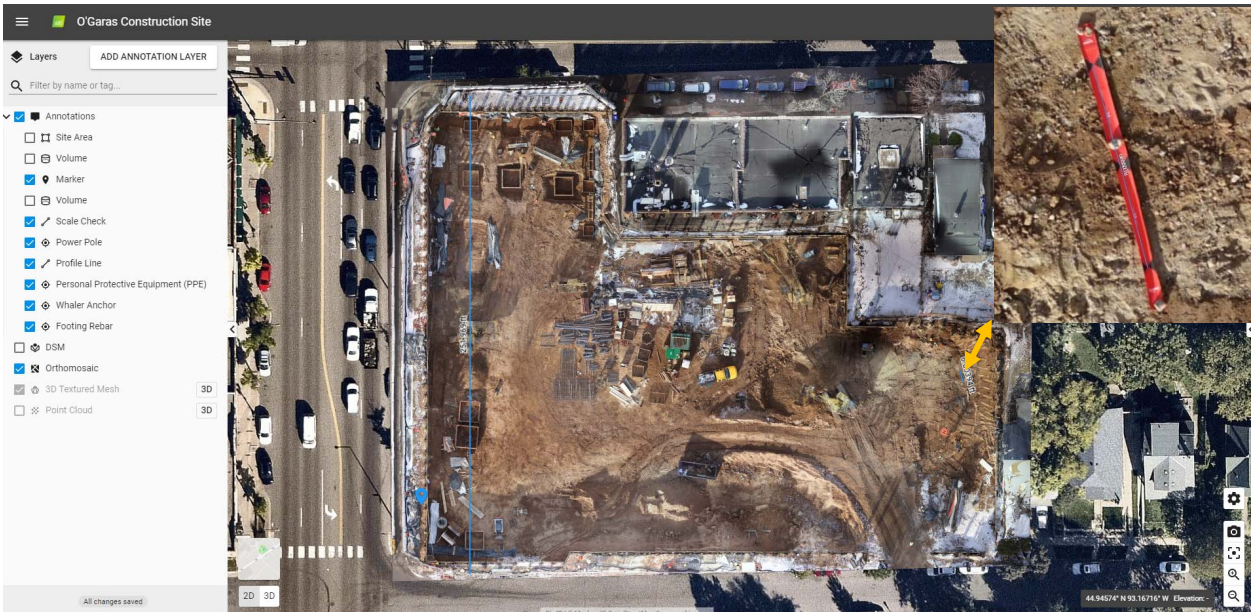
The high-resolution images were post processed using Pix4D Software to create the project deliverables. The Aeropoint GCP's were incorporated into the model to ensure both relative and absolute accuracy. Deliverables included an orthomosaic map of the area, a point cloud and a triangular mesh model of the site. The processing was performed locally on a high-end computer and also on Pix4D's cloud processing service.

Results

The field investigation proved to be an efficient and safe way to collect and process a large amount of data efficiently and cost effectively. The resulting maps and models of the area were useful to engineers and project managers involved in the project in several ways. The resulting model could be used as a check to identify site safety issues and hazards. The construction site model can also be used to plan locations for equipment and supplies. Since the model is dimensionally correct measurements can be made including lengths, areas and volumes. The model was annotated and shared with project staff.

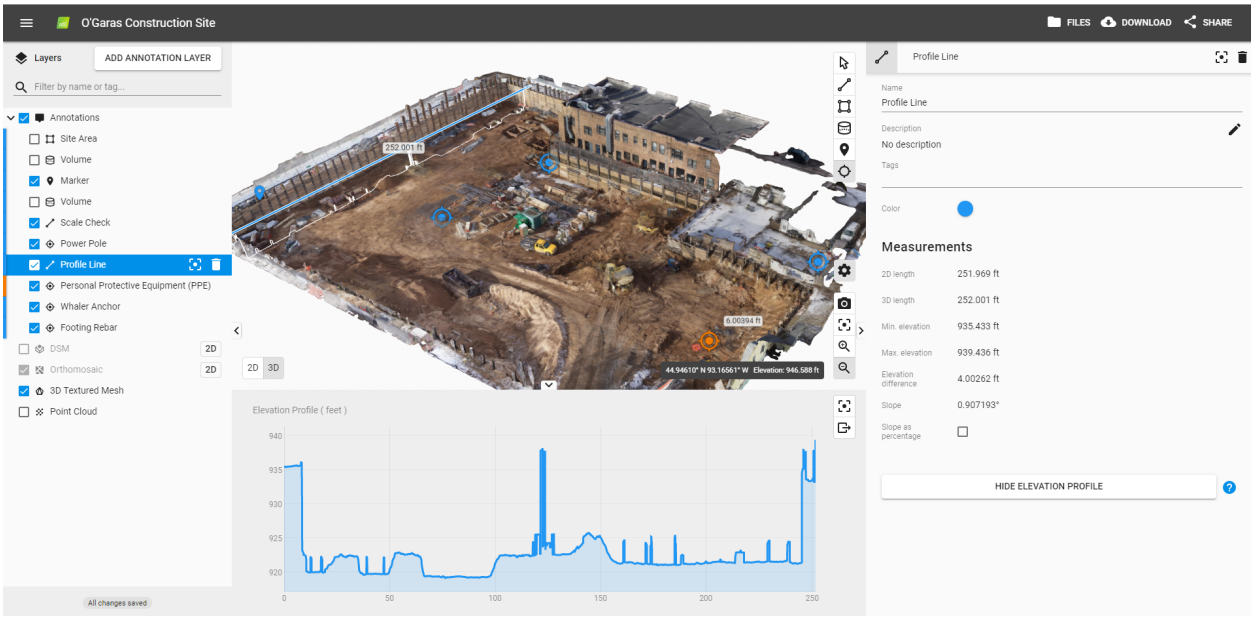


3D Model of O'Gara's Construction Site

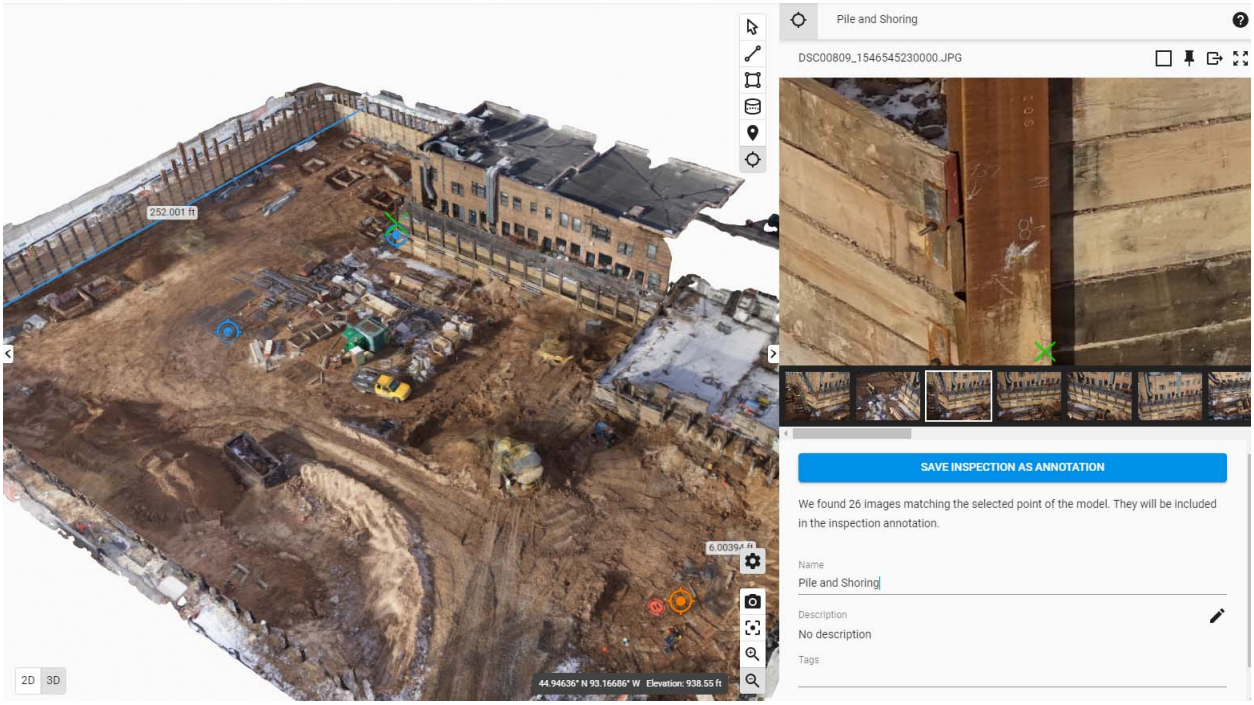


Orthomosaic of O'Gara's Construction Site

The orthomosaic map of the area was used to compare the extents of the slide to property lines to determine if private property was affected by the slide. The map is dimensionally correct and was used to measure distances and convey the extents of the slide.



Elevation Profile of Site



Virtual Inspector Tool

O'Gara's Construction Site Cloud Model:
https://cloud.pix4d.com/pro/project/415394?shareToken=d85868ab-6cb2-4312-8ef6-1c3672311bc1

Conclusions

Drone hardware and processing software are proving to improve project workflows in many ways. Drones are often discussed as a future technology, but the market has matured to the point where it is a viable and implementable technology. Drones are improving safety, reducing costs and generating deliverables that improve engineers and project managers abilities to improve project outcomes. Big data has had an impact on many industries and is now having an impact on the civil industry with exciting results.

VIRTUAL IMAGING TECHNOLOGIES AS DECISION-MAKING TOOLS FOR GEO-HAZARDS

Arpana P. Sabu, WSP USA, New York, NY, USA, Arpana.Sabu@wsp.com
Guillermo Diaz-Fanas, WSP USA, New York, NY, USA, Guillermo.DiazFanas@wsp.com
Themis Vaxevanis, WSP USA, New York, NY, USA, Themis.Vaxevanis@wsp.com
Sissy Nikolaou, WSP USA, New York, NY, USA, Sissy.Nikolaou@wsp.com

ABSTRACT

Geo-failures from extreme events (landslides, wild fires, earthquakes, floods, etc.) have increased exponentially in recent years around the world and within the USA. When catastrophic failures occur, they usually involve hundreds of fatalities especially in cases of unexpected triggering events, such as large intensity earthquakes or heavy flash floods. Protective actions against identified potential geohazards can mitigate the associated risks and the future occurrences and prevent these occurrences from becoming disasters, targeting the essence of resilience in geotechnical engineering. Imaging and other virtual design and construction tools can be used to identify weaknesses that trigger geohazards and can, in combination with numerical simulations, guide decision making. In spatially distributed problems, 3D visualization and LiDAR-type of technologies are essential in providing geotechnical engineers a deeper understanding of precarious soil zones and support finding appropriate solutions.

This paper will present the value of using virtual design and construction technologies though the case study of the Iztapalapa suburb of Mexico, about 20 km southeast of Mexico City. Iztapalapa was developed within irregular topography and has a long history of severe soil subsidence. Following the 2017 Puebla-Morelos earthquake, the town experienced large settlements resulting in extensive damage to the already frail buildings and unregulated infrastructure. The soil subsidence was visualized by mapping available historic and geotechnical data. The visualization helped to identify areas where additional investigations were needed. Additionally, this paper presents a case study of a series of landslides from the 2016 M_w7.8 Muisne Ecuador Earthquake, which demonstrates the advantages of using novel technologies to collect data and create cloud datasets from drones and digital photos to understand and evaluate geo-vulnerabilities in anticipation of an extreme event and during rapid reconnaissance to plan for long-term instrumentation, which can enhance geo-disaster prevention and overall community resilience.

INTRODUCTION

Iztapalapa is a southeastern borough of Mexico City (CDMX) located within the Mexico Basin (Figure 1). This borough is a densely populated area of CDMX with a total of 1.8 million inhabitants, and has a third of its population living in poverty (Gonzalez-Hernandez et al., 2015) with limited to no access to clean drinking water. Iztapalapa also suffers from high rates of crime, drug trafficking, sex trade and illegal buildings. As the population continues to grow, the already non-regulated and fatigued infrastructure is unable to meet the community needs, especially during and after natural hazard occurrences. The region of CDMX is one of the world's most seismically active regions that is also exposed to other geo-hazards such as floods, volcanic eruptions, and continuous settlement due to water pumping that has reached 11 meters over the past 100 years (Nikolaou et al, 2019). While the soil subsidence alone has caused significant infrastructure damage in Iztapalapa and throughout the rest of the city, recent earthquakes have also contributed to those damages.

CDMX has seen many earthquakes in its history that have resulted in loss of life and widespread damage to infrastructure, much of it resulting from vertical and lateral soil movements (Figure 2). The geologic history of the region, irregular topography, and exposure to natural disasters, make the subsurface conditions of the area very complex.

© 2019 Deep Foundations Institute

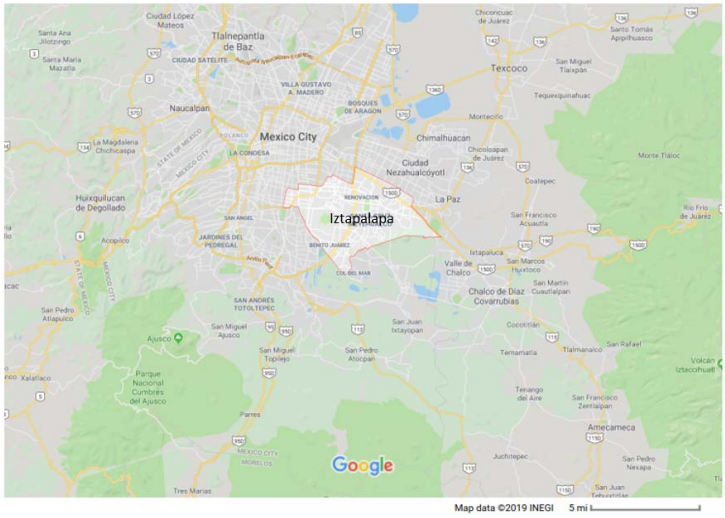


Figure 1. Google map image of Iztapalapa



Figure 2. Sidewalk and pavement damage (left) and soil subsidence (right) in Iztapalapa following the 2017 Puebla-Morelos earthquake (WSP, 2018)

HISTORY OF LAKES AND GEOLOGIC SETTING

Through centuries of volcanic activity in the region, the valley of Mexico City developed into a closed basin located in the highest part of the Mexican plateau, surrounded by mountains and volcanoes. The valley used to be a system of lakes, popularly known as Lake Texcoco, with the city built on the surrounding islands (Ovando-Shelley et al. 2013). The region was settled by the Aztecs who expanded the use of "chinampas" throughout the valley. Chinampas, also known as floating gardens, were a sustainable agriculture technique for cultivation of the land on the shallow lake beds in the valley (Figure 3). Due to lack of natural water outlets in the basin, flooding was common during the rainy season. Canals were built around the chinampas for diversion of water flow, and were often used for navigation by the people. The Aztecs also dug ditches to collect the rainwater and sediments, and once full, excavated the material to place on the chinampas. The material acted as a fertilizing agent for farming the land. However, after the Spanish conquered the region in the 16th century, this natural drainage system was abandoned and the process of draining Lake Texcoco commenced, expanding the land for colonial settlements. While some of the flooding risks were mitigated by this solution, the city was then forced to import water for consumption (Nikolaou et al. 2019). This practice has continued to present day, resulting in a lack of clean drinking water that has plagued the region, along with rapid and

irregular changes in groundwater levels that has caused large movements of the lacustrine soil deposits on which the lake rested. Aside from existence of small bodies of water, much of the lake has disappeared. Figure 4 shows the evolution of lake system and the location of the chinampas relative to the area of study.



Figure 3. Aztec Chinampas model by Te Mahi

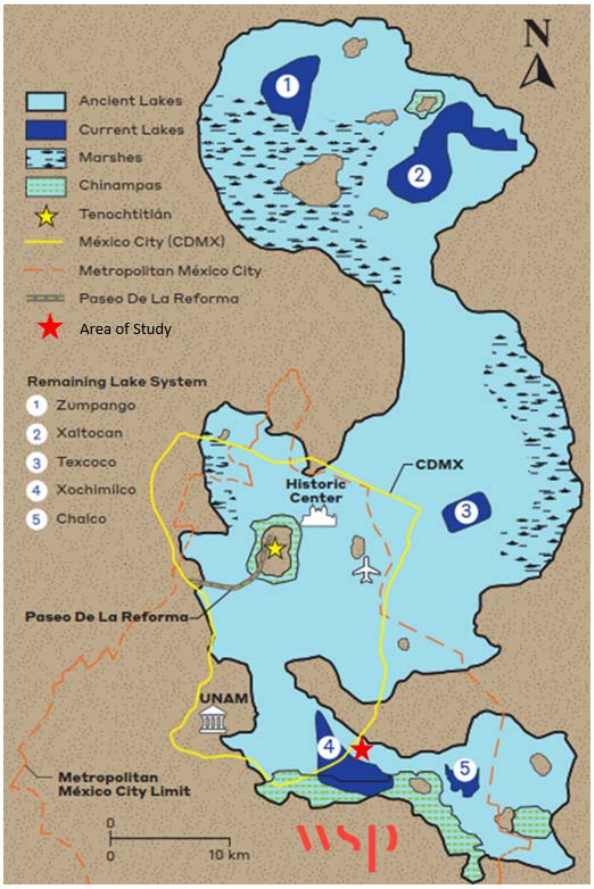


Figure 4. Ancient Texcoco lake system, surroundings, and area of study. (Nikolaou et al. 2019)

Iztapalapa lies on the drained lake bed comprised of lacustrine clay deposits. These deposits are often overlain by alluvial soils or artificial fill materials (Juarez-Camarena et al. 2016). The clays are often interlayered with sand, silt or volcanic ash material. Iztapalapa is home to many volcanoes, including Cerro de la Estrella, one of the city's most iconic viewpoints and the location used by the Aztecs as ceremonial grounds. A range of volcanos also stretches along the southeastern border of Iztapalapa. Due to Iztapalapa's proximity to adjacent volcanoes, large pockets of volcanic ash are observed in the area as well.

GEOTECHNICAL CONDITIONS

Due to its proximity to adjacent volcanos, irregular topography, and highly compressible clay sediments, Iztapalapa's soil configuration is complex and subject to differential soil settlements. To further understand the site conditions, all available geotechnical data in and around Iztapalapa was gathered with the assistance of Universidad Nacional Autónoma de Mexico (UNAM). The existing geotechnical data included 52 geotechnical borings ranging from 10 to 20 meters deep with some corresponding laboratory data. Figure 5 shows the area of study and the boring locations. This data will be used to identify critical regions within the area of study that are highly sensitive to soil subsidence. Identifying such areas will allow the city to make informed decisions on how to prioritize the rebuilding effort and if needed, search for alternative locations for community rebuilding to avoid troubled areas.

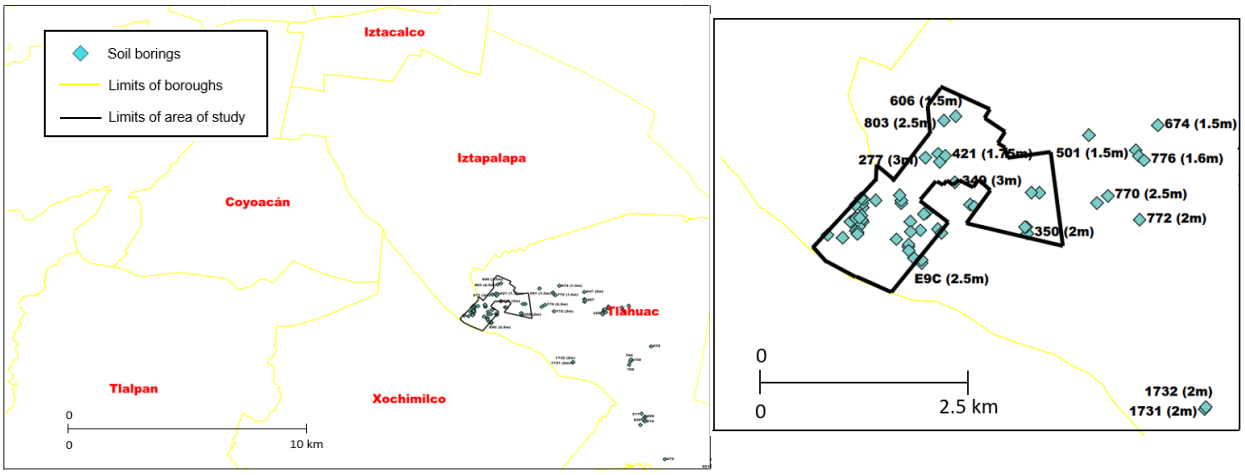


Figure 5. Area of study and boring location plan

The geotechnical investigation indicates that the study area is typically overlain by a layer of fill material consisting of sand with varied amounts of gravel and silt. In many borings, underlying the fill is a layer of medium dense to dense sand and/or volcanic ash. The volcanic ash is found in several borings and often in localized pockets. For some borings, volcanic ash is found at deeper depths, making it difficult to identify the extent of the layer. Following the sand or volcanic ash material are the very soft to medium stiff clay deposits, starting from about 1 to 9 meters below ground surface. The clay deposits are typically highly compressible and highly plastic, with low shear-strengths. This layer is sometimes interlayered with silt, sand, or pyroclastic materials. The water contents for the lacustrine clay deposits range from 50% to 400%, with a large scatter and most water contents below 300%. The plasticity index of the clay ranges from 20 to 110, also with a large scatter.

Two of the borings from the geotechnical investigation are shown in Figure 6 and show the general variance in soil layers. Using these two borings, two settlement analyses were performed to assess the differential settlements. Due to the lack of laboratory data, consolidation parameters were based on empirical correlations, local experience and engineering judgment.

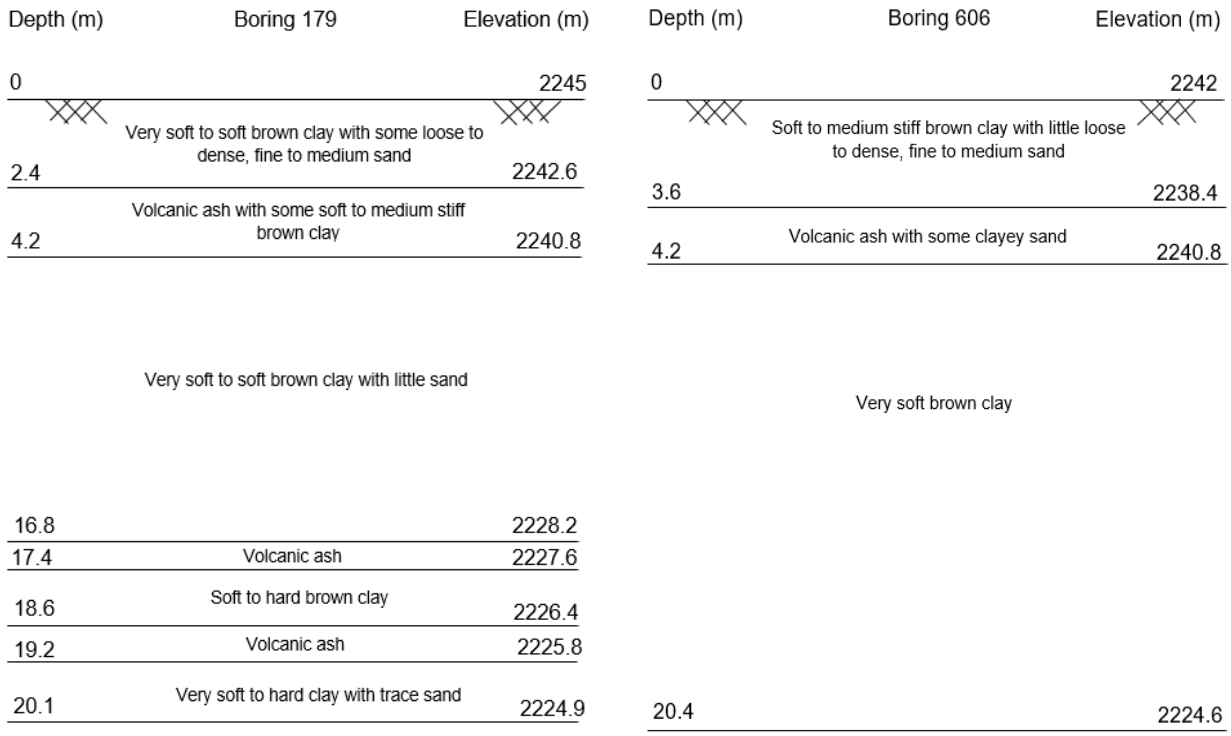


Figure 6. Example Geotechnical Soil Borings

The settlement models assumed one-dimensional consolidation settlement resulting from the clay layers under the same loading conditions and are shown in Figure 7. The analyses resulted in a differential settlement of approximately 0.1 meters, while the actual observed differential settlements are far greater and on the order of a couple meters. The model is unable to fully capture the observed settlement and thus shows that more information is needed to understand the soil behavior and identify the critical zones in the study area.

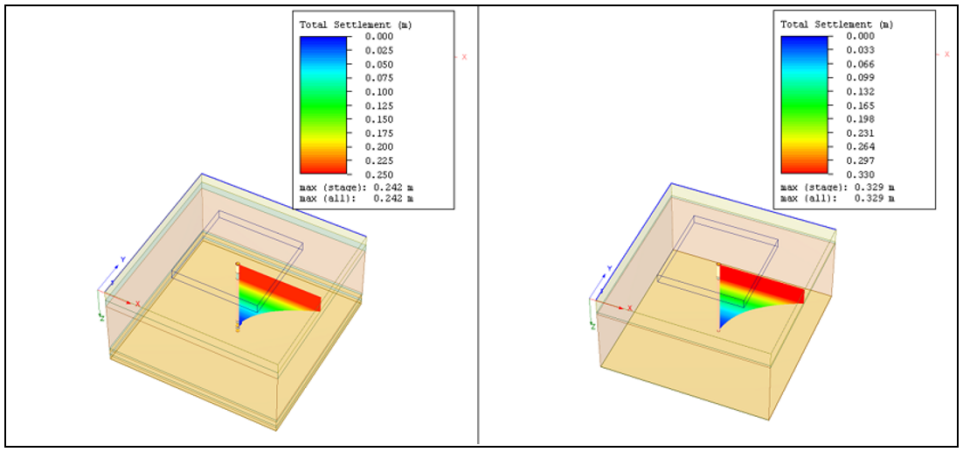


Figure 7. Settlement analysis models for boring 179 (left) and boring 606 (right)

The irregular topography of the study area is not considered in the analysis and is exemplified by the surveyed borings, with the ground surface elevation varying up to 12 meters. Other factors that were not accounted for include significant ground fracturing, locations of water bodies, loading history, and existing water pumping wells, which may be expediting the settlement in localized areas and contributing to some of the geotechnical characteristics of the soil. This information can be used in conjunction with the geotechnical data and analysis to understand and explain the soil behavior.

USE OF GEOGRAPHIC INFORMATION SYSTEM (GIS) FOR VISUALIZATION

Geographic information system (GIS) can be used to gather and integrate various data types into one system. It can overlay multiple geographic data using maps, images, and inputted data, allowing the user to visualize all data and illuminate geographic patterns that are otherwise difficult to deduce. This technology can be used two or three dimensionally to understand the soil behavior of the region and identify some driving factors of it. Topographic data for the GIS model can be collected by surveying methods or existing maps and data after digitizing them.

For this study, all existing data for the area of study and its surroundings was first collected with the assistance of local agencies and digitized into individual maps. The data included:

- The location and extents of the original Lake Texcoco
- The location of the area of study
- The borings performed as part of the geotechnical investigation of the area of study
- The limits and extents of the nearby towns and delegations
- Existing water bodies and currents
- The locations of all known water pumping wells
- The locations of known faults and fractures
- Geotechnical and seismic zoning
- The range of soil subsidence observed
- The locations of structures that were damaged or collapsed during the 2017 Puebla-Morelos earthquake
- Existing canals and aqueducts

Using a computer-aided design and drafting software, each data map was generated into individual layers. The layers

were then overlaid to obtain a sophisticated map, in which all layers could be visualized at once. Figure 8 shows the GIS model with the area of study polygon overlaid by the location of the original lake. With the overlaying of the data, it was evident that the area of study lay in the original lake zone, with some existing bodies of water lying south of the area of study. The adjacent map adds a layer to the GIS model covering the areas affected by the 2017 seismic event.

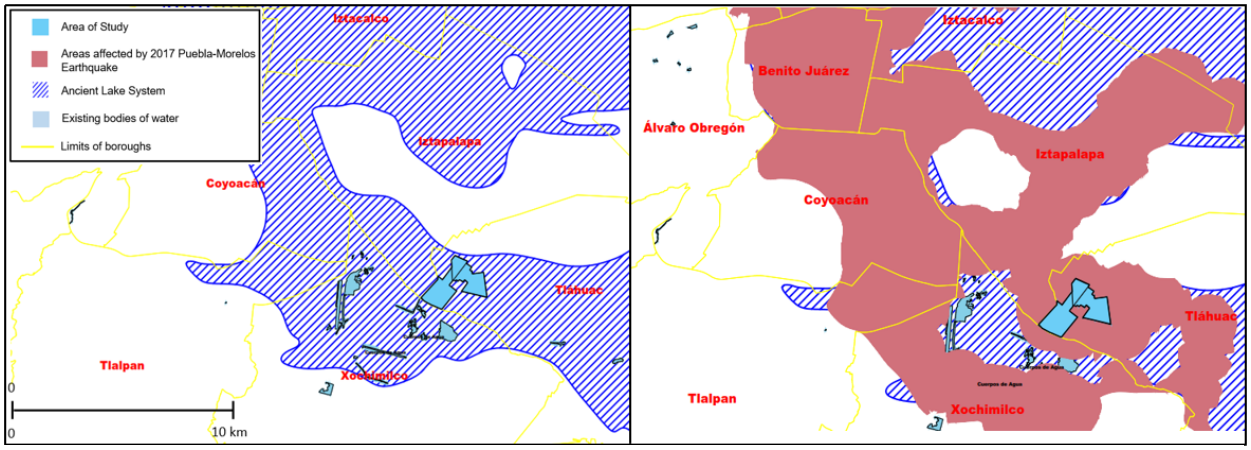


Figure 8. Overview of GIS model showing select layers of collected data: ancient lake system and area of study (left); ancient lake system, area of study, areas affected by 2017 seismic event (right)

The GIS model helped identify that the southwest section of the study area as critical and in need of additional geotechnical investigation and consideration. Figure 9 highlights this section and overlays multiple layers in the model to show geological features that may be related to the high degree of subsidence observed. Two major fault lines can be seen cutting through the highlighted region along with multiple fractures. The GIS layer with the existing water pumping wells is also shown, many of which can be seen along the border of the highlighted area and are likely resulting in expedited settlements near the border. Based on the topographic data collected during the soil drillings, the ground surface elevation varies up to 12 meters in the highlighted region, while the variance in the remainder of the polygon is approximately 5 meters.

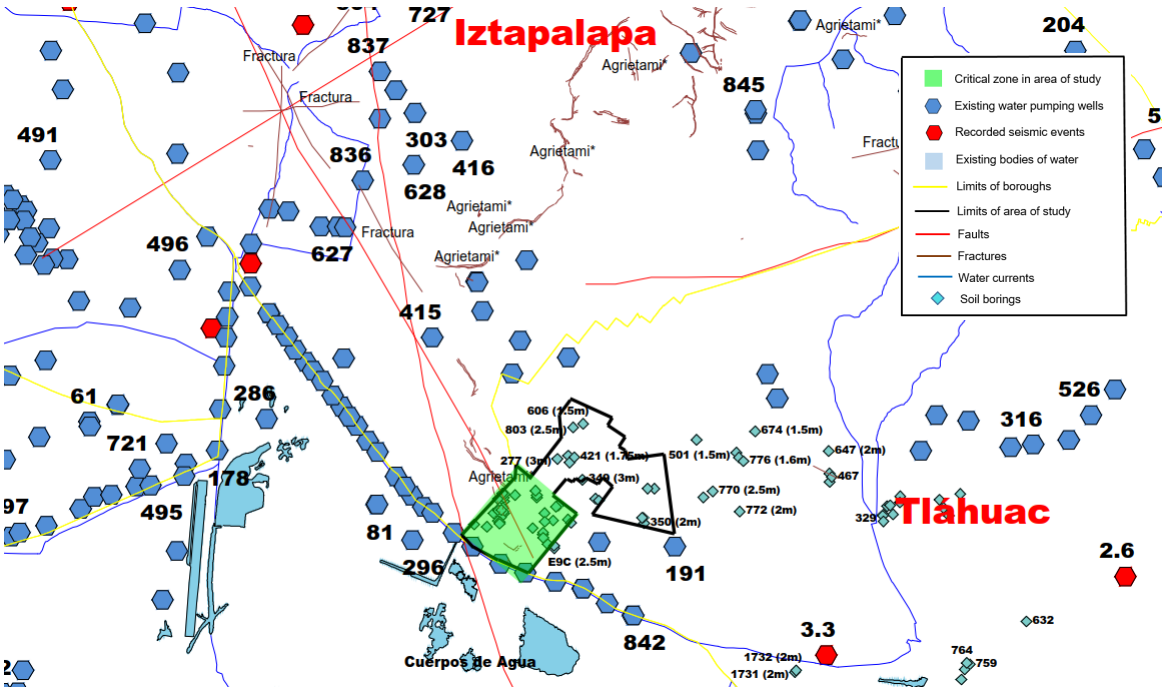


Figure 9. GIS model showing select layers and identifying critical zone

Using this live GIS map, future recordings of observed subsidence, damages, or other information can be added to the database to supplement it.

APPLICATION OF 3D IMAGING SOFTWARE AND TOOLS CASE STUDY: 2016 Mw7.8 MUISNE ECUADOR EARTHQUAKE

The M_w7.8 Muisne, Ecuador earthquake caused major destruction to the Ecuadorian infrastructure when it struck on April 16, 2016. Virtual technologies were used in the aftermath of the earthquake to understand and visualize the earthquake-induced damage across the western coast of Ecuador. A case study carried out by a reconnaissance mission led by GEER-ATC (Nikolaou, et al. 2016) showed the use of 3D imaging to better assess a series of landslides that followed the earthquake's main shock. Using drone images and a 3D point cloud, a space model was generated to understand the pattern of failure, mass movement, and rainfall that triggered the macro-failure (Nikolaou, et al, 2018). The Phantom 4 and Inspire 1 Pro drones were used to collect the data and can be seen in Figure 10.



Figure 10. Reconnaissance drones: Phantom 4 (left); Inspire 1 Pro (right) (Nikolaou et al. 2016)

A 3D point cloud (3DPC) was created to visualize and understand the site failure. This system can generate images and 3D models from before, during, and after geo-hazardous events. An on-site drone was flown over the site to capture a dense 3DPC using time-lapse mode and 50% overlap (Nikolaou et al. 2018). Figure 11 shows an example of the sequence of drone images and its overlapping.

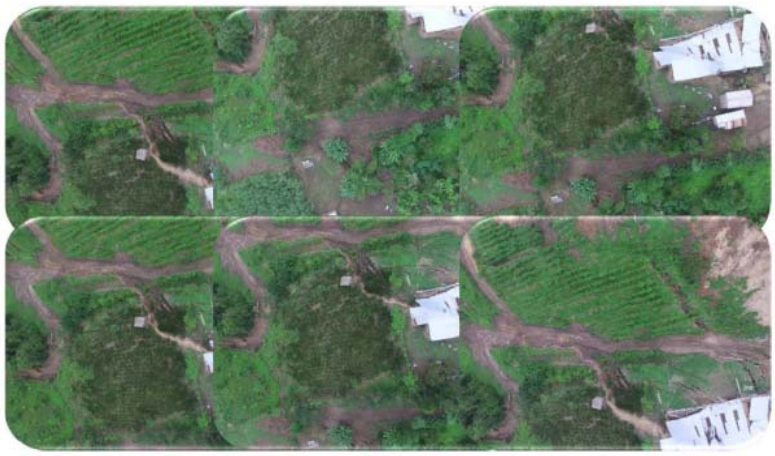


Figure 11. Sequence of drone images (Nikolaou et al. 2016)

Once the images were transferred to a 3D processing software, images and 3D models from before and after the hazardous event were overlaid to compare and assess changes and damages. Figure 12 shows the 3D surface developed with select sections. Based on the imagery and collected data an estimated 290,000 m^2 of area moved laterally and vertically (Nikolaou et al. 2018). The use of UAV drones allowed for fast and effective response to the affected areas and help understand the extent of damages.

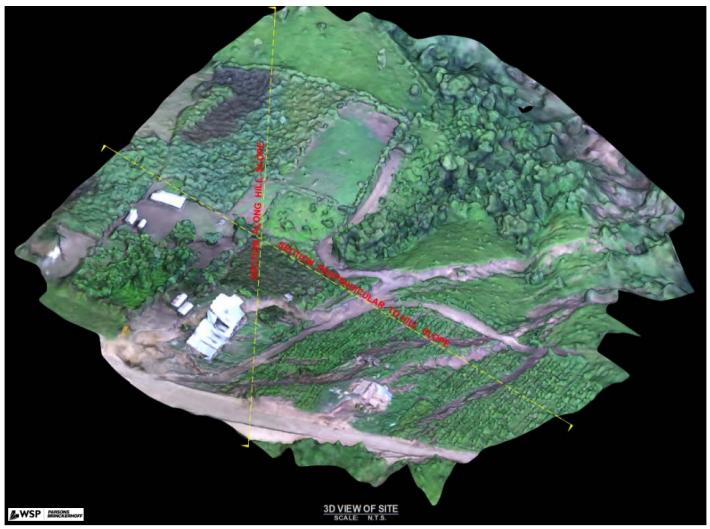


Figure 12. 3D model of site generated using drone images (Nikolaou et al. 2016)

CONCLUSION

Virtual technologies and imagery, including GIS and UAV/drones, can be crucial in understanding the effect and damages due to geo-hazardous events. In Iztapalapa, the 2017 Puebla-Morelos earthquake resulted in significant damages and soil subsidence to an already geologically complex region with large amounts of differential settlements. Using GIS models, available information was compiled into 2D maps to identify the southwest portion of the area of study as critical. This area consisted of existing faults, water pumping wells, and irregular topography. With this information, resources can be more effectively allocated for further field investigation. UAV/drone technology was used immediately after the 2016 Muisne earthquake in Ecuador to understand the mechanisms and pattern of the series of earthquake-induced landslides. Using the existing and collected images before and after the event helped understand the extent of damages, the investment needed for recovery, and identify areas that may be more prone to such geo-hazardous effects.

This paper uses two case studies using different virtual technology methods to demonstrate that virtual technologies can be useful in quantifying damages after geo-hazardous events and understanding how the site conditions are being affected by them. This information can be used to mitigate damages resulting from future events and guide informed decisions on recovery processes.

REFERENCES

1. Ovando-Shelley, E., Ossa, A., Santoyo, E., 2013. Effects of regional subsidence and earthquakes on architectural monuments in Mexico City. Boletin de la Sociedad Geologica Mexicana, vol. 65, (1), pp. 157-167.
2. Nikolaou S., Diaz-Fanas, G., Garini, E., McElvain B., 2019. Dried lakes do tell tales – seismic soil amplification in Mexico City. Geostrata March/April, pp. 40-46.
3. Nikolaou S., Diaz-Fanas, G., Vaxevanis, T., Mezher, J., 2018. Drone and imaging virtual tools for earthquake reconnaissance 2016 Muisne, Ecuador earthquake. Eleventh U.S National Conference on Earthquake Engineering, Integrating Science, Engineering & Policy.
4. Gonzalez-Hernandez, M., Carreon-Freyre, D., Gutierrez-Calderon R., Cerca, M., Flores-Garcia, W., 2015. Mass movement processes triggered by land subsidence in Iztapalapa, the eastern part of Mexico City. PIAHS (372), pp. 261-265.
5. Juarez-Camarena, M., Auvinet-Guichard, G., Mrndez-Sanchez, E., 2016. Geotechnical zoning of Mexico valley subsoil. Ingenieria Investigacion y Tecnologia, vol. XVII (3), pp. 297-308.
6. Nikolaou S., Vera-Grunauer X., Gilsanz R., eds. GEER -ATC Earthquake Reconnaissance: April 16 2016, Muisne, Edcuador 2016; Geotechnical Extreme Events Reconnaissance Association, Report GEER-049.

COST EFFECTIVE EXCAVATION SUPPORT IN SEATTLE

Richard D. Luark, Terracon Consultants, Inc., Mountlake Terrace, Washington, USA, 425-301-8782, Richard.Luark@terracon.com
Fernanda S. Madrona, Terracon Consultants, Inc., Mountlake Terrace, Washington, USA, 240-472-5506, Fernanda.Madrona@terracon.com

ABSTRACT

Deep foundation construction in highly developed urban settings pose unique challenges of working with deep excavations in a relatively confined area while preserving the integrity of nearby structures. For construction of the below grade parking for two, 40-story residential high-rise towers, shoring walls were required to support the maximum 70-foot-deep vertical excavation in downtown Seattle, Washington. The design of the excavation support system consisted of soil nails combined with closely spaced vertical elements to allow the top row of soil nails to be installed up to 10 feet below the ground surface avoiding conflicts with adjacent underground utilities. To limit deflections next to a seven-story building, the upper rows of soil nails were post tensioned. An instrumentation program was implemented to monitor the deflections in the shoring walls by means of vertical inclinometers and optical survey monitoring. The shoring wall performance, designed to limit deflection to less than 1-inch to meet the City of Seattle requirements, was validated by the instrumentation program. This paper provides a discussion of the design and construction of the shoring walls as well as the monitoring data collected from the instrumentation system.

Keywords: deep excavation, soil nailing, vertical elements, instrumentation program, monitoring data

PROJECT INFORMATION

The project consisted of two residential high-rise towers, with five levels of below grade parking, located at 707 Terry Avenue Seattle, Washington. The project site covers a half city block, approximately 120 feet by 240 feet, and is bounded by Terry Avenue to the east, Columbia Street to the north, Cherry Street to the south, and an alley to the West. Prior to the development, site was occupied by surface parking. A 7-story concrete building with two stories of below grade parking, owned by the Archdiocese of Seattle is located just west of the 16-foot-wide alley. Numerous below grade utilities consisting of electrical, telecommunications, gas, water, sanitary sewer, steam, and storm drains, surround the project. The perimeter below grade parking walls extended within inches of the property boundaries. Topographic relief across the site was on the order of 8 feet. Figure 1 illustrates the site plan view.

Terracon Consultants Inc. (Terracon) designed the temporary shoring system for the Northwest Division of Malcolm Drilling Company, Inc. (Malcolm). The geotechnical engineer of record for the project is GeoEngineers of Redmond, Washington.

© 2019 Deep Foundations Institute

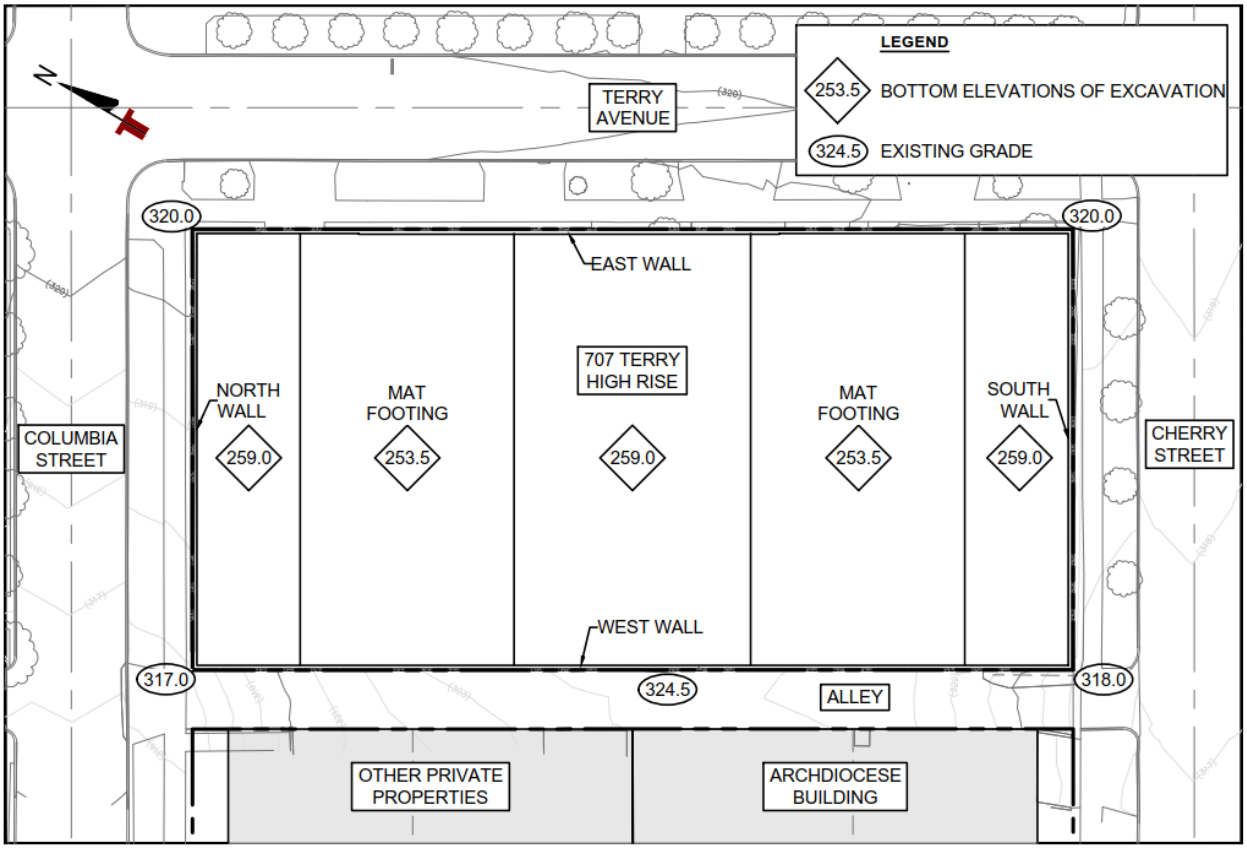


Fig. 1. Site Plan

SUBSURFACE CONDITIONS

Site geology consisted of a layer of fill soils overlying glacially consolidated soils consisting of a discontinuous layer of Glacial Till underlain by Advance Outwash Sands that extended to the full depth of the excavation. The Advanced Outwash Sand unit consisted of dense to very dense sand with variable silt and gravel content. Interbeds of silty sand and silt, was well as gravel, are present within the Advance Outwash Unit. The groundwater table was below the base of the proposed excavation required to construct the below grade parking levels and foundations.

SHORING WALL SELECTION AND DESIGN PARAMETERS

Based on previous experience with temporary soil nail design and construction in the vicinity of the 707 Terry Project, a composite soil nail shoring system, consisting of vertical elements combined with traditional soil nailing, was selected for the preliminary design developed for the cost estimate. The composite soil nail shoring system was proposed as a value engineering alternative to the post tensioned anchored system that was originally designed and permitted for the project. The upper vertical elements consisted of light wide flange beams set in small diameter drilled shafts backfilled with lean concrete. The upper vertical elements supported the soil as cantilever piles allowing for the top row of soil nails to be set lower to avoid utility conflicts, while the vertical elements that extend to the base of the excavation provided temporary face stability during soil nail and shotcrete installation.

The design parameters selected for the soil nail design are listed in Table 1. A nominal 6-inch diameter soil nail drill hole was assumed for the pullout calculations.

Table 1. Soil Nail Design Parameters

Soil Unit	Moist Unit Weight (PCF)	Friction Angle (Degree)	Cohesion (psf)	Ultimate Soil Nail Pullout Resistance (k/ft)
Fill	125	33	0	2
Glacial Till	135	38	200	6
Advance Outwash	135	40	0	6

The vertical elements were designed in with a triangular active earth pressure equal to 27H in pounds per square foot (psf), where H equals the height of the cantilever condition to allow installation of the first row of soil nails. A passive design pressure of 400D psf, where D equal the embedment depth and acts over 2.5 times the lean concrete shaft diameter.

To model the building surcharge load on the west shoring wall, a surcharge pressure of 250 psf was used for each story of the concrete structure, resulting in surcharge pressures of 750 psf and 1,750 psf for three and seven stories, respectively. Traffic surcharge loads were modeled as 250 psf vertical pressure for the north, south, and west shoring walls. The east shoring wall was designed with a construction surcharge loads with 500 psf uniform surcharge pressure.

SHORING SYSTEM DESIGN

Malcolm was awarded the design and construction of the value engineered shoring system for the 707 Terry Project, with Terracon as the shoring designer of record. The design included incorporation of the support of the conveyor system on the top of the east shoring wall as well as support of hanging stairwells on the south and north shoring walls.

Vertical elements were spaced three feet on center around the entire perimeter of the excavation, with every third vertical element extending below the base of the excavation. The purpose of the deep vertical elements was to provide face support for the vertical excavation required to install the shotcrete facing and to provide stiffness of the shoring system to limit deflections to within the City of Seattle required 1-inch or less. The vertical elements consisted of light wide flange sections set in 18 to 24-inch diameter drill holes which were backfilled with lean concrete. The vertical elements were designed with the Shoring Suite computer program by CivilTech Corp. This program determines the moment, shear, deflection, and embedment required to satisfy force and moment equilibrium. Connection of the top row of soil nails to the vertical elements was accomplished with rectangular HSS walers spanning between every other pair of vertical elements. The vertical element beam sizes ranged from a W10 X 12 set in an 18-inch diameter drill hole to a W 14 X 26 set in a 24-inch diameter drill hole. Vertical element lengths ranged from 19 to 78 feet for support of the cantilever height to install the first row of soil nails, while length of every third vertical element extended below the base of the excavation an average of 10 feet. The geotechnical engineer of record recommend that every third vertical element extend ten feet below the base of the excavation.

The City of Seattle Department of Transportation requires that shoring elements placed in upper four feet of the right of way be removed after they are no longer required. Therefore, the vertical elements were designed with removable tops. This was accomplished by fabricating two steel plates on each side of the steel pile web, with upper portion of the plates welded to the flanges. The back web and flange were precut during fabrication, with the front pile flange left intact. As the excavation progressed down to the bottom of the removable pile top, the front flange was field cut. Wood lagging was placed in the upper four to five feet of the excavation to support the soil between the vertical elements, which allowed for easy removal of the pile tops once the shoring system was no longer required. Below the removable pile tops, the temporary

facing consisted of a layer of reinforced shotcrete. The shotcrete facing above the second row of soils nails was connected to the vertical elements with headed studs welded to the front flange of the steel piles.

The soil nails and shotcrete facing were designed with the Snail computer program Version 2.0.3.1, Copyright© 2016 State of California, which is based on the FHWA design criteria for soil nail walls. As the soil nail walls were temporary, a minimum factor of safety of 1.35 on the soil shear strength was used in the design, combined with appropriate factors on the soil nail pullout, reinforcement bar yield strength and head strength (punching shear and flexure). A minimum soil shear strength factor of safety of 1.2 was used in the design for the interim stability condition during construction of the composite soil nail wall. Per the FHWA soil nail design manual, the soil nails can decrease in length from the upper portion of the excavation to the lower, with approximately the upper half of the soil nails a constant length; however; for the portion of the soil nail wall adjacent to the Archdiocese Building, which had two stories of below grade structure, the upper soil nails were limited to 15 feet in length. Figure 2 illustrates the soil nail cross section adjacent to the Archdiocese Building. For most of the excavation, the soil nails were spaced five foot vertically and six foot horizontally (5 x 6 nail pattern), except adjacent the Archdiocese Building where soil nail horizontal spacing ranged from three to five feet. The soil nail lengths and bar sizes varied depending on wall heights and surcharge loads with the longest soil nail being 55 feet in length and the strongest soil nail reinforcement of 1.25" diameter grade 150 thread bar. Soil nail inclinations varied from 15 to 20 degrees from horizontal. The soil nails were connected to the shotcrete facing with half inch-thick square steel head plates, nine by nine inches in dimension.

The reinforced shotcrete facing ranged from 4 to 5 inches in thickness with a specified unconfined compressive strength of 4,500 psi. Reinforcement consisted of two #5 continuous horizontal waler bars and two discontinuous 30-inch-long #5 vertical "tic tack toe" bars, both spaced 6-inches on center beneath the soil nail head plate. Continuous reinforcement consisted of welded wire fabric (WWF), 4 X 4 – W4.0 X W4.0 for the 4-inch shotcrete thick facing and 4 X 4 – W6.0 X W6.0 for the 5-inch shotcrete facing.

Per the geotechnical engineer of record recommendations, soil nail rows 4 through 8 adjacent to the Archdiocese Building, were designed with a post tension load of 30 kips to limit deflection of the shoring system and potential movement of the building. A 3-foot-long unbonded zone with a PVC bond breaker around the top of the soil nail bar was specified for the post tension soil nails.

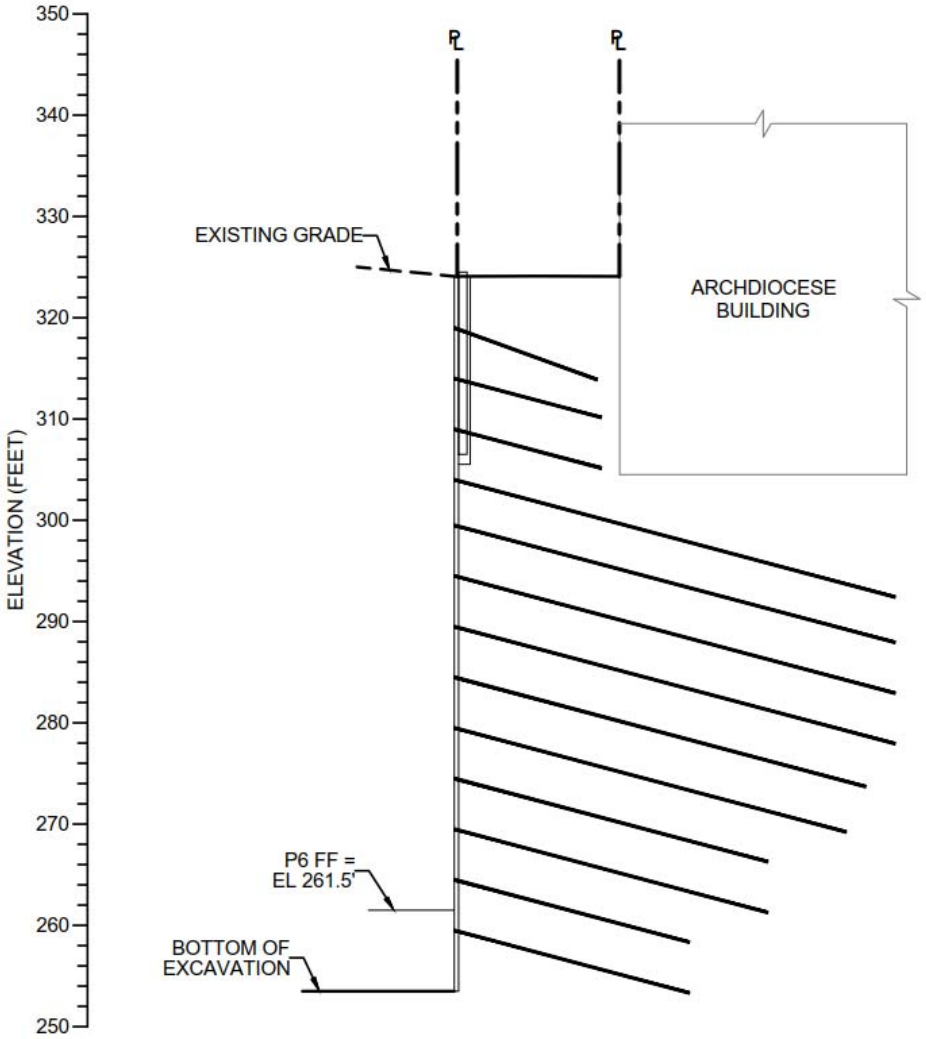


Fig. 2. Cross Section of the West Shoring Wall at The Building

PERMITTING AND CONSTRUCTION

To shorten the permitting time for the value engineered composite soil nail shoring system, the drawings and supporting calculations were submitted after the original post tensioned anchor shoring system was approved. Post permit submittals are given priority by the City of Seattle, which shortened the approval time for the composite soil nail shoring to approximately 4 weeks versus the 6 to 8 months typically required for shoring based on an initial submittal.

Construction of the shoring system started on August 30, 2018 with installation of the vertical elements, followed by installation of the timber lagging between the vertical element in the upper four to five feet of the excavation, with shotcrete facing below. After drilling the top row of soil nails, the connection of the soil nail head to the vertical elements was completed with horizontal HSS rectangular walers. Most of the soil nails were installed using hollow stem continuous flight augers combed with compressed air to evacuate the soil cutting. Once the excavation depth reached approximately 20 feet, a soil conveyor was installed on the top of the east shoring wall. The conveyor was supported on a steel frame bearing on a concrete pad,

which was connected to the top of the vertical elements that extended below the base of the excavation final depth. Two, 6-inch diameter post tensioned anchors were installed at the back of the steel frame to hold down the back of the conveyor frame at the top of the excavation. Where the hanging stairwells and conveyor limited continuous flight auger installation, an air rotary drill rig installed the soil nails using 2-meter-long drill steel.

To confirm the soil nail allowable design pullout capacity of 3,000 pounds per foot (3 kips/ft) with a factor of safety of two, two sacrificial soil nails were tested to 6 kips/ft. During production, five percent of the nails were tested to 150 percent of the allowable pullout for quality control purposes. During proof testing of the upper soil nails, several of the test nails failed; however, it was observed that the bond between the soil nail bar and the grout failed, rather than a bond failure at the soil grout interface. In the areas where failed proof tests were observed, additional soil nails were added to compensate.

The photograph in Figure 3 shows an anchor being installed with 4-inch hollow stem augers. Figure 4 and 5 show the progress of the excavation. More specifically, Figure 5 shows the shoring walls, the conveyor support, and the building adjacent to the west shoring wall when the excavation was nearly completed. Construction of the shoring walls were completed on November 14, 2018 for a total duration of 12 weeks for the shoring and mass excavation phase of the project. The excavation contractor was allowed by the City of Seattle to excavate and haul soil at night, which allowed Malcolm to have open drilling during the day for shoring installation. The night time excavation and hauling were a significant factor that allowed the excavation and shoring to be constructed in 12 weeks.

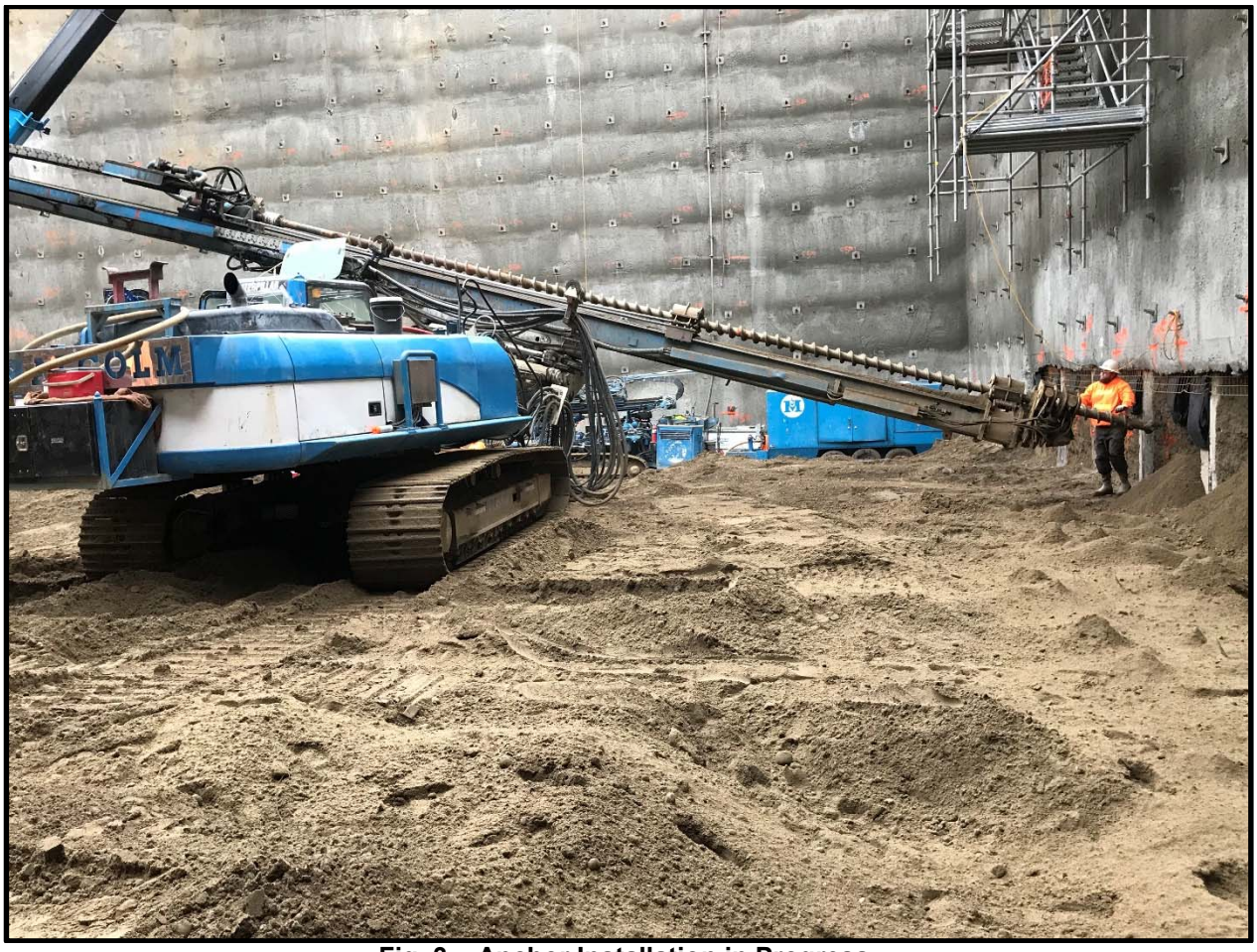


Fig. 3 – Anchor Installation in Progress

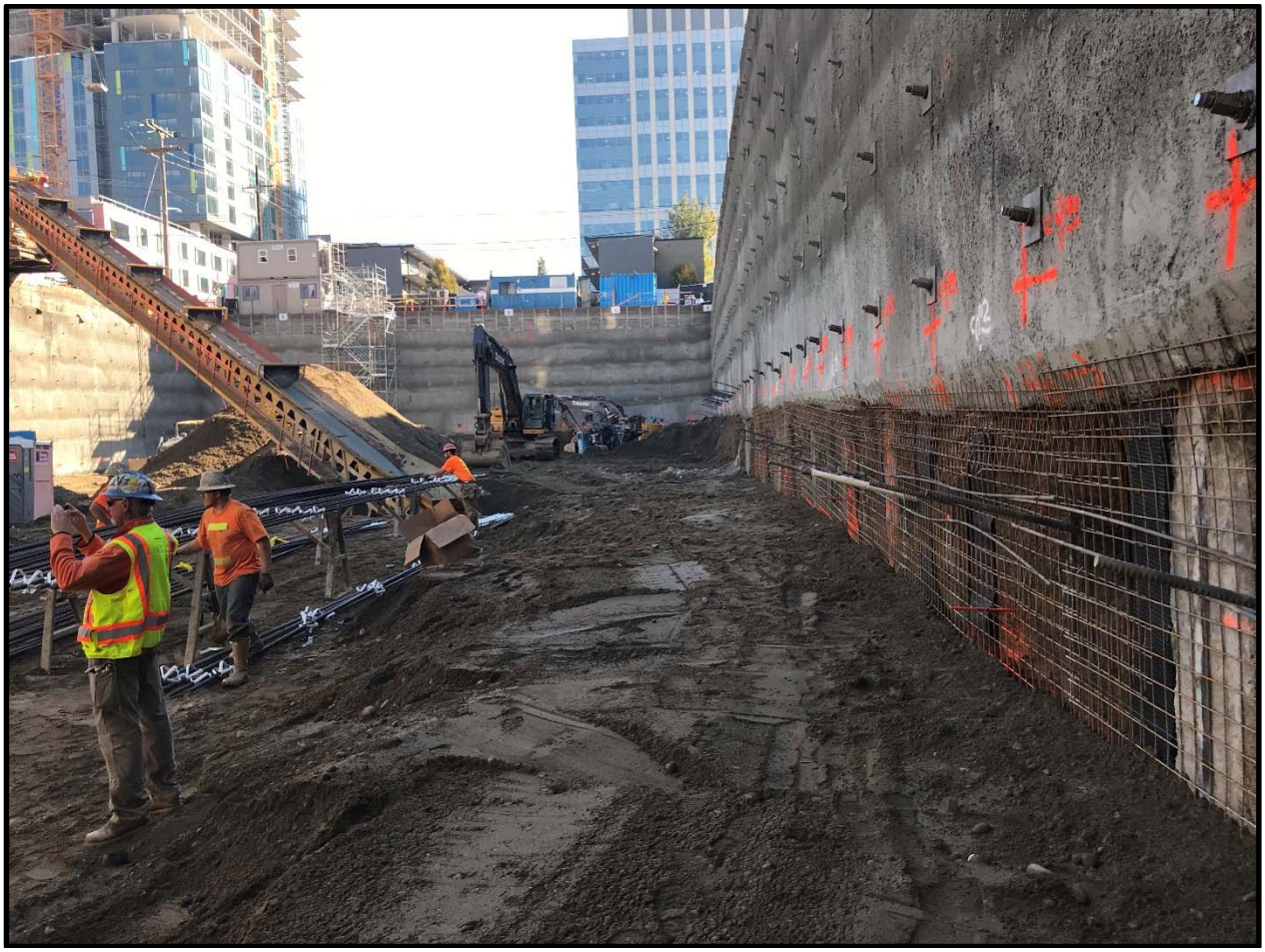


Fig. 4 - Shoring Walls Excavation in Progress

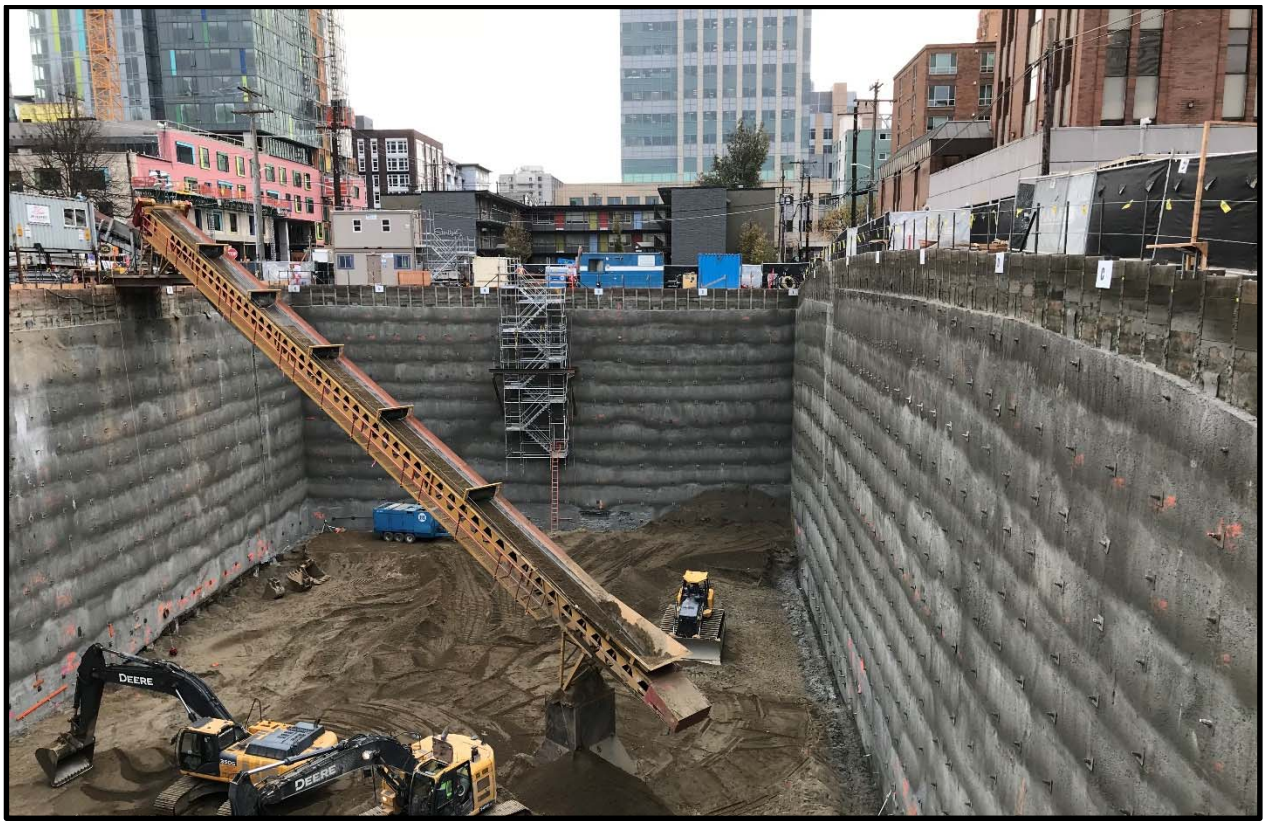


Fig. 5 - Shoring Walls Near the Base of the Excavation

SHORING MONITORING AND MEASURED DISPLACEMENTS

The City of Seattle requires that shoring walls be designed for a maximum 1-inch of deflection at the top of the shoring and that optical survey monitoring, with an accuracy of 0.01 feet, be performed twice weekly by a licensed surveyor during construction to monitor the performance of the shoring. Optical survey monitoring points were established on every other vertical element or about 6 feet on center around the entire perimeter of the shoring. Survey monitoring points were also established on the Archdiocese building and the adjacent streets.

A total of 4 inclinometer casings were installed on the backside of the long vertical elements located near the midpoint of each of the four shoring walls. The inclinometer measurements were taken periodically during construction of the shoring walls. Figure 6 illustrates the west shoring wall inclinometer measurements completed by GeoEngineers.

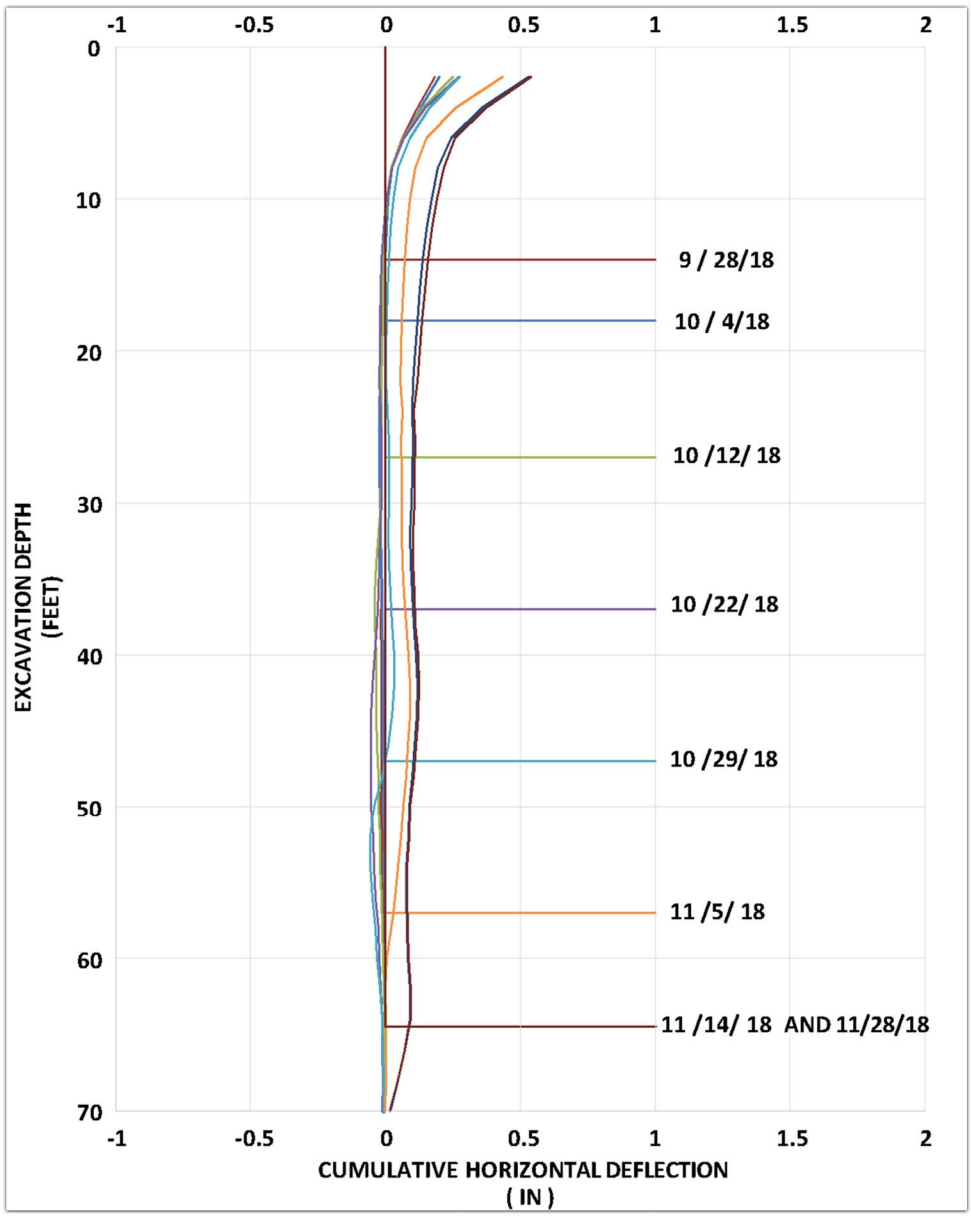


Fig. 6. West Shoring Wall Inclinometer Measurements

Based on the inclinometer measurements, the composite soil nail wall deflection was on the order of ½-inch for the west shoring wall, which is representative of the displacements measured in the three other inclinometers. The optical survey monitoring measured a maximum horizontal displacement of 0.9 inches at the top of the shoring wall; however, the average horizontal displacement was on the order of ½-inch.

SUMMARY AND CONCLUSIONS

The composite soil nail shoring proved to be more cost effective than the originally proposed post tensioned anchored shoring system. The estimated maximum shoring deflection of 1-inch was validated by the optical survey monitoring and inclinometer measurements performed to monitor the performance of the composite soil nail shoring walls. The presence of dense to very dense glacially consolidated unit allowed for the use of a composite soil nail shoring wall system, while limiting defections to within the City of Seattle requirement of a maximum of 1-inch. The use of wood lagging in the upper four to five feet of the shoring

walls allowed for incorporation of removable pile tops into the design and construction. Soil nailing also eliminated the need for block outs in the permanent building walls required to de-tension a post tensioned anchored system.

REFERENCES:

Byrne, R.J., Cotton, D., Porterfield, J., Wolschlag, C., and Ueblacker, G., (1998). "Manual for Design and Construction Monitoring of Soil Nail Walls," Report FHWA-DP-96-69R, Federal Highway Administration, Washington, D.C.

CALTRANS (1991). "A User's Manual for the SNAIL Program, Version 2.02 – Updated PC Version," California Department of Transportation, Division of New Technology, Material and Research, Office of Geotechnical Engineering, Sacramento, California.

CivilTech Software (2007). Shoring Suite Version 8 User's Manual, CivilTech Software, Bellevue, Washington.

FHWA (1993). "French National Research Project Clouterre, 1991-Recommendations Clouterre 1991," (English Translation) Soil Nailing Recommendations, Publication FHWA-SA-93-026, Federal Highway Administration, Washington, D.C.

Lazarte, Carlos.A. Ph.D., P.E., Elias, Victor, P.E., Espinoza, David R., Ph.D., P.E., Sabatini, Ph.D., P.E. (2003). "Geotechnical Engineering Circular No. 7, Soil Nail Walls", Report No. FHWA A0-IF-03-017.

Sabatini, P.J. et al. (1999). "Ground Anchors and Anchored Systems," Geotechnical Engineering Circular No. 4, Publication FHWA-IF-99-015, Federal Highway Administration, Washington, D.C.

DEEP EXCAVATION SUPPORT: INNOVATIVE SHORING DESIGN IN AN URBAN ENVIRONMENT

Richard D. Luark, Terracon Consultants, Inc., Mountlake Terrace, Washington, USA, 425-301-8782, Richard.Luark@terracon.com
Fernanda S. Madrona, Terracon Consultants, Inc., Mountlake Terrace, Washington, USA, 240-472-5506, Fernanda.Madrona@terracon.com

ABSTRACT

Designing temporary retaining systems that allow for deeper excavation amid the existing urban infrastructure has become a challenge. A 60-foot-deep excavation in downtown Seattle was required to construct five levels of below grade parking for a 35-story high-rise building, Tower 12, next to an existing 20-story tower with three levels of below grade parking, separated from the project by an 18-foot wide alley. The solution was to combine two temporary excavation support systems, soil nailing and anchored soldier piles, to work within the site constraints. Densely-arranged, short-length soil nails were used to support the upper 30 feet of the excavation, while the lower 30 feet of the excavation was supported with soldier piles combined with steeply-inclined, high-capacity ground anchors, which extended below the adjacent building foundations. The combined temporary support system eliminated the need for internal bracing, reducing construction cost and schedule. The performance of the combined soil nail and soldier pile system was monitored with an inclinometer and optical survey monitoring, which demonstrated the performance of the combined temporary support system. This paper provides a discussion of the advantages of combining different excavation systems and an analysis of movement monitoring data collected.

Keywords: deep excavation, soil-structure interaction, soil nailing, anchored soldier piles, movement monitoring

SITE CONDITIONS AND PROJECT INFORMATION

Tower 12 consists of a 0.45-acre development with 36-stories of mixed, residential and commercial use with four levels of below grade parking. The project site is bounded by the Cristalla Condominium to the north, Virginia street to the south, 2nd Avenue to the East, and an 18-foot wide private alley to the west. The One Pacific Tower Condominium, which has three levels of below grade parking, was located to the west across the alley. A site layout plan is presented as Figure 1.

As shown in Figure 1, the construction of the west wall required a maximum 51-foot-deep excavation, from elevation (EL) 162 feet to EL 111 feet. Adjacent to the west wall, the existing alley grade varies from elevation 154 to 161 feet, leaving a narrow block of soil 18 feet wide and up to 42 feet high to be shored along the alley in order to reach the One Pacific Tower bottom of mat foundation at EL of about 120 feet. In addition to the existing One Pacific Tower Basement wall, site constraints included existing utilities along the alley such as an existing 4.5-feet wide by 7-feet high vault, with bottom at approximate EL 146 located 10 feet from the back face of the proposed Tower 12 basement wall.

© 2019 Deep Foundations Institute

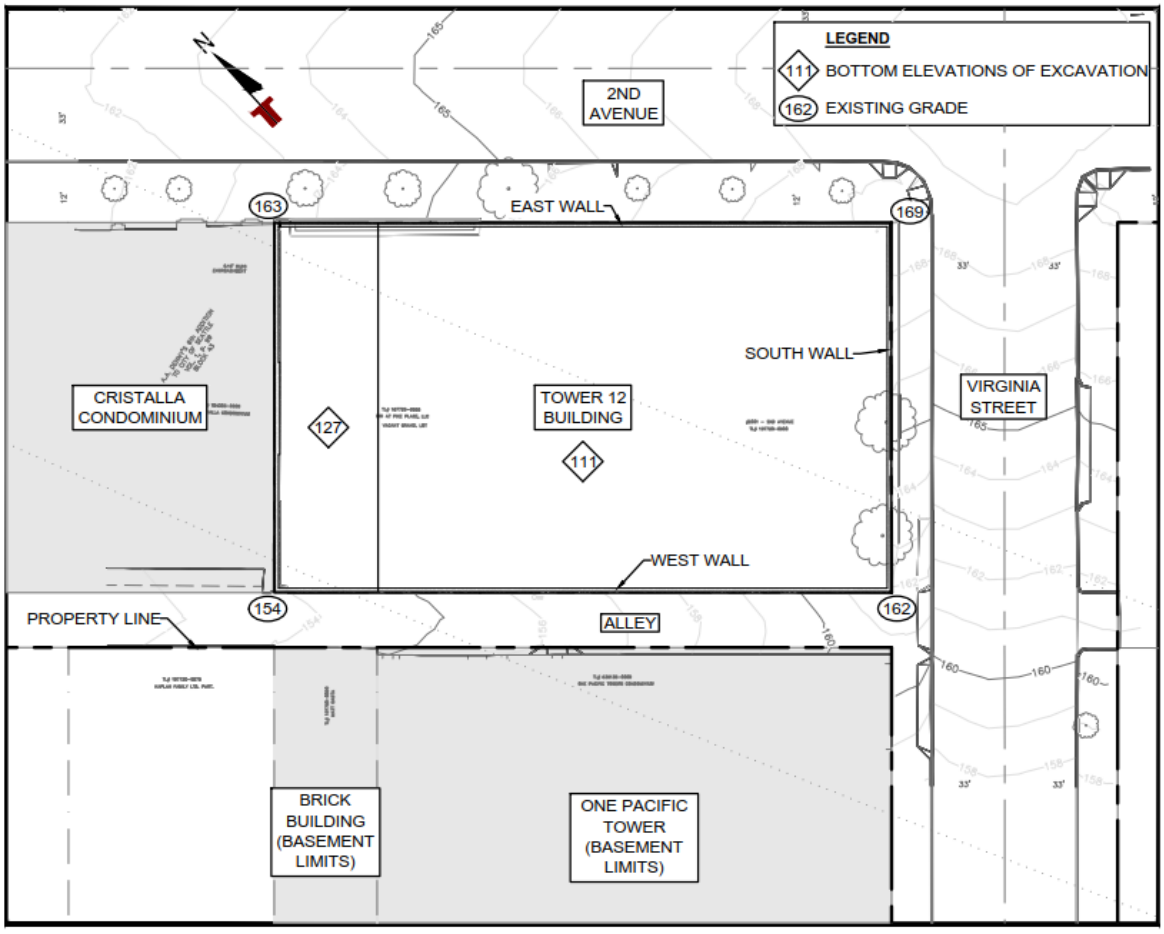


Fig. 1. Site Plan

Terracon Consultants, Inc. (Terracon) was both the geotechnical engineer and shoring designer of record for the project. In addition, Terracon provided geotechnical special inspection during installation of the shoring system and foundation for the high-rise building. DBM Contractors, Inc, was the shoring subcontractor, with PCL as the general contractor.

SOIL AND GROUNDWATER ENVIRONMENT

The Seattle area is generally underlain by a glacial sequence of soil consisting of recessional outwash, till, advance outwash, and lacustrine deposits associated with the Vashon Stade glaciation. Also present are older glacial and interglacial deposits. The project site lies within the area of the Denny regrade of the 1900s, and significant cuts and fills were made to achieve the current ground elevations. Review of the 1910 City of Seattle topographic maps indicated that the ground surface at that time was within 10 feet of the existing site grades. According to Troost, K.G., et al. (2005), the site is underlain by Q_{pf}, which is identified as deposits of pre-Fraser glaciation age. These deposits consist of interbedded sand, gravel, silt, and clay layers. The soils on the site adjacent to the west shoring wall generally consisted of 6 to 8 feet of sandy silty clay fill over very stiff to hard native clay and silt deposits of varying plasticity. Several perched water tables have been inferred in the area above the regional groundwater table, which is at an elevation of about 20 feet (NAVD88). Perched groundwater was anticipated at a depth below existing ground surface of 14 to 16 feet (approximate elevation 140 to 147 feet). Below this elevation, seepage was anticipated within sandier zones that are present within the clay and silt deposits. Three soil borings were drilled at the

vicinity of the West Wall. The soil profile is shown in Figure 2. Also illustrated in Figure 2 are the limits of west wall and the projection or section of adjacent buildings basement walls.

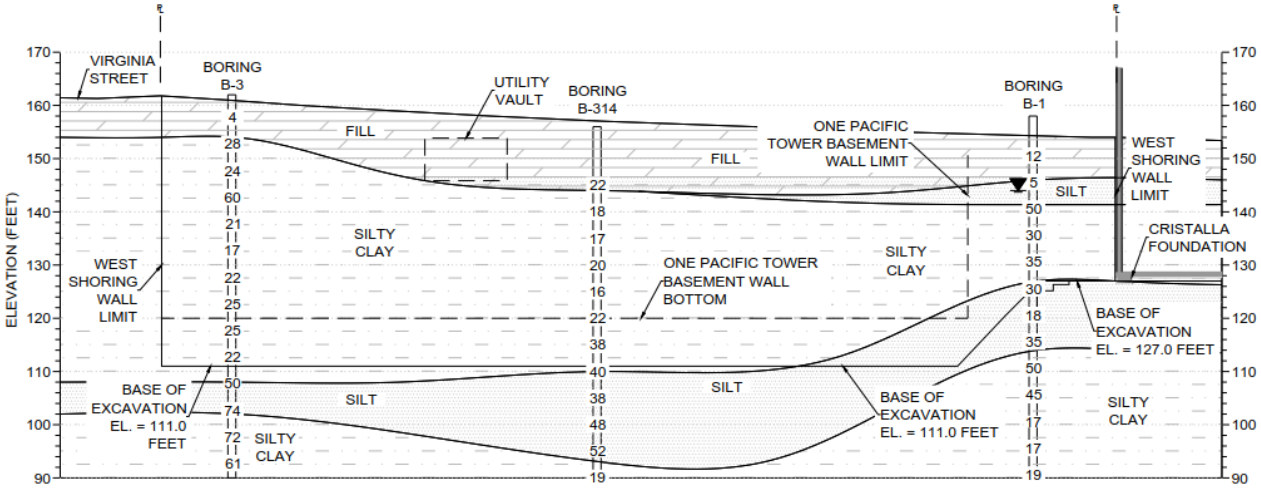


Fig. 2. Soil Conditions and Site Constraints

As we can see from Figure 2, the site is generally underlain by soft to very stiff fill over glacially consolidated fine-grained deposits including fat clay and nonplastic to low-plasticity silt.

WEST WALL EXCAVATION SUPPORT PLAN

The One Pacific Tower building basement limited the horizontal distance available for placement of anchors in the upper half of the excavation along the west wall. Therefore, the solution to support the excavation along the west wall was to combine two different support systems, soil nailing and anchored soldier piles, to work within the site constraints. A soil nail wall was used to support the upper 30 feet of the excavation, from the alley existing grade down to EL 135 feet where the wall transition to a soldier pile and tieback shoring extending to the base of the excavation at approximate EL 111. Consequently, the bottom 30 feet of the excavation was supported with soldier pile with steeply-inclined, high-capacity (200,000 pound) ground anchors, which extended below the adjacent basement wall of the One Pacific Tower building. The solution is shown on the West Wall Section illustration presented as Figure 3. Notice how the geometry of the existing basement and underground utilities were accommodated with the combination retaining wall system. This system also eliminated the need for internal bracing, which would have increased the project's construction cost and schedule.

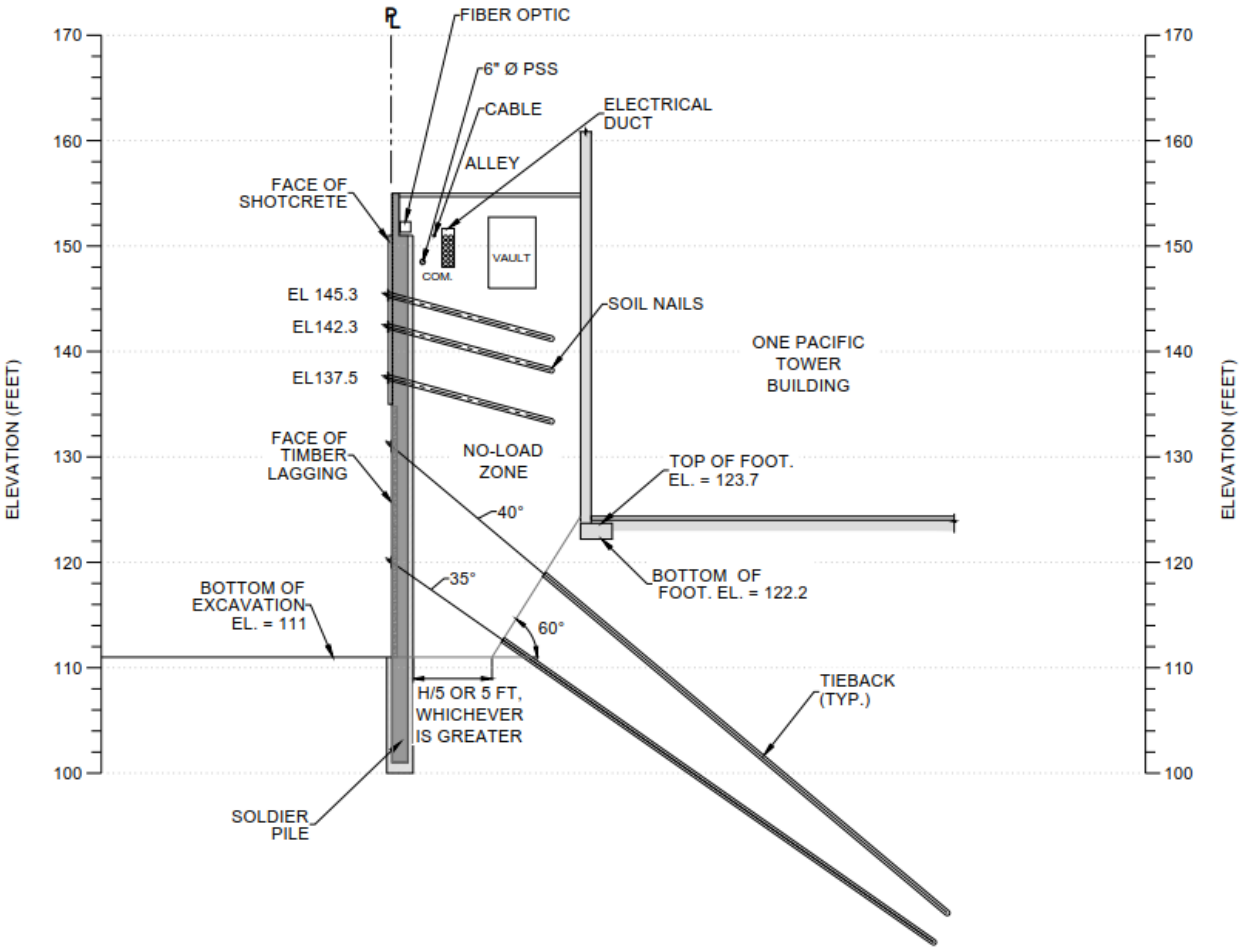


Fig. 3. West Wall Cross Section

SHORING WALL DESIGN

Based on the subsurface conditions encountered during site investigation and our experience with the geology in the area, the soil strength parameters in Table 1 were adopted for the design of the soil nail wall system.

Table 1. Soil Shear Strength Parameters

Soil Unit	Moist Unit Weight (pcf)	Friction Angle (deg)	Cohesion (psf)	Ultimate Soil Nail Pull Out Resistance (kip/ft)
Fill	120	30	0	2
Native Silt and Clay	125	30	200	4

SnailWin version 3.10 was used to design nails at the upper 30-foot high soil nail wall, which included a 250psf vertical traffic surcharge load. Nails lengths of 16 feet were used, limited by the width of the existing alley. Therefore, the soil nail wall design consisted of spacing the soil nails to meet a minimum factor of safety of 1.35 on the soil shear strength. Rsoil nails spacing was 4 feet by 4 feet, both horizontally and vertically. Soil nail wall facing consisted of 4-inch-thick shotcrete reinforced with a WWF 4x4 –

W4.0XW4.0 mesh. The soldier piles required for the post tensioned anchored wall below the soil nail wall extended up to existing grade and acted as vertical elements to provide structural support of the soil until the first row of nails, located at about 9 feet below the alley surface, could be installed.

Additional vertical elements consisting of W12x35 steel beams, set in 18-inch diameter pre-drilled boreholes and backfilled with lean concrete were placed between the soldier piles to provide face stability and increased stiffness to minimize deformations. At the location of the existing electrical vault, an approximate 14-feet deep excavation prior to support with soil nails was required. Therefore, in this location, additional W18x76 soldier piles, extending 10 feet below the bottom of the soil nail wall, were installed.

For the design of the soldier pile system with tiebacks, the upper soil nail wall was assumed to act as a surcharge load on the soldier pile wall below. Although the soil nail wall and soldier pile wall were structurally connected, it was assumed that the soil nail wall would not place lateral loads on the soldier piles above an elevation of 135 feet. Below this elevation, the soil nail wall was modelled as a lateral surcharge equal to 0.4 times the overburden weight acting over the soldier pile below. Lateral surcharge pressures from adjacent building foundations were based on the Boussinesq's equation modified by Teng, using Shoring suite V8 Program by CivilTech. The maximum soil nail wall height is 27 feet, which equals to a 1,332 psf surcharge on the soldier pile wall.

The apparent earth pressure diagram used in the design of the soldier pile wall followed the methodology recommended by FHWA-IF-99-015, taking into consideration soil conditions. As shown in Figure 4, the lateral earth pressure distribution for the shoring system below the soil nail wall consisted of a trapezoidal distribution with a maximum pressure equal to 26 H, in psf, where H is the height of the excavation in feet, with a truncated top beginning at 2/3 H_1, where H_1 is the depth to the first tieback, and truncated at the bottom at $2/3H_{n+1}$, where H_{n+1} is the height to the last row of tiebacks from the base of the excavation. An allowable passive pressure equal to 300 pcf acting over two times the concrete pile diameter or the pile center to center spacing, whichever is less, on the embedded portion of the soldier pile was used for the design.

Tiebacks were located sufficiently far behind the excavation shoring to stabilize the excavation face, which is the known "no load" zone. The "no load" zone adopted was equal to a lateral distance from the base of the excavation equal to the exposed wall height (H in feet) divided by 5, or 5, whichever is greater, and a line sloping up and back at 60 degrees from horizontal.

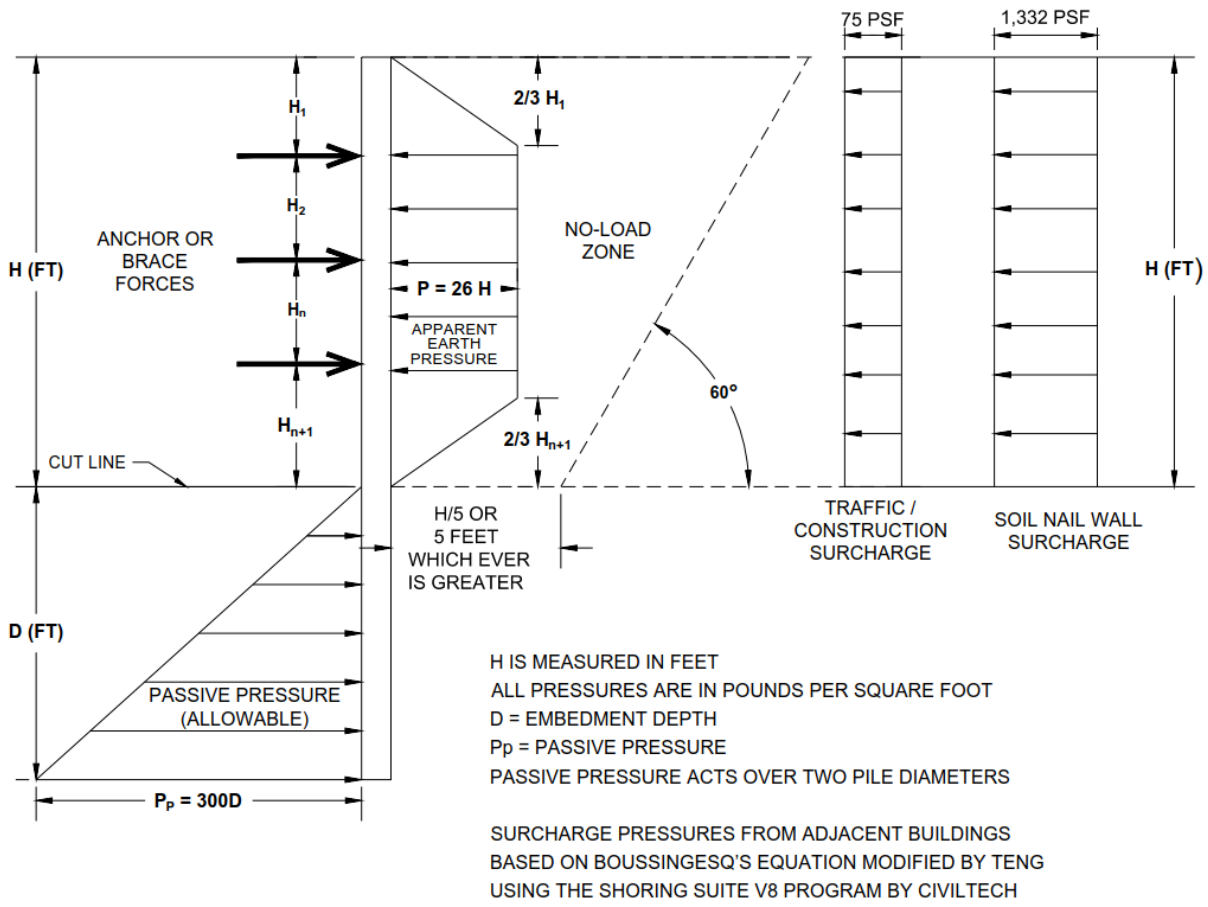


Fig. 4. West Wall Pressure Diagram

The beams for the soldier pile wall consisted of W18x76 steel beams set in 30-inch diameter pre-drilled boreholes backfilled with lean concrete above the cut line and structural concrete in the toe. The soldier piles were generally spaced at 8 feet on center and extended below the base of the excavation at a minimum embedment of 10 feet. In general, the W18x76 beams spaced 8-feet on center can support a 12-foot excavation with estimated deflections of less than 1-inch. Tieback lengths of up to 66 feet were required for the first row and 53 feet for the second row of tiebacks. Tieback capacities of up to 211 kips was required to balance applied pressures. The maximum calculated deflection estimated during design phase on the W18x76 beams was 1 inch as based on the Shoring Suite V8 computer program by CivilTech and experience.

WALL CONSTRUCTION

Installation of the soldier piles for the Tower 12 project started on April 15, 2015 with completion of the shoring system and mass excavation on June 24, 2015. A photograph of the hybrid shoring system near completion is shown in Figure 5.



Fig. 5. Wall During Construction

Verification tests up to 200% of the design load were also performed to verify bonding strengths assumed in design of 4 kip/ft (ultimate) in the native silts and clay. Proof tests were performed on all production anchors, with maximum load of 130% of the design load. Wall construction was successful and performed within budget and schedule.

MOVEMENT MONITORING DURING CONSTRUCTION

The performance of the temporary retaining wall was monitored with one inclinometer behind the west wall as well as optical survey monitoring of the top of the entire excavation, adjacent roadways, and buildings. The monitoring program demonstrated the performance of the unique design met the City's maximum deflection requirement of 1 inch, as presented in Figure 6 and 7.

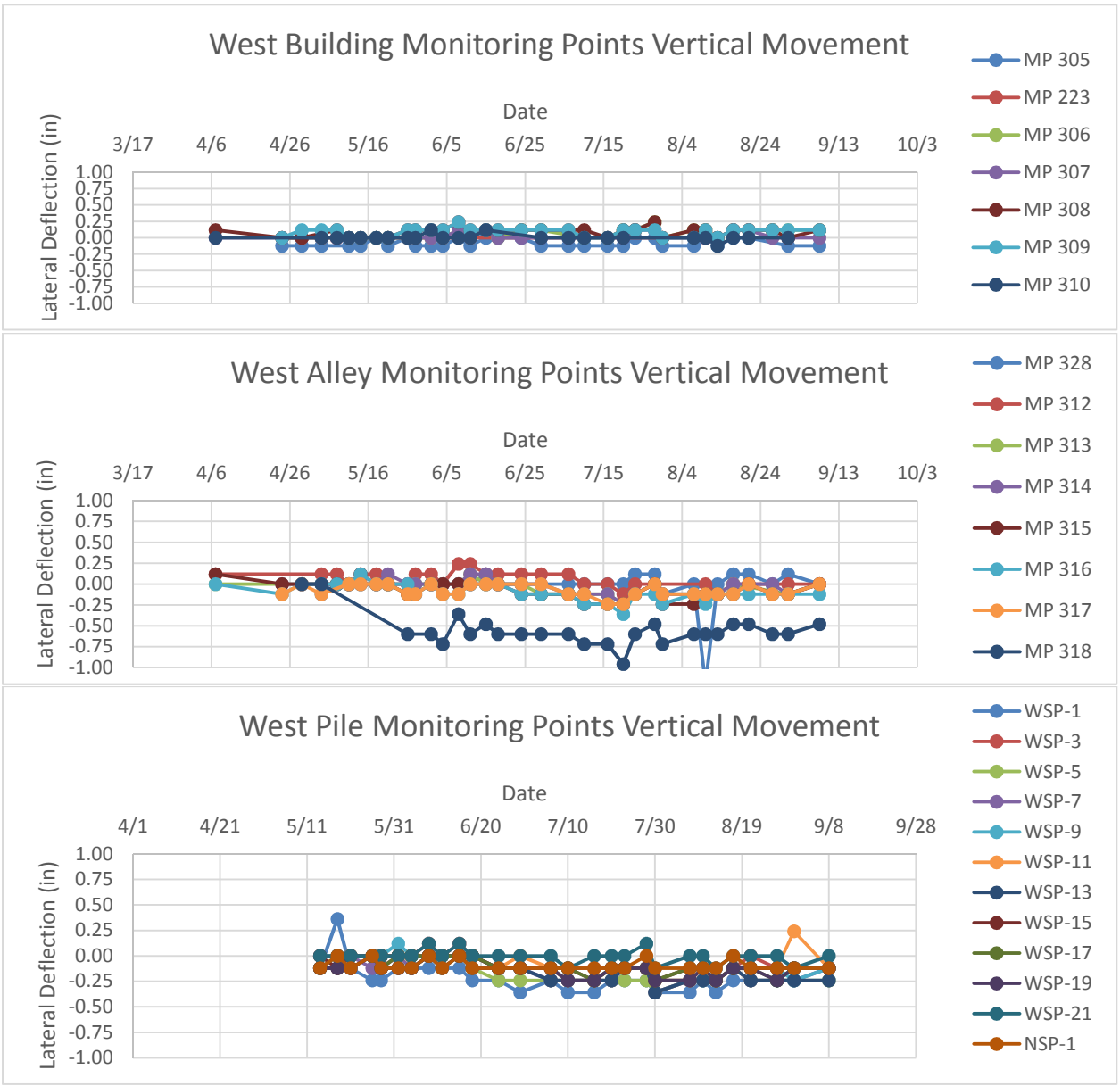


Fig. 6. Results of Monitoring Program (Surveying)

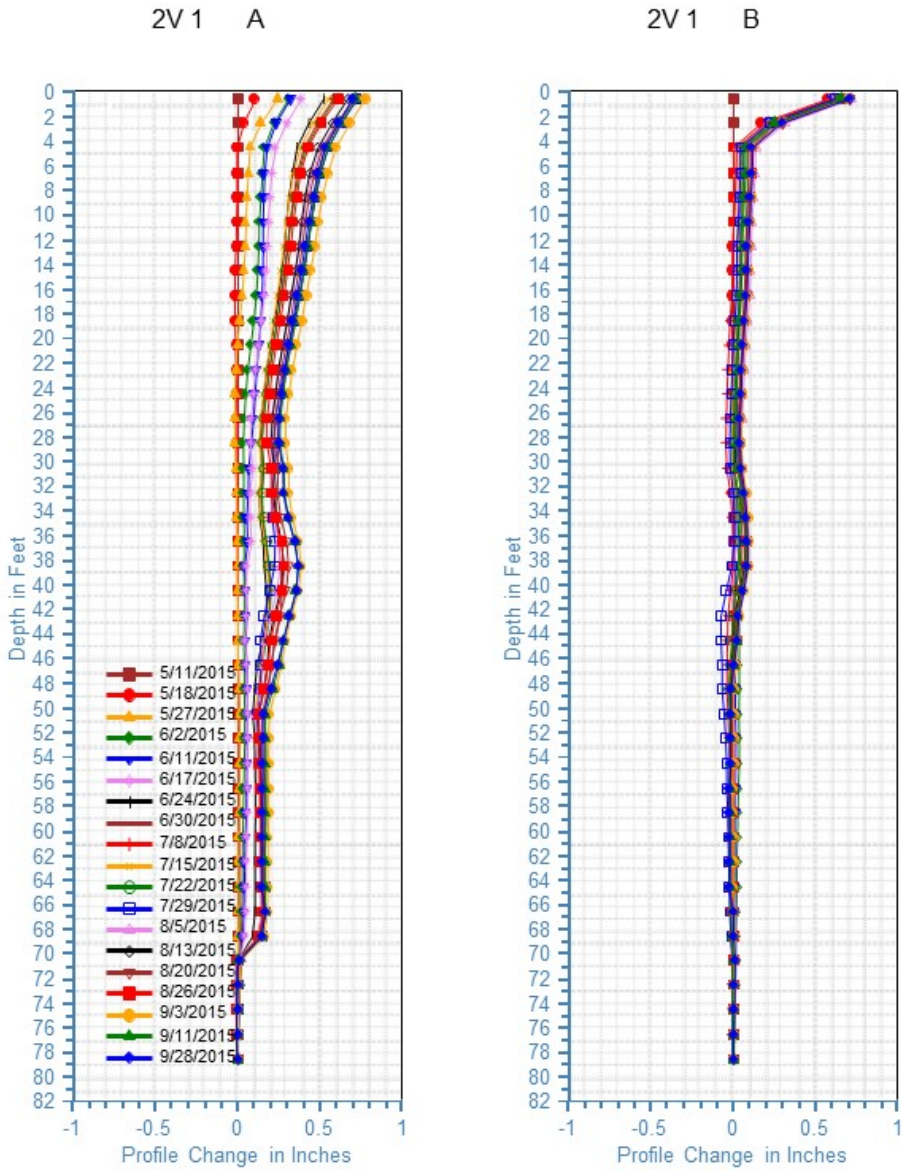


Fig. 7. Results of Monitoring Program (Inclinometer)

Figures 6 and 7 show that the actual measured wall deflections, which reached about 0.8 inch, are in agreement with the predicted deflections during design. Maximum lateral wall movements for anchored walls constructed in sands and stiff clays average approximately 0.2%H with a maximum of approximately 0.5%H where H is the height of the wall (Sabatini et al., 1999). An 0.8-inch deflection corresponds to a wall movement of 0.13% of H.

SUMMARY AND CONCLUSIONS

In this project, the use of a traditional soldier pile shoring for the entire height of the west shoring wall was not possible due to the basement levels and foundations of the One Pacific Tower. The combined temporary support system consisting of soil nailing over a soldier pile wall with post tensioned anchors eliminated the need for internal bracing, which would have increased the project's construction cost and schedule. Monitoring of lateral displacements with an inclinometer and optical survey during construction validated

the performance of the system, which measured deflections to be less than the predicted deflections during design.

REFERENCES

CALTRANS (1991). "A User's Manual for the SNAIL Program, Version 2.02 – Updated PC Version," California Department of Transportation, Division of New Technology, Material and Research, Office of Geotechnical Engineering, Sacramento, California.

CivilTech Software (2007). Shoring Suite Version 8 User's Manual, CivilTech Software, Bellevue, Washington.

Troost, K.G., et al., 2005. "The geologic map of Seattle – a progress report."

Sabatini, P.J., Pass, D.G., and Bachus, R.C., 1999. "Ground Anchors and Anchored Systems," Geotechnical Engineering Circular No. 4, Report No. FHWA-IF-99-015, Federal Highway Administration, Washington, DC.

JET GROUT UNDERPINNING OF SENSITIVE STRUCTURES IN URBAN ENVIRONMENTS

John H. Gill, Hayward Baker, Inc., Cumberland, RI, USA, 401-334-2565, JHGill@HaywardBaker.com
Alexander Ciccone, Hayward Baker, Inc., Middletown, CT , USA, 860-685-9095, Alexander.Ciccone@haywardbaker.com

ABSTRACT

Jet grouting is a highly versatile ground modification technique that can offer significant commercial and technical advantages over traditional concrete pit underpinning applications. Despite these advantages, jet grouting remains an underutilized technique in the construction industry due to its perceived complexity, cost, and risk. When performed thoughtfully, underpinning by jet grouting offers significant safety and schedule advantages over traditional underpinning approaches. The New England construction market has seen a recent acceptance in the use of jet grout underpinning on congested project sites across a variety of subsurface conditions. The reduction of the cement batch plant footprint due to equipment advances has allowed the use of this technique in urban sites where its use would be previously infeasible. Furthermore, jet grout underpinning has been utilized for support of historic and sensitive structures with generally lower tolerance to settlement than is typically feasible with conventional pit underpinning. Robust, real-time geotechnical instrumentation monitoring systems have helped reduce the uncertainty and further expand the feasibility of jet grout underpinning applications. When properly designed and constructed by qualified and experienced jet grouting contractors, the flexibility of soilcrete for design and construction may be utilized to overcome the many inherent challenges which complicate underpinning and earth retention systems.

Keywords: jet grouting, underpinning, sensitive structures

INTRODUCTION

The construction of buildings and infrastructure in our increasingly dense urban spaces often requires excavations below the elevation of existing structures immediately adjacent to the proposed work. Where a proposed excavation system encroaches into an existing structure's zone of influence, additional measures, such as the construction of an underpinning or excavation support system, are required to safely excavate and minimize the impacts on the adjacent structures.

Jet grouting is one method of underpinning that offers significant commercial and technical advantages over many other techniques. Though it was first used to the United States in the 1980s and has grown in popularity elsewhere, jet grout underpinning remains underutilized domestically due to its perceived cost and risk premium. Jet grouting has significant technical advantages over other underpinning methods due to its applicability in a wide range of soil types and its flexibility of design and installation. The jet grouting process is capable of limiting the movement of foundations during construction and excavation to lower thresholds than most traditional underpinning methods (Droof, Furth, & Scarborough, 1995). Its use for underpinning historic and sensitive structures with lower settlement criteria provides additional evidence to its technical utility. Through thoughtful design, adequate planning, and experienced installation, jet grouting can be an appropriate underpinning solution that can provide significant cost and schedule savings.

This discussion highlights the application of jet grouting for building underpinning, and seeks to provide readers with the tools and insights necessary to efficiently propose, design, and utilize jet grouting on prospective projects. It further highlights the authors' own lessons learned on recent jet grouting projects to further encourage its use.

© 2019 Deep Foundations Institute

TRADITIONAL UNDERPINNING APPLICATIONS

Underpinning systems provide vertical support of a structure, utility or feature through direct, engineered contact. They may also be designed to resist the laterally applied structural, geotechnical, or surcharge loads. The underpinning process itself typically involves the alteration of the vertical or lateral load distribution of a stable (at rest) footing. A redistribution and addition of forces on the footing and underpinning system occurs during the temporary construction operation as well as the excavated condition, likely resulting in movement of the footing and supported structure (Burke, 2007). The design and construction of all underpinning methods seek to limit these vertical and horizontal movements.

All underpinning methods share the primary purpose of extending an existing foundation to a lower elevation to improve the performance of the foundation. Often an excavation on one side of the footing and underpinning system is required, generating an unbalanced lateral load on the system.

Pit underpinning remains the most common method of underpinning and involves digging discrete individual pits, typically no larger than four feet square, to a depth required for stability in the excavated case. The underpinning contractor must manually loosen soil, typically with small shovels or pneumatic tools, and remove it from the pit with buckets hoisted to the surface. The face of the pit is lagged with timber boards as it is dug, and upon reaching terminal design depth, it is backfilled with unreinforced concrete. An example of typical conditions during the performance of pit underpinning is presented in Fig. 1.



Fig. 1. Typical pit underpinning operation below an existing discrete foundation.

As the applied load over the existing footing is temporarily transferred to the adjacent portions of the footing pit, underpinning must be carefully sequenced to avoid overstressing the footing or soil. As a result, pit underpinning is a tedious process, requiring significant labor and time to perform even limited scopes. Furthermore, it requires workers to enter potentially confined spaces at a depth below existing structures, generating conditions which must be carefully monitored for environmental exposure as well as structural stability of the foundation and pit

Other underpinning methods involves drilling or driving piles through or directly adjacent to existing footings, and connecting the new piles to the existing footings with steel connection details. During

excavation, lagging may be applied to the piles to provide lateral restraint of soil, or a shotcrete and soil nail face may be installed to provide lateral restraint independent of the vertical support piles.

JET GROUT UNDERPINNING

Jet grouting is an in situ soil improvement method with a wide range of applications; however, it is particularly technically and commercially suited to underpinning and excavation support (Burke & Koelling, 1995). Jet grouting is installed above grade, under safer working conditions, and with significantly reduced durations relative to traditional pit underpinning. As such, it offers a commercially attractive solution for most underpinning projects.

The jet grouting process involves drilling a small diameter borehole below grade and introducing hydraulic and often pneumatic energy from the end of the drill string to erode, mix, and partially replace the existing soil with an engineered cementitious grout. (Burke, 2002). The product of the in situ soil and grout mixture is known as soilcrete and typically has design strengths of 50 to 2000 psi, rendering it capable of providing combined vertical and lateral support in underpinning applications. Individual, overlapping, columns are created by drilling and grouting sequential locations which must be thoughtfully staged, such as in pit underpinning, so as to not concurrently undermine a significant portion of foundation.

Significant flexibility exists in the installation procedures and the resulting geometry of soilcrete. Design engineers specifying jet grouting on any project must consider these flexibilities, and often rely on specialist expertise and experience to furnish an appropriate system, installation procedure, and geometry. In typical jet grouting projects more than one jet grouting system (single, double, or triple fluid) may be appropriate. System selection and variation is typically performed by the grouting contractor.

This discussion does not focus on jet grouting principals, or system selection, however for readers interested in additional information on the process of jet grouting, a vast body of technical literature is available within prior Deep Foundations Institute publications.

Applicable soil conditions for jet grout underpinning

As an erosive process, jet grouting does not rely on soil permeability and can be tuned to specific soil types and conditions, making it even applicable to sites with highly heterogenous soil profiles. Jet grouting mixes and replaces a portion of the soil in the treatment zone. The effectiveness of the grouting and the quality (i.e. the homogeneity, strength, and permeability) of the soilcrete product are therefore dependent on the jet grout system selection, the erosional properties of the soil, and the injected grout.

The jet grouting system, grouting parameters, and installation procedures must be modified to match the soil conditions.

Non-cohesive sands, non-plastic silts, and gravels exhibit high erodibility and tend to result in soilcrete products of higher strength and consistency. Highly plastic clays and silts require relatively higher cutting energy to erode. These soils tend to erode in clumps rather than dispersing into particles. Measures must be taken to address the clumps' tendency to clog the borehole annulus or remain in the soilcrete product undispersed. This is further discussed below in regards to heave potential.

Jetting can be particularly advantageous in high water table applications and where pitting, lagging, or shotcreting would require dewatering. Figure 2 depicts a recent application where a saturated organic soil was economically grouted below an existing pile supported structure to provide a stable 4 to 8-FT cut. The soilcrete effectively eliminated water flow by extending into a marine clay layer. Pit underpinning, micropile and lagging, helical piles and shotcrete were considered but lacked the advantages offered by jetting.



Fig. 2. Soilcrete provided an economical underpinning of a 200-FT section of wall along a pile supported structure. The soilcrete provided a stable means of excavating 4 to 8-FT in saturated organic soils.

Soilcrete properties for underpinning applications

Due to the inherent variation of soil and heterogeneity of soilcrete, large gradations in soilcrete strength are common between soil types and within individual soil strata. The soil-cement spoil mixture exiting the borehole is an appropriate estimation of the quality of soilcrete created in situ. Both the soilcrete spoil and the in-place soilcrete product gain strength at a slower rate than structural concrete, with strength gain typically expected 28 days. Overnight strength gain of underpinning columns is sufficient to grout adjacent locations the following working shift.

Occasional low strengths may be encountered during compressive testing of soilcrete cores or spoil samples due to small soil inclusions. As the underpinning system is governed by the strength of the mass, such inclusions are rarely cause for concern, however variation in strength should be anticipated and accounted for in design. When specifying required strength of soilcrete, it is appropriate to provide a minimum design strength and an allowable standard deviation of break results such as in any jet grout or soil mixing application. For example, a typical specification may require 95 percent of soilcrete samples to exceed 200 psi.

Bleed of the underpinning columns, both due to the curing process of cement and permeation into surrounding soil, must be controlled to prevent tops of soilctrete columns from dropping below bottom of footings. Working from a grade slightly above bottom of footing and topping off columns at the end of shift are best practices to prevent such occurrence.

Design principals

Most underpinning designs rely on fundamental moment equilibrium analyses and numerical calculations. Once the feasibility of the system has been established, the designer must develop a baseline estimation of the required soilcrete mass needed to stabilize the existing footing. The vertical load on the existing footing is estimated, and a simplified geostatic force analysis of the underpinning system is performed to determine the required depth and width of grouting necessary to resist overturning, sliding and bearing capacity failure

(Fig. 3). This existing pinning force restrains the underpinning system, so unfactored loads should be considered in sliding and overturning calculations.

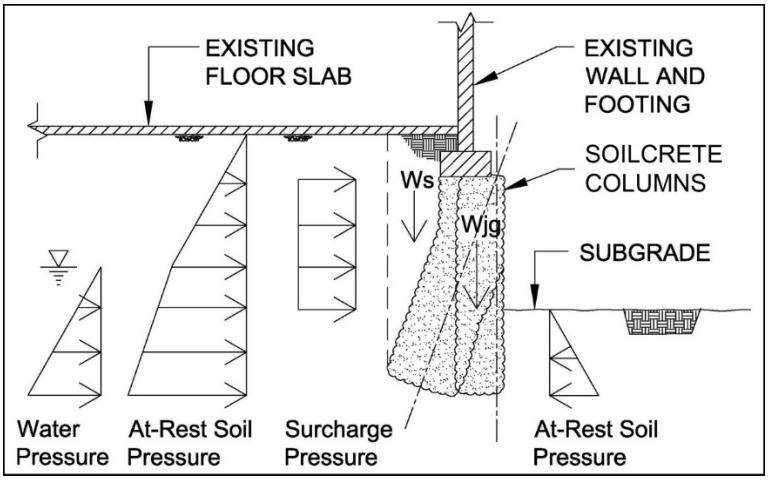


Fig. 3. – Typical design section of a gravity wall jet grout underpinning solution.

Where underpinning depth exceeds four to six feet, more than one row of soilcrete columns or external reinforcements are likely required to resolve the sliding and overturning moment of the system. External restraints such as soil nails or tiebacks drilled through the column, can be applied to resolve excess sliding and overturning moments of the system. Underpinning with additional tiebacks for stability under a sensitive structure is depicted in Fig. 4.



Fig. 4. – Tiebacks or soil nails are commonly employed to provide additional restraint for deeper applications.

For internal stability reinforcement bars can be lowered into the soilcrete column before curing to increase the bending and tensile capacity of the soilcrete mass. Bearing capacity and settlement rarely govern underpinning design, however, they should be verified especially where active tiebacks apply increased vertical load to the system. Consideration must be given to the potential for settlement due to the transfer of existing foundation loads to new soil depths (Burke, Johnson & Heller, 1989).

Burke and Koelling aptly noted that jet grout underpinning requires "experience-based design", demanding particularly high levels of communication between contractors, owners, and design engineers during the design and construction phases (1995). Jet grout contractor feedback should be incorporated regarding anticipated soilcrete column sizes and proposed layouts, including any equipment or access constraints. It is rarely possible drill directly flush to the building façade, for example, so some thought should be given to the proximity to existing structures and the method of attaining grout directly under the existing footing.

INSTALLATION RECCOMENDATIONS

Quality and verification of the soilcrete product

The quality and consistency of the as-built soilcrete geometry must be carefully considered on any jet grout underpinning project. The soilcrete size, connectivity, strength, consistency, and permeability all potentially impact the underpinning system performance.

Common measures of assessing and controlling the risks of the soilcrete product vary with project size and application. In lower risk applications, a reasonable baseline testing program may include simply exhuming one or more pre-production test column, sampling and testing soilcrete spoil samples, and even coring a small percentage of completed production columns. An example of exhumed test columns as part of a jet grout underpinning project is presented in Fig. 5. Where significant risk of column inconsistency is present, redundancies may be built into column layout and design.



Fig. 5. Exhumed test columns as part of a typical jet grout underpinning project.

Though less common in underpinning projects, in applications where higher levels testing of column geometry and consistency are crucial, column geometry may be verified by acoustical testing.

Sequencing of installation

While drilling of jet grout columns can typically penetrate in place obstructions, the risk of shadowing of soilcrete columns around these obstructions (incomplete column creation due to reflection of the jet off an in-place feature) must be monitored and accounted for during construction. Shadowing may also occur

around in place soilcrete geometries, so carful sequencing of column construction is essential. Consideration must be given to where adjacent columns should be constructed “wet-on-wet”, or where an initial setup period is necessary. The in situ vertical and lateral soil stresses from adjacent foundations and structures may also impact the allowable geometry and sequencing of jet grouting construction.

Data acquisition and geostructural monitoring

Due to the injection of fluids at high flow rates, one item of concern on any jet grout underpinning project is the potential for heave or settlement of the structure. At this point, most active specialty grouting contractors utilize real-time data acquisition systems on the drill rig and grout pump to monitor and record jetting parameters. These real-time measurements allow for the drill operator to exercise rapid response, and also facilitates the inspection of as-built logs by the construction team to verify installation consistency.

More recently, the more frequent adoption of geo-structural instrumentation systems packages with real time data recording, processing, and communication allows owners, construction managers, and specialty contractors to rapidly respond to any unexpected movement if it does occur. This instrumentation typically involves any combination of hydrostatic level systems, automated total station survey readings, strain gauges, and tilt meters. Automated systems are capable of obtaining readings several times per minute with greater precision than traditional optical methods. The immediate feedback during grouting and excavation allows modification to installation techniques or design revisions (Fig. 6).

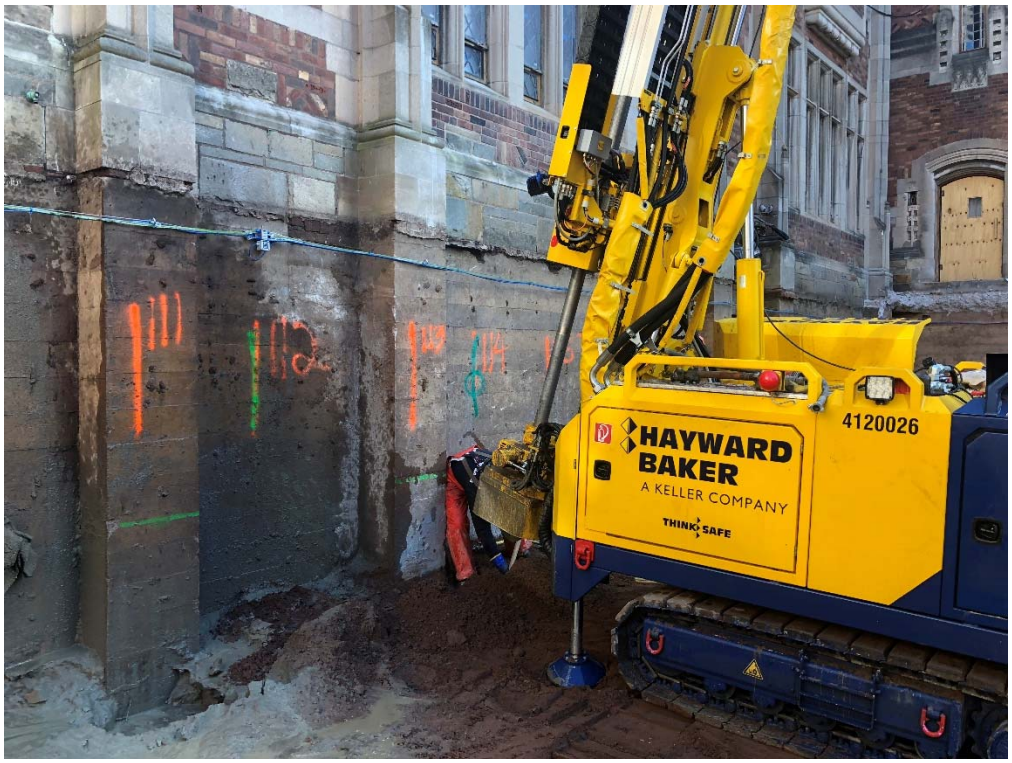


Fig. 6. Jet grout underpinning being performed with a liquid level system and optical prisms for automated total station monitoring fixed to the foundation wall to monitor real time building response.

Spoil management and the importance of spoil relief

Inherent with any jet grouting operation is the generation of spoil, the byproduct of the erosive process. The spoil is relieved through the borehole annulus and must be diverted to temporary holding pits or tanks. Spoil yields vary considerably with system selection, column geometry, sequencing, the grout flow rate, and the monitor extraction rate.

Jet grout spoil will typically move under a gravity head, and with some mechanical assistance from excavator buckets, from the borehole to spoil containment pits near the work area (Fig. 7). When working indoors or in limited footprint work spaces, vacuum trucks are a common means to control and remove spoil during jet grouting operations. For neat cement grouts common in underpinning, soilcrete spoil will cure within 12 hours to a consistency appropriate for excavation and transport for disposal or reuse.



Fig. 7. A spoil trench building being underpinned by jet grouting. A spoil containment area can be seen in the rear ground.

Care must be taken to ensure continuous spoil return through an unrestricted borehole annulus during both drilling and grouting to prevent heave or fracture. While non-cohesive soils generally relieve easily from the borehole, highly plastic clays and silts tend to erode in clumps that can clog the borehole annulus (Fig. 4). Any observed reductions in spoil return must be immediately addressed by reducing the flow rate of injection fluids.

The means and methods for creating a consistent spoil return should be planned and implemented by the grouting contractor. These methods vary depending on soil and groundwater conditions, the depth of the treatment zone, and the proximity and characteristics of underpinned structures. Common methods employed to increase spoil return consistency include:

- Variation in jet grouting system selection
- Variation in air or cutting fluid flow rate
- Variation in cutting fluid viscosity
- Increasing borehole diameter to provide ensure a larger annulus around the drill string
- Predrilling adjacent spoil relief holes within the target treatment zone of each column
- Using casing above the treatment zone to prevent caving of the borehole and reduce side friction
- Reaming of the borehole with the drill string
- Precutting the column to target a smaller initial column geometry

More than one solution to maintaining spoil return may be appropriate for any given project, and addressing these concerns should be left to the creativity and experience of the grouting contractor.

Preparation of the face

Where zero clearance between the planes of the existing footings and the proposed foundation wall is required, jet grouting offers the ability to drill under the footing at a batter and generate a block of soilcrete beyond the proposed extent of the wall. Where soilcrete mass extends beyond the proposed foundation wall due to installation geometry it should be carefully removed with fine excavator teeth, a bladed excavator bucket, or a rotary milling attachment. Semi-circular columns may also be utilized to limit soilcrete generation within the proposed building area. An example of a zero-clearance building excavation utilizing semi-circular underpinning construction is shown in Fig. 8.

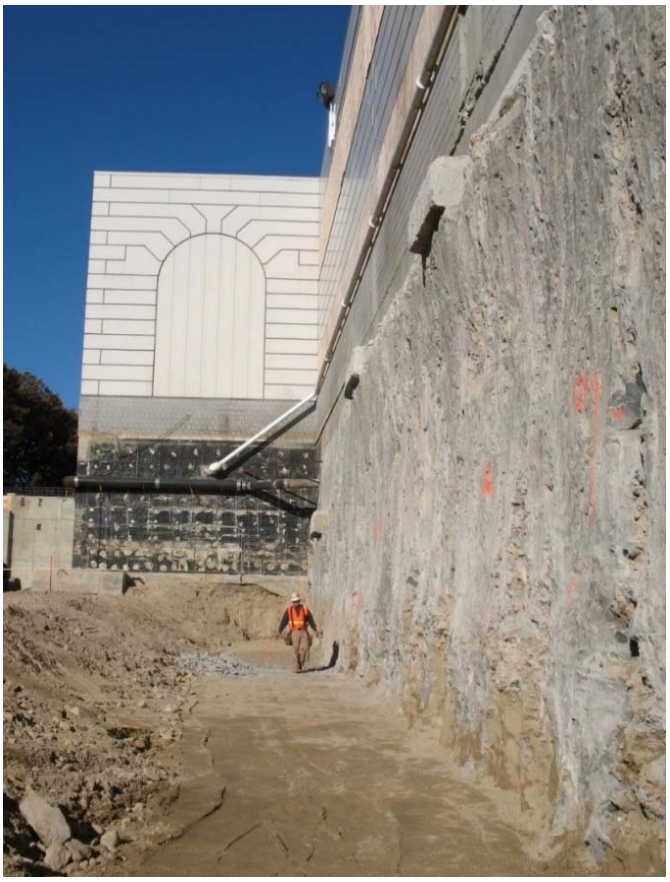


Fig. 8 – A 20-foot excavation with zero clearance to the proposed structure was facilitated through a gravity wall of jet grout underpinning.

ADVANTAGES OF JET GROUT UNDERPINNING

Jet grouting is particularly apt for use in building underpinning and excavation support. Soilcrete may be utilized as a small component of an underpinning design, such as connections between existing structural elements, or as the entire system supporting a building next to an excavation.

Underpinning an existing building is typically performed at the onset of a project, and considerable pressure to improve schedule performance is often placed on the contractor. Jet grout underpinning can be performed significantly faster than traditional pit underpinning or piled underpinning methods.

These potential time savings vary based on the underpinning extent, access conditions, and depth of underpinning treatment required. Schedule savings of more than 50% are typically experienced on projects with more than 150 linear feet of underpinning to a depth of more than five feet. From the experience of the author, this reduced schedule at the onset of a project is often the driving factor encouraging project teams to consider jet grouting.

Jet grouting is well suited for structures with footings of poor condition at bottom. Compared with other underpinning methods, where engineered connection details are required between piles, jet grouting provides intimate positive connections with foundations. This connection allows for buildings to be underpinned with minimal settlements, making it a desirable solution for historic structures (Droof, Furth, & Scarborough, 1995; Massoudi, 2008). Installation is often performed slightly above the existing footing grade, and a positive head of grout is maintained during curing. Without stabilizing additives, cement grout

will bleed during curing and columns may therefore require "topping-off" with fresh grout to maintain a head above bottom of footing elevation.

The drilled-in system is vibration and shock free, and is therefore often recommended around subways, hospitals, and other sensitive building renovations where driven or vibrated piles would be unacceptable. Figure 9 depicts jet grout underpinning installed within 100 feet of the operating room of a historic hospital.



Fig. 9. Jet grout underpinning of a historic hospital building and emergency generator.

Flexibility of design and construction

Jet grout systems provide the designer and contractor significant flexibility in planning for and installing columns where rock, utilities, or obstructions may be present. Utilizing small diameter jet grout drill tools, overcoming these obstacles is more feasible than it is with driven or drilled pile systems, or pit with underpinning. During grouting, obstructions can be incorporated into the soilcrete product by strategically constructing the columns around them. The ability to batter columns around anticipated or unanticipated conditions combined with the flexibility to install soilcrete columns of varied diameters allows for rapid field decisions.



Fig. 10. Jet grout underpinning and excavation support of utility structures installed by battering under the utility where sheet piles (left) and secant piles (right) could not pass through critical utilities.

Access and safety

Underpinning projects often require restricted access foundation renovations through basements, tight alleys or with low headroom restrictions under building overhangs. Jet grouting rigs may be configured to meet these demanding operational requirements (Farr, Camper, & Byford, 2012).

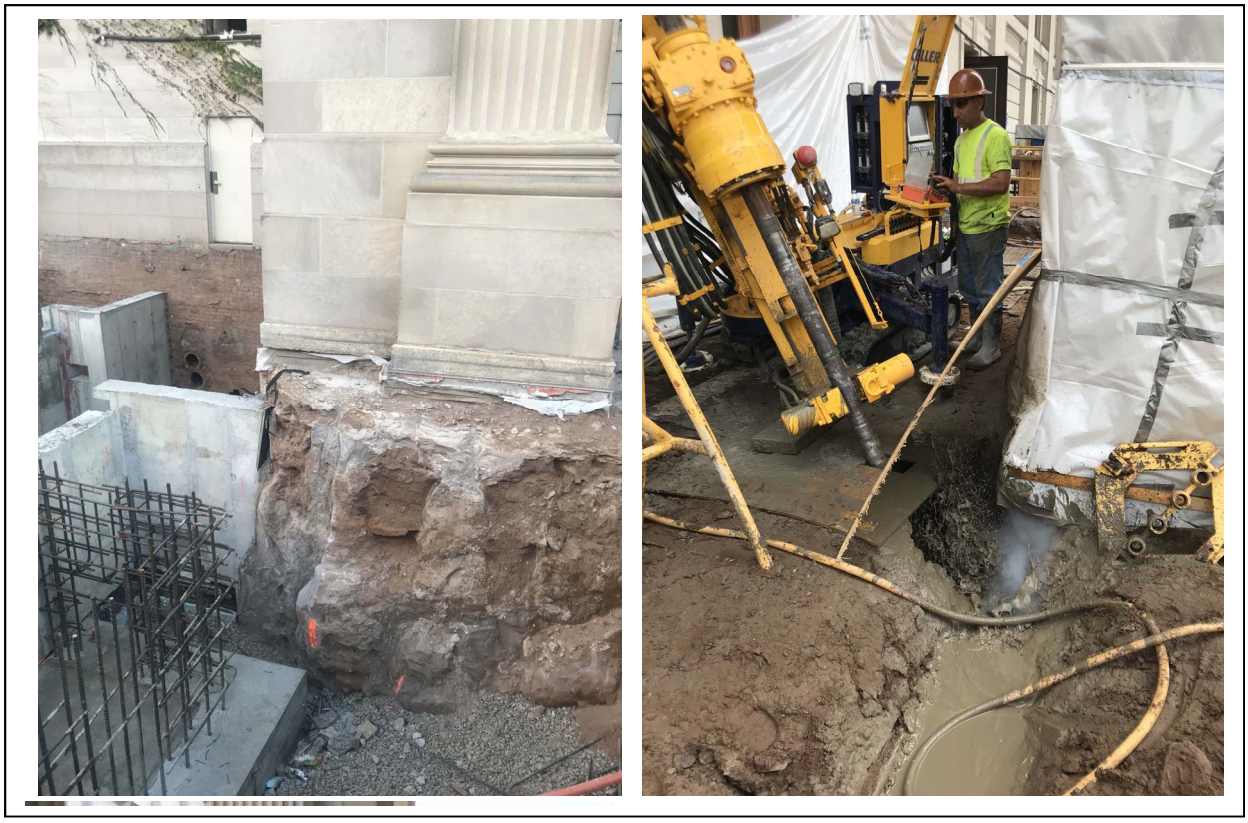


Fig. 11. Restricted access rigs may be used to underpin within basements or tight spaces such as shown behind this sensitive foundation.

When compared with conventional pit underpinning, jet grouting offers a significant safety advantage by removing workers from the confined space below the existing building foundation. Because of this, it is generally regarded as a safer application, provided adequate engineered controls are applied to address the hazards of large equipment, grout, and high-pressure hose lines.

Equipment advancement

Due to the size of the batch plant, work area, and ancillary support tooling and equipment, a jet grouting operation often takes up a considerable portion of a project work site. Recent developments from both equipment manufacturers and specialty contractors have focused on reducing the required footprint of these plants through tiered vertical storage and towable all-in-one batch plants. This is especially true in underpinning given the smaller pumps needed to create 3 to 5-FT columns diameter columns commonly utilized. These smaller pumps have helped reduce mobilization costs and times to expand the attraction of grouting. An example of a modern tiered plant is shown in Fig. XX.



Fig. XX. Tiered batch plants for congested urban sites are one example of equipment advances extending the use of jet grout underpinning.

Use for controlled lift

Jet grouting is not generally applied in scenarios where controlled lift is required by the process itself. The intimate connection between the soilcrete and the footing provides permanent fixity. Other grouting methods such as compaction grouting are often used to increase the bearing capacity of the soil and employed to lift the structure. Piled solutions, such as micropiles, helical piles, or driven piles, offer the ability to couple with a small hydraulic jack between the footing or wall bracket and the pile to raise or lower the structure. In a recent application shown in Fig. XX, soilcrete provided underpinning of slabs and footings as well as a reaction for bracing members to be jacked for controlled lift of select columns.



Fig. XX – Exposed soilcrete columns, left, provide excavation support and underpinning of building slabs and footings. Where controlled lift of foundations was required, soilcrete provided a reaction for structural building jacking. At right, soilcrete has been prepared for single sided foundation wall placement.

SUMMARY AND CONCLUSIONS

Partially due to its relatively limited use and exposure, jet grouting is often perceived in the engineering and construction communities as a risky and expensive solution to underpinning projects. Careful consideration of the project conditions, expectations and risks enables jet grouting to be a viable solution to be tuned to any application. Robust, real-time geotechnical instrumentation monitoring systems have helped reduce the uncertainty and thereby further expand the feasibility of jet grout underpinning applications. When properly designed and constructed by qualified and experienced jet grouting contractors, the flexibility of soilcrete for design and construction may be utilized to overcome the many inherent challenges which complicate underpinning and earth retention systems.

REFERENCES

Burke, G.K. (2002). The State of the Art of Jet Grouting in the United States. NeuviOme conference internationale sur les pieux et les fondations profondes. Nice, France. pp. 74-88.

Burke, G.K. (2004). Jet Grouting Systems: Advantages and Disadvantages. Proceedings of the GeoSupport Conference 2004. Orlando, Florida. pp. 875-886.

Burke, G.K. (2007). New Methods for Underpinning and Earth Retention. Proceedings of Geo-Denver 2007: Grouting for Ground Improvement. Denver, Colorado. pp. 1-12.

Burke, G.K. (2012). The State of the Practice of Jet Grouting. Proceedings of the Fourth International Conference on Grouting and Deep Mixing. New Orleans, Louisiana. pp. 74-88.

Burke, G. K., & Koelling, M. A. (1995). Special Applications for Jet Grouting: Underpinning, Excavation Support and Groundwater Control. Proceedings of Canadian Geotechnical Conference. Vancouver, BC. pp. 1-10.

Burke, G.K. & Welsh, J.P. (1991). Underpinning by Jet Grouting. Deep Foundations Institute 16th Annual Members' Conference. Chicago, Illinois. pp. 323-340.

Burke, G.K., Johnson, L.F. & Heller, R.A., (1989). Jet grouting for underpinning and excavation support. Proceedings of the ASCE 1989 Foundation Engineering Congress, Foundation Engineering: Current Principals and Practices, Col 1 and 2, Evanston, Illinois. pp. 291-306.

Chepurnova, A. (2014). Assessing the influence of jet-grouting underpinning on the nearby buildings. Journal of Rock Mechanics and Geotechnical Engineering, Vol 6, (2), pp. 105-112.

Droof, E.R., Furth, A.J., & Scarborough, J.A., (1995). Jet Grouting to Support Historic Buildings. Proceedings of the ASCE National Convention: Foundation Upgrading and Repair for Infrastructure Improvement. San Diego, California. pp. 42-55.

Essler, R., (2012). The Design of Jet Grouting from Concept to Execution. Proceedings of the Fourth International Conference on Grouting and Deep Mixing. New Orleans, Louisiana. pp. 2071-2081.

Farr, S.J., Camper, K.E., & Byford, B.M. (2012). Jet Grouting for Earth Retention Performed in Low Headroom for Subway Station Expansion. Proceedings of the Fourth International Conference on Grouting and Deep Mixing. New Orleans, Louisiana. pp. 963-971.

Kimpritis, T. (2013). The control of column diameter and strength in Jet Grouting processes and the influence of ground conditions. (Master's thesis, Imperial College London, Department of Civil and Environmental Engineering). Retrieved from http://hdl.handle.net/10044/1/23836

Massoudi, N.M., (2008). Jet Grouting for Support of Excavations Near Historic Structures. Proceedings of GeoCongress 2008: Geosustainability and Geohazard Mitigation. New Orleans, Louisiana. pp. 955-958.

Tirolo V. (2012). Underpinning and Risk - Looking Back and Looking Forward. Lecture presented to ASCE Metropolitan Section / Geo-Institute Chapter: Support of Excavation: Design Construction Instrumentation and Risk in New York, New York.

Wang J.G., Oh B., Lim S.W. & Kumar G.S. (1999). Effect of different jet-grouting Installations on neighboring structures. Proceedings of the 5th International Symposium on Field Measurements in Geomechanics – FMGM99, Singapore. pp. 511–516.

Yoshida, H. (2012). Recent Developments in Jet Grouting. Proceedings of the Fourth International Conference on Grouting and Deep Mixing. New Orleans, Louisiana. pp. 1548-1561.

2019

DFI44 PROCEEDINGS

DEEP FOUNDATIONS INSTITUTE

326 Lafayette Avenue
Hawthorne, NJ 07506
USA
Tel: (973) 423-4030 | Fax: (973) 423-4031
staff@dfi.org | www.dfi.org